ANNUAL ISSUE 2010

PROGRESS IN PHYSICS

"All scientists shall have the right to present their scientific research results, in whole or in part, at relevant scientific conferences, and to publish the same in printed scientific journals, electronic archives, and any other media." — Declaration of Academic Freedom, Article 8

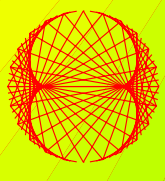

ISSN 1555-5534

The Journal on Advanced Studies in Theoretical and Experimental Physics, including Related Themes from Mathematics

PROGRESS IN PHYSICS

A quarterly issue scientific journal, registered with the Library of Congress (DC, USA). This journal is peer reviewed and included in the abstracting and indexing coverage of: Mathematical Reviews and MathSciNet (AMS, USA), DOAJ of Lund University (Sweden), Zentralblatt MATH (Germany), Scientific Commons of the University of St. Gallen (Switzerland), Open-J-Gate (India), Referativnyi Zhurnal VINITI (Russia), etc.

To order printed issues of this journal, contact the Editors. Electronic version of this journal can be downloaded free of charge:
http://www.ptep-online.com

Postal address

Department of Mathematics and Science,
University of New Mexico,
200 College Road,
Gallup, NM 87301, USA

ISSN: 1555-5534 (print)
ISSN: 1555-5615 (online)

Standard Address Number: 297-5092
Printed in the United States of America

JANUARY 2010 **VOLUME 1**

CONTENTS

Information for Authors and Subscribers

Progress in Physics has been created for publications on advanced studies in theoretical and experimental physics, including related themes from mathematics and astronomy. All submitted papers should be professional, in good English, containing a brief review of a problem and obtained results.

All submissions should be designed in LaTeX format using *Progress in Physics* template. This template can be downloaded from *Progress in Physics* home page http://www.ptep-online.com. Abstract and the necessary information about author(s) should be included into the papers. To submit a paper, mail the file(s) to the Editor-in-Chief.

All submitted papers should be as brief as possible. We accept brief papers, no larger than 8 typeset journal pages. Short articles are preferable. Large papers can be considered in exceptional cases to the section *Special Reports* intended for such publications in the journal. Letters related to the publications in the journal or to the events among the science community can be applied to the section *Letters to Progress in Physics*.

All that has been accepted for the online issue of *Progress in Physics* is printed in the paper version of the journal. To order printed issues, contact the Editors.

This journal is non-commercial, academic edition. It is printed from private donations. (Look for the current author fee in the online version of the journal.)

The Kruskal-Szekeres "Extension": Counter-Examples

Stephen J. Crothers

Queensland, Australia
thenarmis@gmail.com

The Kruskal-Szekeres "coordinates" are said to "extend" the so-called "Schwarzschild solution", to remove an alleged "coordinate singularity" at the event horizon of a black hole at $r = 2m$, leaving an infinitely dense point-mass singularity at "the origin" $r = 0$. However, the assumption that the point at the centre of spherical symmetry of the "Schwarzschild solution" is at "the origin" $r = 0$ is erroneous, and so the Kruskal-Szekeres "extension" is invalid; demonstrated herein by simple counter-examples.

1 Introduction

According to the astrophysical scientists the solution for Einstein's static vacuum gravitational field must satisfy the following conditions [1–11]:

(a) It must be static; i.e. all the components of the metric tensor must be independent of time and the geometry must be unchanged under time reversal;

(b) It must be spherically symmetric;

(c) It must satisfy the equations $R_{\mu\nu} = 0$; no matter present;

(d) It must be asymptotically Minkowski spacetime.

The so-called "Schwarzschild solution" (which is not in fact Schwarzschild's solution at all) is (using $c = 1$ and $G = 1$),

$$ds^2 = \left(1 - \frac{2m}{r}\right)dt^2 - \left(1 - \frac{2m}{r}\right)^{-1} dr^2 - \\ - r^2\left(d\theta^2 + \sin^2\theta\, d\varphi^2\right). \qquad (1)$$

The astrophysical scientists merely inspect this line-element and thereby assert that there are singularities at $r = 2m$ and at $r = 0$ [3, 4, 7, 9]; the former they claim to be a "coordinate" or "removable" singularity which denotes the "radius" of an event horizon of a black hole of mass m located at the "real" or "physical" singularity at $r = 0$. They call $r = 2m$ the "Schwarzschild radius" and $r = 0$ "the origin".

It is plainly evident that metric (1) changes its signature from $(+,-,-,-)$ to $(-,+,-,-)$ when $0 < r < 2m$, despite the fact that metric (1) is supposed to be a generalisation of Minkowski spacetime, described by (using $c = 1$),

$$ds^2 = dt^2 - dr^2 - r^2\left(d\theta^2 + \sin^2\theta\, d\varphi^2\right) \qquad (2)$$

$$0 \leqslant r < \infty,$$

which has *fixed* signature $(+,-,-,-)$; and so there is in fact no possibility for Minkowski spacetime to change signature from $(+,-,-,-)$ to $(-,+,-,-)$ [5]. Consequently, $0 \leqslant r < 2m$ on Eq. (1) has no counterpart in Minkowski spacetime. Nonetheless, although the astrophysical scientists *deliberately* fix the signature to $(+,-,-,-)$ at the very outset of their derivation of Eq. (1) [1–9, 11, 12], in order to maintain the signature of Minkowski spacetime, they nonetheless allow a change of signature to occur in Eq. (1) to $(-,+,-,-)$ [3, 4, 7, 9, 10, 13, 14] according to their assumption that $0 \leqslant r < \infty$ applies to Eq. (1); in direct violation of their initial construction. They then invoke a complicated "change of coordinates" to make the singularity at $r = 2m$ disappear; the Kruskal-Szekeres coordinates [3, 4, 9, 13, 14]. The astrophysical scientists merely assume that the point at the centre of spherical symmetry of the manifold described by Eq. (1) is located at "the origin", $r = 0$. To justify their assumptions on the variable r, which they evidently conceive of as radial distance in "Schwarzschild" spacetime (e.g. "Schwarzschild radius"), they also claim that because the Riemann tensor scalar curvature invariant (the "Kretschmann scalar"), given by $f = R_{\alpha\beta\gamma\delta}R^{\alpha\beta\gamma\delta}$, is finite at $r = 2m$ and unbounded at $r = 0$, there must be a "real" singularity only at $r = 0$. This argument they apply *post hoc*, without any proof that General Relativity requires such a condition on the Kretschmann scalar.

The assumption that "the origin" $r = 0$ marks the point at the centre of spherical symmetry of the manifold described by (1) is demonstrably false. Furthermore, a geometry is fully determined by its line-element [5, 15], not by arbitrary values assigned to any curvature invariant which is calculated from the line-element itself in the first place. Given a line-element of the form of Eq. (1) the admissible values of its associated curvature invariants and the location of its centre of spherical symmetry are fully fixed by it, and so they cannot be arbitrarily determined by simple inspection and *ad hoc* assumptions.

To illustrate the inadmissibility of the methods applied by the astrophysical scientists in their analysis of Eq. (1), I shall adduce counter-examples that satisfy all the required conditions (a)–(d) and their additional assumptions concerning r and the Kretschmann scalar, but nevertheless clearly contradict the claims made by the astrophysical scientists in relation to Eq. (1). By these counter-examples I will demonstrate, by application of the very same methods the astrophysical scientists apply to Eq. (1), that there are "spacetimes" in which the

singularity of a "black hole" is encountered before the event horizon, and that this event horizon can be "removed" by application of the Kruskal-Szekeres method. I will also give an example that not only inverts the locations of the event horizon and the singularity, relative to Eq. (1), but also locates them both at places other than the "origin" $r = 0$ at which the metric is well-defined. It is in fact rather easy to generate an infinite number of such counter-examples (but just one is sufficient to invalidate the Kruskal-Szekeres "extension").

These counter-examples amplify the fact that the usual assumption on Eq. (1) that "the origin" $r = 0$, simply by inspection, marks the point at the centre of spherical symmetry of the manifold it describes, is entirely false, and that the additional assumption that the Kretschmann scalar must be unbounded at a "real" or "physical" singularity is also false. This should not really be all that surprising, bearing in mind that the usual assumptions are just that, for which no proofs have ever been produced. It follows that there is no black hole associated with Eq. (1), and that the Kruskal-Szekeres "extension" is fallacious.

It is easily proven that r in Eq. (1) is the inverse square root of the Gaussian curvature of the spherically symmetric geodesic surface in the spatial section [16, 17, 19]. Being directly related to a curvature invariant, its values are fixed by the intrinsic geometry, fixed by the form of the line-element itself, as are all other related curvature invariants.

It must also be remarked that the transition from Minkowski spacetime to Schwarzschild spacetime involves no matter whatsoever. Therefore Schwarzschild spacetime is not in fact a generalisation of the laws of Special Relativity; only a generalisation of the geometry of Minkowski spacetime. The speed of light in vacuum, c, which appears in the Minkowski line-element is not a photon; it is a speed, the maximum speed with which a point is permitted to move in Minkowski spacetime. Similarly, the appearance of the constant c in Schwarzschild spacetime does not imply the presence of a photon there either. A photon must be present *a priori* to assign the speed c to the photon. Neither photons nor masses are present, by construction, in the generalisation of Minkowski spacetime to Schwarzschild spacetime, owing to the equations $R_{\mu\nu} = 0$ according to condition (c). Minkowski spacetime is not Special Relativity — the latter requires the *a priori* presence of matter, the former does not. Schwarzschild spacetime is a spacetime that by construction contains no matter, and hence no sources.

2 Counter-examples

Consider the metric

$$ds^2 = \left(1 - \frac{2m}{2m-r}\right) dt^2 - \left(1 - \frac{2m}{2m-r}\right)^{-1} dr^2 - \\ - (r-2m)^2 \left(d\theta^2 + \sin^2\theta\, d\varphi^2\right). \tag{3}$$

First, it is clear that Eq. (3) satisfies all the conditions (a)–(d), and so metric (3) is as good as metric (1). I now apply to Eq. (3) the very same methods that the astrophysical scientists apply to Eq. (1) and so assume that $0 \leqslant r < \infty$ on Eq. (3), and that "the origin" $r = 0$ marks the point at the centre of spherical symmetry of the manifold. By inspection there are two "singularities"; at $r = 2m$ and at $r = 0$, just as in the case of Eq. (1). When $r > 2m$ the signature of (3) is $(+,-,-,-)$, just as in Eq. (1). When $0 < r < 2m$ the signature is $(-,+,-,-)$, again just as in Eq. (1). Now when $r = 2m$, the coefficient of dt^2 in Eq. (1) is zero, but in Eq. (3) it is undefined. Similarly, when $r = 0$, the coefficient of dt^2 in Eq. (1) is undefined but in Eq. (3) it is zero. Furthermore, when $r = 2m$, the Kretschmann scalar is $f = 3/4m^4$ in Eq. (1) but is undefined in Eq. (3), and when $r = 0$, the Kretschmann scalar is $f = 3/4m^4$ in Eq. (3) but is undefined in Eq. (1). Therefore, according to the methods of the astrophysical scientists there is an infinitely dense point-mass singularity at $r = 2m$ and an event horizon at $r = 0$ in Eq. (3) (or alternatively a singularity of finite density and radius $r = 2m$ so that the event horizon is within the singularity). Thus the singularity is encountered before the event horizon, and the "Schwarzschild radius" of the black hole in Eq. (3) is $r = 0$. Again, following the very same methods that the astrophysical scientists apply to Eq. (1), apply the Kruskal-Szekeres method to remove the "coordinate singularity" at $r = 0$ in Eq. (3) by setting

$$u = \left(1 - \frac{2m-r}{2m}\right)^{\frac{1}{2}} e^{\frac{2m-r}{4m}} \sinh\frac{t}{4m},$$

$$v = \left(1 - \frac{2m-r}{2m}\right)^{\frac{1}{2}} e^{\frac{2m-r}{4m}} \cosh\frac{t}{4m}.$$

Then metric (3) becomes,

$$ds^2 = \frac{32m^3}{r-2m} e^{\frac{r-2m}{2m}} \left(du^2 - dv^2\right) + \\ + (r-2m)^2 \left(d\theta^2 + \sin^2\theta\, d\varphi^2\right), \tag{4}$$

where r is a function of u and v, by means of

$$\left(\frac{r}{2m}\right) e^{\frac{2m-r}{2m}} = v^2 - u^2.$$

It is now apparent that Eq. (4) is not singular at $r = 0$. The singularity at the event horizon with its "Schwarzschild radius" $r = 0$ has been removed. The metric is singular only at $r = 2m$ where according to the astrophysical scientists there must be an infinitely dense point-mass singularity (or alternatively a singularity of finite density and radius $r = 2m$ so that the event horizon is within the singularity).

In obtaining Eq. (4) I have done nothing more than that which the astrophysical scientists do to Eq. (1), and since (1) and (3) satisfy conditions (a)–(d), the one is as good as the other, and so Eq. (3) is as valid as Eq. (1) insofar as the methods of the astrophysical scientists apply. Thus, the methods

employed by the astrophysical scientists are flawed. To amplify this even further, consider the metric,

$$ds^2 = \left(1 - \frac{2m}{4m-r}\right)dt^2 - \left(1 - \frac{2m}{4m-r}\right)^{-1} dr^2 - \\ -(r-4m)^2\left(d\theta^2 + \sin^2\theta\, d\varphi^2\right). \quad (5)$$

It is clear that this metric also satisfies conditions (a)–(d), and so Eq. (5) is as good as eqs. (1) and (3). Once again, applying the very same methods of the astrophysical scientists, assume that $0 \leqslant r < \infty$ and that $r = 0$ is the "origin". Then by inspection there are singularities at $r = 4m$ and at $r = 2m$. For $r > 4m$ the signature of (5) is $(+,-,-,-)$; for $2m < r < 4m$ it is $(-,+,-,-)$ and for $0 \leqslant r < 2m$ it is $(+,-,-,-)$. Now at $r = 4m$ the coefficient of dt^2 is unbounded and at $r = 2m$ it is zero. But at $r = 0$ it is neither zero nor unbounded — the metric is well-defined there. Furthermore, at $r = 4m$ the Kretschmann scalar is unbounded and at $r = 2m$ it is $f = 3/4m^4$, but at $r = 0$ it is $f = 3/256m^4$. Thus, according to the methods of the astrophysical scientists there is an event horizon at $r = 2m$ with "Schwarzschild radius" $r = 2m$, and an infinitely dense point-mass singularity at $r = 4m$ (or alternatively a singularity of finite density and radius $r = 4m$ so that the event horizon is within the singularity). So the singularity is encountered before the event horizon. The "coordinate" event horizon singularity at "Schwarzschild radius" $r = 2m$ can be removed by again applying the Kruskal-Szekeres method, by setting

$$u = \left(\frac{4m-r}{2m} - 1\right)^{\frac{1}{2}} e^{\frac{4m-r}{4m}} \cosh\frac{t}{4m}$$

$$v = \left(\frac{4m-r}{2m} - 1\right)^{\frac{1}{2}} e^{\frac{4m-r}{4m}} \sinh\frac{t}{4m}$$

for $r < 2m$, and

$$u = \left(1 - \frac{4m-r}{2m}\right)^{\frac{1}{2}} e^{\frac{4m-r}{4m}} \sinh\frac{t}{4m}$$

$$v = \left(1 - \frac{4m-r}{2m}\right)^{\frac{1}{2}} e^{\frac{4m-r}{4m}} \cosh\frac{t}{4m}$$

for $r > 2m$.

Metric (5) then becomes

$$ds^2 = \frac{32m^3}{r-4m} e^{\frac{r-4m}{2m}}\left(du^2 - dv^2\right) + \\ (r-4m)^2\left(d\theta^2 + \sin^2\theta\, d\varphi^2\right), \quad (6)$$

where r is a function of u and v, by means of

$$\left(\frac{2m-r}{2m}\right) e^{\frac{4m-r}{2m}} = u^2 - v^2.$$

It is apparent that Eq. (6) is singular only at $r = 4m$, where, according to the astrophysical scientists, there is an infinitely dense point-mass singularity (or alternatively a singularity of finite density and radius $r = 4m$ so that the event horizon is within the singularity). At the event horizon with "Schwarzschild radius" $r = 2m$, the metric is not singular. At the "origin", $r = 0$ the metric is well-defined, and since Eq.'s (1), (3) and (5) satisfy conditions (a)–(d), any one is as good as any other, and so Eq. (5) is as valid as Eq. (1) insofar as the methods of the astrophysical scientists apply. Since metrics (1), (3) and (5) all satisfy conditions (a)-(d) there is no *a priori* reason to favour one over the other. Moreover, all the faults associated with metrics (3) and (5) are shared by metric (1), insofar as the methods of the astrophysical scientists are concerned, despite them all satisfying the required conditions (a)–(d). Those faults lie in the assumptions of the astrophysical scientists, as applied to all the Schwarzschild spacetime metrics above.

It is of utmost importance to note that Eq. (1) is not in fact Schwarzschild's solution. Here is Schwarzschild's actual solution.

$$ds^2 = \left(1 - \frac{\alpha}{R}\right)dt^2 - \left(1 - \frac{\alpha}{R}\right)^{-1} dR^2 - R^2\left(d\theta^2 + \sin^2\theta\, d\varphi^2\right),$$

$$R = \left(r^3 + \alpha^3\right)^{\frac{1}{3}}, \quad 0 < r < \infty, \quad \alpha = const.$$

Here r is not a distance of any kind in the manifold; and it is not the inverse square root of the Gaussian curvature of the spherically symmetric geodesic surface in the spatial section of Schwarzschild's solution — it is a parameter (and so it is also in Eq. (1)). Schwarzschild's solution contains only one singularity, when $r = 0$, and so it precludes the black hole. The so-called "Schwarzschild solution" is a corruption, due to David Hilbert [22, 23], of Schwarzschild's solution, and the solution obtained independently by Johannes Droste [24].

The correct generalised treatment of Schwarzschild geometry is given in [16–21].

3 The usual derivation of the "Schwarzschild solution"

The astrophysical scientists begin with Eq. (2) and propose a generalisation of the form (or equivalent thereof),

$$ds^2 = e^{2\lambda}dt^2 - e^{2\beta}dr^2 - r^2\left(d\theta^2 + \sin^2\theta\, d\varphi^2\right), \quad (7)$$

the exponential functions being introduced to maintain the signature of Minkowski spacetime, $(+,-,-,-)$, thereby ensuring that the coordinates r, θ, φ remain space-like quantities and t remains a time-like quantity [1–9, 11, 12]. Both λ and β are real-valued analytic functions of only the real variable r. Eq. (1) is then obtained in accordance with conditions (a)–(d). Despite the fixed signature of Eq. (7), the astrophysical scientists permit a change of signature in their resultant Eq. (1), in violation of their construction of Eq. (7), by which they produce a black hole by the Kruskal-Szekeres method. Note that the change of signature in Eq. (1) to $(-,+,-,-)$, in violation of the construction of Eq. (7), causes the rôles

of the quantities t and r to be exchanged, i.e. t becomes a space-like quantity and r becomes a time-like quantity. This means that all the components of the metric tensor of Eq. (1) become functions of the time-like quantity r: but this is then a non-static metric, in violation of condition (a).

There is no matter present in the derivation of Eq. (1) from Eq. (7), since all matter, including sources, is eliminated by construction, according to condition (c), i.e. $R_{\mu\nu} = 0$, and since there is no matter present in Eq. (2) either. It is however claimed by the astrophysical scientists that matter is nonetheless present as a source of the alleged gravitational field "outside a body", and that the field caused by this source, permeating the spacetime "outside" it, in the spacetime of $R_{\mu\nu} = 0$, is Schwarzschild spacetime, obtained from Eq. (7). The constant appearing in the line-element for the "Schwarzschild solution" the astrophysical scientists arbitrarily assign as mass, *post hoc*, by simply inserting Newton's expression for escape velocity: a two-body relation into an alleged one-body problem (their "outside a body"). But it is obviously impossible for Schwarzschild spacetime, which is alleged by the astrophysical scientists by construction to contain one mass in an otherwise totally empty Universe, to reduce to or otherwise contain a relation that is defined in terms of the *a priori* interaction of two masses. Their invalid resort to Newtonian theory is amplified by writing Eq. (1) in terms of c and G explicitly,

$$ds^2 = \left(c^2 - \frac{2Gm}{r}\right)dt^2 - c^2\left(c^2 - \frac{2Gm}{r}\right)^{-1} dr^2 - \\ - r^2\left(d\theta^2 + \sin^2\theta d\varphi^2\right).$$

The term $2Gm/r$ is now immediately recognised as the square of the Newtonian escape velocity from a mass m at radius r. And so the astrophysical scientists assert that for a black hole the "escape velocity" is that of light in vacuum at an event horizon ("Schwarzschild radius") $r_s = 2Gm/c^2$. But escape velocity is a concept that involves *two bodies* - one body escapes from another body. Even though one mass appears in the expression for Newton's escape velocity, it cannot be determined without recourse to a fundamental two-body gravitational interaction by means of Newton's theory of gravitation. The *post hoc* introduction of mass into the "Schwarzschild solution" is thus, inadmissible. Furthermore, the quantity r appearing in Newton's expression for escape velocity is a radial distance, but it is not radial distance in Schwarzschild spacetime because it is not even a distance in Schwarzschild spacetime.

4 Conclusions

The foregoing counter-examples show that the methods used by the astrophysical scientists in analysing Eq. (1), by which they construct the black hole, are invalid. Instead of using the line-element to determine all the intrinsic geometric properties of the manifold, as they should, they instead make false assumptions, by mere inspection, as to the "origin", the geometric identity of the quantity r, the values of the Riemann tensor scalar curvature invariant (the Kretschmann scalar), and the presence of matter. The fact is that the quantity r appearing in all the line-elements discussed herein is not even a distance, let alone a radial one, in any of the line-elements. Moreover, in Eq. (1), $r = 0$ certainly does not mark the "origin" or point at the centre of spherical symmetry of the "Schwarzschild" solution, contrary to the arbitrary assertions of the astrophysical scientists. The identity of the point at the centre of spherical symmetry is also determined from the line-element, by calculation. The astrophysical scientists have never correctly identified the geometric identity of r in Eq. (1). Without knowing the true identity of r, and by making their concomitant additional false assumptions, they have violated the intrinsic geometry of the line-element. It is from these violations that the black hole has been constructed by the astrophysical scientists. There is in truth no solution to Einstein's field equations that predicts the black hole.

Minkowski spacetime is not Special Relativity: there is no matter involved in the transition from Minkowski spacetime to Schwarzschild spacetime, and so Schwarzschild spacetime does not generalise the laws of Special Relativity, and so does not describe Einstein's gravitational field.

Submitted on August 16, 2009 / Accepted on August 22, 2009

References

1. Einstein A. The meaning of relativity. Science Paperbacks and Methuen & Co. Ltd., 1967, 56–57.
2. Schwarzschild K. On the gravitational field of a mass point according to Einstein's theory. *Sitzungsber. Preuss. Akad. Wiss., Phys. Math. Kl.*, 189, 1916.
3. Schutz B. F. A first course in general relativity. Cambridge University Press, UK, 1990.
4. Misner, C. W., Thorne K. S., Wheeler, J. A. Gravitation. W. H. Freeman and Company, New York, 1970.
5. Tolman R. C. Relativity, thermodynamics, and cosmology. Dover Publications Inc., New York, 1987.
6. Pauli W. The theory of relativity. Dover Publications, Inc., New York, 1981.
7. Dirac P. A. M. General theory of relativity. Princeton Landmarks in Physics Series, Princeton University Press, Princeton, New Jersey, 1996.
8. Landau L., Lifshitz E. The classical theory of fields. Addison-Wesley Publishing Company, Inc., Reading, Massachusettes, 1951.
9. Foster J., Nightingale J. D. A short course in General Relativity. Springer-Verlag, New York, Inc., 1995.
10. Finkelstein D. Past-future asymmetry of the gravitational field of a point particle. *Phys. Rev.*, 1958, v. 110, no. 4, 965–967.
11. Eddington A. S. The mathematical theory of relativity. Cambridge University Press, Cambridge, 2nd edition, 1960.
12. Weyl H. Space, time, matter. Dover Publications Inc., New York, 1952.
13. Kruskal M. Maximal extension of Schwarzschild manifold. *Phys. Rev.*, 1960, v. 119, no. 5, 1743–1745.
14. Szekeres G. On the singularities of a Riemannian manifold. *Math. Debrecea*, 1960, v. 7, 285–301.

15. Efimov N. V. Higher geometry. Mir Publishers, Moscow, 1980.
16. Crothers S. J. Gravitation on a spherically symmetric metric manifold. *Progress in Physics*, 2007, v. 2, 68–74.
17. Crothers S. J. The Schwarzschild solution and its implications for gravitational waves. *Mathematics, Physics and Philosophy in the Interpretations of Relativity Theory*, Proceedings of the Conerence, Budapest, 4–6 September, 2009.
18. Crothers S. J. On the geometry of the general solution for the vacuum field of the point-mass. *Progress in Physics*, 2005, v. 2, 3–14.
19. Crothers S. J. Certain conceptual anomalies in Einstein's theory of relativity. *Progress in Physics*, 2008, v. 1, 52–57.
20. Crothers S. J. On isotropic coordinates and Einstein's gravitational field. *Progress in Physics*, 2006, v. 3, 7–12.
21. Crothers S. J. On the ramifications of the Schwarzschild space-time metric. *Progress in Physics*, 2005, v. 1, 74–80.
22. Abrams L. S. Black holes: the legacy of Hilbert's error. *Can. J. Phys.*, 1989, v. 67, 919.
23. Antoci S. David Hilbert and the origin of the "Schwarzschild" solution. 2001, www.sjcrothers.plasmaresources.com/hilbert.pdf
24. Droste J. The field of a single centre in Einstein's theory of gravitation, and the motion of a particle in that field. *Ned. Acad. Wet., S. A.*, 1917, v. 19, 197.
25. Brillouin M. The singular points of Einstein's Universe. *Journ Phys. Radium*, 1923, v. 23, 43.

Is Fundamental Particle Mass 4π Quantized?

Robert A. Stone Jr.
1313 Connecticut Ave, Bridgeport, CT 06484, USA
E-mail: robert.a.stone.jr@gmail.com

The Standard Model lacks an explanation for the specific mass values of the fundamental particles. This is to report that a single spin quantized mass formula can produce the masses of the proton, the W, and the three electron generations. The 4π mass quantization pattern limits the electron generations to three, while the particle's generational property is one of the components of the proposed intra-particle quantization process. Although the developed relationships are presently phenomenological, so was Bohr's atomic quantization proposal that lead to quantum mechanics.

1 Introduction

In an attempt to understand the reason for particle mass values, several authors have looked for mass relationships among the known particles.

Nambu [1] suggested that quark composite particle mass may be quantized, showing a 70 MeV quantization pattern.

Palazzi [2] (2007) revisits this hypothesis for mesons showing that this quantization pattern is statistically real.

Ne'eman and Sijacki [3] use the SL(4,R) group and spin (1/2,3/2,5/2, etc.) to produce the Regge trajectory like behavior of quark particle masses suggesting the possibility that mass may be spin quantized.

What has not been seen is that given the experimental and theoretical uncertainty, the measured $W^{\pm}$ mass of 80398 ± 25 MeV [4] is exactly $2m_{\mathrm{p}}/m_{\mathrm{e}}$ (3672.30534) times the mass value symmetrically between the electron and the proton ($\sqrt{m_p\, m_e}$ = 21.89648319 MeV), i.e. 80410.57 MeV.

2 Fundamental particle mass, a spin quantized process?

Taking a mass symmetric approach to fundamental particle mass leads to an eloquently simple spin quantized mass relationship between the stable spin 1/2 electron and proton mass and the unstable spin 1 $W^{\pm}$ particle mass given by

$$m_x = M_{\mathrm{sp}}\,(2S\,m_p/m_e)^{(SCM)}, \qquad (1)$$

where x is {p,e,W}, the mass symmetry point M_{sp} is 21.89648319 MeV, S is the spin quantum number $\{\frac{1}{2},1\}$, C is the charge quantum number $\{\pm1\}$, and M is the matter type quantum number {matter = +, anti-matter = −}.

Thus equation (1) is both mass and charge up/down symmetric, spin quantized and indicates Nature may be fundamentally mass symmetric.

As indicated in §9, this mass up/down symmetry is in keeping with the measured cosmological constant.

3 Nature's constants, as functions of 4π

Proposing natures coupling constants are a function of 4π and the fine structure coupling constant and the weak (angle) coupling constant are connected to mass, yields the following 4π definitions.

The fine structure constant $\alpha_{\mathrm{cs}} = \pi\varsigma(4\pi\varrho)^{-2}/(2\sqrt{2})$, the charged weak angle $\alpha_{\mathrm{sg}} = 2\sqrt{2}(4\pi\varrho)^{-1}$ (∼.2344 vs .2312 [5]), where "g" is the other force that couples to produce the weak coupling constant. The relationship to mass is $\pi m_{\mathrm{e}}/m_{\mathrm{p}} = \alpha_{\mathrm{cs}}\alpha_{\mathrm{sg}} = \alpha_{\mathrm{cg}} = \pi\varsigma(4\pi\varrho)^{-3}$ and thus $m_{\mathrm{p}}/m_{\mathrm{e}} = (4\pi\varrho)^3/\varsigma$. The uncharged (neutrino) weak angle $\alpha_{\mathrm{sg}(1)} = 2\sqrt{2}(4\pi1)^{-1}$ (∼.2251 vs .2277 [6]). The new constant $\varrho = \alpha_{cs}\,\alpha_{sg(1)}\,m_{\mathrm{p}}/(m_{\mathrm{e}}\,\pi) = 0.959973785$ and $\varsigma = (4\pi\varrho)^3\,m_{\mathrm{e}}/m_{\mathrm{p}} = 0.956090324$.

4 Fundamental particle mass, a 4π quantized process?

Equation (1) rewritten with the 4π definition of $m_{\mathrm{p}}/m_{\mathrm{e}}$ results in

$$m_x = M_{\mathrm{sp}}\,(2S\,(4\pi\varrho)^3/\varsigma)^{(SCM)}. \qquad (2)$$

In addition to being spin quantized, equation (2) indicates that the fundamental particle mass quantization process is a function of $(4\pi)^x$. For example, the pure theory $m_{\mathrm{p}(1,1)}/m_{\mathrm{e}(1,1)}$ ratio ($\varrho = 1, \varsigma = 1$) is exactly $(4\pi)^3$ where the deviation from the pure theory 4π quantization process is given by ϱ.

5 Three electron generations, a 4π quantized process?

The electron generational mass ratios also appear to be a function of $(4\pi\varrho_x)^x$ or more precisely $(4\pi\varrho_x)^{(3-x)}$.

The first ($x = 1$) mass ratio μ to e (i.e $m_{\mathrm{e}_1}/m_{\mathrm{e}_0}$) is $\sqrt{2}(4\pi\varrho_1)^{(3-1)}$ where $\varrho_1 = .962220482$ while the second ($x = 2$) mass ratio $m_{\mathrm{e}_2}/m_{\mathrm{e}_1}$ is $\sqrt{2}(4\pi\varrho_2)^{(3-2)}$ with $\varrho_2 = .946279794$.

Note that ϱ and ϱ_x are believed to be the deviation from pure theory for two separate frequency components of the quantization processes.

Thus the form of the first and second (x=1,2) generation mass ratios $(m_{\mathrm{e}(x)}/m_{\mathrm{e}(x-1)})$ is $\sqrt{2}(4\pi\varrho_x)^{3-x}$. The deviation from the generational pure theory 4π quantization process increases (smaller ϱ_x) with higher generations.

This $\sqrt{2}(4\pi)^{3-x}$ pattern also results in the $x = 3$ mass ratio $(m_{\mathrm{e}_3}/m_{\mathrm{e}_2})$ of $(4\pi)^{(3-3)}$, i.e. no higher $(4\pi)^x$ quantized mass states and thus no higher generations.

The similarity of 4π quantization allows the fundamental particle equation (1) to be combined with the generational re-

lationship into a single phenomenological equation given by,

$$m_x = M_{\mathrm{sp}(n)}\,(2S\,(4\pi\varrho)^3/\varsigma)^{(SCM)}, \qquad (3)$$

where $M_{\mathrm{sp}(n)} = M_{\mathrm{sp}}\ S^{-n/2}(4\pi\varrho_n)^{(6Sn-Sn(n+1))}$ and $\varrho_n = 1 - \log(1 + 64.75639\ n/S)/(112S)$ are used and generation n is {0,1,2}.

From (3), the m_{e_1} (μ) mass is 105.6583668 MeV (μ = 105.6583668 ± .0000038 MeV [4]) and the m_{e_2} (τ) mass is 1776.83 MeV (τ = 1776.84 ± .17 MeV [4]).

Remember that even though both ϱ_n, and ϱ represent deviations from the pure theory $(4\pi)^x$ quantization nature of these particles' masses, their cause is understood to be related to two separate quantization process components.

6 The Standard Model and quantization

First, the quantization proposition is not in conflict with the existence of quarks. Rather quantization is an additional constraint. The quantization proposition is that if there is a (pseudo-) stable frequency quantized state, then there is an observed (persistent) massed particle resulting in;

1) a specific stable quantization state energy/mass or

2) a pseudo-stable quantized decay mass value.

Thus the quantization process constrains the stable particle base mass or unstable particle decay point mass while the types and symmetries of quarks construct the particle variations seen in the "particle zoo".

That quark composite particle masses are quantized was first suggested by Nambu [1] and recently statistically validated by Palazzi [2]. The quantization increments cited are 70 (n=integer) and 35 MeV (n=odd or n=even) which are approximately $M_{\mathrm{sp}}\ \pi$ and $M_{\mathrm{sp}}\ \pi/2$. Thus for example η (547) has n=16 [2] and using $M_{\mathrm{sp}}\ n\pi/2$ gives $m_\eta = M_{\mathrm{sp}}\ 8\pi \simeq 550$.

A Regge trajectory like spin quantum number based quantization pattern is given by Ne'eman and Sijacki [3] where the particle's measured mass vary about the predicted points. For the (3/2,1) group the points are approximately $(20, 22, 24)\ \pi\ M_{\mathrm{sp}}$, for the (5/2,2) group they are approximately $(24, 26, 28, 30, 32)\ \pi\ M_{\mathrm{sp}}$, and for the (7/2,3) group they are approximately $(28, 30, 32, 34, 36, 38, 40)\ \pi\ M_{\mathrm{sp}}$.

Second, a quantizing mechanism as fundamental to the nature of massed particles is a natural explanation given QM's quantized nature.

Third, an intra-particle quantization process minimally needs two intra-particle frequency components. Equation (3) suggests one component is related to the particle's "invariant" mass/energy and a second component is related to the generational mass symmetry point. A generational component could be the source for and thus explain the generational exchange seen in the muon neutrino nucleon interaction $\nu_\mu + N \rightarrow P^+ + \mu^-$. The generational component's effect on the charged particle mass symmetry point is $M_{\mathrm{sp}(n)}$.

Is the massed particle a "quantized photon"?

Is the first photonic component of the quantization process the underlying reason for the universality of Maxwell's equations for both photons and charged particles?

Is the second quantizing component responsible for the intra-particle mass and charge quantization, for the generational property, as well as the (inter-particle?) quantization of QM?

7 Equation 1 and new particles

If quantization is the source of (1) then, quark structure permitting, there may be a second generation proton. From the phenomenological equation (3), $m_{\mathrm{p}_2} \simeq 194$ GeV. This second generation proton is within LHC's capabilities.

Note that equation (3) is phenomenological and another option exists for merging the electron generations.

Equation (1) also indicates the possibility of a new "lepton like" (mass down charge down) spin 1 light $W^\pm$ particle with a mass of $\sim$ 5.96 KeV (m_{lW}). If such low frequency/energy quantization is possible, the $lW^\pm$'s decay, like the $W^\pm$'s decay, would be instantaneous. At KeV energy, attempted quantization may only result in enhanced photon production. At MeV energies, $lW^\pm$ pair production with instantaneous decay would look like an electron positron pair production but would actually be $lW^- \rightarrow e^- + \bar{\nu}$ and $lW^+ \rightarrow e^+ + \nu$ decays.

Finally, the super-symmetric (charge and mass symmetric) view that results from equation (1) can make some fundamental Standard Model problems go away.

8 The matter only universe problem

The present SM has only a matter anti-matter mass creation process, yet we appear to have a matter only universe. This aspect is presently unaccounted for.

The super-symmetric view indicated by the charge and mass up/down symmetry of (1) and (2) enables the possibility of an alternate mechanism for fundamental particle creation.

This alternate process symmetrically breaks the electron and proton of the same mass (for eq. (2), at $\varrho = (4\pi)^{-1}, \varsigma = 1$, $m_e = m_p$) into a proton of higher mass (up) and an electron of lower mass (down), yielding a matter only universe.

9 The cosmological constant problem

Given the symmetric mass up/down symmetry breaking of (2) that produces a matter only universe, the symmetry breaking contribution to the cosmological constant can be zero and thus consistent with the observed cosmological constant value. Based on the Standard Model's view, QCD's contribution to the cosmological constant produces a value that is off by 10^{46}, i.e 46 orders of magnitude wrong [7], with no substantive resolution. Using the Standard Model view for the electroweak contribution results in an even greater error.

The preciseness of the predicted $W^\pm$ particle mass of equation (1) and the pattern of quantization shown via (2)

and (3) call into question many of the Standard Model views and assumptions about the causality of the observed "invariant mass" values.

However, it is precisely the Standard Model view and the Standard Model symmetry breaking approach that results in these fundamental Standard Model problems. Maybe we should listen to these fundamental problems with more care.

10 Summary

The Standard Model is highly successful in many areas, especially QM and QED. One of the open questions for the Standard Model is the cause of the specific invariant mass values of fundamental particles.

The accepted Standard Model view hides the fact that the measured $W^{\pm}$ mass of 80398 ± 25 MeV [4] is exactly $2m_{\mathrm{p}}/m_{\mathrm{e}}$ (3672.30534) times the mass value symmetrically between the electron and the proton ($M_{\mathrm{sp}} = (m_{\mathrm{p}}\, m_{\mathrm{e}})^{1/2}$) and the Standard Model gives no reason for the electron generations nor their masses.

A mass and charge symmetric, 4π quantized and spin quantized mass formula is given that produces the exact $W^{\pm}$ particle mass. The electron generation mass ratios can be produced using a 4π related magnitude, i.e $m_{\mathrm{e}(x)}/m_{\mathrm{e}(x-1)} = \sqrt{2}(4\pi\varrho_x)^{3-x}$ for x=(1,2).

The common 4π formulation allows the single mass formula (3) to produce the masses of the proton, the W, and the three electron generations.

Equations (1), (2) and (3) strongly suggest several new aspects.

First, in addition to the atomic orbital quantization of QM, there is an intra-particle quantization mechanism which gives the fundamental particles and generations their invariant mass values.

Second, the fundamental particle quantization process is spin $\{\frac{1}{2},1\}$ and 4π quantized.

Third, equation (1) indicates that nature is actually highly symmetric, being charge and mass up/down symmetric.

This symmetry allows for the possibility of an alternate matter creation process for the early universe which results in creating only matter.

In addition the mass and charge super-symmetric view of equation (1) should yield a near zero cosmological constant in keeping with the observed value.

A quantization proposition is not in conflict with the existence of quarks.

A dual approach is required to explain the 4π and spin mass pattern of equation (1), the 4π electron generation mass pattern, and Palazzi's [2] results.

This dual approach involves a quantizing mechanism as the source of the stability and mass value of the spin 1/2 particles, the mass values of the fundamental $W^{\pm}$ particles, and the decay point mass of quark composites, while the types and symmetries of quarks construct the variations seen in the "particle zoo".

The quantized view of equation (3) indicates that one of the intra-particle quantization components can be the source for the generational identity and a foundation for the generational exchange seen in the muon neutrino interaction $\nu_{\mu} + N \rightarrow P^{+} + \mu^{-}$.

Is "A quantized form of energy." the answer to the question "What is mass?".

If relationship (1) and the quantization interpretation of (1), (2) and (3) are fundamental, then the recognition of an intra-particle quantization process is required to move the Standard Model to a massed particle model.

Submitted on August 16, 2009 / Accepted on August 25, 2009

References

1. Nambu Y. An empirical mass spectrum of elementary particles. *Prog. Theor. Phys.*, 1952, v. 7, 595.
2. Palazzi P. The meson mass system. *Int. J. of Mod. Phys.*, 2007, v. A22 (2/3), 546–549.
3. Ne'eman Y., Sijacki Dj. SL(4,R) Classification for hadrons. *Phys. Lett.*, 1985, v. B157 (4), 267–274.
4. Amsler C. et al. *Phys. Lett.*, 2008, v. B667, 1; Updated Particle Data Group, Particle Listings 2009 http://pdg.lbl.gov/2009/listings/rpp2009-list-electron.pdf, rpp2009-list-muon.pdf, rpp2009-list-tau.pdf, rpp2009-list-p.pdf, rpp2009-list-w-boson.pdf.
5. Particle Data Group, Physical Constants 2009: http://pdg.lbl.gov/2009/constants/rpp2009-phys-constants.pdf
6. Zeller G.P. et al. (NuTeV collaboration) Precise determination of electroweak parameters in neutrino-nucleon scattering. *Phys. Rev. Lett.*, 2002, v. 88, 091802.
7. Carroll S.M. The cosmological constant. *Living Rev. Relativity*, 2001, v. 4, 1; arXiv: astro-ph/0004075.

From Inspired Guess to Physical Theory: Finding a Theory of Gravitation

Pieter Wagener

Department of Physics, NMMU South Campus, Port Elizabeth, South Africa
E-mail: Pieter.Wagener@nmmu.ac.za

A theory of gravitation satisfying all experimental results was previously proposed in this journal. The dynamics was determined by a proposed Lagrangian. In this paper it is shown how this Lagrangian can be derived heuristically. A Newtonian approach is used, as well as other methods.

1 Introduction

A theory proposed in previous articles in this journal [1–4] relied on two postulates, one of which is that the dynamics of a system is determined by a Lagrangian,

$$L = -m_0\left(c^2 + v^2\right)\exp\frac{R}{r}\,, \tag{1}$$

where m_0 is the *gravitational rest mass* of a test body moving at velocity $\mathbf{v}$ in the vicinity of a massive, central body of mass M, $\gamma = 1/\sqrt{1 - v^2/c^2}$ and $R = 2GM/c^2$ is the Schwarzschild radius of the central body.

This Lagrangian leads to equations of motion that satisfy all experimental observation of gravitational effects. It also leads to expressions for electromagnetic and nuclear interactions. In this regard it gives the fine spectrum of the hydrogen atom and the Yukawa potential for the nuclear force.

No explanation was given of how this Lagrangian had been determined, but only that its validity is confirmed by the consistency of its resultant equations of motion and agreement with experiment.

It is informative to show how such a Lagrangian can be derived. The procedure leads to an understanding of the creation and development of physical theories.

When a Lagrangian embodies the fundamentals of a physical model it cannot be derived from first principles. What is needed is an inspired guess to start with. The equations of motion derived from the initial Lagrangian are compared with observation. If they do not fit satisfactorily with the first try, then one adjusts the Lagrangian to conform closer to experimental results. This modelling cycle is repeated until a satisfactory agreement is found with observation.

In the case of the above Lagrangian various approaches are possible. We consider some of them.

2 Newton's approach

We follow a *Gedanken* speculation of how Isaac Newton would have derived a law of gravitation if he had been aware of the modern classical tests for a theory of gravitation.

The development of theories of gravitation at the beginning of the previous century is well documented [5, 6]. The essential test for a theory of gravitation at that time was whether it explained the anomalous perihelion precession of the orbit of Mercury, first calculated by Leverrier in 1859. This was satisfactorily explained by Einstein's theory of general relativity. Further predictions of this theory, i.e. the bending of light by a massive body and of gravitational redshift, have subsequently become part of the three benchmark tests for a model of gravitation.

2.1 Modern Newton

It is not generally known that Newton first derived his inverse square law of gravitation by first considering circular orbits [7, 8]. He applied Huygens's law for the acceleration in a circular orbit,

$$a = \frac{v^2}{r}\,, \tag{2}$$

and Kepler's third law to arrive at the inverse-square relation. He then proceeded to show in his *Philosophiae Naturalis Principia Mathematica* (there is some doubt about this [9]) that elliptical motion follows in general from this relation.

We follow a similar procedure by assuming a scenario along which Newton could have reasoned today to arrive at a refinement of his law of gravitation.

He would have been aware of the three classical tests for a theory of gravitation and that particles traveling near the speed of light obey relativistic mechanics. Following an iterative procedure he would have started with the simple model of circular orbits, derived the appropriate law of gravity, but modified to accommodate relativistic effects and then generalised it to include the other conical sections. It would finally be compared with other experimental results.

2.2 Finding a Lagrangian

For motion in a circular orbit under the gravitational attraction of a mass M one must have:

$$\frac{v^2}{r} = \frac{GM}{r^2}\,. \tag{3}$$

Because of relativistic considerations, the ratio v^2/c^2 must be compared relative to unity, i.e.

$$1 - \frac{v^2}{c^2} = 1 - \frac{GM}{r\,c^2}\,. \tag{4}$$

Note that (4) is not an approximation of (2) for $v \ll c$. If we surmise that the inverse square law is only valid for $r \gg R$, one could incorporate higher order gravitational effects by generalising the right-hand side of (4) to a polynomial. Furthermore, to allow other motion besides circles, we multiply the right-hand side by an arbitrary constant K:

$$1 - \frac{v^2}{c^2} = \left(1 + \frac{a'R}{r} + \frac{b'R^2}{r^2} + \ldots\right) K\,, \qquad = KP'(r)\,, \tag{5}$$

or

$$\left(1 - \frac{v^2}{c^2}\right) P(r) = K\,, \tag{6}$$

where

$$P(r) = 1 + \frac{aR}{r} + \frac{bR^2}{r^2} \ldots\,, \tag{7}$$

is the inverse of $P'(r)$.

In order to compare (6) with experiment, we have to convert it to some standard form in physics. To do this we first rewrite (6) as:

$$(1 - K)\,\frac{c^2}{2} = \frac{v^2}{2} - \frac{GMa}{r} - \frac{av^2R}{2r} + \ldots \tag{8}$$

If we multiply this equation by a constant, m_0, with the dimension of mass, we obtain a conservation equation with the dimensions of energy:

$$(1 - K)\,\frac{m_0 c^2}{2} = \frac{m_0 v^2}{2} - \frac{GMm_0 a}{r} - \frac{m_0 a v^2 R}{2r} + \ldots \tag{9}$$

For $r \gg R$, this equation must approach the Newtonian limit:

$$\frac{m_0 v^2}{2} - \frac{m_0 MGa}{r} = E_N\,, \tag{10}$$

where E_N is the total Newtonian energy. Comparison of (10) with the Newtonian expression gives $a = 1$.

To simplify the notation, we define a constant E with dimensions of energy, such that

$$K = \frac{E}{m_0 c^2}\,. \tag{11}$$

From (6),

$$E = m_0 c^2 \left(1 - \frac{v^2}{c^2}\right) P(r)\,. \tag{12}$$

If we consider (12) as the total energy of the system, we can find a corresponding Lagrangian by separating the potential and kinetic energies:

$$T = -\,m_0 v^2 P(r)\,,$$
$$V = m_0 c^2 P(r)\,.$$

The corresponding Lagrangian is therefore:

$$L = T - V = -\,m_0 \left(c^2 + v^2\right) P(r)\,. \tag{13}$$

Applying the Euler-Lagrange equations to this Lagrangian one can find the equations of motion of the system. The conservation of energy (12) follows again, while for the conservation of angular momentum we find

$$P(r) r^2\,\dot{\theta} \;=\; \text{constant} \;=\; h. \tag{14}$$

The equations of motion for the system can then be derived from (12) and (14) as a generalised Kepler problem. From these equations one finds a differential equation of motion of the form

$$\frac{d\theta}{du} = Au^2 + Bu + C\,, \tag{15}$$

where

$$u = \frac{1}{r}\,,$$
$$A = bR^2\,\frac{4 - E}{2h} - 1\,, \tag{16}$$
$$B = \frac{R(2 - E)}{h^2}\,, \tag{17}$$
$$C = \frac{1 - E}{h^2}\,. \tag{18}$$

The convention $m_0 = c = 1$ was used, and terms higher than R^2/r^2 were ignored.

2.3 Perihelion precession

In the case of an ellipse, the presence of the coefficient A gives rise to a precession of the perihelion. For one revolution this can be calculated as:

$$\frac{6b\pi cR}{\bar{a}(1 - e^2)}\,, \tag{19}$$

where $\bar{a}$ is the semi-major axis and e is the eccentricity of the ellipse. Comparison with the observed value for Mercury gives $b = 1/2$. With this result the polynomial of (7) becomes:

$$P(r) = 1 + \frac{R}{r} + \frac{R^2}{2r^2} + \ldots \tag{20}$$

Equation (20) could be regarded as simply a fit to experimental data. The theoretical physicist, however, will look for a pattern or a generalisation of some underlying physical law. The form of the equation leads one to propose that the above terms are the first three terms in the Taylor expansion of

$$P(r) = \exp\frac{R}{r}\,. \tag{21}$$

Confirmation of this form, which is aesthetically more acceptable, must come from other experimental results, such as the bending of light by a massive object. This is shown in the first article referred to above [1].

The Lagrangian of (13) can now be rewritten in the form of (1):

$$L = -\,m_0 \left(c^2 + v^2\right) \exp\frac{R}{r}\,, \tag{22}$$

or in terms of the potential Φ as

$$L = -m_0\left(c^2 + v^2\right)\exp\frac{2\Phi}{c^2}\,. \tag{23}$$

The conservation of energy equation (12) can be written as

$$E = m_0 c^2\,\frac{e^{R/r}}{\gamma^2}\,. \tag{24}$$

We define a variable *gravitational mass* as

$$m = \frac{m_0}{\gamma^2}, \tag{25}$$

so that (24) can also be written as

$$E = m c^2\, e^{R/r}. \tag{26}$$

3 A gravitational redshift approach

We continue with the hypothetical Newton, but starting from another experimental observation. In the presence of a body of mass M a photon undergoes a frequency shift relative to its frequency ν_0 in the absence of the body:

$$\nu = \nu_0\left(1 - \frac{R}{2r}\right),$$

where ν_0 is an invariant.

In line with our inspired guess approach, we surmise that the right-hand side of this equation is a first order approximation to

$$\nu = \nu_0\, e^{-R/2r}, \tag{27}$$

or

$$\nu_0 = \nu e^{R/2r}. \tag{28}$$

Substituting time for the frequency, $\nu = 1/t$ and rearranging:

$$dt = B\, e^{R/2r} d\tau\,, \tag{29}$$

where $d\tau$ is an invariant time interval, or proper time, and B is a proportionality constant. Substituting the special relativity relation $dt = \gamma d\tau$ in (29),

$$\frac{1}{B} = \frac{e^{R/2r}}{\gamma}\,. \tag{30}$$

This is a conservation equation involving the variables r, v and M. In order to relate this equation to the classical conservation of energy equation and its Newtonian limit, the equation must be squared and multiplied by $m_0 c^2$:

$$\frac{m_0 c^2}{B^2} = m_0 c^2\,\frac{e^{R/r}}{\gamma^2}\,. \tag{31}$$

This is the same equation as (24) for $E = m_0 c^2/B^2$.

From (11) we note that $B^2 = 1/K$. Separating the kinetic and potential energy terms we again find the Lagrangian of (1).

4 An Einstein approach

It is understandable that the large corpus of publications on general relativity (GR) over the past few decades tend to underrate the heuristic approach, or inspired guesses, which are used to derive the field equations of GR. The classic texts do not. On page 152 of Weinberg's *Gravitation and Cosmology* [10] the author emphasises the guesswork that leads to the field equations. Eddington [11, p.82] mentions that "This preliminary argument need not be rigorous; the final test is whether the formulae suggested by it satisfy the equations to be solved". This is a classical heuristic argument.

One can therefore wonder why the heuristic derivation was not continued to generalise the metric of GR,

$$ds^2 = \left(1 - \frac{R}{r}\right)dt^2 - \\ - \frac{1}{1 - \frac{R}{r}}\,dr^2 - r^2 d\theta^2 - r^2\sin^2\theta\, d\phi^2, \tag{32}$$

to an exponential form:

$$ds^2 = e^{-R/r}dt^2 - e^{R/r}(dr^2 + r^2 d\theta^2 + r^2\sin^2\theta\, d\phi^2)\,. \tag{33}$$

The equations of motion derived from this metric are the same as those derived from the Lagrangian of (1), but are conceptually and mathematically simpler [1]. From the resulting conservation equations one can, similarly to the procedures above, derive our Lagrangian.

5 Nordström's first theory

Although not an example of a heuristic derivation, Gunnar Nordström's first theory [12, 13] is an intriguing example of how theories of gravitation could have taken a different direction in 1912.

Nordström's theory, a noncovariant one, is based on a Lagrangian,

$$L = \exp\frac{R}{2r}\,. \tag{34}$$

In the case of a static, spherically symmetrical field the Lagrangian gives a conservation equation,

$$\gamma\exp\left(-\frac{R}{2r}\right) = A_N\,. \tag{35}$$

Comparison with (30) shows that $A_N = B$. Nordström's first theory therefore gives the same conservation of energy equation as our theory.

The absence of the $\left(c^2 + v^2\right)$ term in Nordström's Lagrangian accounts for its difference from our theory and Nordström's wrong predictions. This shows up in his conservation of angular momentum,

$$r^2\,\frac{d\theta}{dt} = h\,, \tag{36}$$

where h = constant.

Nordström's theory [14] also gives a variation of mass,

$$m = m_0\, e^{-R/2r}. \tag{37}$$

From (11) and (26) our theory gives

$$m = Km_0\, e^{-R/r}. \tag{38}$$

The close correlation between our theory and that of Nordström raises the possibility of Nordström, or anyone else reading his paper of 1912, deriving the Lagrangian of (1). If this had happened, and the resultant agreement with Mercury's perihelion precession were found, then the study of gravitation could have followed a different direction.

Submitted on September 12, 2009 / Accepted on September 18, 2009

References

1. Wagener P. C. A classical model of gravitation. *Progress in Physics*, 2008 v.3, 21–23.
2. Wagener P. C. A unified theory of interaction: Gravitation and electrodynamics. *Progress in Physics*, 2008, v.4, 3–9.
3. Wagener P. C. A unified theory of interaction: Gravitation, electrodynamics and the strong force. *Progress in Physics*, 2009, v.1, 33–35.
4. Wagener P. C. Experimental verification of a classical model of gravitation. *Progress in Physics*, 2009, v.3, 24–26.
5. Whitrow G.J. and Morduch G.E. In: Beer A., editor. *Vistas in Astronomy*. Pergamon, London,1965, v.6, 1–67.
6. Pais A. Subtle is the Lord: the science and the life of Albert Einstein. Oxford Univ. Press, Oxford, 1982.
7. Westfall R.S. Never at rest. Cambridge Univ. Press, Cambridge, 1986.
8. Guth E. In: Carmeli M., Fickler S.I. and Witten L., editors. *Relativity*. Plenum Press, New York, 1970, 161.
9. Weinstock R. Dismantling a centuries-old myth: Newton's principia and inverse-square orbits. *Am. J. Phys.*, 1982, v.50, 610.
10. Weinberg S. Gravitation and cosmology. John Wiley, New York, 1972.
11. Eddington A.S. The mathematical theory of relativity. 2 ed. Cambridge Univ. Press, Cambridge, 1960.
12. Nordström G. *Phys. Z.*, 1912, v.13, 1126.
13. Nordström G. *Ann. Phys. (Leipzig)*, 1913, v.40, 856.
14. Behacker M. *Physik. Zeitschr.*, 1913, v.14, 989.

Resolving Inconsistencies in de Broglie's Relation

Pieter Wagener

Department of Physics, NMMU South Campus, Port Elizabeth, South Africa
E-mail: Pieter.Wagener@nmmu.ac.za

Modern quantum theory is based on de Broglie's relation between momentum and wave-length. In this article we investigate certain inconsistencies in its formulation and propose a reformulation to resolve them.

1 Inconsistencies in de Broglie's relation

Edward MacKinnon made a critical analysis [1–3] of Louis de Broglie's doctoral thesis of 1924 [4]. With this thesis de Broglie is credited with deriving the first relationship between the momentum of a particle and its associated quantum wavelength. MacKinnon's discussion draws some remarkable conclusions. He points out that the most paradoxical feature of de Broglie's thesis is the fact that, although his fundamental argument is essentially relativistic, the only successful applications of his ideas were essentially nonrelativistic. It is well known that his relationship $\lambda = h/mv$ was applied to the Bohr atom and later to the derivation of Schrödinger's equation, both of which are strictly nonrelativistic models. What is not so well known is that the arguments leading to $\lambda = h/mv$ are very much relativistic. De Broglie's problem was to find the relativistic transformation of

$$h\nu_0 = \widetilde{m}_0 c^2, \tag{1}$$

where the relativistic rest mass $\widetilde{m}_0$ and the frequency ν_0 are invariant.

His considerations led him to assign three different frequencies to the same particle:

$$\nu_0 = \frac{\widetilde{m}_0 c^2}{h},$$

the internal frequency in the rest system;

$$\nu_1 = \nu_0 \sqrt{1 - v^2/c^2},$$

the internal frequency as measured by an external observer who sees the system moving with velocity v;

$$\nu = \frac{\nu_0}{\sqrt{1 - v^2/c^2}},$$

the frequency this observer would associate with the particle's total energy.

MacKinnon further points out that de Broglie emphasized the frequency associated with an electron, rather than the wavelength. His wavelength-momentum relationship occurs only once in the thesis, and then only as an approximate expression for the length of the stationary phase waves characterizing a gas in equilibrium. Most of MacKinnon's article is devoted to analyzing the reasons why de Broglie's formula proved successful, despite the underlying conceptual confusion. He finally expresses amazement that this confusion could apparently have gone unnoticed for fifty years.

In addition to MacKinnon's criticism, one can also have doubts about some of the applications of de Broglie's formula in quantum mechanics, particularly to electron diffraction. In standard physics texts [5, p. 567], in order to apply the de Broglie relation, the following assumption is made

$$\widetilde{E}^2 = |\mathbf{p}|^2 c^2 + \widetilde{m}_0^2 c^4 \simeq |\mathbf{p}|^2 c^2. \tag{2}$$

The notation is in accordance with previous articles by the author in this journal [6, 8].

From this equation the momentum of the electron is calculated as $|\mathbf{p}| = \widetilde{E}/c$, and from the de Broglie relation it follows that $\lambda = hc/\widetilde{E}$.

Various explanations are given to support the approximation of (2). The most common is to assume that it is allowed for $\widetilde{E} \gg \widetilde{m}_0 c^2$. Although this assumption satisfies experiment, it is not mathematically or conceptually acceptable. Electron diffraction becomes measurable at high energies and velocities, where relativistic equations are applicable. For these equations to be mathematically consistent all terms must be retained, particularly those in the conservation of energy equation. Another approach is to ignore (2) and to apply a semi-nonrelativistic result, $\widetilde{E} = p^2/2\widetilde{m}$ or $T = \mathbf{p}^2/2\widetilde{m}$ [5, p.147], where $\widetilde{m} = \gamma\widetilde{m}_0$ is the relativistic mass of a particle and T is its kinetic energy. This is clearly untenable because of the high velocities.

Another justification for the approximation is that it works for "experimental purposes" [9]. These assumptions might not be serious to verify predictions expeerimentally, but in the spirit of present attempts to formulate a quantum theory of gravity, these assumptions warrants closer scrutiny.

The use of the above approximation is sometimes subtle and not so apparent. In a popular textbook [10, Problem 12.10] the following equation is given for the conservation of energy in Compton scattering:

$$\frac{hc}{\lambda} + m_0 c^2 = \frac{hc}{\lambda'} + mc^2, \tag{3}$$

where m_0 and m are respectively the rest and final mass of the electron.

The equation is inconsistent since wave and corpuscular expressions are combined in one equation. The expression hc/λ is simply a shortcut for $\sqrt{p^2c^2 + m_{\nu_0}^2 c^4}$, where the rest mass of the photon $m_{\nu 0}$ is set to zero and de Broglie's relation is then applied to p. In general, the assumption of $\widetilde{m}_0 = 0$ for a photon has had an uneasy niche in theoretical physics [1].

In a previous paper [6] we presented a unified theory of gravitation and electromagnetism. We show below that the model of that theory resolves the inconsistencies discussed above.

2 A scalar momentum

In the aforementioned paper the following conservation of energy equation, derived in an earlier paper [7], was given for the gravitational model:

$$E = m_0 c^2 \frac{e^{2\Phi/c^2}}{\gamma^2} = \text{total energy}\,, \tag{4}$$

where

$$\left.\begin{aligned} \Phi &= \text{ gravitational potential,} \\ m_0 &= \text{gravitational rest mass of a test body} \\ &\quad \text{moving about a central mass } M. \end{aligned}\right\} \tag{5}$$

We have generalized the exponential term in this paper to a general potential $\Phi = Rc^2/2r$, where $R = 2GM/c^2$ is the Schwarzschild radius of the central body.

We now define a scalar momentum appropriate to our model.

A constant P_0 with dimensions of linear momentum can be defined in terms of the energy E as

$$P_0^2 = m_0 E. \tag{6}$$

Eq. (4) can then be written as

$$P_0 = \frac{m_0 c}{\gamma} \exp\frac{\Phi}{c^2}\,, \tag{7}$$

or, if the mass constant m_0 is not required in the energy equation, as

$$E = \frac{P_0 c}{\gamma} \exp\frac{\Phi}{c^2}\,, \tag{8}$$

$$= Pc \exp\frac{\Phi}{c^2}\,, \tag{9}$$

where

$$P = \frac{P_0}{\gamma}. \tag{10}$$

In reference [6] we found the following relationship between the gravitational and electromagnetic energies:

$$E = \widetilde{E}\, e^{\Phi/c^2}, \tag{11}$$

where $\widetilde{E} = \widetilde{m}c^2$ is the energy function of Special Relativity.

Comparing (9) and (11) we get

$$\widetilde{E} = Pc\,. \tag{12}$$

3 Derivation of de Broglie's relation

3.1 Preliminaries

Using the relationship between frequency ν and wavelength λ,

$$c = \lambda\nu = \sigma\omega\,, \tag{13}$$

where

$$\sigma = \frac{\lambda}{2\pi} = \frac{c}{2\pi\nu} = \frac{c}{\omega}\,, \tag{14}$$

we rewrite (12) as

$$\widetilde{E} = P\sigma\omega. \tag{15}$$

Since time does not appear explicitly in the above equation for $\widetilde{E}$, we can write down an equivalent Hamiltonian as

$$\widetilde{H} = P\sigma\omega. \tag{16}$$

This form of the Hamiltonian resembles that of the simple harmonic oscillator, after a canonical transformation with generating function $F = (\widetilde{m}_0/2)\, q^2 \cot Q$, where q and Q are the appropriate canonical variables. The significance of this transformation was first pointed out by Max Born [11, §7].

Briefly, it states that the Hamiltonian of a simple harmonic oscillator, given by

$$\widetilde{H} = \frac{p^2}{2\widetilde{m}_0} + \frac{\widetilde{m}_0\,\omega^2 q^2}{2}\,, \tag{17}$$

can, by a canonical transformation with the above generating function, be expressed as

$$\widetilde{H} = \Lambda\omega, \tag{18}$$

where Λ = constant.

If our system behaves as an oscillator it follows from (16) and (18) that

$$P\sigma = \text{constant}. \tag{19}$$

This result prompts us to provisionally write the constant in (19) as $\hbar$, Planck's constant divided by 2π. This step is taken *a priori*, and its validity will depend on the overall consistency of the subsequent results. Keeping this supposition in mind, we rewrite (19) as

$$P\sigma = \hbar, \tag{20}$$

and (15) as

$$\widetilde{E} = \hbar\omega = h\nu. \tag{21}$$

3.2 The photo-electric effect

Eq. (21), combined with $\widetilde{E} = \widetilde{m}c^2$, gives the photo-electric effect, $\widetilde{m}c^2 = \hbar\omega = h\nu$. Eq. (21) also confirms the use of the constant h in the expression for gravitational redshift,

$$E = \widetilde{E} \exp\frac{R}{2r} = h\nu \exp\frac{R}{2r}\,. \tag{22}$$

Eq. (22) is significant in that it contains both h and G in one relation.

The results of (21) and (22) further confirm the consistency of the derivation of (20).

We emphasize that the ω_0, or ω, used above is an internal property of the test particle; it is not its angular velocity about a central body. We cannot say with certainty what the internal physical structure of the test particle should be; only that if some periodic mechanism exists with respect to the test particle the frequency of that mechanism is controlled by the above equations. This, for example, determines the gravitational redshift. As a model for such a type of test particle we shall simply refer to it as a virtual oscillator.

3.3 Derivation

From (14) and (20),

$$P = \frac{h}{\lambda}\,. \tag{23}$$

Although (23) is similar to the de Broglie relationship between momentum and wavelength, the momentum P is not equal to the classical momentum,

$$\mathbf{p} = \widetilde{m}\mathbf{v}\,. \tag{24}$$

Nevertheless, we shall see that (23) is consistent with the application of the de Broglie relation, and actually resolves some ambiguities in quantum mechanics [1].

3.4 The relationship between p and P

From (12) and $\widetilde{E} = \widetilde{m}c^2$ we obtain

$$P = \widetilde{m}c. \tag{25}$$

From this we can see that $P = \widetilde{E}/c$ can be regarded as the fourth component of the relativistic four-vector, p_i:

$$p_i = \left(\mathbf{p}, \frac{\widetilde{E}}{c}\right), \quad i = 1, 2, 3, 4, \tag{26}$$

or

$$p_i = (\mathbf{p}, P), \quad i = 1, 2, 3, 4. \tag{27}$$

To find a direct relation between $\mathbf{p}$ and P we note from (24) and (25) that

$$\mathbf{p} = \frac{P\mathbf{v}}{c} \quad \text{or} \quad \mathbf{p}c = P\mathbf{v}\,. \tag{28}$$

The well-known expression of Special Relativity,

$$\widetilde{E}^2 = \mathbf{p}^2c^2 + \widetilde{m}_0^2c^4, \tag{29}$$

can be rewritten, using (28), as

$$\widetilde{E}^2 = P^2v^2 + \widetilde{m}_0^2c^4. \tag{30}$$

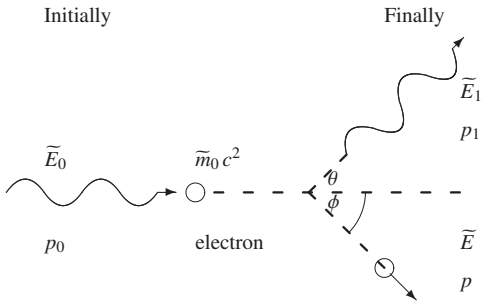

Fig. 1: Compton scattering

4 Applications of de Broglie's relation

The relation of (23), $P = h/\lambda$, is clearly different from the conventional de Broglie relationship. This form is, however, not in conflict with either theory or experiment, but actually simplifies the various formulations.

4.1 Compton scattering

For a photon, $v = c$, and it follows from (23) and (28) that

$$P = |\mathbf{p}| = \frac{h}{\lambda}\,. \tag{31}$$

An advantage of (31) is that, when applied to Compton scattering, it is not necessary to make the assumption $\widetilde{m}_0 = 0$ in (29). It must also be noted that the assumption $\widetilde{m}_0 = 0$ for a photon is not required in our theory; only $v = c$. The paradox of the photon rest mass is resolved in reference [6].

The Compton effect is described schematically in Fig. 1. The equations below follow from this diagram.

Conservation of momentum:

$$p_0 = p_1\cos\theta + p\cos\phi\,, \tag{32}$$

$$p_1\sin\theta = p\sin\phi\,. \tag{33}$$

From (32) and (33),

$$p^2 = p_0^2 + p_1^2 - 2\,p_0\,p_1\cos\theta, \tag{34}$$

and applying (31) gives

$$p^2 = \frac{h^2}{\lambda_0^2} + \frac{h^2}{\lambda_1^2} - \frac{2h^2\cos\theta}{\lambda_0\lambda_1}\,. \tag{35}$$

Since

$$\widetilde{E}^2 = p^2c^2 + \widetilde{m}_0^2c^4,$$

it follows that

$$\frac{\widetilde{E}^2}{c^2} - \widetilde{m}_0^2c^2 = \frac{h^2}{\lambda_0^2} + \frac{h^2}{\lambda_1^2} - \frac{2h^2\cos\theta}{\lambda_0\lambda_1}\,. \tag{36}$$

Conservation of energy:

$$\widetilde{E}_0 + \widetilde{m}_0c^2 = \widetilde{E}_1 + \widetilde{E}\,, \tag{37}$$

therefore

$$(\widetilde{E} - \widetilde{m}_0 c^2)^2 = \widetilde{E}_0^2 + \widetilde{E}_1^2 - 2\widetilde{E}_0 \widetilde{E}_1 .$$

From (31) and rearranging,

$$\frac{\widetilde{E}^2}{c^2} + \widetilde{m}_0^2 c^2 - 2\widetilde{E}\widetilde{m}_0 = \frac{h^2}{\lambda_0^2} + \frac{h^2}{\lambda_1^2} - \frac{2h^2}{\lambda_0 \lambda_1} . \qquad (38)$$

Eq. (38) minus (36), and rearranging:

$$\widetilde{m}_0 c^2 - \widetilde{E} = -\frac{h^2(1 - \cos\theta)}{\widetilde{m}_0 \lambda_0 \lambda_1} . \qquad (39)$$

Subsituting (12) and (31) in (39) gives

$$\lambda_1 - \lambda_0 = \frac{h(1 - \cos\theta)}{\widetilde{m}_0 c} , \qquad (40)$$

the standard formulation for Compton scattering.

4.2 Electron diffraction

Another advantage of our formulation applies to electron diffraction. From the results $P = h/\lambda$ and $\widetilde{E} = \hbar\omega$ it follows directly that $\widetilde{E} = Pc$. This obviates the approximation used in standard texts on electron diffraction, i.e. $\widetilde{E}^2 \cong \mathbf{p}^2 c^2$.

5 Conclusion

The above derivation and formulation of de Broglie's relation resolves the inconsistencies in de Broglie's original derivation. It also obviates the questionable approximations made in Compton scattering and electron diffraction.

Submitted on October 08, 2009 / Accepted on October 12, 2009

References

1. MacKinnon E. De Broglie's thesis: A critical retrospective. *Am. J. Phys*, 1976, v.44, 1047–1055.
2. MacKinnon E. *Am. J. Phys*, 1977, v.45, 872.
3. Schlegel R. *Am. J. Phys.*, 1977, v.45, 871.
4. De Broglie L. *Ann. Phys. (Paris)*, 1925, v.3, 22.
5. Eisberg R.M. *Fundamentals of modern physics*. John Wiley, New York, 1961.
6. Wagener P.C. A unified theory of interaction: gravitation and electrodynamics. *Progress in Physics*, 2008, v.4, 3–9.
7. Wagener P.C. A classical model of gravitation. *Progress in Physics*, 2008, v.3, 21–23.
8. Wagener P.C. A unified theory of interaction: gravitation, electrodynamics and the strong force. *Progress in Physics*, 2009, v.1, 33–35.
9. Wagner M. Elemente der Theoretischen Physik 1. Friedr. Vieweg, Braunschweig, 1980.
10. Gautreau R. and Savin W. Modern physics: Schaum outline series. McGraw-Hill, 1978.
11. Born M. The mechanics of the atom. Frederick Ungar Publ. Co., New York, 1960.

Solving Many Point Particle Interactions Using the Kepler Route

Riadh H. Al Rabeh
College of Engineering, University of Basra, Iraq
Present address: Lydgate Close, Manningtree, Essex, UK. E-mail: alrabeh_rh@yahoo.com

Events in nature can be described using fields and their associated partial differential equations, or equivalently, the mechanics of interaction of point particles described by ordinary differential equations. The field approach can be looked at as the statistical average of the particle approach and in this sense is more economical for computing. The particle approach, on the other hand, is more fundamental but requires enormous computing power as the model has to follow the movements of every individual particle in the interaction. The present work aims at reducing such computing task by solving the problem of many particle interactions (under a central force environment) in an analytical form for one pair of particles using a Kepler type formula- giving the position of the particle as a function of time only. The resulting (analytical) formula is then used to write the result of the many-particle interaction using simple vector superposition. This approach takes less computing time and can give greater numerical stability when the distances between the particles become small and the force grows as the inverse square of the separation distance.

1 Introduction

The problems of physics can be equally described using interacting particles or fields. The flow of fluids, for example, is the result of basic interactions of an enormous number of small particles moving under an inverse square force system. Such processes can be described correctly using force fields that lead to PDE's like those for fluid mechanics and electrodynamics of material media. It is also possible to achieve a description of the same phenomena using interacting particles following what truly happens in the real world. In the present approach, all particles are assumed identical point masses that may carry charges too. The particles interact under a central force environment in which only the separation distance is of any significance. The coupling constants of such interactions can correspond to any of the known forces of nature — gravitation, electrostatic, or any other similarly behaving force. The resultant coupling constant is simply the arithmetic sum of such constants for all the component forces, with a negative sign to distinguish attractive forces from repulsive forces. The numerical values of the individual constants determine the relative strength of each force. In the most basic interaction involving say a doublet of two oppositely charged point masses, the Coulomb force is the most dominant. When very large groups of particles are considered, magnetic, and gravitational forces start becoming more significant.

By using the particle approach, it is possible to do away with the need for closure models (constitutive equations) that describe the properties of matter - such as the elasticity constants in dynamics and the permittivity and permeability of electrodynamics. In fact, one can use the particle interaction model to derive or check the validity of such closure models. The real difficulty with the particle approach is the computing burden which involves solving one ODE corresponding to every single particle in the interaction. We try to address this problem here by performing an initial integration of the ODE, then using vector superposition find the answer of the original many particle interaction problems. In addition to the obvious gain in computing time, the stability of the solution can be enhanced as the singularity is shifted from Inverse Square to simple Inverse of the separation distance. The accumulation error also reduces as a result in long time predictions.

Predicting the behavior of a single particle is well known- as in calculating the position of the landing of a projectile before it is fired for example. The same can be said, at least in principle, for predicting the behavior of multi-point interactions. The equation of motion tells us that once we fix the initial states of position and velocity of every participating point particle, the outcome is determined. The normal way to solve such problems is to find the velocity of each particle from the acceleration by integration (after superposition of all forces) then do a second integration to find the new position and this is to be performed over a large set of simultaneous Ode's since every particle effects every other. In the present work we instead calculate (analytically) the velocity and position in terms of time only for every particle then use vector superposition to find the final picture.

As we are dealing with point particles only, moments of forces and angular momentum and spin are not considered. The gain is an enhanced stability and reduced computing time coming from the fact that we integrate analytically first then use superposition (simple algebraic operation) for displacement as opposed to affecting the superposition of forces first then integrating for the displacement for every point particle. The method can be described as a multi-particle generalization of the Kepler method originally put (and still in use) for the motion of planets.

2 Theory

In an inverse square interaction (electrostatic/gravitational) of point masses, the expression for the force (acceleration since mass is unity) of a pair of such point masses is given by

$$a = \frac{d^2r}{dt^2} = \frac{k}{r^2}\,, \tag{1}$$

where $a = a(t)$, $r = r(t)$ are the acceleration and separation distances between an isolated pair of particles as a function of time t, and k is the coupling constant (negative for attractive and positive for repulsive forces). The magnitude of k is dependent on the type of interaction and equals the sum of the k's of all the forces at play. For example, in the case of repulsive Coulomb forces $k = \frac{1}{4}\pi\epsilon_0$ and for gravitational forces $k = -G$, where ϵ_0 is the permittivity of empty space and G is the universal gravitational constant. For a small number of interacting particles, the Coulomb forces by far dominate all other forces. All charges and masses of all particles are assumed unity as given above. The actual values can be incorporated in the coupling constant. As the interacting masses are points, there is no need to consider angular velocity, spin, angular momentum or any form of moments of forces on the particle. Mass can simply be taken as the number of particles in any setup.

For a group of interacting particles, the net acceleration of particle j is given by

$$\left.\begin{aligned} a_j &= \frac{dv_j}{dt} = \sum_i \frac{k_{ij}\, r_{ij}}{r_{ij}^3} \\ r_{ij} &= |r_{ij}|\,, \qquad i, j = 1, 2, \ldots N \end{aligned}\right\}, \tag{2}$$

where a_j is the resultant acceleration, v is velocity, k_{ij} is the total coupling constant between particles i and j, and $r_{ij} = r_j - r_i$ is the vector from i to j positions and N is the total number of particles. Equation (2) is a set of simultaneous Ode's that must be integrated once in order to find $v_j(t)$ and twice to find the position $r_j(t)$. For a large number of particles, the task becomes formidable. One way to reduce this burden is by going back to (1) and performing the integration for a pair of particles first, then use the resulting closed form formula to perform superposition of displacements and find the result of the interaction. Since the function $r(t)$ is not known before hand, we follow the Kepler route [2].

Assume a solution in the form $r = t^n$, where t is time and n is an exponent. Substituting in (1) we find that for the equality to hold for any r, the value of n should be $\frac{2}{3}$, and hence,

$$r = \frac{9}{4}\, k t^{2/3}. \tag{3}$$

This result can be directly checked by differentiating twice and substituting back to recover the original inverse square law. We are using scalar quantities because the force, acceleration and displacement are all along the separation line. The form of (3) is similar to Kepler's third law for orbital motion. In the original Kepler form the distance r refers to the average radius of the orbit and t refers to the mean time of one revolution. Formula (3) however, is more general and refers to motion along the line joining any two interacting particles under an inverse square relation. It is seen that the same formula is suitable for both types of motions. In fact direct substitution in the centrifugal force formula v^2/r using (3), with $v = dr/dt$ gives the same relation between r and t as that derived form (3). A similar result is obtained if we substitute for the Coriolis and the magnetic (Ampere) forces. In fact, such a substitution in the general acceleration definition d^2r/dt^2 reduces it to an inverse square relation. Kepler formula is also shown to be a direct consequence of mechanical similarity [1], and the form $1/r^n$ satisfy similarity for any n, but only $n = (2, -2)$ produces bounded motion, which corresponds to the inverse square force and to the space oscillator type (spring oscillators) interaction forces. The spring type force is also shown to be a special case of the inverse square law for small displacements around an equilibrium point. When (3) is differentiated with respect to time we get

$$v(t) = \frac{dr}{dt} = \frac{2}{3}\, k t^{-1/3} = k r^{-1/2} \tag{4}$$

further differentiation gives

$$a(t) = \frac{d^2r}{dt^2} = \left(-\frac{2}{9}\right) k t^{-4/3} = \left(-\frac{2}{9}\right) k r^{-2} \tag{5}$$

thus we have recovered the inverse square law. Substituting from (4) for the centrifugal force gives

$$\frac{v^2}{r} = \frac{4}{9}\, k^2 t^{-4/3} = k^2 r^{-2} \tag{6}$$

which is, apart from a constant, has the same form of dependency of t on r. The velocity is given by

$$v_j = v_{j_0} - \frac{2}{3}\, t^{1/3} \sum_i \frac{r_j - r_i}{|r_j - r_i|}\,, \quad j, i = 1; n\,, \quad i \neq j \tag{7}$$

and the position r_j is given by the vector relation

$$r_j = r_{j_0} + v_{j_0} t + \frac{9}{4}\, t^{2/3} \sum_i \frac{r_j - r_i}{|r_j - r_i|}\,, \tag{8}$$

where r is the net position vector of all particles and is given, for each, as the vector sum of $n - 1$ vector displacements in addition to the initial position of the particles r_0 and the initial velocity v_0 multiplied by the time t.

The form in (8) is similar to the usual form of the equation of motion for n interacting particles which can be written as

$$r_j = r_{j0} + (dt)\, v_{j0} + (dt)^2 \sum_i \frac{r_j - r_i}{|r_j - r_i|^3} \tag{9}$$

with the obvious difference that (9) involves dt rather than t and therefore must be advanced in very small steps to reach the final solution.

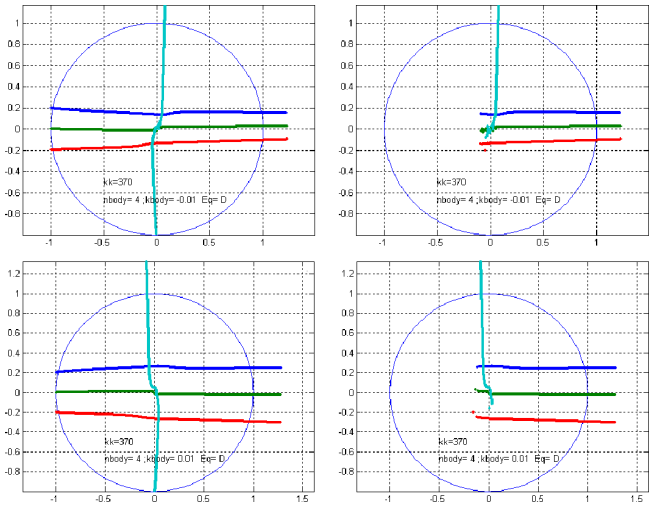

Fig. 1: Four point particles interacting under attractive (top) and repulsive inverse square forces (bottom). Prediction using (8) starts from time step $kk = 1$ (left) and $kk = 150$ (right), showing the capability of writing the correct solution for many particles at any time without going through time evolution.

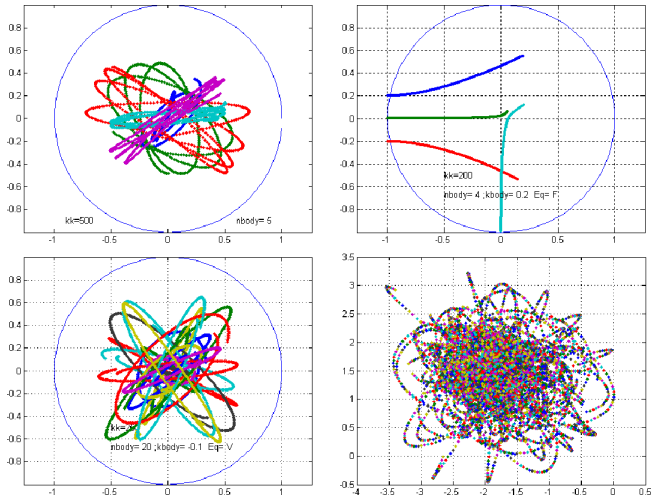

Fig. 3: T: interaction using force (9) for five bodies (confined) and three bodies (not confined). B: interaction using velocity formula (7) for 20 & 200 particles under attractive forces with and without a restraining circular boundary.

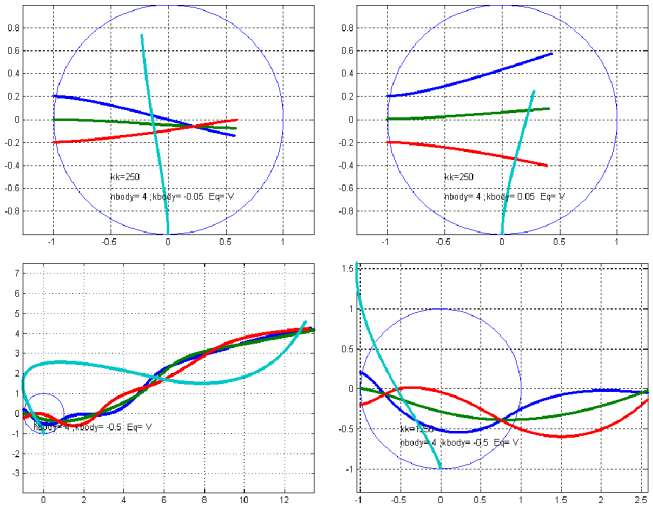

Fig. 2: Predictions using (7) keeping the circular boundary neutral. T: four point particles interacting under attractive and repulsive inverse square forces. B: four point particles interacting under attraction forces for longer time showing the stability of the velocity solution at close encounters. Particle paths interweave as a result of the attraction forces and the (inertia) forces.

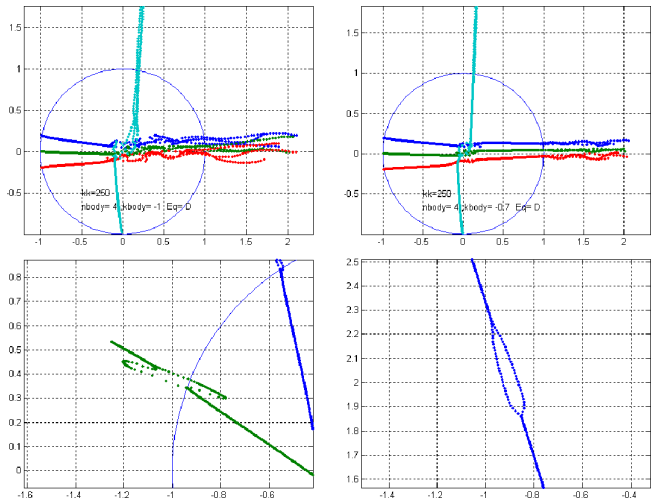

Fig. 4: Instability in the distance formula (8) at small interaction distances. Each particle path branches into three but recovers back to a single path as the particles further separate (top figures). The path disintegrates to only two branches at the encounter of a particle and a wall of particles. The minimum separation distance needed for such behaviour increasing with the increase in the value of the separation constant.

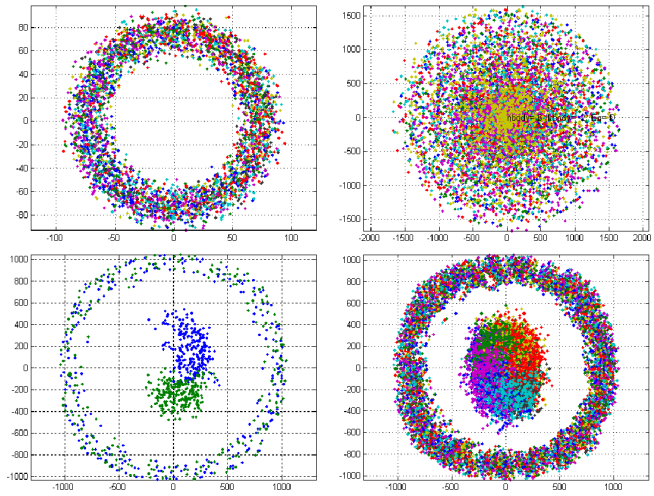

Fig. 5: Rotation, stratification and condensation for large numbers using (8). T: 150 particles under attractive forces only but at different coupling constants. B: one time step and many time steps results of the interaction of 500 particles of equal mix of charges.

3 Results

In this section we concentrate on showing that (7) and (8) give the expected behavior in the case of interacting particles under attraction or repulsion for the case of free particles and for the case of particles trapped inside a constraining circular wall. Comparison is then given with predictions using the usual integration of the inverse square law (9). The distances and coupling constants in these tests are arbitrary- chosen to produce magnified effects of the forces involved. The actual values used are marked on each figure.

Figure 1 shows four particles moving to the right with initial velocities mainly in the horizontal direction. The relative values of initial kinetic energy and the coupling constant determine the behavior of the interacting particles. When the initial velocity is large, as expected, the particles do not change direction appreciably, and when it is small, the repulsion and attraction forces have bigger effect — creating appreciable changes in the particle path. The trajectories are calculated using the displacement expression (8). When using this method it is possible to write the solution at any required time instant as shown in the right hand side frames, wherein the solution is now started at an advanced time location (at the 150th time step kk) and still agreeing with the results of the previous solutions starting at the first time step ($t = 0$) — using the same original set of initial conditions.

Figure 2 shows the results using the velocity expression (7) for the case of attractive and repulsive forces. The stability of the solution is clearly demonstrated by the last frame showing an interweaving paths forced by the equally effective inertial and attractive forces. The velocity formula gives more stable solutions at closer encounters because of the absence of the inverse square term from (7), being replaced by a quantity dependent on t. We should note here also that we still have the direction cosines to consider for the vector superposition. This, however, has a more favorable behavior at very small separation distances since the quantities x_{ij}/r_{ij}, go to unity as r goes to zero.

In Figure 3, the top two frames show the results of using the force formula (9) for the case of four free particles and five particles respectively confined in a circular boundary. The bottom two frames show the result for large number of particles, when using the velocity formula (7), in which 20 particles are confined in a circular boundary and 200 particles under attraction without a restraining boundary.

Problems have been experienced when using the distance formula (8) when the separation distance is small. As shown in Figure 4, the particle path divides into 3 branches but recovers afterwards as the two bodies separate and the separation distance increases depending also on the strength of the coupling constant. Note the effects on the path even before the target is reached. At the interaction with a wall of charges, the path divides instead, into two parts and recovers back again. This phenomenon requires further investigation as it is found to occur only at larger separation distances if the coupling constant is increased. It is numerical in origin, which is somehow different to what one would expect of this formula.

Figure 5 shows the results of using (9) for a large number of particle interactions. Results for 150 and 500 particles under attractive forces are shown. The results show signs of rotation and pulsation behavior as well as coagulation to form separated groups.

4 Conclusion

It has been shown that it is possible to reduce the computation time and enhance the solution stability for multi-point particle interactions. As a result it has been possible to follow the interaction of very large number of particles using modest computer memory and time. In the author opinion the method shown here is worthy of further development and use to numerically investigate the fascinating world of particle interactions. Evidence of grouping appears when the number of interacting particles is large and without the need of retaining external boundaries or forces.

A consistent phenomenon of path splitting into three and two branches has been observed. It is a direct result of evaluating distances using the square root, as it is treatable by adding a very small constant value to the inverse of the rooted quantities. Clearly this phenomenon needs to be corrected first before the present method acquires its full potential.

Submitted on September 12, 2009 / Accepted on October 19, 2009

References

1. Landau L.D., Lifshitz, E.M. Mechanics. Pergamon press, 1960.
2. Murray C.D. and Dermott S.F. Solar system synamics. Cambridge University Press, 2000.

On a Formalization of Cantor Set Theory for Natural Models of the Physical Phenomena

Alexander S. Nudel'man

Sobolev Institute of Mathematics, Siberian Branch of Russian Academy of Science, Novosibirsk, Russia
E-mail: anudelman@yandex.ru

This article presents a set theory which is an extension of ZFC. In contrast to ZFC, a new theory admits absolutely non-denumerable sets. It is feasible that a symbiosis of the proposed theory and Vdovin set theory will permit to formulate a (presumably) non-contradictory axiomatic set theory which will represent the core of Cantor set theory in a maximally full manner as to the essence and the contents of the latter. This is possible due to the fact that the generalized principle of choice and the generalized continuum hypothesis are proved in Vdovin theory. The theory, being more complete than ZF and more natural according to Cantor, will allow to construct and study (in its framework) only natural models of the real physical phenomena.

This paper is dedicated to the memory of Alexander M. Vdovin (1949–2007)

I. It is generally accepted that the (presumably) non-contradictory Zermelo-Fraenkel set theory ZF with the axiom of choice is the most accurate and complete axiomatic representation of the core of Cantor set theory. However, it is acknowledged [3, p. 109], that "Cantor's set theory is so copious as to admit absolutely non-denumerable sets while axiomatic set theory [in particular, ZFC] is so limited [Skolem's paradox] that every non-denumerable set becomes denumerable in a higher system or in an absolute sense". An axiomatic set theory defined here and abbreviated as ZFK admits absolutely non-denumerable sets, as it does Cantor theory.

It is feasible that a symbiosis of the proposed theory and Vdovin set theory [1, 2] will permit to formulate a (presumably) non-contradictory axiomatic set theory which will represent the core of Cantor set theory in a maximally full manner as to the essence and the contents. This is possible due to the fact that the generalized principle of choice and the generalized continuum hypothesis are proved in Vdovin theory.

II. Our definition of ZFK will be based on the traditional (classical) concept of formalized theory explained in [4]. But ZFK is a theory which is axiomatic not completely in the traditional sense, so the syntactic aspects of this theory will be described with references to the principal interpretation of ZFK.

Formulae of ZFK are formulae of the signature $\langle \in, S \rangle$, where $\in$ — is a two-place predicate symbol for denoting the (standard) membership relation on the collection S_k of all Cantor's (intuitive) sets, and S — is a null-place functional symbol (a constant) denoting the family of all axiomatized sets, and in the ZFK formulae containing the symbol "S", the latter symbol is always placed to the right of the symbol "$\in$".

In what follows, we use the conventional notation and abbreviations of ZF. In particular, the relativization of a formula φ to the family S is denoted by $[\varphi]^S$. Besides, depending on the context, records "$\in$" and "S" denote either the signature symbols or denoted by them the relation and the family, respectively. Cantor's (intuitive) sets of S_k will be called k-sets, and the axiomatized sets of S will be simply called as sets.

The axioms of ZFK are divided into two groups: G and G_k. The axioms of group G describe the axiomatized sets, and the axioms of group G_k characterize the relationship between Cantor's (intuitive) sets and the axiomatized sets.

The axioms of group G are the axioms of ZFC (formulae of the signature $\langle \in \rangle$), with exception of the axiom of empty set, which are relativized to the family S.

The axioms of group G_k:

1) Axiom of embedding S into S_k

$$\forall x \in S \; \exists y \, (y = x).$$

2) Axiom of (absolutely) empty set

$$\exists x \in S \; \forall y \, (y \notin x).$$

3) Axiom of transitivity of S in S_k

$$\forall x \in S \, \forall y \, (y \in x \to y \in S).$$

4) Axiom (schema) of generalization

$$[\varphi]^S \to \varphi,$$

where φ — is a formula of ZFK.

5) Axiom (schema) of mappings to S_k

$$\forall t \, (\forall v, w_1, w_2 (\varphi(v, w_1, t) \,\&\, \varphi(v, w_2, t) \to w_1 = w_2) \to$$
$$\to \forall x \exists y \forall z (z \in y \leftrightarrow \exists v \in x \, \exists w (z = \langle v, w \rangle \,\&\, \varphi(v, w, t)))),$$

where φ — is a formula of ZFK and the variable y does not occur free in φ.

6) Axiom of general replacement

$$\forall x\,(\mathrm{map}(x)\,\&\,\mathrm{dom}(x)\in S\,\&\,\mathrm{rang}(x)\subseteq S\;\rightarrow$$
$$\rightarrow\mathrm{rang}(x)\in S\,\&\,x\in S),$$

where map(x) is the formula

$$\forall z\,(z\in x\rightarrow\exists v,w\,(z=\langle v,w\rangle))\,\&\,\forall v,w_1,w_2\,(\langle v,w_1\rangle\in$$
$$x\,\&\,\langle v,w_2\rangle\in x\rightarrow w_1=w_2),$$

and k-sets dom(x) and rang(x) satisfy

$$\forall v\,(v\in\mathrm{dom}(x)\leftrightarrow\exists w\,(\langle v,w\rangle\in x))$$

and

$$\forall w\,(w\in\mathrm{rang}(x)\leftrightarrow\exists v\,(\langle v,w\rangle\in x)).$$

The logic underlying ZFK is the calculus of predicates in the language of ZFK.

III. It is well known [3, p. 27] that "An axiomatic system is in general constructed in order to axiomatize a certain scientific discipline previously given in a pre-systematic, "naive", or 'genetic' form". ZFK formulated here has been constructed, like ZFC, to axiomatize the "naive" set theory of G. Cantor, or more precisely, to axiomatize its non-contradictory core. But ZFK has a more explicit and tight connection to Cantor set theory than it does ZFC, since ZFK in its principal interpretation defines the collection of all k-sets of S_k (more precisely, $\langle S_k;\in\rangle$) as Cantor pre-axiomatic "world" of sets, and the family S (more precisely, $\langle S;\in\cap(S\times S)\rangle$, where $S\subseteq S_k$) as the axiomatic fragment of Cantor "world" of sets.

It seems natural that ZFK is non-contradictory if ZFC is non-contradictory. Let us show that it is true.

Suppose that ZFC is a non-contradictory theory. Then, ZFC has a model and, in particular, a standard transitive model $\mathfrak{M}=\langle M;\in\cap(M\times M)\rangle$ such that for any set $m\in M$ absolutely all its subsets belong to the family M. It is clear that the model $\mathfrak{M}$ (the family M) includes absolutely denumerable sets. We consider the family M as the interpretation of the signature symbol "S" and will show that any axiom of ZFK is either true in the model $\mathfrak{M}$ or it does not deny the existence of such a model.

It is natural that all axioms of group G are true in the model $\mathfrak{M}$.

Axioms G_k–1 and G_k–2 affirm an obvious fact: any ZFC-set (a set of the family M) is also a set of Cantor "world" of sets S_k.

Axiom G_k–3 affirms natural transitivity of the family M.

Axiom G_k–4 affirms an obvious fact: any statement concerning sets of the family M is also true for sets of Cantor "world" of sets S_k due to the fact that ZFC is a formalization of the (presumably) non-contradictory core of Cantor set theory.

Axiom G_k–5) is a natural generalization of ZFC axiom of replacement which is true in the model $\mathfrak{M}$.

Axiom G_k–6), in fact, affirms that the model $\mathfrak{M}$ is naturally $\subseteq$-complete in the sense that any subset of the family M belongs to that M if its power is equal to the power of a certain set of M.

IV. Let $x\in S$. Then, a k-set $\{y\mid y\subseteq x\,\&\,y\in S\}$ is denoted by $P(x)$. It is clear that $P(x)\in S$ ($P(x)$ is a set) by axioms of group G and G_k–1).

THEOREM (*ZFK*).

$$\forall x\in S\,\forall y\,(y\subseteq x\rightarrow y\in P(x)).$$

Proof. Let us suppose that the contrary is fulfilled and let k-sets x_0 and y_0 be such that $x_0\in S$, $y_0\subseteq x_0$ and $y_0\notin P(x)$. If $y_0\in S$, than $y_0\in P(x)$ by an axiom of group G. Therefore, $y_0\notin S$. Since $\varnothing\in S$, then $y_0\neq\varnothing$. Since $y_0\subseteq x_0\in S$ and S is transitive in S_k (the axiom G_k–3)) then $y_0\subseteq S$.

Denote by z_0 some element of a k-set y_0. The axiom G_k–5) says that there is a k-set (k-function) f such that

$$f=\{\langle v,w\rangle\mid v\in x_0,(v\in y_0\rightarrow w=v),(v\notin y_0\rightarrow w=z_0)\}.$$

Since map(f), dom$(f)=x_0\in S$ and rang$(f)=y_0\subseteq S$, then $y_0\in S$ by the axiom G_k–6). A contradiction.

V. Let x be a k-set ($x\in S$ or $x\notin S$). Then $P_k(x)$ denotes k-set $\{y\mid y\subseteq x\}$. Since $x\in S_k$, then $P_k(x)\in S_k$ (by the axiom of generalization), i. e. $P_k(x)$ is an element of Cantor pre-axiomatic "world" of sets, whose power by the theorem of G. Cantor is **absolutely** greater than the power of the k-set x.

Let ω be a denumerably infinite set in S. Since $\omega\in S$ then $\omega\in S_k$ (the axiom G_k–1)). It is clear that the k-set $P_k(\omega)$ is absolutely non-denumerable. **THEOREM** says that any k-set y of S_k is such that $y\subseteq\omega$ (i. e. $y\in P_k(\omega)$) is an element of the set $P(\omega)$ of S. Therefore, the equality $P(\omega)=P_k(\omega)$ is always fulfilled. Thus the set $P(\omega)$ is **absolutely non-denumerable** in any axiomatized model of ZFK, i. e. in any model of the type $\langle S;\in\cap(S\times S)\rangle$.

Thus the concept "The set of all subsets of a set X" which is formalized by the axioms of ZFK is absolute (in view of the **THEOREM**) in the sense that it coincides with Cantor concept "The set of all (absolutely all existing in the Cantor 'world' of sets) subsets of a set X".

VI. Finally it should be noted that a symbiosis of the set theory of Vdovin A. M. and the proposed theory may permit to formulate an axiomatic non-contradictory (presumably) set theory, the only standard model of which will be the most important fragment of Cantor "world"of sets. This is ensured by the fact that Vdovin set theory proves the axioms of ZF, the generalized principle of choice, and the generalized continuum-hypothesis which are natural for Cantor "world" of sets, and the theory presented above proves the absolute

character of the concept "The set of all subsets of a set X" which is natural for Cantor "world" of sets, as well.

Since ZF is a generally acknowledged theory and it is applied as a framework for mathematical disciplines used to describe (study) the real physical world, the natural (Cantor-like) character of the future set theory will permit to develop and investigate only natural models of real physical phenomena.

The author expresses his sincere gratitude to Gregory B. Malykin, ScD in Physics and Mathematics, (senior staff researcher of the Institute of Applied Physics of the Russian Academy of Sciences, Nizhny Novgorod) for a fruitful dialogue that helped me to clarify some of my considerations. The author is also thankful for the kind invitation to participate in the series of papers, released in commemoration of Alexander M. Vdovin (1949–2007), the creator of a new axiomatics of the set theory.

Submitted on May 06, 2009 / Accepted on August 18, 2009

References

1. Vdovin A. M. Foundations of a new axiomatic set theory. *Izv. Akad. Nauk SSSR Ser. Mat.*, 1990, v. 54, 1113–1118; English transl. in *Math. USSR Izv.*, 1991, v. 37.
2. Vdovin A. M. Extension of a new axiomatic set theory. *Izv. Akad. Nauk SSSR Ser. Mat.*, 1993, v. 57, 208–212; English transl. in *Math. USSR Izv.*, 1994, v. 42.
3. Fraenkel A. A. and Bar-Hillel Y. Foundations of set theory. North-Holland, Amsterdam, 1958.
4. Ershov Yu. L., Palyutin E. A. Mathematical logic. Mir Publishers, Moscow, 1984.

"The Arrow of Time" in the Experiments in which Alpha-Activity was Measured Using Collimators Directed at East and West

Simon E. Shnoll*, Ilya A. Rubinstein†, and Nikolai N. Vedenkin†

*Department of Physics, Moscow State University, Moscow 119992, Russia
*Inst. of Theor. and Experim. Biophysics, Russian Acad. of Sci., Pushchino, Moscow Region, 142290, Russia
*Puschino State University, Prospect Nauki 3, Pushchino, Moscow Region, 142290, Russia
†Skobeltsin's Institute of Nuclear Physics, Moscow State University, Moscow 119991, Russia
E-mail: shnoll@mail.ru

In our previous paper (Shnoll and Rubinstein, Progress in Physics, 2009, v. 2, 83–95), we briefly reported about a phenomenon, which can be called the "arrow of time": when we compared histograms constructed from the results of 239-Pu alpha-activity measurements that were obtained using West- and East-directed collimators, daytime series of the "eastern" histograms were similar to the inverted series of the following night, whereas daytime series of the "western" histograms resembled the inverted series of the preceding night. Here we consider this phenomenon in more detail.

1 Introduction

As follows from all our past results, the fine structure of the spectrum of amplitude fluctuations (the shape of the corresponding histograms) is determined by the motion (orientation) of the object studied (the laboratory) in relation to spatial inhomogeneities [2]. The spatial pattern (arrangement in space) of these inhomogeneities is stable: as the Earth rotates about its axis and moves along the circumsolar orbit, similar histogram shapes are realized repeatedly with the corresponding periods (daily, near-monthly, yearly) [3, 4]. The inhomogeneities themselves are analogous to the "numerals on the dial of the celestial sphere", which determine one or another shape of histograms. In the experiments with rotating collimators, beams of α-particles periodically go in the direction of the same inhomogeneities, and similar histograms appear with the corresponding periods [5]. Earlier, when the collimator-equipped devices were immobile (with one collimator directed West and another East), we showed that histograms from either of the collimators would have their analogs (similar shapes) from the other collimator lagging behind by half a day [6] (i.e., by the time needed for the collimators, rotating with the Earth, to face the same spatial inhomogeneities). In the experiments with "daily palindromes", however, this periodicity turned out to be asymmetrical. Asymmetry manifested itself in the daytime series of the "eastern" histograms being similar to the inverted series of the *following* night and the daytime series of the "western" histograms being similar to the inverted series of the *preceding* night [1]. Below we describe this phenomenon in more detail and discuss its possible nature.

2 Materials and methods

The material for this study was series of histograms constructed from the results of long-term measurements of α-activity registered from two ^{239}Pu preparations using two independent collimator-equipped devices. The collimators were used to isolate beams of α-particles flying at certain directions. In this study, one collimator was directed East and another was directed West. The technical information on the devices, which were constructed by I. A. Rubinstein and N. N. Vedenkin, can be found in [2]. The analysis of histogram series consists in the estimation of histogram similarity depending on the interval between them. A detailed description of the methodology for constructing and comparing histograms, as well as for obtaining distributions of the number of similar pairs over the length of the interval between the histograms compared, is given in [2]. To characterize correlations in

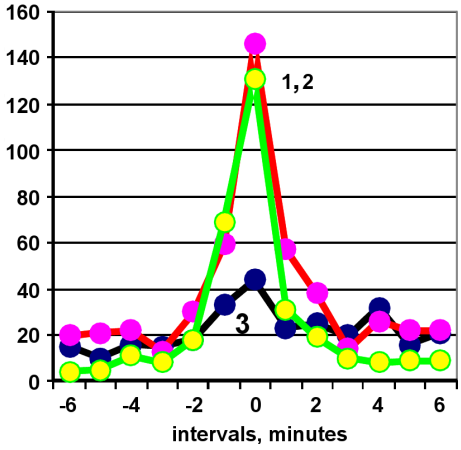

Fig. 1: Illustration of the "palindrome phenomenon". A high probability of histograms of the same order numbers to be similar in the direct daytime/inverse nighttime sequences (line 1) and the direct nighttime/inverse daytime ones (line 2). A low probability of histograms to be similar at comparing the direct daytime and nighttime sequences (line 3). The counter did not contain a collimator. Date of measurements, September 23, 2005. Every line sums up the results of approximately 10000 pairwise comparisons. *X* axis, interval between the histograms compared (min); *Y* axis, the number of similar pairs.

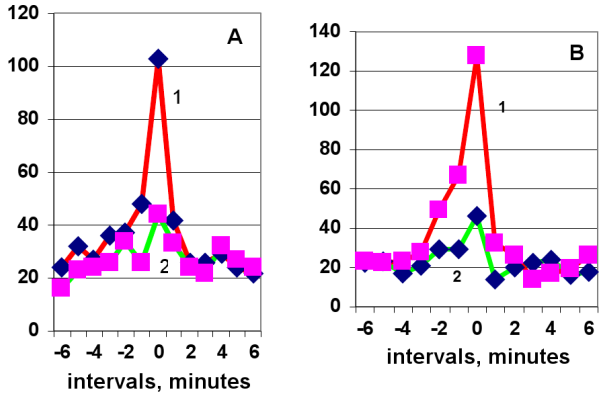

Fig. 2: Palindrome effects in the simultaneous measurements of ^{239}Pu α-activity with two independent collimator-equipped devices directed East (A) and West (B). Date of measurements, September 22–23, 2003. The axes as in Fig. 1. (A) "East": (1) "day" versus the *following* inverse "night"; (2) "day" versus the *preceding* inverse "night". (B) "West": (1) "day" versus the *preceding* inverse "night"; (2) "day" versus the *following* inverse "night".

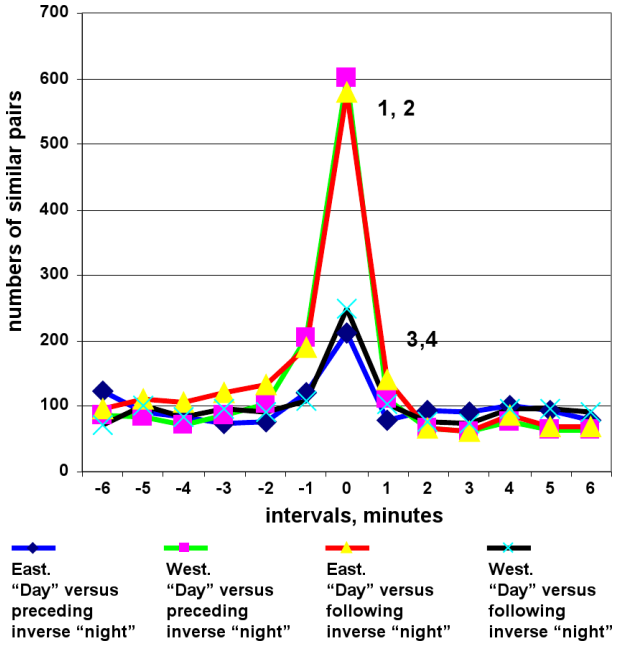

Fig. 3: In the measurements of ^{239}Pu α-activity with the West-directed collimator, a direct sequence of daytime histograms is similar to the reverse histogram sequence of the *preceding* night; in the measurements of ^{239}Pu α-activity with the East-directed collimator, a direct sequence of daytime histograms is similar to the reverse histogram sequence of the *following* night. A sum of four experiments.

the change of the histogram shape over time, we used the "palindrome phenomenon" [7] — the high probability of a sequence of histograms constructed from the results of daytime measurements (from 6:00 to 18:00, by local longitude time) to be similar to the *inverse* sequence of histograms constructed from the results of nighttime measurements (from 18:00 to 6:00 of the next day). Fig. 1 demonstrates this phenomenon. The source material is series of ^{239}Pu α-activity measurements registered with a counter without collimator (frequency of measurement, 1 point per second). From these data, 1-min histogram sequences were constructed (60 points per histogram), with the histograms smoothed 7-fold by the moving summation method (for visual convenience). Two histogram sequences were compared: (1) from 6:00 to 18:00 by accurate local time ("daytime" sequence) and (2) from 18:00 to 6:00 of the next day ("nighttime" series), each sequence consisting of 720 histograms. The sequences could be direct (from no. 1 to 720) or inverse (from no. 720 to 1).

As seen in Fig. 1, if compared are the direct daytime and nighttime sequences, the similarity (the probability to be similar) of histograms of the same order numbers is low (line 3). In contrast, the direct daytime/inverse nighttime (line 1) or inverse daytime/direct nighttime (line 2) comparisons reveal a high similarity of the same histogram numbers — the "effect of palindrome" [7].

3 Results

The phenomenon of palindrome was easily reproduced in the analysis of measurements performed in different seasons without a collimator. However, the analysis of data obtained in the experiments with collimators (western and eastern) showed varying results; the phenomenon became irregular. In the experiments with the western collimator, palindromes were reproduced regularly when a direct daytime sequence was compared with the inverse sequence of the preceding night; with the eastern collimator, it must have been a direct daytime sequence versus the inverse sequence of the following night. This phenomenon is illustrated in Fig. 2.

Fig. 2 shows that in the measurements with the eastern collimator, a clear palindrome can be seen when the direct sequence of histograms obtained from 6:00 to 18:00 on September 22 ("day") is compared with the inverse sequence of histograms obtained from 18:00 on September 22 to 6:00 on September 23 ("night"). At the same time, comparing the direct sequence of nighttime histograms (measurements from 18:00 on September 22 to 6:00 on September 23) with the inverse sequence of the following daytime histograms (measurements from 6:00 to 18:00 on September 23) shows no palindromes.

In the experiments with the "western" collimator, the situation is opposite. A clear palindrome is seen when the direct sequence of histograms obtained from 6:00 to 18:00 on September 22 ("day") is compared with the inverse sequence of histograms obtained from 18:00 on September 21 to 6:00 on September 22 ("night"). No palindromes is revealed when the direct sequence of histograms obtained from 6:00 to 18:00 on September 22 ("day") is compared with the inverse sequence of histograms obtained from 18:00 on September 22 to 6:00 on September 23 ("night"). To put it briefly: the eastern collimator will give palindromes upon the direct-day-to-*following*-inverse-night comparing; the western collima-

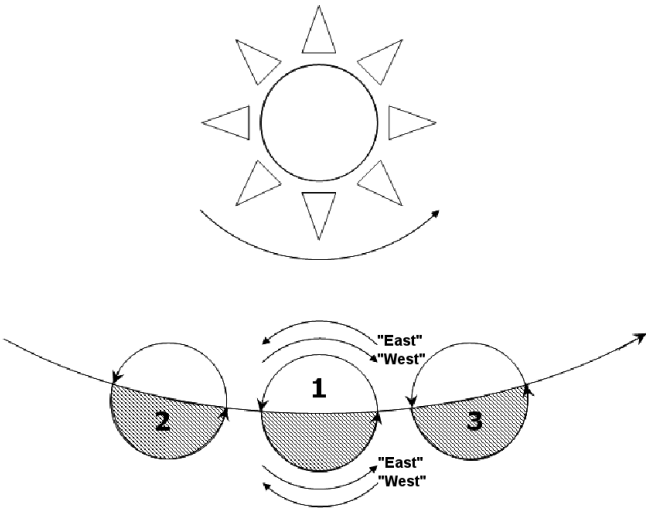

Fig. 4: The relation between the directions of motion during the daily rotation of the Earth, its translocation along the circumsolar orbit, the rotation of the Sun about its axis and the directions of α-particles flying through the "western" and "eastern" collimators.

tor will show palindromes upon the direct-day-to-*preceding*-inverse-night comparing. Since the regularities found were of principle importance, we conducted more than 25 analogous experiments. The regularities were reproduced well and did not depend on the season. This can be seen in Fig. 3, which represents a summary result of four independent experiments.

4 Discusion

The phenomenon under discussion concerns regularities revealed in the experiments, in which ^{239}Pu α-activity was measured with collimator-equipped devices. The collimator were directed either West or East, and the sequence of histograms obtained with the western collimator from 6:00 to 18:00 by local time ("day") turned out to be similar to the inverse sequence of the preceding night (from 18:00 to 6:00), whereas the sequence of daytime histograms obtained with the eastern collimator were similar to the inverse sequence of the following night.

Here we would remind the reader that the matter does not concern any "effects on α-decay"; it concerns changes of the fine structure of amplitude fluctuation spectra (the shape of the corresponding histograms). The intensity of α-decay, a mean number of decay acts per time unit, does not depend on the direction of the collimator; it will fluctuate according to the Poisson statistics — proportionally to $\pm\sqrt{N}$, where N is the decay intensity.

Earlier we established that the changes of the histogram shape would depend on the orientation of collimators in space [8]. It seems that certain histogram shapes correspond to certain directions, possibly, to the spatial locations of gravitational inhomogeneities. Changes of the histogram shape are determined by the motion of our objects in relation to these quite long-living (for more than a year) stable inhomogeneities. Now we see that apart from the dependence on the spatial vector, there is also a dependence on the vector of time.

Fig. 4 schematically illustrates spatial relations in the experiments described above. There are two devices in the laboratory (on the Earth), which differ only by the orientation of the collimators: one isolates a beam of α-particles flying West (i.e., against the direction that the Earth rotates in) and the other is directed East (i.e., along the Earth rotation). The Earth rotates about its axis and moves along the circumsolar orbit. Both these motions, as well as rotation of the Sun, have the same direction: they are directed counterclockwise. However, combining the first two motions results in the rotation of the Earth to be counter-directed to its translocation along the orbit in the daytime and co-directed in the nighttime [9]. Accordingly, α-particles from the "eastern" collimator would fly *against* the orbital Earth motion in the daytime and *along* this motion in the nighttime, this being the opposite for the "western" collimator. Hence, the collimators alternatively (one during the day- and the other during the nighttime) take the same orientation — either "along" or "against" the orbital motion of the Earth. Therefore, the phenomenon discussed cannot be explained by the change of the collimator orientation towards the Earth motion along the circumsolar orbit.

> Thus, the "arrow of time" in our experiments is determined only by the difference in the orientation of the collimators in relation to the direction of the Earth rotation about its axis.

Acknowledgements

The authors are thankful to D. D. Rabounski, D. P. Kharakoz, A. V. Agafonov and V. A. Kolombet for valuable discussions on the subject of the paper. We also thank our colleagues who discussed this phenomenon on a meeting of the "Seminar on the Problem of Time" organized by A. P. Levich (October 13, 2009). In the paper, however, we confined ourselves only to the description of the phenomenon.

Submitted on August 26, 2009 / Accepted on October 04, 2009

References

1. Shnoll S. E. and Rubinstein I. A. Regular changes in the fine structure of histograms revealed in the experiments with collimators which isolate beams of alpha-particles flying at certain directions. *Progress in Physics*, 2009, v. 2, 83–95.
2. Shnoll S. E. Cosmic physical factors in random processes. Svenska fysikarkivet, Stockholm, 2009, 388 pages.
3. Shnoll S. E., Zenchenko K. I. and Udaltsova N. V. Cosmophysical effects in the structure of daily and yearly periods of changes in the shape of histograms constructed from the measurements of ^{239}Pu alpha-activity. *Biophysics*, 2004, v. 49(1), 155–164.
4. Shnoll S. E. The "scattering of the results of measurements" of processes of diverse nature is determined by the Earth's motion in the inhomogeneous space-time continuum. The effect of "half-year palindromes". *Progress in Physics*, 2009, v. 1, 3–7.

5. Shnoll S. E., Rubinshtein I. A., Zenchenko K. I., Shlekhtarev V. A., Kaminsky A. V., Konradov A. A., Udaltsova N. V. Experiments with rotating collimators cutting out pencil of alpha-particles at radioactive decay of Pu-239 evidence sharp anisotropy of space. *Progress in Physics*, 2005, v. 1, 81–84.
6. Shnoll S. E. Changes in fine structure of stochastic distributions as a consequence of space-time fluctuations. *Progress in Physics*, 2006, v. 2, 39–45.
7. Shnoll S. E., Panchelyuga V. A. and Shnoll A. E. The palindrome effect. *Progress in Physics*, 2008, v. 2, 151–153.
8. Shnoll S. E., Zenchenko K. I., Berulis I. I., Udaltsova N. V. and Rubinstein I. A. Fine structure of histograms of alpha-activity measurements depends on direction of alpha particles flow and the Earth rotation: experiments with collimators. arXiv: physics/0412007.
9. Perelman Ya. I. Physics for entertainment. Book 1. Nauka Press, 22nd Edition, 1986, p. 16–21.

SPECIAL REPORT

Two-World Background of Special Relativity. Part I

Akindele O. J. Adekugbe
P. O. Box 2575, Akure, Ondo State 340001, Nigeria
E-mail: adekugbe@alum.mit.edu

A new sheet of spacetime is isolated and added to the existing sheet, thereby yielding a pair of co-existing sheets of spacetimes, which are four-dimensional inversions of each other. The separation of the spacetimes by the special-relativistic event horizon compels an interpretation of the existence of a pair of symmetrical worlds (or universes) in nature. Further more, a flat two-dimensional intrinsic spacetime that underlies the flat four-dimensional spacetime in each universe is introduced. The four-dimensional spacetime is outward manifestation of the two-dimensional intrinsic spacetime, just as the Special Theory of Relativity (SR) on four-dimensional spacetime is mere outward manifestation of the intrinsic Special Theory of Relativity (ϕSR) on two-dimensional intrinsic spacetime. A new set of diagrams in the two-world picture that involves relative rotation of the coordinates of the two-dimensional intrinsic spacetime is drawn and intrinsic Lorentz transformation derived from it. The Lorentz transformation in SR is then written directly from intrinsic Lorentz transformation in ϕSR without any need to draw diagrams involving relative rotation of the coordinates of four-dimensional spacetime, as usually done until now. Indeed every result of SR can be written directly from the corresponding result of ϕSR. The non-existence of the light cone concept in the two-world picture is shown and good prospect for making the Lorentz group SO(3,1) compact in the two-world picture is highlighted.

1 Introduction

The concept of other universe(s) or world(s) is not new in physics. In 1898, Schuster contemplated a universe containing negative mass [1]. The discovery in particle physics of the existence of an anti-particle to every particle afterwards, led some physicists to suggest the existence of an anti-atom (composed of anti-particles) to every atom (composed of particles); an anti-molecule to every molecule and an anti-macroscopic-object to every macroscopic object. Then in order to explain the preponderance of particles and matter over anti-particles and anti-matter respectively in this our universe, the existence of an anti-universe containing a preponderance of anti-matter over matter was suggested, as discussed in [2, see p. 695], for instance. However it has remained unknown until now whether the speculated universe containing negative mass of Schuster and an anti-universe containing a preponderance of anti-matter exist or not.

The purpose of this article is to show formally that the Special Theory of Relativity rests on a background of a two-world picture, in which an identical partner universe in a different spacetime to this universe of ours in our spacetime co-exist, and to commence the development of the two-world picture thus introduced. The placement of the other universe relative to our universe, as well as the configuration of matter in it shall be derived. The symmetry of state and symmetry of laws between the two universes shall be established. The definite interaction between the two universes in relativistic phenomena shall also be shown.

This article may be alternatively entitled as *Isolating a Symmetry-Partner Universe to Our Universe in the Context of the Special Theory of Relativity*. Apart from the derivation of the Lorentz transformation (LT) and its inverse with the aid of a new set of spacetime/intrinsic spacetime diagrams on the combined spacetimes/intrinsic spacetimes of the two co-existing identical "anti-parallel" universes, there are no further implications on the other results of SR usually derived from the LT and its inverse in the existing one-world picture. However SR must be deemed to be tremendously expanded or made more complete by exposing its two-world background and by the addition of a parallel two-dimensional intrinsic Special Theory of Relativity (ϕSR) on a flat two-dimensional intrinsic spacetime that underlies the flat four-dimensional spacetime of SR in each of the two universes.

There are several new implications of the two-world picture for SR as well, which include the non-existence of the light cone concept, good prospect for making SO(3,1) compact, a feat that has proved impossible in the existing one-world picture and inter-universe transitions of symmetry-partner particles between the two universes (at super-high energy regimes), on which the prospect for experimental test ultimately of the two-world picture rests. This initial articles goes as far as a single article can on the vast subject of two-world symmetry that lies at the foundation of the Special Theory of Relativity and possibly the whole of physics.

2 Two schemes towards the Lorentz boost

As can be easily demonstrated, the two schemes summarized in Table 1 both lead to the Lorentz boost, (which shall also

Scheme I	Scheme II
$x = x' \cosh\alpha + ct' \sinh\alpha$	$x = x' sec\psi + ct' \tan\psi$
$ct = ct' \cosh\alpha + x' \sinh\alpha$	$ct = ct' \sec\psi + x' \tan\psi$
$y = y'\ ;\ z = z'$	$y = y'\ ;\ z = z'$
$\cosh\alpha = \dfrac{1}{\sqrt{1 - v^2/c^2}} = \gamma$	$\sec\psi = \dfrac{1}{\sqrt{1 - v^2/c^2}} = \gamma$
$\sinh\alpha = \dfrac{v/c}{\sqrt{1 - v^2/c^2}} = \beta\gamma$	$\tan\psi = \dfrac{v/c}{\sqrt{1 - v^2/c^2}} = \beta\gamma = \beta\gamma$
$\tanh\alpha = v/c = \beta$	$\sin\psi = v/c = \beta$

Table 1: Two schemes towards the derivation of the Lorentz boost graphically.

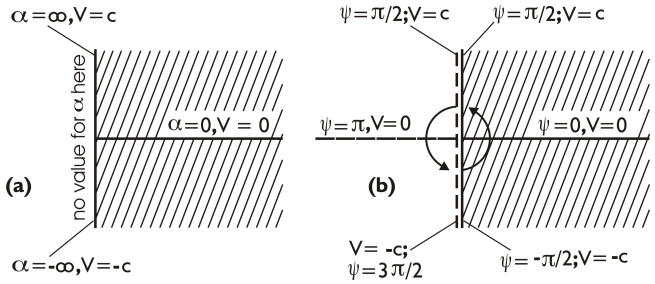

Fig. 1: a) All values of the number α generate the positive half-plane in Scheme I and b) all values of the angle ψ in the first cycle generate the positive and negative half-planes in Scheme II.

be referred to as the Lorentz transformation (LT)) and the Lorentz invariance (LI). Although the $\gamma = \cosh\alpha$ parametrization of the LT in Scheme I is more familiar, the $\gamma = \sec\psi$ parametrization in Scheme II is also known.

Now by letting $v/c = 0$ in Table 1 we obtain the following:

$$\cosh\alpha = 1;\ \sinh\alpha = \tanh\alpha = 0 \ \Rightarrow\ \alpha = 0\,,$$
$$\sec\psi = 1;\ \tan\psi = \sin\psi = 0 \ \Rightarrow\ \psi = 0\,.$$

By letting $v/c = 1$ we have

$$\cosh\alpha = \sinh\alpha = \infty;\ \tanh\alpha = 1 \ \Rightarrow\ \alpha = \infty\,,$$
$$\sec\psi = \tan\psi = \infty;\ \sin\psi = 1 \ \Rightarrow\ \psi = \tfrac{\pi}{2}, \tfrac{5\pi}{2}, \tfrac{9\pi}{2}, \ldots$$

And by letting $v/c = -1$ we have

$$\cosh\alpha = \infty;\ \sinh\alpha = -\infty;\ \tanh\alpha = -1 \ \Rightarrow\ \alpha = -\infty\,,$$
$$\sec\psi = \infty;\ \tan\psi = -\infty;\ \sin\psi = -1 \ \Rightarrow\ \psi = -\tfrac{\pi}{2}, \tfrac{3\pi}{2}, \tfrac{7\pi}{2}, \ldots$$

Thus there are the following equivalent ranges of values of the parameter α and the angle ψ between the two schemes:

$$0 \leqslant \alpha \leqslant \infty \ \text{(Scheme I)} \quad \equiv \quad 0 \leqslant \psi \leqslant \tfrac{\pi}{2} \ \text{(Scheme II)}$$
$$-\infty \leqslant \alpha \leqslant \infty \ \text{(Scheme I)} \quad \equiv \quad -\tfrac{\pi}{2} \leqslant \psi \leqslant \tfrac{\pi}{2} \ \text{(Scheme II)}$$

The second range, which is $-\infty \leqslant \alpha \leqslant \infty$ (Scheme I) or $-\frac{\pi}{2} \leqslant \psi \leqslant \frac{\pi}{2}$ (Scheme II), generates the positive half-plane shown shaded in Figs. 1a and 1b.

If we consider Scheme I, then clearly there is only the positive half-plane as illustrated in Fig. 1a. This is so since the range $-\infty \leqslant \alpha \leqslant \infty$ generates the positive half-plane only, and there are no other values of α outside this range. Thus going to the negative half-plane is impossible in the context of SR in Scheme I.

If we consider Scheme II, on the other hand, then the range $-\frac{\pi}{2} \leqslant \psi \leqslant \frac{\pi}{2}$, which generates the positive half-plane in Fig. 1b is not exhaustive of the values of angle ψ in the first cycle. There is also the range $\frac{\pi}{2} \leqslant \psi \leqslant \frac{3\pi}{2}$, which generates the negative half-plane. Thus going into the negative half-plane is possible in SR in the context of Scheme II. There is actually no gap between the solid line and the broken line along the vertical as appears in Fig. 1b.

It must quickly be pointed out that there has not seemed to be any need to consider the second range $\frac{\pi}{2} \leqslant \psi \leqslant \frac{3\pi}{2}$ (or the negative half-plane) in Fig. 1b in physics until now because the parity inversion and time reversal associated with it can be achieved by reflection of coordinates of 3-space in the first range $-\frac{\pi}{2} \leqslant \psi \leqslant \frac{\pi}{2}$ (or in the positive half-plane) that also includes time reversal. However we consider it worthy of investigation whether the range $\frac{\pi}{2} \leqslant \psi \leqslant \frac{3\pi}{2}$ and the parity inversion it implies exist naturally apart from the possibility of parity inversion by coordinate reflection in the positive half-plane. Reasoning that parity inversion and time reversal will not be the only physical significance of the second range $\frac{\pi}{2} \leqslant \psi \leqslant \frac{3\pi}{2}$ (or the negative half-plane) in Fig. 1b, should it exist in nature, we deem it judicious to carry both ranges $-\frac{\pi}{2} \leqslant \psi \leqslant \frac{\pi}{2}$ and $\frac{\pi}{2} \leqslant \psi \leqslant \frac{3\pi}{2}$ along in the present development with the hope that the theory shall ultimately justify the existence of the second range or otherwise.

In translating Figs. 1a and 1b into spacetime diagrams, the positive horizontal lines along which, $v = 0$, $\alpha = 0$ and $\psi = 0$, in the figure, correspond to the 3-dimensional Euclidean space Σ with mutually orthogonal dimensions x, y and z in the Cartesian system of coordinates; the positive vertical lines along which, $v = c$, $\alpha = \infty$ and $\psi = \frac{\pi}{2}$, correspond to the positive time dimension ct, while the negative vertical lines along which $v = -c$, $\alpha = -\infty$ and $\psi = -\frac{\pi}{2}$, correspond to the negative time dimension (or the time reversal dimension) $-ct^*$. In addition, the horizontal line in the negative half-plane in Fig. 1b corresponds to a negative 3-dimensional Euclidean space (not known in physics until now) to be denoted by $-\Sigma^*$ with mutually orthogonal dimensions $-x^*$, $-y^*$ and $-z^*$ in the rectangular system. Thus Figs. 1a and 1b translate into the space-time diagrams of Figs. 2a and 2b respectively. Representation of the Euclidean 3-spaces by lines along the horizontal and the time dimensions by vertical normal lines to the "space axes", as done in Figs. 2a and 2b, is a well known practice in the graphical representation of four-dimensional spacetime, exemplified by the modern Minkowski diagrams [3].

Figure 2a pertains to Scheme I in Table 1. The four-dimensional spacetime with dimensions x, y, z and ct is the

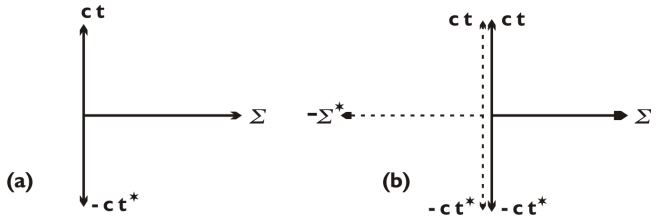

Fig. 2: The spacetime domains generated by a) all values of the number α in Scheme I and b) all values of the angle ψ in the first cycle in Scheme II.

Minkowski space as known. In addition, there is the negative time dimension $-ct^*$ that serves the role of time reversal dimension, (which is different from the *past time* axis in the past light cone). There are no second and third quadrants in Fig. 2a, since the negative half-plane is inaccessible in Scheme I.

Figure 2b pertains to Scheme II in Table 1. There are two "anti-parallel" Minkowski spaces in Fig. 2b namely, the one with positive dimensions, $(\Sigma, ct) \equiv (x, y, z, ct)$, generated by the range of angles $0 \leqslant \psi \leqslant \frac{\pi}{2}$ in the first quadrant in Fig. 1b, to be referred to as the positive Minkowski space, and the other with all negative dimensions, $(-\Sigma^*, -ct^*) \equiv (-x^*, -x^*, -y^*, -ct^*)$, generated by the range of angles $\pi \leqslant \psi \leqslant \frac{3\pi}{2}$ in the third quadrant, to be referred to as the negative Minkowski space. There are in addition the negative time dimension $-ct^*$ that serves the role of the time reversal dimension to the positive Minkowski space, while the positive time dimension ct serves the role of time reversal dimension to the negative Minkowski space.

It shall again be quickly added that the spacetime dimensions of the negative Minkowski space constitute parity inversion and time reversal with respect to the spacetime dimensions of the positive Minkowski space and conversely. Figure 2b says that this situation exists naturally, quite apart from the fact that parity inversion (by coordinate reflection), $x \to -x$; $y \to y$; $z \to z$ or $x \to -x$; $y \to -y$; $z \to -z$ and time reversal $t \to -t$ are achievable within the positive half-plane, that is within the positive Minkowski space (fist quadrant) plus the fourth quadrant in Figs. 2a and 2b. Schemes I and II have been known to imply the existence of the positive half plane only in physics until now. The investigation of the implications of the existence naturally of the negative half-plane in parallel with the positive half-plane in Figs. 1b and 2b shall be started in this paper.

3 Minkowski's diagrams as graphical representation of Lorentz transformation in Scheme I

There is essentially nothing new in this section. Its inclusion is necessary so that the derivation newly of the LT and its inverse graphically in the context of Scheme II from the next section can be compared with the known derivation of the LT and its inverse graphically in the context of Scheme I, which shall be re-presented in this section.

For the relative motion of two frames, (which involves positive time dimension), the time reversal dimension $-ct^*$ is irrelevant, leaving only the first quadrant in Fig. 2a, (in the context of Scheme I). Thus relative rotations of the spacetime coordinates of the particle's (or primed) frame and the observer's (or unprimed) frame, for every pair of frames in relative motion, are limited to the interior of the first quadrant in Scheme I, which corresponds to the first quadrant in Figs. 1a and 2a. As is clear from Fig. 2a, Scheme I pertains to a one-world picture, including the time reversal dimension.

Now the Lorentz transformation (LT) is usually derived analytically in the Special Theory of Relativity (SR), following Albert Einstein's 1905 paper [4]. In his paper, Einstein inferred from two principles of relativity, the LT and its inverse for motion along the x'-direction of the coordinate system (ct', x', y', z') attached to a particle moving at speed v relative to an observer's frame (ct, x, y, z), where the coordinates x' and x are taken to be collinear, respectively as follows:

$$t' = \gamma\left(t - \frac{v}{c^2}\,x\right);\;\; x' = \gamma\,(x - vt);\;\; y' = y;\;\; z' = z \qquad (1)$$

and

$$t = \gamma\left(t' + \frac{v}{c^2}\,x'\right);\;\; x = \gamma\,(x' + vt');\;\; y = y';\;\; z = z', \qquad (2)$$

where $\gamma = (1 - v^2/c^2)^{-1/2}$. As demonstrated in Einstein's paper, each of systems (1) and (2) satisfies the Lorentz invariance,

$$c^2t'^2 - x'^2 - y'^2 - z'^2 = c^2t^2 - x^2 - y^2 - z^2. \qquad (3)$$

Somewhat later, Minkowski explored the graphical (or coordinate- geometrical) implication of the LT and its inverse [5]. In the graphical approach, the first two equations of the inverse LT, system (2), is interpreted as representing rotations of the coordinates x' and ct' of the particle's (or primed) frame relative to the coordinates x and ct respectively of the observer's (or unprimed) frame, while the last two equations are interpreted as representing no special-relativistic rotations of coordinates y' and z' relative to y and z respectively (since relative motion of SR does not occur along these coordinates).

The Minkowski spacetime diagrams from which the LT and its inverse have sometimes been derived for two frames in relative motion along their collinear x'- and x-axes, are shown as Figs. 3a and 3b, where the surface of the future light cone is shown by the broken lines.

The coordinates y' and z' of the particle's frame, as well as the coordinates y and z of the observer's frame remain not rotated from the horizontal, and have not been shown in Figs. 3a and 3b. The net coordinate projection along the horizontal in Fig. 3a, which in ordinary Euclidean geometry would be $x' \cos\phi + ct' \sin\phi$, is given in the Minkowski geometry as $x' \cosh\alpha + ct' \sinh\alpha$. This is the net coordinate projection to be denoted by x, along the X-axis of the observer's frame.

Similarly the net coordinate projection along the vertical in Fig. 3a is $ct' \cosh\alpha + x' \sinh\alpha$ in the Minkowski geometry. This is the net coordinate projection, to be denoted by ct, along the cT-axis of the observer's frame. Thus the following familiar transformation of coordinates has been derived from Fig. 3a:

$$\left.\begin{aligned} ct &= ct' \cosh\alpha + x' \sinh\alpha; \\ x &= x' \cosh\alpha + ct' \sinh\alpha; \;\; y = y' ; \;\; z = z' \end{aligned}\right\}, \qquad (4)$$

where the trivial transformations, $y = y'$ and $z = z'$ of the coordinates along which relative motion of SR does not occur have been added.

The inverse of system (4) that can be similarly derived from Fig. 3b is the following:

$$\left.\begin{aligned} ct' &= ct \cosh\alpha - x \sinh\alpha; \\ x' &= x \cosh\alpha - ct \sinh\alpha; \;\; y' = y ; \;\; z' = z \end{aligned}\right\}, \qquad (5)$$

System (5) can be presented in a matrix form as follows:

$$\begin{pmatrix} ct' \\ x' \\ y' \\ z' \end{pmatrix} = \begin{pmatrix} \cosh\alpha & -\sinh\alpha & 0 & 0 \\ -\sinh\alpha & \cosh\alpha & 0 & 0 \\ 0 & 0 & 1 & 0 \\ 0 & 0 & 0 & 1 \end{pmatrix} \begin{pmatrix} ct \\ x \\ y \\ z \end{pmatrix} \qquad (6)$$

which of the form $\mathbf{x}' = L\,\mathbf{x}$.

By considering the spatial origin, $x' = y' = z' = 0$, of the primed frame, system (4) reduces as follows:

$$x = ct' \sinh\alpha \quad \text{and} \quad ct = ct' \cosh\alpha\,. \qquad (7)$$

Division of the first into the second equation of system (7) gives

$$\frac{x}{ct} = \frac{v}{c} = \tanh\alpha\,, \qquad (8)$$

where, $x/t = v$, is the speed of the primed frame relative to the unprimed frame.

Using (8) along with $\cosh^2\alpha - \sinh^2\alpha = 1$ gives the following:

$$\cosh\alpha = \frac{1}{\sqrt{1 - v^2/c^2}} \equiv \gamma\,, \qquad (9a)$$

$$\sinh\alpha = \frac{v/c}{\sqrt{1 - v^2/c^2}} \equiv \beta\gamma\,. \qquad (9b)$$

Substitution of equations (9a) and (9b) into systems (4) and (5) gives the LT and its inverse in the usual forms of systems (1) and (2).

The transformation from the usual trigonometric ratios, cosine and sine, of the angle ϕ in Figs. 3a and 3b, where $\tan\phi = v/c$; $-\frac{\pi}{4} < \phi < \frac{\pi}{4}$ (the light-cone), to hyperbolic functions, cosh and sinh of a number α in expressing coordinate projections on spacetime, in order to reproduce the Lorentz transformation in the Minkowski graphical approach, is compelled by the need for the parameter α to take on values in the unbounded range $(-\infty, \infty)$ (in Fig. 1a) of Scheme I, as the speed v of the particle relative to the observer takes on values in the unbounded range $(-c, c)$. In other words, the need to transform from the trigonometric ratios, cosine and sine, of the angle ϕ in Figs. 3a and 3b to hyperbolic functions, cosh and sinh, of a number α is compelled by the need to restrict to the positive half-plane of Fig. 1a or to the one-world picture in Special Relativity until now.

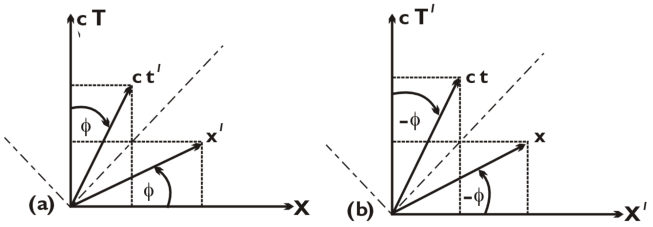

Fig. 3: The Minkowski diagrams sometimes used to derive the Lorentz transformation and its inverse in the existing one-world picture.

There is also a known mathematical significance to the LT system (5) or (6) and its inverse system (4) derived from the Minkowski diagrams of Figs. 3a and 3b. This is the fact that the 4×4 matrix L that generates the Lorentz boost (6), which contains the parameter α in the unbounded range $(-\infty, \infty)$, is a member of the pseudo-orthogonal Lorentz group SO(3,1), which is a non-compact Lie group with an unbounded parameter space [6]. Moreover the matrix L is non-singular for any finite value of α as required for all group SO(3,1) matrices. This implies that non-physical discontinuities do not appear in the Minkowski space generated. Singularities appear in systems (4) and (5) for the extreme values of α namely, $\alpha = \infty$ and $\alpha = -\infty$ only, which are not included in the range of α. These extreme values of α correspond to speeds $v = c$ and $v = -c$ respectively, which material particles cannot attain in relative motion.

The Lorentz boost is just a special Lorentz transformation. The general Lorentz transformation Λ is written in the factorized form [6] as follows:

$$\Lambda = R(\gamma, \beta, 0)\, L_3(\alpha)\, R(\phi, \theta, \varphi)^{-1}, \qquad (10)$$

where $L_3(\alpha)$ is the Lorentz boost along the z-axis with speed $v = c\tanh\alpha$; $0 \leqslant \alpha < \infty$, and the Euler angles for rotation in the Euclidean 3-space have their usual finite ranges.

Since the group SO(3) matrices are closed and bounded, and are hence compact, the compactness or otherwise of Λ is determined by the Lorentz boost. Thus since the Lorentz boost is non-compact, the Lorentz group SO(3,1) is non-compact as known. There is no way of making SO(3,1) compact within the Minkowski one-world picture since the parameter α naturally lies within the unbounded range $-\infty < \alpha < \infty$ in this picture. Thus the Minkowski diagrams of Figs. 3a and 3b and the LT and its inverse of systems (5) and (4) or the implied transformation matrix L in Eq. (6) derived from them, have been seen as physical significance of

the Lorentz group in mathematics, or perhaps the other way round.

From the point of view of physics, on the other hand, one observes that the coordinates x' and ct' of the primed frame are non-orthogonal (or are skewed) in Fig. 3a, and the coordinates x and ct of the unprimed frame are skewed in Fig. 3b. These coordinates are orthogonal in the absence of relative motion of the frames. Even in relative motion, an observer at rest relative to the primed frame could not detect the uniform motion of his frame. Hence the primed frame is stationary relative to an observer at rest relative to it with or without the motion of the primed frame relative to the unprimed frame. Yet Fig. 3a shows that the coordinates of the primed frame are skewed with respect to an observer at rest relative to it while it is in uniform motion relative to the unprimed frame. This skewness of the spacetime coordinates of a frame is then an effect of the uniform motion of the frame, which an observer at rest relative to it could detect. This contradicts the fact that an observer cannot detect any effect of the uniform motion of his frame. Skewness of rotated coordinates cannot be avoided in Minkowski's diagrams because relative rotation of coordinates must be restricted to the first quadrant in Scheme I (or in the one-world picture), as deduced earlier.

Skewness of spacetime coordinates of frames of reference is not peculiar to the Minkowski diagrams. It is a general feature of all the existing spacetime diagrams (in the one-world picture) in Special Relativity. There are at least two other spacetime diagrams in Special Relativity, apart from the Minkowski diagrams namely, the Loedel diagram [7] and the Brehme diagram [8]. The spacetime coordinates of two frames in relative motion are skewed in the Loedel and Brehme diagrams shown as Figs. 4a and 4b respectively, for two frames in relative motion along their collinear x'- and x-axes.

Skewness of the coordinates of a frame of reference in uniform relative motion is undesirable because it is an effect of uniform motion of a frame which an observer at rest relative to the frame could detect, which negates the fundamental principle that no effect of uniform motion is detectable, as mentioned earlier. Moreover it gives apparent preference for one of two frames of reference in uniform relative motion, which, again, is a contradiction of a tenet of Special Relativity.

4 Geometric representation of Lorentz transformation in Scheme II

Having discussed the existing geometric representation of the Lorentz transformation and its inverse in Special Relativity in the context of Scheme I in Table 1 (or in the one-world picture) in the preceding section, we shall develop a new set of spacetime diagrams that are compatible with the Lorentz transformation and its inverse in the context of Scheme II in Table 1 in the rest of this paper. We shall, in particular, watch out for the possibility of making the Lorentz group SO(3,1)

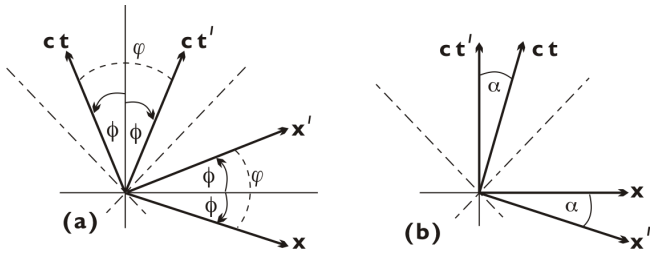

Fig. 4: a) The Loedel diagram and b) the Brehme diagram for two frames in uniform relative motion.

compact and for removing the skewness of rotated spacetime coordinates of frames of reference in the existing spacetime diagrams of Special Relativity (in the one-world picture or in the context of Scheme I).

4.1 Co-existence of two identical universes in the context of Scheme II

As shall be sufficiently justified with progress in this article, the co-existence of two anti-parallel Minkowski spaces in Fig. 2b implies the co-existence of two "anti-parallel" worlds (or universes) in nature. The dimensions x, y, z and ct of the positive Minkowski space, which are accessible to us by direct experience, are the dimensions of our universe (or world). The dimensions $-x^*, -y^*, -z^*$ and $-ct^*$ of the negative Minkowski space, which are inaccessible to us by direct experience, and hence, which have remained unknown until now, are the dimensions of another universe. Dummy star label has been put on the dimensions of the other universe, which are non-observable to us in our universe, in order to distinguish them from the dimensions of our universe.

The negative spacetime dimensions $-x^*, -y^*, -z^*$ and $-ct^*$ are inversions in the origin (or four-dimensional inversion) of the positive spacetime dimensions x, y, z and ct. Thus the spacetime dimensions of the universe with negative dimensions, to be referred to as the negative universe for brevity, and the spacetime dimensions of our universe, (to sometimes be referred to as the positive universe), have an inversion-in-the-origin symmetry. There is a one-to-one mapping of points in spacetimes between the positive (or our) universe and the negative universe. In other words, to every point in spacetime in our universe, there corresponds a unique symmetry-partner point in spacetime in the negative universe.

In addition to the inversion in the origin relationship between the spacetime dimensions of the positive and negative universes, we shall prescribe a reflection symmetry of spacetime geometry between the two universes. In other words, if we denote the spacetime manifold of the positive universe by $\mathbf{M}$ and that of the negative universe by $-\mathbf{M}^*$, then spacetime geometry at a point in spacetime in the positive universe shall be prescribed by $\mathbf{M}$ and the metric tensor $g_{\mu\nu}$ at that point, that is, by $(\mathbf{M}, g_{\mu\nu})$, while spacetime geometry shall be prescribed at the symmetry-partner point in the negative universe by $(-\mathbf{M}^*, g_{\mu\nu})$, where it must be remembered that the metric

tensor is invariant with reflections of coordinates. Symmetry of spacetime geometry between the two universes can only be prescribed at this point of development of the two-world picture.

Now Mach's principle is very fundamental. We shall make recourse to the principle here for the purpose of advancing our argument for the symmetry of state between the positive and negative universes, while knowing that the principle in itself has noting to do with Special Relativity. Essentially the Mach's principle states that the geometry of a space is determined by the distribution of mass - energy in that space [9, see p. 400]. It follows from the foregoing paragraph and Mach's principle that there is a reflection symmetry of the distribution of mass-energy in spacetimes between the two universes. Actually this is also a prescription at this point since the symmetry of spacetime geometry is a prescription.

Reflection symmetry of geometry of spacetime and of the distribution of mass-energy in spacetime also imply reflection symmetry of motions of particles and objects, natural or caused by animate object, between the two universes. In other words, corresponding to an event, natural or man-made, taking place within a local region of spacetime in our universe, there is an identical event within the symmetry-partner local region of spacetime in the negative universe. (This is the symmetry of state between the two universes). The two universes are perfectly identical in state at all times. The perfect symmetry of natural and man-made events (or perfect symmetry of state) between the two universes is a prescription at this point.

There is also a perfect symmetry of laws between the two universes, which implies that natural laws take on perfectly identical forms in the two universes. Symmetry of laws between the two universes is simply the extension of the invariance of laws found in our universe to the negative universe, which follows partly from the validity of local Lorentz invariance in the negative universe to be demonstrated shortly. The two universes could not possess symmetry of state if the laws that guide events and phenomena in them are different. The perfect symmetry of laws between the two universes shall be demonstrated with the advancement of the two-world picture.

The negative spacetime dimensions of the negative universe implies that distance in space, which is a positive scalar quantity in our (positive) universe, is a negative scalar quantity in the negative universe, and that interval of time, which is a positive quantity in the positive universe is a negative quantity in the negative universe; (it does not connote going to the past in our time dimension). This can be easily ascertained from the definition of distance, which is given in 3-space in the negative universe as, $d = \sqrt{(-x^*)^2 + (-y^*)^2 + (-z^*)^2}$. If we consider motion along the dimension $-x^*$ solely, then we must let $-y^* = -z^* = 0$, to have $d = \sqrt{(-x^*)^2} = -x^*$. Likewise the distance element of Special Relativity in the negative universe is, $ds^* = \sqrt{(-ct^*)^2 - (-x^*)^2 - (-y^*)^2 - (-z^*)^2}$. If we let $-x^* = -y^* = -z^* = 0$, for propagation in time only, then $ds^* = \sqrt{(-ct^*)^2} = -ct^*$. Interestingly the negative worldline element ($ds^* < 0$) in the negative universe is the negative root ($-ds$) of the quadratic line element ds^2, which is usually discarded since it conveys nothing to us from the point of view of experience in the positive universe.

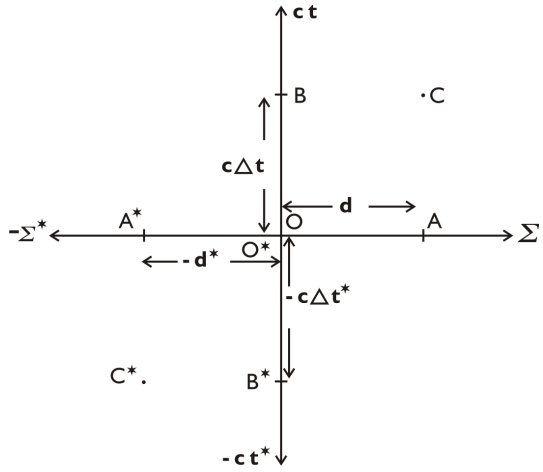

Fig. 5: Combined positive and negative Minkowski's spaces of the positive and negative universes.

4.2 Non-separation of symmetry-partner points in spacetimes in the positive and negative universes

It shall be shown here that a point in spacetime in our (or positive) universe is effectively not separated in space or in time dimension from its symmetry-partner point in spacetime in the negative universe, for every pair of symmetry-partner points in spacetimes in the two universes. Now let us consider the larger spacetime of combined positive and negative universes, Fig. 2b, which is re-illustrated as Fig. 5.

Point A* in the negative Euclidean 3-space $-\Sigma^*$ of the negative universe is the symmetry-partner to point A in the positive Euclidean 3-space Σ of the positive universe. Point B* in the negative time dimension $-ct^*$ of the negative universe is the symmetry-partner to point B in the positive time dimension ct of the positive universe. Hence points C* and C are symmetry-partner points on four-dimensional spacetimes in the two universes.

Now let points A and O in the positive 3-space Σ of the positive universe be separated by a positive distance d, say, since distances in space are positive scalar quantities in the positive universe. Then the symmetry-partner points A* and O* in the negative 3-space $-\Sigma^*$ of the negative universe are separated by negative distance $-d^*$, since distances in space are negative scalar quantities in the negative universe. Hence the distance in 3-space between point A in the positive universe and its symmetry-partner point A* in the negative universe is, $d - d^* = 0$, since d and $-d^*$ are equal in magnitude. This implies that the symmetry-partner points A and A* are effectively separated by zero distance in space with respect to

observers (or people) in the positive and negative universes.

Likewise, if the interval of positive time dimension ct between point O and point B is the positive quantity $c\Delta t$, then the interval of the negative time dimension $-ct^*$ between point O* and point B* is the negative quantity $-c\Delta t^*$, since intervals of time are negative quantities in the negative universe. Hence the interval of time dimension between point B in ct in the positive universe and its symmetry-partner point B* in $-ct^*$ in the negative universe is, $c\Delta t - c\Delta t^* = 0$. This implies that the symmetry-partner points B and B* in the time dimensions are effectively separated by zero interval of time dimension with respect to observers (or people) in the positive and negative universes. It then follows that the time t of an event in the positive universe is effectively separated by zero time interval from the time $-t^*$ of the symmetry-partner event in the negative universe. Thus an event in the positive universe and its symmetry-partner in the negative universe occur simultaneously.

It follows from the foregoing two paragraphs that symmetry-partner points C and C* in spacetimes in the positive and negative universes are not separated in space or time, and this is true for every pair of symmetry-partner points in spacetimes in the two universes. Although symmetry-partner points in spacetimes in the positive and negative universes coincide at the same point, or are not separated, they do not touch because they exist in different spacetimes.

One consequence of the foregoing is that local spacetime coordinates, $(\Sigma, ct) \equiv (x, y, z, ct)$, originating from a point O in the positive universe and the symmetry-partner local spacetime coordinates, $(-\Sigma^*, -ct^*) \equiv (-x^*, -y^*, -z^*, -ct^*)$, originating from the symmetry-partner point O* in spacetime in the negative universe can be drawn from the same point on paper, as done in Fig. 5, and geometrical construction whose predictions will conform with observation or experiment in each of the two universes can be based on this in the two-world picture, as shall be done in the rest of this section.

4.3 Introducing a flat two-dimensional intrinsic spacetime underlying the flat four-dimensional spacetime

Since it is logically required for this article to propagate beyond this point and since space limitation in this paper does not permit the presentation of its derivation, which shall be presented elsewhere, we shall present (as *ansatz*) at this point certain flat two-dimensional intrinsic spacetime with dimensions to be denoted by $\phi\rho$ and $\phi c\phi t$, where $\phi\rho$ is intrinsic space dimension (actually a one-dimensional intrinsic space) and $\phi c\phi t$ is intrinsic time dimension, which underlies the flat four-dimensional spacetime (the Minkowski space) of the Special Relativity, usually denoted by (x^0, x^1, x^2, x^3); $x^0 = ct$, but which shall be denoted by (Σ, ct) in this article for convenience, where Σ is the Euclidean 3-space with dimensions x^1, x^2 and x^3.

Every particle or object with a three-dimensional inertial mass m in the Euclidean 3-space Σ has its one-dimensional intrinsic mass to be denoted by ϕm underlying it in the one-dimensional intrinsic space $\phi\rho$. The one-dimensional intrinsic space $\phi\rho$ underlying the Euclidean 3-space Σ is an isotropic dimension with no unique orientation in Σ. This means that $\phi\rho$ can be considered to be orientated along any direction in Σ. The straight line intrinsic time dimension $\phi c\phi t$ likewise lies parallel to the straight line time dimension ct along the vertical in the graphical presentation of the flat spacetime of SR of Fig. 2 or Fig. 5.

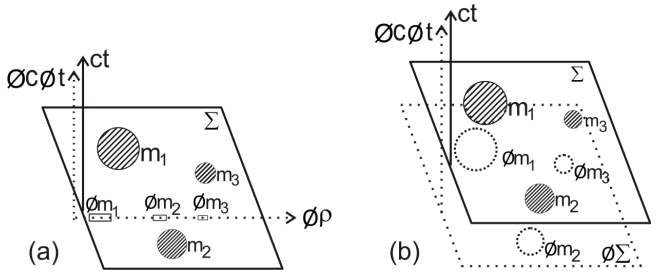

Fig. 6: a) The flat 4-dimensional spacetime and its underlying flat 2-dimensional intrinsic spacetime with the inertial masses of three objects scattered in the Euclidean 3-space and their one-dimensional intrinsic inertial masses aligned along the isotropic one-dimensional intrinsic space with respect to observers in spacetime. b) The flat 2-dimensional intrinsic spacetime with respect to observers in spacetime in a is a flat four-dimensional intrinsic spacetime containing 3-dimensional intrinsic inertial masses of particles and objects in 3-dimensional intrinsic space with respect to intrinsic-mass-observers in intrinsic spacetime.

If we temporarily consider the Euclidean 3-space Σ as an hyper-surface, $t = const$, represented by a plane-surface along the horizontal (instead of a line along the horizontal as in the previous diagrams) and the time dimension ct as a vertical normal line to the hyper-surface, then the graphical representation of the flat four-dimensional spacetime (Σ, ct) and its underlying flat two-dimensional intrinsic spacetime $(\phi\rho, \phi c\phi t)$ in the context of SR described in the foregoing paragraph is depicted in Fig. 6a.

Figure 6a is valid with respect to observers in the flat physical four-dimensional spacetime (Σ, ct). The one-dimensional intrinsic masses of all particles and objects are aligned along the singular isotropic one-dimensional intrinsic space $\phi\rho$, whose inertial masses are scattered arbitrarily in the physical Euclidean 3-space Σ with respect to these observers, in (Σ, ct), as illustrated for three such particles and objects in Fig. 6a.

On the other hand, the intrinsic space is actually a flat three-dimensional domain to be denoted by $\phi\Sigma$, with mutually orthogonal dimensions $\phi x^1, \phi x^2$ and ϕx^3, at leat in the small, with respect to intrinsic-mass-observers in $\phi\Sigma$. The intrinsic masses ϕm of particles and objects are likewise three-dimensional with respect to the intrinsic-mass-observers in $\phi\Sigma$. The intrinsic mass ϕm of a particle or object in the intrinsic space $\phi\Sigma$ lies directly underneath the inertial mass m

of the particle or object in the physical Euclidean 3-space Σ, as illustrated for three such particles or objects in Fig. 6b.

The flat four-dimensional physical spacetime (Σ, ct) containing the three-dimensional inertial masses m of particles and objects in the Euclidean 3-space Σ is the outward manifestation of the flat four-dimensional intrinsic spacetime $(\phi\Sigma, \phi c\phi t)$ containing the three-dimensional intrinsic masses ϕm of the particles and objects in $\phi\Sigma$ in Fig. 6b. It is due to the fact that the flat three-dimensional intrinsic space $\phi\Sigma$ is an isotropic space, that is, all directions in $\phi\Sigma$ are the same, with respect to observers in the physical Euclidean 3-space Σ that the dimensions ϕx^1, ϕx^2 and ϕx^3 of $\phi\Sigma$, which are mutually orthogonal, at least locally, with respect to the intrinsic-mass-observers in $\phi\Sigma$, are effectively directed along the same non-unique direction in $\phi\Sigma$, thereby effectively constituting a singular one-dimensional intrinsic space (or an intrinsic space dimension) $\phi\rho$ with no unique orientation in $\phi\Sigma$ and consequently with no unique orientation in the physical Euclidean 3-space Σ overlying $\phi\Sigma$ with respect to observers on the flat spacetime (Σ, ct), as illustrated in Fig. 6a.

As follows from the foregoing paragraph, Fig. 6a is the correct diagram with respect to observers in spacetime (Σ, ct). It is still valid to say that the flat four-dimensional spacetime (Σ, ct) is the outward (or physical) manifestation of the flat two-dimensional intrinsic spacetime $(\phi\rho, \phi c\phi t)$ and that three-dimensional inertial mass m in Σ is the outward (or physical) manifestation of one-dimensional intrinsic mass ϕm with respect to observers in (Σ, ct) in Fig. 6a. Observers on the flat four-dimensional spacetime (Σ, ct) must formulate intrinsic physics in intrinsic spacetime as two-dimensional intrinsic theories on flat intrinsic spacetime $(\phi\rho, \phi c\phi t)$.

It is for convenience that the three-dimensional Euclidean space Σ shall be represented by a line along the horizontal as done in Figs. 2a and 2b and Fig. 5 and as shall be done in the rest of this article, instead of a plane surface along the horizontal in Figs. 6a and 6b. Thus the flat four-dimensional spacetime and its underlying flat two-dimensional intrinsic spacetime shall be presented graphically in the two-world picture as Fig. 7. The origins O and O* are not actually separated contrary to their separation in Fig. 7.

Figure 7 is Fig. 5 modified by incorporating the flat two-dimensional intrinsic spacetimes underlying the flat four-dimensional spacetimes of the positive and negative universes into Fig. 5. Figure 7 is a fuller diagram than Fig. 5. As mentioned earlier, the intrinsic spacetime and intrinsic parameters in it along with their properties and notations shall be derived elsewhere.

The intrinsic spacetime dimensions $\phi\rho$ and $\phi c\phi t$ and one-dimensional intrinsic masses ϕm of particles and objects in the intrinsic space $\phi\rho$ are hidden (or non-observable) to observers on the flat four-dimensional spacetime (Σ, ct). The symbol ϕ attached to the intrinsic dimensions, intrinsic coordinates and intrinsic masses is used to indicate their intrinsic (or hidden) natures with respect to observers in spacetime.

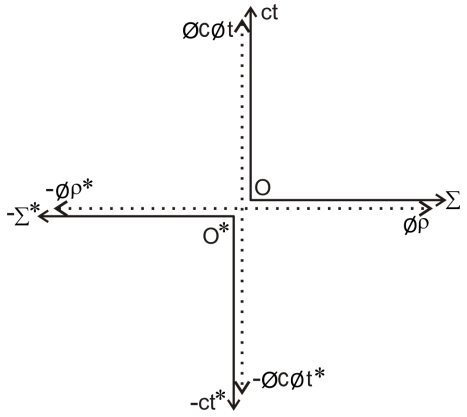

Fig. 7: Combined flat four-dimensional spacetimes and combined underlying flat two-dimensional intrinsic spacetimes of the positive and negative universes.

When the symbol ϕ is removed from the flat two-dimensional intrinsic spacetime $(\phi\rho, \phi c\phi t)$ we obtain the observed flat four-dimensional spacetime (Σ, ct) and when ϕ is removed from the one-dimensional intrinsic mass ϕm in $\phi\rho$ we obtain the observed three-dimensional inertial mass m in the Euclidean 3-space Σ.

As the inertial mass m moves at velocity $\vec{v}$ in the Euclidean 3-space Σ of the flat four-dimensional spacetime (Σ, ct) relative to an observer in (Σ, ct), the intrinsic mass ϕm performs intrinsic motion at intrinsic speed ϕv in the one-dimensional intrinsic space $\phi\rho$ of the flat two-dimensional intrinsic spacetime $(\phi\rho, \phi c\phi t)$ relative to the observer in (Σ, ct), where $|\phi v| = |\vec{v}|$. The inertial mass m of a particle in Σ and its intrinsic mass ϕm in $\phi\rho$ are together always in their respective spaces, irrespective of whether m is in motion or at rest relative to the observer.

Finally in the *ansatz* being presented in this sub-section, the intrinsic motion of the intrinsic rest mass ϕm_0 of a particle at intrinsic speed ϕv in an intrinsic particle's frame $(\phi\tilde{x}', \phi c\phi\tilde{t}')$ relative to the observer's intrinsic frame $(\phi\tilde{x}, \phi c\phi\tilde{t})$ on flat two-dimensional intrinsic spacetime $(\phi\rho, \phi c\phi t)$ pertains to two-dimensional intrinsic Special Theory of Relativity to be denoted by ϕSR, while the corresponding motion of the rest mass m_0 of the particle at velocity $\vec{v}$ in the particle's frame $(\tilde{x}', \tilde{y}', \tilde{z}', c\tilde{t}')$ relative to the observer's frame $(\tilde{x}, \tilde{y}, \tilde{z}, c\tilde{t})$ on the flat four-dimensional spacetime (Σ, ct), pertains to the Special Theory of Relativity (SR) as usual. The SR on flat four-dimensional spacetime (Σ, ct) is mere outward manifestation of ϕSR on the underlying flat two-dimensional intrinsic spacetime $(\phi\rho, \phi c\phi t)$.

The intrinsic motion at intrinsic speed ϕv of the intrinsic rest mass ϕm_0 of a particle in the particle's intrinsic frame $(\phi\tilde{x}', \phi c\phi\tilde{t}')$ relative to the observer's intrinsic frame $(\phi\tilde{x}, \phi c\phi\tilde{t})$, gives rise to rotation of the intrinsic coordinates $\phi\tilde{x}'$ and $\phi c\phi\tilde{t}'$ relative to the intrinsic coordinates $\phi\tilde{x}$ and $\phi c\phi\tilde{t}$ on the vertical intrinsic spacetime plane (which are on the $(\phi\rho, \phi c\phi t)$-plane) in Fig. 7. It must be observed that rotation

of the intrinsic coordinate $\phi\tilde{x}'$ can take place on the vertical intrinsic spacetime plane only in Fig. 6a or Fig. 7.

Two-dimensional intrinsic spacetime diagram and its inverse must be drawn on the vertical $(\phi\rho, \phi c\phi t)$-plane in the two-world picture and intrinsic Lorentz transformation (ϕLT) and its inverse derived from them in the context of ϕSR. The intrinsic Lorentz invariance (ϕLI) on the flat two-dimensional intrinsic spacetime must be validated and every result in the context of the two-dimensional intrinsic Special Theory of Relativity (ϕSR), each of which has its counterpart in SR, must be derived from the ϕLT and its inverse in the manner the results of SR are derived from the LT and its inverse.

Once ϕSR has been formulated as described above, then SR being mere outward (or physical) manifestation on the flat four-dimensional spacetime (Σ, ct) of ϕSR on the flat two-dimensional intrinsic spacetime $(\phi\rho, \phi c\phi t)$, the results of SR namely, the LT and its inverse, the Lorentz invariance (LI) on the flat four-dimensional spacetime and every other results of SR can be written directly from the corresponding results of ϕSR, without having to draw spacetime diagrams involving the rotation of the coordinates $(\tilde{x}', \tilde{y}', \tilde{z}', c\tilde{t}')$ of the primed frame relative to the coordinates $(\tilde{x}, \tilde{y}, \tilde{z}, c\tilde{t})$ of the unprimed frame on the flat four-dimensional spacetime (Σ, ct) in the context of SR. This procedure shall be demonstrated in the next sub-section.

4.4 New spacetime/intrinsic spacetime diagrams for derivation of Lorentz transformation/intrinsic Lorentz transformation in the two-world picture

Consider two frames of reference with extended unprimed straight line affine coordinates $\tilde{x}, \tilde{y}, \tilde{z}, c\tilde{t}$ and extended primed straight line affine coordinates $\tilde{x}', \tilde{y}', \tilde{z}', c\tilde{t}'$ respectively on the flat metric four-dimensional spacetime (Σ, ct). Let a three-dimensional observer (or a 3-observer), Peter, say, be located in 3-space of the unprimed frame and another 3-observer, Paul, say, be located in 3-space of the primed frame.

Corresponding to the 3-dimensional observer Peter in the 3-space of the unprimed frame, there is the one-dimensional observer (or 1-observer) in the time dimension of the unprimed frame to be denoted by $\tilde{\text{P}}$eter. Likewise corresponding to the 3-observer Paul in 3-space of the primed frame is the one-dimensional observer (or 1-observer) $\tilde{\text{P}}$aul in the time dimension of the primed frame. Thus there is the 4-observer (Peter, $\tilde{\text{P}}$eter) in the unprimed frame $(\tilde{x}, \tilde{y}, \tilde{z}, c\tilde{t})$ and the 4-observer (Paul, $\tilde{\text{P}}$aul) in the primed frame $(\tilde{x}', \tilde{y}', \tilde{z}', c\tilde{t}')$ in the positive universe. There is the symmetry-partner 4-observer (Peter*, $\tilde{\text{P}}$eter*) in the symmetry-partner unprimed frame $(-\tilde{x}^*, -\tilde{y}^*, -\tilde{z}^*, -c\tilde{t}^*)$ and symmetry-partner 4-observer (Paul*, $\tilde{\text{P}}$aul*) in the symmetry-partner primed frame $(-\tilde{x}'^*, -\tilde{y}'^*, -\tilde{z}'^*, -c\tilde{t}'^*)$ in the negative universe.

Before proceeding further, let us shine some light on the concepts of metric spacetime and affine spacetime that have been introduced in the preceding two paragraphs. As well known, the metric spacetime (Σ, ct) is the physical four-dimensional spacetime, which is flat with constant Lorentzian metric tensor in the context of SR (and is postulated to be curved with Riemannian metric tensor in the context of the General Theory of Relativity, GR). The matter (or mass) of particles and objects are contained in the metric 3-space Σ (with Euclidean metric tensor in the context of SR). Thus particles and objects exist and move in the four-dimensional metric spacetime in the theories of relativity. The coordinates or dimensions of the metric spacetime shall be denoted by x, y, z and ct without label (in the Cartesian system of coordinates of 3-space) in this article.

On the other hand, the coordinates of an affine spacetime shall be differentiated from those of a metric spacetime by an over-head tilde label as $\tilde{x}$, $\tilde{y}$, $\tilde{z}$ and $c\tilde{t}$. These are mere mathematical entities without physical (or metrical) quality used to identify the positions and to track the motion of material points relative to a specified origin in a metric spacetime. The affine coordinates $\tilde{x}$, $\tilde{y}$, $\tilde{z}$ and $c\tilde{t}$ are straight line coordinates that can be of any extensions in the flat metric spacetime of SR. Just as it is said that "the path of a fish in water cannot be known", so is the path (i.e. the locus of the affine coordinates) of a material point through a metric spacetime non-discernible or without metrical quality. An affine spacetime can be described as mere mathematical scaffolding without physical (or metrical) significance for identifying possible positions of material particles in the metric spacetime. The extended three-dimensional affine space constituted by the affine coordinates $\tilde{x}$, $\tilde{y}$ and $\tilde{z}$ cannot hold matter (or mass of particles and objects).

Now corresponding to the unprimed frame $(\tilde{x}, \tilde{y}, \tilde{z}, c\tilde{t})$ of the 4-observer (Peter, $\tilde{\text{P}}$eter) prescribed on the flat four-dimensional metric spacetime (Σ, ct) earlier, is the unprimed intrinsic frame $(\phi\tilde{x}, \phi c\phi\tilde{t})$ of intrinsic 2-observer (ϕPeter, $\phi\tilde{\text{P}}$eter) in the two-dimensional metric intrinsic spacetime $(\phi\rho, \phi c\phi t)$ underlying (Σ, ct) in the first quadrant in Fig. 7 and corresponding to the primed frame $(\tilde{x}', \tilde{y}', \tilde{z}', c\tilde{t}')$ of the 4-observer (Paul, $\tilde{\text{P}}$aul) prescribed in the metric spacetime (Σ, ct) is the primed intrinsic frame $(\phi\tilde{x}', \phi c\phi\tilde{t}')$ of intrinsic 2-observer (ϕPaul, $\phi\tilde{\text{P}}$aul) in the two-dimensional metric intrinsic spacetime $(\phi\rho, \phi c\phi t)$ underlying (Σ, ct) in Fig. 7. The intrinsic coordinates $\phi\tilde{x}$ and $\phi c\phi\tilde{t}$ of the unprimed intrinsic frame in $(\phi\rho, \phi c\phi t)$ are extended straight line affine intrinsic coordinates like the coordinates $\tilde{x}, \tilde{y}, \tilde{x}$ and $c\tilde{t}$ of the unprimed frame in (Σ, ct). The intrinsic coordinates $\phi\tilde{x}'$ and $\phi c\phi\tilde{t}'$ of the primed intrinsic frame in $(\phi\rho, \phi c\phi t)$ are likewise extended straight line affine intrinsic coordinates like the coordinates $\tilde{x}', \tilde{y}', \tilde{x}'$ and $c\tilde{t}'$ of the primed frame in (Σ, ct).

The summary of all of the foregoing is that we have prescribed a pair of frames with extended straight line affine coordinates namely, $(\tilde{x}, \tilde{y}, \tilde{z}, c\tilde{t})$ of 4-observer (Peter, $\tilde{\text{P}}$eter) and $(\tilde{x}', \tilde{y}', \tilde{z}', c\tilde{t}')$ of 4-observer (Paul, $\tilde{\text{P}}$aul) on the flat four-dimensional metric spacetime (Σ, ct) and underlying pair of intrinsic frames with extended straight line affine intrinsic co-

ordinates namely, $(\phi\tilde{x}, \phi c\phi\tilde{t})$ of intrinsic 2-observer (ϕPeter, $\phi\tilde{\text{P}}$eter) and $(\phi\tilde{x}', \phi c\phi\tilde{t}')$ of intrinsic 2-observer (ϕPaul, $\phi\tilde{\text{P}}$aul) on the flat two-dimensional metric intrinsic spacetime $(\phi\rho, \phi c\phi t)$ that underlies (Σ, ct) in the first quadrant (or in our universe) in Fig. 7.

The perfect symmetry of state between the positive and negative universes requires that there are identical symmetry-partner pair of frames with extended straight line affine coordinates $(-\tilde{x}^*, -\tilde{y}^*, -\tilde{z}^*, -c\tilde{t}^*)$ of symmetry-partner 4-observer (Peter*, $\tilde{\text{P}}$eter*) and $(-\tilde{x}'^*, -\tilde{y}'^*, -\tilde{z}'^*, -c\tilde{t}'^*)$ of symmetry-partner 4-observer (Paul*, $\tilde{\text{P}}$aul*) on the flat four-dimensional metric spacetime $(-\Sigma^*, -ct^*)$ and underlying pair of intrinsic frames with extended straight line affine intrinsic coordinates namely, $(-\phi\tilde{x}^*, -\phi c\phi\tilde{t}^*)$ of intrinsic 2-observer (ϕPeter*, $\phi\tilde{\text{P}}$eter*) and $(-\phi\tilde{x}'^*, -\phi c\phi\tilde{t}'^*)$ of intrinsic 2-observer (ϕPaul*, $\phi\tilde{\text{P}}$aul*) on the flat two-dimensional metric intrinsic spacetime $(-\phi\rho^*, -\phi c\phi t^*)$ that underlies $(-\Sigma^*, -ct^*)$ in the third quadrant (or in negative universe) in Fig. 7.

As done at the beginning of section 2, let us consider the propagation at a constant speed v of the rest mass m_0 of a particle along the coordinate $\tilde{x}'$ of the particle (or primed) frame $(\tilde{x}', \tilde{y}', \tilde{z}', c\tilde{t}')$ relative to the 3-observer Peter in the 3-space $\tilde{\Sigma}(\tilde{x}, \tilde{y}, \tilde{z})$ of the observer's frame $(\tilde{x}, \tilde{y}, \tilde{z}, c\tilde{t})$ in the positive universe (or our universe), where the coordinates $\tilde{x}'$ and $\tilde{x}$ shall be taken to be collinear. Correspondingly, the intrinsic rest mass ϕm_0 of the particle is in intrinsic motion at intrinsic speed ϕv along the intrinsic coordinate $\phi\tilde{x}'$ of the particle's intrinsic frame (or the primed intrinsic frame) $(\phi\tilde{x}', \phi c\phi\tilde{t}')$ relative to the intrinsic observer's frame $(\phi\tilde{x}, \phi c\phi\tilde{t})$ with respect to the intrinsic 1-observer ϕPeter in the one-dimensional intrinsic space $(\phi\tilde{x})$ of the observer's frame and hence with respect to the 3-observer Peter in $\tilde{\Sigma}(\tilde{x}, \tilde{y}, \tilde{z})$ overlying $\phi\tilde{x}$, where the intrinsic coordinates $\phi\tilde{x}'$ and $\phi\tilde{x}$ are necessarily collinear since they are affine intrinsic coordinates in the singular isotropic one-dimensional metric intrinsic space $\phi\rho$.

The intrinsic motion at intrinsic speed ϕv of the intrinsic rest mass ϕm_0 of the particle along the intrinsic coordinate $\phi\tilde{x}'$ of the particle's intrinsic frame $(\phi\tilde{x}', \phi c\phi\tilde{t}')$ relative to the observer's intrinsic frame $(\phi\tilde{x}, \phi c\phi\tilde{t})$ described in the foregoing paragraph, will cause the anti-clockwise rotation of the extended straight line affine intrinsic coordinates $\phi\tilde{x}'$ and $\phi c\phi\tilde{t}'$ of the primed intrinsic frame at equal intrinsic angle $\phi\psi$ relative to the extended straight line affine intrinsic coordinates $\phi\tilde{x}$ and $\phi c\phi\tilde{t}$ respectively of the unprimed intrinsic frame.

The perfect symmetry of state between the positive and negative universes discussed earlier, implies that the rest mass of the symmetry-partner particle (its sign is yet to be determined), is in simultaneous motion at constant speed v along the coordinate $-\tilde{x}'^*$ of the particle's frame $(-\tilde{x}'^*, -\tilde{y}'^*, -\tilde{z}'^*, -c\tilde{t}'^*)$ relative to the symmetry-partner 3-observer* Peter* in the 3-space $-\tilde{\Sigma}^*(-\tilde{x}^*, -\tilde{y}^*, -\tilde{z}^*)$ of the observer's frame $(-\tilde{x}^*, -\tilde{y}^*, -\tilde{z}^*, -c\tilde{t}^*)$ in the negative universe. Correspondingly, the intrinsic rest mass of the symmetry-partner particle is in intrinsic motion at constant intrinsic speed ϕv along the intrinsic coordinate $-\phi\tilde{x}'^*$ of the particle's intrinsic frame $(-\phi\tilde{x}'^*, -\phi c\phi\tilde{t}'^*)$ relative to the intrinsic observer's frame $(-\phi\tilde{x}^*, -\phi c\phi\tilde{t}^*)$, with respect to the intrinsic 1-observer* ϕPeter* in the intrinsic space $-\phi\tilde{x}^*$ of the intrinsic observer's frame and consequently with respect to the 3-observer* Peter* in the 3-space $-\tilde{\Sigma}^*(-\tilde{x}^*, -\tilde{y}^*, -\tilde{z}^*)$ of the observer's frame overlying $-\phi\tilde{x}^*$ in the negative universe. Consequently the extended affine intrinsic coordinates $-\phi\tilde{x}'^*$ and $-\phi c\phi\tilde{t}'^*$ of the particle's frame will be rotated anti-clockwise at equal intrinsic angle $\phi\psi$ relative to the extended straight line affine intrinsic coordinates $-\phi\tilde{x}^*$ and $-\phi c\phi\tilde{t}^*$ respectively of the observer's intrinsic frame.

Now on the larger spacetime/intrinsic spacetime of combined positive universe and negative universe depicted in Fig. 7, the extended straight line affine intrinsic time coordinate $\phi c\phi\tilde{t}'$ of the primed intrinsic frame in the first quadrant can rotate into the second quadrant with respect to the 3-observer (Peter) in the 3-space $\tilde{\Sigma}(\tilde{x}, \tilde{y}, \tilde{z})$ along the horizontal in the first quadrant in Fig. 7. This is so since the intrinsic angle $\phi\psi$ has values in the negative half-plane in Fig. 1b, which correspond to the second and third quadrants in Fig. 7. Similarly the extended straight line affine intrinsic time coordinate $-\phi c\phi\tilde{t}'^*$ of the primed intrinsic frame in the third quadrant can rotate into the fourth quadrant with respect to 3-observer* (Peter*) in the 3-space $-\tilde{\Sigma}^*$ along the horizontal in the third quadrant, since $\phi\psi$ has value in the positive half-plane in Fig. 1b, which corresponds to the fourth and first quadrants in Fig. 7, with respect to 3-observers* in $-\Sigma^*$ along the horizontal in the third quadrant in Fig.7. Thus the rotation of the intrinsic coordinates $\phi\tilde{x}'$ and $\phi c\phi\tilde{t}'$ relative to $\phi\tilde{x}$ and $\phi c\phi\tilde{t}$ respectively in Fig. 8a is possible (or will ensue) in the two-world picture.

The intrinsic coordinate $\phi\tilde{x}$ is the projection along the horizontal of the inclined $\phi\tilde{x}'$ in Fig. 8a. That is, $\phi\tilde{x} = \phi\tilde{x}' \cos\phi\psi$. Hence we can write,

$$\phi\tilde{x}' = \phi\tilde{x} \sec\phi\psi \,.$$

This transformation of affine intrinsic space coordinates is all that should have been possible with respect to the intrinsic 1-observer ϕPeter in the intrinsic space $\phi\tilde{x}$ of the intrinsic observer's frame along the horizontal and consequently with respect to 3-observer (Peter) in the 3-space $\tilde{\Sigma}(\tilde{x}, \tilde{y}, \tilde{z})$ of the observer's frame from Fig. 8a, but for the fact that the negative intrinsic time coordinate $-\phi c\phi\tilde{t}'^*$ of the negative universe rotated into the fourth quadrant also projects component $-\phi c\phi\tilde{t}' \sin\phi\psi$ along the horizontal, which must be added to the right-hand side of the last displayed equation yielding,

$$\phi\tilde{x}' = \phi\tilde{x} \sec\phi\psi - \phi c\phi\tilde{t}' \sin\phi\psi \,.$$

The dummy star label used to differentiate the coordinates and parameters of the negative universe from those of the positive universe has been removed from the component $-\phi c\phi t'^* \sin\phi\psi$ projected along the horizontal by the coordi-

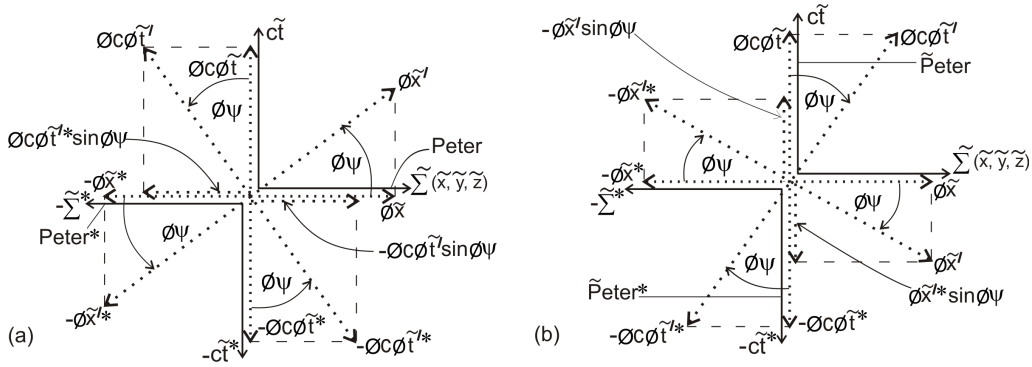

Fig. 8: a) The diagram used to derive partial intrinsic Lorentz transformations / partial Lorentz transformations with respect to 3-observers in the 3-spaces in the positive and negative universes. b) The complementary diagram to a used to derive partial intrinsic Lorentz transformations / partial Lorentz transformations with respect to 1-observers in the time dimensions in the positive and negative universes.

nate $-\phi c\,\phi\tilde{t}'^{*}$ of the negative universe rotated into the fourth quadrant in Fig. 8a, since the projected component is now an intrinsic coordinate in the positive universe.

But the intrinsic coordinates $\phi c\,\phi\tilde{t}$ and $\phi c\phi\tilde{t}'$ are also related as, $\phi c\,\phi\tilde{t} = \phi c\,\phi\tilde{t}'\cos\phi\psi$ hence $\phi c\phi\tilde{t}' = \phi c\,\phi\tilde{t}\sec\phi\psi$, along the vertical in the same Fig. 8a. By replacing $\phi c\phi\tilde{t}'$ by $\phi c\,\phi\tilde{t}\sec\phi\psi$ in the last displayed equation we have

$$\phi\tilde{x}' = \phi\tilde{x}\sec\phi\psi - \phi c\phi\tilde{t}\tan\phi\psi \qquad (11)$$

(w.r.t. 3-observer Peter in $\tilde{\Sigma}$).

Likewise the affine intrinsic time coordinate $\phi c\phi\tilde{t}$ is the projection along the vertical of the inclined affine intrinsic coordinate $\phi c\,\phi\tilde{t}'$ in Fig. 8b. Hence $\phi c\,\phi\tilde{t} = \phi c\phi\tilde{t}'\cos\phi\psi$ or

$$\phi c\,\phi\tilde{t}' = \phi c\,\phi\tilde{t}\sec\phi\psi\,.$$

This affine intrinsic time coordinate transformation is all that should have been possible with respect to the 1-observer P̃eter in the time dimension $c\tilde{t}$ of the observer's frame from Fig. 8b, but for the fact that the inclined negative intrinsic space coordinate $-\phi\tilde{x}'^{*}$ of the negative universe rotated into the second quadrant also projects component $-\phi\tilde{x}'\sin\phi\psi$ along the vertical, which must be added to the right-hand side of the last displayed equation yielding,

$$\phi c\,\phi\tilde{t}' = \phi c\,\phi\tilde{t}\sec\phi\psi - \phi\tilde{x}'\sin\phi\psi\,.$$

The dummy star label has again been removed from the component $-\phi\tilde{x}'^{*}\sin\phi\psi$ projected along the vertical in the second quadrant by the inclined intrinsic coordinate $-\phi\tilde{x}'^{*}$ of the negative universe rotated into the second quadrant, since the projected component is now an intrinsic coordinate in the positive universe.

But the intrinsic coordinate $\phi\tilde{x}$ is related to $\phi\tilde{x}'$ along the horizontal in the same Fig. 8b as, $\phi\tilde{x} = \phi\tilde{x}'\cos\phi\psi$ or $\phi\tilde{x}' = \phi\tilde{x}\sec\phi\psi$ along the horizontal in Fig. 8b. Then by replacing $\phi\tilde{x}'$ by $\phi\tilde{x}\sec\phi\psi$ in the last displayed equation we have

$$\phi c\,\phi\tilde{t}' = \phi c\tilde{t}\sec\phi\psi - \phi\tilde{x}\tan\phi\psi \qquad (12)$$

(w.r.t. 1-observer P̃eter in $c\tilde{t}$).

The concept of 1-observer in the time dimension added to 3-observer in 3-space to have 4-observer in four-dimensional spacetime introduced above is in agreement with the known four-dimensionality of particles and bodies in 4-geometry of relativity. Anti-clockwise (or positive) rotation of the intrinsic space coordinate $\phi\tilde{x}'$ by intrinsic angle $\phi\psi$ towards the intrinsic time coordinate $\phi c\,\phi\tilde{t}$ along the vertical with respect to the 3-observer (Peter) in the 3-space $\tilde{\Sigma}(\tilde{x},\tilde{y},\tilde{z})$ of the observer's frame in Fig. 8a, corresponds to clockwise (or positive) rotation of the intrinsic time coordinate $\phi c\,\phi\tilde{t}'$ by equal intrinsic angle $\phi\psi$ towards the intrinsic space coordinate $\phi\tilde{x}$ along the horizontal with respect to the 1-observer (P̃eter) in the time dimension $c\tilde{t}$ of the observer's frame in Fig. 8b. The explanation of the fact that anti-clockwise rotation of the primed intrinsic spacetime coordinates relative to unprimed intrinsic spacetime coordinates is positive rotation with respect to 3-observers in 3-spaces in Fig. 8a, while clockwise rotation of primed intrinsic spacetime coordinates relative to unprimed intrinsic spacetime coordinates is positive rotation with respect to 1-observers in the time dimensions in Fig. 8b, requires further development of the two-world picture than in this paper. It shall be presented elsewhere.

The partial intrinsic Lorentz transformation of affine intrinsic space coordinates (11) with respect to the 3-observer Peter in the 3-space $\tilde{\Sigma}(\tilde{x},\,\tilde{y},\,\tilde{z})$ of the observer's frame and the partial intrinsic Lorentz transformation of affine intrinsic time coordinates (12) with respect to the 1-observer P̃eter in the time dimension $c\tilde{t}$ of the observer's frame must be collected to obtain the intrinsic Lorentz transformation of extended straight line affine intrinsic spacetime coordinates with respect to 4-observers (Peter, P̃eter) in the observer's frame as follows:

$$\left.\begin{array}{c} \phi c\,\phi\tilde{t}' = \phi c\,\phi\tilde{t}\sec\phi\psi - \phi\tilde{x}\tan\phi\psi \\ \text{(w.r.t. 1-observer P̃eter in } c\tilde{t}) \\ \phi\tilde{x}' = \phi\tilde{x}\sec\phi\psi - \phi c\phi\tilde{t}\tan\phi\psi \\ \text{(w.r.t. 3-observer Peter in } \tilde{\Sigma}) \end{array}\right\}, \qquad (13)$$

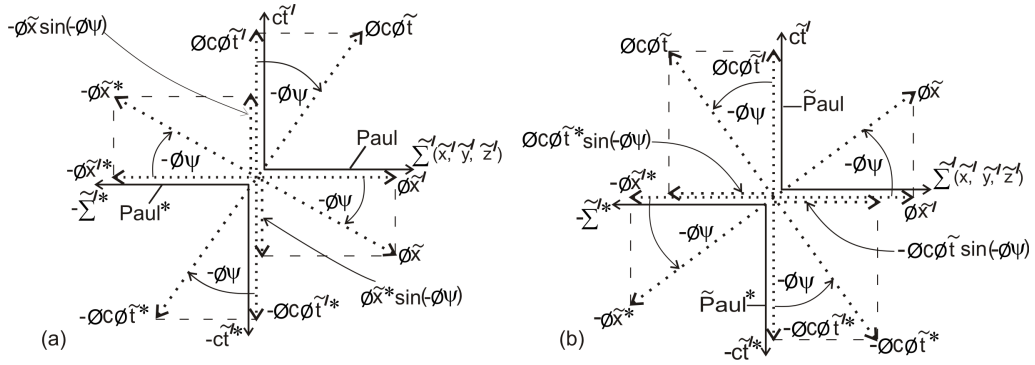

Fig. 9: The inverse diagrams to Figures 8a and 8b respectively, used to derive inverse intrinsic Lorentz transformations / inverse Lorentz transformations in the positive and negative universes.

where $-\frac{\pi}{2} < \phi\psi < \frac{\pi}{2}$ (temporarily).

The range $-\frac{\pi}{2} < \phi\psi < \frac{\pi}{2}$ of the intrinsic angles $\phi\psi$ in system (13) in the positive universe is temporary as indicated. This temporary range shall be modified later in this section. The fact that the intrinsic angle $\phi\psi$ can have values in the range $[0, \frac{\pi}{2})$ in the first quadrant in Figs. 8a and 8b in the two-world picture, instead of the range $[0, \frac{\pi}{4})$ of the angle ϕ in the Minkowski diagrams, (Figs. 3a and 3b in the one-world picture), is due to the non-existence of light-cones in the two-world picture, as shall be established shortly.

In order to obtain the inverses of equations (11) and (12) and hence the inverse to system (13), let us draw the inverses of Figs. 8a and 8b. The inverse to Fig. 8a obtained by rotating all intrinsic coordinates clockwise by negative intrinsic angle $-\phi\psi$ with respect to 3-observer in the 3-spaces $\tilde{\Sigma}$ and $-\tilde{\Sigma}^*$ in Fig. 8a is depicted in Fig. 9a and the the inverse to Fig. 8b obtained by rotating all intrinsic coordinates anti-clockwise by negative intrinsic angle $-\phi\psi$ with respect to 1-observer in the time dimensions $c\tilde{t}$ and $-c\tilde{t}^*$ in Fig. 8b is depicted in Fig. 9b.

The clockwise sense of negative rotation (i.e. by negative intrinsic angle) of intrinsic coordinates in Fig. 9a is valid with respect to the 3-observer (Paul) in the 3-space $\tilde{\Sigma}'$ of the primed (or particle's) frame with respect to whom positive rotation is anti-clockwise. Hence the transformation of intrinsic coordinates derived from Fig. 9a is valid with respect to the 3-observer (Paul) in $\tilde{\Sigma}'$. On the other hand, the anti-clockwise sense of negative rotation of intrinsic coordinates in Fig. 9b is valid relative to the 1-observer ($\tilde{\text{P}}$aul) in the time dimension $c\tilde{t}'$, with respect to whom positive rotation is clockwise. Hence the intrinsic coordinate transformation derived from Fig. 9b is valid relative to the 1-observer (Paul) in $c\tilde{t}'$.

Again the affine intrinsic time coordinate $\phi c\phi\tilde{t}'$ is the projection along the vertical of the inclined $\phi c\phi\tilde{t}$ in Fig. 9a. That is, $\phi c\phi\tilde{t}' = \phi c\,\phi\tilde{t}\cos(-\phi\psi) = \phi c\phi\tilde{t}\cos\phi\psi$. Hence we can write,

$$\phi c\,\phi\tilde{t} = \phi c\,\phi\tilde{t}'\sec\phi\psi\,.$$

This transformation of affine intrinsic time coordinates is all that should have been possible along the vertical in Fig. 9a by the 3-observer (Paul) in $\tilde{\Sigma}'$ of the particle's frame, but for the fact that the unprimed negative intrinsic space coordinate $-\phi\tilde{x}^*$ of the negative universe rotated into the second quadrant projects component, $-\phi\tilde{x}\sin(-\phi\psi) = \phi\tilde{x}\sin\phi\psi$, along the vertical, which must be added to the right-hand side of the last displayed equation to have as follows:

$$\phi c\,\phi\tilde{t} = \phi c\,\phi\tilde{t}'\sec\phi\psi + \tilde{x}\sin\phi\psi\,.$$

The dummy star label has again been removed from the component $-\phi\tilde{x}^*\sin(-\phi\psi)$ projected along the vertical in the second quadrant by the negative intrinsic space coordinate $-\phi\tilde{x}^*$ of the negative universe rotated into the second quadrant in Fig. 9a, since the projected component is now an intrinsic coordinate in the positive universe.

But $\phi\tilde{x}$ and $\phi\tilde{x}'$ are related as $\phi\tilde{x}\cos(-\phi\psi) = \phi\tilde{x}'$ hence, $\phi\tilde{x} = \phi\tilde{x}'\sec\phi\psi$, along the horizontal in the same Fig. 9a. By using this in the last displayed equation we have

$$\phi c\,\phi\tilde{t} = \phi c\phi\tilde{t}'\sec\phi\psi + \phi\tilde{x}'\tan\phi\psi \qquad (14)$$

(w.r.t. 3-observer Paul in $\tilde{\Sigma}'$).

Likewise the affine intrinsic space coordinate $\phi\tilde{x}$ is related to $\phi\tilde{x}'$ and the component $-\phi c\phi\tilde{t}\sin(-\phi\psi)$ projected along the horizontal with respect to the 1-observer $\tilde{\text{P}}$aul in the time dimension $c\tilde{t}'$ of the particle's frame in Fig. 9b as

$$\phi\tilde{x} = \tilde{x}'\sec\phi\psi + \phi c\,\phi\tilde{t}\sin\phi\psi\,.$$

Then by using the relation, $\phi c\,\phi\tilde{t} = \phi c\phi\tilde{t}'\sec\phi\psi$, which also holds along the vertical in the same Fig. 9b in the last displayed equation, we have

$$\phi\tilde{x} = \phi\tilde{x}'\sec\phi\psi + \phi c\phi\tilde{t}'\tan\phi\psi \qquad (15)$$

(w.r.t. 1-observer $\tilde{\text{P}}$aul in $c\tilde{t}'$).

By collecting the partial intrinsic coordinate transformations (14) and (15) we obtain the inverse intrinsic Lorentz transformation to system (13) with respect to 4-observer

(Paul, $\tilde{\text{P}}$aul) in the particle's (or primed) frame as follows:

$$\left.\begin{array}{c} \phi c\,\phi\tilde{t} = \phi c\phi\tilde{t}'\sec\phi\psi + \phi\tilde{x}'\tan\phi\psi \\ \text{(w.r.t. 3-observer Paul in } \tilde{\Sigma}') \\ \phi\tilde{x} = \phi\tilde{x}'\sec\phi\psi + \phi c\phi\tilde{t}'\tan\phi\psi \\ \text{(w.r.t. 1-observer } \tilde{\text{P}}\text{aul in } c\tilde{t}') \end{array}\right\}, \tag{16}$$

where $-\frac{\pi}{2} < \phi\psi < \frac{\pi}{2}$ (temporarily).

Again the range $-\frac{\pi}{2} < \phi\psi < \frac{\pi}{2}$ of the intrinsic angles $\phi\psi$ in system (16) in the positive universe is temporary as indicated. It shall be modified shortly in this section.

By considering the origin $\phi\tilde{x}' = 0$ of the intrinsic space coordinate $\phi\tilde{x}'$ of the primed intrinsic frame, system (16) simplifies as follows:

$$\phi\tilde{x} = \phi c\,\phi\tilde{t}'\tan\phi\psi \quad \text{and} \quad \phi c\,\phi\tilde{t} = \phi c\,\phi\tilde{t}'\sec\phi\psi\,. \tag{17}$$

Then by dividing the first into the second equation of system (17) we have

$$\frac{\phi\tilde{x}}{\phi c\,\phi\tilde{t}} = \sin\phi\psi\,.$$

But, $\phi\tilde{x}/\phi\tilde{t} = \phi v$, is the intrinsic speed of the primed intrinsic frame relative to the unprimed intrinsic frame. Hence,

$$\sin\phi\psi = \phi v/\phi c = \phi\beta \tag{18}$$

$$\sec\phi\psi = \frac{1}{\sqrt{1-\phi v^2/\phi c^2}} = \phi\gamma\,. \tag{19}$$

By using relations (18) and (19) in systems (13) we have

$$\phi c\,\phi\tilde{t}' = \frac{1}{\sqrt{1-\phi v^2/\phi c^2}}\left(\phi c\,\phi\tilde{t} - \frac{\phi v}{\phi c}\,\phi\tilde{x}\right)$$

(w.r.t. 1-observer $\tilde{\text{P}}$eter in $c\tilde{t}$),

$$\phi\tilde{x}' = \frac{1}{\sqrt{1-\phi v^2/\phi c^2}}\left(\phi\tilde{x} - \frac{\phi v}{\phi c}\,\phi c\,\phi\tilde{t}\right)$$

(w.r.t. 3-observer Peter in $\tilde{\Sigma}$), or

$$\left.\begin{array}{c} \phi\tilde{t}' = \phi\gamma\left(\phi\tilde{t} - \dfrac{\phi v}{\phi c^2}\,\phi\tilde{x}\right) \\ \text{(w.r.t. 1-observer } \tilde{\text{P}}\text{eter in } c\tilde{t}) \\ \phi\tilde{x}' = \phi\gamma\,(\phi\tilde{x} - \phi v\,\phi\tilde{t}) \\ \text{(w.r.t. 3-observer Peter in } \tilde{\Sigma}) \end{array}\right\}. \tag{20}$$

And by using equations (18) and (19) in system (16) we have

$$\phi c\,\phi\tilde{t} = \frac{1}{\sqrt{1-\phi v^2/\phi c^2}}\left(\phi c\,\phi\tilde{t}' + \frac{\phi v}{\phi c}\,\phi\tilde{x}'\right)$$

(w.r.t. 3-observer Peter in $\tilde{\Sigma}'$),

$$\phi\tilde{x} = \frac{1}{\sqrt{1-\phi v^2/\phi c^2}}\left(\phi\tilde{x}' + \frac{\phi v}{\phi c}\,\phi c\,\phi\tilde{t}'\right)$$

(w.r.t. 1-observer $\tilde{\text{P}}$eter in $c\tilde{t}'$), or

$$\left.\begin{array}{c} \phi\tilde{t} = \phi\gamma\left(\phi\tilde{t}' + \dfrac{\phi v}{\phi c^2}\,\phi\tilde{x}'\right) \\ \text{(w.r.t. 3-observer Paul in } \tilde{\Sigma}') \\ \phi\tilde{x} = \phi\gamma\,(\phi\tilde{x}' + \phi v\phi\tilde{t}') \\ \text{(w.r.t. 1-observer } \tilde{\text{P}}\text{aul in } c\tilde{t}') \end{array}\right\}. \tag{21}$$

Systems (20) and (21) are the explicit forms of the intrinsic Lorentz transformation (ϕLT) of extended affine intrinsic coordinates and its inverse respectively on the flat two-dimensional metric intrinsic spacetime $(\phi\rho, \phi c\,\phi t)$ that underlies the flat four-dimensional metric spacetime (Σ, ct) in the positive universe in Fig. 7.

As can be easily verified, either system (13) or (16) or its explicit form (20) or (21) implies intrinsic Lorentz invariance (ϕLI) on $(\phi\rho, \phi c\,\phi t)$:

$$\phi c^2\phi\tilde{t}^2 - \phi\tilde{x}^2 = \phi c^2\phi\tilde{t}'^2 - \phi\tilde{x}'^2\,. \tag{22}$$

Just as the 4-observer (Peter, $\tilde{\text{P}}$eter) in the unprimed frame $(\tilde{x}, \tilde{y}, \tilde{z}, c\tilde{t})$ derives system (13) given explicitly as system (20) from Figs. 8a and 8b and the 4-observer (Paul, $\tilde{\text{P}}$aul) in the primed frame derives the system (16) given explicitly as system (21) from Figs. 9a and 9b in the positive universe, the symmetry-partner 4-observer* (Peter*, $\tilde{\text{P}}$eter*) in the unprimed frame $(-\tilde{x}^*, -\tilde{y}^*, -\tilde{z}^*, -c\tilde{t}^*)$ in the negative universe derives the ϕLT and its inverse from Figs. 8a and 8b and the symmetry-partner observer* (Paul*, $\tilde{\text{P}}$aul*) in the primed frame $(-\tilde{x}'^*, -\tilde{y}'^*, -\tilde{z}'^*, -c\tilde{t}'^*)$ in the the negative universe derives the inverse ϕLT from Figs. 9a and 9b, and the 4-observers (Peter*, $\tilde{\text{P}}$eter*) and (Paul*, $\tilde{\text{P}}$aul*) write

$$\left.\begin{array}{c} -\phi c\,\phi\tilde{t}'^* = -\phi c\,\phi\tilde{t}^*\sec\phi\psi - (-\phi\tilde{x}^*)\tan\phi\psi \\ \text{(w.r.t. 1-observer}^* \ \tilde{\text{P}}\text{eter}^* \text{ in } -c\tilde{t}^*) \\ -\phi\tilde{x}'^* = -\phi\tilde{x}^*\sec\phi\psi - (-\phi c\phi\tilde{t}^*)\tan\phi\psi \\ \text{(w.r.t. 3-observer}^* \text{ Peter}^* \text{ in } -\tilde{\Sigma}^*) \end{array}\right\} \tag{23}$$

and

$$\left.\begin{array}{c} -\phi c\,\phi\tilde{t}^* = -\phi c\phi\tilde{t}'^*\sec\phi\psi + (-\phi\tilde{x}'^*)\tan\phi\psi \\ \text{(w.r.t. 3-observer}^* \text{ Paul}^* \text{ in } -\tilde{\Sigma}'^*) \\ -\phi\tilde{x}^* = -\phi\tilde{x}'^*\sec\phi\psi + (-\phi c\phi\tilde{t}'^*)\tan\phi\psi \\ \text{(w.r.t. 1-observer}^* \ \tilde{\text{P}}\text{aul}^* \text{ in } -c\tilde{t}'^*) \end{array}\right\}, \tag{24}$$

where $-\frac{\pi}{2} < \phi\psi < \frac{\pi}{2}$ (temporarily).

The range $-\frac{\pi}{2} < \phi\psi < \frac{\pi}{2}$ of the intrinsic angles $\phi\psi$ in systems (23) and (24) in the negative universe is temporary as indicated. It shall be modified shortly in this section.

Systems (23) and (24) can also be put in their explicit

forms respectively as follows by virtue of Eqs. (18) and (19):

$$\left.\begin{array}{c} -\phi\tilde{t}'^{*} = \phi\gamma\left(-\phi\tilde{t}^{*} - \dfrac{\phi v}{\phi c^2}\left(-\phi\tilde{x}^{*}\right)\right) \\ \text{(w.r.t. 1-observer}^{*}\ \tilde{\text{P}}\text{eter}^{*}\ \text{in}\ -c\tilde{t}^{*}) \\ -\phi\tilde{x}'^{*} = \phi\gamma\left(-\phi\tilde{x}^{*} - \phi v(-\phi\tilde{t}^{*})\right) \\ \text{(w.r.t. 3-observer}^{*}\ \text{Peter}^{*}\ \text{in}\ -\tilde{\Sigma}^{*}) \end{array}\right\} \quad (25)$$

and

$$\left.\begin{array}{c} -\phi\tilde{t}^{*} = \phi\gamma\left(-\phi\tilde{t}'^{*} + \dfrac{\phi v}{\phi c^2}\left(-\phi\tilde{x}'^{*}\right)\right) \\ \text{(w.r.t. 3-observer}^{*}\ \text{Paul}^{*}\ \text{in}\ -\tilde{\Sigma}'^{*}) \\ -\phi\tilde{x}^{*} = \phi\gamma\left(-\phi\tilde{x}'^{*} + \phi v(-\phi\tilde{t}'^{*})\right) \\ \text{(w.r.t. 1-observer}^{*}\ \tilde{\text{P}}\text{aul}^{*}\ \text{in}\ -c\tilde{t}'^{*}) \end{array}\right\}. \quad (26)$$

Again system (23) or (24) or the explicit form (25) or (26) implies intrinsic Lorentz invariance on the flat two-dimensional intrinsic spacetime $(-\phi\rho^{*}, -\phi c\phi t^{*})$ in the negative universe:

$$(-\phi c^2\phi\tilde{t}^{*})^2 - (-\phi\tilde{x}^{*})^2 = (-\phi c^2\phi\tilde{t}'^{*})^2 - (-\phi\tilde{x}'^{*})^2. \quad (27)$$

The intrinsic LT of system (13) and its inverse of system (16) or their explicit forms of systems (20) and (21) and the intrinsic Lorentz invariance (22) they imply, pertain to two-dimensional intrinsic Special Theory of Relativity (ϕSR) on the flat two-dimensional metric intrinsic spacetime $(\phi\rho, \phi c\phi t)$ that underlies the flat four-dimensional metric spacetime (Σ, ct) in the positive universe in Fig. 7. In symmetry, the intrinsic LT and its inverse of system (23) and (24) or their explicit forms (25) and (26) and the intrinsic Lorentz invariance (27) they imply pertain to the intrinsic Special Theory of Relativity (ϕSR) on flat two-dimensional metric intrinsic spacetime $(-\phi\rho^{*}, -\phi c\phi t^{*})$ that underlies the flat four-dimensional metric spacetime $(-\Sigma^{*}, -ct^{*})$ in the negative universe.

Having derived the intrinsic LT of system (13) on page 40 and its inverse of system (16) on page 42 and their explicit forms of systems (20) and (21) in the context of intrinsic 2-geometry ϕSR in the positive universe, we must now obtain their outward (or physical) manifestations on the flat four-dimensional spacetime in the context of 4-geometry Special Theory of Relativity (SR). We do not have to draw a new set of diagrams in the two-world picture in which extended straight line affine spacetime coordinates $\tilde{x}'$ and $c\tilde{t}'$ of the primed frame are rotated relative to the extended affine coordinates $\tilde{x}$ and $c\tilde{t}$ respectively of the unprimed frame on the vertical (x, ct)-plane, while the affine coordinates $\tilde{y}'$ and $\tilde{z}'$ of the primed frame along which relative motion of SR do not occur are not rotated on the vertical spacetime plane. Indeed such diagram does exist. Figures 8a and 8b and their inverses Figs. 9a and 9b, in which the intrinsic spacetime coordinates are rotated being the only diagrams of Special Relativity/intrinsic Special Relativity (SR/ϕSR) in the two-world picture.

As discussed earlier, the flat four dimensional metric spacetime $(\Sigma, ct) \equiv (x, y, z, ct)$ is the outward (or physical) manifestation of the flat two-dimensional metric intrinsic spacetime $(\phi\rho, \phi c\phi t)$ in Fig. 7. Likewise the extended mutually orthogonal straight line affine coordinates $\tilde{x}, \tilde{y}$ and $\tilde{z}$ constitute a flat affine 3-space, shown as a straight line and denoted by $\tilde{\Sigma}(\tilde{x}, \tilde{y}, \tilde{z})$ along the horizontal in the first quadrant. It is the outward manifestation of the extended straight line affine intrinsic coordinate $\phi\tilde{x}$ underlying it in Figs. 8a and 8b. And the extended straight line affine time coordinate $c\tilde{t}$ is the outward (or physical) manifestation of the extended straight line affine intrinsic time coordinate $\phi c\phi\tilde{t}$ along the vertical in Figs. 8a and 8b. The extended straight line affine spacetime coordinates $\tilde{x}', \tilde{y}', \tilde{z}'$ and $c\tilde{t}$ are likewise the outward manifestations of the extended affine intrinsic spacetime coordinates $\phi\tilde{x}'$ and $\phi c\phi\tilde{t}'$ in Figs. 9a and 9b.

It follows by virtue of the foregoing paragraph that the LT and its inverse in the context of SR are the outward (or physical) manifestations of the intrinsic Lorentz transformation (ϕLT) of system (13) or (20) and its inverse of system (16) or (21). We must simply remove the symbol ϕ in systems (13) and (16) to have the LT and its inverse in SR respectively as follows:

$$\left.\begin{array}{c} c\tilde{t}' = c\tilde{t}\sec\psi - \tilde{x}\tan\psi \\ \text{(w.r.t. } \tilde{\text{P}}\text{eter in } c\tilde{t}) \\ \tilde{x}' = \tilde{x}\sec\psi - c\tilde{t}\tan\psi\,,\ \ \tilde{y}' = \tilde{y}\,,\ \ \tilde{z}' = \tilde{z} \\ \text{(w.r.t. Peter in } \tilde{\Sigma}) \end{array}\right\} \quad (28)$$

and

$$\left.\begin{array}{c} c\tilde{t} = c\tilde{t}'\sec\psi + \tilde{x}'\tan\psi \\ \text{(w.r.t. Paul in } \tilde{\Sigma}') \\ \tilde{x} = \tilde{x}'\sec\psi + c\tilde{t}'\tan\psi\,,\ \ \tilde{y} = \tilde{y}'\,,\ \ \tilde{z} = \tilde{z}' \\ \text{(w.r.t. } \tilde{\text{P}}\text{aul in } c\tilde{t}') \end{array}\right\}, \quad (29)$$

where $-\frac{\pi}{2} < \psi < \frac{\pi}{2}$ (temporarily).

The trivial transformations $\tilde{y} = \tilde{y}'$ and $\tilde{z} = \tilde{z}'$ of the coordinates along which relative motion of SR does not occur have been added to the first and second equations of systems (28) obtained by simply removing symbol ϕ from system (13) on page 40 and to the first and second equations of system (29) obtained by simply removing symbol ϕ from system (16) on page 42, thereby making the resulting LT of system (28) and its inverse of system (29) consistent with the 4-geometry of SR. The angle ψ being the outward manifestation in spacetime of the intrinsic angle $\phi\psi$ in intrinsic spacetime, has the same temporary range in systems (28) and (29) as does $\phi\psi$ in systems (13) and (16). This temporary range of ψ shall also be modified shortly in this section.

System (28) indicates that the affine spacetime coordinates $\tilde{x}'$ and $c\tilde{t}'$ are rotated at equal angle ψ relative to the affine spacetime coordinates $\tilde{x}$ and $c\tilde{t}$ respectively, while $\tilde{y}$ is not rotated relative $\tilde{y}$ and $\tilde{z}'$ is not rotated relative to $\tilde{z}$ by angle ψ in the context of SR and system (29) indicates that $\tilde{x}$

and $c\tilde{t}$ are rotated by equal negative angle $-\psi$ relative to $\tilde{x}'$ and $c\tilde{t}'$ respectively. However the relative rotations of the affine coordinates of the four-dimensional spacetime do not exist in reality, as discussed earlier. The indicated rotations in systems (28) and (29) may be referred to as intrinsic (i.e. non-observable or hypothetical) relative rotations of affine spacetime coordinates only, which is what the actual relative rotations of affine intrinsic spacetime coordinates in Figs. 8a and 8b and Figs. 9a and 9b represent.

By considering the spatial origin $\tilde{x}' = \tilde{y}' = \tilde{z}' = 0$ of the primed frame, system (29) reduces as follows:

$$c\tilde{t} = c\tilde{t}' \sec\psi \quad \text{and} \quad \tilde{x} = \tilde{x}' \tan\psi . \tag{30}$$

And by dividing the second equation into the first equation of system (30) we have

$$\frac{\tilde{x}}{c\tilde{t}} = \sin\psi .$$

But, $\tilde{x}/\tilde{t}=v$, is the speed of the primed frame ($\tilde{x}'$, $\tilde{y}'$, $\tilde{z}'$, $c\tilde{t}'$) frame relative to the unprimed frame ($\tilde{x}$, $\tilde{y}$, $\tilde{z}$, $c\tilde{t}$), for relative motion along the collinear $\tilde{x}$ and $\tilde{x}'$ coordinates of the frames. Hence

$$\sin\psi = v/c = \beta , \tag{31}$$

$$\sec\psi = \frac{1}{\sqrt{1 - v^2/c^2}} = \gamma . \tag{32}$$

Relations (31) and (32) on flat four-dimensional spacetime corresponds to relations (18) and (19) respectively on flat two-dimensional intrinsic spacetime. By using Eqs. (31) and (32) in systems (28) and (29) we obtain the LT and its inverse in their usual explicit forms respectively as follows:

$$\left.\begin{gathered} \tilde{t}' = \gamma\left(\tilde{t} - \frac{v}{c^2}\,\tilde{x}\right) \\ \text{(w.r.t. } \tilde{\text{P}}\text{eter in } c\tilde{t}\text{)} \\ \tilde{x}' = \gamma\left(\tilde{x} - v\tilde{t}\right),\ \ \tilde{y}' = \tilde{y},\ \ \tilde{z}' = \tilde{z} \\ \text{(w.r.t. Peter in } \tilde{\Sigma}\text{)} \end{gathered}\right\} \tag{33}$$

and

$$\left.\begin{gathered} \tilde{t} = \gamma\left(\tilde{t}' + \frac{v}{c^2}\,\tilde{x}'\right) \\ \text{(w.r.t. Paul in } \tilde{\Sigma}'\text{)} \\ \tilde{x} = \gamma\left(\tilde{x}' + v\tilde{t}'\right),\ \ \tilde{y} = \tilde{y}',\ \ \tilde{z} = \tilde{z}' \\ \text{(w.r.t. } \tilde{\text{P}}\text{eter in } c\tilde{t}'\text{)} \end{gathered}\right\} . \tag{34}$$

Systems (33) and (34) are the outward (or physical) manifestations on flat four-dimensional spacetime (Σ, ct) in the context of SR of systems (20) and (21) respectively on the flat two-dimensional intrinsic spacetime $(\phi\rho, \phi c\phi t)$ in the context of ϕSR in the positive universe.

Systems (28) and (29) or the explicit form (33) or (34) implies Lorentz invariance (LI) in SR in the positive universe:

$$c^2\tilde{t}^2 - \tilde{x}^2 - \tilde{y}^2 - \tilde{z}^2 = c^2\tilde{t}'^2 - \tilde{x}'^2 - \tilde{y}'^2 - \tilde{z}'^2 . \tag{35}$$

This is the outward manifestation on flat four-dimensional spacetime of SR of the intrinsic Lorentz invariance (ϕLI) (22) on page 42 on flat two-dimensional intrinsic spacetime of ϕSR. Just as the intrinsic LT and its inverse of system (13) on page 40 and (16) on page 42 in the context of ϕSR are made manifest in systems (28) and (29) respectively in SR in the positive universe, the intrinsic LT and its inverse of systems (23) and (24) in ϕSR are made manifest in LT and its inverse in SR in the negative universe respectively as follows:

$$\left.\begin{gathered} -c\tilde{t}'^{*} = -c\tilde{t}^{*}\sec\psi - (-\tilde{x}^{*})\tan\psi \\ \text{(w.r.t. } \tilde{\text{P}}\text{eter}^{*} \text{ in } -c\tilde{t}^{*}\text{)} \\ -\tilde{x}'^{*} = -\tilde{x}^{*}\sec\psi - (-c\tilde{t}^{*})\tan\psi , \\ -\tilde{y}'^{*} = -\tilde{y}^{*},\quad -\tilde{z}'^{*} = -\tilde{z}^{*} \\ \text{(w.r.t. Peter}^{*} \text{ in } -\tilde{\Sigma}^{*}\text{)} \end{gathered}\right\} \tag{36}$$

and

$$\left.\begin{gathered} -c\tilde{t}^{*} = -c\tilde{t}'^{*}\sec\psi + (-\tilde{x}'^{*})\tan\psi \\ \text{(w.r.t. Paul}^{*} \text{ in } -\tilde{\Sigma}'^{*}\text{)} \\ -\tilde{x}^{*} = -\tilde{x}'^{*}\sec\psi + (-c\tilde{t}'^{*})\tan\psi , \\ -\tilde{y}^{*} = -\tilde{y}'^{*},\quad -\tilde{z}^{*} = -\tilde{z}'^{*} \\ \text{(w.r.t. } \tilde{\text{P}}\text{aul}^{*} \text{ in } -c\tilde{t}'^{*}\text{)} \end{gathered}\right\} . \tag{37}$$

And by using equations (31) and (32) in systems (36) and (37) we obtain the LT and it inverse in their usual explicit forms in the negative universe as follows:

$$\left.\begin{gathered} -\tilde{t}'^{*} = \gamma\left(-\tilde{t}^{*} - \frac{v}{c^2}\,(-\tilde{x}^{*})\right) \\ \text{(w.r.t. } \tilde{\text{P}}\text{eter}^{*} \text{ in } -c\tilde{t}^{*}\text{)} \\ -\tilde{x}'^{*} = \gamma\left(-\tilde{x}^{*} - v\,(-\tilde{t}^{*})\right),\ \ -\tilde{y}'^{*} = -\tilde{y}^{*},\ \ -\tilde{z}'^{*} = -\tilde{z}^{*} \\ \text{(w.r.t. Peter}^{*} \text{ in } -\tilde{\Sigma}^{*}\text{)} \end{gathered}\right\} \tag{38}$$

and

$$\left.\begin{gathered} -\tilde{t}^{*} = \gamma\left(-\tilde{t}'^{*} + \frac{v}{c^2}\,(-\tilde{x}'^{*})\right) \\ \text{(w.r.t. Paul}^{*} \text{ in } -\tilde{\Sigma}'^{*}\text{)} \\ -\tilde{x}^{*} = \gamma\left(-\tilde{x}'^{*} + v\,(-\tilde{t}'^{*})\right),\ \ -\tilde{y}^{*} = -\tilde{y}'^{*},\ \ -\tilde{z}^{*} = -\tilde{z}'^{*} \\ \text{(w.r.t. } \tilde{\text{P}}\text{aul}^{*} \text{ in } -c\tilde{t}'^{*}\text{)} \end{gathered}\right\} . \tag{39}$$

Systems (38) and (39) are the outward manifestations on flat four-dimensional spacetime $(-\Sigma^{*}, -ct^{*})$ of SR of systems (25) and (26) respectively on flat two-dimensional intrinsic spacetime $(-\phi\rho^{*}, -\phi c\phi t^{*})$ of ϕSR in the negative universe. Either the LT (36) or its inverse (37) or the explicit form (38) or (39) implies Lorentz invariance in SR in the negative universe:

$$\begin{aligned} (-c\tilde{t}^{*})^2 - (-\tilde{x}^{*})^2 - (-\tilde{y}^{*})^2 - (-\tilde{z}^{*})^2 = \\ = (-c\tilde{t}'^{*})^2 - (-\tilde{x}'^{*})^2 - (-\tilde{y}'^{*})^2 - (-\tilde{z}'^{*})^2 . \end{aligned} \tag{40}$$

This is the outward manifestation on the flat four-dimensional spacetime of SR of the intrinsic Lorentz invariance (27)

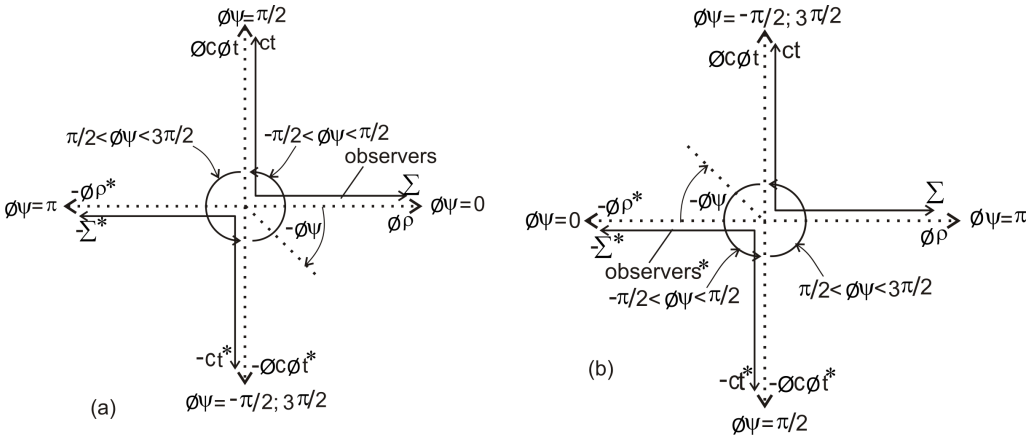

Fig. 10: The concurrent open intervals $(-\frac{\pi}{2}, \frac{\pi}{2})$ and $(\frac{\pi}{2}, \frac{3\pi}{2})$ within which the intrinsic angle $\phi\psi$ could take on values: a) with respect to 3-observers in the positive universe and b) with respect to 3-observers in the negative universe.

on page 43 on flat two-dimensional intrinsic spacetime of ϕSR in the negative universe. The restriction of the values of the intrinsic angle $\phi\psi$ to a half-plane $(-\frac{\pi}{2} < \phi\psi < \frac{\pi}{2})$ with respect to observers in the positive universe in systems (13) and (16) and with respect to observers* in the negative universe in systems (23) and (24) is a temporary measure as indicated in those systems. The intrinsic angle $\phi\psi$ actually takes on values on the entire plane $[-\frac{\pi}{2} \leqslant \phi\psi \leqslant \frac{3\pi}{2}]$ with respect to observers in the positive and negative universes, except that certain values of $\phi\psi$ namely, $-\frac{\pi}{2}, \frac{\pi}{2}$ and $\frac{3\pi}{2}$, must be excluded, as shall be discussed more fully shortly. The values of $\phi\psi$ in the first cycle as well as negative senses of rotation (by negative intrinsic angle $-\phi\psi$) with respect to 3-observers in the 3-spaces in the positive and negative universes are shown in Figs. 10a and 10b respectively.

We have thus obtained a (new) set of spacetime/intrinsic spacetime diagrams namely, Figs. 8a and 8b and their inverses Figs. 9a and 9b in the context of Scheme II in Table 1 or in the two-world picture, for deriving intrinsic Lorentz transformation (ϕLT) and its inverse in terms of extended straight line affine intrinsic spacetime coordinates $\phi\tilde{x}', \phi c\phi\tilde{t}'$ and $\phi\tilde{x}, \phi c\phi\tilde{t}$ on the flat two-dimensional metric intrinsic spacetime $(\phi\rho, \phi c\phi t)$ of the two-dimensional intrinsic Special Theory of Relativity (ϕSR) in both the positive and negative universes and for deriving the Lorentz transformation (LT) and its inverse in terms of extended straight line affine spacetime coordinates $\tilde{x}$, $\tilde{y}$, $\tilde{z}$, $c\tilde{t}$ and $\tilde{x}'$, $\tilde{y}'$, $\tilde{z}'$, $c\tilde{t}'$, as outward (or physical) manifestations on the flat four-dimensional spacetime of SR of the intrinsic Lorentz transformation (ϕLT) and its inverse of ϕSR in both the positive and negative universes. Figures 8a and 8b and their inverses Figs. 9a and 9b must replace the Minkowski diagrams of Figs. 3a and 3b in the context of Scheme I in Table 1 or in the one-world picture.

The skewness of the rotated spacetime coordinates in the Minkowski diagrams of Figs. 3a and 3b (and in the Loedel and Brehme diagrams of Figs. 4a and 4b), from which the LT and its inverse have sometimes been derived until now in the existing one-world picture, has been remarked to be undesirable earlier in this paper because the observer at rest with respect to the frame with rotated spacetime coordinates could detect the skewness of the coordinates of his frame as an effect of the uniform motion of his frame. Moreover the skewness of the rotated coordinates of the "moving" frame vis-a-vis the non-skewed coordinates of the "stationary" frame (in the Minkowski diagrams) gives apparent preference to one of two frames in uniform relative motion. On the other hand, neither the skewness of the rotated intrinsic spacetime coordinates of the "moving" frame nor of the "stationary" frame occurs in Figs. 8a, 8b, 9a and 9b. The diagrams of Figs. 8a, 8b, 9a and 9b in the two-world picture do not give apparent preference for any one of the pair of intrinsic frames in relative intrinsic motion and consequently do not give apparent preference for any one of the pair of frames on four-dimensional spacetime in relative motion, since both intrinsic frames have mutually orthogonal intrinsic spacetime coordinates in each of those figures.

Although the negative universe is totally elusive to people in our (or positive) universe, just as our universe is totally elusive to people in the negative universe, from the point of view of direct experience, we have now seen in the above that the intrinsic spacetime coordinates of the two universes unite in prescribing intrinsic Lorentz transformation and intrinsic Lorentz invariance on the flat two-dimensional intrinsic spacetime and consequently in prescribing Lorentz transformation and Lorentz invariance on flat four-dimensional spacetime in each of the two universes. It can thus be said that there is intrinsic (or non-observable) interaction of four-dimensional spacetime coordinates of the two universes in Special Relativity.

The singularities at $\phi\psi = \frac{\pi}{2}$ and $\phi\psi = -\frac{\pi}{2}$ or $\phi\psi = \frac{3\pi}{2}$ in systems (13) and (16), (of Scheme II in Table 1 or in the two-world picture), correspond to the singularities at $\alpha = \infty$ and $\alpha = -\infty$ in the coordinate transformation of systems (4) and (5) in the Minkowski one-world picture. Being smooth

for all values of α, except for the extreme values, $\alpha = \infty$ and $\alpha = -\infty$, at its boundary represented by the vertical line in Fig. 1a, which corresponds to a line along the ct- and $-ct^*$-axes in Fig. 2a, the only (positive) Minkowski space including the time reversal dimension, (to be denoted by $(\Sigma, ct, -ct^*)$), in Fig. 2a in the one-world picture is usually considered to be sufficiently smooth. Similarly being smooth for all values of the intrinsic angle $\phi\psi$ in the first cycle, except for $\phi\psi = -\frac{\pi}{2}, \frac{\pi}{2}$ and $\phi\psi = \frac{3\pi}{2}$ along their interface in Fig. 2b, the positive Minkowski space including the time reversal dimension $(\Sigma, ct, -ct^*)$ and the negative Minkowski space including time reversal dimension $(-\Sigma^*, -ct^*, ct)$ of the two-world picture in Fig. 2b must be considered to be sufficiently smooth individually.

An attempt to compose the positive Minkowski space including the time reversal dimension $(\Sigma, ct, -ct^*)$ and the negative Minkowski space including time reversal dimension $(-\Sigma^*, -ct^*, ct)$ into a single space, over which $\phi\psi$ has values within the range $[-\frac{\pi}{2}, \frac{3\pi}{2}]$ or $[0, 2\pi]$, cannot work since the resultant space possesses interior (and not boundary) discontinuities at $\phi\psi = \frac{\pi}{2}$ in the case of the range $[-\frac{\pi}{2}, \frac{3\pi}{2}]$ and $\phi\psi = -\frac{\pi}{2}$, $\phi\psi = \frac{\pi}{2}$ and $\phi\psi = \frac{3\pi}{2}$ in the case of the range $[0, 2\pi]$, thereby making the single space generated non-smooth. This implies that the larger spacetime domain of combined positive and and negative universes cannot be considered as a continuum of event domain or as constituting a single world or universe. The lines of singularity $\phi\psi = \frac{\pi}{2}$ and $\phi\psi = -\frac{\pi}{2}$ along the vertical ct- and and $-ct^*$-axes respectively represent event horizons, (the special-relativistic event horizons), to observers in 3-spaces Σ and $-\Sigma^*$ in the positive and negative universes respectively. These event horizons at $\phi\psi = \frac{\pi}{2}$ and $-\frac{\pi}{2}$ show up as singularities in the intrinsic Lorentz transformation (ϕLT) and its inverse of systems (13) and (16) and consequently in the LT and its inverse of systems (28) and (29) in the positive universe and in ϕLT and its inverse of systems (23) and (24) and consequently in the LT and its inverse of systems (36) and (37) in the negative universe.

The observers in 3-space on one side of the event horizons along the dimensions ct and $-ct^*$ in Fig. 5 and Fig. 7 cannot observe events taking place on the other side. This makes a two-world interpretation of Scheme II in Table 1 with the spacetime/intrinsic spacetime diagram of Fig. 7 mandatory.

4.5 Reduction of the LT and its inverse to length contraction and time dilation formulae from the point of view of what can be measured with laboratory rod and clock

Nature makes use of all the terms of the LT, system (28) or (33), and its inverse, system (29) or (34) to establish Lorentz invariance. However man could not detect all the terms of the LT and its inverse with his laboratory rod and clock. First of all, it is the last three equations of system (28) or (33) written by or with respect to the 3-observer (Peter) in 3-space in the unprimed frame with affine coordinates $\tilde{x}, \tilde{y}$ and $\tilde{z}$ and the first equation of system (29) or (34) written by or with respect to the 3-observer Paul in 3-space in the primed frame with affine coordinates $\tilde{x}', \tilde{y}'$ and $\tilde{z}'$ that are relevant for the measurements of distance in space by a rod in 3-space and of time duration by a clock kept in 3-space respectively of a special-relativistic event by 3-observers in 3-space. By collecting those equations we have the following:

$$\tilde{x}' = \tilde{x}\sec\psi - c\tilde{t}\tan\psi\,, \quad \tilde{y}' = \tilde{y}\,, \quad \tilde{z}' = \tilde{z} \tag{41a}$$

(w.r.t. 3-observer Peter in $\tilde{\Sigma}$), and

$$c\tilde{t} = c\tilde{t}'\sec\psi + \tilde{x}'\tan\psi \tag{41b}$$

(w.r.t. 3-observer Paul in $\tilde{\Sigma}'$).

Now when Peter picks his laboratory rod to measure length, he will be unable to measure the term $-c\tilde{t}\tan\psi$ of the first equation of system (41a) with his laboratory-rod. Likewise when Paul picks his clock to measure time duration, he will be unable to measure the term $\tilde{x}'\tan\psi$ in (41b) with his clock. Thus from the point of view of what can be measured by laboratory rod and clock by observers in 3-space, system (41a) and Eq. (41b) reduce as follows:

$$\tilde{x} = \tilde{x}'\cos\psi\,, \quad \tilde{y} = \tilde{y}'\,, \quad \tilde{z} = \tilde{z}'\,, \quad \tilde{t} = \tilde{t}'\sec\psi\,. \tag{42}$$

System (42) becomes the following explicit form in terms of particle's speed relative to the observer by virtue of Eq. (32) on page 44:

$$\left.\begin{aligned} \tilde{x} &= \tilde{x}'\sqrt{1 - v^2/c^2}\,, \quad \tilde{y} = \tilde{y}'\,, \quad \tilde{z} = \tilde{z}' \\ \tilde{t} &= \frac{\tilde{t}'}{\sqrt{1 - v^2/c^2}} \end{aligned}\right\}. \tag{43}$$

These are the well known length contraction and time dilation formulae for two frames in relative motion along their collinear $\tilde{x}$- and $\tilde{x}'$-axes in SR. Showing that they pertain to the measurable sub-space of the space of SR is the essential point being made here.

4.6 The generalized form of intrinsic Lorentz transformation in the two-world picture

Now let us rewrite the intrinsic Lorentz transformation (ϕLT) and its inverse of systems (13) on page 40 and (16) on page 42 in the positive universe in the generalized forms in which they can be applied for all values of $\phi\psi$ in the concurrent open intervals $(-\frac{\pi}{2}, \frac{\pi}{2})$ and $(\frac{\pi}{2}, \frac{3\pi}{2})$ in Fig. 10a by factorizing out $\sec\phi\psi$ to have respectively as follows:

$$\left.\begin{aligned} \phi c\phi\tilde{t}' &= \sec\phi\psi\,(\phi c\phi\tilde{t} - \phi\tilde{x}\sin\phi\psi) \\ \phi\tilde{x}' &= \sec\phi\psi\,(\phi\tilde{x} - \phi c\phi\tilde{t}\sin\phi\psi) \end{aligned}\right\} \tag{44}$$

and

$$\left.\begin{aligned} \phi c\phi\tilde{t} &= \sec\phi\psi\,(\phi c\phi\tilde{t}' + \phi\tilde{x}'\sin\phi\psi) \\ \phi\tilde{x} &= \sec\phi\psi\,(\phi\tilde{x}' + \phi c\phi\tilde{t}'\sin\phi\psi) \end{aligned}\right\}. \tag{45}$$

The 3-observers in the Euclidean 3-space Σ of the positive universe "observe" intrinsic Special Relativity (ϕSR) and consequently observe Special Relativity (SR) for intrinsic angles $\phi\psi$ in the range $(-\frac{\pi}{2}, \frac{\pi}{2})$. However as Fig. 10a shows, 3-observers in the positive universe could construct ϕSR and hence SR relative to themselves for all intrinsic angles $\phi\psi$ in the concurrent open intervals $(-\frac{\pi}{2}, \frac{\pi}{2})$ and $(\frac{\pi}{2}, \frac{3\pi}{2})$, by using the generalized intrinsic Lorentz transformation (ϕLT) and its inverse of systems (44) and (45) and obtaining the LT and its inverse as outward manifestations on flat four-dimensional spacetime of the ϕLT and its inverse so derived, although they can observe Special Relativity for intrinsic angles $\phi\psi$ in $(-\frac{\pi}{2}, \frac{\pi}{2})$ in Fig. 10a only.

Likewise the ϕLT and its inverse in the negative universe of systems (25) on page 43 and (26) on page 43, shall be written in the generalized forms in which they can be applied for all intrinsic angles $\phi\psi$ in the concurrent open intervals $(-\frac{\pi}{2}, \frac{\pi}{2})$ and $(\frac{\pi}{2}, \frac{3\pi}{2})$ in Fig. 10b respectively as follows:

$$\left.\begin{aligned} -\phi c\,\phi\tilde{t}'^{*} &= \sec\phi\psi\,(-\phi c\,\phi\tilde{t}^{*} - (-\phi\tilde{x}^{*})\sin\phi\psi) \\ -\phi\tilde{x}'^{*} &= \sec\phi\psi\,(-\phi\tilde{x}^{*} - (-\phi c\phi\tilde{t}^{*})\sin\phi\psi) \end{aligned}\right\} \quad (46)$$

and

$$\left.\begin{aligned} -\phi c\,\phi\tilde{t}^{*} &= \sec\phi\psi\,(-\phi c\,\phi\tilde{t}'^{*} + (-\phi\tilde{x}'^{*})\sin\phi\psi) \\ -\phi\tilde{x}^{*} &= \sec\phi\psi\,(-\phi\tilde{x}'^{*} + (-\phi c\phi\tilde{t}'^{*})\sin\phi\psi) \end{aligned}\right\}. \quad (47)$$

The 3-observers* in the Euclidean 3-space $-\Sigma^{*}$ of the negative universe "observe" intrinsic Special Relativity (ϕSR) and hence observe Special Relativity (SR) for intrinsic angles $\phi\psi$ in the open interval $(-\frac{\pi}{2}, \frac{\pi}{2})$ in Fig. 10b. Again as Fig. 10b shows, 3-observers* in the negative universe could construct ϕSR and hence SR relative to themselves for all intrinsic angles $\phi\psi$ in the concurrent open intervals $(-\frac{\pi}{2}, \frac{\pi}{2})$ and $(\frac{\pi}{2}, \frac{3\pi}{2})$, by using the generalized ϕLT and its inverse of ϕSR of systems (46) and (47) and obtaining LT and its inverse of SR as outward manifestations on flat four-dimensional spacetime of the ϕLT and its inverse so constructed, although they can observe SR for intrinsic angles $\phi\psi$ in $(-\frac{\pi}{2}, \frac{\pi}{2})$ in Fig. 10b only.

The fact that the intrinsic Lorentz transformation (ϕLT) and its inverse represent continuous rotation of intrinsic spacetime coordinates $\phi\tilde{x}'$ and $\phi c\,\phi\tilde{t}'$ of the primed frame relative to the intrinsic spacetime coordinates $\phi\tilde{x}$ and $\phi c\,\phi\tilde{t}$ respectively of the unprimed frame through all intrinsic angles $\phi\psi$ in the closed range $[0, 2\pi]$, excluding rotation by $\phi\psi = -\frac{\pi}{2}, \frac{\pi}{2}$ and $\phi\psi = \frac{3\pi}{2}$, is clear from the concurrent open intervals $(-\frac{\pi}{2}, \frac{\pi}{2})$ and $(\frac{\pi}{2}, \frac{3\pi}{2})$ of the intrinsic angle $\phi\psi$ in Figs. 10a and 10b over which the generalized ϕLT and its inverse of systems (44) and (45) in the positive universe and systems (46) and (47) in the negative universe could be applied. We shall not be concerned with the explanation of how the intrinsic coordinates $\phi\tilde{x}'$ and $\phi c\,\phi\tilde{t}'$ of the particle's intrinsic frame can be rotated continuously relative to the intrinsic coordinates $\tilde{x}$ and $\phi c\,\phi\tilde{t}$ of the observer's intrinsic frame through intrinsic angles $\phi\psi$ in the range $[0, 2\pi]$, while avoiding $\phi\psi = \frac{\pi}{2}$ and $\phi\psi = \frac{3\pi}{2}$ in this paper.

4.7 Non-existence of light cones in the two-world picture

The concept of light-cone does not exist in the two-world picture. This follows from the derived relation, $\sin\phi\psi = \phi v/\phi c$, (Eq. (18) on page 42), which makes the intrinsic speed ϕv of relative intrinsic motion of every pair of intrinsic frames lower than the intrinsic light speed ϕc, $(\phi v < \phi c)$, for all values of $\phi\psi$ in the concurrent open intervals $(-\frac{\pi}{2}, \frac{\pi}{2})$ and $(\frac{\pi}{2}, \frac{3\pi}{2})$ in Fig. 10a in the context of ϕSR and consequently speed v of relative motion of every pair of frames lower than the speed of light c, $(v < c)$, for all intrinsic angles $\phi\psi$ in the concurrent open intervals $(-\frac{\pi}{2}, \frac{\pi}{2})$ and $(\frac{\pi}{2}, \frac{3\pi}{2})$ in Fig. 10a. The intrinsic angle $\phi\psi = \frac{\pi}{2}$ corresponds to intrinsic speed $\phi v = \phi c$ and $\phi\psi = -\frac{\pi}{2}$ or $\phi\psi = \frac{3\pi}{2}$ corresponds to $\phi v = -\phi c$, which are excluded from ϕSR. They correspond to speed $v = c$ and $v = -c$ respectively, which are excluded from SR.

We therefore have a situation where all intrinsic angles $\phi\psi$ in the closed range $[0, 2\pi]$, except $\phi\psi = \frac{\pi}{2}$ and $\phi\psi = \frac{3\pi}{2}$, (in Fig. 10a), are accessible to intrinsic Special Relativity (ϕSR) with intrinsic timelike geodesics and consequently to SR with timelike geodesics with respect to observers in the positive universe. All intrinsic angles $\phi\psi$ in the closed interval $[0, 2\pi]$, except $\phi\psi = \frac{\pi}{2}$ and $\phi\psi = \frac{3\pi}{2}$, (in Fig. 10b), are likewise accessible to ϕSR with intrinsic timelike geodesics and hence to SR with timelike geodesics with respect to observers* in the negative universe.

Intrinsic spacelike geodesics of for which $\phi v > \phi c$ and spacelike geodesics for which $v > c$ do not exist for any value of the intrinsic angle $\phi\psi$ in the four quadrants, that is, for $\phi\psi$ in the closed range $[0, 2\pi]$, on the larger spacetime/intrinsic spacetime domain of combined positive and negative universes in Fig. 7. Since the existence of light cones requires regions of spacelike geodesics outside the cones, the concept of light cones does not exist in the two-world picture.

4.8 Prospect for making the Lorentz group compact in the two-world picture

The impossibility of making the Lorentz group SO(3,1) compact in the context of the Minkowski geometry in the one-world picture has been remarked earlier in this paper. It arises from the fact that the unbounded parameter space $-\infty < \alpha < \infty$ of the Lorentz boost (the matrix L in (6) on page 33), in the one-world picture, is unavoidable. Compactification of the Lorentz group in the two-world picture would be interesting.

Now the new intrinsic matrix ϕL^{*} that generates the intrinsic Lorentz boost, $\phi\mathbf{x} \rightarrow \phi\mathbf{x}' = \phi L^{*}\phi\mathbf{x}$, on the flat two-dimensional intrinsic spacetime in Eq. (13) on page 40 in the positive universe or (23) on page 42 in the negative universe in the two-world picture is the following:

$$\phi L^{*} = \begin{pmatrix} \sec\phi\psi & -\tan\phi\psi \\ -\tan\phi\psi & \sec\phi\psi \end{pmatrix}, \quad (48)$$

where $\phi\psi$ takes on values in the concurrent open intervals $(-\frac{\pi}{2}, \frac{\pi}{2})$ and $(\frac{\pi}{2}, \frac{3\pi}{2})$ in the positive and negative universes, as

explained earlier and illustrated in Figs. 10a and 10b.

The corresponding new matrix L^* that generates the Lorentz boost, $\mathbf{x} \to \mathbf{x}' = L^*\mathbf{x}$, on flat four-dimensional spacetime in Eq. (28) on page 43 in the positive universe or (36) on page 44 in the negative universe in the two-world picture is the following

$$L^* = \begin{pmatrix} \sec\psi & -\tan\psi & 0 & 0 \\ -\tan\psi & \sec\psi & 0 & 0 \\ 0 & 0 & 1 & 0 \\ 0 & 0 & 0 & 1 \end{pmatrix} \qquad (49)$$

where, ψ takes on values in the concurrent open intervals $(-\frac{\pi}{2}, \frac{\pi}{2})$ and $(\frac{\pi}{2}, \frac{3\pi}{2})$ like $\phi\psi$, in the positive and negative universes.

The matrix L^* can be said to be the outward manifestation on flat four-dimensional spacetime of SR of the intrinsic matrix ϕL^* on flat two-dimensional intrinsic spacetime of ϕSR. It must be recalled however that while the intrinsic angle $\phi\psi$ in (48) measures actual rotation of intrinsic coordinates $\phi\tilde{x}'$ and $\phi c\phi\tilde{t}'$ of the primed frame relative to the intrinsic coordinates $\phi\tilde{x}$ and $\phi c\phi\tilde{t}$ of the unprimed frame, (as in Figs. 8a, 8b, 9a and 9b), in the context of ϕSR, the angle ψ in (49) represents intrinsic (i.e. non-observable or hypothetical) rotation of spacetime coordinates $\tilde{x}'$ and $c\tilde{t}'$ of the primed frame relative to $\tilde{x}$ and $c\tilde{t}$ of the unprimed frame.

The concurrent open intervals $(-\frac{\pi}{2}, \frac{\pi}{2})$ and $(\frac{\pi}{2}, 3\pi)$ wherein the intrinsic angle $\phi\psi$ and the angle ψ take on values in the positive and negative universes imply that the intrinsic matrix ϕL^* (the intrinsic Lorentz boost) and the Lorentz boost L^* in the two-world picture are unbounded. It must be recalled that the matrix L that generates the Lorentz boost in the Minkowski one-world picture given by Eq. (6) on page 33 is likewise unbounded because the parameter α in that matrix takes on values in the unbounded interval $(-\infty, \infty)$.

Also by letting $\phi\psi \to \frac{\pi}{2}$ and $\phi\psi \to -\frac{\pi}{2}$ or $\frac{3\pi}{2}$ in the intrinsic matrix ϕL^*, we have $\sec\phi\psi = \tan\phi\psi \to \infty$ and $\sec\phi\psi = \tan\phi\psi \to -\infty$ respectively, which shows that ϕL^* (or the intrinsic Lorentz boost) and hence the Lorentz boost L^* in the two-world picture are not closed. Whereas $\alpha \to \infty$, $\cosh\alpha \to \infty$, $\sinh\alpha \to \infty$, and $\alpha \to -\infty$, $\cosh\alpha \to \infty$, $\sinh\alpha \to -\infty$ in matrix L, which implies that the Lorentz boost in the Minkowski one-world picture is closed (since no entry of L is outside the range $-\infty < \alpha < \infty$ of the parameter α [6]). Thus L is not bounded but is closed, while ϕL^* and L^* are not bounded and not closed. The matrices L, L^* and the intrinsic matrix ϕL^* are therefore non-compact.

It is required that ϕL^* be both closed and bounded for it to be compact. Likewise the matrix L^*. It follows from this and the foregoing paragraphs that making the the intrinsic Lorentz boost (48) and consequently the Lorentz boost (49) in the two-world picture compact has not been achieved in this paper. As deduced in sub-section 1.1, making the Lorentz boost compact implies making SO(3,1) compact. Thus SO(3,1) has yet not been made compact in the two-world picture since the Lorentz boost has yet not been made compact.

There is good prospect for making SO(3,1) compact in the two-world picture however. This is so since the intrinsic matrix ϕL^* and consequently the matric L^* (the Lorentz boost in the two-world picture) will become compact by justifiably replacing the concurrent open intervals $(-\frac{\pi}{2}, \frac{\pi}{2})$ and $(\frac{\pi}{2}, \frac{3\pi}{2})$, in which the intrinsic angle $\phi\psi$ and the angle ψ take on values in ϕL^* and L^* respectively, by the concurrent closed intervals $[-(\frac{\pi}{2} - \epsilon), \frac{\pi}{2} - \epsilon]$ and $[\frac{\pi}{2} - \epsilon, \frac{3\pi}{2} - \epsilon]$, where ϵ is a small non-zero angle. This will make each of ϕL^* and L^* to be both closed and bounded and hence to be compact. It will certainly require further development of the two-world picture than in this initial paper to make SO(3,1) compact in two-world − if it will be possible.

This paper shall be ended at this point with a final remark that although the possibility of the existence of a two-world picture (or symmetry) in nature has been exposed, there is the need for further theoretical justification than contained in this initial paper and experimental confirmation ultimately, in order for any one to conclude the definite existence of the two-world picture. The next natural step will be to include the light-axis and the distinguished frame of reference of electromagnetic waves in the two-world picture that encompasses no light cones and to investigate the signs of mass and other physical parameters, as well as the possibility of invariance of natural laws in the negative universe.

Acknowledgements

I am grateful to Professors John Wheeler (of blessed memory), Jerome Friedman and Christopher Isham for encouragement in words to continue with this investigation over the years and to Professor A. Maduemezia for assistance with the Lorentz group.

Submitted on September 30, 2009 / Accepted on October 16, 2009

References

1. Bonnor W. B. Negative mass in general relativity. *Gen. Relat. & Grav.*, 1989, v. 21, 1143–1157.
2. Segre E. Nuclei and particles. W. A. Benjamin Inc., Reading, 1977.
3. . Muirhead H. The Special Theory of Relativity. The McMillan Book Company, New York, 1973.
4. Einstein A. On the electrodynamics of moving bodies. In: *The Principle of Relativity*, a collection of memoirs on relativity, with notes by A. Sommerfeld, translated by W. Perrett and G. B. Jeffery, Methuen, 1923 (with reprints by Dover Publications).
5. Minkowski H. Space and time. *Ibid.*
6. Tung W. Group theory in physics. World Scientific Publishing Co. Pte Ltd., Singapore, 1985.
7. Loedel E. Geometric representation of Lorentz transformation. *Am. J. Phys.*, 1957, v. 25, 327.
8. Brehme R. W. A geometric representation of Galilean and Lorentz transformations. *Am. J. Phys.*, 1962, v. 30, 489.
9. Adler R., Bazin M., Schiffer M. Introduction to General Relativity. Second edition, McGraw-Hill Book Company, New York, 1975.

SPECIAL REPORT

Two-World Background of Special Relativity. Part II

Akindele O. J. Adekugbe
P. O. Box 2575, Akure, Ondo State 340001, Nigeria
E-mail: adekugbe@alum.mit.edu

The two-world background of the Special Theory of Relativity started in part one of this article is continued in this second part. Four-dimensional inversion is shown to be a special Lorentz transformation that transforms the positive spacetime coordinates of a frame of reference in the positive universe into the negative spacetime coordinates of the symmetry-partner frame of reference in the negative universe in the two-world picture, contrary to the conclusion that four-dimensional inversion is impossible as actual transformation of the coordinates of a frame of reference in the existing one-world picture. By starting with the negative spacetime dimensions in the negative universe derived in part one, the signs of mass and other physical parameters and physical constants in the negative universe are derived by application of the symmetry of laws between the positive and negative universes. The invariance of natural laws in the negative universe is demonstrated. The derived negative sign of mass in the negative universe is a conclusion of over a century-old effort towards the development of the concept of negative mass in physics.

1 Introduction

A brief summary of the new geometrical representation of Lorentz transformation and its inverse in the two-world picture and the other associated issues presented in part one of this article [1], is appropriate at the beginning of this second part.

Having deduced from the $\gamma = \sec\psi$ parametrization of the Lorentz boost that a pair of flat four-dimensional spacetimes (or a pair of Minkowski's spaces), which are four-dimensional inversions of each other namely, $(\Sigma, ct) \equiv (x^1, x^2, x^3, ct)$ and $(-\Sigma^*, -ct^*) \equiv (-x^{1*}, -x^{2*}, -x^{3*}, -ct^*)$, co-exist in nature and that this implies the co-existence in nature of a pair of symmetrical worlds (or universes), referred to as our (or positive) universe and negative universe, a pair of two-dimensional intrinsic spacetimes denoted respectively by $(\phi\rho, \phi c\phi t)$ and $(-\phi\rho^*, -\phi c\phi t^*)$, which underlie the flat four-dimensional spacetimes (Σ, ct) of the positive universe and $(-\Sigma^*, -ct^*)$ of the negative universe respectively, were introduced (as *ansatz*) in [1]. The derived graphical representation of the larger spacetime/intrinsic spacetime of the co-existing "anti-parallel" worlds (or universes) was then derived and presented as Fig. 7 of [1].

A new set of intrinsic spacetime diagrams that involve rotations of the primed affine intrinsic spacetime coordinates $\phi\tilde{x}'$ and $\phi c\phi\tilde{t}'$ relative to the unprimed affine intrinsic spacetime coordinates $\phi\tilde{x}$ and $\phi c\phi\tilde{t}$ of a pair of frames in relative motion in the positive universe, which are united with the symmetrical rotations of the primed affine intrinsic spacetime coordinates $-\phi\tilde{x}'^*$ and $-\phi c\,\phi\tilde{t}'^*$ relative to the unprimed affine intrinsic spacetime coordinates $-\phi\tilde{x}^*$ and $-\phi c\phi\tilde{t}^*$ of the symmetry-partner pair of frames in simultaneous identical relative motion in the negative universe, are then drawn on the larger spacetime/intrinsic spacetime of combined positive and negative universes, as Figs. 8a, 8b, 9a and 9b of [1]. The intrinsic Lorentz transformations (ϕLT) and its inverse are derived from the set of intrinsic spacetime diagrams and intrinsic Lorentz invariance (ϕLI) validated in the context of the intrinsic Special Theory of Relativity (ϕSR) on each of the flat two-dimensional intrinsic spacetimes $(\phi\rho, \phi c\phi t)$ of the positive universe and $(-\phi\rho^*, -\phi c\phi t^*)$ of the negative universe.

The flat four-dimensional spacetimes (Σ, ct) and $(-\Sigma^*, -ct^*)$ being the outward (or physical) manifestations of their underlying flat two-dimensional intrinsic spacetimes $(\phi\rho, \phi c\phi t)$ and $(-\phi\rho^*, -\phi c\phi t^*)$ respectively and the Special Theory of Relativity (SR) on each of the spacetimes (Σ, ct) and $(-\Sigma^*, -ct^*)$ being mere outward manifestations of the intrinsic Special Theory of Relativity (ϕSR) on each of $(\phi\rho, \phi c\phi t)$ and $(-\phi\rho^*, -\phi c\phi t^*)$ respectively, the Lorentz transformation (LT) and its inverse are written directly and Lorentz invariance (LI) validated on each of the flat four-dimensional spacetimes (Σ, ct) and $(-\Sigma^*, -ct^*)$, as outward manifestations of intrinsic Lorentz transformation (ϕLT) and its inverse and intrinsic Lorentz invariance (ϕLI) derived graphically on each of $(\phi\rho, \phi c\phi t)$ and $(-\phi\rho^*, -\phi c\phi t^*)$.

There is consequently no need to draw spacetime diagrams involving relative rotations of the primed affine spacetime coordinates $\tilde{x}'$ and $c\tilde{t}'$ relative to the unprimed affine spacetime coordinates $\tilde{x}$ and $c\tilde{t}$ of a pair of frames in relative motion along their collinear $\tilde{x}'-$ and $\tilde{x}-$ axes in the positive universe, which would be united with the symmetrical rotations of the primed affine spacetime coordinates $-\tilde{x}'^*$ and $-c\tilde{t}'^*$ relative to the unprimed affine spacetime coordinates $-\tilde{x}^*$ and $-c\tilde{t}^*$ of the symmetry-partner pair of frames in simultaneous identical relative motion in the negative universe, on the larger spacetime of combined positive and negative

universes, in deriving LT and its inverse and in validating LI in the positive and negative universes. Indeed such diagrams do not exist and if drawn, they must be understood that they are intrinsic (that is, non-observable) or hypothetical diagrams only, as noted in [1].

The fact that the derived intrinsic Lorentz transformation represents rotation of intrinsic spacetime coordinates $\phi\tilde{x}'$ and $\phi c\phi\tilde{t}'$ of a particle's frame relative to intrinsic spacetime coordinates $\phi\tilde{x}$ and $\phi c\phi\tilde{t}$ respectively of the observer's frame at intrinsic angle $\phi\psi$, where $\phi\psi$ can vary continuously in the entire range $[0, 2\pi]$, except that $\phi\psi = \frac{\pi}{2}$ and $\phi\psi = \frac{3\pi}{2}$ must be avoided, are shown in [1]. The non-existence of the light cone concept and good prospect for making SO(3,1) compact in the two-world picture are also shown in [1].

The next natural step in the theoretical justification of the two-world background of the Special Theory of Relativity started in part one of this article, to which this second part is devoted, is the derivations of the signs of mass and other physical parameters and physical constants and investigation of Lorentz invariance of natural laws in the negative universe. The matter arising from [1] namely, the formal derivation (or isolation) of the flat two-dimensional intrinsic spacetimes $(\phi\rho, \phi c\phi t)$ and $(-\phi\rho^*, -\phi c\phi t^*)$ that underlie the flat four-dimensional spacetimes (Σ, ct) and $(-\Sigma^*, -ct^*)$ respectively, which were introduced (as *ansatz*) in [1], requires further development of the two-world picture than in this second part of this article to resolve.

2 Four-dimensional inversion as special Lorentz transformation of the coordinates of a frame of reference in the two-world picture

The intrinsic Lorentz transformation (ϕLT) and its inverse in the two-world picture have been written in the generalized forms of equations (44) and (45) of part one of this article [1]. They can be applied for all intrinsic angles $\phi\psi$ in the first cycle, while avoiding $\phi\psi = -\frac{\pi}{2}$, $\phi\psi = \frac{\pi}{2}$ and $\phi\psi = \frac{3\pi}{2}$, of relative rotation of the affine intrinsic spacetime coordinates $\phi\tilde{x}'$ and $\phi c\phi\tilde{t}'$ of the intrinsic particle's (or primed) frame $(\phi\tilde{x}', \phi c\phi\tilde{t}')$ relative to the affine intrinsic coordinates $\phi\tilde{x}$ and $\phi c\phi\tilde{t}$ of the intrinsic observer's (or unprimed) frame $(\phi\tilde{x}, \phi c\phi\tilde{t})$ on the larger two-dimensional intrinsic spacetime of combined positive and negative universes. They are reproduced here as follows

$$\left.\begin{aligned} \phi c\phi\tilde{t}' &= \sec\phi\psi(\phi c\phi\tilde{t} - \phi\tilde{x}\sin\phi\psi) \\ \phi\tilde{x}' &= \sec\phi\psi(\phi\tilde{x} - \phi c\phi\tilde{t}\sin\phi\psi) \end{aligned}\right\} \quad (1)$$

and

$$\left.\begin{aligned} \phi c\phi\tilde{t} &= \sec\phi\psi(\phi c\phi\tilde{t}' + \phi\tilde{x}'\sin\phi\psi) \\ \phi\tilde{x} &= \sec\phi\psi(\phi\tilde{x}' + \phi c\phi\tilde{t}'\sin\phi\psi) \end{aligned}\right\}, \quad (2)$$

where, as mentioned above, the intrinsic angle $\phi\psi$ can take on values in the range $[0, 2\pi]$, while avoiding $\phi\psi = \frac{\pi}{2}$ and $\phi\psi = \frac{3\pi}{2}$.

Systems (1) and (2) on the flat two-dimensional intrinsic spacetime (or in the intrinsic Minkowski space) $(\phi\rho, \phi c\phi t)$ of intrinsic Special Theory of Relativity (ϕSR) are made manifest outwardly (or physically) on the flat four-dimensional spacetime (the Minkowski space) (Σ, ct) of the Special Theory of Relativity (SR) in the positive universe respectively as follows, as developed in [1]

$$\left.\begin{aligned} c\tilde{t}' &= \sec\psi(c\tilde{t} - \tilde{x}\sin\psi) \\ \tilde{x}' &= \sec\psi(\tilde{x} - c\tilde{t}\sin\psi), \quad \tilde{y}' = \tilde{y}, \quad \tilde{z}' = \tilde{z} \end{aligned}\right\} \quad (3)$$

and

$$\left.\begin{aligned} c\tilde{t} &= \sec\psi(c\tilde{t}' + \tilde{x}'\sin\psi), \\ \tilde{x} &= \sec\psi(\tilde{x}' + c\tilde{t}'\sin\psi), \quad \tilde{y} = \tilde{y}', \quad \tilde{z} = \tilde{z}' \end{aligned}\right\}, \quad (4)$$

where, again, the angle ψ can take on values in $[0, 2\pi]$, excluding $\psi = \frac{\pi}{2}$ and $\psi = \frac{3\pi}{2}$.

However, it must be noted, as discussed in [1], that while the intrinsic angle $\phi\psi$ measures actual rotation of the affine intrinsic coordinates $\phi\tilde{x}'$ and $\phi c\phi\tilde{t}'$ of the intrinsic particle's frame $(\phi\tilde{x}', \phi c\phi\tilde{t}')$ relative to the intrinsic coordinates $\phi\tilde{x}$ and $\phi c\phi\tilde{t}$ respectively of the intrinsic observer's frame $(\phi\tilde{x}, \phi c\phi\tilde{t})$ in system (1), the angle ψ refers to intrinsic (i.e. non-observable) or hypothetical rotation of the coordinates $\tilde{x}'$ and $c\tilde{t}'$ of the particle's frame ($\tilde{x}'$, $\tilde{y}'$, $\tilde{z}'$, $c\tilde{t}'$) relative to the coordinates $\tilde{x}$ and $c\tilde{t}$ of the observer's frame ($\tilde{x}$, $\tilde{y}$, $\tilde{z}$, $c\tilde{t}$) respectively in system (3). The affine spacetime coordinates $\tilde{x}'$, $\tilde{y}'$, $\tilde{z}'$, $c\tilde{t}'$ of the particle's frame are not rotated relative to the coordinates $\tilde{x}$, $\tilde{y}$, $\tilde{z}$, $c\tilde{t}$ of the observer's frame and conversely in the present geometrical representation of Lorentz transformation and its inverse in the two-world picture started in [1].

We shall for now assume the possibility of continuous rotation of the intrinsic coordinates $\phi\tilde{x}'$ and $\phi c\phi\tilde{t}'$ of the intrinsic particle's frame by intrinsic angle $\phi\psi = \pi$, while avoiding $\phi\psi = \frac{\pi}{2}$, relative to the intrinsic coordinates $\phi\tilde{x}$ and $\phi c\phi\tilde{t}$ of the intrinsic observer's frame in the two-world picture, as developed in [1]. As also mentioned in [1], the explanation of how rotation through all angles ψ in $[0, \pi]$ while avoiding $\psi = \frac{\pi}{2}$ can be achieved shall not be of concern in this paper.

Then by letting $\phi\psi = \pi$ we have $\sec\phi\psi = -1$, $\sin\phi\psi = 0$ and system (1) simplifies as follows

$$\phi c\phi\tilde{t}' = -\phi c\phi\tilde{t} \quad \text{and} \quad \phi\tilde{x}' = -\phi\tilde{x}. \quad (5)$$

The meaning of system (5) is that upon rotation through intrinsic angle $\phi\psi = \pi$ of the intrinsic coordinates $\phi\tilde{x}'$ and $\phi c\phi\tilde{t}'$ of the intrinsic particle's frame relative to the intrinsic coordinates $\phi\tilde{x}$ and $\phi c\phi\tilde{t}$ respectively of the intrinsic observer's frame in the positive universe, the rotated intrinsic coordinates $\phi\tilde{x}'$ and $\phi c\phi\tilde{t}'$ transform into (or become) intrinsic coordinates of an observer's frame with negative sign $-\phi\tilde{x}$ and $-\phi c\phi\tilde{t}$ respectively.

The outward manifestation on flat four-dimensional spacetime of system (5) is the following

$$c\tilde{t}' = -c\tilde{t}, \quad \tilde{x}' = -\tilde{x}, \quad \tilde{y}' = -\tilde{y}, \quad \tilde{z}' = -\tilde{z}. \quad (6)$$

System (6) is valid because the intrinsic space coordinates $\phi\tilde{x}'$ and $-\phi\tilde{x}$ are made manifest in the coordinates $\tilde{x}'$, $\tilde{y}'$, $\tilde{z}'$ of 3-space $\tilde{\Sigma}'$ and the coordinates $-\tilde{x}$, $-\tilde{y}$, $-\tilde{z}$ of 3-space $-\tilde{\Sigma}$ respectively, as explained in [1].

Although the coordinates $c\tilde{t}'$ and $\tilde{x}'$ of the particle's frame are not rotated relative to the coordinates $c\tilde{t}$ and $\tilde{x}$ of the observer's frame, once the intrinsic coordinates $\phi\tilde{x}'$ and $\phi c\phi\tilde{t}'$ of the intrinsic particle's frame are rotated by intrinsic angle $\phi\psi = \pi$ relative to the intrinsic coordinates $\phi\tilde{x}$ and $\phi c\phi\tilde{t}$ of the intrinsic observer's frame, thereby giving rise to system (5), then system (6) will arise automatically as the outward manifestation of system (5). It may be observed that system (6) cannot be derived by letting $\psi = \pi$ in system (3).

According to system (5), the intrinsic particle's frame whose intrinsic coordinates $\phi\tilde{x}'$ and $\phi c\phi\tilde{t}'$ are inclined at intrinsic angle $\phi\psi = \pi$ relative to the respective intrinsic coordinates $\phi\tilde{x}$ and $\phi c\phi\tilde{t}$ of the intrinsic observer's frame in the positive universe, although is at rest relative to the observer's frame, since $\sin\phi\psi = \phi v/\phi c = 0 \Rightarrow \phi v = 0$ for $\phi\psi = \pi$, it possesses negative intrinsic spacetime coordinates relative to the intrinsic observer's frame in the positive universe. This implies that the intrinsic particle's frame has made transition into the negative universe. As confirmation of this fact, letting $\phi\psi = \pi$ in Fig. 8a of [1] causes the inclined intrinsic coordinate $\phi\tilde{x}'$ to lie along $-\phi\tilde{x}^*$ along the horizontal in the third quadrant and the inclined intrinsic coordinate $\phi c\phi\tilde{t}'$ to lie along $-\phi c\phi\tilde{t}^*$ along the vertical in the third quadrant in that figure.

The negative intrinsic coordinates $-\phi\tilde{x}$ and $-\phi c\phi\tilde{t}$ in system (5) are clearly the intrinsic coordinates of the symmetry-partner intrinsic observer's frame in the negative universe. Then by putting a dummy star label on the unprimed negative intrinsic coordinates in system (5) as our conventional way of denoting the coordinates/intrinsic coordinates and parameters/intrinsic parameters of the negative universe, in order to differentiate them from those of the positive universe we have

$$\phi c\phi\tilde{t}' = -\phi c\phi\tilde{t}^*, \quad \phi\tilde{x}' = -\phi\tilde{x}^*. \tag{7}$$

Likewise, by putting dummy star label on the negative spacetime coordinates in system (6), since they are the coordinates if the symmetry-partner observer's frame in the negative universe we have

$$c\tilde{t}' = -c\tilde{t}^*, \quad \tilde{x}' = -\tilde{x}^*, \quad \tilde{y}' = -\tilde{y}^*, \quad \tilde{z}' = -\tilde{z}^*. \tag{8}$$

System (8) is the outward manifestation on flat four-dimensional spacetime of system (7). System (7) is the form taken by the generalized intrinsic Lorentz transformation (1) for $\phi\psi = \pi$ and system (8) is the form taken by the generalized Lorentz transformation (3) for $\psi = \pi$.

Since the intrinsic particle's frame $(\phi\tilde{x}', \phi c\phi\tilde{t}')$ is at rest relative to the symmetry-partner intrinsic observer's frame $(-\phi\tilde{x}^*, -\phi c\phi\tilde{t}^*)$ in the negative universe in system (7), which is so since $\sin\phi\psi = \phi v/\phi c = 0 \Rightarrow \phi v = 0$, as mentioned earlier, the intrinsic coordinates $-\phi\tilde{x}^*$ and $-\phi c\phi\tilde{t}^*$ of the intrinsic "stationary" observer's frame are identical to the coordinates $-\phi\tilde{x}'^*$ and $-\phi c\phi\tilde{t}'^*$ of the symmetry-partner intrinsic particle's frame in the negative universe. Consequently system (7) is equivalent to the following transformation of the primed intrinsic coordinates of the intrinsic particle's frame in the positive universe into the primed intrinsic coordinates of the symmetry-partner intrinsic particle's frame in the negative universe:

$$\phi c\phi\tilde{t}' = -\phi c\phi\tilde{t}'^*, \quad \phi\tilde{x}' = -\phi\tilde{x}'^*$$

or

$$\phi c\phi\tilde{t}' \to -\phi c\phi\tilde{t}'^*, \quad \phi\tilde{x}' \to -\phi\tilde{x}'^*. \tag{9}$$

This is inversions in the origin (or intrinsic two-dimensional inversions) of the intrinsic coordinates $\phi\tilde{x}'$ and $\phi c\phi\tilde{t}'$ of the intrinsic particle's frame $(\phi\tilde{x}', \phi c\phi\tilde{t}')$ in the positive universe, which arises by virtue of actual rotations of the intrinsic coordinates $\phi\tilde{x}'$ and $\phi c\phi\tilde{t}'$ by intrinsic angle $\phi\psi = \pi$ relative to the intrinsic coordinates $\phi\tilde{x}$ and $\phi c\phi\tilde{t}$ respectively of the intrinsic observer's frame $(\phi\tilde{x}, \phi c\phi\tilde{t})$ in the positive universe. The intrinsic two-dimensional inversion (9) is still the generalized intrinsic Lorentz transformation (1) for $\phi\psi = \pi$.

The outward manifestation on the flat four-dimensional spacetime of system (9), which also follows from system (8), is the following

$$c\tilde{t}' = -c\tilde{t}'^*, \ \ \tilde{x}' = -\tilde{x}'^*, \ \ \tilde{y}' = -\tilde{y}'^*, \ \ \tilde{z}' = -\tilde{z}'^*$$

or

$$c\tilde{t}' \to -c\tilde{t}'^*, \ \ \tilde{x}' \to -\tilde{x}'^*, \ \ \tilde{y}' \to -\tilde{y}'^*, \ \ \tilde{z}' \to -\tilde{z}'^*. \tag{10}$$

This is the corresponding inversions in the origin (or four-dimensional inversions) of the coordinates $\tilde{x}'$, $\tilde{y}'$, $\tilde{z}'$ and $c\tilde{t}'$ of the particle's frame in the positive universe, which arises as outward manifestation of system (9). The four-dimensional inversion (10) is still the generalized Lorentz transformation of system (3) for $\psi = \pi$. It shall be reiterated for emphasis that the coordinates $\tilde{x}'$, $\tilde{y}'$, $\tilde{z}'$ and $c\tilde{t}'$ of the particle's frame in the positive universe are not actually rotated by angle $\psi = \pi$ relative to the coordinates $\tilde{x}$, $\tilde{y}$, $\tilde{z}$ and $c\tilde{t}$ of the observer's frame in the positive universe, but that system (10) arises as a consequence of system (9) that arises from actual rotation of intrinsic coordinates.

Corresponding to system (9) expressing inversions in the origin of intrinsic coordinates of the intrinsic particle's frame, derived from the intrinsic Lorentz transformation (1) for $\phi\psi = \pi$, is the following inversions in the origin of the unprimed intrinsic coordinates of the intrinsic observer's frame, which can be derived from the inverse intrinsic Lorentz transformation (2) for $\phi\psi = \pi$:

$$\phi c\phi\tilde{t} = -\phi c\phi\tilde{t}^*, \quad \phi\tilde{x} = -\phi\tilde{x}^*$$

or

$$\phi c\phi\tilde{t} \to -\phi c\phi\tilde{t}^*, \quad \phi\tilde{x} \to -\phi\tilde{x}^*. \tag{11}$$

And the outward manifestation on flat four-dimensional spacetime of system (11) is the following four-dimensional

inversions of the coordinates of the observer's frame

$$c\tilde{t} = -c\tilde{t}^*, \quad \tilde{x} = -\tilde{x}^*, \quad \tilde{y} = -\tilde{y}^*, \quad \tilde{z} = -\tilde{z}^*$$

or

$$c\tilde{t} \to -c\tilde{t}^*, \quad \tilde{x} \to -\tilde{x}^*, \quad \tilde{y} \to -\tilde{y}^*, \quad \tilde{z} \to -\tilde{z}^*. \quad (12)$$

We have thus shown that intrinsic two-dimensional inversion is the special intrinsic Lorentz transformation (1) or its inverse (2) for $\phi\psi = \pi$. It transforms the intrinsic spacetime coordinates of a frame in the positive universe into the intrinsic spacetime coordinates of the symmetry-partner frame in the negative universe or conversely. Four-dimensional inversion is likewise the special Lorentz transformation (3) or its inverse (4) for $\psi = \pi$, which transforms the spacetime coordinates of a frame in the positive universe into the spacetime coordinates of the symmetry-partner frame in the negative universe or conversely.

On the other hand, it has been concluded in the context of the existing one-world background of the Special Theory of Relativity (or in the one-world picture) that four-dimensional inversion in impossible as actual transformation of the coordinates of a frame of reference. This, as discussed in [2, see p.39], for example, is due to the fact four-dimensional inversion carries the time axis from the future light cone into the past light cone, which is impossible without going through regions of spacelike geodesics that requires the introduction of imaginary spacetime coordinates in the one-world picture.

The light cone concept does not exist in the two-world picture, as deduced in sub-section 4.7 of [1]. Consequently continuous relative rotation of intrinsic spacetime coordinates of two frames through all intrinsic angles $\phi\psi$ in $[0, 2\pi]$, while avoiding $\phi\psi = \frac{\pi}{2}$ and $\phi\psi = \frac{3\pi}{2}$, is possible, (granting that how $\phi\psi = \frac{\pi}{2}$ and $\phi\psi = \frac{3\pi}{2}$ are avoided shall be explained,) without going into regions of spacelike geodesics in the two-world picture. Four-dimensional inversion, (which does not involve actual relative rotation of spacetime coordinates of two frames), being mere outward manifestation of intrinsic two-dimensional inversion that involves actual relative rotation of intrinsic spacetime coordinates of two frames, is therefore possible as transformation of the coordinates of a frame of reference in the two-world picture.

3 Sign of mass in the negative universe derived from generalized mass expression in Special Relativity in the two-world picture

Now the intrinsic particle's frame $(\phi\tilde{x}', \phi c\phi\tilde{t}')$ contains the intrinsic rest mass ϕm_0 of the particle at rest relative to it and the particle's frame $(\tilde{x}', \tilde{y}', \tilde{z}', c\tilde{t}')$ contains the rest mass m_0 of the particle at rest relative to it in the positive universe. The question arises; what are the signs of the intrinsic rest mass and rest mass of the symmetry-partner particle contained in the symmetry-partner intrinsic particle's frame $(-\phi\tilde{x}'^*, -\phi c\phi\tilde{t}'^*)$ and symmetry-partner particle's frame $(-\tilde{x}'^*, -\tilde{y}'^*, -\tilde{z}'^*, -c\tilde{t}'^*)$ respectively in the negative universes? The answer to this question shall be sought from the the generalized intrinsic mass relation in the context of the intrinsic Special Theory of Relativity (ϕSR) and from the corresponding generalized mass relation in the context of the Special Theory of Relativity (SR) in the two-world picture in this section and by requiring the symmetry of laws between the positive and negative universes in the next section.

The well known mass relation on flat four-dimensional spacetime (Σ, ct) in the context of SR is the following

$$m = \frac{m_0}{\sqrt{1 - v^2/c^2}}. \quad (13)$$

The corresponding intrinsic mass relation on the flat two-dimensional intrinsic spacetime $(\phi\rho, \phi c\phi t)$ in the context of the intrinsic Special Theory of Relativity (ϕSR) is

$$\phi m = \frac{\phi m_0}{\sqrt{1 - \phi v^2/\phi c^2}}. \quad (14)$$

The three-dimensional masses m_0 and m in the three-dimensional Euclidean space are the outward manifestation of the one-dimensional intrinsic masses ϕm_0 and ϕm respectively in the one-dimensional intrinsic space, as illustrated in Fig. 6a of [1].

Then by using the relation, $\sec\phi\psi = (1 - \phi v^2/\phi c^2)^{-\frac{1}{2}}$ and $\sec\psi = (1 - v^2/c^2)^{-\frac{1}{2}}$ derived and presented as Eqs. (19) and (32) respectively in [1], Eqs. (14) and (13) can be written respectively as follows

$$\phi m = \phi m_0 \sec\phi\psi \quad (15)$$

and

$$m = m_0 \sec\psi. \quad (16)$$

Eqs. (15) and (16) are the generalized forms in the two-world picture of the intrinsic mass relation in the context of ϕSR and mass relation in the context of SR respectively. They can be applied for all intrinsic angle $\phi\psi$ and all angles ψ in the range $[0, 2\pi]$, except that $\phi\psi = \frac{\pi}{2}$ and $\phi\psi = \frac{3\pi}{2}$ must be avoided.

By letting $\phi\psi = \pi$ in Eq. (15) and $\psi = \pi$ in Eq. (16) we have

$$\phi m = -\phi m_0 \equiv -\phi m_0^* \quad (17)$$

and

$$m = -m_0 \equiv -m_0^*. \quad (18)$$

However the intrinsic particle's frame is stationary relative to the intrinsic observer's frame for $\phi\psi = \pi$, since then $\sin\phi\psi = \phi v/\phi c = 0 \Rightarrow \phi v = 0$, as noted earlier. Consequently the intrinsic special-relativistic mass $\phi m = \phi m_0(1 - \phi v^2/\phi c^2)^{-\frac{1}{2}}$ must be replaced by the intrinsic rest mass ϕm_0 in (17) and the special-relativistic mass $m = m_0(1 - v^2/c^2)^{-\frac{1}{2}}$ must be replaced by the rest mass m_0 in (18) to have respectively as follows

$$\phi m_0 = -\phi m_0^* \text{ or } \phi m_0 \to -\phi m_0^* \quad (19)$$

and

$$m_0 = -m_0^* \text{ or } m_0 \to -m_0^*. \quad (20)$$

Just as the positive intrinsic coordinates $\phi\tilde{x}'$ and $\phi c\phi\tilde{t}'$ of the intrinsic particle's frame in the positive universe

transform into the negative intrinsic coordinates $-\phi\tilde{x}'^*$ and $-\phi c\,\phi\tilde{t}'^*$ of the symmetry-partner intrinsic particle's frame in the negative universe expressed by system (9), by virtue of the generalized intrinsic Lorentz transformation (1) for $\phi\psi = \pi$, the positive intrinsic rest mass ϕm_0 of the particle contained in the intrinsic particle's frame $(\phi\tilde{x}', \phi c\,\phi\tilde{t}')$ in the positive universe, transforms into negative intrinsic rest mass $-\phi m_0^*$ contained in the intrinsic particle's frame $(-\phi\tilde{x}'^*, -\phi c\,\phi\tilde{t}'^*)$ in the negative universe, by virtue of the generalized intrinsic mass relation (15) for $\phi\psi = \pi$. The negative intrinsic rest mass $-\phi m_0^*$ is certainly the intrinsic rest mass of the symmetry-partner particle in the negative universe.

Likewise as the positive coordinates $\tilde{x}'$, $\tilde{y}'$, $\tilde{z}'$ and $c\tilde{t}'$ of a particle's frame in the positive universe transform into negative coordinates $-\tilde{x}'^*$, $-\tilde{y}'^*$, $-\tilde{z}'^*$ and $-c\tilde{t}'^*$ of the symmetry-partner particle's frame in the negative universe, expressed by system (10), by virtue of the generalized Lorentz transformation (3) for $\psi = \pi$, the positive rest mass m_0 of the particle contained in the particle's frame $(\tilde{x}', \tilde{y}', \tilde{z}', c\tilde{t}')$ in the positive universe, transforms into negative rest mass $-m_0^*$ contained in the symmetry-partner particle's frame $(-\tilde{x}'^*, -\tilde{y}'^*, -\tilde{z}'^*, -c\tilde{t}'^*)$ in the negative universe, by virtue of the generalized relativistic mass relation (16) for $\psi = \pi$. Again the negative rest mass $-m_0^*$ is certainly the rest mass of the symmetry-partner particle in the negative universe.

It follows from the foregoing two paragraphs that the intrinsic particle's frame containing positive intrinsic rest mass of the particle in the positive universe, to be denoted by $(\phi\tilde{x}', \phi c\,\phi\tilde{t}';\ \phi m_0)$, corresponds to the symmetry-partner intrinsic particle's frame containing negative intrinsic rest mass $(-\phi\tilde{x}'^*, -\phi c\,\phi\tilde{t}'^*;\ -\phi m_0^*)$ in the negative universe. The particle's frame containing the positive rest mass of the particle $(\tilde{x}', \tilde{y}', \tilde{z}', c\tilde{t}';\ m_0)$ in the positive universe, likewise corresponds to the symmetry-partner particle's frame containing negative rest mass $(-\tilde{x}', -\tilde{y}'^*, -\tilde{z}'^*, -c\tilde{t}'^*; -m_0^*)$ in the negative universe.

The conclusion that follows from the foregoing is that intrinsic rest masses and rest masses of material particles and objects (that appear in classical, that is, in non-special-relativistic intrinsic physics and physics) are negative quantities in the negative universe. The special-relativistic intrinsic masses $\phi m = \gamma(\phi v)\phi m_0$ and special-relativistic masses $m = \gamma(v)m_0$ of material particles and objects that appear in special-relativistic intrinsic physics and special-relativistic physics respectively are therefore negative quantities in the negative universe.

4 Derivation of the signs of physical parameters and physical constants in the negative universe by application of symmetry of laws between the positive and negative universes

Four-dimensional inversion is the transformation of the positive spacetime coordinates of a frame in the positive universe into the negative spacetime coordinates of the symmetry-partner frame in the negative universe, as systems (10) and (12) show. Thus the simultaneous negation of spacetime coordinates in the classical or special-relativistic form of a natural law amounts to writing that law in the negative universe.

Now the prescribed perfect symmetry of state between the positive and negative universes discussed in sub-section 4.1 of part one of this article [1], will be impossible unless there is also a perfect symmetry of laws between the two universes. That is, unless natural laws take on identical forms in the two universes. Perfect symmetry of laws between the positive and negative universes is immutable, as shall be demonstrated shortly in this article. It must be recalled that Lorentz invariance in the negative universe, (which is an important component of the invariance of laws in the negative universe), has been validated from the derived LT and its inverse in the negative universe of systems (38) and (39) of [1].

The simultaneous negation of space and time coordinates in a natural law in the positive universe in the process of writing it in the negative universe will change the form of that law in general unless physical quantities and constants, such as mass, electric charge, temperature, flux, etc, which also appear in the law (usually as differential coefficients in the instantaneous differential laws) are given the appropriate signs. By combining the simultaneous negation of space and time dimensions with the invariance of laws, the signs of physical quantities and constants in the negative universe can be derived. The derivations of the signs of the fundamental quantities namely, mass, electric charge and absolute temperature in the negative universe shall be done below. The signs of all derived (or non-fundamental) physical quantities and physical constants can then be inferred from their dimensions, as shall be demonstrated.

Consider a body of constant mass m being accelerated by a force $\vec{F}$ directed along the positive X-axis of the frame attached to it. In the positive universe, Newton's second law of motion for this body is the following

$$\vec{F} = \left(m\,\frac{d^2x}{dt^2}\right)\hat{\imath}\,. \tag{21}$$

Since the dimensions of 3-space of the negative universe is inversion in the origin of the dimensions of 3-space of the positive universe, the dimensions, unit vector and force, $(x,\ y,\ z,\ t;\ \hat{\imath};\ \vec{F}\,)$, in the positive universe correspond to $(-x^*,\ -y^*,\ -z^*,\ -t^*;\ -\hat{\imath}^*;\ -\vec{F}^*)$ in the negative universe. Thus in the negative universe, we must let $x \to -x^*$, $t \to -t^*$, $\hat{\imath} \to -\hat{\imath}^*$ and $\vec{F} \to -\vec{F}^*$, while leaving m unchanged meanwhile in (21) to have as follows

$$-\vec{F}^* = \left(m\,\frac{d^2(-x^*)}{d(-t^*)^2}\right)(-\hat{\imath}^*) = \left(m\,\frac{d^2x^*}{dt^{*2}}\right)\hat{\imath}^*. \tag{22}$$

While Eq. (21) states that a body pushed towards the positive x-direction by a force $\vec{F}$, moves along the positive x-direction, (away from the force), in the positive universe,

Eq. (22) states that a body pushed in the $-x^*$-direction in the negative universe by a force $-\vec{F}^*$, moves in the $+x^*$-direction, with unit vector $+\hat{\imath}^*$, (towards the force), in the negative universe. This implies that Newton's second law of motion is different in the negative universe, contrary to the required invariance of natural laws in that universe.

In order for (22) to retain the form of (21), so that Newton's second law of motion remains unchanged in the negative universe, we must let $m \to -m^*$ in it to have as follows

$$-\vec{F}^* = \left(-m^* \frac{d^2x^*}{dt^{*2}}\right)(\hat{\imath}^*) = \left(m^* \frac{d^2x^*}{dt^{*2}}\right)(-\hat{\imath}^*), \qquad (23)$$

which is of the form of (21) upon cancelling the signs. The fact that we must let $m \to -m^*$ in (22) to arrive at (23) implies that mass is a negative quantity in the negative universe.

Newton's second law has been chosen because it involves spacetime coordinates and mass and no other physical quantity or constant. However the negation of mass in the negative universe does not depend on the natural law adopted, it follows from any chosen law once the signs in the negative universe of other physical quantities and physical constants that appear in that law have been correctly substituted, in addition to the simultaneous negation of space and time coordinates in the law.

The negation of mass also follows from the required invariance of the metric tensor with the reflection of spacetime dimensions. For if we consider the Schwarzschild metric in empty space at the exterior of a spherically symmetric gravitational field source, for example, then the non-trivial components of the metric tensor are, $g_{00} = -g_{11}^{-1} = 1 - 2GM/rc^2$. By letting $r \to -r^*$, we must also let $M \to -M^*$ in order to preserve the metric tensor in the negative universe. It can be verified that this is true for all other metric tensors in General Relativity.

Thus negative mass in the negative universe has again been derived from the symmetry of natural laws between the positive and negative universes, which has been derived from the generalized mass relation in the Special Theory of Relativity in the two-world picture in the preceding section.

For electric charge, the electrostatic field $\vec{E}$ emanating from a particle (assumed spherical in shape) with net electric charge q in the positive universe is given at radial distance r from the centre of the particle as follows

$$\vec{E} = \frac{q\vec{r}}{4\pi\epsilon_0 r^3}. \qquad (24)$$

The symmetry-partner electrostatic field emanating from the symmetry-partner particle in the negative universe is inversion in the origin of the electrostatic field in the positive universe. Hence the electrostatic field in the negative universe points in opposite direction in space as its symmetry-partner field $\vec{E}$ of Eq. (24) in the positive universe. This implies that the symmetry-partner electrostatic field in the negative universe is $-\vec{E}^*$. By letting $r \to -r^*$, $\vec{r} \to -\vec{r}^*$ and $\vec{E} \to -\vec{E}^*$ in (24), while retaining q and ϵ_0 meanwhile we have

$$-\vec{E}^* = \frac{q(-\vec{r}^*)}{4\pi\epsilon_0(-r*)^3} = \frac{q\vec{r}^*}{4\pi\epsilon_0 r^{*3}} \qquad (25)$$

In order for (25) to retain the form of (24), so that Coulomb's law remains unchanged in the negative universe, we must let $q/\epsilon_0 \to -(q^*/\epsilon_0^*)$ to have

$$-\vec{E}^* = -\frac{q^*\vec{r}^*}{4\pi\epsilon_0^* r^{*3}}, \qquad (26)$$

which is of the form of Eq. (24) upon cancelling the signs. The negative sign of $-(q^*/\epsilon_0^*)$ is associated with the electric charge, while the electric permittivity of free space retains its positive sign in the negative universe. This can be ascertained from the relation for the divergence of electric field namely,

$$\vec{\nabla} \cdot \vec{E} = \frac{\rho}{\epsilon_0}. \qquad (27)$$

In the negative universe, we must let $\vec{\nabla} \to -\vec{\nabla}^*$, $\vec{E} \to -\vec{E}^*$, $\rho \to \rho^*$, (since $\rho = q/V \to -q^*/(-V^*) = q^*/V^* = \rho^*$), while retaining ϵ_0 meanwhile in (27) to have

$$-\vec{\nabla}^* \cdot (-\vec{E}^*) = \frac{\rho^*}{\epsilon_0}. \qquad (28)$$

In order for (28) to retain the form of (27), we must let $\epsilon_0 \to \epsilon_0^*$, which confirms the positivity of the electric permittivity of free space in the negative universe. The conclusion then is that the electric charge of a particle in the negative universe has opposite sign as the electric charge of its symmetry-partner in the positive universe.

We are now left to determine the sign in the negative universe of the last fundamental quantity namely, absolute temperature. It has been found impossible to determine the sign of absolute temperature in the negative universe in a unique manner from consideration of the equations of thermodynamics, kinetic theory of gases and transport phenomena. It has been necessary to make recourse to the more fundamental notions of the "arrow of entropy" and "arrow of time" in order to propagate. These notions have been made tangible by the works of Prigogine [3].

We know that entropy always increases or always "flows" along the positive direction of the "entropy axis" S in our (or the positive) universe, even as time always increases or always "flows" into the future direction, that is, along the positive time axis ct in our universe. Thus the arrow of time and the arrow of entropy lie parallel to each other in our universe. Or in the words of Prigogine, "a [positively directed] arrow of time is associated with a [positively directed] arrow of entropy". Thus absolute entropy is a positive quantity in our (or positive) universe, just as time is a positive quantity in our (or positive) universe. The arrow of time and the arrow of entropy likewise lie parallel to each other in the negative universe. We then infer from this that entropy is negatively directed and is hence a negative quantity in the negative uni-

verse, since time is negatively directed and is hence a negative quantity in the negative universe.

Having determined the sign of absolute entropy in the negative universe from the above reasoning, it is now an easy matter to determine the sign of absolute temperature in the negative universe. For let us write the following fundamental relation for absolute entropy in our universe:

$$S = k \ln W , \tag{29}$$

where k is the Boltzmann constant and W is the number of micro-states in an ensemble in the quantum-mechanical formulation [4]. In the negative universe, we must let $S \to -S^*$ and $W \to W^*$ while retaining k meanwhile to have as follows

$$-S^* = k \ln W^* . \tag{30}$$

In order for (30) to retain the form of (29) we must let $k \to -k^*$, in (30), to have as follows

$$-S^* = -k^* \ln W^* , \tag{31}$$

which is of the form of (29) upon cancelling the signs. Thus the Boltzmann constant is a negative quantity in the negative universe.

The average energy ε of a molecule, for one degree-of-freedom motion of a diatomic molecule in a gas maintained at thermal equilibrium at temperature T, is given as follows

$$\varepsilon = \frac{2}{3} k T , \tag{32}$$

where, again, k is the Boltzmann constant. In the negative universe, we must let $\varepsilon \to -\varepsilon^*$, (since the kinetic energy $\frac{1}{2}mv^2$ of molecules, like mass m, is a negative quantity in the negative universe), and $k \to -k^*$, in (32) while retaining T meanwhile to have as follows

$$-\varepsilon^* = \frac{2}{3} (-k^*) T , \tag{33}$$

which is of the form of (32) upon cancelling the signs. The transformation, $T \to T^*$, required to convert Eq. (33) into Eq. (32) implies that absolute temperature is a positive quantity in the negative universe.

In summary, the fundamental quantities namely, mass m, electric charge Q and absolute temperature T, transform between the positive and negative universes as, $m \to -m^*$, $Q \to -Q^*$ and $T \to T^*$.

By writing various natural laws in terms of negative spacetime dimensions, negative mass, negative electric charge and positive absolute temperature and requiring the laws to retain their usual forms in the positive universe, the signs of other physical quantities and constants in the negative universe can be derived. However a faster way of deriving the signs in the negative universe of derived physical quantities and constants is to check the signs of their dimensions in the negative universe, as demonstrated for a few quantities and constants below.

Let us consider the Boltzmann constant k and absolute entropy S, whose negative signs in the negative universe have been deduced above. They both have the unit, Joule/Kelvin, or dimension $ML^2/T^2\Theta$ in the positive universe, where M represents mass "dimension", L represents length dimension, T represents time dimension and Θ represents absolute temperature "dimension". In the negative universe, we must let $M \to -M^*$, $L \to -L^*$, $T \to -T^*$ and $\Theta \to \Theta^*$, to have the dimensions of Boltzmann constant and absolute entropy in the negative universe as $-M^*(-L^*)^2/(-T^*)^2\Theta^* = -M^*L^{*2}/T^{*2}\Theta^*$. The Boltzmann constant and absolute entropy are negative quantities in the negative universe, since their common dimension is negative in the negative universe.

The Planck constant has the unit Joule/second and dimension ML^2/T^3 in the positive universe. In the negative universe, it has dimension of $-M^*(-L^*)^2/(-T^*)^3)$, which is positive. Hence the Planck constant is a positive quantity in the negative universe.

The specific heat capacity c_p has the unit Joule/kg×Kelvin and dimension $L^2/T^2\Theta$ in the positive universe. In the negative universe it has dimension $(-L^*)^2/\ (-T^*)^2\Theta^*$, which is positive. Hence specific heat capacity is a positive quantity in the negative universe.

The electric permittivity of space ϵ has the unit of Joule×metre/Coulomb^2 and dimension ML^3/T^2C^2 in the positive universe, where C is used to represent the charge "dimension". In the negative universe, it has dimension $(-M^*)(-L^*)^3/(-T^*)^2(-C^*)^2 = M^*L^{*3}/T^{*2}C^{*2}$, which is positive. Hence the electric permittivity of space is a positive quantity in the negative universe. This fact has been derived earlier in the process of deriving the sign of electric charge in the negative universe. Likewise magnetic permeability of space μ has dimension ML/C^2 in the positive universe and dimension $-M^*(-L^*)/(-C^*)^2 = M^*L^*/C^{*2}$, in the negative universe. It is hence a positive quantity in both the positive and negative universes.

An angular measure in space in the positive universe has the same sign as the symmetry-partner angular measure in the negative universe. This follows from the fact that an arc length, $s = r\theta$ [metre], in the positive universe corresponds to a negative arc length, $s^* = -(r^*\theta^*)$ [−metre*], in the negative universe. In other words, an arc length in the positive universe and its symmetry-partner in the negative universe transform as, $r\theta \to -(r^*\theta^*)$. But the radii of the symmetry-partner arcs transform as, $r \to -r^*$. It follows from these two transformations that an angular measure in space in the positive universe has the same sign as its symmetry-partner in the negative universe, that is, $\pm\theta \to \pm\theta^*$ and $\pm\varphi \to \pm\varphi^*$, etc.

Finally, a dimensionless quantity or constant in the positive universe necessarily has the same sign as its symmetry-partner in the negative universe, as follows from the above. Examples of dimensionless constants are the dielectric constants, ϵ_r and μ_r.

Table 1 gives a summary of the signs of some physical

Physical quantity/constant	Symbol	Intrinsic quantity/ constant	Sign	
			positive universe	negative universe
Distance/dimension of space	$dx\,;\ x$	$d\phi x\,;\ \phi x$	+	−
Interval/dimension of time	$dt\,;\ t$	$d\phi t\,;\ \phi t$	+	−
Mass	m	ϕm	+	−
Electric charge	q	q	+ or −	− or +
Absolute entropy	S	ϕS	+	−
Absolute temperature	T	T	+	+
Energy (total, kinetic)	E	ϕE	+	−
Potential energy	U	ϕU	+ or −	− or +
Radiation energy	$h\nu$	$h\phi\nu$	+	−
Electrostatic potential	Φ_E	$\phi\Phi_E$	+ or −	+ or −
Gravitational potential	Φ_g	$\phi\Phi_g$	−	−
Electric field	$\vec{E}$	ϕE	+ or −	− or +
Magnetic field	$\vec{B}$	ϕB	+ or −	− or +
Planck constant	h	h	+	+
Boltzmann constant	k	ϕk	+	−
Thermal conductivity	k	ϕk	+	−
Specific heat capacity	c_p	ϕc_p	+	+
Speed	v	ϕv	+	+
Electric permittivity	ϵ_0	$\phi\epsilon_0$	+	+
Magnetic permeability	μ_0	$\phi\mu_0$	+	+
Angle	θ, φ	$\phi\theta, \phi\varphi$	+ or −	+ or −
Parity	Π	$\phi\Pi$	+ or −	− or +
⋮	⋮	⋮	⋮	⋮

Table 1: The signs of physical parameters/intrinsic parameters and physical constants/intrinsic constants in the positive and negative universes.

quantities and physical constants in the positive and negative universes. The signs in the positive and negative universes of other physical quantities and constants that are not included in Table 1 can be easily determined from the signs of their dimensions in the negative universe. The appropriateness of the names positive universe and negative universe is made clearer by Table 1.

5 Demonstrating the invariance of the natural laws in the negative universe

It shall be shown in this section that the simultaneous negations of spacetime dimensions and mass, along with simultaneous reversal of the sign of electric charge, retention of the positive sign of absolute temperature and substitution of the signs of other physical quantities and physical constants in the negative universe summarized in column 5 of Table 1 in its complete form, render all natural laws unchanged. However only the invariance of a few laws in the negative universe namely, mechanics (classical and special-relativistic), quantum mechanics, electromagnetism and propagation of light, the theory of gravity, cosmology and fundamental interactions in elementary particle physics shall be demonstrated for examples.

5.1 Further on the invariance of classical mechanics, classical gravitation and Special Relativity in the negative universe

Demonstrating the invariance of classical mechanics in the negative universe consists essentially in showing that Newton's laws of motion for a body under an impressed force and due to interaction of the body with an external force field are invariant under the simultaneous operations of inversion of all coordinates (or dimensions) of 3-space (parity inversion), time reversal and mass negation. The laws are given respectively as follows in the positive universe:

$$\vec{F}_{\text{mech}} = m\,\frac{d^2r}{dt^2}\,\hat{r} \tag{34}$$

and

$$\vec{F}_{\text{field}} = m\,(-\nabla\Phi)\,\hat{k}\,, \tag{35}$$

where $\hat{r}$ and $\hat{k}$ are unit vectors in the directions of the forces $\vec{F}_{\text{mech}}$ and $\vec{F}_{\text{field}}$ respectively.

In the negative universe, we must let $\vec{F}_{\text{mech}} \to -\vec{F}^*_{\text{mech}}$, $\vec{F}_{\text{field}} \to -\vec{F}^*_{\text{field}}$, $m \to -m^*$, $r \to -r^*$, $t \to -t^*$, $\nabla \to -\nabla^*$, $\Phi \to \Phi^*$ (for gravitational and elastic potentials), $\hat{r} \to -\hat{r}^*$ and $\hat{k} \to -\hat{k}^*$ in (34) and (35) to have as follows

$$-\vec{F}^*_{\text{mech}} = -\,m^*\,\frac{d^2(-r^*)}{d(-t^*)^2}\,(-\hat{r}^*) = m^*\,\frac{d^2r^*}{dt^{*2}}\,(-\hat{r}^*) \tag{36}$$

and

$$-\vec{F}^{*}_{\text{field}} = -m^{*}(-(-\nabla^{*})(\Phi^{*}))(-\hat{k}^{*}) = m^{*}(-\nabla^{*}\Phi^{*})(-\hat{k}^{*}) \quad (37)$$

Equations (36) and (37) are the same as Eqs. (34) and (35) respectively upon cancelling the signs.

The invariance in the negative universe of the classical laws of motion (34) and (35) in the positive universe implies that a body of negative mass $-m^{*}$ in the negative universe moves along a trajectory, when impressed upon by an external mechanical force $-\vec{F}^{*}_{\text{mech}}$, or when it is moving within a force field with potential function Φ^{*} in the negative universe, which is identical to the trajectory followed by the symmetry-partner body of positive mass m in the positive universe, which is impressed upon by an external symmetry-partner mechanical force $\vec{F}_{\text{mech}}$ or which is moving within a symmetry-partner force field with potential function Φ in the positive universe.

The invariance in the negative universe of trajectories of a body implied by the invariance in the negative universe of the differential classical laws of motion (34) and (35) for the body, established above can be alternatively formulated as the invariance in the negative universe of the variational formula of Maupertuis. In the positive universe, this is given as follows

$$\delta \int_{p_1}^{P_2} \left(\frac{2}{m}(E-U)\right)^{1/2} dt = 0\,. \quad (38)$$

In the negative universe, we must let $m \to -m^{*}$, $E \to -E^{*}$, $U \to -U^{*}$ and $dt \to -dt^{*}$ in (38) to have as follows

$$\delta \int_{p_1^{*}}^{p_2^{*}} \left(\frac{2}{-m^{*}}(-E^{*}-(-U^{*}))\right)^{1/2} (-dt^{*}) = = \delta \int_{p_1^{*}}^{p_2^{*}} \left(\frac{2}{m^{*}}(E^{*}-U^{*})\right)^{1/2} dt^{*} = 0\,. \quad (39)$$

The summary of the above is that although inertial mass, kinetic energy, distances in space and periods of time are negative in the negative universe, material particles in the negative universe perform identical motions under impressed forces and external force fields as their symmetry-partners perform under symmetry-partner impressed forces and external force fields in the positive universe. Thus outward external forces lead to outward motions of bodies both in the positive and negative universes. Attractive gravitational field in the positive universe correspond to symmetry-partner repulsive gravitational field in the negative universe, but they both give rise to attractive motions of particles (towards the field sources) in both universes. In brief, the transformation of classical mechanics in the positive universe into the negative universe does not give rise to strange motions and associated strange phenomena.

Demonstrating the invariance of classical gravitation (or classical gravitational interaction) in the negative universe consists in showing the invariance in the negative universe of the Newtonian law of gravity in differential form and the implied Newtonian law of universal gravity,

$$\vec{\nabla}\cdot\vec{g} = -4\pi G\varrho \quad (40)$$

or

$$\nabla^{2}\Phi = 4\pi G\varrho \quad (41)$$

and

$$\vec{F} = m\vec{g} = -\frac{GMm\vec{r}}{r^{3}}\,, \quad (42)$$

where

$$\varrho = m/V \ (\text{mass}-\text{density}), \quad (43)$$

$$\Phi = -GM/r\,, \quad (44)$$

$$\vec{g} = -GM\vec{r}/r^{3}. \quad (45)$$

In writing equations (43)–(45) in the negative universe, we must let $m \to -m^{*}$; $M \to -M^{*}$; $r \to -r^{*}$ and $V \to -V^{*}$ (volume of m) to have

$$\frac{m}{V} \to \frac{-m^{*}}{-V^{*}} = \frac{m^{*}}{V^{*}} \Rightarrow \varrho \to \varrho^{*} \quad (46)$$

$$-\frac{GM}{r} \to -\frac{G(-M^{*})}{-r^{*}} = -\frac{GM^{*}}{r^{*}} \Rightarrow \Phi \to \Phi^{*} \quad (47)$$

and

$$-\frac{GM\vec{r}}{r^{3}} \to -\frac{G(-M)(-\vec{r}^{*})}{(-r^{*})^{3}} = \frac{GM^{*}\vec{r}^{*}}{r^{*3}} \Rightarrow \vec{g} \to -\vec{g}^{*}. \quad (48)$$

By using the transformations (46)–(48) along with $\vec{\nabla} \to -\vec{\nabla}^{*}$ in equations (40)–(42) we have

$$(-\vec{\nabla}^{*})\cdot(-\vec{g}^{*}) = -4\pi G\varrho^{*}$$

or

$$\vec{\nabla}^{*}\cdot\vec{g}^{*} = -4\pi G\varrho^{*}, \quad (49)$$

$$(-\nabla^{*})^{2}\Phi^{*} = 4\pi G\varrho^{*}$$

or

$$\nabla^{*2}\Phi^{*} = 4\pi G\varrho^{*} \quad (50)$$

and

$$\vec{F}^{*} = (-m^{*})(-\vec{g}^{*}) = -\frac{G(-M^{*})(-m^{*})(-\vec{r}^{*})}{(-r^{*})^{3}}$$

or

$$\vec{F}^{*} = m^{*}\vec{g}^{*} = -\frac{GM^{*}m^{*}\vec{r}^{*}}{r^{*3}}\,. \quad (51)$$

A comparison of equations (40)–(42) in the positive universe with the corresponding equations (49)–(51) in the negative universe, shows that the Newtonian law of gravity in differential form and the implied Newtonian law of universal gravity are invariant in the negative universe. The invariance of classical gravitation (or classical gravitational interaction) in the negative universe has thus been demonstrated. This is true despite the fact that gravitational potential does not change sign while gravitational field (or gravitational acceleration) changes sign in the negative universe according to equations (47) and (48).

Demonstrating the invariance of Special Relativity in the negative universe consists in showing the invariance of Lorentz transformation, time dilation and length contraction formulae and the special-relativistic expressions for mass and other quantities in that universe. Now in the positive universe, for motion at speed v of a particle of rest mass m_0 along the x-axis of the coordinate system attached to it relative to an observer, the Lorentz transformation of the coordinates $(\tilde{x}', \tilde{y}', \tilde{z}', c\tilde{t}')$ of the primed (or particle's) frame into the coordinates $(\tilde{x}, \tilde{y}, \tilde{z}, c\tilde{t})$ of the unprimed (or observer's) frame has been written as system (3). The special-relativistic mass is given in the positive universe by the usual expression (13), which shall be re-written here as

$$m = \gamma m_0 \,. \tag{52}$$

In the negative universe, we must let $(\tilde{x}', \tilde{y}', \tilde{z}', c\tilde{t}'; m_0) \to (-\tilde{x}'^*, -\tilde{y}'^*, -\tilde{z}'^*, -c\tilde{t}'^*; -m_0^*)$, and also $(\tilde{x}, \tilde{y}, \tilde{z}, c\tilde{t}; m) \to (-\tilde{x}^*, -\tilde{y}^*, -\tilde{z}^*, -c\tilde{t}^*; -m^*)$, yielding the Lorentz transformation of the coordinates of the frame of reference attached to the symmetry-partner particle in motion relative to the symmetry-partner observer in the negative universe written as system (38) in [1], which shall be re-written here as follows

$$\left.\begin{aligned} -\tilde{x}'^* &= \gamma\left(-\tilde{x}^* - v(-\tilde{t}^*)\right) \\ -\tilde{t}'^* &= \gamma\left(-\tilde{t}^* - \frac{v}{c^2}\,(-\tilde{x}^*)\right) \\ -\tilde{y}'^* &= -\tilde{y}^*, \quad -\tilde{z}'^* = -\tilde{z}^* \end{aligned}\right\}, \tag{53}$$

while the expression for special-relativistic mass in the negative universe becomes the following

$$-m^* = -\gamma m_0^* . \tag{54}$$

The expressions for time dilation and length contraction in the negative universe are similarly given respectively as follows

$$\Delta(-\tilde{t}^*) = \gamma\,\Delta(-\tilde{t}'^*)\,, \tag{55}$$

$$\Delta(-\tilde{x}^*) = \gamma^{-1}\,\Delta(-\tilde{x}'^*)\,. \tag{56}$$

Although the negative signs must be retained in (53), (54), (55) and (56) in the negative universe, mathematically the signs cancel, thereby making Lorentz transformation and the other equations of Special Relativity to retain their usual forms in the negative universe. Thus Lorentz invariance, (and local Lorentz invariance in gravitational fields), hold in the negative universe.

5.2 Invariance of quantum mechanics in the negative universe

The time-dependent Schrödinger wave equation is the following in the positive universe

$$H(\vec{r},\, t,\, m,\, q)\,|\Psi(\vec{r},\, t,\, m,\, q)\rangle = i\hbar\,\frac{\partial}{\partial t}\,|\Psi(\vec{r},\, t,\, m,\, q)\rangle\,. \tag{57}$$

By writing (57) in the negative universe, while leaving Ψ unchanged meanwhile, we have

$$-H^*(-\vec{r}^*,\, -t^*,\, -m^*,\, -q^*)\,|\Psi(\vec{r},\, t,\, m,\, q)\rangle = i\hbar^*\frac{\partial}{\partial(-t^*)}\,|\Psi(\vec{r},\, t,\, m,\, q)\rangle\,, \tag{58}$$

where the fact that the Boltzmann constant transforms as $\hbar \to \hbar^*$ between the positive and negative universes in Table 1 has been used.

Now the wave function should transform between the positive and negative universes either as

$$\Psi(\vec{r},\, t,\, m,\, q) \to \Psi^*(-\vec{r}^*,\, -t^*,\, -m^*,\, -q^*) = \Psi^*(\vec{r}^*,\, t^*,\, m^*,\, q^*) \tag{59}$$

or as

$$\Psi(\vec{r},\, t,\, m,\, q) \to -\Psi^*(-\vec{r}^*,\, -t^*,\, -m^*,\, -q^*) = -\Psi^*(\vec{r}^*,\, t^*,\, m^*,\, q^*)\,. \tag{60}$$

The parity of the wave function is conserved in (59) and inverted in (60).

Let us consider the following wave function in the positive universe,

$$\Psi(\vec{r},\, t) = A\sin\left(\vec{k}\cdot\vec{r} - \omega t\right) \tag{61}$$

The symmetry-partner wave function in the negative universe is obtained by letting $\vec{r} \to -\vec{r}^*$, $\vec{k} \to -\vec{k}^*$, $\omega \to -\omega^*$, $t \to -t^*$ and $A \to -A^*$ in (61) to have

$$\begin{aligned} \Psi^*(\vec{r},\, t) &= -A^*\sin\left(-\vec{k}^*\cdot(-\vec{r}^*) - (-\omega^*)(-t^*)\right) \\ &= -A^*\sin\left(\vec{k}^*\cdot\vec{r}^* - \omega^* t^*\right)\,. \end{aligned} \tag{62}$$

The transformation $A \to -A^*$ is necessary since inversion in the origin of the coordinates of a Euclidean 3-space inverts the amplitude of a wave in that space. On the other hand, the phase of a wave function, being a dimensionless number, does not change sign in the negative universe. Thus the transformation (60) and not (59) is the correct transformation of the wave function between the positive and negative universes. This is obviously so since (60) is a parity inversion situation, which is in agreement with the natural parity inversion of a wave, $\Pi \to -\Pi$, between the positive and negative universes included in Table 1. By incorporating the transformation (60) into (58) we obtain the following

$$-H^*(-\vec{r}^*, -t^*, -m^*, -q^*)\,|-\Psi^*(-\vec{r}^*, -t^*, -m^*, -q^*)\rangle = -i\hbar^*\,\frac{\partial}{\partial t^*}\,|-\Psi^*(-\vec{r}^*, -t^*, -m^*, -q^*)\rangle$$

or

$$H^*(\vec{r}^*, t^*, m^*, q^*)\,|\Psi^*(\vec{r}^*, t^*, m^*, q^*)\rangle = i\hbar^*\frac{\partial}{\partial t^*}\,|\Psi^*(\vec{r}^*, t^*, m^*, q^*)\rangle\,. \tag{63}$$

This is of the form of Eq. (57). The invariance of the Schrödinger wave equation in the negative universe has thus been established. It is straight forward to demonstrate the invariance in the negative universe of the Dirac's equation for the electron and of Gordon's equation for bosons.

5.3 Invariance of Maxwell equations in the negative universe

The Maxwell equations in a medium with electric charge density ρ and electric current density $\vec{J}$ are given in the positive universe as follows

$$\left.\begin{aligned} &\vec{\nabla}\cdot\vec{E}=\frac{\rho}{\epsilon}, && \vec{\nabla}\cdot\vec{B}=0\\ &\vec{\nabla}\times\vec{B}=\mu\vec{J}+\epsilon\mu\,\frac{\partial\vec{E}}{\partial t}, && \vec{\nabla}\times\vec{E}=-\frac{\partial\vec{B}}{\partial t}\end{aligned}\right\}. \tag{64}$$

Now, $\rho=\frac{charge}{volume}$, is the electric charge density of the medium in the positive universe. The charge density of the symmetry-partner medium in the negative universe is the positive quantity, $\frac{-charge^*}{-volume^*}=\frac{charge^*}{volume^*}=\rho^*$. The magnitude of an electric current is, $I=\frac{charge}{time}$ or $I=\rho vA$, in the positive universe and the magnitude of its symmetry-partner in the negative universe is the positive quantity, $\frac{-charge^*}{-time^*}=\frac{charge^*}{time^*}=I^*$ or $\rho^* vA^*=I^*$, since speed v and area A do not change sign in the negative universe. Similarly the magnitude of an electric current density of a medium in the positive universe is, $J=\frac{current}{area}$, and the magnitude of the current density of the symmetry-partner medium in the negative universe is, $\frac{current^*}{area^*}=J^*$. Thus in obtaining the Maxwell equations in the negative universe, we must let $\vec{E}\to-\vec{E}^*$, $\vec{B}\to-\vec{B}^*$, $\rho\to\rho^*$, $\vec{J}\to\vec{J}^*$, $\vec{\nabla}\to-\vec{\nabla}^*$, $\epsilon\to\epsilon^*$, $\mu\to\mu^*$ and $t\to-t^*$ in system (65) to have as follows

$$\left.\begin{aligned} &-\vec{\nabla}^*\cdot(-\vec{E}^*)=\frac{\rho^*}{\epsilon^*}, && -\vec{\nabla}^*\cdot(-\vec{B}^*)=0\\ &-\vec{\nabla}^*\times(-\vec{B}^*)=\mu^*\vec{J}^*+\epsilon^*\mu^*\,\frac{\partial(-\vec{E}^*)}{\partial(-t^*)}\\ &-\vec{\nabla}^*\times(-\vec{E}^*)=-\frac{\partial(-\vec{B}^*)}{\partial(-t^*)}\end{aligned}\right\}. \tag{65}$$

System (65) with the negative signs is the form the Maxwell equations are written by physicists* in the negative universe. The signs cancel mathematically thereby making system (65) to retain the form of system (64) and thereby establishing the invariance of Maxwell equations in the negative universe.

The law of propagation of electromagnetic waves derived from the Maxwell equations remain invariant in the negative universe as a consequence of the above. The equations are given in the positive universe as follows

$$\nabla^2\vec{E}=\frac{1}{c^2}\frac{\partial^2\vec{E}}{\partial t^2}, \qquad \nabla^2\vec{B}=\frac{1}{c^2}\frac{\partial^2\vec{B}}{\partial t^2}, \tag{66}$$

while in the negative universe, the electromagnetic wave equations are given as follows

$$\left.\begin{aligned} &(-\nabla^*)^2(-\vec{E}^*)=\frac{1}{c^2}\frac{\partial^2(-\vec{E}^*)}{\partial(-t^*)^2}\\ &(-\nabla^*)^2(-\vec{B}^*)=\frac{1}{c^2}\frac{\partial^2(-\vec{B}^*)}{\partial(-t^*)^2}\end{aligned}\right\}. \tag{67}$$

Thus as the perpendicular electric field and magnetic field $\vec{E}$ and $\vec{B}$ propagate as electromagnetic wave at the speed of light in the positive universe, the symmetry-partner perpendicular fields $-\vec{E}^*$ and $-\vec{B}^*$ propagate as the identical symmetry-partner electromagnetic wave at the speed of light in the negative universe.

The foregoing shows that although electric charge as well as electric field and magnetic field change signs in the negative universe, the laws of propagation of electric and magnetic fields and electromagnetic waves remain invariant in the negative universe.

5.4 Invariance of General Relativity and cosmology in the negative universe

Since system of coordinates does not enter the covariant tensor formulation of Einstein's field equations, the equations are equally valid for the negative dimensions of the negative universe. The most general form of Einstein's field equations in the positive universe is the following

$$R^\nu_\mu-\frac{1}{2}\,R\,g^\nu_\mu+\Lambda\,g^\nu_\mu=-\frac{8\pi G}{c^2}\,T^\nu_\mu, \tag{68}$$

where the energy-momentum tensor T^ν_μ is defined as follows

$$T^\nu_\mu=(p+\rho)\,u^\nu u_\mu-p\,g^\nu_\mu, \tag{69}$$

Λ is the cosmological constant, p and ρ are the pressure and density of the universe respectively, while the other quantities in (68) and (69) are as defined in the theory. Λ is usually set to zero in General Relativity when considering local gravitational problems but retained in cosmological problems.

For the static exterior field of a spherical body, we must let $\Lambda=T^\nu_\mu=0$ in (68) and require the vanishing of the Ricci tensor to have as follows

$$R_{\mu\nu}=0 \tag{70}$$

Adopting a metric with signature $(+---)$, the Schwarzschild solution to the field equation (70) is the following

$$ds^2=c^2dt^2\left(1-\frac{2GM}{rc^2}\right)-\frac{dr^2}{\left(1-\frac{2GM}{rc^2}\right)}-\\ -r^2\left(d\theta^2+\sin^2\theta\,d\varphi^2\right). \tag{71}$$

By letting $t\to-t^*$, $r\to-r^*$, $\theta\to\theta^*$, $\varphi\to\varphi^*$ and $M\to-M^*$ in (71) we find that the Schwarzschild line element or metric tensor remains invariant in the negative universe. Other forms of exterior line elements or metric tensors, such as Kerr's line element, as well as interior metric tensors remain invariant in the negative universe as well. This is so because ds^2 is quadratic in intervals cdt, dr, $rd\theta$ and $r\sin\theta d\varphi$, and the components of the metric tensor are dimensionless. This concludes the invariance of general relativity in the negative universe.

Now the metric of spatially homogeneous universe in comoving coordinates is the Robertson-Walker metric

$$ds^2 = c^2dt^2 - R(t)^2\left(\frac{du^2 + u^2\left(d\theta^2 + \sin^2\theta\, d\varphi^2\right)}{\left(1 + \frac{k}{4}u^2\right)^2}\right), \quad (72)$$

where $u = r/r_0$ and the constant k is -1, 0 or $+1$, corresponding to spherical space, Euclidean space or pseudo-spherical space. Assuming that the universe is filled with perfect fluid, the field equation (68) along with the energy-momentum tensor (69) have been cast in the following forms, from which various models of the universe have been derived in General Relativity, as can be found in the standard texts on General Relativity

$$\frac{8\pi G\rho}{c^2} = -\Lambda + \left[\frac{3k}{R(t)^2} + \frac{3\dot{R}(t)^2}{c^2R(t)^2}\right], \quad (73)$$

$$\frac{8\pi G}{c^2}\left(\frac{p}{c^2}\right) = \Lambda - \left[\frac{k}{R(t)^2} + \frac{\dot{R}(t)^2}{c^2R(t)^2} + \frac{2\ddot{R}(t)}{c^2R(t)}\right], \quad (74)$$

$$R(t) = R_0\exp(Ht), \quad R_0 = R(t=0), \quad (75)$$

where $R(t)$ is the "radius" of the universe, H is the Hubble constant given by

$$H = \frac{\dot{R}(t)}{R(t)} = \frac{1}{R(t)}\frac{dR(t)}{dt} \quad (76)$$

and the cosmological constant Λ is related to the Hubble constant H as follows

$$\Lambda = \frac{3H^2}{c^2}. \quad (77)$$

The parameters that appear in cosmological model, that is, in Eqs. (73) through (75), are the global time t, the "radius" of the universe $R(t)$, the mass-density of the universe ρ, the pressure of the universe p, the Hubble constant H, and the cosmological constant Λ. Also the rate of expansion $\dot{R}(t)$, as well as the acceleration $\ddot{R}(t)$, of the expanding universe enter into the equations. In the negative universe, we must let $t \to -t^*$, $R(t) \to -R^*(-t^*)$, $p \to p^*$, $H \to -H^*$, $\Lambda \to \Lambda^*$, $\dot{R}(t) \to \dot{R}^*(-t^*)$ and $\ddot{R}(t) \to -\ddot{R}^*(-t^*)$ in (73) through (75). Doing this, we find that the equations remain unchanged, so that physicists* in the negative universe formulate identical cosmological models as those in the positive universe. Consequently observers* in the negative universe make observation of that universe that are identical to the observation made of the positive universe by observers in the positive universe at all epochs.

It is easy and straight forward to demonstrate the invariance of the kinetic theory of gas, the laws of propagation of heat (conduction, convection and radiation) in continuous media, transport phenomena and other macroscopic laws of physics by following the procedure used to demonstrate the invariance of some macroscopic natural laws above with the aid of the complete form of Table 1.

5.5 Invariance of fundamental interactions in the negative universe

In a formal sense, the invariance in the negative universe of quantum chromodynamics, quantum electrodynamics, the electro-weak theory and quantum gravity must be demonstrated with the aid of the complete form of Table 1 in order to show the invariance in the negative universe of strong, electromagnetic, weak and gravitational interactions among elementary particles, as has been done for the macroscopic natural laws in this section. However we shall not attempt this. Rather we shall make recourse to the CPT theorem to demonstrate the invariance of the strong, electromagnetic and weak interactions in this section.

The CPT theorem, in a simplified form in [5, see p. 712], for instance, states that any hermitian interaction relativistically invariant, commutes with all products of the three operators C (charge conjugation), P (parity inversion), and T (time reversal) in any order. Even if an interaction is not invariant under one or two of the three operations, it must be invariant under CPT. The invariance of strong, weak and electromagnetic interactions under CPT is a well established fact in elementary particle physics [5].

Now the spacetime dimensions $-x^*$, $-y^*$, $-z^*$ and $-ct^*$ (in the Cartesian system of the dimensions of 3-space) of the third quadrant (or of the negative universe) are the products of natural parity inversion operation (P) and time reversal operation (T), (or of natural operation PT), on the spacetime dimensions x, y, z and ct of the first quadrant (or of the positive universe) in Fig. 5 or Fig. 7 of [1]. This implies, for instance, that the parity of a Schrodinger wave in the negative universe is natural inversion of parity of the symmetry-partner Schrodinger wave in the positive universe. The natural parity inversion of classical quantum-mechanical waves between the positive and negative universes equally applies to intrinsic parties of relativistic quantum mechanics and quantum field theories.

As also derived earlier in this paper and included in Table 1, the electric charge Q of a particle in the positive universe corresponds to an electric charge of equal magnitude but of opposite sign $-Q^*$ of the symmetry-partner particle in the negative universe. Thus the electric charge of a particle in the negative universe is the product of natural charge conjugation operation (C) on the electric charge of its symmetry-partner particle in the positive universe.

It follows from the foregoing two paragraphs that strong, weak and electromagnetic interactions among elementary particles in the negative universe are the products of natural operations of parity inversion (P), time reversal (T) and charge conjugation (C), in any order, (or of natural operation CPT), on strong, weak and electromagnetic interactions among elementary particles in the positive universe. The invariance of strong, weak and electromagnetic interactions among elementary particles in the negative universe follow

from this and the CPT theorem.

The invariance of classical gravitation and the General Theory of Relativity (or of gravitational interaction) at the macroscopic level in the negative universe has been demonstrated earlier in this section. The invariance in the negative universe of gravitational interaction among elementary particles follow from this. This section shall be ended with a remark that all natural laws, including the fundamental interactions among elementary particles, take on the same forms in the positive and negative universes and this is perfect symmetry of laws between the positive and negative universes.

6 On the concept of negative mass in physics

The concept of negative mass is not new in physics. The earliest speculations include the elaborate theory of negative mass by Föppl in 1897 and Schuster's contemplation of a universe with negative mass in 1898 [6] . However, as mentioned in [6], the fundamental modern paper on negative mass can be deemed to begin with Bondi [7]. As also stated in [6], Bondi pointed out that the mass in classical mechanics actually consists of three concepts namely, inertial mass, m_i, passive gravitational mass m_p, and active gravitational mass m_a. In Newton's theory of gravity, $m_i = m_p = m_a$. Also in the General Theory of Relativity, the principle of equivalence requires that, $m_i = m_p = m_a$. Although all three mass concepts are usually taken to be positive in physics, the theories do not compel this, as noted in [6].

Several papers on negative mass listed in [6] have appeared after Bondi's paper [7]. As noted in [6], most of those papers investigate the interaction and possible co-existence of particles with masses of both signs. The paper by Bonnor [6] is an important reappraisal of the concept of negative mass in the more recent time. In his analysis, Bonnor starts with the assumption m_i, $m_p > 0$, $m_a < 0$. He arrives at the result that either $m_i < 0$, $m_p < 0$ and $m_a < 0$ for all particles and bodies or $m_i > 0$, $m_p > 0$ and $m_a > 0$ for all particles and bodies. He then chooses to work with the former case, that is, all three mass concepts negative in an hypothetical universe. He substitutes negative mass into mechanics, relativity, gravitation as well as cosmology and finds that observers located in the hypothetical universe would observe strange phenomena, such as pebbles or sand falling on a stretched membrane producing tension and not compression of the membrane, and a push on a trolley causing it to accelerate towards the person who pushed it, etc. It is certain that this our universe is not the hypothetical universe containing negative mass in [6].

The hypothetical universe containing negative mass in [6] is not the negative universe isolated in the two parts of this article either. This is so because only mass is made negative while space and time dimensions, as well as other physical quantities and constants retain their signs (in our universe) in the hypothetical universe of [6]. This proviso leads to the deduced observation of strange phenomena in the hypothetical universe. On the other hand, the negative universe of this article contains negative mass along with the negation of space and time dimensions, as well as the signs of other physical quantities and constants summarized in column 5 of Table 1. As demonstrated in the preceding section, the laws of physics retain their usual forms in the negative universe, and observers located in the negative universe observe phenomena in their universe that are identical to the phenomena observed in our (or positive) universe. There are no strange phenomena in the negative universe of the two parts of this article.

This section is perhaps the conclusion of over a century-old effort towards the development of the concept of negative mass in physics. Schuster's speculation one hundred and ten years ago of a universe containing negative mass must have now been realized. This second part of this article shall be ended at this point, while possible further development of the two-world background of Special Relativity (or the two-world picture) shall be investigated elsewhere.

Submitted on October 28, 2009 / Accepted on November 03, 2009

References

1. Adekugbe A. O. J. Two-world background of Special Relativity. Part I. *Progress in Physics*, 2010, v. 1, 30–48.
2. Berestetskii V. B., Lifshitz E. M. and Pitaevskii L. P. Quantum Electrodynamics. Pergamon Press Ltd, Oxford, 1982.
3. Prigogine I. The arrow of time: an inaugural lecture by Ilya Prigogine at the Second International Centre of Relativistic Astrophysics (ICRA) Network Workshop, February 1–5, 1999, Converso O. and Sigismondi C., Editors, Publication no. 4 of ICRA Network, Pescara, Italy, 1999.
4. Akin-Ojo R. *International Journal of Theoretical Physics*, 1988, v. 27, 1023.
5. Segre E. Nuclei and particles. W. A. Benjamin, Incorporated, Reading, 1977.
6. Bonnor W. B. Negative mass in General Relativity. *Gen. Relat. Grav.*, 1989, v. 21, 1143.
7. Bondi H. Negative mass in General Relativity. *Rev. Mod. Phys.*, 1957, v. 29(3), 423–428.

Fractal Scaling Models of Natural Oscillations in Chain Systems and the Mass Distribution of the Celestial Bodies in the Solar System

Hartmut Müller

Global Scaling Research Institute in memoriam Leonhard Euler, Munich, Germany. E-mail: info@globalscaling.de

The present paper interprets matter as a chain system of quantum harmonic oscillators. A fractal spectral model of resonant oscillations in chain systems of protons generates a scaling mass spectrum, that reproduces the mass distribution of the celestial bodies in the Solar System.

1 Introduction

Fractal scaling models [1] of natural oscillations in chain systems of harmonic oscillators are not based on any statements about the nature of the link or interaction between the elements of the oscillating chain system. Therefore the model statements are quite generally, what opens a wide field of possible applications.

In comparison with empty cosmic space, celestial bodies (stars, planets, moons, asteroids) are compressed matter and the contribution of nucleons to the bodies mass is about 99%. In the framework of the standard particle model, protons and neutrons are baryons, in which the proton connects to a lower quantum energy level and a much more stable state than the neutron. In addition, the proton and neutron have similar rest masses, what permits us to interpret protons and neutrons as similar quantum oscillators with regard to their rest masses.

Based on a fractal scaling model [1] of natural oscillations in this paper we will interpret matter as a chain system of many oscillating protons and find out spectral ranges where the oscillation process stability and energy efficiency are relative high or low.

2 Methods

On the base of continued fraction method [1] we will search the natural frequencies of a chain system of many vibrating protons on the lowest energy level (ground stage) in this form:

$$f = f_p \exp(S), \tag{1}$$

f is a natural frequency of a chain system of vibrating protons, f_p is the natural oscillation frequency of one proton, S is a finite continued fraction with integer elements:

$$S = n_0 + \cfrac{1}{n_1 + \cfrac{1}{n_2 + \ddots + \frac{1}{n_k}}} = [n_0; n_1, n_2, \ldots, n_k], \tag{2}$$

where $n_0, n_1, n_2, \ldots, n_k \in Z$. The continued fractions (2) are in the canonical form and have a discrete spectrum of eigenvalues. With the help of the Lagrange transformation [2] every continued fraction with integer partial denominators can be represented as a continued fraction with natural partial denominators, that's always convergent. In this paper we will investigate spectra generated by convergent continued fractions (2). The present paper follows the Terskich [3] definition of a chain system, where the interaction between the elements proceeds only in their movement direction.

Model spectra (2) are not only logarithmic-invariant, but also fractal, because the discrete hyperbolic distribution of natural frequencies repeats itself on each spectral level k. We investigate continued fractions (2) with a finite quantity of layers k, which generate discrete spectra, because in this case all continued fractions S represent rational numbers. Therefore the free link n_0 and the partial denominators n_1 can be interpreted as "quantum numbers".

The partial denominators n_1 run through positive and negative integer values. Maximum spectral density areas (spectral nodes) arise automatically on the distance of one logarithmic unit, where $|n_1| \to \infty$. Fig.1 shows the spectrum on the first layer $k = 1$ for $|n_1| = 2, 3, 4, \ldots$ and $|n_0| = 0, 1, 2, \ldots$ (logarithmic representation). Integer S-values are labeled.

Fig. 1: The spectrum (2) on the first layer $k = 1$, for $|n_1| = 2, 3, 4, \ldots$ and $|n_0| = 0, 1, 2, \ldots$ (logarithmic representation). Integer S-values are labeled.

Ranges of relative low spectral density (spectral gaps) and ranges of relative high spectral density (spectral nodes) arise on each spectral layer. In addition to the first spectral layer, Fig. 2 shows the second spectral layer $k = 2$ for $|n_2| = 2, 3, 4, \ldots$ and $|n_1| = 2$ (logarithmic representation).

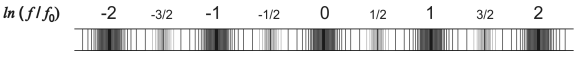

Fig. 2: The spectrum (2) on the first layer $k = 1$, for $|n_0| = 0, 1, 2, \ldots$ and $|n_1| = 2, 3, 4, \ldots$ and, in addition, the second layer $k = 2$ for $|n_1| = 2$ and $|n_2| = 2, 3, 4, \ldots$ (logarithmic representation).

In the spectral node ranges, where the spectral density reachs local maximum, natural frequencies are distributed maximum densely, so that near a spectral node almost each frequency is a natural frequency. The energy efficiency of

Celestial body	Body mass m, kg	$\ln(m/m_p)$	S	d, %
15 Eunomia (A)	3.12×10^{19} [8]	106.54	[106; 2]	0.037
Mimas (S)	$(3.7493 \pm 0.0031) \times 10^{19}$ [7]	106.73	[106; 2]	0.216
Miranda (U)	$(6.59 \pm 0.75) \times 10^{19}$ [8]	107.29	[107; 2]	−0.195
10 Hygiea (A)	$(8.98 \pm 0.01) \times 10^{19}$ [8]	107.60	[107; 2]	0.093
Enceladus (S)	$(1.08022 \pm 0.00101) \times 10^{20}$ [7]	107.78	[108]	−0.204
2 Pallas (A)	$(2.11 \pm 0.26) \times 10^{20}$ [8]	108.50	[108; 2]	0.001
4 Vesta (A)	$(2.67 \pm 0.02) \times 10^{20}$ [8]	108.69	[108; 2]	0.175
Tethys (S)	$(6.17449 \pm 0.00132) \times 10^{20}$ [7]	109.53	[109; 2]	0.028
1 Ceres (P)	$(9.43 \pm 0.07) \times 10^{20}$ [8, 9]	109.95	[110]	−0.045
Dione (S)	$(1.095452 \pm 0.000168) \times 10^{21}$ [7]	110.10	[110]	0.091
Umbriel (U)	$(1.172 \pm 0.135) \times 10^{21}$ [10]	110.10	[110]	0.091
Ariel (U)	$(1.350 \pm 0.120) \times 10^{21}$ [10]	110.23	[110]	0.209
Charon (P)	$(1.52 \pm 0.06) \times 10^{21}$ [11]	110.43	[110; 2]	−0.064
Iapetus (S)	$(1.805635 \pm 0.000375) \times 10^{21}$ [7]	110.60	[110; 2]	0.090
Rhea (S)	$(2.306518 \pm 0.000353) \times 10^{21}$ [7]	110.84	[111]	−0.144
Oberon (U)	$(3.014 \pm 0.075) \times 10^{21}$ [12]	111.12	[111]	0.108
Titania (U)	$(3.53 \pm 0.09) \times 10^{21}$ [12]	111.28	[111; 2]	−0.197
Haumea (P)	$(4.006 \pm 0.040) \times 10^{21}$ [13]	111.40	[111; 2]	−0.090
Pluto (P)	$(1.305 \pm 0.007) \times 10^{22}$ [11]	112.57	[112; 2]	0.018
Eris (P)	$(1.67 \pm 0.02) \times 10^{22}$ [14]	112.83	[113]	−0.150
Triton (N)	2.14 ± 10^{22} [15]	113.07	[113]	0.062
Europa (J)	4.80 ± 10^{22} [16]	113.88	[114]	−0.105
Moon (E)	7.3477 ± 10^{22}	114.30	[114; 2]	−0.175
Io (J)	$(8.9319 \pm 0.0003) \times 10^{22}$ [16]	114.50	[114; 2]	0.001
Callisto (J)	$(1.075938 \pm 0.000137) \times 10^{23}$ [17]	114.69	[114; 2]	0.166
Titan (S)	$(1.3452 \pm 0.0002) \times 10^{23}$ [7]	114.91	[115]	−0.078
Ganymede (J)	$(1.4819 \pm 0.0002) \times 10^{23}$ [16]	115.00	[115]	0.001
Mercury	$(3.3022 \pm 0.0001) \times 10^{23}$	115.81	[116]	−0.164
Mars	$(6.4185 \pm 0.0001) \times 10^{23}$	116.47	[116; 2]	−0.026
Venus	$(4.8685 \pm 0.0001) \times 10^{24}$	118.50	[118; 2]	0.001
Earth	$(5.9722 \pm 0.0006) \times 10^{24}$ [18]	118.69	[118; 2]	0.160
Uranus	$(8.6810 \pm 0.0013) \times 10^{25}$ [12]	121.38	[121; 2]	−0.099
Neptune	$(1.0243 \pm 0.0015) \times 10^{26}$	121.55	[121; 2]	0.041
Saturn	$(5.6846 \pm 0.0001) \times 10^{26}$	123.27	[123; 2]	−0.186
Jupiter	$(1.8986 \pm 0.0001) \times 10^{27}$	124.47	[124; 2]	−0.024
Sun	$(1.9884 \pm 0.0002) \times 10^{30}$ [18]	131.42	[131; 2]	−0.061

Table 1: The masses of celestial bodies — planets, dwarf planets (P), asteroids (A), moons of Jupiter (J), Saturn (S), Uranus (U), Neptune (N) and Earth (E) and the S-values (6) of the nearest spectral nodes. The relative deviation $d = \big(\ln(m/m_p) - S\big)/S$ is indicated in percents.

natural oscillations is very high. Therefore, if a frequency of an oscillation process is located near a node of the fractal spectrum (2), the process energy efficiency (degree of effectiveness) should be relative high. More detailed this topic is described in [1].

Let's assume that the oscillation amplitudes are low, the oscillations are harmonic and the energy level E_f of the vibrating protons depends only on their oscillation frequency (h is the Planck constant):

$$E_f = hf\,. \tag{3}$$

Atomic nucleuses arise in the result of high energy processes of nucleosynthesis. Einstein's formula defines not only the connection between the rest energy and rest mass of nucleons, but also between binding energy and the mass defect of an atomic nucleus. Therefore we assume that the rest mass m of our model matter corresponds to the energy E_m:

$$E_m = mc^2\,. \tag{4}$$

Let's assume that the basis of nucleosynthesis is harmonic oscillations of protons and the energy (4) is identically

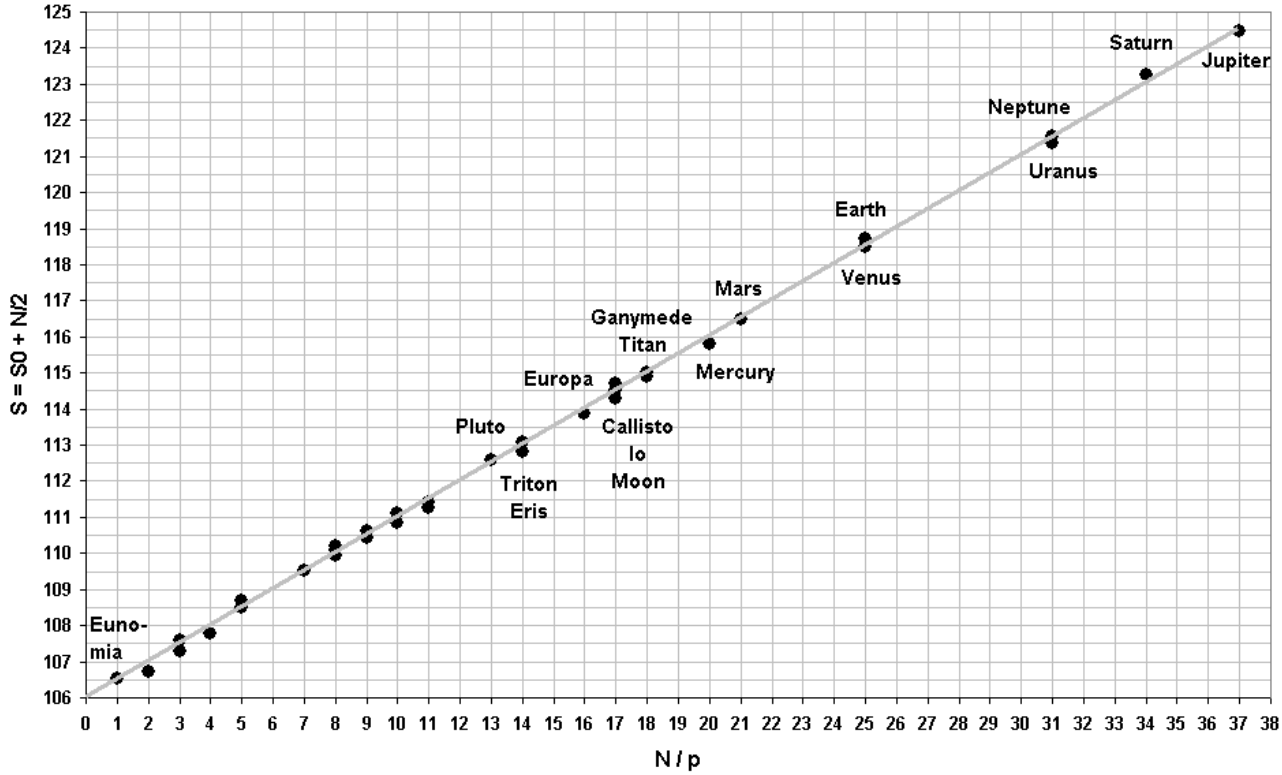

Fig. 3: The S-trajectory for $S_0 = [106]$ and $p = 1$. Logarithmic scaling of Eunomia to Jupiter body mass.

with (3). In this case we can write:

$$m = f\frac{h}{c^2}\,. \tag{5}$$

In the framework of our oscillation model (1) the equation (5) means not only that mass can be changed into energy, but also that quantum oscillations generate the mass spectrum of our model matter. Under consideration of (1) now we can create a fractal scaling model of the natural mass spectrum of our model matter of vibrating protons. This mass spectrum is described by the same continued fraction (2), for $m_p = f_p\frac{h}{c^2}$:

$$\ln\frac{m}{m_p} = [n_0; n_1, n_2, \ldots, n_k]\,. \tag{6}$$

Consequently, the frequency spectrum (2) and the mass spectrum (6) are isomorphic, and m_p is the proton rest mass $1.672621637(83) \times 10^{-27}$ kg [4]. As mentioned already, we assume that mass generation processes are based on quantum natural oscillation processes. Celestial bodies are compressed matter, which consist of nucleons over 99%. Therefore we expect that the distribution of the celestial bodies in the proton resonance mass spectrum is not random and near spectral nodes the formation probability of massive bodies is maximum. Like in the Kundt's tube [5], near resonance nodes the matter accumulation reachs maximum intensity. The mass spectrum (6) is fractal and consequently it has a clear hierarchical structure, in which continued fractions (2) of the form $[n_0]$ and $[n_0; 2]$ define main spectral nodes, as Fig. 2 shows.

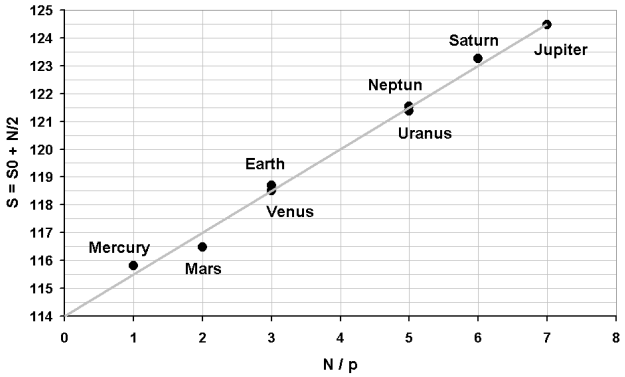

Fig. 4: The S-trajectory for $S_0 = [114]$ and $p = 3$. Possibly, the extrasolar planet Gliese 581d could be a candidate of the node $S = [120]$.

3 Results

In the present paper we will compare the scaling mass spectrum (6) of our model matter in the range of 10^{19} kg to 10^{30} kg with the mass distribution of well-known celestial bodies. These are asteroids, planetoids, moons and planets of the Solar System (including the Sun), which masses were measured precisely enough and which are massive enough to be rounded by their own gravity.

For example, to locate the mass of the planet Venus in the scaling mass spectrum (6) of our model matter, one divides the Venus body mass by the proton rest mass and represents

Particle	Rest mass m, MeV/c^2 [20]	$\ln(m/m_p)$	S	d, %
electron	0.510998910 ± 0.000000013	−7.515	[−7; −2]	−0.206
proton	938.27203 ± 0.00008	0.000	[0]	0.000
W	80398 ± 25	4,451	[4; 2]	1,089
Z	91187.6 ± 2.1	4,577	[4; 2]	1,711

Table 2: The rest masses of the electron, proton and the W-Z-bosons and the S-values (6) of the nearest spectral nodes. The relative deviation $d = \left(\ln\left(m/m_p\right) - S\right)/S$ is indicated in percent.

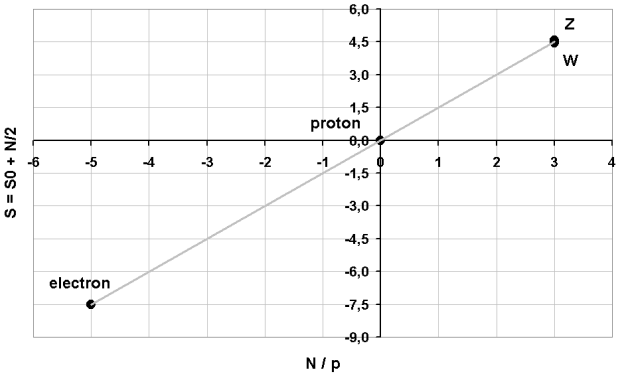

Fig. 5: The electron and W-Z-bosons rest masses lie on the S-trajectory for $S_0 = [0]$ and $p = 3$. It's the same S-trajectory that shows Fig. 4, but prolonged down to negative N.

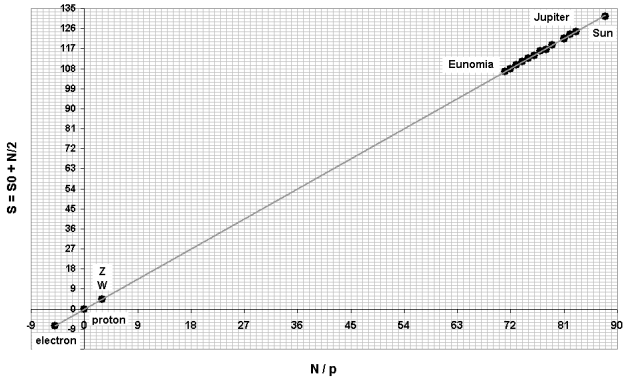

Fig. 6: The S-trajectory for $S_0 = [0]$ and $p = 3$. Logarithmic scaling of the electron rest mass to the body mass of the Sun.

the logarithm as a continued fraction:

$$S_{venus} = \ln\frac{m_{venus}}{m_p} = \ln\left(\frac{4.869\times10^{24}\,\mathrm{kg}}{1.67262\times10^{-27}\,\mathrm{kg}}\right) \cong \cong 118.50 = 118 + \frac{1}{2}. \quad (7)$$

The analysis (6) of the Venus body mass takes the result $n_0 = 118$, $n_1 = 2$. This means, that the Venus body mass corresponds to a spectral node on the first layer $k = 1$ of the spectrum (6). The Sun mass is near the spectral node [131; 2]. It's also correct for the Alpha Centauri A and B masses. The Alpha Aquilae (Altair) mass is about 1.7 solar masses, that's near the node [132]. Table 1 shows the logarithms (6) calculated from the measured masses m of the celestial bodies and the S-values of the nearest spectral nodes.

Table 1 shows, that spectral nodes are occupied by bodies which have maximum mass in a local group or family. For example, the spectral node [115] is occupied by Ganymede and Titan, the most massive moons of Jupiter and Saturn, the spectral node [113] is occupied by Triton, the most massive moon of Neptune, the body mass of Eris, the largest defined dwarf planet, is also near the spectral node [113], but the spectral node [110] is occupied by Ceres, the most massive body of the asteroid belt. Mercury's mass is near the node [116]. Possibly, not Eris, but Mercury is the most massive dwarf planet in the Solar System. Actually, Mercury behaves like a dwarf planet, because it has the highest eccentricity of all the Solar System planets and it has the smallest axial tilt.

For the nodes $[n_0]$ and $[n_0; 2]$ the finite continued fraction (2) is $S = n_0 + 1/n_1$ and the corresponding discrete mass values can be defined by linear S-trajectories, in which $N \in Z$:

$$S = S_0 + \frac{N}{2}. \quad (8)$$

The prime divisibility of $N = pn$, in which p is a prime factor of N, defines sets of S-trajectories which form different sequences of mass-values m of the discrete spectrum (6).

S-trajectories (8) present the discrete scaling mass distribution (6) very clear and can be interpreted as exponential equivalents to linear square-mass trajectories, which are a well-known systematic feature in the hadrons spectrum [6]. Fig. 3 shows the S-trajectory for $S_0 = [106]$ and $p = 1$. Largest bodies are labeled. Possibly, vacant nodes are occupied by extrasolar bodies or bodies still to be discovered in the Solar System.

Possibly, the existence of the discrete spectrum (6) in the range of celestial bodies masses can be interpreted as "macroscopic quantization" [19]. The larger the bodies the more distinctive is this phenomenon. This can be recognized well at the example of the 8 largest planets in the Solar System, as Fig. 4 shows.

For $S_0 = [0]$ and every p is $m_0 = m_p$, so that every S-trajectory can be prolonged down to the proton rest mass. Also the electron and W-Z-bosons rest masses lie on the S-trajectory for $S_0 = [0]$ and $p = 3$, as Fig. 5 shows. Already within the eighties the scaling exponent 3/2 was found in the distribution of particle masses by Valery A. Kolombet [21].

Table 2 shows the logarithms (6) calculated from the measured particle rest masses, and the S-values of the nearest spectral nodes.

The S-trajectory in Fig. 5 is the same as the S-trajectory in Fig. 4, but prolonged down to the electron rest mass for $S = [-7; -2]$. Possibly, there is a fundamental link between particle rest masses and the masses of celestial bodies. Fig. 6 shows the S-trajectory for $S_0 = [0]$ and $p = 3$ in the range of $-9 \leqslant S \leqslant 135$, of the electron rest mass to the body mass of the Sun.

4 Resume

In the framework of the present model discrete scaling distributions arise as result of natural oscillations in chain systems of harmonic oscillators. Particularly, the observable mass distribution of celestial bodies arise as result of natural oscillations in chain systems of protons, that can be understood as contribution to the fundamental link between quantum- and astrophysics. Possibly, the high energy efficiency of natural oscillations is the cause of the fractal scaling distribution of matter in the universe.

Acknowledgements

The author is deeply grateful to S. E. Shnoll, V. A. Panchelyuga and V. A Kolombet for valuable discussions and support.

Submitted on October 28, 2009 / Accepted on November 10, 2009

References

1. Muller H. Fractal scaling models of resonant oscillations in chain systems of harmonic oscillators. *Progress in Physics*, 2009.
2. Khintchine A. Ya. Continued fractions. University of Chicago Press, Chicago, 1964.
3. Terskich V. P. The continued fraction method. Leningrad, 1955 (*in Russian*).
4. Physical constants. Particle Data Group, www.pdg.lbl.gov
5. Kundt A. Uber eine neue Art akustischer Staubfiguren und uber die Anwendung derselben zur Bestimmung der Schallgeschwindigkeit in festen Korpern und Gasen. *Annalen der Physik*, Leipzig, 1866, v. 127 (4), 497–523.
6. Forkel H., Beyer M., Frederico T. Linear square-mass trajectories of radially and orbitally excited hadrons in holographic QCD. arXiv: 0705.1857v2.
7. Jacobson R., Antreasian P., Bordi J. et al. The Gravity Field of the Saturnian System from Satellite Observations and Spacecraft Tracking Data. *Astronomical Journal*, 2006, v. 132, 2520–2526.
8. Baer J., Steven R. Astrometric masses of 21 asteroids, and an integrated asteroid ephemeris. Celestial Mechanics and Dynamical Astronomy. *Springer Science and Business Media*, 2008, v. 100, 27–42.
9. Carry B. et al. Near-Infrared Mapping and Physical Properties of the Dwarf-Planet Ceres. *Astronomy and Astrophysics*, 2007, v. 478, 235-244.
10. Uranus System Nomenclature Table Of Contents. Gazetteer of Planetary Nomenclature. USGS Astrogeology, 2009.
11. Marc W., William M, Eliot F et al. Orbits and photometry of Pluto's satellites: Charon, S/2005 P1, and S/2005 P2. *Astronomical Journal*, 2006, v. 132 (1), 290–298.
12. Jacobson R, Campbell J, Taylor A, Synnott S. The masses of Uranus and its major satellites from Voyager tracking data and Earth based Uranian satellite data. *Astronomical Journal*, 1992, v. 103 (6), 2068–2078.
13. Ragozzine D., Brown M. Orbits and Masses of the Satellites of the Dwarf Planet Haumea = 2003 EL61. *Astronomical Journal*, 2009. arXiv: 0903.4213v1.
14. Brown M, Schaller E. The Mass of Dwarf Planet Eris. *Science*, 2007, v. 316 (5831), 1585.
15. Neptune System Nomenclature Table Of Contents. Gazetteer of Planetary Nomenclature. USGS Astrogeology, 2009.
16. Showman A., Malhotra R. The Galilean Satellites. *Science*, 1999, v. 286, 77–84.
17. Anderson J., Jacobson R. et al. Shape, mean radius, gravity field and interior structure of Callisto. *Icarus*, v. 153, 157–161.
18. Astrophysical Constants and Parameters. Particle Data Group, www.pdg.lbl.gov
19. Shnoll S. et al. Realization of discrete states during fluctuations in macroscopic processes, *Physics Uspekhi*, 1998, v. 41 (10), 1025–1035.
20. Particle listings. Particle Data Group, www.pdg.lbl.gov
21. Kolombet V. Macroscopic fluctuations, masses of particles and discrete space-time, *Biofizika*, 1992, v. 36, 492–499 (in Russian).

Dynamical 3-Space Predicts Hotter Early Universe: Resolves CMB-BBN ^{7}Li and ^{4}He Abundance Anomalies

Reginald T. Cahill

School of Chemistry, Physics and Earth Sciences, Flinders University, Adelaide 5001, Australia
E-mail: Reg.Cahill@flinders.edu.au

The observed abundances of ^{7}Li and ^{4}He are significantly inconsistent with the predictions from Big Bang Nucleosynthesis (BBN) when using the ΛCDM cosmological model together with the value for $\Omega_B h^2 = 0.0224 \pm 0.0009$ from WMAP CMB fluctuations, with the value from BBN required to fit observed abundances being $0.009 < \Omega_B h^2 < 0.013$. The dynamical 3-space theory is shown to predict a 20% hotter universe in the radiation-dominated epoch, which then results in a remarkable parameter-free agreement between the BBN and the WMAP value for $\Omega_B h^2$. The dynamical 3-space also gives a parameter-free fit to the supernova redshift data, and predicts that the flawed ΛCDM model would require $\Omega_\Lambda = 0.73$ and $\Omega_M = 0.27$ to fit the 3-space dynamics Hubble expansion, and independently of the supernova data. These results amount to the discovery of new physics for the early universe that is matched by numerous other successful observational and experimental tests.

1 Introduction

Astrophysical observed abundances of ^{7}Li and ^{4}He are significantly inconsistent with the predictions from Big Bang Nucleosynthesis (BBN) when using the ΛCDM cosmological model, with the value for* $\Omega_B h^2 = 0.0224 \pm 0.0009$ from WMAP CMB fluctuations being considerably different from the value from BBN required to fit observed abundances $0.009 < \Omega_B h^2 < 0.013$ (Coc *et al.* [1]).

The most significant long-standing discrepancy is that of ^{7}Li because the pre-Galactic lithium abundance inferred from observations of metal-poor (Population II) stars is at least 2–3 times smaller than predicted by BBN–ΛCDM. The ^{7}Li problem has been most difficult to understand as its primordial abundance should be the most reliable, because of the higher observational statistics and an easier extrapolation to primordial values. Various possible resolutions were discussed in [2], with the conclusion that the lithium problem most likely points to new physics.

It is shown herein that the new physics of a dynamical 3-space [4–6] results in a 20% hotter universe during the radiation dominated epoch, and in a parameter-free analysis the BBN abundances are brought into close agreement with the WMAP value for the baryonic density $\Omega_B h^2 = 0.0224 \pm 0.0009$. The dynamical 3-space also gives a parameter free account of the supernova redshift data, and fitting the ΛCDM to the dynamical 3-space model requires $\Omega_\Lambda = 0.73$ and $\Omega_m = 0.27$, independently of the supernova data. There are numerous other experimental and observational confirmations of the new physics [4, 5], including a recent analysis of the NASA/JPL spacecraft earth-flyby Doppler-shift anomalies [7,8]. The conclusion is that the ΛCDM is flawed, with precision data from the supernova redshifts [10–12], and WMAP CMB fluctuations [3] in conjunction with BBN computations finally ruling out this model. As briefly noted below that ΛCDM is essentially Newtonian gravity, and various data have indicated the failure of Newtonian gravity.

*$H_0 = 100\,h$ km/s/Mpc defines h. Ω_B is baryon density relative to critical density ρ_c.

2 Dynamical 3-space

Newton's inverse square law of gravity [9] has the differential form

$$\nabla \cdot \mathbf{g} = -4\pi G\rho\,, \qquad \nabla \times \mathbf{g} = 0\,, \tag{1}$$

for the matter acceleration field $\mathbf{g}(\mathbf{r}, t)$. Application of this to spiral galaxies and the expanding universe has lead to many problems, including, in part, the need to invent dark energy and dark matter. However (1) has a unique generalisation that resolves these problems. In terms of a velocity field $\mathbf{v}(\mathbf{r}, t)$ (1) has an equivalent form [4, 5]

$$\nabla \cdot \left(\frac{\partial \mathbf{v}}{\partial t} + (\mathbf{v} \cdot \nabla)\,\mathbf{v} \right) = -4\pi G\rho\,, \qquad \nabla \times \mathbf{v} = 0\,, \tag{2}$$

where now

$$\mathbf{g} = \frac{\partial \mathbf{v}}{\partial t} + (\mathbf{v} \cdot \nabla)\,\mathbf{v}, \tag{3}$$

is the Euler acceleration of the substratum that has velocity $\mathbf{v}(\mathbf{r}, t)$. Because of the covariance of v under a change of the spatial coordinates only relative internal velocities have an ontological existence — the coordinates $\mathbf{r}$ then merely define a mathematical embedding space. In the form (2) Newton's law permits a unique generalisation by adding a term of the same order but which can preserve the inverse square law outside of spherical masses,

$$\nabla \cdot \left(\frac{\partial \mathbf{v}}{\partial t} + (\mathbf{v} \cdot \nabla)\,\mathbf{v} \right) + \frac{\alpha}{8} \left((\mathrm{tr}\, D)^2 - \mathrm{tr}\,(D^2) \right) = -4\pi G\rho,$$

$$\nabla \times \mathbf{v} = 0\,, \qquad D_{ij} = \frac{1}{2}\left(\frac{\partial v_i}{\partial x_j} + \frac{\partial v_j}{\partial x_i}\right). \tag{4}$$

Eqn. (4) has two fundamental constants: G and α. Experimental bore-hole g anomaly data reveals that α is the fine structure constant $\approx 1/137$ to within experimental errors [4, 5]. Eqn (4) has a rich variety of solutions: (i) black holes with a non-inverse square law acceleration field that explains the supermassive black hole mass spectrum and the flat rotation curves of spiral galaxies without the need for dark matter — these black holes may be primordial as well as induced, (ii) the bore-hole g-anomaly, (iii) gravitational light bending, (iv) a parameter free fit to the supernova data [6] without the need for dark energy or dark matter, and other effects. As well the 3-space field $\mathbf{v}(\mathbf{r}, t)$ has been directly detected in numerous laboratory experiments, and now in Doppler shift data from spacecraft earth-flybys [8].

Eqn (4) gives a different account of the Hubble expansion of the universe, and here we outline a new account of the thermal history of the universe. The results are very different from the predictions of the Friedmann equation — the standard equation of cosmology since its inception (FRW-GR). In the Friedmann equations the expansion of the universe is determined solely by the presence of matter or energy, as would be expected since it derives from (1), and it then requires, at the present epoch, some 73% dark energy, 23% dark matter and 4% baryonic matter. Eqn (4), in contrast, requires only the normal matter — this is because (4) has an expanding 3-space solution even in the absence of matter/energy. Fitting the Friedmann Hubble function $H(z)$ to the Hubble function from (4), using the usual distance-redshift modulus as a measure, indeed permits these dark energy and dark matter quantities to be simply predicted, independently of the observed supernova data, for these are the values that best-fit the ΛCDM to the observed uniformly expanding 3-space Hubble solution.

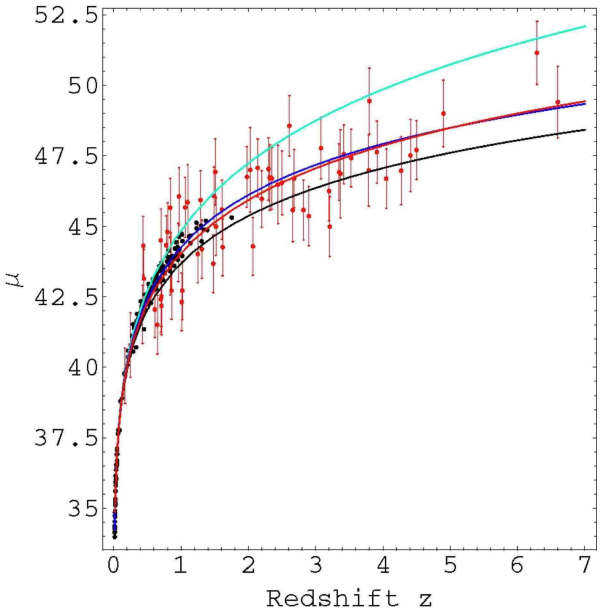

Fig. 1: Hubble diagram showing the supernovae data using several data sets, and the Gamma-Ray-Bursts data (with error bars). Upper curve (green) is ΛCDM "dark energy" only $\Omega_\Lambda = 1$, lower curve (black) is ΛCDM matter only $\Omega_M = 1$. Two middle curves show best-fit of ΛCDM "dark energy"—"dark-matter" (blue) and dynamical 3-space prediction (red), and are essentially indistinguishable. We see that the best-fit ΛCDM "dark energy"—"dark-matter" curve essentially converges on the uniformly-expanding parameter-free dynamical 3-space prediction. The supernova data shows that the universe is undergoing a uniform expansion, although not reported as such in [10–12], wherein a fit to the FRW-GR expansion was forced, requiring "dark energy", "dark matter" and a future "exponentially accelerating expansion".

3 Expanding universe from dynamical 3-space

Let us now explore the expanding 3-space from (4). Critically, and unlike the FLRW-GR model, the 3-space expands even when the energy density is zero. Suppose that we have a radially symmetric effective density $\rho(r, t)$, modelling normal matter and EM radiation, and that we look for a radially symmetric time-dependent flow $\mathbf{v}(\mathbf{r}, t) = v(r, t)\,\hat{\mathbf{r}}$ from (4). Then $v(r, t)$ satisfies the equation, with $v' = \frac{\partial v(r,t)}{\partial r}$,

$$\frac{\partial}{\partial t}\left(\frac{2v}{r} + v'\right) + vv'' + 2\frac{vv'}{r} + (v')^2 + \\ + \frac{\alpha}{4}\left(\frac{v^2}{r^2} + \frac{2vv'}{r}\right) = -4\pi G\rho(r, t). \tag{5}$$

Consider first the zero energy case $\rho = 0$. Then we have a Hubble solution $v(r, t) = H(t)r$, a centreless flow, determined by

$$\dot{H} + \left(1 + \frac{\alpha}{4}\right)H^2 = 0, \tag{6}$$

with $\dot{H} = \frac{dH}{dt}$. We also introduce in the usual manner the scale factor $a(t)$ according to $H(t) = \frac{\dot{a}}{a}$. We then obtain the solution

$$H(t) = \frac{1}{(1 + \frac{\alpha}{4})\,t} = H_0\,\frac{t_0}{t}; \qquad a(t) = a_0\left(\frac{t}{t_0}\right)^{4/(4+\alpha)} \tag{7}$$

where $H_0 = H(t_0)$ and $a_0 = a(t_0) = 1$, with t_0 the present age of the universe. Note that we obtain an expanding 3-space even where the energy density is zero — this is in sharp contrast to the FLRW-GR model for the expanding universe, as shown below. The solution (7) is unique — it has one free parameter — which is essentially the age of the universe $t_0 = t_H = 1/H_0$, and clearly this cannot be predicted by physics, as it is a purely contingent effect — the age of the universe when it is observed by us. Below we include the small effect of ordinary matter and EM radiation.

We can write the Hubble function $H(t)$ in terms of $a(t)$ via the inverse function $t(a)$, i.e. $H(t(a))$ and finally as $H(z)$,

where the redshift observed now, relative to the wavelengths at time t, is $z = a_0/a - 1$. Then we obtain

$$H(z) = H_0(1+z)^{1+\alpha/4}. \tag{8}$$

To test this expansion we need to predict the relationship between the cosmological observables, namely the apparent photon energy-flux magnitudes and redshifts. This involves taking account of the reduction in photon count caused by the expanding 3-space, as well as the accompanying reduction in photon energy. The result is that the dimensionless "energy-flux" luminosity effective distance is then given by

$$d_L(z) = (1+z)\int_0^z \frac{H_0\, dz'}{H(z')} \tag{9}$$

and the distance modulus is defined as usual by

$$\mu(z) = 5\log_{10}(d_L(z)) + m\,. \tag{10}$$

Because all the selected supernova have the same absolute magnitude, m is a constant whose value is determined by fitting the low z data.

Using the Hubble expansion (8) in (9) and (10) we obtain the middle curve (red) in Fig. 1, yielding an excellent agreement with the supernovae and GRB data. Note that because $\alpha/4$ is so small it actually has negligible effect on these plots. But that is only the case for the homogeneous expansion — the α dynamics can result in large effects such as black holes and large spiral galaxy rotation effects when the 3-space is inhomogeneous, and particularly precocious galaxy formation. Hence the dynamical 3-space gives an immediate account of the universe expansion data, and does not require the introduction of a cosmological constant or "dark energy" nor "dark matter".

4 Expanding universe — matter and radiation only

When the energy density is not zero we need to take account of the dependence of $\rho(r,t)$ on the scale factor of the universe. In the usual manner we thus write

$$\rho(r,t) = \frac{\rho_m}{a(t)^3} + \frac{\rho_r}{a(t)^4}, \tag{11}$$

for ordinary matter and EM radiation. Then (5) becomes for $a(t)$

$$\frac{\ddot{a}}{a} + \frac{\alpha}{4}\frac{\dot{a}^2}{a^2} = -\frac{4\pi G}{3}\left(\frac{\rho_m}{a^3} + \frac{\rho_r}{a^4}\right), \tag{12}$$

giving

$$\dot{a}^2 = \frac{8\pi G}{3}\left(\frac{\rho_m}{a} + \frac{\rho_r}{2a^2}\right) - \frac{\alpha}{2}\int \frac{\dot{a}^2}{a}\, da + f\,, \tag{13}$$

where f is the integration constant. In terms of $\dot{a}^2$ this has the solution

$$\dot{a}^2 = \frac{8\pi G}{3}\left(\frac{\rho_m}{(1-\frac{\alpha}{2})\,a} + \frac{\rho_r}{(1-\frac{\alpha}{4})\,2a^2} + ba^{-\alpha/2}\right), \tag{14}$$

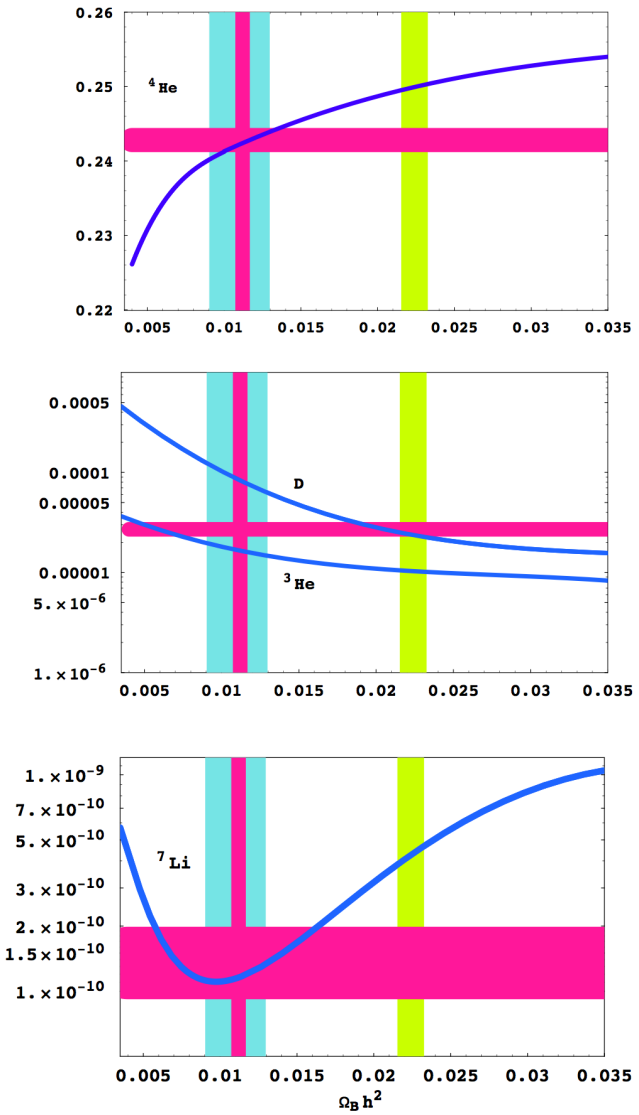

Fig. 2: Shows the Big Bang nucleosynthesis (BBN) number abundances for: the ^{4}He mass fraction (top), D and ^{3}He (middle) and ^{7}Li (bottom) relative to hydrogen vs $\Omega_B h^2$, as blue curves, from Coc *et al.* [1]. Horizontal (red) bar-graphs show astrophysical abundance observations. The vertical (yellow) bar-graphs show the values $\Omega_B h^2 = 0.0224 \pm 0.0009$ from WMAP CMB fluctuations, while the (blue) bar-graph $0.009 < \Omega_B h^2 < 0.013$ shows the best-fit at 68% CL from the BBN for the observed abundances [1]. We see that the WMAP data is in significant disagreement with the BBN results for $\Omega_B h^2$, giving, in particular, the ^{7}Li abundance anomaly within the ΛCDM model. The dynamical 3-space model has a different and hotter thermal history in the radiation dominated epoch, and the corresponding BBN predictions are easily obtained by a re-scaling of the WMAP value $\Omega_B h^2$ to $\Omega_B h^2/2$. The resultant $\Omega_B h^2 = 0.0112 \pm 0.0005$ values are shown by the vertical (red) bar-graphs that center on the BBN $0.009 < \Omega_B h^2 < 0.013$ range, and which is now in remarkable agreement with BBN computations. So while the BBN — WMAP inconsistency indicates a failure of the Friedmann FRW-GR Big Bang model, it is another success for the new physics entailed in the dynamical 3-space model. Plots adapted from [1].

which is easily checked by substitution into (13), and where b is the integration constant. We have written an overall factor of $8\pi G/3$ even though b, in principle, is independent of G. This gives b convenient units of matter density, but which does not correspond to any actual energy. From now on we shall put $\alpha = 0$. Finally we obtain from (14)

$$t(a) = \int_0^a \frac{da}{\sqrt{\frac{8\pi G}{3}\left(\frac{\rho_m}{a} + \frac{\rho_r}{2a^2} + b\right)}}\,. \qquad (15)$$

When $\rho_m = \rho_r = 0$, (15) reproduces the expansion in (7), and so the density terms in (14) give the modifications to the dominant purely-spatial expansion, which we have noted above already gives an excellent account of the red-shift data. Having $b \neq 0$ simply asserts that the 3-space can expand even when the energy density is zero — an effect missing from FLRW-GR cosmology. From (14) we obtain*

$$\overline{H}(z)^2 = H_0{}^2\left(\overline{\Omega}_m(1+z)^3 + \frac{\overline{\Omega}_r(1+z)^4}{2} + \overline{\Omega}_s(1+z)^2\right), \qquad (16)$$

$$\overline{\Omega}_m \equiv \rho_m/\rho_c\,, \quad \overline{\Omega}_r \equiv \rho_r/\rho_c\,, \quad \overline{\Omega}_s \equiv b/\rho_c\,, \qquad (17)$$

$$\overline{\Omega}_m + \frac{\overline{\Omega}_r}{2} + \overline{\Omega}_s = 1\,, \qquad (18)$$

$$H_0 = \left(\frac{8\pi G}{3}\left(\rho_m + \frac{\rho_r}{2} + b\right)\right)^{1/2} \equiv \left(\frac{8\pi G}{3}\rho_c\right)^{1/2}, \qquad (19)$$

which defines the usual critical energy density ρ_c, but which here is merely a form for H_0 — it has no interpretation as an actual energy density, unlike in FRW-GR. Note the factor of 2 for $\overline{\Omega}_r$, which is a key effect in this paper, and is not in FRW-GR. In the dynamical 3-space model these $\overline{\Omega}$'s do not correspond to the composition of the universe, rather to the relative dynamical effects of the matter and radiation on the intrinsic 3-space expansion dynamics. $H_0 = 73$ km/s/Mpc with $\overline{\Omega}_m \approx \Omega_B = 0.04$ and $\overline{\Omega}_s = 0.96$ gives an age for the universe of $t_0 = 12.6$ Gyrs, while (22) with $\Omega_M = 0.27$ and $\Omega_\Lambda = 0.73$ gives $t_0 = 13.3$ Gyrs, $\overline{\Omega}_r = \Omega_r = 8.24 \times 10^{-5}$.

5 Friedmann-GR standard ΛCDM cosmology model

We now discuss the strange feature of the standard model dynamics which requires a non-zero energy density for the universe to expand. The well known Friedmann equation is

$$\left(\frac{\dot{a}}{a}\right)^2 = \frac{4\pi G}{3}\left(\frac{\rho_M}{a^3} + \frac{\rho_r}{a^4} + \Lambda\right), \qquad (20)$$

where now $\rho_M = \rho_m + \rho_{DM}$ is the matter composition of the universe, and includes ordinary matter and dark matter, and Λ is the cosmological constant or dark energy, expressed in mass density units. The differences between (13) and (20) need to be noted: apart from the α term (20) has no integration constant which corresponds to a purely spatial expansion, and in compensation requires the *ad hoc* dark matter and dark energy terms, whose best-fit values are easily predicted; see below. It is worth noting how (20) arises from Newtonian gravity. For radially expanding homogeneous matter (1) gives for the total energy E of a test mass (a galaxy) of mass m

$$\frac{1}{2}mv^2 - \frac{GmM(r)}{r} = E\,, \qquad (21)$$

where $M(r)$ is the time-independent amount of matter within a sphere of radius r. With $E = 0$ and $M(r) = \frac{4}{3}\pi r^3\rho(t)$ and $\rho(t) \sim 1/r(t)^3$ (21) has the Hubble form $v = H(t)r$. In terms of $a(t)$ this gives (20) after an *ad hoc* and invalid inclusion of the radiation and dark energy terms, as for these terms $M(r)$ is not independent of time, as assumed above. These terms are usually included on the basis of the stress-energy tensor within GR. Eqn. (20) leads to the analogue of (15),

$$t(a) = \int_0^a \frac{da}{\sqrt{\frac{8\pi G}{3}\left(\frac{\rho_M}{a} + \frac{\rho_r}{a^2} + \Lambda a^2\right)}}\,, \qquad (22)$$

$$H(z)^2 = H_0^2\left(\Omega_M(1+z)^3 + \Omega_r(1+z)^4 + \Omega_\Lambda(1+z)^2\right), \qquad (23)$$

$$\Omega_M \equiv \rho_M/\rho_c, \quad \Omega_r \equiv \rho_r/\rho_c, \quad \Omega_\Lambda \equiv \Lambda/\rho_c\,, \qquad (24)$$

$$\Omega_M + \Omega_r + \Omega_\Lambda = 1\,, \qquad (25)$$

$$H_0 = \left(\frac{8\pi G}{3}(\rho_M + \rho_r + \Lambda)\right)^{1/2} \equiv \left(\frac{8\pi G}{3}\,\rho_c\right)^{1/2}. \qquad (26)$$

This has the same value of ρ_c as in (19), but now interpreted as an actual energy density. Note that $\overline{\Omega}_r = \Omega_r$, but that $\overline{\Omega}_m \neq \Omega_M$, as Ω_M includes the spurious "dark matter".

6 Predicting the ΛCDM parameters Ω_Λ and Ω_{DM}

The "dark energy" and "dark matter" arise in the FLRW-GR cosmology because in that model space cannot expand unless there is an energy density present in the space, if that space is flat and the energy density is pressure-less. Then essentially fitting the Friedmann model $\mu(z)$ to the dynamical 3-space cosmology $\mu(z)$ we obtain $\Omega_\Lambda = 0.73$, and so $\Omega_M = 1 - \Omega_\Lambda = 0.27$. These values arise from a best fit for $z \in \{0, 14\}$ [6]. The actual values for Ω_Λ depend on the redshift range used, as the Hubble functions for the FLRW-GR and dynamical 3-space have different functional dependence on z. These values are of course independent of the actual observed redshift data. Essentially the current standard model of cosmology ΛCDM is excluded from modelling a uniformly expanding dynamical 3-space, but by choice of the parameter Ω_Λ the ΛCDM Hubble function $H(z)$ can be made to best-fit the data. However $H(z)$ has the wrong functional form; when applied to the future expansion of the universe the Friedmann dynamics produces a spurious exponentially expanding universe.

*From now-on an "overline" is used to denote the 3-space values. Note that $\overline{H}_0 \equiv H_0$ — the current observable value.

7 Dynamical 3-space and hotter early universe

The 3-space dynamics and the ΛCDM dynamics give different accounts of the expansion of the universe, particularly the thermal history and density during the radiation dominated epoch. ΛCDM gives in that epoch from (22)

$$a(t) = \sqrt{2H_0 t \sqrt{\Omega_r}}\,,$$

while (15) gives

$$a(t) = \sqrt{2H_0 t \sqrt{\Omega_r/2}}\,.$$

Because the CMB is thermal radiation its temperature varies as $T(t) = (2.725 \pm 0.001)/a(t)$ °K, and so the 3-space dynamics predicts an early thermal history that is 20% hotter. This means that a re-analysis of the BBN is required. However this is easily achieved by a scaling analysis. Essentially we can do this by effectively using $H_0/\sqrt{2}$ in place of H_0 in the radiation-dominated epoch, as this takes account of the $\Omega_r/2$ effect. In terms of $\Omega_B h^2$, which determines the BBN, this amounts to the re-scaling $\Omega_B h^2 \to \Omega_B h^2/2$. This immediately brings the WMAP $\Omega_B h^2 = 0.0224 \pm 0.0009$ down to, effectively, $\Omega_B h^2 = 0.0112 \pm 0.0005$, and into excellent agreement with the BBN value $0.009 < \Omega_B h^2 < 0.013$, as shown in Fig. 2, and discussed in detail in the figure caption.

8 Conclusions

It has been shown that the significant inconsistency between observed abundances of ^{7}Li and ^{4}He with the predictions from Big Bang Nucleosynthesis (BBN) when using the ΛCDM cosmological model together with the value for $\Omega_B h^2 = 0.0224 \pm 0.0009$ from WMAP CMB fluctuations, with the value from BBN required to fit observed abundances being $0.009 < \Omega_B h^2 < 0.013$, are resolved with remarkable precision by using the dynamical 3-space theory. This theory is shown to predict a 20% hotter universe in the radiation-dominated epoch, which then results in a remarkable agreement between the BBN and the WMAP value for $\Omega_B h^2$. The dynamical 3-space also gives a parameter-free fit to the supernova redshift data, and predicts that the flawed ΛCDM model would require $\Omega_\Lambda = 0.73$ and $\Omega_M = 0.27$ to fit the 3-space dynamics Hubble expansion, and independently of the supernova data. These results amount to the discovery of new physics for the early universe. This new physics has also explained (i) the bore-hole g anomaly, (ii) black-hole mass spectrum, (iii) flat rotation curves in spiral galaxies, (iv) enhanced light bending by galaxies, (v) anomalies in laboratory measurements of G, (vi) light speed anisotropy experiments including the explanation of the Doppler shift anomalies in spacecraft earth-flybys, and (vii) the detection of so-called gravitational waves. As well because (4) is non-local it can overcome the horizon problem. The new physics unifies cosmology with laboratory based phenomena, indicating a new era of precision studies of the cosmos.

Submitted on November 04, 2009 / Accepted on November 12, 2009

References

1. Coc A., Vangioni-Flam E., Descouvemont P., Adahchour A. and Angulo C. Updated Big Bang nucleosynthesis compared with WMAP observations and abundance of elements. *ApJ*, 2004, v. 600, 544–552.
2. Cyburt R.H., Fields B.D. and Olive K.A. A bitter pill: the primordial Lithium problem worsens. *JCAP*, 2008, 0811:012.
3. Spergel D.N. *et al. ApJ. Suppl.*, 2003, v. 148, 175.
4. Cahill R.T. Dynamical 3-space: a review. In *Ether Space-time and Cosmology*: *New Insights into a Key Physical Medium*, Duffy M. and Lévy J., eds., *Apeiron*, 2009, 135–200.
5. Cahill R.T. Process physics: from information theory to quantum space and matter. Nova Science Pub., New York, 2005.
6. Cahill R.T. Unravelling the Dark Matter — Dark Energy paradigm. *Apeiron*, 2009, v. 16, no. 3, 323–375.
7. Anderson J.D., Campbell J.K., Ekelund J.E., Ellis J. and Jordan J.F. Anomalous orbital-energy changes observed during spacecraft flybys of Earth. *Phys. Rev. Lett.*, 2008, v. 100, 091102.
8. Cahill R.T. Combining NASA/JPL one-way optical-fiber light-speed data with spacecraft Earth-flyby Doppler-shift data to characterise 3-space flow. *Progress in Physics*, 2009, v. 4, 50–64.
9. Newton I. Philosophiae naturalis principia mathematica. 1687.
10. Riess A.G. *et al. Astron. J.*, 1998, v. 116, 1009.
11. Perlmutter S. *et al. Astrophys. J.*, 1999, v. 517, 565.
12. Perlmutter S. and Schmidt B.P. Measuring cosmology with supernovae. In: *Supernovae and Gamma Ray Bursters*, Weiler K, Ed., Springer, Lecture Notes in Physics, v. 598, 2003, 195–217.

SPECIAL REPORT

Dynamics of Particles in Non Scaling Fixed Field Alternating Gradient Accelerators

James K. Jones*, Bruno D. Muratori†, Susan L. Smith‡, and Stephan I. Tzenov‖

*STFC Daresbury Laboratory, Daresbury, Warrington, Cheshire, WA4 4AD, United Kingdom. E-mail: james.jones@stfc.ac.uk
†STFC Daresbury Laboratory, Daresbury, Warrington, Cheshire, WA4 4AD, United Kingdom. E-mail: bruno.muratori@stfc.ac.uk
‡STFC Daresbury Laboratory, Daresbury, Warrington, Cheshire, WA4 4AD, United Kingdom. E-mail: susan.smith@stfc.ac.uk
‖STFC Daresbury Laboratory, Daresbury, Warrington, Cheshire, WA4 4AD, United Kingdom. E-mail: stephan.tzenov@stfc.ac.uk

Non scaling Fixed-Field Alternating Gradient (FFAG) accelerators have an unprecedented potential for muon acceleration, as well as for medical purposes based on carbon and proton hadron therapy. They also represent a possible active element for an Accelerator Driven Subcritical Reactor (ADSR). Starting from first principle the Hamiltonian formalism for the description of the dynamics of particles in non-scaling FFAG machines has been developed. The stationary reference (closed) orbit has been found within the Hamiltonian framework. The dependence of the path length on the energy deviation has been described in terms of higher order dispersion functions. The latter have been used subsequently to specify the longitudinal part of the Hamiltonian. It has been shown that higher order phase slip coefficients should be taken into account to adequately describe the acceleration in non-scaling FFAG accelerators. A complete theory of the fast (serpentine) acceleration in non-scaling FFAGs has been developed. An example of the theory is presented for the parameters of the Electron Machine with Many Applications (EMMA), a prototype electron non-scaling FFAG to be hosted at Daresbury Laboratory.

1 Introduction

Fixed-Field Alternating Gradient (FFAG) accelerators were proposed half century ago [1–4], when acceleration of electrons was first demonstrated. These machines, which were intensively studied in the 1950s and 1960s but never progressed beyond the model stage, have in recent years become the focus of renewed attention. Acceleration of protons has been recently achieved at the KEK Proof-of-Principle (PoP) proton FFAG [5].

To avoid the slow crossing of betatron resonances associated with a typical low energy-gain per turn, the first FFAGs designed and constructed so far have been based on the "scaling" principle. The latter implies that the orbit shape and betatron tunes must be kept fixed during the acceleration process. Thus, magnets must be built with constant field index, while in the case of spiral-sector designs the spiral angle must be constant as well. Machines of this type use conventional magnets with the bending and focusing field being kept constant during acceleration. The latter alternate in sign, providing a more compact radial extension and consequently smaller aperture as compared to the AVF cyclotrons. The ring essentially consists of a sequence of short cells with very large periodicity.

Non scaling FFAG machines have until recently been considered as an alternative. The bending and the focusing is provided simultaneously by focusing and defocusing quadrupole magnets repeating in an alternating sequence. There is a number of advantages of the non-scaling FFAG lattice as compared to the scaling one, among which are the relatively small transverse magnet aperture (tending to be much smaller than the one for scaling machines) and the lower field strength. Unfortunately this lattice leads to a large betatron tune variation across the required energy range for acceleration as opposed to the scaling lattice. As a consequence several resonances are crossed during the acceleration cycle, some of them nonlinear created by the magnetic field imperfections, as well as half-integer and integer ones. A possible bypass to this problem is the rapid acceleration (of utmost importance for muons), which allows betatron resonances no time to essentially damage beam quality.

Because non-scaling FFAG accelerators have otherwise very desirable features, it is important to investigate analytically and numerically some of the peculiarities of the beam dynamics, the new type of fast acceleration regime (so-called serpentine acceleration) and the effects of crossing of linear as well as nonlinear resonances. Moreover, it is important to examine the most favorable phase at which the cavities need to be set for the optimal acceleration. Some of these problems will be discussed in the present paper.

An example of the theory developed here is presented for the parameters of the Electron Machine with Many Applications (EMMA) [6], a prototype electron non-scaling FFAG to be hosted at Daresbury Laboratory. The Accelerators and Lasers In Combined Experiments (ALICE) accelerator [7] is used as an injector to the EMMA ring. The energy delivered by this injector can vary from a 10 to 20 MeV single bunch train with a bunch charge of 16 to 32 pC at a rate of 1 to 20

Hz. ALICE is presently designed to deliver bunches which are around 4 ps and 8.35 MeV from the exit of the booster of its injector line. These are then accelerated to 10 or 20 MeV in the main ALICE linac after which they are sent to the EMMA injection line. The EMMA injection line ends with a septum for injection into the EMMA ring itself followed by two kickers so as to direct the beam onto the correct, energy dependent, trajectory. After circulation in the EMMA ring, the electron bunches are extracted using what is almost a mirror image of the injection setup with two kickers followed by an extraction septum. The beam is then transported to a diagnostic line whose purpose it is to analyze in as much detail as possible the effect the non-scaling FFAG has had on the bunch.

The paper is organized as follows. Firstly, we review some generalities and first principles of the Hamiltonian formalism [8–10] suitably modified to cover the case of a non-scaling FFAG lattice. Firstly, a sequence of canonical transformations within the synchrobetatron framework is applied to determine the energy dependent reference orbit. Stability of motion about the stationary reference orbit is described in terms of betatron oscillations with energy dependent Twiss parameters and betatron tunes. Dispersion, measuring the effect of energy variation on the path length along the reference orbit is an essential feature of non-scaling FFAGs. Within the developed synchrobetatron formalism higher order dispersion functions have been introduced and their contribution to the longitudinal dynamics has been further analyzed. Finally, a complete description of the so-called serpentine acceleration in non-scaling lepton FFAGs is given together with conclusions. The calculations of the reference orbit and phase stability are detailed in the appendices.

2 Generalities and first principles

Let the ideal (design) trajectory of a particle in an accelerator be a planar curve with curvature K. The Hamiltonian describing the motion of a particle in a natural coordinate system attached to the orbit thus defined is [8]:

$$H = -(1+Kx)\times$$
$$\times\sqrt{\frac{(\mathcal{H}-q\varphi)^2}{c^2}-m_{p_0}^2c^2-(P_x-qA_x)^2-(P_z-qA_z)^2}\;-$$
$$-\;q(1+Kx)A_s\,, \tag{1}$$

where m_{p_0} is the rest mass of the particle. The guiding magnetic field can be represented as a gradient of a certain function $\psi(x,z;s)$

$$\mathbf{B}=\nabla\psi\,, \tag{2}$$

where the latter satisfies the Laplace equation

$$\nabla^2\psi=0\,. \tag{3}$$

Using the median symmetry of the machine, it is straightforward to show that ψ can be written in the form

$$\psi=\left(a_0+a_1x+\frac{a_2x^2}{2!}+\dots\right)z-$$
$$-\left(b_0+b_1x+\frac{b_2x^2}{2!}+\dots\right)\frac{z^3}{3!}+(c_0+c_1x+\dots)\frac{z^5}{5!}+\dots\,. \tag{4}$$

Inserting the above expression into the Laplace equation (3), one readily finds relations between the coefficients b_k and c_k on one hand and a_k on the other

$$b_0=a_0''+Ka_1+a_2\,, \tag{5}$$

$$b_1=-2Ka_0''-K'a_0'+a_1''-K^2a_1+Ka_2+a_3\,, \tag{6}$$

$$b_2=6K^2a_0''+6KK'a_0'-4Ka_1''-2K'a_1'+$$
$$+a_2''+2K^3a_1-2K^2a_2+Ka_3+a_4\,, \tag{7}$$

$$c_0=b_0''+Kb_1+b_2\,. \tag{8}$$

Prime in the above expressions implies differentiation with respect to the longitudinal coordinate s. The coefficients a_k have a very simple meaning

$$a_0=(B_z)_{x,z=0},\qquad a_1=\left(\frac{\partial B_z}{\partial x}\right)_{x,z=0},$$
$$a_2=\left(\frac{\partial^2B_z}{\partial x^2}\right)_{x,z=0}. \tag{9}$$

In other words, this implies that, provided the vertical component B_z of the magnetic field and its derivatives with respect to the horizontal coordinate x are known in the median plane, one can in principle reconstruct the entire field chart.

The vector potential $\mathbf{A}$ can be represented as

$$A_x=-z\,\overline{F}(x,z;s),\;\;A_z=x\,\overline{F}(x,z;s),\;\;A_s=\overline{G}(x,z;s), \tag{10}$$

where the Poincaré gauge condition

$$xA_x+zA_z=0\,, \tag{11}$$

written in the natural coordinate system has been used. From Maxwell's equation

$$\mathbf{B}=\nabla\times\mathbf{A}\,, \tag{12}$$

we obtain

$$2\overline{F}+(x\,\partial_x+z\,\partial_z)\,\overline{F}=B_s\,, \tag{13}$$

$$\frac{Kx}{1+Kx}\,\overline{G}+(x\,\partial_x+z\,\partial_z)\,\overline{G}=z\,B_x-x\,B_z\,. \tag{14}$$

Applying Euler's theorem for homogeneous functions, we can write

$$\overline{F}=\frac{1}{2}\,B_s^{(0)}+\frac{1}{3}\,B_s^{(1)}+\frac{1}{4}\,B_s^{(2)}+\dots\,, \tag{15}$$

$$\overline{G}_u = \left(1 + \frac{Kx}{2}\right) B_u^{(0)} + \left(\frac{1}{2} + \frac{Kx}{3}\right) B_u^{(1)} + \\ + \left(\frac{1}{3} + \frac{Kx}{4}\right) B_u^{(2)} + \dots , \tag{16}$$

$$\overline{G} = \frac{z\overline{G}_x - x\overline{G}_z}{1 + Kx} . \tag{17}$$

Here $u = (x, z)$ and $B_\alpha^{(k)}$ denotes homogeneous polynomials in x and z of order k, representing the corresponding parts of the components of the magnetic field $\mathbf{B} = (B_x, B_z, B_s)$. Thus, having found the magnetic field represented by equation (4), it is straightforward to calculate the vector potential $\mathbf{A}$.

The accelerating field in AVF cyclotrons and FFAG machines can be represented by a scalar potential φ (the corresponding vector potential $\mathbf{A} = 0$). Due to the median symmetry, we have

$$\varphi = A_0 + A_1 x + \frac{A_2 x^2}{2!} + \dots - \left(B_0 + B_1 x + \frac{B_2 x^2}{2!} + \dots\right)\frac{z^2}{2!} + \\ + (C_0 + C_1 x + \dots)\frac{z^4}{4!} + \dots . \tag{18}$$

Inserting the above expansion into the Laplace equation for φ, we obtain similar relations between B_k and C_k on one hand and A_k on the other, which are analogous to those relating b_k, c_k and a_k.

We consider the canonical transformation, specified by the generating function

$$S_2\left(x,\, z,\, \mathcal{T},\, \widehat{P}_x,\, \widehat{P}_z,\, E;\, s\right) = x\widehat{P}_x + z\widehat{P}_z + \mathcal{T}E + \\ + q\int \mathrm{d}\mathcal{T}\varphi(x, z, \mathcal{T}; s) , \tag{19}$$

where

$$\mathcal{T} = -t \tag{20}$$

is a canonical variable canonically conjugate to $\mathcal{H}$. The relations between the new and the old variables are

$$\widehat{u} = \frac{\partial S_2}{\partial \widehat{P}_u} = u, \qquad u = (x, z), \qquad \widehat{\mathcal{T}} = \frac{\partial S_2}{\partial E} = \mathcal{T} , \tag{21}$$

$$P_u = \frac{\partial S_2}{\partial u} = \widehat{P}_u - q\int \mathrm{d}\mathcal{T} E_u(x,\, z,\, \mathcal{T};\, s) = \\ = \widehat{P}_u - q\widetilde{E}_u(x,\, z,\, \mathcal{T};\, s), \qquad E_u = -\frac{\partial\varphi}{\partial u} , \tag{22}$$

$$\mathcal{H} = \frac{\partial S_2}{\partial \mathcal{T}} = E + q\varphi(x,\, z,\, \mathcal{T};\, s) = \\ = m_{p_0}\gamma c^2 + q\varphi(x, z, \mathcal{T}; s) . \tag{23}$$

The new Hamiltonian acquires now the form

$$\widehat{H} = -(1 + Kx)\times \\ \times\sqrt{\frac{E^2}{c^2} - m_{p_0}^2 c^2 - \left(\widehat{P}_x - q\widetilde{E}_x - qA_x\right)^2 - \left(\widehat{P}_z - q\widetilde{E}_z - qA_z\right)^2} - \\ - q(1 + Kx)\left(A_s + \widetilde{E}_s\right), \tag{24}$$

where

$$\widetilde{E}_s = \int \mathrm{d}\mathcal{T} E_s(x,\, z,\, \mathcal{T};\, s) = \\ = -\frac{1}{1 + Kx}\int \mathrm{d}\mathcal{T}\,\frac{\partial\varphi(x,\, z,\, \mathcal{T};\, s)}{\partial s} . \tag{25}$$

We introduce the new scaled variables

$$\widetilde{P}_u = \frac{\widehat{P}_u}{p_0} = \frac{\widehat{P}_u}{m_{p_0}c}, \quad \Theta = c\mathcal{T}, \quad \gamma = \frac{E}{E_p} = \frac{E}{m_{p_0}c^2} . \tag{26}$$

The new scaled Hamiltonian can be expressed as

$$\widetilde{H} = \frac{\widehat{H}}{p_0} = -(1 + Kx)\times \\ \times\sqrt{\gamma^2 - 1 - \left(\widetilde{P}_x - \widetilde{q}\widetilde{E}_x - \widetilde{q}A_x\right)^2 - \left(\widetilde{P}_z - \widetilde{q}\widetilde{E}_z - \widetilde{q}A_z\right)^2} - \\ - \widetilde{q}(1 + Kx)\left(A_s + \widetilde{E}_s\right), \tag{27}$$

where

$$\widetilde{q} = \frac{q}{p_0} . \tag{28}$$

The quantities $\widetilde{E}_x$ and $\widetilde{E}_z$ can be neglected as compared to the components of the vector potential $\mathbf{A}$, so that

$$\widetilde{H} = \beta\gamma(1 + Kx)\times \\ \times\left[-\sqrt{1 - \left(\overline{P}_x - \overline{q}A_x\right)^2 - \left(\overline{P}_z - \overline{q}A_z\right)^2} - \overline{q}A_s\right] - \\ - \widetilde{q}(1 + Kx)\,\widetilde{E}_s , \tag{29}$$

where now

$$\overline{q} = \frac{q}{p} = \frac{q}{\beta\gamma p_0}, \quad \overline{P}_u = \frac{\widehat{P}_u}{p} = \frac{\widehat{P}_u}{\beta\gamma p_0}, \quad u = (x, z) . \tag{30}$$

Since $\overline{P}_u$ and u are small deviations, we can expand the square root in power series in the canonical variables x, $\overline{P}_x$ and z, $\overline{P}_z$. Tedious algebra yields

$$\widetilde{H} = \widetilde{H}_0 + \widetilde{H}_1 + \widetilde{H}_2 + \widetilde{H}_3 + \widetilde{H}_4 + \dots , \tag{31}$$

$$\widetilde{H}_0 = -\beta\gamma - \widetilde{q}(1 + Kx)\,\widetilde{E}_s , \tag{32}$$

$$\widetilde{H}_1 = \beta\gamma\,(\overline{q}a_0 - K)\,x , \tag{33}$$

$$\widetilde{H}_2 = \frac{\beta\gamma}{2}\left(\overline{P}_x^2 + \overline{P}_z^2\right) + \frac{\widetilde{q}}{2}\left[(Ka_0 + a_1)x^2 - a_1 z^2\right], \tag{34}$$

$$\widetilde{H}_3 = \frac{\beta\gamma}{2}\,Kx\left(\overline{P}_x^2 + \overline{P}_z^2\right) + \frac{\widetilde{q}a_0' z}{3}\left(z\,\overline{P}_x - x\,\overline{P}_z\right) +$$

$$+\frac{\widetilde{q}}{3}\left[\left(Ka_1+\frac{a_2}{2}\right)x^3-\left(Ka_1+a_2+\frac{b_0}{2}\right)xz^2\right], \qquad (35)$$

$$\widetilde{H}_4=\frac{\beta\gamma}{8}\left(\overline{P}_x^2+\overline{P}_z^2\right)^2+\frac{\widetilde{q}xz}{12}\left(Ka_0'+3a_1'\right)\left(z\overline{P}_x-x\overline{P}_z\right)+$$
$$+\frac{\overline{q}^2\beta\gamma a_0'^2z^2}{18}\left(x^2+z^2\right)++\frac{\widetilde{q}}{4}\left[\left(\frac{Ka_2}{2}+\frac{a_3}{6}\right)x^4-\right.$$
$$\left.-\left(Ka_2+\frac{a_3}{3}+\frac{Kb_0}{2}+\frac{b_1}{2}\right)x^2z^2+\frac{b_1}{6}z^4\right]. \qquad (36)$$

The Hamiltonian decomposition (31) represents the milestone of the synchrobetatron formalism. For instance, $\widetilde{H}_0$ governs the longitudinal motion, $\widetilde{H}_1$ describes linear coupling between longitudinal and transverse degrees of freedom and is the basic source of dispersion. The part $\widetilde{H}_2$ is responsible for linear betatron motion and chromaticity, while the remainder describes higher order contributions.

3 The synchro-betatron formalism and the reference orbit

In the present paper we consider a FFAG lattice with polygonal structure. To define and subsequently calculate the stationary reference orbit, it is convenient to use a global Cartesian coordinate system whose origin is located in the center of the polygon. To describe step by step the fraction of the reference orbit related to a particular side of the polygon, we rotate each time the axes of the coordinate system by the polygon angle $\Theta_p = 2\pi/N_L$, where N_L is the number of sides of the polygon.

Let X_e and P_e denote the reference orbit and the reference momentum, respectively. The vertical component of the magnetic field in the median plane of a perfectly linear machine can be written as

$$B_z(X_e;s)=a_1(s)[X_e-X_c-d(s)]\,,$$
$$a_0(X_e;s)=B_z(X_e;s)\,, \qquad (37)$$

where s is the distance along the polygon side, and X_c is the distance of the side of the polygon from the center of the machine

$$X_c=\frac{L_p}{2\tan(\Theta_p/2)}\,. \qquad (38)$$

Here L_p is the length of the polygon side which actually represents the periodicity parameter of the lattice. Usually X_c is related to an arbitrary energy in the range from injection to extraction energy. In the case of EMMA it is related to the 15 MeV orbit. The quantity $d(s)$ in equation (37) is the relative offset of the magnetic center in the quadrupoles with respect to the corresponding side of the polygon. In what follows [see equations (47) and (50)] d_F corresponds to the offset in the focusing quadrupoles and d_D corresponds to the one in the defocusing quadrupoles. Similarly, a_F and a_D stand for the particular value of a_1 in the focusing and the defocusing quadrupoles, respectively.

A design (reference) orbit corresponding to a local curvature $K(X_e;s)$ can be defined according to the relation

$$K(X_e;s)=\frac{q}{p_0\beta_e\gamma_e}B_z(X_e;s)\,, \qquad (39)$$

where γ_e is the energy of the reference particle. In terms of the reference orbit position $X_e(s)$ the equation for the curvature can be written as

$$X_e''=\frac{q}{p_0\beta_e\gamma_e}\left(1+X_e'^2\right)^{3/2}B_z(X_e;s)\,, \qquad (40)$$

where the prime implies differentiation with respect to s.

To proceed further, we notice that equation (40) parameterizing the local curvature can be derived from an equivalent Hamiltonian

$$H_e(X_e,P_e;s)=-\sqrt{\beta_e^2\gamma_e^2-P_e^2}-\widetilde{q}\int \mathrm{d}X_eB_z(X_e;s)\,. \qquad (41)$$

Taking into account Hamilton's equations of motion

$$X_e'=\frac{P_e}{\sqrt{\beta_e^2\gamma_e^2-P_e^2}}, \qquad P_e'=\widetilde{q}B_z(X_e;s)\,, \qquad (42)$$

and using the relation

$$P_e=\frac{\beta_e\gamma_eX_e'}{\sqrt{1+X_e'^2}}\,, \qquad (43)$$

we readily obtain equation (40). Note also that the Hamiltonian (41) follows directly from the scaled Hamiltonian (27) with $x=0$, $\widetilde{P}_x=P_e$, $\widetilde{P}_z=0$, $A_x=A_z=0$ and the accelerating cavities being switched off respectively.

Hamilton's equations of motion (42) can be linearized and subsequently solved approximately by assuming that

$$P_e\ll\beta_e\gamma_e\,. \qquad (44)$$

Thus, assuming electrons ($q=-e$), we have

$$P_e=\beta_e\gamma_eX_e'\,, \qquad X_e''=-\frac{ea_1(s)}{p_0\beta_e\gamma_e}(X_e-X_c-d(s))\,. \qquad (45)$$

The three types of solutions to equations (45) are as follows:

Drift Space

$$X_e=X_0+\frac{P_0}{\beta_e\gamma_e}(s-s_0)\,, \qquad P_e=P_0\,, \qquad (46)$$

where X_0 and P_0 are the initial position and reference momentum and s is the distance in longitudinal direction.

Focusing Quadrupole

$$X_e=X_c+d_F+(X_0-X_c-d_F)\cos\omega_F(s-s_0)+$$
$$+\frac{P_0}{\beta_e\gamma_e\omega_F}\sin\omega_F(s-s_0)\,, \qquad (47)$$

$$P_e = -\beta_e\gamma_e\omega_F(X_0 - X_c - d_F)\sin\omega_F(s - s_0) + \\ + P_0\cos\omega_F(s - s_0)\,, \tag{48}$$

where

$$\omega_F^2 = \frac{ea_F}{p_0\beta_e\gamma_e}\,. \tag{49}$$

Defocusing Quadrupole

$$X_e = X_c + d_D + (X_0 - X_c - d_D)\cosh\omega_D(s - s_0) + \\ + \frac{P_0}{\beta_e\gamma_e\omega_D}\sinh\omega_D(s - s_0)\,, \tag{50}$$

$$P_e = \beta_e\gamma_e\omega_D(X_0 - X_c - d_D)\sinh\omega_D(s - s_0) + \\ + P_0\cosh\omega_D(s - s_0)\,, \tag{51}$$

where

$$\omega_D^2 = \frac{ea_D}{p_0\beta_e\gamma_e}\,. \tag{52}$$

In addition to the above, the coordinate transformation at the polygon bend when passing to the new rotated coordinate system needs to be specified. The latter can be written as

$$X_e = X_c + \frac{X_0 - X_c}{\cos\Theta_p - P_0\sin\Theta_p/\beta_e\gamma_e}\,,$$

$$P_e = \beta_e\gamma_e\tan\left[\Theta_p + \arctan\left(\frac{P_0}{\beta_e\gamma_e}\right)\right]. \tag{53}$$

Once the reference trajectory has been found the corresponding contributions to the total Hamiltonian (31) can be written as follows

$$\widetilde{H}_0 = -\beta\gamma + \frac{Z}{AE_p}\left(\frac{\mathrm{d}\Delta E}{\mathrm{d}s}\right)\int \mathrm{d}\Theta\sin\phi(\Theta)\,, \tag{54}$$

$$\widetilde{H}_1 = -(\beta\gamma - \beta_e\gamma_e)K\tilde{x}\,, \tag{55}$$

$$\widetilde{H}_2 = \frac{1}{2\beta\gamma}\left(\widetilde{P}_x^2 + \widetilde{P}_z^2\right) + \frac{1}{2}\left[\left(g + \beta_e\gamma_e K^2\right)\tilde{x}^2 - g\tilde{z}^2\right], \tag{56}$$

$$\widetilde{H}_3 = \frac{K\tilde{x}}{2\beta\gamma}\left(\widetilde{P}_x^2 + \widetilde{P}_z^2\right) + \frac{Kg}{6}\left(2\tilde{x}^3 - 3\tilde{x}\tilde{z}^2\right), \tag{57}$$

$$\widetilde{H}_4 = \frac{\left(\widetilde{P}_x^2 + \widetilde{P}_z^2\right)^2}{8\beta^3\gamma^3} - \frac{K^2 g}{24}\,\tilde{z}^4. \tag{58}$$

Here, we have introduced the following notation

$$g = \frac{qa_1}{p_0}\,. \tag{59}$$

Moreover, Z is the charge state of the accelerated particle, A is the mass ratio with respect to the proton mass in the case of ions, and $\phi(\Theta)$ is the phase of the RF. For a lepton accelerator like EMMA, $A = Z = 1$. In addition, $(\mathrm{d}\Delta E/\mathrm{d}s)$ is the energy gain per unit longitudinal distance s, which in thin lens approximation scales as $\Delta E/\Delta s$, where Δs is the length of the cavity. It is convenient to pass to new scaled variables as follows

$$\tilde{p}_u = \frac{\widetilde{P}_u}{\beta_e\gamma_e}\,, \qquad h = \frac{\gamma}{\beta_e^2\gamma_e}\,, \tag{60}$$

$$\tau = \beta_e\Theta\,, \qquad \Gamma_e = \frac{\beta\gamma}{\beta_e\gamma_e} = \sqrt{\beta_e^2h^2 - \frac{1}{\beta_e^2\gamma_e^2}}\,. \tag{61}$$

Thus, expressions (54)–(58) become

$$\widetilde{H}_0 = -\Gamma_e + \frac{Z}{A\beta_e^2E_e}\left(\frac{\mathrm{d}\Delta E}{\mathrm{d}s}\right)\int \mathrm{d}\tau\sin\phi(\tau)\,, \tag{62}$$

$$\widetilde{H}_1 = -(\Gamma_e - 1)\,K\tilde{x}\,, \tag{63}$$

$$\widetilde{H}_2 = \frac{1}{2\Gamma_e}\left(\tilde{p}_x^2 + \tilde{p}_z^2\right) + \frac{1}{2}\left[\left(g_e + K^2\right)\tilde{x}^2 - g_e\tilde{z}^2\right], \tag{64}$$

$$\widetilde{H}_3 = \frac{K\tilde{x}}{2\Gamma_e}\left(\tilde{p}_x^2 + \tilde{p}_z^2\right) + \frac{Kg_e}{6}\left(2\tilde{x}^3 - 3\tilde{x}\tilde{z}^2\right), \tag{65}$$

$$\widetilde{H}_4 = \frac{\left(\tilde{p}_x^2 + \tilde{p}_z^2\right)^2}{8\Gamma_e^3} - \frac{K^2g_e}{24}\,\tilde{z}^4, \tag{66}$$

$$E_p = m_{p_0}c^2, \qquad g_e = \frac{g}{\beta_e\gamma_e}\,. \tag{67}$$

The longitudinal part of the reference orbit can be isolated via a canonical transformation

$$F_2\left(\tilde{x}, \tilde{\widehat{p}}_x, \tilde{z}, \tilde{\widehat{p}}_z, \tau, \eta; s\right) = \tilde{x}\tilde{\widehat{p}}_x + \tilde{z}\tilde{\widehat{p}}_z + (\tau + s)\left(\eta + \frac{1}{\beta_e^2}\right), \tag{68}$$

$$\sigma = \tau + s\,, \qquad \eta = h - \frac{1}{\beta_e^2}\,, \tag{69}$$

where σ is the new longitudinal variable and η is the energy deviation with respect to the energy γ_e of the reference particle.

4 Dispersion and betatron motion

The (linear and higher order) dispersion can be introduced via a canonical transformation aimed at canceling the first order Hamiltonian $\widetilde{H}_1$ in all orders of η. The explicit form of the generating function is

$$G_2(\tilde{x}, \widehat{p}_x, \tilde{z}, \widehat{p}_z, \sigma, \widehat{\eta}; s) = \sigma\widehat{\eta} + \tilde{z}\widehat{p}_z + \tilde{x}\widehat{p}_x + \\ + \sum_{k=1}^{\infty}\widehat{\eta}^k\left[\tilde{x}\mathcal{X}_k(s) - \widehat{p}_x\mathcal{P}_k(s) + \mathcal{S}_k(s)\right], \tag{70}$$

$$\tilde{x} = \widehat{x} + \sum_{k=1}^{\infty}\widehat{\eta}^k\mathcal{P}_k\,, \qquad \tilde{p}_x = \widehat{p}_x + \sum_{k=1}^{\infty}\widehat{\eta}^k\mathcal{X}_k\,, \tag{71}$$

$$\sigma = \widehat{\sigma} + \sum_{k=1}^{\infty}k\widehat{\eta}^{k-1}(\mathcal{P}_k\widehat{p}_x - \mathcal{X}_k\widehat{x}) - \\ - \sum_{k=1}^{\infty}k\widehat{\eta}^{k-1}\left(\mathcal{S}_k + \mathcal{X}_k\sum_{m=1}^{\infty}\widehat{\eta}^m\mathcal{P}_m\right). \tag{72}$$

Equating terms of the form $\widehat{x}\widehat{\eta}^n$ and $\widehat{p}_x\widehat{\eta}^n$ in the new transformed Hamiltonian, we determine order by order the conventional (first order) and higher order dispersions. The first order in $\widehat{\eta}$ (terms proportional to $\widehat{x}\widehat{\eta}$ and $\widehat{p}_x\widehat{\eta}$) yields the well-known result

$$\mathcal{P}_1' = \mathcal{X}_1\,, \qquad \mathcal{X}_1' + \left(g_e + K^2\right)\mathcal{P}_1 = K\,. \tag{73}$$

Since in the case, where betatron motion ($\widehat{x} = 0, \widehat{p}_x = 0$) can be neglected the new longitudinal coordinate $\widehat{\sigma}$ should not depend on the new longitudinal canonical conjugate variable $\widehat{\eta}$, the second sum in equation (72) must be identically zero. We readily obtain $\mathcal{S}_1 = 0$, and

$$\mathcal{S}_2 = -\frac{\mathcal{X}_1\mathcal{P}_1}{2}\,. \tag{74}$$

In second order we have

$$\mathcal{P}_2' = \mathcal{X}_2 - \mathcal{X}_1 + K\mathcal{X}_1\mathcal{P}_1\,, \tag{75}$$

$$\mathcal{X}_2' + \left(g_e + K^2\right)\mathcal{P}_2 = -Kg_e\mathcal{P}_1^2 - \frac{K\mathcal{X}_1^2}{2} - \frac{K}{2\gamma_e^2}\,, \tag{76}$$

and in addition the function $\mathcal{S}_3(s)$ is expressed as

$$\mathcal{S}_3 = -\frac{1}{3}\left(\mathcal{X}_1\mathcal{P}_2 + 2\mathcal{X}_2\mathcal{P}_1\right). \tag{77}$$

Close inspection of equations (73), (75) and (76) shows that $\mathcal{P}_1$ is the well-known linear dispersion function, while $\mathcal{P}_2$ stands for a second order dispersion and so on. Up to third order in $\widehat{\eta}$ the new Hamiltonian describing the longitudinal motion and the linear transverse motion acquires the form

$$\widehat{H}_0 = -\frac{\widetilde{\mathcal{K}}_1\widehat{\eta}^2}{2} + \frac{\widetilde{\mathcal{K}}_2\widehat{\eta}^3}{3} + \frac{Z}{A\beta_e^2E_e}\left(\frac{\mathrm{d}\Delta E}{\mathrm{d}s}\right)\int \mathrm{d}\tau\sin\phi(\tau)\,, \tag{78}$$

$$\widehat{H}_2 = \frac{1}{2}\left(\widehat{p}_x^2 + \widehat{p}_z^2\right) + \frac{1}{2}\left[\left(g_e + K^2\right)\widehat{x}^2 - g_e\widehat{z}^2\right], \tag{79}$$

where

$$\widetilde{\mathcal{K}}_1 = K\mathcal{P}_1 - \frac{1}{\gamma_e^2}\,, \quad \widetilde{\mathcal{K}}_2 = \frac{K\mathcal{P}_1}{\gamma_e^2} - K\mathcal{P}_2 - \frac{\mathcal{X}_1^2}{2} - \frac{3}{2\gamma_e^2}\,. \tag{80}$$

For the sake of generality, let us consider a Hamiltonian of the type

$$\widehat{H}_b = \sum_{u=(x,z)}\left[\frac{\mathcal{F}_u}{2}\,\widehat{p}_u^2 + \mathcal{R}_u\widehat{u}\widehat{p}_u + \frac{\mathcal{G}_u}{2}\,\widehat{u}^2\right]. \tag{81}$$

A generic Hamiltonian of the type (81) can be transformed to the normal form

$$\mathcal{H}_b = \sum_{u=(x,z)}\frac{\chi_u'}{2}\left(\overline{P}_u^2 + \overline{U}^2\right), \tag{82}$$

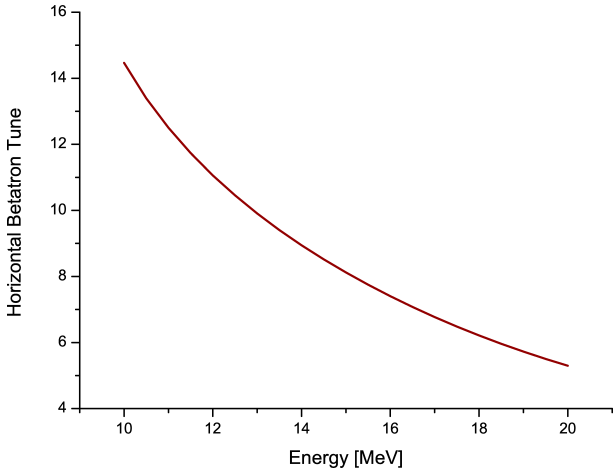

Fig. 1: Horizontal betatron tune for the EMMA ring as a function of energy.

by means of a canonical transformation specified by the generating function

$$\mathcal{F}_2\left(\widehat{x},\,\overline{P}_x,\,\widehat{z},\,\overline{P}_z;\,s\right) = \sum_{u=(x,z)}\left(\frac{\widehat{u}\overline{P}_u}{\sqrt{\beta_u}} - \frac{\alpha_u\widehat{u}^2}{2\beta_u}\right). \tag{83}$$

Here the prime implies differentiation with respect to the longitudinal variable s. The old and the new canonical variables are related through the expressions

$$\widehat{u} = \overline{U}\,\sqrt{\beta_u}, \qquad \widehat{p}_u = \frac{1}{\sqrt{\beta_u}}\left(\overline{P}_u - \alpha_u\overline{U}\right). \tag{84}$$

The phase advance $\chi_u(s)$ and the generalized Twiss parameters $\alpha_u(s), \beta_u(s)$ and $\gamma_u(s)$ are defined as

$$\chi_u' = \frac{\mathrm{d}\chi_u}{\mathrm{d}s} = \frac{\mathcal{F}_u}{\beta_u}, \tag{85}$$

$$\alpha_u' = \frac{\mathrm{d}\alpha_u}{\mathrm{d}s} = \mathcal{G}_u\beta_u - \mathcal{F}_u\gamma_u, \tag{86}$$

$$\beta_u' = \frac{\mathrm{d}\beta_u}{\mathrm{d}s} = -2\,\mathcal{F}_u\alpha_u + 2\mathcal{R}_u\beta_u\,. \tag{87}$$

The third Twiss parameter $\gamma_u(s)$ is introduced via the well-known expression

$$\beta_u\gamma_u - \alpha_u^2 = 1\,. \tag{88}$$

The corresponding betatron tunes are determined according to the expression

$$\nu_u = \frac{N_p}{2\pi}\int_s^{s+L_p}\frac{\mathrm{d}\theta\,\mathcal{F}_u(\theta)}{\beta_u(\theta)}\,. \tag{89}$$

Typical dependence of the horizontal and vertical betatron tunes on energy in the EMMA non-scaling FFAG is shown in Figures 1 and 2.

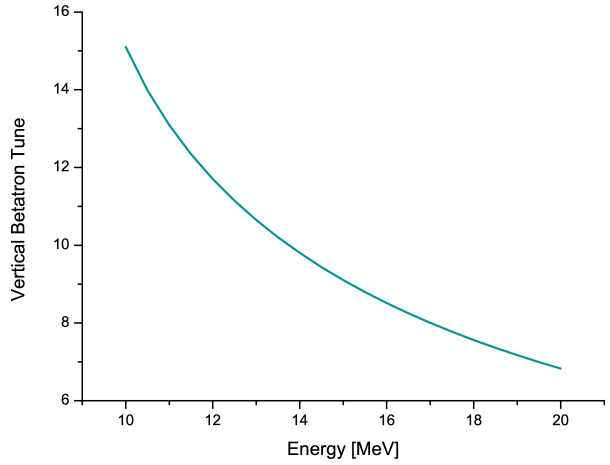

Fig. 2: Vertical betatron tune for the EMMA ring as a function of energy.

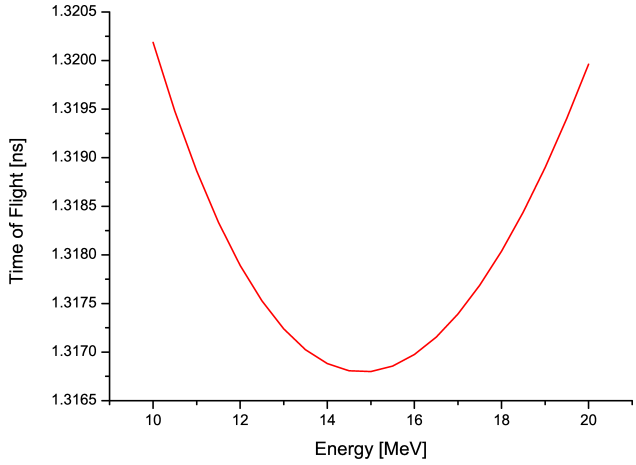

Fig. 3: Time of flight as a function of energy for a single 0.394481 meter EMMA cell.

It is worthwhile noting that the canonical transformation specified by the generating function (70) allowed us to cancel terms linear in the transverse canonical coordinates $\widehat{x}$ and $\widehat{p}_x$. In order to take a due account of the dependence of the longitudinal dynamics on the transverse one it is necessary to retain terms in the resulting Hamiltonian that are proportional to higher powers in $\widehat{\eta}$, $\widehat{x}$, $\widehat{p}_x$ and $\widehat{p}_z$. Up to first order in $\widehat{\eta}$, this gives rise to additional terms in the longitudinal Hamiltonian of the form

$$\widehat{H}_{0ad} = -\frac{\widehat{\eta}}{2}\left(\widehat{p}_x^2 + \widehat{p}_z^2\right) - \frac{K\widehat{\eta}\widehat{x}}{2}\left(\widehat{p}_x^2 + \widehat{p}_z^2\right) + \dots . \qquad (90)$$

The lengthening of the time of flight for one period of the machine due to betatron oscillations can be expressed as

$$\Delta\Theta = -\frac{1}{2\beta_e}\int_s^{s+L_p} \mathrm{d}\theta\left[1 + K(\theta)\widehat{x}(\theta)\right]\left[\widehat{p}_x^2(\theta) + \widehat{p}_z^2(\theta)\right]. \qquad (91)$$

5 Acceleration in a non-scaling FFAG accelerator

The process of acceleration in a non-scaling FFAG accelerator can be studied by solving Hamilton's equations of motion for the longitudinal degree of freedom. The latter are obtained from the Hamiltonian (41) supplemented by an additional term [similar to that in equation (54)], which takes into account the electric field of the RF cavities. They read as

$$\frac{\mathrm{d}\Theta}{\mathrm{d}s} = -\frac{\gamma}{\sqrt{\beta^2\gamma^2 - P^2}}, \qquad (92)$$

$$\frac{\mathrm{d}\gamma}{\mathrm{d}s} = -\frac{ZeU_c}{2AE_p}\sum_{k=1}^{N_c}\delta_p(s - s_k)\sin\left(\frac{\omega_c\Theta}{c} - \varphi_k\right). \qquad (93)$$

Here U_c is the cavity voltage, ω_c is the RF frequency, N_c is the number of cavities and φ_k is the corresponding cavity phase.

One could use the results obtained in the previous section with the additional requirement that the phase slip coefficient $\widetilde{\mathcal{K}}_1$ averaged over one period vanishes. Instead, we shall use an equivalent but more illustrative approach. The path length in a FFAG arc and therefore the time of flight Θ is often well approximated as a quadratic function of energy. The acceleration process is then described by a longitudinal Hamiltonian, which contains terms proportional to the zero-order (conventional phase slip) factor and first-order phase slip factor. It usually suffices to take into account only terms to second order in the energy deviation

$$\Theta = \Theta_0 + 2\mathcal{A}\gamma_m\gamma - \mathcal{A}\gamma^2, \qquad (94)$$

as suggested by Figure 3.

Here γ_m corresponds to the reference energy with a minimum time of flight. Provided the time of flight Θ_i at injection energy γ_i and the time of flight Θ_m at reference energy γ_m are known, the constants entering equation (94) can be expressed as

$$\mathcal{A} = \frac{\Theta_m - \Theta_i}{(\gamma_m - \gamma_i)^2}, \qquad \Theta_0 = \Theta_m - \mathcal{A}\gamma_m^2. \qquad (95)$$

Next, we pass to a new variable

$$\widehat{\gamma} = \gamma - \gamma_m, \qquad \Theta = \Theta_m - \mathcal{A}\widehat{\gamma}^2, \qquad (96)$$

similar to the variable $\widehat{\eta}$ introduced in the previous section. Then, Hamilton's equation of motion (92) can be rewritten in an equivalent form

$$\frac{\mathrm{d}\Theta}{\mathrm{d}s} = \frac{\Theta_m}{L_p} - \frac{\mathcal{A}\widehat{\gamma}^2}{L_p}. \qquad (97)$$

In what follows, it is convenient to introduce a new phase $\widetilde{\varphi}$ and the azimuthal angle θ along the machine circumference as an independent variable according to the relations

$$\mathrm{d}s = R\mathrm{d}\theta, \qquad \widetilde{\varphi} = \frac{\omega_c\Theta}{c}, \qquad R = \frac{N_L L_p}{2\pi}. \qquad (98)$$

It is straightforward to verify (see the averaging procedure below) that the necessary condition to have acceleration is

$$\frac{\omega_c N_L |\Theta_m|}{2\pi c} = h\,, \tag{99}$$

where h is an integer (a harmonic number). Averaging Hamilton's equations of motion

$$\frac{\mathrm{d}\widetilde{\varphi}}{\mathrm{d}\theta} = -h - ha\widehat{\gamma}^2, \qquad a = \frac{\mathcal{A}}{|\Theta_m|}\,, \tag{100}$$

$$\frac{\mathrm{d}\widehat{\gamma}}{\mathrm{d}\theta} = -\frac{ZeU_c}{2AE_p}\sum_{k=1}^{N_c}\delta_p(\theta-\theta_k)\sin\left(\widetilde{\varphi}-\varphi_k\right), \tag{101}$$

we rewrite them in a simpler form as

$$\frac{\mathrm{d}\varphi}{\mathrm{d}\theta} = ha\widehat{\gamma}^2, \qquad \frac{\mathrm{d}\widehat{\gamma}}{\mathrm{d}\theta} = \lambda\sin\varphi\,, \tag{102}$$

where

$$\varphi = -\widetilde{\varphi} - h\theta + \psi_0, \qquad \lambda = \frac{ZeU_c\mathcal{D}}{4\pi AE_p}\,, \tag{103}$$

$$\mathcal{D} = \sqrt{\mathcal{A}_c^2 + \mathcal{A}_s^2}\,, \qquad \psi_0 = \arctan\left(\frac{\mathcal{A}_s}{\mathcal{A}_c}\right), \tag{104}$$

$$\mathcal{A}_c = \sum_{k=1}^{N_c}\cos\left(h\theta_k+\varphi_k\right), \quad \mathcal{A}_s = \sum_{k=1}^{N_c}\sin\left(h\theta_k+\varphi_k\right). \tag{105}$$

The effective longitudinal Hamiltonian, which governs the equations of motion (102) can be written as

$$H_0 = \frac{ha}{3}\widehat{\gamma}^3 + \lambda\cos\varphi\,. \tag{106}$$

Since the Hamiltonian (106) is a constant of motion, the second Hamilton equation (102) can be written as

$$\frac{\mathrm{d}\widehat{\gamma}}{\mathrm{d}\theta} = \pm\lambda\sqrt{1-\frac{1}{\lambda^2}\left(H_0 - \frac{ha}{3}\widehat{\gamma}^3\right)^2}\,. \tag{107}$$

Let us first consider the case of the central trajectory, for which $H_0 = 0$. It is of utmost importance for the so called gutter (or serpentine) acceleration. Equation (107) can be solved in a straightforward manner to give

$$\theta = \frac{J}{b}\,{}_2F_1\left(\frac{1}{6},\,\frac{1}{2};\,\frac{7}{6};\,J^6\right) - \frac{C}{b}\,, \tag{108}$$

where

$$J = \widehat{\gamma}\sqrt[3]{\frac{ha}{3\lambda}}\,, \qquad b = \lambda\sqrt[3]{\frac{ha}{3\lambda}}\,, \tag{109}$$

$$C = {}_2F_1\left(\frac{1}{6},\,\frac{1}{2};\,\frac{7}{6};\,J_i^6\right)J_i\,. \tag{110}$$

In the above expressions ${}_2F_1(\alpha,\beta;\gamma;x)$ denotes the Gauss hypergeometric function of the argument x. This case is illustrated in Figure 4.

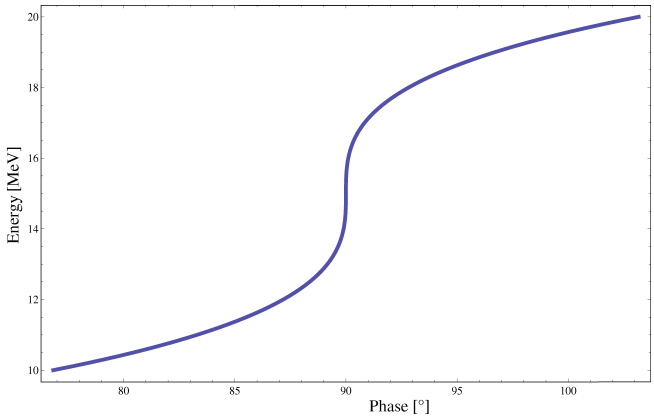

Fig. 4: An example of the so-called serpentine acceleration for the EMMA ring for the central trajectory, where the longitudinal $H_0 = 0$. The harmonic number is assumed to be 11, with the RF wavelength 0.405m. The parameter a from Eq. (100) is taken to be 2.686310^{-5}.

In the general case where $H_0 \neq 0$, we have

$$\theta = \frac{J}{b\sqrt{a_1 c}}\,F_1\left(\frac{1}{3};\,\frac{1}{2},\,\frac{1}{2};\,\frac{4}{3};\,\frac{J^3}{a_1},\,-\frac{J^3}{c}\right) - \frac{C_1}{b}\,, \tag{111}$$

where

$$a_1 = 1 + \frac{H_0}{\lambda}\,, \qquad c = 1 - \frac{H_0}{\lambda}\,, \tag{112}$$

$$C_1 = \frac{J_i}{\sqrt{a_1 c}}\,F_1\left(\frac{1}{3};\,\frac{1}{2},\,\frac{1}{2};\,\frac{4}{3};\,\frac{J_i^3}{a_1},\,-\frac{J_i^3}{c}\right). \tag{113}$$

Here now, $F_1(\alpha;\beta,\gamma;\delta;x,y)$ denotes the Appell hypergeometric function of the arguments x and y. The phase portrait corresponding to the general case for a variety of values of the longitudinal Hamiltonian H_0 is illustrated in Figure 5. The important question on whether the serpentine acceleration along the separatrix $H_0 = 0$ is stable is addressed in Appendix B.

A qualitative analysis of the fast serpentine acceleration has been presented earlier [11, 12]. However, to the best of our knowledge the results presented here comprise the first attempt to describe the process quantitatively. Although the exact solution is expressed in the form of standard and generalized hypergeometric functions, it can be easily incorporated in modern computational environments like Mathematica.

6 Concluding remarks

Based on the Hamiltonian formalism, the synchro-betatron approach for the description of the dynamics of particles in non-scaling FFAG machines has been developed. Its starting point is the specification of the static reference (closed) orbit for a fixed energy as a solution of the equations of motion in the machine reference frame. The problem of dynamical stability and acceleration is sequentially studied in the natural coordinate system associated with the reference orbit thus determined.

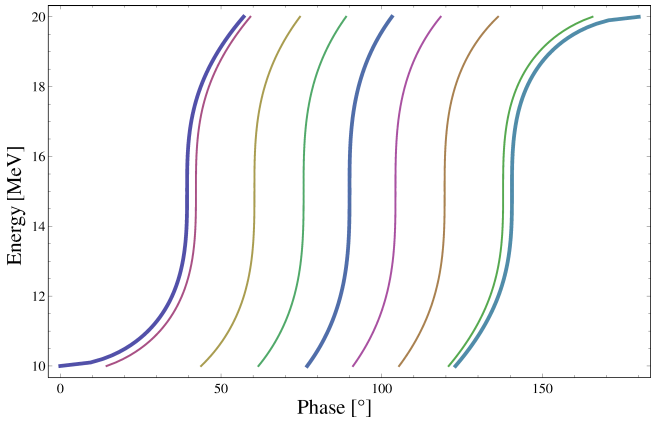

Fig. 5: Examples of serpentine acceleration for the EMMA ring, with varying value of the longitudinal Hamiltonian. The limits of stability are given at values of the longitudinal Hamiltonian of ±0.31272, corresponding to either a 0 phase at 10MeV, or a π phase at 20MeV.

It has been further shown that the dependence of the path length on the energy deviation can be described in terms of higher order (nonlinear) dispersion functions. The method provides a systematic tool to determine the dispersion functions and their derivatives to every desired order, and represents a natural definition through constitutive equations for the resulting Twiss parameters.

The formulation thus developed has been applied to the electron FFAG machine EMMA. The transverse and longitudinal dynamics have been explored and an initial attempt is made at understanding the limits of longitudinal stability of such a machine.

Unlike the conventional synchronous acceleration, the acceleration process in FFAG accelerators is an asynchronous one in which the reference particle performs nonlinear oscillations around the crest of the RF waveform. To the best of our knowledge, it is the first time that such a fully analytic (quantitative) theory describing the acceleration in non-scaling FFAGs has been developed.

A Calculation of the reference orbit

The explicit solutions of the linearized equations of motion (45) can be used to calculate approximately the reference orbit. To do so, we introduce a state vector

$$\mathbf{Z}_e = \begin{pmatrix} X_e \\ P_e \end{pmatrix}. \tag{114}$$

The effect of each lattice element can be represented in a simple form as

$$\mathbf{Z}_{out} = \widehat{\mathcal{M}}_{el}\mathbf{Z}_{in} + \mathbf{A}_{el}\,. \tag{115}$$

Here $\mathbf{Z}_{in}$ is the initial value of the state vector, while $\mathbf{Z}_{out}$ is its final value at the exit of the corresponding element. The transfer matrix $\widehat{\mathcal{M}}_{el}$ and the shift vector $\mathbf{A}_{el}$ for various lattice elements are given as follows:

1. *Polygon Bend.*

Within the approximation (44) considered here we can linearize the second of equations (53) and write

$$\widehat{\mathcal{M}}_p = \begin{pmatrix} 1/\cos\Theta_p & -X_c\tan\Theta_p/\big(\beta_e\gamma_e\cos\Theta_p\big) \\ 0 & 1/\cos^2\Theta_p \end{pmatrix},$$

$$\mathbf{A}_p = \begin{pmatrix} X_c\big(1-1/\cos\Theta_p\big) \\ \beta_e\gamma_e\tan\Theta_p \end{pmatrix}. \tag{116}$$

2. *Drift Space.*

$$\widehat{\mathcal{M}}_O = \begin{pmatrix} 1 & L_O/\beta_e\gamma_e \\ 0 & 1 \end{pmatrix}, \qquad \mathbf{A}_O = 0\,, \tag{117}$$

where L_O is the length of the drift. Every cell of the EMMA lattice includes a short drift of length L_0 and a long one of length L_1.

3. *Focusing Quadrupole.*

The transfer matrix can be written in a straightforward manner as

$$\widehat{\mathcal{M}}_F = \begin{pmatrix} \cos(\omega_F L_F) & \sin(\omega_F L_F)/(\beta_e\gamma_e\omega_F) \\ -\beta_e\gamma_e\omega_F\sin(\omega_F L_F) & \cos(\omega_F L_F) \end{pmatrix}, \tag{118}$$

$$\mathbf{A}_F = \begin{pmatrix} (X_c+d_F)[1-\cos(\omega_F L_F)] \\ \beta_e\gamma_e\omega_F(X_c+d_F)\sin(\omega_F L_F) \end{pmatrix}, \tag{119}$$

where L_F is the length of the focusing quadrupole.

4. *Defocusing Quadrupole.*

The transfer matrix in this case can be written in analogy to the above one as

$$\widehat{\mathcal{M}}_D = \begin{pmatrix} \cosh(\omega_D L_D) & \sinh(\omega_D L_D)/(\beta_e\gamma_e\omega_D) \\ \beta_e\gamma_e\omega_D\sinh(\omega_D L_D) & \cosh(\omega_D L_D) \end{pmatrix}, \tag{120}$$

$$\mathbf{A}_D = \begin{pmatrix} (X_c+d_D)[1-\cosh(\omega_D L_D)] \\ -\beta_e\gamma_e\omega_D(X_c+d_D)\sinh(\omega_D L_D) \end{pmatrix}, \tag{121}$$

where L_D is the length of the defocusing quadrupole.

Since the reference orbit must be a periodic function of s with period L_p, it clearly satisfies the condition

$$\mathbf{Z}_{out} = \mathbf{Z}_{in} = \mathbf{Z}_e\,. \tag{122}$$

Thus, the equation for determining the reference orbit becomes

$$\mathbf{Z}_e = \widehat{\mathcal{M}}\mathbf{Z}_e + \mathbf{A}, \quad \text{or} \quad \mathbf{Z}_e = \big(1-\widehat{\mathcal{M}}\big)^{-1}\mathbf{A}\,. \tag{123}$$

Here $\widehat{\mathcal{M}}$ and $\mathbf{A}$ are the transfer matrix and the shift vector for one period, respectively. The inverse of the matrix $1-\widehat{\mathcal{M}}$

can be expressed as

$$\left(1-\widehat{\mathcal{M}}\right)^{-1}=\frac{\cos^3\Theta_p}{1+\left(1-\mathrm{Sp}\widehat{\mathcal{M}}\right)\cos^3\Theta_p}\times \times\begin{pmatrix}1-\mathcal{M}_{22} & \mathcal{M}_{12}\\ \mathcal{M}_{21} & 1-\mathcal{M}_{11}\end{pmatrix}. \quad (124)$$

For the EMMA lattice in particular, the components of the one period transfer matrix and shift vector can be written explicitly as

$$\mathcal{M}_{11}=\frac{1}{c_p}\left[c_Fc_D+\left(\frac{\omega_D}{\omega_F}-L_0L_1\omega_F\omega_D\right)s_Fs_D+ +\left(L_0+L_1\right)\omega_Dc_Fs_D-L_1\omega_Fs_Fc_D\right], \quad (125)$$

$$\mathcal{M}_{12}=\frac{1}{\beta_e\gamma_ec_p}\left\{\left(\frac{L_0+L_1}{c_p}-X_ct_p\right)c_Fc_D+ +\left[\left(L_0L_1\omega_F\omega_D-\frac{\omega_D}{\omega_F}\right)X_ct_p-\frac{\omega_FL_1}{\omega_Dc_p}\right]s_Fs_D+ +\left[\frac{1}{\omega_Dc_p}-\left(L_0+L_1\right)\omega_DX_ct_p\right]c_Fs_D+ +\left(\frac{1}{\omega_Fc_p}+L_1\omega_FX_ct_p-\frac{L_0L_1\omega_F}{c_p}\right)s_Fc_D\right\}, \quad (126)$$

$$\mathcal{M}_{21}=-\frac{\beta_e\gamma_e}{c_p}(\omega_Fs_Fc_D+L_0\omega_F\omega_Ds_Fs_D-\omega_Dc_Fs_D), \quad (127)$$

$$\mathcal{M}_{22}=\frac{1}{c_p}\left[\frac{c_Fc_D}{c_p}+\left(L_0\omega_F\omega_DX_ct_p-\frac{\omega_F}{\omega_Dc_p}\right)s_Fs_D+ +\omega_F\left(X_ct_p-\frac{L_0}{c_p}\right)s_Fc_D-\omega_DX_ct_pc_Fs_D\right], \quad (128)$$

$$A_1=X_c+d_F+(d_D-d_F)(c_F-L_1\omega_Fs_F)+\left(\frac{X_c}{c_p}+d_D\right)\times \times\left[L_1\omega_Fs_Fc_D-c_Fc_D-\left(L_0+L_1\right)\omega_Dc_Fs_D- -\frac{\omega_Ds_Fs_D}{\omega_F}+L_0L_1\omega_F\omega_Ds_Fs_D\right]+ +t_p\left[(L_0+L_1)c_Fc_D+\frac{c_Fs_D}{\omega_D}+ +\frac{s_Fc_D}{\omega_F}-\frac{L_1\omega_Fs_Fs_D}{\omega_D}-L_0L_1\omega_Fs_Fc_D\right], \quad (129)$$

$$A_2=-\beta_e\gamma_e\omega_F\left(d_D-d_F\right)s_F+\beta_e\gamma_e\left(\frac{X_c}{c_p}+d_D\right)\times \times(\omega_Fs_Fc_D+\omega_F\omega_DL_0s_Fs_D-\omega_Dc_Fs_D)+ +\beta_e\gamma_et_p\left(c_Fc_D-\frac{\omega_Fs_Fs_D}{\omega_D}-\omega_FL_0s_Fc_D\right). \quad (130)$$

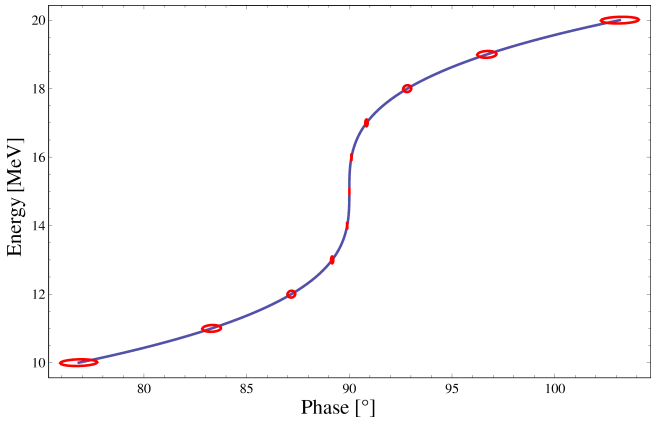

Fig. 6: Phase stability of the standard EMMA ring, for the central trajectory at $H_0=0$. The errors are given as 0.1MeV in energy and 1.3° in phase.

For the sake of brevity, the following notations

$$c_p=\cos\Theta_p,\quad c_F=\cos\left(\omega_FL_F\right),\quad c_D=\cosh\left(\omega_DL_D\right), \quad (131)$$

$$t_p=\tan\Theta_p,\quad s_F=\sin\left(\omega_FL_F\right),\quad s_D=\sinh\left(\omega_DL_D\right), \quad (132)$$

have been introduced in the final expressions for the components of the one period transfer matrix and shift vector.

B Phase stability in FFAGs

To study the stability of the serpentine acceleration in FFAG accelerators, we write the longitudinal Hamiltonian (106) in an equivalent form

$$H_0=\lambda\left(J^3+\cos\varphi\right). \quad (133)$$

Hamilton's equations of motion can be written as

$$\frac{\mathrm{d}\varphi}{\mathrm{d}\theta}=3bJ^2,\qquad \frac{\mathrm{d}J}{\mathrm{d}\theta}=b\sin\varphi\,. \quad (134)$$

Let $\varphi_a(\theta)$ and $J_a(\theta)$ be the exact solution of equations (134) described already in Section V. Let us further denote by φ_1 and J_1 a small deviation about this solution such that $\varphi=\varphi_a+\varphi_1$ and $J=J_a+J_1$. Then, the linearized equations of motion governing the evolution of φ_1 and J_1 are

$$\frac{\mathrm{d}\varphi_1}{\mathrm{d}\theta}=6bJ_aJ_1\,,\qquad \frac{\mathrm{d}J_1}{\mathrm{d}\theta}=b\varphi_1\cos\varphi_a\,. \quad (135)$$

The latter should be solved provided the constraint

$$3J_a^2J_1-\varphi_1\sin\varphi_a=0\,, \quad (136)$$

following from the Hamiltonian (133) holds. Differentiating the second of equations (135) with respect to θ and eliminating φ_1, we obtain

$$\frac{\mathrm{d}^2J_1}{\mathrm{d}\theta^2}-\frac{6b^2H_0}{\lambda}J_aJ_1+15b^2J_a^4J_1=0\,. \quad (137)$$

Next, we examine the case of separatrix acceleration with $H_0 = 0$. In Section V we showed that to a good accuracy the energy gain $[J_a(\theta) = b\theta + J_i]$ is linear in the azimuthal variable θ. Therefore, equation (137) can be written as

$$\frac{\mathrm{d}^2 J_1}{\mathrm{d}J_a^2} + 15 J_a^4 J_1 = 0\,. \tag{138}$$

The latter possesses a simple solution of the form

$$J_1 = \sqrt{|J_a|}\left[C_1 \mathcal{J}_{1/6}\left(\sqrt{\frac{5}{3}}\,|J_a|^3\right) + C_2 \mathcal{Y}_{1/6}\left(\sqrt{\frac{5}{3}}\,|J_a|^3\right)\right], \tag{139}$$

where $\mathcal{J}_\alpha(z)$ and $\mathcal{Y}_\alpha(z)$ stand for the Bessel functions of the first and second kind, respectively. In addition the constants C_1 and C_2 should be determined taking into account the initial conditions

$$\frac{\mathrm{d}J_1(J_i)}{\mathrm{d}J_a} = \varphi_1(J_i)\cos\varphi_i\,, \qquad J_1(J_i) = J_{1i}\,. \tag{140}$$

Submitted on November 12, 2009 / November 16, 2009

References

1. Kolomensky A.A. and Lebedev A.N. Theory of cyclic accelerators. North-Holland Publishing Company, 1966.
2. Kolomensky A.A. et al. Some questions of the theory of cyclic accelerators. Edition AN SSSR, 1956, v.26, no. 2, 7.
3. Symon K.R. et al. *Phys. Rev.*, 1956, v.103, 1837.
4. Kerst D.W. et al. *Review of Science Instruments*, 1960, v.31, 1076.
5. Aiba M. et al. Development of a FFAG proton synchrotron. *Proceedings of EPAC*, 2000, 581.
6. Edgecock R. et al. EMMA — the world's first non-scaling FFAG. *Proceedings of EPAC*, 2008, 3380.
7. Smith S.L. The status of the Daresbury Energy Recovery Linac Prototype (ERLP). *Proceedings of ERL*, 2007, 6.
8. Tzenov S.I. Contemporary accelerator physics. World Scientific, 2004.
9. Symon K.R. Derivation of Hamiltonians for accelerators. ANL/APS/TB-28, 1997.
10. Suzuki T. Equation of motion and Hamiltonian for synchrotron oscillations and synchrotron-betatron coupling. *KEK Report*, 1996, 96–10.
11. Koscielniak S. and Johnstone C. *Nuclear Instrum. and Methods A*, 2004, v. 523, 25.
12. Scott Berg J. *Physical Review Special Topics Accel. Beams*, 2006, v.9, 034001.

On Some New Ideas in Hadron Physics

Florentin Smarandache* and Vic Christianto†
*Department of Mathematics, University of New Mexico, Gallup, NM 87301, USA
E-mail: smarand@unm.edu
†Sciprint.org — a Free Scientific Electronic Preprint Server, http://www.sciprint.org
E-mail: vxianto@yahoo.com, admin@sciprint.org

We shortly review a series of novel ideas on the physics of hadrons and nuclear matter. Despite being vastly different in scope and content, these models share a common attribute, in that they offer unconventional viewpoints on infrared QCD and nuclear phenomena. In a sense, they are reminiscent of the plethora of formulations that have been developed over the years on classical gravitation: many seemingly disparate approaches can be effectively used to describe and explore the same physics.

1 Introduction

Given the extent and complexity of hadron and nuclear phenomena, any attempt for an exhaustive review of new ideas is outright unpractical. We survey here only a limited number of models and guide the reader to appropriate references for further information. The paper is divided in several sections according to the following plan:

1. The first section discusses the Brightsen model and the Nuclear String hypothesis;
2. Models inspired by Kerr-Newman twistor model and the AdS/CFT conjecture are introduced in the second section;
3. The last section discusses CGLE model of hadron masses and non-equilibrium phase transitions in infrared QCD.

The selection of topics is clearly incomplete and subjective. As such, it may not necessarily reflect the prevalent opinion of theorists working in this field. Our intent is to simply stimulate a constructive exchange of ideas in this active area of research.

2 Brightsen mdodel and the nuclear string hypothesis

In this hadron model, developed by M.Pitkanen [1] based on his TGD theory, it is supposed that ^{4}He nuclei and $A < 4$ nuclei and possibly also nucleons appear as basic building blocks of nuclear strings. This seems like some kind of improvement of the Close Packed Spheron model of L. Pauling in 1960s, which asserts that nuclei is composite form of small numbers of interacting boson-fermion nucleon clusters, i.e. ^{3}He (PNP), triton (NPN) and deuteron (NP). Another extension of Pauling model is known as Brightsen's cluster nuclei model, which has been presented and discussed by F. Smarandache and D. Rabounski [2].

Interestingly, it can be shown that the Close Packed model of nuclei may explain naturally why all the upper quarks have fractional electric charge at the order of $Q = +\frac{2}{\sqrt{3}}$. So far this is one of the most mysterious enigma in the hadron physics. But as described by Thompson [4], in a closed-packed crystal sheet model, the displacement coefficients would be given by a matrix where the 1-1 component is:

$$c_{11} = \frac{2\rho}{\sqrt{3}} - 1\,, \tag{1}$$

where the deformation can be described by the resolved distance between columns, written as ρd. Here d represents diameter of the nuclei entity. Now it seems interesting to point out here that if we supposed that $\rho = 1 + \frac{\sqrt{3}}{2}$, then c from equation (3) yields exactly the same value with the upper quark's electric charge mentioned above. In other words, this seems to suggest plausible deep link between QCD/quark charges and the close-packed nuclei picture [3].

Interestingly, the origin of such fractional quark charge can also be described by a geometric icosahedron model [4]. In this model, the concept of quark generation and electroweak charge values are connected with (and interpreted as) the discrete symmetries of icosahedron geometry at its 12 vertices. Theoretical basis of this analog came from the fact that the gauge model of electroweak interactions is based on SU(2)×U(1) symmetry group of internal space. Meanwhile, it is known that SU(2) group corresponds to the O(3) group of 3D space rotations, hence it appears quite natural to connect particle properties with the discrete symmetries of the icosahedron polygon.

It is worth to mention here that there are some recent articles discussing plausible theoretical links between icosahedron model and close-packed model of nuclei entities, for instance by the virtue of Baxter theory [5]. Furthermore, there are other articles mentioning theoretical link between the close-packed model and Ginzburg-Landau theory. There is also link between Yang-Baxter theory and Ginzburg-Landau theory [6]. In this regards, it is well known that cluster hydrogen or cluster helium exhibit superfluidity [7, 8], therefore it suggests deep link between cluster model of Pauling or Brightsen and condensed matter physics (Ginzburg-Landau theory).

The Brightsen model supports a hypothesis that antimatter nucleon clusters are present as a parton (*sensu* Feynman) superposition within the spatial confinement of the proton

($^1H_1$), the neutron, and the deuteron ($^1H_2$). If model predictions can be confirmed both mathematically and experimentally, a new physics is suggested. A proposed experiment is connected to orthopositronium annihilation anomalies, which, being related to one of known unmatter entity, orthopositronium (built on electron and positron), opens a way to expand the Standard Model.

Furthermore, the fact that the proposed Nuclear String hypothesis is derived from a theory which consists of many-sheeted spacetime framework called TGD seems to suggest a plausible link between this model and Kerr-Schild twistor model as described below.

3 Multiparticle Kerr-Schild twistor model and AdS/CFT Light-Front Holography model

Kerr's multiparticle solution can be obtained on the basis of the Kerr theorem, which yields a many-sheeted multi-twistorial spacetime over M^4 with some unusual properties. Gravitational and electromagnetic interaction of the particles occurs with a singular twistor line, which is common for twistorial structures of interacting particles [6].

In this regards the Kerr-Newman solution can be represented in the Kerr-Schild form [9]:

$$g_{\mu\nu} = \eta_{\mu\nu} + 2hk_\mu k_\nu \,, \qquad (2)$$

where $\eta_{\mu\nu}$ is the metric of auxiliary Minkowski spacetime.

Then the Kerr theorem allows one to describe the Kerr geometry in twistor terms. And using the Kerr-Schild formalism, one can obtain exact asymptotically flat multiparticle solutions of the Einstein-Maxwell field equations. But how this model can yield a prediction of hadron masses remain to be seen. Nonetheless the axial stringy system corresponds to the Kerr-Schild null tetrad can be associated with superconducting strings. Interestingly one can find an interpretation of Dirac equation from this picture, and it is known that Dirac equation with an effective QCD potential can describe hadron masses.

What seems interesting from this Kerr-Schild twistor model, is that one can expect to give some visual interpretation of the electromagnetic string right from the solution of Einstein-Maxwell field equations. This would give an interesting clue toward making the string theory a somewhat testable result. Another approach to connect the superstring theory to hadron description will be discussed below, called Light-Front Holography model.

Brodsky et al. [10, 11] were able to prove that there are theoretical links, such that the Superstring theory reduces to AdS/CFT theory, and Ads/CFT theory reduces to the so-called Light Front Holography, which in turn this model can serve as first approximation to the Quantum Chromodynamics theory.

Starting from the equation of motion in QCD, they identify an invariant light front coordinate which allows separation of the dynamics of quark and gluon binding from the kinematics of constituent spin and internal orbital angular momentum. Of most interesting here is that this method gives results in the from of 1-parameter light-front Schrödinger equation for QCD which determines the eigenspectrum and the light-front wavefunctions of hadrons for general spin and orbital angular momentum.

The light-front wave equation can be written as [8]:

$$\left(-\frac{d^2}{d\zeta^2} - \frac{1-4L^2}{4\zeta^2} + U(\zeta)\right)\phi(\zeta) = M^2\phi(\zeta)\,, \qquad (3)$$

which is an effective single-variable light-front Schrödinger equation which is relativistic, covariant, and analytically tractable; here M represents the mass spectra.

Nonetheless, whether this Light-Front Holography picture will yield some quantitative and testable predictions of hadron masses, remains to be seen.

4 Concluding note

We shortly review a series of novel ideas on the physics of hadrons and nuclear matter. Despite being vastly different in scope and content, these models share a common attribute, in that they offer unconventional viewpoints on hadron, nuclear phenomena, and infrared QCD. In a sense, they are reminiscent of the plethora of formulations that have been developed over the years on classical gravitation: many seemingly disparate approaches can be effectively used to describe and explore the same physics.

These very interesting new approaches, therefore, seem to suggest that there is a hitherto hidden theoretical links between different approaches.

In our opinion, these theoretical links worth to discuss further to prove whether they provide a consistent picture, in particular toward explanation of the hadron mass generation mechanism and spontaneous symmetry breaking process.

The present article is a first part of our series of review of hadron physics. Another part is under preparation.

Acknowledgements

One of the authors (VC) wishes to express his gratitude to Profs. A. Yefremov and M. Fil'chenkov for kind hospitality in the Institute of Gravitation and Cosmology, PFUR.

Submitted on February 09, 2009 / Re-submitted on November 09, 2009
Accepted on November 27, 2009

References

1. Pitkanen M. Nuclear string hypothesis. In: F. Smarandache & V. Christianto (eds.) *Hadron Models and Related New Energy Issues*, InfoLearnQuest Publ., USA, 2008.
2. Smarandache F., Rabounski D. Unmatter entities inside nuclei, predicted by the Brightsen Nucleon Cluster Model. *Progress in Physics*, 2005, v. 2.
3. Thompson J.M.T. Instabilities and catastrophes in science and engineering. John Wiley & Sons Ltd, New York, 1982, pp. 96 and 101.

4. Vladimirov Yu.S. Quark icosahedron, charges and Weinberg's angle. *Grav. & Cosmology*, 2004, v. 10, no. 1–2(37–38), 63–70.
5. Esposito G. & Marmo G. arXiv: math-ph/0511063.
6. Gomez C. & Sierra G. arXiv: hep-th/9309007.
7. Mezzacapo F. & Boninsegni M. Structure, superfluidity and quantum melting of hydrogen cluster. arXiv: cond-mat/ 0611775.
8. Serot B.D. & Walecka J.D. arXiv: nucl-th/0010031; nucl-th/9701058.
9. Burinskii A. Axial stringy system of the Kerr spinning particle. *Grav. & Cosmology*, 2004, v. 10, no. 1–2(37–38), 50–60.
10. Brodsky S. Dynamic versus static hadronic structure functions. arXiv: 0901.0781.
11. de Teramond G. F. & Brodsky S. J. Light-front holography: a first approximation to QCD. arXiv: 0809.4899.

LETTERS TO PROGRESS IN PHYSICS

LETTERS TO PROGRESS IN PHYSICS

Coordinate Transformations and Metric Extension: a Rebuttal to the Relativistic Claims of Stephen J. Crothers

Jason J. Sharples

School of Physical, Environmental and Mathematical Sciences, University of New South Wales
at the Australian Defence Force Academy, Canberra 2600, Australia
E-mail: j.sharples@adfa.edu.au

The concept of coordinate transformation is fundamental to the theory of differentiable manifolds, which in turn plays a central role in many modern physical theories. The notion of metric extension is also important in these respects. In this short note we provide some simple examples illustrating these concepts, with the intent of alleviating the confusion that often arises in their use. While the examples themselves can be considered unrelated to the theory of general relativity, they have clear implications for the results cited in a number of recent publications dealing with the subject. These implications are discussed.

1 Introduction

Differentiable manifolds play a central role in modern physical theories. Roughly speaking, a differentiable manifold (hereafter manifold) is a topological space whose local equivalence to Euclidean space permits a global calculus. In more precise mathematical terms, a manifold is a topological space M with a collection of coordinate systems that cover all of M. Thus the concept of a coordinate system is fundamental to the notion of manifold.

A coordinate system is defined as a mapping ϕ (with certain properties) from an open set U of a topological space onto an open set $\phi(U)$ of Euclidean space. The open set U is called the coordinate neighborhood of ϕ and the functions $x^1, \ldots, x^n$ on U such that $\phi = \left(x^1, \ldots, x^n\right)$, are the coordinate functions, or more simply the coordinates. A manifold can have an infinite number of equally valid coordinates defined on it.

As an example consider the topological space S^2 (the unit sphere). Further consider the northern and southern hemispheres of the sphere, which are both open subsets of S^2. On each of the hemispheres we can define stereographic coordinates by projecting the respective hemispheres onto two-dimensional Euclidean space. Each of the projections defines a coordinate system, which when taken together cover all of S^2. Thus S^2 is a manifold.

The notion of a metric tensor g on a manifold M is fundamental to the theory of differential geometry (indeed, the metric tensor is alternatively called the first fundamental form). Explicitly, g is a type-(0,2) tensor that defines a scalar product $g(p)$ on the tangent space $T_p(M)$, for each point $p \in M$. On a domain U, corresponding to a particular coordinate system $\{x^1, \ldots, x^n\}$, the components of the metric tensor are $g_{ij} = g(\partial_i, \partial_j)$. It is important to note that the metric components g_{ij} are functions, not tensors. The metric tensor itself is given by $g = g_{ij}\, dx^i \otimes dx^j$, where summation over the indices is implied. It must be stressed that a metric, by virtue of the fact that it is a tensor, is independent of the coordinate system which is used to express the component functions g_{ij}.

The metric tensor can be represented by its line-element ds^2, which gives the associated quadratic form of $g(p)$. We stress that a line-element is *not* a tensor. A line-element can be expressed in terms of a coordinate system as

$$ds^2 = g_{ij}\, dx^i\, dx^j.$$

Representing the metric in a particular coordinate system by the associated quadratic form is equivalent to expressing it as a square matrix with respect to the coordinate basis. For example, on the unit sphere the metric σ is often written in terms of the line-element with respect to spherical coordinates $\{\theta, \varphi\}$ as

$$ds^2 = d\theta^2 + \sin^2\theta\, d\varphi^2,$$

or equivalently as the matrix

$$[\sigma]_{\{\theta,\varphi\}} = \begin{pmatrix} 1 & 0 \\ 0 & \sin^2\theta \end{pmatrix}.$$

It is important when practicing differential geometry to distinguish between coordinate dependent quantities and coordinate invariant quantities. We have already seen some examples of these: the metric tensor is coordinate invariant (as is any tensor), while the line-element is coordinate dependent. Another example of a coordinate dependent quantity are the Christoffel symbols

$$\Gamma^i_{jk} = g^{im}\left(\partial_k g_{mj} + \partial_j g_{mk} - \partial_m g_{jk}\right)$$

while the scalar curvature (Kretschmann scalar), which is derived from them as

$$f = g^{ab}\left(\partial_c \Gamma^c_{ab} - \partial_b \Gamma^c_{ac} + \Gamma^d_{ab}\Gamma^c_{cd} - \Gamma^d_{ac}\Gamma^c_{bd}\right),$$

is coordinate invariant. Another example of a coordinate invariant quantity is the metric length of a path in a manifold.

Suppose now that we have two different sets of coordinates defined on an open set $U \subset M$. That is to say that we have two mappings ϕ_1 and ϕ_2 that act from U onto two (possibly different) open sets V_1 and V_2 in Euclidean space. It is apparent that we can change from one coordinate system to the other with the maps $\phi_2 \circ \phi_1^{-1}$ or $\phi_1 \circ \phi_2^{-1}$. Such maps define a change of coordinates or *coordinate transformation*. Alternatively if we have a mapping ζ from V_1 into V_2 and a coordinate system (mapping) ϕ from U onto V_1, then the mapping $\zeta \circ \phi$ also defines a coordinate system. In this context ζ is the coordinate transformation. Coordinate invariant quantities, such as the metric, the scalar curvature and lengths, do not change under the action of a coordinate transformation

In what follows we illustrate these concepts by means of some simple examples and discuss some of their implications.

2 Some simple examples

We begin by illustrating the concept of coordinate transformation with a simple example in ordinary Euclidean 3-space (E^3). Suppose that (r, θ, φ) are the usual spherical coordinates on E^3 and consider the spherically symmetric line-element

$$ds^2 = r^2\, dr^2 + r^2\, d\Omega^2, \tag{1}$$

where $d\Omega^2 = d\theta^2 + \sin^2\theta\, d\varphi^2$ is the usual shorthand for the line-element on the unit sphere S^2.

Defining a new radial coodinate ρ by $2\rho = r^2$, the line-element can be written in terms of the coordinates (ρ, θ, φ) as

$$ds^2 = d\rho^2 + 2\rho\, d\Omega^2. \tag{2}$$

Note that if ρ is held constant then the line-element reduces to the standard line-element for a sphere of radius $\sqrt{2\rho} = r$.

Note that the coordinate transformation has changed nothing. The metrics corresponding to the line-elements given by (1) and (2) are exactly the same tensor, they have just been expressed in two different sets of coordinates. To illustrate this consider calculating metric length along a radial line. Specifically, consider the path defined in terms of the (r, θ, ϕ) coordinates by

$$\gamma_a = \{(r, \theta, \varphi) : r \in (0, a),\ \theta = \pi/4,\ \varphi = 0\}.$$

Equivalently, we can define the path in terms of the (ρ, θ, φ) coordinates as

$$\gamma_a = \{(\rho, \theta, \varphi) : \rho \in (0, a^2/2),\ \theta = \pi/4,\ \varphi = 0\}.$$

Thus calculating the metric length of the path γ_a with respect to the line-element (1) we find

$$L(\gamma_a) = \int_{r=0}^{r=a} r\, dr = \frac{a^2}{2},$$

while if we calculate it with respect to the line-element (2) we find that

$$L(\gamma_a) = \int_{\rho=0}^{\rho=a^2/2} d\rho = \frac{a^2}{2}\,.$$

This confirms that the metric length does not depend on the particular coordinate expression (line-element) representing the metric.

This example also illustrates another interesting property of the metric corresponding to (1) or (2). If we set $\rho = b$, where b is a constant, the line-element (2) reduces to the 2D line-element:

$$ds^2 = 2b\, d\Omega^2.$$

This is the line-element of a 2-sphere with a radius of curvature of $\sqrt{2b}$, i.e. the Gaussian curvature is $1/2b$. However, calculating the metric distance d from the origin ($\rho = 0$) to this sperical shell ($\rho = b$), we find that

$$d = \int_0^b d\rho = b.$$

Hence, the metric radius and the radius of curvature are not equal in general. Repeating the calulation with (1) yields the same result.

As another example consider the two-dimensional, non-Euclidean metric

$$ds_1^2 = -x^2\, dt^2 + dx^2, \tag{3}$$

where it is assumed that $t \in (-\infty, \infty)$ and $x \in (0, \infty)$. In terms of the coordinates $\{t, x\}$ the metric tensor g_1 can therefore be represented as

$$[g_1]_{\{t,x\}} = \begin{pmatrix} -x^2 & 0 \\ 0 & 1 \end{pmatrix}, \tag{4}$$

with a metric determinant of $|g_1| = -x^2$, which suggests that as $x \to 0$ the metric becomes singular.

However, calculating the scalar curvature of the metric we find that $R_{g_1} = 0$, which is independent of x. The metric g_1 therefore defines a flat manifold (N, g_1). The fact that the singularity arises in the coordinate dependent form of the metric, but not in the coordinate invariant scalar curvature, indicates that the apparent singularity may in fact be due solely to a breakdown in the coordinate system $\{t, x\}$ that was chosen to represent the metric, i.e. it may merely be a *coordinate singularity* rather than a true singularity of the manifold described by g_1. A coordinate singularity can be removed by a good choice of coordinates, whereas a true singularity cannot.

Introducing new coordinates $\{T, X\}$, which are defined in terms of the old coordinates $\{t, x\}$ by

$$X = x \cosh t$$
$$T = x \sinh t,$$

the line-element ds_1^2 may be written as

$$ds_1^2 = -dT^2 + dX^2. \tag{5}$$

Note that $t \in (-\infty, \infty)$ and $x \in (0, \infty)$ implies that $T \in (-\infty, \infty)$ and $X \in (0, \infty)$ also.

In terms of the $\{T, X\}$ coordinates, the metric tensor g_1 is represented by

$$[g_1]_{\{T,X\}} = \begin{pmatrix} -1 & 0 \\ 0 & 1 \end{pmatrix}. \tag{6}$$

and so the metric determinant is $|g_1| = -1$. The apparent singularity has been removed by invoking a good choice of coordinates.

We note further that even though the line-element (5) was only defined for $X \in (0, \infty)$ there is now nothing stopping us from extending the definition to include $X \in (-\infty, \infty)$. We thus make the distinction between the line-element ds_1^2, defined above, and the line-element ds_2^2 defined as

$$ds_1^2 = -d\tau^2 + d\xi^2, \tag{7}$$

with coordinates $\tau, \xi \in (-\infty, \infty)$. The metric corresponding to the line-element (7), denoted by g_2, defines a manifold (M, g_2) that can be thought of as 2D Minkowski space. By restricting the coordinate ξ to the semi-finite interval $(0, \infty)$ we recover the metric g_1, that is

$$g_2|_{\xi>0} = g_1.$$

It follows that the manifold (N, g_1) is a submanifold of the Minkowski space (M, g_2). Alternatively we say that (M, g_2) is a *coordinate extension* of the manifold (N, g_1). The manifold (N, g_1) is known as the *Rindler wedge* and corresponds to that part of (M, g_2) defined by $|\tau| < \xi$.

3 Implications

In [1] the author notes that the line-element written in terms of coordinates $\{t, r, \theta, \varphi\}$ as

$$ds^2 = A(r)\,dt^2 + B(r)\,dr^2 + C(r)\,d\Omega^2 \tag{8}$$

corresponds to the most general spacetime metric that is static and spherically symmetric. He then goes on to claim that the line-element written in terms of coordinates $\{t, \rho, \theta, \phi\}$ as

$$ds^2 = A^*(\rho)\,dt^2 + B^*(\rho)\,d\rho^2 + \rho^2\,d\Omega^2 \tag{9}$$

does *not* correspond to the most general metric that is static and spherically symmetric*. This claim is false, as we will now demonstrate.

Consider the line-element (9) and define the coordinate transformation $\rho = \sqrt{C(r)}$, where C is some function independent of the functions A^* and B^*. Taking the differential we find that

$$d\rho = \frac{C'(r)}{2\sqrt{C(r)}}\,dr$$

and so the line-element (9) can be written in terms of the coordinates $\{t, r, \theta, \varphi\}$ as

$$ds^2 = E(r)\,dt^2 + D(r)\,dr^2 + C(r)\,d\Omega^2, \tag{10}$$

where

$$E(r) = A^*\left(\sqrt{C(r)}\right) \quad \text{and} \quad D(r) = \frac{B^*\left(\sqrt{C(r)}\right) C'(r)^2}{4C(r)}.$$

Since the functions A^* and B^* are independent of the function C, the functions E and D are also independent of the function C. The line-element (10) is identical to (8) and it follows that the metrics represented by (8) and (9) are the same metric (just expressed in terms of different coordinates), and therefore that both line-elements represent the most general static, sperically symmetric spacetime metric.

Based on the claim of [1], just shown is false, the author goes on to conclude that solutions of the gravitational field equations that are derived from the metric ansatz (9) are particular solutions rather than general solutions. These claims are also false for the same reasons as illustrated above.

The foregoing considerations therefore have bearing on the relativistic arguments contained in [1] and subsequent papers by the author. For example, in [1–8] the author repeatedly makes the following claims:

1. The coordinate ρ, appearing in (9), is not a proper radius;
2. The "Schwarzschild" solution, as espoused by Hilbert and others is different to the Schwarzschild solution obtained originally by Schwarzschild [9];
3. The original Schwarzschild solution is a complete (i.e. inextendible) metric;
4. There are an infinite number of solutions to the static, spherically symmetric solutions to the field equations correponding to a point mass;
5. For line-elements of Schwarzschild form†, the scalar curvature f remains bounded everywhere, and hence there is no "black hole".

We will now address and dismiss each of these claims.

Claim 1. The claim that ρ is not a proper radius stems from a calculation in [1]. The author defines the proper radius as

$$R_p = \int \sqrt{B(r)}\,dr \tag{11}$$

where B is the function appearing in (8). Strictly speaking this is not a radius, per se, but a *function* of the coordinate r. In more precise terms, the proper radius should be defined as the metric length of the radial path γ_a defined by‡

$$\gamma_a = \{(t, r, \theta, \varphi) : r \in (a_1, a_2),\ t, \theta, \varphi = \text{constant}\}.$$

This then implies that the proper radius is defined as

$$R_p = L_1(\gamma_a) = \int_{a_1}^{a_2} \sqrt{B(r)}\,dr\,. \tag{12}$$

*Note that in [1] the author has used r again instead of ρ. We use the different symbol ρ to avoid confusion.

†Line-elements of "Schwarzschild form" are defined in [2].

‡We believe that this is what the definition in [1] was actually aiming at.

The claim in [1] relates to the fact that R_p, as defined by (11), is equal to r only if $B(r) = 1$. This conclusion is based on an imprecise definition of the proper radius and does not take into account the effect of coordinate transformation. If we work in terms of the coordinates appearing in the line-element (9), which we have already shown represents the same metric as (8), then the path γ_a is defined as

$$\gamma_a = \{(t, \rho, \theta, \varphi) : \rho \in (\rho_1, \rho_2),\ t, \theta, \varphi = \text{constant}\},$$

with $\rho_1 = \sqrt{C(a_1)}$ and $\rho_2 = \sqrt{C(a_2)}$. In terms of the line-element (9) the metric length of γ_a is given by

$$L_2(\gamma_a) = \int_{\sqrt{C(a_1)}}^{\sqrt{C(a_2)}} \sqrt{B^*(\rho)}\, d\rho.$$

Noting the effect of the coordinate transformation, that was established earlier, we then find that

$$\begin{aligned} R_p = L_1(\gamma_a) &= \int_{a_1}^{a_2} \sqrt{B(r)}\, dr \\ &= \int_{a_1}^{a_2} \left[B^*(\sqrt{C(r)}\right]^{1/2} \frac{C'(r)}{2\sqrt{C(r)}}\, dr \\ &= \int_{\sqrt{C(a_1)}}^{\sqrt{C(a_2)}} \sqrt{B^*(\rho)}\, d\rho \\ &= L_2(\gamma_a)\,. \end{aligned}$$

Hence the proper radius does not depend on the form of the line-element. Proper radius (i.e. a metric length) can be equivalently defined in terms of either of the "radial" coordinates r or ρ.

Claims 2 and 3. The original Schwarzschild solution obtained in [9] is given as the line-element

$$ds^2 = A(R)dt^2 - A(R)^{-1}dR^2 - R^2 d\Omega^2, \qquad (13)$$

where

$$A(R) = 1 - \frac{\alpha}{R} \quad \text{and} \quad R = (r^3 + \alpha^3)^{1/3}.$$

The coordinate $r \in (0, \infty)$ that appears is the standard spherical radial coordinate. The expression $R = (r^3 + \alpha^3)^{1/3}$ defines a transformation of the radial coordinate r into the auxilliary radial coordinate R. The constant α is related to the value of the mass at the origin [9]. Indeed, by imposing the additional boundary condition at infinity, that the solution be consistent with the predictions of Newtonian gravitational theory, it is found that the constant $\alpha = 2m$, where m is the mass at the origin. The line-element (13) can therefore be written as

$$ds^2 = \left(1 - \frac{2m}{R}\right)dt^2 - \left(1 - \frac{2m}{R}\right)^{-1} dR^2 - R^2 d\Omega^2, \qquad (14)$$

with $R \in (2m, \infty)$. Note that if R and t are held constant (say $R = a$ and $t = t_0$) the line-element reduces to that of a 2-sphere with radius $a > 2m$. The line-element therefore defines a manifold that is foliated by 2-spheres with radii greater than $2m$.

The line-element is of precisely the same form as the line-element derived by Hilbert [10], i.e.

$$ds^2 = \left(1 - \frac{2m}{\rho}\right)dt^2 - \left(1 - \frac{2m}{\rho}\right)^{-1} d\rho^2 - \rho^2 d\Omega^2, \qquad (15)$$

where $\rho \in (0, 2m) \cup (2m, \infty)$. The only difference is that (14) is defined over a subset of the domain over which (15) is defined. To obtain the line-element (15) the radial coordinate has been extended to values less than $2m$ in much the same way that the metric corresponding to (5) was extended to the metric corresponding to (7). The only real difference is that in the case at hand there remains a coordinate singularity at $R = 2m$, and so in terms of the coordinates used, the extended manifold must be viewed as a disjoint union of the regions corresponding to $R < 2m$ and $R > 2m$. Both of the disjoint regions satisfy the static, spherically symmetric field equations. In fact it is well-known that there exist coordinates in which the difficulty at $R = 2m$ can be removed, resulting in a single manifold that satisfies the field equations. As a point of historical interest we note that the extended metric is also known as the "Schwarzschild" metric in honour of Schwarzschild's contribution to the field, despite the fact that his original solution is only a subset of the complete solution.

From the above considerations it clear that the manifold corresponding to the line-element (13) is incomplete. Indeed, in deriving this form of the line-element, Schwarzschild imposed a very specific boundary condition, namely that the line-element is continuous everywhere except at $r = 0$, where $r \in (0, \infty)$ is the standard spherical radial coordinate. Imposition of this boundary condition has significant implications for the solution obtained. In particular, as a consequence of the boundary condtion the coordinate R is shifted away from the origin. Indeed, if $r \in (0, \infty)$ then $R \in (\alpha, \infty)$. Hence the manifold represented by (13) is foliated by 2-spheres of radius greater than $\alpha = 2m$ — the spacetime has a hole in its centre!

Claim 4. In [2] the author derives the general solution for the static, spherically symmetric field due to a point mass as

$$ds^2 = \left(\frac{\sqrt{C_n} - \alpha}{\sqrt{C_n}}\right)dt^2 - \left(\frac{\sqrt{C_n}}{\sqrt{C_n} - \alpha}\right)\frac{C_n'^2}{4C_n}dr^2 - C_n\, d\Omega^2, \qquad (16)$$

where r is the standard radial spherical coordinate and

$$C_n(r) = \left[(r - r_0)^n + \alpha^n\right]^{2/n} \qquad (17)$$

with $r_0 \geqslant 0$ and $n > 0$ arbitrary constants. The author also notes that (16) is only defined for $r > r_0$.

Let us now see the effect of transforming coordinates. Firstly, let $\rho = r - r_0$ so that the coordinate ρ is simply a shifted

version of the coordinate r. Taking differentials implies that $d\rho = dr$ and so we may equivalently write the line-element (16) as

$$ds^2 = \left(\frac{\sqrt{C_n}-\alpha}{\sqrt{C_n}}\right)dt^2 - \left(\frac{\sqrt{C_n}}{\sqrt{C_n}-\alpha}\right)\frac{C_n'^2}{4C_n}d\rho^2 - C_n\, d\Omega^2, \quad (18)$$

where now

$$C_n(\rho) = [\rho^n + \alpha^n]^{2/n}$$

and the line-element is defined for $\rho > 0$.

Secondly, define another change of coordinates by $R = \sqrt{C_n(\rho)}$. This is essentially a rescaling of the radial coordinate ρ. Taking differentials we find that

$$dR = \frac{C_n'}{2\sqrt{C_n}}\, d\rho\,.$$

Thus in terms of the coordinate R the line-element may be written as

$$ds^2 = \left(\frac{R-\alpha}{R}\right)dt^2 - \left(\frac{R}{R-\alpha}\right)dR^2 - R^2\, d\Omega^2, \quad (19)$$

where the coordinate $R > \alpha$.

Hence we have shown that what appeared to be an infinitude of particular solutions are actually just different coordinate expressions of the same solution, which without loss of generality can be expressed in "Schwarzschild coordinates" $\{t, R, \theta, \varphi\}$ by (19). This solution is incomplete, as we have already seen, since the line-element and the corresponding metric are only defined when the coordinate $R > \alpha$. The solution is known as the *exterior* Schwarzschild solution.

Another way of seeing that the metrics corresponding to the line-elements defined by (16) are all the same, is by invoking Birkoff's Theorem [11]. This theorem establishes, with mathematical certainty, that the Schwarzschild solution (exterior, interior or both) is the only solution of the spherically symmetric vacuum field equations*.

Claim 5. In [2] the author notes that the scalar curvature of the metric corresponding to (16) is given by

$$f = \frac{12\alpha^2}{C_n^3} = \frac{12\alpha^2}{[(r-r_0)^n + \alpha^n]^{6/n}}$$

and that as $r \to r_0$ there is no curvature singularity. He then concludes that a "black hole" singularity cannot exist.

In fact, as we have just seen, the line-element (16) only corresponds to the exterior Schwarzschild solution, which is a manifold foliated by 2-spheres with radial coordinate $R > \alpha$. The calculation in [2] therefore only proves that the exterior solution has no curvature singularity. This is a well known fact. Writing (16) in its equivalent form (19) and extending the coordinate R to obtain the *interior* Schwarzschild solution ($0 < R < \alpha$), the scalar curvature is given by

$$f = \frac{12\alpha^2}{R^3}\,,$$

from which it is clear that

$$\lim_{R\to 0} f = \infty\,.$$

Hence there is a curvature singularity at $R = 0$. Since the vector ∂_R is timelike for $0 < R < \alpha$, the singularity corresponds to a black hole.

4 Conclusions

We have presented a number of simple examples which hopefully elucidate the concepts of coordinate transformation and metric extension in differential geometry. Implications of the concepts were also discussed, with particular focus on a number of the relativistic claims of [1–8]. It was proven that each of these claims was false. The claims appear to arise from a lack of understanding of the notions of coordinate transformation and metric (coordinate) extension. Any conclusions contained in [1–8] that are based on such claims should therefore be considered as unproven. In particular, the claim that the black hole "is not consistent at all with general relativity" is completely false.

General relativity is a difficult topic, which is grounded in advanced mathematics (indeed, Einstein himself is quoted as saying something along the lines of "Ever since the mathematicians took hold of relativity, I no longer understand it myself!"). A sound understanding of differential geometry is a prerequisite for understanding the theory in its modern form. Thus to paraphrase Lao Tzu [12] — beware of the half-enlightened master.

Postscript

The article by Stephen J. Crothers in the current issue [13] provides a good illustration of the problems discussed above. For example, in his first "counter-example" he considers a metric which is easily seen to be the Schwarzschild metric written in terms of an 'inverted' radial coordinate. Using x to denote the inverted radial coordinate (denoted by r in [13]), and R to denote the usual Schwarzschild radius, the transformation is $R = 2m - x$. In particular, $R = 0$ corresponds to $x = 2m$, and $R = 2m$ corresponds to $x = 0$. It is thus not surprising that the coordinate singualrity is at $x = 0$ and the point singularity is at $x = 2m$. The other counter-examples in [13] can be dismissed through similar arguments.

The author is grateful to S. J. Crothers for a number of discussion that resulted in the writing of this paper.

Submitted on August 06, 2009 / Accepted on August 14, 2009

*The assumption of staticity is not actually required, hence all spherically symmetric spacetimes satisfying the vacuum field equations are static.

References

1. Crothers S. J. On the geometry of the general solution for the vacuum field of the point-mass. *Progress in Physics*, 2005, v. 2, 3–14.
2. Crothers S. J. On the general solution to Einstein's vacuum field and its implications for relativistic degeneracy. *Progress in Physics*, 2005, v. 1, 68–73.
3. Crothers S. J. On the ramifications of the Schwarzschild space-time metric. *Progress in Physics*, 2005, v. 1, 77–80.
4. Crothers S. J. On the generalisation of Kepler's 3rd Law for the vacuum field of the point-mass. *Progress in Physics*, 2005, v. 2, 70–75.
5. Crothers S. J. On the vacuum field of a sphere of incompressible fluid. *Progress in Physics*, 2005, v. 2, 76–81.
6. Crothers S. J. On the general solution to Einstein's vacuum field for the point-mass when $\lambda \neq 0$ and its implications for relativistic cosmology. *Progress in Physics*, 2005, v. 3, 8–18.
7. Crothers S. J. Introducing distance and measurement in general relativity: changes for the standard tests and the cosmological large scale. *Progress in Physics*, 2005, v. 3, 41–47.
8. Crothers S. J. A short discussion of relativistic geometry. *Bulletin of Pure and Applied Sciences*, 2005, v. 3(2), 267–273.
9. Schwarzschild K. Über das Gravitationsfeld eines Massenpunktes nach der Einsteinschen Theorie. *Sitzungsberichte der Königlich Preussischen Akademie der Wissenschaften*, 1916, 189–196 (published in English as: Schwarzschild K. On the gravitational field of a point mass according to Einstein's theory. *The Abraham Zelmanov Journal*, 2008, vol. 1, 10–19).
10. Hilbert, D. *Nachr. Ges. Wiss. Gottingen, Math. Phys. Kl.*, 1917, v. 53.
11. Birkoff, G.D. *Relativity and Modern Physics*, Cambridge, MA: Harvard University Press.
12. Lao Tzu. Tao Te Ching. Penguin, 1963.
13. Crothers S.J. The Kruskal-Szekeres "extension": Counter-examples *Progress in Physics*, 2010, v. 1, 3–7.

LETTERS TO PROGRESS IN PHYSICS

On Crothers' Assessment of the Kruskal-Szekeres "Extension"

Ulrich E. Bruchholz

Wurzen, Germany. E-mail: Ulrich.Bruchholz@t-online.de; http://www.bruchholz-acoustics.de

I agree with Crothers in it that any introduction of Kruskal-Szekeres coordinates is unnecessary. The solution of problems from so-called Schwarzschild solutions appears amazingly simpler than discussed in Crothers' paper.

S. J. Crothers [1] discusses the introduction of Kruskal-Szekeres coordinates, which pursue the target to avoid certain forms of singularity and the change of signature. Crothers argues that this measure is off target. — Let me note following:

1. The Kruskal-Szekeres coordinates as quoted with the equations before Eq. (4) of [1] mingle time and length. That is physically self-defeating. Moreover, any real coordinate transformation does not change the situation with the original coordinates.

2. The solution according to Eq. (1) of [1] is physically difficult for the coordinate singularity. We should take notice of this fact instead of doing inept tries, see item 1.

3. The general central symmetric and time-independent solution of $R_{\mu\nu} = 0$ is the first part of Schwarzschild's actual solution

$$ds^2 = \Big(1 - \frac{\alpha}{R}\Big)dt^2 - \Big(1 - \frac{\alpha}{R}\Big)^{-1} dR^2 - \\ - R^2(d\theta^2 + \sin^2\theta\, d\varphi^2)\,,$$

in which R is an *arbitrary* function of r within the limit that metrics must be asymptotically Minkowski spacetime, i.e. $R \Rightarrow r$ for great r. α is an integration constant related to the mass,

$$\alpha = \frac{\kappa m}{4\pi}\,.$$

This solution is based on "virtual" coordinate transformation, which is possible for the degrees of freedom from Bianchi identities.

4. Above solution implies also an isotropic solution without singularity at the event horizon

$$ds^2 = \Big(\frac{r - r_g}{r + r_g}\Big)^2 dt^2 - \\ -\Big(1 + \frac{r_g}{r}\Big)^4 \left(dr^2 + r^2(d\theta^2 + \sin^2\theta\, d\varphi^2)\right)$$

with

$$r_g = \frac{\alpha}{4} = \frac{\kappa m}{16\pi}\,.$$

The event horizon (at $r = r_g$) turns up to be a geometric boundary with $g = 0$.

5. Any change of signature is physically irrelevant, because areas with different signature (from normal, according to observer's coordinates) are not locally imaged. Therefore, any singularity in such an area is absolutely irrelevant.

6. It is deduced from the geometric theory of fields [2] that particles do not follow any analytic solution, no matter whether obtained from General Relativity or any quantum theory. One can specify the field only numerically. It has to do with chaos. — It was interesting to see if the discussed analytic solutions are possible at all, or if macroscopic solutions are decided by chaos too.

Submitted on October 17, 2009 / Accepted on November 09, 2009

References

1. Crothers S. J. The Kruskal-Szekeres "extension": counter-examples. *Progress in Physics*, 2010, v. 1, 3–7.
2. Bruchholz U. E. Key notes on a geometric theory of fields. *Progress in Physics*, 2009, v. 2, 107–113.

LETTERS TO PROGRESS IN PHYSICS

An Einstein-Cartan Fine Structure Constant Definition

Robert A. Stone Jr

1313 Connecticut Ave, Bridgeport, CT 06607 (USA). E-mail: robert.a.stone.jr@gmail.com

The fine structure constant definition given in Stone R. A. Jr. *Progress in Physics*, 2010, v.1, 11–13 [1] is compared to an Einstein-Cartan fine structure constant definition. It is shown that the Einstein-Cartan definition produces the correct pure theory value, just not the measure value. To produce the measured value, the pure theory Einstein-Cartan fine structure constant requires only the new variables and spin coupling of the fine structure constant definition in [1].

1 Introduction

Stone in [1] gives Nature's coupling constants, the fine structure constant and the weak angle, and a single mass formula for the W, the proton, the electron and electron generations all as functions of $(4\pi)^n$.

If these 4π coupling constant definitions are correct, then if a literature search found another theoretical definition, one would expect a similar form for the two definitions.

In [1] the fine structure constant (FSC), designated as α_{cs} (α charge to spin), is defined as $\pi\varsigma(4\pi\varrho)^{-2}/(2\sqrt{2})$ with $\varrho = \alpha_{cs}\,\alpha_{sg\,(1)}\,m_p/(m_e\,\pi) = 0.959973785$ where $\alpha_{sg\,(1)}=2\sqrt{2}/4\pi$ and $\varsigma = (4\pi\varrho)^3\,m_e/m_p = 0.956090324$.

2 An Einstein-Cartan model

Many Einstein-Cartan models are scale independent models where the force magnitude (scale) is related to some internal variable like a length, e.g. l_0. The pure theory scale is l_0 while potential deviation from the pure theory is represented by l. The Einstein-Cartan model of Horie's [2] is such a model.

Equation (4.2) in Horie's paper [2] gives the Einstein-Cartan theoretical definition for the FSC as

$$\alpha_{cs} = \frac{1}{64\pi}\,\frac{l_0^2}{l^2}\,, \tag{1}$$

where l assumed to be less than and approximately l_0.

When $l = l_0$, (1) gives the FSC value of approximately 4.97×10^{-3}. To match the measured FSC value requires l_0/l to equal about 1.2113 ($l_0^2/l^2 \simeq 1.4672$), a value for l not approximately l_0.

The 4π definition of the fine structure coupling constant is given in [1] as $\alpha_{cs} = \pi\varsigma(4\pi\varrho)^{-2}/(2\sqrt{2})$ and the charged particle weak angle coupling constant as $\alpha_{sg} = 2\sqrt{2}(4\pi\varrho)^{-1}$.

Noting that the $\sqrt{2}$ appears with both spin couplings suggests that the origin of the $\sqrt{2}$ is related to the coupling of the other force in the coupling constant to spin.

From the underlying approach, this is true. However the $\sqrt{2}$ is mathematically on the side of the other force because the coupling of spin to charge (and g) is larger than expected by present approaches.

Thus in order to reflect the underlying approach of the 4π definitions, α_{cs} is better written as

$$\alpha_{cs} = \frac{1}{16\pi}\,\frac{1}{4}\;\;\sqrt{2}\;\;\frac{1}{\varrho^2}\;\;\varsigma. \tag{2}$$

Rewriting Horie's equation (1) in a similar form yields

$$\alpha_{cs} = \frac{1}{16\pi}\,\frac{1}{4}\;\;1\;\;\frac{1}{(l/l_0)^2}\;\;1. \tag{3}$$

Where as Horie's pure theory Einstein-Cartan model assumes 1 for the coupling, the underlying source coupling value in α_{cs} (and α_{sg}) is larger by $\sqrt{2}$.

Where as Horie's pure theory Einstein-Cartan model can not give a value for l/l_0 for α_{cs}, the definition in [1] gives the value as ϱ. Note that using the correct spin coupling ($\sqrt{2}$) now results in $l \lessapprox l_0$ as expected.

Lastly, Horie's pure theory Einstein-Cartan model simply lacks an additional factor ς that appears on the charge side of the coupling constants α_{cs} and α_{cg} [1].

Thus, as a pure theory model, Horie's result is correct. To produce the measured FSC value, Horie's pure theory model only needs the correct spin coupling ($\sqrt{2}$), the correct l/l_0 value (ϱ) and the ς adjustment that come from the approach that produced the 4π definition of Nature's constants.

3 Summary

In [1], several 4π coupling constant definitions were given including the fine structure constant.

It is shown that the 4π fine structure constant definition of [1] is in keeping with Horie's complex connection pure theory Einstein-Cartan fine structure constant definition [2].

Thus not only does the 4π definitions in [1] produce the two weak angle values as experimentally observed, the fine structure constant definition has the three missing constants required by a pure theory Einstein-Cartan fine structure constant definition to produce the measured value.

Submitted on November 13, 2009 / Accepted on November 22, 2009

References

1. Stone R. A. Jr. Is fundamental particle mass 4π quantized? *Progress in Physics*, 2010, v. 1, 11–13.
2. Horie K. Geometric interpretation of electromagnetism in a gravitational theory with space-time torsion. arXiv: hep-th/9409018.

LETTERS TO PROGRESS IN PHYSICS

Valery N. Smirnov (1939–2009) and His Detector

Victor A. Panchelyuga

Research Institute of Hypercomplex Systems in Geometry and Physics, Friazino, Russia
Institute of Theoretical and Experimental Biophysics, Russian Academy of Sscience, Pushchino, Russia
E-mail: panvic333@yahoo.com

Dr. Valery N. Smirnov who passed away recently, was an experimental physicist working on accelerator physics. Despite this fact, the main achievement of his scientific creation was the detector for measurement of perturbations in gravitational fields. This detector, having originally construction suggested by Smirnov, was launched at Moscow Engineer Physical Institute, Russia. Valery N. Smirnov continued his observations with the detector until his last days. We therefore refer to this device as Smirnov's detector.

Dr. Valery N. Smirnov. Pictured in the last decade.

Valery N. Smirnov was born in October 6, 1939, in Magadan, Russia, where his parents worked as reporters. In 1945, his family returned to Moscow, where he lived all his life.

After high school, in 1958, he was employed at the Institute of Radio Engineering. In 1960 he entered to Moscow Engineer Physical Institute, where was gaduated in 1966. Then he returned to the Institute of Radio Engineering. In 1975 he was employed at Kurchatov Institute of Atomic Energy, as an experimental physicist in the field of accelerator physics. Smirnov designed "Fakel" (tourch), the linear accelerator, and also numerous other accelerators for Kurchatov Institute. In 1983, he awarded Kurchatov Prize for the best engineering work done in the field. As one of the stuff of Kurchatov Institute, Smirnov produced some studies at Chernobyl Nuclear Power Station, in 1987 and 1989, after the catastroph. He was gratituded by the Government for this job.

Some persons work in order only to earn money for live. In contrast, Smirnov spent all his life for scientific studies. He found the main task of his scientific creation when read the papers, published by Prof. Nikolai A. Kozyrev, the famous astronomer and physicist of Pulkovo Observatory, Leningrad. Kozyrev pointed out that, in his regular experiments with gyposcopes, the devices experienced small fluctuations at the moments connected to the dynamics of celestial bodies, e.g. the planets. This effect remained unexplained.

Smirnov supposed that the source of this effect is hidden in the imperfect suspension of Kozyrev's gyroscope. Thus, every period of revolution may be broken due to an external influence. In aim to study his supposition, Smirnov designed a special device, containing a gyroscope which was rotating in a special regime of braking (different braking regimes were ruled by special control electronics). Experiments conducted by him confirmed his initially supposition: the device showed steady sensitivity to the specific moments of celestial bodies dynamics, exact according to Kozyrev.

During the years and until his last days, Smirnov conducted regular observations with the device. He also improved its contruction, making it more sensitive. The experimental results and the technical descriptions were presented by him in the publication [1]. Complete review of the experiments will be submitted to *Progress in Physics* later.

Dr. Valery N. Smirnov passed away in November 4, 2009, being full of new plans for research and creative ideas. In our memory he is still live amongst us, with his device we refer to as Smirnov's detector.

Submitted on November 15, 2009 / Accepted on December 01, 2009

References

1. Smirnov V. N., Egorov N. V., Schedrin I. S. A new detector for perturbations in gravitational field. *Progress in physics*, 2008, v. 2, 129–133.

NEW PARADIGMS IN PHYSICS

A New Paradigm: From Quantum Fields to the Planck Vacuum

William C. Daywitt

National Institute for Standards and Technology (retired), Boulder, Colorado, USA E-mail: wcdaywitt@earthlink.net

The current paradigm in fundamental physics assumes that Newton's gravitational constant G, Planck's (reduced) constant $\hbar$, and the fine structure constant α are primary constants — i.e., these constants are associated with something basic in nature and are thus not reducible to something more fundamental. This assumption leads, for example, to the conclusion [1] that quantum fields are the fundamental building blocks out of which the visible universe is constructed.

The Planck vacuum (PV) theory [2] derives the three constants

$$G = \frac{e_*^2}{m_*^2}\,, \tag{1}$$

$$\hbar = \frac{e_*^2}{c}\,, \tag{2}$$

$$\alpha = \frac{e^2}{e_*^2}\,, \tag{3}$$

where e_* is the bare electronic charge, m_* is the Planck mass, c is the speed of light, and e is the experimentally observed electronic charge. In effect, then, a new paradigm* has emerged where the PV is the source of the visible universe and its properties.

What follows is a brief survey of some equations that demonstrate how the current and new paradigms are related. The details leading to the equations are unimportant here and are left to the references. What is important is how the current primary constants on the left side of (1)–(3) are replaced by the new primary constants e_* and m_* on the right and in the equations to follow.

The Compton relation [3, p.433]

$$\lambda_c = \frac{h}{mc} \qquad \text{or} \qquad r_c mc = \hbar \tag{4}$$

associates a Compton wavelength λ_c (or a Compton radius $r_c = \lambda_c/2\pi$) with the particle mass m, while the de Broglie relation [3, p.81]

$$p = \frac{\hbar}{r_d} \tag{5}$$

relates the particle's relativistic momentum ($p = m\gamma v$) to its de Broglie radius $r_d = r_c/\beta\gamma$, where $\beta = v/c$ and $\gamma = 1/\sqrt{1-\beta^2}$. The PV theory explains these relations [2] [4] in terms of the magnitudes, mc^2/r and e_*^2/r^2, of the two distortion forces the particle exerts on the PV, the radius at which these two forces are equal being the Compton radius r_c. The calculations lead to the string of Compton relations

$$r_* m_* c = r_c mc = e_*^2/c\,, \tag{6}$$

where r_c is the Compton radius of any of the elementary particles, m is the particle mass, and r_* and m_* are the Compton radius and mass of the individual Planck particles making up the negative-energy PV state.

The Compton relations (6) yield the free-space permittivities [2]

$$\epsilon = \frac{1}{\mu} = \frac{e_*^2}{r_* m_* c^2} = 1\,, \tag{7}$$

while the static electric force between two charges e becomes

$$F_{el} = \frac{e^2}{r^2} = \alpha\,\frac{e_*^2}{r^2} \tag{8}$$

showing the fine structure constant α to be closely related to the PV polarizability.

The Heisenberg uncertainty relations

$$\Delta p \cdot \Delta q \geqslant \frac{\hbar}{2} = \frac{e_*^2/c}{2} \tag{9}$$

where p and q correspond to any two canonically conjugate operators, remain a wave-particle-duality mystery in the current paradigm. The PV theory explains these relations in the following manner: the so-called free particle interacts continually with the invisible PV continuum; as this continuum, like any continuum, can support wavelike disturbances, the reaction of the PV to the particle perturbations produces a wavelike reaction in the particle; then (9), which is currently ascribed to the particle, is actually a straightforward mathematical property of the perturbed continuum [3, p.105].

The gravitational equations of Newton and Einstein transform from the current paradigm to the new paradigm in the following way [5]:

$$F_{gr} = -\frac{mMG}{r^2} = \frac{(-mc^2/r)(-Mc^2/r)}{-m_* c^2/r_*} \tag{10}$$

and

$$G_{\mu\nu} = \frac{8\pi G}{c^4}\,T_{\mu\nu} \quad \rightarrow \quad \frac{G_{\mu\nu}/6}{1/r_*^2} = \frac{T_{\mu\nu}}{\rho_* c^2}\,, \tag{11}$$

*Merriam-Webster Online Dictionary, 2009. Paradigm: a philosophical and theoretical framework of a scientific school or discipline within which theories, laws, and generalizations and the experiments performed in support of them are formulated.

where $c^4/G\,(=\, m_* c^2/r_*)$ and $1/r_*^2$ are the ultimate curvature force and Gaussian curvature sustainable by the PV, and ρ_* $(=\, m_*/(4\pi r_*^3/3))$ is the Planck-particle mass density of the PV.

Finally, the quantum vacuum consists of an electromagnetic (photon) component and a massive-particle ($k_c\, =\, 1/r_c$) component [4]. The energy densities of the two transform as

$$\frac{c\hbar}{2\pi^2}\int k^3 dk \quad \rightarrow \quad \frac{1}{8}\frac{e_*^2/r_*}{r_*^3} \tag{12}$$

and

$$\frac{c\hbar}{4\pi^2}\int k^2\left(k_c^2+k^2\right)^{1/2} dk \quad \rightarrow \quad \frac{1}{16}\frac{e_*^2/r_*}{r_*^3} \tag{13}$$

from the current to the new paradigm respectively.

Submitted on July 29, 2009 / Accepted on September 19, 2009

References

1. Weinberg S. The search for unity: notes for a history of quantum field theory. *Daedalus 106*, 1977, 17.
2. Daywitt W.C. The Planck vacuum. *Progress in Physics*, 2009, v. 1, 20.
3. Leighton R.B. Principles of modern physics. McGraw-Hill Book Co., NY, Toronto, London, 1959.
4. Daywitt W.C. The source of the quantum vacuum. *Progress in Physics*, 2009, v. 1, 27.
5. Daywitt W.C. Limits to the validity of the Einstein field equations and General Relativity from the viewpoint of the negative-energy Planck vacuum state. *Progress in Physics*, 2009, v. 3, 27.

NEW PARADIGMS IN PHYSICS

New Ideas for the Extra Dimensions and for Deriving the Basic Laws of Physics

Riadh H. Al Rabeh

College of Engineering, University of Basra, Iraq
Present address: Lydgate Close, Manningtree, Essex, UK. E-mail: alrabeh_rh@yahoo.com

As geometry is constructed from points and their separating distances, physics may be similarly constructed using identical material points and their separating distances with the additional requirement that all points have infinitesimal masses and move all the time at the speed of light. Pairs of such points can get locked together in circles to make doublet particles that can have any speed from zero to that of light, at which point the doublet disintegrates. Using this construct together with the rich mathematical properties of a 3D space, a mechanical definition of time, and simple symmetry rule for displacement, it is possible to derive many of the fundamental laws of physics such as the inverse square laws of gravitation and static electricity, many of the relativistic and quantum mechanical results such as the mass-energy conversion of Einstein and the quantized energy levels of Planck and Bohr. In addition, a better understanding of some illusive terms like inertia and force becomes possible. No arbitrary constants are needed in the process. Extra dimensions (variables that are not a distance) are created as a result of this setup — but they are all found to be discrete. Mass, charge, spin, and time are some notable examples.

1 Introduction

We use common ideas, simple constructs and simple mathematics to shed light on the origin of the grand laws of physics that have hitherto remained untied together. That this is possible was a big astonishment to the author having spent years of search to achieve the same using fields and waves excluding discrete masses. We first postulate the existence of a 3D Euclidian space containing a large number of material points (point masses). The distance between the points is to be a continuous function, which goes well with our intuition, as we never observed material objects jump without passing through all joining points in between. We then realize that this postulate endows the space with an enormously rich structure [1] due to the fact that the distance becomes analytic and infinitely differentiable. The masses must be infinitesimal in order to move continuously at the speed of light without violating Einstein's and other results in this regard. We are tacitly assuming that no space can be defined without material points. As to what is a material point is left undefined.

Material points can acquire other properties like electric charge etc which we will come to meet later. When the separating distance between two material points of suitable attributes is small, they trap each other to make a doublet particle. This combined structure can have any speed — from zero to that of light, in which case it disintegrates into two point particles. Bound states of equal masses do exist in physics as in the case of the exotic particle "positronium" [2]. The normal mass of a material body, composed of a large number of such doublet particles, is simply the total number of doublets and hence it is discrete. We note that an immediate benefit of this setup is a simple mechanism for converting mass into energy and visa versa if we associate energy flux with point particle flux. In fact it amounts to an ultimate unification of the of mass and energy concepts. We also note that a space with continuously moving material points may be an alternative and fairly convincing way of interpreting Einstein's space time continuum ideas. This becomes even more apparent as we arrive at the same relativistic results using the simple doublet structure.

To reach to the more fundamental laws of physics, we shall put a simple mechanical definition for time and a symmetry rule that governs the displacement of point particles (and doublets as a result) in space. We shall consider such grand ideas with the simplicity they deserve, as Einstein have suggested in more than one occasion — what is needed is simple physical interpretations rather than complicated mathematical descriptions [3]. The transformation between point and doublet particles may be looked at as a process of equilibrium or a continuous forward and backward transformation — an evaporation condensation process if you like, and one that can be observed on larger and larger scales in nature. The trapping and escape of photons in matter(radiation), of electrons out and into the nucleus of different materials, of whole molecules from the surfaces of any liquid and the trapping and escape of large masses in volcano eruptions on planets and stars are few such examples.

Doublet particles are to be taken to represent the simplest form of condensed matter, whereas singlet particles are to represent energy flux. Singlet particles may also combine (along their flight path) in any number and remain as different energy fluxes as long as they do not take the form of circularly bound doublets. Doublets can also come together(condense) and combine to form massive particles. In [4] the doublet

structure is examined further and it is shown that the geometrical rules for the combination(packing) of doublets seem to fit well measured values of different forms of condensed matter.

2 Theory

2.1 Space and Time

Intuitively, it is not possible to define space when it is devoid of matter [6, 7]. Our starting point therefore is to assume the existence of material points with infinitesimal masses that move all the time at the characteristic speed of the space — the speed of light c. The numerical value of $c = 2.99\times10^8$ comes from our arbitrary choice for the units of distance and of time. A 3D Euclidean space may(at one instance) be structured out of *all* such material points and the distances that separate them. This space is continuous to go with our intuition — that is to say when material points move, they do not jump, but pass by all the joining points along the path of motion as given earlier.

We then note that time itself can not be defined in a space devoid of motion. Just imagine one is at night in a desert with nothing moving — no moon, no stars and not even a heart beat. In this setup there is no way to see time flowing. So we are led to say that time must be connected with the motion of material points. To get a sense of time we need an observer point and a moving point, since if we move along a straight line without being able to observe anything else moving, we will not be able to see time flowing either. The problem now is that any observation over a distance must rely on light propagation and will introduce the well known complication of a finite value of c.

A simple case however, where this is not a problem is the case of two material points moving on a circle in a doublet formation and the observer point is sitting on the path of this doublet. We can then define time as the *number* of visits of the doublet members. This number has all the characteristics of time since it is an *ever increasing* variable (pointing in one direction- hence the arrow of time expression) and it is *symmetric* in the sense that the zero of count (zero of time) can be placed anywhere. It is, however, *discrete* according to this picture. It is also an independent variable in the sense that it can have any integral value for any value of the other three spatial coordinates. This is well in tune with our intuition of the variable "time", as we always rely in our time measurements on some sort of oscillation and count the number of such oscillations to measure time. If light can be sent to come back in a straight line to a distant point, the distance to that point can be judged from the knowledge of the period taken as given by the number of rotations(visits) of our local doublet members and the assumption that the characteristic speed c is constant all the time. Time can thus be looked at as a measure of the distance travelled by any material object to the distance travelled by a material point as given by the circumference and the number of rotations of our local doublet.

A mathematical fact is that if a particle in an *isolated* system follows one path exactly more than once, it will continue to do so for ever. We can convince ourselves with this if we remembered that the number of points along an even a *differential line segment* of such path is more than enough to fix any number of *constants* in the solution of the differential equation of motion — thus ensuring that the path is fixed and unchanged in subsequent visits. This conclusion is possible only if the line of motion is continuous and analytic (infinitely differentiable) which is the reason for our original assumption. The emergence of such eternal stability can prove useful in explaining the eternal stability of some of the elementary particles like the photon and the electron when in isolation.

We also note that the rich mathematical properties of the path of motion in space lead to new variables or dimensions that are independent of the original three spatial dimensions. Any extra dimension derivable this way appears to be not a distance and only discrete however. We notice also that the creation of such extra variables comes out of a process of a closure or folding in the path of motion and turning it into a multi-valued variable in which every point is described not only by its three space coordinates, but also by other numbers derived from the multiplicity at that space point. We mention angle measurement as one more example of such multiplicity.

Since the velocity of a moving point is a mathematical derivative with respect to time, and as time is represented by a number, we conclude that the process of determining the velocity and acceleration, (or the process of going from static to kinematic and dynamic), is a process of comparison (ratio) of the motion of a larger system with that of a simpler and standard one like a doublet. In other words, the motion of the simple doublet is effectively being used as a yardstick to gauge the velocity and acceleration of more complicated systems. This definition of time breaks down of course for periods that are smaller than one unit of measurement (determined by the smallest possible doublet) whatever that may be. Since time is discrete, velocity, acceleration, force, momentum and any similarly related variable are all discrete. This will later lead to the Heisenberg uncertainty principle.

2.2 Laws of motion — action and reaction

We put here a simple rule for the displacement of material points that goes with the state of natural symmetry possessed by two material points (in isolation) in the form; "*The displacement of any material point must be accompanied by the displacement of another point by the same amount in an opposite direction*". For two isolated points it might be argued that it does not matter if one point made the entire move and the other stays a foot, as the outcome would be the same. This is clearly not the case, since in reality we will have many more points and our rule should apply to every pair of them.

Since mass is composed of many material points of the

same value, and motion is to be discrete, the displacement of ten points one distance can be compensated for by the displacement of one point ten times that distance in the opposite direction, and our equivalent statement of action and reaction becomes; "*The sum of mass times displacement is zero at any point and along any direction*". In other words, the center of mass of an isolated system of points never moves. We can also see that as time is now just a number, differentiation of the displacement with respect to time gives; "*The sum of mass times velocity (linear momentum) is zero at any point and along any direction*", and differentiating again gives; "*The sum of mass times acceleration (force) is zero at any point and along any direction*". Thus we see that it is possible to recover both the second and third Laws of motion of Newton from a simple rule of displacement. We take this to be a strong support of the correctness of this postulate as a rule of displacement.

Our rule of displacement, which we shall call the "*balanced displacement*" (BD) rule, may be considered as the equivalent of Newton's first law of motion since it tells that points can not change their state of motion independently... if a material point moves, another must also move by the same amount and in the opposite direction, and things can then stay like this forever as long as the BD rule is true. The BD rule also provides a neat explanation of the source of inertia of massive bodies. It is simply a balanced displacement requirement. As if the world is sitting on a knife edge and moving anything must be done symmetrically to keep the balance .

Displacement can be resolved into three directions, the first along the separation distance between two moving points plus two components normal to this direction. The two normal components combine to define the spin direction of the doublet. The doublet particle can have left or right hand spin property. Such spin, once initiated, will continue unchanged since the BD rule works correctly all the time– that is until an interaction occurs with another group of points.

The displacement along a radial line separating two moving points can have two directions; to the inward and to the outward directions. This produces the attraction and repulsion type effects. The probability for material points to take any one of six possible motions along three perpendicular directions is presumably equal, this provides a plausible reason for the existence of antiparticles, and the fact that antiparticles can be anti in all their attributes and have the same mass. Thus we have by now two types of coupling constants and two different spins — all new variables and all discrete, since they can only take the values $(+/-$ a constant) representing each of the two opposing directions. Larger values of charge, spin etc must now be in multiples of this constant value.

An interesting conclusion of all this is that the sum of displacements of all material points in the universe is zero at any time and hence the center of mass in the universe never moves. It is also not hard to see that as a result of the BD rule being applicable to every two points separated by a distance, there is a universal entanglement situation of every single point mass in the universe. If we now imagine doing a back play of all the events of displacements that has occurred since the start of time, we may reach the original point start(the big bang point!). The clear impossibility of such undoing, should tell us that it is impossible to go back in time. We could also say here that time must have started with the first motion and will only stop when everything else stops moving.

As pointed above, the BD rule can give us a neat explanation of inertia which some believed it to be a property of matter and others to be due to the effect of distant masses (the Mach principle). In the present setup we see that it is a result of the symmetry of displacement — i.e. a property of space and matter together with distant and near masses all involved. One interesting example to make the picture clear is the case of the rotation of a thin disc in isolation. Every two diametrically opposed points of the disc follow happily the BD rule and, as such, constitute a self contended system that will, if not disturbed, remain as it is for ever. If we move the disc along the axis of rotation, we must create a movement of other masses equivalent to that of the disc in the opposite direction — as in propelling it with the gases of a rocket for example. The rotational motion of the disc remains unaffected in this case. If we now try to move the disk on a curved path, we need to provide an equivalent opposite motion to the curving and rotating material points of the disc in its new complex motion, and it is this that shows as the gyroscopic effect.

2.3 The inverse square laws

The interaction between two isolated material points can only be a function of the separation distance — because of isolation. Such interaction, as a result, becomes homogenous in the coordinates — that is to say there can be no preference of one coordinate to the other. For such cases we quote few lines from [8] "...the multiplication of a Lagrangian by a constant does not effect the equation of motion. This fact makes it possible, in a number of important cases, some useful inferences concerning the properties of the motion without the necessity of actually integrating the equation of motion. Such cases include those where the potential energy is a homogenous function of the coordinates, i.e. satisfying the condition $U(ar^1, ar^2, \ldots, ar^n) = a^k U(r^1, r^2, \ldots r^n)$, where a is a scaling constant, k is the order of the potential function and n is the number of coordinates". This then lead the reference to the following conclusion "If the potential energy of the system is a homogenous function of degree k in the (Cartesian) coordinates, the equation of motion permits a series of geometrically similar paths and the times of the motion between corresponding points are in the ratio $t'/t = (l'/l)^{1-k/2}$, where l'/l is the ratio of the linear dimensions of the two paths". To follow our notations, put r for l', t' for t to get $r = Kt^{2/(2-k)}$, where $K = l'/(t')^{2/3}$ is a coupling constant and is made up of the values of the radius and the time of one rotation "of a

standard doublet in our case" and r is the separation distance between the two points.

There are only two values for k [8] that result in a bound motion. These are $k = (-1, 2)$. The first gives $r = Kt^{2/3}$ and the second leads to a spring type force or what is known as a "space oscillator". The space oscillator case can be shown to be not a new case and occurs in a field of inverse square when the displacement is small, the region is small with a large number of interacting particles [8]. The first case (the two third power formula) is one form of the famous Kepler third law of motion and if differentiated twice gives the inverse square law $d^2r/dt^2 = (-2/9)K/r^2$ in confirmation of our starting assumption. In [5] this form of the inverse square law (involving time only) was used to predict the motion of many point particles with a notable gain on computing time. The quantity $(-2/9)K$ is the coupling constant of the interaction which takes the value of the universal gravitational constant $K_g = (-2/9)K = G$ for gravity forces or the Coulomb coupling constant $K_e = 1/4\pi\epsilon_0$ for electrostatic forces. The value of G is therefore calculable(in principle) from the dimensions of the doublet used in the dynamic scaling of the problem — when this is known.

The values of the coupling constant for the gravitation and electrostatic forces come from our arbitrary definitions of the units of mass and charge. By now we had four constants; the speed of light c, the Planck's constant h, the gravitational constant G and the permittivity of free space ϵ_0. Our arbitrary physical units from which these are derived are the meter, the second, the kilogram and the Coulomb.

When we have more than two material points, vector superposition of forces, velocities and displacements must be used, with the force (= acceleration since we have equal mass) for each pair calculated separately then added for the lot. For N material points, there are $N - 1$ interacting pairs of points as we exclude the interaction of a point with itself. If N is large, $N - 1$ can be replaced with N. For the case of a large collection of points that are effectively *sitting at the same point*, the center of mass of any such body obeys the same rules of motion given above, since mathematically the two are equivalent. The final interaction force is a resultant of the interaction of all pairs in each collection and will thus be a multiple of the total number of interacting pairs, or equivalently by the product of the masses of any two interacting groups having the same center of mass. This reproduces Newton's law for gravitational interaction and the Coulomb charge interaction and the product of the two masses/charges will appear in the coupling constant.

2.4 The size of a doublet

Take the case of pairs of points with an attractive force locked in doublets to form particles. These doublets will have fixed masses(by assumption) and also fixed spin velocity since the tangential speed of all the material points making a doublet is fixed at c at all times. It has a fixed radius also since the speed of the constituents are fixed and the coupling constant is also fixed. This creates a particle with fixed and well defined properties. Since the product of the mass of two point masses $2\delta m$, the speed v, and the radius of the doublet r is given by; $2\delta mcr = \delta mcd$, where $d = 2r$; has the units of energy and time (or that of angular momentum) and is the same as that of the Planck's constant, we conclude that a limit must be placed on the smallest allowable doublet, giving $\delta md = \hbar/c$, where $\hbar$ is the reduced Planck constant. This also suggests that (δmd) is a new fundamental physical unit involving mass and distance combined together (= 3.5177×10^{-43} kg m). The numerical value of this constant (or equivalently of the Planck's constant) comes from our arbitrary choice for the unit of mass in addition to that of distance and time used earlier. The quantity $(\delta mcd = \hbar)$ is the angular momentum and also the spin of our doublet particle and it is the unit of measurement of spin. As we have now a lower bound on spin, the orbital momentum of any one or more particles can only be a multiple of this value $\hbar$.

3 Further results

3.1 Heisenberg uncertainty

Since $\delta mvd = \hbar$ can be rewritten as $pd = \hbar$, where $p = \delta mv$ is momentum for one material point, we get (putting Δx for d) the uncertainty principle of Heisenberg usually written as $\Delta p \Delta x = \hbar$. Accordingly, the uncertainty principle refers to the smallest possible angular momentum in nature. As material points always move at c and must have some effective size, it is only natural that there is a minimum radius for the circle of rotation of a doublet. For larger masses, Δx is smaller according to this principle. This need not cause any contradiction. It can be taken in this setup to represent the region inside which the center of mass of all doublets is likely to be located. It becomes smaller as the mass increases, very much like the uncertainty (scatter) in the average of a large number of collected data growing smaller and smaller as the number of data points is larger. Interestingly when this is extended to take the mass of the entire universe, it becomes equivalent to saying that the center of mass of the universe is firmly fixed at a point.

3.2 Einstein mass and energy conversion

As all points making a doublet particle move at the speed of light, the kinetic energy in any doublet must be a function of c^2 and accordingly we can write $E = mc^2$, with m defined as the number of doublets in any larger particle. As we have two point masses in any doublet particle, the more general formula $E = 0.5mv^2$ for kinetic energy is still valid if applied to a single point constituent of a doublet.

3.3 Planck's energy of radiation

For points moving with a speed c around a circle or escaping out of it, we have $c = \omega r$, and $mvr = mc(c/\omega) = h/2\pi$ using the results above. Using $\omega = 2\pi f$, we have $fh = mc^2$ or $E = hf$. This is Planck relation for the energy of radiation of frequency f. Also if we put $p = mc$, we get $E = cp$ for points moving at c. This is the momentum-energy relation for a particle with infinitesimal mass (zero mass in the literature).

3.4 Einstein's relativistic mass

Since points forming a doublet can have two motions — one along a circle with velocity c and one along the center line with velocity v (less than c), the ratio of the kinetic energy of the doublet particle to its total energy must be like $(v/c)^2$, *i.e.* $E_k/E = (v/c)^2$ since both quantities refer to the same set of masses. Also, as we had $E = mc^2$, we get $E_k^2 = E^2(v^2/c^2) = = (E^2/c^2)v^2 = p^2c^2$, which then gives the relation for the total energy as $E^2 = E_0^2 + c^2p^2$. This is the well known relativistic formula for the total energy of a particle in terms of its rest energy and kinetic energy. Here it is derived using the simple doublet structure alone.

3.5 Bohr's energy levels

For a group containing n doublet particles bound together, the single doublet formula given above in the form; $mvd = \hbar$ becomes $m_n vd = n\hbar$ giving the well known Bohr formula for the spin of bound electrons. This formula, despite its success in being very close to experiment, has been criticized as not being based on a model. The doublet model as explained above can be given in support of this very useful, simple and experimentally correct formula. The Bohr formula is normally combined with the centrifugal force expression $F_c = mv^2/r$ and static electric force $F_e = e^2/4\pi\epsilon_0 r^2$ [9] to derive another expression for the energy levels in an atom (and other bound structures) in the form $r_b = (n^2/Z)(4\pi\epsilon_0 h^2/m_e e^2)$, where Z is the total charge of an atom and n is an integer multiple of the spin of the atom. For a single charge atom like hydrogen and lowest spin level corresponding to $n = 1$, we get the Bohr radius $r = r_b = \epsilon_0 h^2/\pi m_e e^2 = 5.2917{\times}10^{-11}$ m. This formula has been declared wrong, in some of the literature, because it predicts the spin squared as $n^2\hbar^2$ rather $n(n-1)\hbar^2$ as predicted by the wave function theory of quantum mechanics (which has a better agreement with experiment). In the author opinion this is an unfair conclusion, since in any n discrete interactions, a particle does not interact with itself(as given above), leaving only $n(n-1)$ interactions that should replace the n^2 term in the Bohr formula and bring it inline with the corresponding quantum formula.

When a group of doublets form a larger structure, the volume of the new structure will intuitively depend on the number of doublets if these happen to occupy different volumes and not share the same center of rotation. This fits well with the observations about the nucleus of any atom being a function of the number of the nucleons only. The application of this fact lead to the one third power law for the radius of an atom R in terms of the atomic number A [9] giving $R = r_0 A^{1/3}$; where $r_0 = 1.4{\times}10^{-15}$ m is an experimental constant. For the nucleus of hydrogen $A = 1$ and r_0 becomes the diameter of a proton. We shall compare this value with that of the electron as calculated in the next section.

3.6 The fine structure constant

When the gravitational and magnetic forces are small, the electrical Coulomb forces $F_e = e^2/4\pi\epsilon_0 r^2$ for electrons are nearly equal to the centrifugal forces $F_c = m_e v^2/r$. In the case $v = c$; $r_e = e^2/4\pi\epsilon_0 m_e c^2 = 2.817{\times}10^{-15}$, giving the classic radius of the electron. This formula is normally derived in the literature (see [10]) from the potential distribution around the electron due to its charge using energy conservation. The present derivation relies on the doublet model alone. In a doublet however, we have two material points (two masses) contributing to the force which seems to suggest a different value for r_e, giving $r_e = 1.4010{\times}10^{-15}$ instead. This is probably more plausible as an electron radius, and it is to one's surprise, exactly the same as that for the proton as we found from the hydrogen nucleus in the previous paragraph. If this is correct, it indicates a similarity in the packing in both the electron and the proton despite the large difference in mass. One possible explanation is that this is the result of many doublets occupying the same volume and sharing the same center of rotation — increasing the energy content but not the size. Experimentally, the electron has, so far, behaved as a point charge with no internal details apparent. The proton on the other do have an internal structure.

If in the expressions for the centrifugal and static forces above, the velocity v is less than c, we could calculate v using $mvd = \hbar$ and obtain; $v^2 = e^2/2\epsilon_0 h$, and $v/c = e^2/2\epsilon_0 hc = = 1/137.036$. This is the fine structure constant and it now points to the relative velocity of the electron in an orbit to that of light (or that of the material points in a doublet), and can therefore be looked at as a form of a packing factor. If the expression for the doublet radius is divided by the radius of the electron using $mvd_c = \hbar$; we get $d_e/d_c = e^2/4\pi\epsilon_0\hbar c = = 1/137.036$, giving the "fine structure constant" again — now it is a clear packing factor. The quantity d_c is the Compton wavelength of the electron. The ratio of the Compton diameter d_c and the Bohr diameter d_b as found above gives $d_c/d_b = e^2/2\epsilon_0 hc$, that is the fine structure constant again — now representing the next level of particle packing. All these are well known results, but now we have a clearer reasoning for their existence– using expressions derived from the structure of the doublet alone.

3.7 Planck's length scale

The Coulomb force between two point charges is given by $F_e = q^2/4\pi\epsilon_0 r^2$; and the magnetic force between two moving

point charges is given by Ampere's law $F_m = \mu_0 q^2 v^2 / 4\pi r^2$. This can be modified using the identity $c^2 = 1/\epsilon_0\mu_0$ to give $F_m = (q^2/4\pi\epsilon_0 r^2)(v/c)^2$. Thus if $v = c$ the electric and magnetic forces between two point charges are equal regardless of the value of the separation distance r or charge q, since they cancel out. This is very interesting because it allows the *packing* of doublets without having to overcome the huge electrostatic repulsion forces. This is an *asymptotic freedom* type condition. Such equality is normally broken as the particles go to form a doublet and the electric forces between different doublets become much stronger than the magnetic forces between them, since the speed of the center of a particle doublet is small and the magnetic forces between two doublets, becoming small compared to the electrostatic forces. The situation changes again for a very large collection of moving doublets wherein the magnetic forces become important again because of the shear number of participants (when correctly oriented) rather than the result of very high velocity. We observe this in our daily usage of the magnetic force wherein currents are the result of the orderly movement of a very large number of particles.We note here that Ampere's law is also derivable from the inverse square law when the charges are in motion.

When the electric and the magnetic forces are balanced at the velocity limit c, only gravity and centrifugal forces are left in play. Gravity force is given by $F_g = Gm^2/r^2$ and centrifugal forces by $F_c = mv^2/r$; equating the two and taking into account the Planck formula $mvr = \hbar$ with $v = c$, we obtain $r_p = \sqrt{G\hbar/c^3} = 1.616{\times}10^{-35}$ m. This is the Planck length scale and it gives the smallest possible dimension of any doublet structure. When the separation distance increases beyond this length, the equality changes and the centrifugal force becomes more dominant over gravity as in normal interactions. For large astronomical masses the picture changes again and gravity becomes strong and dominant because of the shear number of participating particles.

3.8 Spin and space quantization

In the presence of more than one doublet contained inside a larger particle, it is not unreasonable to think that space and size limitations allow the compaction of only a limited *integral* number of doublets. This leads to an angle quantization, if doublets shared the same spherical space and to volume quantization if doublets are in separate spheres. Angle quantization leads to the well known quantization of angular momentum and volume quantization gives the nucleus a size that is dependent only on the number of nucleons [9].

4 Final remarks

We have started with identical material points together with the continuous distances separating them and formed a 3D Euclidean space for any point in time. We have assumed that all material points have infinitesimal masses and move all the time at the characteristic speed of space and that of light c. The value of c comes from our arbitrary choice of the ratio of the units of mass and time. We formed doublet particles that have a (center of mass) speed from zero to that of light from every two point particles of suitable attributes. This simple construct produced a simple mechanism for the transformation between mass and energy and when further analyzed, produced the correct relativistic energy and quantum mechanical relations too.

Extra dimensions — all discrete are derived from the properties of the 3D space and the differentiable distances existing between any two material points in it — using the fact that through a single point in space one can have multiple paths of motion. The dimension of time is found to correspond to one such multiplicity– the number of rotations of a standard doublet counted at any one space point.

Velocity, acceleration, force, momentum and any variable dependent on time are found to be discrete as a result of the discreteness of time. This naturally lead to the Heisenberg uncertainty principle and the discrete energy and some other ideas associated with quantum mechanics. The need for discrete description of some of the basic variables of physics can be traced as far back as the Greek philosopher Zeno, who put paradoxes that threatened the rational basis of science till very recently. These were only recently resolved using arguments from calculus in which infinitesimal quantities can integrate to finite quantities in a limiting process. Making time discrete is another neat way to clear Zeno's paradoxes.

The process of timing is found to represent a gauging process of the dynamics of larger systems by those of a simpler system like a doublet. The dimensions of spin etc are created in connection with movements in the directions normal to the line joining any two material points. The inverse square laws are only the result of similarity in the motion of different size systems. The coupling constants in the two opposite directions along the line joining two material points can be ± 1 for repulsion and attraction. To work with individual charges, rather than the resultant outcome, is the square root of this giving; $\sqrt{-1} = \pm\, i$, to produce the desired effect of repulsion for similar charges and attraction for different charges, and $\sqrt{1} = 1$ to represent attraction only in the case of gravitational forces — since we do not have negative masses in nature as far as we know. Again if we are only concerned with the combined effect of two charges or two masses, then we only need to consider the real quantities ± 1 for the coupling constant for the gravitational and electrostatic forces.

Only four different forces are needed in the present setup. Two of the forces, the magnetic force and the centrifugal force result from the motion of the *sources* of the other two — that is masses and charges. The last two types of forces disappear at zero velocity. As we have identical point masses, the word "force" becomes not essential and can be replaced with just "acceleration". The mathematical ideas of superposition and center of mass are very useful and should be used for all vec-

tor quantities. Four numerical constants appear in the present formulation. At the same time, we have four arbitrary units to fix. Therefore we could assume that the two make two equivalent sets of values or figures.

A transformation from a singlet particle to doublet particle was taken to occur when two material points are locked in a circular motion to form a doublet. In the absence of external factors, this system is self preserving and eternal, since the two rotating points observe the rule of balanced displacement BD all the time and the linear speed is fixed at that of light all time by assumption. Further the coupling constant is fixed and this fixes the radius of the doublet. This made one doublet exactly similar to any other doublet in size, mass, magnitude of spin, but may differ in the other attributes like the sign of spin, sign of charge etc. This allows for creating antiparticles that are identical in mass, but have anti other attributes. The rule of motion in the form of balanced displacement BD is a generator of the three laws of motion of Newton as it leads directly by differentiation to the conservation of momentum and to the usual action reaction for forces. As the measure of time is discrete, all the quantities connected to time are discrete leading naturally to the Heisenberg uncertainty principle and Planck's discrete energy quanta.

The method of using fields rather than particles is not essentially different. Water is composed of particles, but it is describable in terms of a continuous field of pressure. Also a large number of particles with suitable coupling constants can be described using waves, and a group of waves can become concentrated to resemble a particle(the soliton). Particles however, constitute the simples and more natural model for construction of matter. The phenomenon of interference and others have been sighted in the past as arguments against the particle picture. The Newton's corpuscular theory of light, for example, was rejected by simply asking where the corpuscles go at points of zero amplitude in the interference pattern (the dark spots in the interference pattern). These and other objections, have long been shown to be false since interferences happen only at the surfaces of matter and the energy or photons or corpuscles are readily absorbed by matter itself — very much like hitting a body with two bullets from two opposite directions produces no apparent kinetic energy — it is simply transferred to the molecules in each of the two bodies.

Another problem of interest is that when all particles at sight are connected via deterministic laws, as in the present case, one may suspect the disappearance of the *free* will concept. It is a fact that at this moment I can stop writing this article if I wanted to. How a decision like this can be made if the destiny is decided by the fact that all material points in the *world are entangled* together by the balanced displacement rule and the motion of any material point as a result is decided by the fate of every other one. The author believes this problem is closely related to an earlier situation we met above, wherein material points can "decide" whether to have a left handed or right handed spin or some of the other opposing attributes. At the point of branching or multiplicity of choices of paths that are equally likely, it takes nearly "zero" energy to change ones mind, and this could be why we feel free to take decisions at a moment where more than one action route is possible. In other words, our free will decisions are mainly done on branching and cross roads situations.

Reference [4], considers further the idea of a doublet particle and the geometry of aggregate of doublets, and show that it is possible to use such building blocks to make more complicated pieces of condensed matter and that there is good evidence that the masses of the elements in the periodic table and those of the elementary particles of physics are well correlated with assumptions given for simple doublets.

The Pauli Exclusion Principle, which is a corner stones of modern physics, has not been considered here. This principle is also derivable from the geometry of space and symmetry.

Acknowledgements

The author acknowledges many useful discussions with Dr. J. Hemp (Oxford, UK) and encouragement of Prof. J. Gilson (QMC, London). This work is self supported and the author is very grateful to authors who allowed their work to be made available free on the web and to the wonderful information centers and search engines that allowed such information to reach everyone at the touch of a button.

Submitted on August 25, 2009 / Accepted on September 19, 2009

References

1. Schutz B. Geometrical methods of mathematical physics. Cambridge University Press, 1980.
2. Griffiths D. Introduction to elementary particles. Wiley-VCH Verlag, 2004.
3. Einstein A., Lorentz H.A., Weyl H., Minkowski H. The Principles of Relativity — a collection of papers. Dover, 1952.
4. Al Rabeh R. H. Primes, geometry, and condensed matter. *Progress in Physics*, 2009, v. 3, 54–59.
5. Al Rabeh R. H. Solving multiparticle interactions using the Kepler route. *Progress in Physics*, 2010, v. 1, 19–22.
6. Penrose R. The road to reality. Cape, 2004.
7. Zeh H. D. The physical basis of the direction of time. Springer-Verlag, 2001.
8. Landau L. D., Lifshitz E. M. Mechanics. Pergamon Press, 1960.
9. Alonso M., Finn E. J. University physics, vol. III. Addison-Wesley, 1968.
10. Panofsky W. K. H., Phillips M. Classical electricity and magnetism. Addison-Wesley, 1962.

NEW PARADIGMS IN PHYSICS

Major Gravitational Phenomena Explained by the Micro-Quanta Paradigm

Maurizio Michelini

ENEA — Casaccia Research Centre, Rome, Italy. E-mail: m_michelini@alice.it

Some major problems of physics, which remained unsolved within classical and relativistic gravitation theories, are explained adopting the quantum gravity interaction descending from the micro-quanta paradigm. The energy source of the gravitational power P_{gr}, which heats and contracts the Bok's gas globules harbouring the future stars, is identified and defined as well as the gravitational power generated on the solid/fluid planets. Calculations are carried out to make the comparison between P_{gr} predicted for the solar giant planets and the measured infrared radiation power P_{int} coming from the interior. The case of planets with solid crust (Earth, etc.) requires a particular attention due to the threat to stability produced by the thermal dilatation. An analysis is done of the Earth's planetary equilibrium which may be attained eliminating the temperature rise through the migration of hot internal magma across the crust fractured by earthquakes. The temperatures observed up to 420,000 years ago in Antartica through Vostok and Epica ice cores suggest the possibility that the Earth gravitational power P_{gr} may be radiated in space through these temperature cycles (Glacial Eras). In this general frame the Earth's high seismicity and the dynamics of Plate tectonics may find their origin.

1 Introduction

A preceding paper showed that some fundamental forces, i.e. the Gravitational, the relativistic Inertial forces and the Strong force between nucleons and other particles, have the common origin from the interaction of particles with the uniform flux of micro-quanta [1]. The paradigm is characterised by a very high flux of very small quanta (wavelength equal to the Planck's lengh) which collide with particles determining their motion according to the Relativistic Mechanics. Micro-quanta easily penetrate any large mass, generating the Gravitational and the Strong forces on each particle. Travelling with the speed of light, these quanta explain why all principal interactions travel with this velocity. For these reasons the micro-quanta paradigm represents the underlying reality which supports Special Relativity, a fundameental theory which comes out reinforced by this physical paradigm. The supposed frailty of SR was denounced through several scratching paradoxes, such as the twins paradox, etc. Now the uncertainty on the inertial frames vanishes because the particle kinetic energy depends on the *physical* collisions with the micro-quanta flux. Some new results has been already analised [1], for instance the congruence of the Strong force between nucleons (an explicit expression is given for the first time) with the dynamical structure of the Deuterium nucleus. Here we try to explain some gravitational problems which did not find solution in the frame of the classical and the GR gravitation theories.

2 The quantum gravitational pushing force. Some fundamental concepts

In the last decades some quantum gravitational theories have been proposed, but they found difficulties. All these theories assume, like classical gravitation and General Relativity, that the gravitational mass is the source of the gravitational force, directly or indirectly through the space curvature. The present theory assumes that two masses are not attracted, but are *pushed* towards each other by the gravitational force, because the interaction between two particles is due to collisions with the micro-quanta flux ϕ_0. The cross section $\sigma_i = A_0 m_i$ of any particle is proportional to its inertial mass m_i through the fundamental constant [1] $A_0 \approx 4.7{\times}10^{-11}$ (units SI system). This simple origin of the most general characteristic of particles (i.e. the *mass*) depends on the fact that cross sections are the measure of the particle interaction with the micro-quanta flux filling the Universe. For the sake of simplicity we consider in the following only nucleons since they represent in practice the total mass of any gravitational body. Let's summarise some fundamental concepts. Particles are made of electromagnetic energy supporting a spherical symmetric field which scatters the incident quanta. Due to the very little Compton ratio $K_0 \approx E_0/mc^2 = 3.93{\times}10^{-51}$ between quantum and nucleon rest energy, the colliding quanta follow the optical reflection law. This fact prevents between a pair of particles the beam of quanta directed along the joining line and delimited by the small fractional cross section $\Delta\sigma = K_0\sigma(\sigma/2\pi r^2)$ centered on each particle. Due to the lack of the quantum beam $\psi(r) = \Delta\sigma\phi_0$, each particle feels a force due to an equal beam $\psi(r)$ colliding on the diametrically opposite $\Delta\sigma$. Since each recoiling quantum leaves the momentum $2E_0/c$, the beam $\psi(r)$ gives rise to the radial pushing force

$$f(r) = \frac{2E_0}{c}\,\psi(r) = \frac{2E_0}{c}\,K_0\sigma\phi_0\,\frac{\sigma}{2\pi r^2}\,, \qquad (1)$$

where $E_0 \cong 5.9{\times}10^{-61}$ is the quantum of energy and $\sigma \cong 7.85{\times}10^{-38}$ is the nucleon cross section. This equation must

be compared with the inertial model of particles [1]

$$mc^2 = \sigma\phi_0 E_0 \tau_0 \quad (2)$$

where $\tau_0 = 2\lambda_0/c$ is the simultaneous collision time of the micro-quanta, whose wavelength derived from Eq. (2)

$$\lambda_0 = c^3/2A_0\phi_0 E_0 \approx 4{\times}10^{-35} \quad (3)$$

results very close to the Planck's length. In the time τ_0 a nucleon scatters a high number of quanta

$$\sigma\phi_0\tau_0 = 1/K_0 \cong 2.54{\times}10^{50} \quad (4)$$

which press *uniformly* any *free* particle, without changing its state of motion or rest (Principle of Inertia). The force $f(r)$ which pushes the particles towards each other is just the experienced gravitational force. This may be described rearranging Eq. (1) and imposing that the term in brackets equals the gravitational constant G

$$f(r) = \frac{E_0 K_0 \phi_0 A_0^2}{\pi c}\,\frac{m^2}{r^2} = \frac{Gm^2}{r^2}\,. \quad (5)$$

The rihgt side is the newtonian law, but now G cannot in principle be considered constant and uniform throughout the Universe, although within the solar system it is. The newtonian law gives a simple notation of the pushing gravitational force.

It is largely believed that the newtonian gravitation supports the paradigm of the *gravitational* mass. Let's put a question : Who defined this paradigm? In his famous words "Ipotheses non fingo" Newton did not make assumptions on the mechanism of interaction. Many years ago I was impressed by the fact that Newton never declared that masses *generate* the force drawing them. He said that massive bodies show between them an "action at a distance" requiring that the mutual forces are aligned. This feature has been verified by the astronomers of the XIX century.

For some centuries the physicists found natural that the mass of bodies was the source of the gravitational force measured between them, as the experience about the new electrical phenomena taught us. However it has been recognised that the concept of *mass* as a field source is inappropriate, since it does not produce the "action at a distance"condition. Let's notice that this condition is satisfied by the gravitational pushing force.

The history of science taught us that when in the long run physics stagnates, then some old paradigm obstructs the development. In 1939 some difficulties were recognised with the GR theory. For instance it was found that stars of adequate mass undergo an *unlimited* gravitational collapse. The final product of this collapse was named "black hole", but this concept soon appeared *unphysical*. To be short, the enourmous stellar body vanishes but the great gravitational field remains. Contrary to the common conviction, the *unlimited* gravitational collapse is not linked to the GR theory, which is a rigorous logical construction excepting one point: the arbitrary incorporation in the theory of the (not necessarily *universal*) gravitational constant introducing the empirical gravitational force between the masses.

The unlimited collapse depends in fact on the gravitational mass paradigm, which arbitrarily considers the gravitational force as a *property* of the mass. Recent theoretical studies within the GR mathematical frame [2] esclude the existence of black holes, never really observed. This comes in favour of the new class of observed neutron stars originating from the collapse of large stars with enormous emission of radiation (supernovae).

In the frame of the micro-quanta pushing gravity the mass of particles is not the source of the gravitational force, but is simply a duplicate of the inertial mass. This explains why the Equivalence principle is perfectly verified up to 1 part on 10^{12} by the experiments. As a consequence the large star bodies undergo *limited* collapses, because the increasing gravitational pushing force does not exceed a maximum linked to the micro-quanta flux constants. These collapses originate the neutron stars.

Finally let's recall that in [1] a strong force between nucleons is defined, which is accurate at distances lower than the nuclear diametre. At the usual distances between atomic nuclei, the gravitational force largely exceeds the strong force, giving rise to the concept of *gravitational power*. In the following paragraphs we shall examine the implications of the gravitational power on the evolution of celestial bodies. For instance : i) H_2 galactic gas clouds (Bok globules), ii) dense cold planets, iii) neutron stars. The case of neutron stars will be dealt with subsequently.

3 Gravitational power on the contracting Bok globules

Before considering the solid and liquid aggregation state, let's consider the case of free atoms in gas clouds which interact emitting radiation. The astronomer Bart Bok, observing in 1947 some dark galactic gas globules with low temperature about 8° K and radius around 10^{15} metres, predicted that they might be the forge of the stars. After 43 years J. L. Yun and D. P. Clemens [3] found that practically all Bok globules they observed through CO spectroscopy resulted associated with IR emission, so they could affirm that "almost every Bok globule harbours a young star". They examined a total of 248 globules having an average mass of 11 $M_\odot$ and an average infrared radiation power $P_{rad} \approx 0.5M(L_\odot/M_\odot)$ [4].

At the end of XIX century lord Kelvin and Helmholtz studied a physical mechanism which could explain why the Sun shines from billions years without reducing its luminosity. But they correctly recognised that the gravitational contraction of the outer solar layers cannot explain quantitatively the star luminosity. Only after the advent of Special relativity it was recognised that the solar energy comes from the high temperature fusion of light nuclei through the Einstein's mass-energy equivalence.

To day we don't know which source of energy heats the core of gas globules up to the temperature of star ignition. Of course the gravitational force accelerates the atoms which colliding emit infrared radiation and tend to aggregate towards the cloud centre. The infrared power is generated reducing the atomic kinetic energy, but the average gas temperature, instead of reducing, increases. From which physical source comes the energy which heats the mass and produces radiation? It cannot come from the Einstein's mass-energy equivalence, considering the low gas temperature within the Bok globules.

The problem of correctly defining the source of the gravitational power heating the Bok globules remained unsolved in absence of a theory of the gravitational *interaction* able to specify the rate at which the gravitational waves hit the particles. During the last century the GR theory, which predicts correctly the astronomical observations, didn't solve this problem. The non-existence in GR theory of the standard gravitational waves has been theoretically guessed by several authors and recently shown by A. Loinger [5]. As a matter of fact several groups of physicists are searching for the standard GW's throughout the Universe, but they didn't find a definite result. To define the gravitational power we need to know the collision rate of known waves. It has been shown that each particle of a pair undergoes a pushing force $f(r)$ given by Eq. (1), which recalling Eq. (4) can be written as $f(r) = (2E_0/c\tau_0)(\sigma/2\pi r^2)$, a form expressing clearly the momentum variation in the time τ_0 of the bouncing quantum beam. Assuming that the particle velocity $v \ll c$, which holds up to temperatures of 10^8 °K within the star core, this force originates during the time τ_0 of the beam reflection, so the energy released to the particle by the force along the distance of reflection $l_r = c\tau_0$ is $\Delta L \cong f(r) \times l_r = 2E_0(\sigma/2\pi r^2)$. Then the power given up to the particle in the time τ_0 is $p_i = \Delta L/\tau_0 = f(r) \times c$ [1]. Using for the sake of simplicity the newtonian notation (Eq. 5), the gravitational power received by each nucleus of a pair at a distance x_i becomes

$$p_i = G c m_i^2 / x_i^2 , \tag{6}$$

where m_i is the mass of nuclei, $x_i = (m_i/\delta)^{1/3}$ is the average distance between nuclei within a body of local density $\delta(r)$ where r is the distance along the body radius. Summing up to all nuclei m_i of a celestial body with radius R, the gravitational power released to the body is defined

$$P_{gr} = \int_0^R p_i(r) \, \frac{4\pi r^2 \delta(r)}{m_i(r)} \, dr . \tag{7}$$

First let's assume the limiting case where the atoms are at rest. From Eq. (6) one gets

$$p_i(r) = G c m_i^{4/3} \delta^{2/3}(r) \tag{8}$$

which, substituted in Eq. (7) and considering that the molecular mass (mostly Hydrogen) does not vary along r, gives the gravitational power of a gas cloud at absolute zero temperature

$$P_{gr} = G c m_i^{1/3} \int_0^R 4\pi r^2 \delta^{5/3}(r) \, dr . \tag{9}$$

This situation looks like the atoms of very cold gas clouds. However Eq. (9) is inaccurate because does not consider the high temperature reached in the core of galactic gas globules made of free molecules having velocity $v = (2kT/m_i)^{1/2}$. When the distance $x_i(t)$ between two close molecules sometimes reduces to the molecule diametre, there is a collision with probable emission of a visible photon. More in general, putting x_0 the minimun distance, the two atomic nuclei graze with angular velocity

$$\omega \approx \frac{v}{x_0} = \frac{(2kT/m_i)^{1/2}}{x_0} . \tag{10}$$

For a very small time, the charged nuclei oscillate with amplitude $x(t) = x_0/\cos(\omega t) = 2x_0 \cos(\omega t)/(1 + \cos(2\omega t))$. Since gas oscillators at temperature T produce radiation with wavelength $\lambda = 2.89{\times}10^{-3}/T$ (Wien's law) the corresponding radiation emitted from a gas cloud is linked to

$$\omega = (2\pi c/\lambda) = 6.52{\times}10^{11} \, T . \tag{11}$$

Substituting ω in Eq. (10) one has

$$x_0^2 = 6.49{\times}10^{-47}/T m_i . \tag{12}$$

Putting in Eq. (6) the distance $x_i = x_0$, the gravitational power of a pair just emitting an infrared photon at a distance r along the radius of the body is

$$p_i(r) = 1.54{\times}10^{46} \, G c m_i^3(r) \, T(r) . \tag{13}$$

Susbstituting in Eq. (7) and integrating to all nuclei of a gas globule made of equal molecules one obtains

$$P_{gr} = 1.54{\times}10^{46} \, G c m_i^2 \int_0^R 4\pi r^2 \delta(r) \, T(r) \, dr . \tag{14}$$

Assuming the H_2 molecules of the Bok globules, quick calculations can be made recognising that Eq. (14) contains just the definition of the average temperature T_{av} of a body of mass M. So we have

$$P_{gr} \approx 3.42{\times}10^{-9} \, M T_{av} . \tag{15}$$

To calculate the average temperature through the ideal gas equation of state, we need to calculate the average radius R_{av} of the 248 observed globules, which emit infrared radiation corresponding to an external temperature T_0 comprised between 26° and 254° K [3]. This may be obtained putting the radiation power $P_{rad} = 4\pi R_{av}^2 \kappa_s T_0^4$ equal to the observed radiation $P_{rad} \approx 10^{-4} \, M$ which, substituting the average globule mass, gives $P_{rad} \approx 2.2{\times}10^{27}$ Watt. The resulting $R_{av} \approx 2{\times}10^{12}$

gives an average temperature $T_{av} \approx 5{\times}10^4\,^\circ$K leading to a gravitational power $P_{gr} \approx 3.8{\times}10^{27}$ Watt.

The observed Bok globules denounced an inner hot core. As appearing in Eq. (14), the inner gravitational power is proportional to the high central temperature, which explains why the inner core temperature increases so rapidly.

Part of the gravitational power escapes as radiation according to the energy balance of the globule

$$C_H M(dT_{av}/dt) = P_{gr} - P_{rad} \tag{16}$$

where $C_H = 1.44{\times}10^4$ J/kg×K is the specific heat of the molecular Hydrogen. Since it has been found that $P_{gr} \geqslant P_{rad}$, Eq. (16) states that the globule temperature increases.

Had the theory predicted P_{gr} less than the experimental P_{rad}, it should be considered wrong.

Now we have to proof that this inequality holds during the globule lifetime. The micro-quanta paradigm shows that within the gas clouds P_{gr} increments the molecular kinetic energy and produces photons which undergo many Compton scattering with reduction of their energy before escaping from the globule. In fact the photon mean free path results 10^{11}–10^{12} metres in the periphery of a cold large globule ($R = 10^{15}$) whereas takes a figure of 10^2–10^4 metres within the observed Bok globules ($R = 2{\times}10^{12}$). Since the last case shows an optical thickness much greater than the first case, this means that the fraction $Y = P_{rad}/P_{gr}$ of the infrared radiation escaping from the cold large globule is higher than the fraction $Y = 2.2{\times}10^{27}/3.8{\times}10^{27} \approx 0.55$ escaping from the observed Bok globules. The fraction $Y(R)$ is a function of the globule radius and reduces when the globule contracts, increasing the optical thickness. To evaluate the temporal trend of the globule temperature from Eq. (16) we substitute the definition of P_{gr} and put $P_{rad} = Y(R)P_{gr}$

$$C_H M(dT_{av}/dt) = 3.42{\times}10^{-9} M T_{av}(1 - Y(R)). \tag{17}$$

It appears that T_{av} depends slowly on the mass through the factor $Y(R)$. If one assumes that the observed value $Y \approx 0.55$ does not vary much during the globule lifetime, the solution is

$$T_{av}(t) \approx T_{in} \exp\left(9.96{\times}10^{-14}\, t\right), \tag{18}$$

where T_{in} is the average temperature of the Bok globule at the initial stage $t = 0$. For instance one may put the initial stage when the radius $R \approx 10^{15}$ corresponds to the cold large globule. In this case the average temperature, calculating the right average gravitational pressure, results $T_{in} \approx 3.2{\times}10^4\,^\circ$K, showing that even the cold globule has a hot core. From this initial stage one can calculate the time a Bok globule needs to heat the mass at a temperature T_{av}

$$\Delta t_B \approx 10^{13} \ln \frac{T_{av}}{3.2{\times}10^4}\,. \tag{19}$$

The most important event in the life of Bok globules is the ignition of the nuclear reactions which takes place when the inner core attains a temperature of the order of $10^7\,^\circ$K. Assuming the corresponding average temperature $T_{av} \approx 8{\times}10^5\,^\circ$K, the star ignition occurs after the time

$$\Delta t_F \approx 10^6 \text{ years}. \tag{20}$$

This result agrees with the computation of the star incubation time given by some classical methods. However Herbig's method predicted that globules producing small stars required an increasing incubation time. For instance a star of $0.2M_\odot$ would require more than 10^9 years before it begins to shine. This implies that these small stars would be only a little fraction in the celestial vault, contrary to the common observation.

Conversely, the gravitational power concept satisfies the experimental evidence because the incubation time depends on the firing temperature of fusion reactions, which is the same for the Hydrogen gas globules. Since the ideal gas equation holds in the case of gas globules (escluding the inner core where the high temperature determines plasma conditions), the thermal energy of the body equals substantially the gravitational energy

$$GM^2/2R \cong C_H M T_{av} \tag{21}$$

from which the radius R corresponding to a globule of mass M and average temperature T_{av} can be calculated. The high power generated by the nuclear reactions in the inner core (protostar) gives rise to a radiation wind able to sweep away the external globule layers, revealing a young bright star. It may be useful to recall that the fire of nuclear reactions limits, through the radiation wind, the size of the star mass. The different masses of the stars depend probably on the different increasing rate of the inner core temperature at the moment of the nuclear ignition. This very complex phenomenon has been recently observed and described by an equipe of astronomers which observed the formation of a star group within an infrared dark cloud in the G327.3-0.6 region [6].

4 A new dynamical principle in the Universe

Cosmologists have long debated between the expanding universe described by various GR models and the stationary universe described by the Hoyle-Bondi model, where new matter continuosly emerges apparently from the void space.

The micro-quanta flux is the physical reality underlying the Relativistic Mechanics which rules the motion of particles. The gravitational power on the bodies heats cosmic cold gas clouds at different places in the Universe, which become observable at different times when their electromagnetic emissions come within the sensitivity of the astronomical and astrophysical instruments. The energy heating small and large masses in the Universe is drawn from the collisions of particles with the micro-quanta flux filling the space, giving up to each particle a gravitational power produced by the gravitational force due to the mutual screening of masses. Is this the "creation of matter" mentioned by Hoyle? Strictly

speaking, the gravitational power concept implies only the drawing of energy from the underlying reality. Being the energy equivalent to mass, the answer might be yes.

The new dynamical principle describes, more likely, the model of the Universe depicted by the astronomer H. Arp [7]: the Universe has no origin and is in continuous transformation, drawing locally from its interior the possibility of evolution. Any large gas cloud at temperature near the absolute zero may give rise to crowded star clusters or to new galaxies thanks to the gravitational power, which acts also in many other astrophysical situations. For instance influencing even the behaviour of modest astrophysical bodies, such as the planets.

5 Gravitational power on the planets

In the so-called "inert" celestial bodies, such as the planets, atoms are bound to each other by the forces of the Lennard-Jones potential, which determine the equilibrium distance between them. A planet forms when the density of a contracting small cloud takes values corresponding to the solid or liquid state. Obviously this fact stops the contraction and makes largely inaccurate the ideal gas equation, so the equivalence between the gravitational and thermal energy vanishes. Around their rest-place the atomic nuclei oscillate with amplitude and frequency depending on the temperature. Any nucleus of mass m_i and average velocity v shows an absolute temperature given by

$$kT = \frac{1}{2}\, m_i v^2. \tag{22}$$

The instanteneous velocity $v(t)$ is bound to the oscillation amplitude $x(t) = a\sin(\omega t + \alpha)$ through the relationship

$$v^2(t) = (dx/dt)^2 = a^2\omega^2 \cos^2(\omega t + \alpha) \tag{23}$$

whose average value is $v^2 = \frac{1}{2}\, a^2\omega^2$.Then the oscillation amplitude is given by

$$a = \frac{(4kT/m_i)^{1/2}}{\omega} \tag{24}$$

which is a little different from Eq. (10). The frequency of the emitted photon is linked to the temperature of the gas through the Wien's law which leads to ω given by Eq. (11). Substituting ω and $m_i = Am_0$ into Eq. (24) and putting the numerical values, one gets the radial behaviour of the amplitude depending on $T(r)$ and $A(r)$

$$a(r) = \frac{2.79{\times}10^{-10}}{[T(r)\,A(r)]^{1/2}}\,. \tag{25}$$

The electrical forces rule the motion of the oscillating atoms in thermal equilibrium. But the kinetic energy of the atoms came from the same source that heated the ancient Bok globule which produced our Sun and planets. The primeval planets were hot bodies with outer temperature around 950° K, which lose their energy early by radiating in space, thus allowing life on the Earth during nearly 4 billion years. Abstracting from the heating of solar radiation, all planet surfaces should be presently near the absolute zero. But the astronomers found a sensible infrared radiation which comes from the interior of the giant solar planets [see Table 1]. As explained for the gas globules, also the atoms in the planets receive new kinetic energy from the micro-quanta flux. Each atom receives the major fraction of the gravitational power from the nearest nuclei. The work done on each oscillating atom by the resultant gravitational force always increments its kinetic energy. Let's consider the resultant gravitational force on a nucleus of mass m_i oscillating with amplitude $x(t)$ along the straight line joining some nuclei placed on both sides at equal distance x_i. Pairs of adjacent nuclei are alternatively approaching and removing of a displacement $2x(t)$ due to the thermal motion. Thus the nearest two nuclei gives the greatest contribute, whereas the nuclei at distance $2x_i$ do not contribute and the nuclei at distance $3x_i$ contribute for a few percent, as shown by Eq. (26). Multiplying the resultant force by the velocity c of the colliding quanta gives us (considering that $x \ll x_i$) the released power

$$\begin{aligned} p_i(t) = Gcm_i^2 \Big[&\frac{1}{(x_i - 2x)^2} - \frac{1}{(x_i + 2x)^2} + \\ &+ \frac{1}{(3x_i - 2x)^2} - \frac{1}{(3x_i + 2x)^2} \Big] \cong 8.3\, Gcm_i x\delta\,. \end{aligned} \tag{26}$$

To obtain the time averaged power when the amplitude varies from 0 to a we have to multiply by $\frac{2}{\pi}$, so one gets the radial power distribution $p_i(r) \cong \frac{16.6}{\pi}\; Gcm_i a(r)\delta(r)$ to be substituted in Eq. (7). As a consequence the gravitational power released to a planet results

$$P_{gr} \cong \frac{16.6}{\pi}\, Gc \int_0^R 4\pi r^2 \delta^2(r)\, a(r)\, dr \tag{27}$$

which, substituting the amplitude $a(r)$ from Eq. (25), gives

$$P_{gr} \cong 2.95{\times}10^{-9}\, Gc \int_0^R \frac{4\pi r^2 \delta^2(r)}{[T(r)\,A(r)]^{1/2}}\, dr\,. \tag{28}$$

If the internal parameters were known, Eq. (28) might be simply computed by numerical integration. But the trends of the internal density, nuclear mass and temperature are in general not known (excepting perhaps the Earth) with an accuracy better than 20%. To the aim of doing some quick calculations we observed that the ratio $B = \delta(r)/T(r)A(r)$ results to be, referring to the Earth's internal parameters recently calculated by D. Alphe et al. [8], independent from the radial coordinate and about equal to $B \approx 4{\times}10^{-2}$ (SI system). Let's recall that Earth is the unique planet whose internal structure is known with an accuracy better than 10%. Substituting B in Eq. (28) one may obtain the approximate formula

$$P_{gr} \approx 2.9{\times}10^{-11} M\, (\delta_{av} B)^{1/2}. \tag{29}$$

Planet	Predicted gravitational power P_{gr} (W)	Measured infrared flux ϕ_{ir} (W/m^2)	Internal infrared flux $\Delta\phi_{ir}$ (W/m^2)	Measured internal power P_{int} (W)
Jupiter	4.3×10^{17}	13.89	5.57	3.5×10^{17}
Saturn	9.1×10^{16}	4.40	1.93	8.6×10^{16}
Uranus	9.8×10^{15}	0.69	0.04	3.2×10^{14}
Neptune	1.7×10^{16}	0.72	0.45	3.5×10^{15}
Earth	2.6×10^{15}	?	?	?

Table 1: Predicted gravitational power P_{gr} compared with the measured internal power P_{int} observed for the solar giant planets, according to [10].

5.1 Calculation of the gravitational power on Earth and the giant solar planets

When applied to the Earth, Eq. (29) gives a gravitational power $P_{gr} \approx 2.6\times10^{15}$ Watt. This approximate formula shows an accuracy comparable to that we would obtain introducing the Earth internal parameters directly in the exact Eq. (28). The predicted P_{gr} is 60 times higher than the classical heat flow (4.4×10^{13} Watt) calculated by laborious evaluation of the geothermal gradient measured throughout the continents and adopting an average thermal conductivity κ measured in laboratory for the principal rocks [9]. Of course the value of the geothermal gradient and of κ for the remaining 70% of the planet surface (under the oceans) had to be inferred, due to the difficulties of making measurements. Because the classical heat flow is likely not affected by a computational error higher than 30%, the discrepancy with P_{gr} has to be attributed to the lack of other forms of heat flow across the crust. The contribution of the radioactive isotopes in the rocks to the total power generated inside the planet becomes negligible when compared to P_{gr}. Useful verifications of the computational formula for P_{gr} (Eq. 29) may be done searching for the constant B_i of the giant planets of the solar system for which the infrared radiation coming from the interior has been measured. A recent book by P. G. Irwin [10] analyses the data collected from various interplanetary spacecrafts launched in the last decades towards Jupiter, Saturn, Uranus and Neptune. A draft of the internal structure of these planets is given from which only rough values of B_i may be obtained. However for Jupiter and Saturn the values of B_i are not much different from the Earth's value, whereas lower values were obtained for Uranus and Neptune, whose structure is dominated by H_2O ice instead of molecular Hydrogen.

In Table 1 the gravitational power P_{gr} computed for the giant planets is compared with the internal infrared power $P_{int} = 4\pi R^2(\phi_{ir} - \phi_{Sun})$ derived from the measured infrared flux ϕ_{ir} minus the infrared contribution ϕ_{Sun} due to the solar absorbed/emitted radiation. The difference $\Delta\phi_{ir}$ appears to be numerically accurate for Jupiter, Saturn and Neptune because it amounts to a large fraction of the observed flux ϕ_{ir}. Only for Uranus $\Delta\phi_{ir}$ is a small fraction (5.8%) of the observed flux, so some inaccuracy on the related P_{int} is unavoidable. The agreement between P_{gr} and P_{int} for Jupiter and Saturn confirm that the experimental P_{int} appears to be the gravitational power theoretically predicted. The discrepancy found for Neptune may be likely due to the uncertain factor B. However the high discrepancy between P_{gr} and P_{int} of Uranus has to be attributed to some profound reason. For instance, the fact that the internally generated P_{gr} does not entirely reach the external surface due to the particular peripheral structure of the planet. Let's recall that specific studies suggest that Uranus presents a discontinuity of the internal structure, probably near the surface [11]. As we know, a similar discontinuity (Mohorovich's one) is present also on the Earth. Observing Table 1 one wonders if an experimental method may be adopted (as for the giant planets) to measure the IR flux radiating from the Earth interior. This would give an independent check of the gravitational power generated on the planets.

5.2 The emergent problem of the Earth dilatation

We have seen that the gravitational power discharged on the Earth largely exceeds the classical heat flow by conduction through the crust. The classical method does not consider the heat flow through other ways, for instance the cooling of magma escaping from the Mid Ocean Ridges, from the seismic fractures linked to the Plate tectonics [12] and from volcanic activities on the ocean seafloor. Let's recall that the U.S. Geological Service data show a frequency of about 8 earthquakes per day, Richter magnitude $\geqslant 4$, mostly under the ocean seafloor.

The gravitational power is the physical agent heating and contracting the galactic gas globules. In the case of planets — where the atoms are tightly packaged — P_{gr} can no longer induce a contraction. On the contrary it may induce a thermal expansion which increases the Earth radius. Let's consider the energy balance of the *core + mantle* mass

$$C_{av}M(dT_{av}/dt) = 0.966P_{gr} - P_{ex}(t)\,, \qquad (30)$$

where $C_{av} = 708$ J/kg×K is the average specific heat. It is taken into account that about 3.4% of P_{gr} is generated into the lithosphere. $P_{ex}(t)$ is the power exiting from the mantle towards the lithosphere. To a first approximation, it equals the classical heat flow by conduction across the solid crust 4.4×10^{13} W plus the heat flow of hot magma which cools penetrating the seismic fractures produced through the crust

$$P_{ex}(t) = Q_0(dV/dt) + 4.4\times10^{13}, \qquad (31)$$

where Q_0 is the heat released by 1 m^3 of hot magma which enters the crust at a temperature around 1800° K and (dV/dt) is the volume rate of hot magma entering the crust (Eq. 33). Correspondingly the power entering the crust and accumulating before to be radiated into space, obey the energy balance

$$C_{cr}M_{cr}(dT_{cr}/dt) = 0.034\,P_{gr} + P_{ex}(t) - P_{int}(t)\,, \qquad (32)$$

where $C_{cr} \approx 1200$ J/kg×K is the average specific heat of the rocks and P_{int} is the infrared radiation power coming from the interior.

Eqs. (30, 31, 32) contain the unknown temperature derivatives of the Earth interior and of the crust. $P_{ex}(t)$ and $P_{int}(t)$ are physical quantities to be found. To a first approximation the exiting power P_{ex} may be evaluated assuming that the expansion rate of the *core* + *mantle* exceeds the expansion rate allowed by the solid crust, which consequently undergoes seismic fractures incorporating the increased volume of hot magma. The volume rate of magma entering the crust (and partially escaping from the ocean seafloor and volcanic activity) is given by

$$\frac{dV}{dt} \approx 4\pi R^2 \left(\frac{dR_m}{dt} - \frac{dR_{cr}}{dt} \right). \qquad (33)$$

The temperature derivative dT_{av}/dt produces a dilatation of the *mantle* radius

$$dR_m/dt = R_i \alpha_{av} (dT_{av}/dt) \qquad (34)$$

where it has been considered an average *core* + *mantle* linear expansion coefficient $\alpha_{av} = 1.12{\times}10^{-5}\,^{\circ}\mathrm{K}^{-1}$ based on the usual data at normal temperature. It is not clear how much α might change at temperature $\geqslant 2000^{\circ}$ K (mantle) and $\geqslant 5000^{\circ}$ K (FeNi-core). The *core* + *mantle* expansion originates a radial compression on the solid crust (spherical shell) whose inner radius R_{cr} shows an annual dilatation

$$dR_{cr}/dt = R_i \alpha_{cr} (dT_{cr}/dt)\,, \qquad (35)$$

where the assumed expansion coefficient of the rocks is $\alpha_{cr} \approx 1.3{\times}10^{-5}\,^{\circ}\mathrm{K}^{-1}$.

Let's recall that the 1 m^3 of hot magma at a temperature around 1800° K releases to the crust the heat which is $Q_0 = \delta(c\,\Delta T + H_f) \approx 6.9{\times}10^9$ J/m^3, where $H_{fus} \approx 3.7{\times}10^5$ J/kg is the average heat of fusion/solification of the rocks. Multiplying by Q_0 the magma flow of Eq. (33), one obtains the heat flow due to the cooling of magma entering the crust fractures, to which is added the classical heat flow by conduction. Part of the magma flow escapes from the Mid ocean Ridges, thus removing the tectonic plates [12] which undergo subduction. Rough estimates of the plate dynamics show an amount of new formed crust of the order of $1.3{\times}10^{10}$ m^3/y, that is probably a little fraction of the total.

This scheme gives values of $P_{ex}(t)$ depending on the two unknown temperature derivatives.

The infrared radiation $P_{int}(t)$ coming from the interior remains up to now unspecified. A simple equation comes out summing Eq. (30) and Eq. (32)

$$C_{av} M (dT_{av}/dt) + C_{cr} M_{cr} (dT_{cr}/dt) = P_{gr} - P_{int}(t) \qquad (36)$$

which does no longer need to know $P_{ex}(t)$. When the infrared radiation power $P_{int}(t)$ is less than the gravitational power, this equation states that the Earth temperature increases sensibly along some million years, thus producing the dilatation threat.

5.3 Comparison between the effects on Earth and the giant solar planets

Some points of the present analysis about the Earth thermal dilatation require further specification. The lithosphere began to form upon the fluid planet about 4 billion years ago, to account for the evolution of primeval life on the Earth. If the magma estimated by Eq. (33) escaped during 4 billion years, the volume of the lithosphere would be about 16 times the present value. This requires an explanation. One may wonder which fraction of time the tectonic process was operating. A recent hypothesis [13] suggests that plate dynamics was intermittent along the geological periods. As a matter of fact the process of the magma escaping through seismic fractures has just the characteristics of discontinuity. However this does not match with the continuous feeding of heat to the Earth by the gravitational power.

To this aim it is necessary to make reference to the fluid planets, such as the giant solar planets (namely Jupiter and Saturn) where the mass expands freely and the gravitational power generated in the interior flows up to the outer surface where it is radiated in space. For these planets the energy balance

$$C_{av} M (dT_{av}/dt) = P_{gr} - P_{int}(t) \qquad (37)$$

indicates that, when $P_{gr} = P_{int}$, the internal temperature of the planet is constant. No thermal expansion stresses arise because the solid crust is lacking. Let's now return to the Earth. The major problems are:

1. If in Eq. (30) we neglect P_{ex}, the increase of the average temperature $dT_{av}/dt \approx (P_{gr}/C_{av}M)$ would be of the order of $10^{-5}\,^{\circ}$K/y). Lasting for 10 million years this would increase the internal temperaure of about 100° C. Conversely the *surface* temperature would experience a little increment because an increase of 1° C is sufficient to radiate in space an infrared power equal to the whole P_{gr}. This can be proved recalling that the Earth effective temperature $T_0 = 255^{\circ}$ K, calculated by P. G. Irwin [10] considering the bond albedo, radiates an infrared power equal to the absorbed solar light. If the planet surface were radiating in addition the predicted power P_{gr}, the surface effective temperature would increase from 255° K to 256° K only;
2. If the duration of the Earth increasing temperature is assumed to be 1 billion years, the resulting temperature would have evaporised the planet. Because this din't happen, there was some mechanism which braked the increasing temperature;
3. At the boundary between astenosphere and lithosphere a modest increase of temperature (for instance 100° C) makes fluid some solid rocks, so reducing the mass of

the solid crust. This explains why the volume of the present solid crust is many times smaller than the volume of the total magma escaped during 4 billion years. Let's assume that the escaping magma that annually solidifies within the crust is counterbalanced by an equal volume of liquefied rocks at the boundary with the astenosphere. This requires that the Earth should give up to the crust some heat flow which can be easily furnished by the gravitational power;

4. The risk still remains of the increasing Earth temperature. Up to now we have assumed that the transfer of the internally generated power towards the outer surface depends on the fact that the expanding volume (dilatation) of the hot interior produces many fractures (deep earthquakes) on the solid crust, which are rapidly filled by hot fluid magma. In this frame the Earth appears to be an intrinsically seismic planet.

In a recent work, the pressure exerted by the expanded *core + mantle* on the elastic solid crust has been assumed to produce a continuous passage of some hot fluid minerals through a complex physical-chemical process conveying some thermal power. A plain description of such a process by P. B. Kelemen may be found in *Scientific American* [13], whereas the fundamental concepts may be found in a previous paper [14]. However the potentiality of the process in transferring internal power towards the outer surface does not appear to have been evaluated.

5.4 The ice core data recording the Glacial Eras

The cycles of the temperature (Fig.1) observed from ice cores in Antartica by two independent teams, Vostok [15] and Epica [16], show an impressive result: the most recent four cycles may be nearly placed one upon other. The cycle durations are between 85–122 ky. Each peak is preceded by a temperature strong rise with slope around 1.8° C/ky and is followed by a partial descent with about the same slope. This fact is worth receiving an explanation. The descent continues with a series of small alternated rises and descents characteristics of each cycle. The Antarctica temperature behaviour has been observed together with the concentrations of CO_2 and CH_4 greenhouse gases and of the local insolation.

Deciphering this lot of data is the main trouble of many scientists. Since the peaks of the greenhouse gases are considerably less than their present concentration, the temperature rising in Antarctica could not be due to the greenhous gas effect. In any case the slope of the present climate effect by greenhouse gases (more than 10° C/ky) is not comparable with the antartic cycling phenomena. Most likely, since there is simultaneity between the temperature peaks and the greenhouse gas peaks, the antartic CO_2 and CH_4 concentrations could be due to the increase of temperature in the equatorial and temperate regions, where the decomposition of organic matter in CO_2 and CH_4 was enhanced, so the greenhouse gases migrate rapidly through winds towards the poles.

The cycling temperature amplitude $\Delta T(t)$ in Antartica is notable (each cycle shows an amplitude comprised between 10° C and 13° C). Here it is considered as the increase, over the undisturbed average antartic temperature T_A, due to some thermal power $P_{int}(t)$ coming from the planet interior and radiated to space. Since the average temperature measured at the Vostok site is −64° C, it follows that the minimum temperature of the ice core record (see Fig.1) results $T_A \approx 200°$ K. Let's consider 1 m^2 of surface in Antartica where, in absence of the internal power, the radiation balance is

$$\kappa\epsilon\,(T_A)^4 \approx 110\,\varepsilon\,(\mathrm{W/m^2}) = p_{sun} + p_{atm} \qquad (38)$$

where κ is the Stephan-Boltzmann constant, ε is the snow emissivity, p_{sun} is the specific power from sunlight and p_{atm} is the power released on 1 m^2 by the atmospheric precipitations transported by winds from the oceans. By consequence, in the energy balance the internal power $p_{int}(t) = P_{int}(t)/4\pi R^2$ radiates in space through the temperature increment $\Delta T(t)$

$$p_{int}(t) = \kappa\varepsilon\left[(T_A + \Delta T(t))^4 - T_A^4\right] \cong 4\kappa\varepsilon\, T_A^3 \Delta T(t)\,. \qquad (39)$$

Substituting $T_A \approx 200°$ K in this equation one gets

$$p_{int}(t) \approx 1.81\,\varepsilon\,\Delta T(t) \qquad (40)$$

which shows an internal power rising from 0 up to the maximum $p_{int} \approx 19\,\varepsilon$ W/m^2 and subsequently descending to 0 with a particular series of descents and risings.

We assume that the Earth gravitational power P_{gr} goes beyond the solid crust *via* the hot magma entering the seismic fractures in the crust. The longest duration of magma flow produces the strongest $\Delta T(t)$ rise up to the interglacial peak, which occurs due to the stop of the magma flow consequent to the stop of earthquakes. The seismicity depends on the crust ruptures consequent to the dilatation of the Earth interior (Eq. 33). Resuming, each rising of the $\Delta T(t)$ cycle occurs in presence of the seismic activity. Conversely, when $\Delta T(t)$ descends (due to the radiative emission cooling) the seismic activity should vanish. In this frame each temperature cycle is made of seismic periods alternated with quiet periods.

Some considerations on the nearly equal slopes (excepting the sign) of $\Delta T(t)$ before and after the peak. The constant slope of the strong ascent is due to the increasing magma flow entering the superficial crust. The slope of the descent is linked to the radiative cooling of the superficial mass.

In any case the ice core data imply that the temperatures of the crust $T_{cr}(t)$ and of the Earth interior $T_{av}(t)$ undergo cycles. Assuming in Eq. (36) these temperature cycles, we observe that integrating of the left side along the cycle period gives zero. By consequence the integration of the right side gives

$$P_{gr} \approx (p_{int})_{av}\, 4\pi R^2, \qquad (41)$$

where $(p_{int})_{av}$ is uniform on the Earth surface since the gravitational power flows outside isotropically.

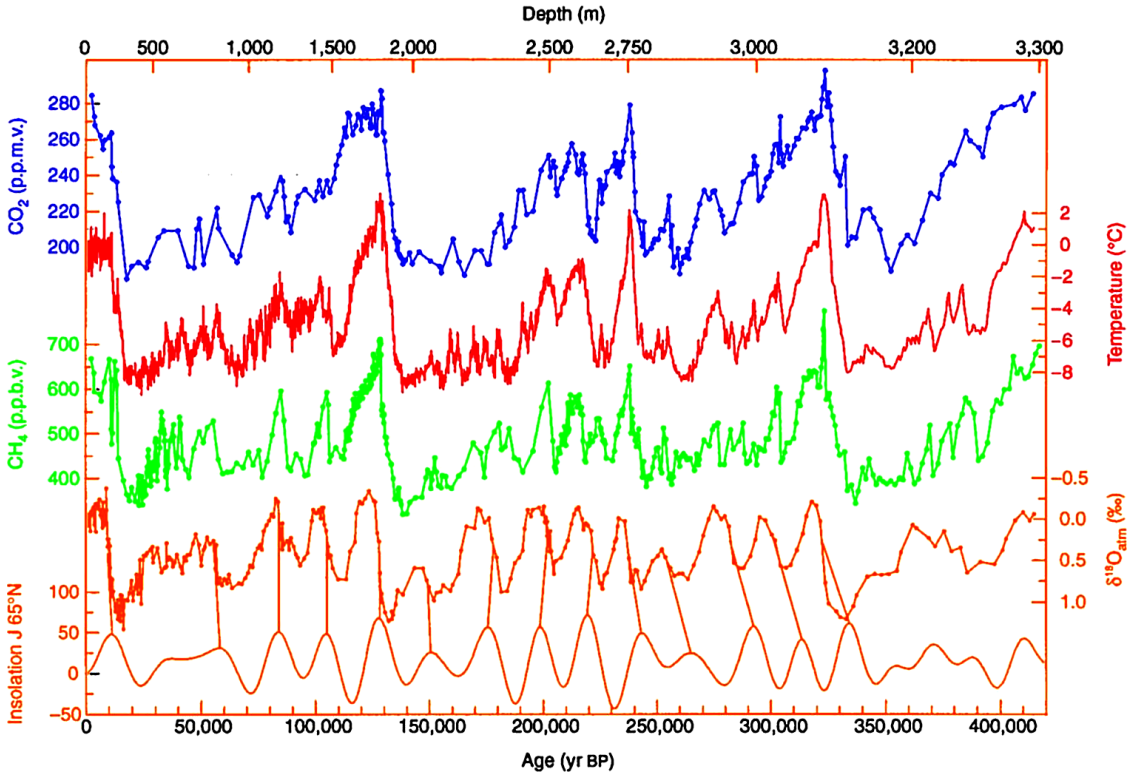

Fig. 1: 420,000 years of ice core data recorded from Vostok, Antartica research station. From bottom to top: Solar variation at $65°N$ due to Milankovitch cycles; ^{18}O isotope of oxygen; levels of methane CH_4; relative temperature respect to local annual temperature; levels of carbon dioxide CO_2.

In particular $(p_{int})_{av}$ may be calculated in Antartica making in Eq. (40) the graphic integration of $\Delta T(t)$, which gives the average $(\Delta T)_{av} \approx 3.9°$ C.

Substituting $(p_{int})_{av}$ in Eq. (41) one gets

$$P_{gr} \approx 1.81\,\varepsilon\,(\Delta T)_{av}\,4\pi R^2 \qquad (42)$$

which, considering the snow emissivity $\varepsilon = 0.82$, gives an independent value of the Earth gravitational power through the ice core data from Antartica

$$P_{gr} \approx 2.9{\times}10^{15}\ \text{Watt}. \qquad (43)$$

This empirical value of P_{gr} is higher than the approximate value $2.6{\times}10^{15}$ derived from the theoretical Eq. (28), where the numerical uncertainties on the Earth internal structure, currently discussed in the literature, are present.

6 Some final considerations

After the conceptual default of classical physics about the energetic mechanism of the contracting gas globules leading to the star birth, the introduction of the *gravitational power concept* permits us to explain the genesis of several celestial bodies from the primeval Hydrogen cold clouds. The new dynamical principle describes an Universe (somewhat similar to the Hoyle-Bondi stationary model) putting light on new phenomena such as the discordant redshifts of quasars studied by the astronomer H. Arp. The fluid giant planets do not feel heavy troubles from the gravitational power they receive. Conversely the gravitational power produces on the Earth and any planet or satellite with solid crust, dangerous physical effects through heating and dilatation. Firstly, the internal dilatation stresses the solid crust producing the planetary seismicity originating fractures rapidly filled by the mantle fluid magma. The process presents periods of emphasis followed by stasis, as confirmed by the periodic changes of the temperature slope derived from the ice core data, which show that Glacial and Interglacial Eras depend on the variable rate of the internally generated heat flowing up to the planet surface.

The present contribution to the unsatisfying knowledge of geodynamics is aimed at finding the common origin of different phenomena: the high planet seismicity, the surface thermal cycles around 100.000 years (Glacial Eras) and the Tectonic dynamics (around some ten million years). Much work needs to be done.

Submitted on October 18, 2009 / Accepted on October 26, 2009

References

1. Michelini M. The common physical origin of the Gravitational, Strong and Weak forces. *Apeiron Journal*, 2008, v. 15, 440.
2. Loinger A. GW's towards fundamental principles of GR. arXiv: phys/0709.0490.
3. Yun J. L., Clemens D. P. Star formation in small globules: Bart Bok was correct! *Astroph. J.*, 1990, v. 365, L73.

4. Clemens D. P., Yun J. L., Heyer M. H. Bok globules and small molecular clouds: Deep IRAS Photometry and CO Spectroscopy. *Astroph. J. Suppl.*, 1991, v. 75, 877.
5. Loinger A. Gravitational collapses to bodies of finite volume. arXiv: phys/0612160.
6. Minier V., André Ph., et al. Evidence of triggered star formation in G327.3-0.6. *Astron. and Astrophys.*, v. 501, L1.
7. Arp H. Catalog of discordant redshift associations. Apeiron Publishers, Montreal, 2003.
8. Alphe D., Gillan M.G., et al., The "ab initio" simulation of the Earth core. *Phil. Trans. Roy. Soc. London*, 2002, v. 360, 1227.
9. Stein C. Global Earth Phyisics. Amer. Geophys. Union, 1995.
10. Irwin P. G. Giant planets of our solar system. Springer Praxis, 2003.
11. Podolak M., Podolak J., Marley M. S. *Amer. Astron. Soc. Bulletin*, 1997, v. 29, 994.
12. Turcotte D. L., Schubert G. The plate tectonics geodynamics. 2nd Edition, Cambridge Univ. Press, 2002.
13. Silver P. G., Behn M. D. Intermittent plate tectonics? *Science*, 2008, v. 319, 85.
14. Kelemen P. B. The origin of the Land under the Sea. *Sci. Am.*, 2008, v. 300, no.2, 52.
15. Spiegelman M., Kelemen P. B., Aharonov E. Causes and consequences of flow organization during melt transport: the reaction infiltration instability in compactible media. *J. Geophys. Res.*, 2001, v. 106, 2061.
16. Petit J. R., et al. Climate and atmospheric history of the past 420,000 years from the Vostok ice core in Antartica. *Nature*, 1999, v. 399, 429–436.
17. Laurent A., Barbante C., et al. Eight glacial cycles from the Antartic ice core. *Nature*, 2004, v. 429, 623–628.

The Journal on Advanced Studies in Theoretical and Experimental Physics, including Related Themes from Mathematics

PROGRESS IN PHYSICS

A quarterly issue scientific journal, registered with the Library of Congress (DC, USA). This journal is peer reviewed and included in the abstracting and indexing coverage of: Mathematical Reviews and MathSciNet (AMS, USA), DOAJ of Lund University (Sweden), Zentralblatt MATH (Germany), Scientific Commons of the University of St. Gallen (Switzerland), Open-J-Gate (India), Referativnyi Zhurnal VINITI (Russia), etc.

To order printed issues of this journal, contact the Editors. Electronic version of this journal can be downloaded free of charge:
http://www.ptep-online.com

Postal address

Department of Mathematics and Science,
University of New Mexico,
200 College Road,
Gallup, NM 87301, USA

ISSN: 1555-5534 (print)
ISSN: 1555-5615 (online)

Standard Address Number: 297-5092
Printed in the United States of America

APRIL 2010 **VOLUME 2**

CONTENTS

Information for Authors and Subscribers

Progress in Physics has been created for publications on advanced studies in theoretical and experimental physics, including related themes from mathematics and astronomy. All submitted papers should be professional, in good English, containing a brief review of a problem and obtained results.

All submissions should be designed in LaTeX format using *Progress in Physics* template. This template can be downloaded from *Progress in Physics* home page http://www.ptep-online.com. Abstract and the necessary information about author(s) should be included into the papers. To submit a paper, mail the file(s) to the Editor-in-Chief.

All submitted papers should be as brief as possible. We accept brief papers, no larger than 8 typeset journal pages. Short articles are preferable. Large papers can be considered in exceptional cases to the section *Special Reports* intended for such publications in the journal. Letters related to the publications in the journal or to the events among the science community can be applied to the section *Letters to Progress in Physics*.

All that has been accepted for the online issue of *Progress in Physics* is printed in the paper version of the journal. To order printed issues, contact the Editors.

This journal is non-commercial, academic edition. It is printed from private donations. (Look for the current author fee in the online version of the journal.)

Two New Type Surface Polaritons Excited into Nanoholes in Metal Films

Vahan Minasyan and Valentin Samoilov
Scientific Center of Applied Research, JINR, Dubna, 141980, Russia
E-mails: mvahan@scar.jinr.ru; scar@off-serv.jinr.ru

We argue that the smooth metal-air interface should be regarded as a distinct dielectric medium, the skin of the metal. Here we present quantized Maxwell's equations for electromagnetic field in an isotropic homogeneous medium, allowing us to solve the absorption anomaly property of these metal films. The results imply the existence of light quasi-particles with spin one and effective mass $m = 2.5{\times}10^{-5} m_e$ which in turn provide the presence of two type surface polaritons into nanoholes in metal films.

1 Introduction

There have been many studies of optical light transmission through individual nanometer-sized holes in opaque metal films in recent years [1–3]. These experiments showed highly unusual transmission properties of metal films perforated with a periodic array of subwavelength holes, because the electric field is highly localized inside the grooves (around 300-1000 times larger than intensity of incoming optical light). Here we analyze the absorption anomalies for light in the visible to near-infrared range observed into nanoholes in metal films. These absorption anomalies for optical light as seen as enhanced transmission of optical light in metal films, and attributed to surface plasmons (collective electron density waves propagating along the surface of the metal films) excited by light incident on the hole array [4]. The enhanced transmission of optical light is then associated with surface plasmon (SP) polaritons. Clearly, the definition of surface metal-air region is very important factor, since this is where the surface plasmons are excited. In contrast to this surface plasmon theory, in which the central role is played by collective electron density waves propagating along the surface of metal films in a free electron gas model, the authors of paper [5] propose that the surface metal-air medium should be regarded as a metal skin and that the ideas of the Richardson-Dushman effect of thermionic emission are crucial [6]. Some of the negatively charged electrons are thermally excited from the metal, and these evaporated electrons are attracted by positively charged lattice of metal to form a layer at the metal-air interface. However, it is easy to show that the thermal Richardson-Dushman effect is insufficient at room temperature $T \simeq 300K$ because the exponent $\exp^{-\frac{\phi}{kT}}$ with a value of the work function $\phi \simeq 1\,\text{eV}$–$10\,\text{eV}$ leads to negligible numbers of such electrons.

In this letter, we shall regard the metal skin as a distinct dielectric medium consisting of neutral molecules at the metal surface. Each molecule is considered as a system consisting of an electron coupled to an ion, creating of dipole. The electron and ion are linked by a spring which in turn defines the frequency ω_0 of electron oscillation in the dipole. Obviously, such dipoles are discussed within elementary dispersion theory [7]. Further, we shall examine the quantization scheme for local electromagnetic field in the vacuum, as first presented by Planck for in his black body radiation studies. In this context, the classic Maxwell equations lead to appearance of the so-called ultraviolet catastrophe; to remove this problem, Planck proposed modelled the electromagnetic field as an ideal Bose gas of massless photons with spin one. However, Dirac [8] showed the Planck photon-gas could be obtained through a quantization scheme for the local electromagnetic field, presenting a theoretical description of the quantization of the local electromagnetic field in vacuum by use of a model Bose-gas of local plane electromagnetic waves, propagated by speed c in vacuum. An investigation of quantization scheme for the local electromagnetic field [9] predicted the existence of light quasi-particles with spin one and finite effective mass $m = 2.5{\times}10^{-5} m_e$ (where m_e is the mass of electron) by introducing quantized Maxwell equations. In this letter, we present properties of photons which are excited in clearly dielectric medium, and we show existence of two new type surface polaritons into nanoholes in metal films.

2 Quantized Maxwell equations

We now investigate Maxwells equations for dielectric medium [7] by quantum theory field [8]

$$\operatorname{curl} \vec{H} - \frac{1}{c}\frac{d\vec{D}}{dt} = 0\,, \tag{1}$$

$$\operatorname{curl} \vec{E} + \frac{1}{c}\frac{d\vec{B}}{dt} = 0\,, \tag{2}$$

$$\operatorname{div} \vec{D} = 0\,, \tag{3}$$

$$\operatorname{div} \vec{B} = 0\,, \tag{4}$$

where $\vec{B} = \vec{B}(\vec{r}, t)$ and $\vec{D} = \vec{D}(\vec{r}, t)$ are, respectively, the local magnetic and electric induction depending on space coordinate $\vec{r}$ and time t; $\vec{H} = \vec{H}(\vec{r}, t)$ and $\vec{E} = \vec{E}(\vec{r}, t)$ are, respectively, the magnetic and electric field vectors, and c is the velocity of light in vacuum. The further equations are

$$\vec{D} = \varepsilon \vec{E}\,, \tag{5}$$

$$\vec{B} = \mu \vec{H}\,, \tag{6}$$

where $\varepsilon > 1$ and $\mu = 1$ are, respectively, the dielectric and the magnetic susceptibilities of the dielectric medium.

The Hamiltonian of the radiation field $\hat{H}_R$ is

$$\hat{H}_R = \frac{1}{8\pi}\int\left(\varepsilon E^2 + \mu H^2\right)dV\,. \tag{7}$$

We now wish to solve a problem connected with a quantized electromagnetic field, a nd begin from the quantized equations of Maxwell. We search for a solution of (1)–(6), in an analogous manner to that presented in [9]

$$\vec{E} = -\frac{\alpha}{c}\frac{d\vec{H}_0}{dt} + \beta\vec{E}_0 \tag{8}$$

and

$$\vec{H} = \alpha\,\mathrm{curl}\,\vec{H}_0 + \beta\vec{H}_0\,, \tag{9}$$

where $\alpha = \frac{\hbar\sqrt{2\pi}}{\sqrt{m}}$ and $\beta = c\sqrt{2m\pi}$ are the constants obtained in [9]. Thus $\vec{E}_0 = \vec{E}_0(\vec{r},t)$ and $\vec{H}_0 = \vec{H}_0(\vec{r},t)$ are, respectively, vectors of electric and magnetic field for one Bose-light-particle of electromagnetic field with spin one and finite effective mass m. The vectors of local electric $\vec{E}_0$ and magnetic $\vec{H}_0$ fields, presented by equations (8) and (9), satisfy to equations of Maxwell in dielectric medium

$$\mathrm{curl}\,\vec{H}_0 - \frac{\varepsilon}{c}\frac{d\vec{E}_0}{dt} = 0\,, \tag{10}$$

$$\mathrm{curl}\,\vec{E}_0 + \frac{1}{c}\frac{d\vec{H}_0}{dt} = 0\,, \tag{11}$$

$$\mathrm{div}\,\vec{E}_0 = 0\,, \tag{12}$$

$$\mathrm{div}\,\vec{H}_0 = 0\,. \tag{13}$$

By using of (10), we can rewrite (9) as

$$\vec{H} = \frac{\alpha\varepsilon}{c}\frac{d\vec{E}_0}{dt} + \beta\vec{H}_0\,. \tag{14}$$

The equations (10)–(13) lead to a following wave-equations:

$$\nabla^2\vec{E}_0 - \frac{\varepsilon}{c^2}\frac{d^2\vec{E}_0}{dt^2} = 0 \tag{15}$$

and

$$\nabla^2\vec{H}_0 - \frac{\varepsilon}{c^2}\frac{d^2\vec{H}_0}{dt^2} = 0 \tag{16}$$

which in turn have the following solutions

$$\vec{E}_0 = \frac{1}{V}\sum_{\vec{k}}\left(\vec{E}_{\vec{k}}\,e^{i(\vec{k}\vec{r}+\frac{kct}{\sqrt{\varepsilon}})} + \vec{E}^{+}_{\vec{k}}\,e^{-i(\vec{k}\vec{r}+\frac{kct}{\sqrt{\varepsilon}})}\right), \tag{17}$$

$$\vec{H}_0 = \frac{1}{V}\sum_{\vec{k}}\left(\vec{H}_{\vec{k}}\,e^{i(\vec{k}\vec{r}+\frac{kct}{\sqrt{\varepsilon}})} + \vec{H}^{+}_{\vec{k}}\,e^{-i(\vec{k}\vec{r}+\frac{kct}{\sqrt{\varepsilon}})}\right), \tag{18}$$

where $\vec{E}^{+}_{\vec{k}}$, $\vec{H}^{+}_{\vec{k}}$ and $\vec{E}_{\vec{k}}$, $\vec{H}_{\vec{k}}$ are, respectively, the second quantization vector wave functions, essentially the vector Bose "creation" and "annihilation" operators for the Bose quasi-particles of electric and magnetic waves with spin one in dielectric medium. With these new terms $\vec{E}_0$ and $\vec{H}_0$, the radiation Hamiltonian $\hat{H}_R$ in (7) takes the form

$$\begin{aligned}\hat{H}_R &= \frac{1}{8\pi}\int\left(\varepsilon E^2 + H^2\right)dV = \\ &= \frac{1}{8\pi}\int\left[\varepsilon\left(-\frac{\alpha}{c}\frac{d\vec{H}_0}{dt} + \beta\vec{E}_0\right)^2 + \right. \\ &\left. + \left(\frac{\alpha\varepsilon}{c}\frac{d\vec{E}_0}{dt} + \beta\vec{H}_0\right)^2\right]dV\,,\end{aligned} \tag{19}$$

where, by substituting into (17) and (18), leads to the reduced form of $\hat{H}_R$

$$\hat{H}_R = \hat{H}_e + \hat{H}_h\,, \tag{20}$$

where the operators $\hat{H}_e$ and $\hat{H}_h$ are

$$\begin{aligned}\hat{H}_e &= \sum_{\vec{k}}\left(\frac{\hbar^2k^2\varepsilon^2}{2m} + \frac{mc^2\varepsilon}{2}\right)\vec{E}^{+}_{\vec{k}}\vec{E}_{\vec{k}} - \\ &- \frac{1}{2}\sum_{\vec{k}}\left(\frac{\hbar^2k^2\varepsilon^2}{2m} - \frac{mc^2\varepsilon}{2}\right)\left(\vec{E}^{+}_{\vec{k}}\vec{E}^{+}_{-\vec{k}} + \vec{E}_{-\vec{k}}\vec{E}_{\vec{k}}\right)\end{aligned} \tag{21}$$

and

$$\begin{aligned}\hat{H}_h &= \sum_{\vec{k}}\left(\frac{\hbar^2k^2\varepsilon}{2m} + \frac{mc^2}{2}\right)\vec{H}^{+}_{\vec{k}}\vec{H}_{\vec{k}} - \\ &- \frac{1}{2}\sum_{\vec{k}}\left(\frac{\hbar^2k^2\varepsilon}{2m} - \frac{mc^2}{2}\right)\left(\vec{H}^{+}_{\vec{k}}\vec{H}^{+}_{-\vec{k}} + +\vec{H}_{-\vec{k}}\vec{H}_{\vec{k}}\right).\end{aligned} \tag{22}$$

In the letter [9], the boundary wave number $k_0 = \frac{mc}{\hbar}$ for electromagnetic field in vacuum was appeared by suggestion that the light quasi-particles interact with each other by repulsive potential $U_{\vec{k}}$ in momentum space

$$U_{\vec{k}} = -\frac{\hbar^2k^2}{2m} + \frac{mc^2}{2} \geqslant 0\,.$$

As result, condition for wave numbers of light quasi-particles $k \leqslant k_0$ is appeared.

On other hand, due to changing energetic level into Hydrogen atom, the appearance of photon with energy hkc is determined by a distance between energetic states for electron going from high level to low one. The ionization energy of the Hydrogen atom $E_I = \frac{m_e e^4}{2\hbar^2}$ is the maximal one for destruction atom. Therefore, one coincides with energy of free light quasi-particle $\frac{\hbar^2k_0^2}{2m}$ which is maximal too because $k \leqslant k_0$. The later represents as radiated photon with energy $\hbar k_0 c$ in vacuum. This reasoning claims the important condition as $\frac{m_e e^4}{2\hbar^2} = \hbar k_0 c$ which in turn determines a effective mass of the light quasi-particles $m = \frac{m_e e^4}{2\hbar^2c^2} = 2.4{\times}10^{-35}$ kg in vacuum.

In analogy manner, we may find the boundary wave number $k_\varepsilon = \frac{mc}{\hbar\varepsilon}$ for light quasi-particles of electromagnetic field

in isotropic homogenous medium by suggestion that light quasi-particles in medium interact with each other by repulsive potentials $U_{E,\vec{k}}$ in (21) and $U_{H,\vec{k}}$ in (22) which correspond, respectively, to electric and magnetic fields in momentum space

$$U_{E,\vec{k}} = -\frac{\hbar^2 k^2 \varepsilon^2}{2m} + \frac{mc^2\varepsilon}{2} \geqslant 0$$

and

$$U_{H,\vec{k}} = -\frac{\hbar^2 k^2 \varepsilon}{2m} + \frac{mc^2}{2} \geqslant 0\,.$$

Obviously, the both expressions in above determine wave numbers of light quasi-particles k satisfying to condition $k \leqslant k_\varepsilon$.

We now apply a new linear transformation of the vector Bose-operators which is a similar to the Bogoliubov transformation [10] for scalar Bose operator, so as to evaluate the energy levels of the operator $\hat{H}_R$ within diagonal form

$$\vec{E}_{\vec{k}} = \frac{\vec{e}_{\vec{k}} + M_{\vec{k}}\,\vec{e}^{+}_{-\vec{k}}}{\sqrt{1 - M^2_{\vec{k}}}} \tag{23}$$

and

$$\vec{H}_{\vec{k}} = \frac{\vec{h}_{\vec{k}} + L_{\vec{k}}\,\vec{h}^{+}_{-\vec{k}}}{\sqrt{1 - L^2_{\vec{k}}}}\,, \tag{24}$$

where $M_{\vec{k}}$ and $L_{\vec{k}}$ are the real symmetrical functions of a wave vector $\vec{k}$.

The operator Hamiltonian $\hat{H}_R$ within using of a canonical transformation takes a following form

$$\hat{H}_R = \sum_{k \leqslant k_\varepsilon} \chi_{\vec{k}}\,\vec{e}^{+}_{\vec{k}}\,\vec{e}_{\vec{k}} + \sum_{k \leqslant k_\varepsilon} \eta_{\vec{k}}\,\vec{h}^{+}_{\vec{k}}\,\vec{h}_{\vec{k}} \tag{25}$$

Hence, we infer that the Bose-operators $\vec{e}^{+}_{\vec{k}}$, $\vec{e}_{\vec{k}}$ and $\vec{h}^{+}_{\vec{k}}$, $\vec{h}_{\vec{k}}$ are, respectively, the vector creation and annihilation operators of two types of free photons with energies

$$\chi_{\vec{k}} = \sqrt{\left(\frac{\hbar^2 k^2 \varepsilon^2}{2m} + \frac{mc^2\varepsilon}{2}\right)^2 - \left(\frac{\hbar^2 k^2 \varepsilon^2}{2m} - \frac{mc^2\varepsilon}{2}\right)^2} = \tag{26}$$
$$= \hbar k v_e$$

and

$$\eta_{\vec{k}} = \sqrt{\left(\frac{\hbar^2 k^2 \varepsilon}{2m} + \frac{mc^2\varepsilon}{2}\right)^2 - \left(\frac{\hbar^2 k^2 \varepsilon}{2m} - \frac{mc^2\varepsilon}{2}\right)^2} = \tag{27}$$
$$= \hbar k v_h\,.$$

where $v_e = c\varepsilon^{\frac{3}{2}}$ and $v_h = c\varepsilon^{\frac{1}{2}}$ are, respectively, velocities of photons excited by the electric and the magnetic field. Thus, we predict the existence of two types photons excited in dielectric medium, with energies $\chi_{\vec{k}} = \hbar k c \varepsilon^{\frac{3}{2}}$ and $\eta_{\vec{k}} = \hbar k c \varepsilon^{\frac{1}{2}}$ that depend on the dielectric response of the homogeneous medium ε. The velocities of the two new type photon modes $v_e = c\varepsilon^{\frac{3}{2}}$ and $v_h = c\varepsilon^{\frac{1}{2}}$ are more than velocity c of photon in vacuum because $\varepsilon > 1$. Obviously, the phase velocity of light is given by $v_p = \frac{c}{\sqrt{\varepsilon}}$, contradicting the results obtained for $v_e = c\varepsilon^{\frac{3}{2}}$ and $v_h = c\varepsilon^{\frac{1}{2}}$. This is the source of the absorption anomalies in isotropic homogeneous media.

3 Skin of metal on the boundary metal-air

A standard model of metal regards it as a gas of free electrons with negative charge $-e$ in a box of volume V , together with a background of lattice ions of opposite charge e to preserve charge neutrality. For the boundary of this metal with the vacuum, we introduce the concept of a metal skin comprising free neutral molecules at the metal surface. The skin then has a thickness similar to the size of the molecule, a small number of Bohr diameter $a = \frac{2\hbar^2}{me^2} = 1$ Å. We assume N_0 molecules per unit area is $N_0 = \frac{3}{4\pi r^3}$ (where $r = \frac{a}{2}$ is the Bohr radius) which in turn determines the dielectric constant of metal's skin ε under an electromagnetic field in the visible to near-infrared range with frequency $\omega \leqslant \omega_0$, by the well known formulae

$$\varepsilon = 1 + \frac{4\pi N_0 e^2}{m_e\,(\omega_0^2 - \omega^2)}\,. \tag{28}$$

As we show in below, namely, the anomalies property of light is observed near resonance frequency ω_0.

4 Two new type surface polaritons excited in metal films

We now show that presented theory explains the absorption anomalies such as enhanced transmission of optical light in metal films. We consider the subwavelength sized holes into metal films as cylindrical resonator with partly filled homogeneous medium [11]. The hole contains vacuum which has boundary with metals skin with width $a = 10^{-4}$ μm but the grooves radius is $d = 0.75$ μm as experimental data [2]. The standing electromagnetic wave is excited by incoming light with frequency ω related to the frequency of cylindrical resonator ω by following system of dispersion equations

$$\left.\begin{array}{c} \dfrac{J_1\left(\frac{\omega d}{c}\right)}{J_0\left(\frac{\omega d}{c}\right)} = \dfrac{J_1\left(\frac{\omega\sqrt{\varepsilon} d}{c}\right)}{J_0\left(\frac{\omega\sqrt{\varepsilon} d}{c}\right)} \\ J_0\left(\dfrac{\omega\sqrt{\varepsilon}\,(d+a)}{c}\right) = 0 \end{array}\right\}, \tag{29}$$

where $J_0(z)$ and $J_1(z)$, are, respectively, the Bessel functions of zero and one orders.

There is observed a shape resonance in lamellar metallic gratings when frequency ω of optical light in the visible to near-infrared range coincides with resonance frequency of dipole ω_0 in metal's skin because the dielectric response is given by

$$\lim_{\omega \to \omega_0} \varepsilon \to \infty\,.$$

Therefore, the energies of two types of surface polaritons tend to infinity. This result confirms that the electric

field is highly localized inside the grooves because the energy of electric field inside the grooves is 300–1000 times higher than energy incoming optical light in air $\chi_{\vec{k}} = \eta_{\vec{k}} = \hbar kc$ as $\varepsilon = 1$ in air. Thus, we have shown the existence of two new type surface polaritons with energies $\chi_{\vec{k}}$ and $\eta_{\vec{k}}$ which are excited into nanoholes.

The resonance frequency of dipole ω_0 in metal's skin is defined from (29), at condition $\varepsilon \to \infty$ in the metal skin, which is fulfilled at $\omega = \omega_0$. In turn, this leads to following equation:

$$J_1\left(\frac{\omega_0 d}{c}\right) = 0\,, \tag{30}$$

because second equation in (29) is fulfilled automatically at condition $\varepsilon \to \infty$.

The equation (30) has a root $\omega_0 = \frac{3.8c}{d}$ which in turn determines the resonance wavelength $\lambda_0 = \frac{2\pi c}{\omega_0} = 1.24\,\mu$m. This theoretical result is confirmed by experiment [2], where the zero-order transmission spectra were obtained with a Cary-5 spectrophotometer using of incoherent light sources with a wavelength range $0.2 \leqslant \lambda \leqslant 3.3\ \mu$m. Thus, the geometry of hole determines the transmission property of light into nanoholes.

In conclusion, we may say that the theory presented above confirms experimental results on metal films, and in turn solves the problem connected with the absorption anomalies in isotropic homogeneous media.

Acknowledgements

We are particularly grateful to Professor Marshall Stoneham F.R.S. (London Centre for Nanotechnology, and Department of Physics and Astronomy, University College of London, Gower Street, London WC1E 6BT, UK) for valuable scientific support and corrected English.

Submitted on November 11, 2009 / Accepted on November 30, 2009

References

1. Lopez-Rios T., Mendoza D., Garcia-Vidal F.J., Sanchez-Dehesa J., Panneter B. Surface shape resonances in lamellar metallic gratings. *Physical Review Letters*, 1998, v. 81 (3), 665–668.
2. Ghaemi H.F.,Grupp D. E., Ebbesen T.W., Lezes H.J. Surface plasmons enhance optical transmission through suwaveleght holes. *Physical Review B*, 1998, v. 58 (11), 6779–6782.
3. Sonnichen C., Duch A.C., Steininger G., Koch M., Feldman J. Launching surface plasmons into nanoholes in metal films. *Applied Physics Letters*, 2000, v. 76 (2), 140–142.
4. Raether H. Surface plasmons. Springer-Verlag, Berlin, 1988.
5. Minasyan V.N. et al. New charged spinless bosons at interface between vacuum and a gas of electrons with low density, Preprint E17-2002-96 of JINR, Dubna, Russia, 2002.
6. Modinos A. Field, thermionic and secondary electron emission spectroscopy. Plenum Press, New York and London 1984.
7. Born M. and Wolf E. Principles of optics. Pergamon press, Oxford, 1980.
8. Dirac P.A.M. The principles of Quantum Mechanics. Clarendon press, Oxford, 1958.
9. Minasyan V.N. Light bosons of electromagnetic field and breakdown of relativistic theory. arXiv: 0808.0567.
10. Bogoliubov N.N. On the theory of superfludity. *Journal of Physics (USSR)*, 1947, v. 11, 23.
11. Minasyan V.N. et al. Calculation of modulator with partly filled by electro-optic crystal. *Journal of Opto-Mechanics Industry (USSR)*, 1988, v. 1, 6.

Physics of Rotating and Expanding Black Hole Universe

U. V. S. Seshavatharam
Honorary Faculty, Institute of Scientific Research on Vedas (I-SERVE), Hyderabad-35, India
Email: seshavatharam.uvs@gmail.com

Throughout its journey universe follows strong gravity. By unifying general theory of relativity and quantum mechanics a simple derivation is given for rotating black hole's temperature. It is shown that when the rotation speed approaches light speed temperature approaches Hawking's black hole temperature. Applying this idea to the cosmic black hole it is noticed that there is "no cosmic temperature" if there is "no cosmic rotation". Starting from the Planck scale it is assumed that- universe is a rotating and expanding black hole. Another key assumption is that at any time cosmic black hole rotates with light speed. For this cosmic sphere as a whole while in light speed rotation "rate of decrease" in temperature or "rate of increase" in cosmic red shift is a measure of "rate of cosmic expansion". Since 1992, measured CMBR data indicates that, present CMB is same in all directions equal to 2.726 °K, smooth to 1 part in 100,000 and there is no continuous decrease! This directly indicates that, at present rate of decrease in temperature is practically zero and rate of expansion is practically zero. Universe is isotropic and hence static and is rotating as a rigid sphere with light speed. At present galaxies are revolving with speeds proportional to their distances from the cosmic axis of rotation. If present CMBR temperature is 2.726 °K, present value of obtained angular velocity is $2.17 \times 10^{-18} \frac{\text{rad}}{\text{sec}} \cong 67 \frac{\text{Km}}{\text{sec} \times \text{Mpc}}$. Present cosmic mass density and cosmic time are fitted with a ln (volume ratio) parameter. Finally it can be suggested that dark matter and dark energy are ad-hoc and misleading concepts.

1 Introduction

Now as recently reported at the American Astronomical Society a study using the Very Large Array radio telescope in New Mexico and the French Plateau de Bure Interferometer has enabled astronomers to peer within a billion years of the Big Bang and found evidence that black holes were the first that leads galaxy growth [1]. The implication is that the black holes started growing first. Initially astrophysicists attempted to explain the presence of these black holes by describing the evolution of galaxies as gathering mass until black holes form at their center but further observation demanded that the galactic central black hole co-evolved with the galactic bulge plasma dynamics and the galactic arms. This is a fundamental confirmation of N. Haramein's theory [2] described in his papers as a universe composed of "different scale black holes from universal size to atomic size".

This clearly suggests that: (1) Galaxy constitutes a central black hole; (2) The central black hole grows first; (3) Star and galaxy growth goes parallel or later to the central black holes growth. The fundamental questions are: (1) If "black hole" is the result of a collapsing star, how and why a stable galaxy contains a black hole at its center? (2) Where does the central black hole comes from? (3) How the galaxy center will grow like a black hole? (4) How its event horizon exists with growing? If these are the observed and believed facts — not only for the author — this is a big problem for the whole science community to be understood. Any how, the important point to be noted here is that "due to some unknown reasons galactic central black holes are growing"! This is the key point for the beginning of the proposed expanding or growing cosmic black hole! See this latest published reference [3] for the "black hole universe".

In our daily life generally it is observed that any animal or fruit or human beings (from birth to death) grows with closed boundaries (irregular shapes also can have a closed boundary). An apple grows like an apple. An elephant grows like an elephant. A plant grows like a plant. A human grows like a human. Through out their life time they won't change their respective identities. These are observed facts. From these observed facts it can be suggested that "growth" or "expansion" can be possible with a closed boundary. By any reason if the closed boundary is opened it leads to "destruction" rather than "growth or expansion". Thinking that nature loves symmetry, in a heuristic approach in this paper author assumes that "through out its life time universe is a black hole". Even though it is growing, at any time it is having an event horizon with a closed boundary and thus it retains her identity as a black hole for ever. Note that universe is an independent body. It may have its own set of laws. At any time if universe maintains a closed boundary to have its size minimum at that time it must follow "strong gravity" at that time. If universe is having no black hole structure any massive body (which is bound to the universe) may not show a black hole structure. That is black hole structure may be a subset of cosmic structure. This idea may be given a chance.

Rotation is a universal phenomenon [4, 5, 6]. We know that black holes are having rotation and are not stationary. Re-

cent observations indicates that black holes are spinning close to speed of light [7]. In this paper author made an attempt to give an outline of "expanding and light speed rotating black hole universe" that follows strong gravity from its birth to end of expansion.

Stephen Hawking in his famous book *A Brief History of Time* [8], in Chapter 3 which is entitled *The Expanding Universe*, says: "*Friedmann made two very simple assumptions about the universe: that the universe looks identical in which ever direction we look, and that this would also be true if we were observing the universe from anywhere else. From these two ideas alone, Friedmann showed that we should not expect the universe to be static. In fact, in 1922, several years before Edwin Hubble's discovery, Friedmann predicted exactly what Hubble found... We have no scientific evidence for, or against, the Friedmann's second assumption. We believe it only on grounds of modesty: it would be most remarkable if the universe looked the same in every direction around us, but not around other points in the universe*". From this statement it is very clear and can be suggested that, the possibility for a "closed universe" and a "flat universe" is 50–50 per cent and one can not completely avoid the concept of a "closed universe". Clearly speaking, from Hubble's observations and interpretations in 1929, the possibility of "galaxy receding" and "galaxy revolution" is 50–50 per cent and one can not completely avoid the concept of "rotating universe".

1.1 Need for cosmic constant speed rotation

1. Assume that a planet of mass M and size R rotates with angular velocity ω_e and linear velocity v_e in such a way that free or loosely bound particle of mass m "lying on its equator" gains a kinetic energy equal to its potential energy and linear velocity of planet's rotation is equal to free particle's escape velocity. That is without any external power or energy, test particle gains escape velocity by virtue of planet's rotation

$$\frac{mv_e^2}{2} = \frac{GMm}{R}\,, \tag{1}$$

$$\omega_e = \frac{v_e}{R} = \sqrt{\frac{2GM}{R^3}}\,. \tag{2}$$

Using this idea, "black hole radiation" and "origin of cosmic rays" can be understood. Now writing $M = \frac{4\pi}{3}R^3\rho_e$ and $\omega_e = \frac{v_e}{R} = \sqrt{\frac{8\pi G\rho_e}{3}}$ it can be written as

$$\omega_e^2 = \frac{8\pi G\rho_e}{3}\,, \tag{3}$$

where density ρ_e is

$$\text{density} = \rho_e = \frac{3\omega_e^2}{8\pi G}\,. \tag{4}$$

In real time this obtained density may or may not be equal to the actual density. But the ratio $\frac{8\pi G\rho_{real}}{3\omega_{real}^2}$ may have some physical meaning. From equation (4) it is clear that proportionality constant being $\frac{3}{8\pi G}$

$$\text{density} \propto \text{angular velocity}^2. \tag{5}$$

Equation (4) is similar to the "flat model concept"of cosmic "critical density"

$$\rho_0 = \frac{3H_0^2}{8\pi G}\,. \tag{6}$$

Comparing equations (4) and (6) dimensionally and conceptually $\rho_e = \frac{3\omega_e^2}{8\pi G}$ and $\rho_0 = \frac{3H_0^2}{8\pi G}$ one can say that

$$H_0^2 \to \omega_e^2 \Rightarrow H_0 \to \omega_e\,. \tag{7}$$

In any physical system under study, for any one "simple physical parameter" there will not be two different units and there will not be two different physical meanings. This is a simple clue and brings "cosmic rotation" into picture. This is possible in a closed universe only. It is very clear that dimensions of Hubble's constant must be "radian per second". Cosmic models that depends on this "critical density" must accept "angular velocity of the universe" in the place of Hubble's constant. In the sense "cosmic rotation" must be included in the existing models of cosmology. If this idea is rejected without any proper reason, alternatively the subject of cosmology can be studied in a rotating picture where the ratio of existing Hubble's constant and estimated present cosmic angular velocity will give some valuable information.

2. After the Big Bang, since 5 billion years if universe is "accelerating" and at present dark energy is driving it- right from the point of Big Bang to the visible cosmic boundary in all directions, thermal photon wavelength must be stretched instantaneously and continuously from time to time and cosmic temperature must decrease instantaneously and continuously for every second. This is just like "rate of stretching of a rubber band of infinite length". Note that photon light speed concept is not involved here. Against to this idea since 1992 from COBE satellite's CMBR data reveals that cosmic temperature is practically constant at 2.726 °K. This observational clash clearly indicates that something is going wrong with accelerating model. Moreover the standard model predicts that the cosmic background radiation should be cooling by something like one part in 10^{10} per year. This is at least 6 orders of magnitude below observable limits. Such a small decrease in cosmic temperature might be the result of cosmic "slowing down" rather than cosmic acceleration. See this latest published reference for cosmic slowing down [9].

3. If universe is accelerating, just like "rate of stretching of a rubber band of infinite length" CMBR photon wavelength stretches and CMBR temperature decreases. Technically from time to time if we are able to measure the changes in cosmic temperature then rate of decrease in cosmic temperature will give the rate of increase in cosmic expansion

accurately. Even though acceleration began 5 billion years before since all galaxies will move simultaneously from our galaxy "rate of increase" in super novae red shift can not be measured absolutely and accurately. Hence it is reasonable to rely upon "rate of decrease" in cosmic temperature rather than "rate of increase" in galaxy red shift.

4. Based on this analysis if "cosmic constant temperature" is a representation of "isotropy" it can be suggested that at present there is no acceleration and there is no space expansion and thus universe is static. From observations it is also clear that universe is homogeneous in which galaxies are arranged in a regular order and there is no mutual attraction in between any two galaxies. Not only that Hubble's observations clearly indicates that there exists a linear relation in between galaxy distance and galaxy speed which might be a direct consequence of "cosmic rotation" with "constant speed". This will be true if it is assumed that "rate of increase in red shift" is a measure of cosmic "rate of expansion". Instead of this in 1929 Hubble interpreted that "red shift" is a measure of cosmic "expansion". This is the key point where Einstein's static universe was discarded with a simple 50–50 percent misinterpretation [10].

5. At present if universe is isotropic and static how can it be stable? The only one solution to this problem is "rotation with constant speed". If this idea is correct universe seems to follow a closed model. If it is true that universe is started with a big bang, the "Big Bang" is possible only with "big crunch" which is possible only with a closed model.

6. At present if universe rotates as a rigid sphere with constant speed then galaxies will revolve with speeds proportional to their distances from the cosmic axis of rotation. This idea matches with the Hubble's observations but not matches with the Hubble's interpretation as "galaxy receding" . From points 2, 3 and 4 it is very clear that at present universe is isotropic and static. Hence the Hubble's law must be re-interpreted as "at present as galaxy distance increases its revolving speed increases". If so H_0 will turn out to be the present angular velocity. In this way cosmic stability and homogeneity can be understood.

7. This "constant speed cosmic rotation" can be extended to the Big Bang also. As time passes while in constant speed of rotation some how if the cosmic sphere expands then "galaxy receding" as well as "galaxy revolution" both will come into picture. In the past while in constant speed of rotation at high temperatures if expansion is rapid for any galaxy (if born) receding is rapid and photon from the galaxy travels towards the cosmic center in the opposite direction of space expansion and suffers a continuous fast rate of stretching and there will be a continuous fast rate of increase in red shift. At present at small temperatures if expansion is slow galaxy receding is small and photon suffers continuous but very slow rate of stretching and there will be a continuous but very slow rate of increase in red shift i.e. red shift practically remains constant. From this analysis it can be suggested that rate of decrease in cosmic temperature or rate of increase in red shift will give the rate of cosmic expansion.

8. In the past we have galaxy receding and at present we can have galaxy revolution. By this time at low temperature and low angular velocity, galaxies are put into stable orbits.

1.2 Need for cosmic strong gravity

1. After Big Bang if universe follows "least path of expansion" then at any time "time of action" will be minimum and "size of expansion" will be minimum and its effects are stable and observable.

2. For any astrophysical body its size is minimum if it follows strong gravity. Being an astrophysical body at any time to have a minimum size of expansion universe will follow strong gravity. No other alternative is available.

3. Following a closed model and similar to the growth of an "apple shaped apple" if universe grows in mass and size it is natural to say that as time is passing cosmic black hole is "growing or expanding".

1.3 Need for light speed cosmic rotation and red shift boundary from 0 to 1

1. From Hubble's observations when the red shift $z \leqslant 0.003$, velocity-distance relation is given by $v = zc$ and ratio of galaxy distance and red shift is equal to $\frac{c}{H_0}$. If H_0 represents the present cosmic angular velocity $\frac{c}{H_0}$ must be the present size of the universe. Hence it can be guessed that cosmic speed of rotation is c. Since from Big Bang after a long time, i.e. at present if rotation speed is c, it means at the time of Big Bang also cosmic rotation speed might be c. Throughout the cosmic journey cosmic rotation speed [7] is constant at c. This is a heuristic idea. One who objects this idea must explain — being bound to the cosmic space, why photon travels at only that much of speed. This idea supports the recent observations of light speed rotation of black holes. Universe is an independent body. It is having its own mechanism for this to happen.

2. Galaxies lying on the equator will revolve with light speed and galaxies lying on the cosmic axis will have zero speed. Hence it is reasonable to put the red shift boundary as 0 to 1. Then their distances will be proportional to their red shifts from the cosmic axis of rotation.

1.4 Origin of cosmic black hole temperature

1. Following the Hawking's black hole temperature formula (see subsection 2.1) it is noticed that black hole temperature is directly proportional to its rotational speed. For a stationary or non-rotating black hole its temperature is zero. As the rotational speed increases black hole's temperature increases and reaches to maximum if its rotational speed approaches to light speed. At any time if we treat universe as black hole when it is stationary its temperature will be zero. Without cosmic black hole rotation there is no cosmic temperature.

2. When the growing cosmic black hole rotates at light speed it attains a maximum temperature corresponding to its mass or angular velocity at that time. As time passes if the cosmic black hole continues to rotate at light speed and expands then rate of decrease in temperature seems to be minimum if rate of increase in size is minimum and thus it always maintains least size of expansion to have minimum drop in temperature.

2 The four assumptions

To implement the Planck scale successfully in cosmology, to develop a unified model of cosmology and to obtain the value of present Hubble's constant (without considering the cosmic red shifts), starting from the Planck scale it is assumed that at any time t: (1) *The universe can be treated as a rotating and growing black hole*; (2) *With increasing mass and decreasing angular velocity universe always rotates with speed of light*; (3A) *Without cosmic rotation there is no "cosmic temperature*"; (3B) *Cosmic temperature follows Hawking black hole temperature formula where mass is equal to the geometric mean of Planck mass M_P and cosmic mass M_t*; (4) *Rate of decrease in CMBR temperature is a measure of cosmic rate of expansion*.

2.1 Derivation for black hole temperature and base for assumptions 1, 2 and 3

A black hole of mass M having size R rotates with an angular velocity ω and rotational speed $v = R\omega$. Assume that its temperature T is inversely proportional to its rotational time period t. Keeping "Law of uncertainty" in view assume that

$$(k_B T) \times t = \frac{\hbar}{2} = \frac{h}{4\pi} . \tag{8}$$

$$T \times t = \frac{\hbar}{2k_B} . \tag{9}$$

where, t = rotational time period, T = temperature, k_B = Boltzmann's radiation constant, h = Planck's constant and $\frac{k_B T}{2} + \frac{k_B T}{2} = k_B T$ is the sum of kinetic and potential energies of a particle in any one direction.

Stephen Hawking in Chapter 11 *The Unification of Physics* of his book [8], says: "*The main difficulty in finding a theory that unifies gravity with the other forces is that general relativity is a "classical" theory; that is, it does not incorporate the uncertainty principle of quantum mechanics. On the other hand, the other partial theories depend on quantum mechanics in an essential way. A necessary first step, therefore, is to combine general relativity with the uncertainty principle. As we have seen, this can produce some remarkable consequences, such as black holes not being black, and the universe not having any singularities but being completely self-contained and without a boundary*". We know that

$$t = \frac{2\pi}{\omega} = \frac{2\pi R}{v} = \frac{4\pi GM}{c^2 v} , \tag{10}$$

$$T = \frac{\hbar c^2 v}{8\pi k_B GM} = \frac{\hbar\omega}{4\pi k_B} , \tag{11}$$

thus if black hole rotational speed v reaches light speed then its temperature reaches to maximum

$$v \to v_{max} = c \Rightarrow T \to T_{max} = \frac{\hbar c^3}{8\pi k_B GM} = \frac{\hbar\omega_{max}}{4\pi k_B} . \tag{12}$$

Note that this idea couples GTR and quantum mechanics successfully. Hawking's black hole temperature formula can be obtained easily. And its meaning is simple and there is no need to consider the pair particle creation for understanding "Hawking radiation". This is the main advantage of this simple derivation. From this idea it is very clear that origin of Hawking radiation is possible in another way also. But it has to be understood more clearly. Information can be extracted from a black hole, if it rotates with light speed. *If a black hole rotates at light speed photons or elementary particles can escape from its "equator only" with light speed and in the direction of black hole rotation and this seems to be a signal of black hole radiation around the black hole equator. With this idea origin of cosmic rays can also be understood*. Note that not only at the black hole equator Hawking radiation can take place at the event horizon of the black hole having a surface area.

This equation (12) is identical to the expression derived by Hawking [11]. From the assumptions and from the obtained expressions it is clear that black hole temperature is directly proportional to the rotational speed of the black hole. Temperature of a stationary black hole is always zero and increases with increasing rotational speed and reaches to maximum at light speed rotation. In this way also GTR and quantum mechanics can be coupled. *But this concept is not the output from Hawking's black hole temperature formula. In any physical system for any physical expression there exists only one true physical meaning. Either Hawking's concept is true or the proposed concept is true. Since the black hole temperature formula is accepted by the whole science community author humbly request the science community to kindly look into this major conceptual clash at utmost fundamental level. Recent observations shows that black holes are spinning close to light speed*. Temperature of any black hole is very small and may not be found experimentally. But this idea can successfully be applied to the universe! By any reason if it is assumed that universe is a black hole then it seems to be surprising that temperature of a stationary cosmic black hole is zero. Its temperature increases with increase in its rotational speed and reaches to maximum if the rotational speed approaches light speed. This is the essence of cosmic black hole rotation. CMBR temperature demands the existence of "cosmic rotation". This is the most important point to be noted here.

Hawking radiation is maintained at event horizon as a (particle and anti particle) pair particle creation. One particle falls into the black hole and the other leaves the black

hole. Since the black hole is situated in a free space and lot of free space is available around the black hole's event horizon this might be possible. But applying this idea to the universe this type of thinking may not be possible. There will be no space for the particle to go out side the cosmic boundary or the cosmic event horizon and there is no scope for the creation of antiparticle also. If so the concept of cosmic black hole radiation and normally believed black hole radiation has to be studied in a different point of view. If there is no particle creation at the cosmic event horizon then there will be no evaporation of the cosmic black hole and hence there is no chance for decay of the cosmic black hole. Due to its internal mechanism it will grow like a black hole.

2.2 Black hole minimum size, maximum rotation speed and stability

Here, the fundamental question to be answered is — by birth, is black hole a rigid stationary sphere or a rigid light speed rotating sphere? See the web reference [7]. *Super massive black holes, according to new research, are approaching the speed of light. Nine galaxies were examined by NASA using the Chandra X-ray Observatory, and found each to contain black holes pumping out jets of gas in to the surrounding space. "Extremely fast spin might be very common for large black holes", said co-investigator Richard Bower of Durham University. This might help us explain the source of these incredible jets that we see stretching for enormous distances across space*. This reference indicates that author's idea is correct. Not only that it suggests that there is something new in black hole's spin concepts. Author suggests that [12, 13, 14] force limit $\frac{c^4}{G}$ keeps the black hole stable or rigid even at light speed rotation. This force can be considered as the "classical limit" of force. It represents the "maximum gravitational force of attraction" and "maximum electromagnetic force". It plays an important role in unification scheme. It is the origin of Planck scale. It is the origin of quantum gravity. Similar to this classical force, classical limit of power can be given by $\frac{c^5}{G}$. It plays a crucial role in gravitational radiation. It represents the "maximum limit" of mechanical or electromagnetic or radiation power. The quantity $\frac{c^4}{G}$ can be derived based on "Newton's law of gravitation and "constancy of speed of light". In solar system force of attraction between sun and planet can be given as

$$F = \left(\frac{m}{M}\right)\left(\frac{v^4}{G}\right), \tag{13}$$

where M = mass of sun, m = mass of planet and v = planet orbital velocity. Since $\frac{m}{M}$ is a ratio $\frac{v^4}{G}$ must have the dimensions of force. Following the constancy of speed of light, a force of the form $\frac{c^4}{G}$ can be constructed. With 3 steps origin of rotating black hole formation can be understood with $\frac{c^5}{G}$ and Mc^2, i.e.

$$\text{torque} = \tau \leqslant Mc^2, \tag{14}$$

$$\text{power} = \tau\omega \leqslant \left(\frac{c^5}{G}\right), \tag{15}$$

$$\omega \leqslant \frac{\mathrm{c}^3}{GM} \Rightarrow \omega_{max} = \frac{\mathrm{c}^3}{GM}. \tag{16}$$

To have maximum angular velocity size should be minimum

$$R_{min} = \frac{c}{\omega_{max}} = \frac{GM}{c^2}. \tag{17}$$

That is, if size is minimum, the black hole can rotate with light speed! Hence the space and matter surrounding its equator can turn at light speed! This is found to be true for many galaxy centers. Acceleration due to gravity at its surface can be given as $\frac{c^4}{GM}$. Rotational force can be given as $MR_{min}\omega_{max}^2 = \frac{c^4}{G}$. This is the ultimate magnitude of force that keeps the black hole stable even at light speed! This is a natural manifestation of space-time geometry.

Note that here in equation (17) only the coefficient 2 is missing compared with Schwarzschild radius. If the concept of "Schwarzschild radius" is believed [15] to be true, for any rotating black hole of rest mass (M) the critical conditions are: (1) *Magnitude of kinetic energy never crosses rest energy*; (2) *Magnitude of torque never crosses potential energy*; (3) *Magnitude of mechanical power never crosses* $\left(\frac{c^5}{G}\right)$.

Based on virial theorem, potential energy is twice of kinetic energy and hence, $\tau \leqslant 2Mc^2$. In this way factor 2 can be obtained easily from equations (14), (15) and (16). Not only that special theory of relativity, classical mechanics and general theory of relativity can be studied in a unified way.

2.3 Planck scale and cosmic black hole temperature

At any time (t) from assumption (1) based on black hole concepts, if mass of the universe is M_t size of the cosmic event horizon can be given by

$$R_t = \frac{2GM_t}{c^2}. \tag{18}$$

From assumption (2) if cosmic event horizon rotates with light speed then cosmic angular velocity can be given by

$$\omega_t = \frac{c}{R_t} = \frac{c^3}{2GM_t}. \tag{19}$$

From assumptions (3A) and (3B),

$$T_t = \frac{\hbar c^3}{8\pi k_B G\sqrt{M_t M_P}}, \tag{20}$$

where $M_t \geqslant M_P$. From equations (19) and (20)

$$4\pi k_B T_t = \hbar\sqrt{\omega_t \omega_P}. \tag{21}$$

This is a very simple expression for the long lived large scale universe! At any time if temperature T_t is known

$$\omega_t = \left(\frac{4\pi k_B T_t}{\hbar}\right)^2\left(\frac{1}{\omega_p}\right). \tag{22}$$

Ultimate gravitational force of attraction between any two Planck particles of mass M_P separated by a minimum distance r_{min} can be given as

$$\frac{GM_PM_P}{r_{min}^2} = \frac{c^4}{G}\,, \tag{23}$$

where $2\pi r_{min} = \lambda_P = \frac{h}{cM_P}$ = Planck wave length. In this way Planck scale mass and energy can be estimated

$$\text{Pl. mass} = M_P = 2.176{\times}10^{-8}\ \text{Kg} = \sqrt{\frac{\hbar c}{G}}\,, \tag{24}$$

$$\text{Pl. size} = R_P = 3.2325{\times}10^{-35}\ \text{meter} = \frac{2GM_P}{c^2}\,, \tag{25}$$

$$\text{Pl. angl. velocity} = \omega_P = 9.274{\times}10^{42}\,\frac{\text{rad}}{\text{sec}} = \frac{c^3}{2GM_P}\,, \tag{26}$$

$$\text{Pl. temperature} = T_P = 5.637{\times}10^{30}\,^\circ\text{K} = \frac{\hbar\omega_P}{4\pi k_B}\,. \tag{27}$$

Substituting the present cosmic CMBR temperature [16] 2.726 °K in equation (22) we get present cosmic angular velocity as $\omega_t = 2.169{\times}10^{-18}\ \frac{\text{rad}}{\text{sec}} \cong 66.93\ \frac{\text{Km}}{\text{sec}\times\text{Mpc}}$. Numerically this obtained value is very close to the measured value of Hubble's constant H_0 [17, 18]. Not only that this proposed unified method is qualitatively and quantitatively simple compared with the "cosmic red shift" and "galactic distance" observations. This procedure is error free and is reliable. *Author requests the science community to kindly look into this kind of rotating and growing universe models. If this procedure is really true and applicable to the expanding universe then accelerating model, dark matter and dark energy are becomes ad-hoc concepts*. At any time it can be shown that

$$M_tR_t\omega_t^2 = M_tc\omega_t = \frac{c^4}{2G}\,. \tag{28}$$

2.4 Cosmic mass density and baryon-photon number density ratio

With this model empirically it is noticed that, mass density

$$\rho_{mass} \cong 3\ln\left(\frac{R_t}{R_P}\right)\left[\frac{aT_t^4}{c^2}\right] \cong 6\ln\left(\frac{T_P}{T_t}\right)\left[\frac{aT_t^4}{c^2}\right]. \tag{29}$$

If $T_t = 2.726\,^\circ\text{K}$, $\omega_t = 2.169{\times}10^{-18}\ \frac{\text{rad}}{\text{sec}}$, $R_t = \frac{c}{\omega_t} = 1.383{\times}10^{26}$ meter and $R_P = 3.232{\times}10^{-35}$ meter, present mass density can be obtained as

$$\rho_{mass} \cong 418.82\times 4.648{\times}10^{-34} = 1.95{\times}10^{-31}\ \frac{\text{gram}}{\text{cm}^3}\,.$$

This is very close to the observed mater density [19] of the universe $(1.75\text{ to }4.1){\times}10^{-31}\ \frac{\text{gram}}{\text{cm}^3}$. If this idea is true the proposed term

$$3\ln\left(\frac{R_t}{R_P}\right) \cong 6\ln\left(\frac{T_P}{T_t}\right), \tag{30}$$

can be given a chance in modern cosmology. Actually this is the term given as

$$\ln\left(\frac{\text{cosmic volume at time, } t}{\text{Planck volume}}\right) \cong 3\ln\left(\frac{R_t}{R_P}\right). \tag{31}$$

The interesting idea is that, if $R_t \to R_P$, and $T_t \to T_P$, the term $3\ln\left(\frac{R_t}{R_P}\right) \to 0$ and mass density at Planck time approaches zero. Conceptually this supports the Big Bang assumption that "at the time of Big Bang matter was in the form of radiation". Not only that as cosmic time increases mass density gradually increases and thermal density gradually decreases. Using this term and considering the present CMBR temperature baryon-photon number density ratio can be fitted as follows

$$\frac{N_B}{N_\gamma} \cong 3\ln\left(\frac{R_t}{R_P}\right)\left[\frac{2.7k_BT_t}{m_nc^2}\right], \tag{32}$$

Here interesting point is that

$$\left[\frac{2.7k_BT_t}{m_nc^2}\right] \cong \frac{\text{average energy per photon}}{\text{rest energy of nucleon}}\,, \tag{33}$$

thus present value can be given as

$$\frac{N_B}{N_\gamma} \cong \frac{1}{3.535{\times}10^9}\,. \tag{34}$$

2.5 The 2 real densities

Since the cosmic black hole always follows closed model and rotates at light speed, at any time size of cosmic black hole is $\frac{c}{\omega_t}$. It's density $= \frac{\text{mass}}{\text{volume}} = \frac{3\omega_t^2}{8\pi G}$. It is no where connected with "critical density" concepts. From equations (18), (19) and (20) it is noticed that

$$\frac{3\omega_t^2}{8\pi G} = 5760\pi\left[\frac{aT_t^4}{c^2}\right]. \tag{35}$$

Finally we can have only 2 real densities, one is "thermal energy density" and the second one is "mass density".

3 Origin of the cosmic red shift, galaxy receding and galaxy revolution

As the cosmic sphere is expanding and rotating galaxies receding and revolving from and about the cosmic axis. As time passes photon from the galaxy travels opposite to the direction of expansion and reaches to the cosmic axis or center. Thus photon shows a red shift about the cosmic center. If this idea is true cosmic red shift is a measure of galactic distances from the cosmic axis of rotation or center. Galaxy receding is directly proportional to the rate of expansion of the rotating cosmic sphere as a whole. In this scenario for any galaxy continuous increase in red shift is a measure of rapid expansion and "practically constant red shift" is a measure of very

slow expansion. That is change in galaxy distance from cosmic axis is practically zero. At any time (t) it can be defined as, cosmic red shift

$$z_t = \frac{\Delta\lambda}{\lambda_{measured}} \leqslant 1. \tag{36}$$

when z_t is very small this definition is close to the existing red shift definition

$$z = \frac{\Delta\lambda}{\lambda_{emitted}}\,. \tag{37}$$

At present time relation between equations (36) and (37) can be given as

$$\frac{z}{z+1} \cong z_t\,. \tag{38}$$

Equation (38) is true only when z is very small. Note that at Hubble's time the maximum red shift observed was $z = 0.003$ which is small and value of H_0 was 530 Km/sec/Mpc. By Hubble's time equation (36) might have been defined in place of equation (37). But it not happened so! When rate of expansion is very slow, i.e. at present, based on $v = r\omega$ concepts

$$v_t \cong z_t c\,, \tag{39}$$

gives revolving galaxies tangential velocity where increase in red shift is very small and practically remains constant and galaxy's distance from cosmic axis of rotation can be given as

$$r_t \cong \frac{v_t}{\omega_t} \cong z_t\left(\frac{c}{\omega_t}\right). \tag{40}$$

Numerically this idea is similar to Hubble's law [20]. This indicates that there is something odd in Hubble's interpretation of present cosmic red shifts and galaxy moments. By this time even though red shift is high if any galaxy shows a continuous increase in red shift then it can be interpreted that the galaxy is receding fast in the sense this light speed rotating cosmic sphere is expanding at a faster rate. Measured galactic red shift data indicates that, for any galaxy at present there is no continuous increase in their red shifts and are practically constants! This is a direct evidence for the slow rate of expansion of the present light speed rotating universe. When the universe was young i.e. in the past, Hubble's law was true in the sense "red shift was a measure of galaxy receding (if born)" and now also Hubble's law is true in the sense "red shift is a measure of galaxy revolution".

As time is passing "galaxy receding" is gradually stopped and "galaxy revolution" is gradually accomplished. Galaxies lying on the equator will revolve with light speed and galaxies lying on the cosmic axis will have zero speed. Hence it is reasonable to put the red shift boundary as 0 to 1. Then their distances will be proportional to their red shifts from the cosmic axis of rotation.

4 The present cosmic time

(1) Time required to complete one radian is $\frac{1}{\omega_t}$ where ω_t is the angular velocity of the universe at time t. At any time this is not the cosmic age. If at present $\omega_t \to H_0$, it will not represent the present age of the universe. (2) Time required to complete one revolution is $\frac{2\pi}{\omega_t}$. (3) Time required to move from Planck volume to existing volume = present cosmic age.

How to estimate this time? Author suggests a heuristic procedure in the following way. With reference to Big Bang picture present cosmic time can be given as

$$t \cong \ln\left(\frac{T_P}{T_t}\right)\sqrt{\frac{3c^2}{8\pi G a T_t^4}} = 4.33{\times}10^{21}\ \text{seconds}. \tag{41}$$

Here $T_t \leqslant T_P$, and interesting idea is that if $T_t \to T_P$, the term $\ln\left(\frac{T_t}{T_P}\right) \to 0$. It indicates that, unlike the Planck time, here in this model cosmic time starts from zero seconds. This idea is very similar to the birth of a living creature. How and why, the living creature has born? This is a fundamental question to be investigated by the present and future mankind. In the similar way, how and why, the "Planck particle" born? has to be investigated by the present and future cosmologists. Proposed time is 9400 times of $\frac{1}{H_0}$. With this large time "smooth cosmic expansion" can be possible. Inflation, magnetic monopoles problem and super novae dimming can be understood by a "larger cosmic time and smooth cosmic expansion". Proportionality constant being unity with the following 3 assumptions "cosmic time" can be estimated

$$t \propto 3\ln\left(\frac{R_t}{R_P}\right), \tag{42}$$

$$t \propto \left[\frac{M_P c^2}{4\pi k_B T_t}\right], \tag{43}$$

$$t \propto \left[\frac{\hbar}{k_B T_t}\right]. \tag{44}$$

After simplification, obtained relation can be given as

$$t = \sqrt{\frac{36\pi}{90}} \times \ln\left(\frac{T_P}{T_t}\right)\sqrt{\frac{3c^2}{8\pi G a T_t^4}}\,, \tag{45}$$

$$t = 1.121{\times}\ln\left(\frac{T_P}{T_t}\right)\sqrt{\frac{3c^2}{8\pi G a T_t^4}} = 4.85{\times}10^{21}\ \text{sec}. \tag{46}$$

5 Conclusion

The force $\frac{c^4}{G}$ and power $\frac{c^5}{G}$ are really the utmost fundamental tools of black hole physics and black hole cosmology. In this paper author presented a biological model for viewing the universe in a black hole picture. In reality its validity has to be studied, understood and confirmed by the science community at utmost fundamental level. At present also regarding the cosmic acceleration some conflicts are there [9].

The concept of dark energy is still facing and raising a number of fundamental problems. If one is able to understand the need and importance of "universe being a black hole for ever", "CMBR temperature being the Hawking temperature" and "angular velocity of cosmic black hole being the present Hubble's constant", a true unified model of "black hole universe" can be developed.

The main advantage of this model is that, it mainly depends on CMBR temperature rather than the complicated red shift observations. From the beginning and up to right now if universe rotates at light speed- "Big Bang nucleosynthesis concepts" can be coupled with the proposed "cosmic black hole concepts". Clearly speaking, in the past there was no Big Bang. Rotating at light speed for ever high temperature and high RPM (revolution per minute) the "small sized Planck particle" gradually transforms into low temperature and low RPM "large sized massive universe".

Acknowledgements

Author is very much grateful to the editors of the journal, Dr. Dimtri Rabounski and Dr. Larissa Borissova, for their kind guidance, discussions, valuable suggestions and accepting this paper for publication. Author is indebted to Institute of Scientific Research on Vedas (I-SERVE, recognized by DSIR as SIRO), Hyderabad, India, for its all-round support in preparing this paper. For considering this paper as poster presentation author is very much thankful to the following organizing committees: "DAE-BRNS HEP 2008, India", "ISRAMA 2008, India", "PIRT-CMS 2008, India", "APSC 2009, India", "IICFA 2009, India" and "JGRG-19, Japan". Author is very much thankful to Prof. S. Lakshminarayana, Dept. of Nuclear Physics, Andhra University, Vizag, India, Dr. Sankar Hazra, PIRT-CMS, Kolkata, India, and Dr. José López-Bonilla, Mexico, for their special encouragement and guidance in publishing and giving a life to this paper. Finally author is very much thankful to his brothers B. Vamsi Krishna (software professional) and B. R. Srinivas (Associate Professor) for encouraging, providing technical and financial support.

Submitted on September 16, 2009 / Accepted on December 06, 2009

References

1. Carilli et al. Black holes lead Galaxy growth, new research shows. Lecture presented to the American Astronomical Society's meeting in Long Beach, California, 4–8 January 2009, National Radio Astronomy Observatory, Socorro, NM: http://www.nrao.edu/pr/2009/bhbulge
2. Haramein N. et al. Scale Unification-A Universal scaling law for organized matter. *Proceedings of the Unified Theories Conference 2008*, Budapest, 2008.
3. Tianxi Zhang. A new cosmological model: black hole Universe. *Progress in Physics*, 2009, v.3.
4. Rabounski D. On the speed of rotation of isotropic space: insight into the redshift problem. *The Abraham Zelmanov Jounal*, 2009, v.2, 208–223.
5. Gentry R.V. New cosmic center Universe model matches eight of Big Bang's major predictions without the F-L paradigm. CERN Electronic Publication EXT-2003-022.
6. Obukhov Y.N. On physical foundations and observational effects of cosmic Rotation. *Colloquium on Cosmic Rotation*, Wissenschaft und Technik Verlag, Berlin, 2000, 23–96.
7. Black holes spinning near the speed of light. http://www.space.com/scienceastronomy080115-st-massive-black-hole.html
8. Hawking S.W. A brief history of time. Bantam Dell Publishing Group, 1988.
9. Shafieloo A. et al. Is cosmic acceleration slowing down? *Phys. Rev. D*, 2009, v.80, 101301; arXiv: 0903.5141.
10. Hubble E.P. A relation between distance and radial velocity among extra-galactic nebulae. *PNAS*, 1929, v.15, 168–173.
11. Hawking S.W. Particle creation by black holes. *Commun. Math. Phys.*, 1975, v.43, 199–220.
12. Haramein N. et al. The origin of spin: a consideration of torque and coriolis forces in Einstein's field equations and Grand Unification Theory. In: *Beyond the Standard Model: Searching for Unity in Physics*, The Noetic Press, 2005, 153–168.
13. Rauscher E.A. A unifying theory of fundamental processes. Lawrence Berkeley National Laboratory Reports UCRL-20808 (June 1971), and *Bull. Am. Phys. Soc.*, 1968, v.13, 1643.
14. Kostro L. Physical interpretations of the coefficients c/G, c^2/G, c^3/G, c^4/G, c^5/G that appear in the equations of General Relativity. In: *Mathematics, Physics and Philosophy in the Interpretations of Relativity Theory*, Budapest, September 4–6, 2009, http://www.phil-inst.hu/~szekely
15. Schwarzschild K. Über das Gravitationsfeld eines Massenpunktes nach der Einsteinschen Theorie. *Sitzungsberichte der Königlich Preussischen Akademie der Wissenschaften*, 1916, 189–196 (published in English as: Schwarzschild K. On the gravitational field of a point mass according to Einstein's theory. *Abraham Zelmanov Journal*, 2008, vol. 1, 10–19).
16. Yao W.-M. et al. Cosmic Microwave Background. *Journal of Physics*, 2006, G33, 1.
17. Kirsnner R.P. Hubble's diagram and cosmic expansion. *PNAS*, 2004, v.101, no.1, 8–13.
18. Huchara J. Estimates of the Hubble constant. Harvard-Smithsonian Center for Astrophysics, 2009, http://www.cfa.harvard.edu/~huchra/hubble.plot.dat
19. Copi C.J. et al. Big bang nucleosythesis and the baryon density of the universe. arXiv: astro-ph/9407006.
20. Rabounski D. Hubble redshift due to the global non-holonomity of space. *The Abraham Zelmanov Jounal*, 2009, v.2, 11–28.

The Radiation Reaction of a Point Electron as a Planck Vacuum Response Phenomenon

William C. Daywitt

National Institute for Standards and Technology (retired), Boulder, Colorado, USA. E-mail: wcdaywitt@earthlink.net

The polarizability of the Planck vacuum (PV) transforms the bare Coulomb field e_*/r^2 of a point charge into the observed field e/r^2, where e_* and e are the bare and observed electronic charges respectively [1]. In uniform motion this observed field is transformed into the well-known relativistic electric and magnetic fields [2, p.380] by the interaction taking place between the bare-charge field and the PV continuum. Given the involvement of the PV in both these transformations, it is reasonable to conclude that the negative-energy PV must also be connected to the radiation reaction or damping force of an accelerated point electron. This short paper examines that conclusion by comparing it to an early indication [3] that the point electron problem may involve more than just a massive point charge.

The nonrelativistic damping force

$$\frac{2e^2}{3c^3}\frac{d\ddot{\mathbf{r}}}{dt} \tag{1}$$

is the one experimentally tested fact around which the classical equations of motion for the point electron are constructed. The relativistic version of the equation of motion due to Dirac [3] can be expressed as [4, p.393]

$$m\,a^\mu = \frac{2e^2}{3c^3}\,\frac{v^\alpha(v_\alpha\dot{a}^\mu - \dot{a}_\alpha v^\mu)}{c^2} + F^\mu \tag{2}$$

where $\mu = 0, 1, 2, 3$; v^μ and a^μ are the velocity and acceleration 4-vectors; the dot above the acceleration vectors represents differentiation with respect to the proper time; and F^μ is the external 4-force driving the electron. The first term on the right side of (2) is the relativistic damping-force 4-vector that leads to (1) in the nonrelativistic limit. In the derivation of (2) Dirac stayed within the framework of the Maxwell equations; so the m on the left side is a derived electromagnetic mass for the electron.

In deriving (2) Dirac was not interested in the physical origin of the damping force (1) — he was interested in a covariant expression for the damping force that recovered (1) in the nonrelativistic limit, whatever it took. In the derivation he utilized a radiation-reaction field proportional to the difference between retarded and advanced fields [4, p.399]:

$$\frac{F^{\mu\alpha}_{\text{ret}} - F^{\mu\alpha}_{\text{adv}}}{2} \longrightarrow \frac{2e}{3c^3}\,\frac{(v^\mu\dot{a}^\alpha - \dot{a}^\mu v^\alpha)}{c} \tag{3}$$

where $F^{\mu\alpha}_{\text{ret}}$ and $F^{\mu\alpha}_{\text{adv}}$ are, respectively, the retarded and advanced electromagnetic field tensors for a point charge. The right side of (3) is the left side evaluated at the point electron. It is significant that this field difference is nonsingular at the position of the electron's charge, for the Maxwell equations then imply that the origin of the damping force and the field (3) *must be attributed to charged sources other than the electron charge* since that charge's Coulomb field diverges as $r \to 0$. This conclusion implies that a third entity, in addition to the electron charge and its mass, is the cause of the damping force.

It can be argued that this third entity is the omnipresent PV if it is assumed that the electron charge interacts with the PV in the near neighborhood of the charge to produce the damping force. Under this assumption, the advanced field in (3) represents in a rough way *the reaction field from the PV converging on the charge*. (To the present author's knowledge, there exists no other simple explanation for this convergent field.) Thus the superficial perception of the advanced field in (3) as a cause-and-effect-violating conundrum is changed into that of an acceptable physical effect involving the PV.

The Wheeler-Feynman model for the damping force [5] [4, pp.394–399] comes to a conclusion similar to the preceding result involving the PV. In their case the third entity mentioned above is a completely absorbing shell containing a compact collection of massive point charges that surrounds the point electron. The total force exerted on the electron by the absorber is [4, eqn.(21–91)]

$$e\sum_{i=1}^{n}\frac{F^{(i)}_{\text{ret}\,\mu\alpha}\,v^\alpha}{c} + \frac{2e^2}{3c^3}\,\frac{(v_\mu\dot{a}_\alpha - \dot{a}_\mu v_\alpha)\,v^\alpha}{c^2} \tag{4}$$

where $F^{(i)}_{\text{ret}\,\mu\alpha}$ is the retarded field tensor due to the i-th charged particle in an absorber containing n particles, and where the v_μs and a_μs are defined in (2). (The reader should note that the index i on the sum is defined somewhat differently here than in [4].) A central property of the electron-plus-absorber system is that there is no radiation outside that system. That is, the disturbance caused by the accelerated electron is confined to a neighborhood (the electron-plus-absorbed) surrounding the electron.

In summary, the importance of the PV theory to (1) and its covariant cousin in the Dirac radiation-reaction equation

(2) is that it explains the advanced field in (3) as a convergent field whose source is the PV. Also, it is interesting to note that the Wheeler-Feynman model for the damping force tends to support the PV model, where the free-space absorber is a rough approximation for the negative-energy PV in the vicinity of the accelerated electron charge.

Submitted on December 01, 2009 / Accepted on December 18, 2010

References

1. Daywitt W.C. The Planck vacuum. *Progress in Physics*, 2009, v. 1, 20.
2. Jackson J.D. Classical electrodynamics. John Wiley & Sons Inc., 1st ed., 2nd printing, NY, 1962.
3. Dirac P.A.M. Classical theory of radiating electrons. *Proc. R. Soc. Lond. A*, 1938, v. 167, 148–169.
4. Panofsky W.K.H., Phillips M. Classical electricity and magnetism. Addison-Wesley Publ. Co. Inc., Mass. (USA) and London (England), 1962.
5. Wheeler J.A, Feynman R.P. Interaction with the absorber as the mechanism of radiation. *Rev. Mod. Phys.*, 1945, v. 17, no. 2 and 3, 157.

A Massless-Point-Charge Model for the Electron

William C. Daywitt

National Institute for Standards and Technology (retired), Boulder, Colorado, USA. E-mail: wcdaywitt@earthlink.net

"It is rather remarkable that the modern concept of electrodynamics is not quite 100 years old and yet still does not rest firmly upon uniformly accepted theoretical foundations. Maxwell's theory of the electromagnetic field is firmly ensconced in modern physics, to be sure, but the details of how charged particles are to be coupled to this field remain somewhat uncertain, despite the enormous advances in quantum electrodynamics over the past 45 years. Our theories remain mathematically ill-posed and mired in conceptual ambiguities which quantum mechanics has only moved to another arena rather than resolve. Fundamentally, we still do not understand just what is a charged particle" [1, p.367]. As a partial answer to the preceeding quote, this paper presents a new model for the electron that combines the seminal work of Puthoff [2] with the theory of the Planck vacuum (PV) [3], the basic idea for the model following from [2] with the PV theory adding some important details.

The Abraham-Lorentz equation for a point electron can be expressed as [4, p.83]

$$m\ddot{\mathbf{r}} = (m_0 + \delta m)\,\ddot{\mathbf{r}} = \frac{2e^2}{3c^3}\frac{d\ddot{\mathbf{r}}}{dt} + \mathbf{F}\,, \tag{1}$$

where

$$\delta m = \frac{4e^2}{3\pi c^2}\int_0^{k_{c*}} dk = \frac{4\alpha m_*}{3\pi^{1/2}} \tag{2}$$

is the electromagnetic mass correction; $e\,(=e_*\sqrt{\alpha}\,)$ is the observed electronic charge; α is the fine structure constant; e_* is the true or bare electronic charge; $k_{c*}\,(=\sqrt{\pi}/r_*)$ is the cutoff wavenumber for the mass correction [2, 5]; m_* and $r_*\,(=e_*^2/m_*c^2)$ are the mass and Compton radius of the Planck particles in the PV; m and m_0 are the observed and bare electron masses; and $\mathbf{F}$ is some external force driving the electron. One of the e_*s in the product $e^2\,(=\alpha e_*^2)$ comes from the free electronic charge and the other from the charge on the individual Planck particles making up the PV. The bare mass is defined via

$$m_0 = m - \delta m \approx -\alpha m_* \tag{3}$$

the approximation following from (2) and the fact that $\alpha m_* \gg m$. In other words, the bare mass is equal to some huge *negative* mass αm_*, an unacceptable result in any classical or semiclassical context.

The problem with the mass in (1) and (3) stems from assigning, ad hoc, a mass to the point charge to create the point electron, a similar problem showing up in quantum electrodynamics. The PV theory, however, derives the string of Compton relations [5]

$$r_* m_* c^2 = r_c m c^2 = e_*^2 \tag{4}$$

that relate the mass m and Compton radius $r_c\,(=e_*^2/mc^2)$ of the various elementary particles to the mass m_* and Compton radius r_* of the Planck particles constituting the negative energy PV. Since the same bare charge e_* is associated with the various masses in (4), it is reasonable to suggest that e_* is massless, implying that the electron charge is also massless. A massless-point-charge electron model is pursued in what follows.

The Puthoff model for a charged particle [2, 5] starts with an equation of motion for the mass m_0

$$m_0\ddot{\mathbf{r}} = e_*\mathbf{E}_{zp}\,, \tag{5}$$

where m_0, considered to be some function of the actual particle mass m, is eliminated from (5) by substituting the damping constant

$$\Gamma = \frac{2e_*^2}{3c^3 m_0} \tag{6}$$

and the electric dipole moment $\mathbf{p} = e_*\mathbf{r}$, where $\mathbf{r}$ represents the random excursions of the point charge about its average position at $\langle\mathbf{r}\rangle = 0$. The force driving the charge is $e_*\mathbf{E}_{zp}$, where $\mathbf{E}_{zp}$ is the zero-point electric field [5, Appendix B]

$$\mathbf{E}_{zp}(\mathbf{r},t) = e_*\mathrm{Re}\sum_{\sigma=1}^{2}\int d\Omega_k\int_0^{k_{c*}} dk\,k^2\widehat{\mathbf{e}}_\sigma(\mathbf{k})\sqrt{k/2\pi^2}\times \\ \times\exp\left[i\left(\mathbf{k}\cdot\mathbf{r}-\omega t+\Theta_\sigma(\mathbf{k})\right)\right] \tag{7}$$

and $\omega = ck$. The details of the equation are unimportant here, except to note that this free-space stochastic field depends only upon the nature of the PV through the Planck particle charge e_* and the cutoff wavenumber k_{c*}.

Inserting (6) into (5) leads to the equation of motion

$$\ddot{\mathbf{p}} = \frac{3c^3\Gamma}{2}\,\mathbf{E}_{zp} \tag{8}$$

for the point charge in the massless-charge electron model, where the mass equation of motion (5) is now discarded. The

mass m of the electron is then defined via the charge's average kinetic energy [2, 5]

$$m \equiv \frac{2e_*^2}{3c^3}\frac{\left\langle \dot{\mathbf{r}}_2^2 \right\rangle}{c^2\Gamma}\,, \tag{9}$$

where $\dot{\mathbf{r}}_2$ represents the planar velocity of the charge normal to its instantaneous propagation vector $\mathbf{k}$, and where

$$\left\langle \dot{\mathbf{r}}_2^2 \right\rangle = \frac{3c^4(k_{c*}\Gamma)^2}{2\pi} \tag{10}$$

is the squared velocity averaged over the random fluctuations of the field.

The cutoff wavenumber and damping constant are determined to be [2, 5]

$$k_{c*} = \frac{\sqrt{\pi}}{r_*} \tag{11}$$

and

$$\Gamma = \left(\frac{r_*}{r_c}\right)\frac{r_*}{c} = \left(\frac{1.62\times10^{-33}}{3.91\times10^{-11}}\right)\frac{r_*}{c} \sim 10^{-66}\ [\text{sec}], \tag{12}$$

where the vanishingly small damping constant is due to the large number ($\sim 10^{99}$ per cm^3) of agitated Planck particles in the PV contributing their fields simultaneously to the zero-point electric field fluctuations in (7). This damping constant is assumed to be associated with the dynamics taking place within the PV and leading to the free-space vacuum field (7).

Inserting (11) and (12) into (9) and (10) yields

$$\frac{\left\langle \dot{\mathbf{r}}_2^2 \right\rangle}{c^2} = \frac{3}{2}\left(\frac{r_*}{r_c}\right)^2 \tag{13}$$

and

$$m = \frac{r_* m_*}{r_c} \tag{14}$$

where the result in (14) agrees with the Compton relations in (4). Equation (13) shows the root-mean-square relative velocity of the massless charge to be

$$\frac{\left\langle \dot{\mathbf{r}}_2^2 \right\rangle^{1/2}}{c} = \sqrt{\frac{3}{2}}\left(\frac{r_*}{r_c}\right) \sim 10^{-23} \tag{15}$$

a vanishingly small fraction of the speed of light. The reason for this small rms velocity is the small damping constant (12) that prevents the velocity from building up as the charge is randomly accelerated.

The equation of motion (8) of the point charge can be put in a more transparent form by replacing the zero-point field (7) with [3]

$$\mathbf{E}_{zp} = \sqrt{\frac{\pi}{2}}\,\frac{e_*}{r_*^2}\,\mathbf{I}_{\text{zp}}\,, \tag{16}$$

where $\mathbf{I}_{\text{zp}}$ is a random variable of zero mean and unity mean square $\left\langle \mathbf{I}_{\text{zp}}^2 \right\rangle = 1$. Making this substitution leads to

$$\ddot{\mathbf{r}} = \sqrt{\frac{9\pi}{8}}\left(\frac{m}{m_*}\right)\frac{c^2}{r_*}\,\mathbf{I}_{\text{zp}} = \sqrt{\frac{9\pi}{8}}\,\frac{c^2}{r_c}\,\mathbf{I}_{\text{zp}}\,, \tag{17}$$

where the factors multiplying $\mathbf{I}_{\text{zp}}$ are the rms acceleration of the point charge. The electron mass m now appears on the *right side* of the equation of motion, a radical departure from equations of motion similar to (1) and (5) that are modeled around Newton's second law with the mass multiplying the acceleration $\ddot{\mathbf{r}}$ on the left of the equation. The final expression follows from the Compton relations in (4) and shows that the acceleration is roughly equivalent to a constant force accelerating the charge from zero velocity to the speed of light in the time r_c/c it takes a photon to travel the electron's Compton radius r_c.

The overall dynamics of the new electron model can be summarized in the following manner. The zero point agitation of the Planck particles within the degenerate negative-energy PV create zero-point electromagnetic fields that exist in free space [5], the evidence being the e_* and k_{c*} in (7), the rms Coulomb field e_*/r_*^2 in (16), and the fact that $\mathbf{E}_{\text{zp}}$ drives the free-space charge e_*. When the charge is injected into free space (presumably from the PV), the driving force $e_*\mathbf{E}_{\text{zp}}$ generates the electron mass in (9), thereby creating the point electron characterized by its bare point charge e_*, its derived mass m, and its Compton radius r_c. Concerning the point-charge aspect of the model, it should be recalled that, experimentally, the electron appears to have no structure at least down to a radius around 10^{-20} [cm], nine orders of magnitude smaller than the electron's Compton radius in (12).

Submitted on December 23, 2009 / Accepted on January 18, 2010

References

1. Grandy W.T. Jr. Relativistic quantum mechanics of leptons and fields. Kluwer Academic Publishers, Dordrecht-London, 1991.
2. Puthoff H.E. Gravity as a Zero-Point-Fluctuation Force. *Phys. Rev. A*, 1989, v.39, no.5, 2333–2342.
3. Daywitt W.C. The Planck vacuum. *Progress in Physics*, 2009, v. 1, 20.
4. de la Peña L., Cetto A.M. The quantum dice — an introduction to stochastic electrodynamics. Kluwer Academic Publishers, Boston, 1996. Note that the upper integral limit for δm in (2) of the present paper is different from that in (3.114) on p.83 of reference [4].
5. Daywitt W.C. The source of the quantum vacuum. *Progress in Physics*, 2009, v. 1, 27.

Quark Confinement and Force Unification

Robert A. Stone Jr.

1313 Connecticut Ave, Bridgeport, CT 06607, USA. E-mail: robert.a.stone.jr@gmail.com

String theory had to adopt a bi-scale approach in order to produce the weakness of gravity. Taking a bi-scale approach to particle physics along with a spin connection produces 1) the measured proton radius, 2) a resolution of the multiplicity of measured weak angle values 3) a correct theoretical value for the Z^0 4) a reason that h is a constant and 5) a "neutral current" source. The source of the "neutral current" provides 6) an alternate solution to quark confinement, 7) produces an effective r like potential, and 8) gives a reason for the observed but unexplained Regge trajectory like $J \sim M^2$ behavior seen in quark composite particle spin families.

1 Introduction

One of the successful aspects of String Theory is its ability to produce both atomic type and gravitational type forces within the same mathematical formalism. The problem was that the resultant gravitational force magnitude was not even close.

This problem continued until the string theorists added extra dimension of about $10^{19\text{th}}$ times larger than plank scale dimensions [1, 2]. The weakness of inter-scale gravity is due to the size difference between the two scales.

But a bi-scale approach raises the question; Is there also a "strong" intra-scale gravity force at the scale that produces the other strong particle level forces?

The particle level gravity proposition (e.g. Recami [3] and Salam [4]) is revisited, as the source of the "neutral current".

Spin in the Standard Model (SM) is not viewed as physical. As shown in [5], it is not the SM mathematics, but the "standard" view of the mathematics that results in the Cosmological Constant Problem while hiding Nature's mass symmetry, a symmetry in keeping with the cosmological constant and a symmetry that results in a single mass formula for the fundamental particles ($W^{\pm}$, $p^{\pm}$, $e^{\mp}$) and electron generations.

The results of [5] could not have occurred without putting aside the SM "standard" view.

This paper proposes that the particle's components real spin is the source of a particle level gravity.

2 The spin connection

It is proposed that spin is the source of a strong particle level gravity and associated intra-scale induced curvature. A spin torsion connection to a "strong" gravity is not new [6].

An intra-scale induced curvature is different than an inter-scale induced curvature. An inter-scale force is related to the difference between scales making G a constant.

The proposed intra-scale gravity magnitude is dependent on the frequency of spin. The higher the energy the higher the frequency (e.g. like $E = h\nu$ used in the development of the Schrödinger equation). The higher the frequency the higher the resultant curvature. Thus this intra-scale gravity value is not a constant.

Given the units of strong particle level gravity (sG) are $\mathrm{gm}^{-1}\mathrm{cm}^3\mathrm{sec}^{-2}$ and spin (h) are $\mathrm{gm}^1\mathrm{cm}^2\mathrm{sec}^{-1}$ the first spin $\frac{1}{2}\hbar$ particle "x" relationship one might propose is

$$\mathrm{C}\,\frac{2\,sG_x\,m_x^2}{c} = \hbar\,, \tag{1}$$

where c is the velocity of light, C is a proportionality constant and the 2 on the lhs comes from the $\frac{1}{2}$ originally in front of $\hbar$.

In [5], a 4π definition of Nature's coupling constants was given for the charged particle weak angle as $\alpha_{\mathrm{sg}}{=}2\sqrt{2}\,(4\pi\varrho)^{-1}$ ($\sim$0.2344 vs 0.2312 [7]) where $\varrho = 0.959973785$.

Equating C with the α_{sg} gives

$$\alpha_{\mathrm{sg}}\,\frac{2\,sG_x\,m_x^2}{c} = \hbar\,. \tag{2}$$

3 The proton radius

Using the traditional gravity radius relationship for proof of concept (see §12), i.e. $\mathrm{R_p} = 2\,sG_{\mathrm{p}}\,m_{\mathrm{p}}/c^2$ and the proton mass (m_{p} [8]) gives the proton radius of

$$\mathrm{R_p} = \frac{2\,sG_{\mathrm{p}}\,m_{\mathrm{p}}}{c^2} = \frac{\hbar}{c\,m_{\mathrm{p}}\,\alpha_{\mathrm{sg}}} = 8.96978{\times}10^{-14}\ \mathrm{cm}\,. \tag{3}$$

From scattering data, Sick [9] gives a proton radius $\mathrm{R_p}$ of $8.95{\times}10^{-14}$cm $\pm$ 0.018 making (3) 0.221% of Sick's value and Ezhela [10] gives a proton radius $\mathrm{R_p}$ of $8.97{\times}10^{-14}$cm $\pm$ 0.02(exp) $\pm$ 0.01(norm) making (3) 0.0024% of Ezhela's value.

4 A force magnitude unification

The proposed spin frequency strong gravity connection results in the three force distance squared ratios of

$$\alpha_{\mathrm{cs}} = 7.2973525310^{-3}\,, \tag{4}$$

$$\alpha_{\mathrm{cg}} = 1.7109648410^{-3}\,, \tag{5}$$

$$\alpha_{\mathrm{sg}} = 0.234463777\,. \tag{6}$$

Thus the string theory conjecture that Nature's space-time is bi-scalar and this paper's conjecture on real spin as the source of a strong particle level gravity curvature results in a unification of forces at the particle level.

5 A weak theory puzzle

One recognized puzzle is that there are three statistically different weak angle values (Salam-Weinberg mass ratio SM theoretical value 0.2227 [11], $\sin^2\hat{\theta}_{\mathrm{W}}(M_{\mathrm{Z}}) = 0.2312$ [7], neutrino $s^2_{\mathrm{W}} = 0.2277$ [11]) rather than a single value as expected by the SM. Note that the conversion between these weak angle forms does not resolve this puzzle.

6 A weak theory solution

The puzzle of three different measured weak angles using the present work is no longer a puzzle.

Unlike the SM view, the theoretical definition, $\alpha_{\mathrm{sg}} = 2\sqrt{2}(4\pi\varrho)^{-1}$, allows for at least two basic weak angle values. When $\varrho = 1$ the pure theory definition gives $\alpha_{\mathrm{sg}(1)} = 2\sqrt{2}(4\pi\,1)^{-1} \sim 0.2251$, close to the measured neutrino weak angle (0.2277 [11]). When using the same value of ϱ used for the fine structure constant definition [5], i.e $\varrho = 0.959973785$, the definition $\alpha_{\mathrm{sg}} = 2\sqrt{2}(4\pi\varrho)^{-1}$ is close to the measured charge particle weak angle (~0.2344 vs 0.2312 [7]).

Thus these two different values, s^2_{W} and $\sin^2\hat{\theta}_{\mathrm{W}}(M_{\mathrm{Z}})$, result from two different spin couplings ($\varrho = 1$ and $\varrho = 0.959973785$) for two different types of particles, neutrino particles and charged particles.

The resolution for the Salam-Weinberg value in part comes from the recognition that the charged particle weak angle is different from the pure theory value, and that the Salam-Weinberg mass ratio is a pure theory value. The other part comes from the expectation that a true pure theory value would use chargeless particle masses.

Using the PDG W mass (m_{W} [8]) and the new constant α_{cg} given in [5] to produce the W particle charge reduced mass value, $m_{\mathrm{W}}(1 - S\,\alpha_{\mathrm{cg}})$ with $S = 1$, yields the pure theory Salam-Weinberg bare mass ratio equation

$$1 - \frac{(m_{\mathrm{W}}(1-\alpha_{\mathrm{cg}}))^2}{m^2_{\mathrm{Z}}} = 0.2253 \simeq \alpha_{\mathrm{sg}(1)} = 0.2251. \qquad (7)$$

Note that using the pure theory approach to the Salam-Weinberg mass ratio reduces the number values for the weak angle to two. Now, as theoretically expected, the pure theory charge reduced bare Salam-Weinberg mass ratio numerically matches the pure theory weak angle value.

7 A theoretical Z^0 mass

Given the theoretical value of the W mass in [5] and rearranging to give the Z^0 theoretical mass produces the m_{Z}

$$m_{\mathrm{Z}} = \frac{m_{\mathrm{W}}(1-\alpha_{\mathrm{cg}})}{(1-\alpha_{\mathrm{sg}(1)})^{\frac{1}{2}}} = 91188.64\ \mathrm{MeV}, \qquad (8)$$

a value within 0.0011% of the measured PDG value of 91187.6 ± 2.1 [8].

8 Confinement and quark's existence

This particle level gravity approach also gives a reason that quarks are only seen inside of particles, but not all particles.

Noting that all quark composite particle masses are greater than the mass symmetry point ($M_{\mathrm{sp}} \sim 21$ MeV), implies that quark particles are only stable inside the higher curvature (compacted) space-time fabric particles above the mass symmetry point and are not stable inside the low curvature (voided) space-time particles below M_{sp}.

9 Confinement, persistence and Regge trajectories

But if quarks can only exist inside high curvature particles then unstable particle decay may not occur at the quarks base mass but when the curvature is not high enough for the quarks to persist.

This means that the measured quark masses may not be their base mass but their decay point masses.

The two natural postulates, 1) that the enclosure curvature makes quarks stable and 2) that a quark decays before reaching its base mass, imply that a given quark orbital spin configuration will decay at or near some given curvature value. This means that for a specific quark particle spin family (e.g. a $S = 1/2,\ 3/2,\ 5/2$ $J(S\hbar)$ family), all members of the family would decay at or around the same curvature.

That a quark spin family all decay at the same curvature, i.e sG is a constant ($sG = C_{decay}$), means that Eq. (2) becomes

$$C' M_x^2 = J(S\hbar). \qquad (9)$$

This equation is the Regge trajectory like ($J \sim M^2$) behavior seen in Chew-Fraustchi plots for unstable quark spin families (see [12] for some examples).

Thus the spin strong gravity connection that produces the correct proton radius and the correct weak angle, also gives a reason why quarks do not exist outside of particles and can produce the observed Regge trajectory like behavior.

10 The proton and quarks

As indicated by the single quantized mass formula for the electron, proton and W particle given in [5], the quantization process' spin dominates the proton and thus the (stable) proton is not a typical (unstable) quark composite particle.

Evidence that the proton is not typical also comes from B. G. Sidharth [13]. Sidharth reproduces numerous composite particle masses using the pion as the "base particle". Sidharth states, "Secondly, it may be mentioned that ... using the proton as the base particle has lead to interesting, but not such comprehensive results".

That the proton is not a quark spin dominated particle may be one of the reasons that QCD has struggled for 40 years, with numerous additions to the model to produce a good proton radius value within 5% and why "solutions", like adding the effect of the s quarks fails to be supported by experimental evidence consistent with no s quarks.

The spin connection with the strong gravity approach immediately results in a proton radius value significantly less than 1%.

11 A r potential from a $1/r$ potential force

What the data for unstable quark composite particles indicates is that there is an *effective r* like confining potential.

What the data does not say is how this r like potential *effect* occurs.

One way of creating this r potential was found by making a new force nature that requires the QCD "equivalent of the photon", the gluon, to not only mediate the force as does the photon, but also participates in it (requires glueballs to exist).

However, there is another way that does not require a new force nature nor force form nor particle nature. Note that what follows is for quark (spin dominated) composite particles, not quantization dominated fundamental particles, i.e. the proton, and is a simplification of a complex situation including the frame dragging of quarks.

For quark composite particles the real spin proposition implies that the quark orbital spin angular momentum can be a significant contribution to the strong gravity value.

The particles strong gravity value would not be a constant but fluctuate with the quarks contribution due to their radius and velocity within the strong gravity enclosure.

That is to say, the higher the internal quark real spin angular momentum value, the higher the curvature and the stronger the confinement force. Mathematically this implies a C/r potential whose "gravitational constant value" C is not constant, but also a function of constituent quark orbital spin angular momentum.

As the quark orbital spin angular momentum contribution is a function of r^2 ($C = C'r^2$) the resulting effective confining potential ($V(r)$) would be $V(r) = C/r = C'r^2/r = C'r$. Thus the quark contribution to the resultant strong gravity confining potential, i.e. *effective behavior*, can act like a r potential.

Phenomenologically/experimentally the essential requirement is that the *effective* confining behavior, not that the actual potential form, is r like. Though not rigorous, this shows the potential to produce the *effective r* like behavior.

12 The particle level gravity proposition

The particle level gravity proposition is not new. Back in the early days of the quark strong force conjecture, there also was a particle level gravity conjecture.

Nobel Prize winner Abdus Salam [4] and Recami [3], via two different particle level gravity approaches, show that both asymptotic freedom and confinement can result from this approach. Both of these two approaches lacked a source of or cause and thus were unable to produce any specific values.

As indicated by Ne'eman and Sijacki [12] "Long ago, we noted the existence of a link between Regge trajectories and what we then thought was plain gravity ... In nuclei, ... the quadrupolar nature of the SL(3,R), SU(3) and Eucl(3) sequences ... all of these features again characterize the action of a gravity like spin-2 effective gauge field. Overall the evidence for the existence of such an effective component in QCD seems overwhelming".

Note that a particle level gravity theory is a spin torsion intra-scale gravity theory that includes the curvature stress energy tensor. Thus it's properties can differ from those associated with traditional inter-scale gravity theory. For example Yilmaz's [14] attempt at inclusion of a gravity stress energy tensor term appears not to have the intra-scale "hard" event horizon associated with the inter-scale Kerr solution.

With respect to the SM, Sivaram [6] indicates that the Dirac spinor can gain mass via a strong gravity field.

Last but not least, in Sivaram's paper [6] on the potential of the strong particle level gravity approach, Sivaram states; "It is seen that the form of the universal spin-spin contact interaction ... bears a striking resemblance to that of the familiar four-fermion contact interaction of Fermi's theory of weak interactions. This suggests the possibility of identifying the coupling of spin and torsion to the vierbein strong gravitational field as the origin of the weak interaction".

Sivaram's association of Fermi's weak theory with the coupling of spin and strong gravity is in keeping with Eq. (2) and the proposition in [5] that α_{sg} is a theoretical definition of the SM charged particle weak mixing angle.

13 Why h is constant and its value source

In particle physics, h is a constant of spin. However, the Standard Model does not answer the question, "Why does particle physics have the spin constant h ?".

The answer naturally results from the real spin extent connection to strong gravity.

The spin extent is limited by the size of the particle. As real spin angular momentum energy is added to the particle, the coupling requires the particle size to contract resulting in extent contraction and resultant increase in frequency to conserve angular momentum, i.e. a spin constant. Field acceleration to a higher spin frequency results in extent contraction to match the higher spin frequency, i.e. a spin constant.

This is the observed Frequency Lorentzian nature of the photon, i.e energy dilation, (wave)length contraction and frequency dilation.

Thus the gravitational curvature constant constrains the spin constant via the coupling value of spin to strong gravity as given in Eq. (2).

14 Summary

To produce gravity's weak value, string theory requires a bi-scale approach where gravity is an inter-scale property. This leads to the conjecture that there is also an intra-scale gravity at the same scale as the other particle forces.

There is also the additional proposition that there is a real spin strong particle level gravity relationship.

If this spin particle level gravity connection is correct then one would expect that it would produce the correct proton radius and it does.

One would also expect that either the α_{sg} value or the α_{cg} value should be a value within the Standard Model.

Not only does α_{sg} match the charged particle weak angle, the pure theory $\alpha_{sg(1)}$ matches the neutrino weak angle.

These propositions resolve the problem of the NuTev [11] neutrino results being 2.5σ from the SM $\sin^2\theta_W^{(on-shell)}$ value. The true $\sin^2\theta_W^{(on-shell)}$ is the Salam-Weinberg bare mass ratio which is near the NuTev result and almost exactly $\alpha_{sg(1)}$.

As shown in [15] the FSC definition (α_{cs}) of this electro-gravitic approach matches an Einstein-Cartan FSC definition.

In keeping with [5], neither the quantization proposition nor the strong particle level gravity proposition are in conflict with the existence of quarks.

This particle level gravity approach does not require a new force form for the confinement of quarks and due to the spin strong gravity connection, can result in an *effective r* potential force for quark spin dominated unstable particles.

A strong gravity confinement source indicates that quarks can only exist inside high curvature particles thus giving a reason why quarks are not seen as free particles. The high curvature quark connection and the quark mass pattern indicates that the "measured" quark masses are not their base "invariant" mass values but decay point mass values. This proposition results in Regge trajectory like behavior.

Though the SM has had great numerical and behavioral success, its propositions (Higgs, QCD, etc.) result in fundamental problems like the Cosmological Constant Problem (10^{34+} off) and no excepted solution to the Matter Only Universe Problem, while not addressing the integration of gravity. Thus despite its numerical success, the SM has not solved the particle puzzle in all of its parts.

In [5], taking a non-standard view of the fundamental particle masses, the quantization proposition not only results in a single mass formula for the W, p, e and electron generations, it can solve the Cosmological Constant Problem and the Matter Only Universe Problem.

In this paper, the proposition of a real spin connection to the strong particle level gravity gives a source for the weak angle. This makes strong particle level gravity the "neutral current" and the foundation for the particle nature of particles.

These papers produce values for the $W^{\pm}$ and Z^0 mass and proton radius that are within the uncertainty in the measured values, naturally results in two weak angle values as experimentally observed, matches these values and explains why Nature has a spin angular momentum constant and thus show this approach potential. Also indicated is the potential of a bi-scalar approach to Nature which can solve the Hierarchy Problem and produce a particle scale Unification of Forces.

Submitted on January 12, 2009 / Accepted on January 18, 2010

References

1. Antoniadis I., Arkani-Hamed N., Dimpopoulus S., and Dvali G. New dimensions at a millimeter to a fermi and superstrings at a TeV. *Phys. Lett.*, 1998, v. B436, 257–263.
2. Arkani-Hamed N., Dimpopoulus S., and Dvali G. The hierarchy problem and new dimensions at a millimeter. *Phys. Lett.*, 1998, v. B429, 263–272.
3. Recami E. and Tonin-Zanchin V. The strong coupling constant: its theoretical derivation from a geometric approach to hadron structure. *Found. Phys. Lett.*, 1994, v, 7(1), 85–92.
4. Salam A. and Sivaram C. Strong Gravity Approach to QCD and Confinement. *Mod. Phys. Lett.*, 1993, v. A8(4), 321–326.
5. Stone R.A. Is Fundamental Particle Mass $\mathbf{4}\pi$ Quantized? *Progress in Physics*, 2010, v. 1, 11–13.
6. Sivaram C. and Sinha K.P. Strong spin-two interactions and general relativity. *Phys. Rep.*, 1979, v. 51, 113–187 (p.152).
7. Particle Data Group, Physical Constants 2009. http://pdg.lbl.gov/2009/constants/rpp2009-phys-constants.pdf
8. Particle Data Group, Particle Listings, 2009. http://pdg.lbl.gov/2009/listings/rpp2009-list-p.pdf, rpp2009-list-z-boson.pdf, rpp2009-list-w-boson.pdf
9. Sick I. On the rms-radius of the proton. *Phys. Lett.*, 2003, v. B576(1), 62–67; also arXiv: nucl-ex/0310008.
10. Ezhela V. and Polishchuk B. Reanalysis of e-p Elastic Scattering Data in Terms of Proton Electromagnetic Formfactors. arXiv: hep-ph/9912401.
11. Zeller G.P. et al. (NuTeV Collaboration) Precise Determination of Electroweak Parameters in Neutrino-Nucleon Scattering. *Phys. Rev. Lett.*, 2002, v. 88, 091802.
12. Ne'eman Y. and Sijacki Dj. Proof of pseudo-gravity as QCD approximation for the hadron IR region and $J \sim M^2$ Regge trajectories. *Phys. Lett.*, 1992, v. B276(1), 173–178.
13. Sidharth B.G. A QCD generated mass spectrum. arXiv: physics/0309037.
14. Yilmaz H. Toward a Field Theory of Gravitation. *Il Nuovo Cimento*, 1992, v. B8, 941–959.
15. Stone R.A. An Einstein-Cartan Fine Structure Constant definition. *Progress in Physics*, 2010, v. 1, L8.

A Derivation of Maxwell Equations in Quaternion Space

Vic Chrisitianto* and Florentin Smarandache†

*Present address: Institute of Gravitation and Cosmology, PFUR, Moscow, 117198, Russia. E-mail: vxianto@yahoo.com
†Department of Mathematics, University of New Mexico, Gallup, NM 87301, USA. E-mail: smarand@unm.edu

Quaternion space and its respective Quaternion Relativity (it also may be called as Rotational Relativity) has been defined in a number of papers, and it can be shown that this new theory is capable to describe relativistic motion in elegant and straightforward way. Nonetheless there are subsequent theoretical developments which remains an open question, for instance to derive Maxwell equations in Q-space. Therefore the purpose of the present paper is to derive a consistent description of Maxwell equations in Q-space. First we consider a simplified method similar to the Feynman's derivation of Maxwell equations from Lorentz force. And then we present another derivation method using Dirac decomposition, introduced by Gersten (1998). Further observation is of course recommended in order to refute or verify some implication of this proposition.

1 Introduction

Quaternion space and its respective Quaternion Relativity (it also may be called as Rotational Relativity has been defined in a number of papers including [1], and it can be shown that this new theory is capable to describe relativistic motion in elegant and straightforward way. For instance, it can be shown that the Pioneer spacecraft's Doppler shift anomaly can be explained as a relativistic effect of Quaternion Space [2]. The Yang-Mills field also can be shown to be consistent with Quaternion Space [1]. Nonetheless there are subsequent theoretical developments which remains an open issue, for instance to derive Maxwell equations in Q-space [1].

Therefore the purpose of the present article is to derive a consistent description of Maxwell equations in Q-space. First we consider a simplified method similar to the Feynman's derivation of Maxwell equations from Lorentz force. Then we present another method using Dirac decomposition, introduced by Gersten [6]. In the first section we will shortly review the basics of Quaternion space as introduced in [1].

Further observation is of course recommended in order to verify or refute the propositions outlined herein.

2 Basic aspects of Q-relativity physics

In this section, we will review some basic definitions of quaternion number and then discuss their implications to quaternion relativity (Q-relativity) physics [1].

Quaternion number belongs to the group of "very good" algebras: of real, complex, quaternion, and octonion, and normally defined as follows [1]

$$Q \equiv a + bi + cj + dk\,. \tag{1}$$

Where a, b, c, d are real numbers, and i, j, k are imaginary quaternion units. These Q-units can be represented either via 2×2 matrices or 4×4 matrices. There is quaternionic multiplication rule which acquires compact form [1]

$$1q_k = q_k 1 = q_k\,, \qquad q_j q_k = -\delta_{jk} + \epsilon_{jkn} q_n\,. \tag{2}$$

Where δ_{kn} and ϵ_{jkn} represents 3-dimensional symbols of Kronecker and Levi-Civita, respectively.

In the context of Quaternion Space [1], it is also possible to write the dynamics equations of classical mechanics for an inertial observer in constant Q-basis. SO(3,R)-invariance of two vectors allow to represent these dynamics equations in Q-vector form [1]

$$m\,\frac{d^2}{dt^2}\,(x_k q_k) = F_k q_k\,. \tag{3}$$

Because of antisymmetry of the connection (generalised angular velocity) the dynamics equations can be written in vector components, by conventional vector notation [1]

$$m\left(\vec{a} + 2\vec{\Omega}\times\vec{v} + \vec{\Omega}\times\vec{r} + \vec{\Omega}\times\left(\vec{\Omega}\times\vec{r}\right)\right) = \vec{F}\,. \tag{4}$$

Therefore, from equation (4) one recognizes known types of classical acceleration, i.e. linear, coriolis, angular, centripetal.

From this viewpoint one may consider a generalization of Minkowski metric interval into biquaternion form [1]

$$dz = (dx_k + i dt_k)\, q_k\,. \tag{5}$$

With some novel properties, i.e.:

- time interval is defined by imaginary vector;
- space-time of the model appears to have six dimensions (6D model);
- vector of the displacement of the particle and vector of corresponding time change must always be normal to each other, or

$$dx_k dt_k = 0\,. \tag{6}$$

One advantage of this Quaternion Space representation is that it enables to describe rotational motion with great clarity.

After this short review of Q-space, next we will discuss a simplified method to derive Maxwell equations from Lorentz force, in a similar way with Feynman's derivation method using commutative relation [3, 4].

3 An intuitive approach from Feynman's derivative

A simplified derivation of Maxwell equations will be discussed here using similar approach known as Feynman's derivation [3–5].

We can introduce now the Lorentz force into equation (4), to become

$$m\left(\frac{d\vec{v}}{dt}+2\vec{\Omega}\times\vec{v}+\vec{\Omega}\times\vec{r}+\vec{\Omega}\times\left(\vec{\Omega}\times\vec{r}\right)\right)= \\ =q_{\otimes}\left(\vec{E}+\frac{1}{c}\,\vec{v}\times\vec{B}\right), \qquad (7)$$

or

$$\left(\frac{d\vec{v}}{dt}\right)=\frac{q_{\otimes}}{m}\left(\vec{E}+\frac{1}{c}\,\vec{v}\times\vec{B}\right)-2\vec{\Omega}\times\vec{v}-\vec{\Omega}\times\vec{r}-\vec{\Omega}\times\left(\vec{\Omega}\times\vec{r}\right). \qquad (8)$$

We note here that q variable here denotes electric charge, not quaternion number.

Interestingly, equation (4) can be compared directly to equation (8) in [3]

$$m\ddot{x}=F-m\left(\frac{d\vec{v}}{dt}\right)+m\vec{r}\times\vec{\Omega}+m2\dot{x}\times\vec{\Omega}+m\vec{\Omega}\times\left(\vec{r}\times\vec{\Omega}\right). \qquad (9)$$

In other words, we find an exact correspondence between quaternion version of Newton second law (3) and equation (9), i.e. the equation of motion for particle of mass m in a frame of reference whose origin has linear acceleration a and an angular velocity $\vec{\Omega}$ with respect to the reference frame [3].

Since we want to find out an "electromagnetic analogy" for the inertial forces, then we can set $F = 0$. The equation of motion (9) then can be derived from Lagrangian $L = T - V$, where T is the kinetic energy and V is a velocity-dependent generalized potential [3]

$$V(x,\dot{x},t)=ma\cdot x-m\dot{x}\cdot\vec{\Omega}\times x-\frac{m}{2}\left(\vec{\Omega}\times x\right)^2, \qquad (10)$$

Which is a linear function of the velocities. We now may consider that the right hand side of equation (10) consists of a scalar potential [3]

$$\phi(x,t)=ma\cdot x-\frac{m}{2}\left(\vec{\Omega}\times x\right)^2, \qquad (11)$$

and a vector potential

$$A(x,t)\equiv m\dot{x}\cdot\vec{\Omega}\times x, \qquad (12)$$

so that

$$V(x,\dot{x},t)=\phi(x,t)-\dot{x}\cdot A(x,t). \qquad (13)$$

Then the equation of motion (9) may now be written in Lorentz form as follows [3]

$$m\ddot{x}=E(x,t)+x\times H(x,t) \qquad (14)$$

with

$$E=-\frac{\partial A}{\partial t}-\nabla\phi=-m\Omega\times x-ma+m\Omega\times(x\times\Omega) \qquad (15)$$

and

$$H=\nabla\times A=2m\Omega. \qquad (16)$$

At this point we may note [3, p. 303] that Maxwell equations are satisfied by virtue of equations (15) and (16). The correspondence between Coriolis force and magnetic force, is known from Larmor method. What is interesting to remark here, is that the same result can be expected directly from the basic equation (3) of Quaternion Space [1]. The aforementioned simplified approach indicates that it is indeed possible to find out Maxwell equations in Quaternion space, in particular based on our intuition of the direct link between Newton second law in Q-space and Lorentz force (We can remark that this parallel between classical mechanics and electromagnetic field appears to be more profound compared to simple similarity between Coulomb and Newton force).

As an added note, we can mention here, that the aforementioned Feynman's derivation of Maxwell equations is based on commutator relation which has classical analogue in the form of Poisson bracket. Then there can be a plausible way to extend directly this "classical" dynamics to quaternion extension of Poisson bracket, by assuming the dynamics as element of the type: $r \in H \wedge H$ of the type: $r = ai \wedge j + bi \wedge k + cj \wedge k$, from which we can define Poisson bracket on H. But in the present paper we don't explore yet such a possibility.

In the next section we will discuss more detailed derivation of Maxwell equations in Q-space, by virtue of Gersten's method of Dirac decomposition [6].

4 A new derivation of Maxwell equations in Quaternion Space by virtue of Dirac decomposition

In this section we present a derivation of Maxwell equations in Quaternion space based on Gersten's method to derive Maxwell equations from one photon equation by virtue of Dirac decomposition [6]. It can be noted here that there are other methods to derive such a "quantum Maxwell equations" (i.e. to find link between photon equation and Maxwell equations), for instance by Barut quite a long time ago (see ICTP preprint no. IC/91/255).

We know that Dirac deduces his equation from the relativistic condition linking the Energy E, the mass m and the momentum p [7]

$$\left(E^2-c^2\vec{p}^{\,2}-m^2c^4\right)I^{(4)}\Psi=0, \qquad (17)$$

where $I^{(4)}$ is the 4×4 unit matrix and Ψ is a 4-component column (bispinor) wavefunction. Dirac then decomposes equation (17) by assuming them as a quadratic equation

$$\left(A^2-B^2\right)\Psi=0, \qquad (18)$$

where

$$A=E, \qquad (19)$$

$$B=c\vec{p}+mc^2. \qquad (20)$$

The decomposition of equation (18) is well known, i.e. $(A+B)(A-B)=0$, which is the basic of Dirac's decomposition method into 2×2 unit matrix and Pauli matrix [6].

By virtue of the same method with Dirac, Gersten [6] found in 1998 a decomposition of one photon equation from relativistic energy condition (for massless photon [7])

$$\left(\frac{E^2}{c^2}-\vec{p}^{\,2}\right)I^{(3)}\Psi=0\,, \tag{21}$$

where $I^{(3)}$ is the 3×3 unit matrix and Ψ is a 3-component column wavefunction. Gersten then found [6] equation (21) decomposes into the form

$$\left[\frac{E}{c}I^{(3)}-\vec{p}\cdot\vec{S}\right]\left[\frac{E}{c}I^{(3)}+\vec{p}.\vec{S}\right]\vec{\Psi}-\begin{pmatrix}p_x\\p_y\\p_z\end{pmatrix}\left(\vec{p}\cdot\vec{\Psi}\right)=0 \tag{22}$$

where $\vec{S}$ is a spin one vector matrix with components [6]

$$S_x=\begin{pmatrix}0&0&0\\0&0&-i\\0&-i&0\end{pmatrix}, \tag{23}$$

$$S_y=\begin{pmatrix}0&0&i\\0&0&0\\-i&0&0\end{pmatrix}, \tag{24}$$

$$S_z=\begin{pmatrix}0&-i&0\\-i&0&0\\0&0&0\end{pmatrix}, \tag{25}$$

and with the properties

$$\left.\begin{aligned}&\left[S_x,S_y\right]=iS_z\,,\quad [S_x,S_z]=iS_y\\&\left[S_y,S_z\right]=iS_x\,,\quad \vec{S}^2=2I^{(3)}\end{aligned}\right\}. \tag{26}$$

Gersten asserts that equation (22) will be satisfied if the two equations [6]

$$\left[\frac{E}{c}I^{(3)}+\vec{p}\cdot\vec{S}\right]\vec{\Psi}=0\,, \tag{27}$$

$$\vec{p}\cdot\vec{\Psi}=0 \tag{28}$$

are simultaneously satisfied. The Maxwell equations [8] will be obtained by substitution of E and p with the ordinary quantum operators (see for instance Bethe, *Field Theory*)

$$E\to i\hbar\frac{\partial}{\partial t} \tag{29}$$

and

$$p\to -ih\nabla \tag{30}$$

and the wavefunction substitution

$$\vec{\Psi}=\vec{E}-i\vec{B}\,, \tag{31}$$

where E and B are electric and magnetic fields, respectively. With the identity

$$\left(\vec{p}\cdot\vec{S}\right)\vec{\Psi}=\hbar\nabla\times\vec{\Psi}\,, \tag{32}$$

then from equation (27) and (28) one will obtain

$$i\frac{\hbar}{c}\frac{\partial\left(\vec{E}-i\vec{B}\right)}{\partial t}=-\hbar\nabla\times\left(\vec{E}-i\vec{B}\right), \tag{33}$$

$$\nabla\cdot\left(\vec{E}-i\vec{B}\right)=0\,, \tag{34}$$

which are the Maxwell equations if the electric and magnetic fields are real [6, 7].

We can remark here that the combination of E and B as introduced in (31) is quite well known in literature [9,10]. For instance, if we use positive signature in (31), then it is known as Bateman representation of Maxwell equations $\operatorname{div}\vec{\epsilon}=0$, $\operatorname{rot}\vec{\epsilon}=\frac{\partial\epsilon}{\partial t}$, $\epsilon=\vec{E}+i\vec{B}$. But the equation (31) with negative signature represents the *complex nature* of electromagnetic fields [9], which indicates that these fields can also be represented in quaternion form.

Now if we represent in other form $\vec{\epsilon}=\vec{E}-i\vec{B}$ as more conventional notation, then equation (33) and (34) will get a quite simple form

$$i\frac{\hbar}{c}\frac{\partial\vec{\epsilon}}{\partial t}=-\hbar\nabla\times\vec{\epsilon}\,, \tag{35}$$

$$\nabla\cdot\vec{\epsilon}=0\,. \tag{36}$$

Now to consider quaternionic expression of the above results from Gersten [6], one can begin with the same linearization procedure just as in equation (5)

$$dz=(dx_k+idt_k)\,q_k\,, \tag{37}$$

which can be viewed as the quaternionic square root of the metric interval dz

$$dz^2=dx^2-dt^2. \tag{38}$$

Now consider the relativistic energy condition (for massless photon [7]) similar to equation (21)

$$E^2=p^2c^2\;\Rightarrow\left(\frac{E^2}{c^2}-\vec{p}^{\,2}\right)=k^2. \tag{39}$$

It is obvious that equation (39) has the same form with (38), therefore we may find its quaternionic square root too, then we find

$$k=\left(E_{qk}+i\vec{p}_{qk}\right)q_k\,, \tag{40}$$

where q represents the quaternion unit matrix. Therefore the linearized quaternion root decomposition of equation (21) can be written as follows [6]

$$\left[\frac{E_{qk}q_k}{c}I^{(3)}+i\vec{p}_{qk}q_k\cdot\vec{S}\right]\left[\frac{E_{qk}q_k}{c}I^{(3)}+i\vec{p}_{qk}q_k\cdot\vec{S}\right]\vec{\Psi}-$$
$$-\begin{pmatrix}p_x\\p_y\\p_z\end{pmatrix}\left(i\vec{p}_{qk}q_k\cdot\vec{\Psi}\right)=0\,. \tag{41}$$

Accordingly, equation (41) will be satisfied if the two equations

$$\left[\frac{E_{qk}\,q_k}{c}\,I^{(3)} + i\,\vec{p}_{qk}\,q_k\cdot\vec{S}\right]\vec{\Psi}_k = 0\,, \tag{42}$$

$$i\,\vec{p}_{qk}\,q_k\cdot\vec{\Psi}_k = 0 \tag{43}$$

are simultaneously satisfied. Now we introduce similar wavefunction substitution, but this time in quaternion form

$$\vec{\Psi}_{qk} = \vec{E}_{qk} - i\vec{B}_{qk} = \vec{\epsilon}_{qk}\,. \tag{44}$$

And with the identity

$$\left(\vec{p}_{qk}\,q_k\cdot\vec{S}\right)\vec{\Psi}_k = \hbar\,\nabla_k\times\vec{\Psi}_k\,. \tag{45}$$

Then from equations (42) and (43) one will obtain the *Maxwell equations in Quaternion-space* as follows

$$i\,\frac{\hbar}{c}\,\frac{\partial\vec{\epsilon}_q k}{\partial t} = -\,\hbar\,\nabla_k\times\vec{\epsilon}_{qk}\,, \tag{46}$$

$$\nabla_k\cdot\vec{\epsilon}_{qk} = 0\,. \tag{47}$$

Now the remaining question is to define quaternion differential operator in the right hand side of (46) and (47).

In this regards one can choose some definitions of quaternion differential operator, for instance the Moisil-Theodoresco operator [11]

$$D\,[\varphi] = \operatorname{grad}\varphi = \sum_{k=1}^{3} i_k\partial_k\varphi = i_1\,\partial_1\varphi + i_2\,\partial_2\varphi + i_3\,\partial_3\varphi\,. \tag{48}$$

where we can define $i_1 = i$; $i_2 = j$; $i_3 = k$ to represent 2×2 quaternion unit matrix, for instance. Therefore the differential of equation (44) now can be expressed in similar notation of (48)

$$\begin{aligned} D\left[\vec{\Psi}\right] = D\,[\vec{\epsilon}] = i_1\,\partial_1 E_1 + i_2\,\partial_2 E_2 + i_3\,\partial_3 E_3 - \\ - i\,(i_1\,\partial_1 B_1 + i_2\,\partial_2 B_2 + i_3\,\partial_3 B_3)\,, \end{aligned} \tag{49}$$

This expression indicates that both electric and magnetic fields can be represented in unified manner in a biquaternion form.

Then we define quaternion differential operator in the right-hand-side of equation (46) by an extension of the conventional definition of curl

$$\nabla\times A_{qk} = \begin{vmatrix} i & j & k \\ \dfrac{\partial}{\partial x} & \dfrac{\partial}{\partial y} & \dfrac{\partial}{\partial z} \\ A_x & A_y & A_z \end{vmatrix}\,. \tag{50}$$

To become its quaternion counterpart, where i, j, k represents quaternion matrix as described above. This quaternionic extension of curl operator is based on the known relation of multiplication of two arbitrary complex quaternions q and b as follows

$$q\cdot b = q_0 b_0 - \left\langle\vec{q},\vec{b}\right\rangle + \left[\vec{q}\times\vec{b}\right] + q_0\vec{b} + b_0\vec{q}\,, \tag{51}$$

where

$$\left\langle\vec{q},\vec{b}\right\rangle := \sum_{k=1}^{3} q_k\,b_k \in C\,, \tag{52}$$

and

$$\left[\vec{q}\times\vec{b}\right] := \begin{vmatrix} i & j & k \\ q_1 & q_2 & q_3 \\ b_1 & b_2 & b_3 \end{vmatrix}\,. \tag{53}$$

We can note here that there could be more rigorous approach to define such a quaternionic curl operator [10].

In the present paper we only discuss derivation of Maxwell equations in Quaternion Space using the decomposition method described by Gersten [6]. Further extension to Proca equations in Quaternion Space seems possible too using the same method [7], but it will not be discussed here.

In the next section we will discuss some physical implications of this new derivation of Maxwell equations in Quaternion Space.

5 A few implications: de Broglie's wavelength and spin

In the foregoing section we derived a consistent description of Maxwell equations in Q-Space by virtue of Dirac-Gersten's decomposition. Now we discuss some plausible implications of the new proposition.

First, in accordance with Gersten, we submit the viewpoint that the Maxwell equations yield wavefunctions which can be used as guideline for interpretation of Quantum Mechanics [6]. The one-to-one correspondence between classical and quantum wave interpretation actually can be expected not only in the context of Feynman's derivation of Maxwell equations from Lorentz force, but also from known exact correspondence between commutation relation and Poisson bracket [3,5]. Furthermore, the proposed quaternion yields to a novel viewpoint of both the wavelength, as discussed below, and also mechanical model of spin.

The equation (39) implies that momentum and energy could be expressed in quaternion form. Now by introducing de Broglie's wavelength $\lambda_{DB} = \frac{\hbar}{p} \rightarrow p_{DB} = \frac{\hbar}{\lambda}$, then one obtains an expression in terms of wavelength

$$k = (E_k + i\vec{p}_k)\,q_k = (E_k q_k + i\vec{p}_k q_k) = \left(E_k q_k + i\,\frac{\hbar}{\lambda_k^{DB} q_k}\right). \tag{54}$$

In other words, now we can express de Broglie's wavelength in a consistent Q-basis

$$\lambda_{DB-Q} = \frac{\hbar}{\sum_{k=1}^{3}(p_k)\,q_k} = \frac{\hbar}{v_{group}\sum_{k=1}^{3}(m_k)\,q_k}\,, \tag{55}$$

therefore the above equation can be viewed as an extended De Broglie wavelength in Q-space. This equation means that

the mass also can be expressed in Q-basis. In the meantime, a quite similar method to define quaternion mass has also been considered elsewhere, but it has not yet been expressed in Dirac equation form as presented here.

Further implications of this new proposition of quaternion de Broglie requires further study, and therefore it is excluded from the present paper.

6 Concluding remarks

In the present paper we derive a consistent description of Maxwell equations in Q-space. First we consider a simplified method similar to the Feynman's derivation of Maxwell equations from Lorentz force. And then we present another method to derive Maxwell equations by virtue of Dirac decomposition, introduced by Gersten [6].

In accordance with Gersten, we submit the viewpoint that the Maxwell equations yield wavefunctions which can be used as guideline for interpretation of quantum mechanics. The one-to-one correspondence between classical and quantum wave interpretation asserted here actually can be expected not only in the context of Feynman's derivation of Maxwell equations from Lorentz force, but also from known exact correspondence between commutation relation and Poisson bracket [3, 6].

A somewhat unique implication obtained from the above results of Maxwell equations in Quaternion Space, is that it suggests that the De Broglie wavelength will have quaternionic form. Its further implications, however, are beyond the scope of the present paper.

In the present paper we only discuss derivation of Maxwell equations in Quaternion Space using the decomposition method described by Gersten [6]. Further extension to Proca equations in Quaternion Space seems possible too using the same method [7], but it will not be discussed here.

This proposition, however, deserves further theoretical considerations. Further observation is of course recommended in order to refute or verify some implications of this result.

Acknowledgements

One of the authors (VC) wishes to express his gratitude to Profs. A. Yefremov and M. Fil'chenkov for kind hospitality in the Institute of Gravitation and Cosmology, PFUR. Special thanks also to Prof. V. V. Kassandrov for excellent guide to Maxwell equations, and to Prof. Y. P. Rybakov for discussions on the interpretation of de Broglie's wavelength.

Submitted on December 11, 2009 / Accepted on January 02, 2010

References

1. Yefremov A. Quaternions: algebra, geometry and physical theories. *Hypercomplex Numbers in Geometry and Physics*, 2004, v. 1(1), 105; arXiv: mathp-ph/0501055.
2. Smarandache F. and Christianto V. Less mundane explanation of Pioneer anomaly from Q-relativity. *Progress in Physics*, 2007, v. 3, no.1.
3. Hughes R.J. On Feynman's proof of the Maxwell equations. *Am. J. Phys.*, 1991, v. 60(4), 301.
4. Silagadze Z.K. Feynman's derivation of Maxwell equations and extra dimensions. *Annales de la Fondation Louis de Broglie*, 2002, v. 27, no.2, 241.
5. Kauffmann L.H. Non-commutative worlds. arXiv: quant-ph/0403012.
6. Gersten A. Maxwell equations as the one photon quantum equation. *Found. Phys. Lett.*, 1998, v. 12, 291–298.
7. Gondran M. Proca equations derived from first principles. arXiv: quant-ph/0901.3300.
8. Terletsky Y.P., and Rybakov Y.P. Electrodynamics. 2nd. Ed., Vysshaya Skola, Moscow, 1990.
9. Kassandrov V.V. Singular sources of Maxwell fields with self-quantized electric charge. arXiv: physics/0308045.
10. Sabadini I., Struppa D.C. Some open problems on the analysis of Cauchy-Fueter system in several variables. A lecture given at Prof. Kawai's *Workshop Exact WKB Analysis and Fourier Analysis in Complex Domain*.
11. Kravchenko V. Quaternionic equation for electromagnetic fields in inhomogenous media. arXiv: math-ph/0202010.

On Some Novel Ideas in Hadron Physics. Part II

Florentin Smarandache* and Vic Chrisitianto†

*Department of Mathematics, University of New Mexico, Gallup, NM 87301, USA. E-mail: smarand@unm.edu
†Present address: Institute of Gravitation and Cosmology, PFUR, Moscow, 117198, Russia. E-mail: vxianto@yahoo.com

As a continuation of the preceding section, we shortly review a series of novel ideas on the physics of hadrons. In the present paper, emphasis is given on some different approaches to the hadron physics, which may be called as "programs" in the sense of Lakatos. For clarity, we only discuss geometrization program, symmetries/unification program, and phenomenology of inter-quark potential program.

1 Introduction

We begin the present paper by reiterating that given the extent and complexity of hadron and nuclear phenomena, any attempt for an exhaustive review of new ideas is outright unpractical. Therefore in this second part, we limit our short review on a number of scientific programs (in the sense of Lakatos). Others of course may choose different schemes or categorization. The main idea for this scheme of approaches was attributed to an article by Lipkin on hadron physics. accordingly, we describe the approaches as follows:

1. The geometrization approach, which was based on analogy between general relativity as strong field and the hadron physics;
2. Models inspired by (generalization of) symmetry principles;
3. Various composite hadron models;
4. The last section discusses phenomenological approach along with some kind of inter-quark QCD potential.

To reiterate again, the selection of topics is clearly incomplete, and as such it may not necessarily reflect the prevalent opinion of theorists working in this field (for more standard review the reader may wish to see [1]). Here the citation is far from being complete, because we only cite those references which appear to be accessible and also interesting to most readers.

Our intention here is to simply stimulate a healthy exchange of ideas in this active area of research, in particular in the context of discussions concerning possibilities to explore elementary particles beyond the Standard Model (as mentioned in a number of papers in recent years).

2 Geometrization approach

In the preceding section we have discussed a number of hadron or particle models which are essentially based on geometrical theories, for instance Kerr-Schild model or Topological Geometrical Dynamics [1].

However, we can view these models as part of more general approach which can be called "geometrization" program. The rationale of this approach can be summarized as follows (to quote Bruchholz): "The deeper reason is that the standard model is based on Special Relativity while gravitation is the principal item of General Relativity" [2].

Therefore, if we follow this logic, then it should be clear that the Standard Model which is essentially based on Quantum Electrodynamics and Dirac equation, is mostly special relativistic in nature, and it only explains the weak field phenomena (because of its linearity). And if one wishes to extend these theories to explain the physical phenomena corresponding to the strong field effects (like hadrons), then one should consider the nonlinear effects, and therefore one begins to introduce nonlinear Dirac-Hartree-Fock equation or nonlinear Klein-Gordon equation (we mentioned this approach in the preceding section).

Therefore, for instance, if one wishes to include a consistent general relativistic approach as a model of strong fields, then one should consider the general covariant generalization of Dirac equation [3]

$$\left(i\gamma^k(x)\,\overline{\nabla}_k - m\right)\psi(x) = 0\,. \tag{1}$$

Where the gamma matrices are related to the 4-vector relative to General Coordinate Transformations (GCT). Then one can consider the interaction of the Dirac field with a scalar external field U which models a self-consistent quark system field (by virtue of changing $m \to m + U$) [3].

Another worth-mentioning approach in this context has been cited by Bruchholz [2], i.e. the Geilhaupt's theory which is based on some kind of Higgs field from GTR and Quantum Thermodynamics theory.

In this regards, although a book has been written discussing some aspects of the strong field (see Grib et al. [3]), actually this line of thought was recognized not so long ago, as cited in Jackson and Okun [4]: "The close mathematical relation between non-Abelian gauge fields and general relativity as connections in fiber bundles was not generally realized until much later".

Then began the plethora of gauge theories, both including or without gravitational field. The essential part of these GTR-like theories is to start with the group of General Coordinate Transformations (GCT). It is known then that the finite dimensional representations of GCT are characterized by the corresponding ones of the SL(4,R) which belongs to GL(4,R) [5]. In this regards, Ne'eman played the pioneering

role in clarifying some aspects related to double covering of SL(n,R) by GL(n,R), see for instance [6]. It can also be mentioned here that spinor SL(2,C) representation of GTR has been discussed in standard textbooks on General Relativity, see for instance Wald (1983). The SL(2,C) gauge invariance of Weyl is the most well-known, although others may prefer SL(6,C), for instance Abdus Salam et al. [7].

Next we consider how in recent decades the progress of hadron physics was mostly driven by symmetries consideration.

3 Symmetries approach

Perhaps it is not quite an exaggeration to remark here that most subsequent developments in both elementary particle physics and also hadron physics were advanced by Yang-Mills' effort to generalize the gauge invariance [8]. And then Ne'eman and Gell-Mann also described hadrons into octets of SU(3) flavor group.

And therefore, it becomes apparent that there are numerous theories have been developed which intend to generalize further the Yang-Mills theories. We only cite a few of them as follows.

We can note here, for instance, that Yang-Mills field somehow can appear more or less quite naturally if one uses quaternion or hypercomplex numbers as basis. Therefore, it has been proved elsewhere that Yang-Mills field can be shown to appear naturally in Quaternion Space too [8].

Further generalization of Yang-Mills field has been discussed by many authors, therefore we do not wish to reiterate all of them here. Among other things, there are efforts to describe elementary particles (and hadrons) using the most generalized groups, such as E8 or E11, see for instance [9].

Nonetheless, it can be mentioned in this regards, that there are other symmetries which have been considered (beside the SL(6,C) mentioned above), for instance U(12) which has been considered by Ishida and Ishida, as generalizations of SU(6) of Sakata, Gursey et al. [10].

One can note here that Gursey's approach was essentially to extend Wigner's idea to elementary particle physics using SU(2) symmetry. Therefore one can consider that Wigner has played the pioneering role in the use of groups and symmetries in elementary particles physics, although the mathematical aspects have been presented by Weyl and others.

4 Composite model of hadrons

Beside the group and symmetrical approach in Standard Model, composite model of quarks and leptons appear as an equivalent approach, as this method can be traced back to Fermi-Yang in 1949, Sakata in 1956, and of course the Gell-Mann-Ne'eman [10]. Nonetheless, it is well known that at that time quark model was not favorite, compared to the geometrical-unification program, in particular for the reason that the quarks have not been observed.

With regards to quarks, Sakata has considered in 1956 three basic hadrons (proton, neutron, and alphaparticle) and three basic leptons (electron, muon, neutrino). This Nagoya School was quite inuential and the Sakata model was essentially transformed into the quark model of Gell-Mann, though with more abstract interpretation. It is perhaps more interesting to remark here, that Pauling's closed-packed spheron model is also composed of three sub-particles.

The composite models include but not limited to superconductor models inspired by BCS theory and NJL (Nambu-Jona-Lasinio theory). In this context, we can note that there are hadron models as composite bosons, and other models as composite fermions. For instance, hadron models based on BCS theory are essentially composite fermions. In developing his own models of composite hadron, Nambu put forward a scheme for the theory of the strong interactions which was based on and has resemblance with the BCS theory of superconductivity, where free electrons in superconductivity becomes hypothetical fermions with small mass; and energy gap of superconductor becomes observed mass of the nucleon. And in this regards, gauge invariance of superconductivity becomes chiral invariance of the strong interaction. Nambu's theory is essentially non-relativistic.

It is interesting to remark here that although QCD is the correct theory for the strong interactions it cannot be used to compute at all energy and momentum scales. For many purposes, the original idea of Nambu-Jona-Lasinio works better.

Therefore, one may say that the most distinctive aspect between geometrization program to describe hadron models and the composite models (especially Nambu's BCS theory), is that the first approach emphasizes its theoretical correspondence to the General Relativity, metric tensors etc., while the latter emphasizes analogies between hadron physics and the strong field of superconductors [3].

In the preceding section we have mentioned another composite hadron models, for instance the nuclear string and Brightsen cluster model. The relativistic wave equation for the composite models is of course rather complicated (compared to the 1-entity model of particles) [10].

5 Phenomenology with Inter-Quark potential

While nowadays most physicists prefer not to rely on the phenomenology to build theories, it is itself that has has its own virtues, in particular in studying hadron physics. It is known that theories of electromagnetic fields and gravitation are mostly driven by some kind of geometrical principles. But to describe hadrons, one does not have much choices except to take a look at experiments data before begin to start theorizing, this is perhaps what Gell-Mann meant while emphasizing that physicists should sail between Scylla and Charybdis. Therefore one can observe that hadron physics are from the beginning affected by the plentitude of analogies with human senses, just to mention a few: strangeness, flavor and colour.

In other words one may say that hadron physics are more or less phenomenology-driven, and symmetries consideration comes next in order to explain the observed particles zoo.

The plethora of the aforementioned theories actually boiled down to either relativistic wave equation (Klein-Gordon) or non-relativistic wave equation, along with some kind of inter-quark potential. The standard picture of course will use the QCD linear potential, which can be derived from Maxwell equations.

But beside this QCD linear potential, there are other types of potentials which have been considered in the literature, to mention a few of them:

a. Trigononometric Rosen-Morse potential [11]

$$v_t(|z|) = -2b\cot|z| + a(a+1)^2\csc|z|\,, \qquad (2)$$

where $z = \frac{r}{d}$;

b. PT-Symmetric periodic potential [12];

c. An Interquark qq-potential from Yang-Mills theory has been considered in [13];

d. An alternative PT-Symmetric periodic potential has been derived from radial biquaternion Klein-Gordon equation [14]. Interestingly, we can note here that a recent report by Takahashi et al. indicates that periodic potential could explain better the cluster deuterium reaction in Pd/PdO/ZrO2 nanocomposite-samples in a joint research by Kobe University in 2008. This experiment in turn can be compared to a previous excellent result by Arata-Zhang in 2008 [15]. What is more interesting here is that their experiment also indicates a drastic mesoscopic effect of D(H) absorption by the Pd-nanocomposite-samples.

Of course, there is other type of interquark potentials which have not been mentioned here.

6 Concluding note

We extend a bit the preceding section by considering a number of approaches in the context of hadron theories. In a sense, they are reminiscent of the plethora of formulations that have been developed over the years on classical gravitation: many seemingly disparate approaches can be effectively used to describe and explore the same physics.

It can be expected that those different approaches of hadron physics will be advanced further, in particular in the context of possibility of going beyond Standard Model.

Acknowledgements

One of the authors (VC) wishes to express his gratitude to Profs. A. Yefremov and M. Fil'chenkov for kind hospitality in the Institute of Gravitation and Cosmology, PFUR. Special thanks to Prof. A. Takahashi for discussion of his experimental results of Pd lattice with his team.

Submitted on December 10, 2009 / Accepted on January 01, 2010

References

1. Georgi H. Effective field theory, HUTP-93/A003. *Ann. Rev. Nucl. and Particle Sci.*, 1993, v.43.
2. Bruchholz U.E. Key notes on a Geometric Theory of Fields. *Progress in Physics*, 2009, v.2, 107.
3. Grib A., et al. Quantum vacuum effects in strong fields. Friedmann Lab. Publishing, St. Petersburg, 1994, pp.24–25.
4. Jackson J.D. and Okun L.B. Historical roots of gauge invariance. *Rev. Mod. Phys.*, 2001, v.73, 676–677.
5. Sijacki D.J. World spinors revisited. *Acta Phys. Polonica B*, 1998, v.29, no.4, 1089–1090.
6. Ne'eman Y. Gravitational interactions of hadrons: band spinor representations of GL(n,R). *Proc. Natl. Acad. Sci. USA*, 1977, v.74, no.10, 4157-4159.
7. Isham C.J., Salam A., and Strathdee J. SL(6,C) gauge invariance of Einstein-like Lagrangians. Preprint ICTP no.IC/72/123, 1972.
8. Chýla J. From Hermann Weyl to Yang and Mills to Quantum Chromodynamics. *Nucl. Phys. A*, 2005, v.749, 23–32.
9. Lisi A.G. An exceptionally simple theory of everything. arXiv: hep-th/0711.0770.
10. Ishida S. and Ishida M. U(12): a new symmetry possibly realizing in hadron spectroscopy. arXiv: hep-ph/0203145.
11. Compean C. and Kirchbach M. Trigonometric quark confinement potential of QCD traits. arXiv: hep-ph/0708.2521; nucl-th/0610001, quant-ph/0509055.
12. Shalaby A.M. arXiv: hep-th/0712.2521.
13. Zarembo K. arXiv: hep-th/9806150.
14. Christianto V. and Smarandache F. Numerical solution of radial biquaternion Klein-Gordon equation. *Progress in Physics*, 2008, v.1.
15. Takahashi A., et al. Deuterium gas charging experiments with Pd powders for excess heat evolution: discussion of experimental result. Abstract to JCF9, 2009.

Lunar Laser-Ranging Detection of Light-Speed Anisotropy and Gravitational Waves

Reginald T. Cahill

School of Chemical and Physical Sciences, Flinders University, Adelaide 5001, Australia
E-mail: Reg.Cahill@flinders.edu.au

The Apache Point Lunar Laser-ranging Operation (APOLLO), in NM, can detect photon bounces from retroreflectors on the moon surface to 0.1ns timing resolution. This facility enables not only the detection of light speed anisotropy, which defines a local preferred frame of reference — only in that frame is the speed of light isotropic, but also fluctuations/turbulence (gravitational waves) in the flow of the dynamical 3-space relative to local systems/observers. So the APOLLO facility can act as an effective "gravitational wave" detector. A recently published small data set from November 5, 2007, is analysed to characterise both the average anisotropy velocity and the wave/turbulence effects. The results are consistent with some 13 previous detections, with the last and most accurate being from the spacecraft earth-flyby Doppler-shift NASA data.

1 Introduction

Light speed anisotropy has been repeatedly detected over more than 120 years, beginning with the Michelson-Morley experiment in 1887 [1]. Contrary to the usual claims, that experiment gave a positive result, and not a null result, and when the data was first analysed, in 2002, using a proper calibration theory for the detector [2, 3] an anisotropy speed, projected onto the plane of the gas-mode interferometer, in excess of 300 km/s was obtained. The problem was that Michelson had used Newtonian physics to calibrate the interferometer. When the effects of a gas in the light path and Lorentz contraction of the arms are taken into account the instrument turns out to be nearly 2000 times less sensitive that Michelson had assumed. In vacuum-mode the Michelson interferometer is totally insensitive to light speed anisotropy, which is why vacuum-mode resonant cavity experiments give a true null result [4]. These experiments demonstrate, in conjunction with the various non-null experiments, that the Lorentz contraction is a real contraction of physical objects, not that light speed is invariant. The anisotropy results of Michelson and Morley have been replicated in numerous experiments [5–15], using a variety of different experimental techniques. The most comprehensive early experiment was by Miller [5], and the direction of the anisotropy velocity obtained via his gas-mode Michelson interferometer has been recently confirmed, to within 5°, using [15] spacecraft earth-flyby Doppler shift data [16]. The same result is obtained using the range data — from spacecraft bounce times.

It is usually argued that light speed anisotropy would be in conflict with the successes of Special Relativity (SR), which supposedly is based upon the invariance of speed of light. However this claim is false because in SR the space and time coordinates are explicitly chosen to make the speed of light invariant wrt these coordinates. In a more natural choice of space and time coordinates the speed of light is anisotropic, as discussed in [18]. Therein the new exact mapping between the Einstein-Minkowski coordinates and the natural space and time coordinates is given. So, rather than being in conflict with SR, the anisotropy experiments have revealed a deeper explanation for SR effects, namely physical consequences of the motion of quantum matter/radiation wrt a structured and dynamical 3-space. In 1890 Hertz [17] gave the form for the Maxwell equations for observers in motion wrt the 3-space, using the more-natural choice of space and time coordinates [18]. Other laboratory experimental techniques are being developed, such as the use of a Fresnel-drag anomaly in RF coaxial cables, see Fig. 6e in [15]. These experimental results, and others, have lead to a new theory of space, and consequently of gravity, namely that space is an observable system with a known and tested dynamical theory, and with gravity an emergent effect from the refraction of quantum matter and EM waves in an inhomogeneous and time-varying 3-space velocity field [19, 20]. As well all of these experiments show fluctuation effects, that is, the speed and direction of the anisotropy fluctuates over time [15, 20] — a form of turbulence. These are "gravitational waves", and are very much larger than expected from General Relativity (GR). The observational data [15] determines that the solar system is in motion through a dynamical 3-space at an average speed of some 486 km/s in the direction RA = 4.29^{h}, Dec = $-75°$, essentially known since Miller's extraordinary experiments in 1925/26 atop Mount Wilson. This is the motion of the solar system wrt a detected local preferred frame of reference (FoR) — an actual dynamical and structured system. This FoR is different to and unrelated to the FoR defined by the CMB radiation dipole, see [15].

Here we report an analysis of photon travel time data from the Apache Point Lunar Laser-ranging Operation (APOLLO) facility, Murphy *et al.* [21], for photon bounces from retroreflectors on the moon. This experiment is very similar to the spacecraft Doppler shift observations, and the results are con-

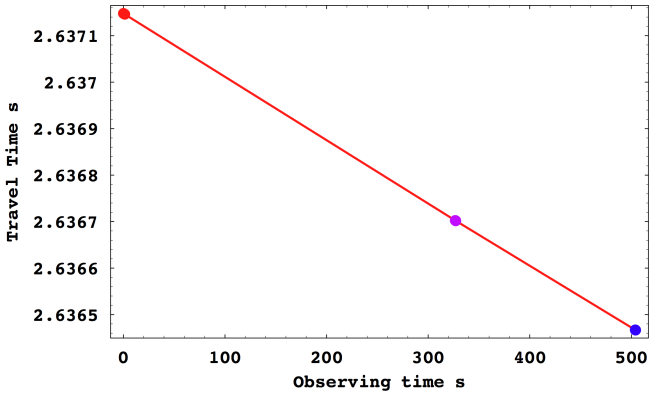

Fig. 1: Total photon travel times, in seconds, for moon bounces from APO, November 5, 2007, plotted against observing time, in seconds, after 1st shot at UTC = 0.5444 hrs. Shots 1–5 shown as 1st data point (size of graphic point unrelated to variation in travel time within each group of shots, typically ±20 ns as shown in Fig. 2, shots 1100-1104 shown as middle point, and shots 2642–2636 shown in last graphic point. Data from Murphy [21], and tabulated in Gezari [22] (Table 1 therein). Straight line reveals linear time variation of bounce time vs observer time, over the observing period of some 500 s. Data reveals that distance travelled decreased by 204 m over that 500 s, caused mainly by rotation of earth. Data from shots 1000–1004 not used due to possible misprints in [22]. Expanded data points, after removal of linear trend, and with false zero for 1st shot in each group, are shown in Fig. 2. The timing resolution for each shot is 0.1 ns.

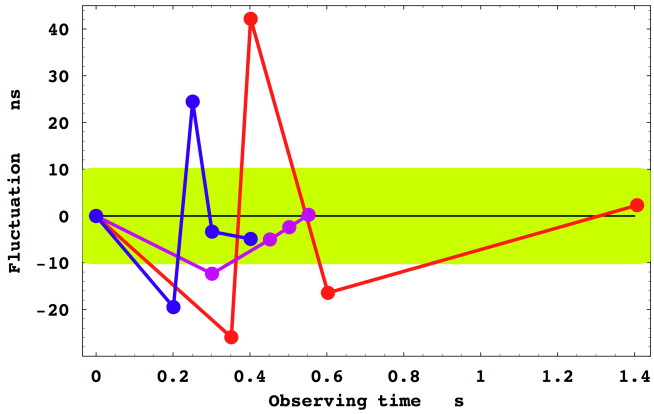

Fig. 2: Fluctuations in bounce time, in ns, within each group of shots, shown as one data point in Fig. 1, and plotted against time, in s, from time of 1st bounce in each group, and after removing the best-fit linear drift in each group, essentially the straight line in Fig. 1. The fluctuations are some ±20 ns. Shaded region shows fluctuation range expected from dynamical 3-space and using spacecraft earth-flyby Doppler-shift NASA data [16] for 3-space velocity [15], and using a fluctuation in RA angle of, for example, 3.4° and a 3-space speed of 490 km/s. Fluctuations in only speed or declination of 3-space produce no measureable effect, because of orientation of 3-space flow velocity to APO-moon direction during these shots. These fluctuations suggest turbulence or wave effects in the 3-space flow. These are essentially "gravitational waves", and have been detected repeatedly since the Michelson-Morley experiment in 1887; see [20] for plots of that fringe shift data.

sistent with the anisotropy results from the above mentioned experiments, though some subtleties are involved, and also the presence of turbulence/ fluctuation effects are evident.

2 APOLLO lunar ranging data

Light pulses are launched from the APOLLO facility, using the 3.5-meter telescope at Apache Point Observatory (APO), NM. The pulses are reflected by the AP15RR retroreflector, placed on the moon surface during the Apollo 15 mission, and detected with a time resolution of 0.1 ns at the APOLLO facility. The APOLLO facility is designed to study fundamental physics. Recently Gezari [22] has published some bounce-time* data, and performed an analysis of that data. The analysis and results herein are different from those in [22], as are the conclusions. The data is the bounce time recorded from 2036 bounces, beginning at UTC = 0.54444 hrs and ending at UTC = 0.55028 hrs on November 5, 2007†. Only a small subset of the data from these 2036 bounces is reported in [22], and the bounce times for 15 bounces are shown in Fig. 1, and grouped into 3 bunches‡. The bounce times, at the plot time resolution, show a linear time variation of bounce time vs observer time, presumably mainly caused by changing distance between APO and retroreflector, which is seen to be decreasing over time of observation. Herein we consider only these bounce times, and not the distance modellings, which are based on the assumption that the speed of light is invariant, and so at best are pseudo-ranges.

Of course one would also expect that the travel times would be affected by the changing orientation of the APO-moon photon propagation directions wrt the light speed anisotropy direction. However a bizarre accident of date and timing occurred during these observations. The direction of the light-speed anisotropy on November 5 may be estimated from the spacecraft earth-flyby analysis, and from Fig. 11 of [15] we obtain RA=6.0^h, Dec=−76°, and with a speed ≈490 km/s. And during these APOLLO observations the direction of the photon trajectories was RA=11^{h}40′, Dec=0°3′. Remarkably these two directions are almost at right angles to each other (88.8°), and then the speed of 490 km/s has a projection onto the photon directions of a mere v_p = 11 km/s.

From the bounce times, alone, it is not possible to extract the anisotropy velocity vector, as the actual distance to the retroreflector is not known. To do that a detailed modelling of the moon orbit is required, but one in which the invariance of the light speed is not assumed. In the spacecraft earth-flyby Doppler shift analysis a similar problem arose, and the resolution is discussed in [15] and [16], and there the asymptotic velocity of motion, wrt the earth, of the spacecraft changed

*Total travel time to moon and back.

†The year of the data is not given in [22], but only in 2007 is the moon in the position reported therein at these UTC times.

‡An additional 5 shots (shot #1000-1004) are reported in [22] — but appear to have identical launch and travel times, and so are not used herein.

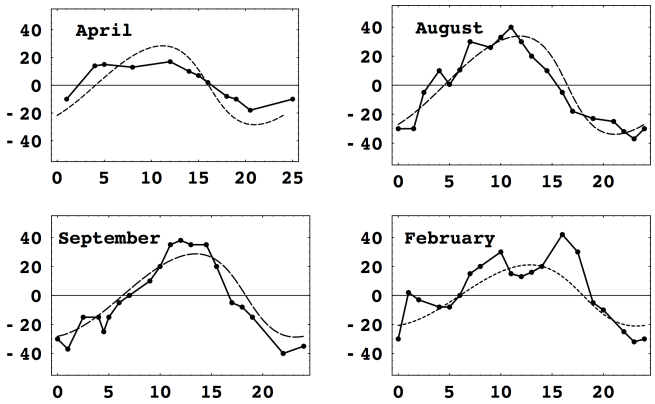

Fig. 3: Azimuth, in degrees, of 3-space flow velocity vs local sidereal time, in hrs, detected by Miller [5] using a gas-mode Michelson interferometer atop Mt Wilson in 1925/26. Each composite day is a collection of results from various days in each indicated month. In August, for example, the RA for the flow being NS (zero azimuth — here measured from S) is ≈5 hrs and ≈17 hrs. The dotted curves show expected results for the RA, determined in [19], for each of these months — these vary due to changing direction of orbital speed of earth and of sun-inflow speed, relative to cosmic speed of solar system, but without wave effects..The data shows considerable fluctuations, at the time resolution of these observations (≈1 hr). These fluctuations are larger than the errors, given as ±2.5° in [5].

from before to after the flyby, and as well there were various spacecraft with different orbits, and so light-speed anisotropy directional effects could be extracted.

3 Bounce-time data analysis

Herein an analysis of the bounce-time data is carried out to try and characterise the light speed anisotropy velocity. If the 3-space flow-velocity vector has projection v_p onto the photon directions, then the round-trip travel time, between co-moving source/reflector/detector system, shows a 2nd order effect in v_p/c, see Appendix,

$$t = \frac{2L}{c} + \frac{L}{c}\frac{v_p^2}{c^2} + \dots \qquad (1)$$

where L is the actual 3-space distance travelled. The last term is the change in net travel time if the photons have speed $c \pm v_p$, relative to the moving system. There is also a 1st order effect in v_p/c caused by the relative motion of the APO site and the retroreflector, but this is insignificant, again because of the special orientation circumstance. These effects are partially hidden by moon orbit modelling if the invariance of light speed is assumed in that modelling. To observe these v_p effects one would need to model the moon orbit taking into account the various gravity effects, and then observing anomalies in net travel times over numerous orientations of the APO-moon direction, and sampled over a year of observations. However a more subtle effect is used now to extract some characteristaion of the anisotropy velocity. In Fig. 2 we have extracted the travel time variations within each group of 5 shots, by removing a linear drift term, and also using a false zero. We see that the net residual travel times fluctuate by some ±20 ns. Such fluctuations are expected, because of the 3-space wave/turbulence effects that have been detected many times, although typically with much longer resolution times. These fluctuations arise from changes in the 3-space velocity, which means fluctuations in the speed, RA and Dec. Changes in speed and declination happen to produce insignificant effects for the present data, because of the special orientation situation noted above, but changes in RA do produce an effect. In Fig. 2 the shaded region shows the variations of 20 ns (plotted as ±10ns because of false zero) caused by a actual change in RA direction of +3.4°. This assumes a 3-space speed of 490 km/s. Fig. 3 shows fluctuations in RA in the anisotropy vector from the Miller experiment [5]. We see fluctuations of some ±2 hrs in RA (≡ ±7.3° at Dec =−76°), observed with a timing resolution of an hour or so. Other experiments show similar variations in RA from day to day, see Fig. 6 in [15], so the actual RA of 6^h in November is not steady, from day to day, and the expected APOLLO time fluctuations are very sensitive to the RA. A fluctuation of +3° is not unexpected, even over 3 s. So this fluctuation analysis appear to confirm the anisotropy velocity extracted from the earth-flyby Doppler-shift NASA data. However anisotropy observations have never been made over time intervals of the order of 1sec, as in Fig. 2, although the new 1st order in v_p/c coaxial cable RF gravitational wave detector detector under construction can collect data at that resolution.

4 Conclusions

The APOLLO lunar laser-ranging facility offers significant potential for observing not only the light speed anisotropy effect, which has been detected repeatedly since 1887, with the best results from the spacecraft earth-flyby Doppler-shift NASA data, but also wave/turbulence effects that have also been repeatedly detected, as has been recently reported, and which are usually known as "gravitational waves"*. These wave effects are much larger than those putatively suggested within GR. Both the anisotropy effect and its fluctuations show that a dynamical and structured 3-space exists, but which has been missed because of two accidents in the development of physics, (i) that the Michelson interferometer is very insensitive to light speed anisotropy, and so the original small fringe shifts were incorrectly taken as a "null effect", (ii) this in turn lead to the development of the 1905 Special Relativity formalism, in which the speed of light was forced to be invariant, by a peculiar choice of space and time coordinates, which together formed the spacetime construct. Maxwell's EM equations use these coordinates, but Hertz as early as 1890 gave the more transparent form which use more

*It may be shown that a dynamical 3-space velocity field may be mapped into a non-flat spacetime metric $g_{\mu\nu}$ formalism, in that both produce the same matter acceleration, but that metric does not satisfy the GR equations [19,20]

natural space and time coordinates, and which explicitly takes account of the light-speed anisotropy effect, which was of course unknown, experimentally, to Hertz. Hertz had been merely resolving the puzzle as to why Maxwell's equations did not specify a preferred frame of reference effect when computing the speed of light relative to an observer. In the analysis of the small data set from APOLLO from November 5, 2007, the APO-moon photon direction just happened to be at 90° to the 3-space velocity vector, but in any case determination, in general, by APOLLO of that velocity requires subtle and detailed modelling of the moon orbit, taking account of the light speed anisotropy. Then bounce-time data over a year will show anomalies, because the light speed anisotropy vector changes due to motion of the earth about the sun, as 1st detected by Miller in 1925/26, and called the "apex aberration" by Miller, see [15]. An analogous technique resolved the earth-flyby spacecraft Doppler-shift anomaly [16]. Nevertheless the magnitude of the bounce-time fluctuations can be explained by changes in the RA direction of some 3.4°, but only if the light speed anisotropy speed is some 490 km/s. So this is an indirect confirmation of that speed. Using the APOLLO facility as a gravitational wave detector would not only confirm previous detections, but also provide time resolutions down to a few seconds, as the total travel time of some 2.64 s averages the fluctuations over that time interval. Comparable time resolutions will be possible using a laboratory RF coaxial cable wave/turbulence detector, for which a prototype has already been successfully operated. Vacuum-mode laboratory Michelson interferometers are of course insensitive to both the light speed anisotropy effect and its fluctuations, because of a subtle cancellation effect — essentially a design flaw in the interferometer, which fortunately Michelson, Miller and others avoided by using the detector in gas-mode (air) but without that understanding.

Appendix

Fig. 4 shows co-moving Earth-Moon-Earth photon bounce trajectories in reference frame of 3-space. Define $t_{AB} = t_B - t_A$ and $t_{BC} = t_C - t_B$. The distance AB is vt_{AB} and distance BC is vt_{BC}. Total photon-pulse travel time is $t_{AC} = t_{AB} + t_{BC}$. Applying the cosine theorem to triangles ABB′ and CBB′ we obtain

$$t_{AB} = \frac{vL\cos(\theta) + \sqrt{v^2L^2\cos^2(\theta) + L^2(c^2 - v^2)}}{(c^2 - v^2)}\,, \qquad (2)$$

$$t_{BC} = \frac{-vL\cos(\theta) + \sqrt{v^2L^2\cos^2(\theta) + L^2(c^2 - v^2)}}{(c^2 - v^2)}\,. \qquad (3)$$

Then to $O(v^2/c^2)$

$$t_{AC} = \frac{2L}{c} + \frac{Lv^2(1 + \cos^2(\theta))}{c^3} + \dots \qquad (4)$$

However the travel times are measured by a clock, located at the APO, travelling at speed v wrt the 3-space, and so undergoes a clock-slowdown effect. So t_{AC} in (4) must be reduced by the factor

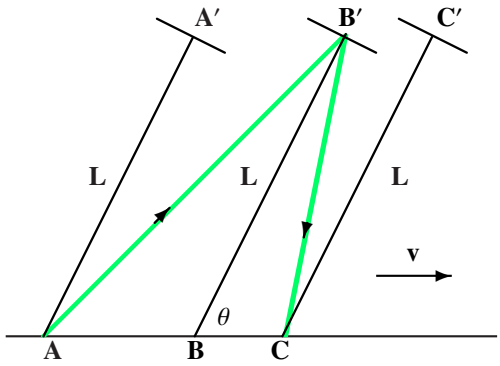

Fig. 4: Co-moving Earth-Moon-Earth photon bounce trajectories in reference frame of 3-space, so speed of light is c in this frame. Earth (APO) and Moon (retroreflector) here taken to have common velocity $\mathbf{v}$ wrt 3-space. When APO is at locations A,B,C, at times $t_A, t_B, t_C, \dots$ the moon retroreflector is at corresponding locations A′, B′, C′, … at same respective times $t_A, t_B, t_C, \dots$ Earth-Moon separation distance L, at same times, has angle θ wrt velocity $\mathbf{v}$, and shown at three successive times: (i) when photon pulse leaves APO at A (ii) when photon pulse is reflected at retroreflector at B′, and (iii) when photon pulse returns to APO at C.

$\sqrt{1 - v^2/c^2}$, giving

$$t_{AC} = \frac{2L}{c} + \frac{Lv^2\cos^2(\theta)}{c^3} + \dots = \frac{2L}{c} + \frac{Lv_P^2}{c^3} + \dots \qquad (5)$$

where v_P is the velocity projected onto L. Note that there is no Lorentz contraction of the distance L. However if there was a solid rod separating AA′ etc, as in one arm of a Michelson interferometer, then there would be a Lorentz contraction of that rod, and in the above we need to make the replacement $L \to L\sqrt{1 - v^2\cos^2(\theta)/c^2}$, giving $t_{AC} = 2L/c$ to $O(v^2/c^2)$. And then there is no dependence of the travel time on orientation or speed v to $O(v^2/c^2)$.

Applying the above to a laboratory vacuum-mode Michelson interferometer, as in [4], implies that it is unable to detect light-speed anisotropy because of this design flaw. The "null" results from such devices are usually incorrectly reported as proof of the invariance of the speed of light in vacuum. This design flaw can be overcome by using a gas or other dielectric in the light paths, as first reported in 2002 [2].

Submitted on January 14, 2010 / Accepted on January 25, 2010

References

1. Michelson A.A. and Morley E.W. *Am. J. Sc.*, 1887, v.34, 333–345.
2. Cahill R.T. and Kitto K. Michelson-Morley experiments revisited. *Apeiron*, 2003, v.10(2), 104–117.
3. Cahill R.T. The Michelson and Morley 1887 experiment and the discovery of absolute motion. *Progress in Physics*, 2005, v.3, 25–29.
4. Braxmaier C. *et al. Phys. Rev. Lett.*, 2002, v.88, 010401; Müller H. *et al. Phys. Rev. D*, 2003, v.68, 116006-1-17; Müller H. *et al. Phys. Rev. D*, 2003, v.67, 056006; Wolf P. *et al. Phys. Rev. D*, 2004, v.70, 051902-1-4; Wolf P. *et al. Phys. Rev. Lett.*, 2003, v.90, no.6, 060402; Lipa J.A., *et al. Phys. Rev. Lett.*, 2003, v.90, 060403; Eisele Ch. *et al. Phys. Rev. Lett.*, 2009, v.103, 090401.
5. Miller D.C. *Rev. Mod. Phys.*, 1933, v.5, 203–242.
6. Illingworth K.K. *Phys. Rev.*, 1927, v.3, 692–696.

7. Joos G. *Ann. d. Physik*, 1930, v.7, 385.
8. Jaseja T.S. *et al. Phys. Rev. A*, 1964, v.133, 1221.
9. Torr D.G. and Kolen P. In *Precision Measurements and Fundamental Constants*, Taylor B.N. and Phillips W.D. eds., Natl. Bur. Stand. (U.S.), Special Publ., 1984, 617 and 675.
10. Krisher T.P., Maleki L., Lutes G.F., Primas L.E., Logan R.T., Anderson J.D. and Will C.M. Test of the isotropy of the one-way speed of light using hydrogen-maser frequency standards. *Phys. Rev. D*, 1990, v.42, 731–734.
11. Cahill R.T. The Roland DeWitte 1991 experiment. *Progress in Physics*, 2006, v.3, 60–65.
12. Cahill R.T. A new light-speed anisotropy experiment: absolute motion and gravitational waves detected. *Progress in Physics*, 2006, v.4, 73–92.
13. Munéra H.A., *et al.* In *Proceedings of SPIE*, 2007, v.6664, K1–K8, eds. Roychoudhuri C. *et al.*
14. Cahill R.T. Resolving spacecraft Earth-flyby anomalies with measured light speed anisotropy. *Progress in Physics*, 2008, v.4, 9–15.
15. Cahill R.T. Combining NASA/JPL one-way optical-fiber light-speed data with spacecraft Earth-flyby Doppler-shift data to characterise 3-space flow. *Progress in Physics*, 2009, v.4, 50–64.
16. Anderson J.D., Campbell J.K., Ekelund J.E., Ellis J. and Jordan J.F. Anomalous orbital-energy changes observed during spaceraft flybys of Earth. *Phys. Rev. Lett.*, 2008, v.100, 091102.
17. Hertz H. On the fundamental equations of electro-magnetics for bodies in motion. *Wiedemann's Ann.*, 1890, v.41, 369; also in: *Electric Waves, Collection of Scientific Papers*, *Dover Publ.*, New York, 1962.
18. Cahill R.T. Unravelling Lorentz covariance and the spacetime formalsim. *Progress in Physics*, 2008, v.4, 19–24.
19. Cahill R.T. Process physics: from information theory to quantum space and matter. Nova Science Publ., New York, 2005.
20. Cahill R.T. Dynamical 3-space: a review. In: *Ether Space-Time and Cosmology: New Insights into a Key Physical Medium*, Duffy M. and Lévy J., eds., Apeiron, 2009, p.135–200.
21. Murphy T.W. Jr., Adelberger E.G., Battat J.B.R., Carey L.N., Hoyle C.D., LeBlanc P., Michelsen E.L., Nordtvedt K., Orin A.E., Strasburg J.D., Stubbs C.W., Swanson H.E. and Williiams E. APOLLO: the Apache Point Observatory Lunar laser-ranging operation: instrument description and first detections. *Publ. Astron. Soc. Pac.*, 2008, v.120, 20–37.
22. Gezari D.Y. Lunar laser ranging test of the invariance of c. arXiv: 0912.3934.

Fundamental Elements and Interactions of Nature: A Classical Unification Theory

Tianxi Zhang

Department of Physics, Alabama A & M University, Normal, Alabama, USA. E-mail: tianxi.zhang@aamu.edu

A classical unification theory that completely unifies all the fundamental interactions of nature is developed. First, the nature is suggested to be composed of the following four fundamental elements: mass, radiation, electric charge, and color charge. All known types of matter or particles are a combination of one or more of the four fundamental elements. Photons are radiation; neutrons have only mass; protons have both mass and electric charge; and quarks contain mass, electric charge, and color charge. The nature fundamental interactions are interactions among these nature fundamental elements. Mass and radiation are two forms of real energy. Electric and color charges are considered as two forms of imaginary energy. All the fundamental interactions of nature are therefore unified as a single interaction between complex energies. The interaction between real energies is the gravitational force, which has three types: mass-mass, mass-radiation, and radiation-radiation interactions. Calculating the work done by the mass-radiation interaction on a photon derives the Einsteinian gravitational redshift. Calculating the work done on a photon by the radiation-radiation interaction derives a radiation redshift, which is much smaller than the gravitational redshift. The interaction between imaginary energies is the electromagnetic (between electric charges), weak (between electric and color charges), and strong (between color charges) interactions. In addition, we have four imaginary forces between real and imaginary energies, which are mass-electric charge, radiation-electric charge, mass-color charge, and radiation-color charge interactions. Among the four fundamental elements, there are ten (six real and four imaginary) fundamental interactions. This classical unification theory deepens our understanding of the nature fundamental elements and interactions, develops a new concept of imaginary energy for electric and color charges, and provides a possible source of energy for the origin of the universe from nothing to the real world.

1 Introduction

In the ancient times, the nature was ever considered to have five elements: space, wind, water, fire, and earth. In traditional Chinese Wu Xing (or five-element) theory, the space and wind are replaced by metal and wood. All the natural phenomena are described by the interactions of the five elements. There are two cycles of balances: generating (or sheng in Chinese) and overcoming (or ke in Chinese) cycles. The generating cycle includes that wood feeds fire, fire creates earth (or ash), earth bears metal, metal carries water, and water nourishes wood; while the overcoming cycle includes that wood parts earth, earth absorbs water, water quenches fire, fire melts metal, and metal chops wood.

According to the modern scientific view, how many elements does the nature have? How do these fundamental elements interact with each other? It is well known that there have been four fundamental interactions found in the nature. They are the gravitational, electromagnetic, weak, and strong interactions. The gravitational interaction is an interaction between masses. The electromagnetic interaction is an interaction between electric charges. The strong interaction is an interaction between color charges. What is the weak interaction? Elementary particles are usually classified into two categories: hadrons and leptons. Hadrons participate in both strong and weak interactions, but leptons can only participate in the weak interaction. If the weak interaction is an interaction between weak charges, what is the weak charge? How many types of weak changes? Are the weak charges in hadrons different from those in leptons? Do we really need weak charges for the weak interaction? All of these are still unclear although the weak interaction has been extensively investigated for many decades. Some studies of particular particles show that the weak charges might be proportional to electric charges.

In this paper, we suggest that the nature has four fundamental elements, which are: mass M, radiation γ, electric charge Q, and color charge C. Any type of matter or particle contains one or more of these four elements. For instances, a neutron has mass only; a photon is just a type of radiation, which is massless; a proton contains both mass and electric charge; and a quark combines mass, electric charge, and color charge together. Mass and radiation are well understood as two forms of real energy. Electric charge is a property of some elementary particles such as electrons and protons and has two varieties: positive and negative. Color charge is a property of quarks, which are sub-particles of hadrons, and has three varieties: red, green, and blue. The nature funda-

mental interactions are the forces among these fundamental elements. The weak interaction is considered as an interaction between color charges and electric charges.

Recently, Zhang has considered the electric charge to be a form of imaginary energy [1]. With this consideration, the energy of an electrically charged particle is a complex number. The real part is proportional to the mass as the Einsteinian mass-energy expression represents, while the imaginary part is proportional to the electric charge. The energy of an antiparticle is given by conjugating the energy of its corresponding particle. Newton's law of gravity and Coulomb's law of electric force were classically unified into a single expression of the interaction between the complex energies of two electrically charged particles. Interaction between real energies (including both mass and radiation) is the gravitational force, which has three types: mass-mass, mass-radiation, and radiation-radiation interactions. Calculating the work done by the mass-radiation interaction on a photon, we derived the Einsteinian gravitational redshift. Calculating the work done by the radiation-radiation interaction on a photon, we obtained a radiation redshift, which is negligible in comparison with the gravitational redshift. Interaction between imaginary energies (or between electric charges) is the electromagnetic force.

In this study, we further consider the color charge to be another form of imaginary energy. Therefore, the nature is a system of complex energy and the four fundamental elements of nature are described as a complex energy. The real part includes the mass and radiation, while the imaginary part includes the electric and color charges. All the fundamental interactions can be classically unified into a single interaction between complex energies. The interaction between real energies is gravitational interaction. By including the massless radiation, we have three types of gravitational forces. The interaction between imaginary energies are electromagnetic (between electric charges), weak (between electric and color charges), and strong (between color charges) interactions. In addition, we have four types of imaginary forces (between real and imaginary energies): mass-electric charge interaction, radiation-electric charge interaction, mass-color charge interaction, and radiation-color charge interaction. Among the four fundamental elements, we have in total ten (six real and four imaginary) fundamental interactions.

2 Fundamental elements of Nature

2.1 Mass — a form of real energy

It is well known that mass is a fundamental property of matter, which directly determines the gravitational interaction via Newton's law of gravity [2]. Mass M is a quantity of matter [3], and the inertia of motion is solely dependent upon mass [4]. A body experiences an inertial force when it accelerates relative to the center of mass of the entire universe. In short, mass there affects inertia here.

According to Einstein's energy-mass expression (or Einstein's first law) [5], mass is also understood as a form of real energy. A rest object or particle with mass M has real energy given by

$$E^M = Mc^2, \tag{1}$$

where c is the speed of light. The real energy is always positive. It cannot be destroyed or created but can be transferred from one form to another.

2.2 Radiation — a form of real energy

Radiation γ refers to the electromagnetic radiation (or light). In the quantum physics, radiation is described as radiation photons, which are massless quanta of real energy [6]. The energy of a photon is given by

$$E^\gamma = h\nu, \tag{2}$$

where $h = 6.6{\times}10^{-34}$ J·s is the Planck constant [7] and ν is the radiation frequency from low frequency (e.g., 10^3 Hz) radio waves to high frequency (e.g., 10^{20} Hz) γ-rays. Therefore, we can generally say that the radiation is also a form of real energy.

2.3 Electric charge — a form of imaginary energy

Electric charge is another fundamental property of matter, which directly determines the electromagnetic interaction via Coulomb's law of electric force [8], which is generalized to the Lorentz force expression for moving charged particles. Electric charge has two varieties of either positive or negative. It appears or is observed always in association with mass to form positive or negative electrically charged particles with different amount of masses. The interaction between electric charges, however, is completely independent of mass. Positive and negative charges can annihilate or cancel each other and produce in pair with the total electric charges conserved. Therefore, electric charge should have its own meaning of physics.

Recently, Zhang has considered the electric charge Q to be a form of imaginary energy [1]. The amount of imaginary energy is defined as

$$E^Q = \frac{Q}{\sqrt{G}}c^2, \tag{3}$$

where G is the gravitational constant. The imaginary energy has the same sign as the electric charge. Then, for an electrically charged particle, the total energy is

$$E = E^M + iE^Q = (1 + i\alpha)Mc^2. \tag{4}$$

Here, $i = \sqrt{-1}$ is the imaginary number, α is the charge-mass ratio defined by

$$\alpha = \frac{Q}{\sqrt{G}M}, \tag{5}$$

in the cgs unit system. Including the electric charge, we have modified Einstein's first law Eq. (1) into Eq. (4). In other words, electric charge is represented as an imaginary mass. For an electrically charged particle, the absolute value of α is a big number. For instance, proton's α is about 10^{18} and electron's α is about -2×10^{21}. Therefore, an electrically charged particle holds a large amount of imaginary energy in comparison with its real or rest energy. A neutral particle such as a neutron, photon, or neutrino has only a real energy. Weinberg suggested that electric charges come from the fifth-dimension [9], a compact circle space in the Kaluza-Klein theory [10–12]. Zhang has shown that electric charge can affect light and gravity [13].

The energy of an antiparticle [14, 15] is naturally obtained by conjugating the energy of the corresponding particle [1]

$$E^* = \left(E^M + iE^Q\right)^* = E^M - iE^Q. \tag{6}$$

The only difference between a particle and its corresponding antiparticle is that their imaginary energies (thus their electric charges) have opposite signs. A particle and its antiparticle have the same real energy but have the sign-opposite imaginary energy. In a particle-antiparticle annihilation process, their real energies completely transfer into radiation photon energies and their imaginary energies annihilate or cancel each other. Since there are no masses to adhere, the electric charges come together due to the electric attraction and cancel each other (or form a positive-negative electric charge pair $(+,-)$). In a particle-antiparticle pair production process, the radiation photon energies transfer to rest energies with a pair of imaginary energies, which combine with the rest energies to form a particle and an antiparticle.

To describe the energies of all particles and antiparticles, we can introduce a two-dimensional energy space. It is a complex space with two axes denoted by the real energy E^M and the imaginary energy iE^Q. There are two phases in this two-dimensional energy space because the real energy is positive. In phase I, both real and imaginary energies are positive, while, in phase II, the imaginary energy is negative. Neutral particles including massless radiation photons are located on the real energy axis. Electrically charged particles are distributed between the real and imaginary energy axes. A particle and its antiparticle cannot be located in the same phase of the energy space. They distribute in two phases symmetrically with respect to the real energy axis.

The imaginary energy is quantized because the electric charge is so. Each electric charge quantum e has the following imaginary energy $E_e = ec^2/\sqrt{G} \sim 10^{27}$ eV, which is about 10^{18} times greater than proton's real energy (or the energy of proton's mass). Dividing the size of proton by the imaginary-real energy ratio (10^{18}), we obtain a scale length $l_Q = 10^{-33}$ cm, the size of the fifth-dimension in the Kaluza-Klein theory. In addition, this amount of energy is equivalent to a temperature $T = 2E_e/k_B \sim 2.4\times10^{31}$K with k_B the Boltzmann constant. In the epoch of big bang, the universe could reach this high temperature. Therefore, big bang of the universe from nothing to a real world, if really occured, might be a process that transfers a certain amount of imaginary energy to real energy. In the recently proposed black hole universe model, however, the imaginary-real energy transformation could not occur because of low temperature [16].

Names	Symbols	Masses	Electric Charge (e)
up	u	2.4 MeV	2/3
down	d	4.8 MeV	−1/3
charm	c	1.27 GeV	2/3
strange	s	104 MeV	−1/3
top	t	171.2 GeV	2/3
bottom	b	4.2 GeV	−1/3

Table 1: Properties of quarks: names, symbols, masses, and electric charges.

2.4 Color charge — a form of imaginary energy

In the particle physics, all elementary particles can be categorized into two types: hadrons and leptons, in accord with whether they experience the strong interaction or not. Hadrons participate in the strong interaction, while leptons do not. All hadrons are composed of quarks. There are six types of quarks denoted as six different flavors: up, down, charm, strange, top, and bottom. The basic properties of these six quarks are shown in Table 1.

Color charge (denoted by C) is a fundamental property of quarks [17], which has analogies with the notion of electric charge of particles. There are three varieties of color charges: red, green, and blue. An antiquark's color is antired, antigreen, or antiblue. Quarks and antiquarks also hold electric charges but the amount of electric charges are frational such as $\pm e/3$ or $\pm 2e/3$. An elementary particle is usually composed by two or more quarks or antiquarks and colorless with electric charge to be a multiple of e. For instance, a proton is composed by two up quarks and one down quarks (uud); a neutron is composed by one up quark and two down quarks (udd); a pion, π^+, is composed by one up quark and one down antiquark ($u\bar{d}$); a charmed sigma, Σ_c^{++}, is composed by two up quarks and one charm quark ($uu\bar{c}$); and so on.

Similar to electric charge Q, we can consider color charge C to be another form of imaginary energy. The amount of imaginary energy can be defined by

$$E^C = \frac{C}{\sqrt{G}}\, c^2. \tag{7}$$

Then, for a quark with mass M, electric charge Q, and color charge C, the total energy of the quark is

$$E = E^M + iE^Q + iE^C = \left[1 + i(\alpha+\beta)\right] Mc^2, \tag{8}$$

where β is given by

$$\beta = \frac{C}{\sqrt{G}M}\,. \tag{9}$$

The total energy of a quark is a complex number.

The energy of an antiquark is naturally obtained by conjugating the energy of the corresponding quark

$$E^* = \left(E^M + iE^Q + iE^C\right)^* = E^M - iE^Q - iE^C = \\ = \left[1 - i(\alpha+\beta)\right] Mc^2. \quad (10)$$

The only difference between a quark and its corresponding antiquark is that their imaginary energies (thus their electric and color charges) have opposite signs. A quark and its antiquark have the same real energy and equal amount of imaginary energy but their signs are opposite. The opposite of the red, green, and blue charges are antired, antigreen, and antiblue charges.

To describe the energies of all particles and antiparticles including quarks and antiquarks, we can introduce a three-dimensional energy space. It is a complex space with three axes denoted by the real energy E^M, the electric imaginary energy iE^Q, and the color imaginary energy iE^C. There are four phases in this three-dimensional energy space. In phase I, all real and imaginary energies are positive; in phase II, the imaginary energy of electric charge is negative; in phase III, the imaginary energies of both electric and color charges are negative; and in phase IV, the imaginary energy of color charge is negative. Neutral particles including massless radiation photons are located on the real-energy axis. Electrically charged particles are distributed on the plane composed of the real-energy axis and the electric charge imaginary-energy axis. Quarks are distributed in all four phases. Particles and their antiparticles are distributed on the plane of the real-energy axis and the electric charge imaginary-energy axis symmetrically with respect to the real-energy axis. Quarks and their antiquarks are distributed in different phases by symmetrically with respect to the real-energy axis and separated by the plane of the real and electric imaginary energy axes.

3 Fundamental interactions of Nature

Fundamental interactions of nature are all possible interactions between the four fundamental elements of nature. Each of the four fundamental elements is a form of energy (either real or imaginary), the fundamental interactions can be unified as a single interaction between complex energies given by

$$\vec{F}_{EE} = -G\frac{E_1E_2}{c^4r^2}\,\hat{\vec{r}}, \quad (11)$$

where E_1 and E_2 are the complex energy given by

$$E_1 = E_1^M + E_1^\gamma + i\left(E_1^Q + E_1^C\right), \quad (12)$$

$$E_2 = E_2^M + E_2^\gamma + i\left(E_2^Q + E_2^C\right). \quad (13)$$

Replacing E_1 and E_2 by using the energy expression (12) and (13), we obtain

$$\vec{F}_{EE} = \vec{F}_{RR} + \vec{F}_{II} + i\vec{F}_{RI} =$$

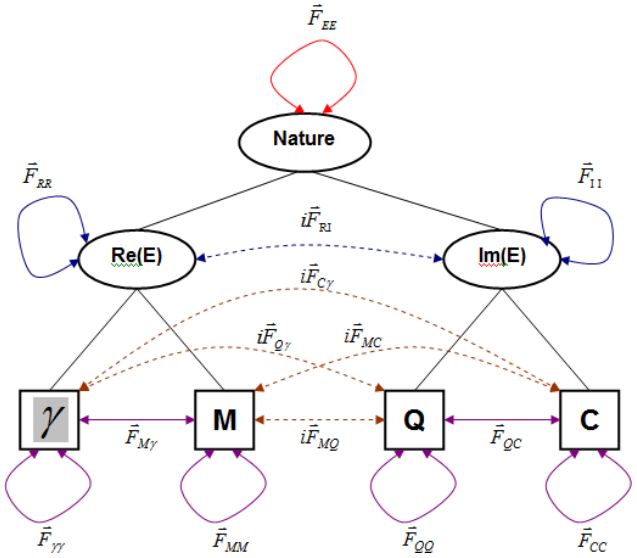

Fig. 1: Fundamental interactions among four fundamental elements of nature: mass, radiation, electric charge and color charge. Mass and radiation are real energies, while electric and color charges are imaginary energies. The nature is a system of complex energy and all the fundamental interactions of nature are classically unified into a single interaction between complex energies. There are six real and four imaginary interactions among the four fundamental elements.

$$= -G\frac{M_1M_2}{r^2}\,\hat{\vec{r}} - G\frac{M_1h\nu_2 + M_2h\nu_1}{c^2r^2}\,\hat{\vec{r}} - G\frac{h\nu_1h\nu_2}{c^4r^2}\,\hat{\vec{r}} + \\ + \frac{Q_1Q_2}{r^2}\,\hat{\vec{r}} + \frac{Q_1C_2 + Q_2C_1}{r^2}\,\hat{\vec{r}} + \frac{C_1C_2}{r^2}\,\hat{\vec{r}} - \\ - i\sqrt{G}\frac{M_1Q_2 + M_2Q_1}{r^2}\,\hat{\vec{r}} - i\sqrt{G}\frac{M_1C_2 + M_2C_1}{r^2}\,\hat{\vec{r}} - \\ - i\sqrt{G}\frac{h\nu_1Q_2 + h\nu_2Q_1}{c^2r^2}\,\hat{\vec{r}} - i\sqrt{G}\frac{h\nu_1C_2 + h\nu_2C_1}{c^2r^2}\,\hat{\vec{r}} \equiv \\ \equiv \vec{F}_{MM} + \vec{F}_{M\gamma} + \vec{F}_{\gamma\gamma} + \vec{F}_{QQ} + \vec{F}_{QC} + \vec{F}_{CC} + \\ + i\vec{F}_{MQ} + i\vec{F}_{MC} + i\vec{F}_{Q\gamma} + i\vec{F}_{C\gamma}\,. \quad (14)$$

It is seen that the interaction between complex energies $\vec{F}_{EE}$ is decoupled into the real-real energy interaction $\vec{F}_{RR}$, the imaginary-imaginary energy interaction $\vec{F}_{II}$, and the real-imaginary energy interaction $i\vec{F}_{RI}$. The real-real energy interaction $\vec{F}_{RR}$ is decoupled into the mass-mass interaction $\vec{F}_{MM}$, the radiation-radiation interaction $\vec{F}_{\gamma\gamma}$, and the mass-radiation interaction $\vec{F}_{M\gamma}$. The imaginary-imaginary energy interaction $\vec{F}_{II}$ is decoupled into the interaction between electric charges $\vec{F}_{QQ}$, the interaction between color charges $\vec{F}_{CC}$, and the interaction between electric and color charges $\vec{F}_{QC}$. The real-imaginary energy interaction $i\vec{F}_{RI}$ is decoupled into the mass-electric charge interaction $i\vec{F}_{MQ}$, the mass-color charge interaction $i\vec{F}_{MC}$, the radiation-electric charge interaction $i\vec{F}_{Q\gamma}$, the radiation-color charge interaction $i\vec{F}_{C\gamma}$. All these interactions as shown in Eq. (14) can be represented by Figure 1 or Table 2.

	M	γ	iQ	iC
M	$\vec{F}_{\rm MM}$	$\vec{F}_{\rm M\gamma}$	$i\vec{F}_{\rm MQ}$	$i\vec{F}_{\rm MC}$
γ		$\vec{F}_{\gamma\gamma}$	$i\vec{F}_{\rm Q\gamma}$	$i\vec{F}_{\rm C\gamma}$
iQ			$\vec{F}_{\rm QQ}$	$\vec{F}_{\rm QC}$
iC				$\vec{F}_{\rm CC}$

Table 2: Fundamental elements and interactions of nature.

3.1 Gravitational force

The force $\vec{F}_{MM}$ represents Newton's law for the gravitational interaction between two masses. This force governs the orbital motion of the solar system. The force $\vec{F}_{M\gamma}$ is the gravitational interaction between mass and radiation. The force $\vec{F}_{\gamma\gamma}$ is the gravitational interaction between radiation and radiation. These three types of gravitational interactions are categorized from the interaction between real energies (see Figure 3 of [1]).

Calculating the work done by this mass-radiation force on a photon, we can derive the Einsteinian gravitational redshift without using the Einsteinian general relativity

$$Z_G = \frac{\lambda_o - \lambda_e}{\lambda_e} = \exp\left(\frac{GM}{c^2 R}\right) - 1. \qquad (15)$$

In the weak field approximation, it reduces

$$Z_G \simeq \frac{GM}{c^2 R}\,. \qquad (16)$$

Similarly, calculating the work done on a photon from an object by the radiation-radiation gravitation $\vec{F}_{\gamma\gamma}$, we obtain a radiation redshift,

$$Z_\gamma = \frac{4GM}{15c^5}\,\sigma A T_c^4 + \frac{G}{c^5}\,\sigma A T_s^4, \qquad (17)$$

where σ is the Stepan-Boltzmann constant, A is the surface area, T_c is the temperature at the center, T_s is the temperature on the surface. Here we have assumed that the inside temperature linearly decreases from the center to the surface. The radiation redshift contains two parts. The first term is contributed by the inside radiation. The other is contributed by the outside radiation. The redshift contributed by the outside radiation is negligible because $T_s \ll T_c$.

The radiation redshift derived here is significantly small in comparison with the empirical expression of radiation redshift proposed by Finlay-Freundlich [18]. For the Sun with $T_c = 1.5{\times}10^7$ K and $T_s = 6{\times}10^3$ K, the radiation redshift is only about $Z_\gamma = 1.3{\times}10^{-13}$, which is much smaller than the gravitational redshift $Z_G = 2.1{\times}10^{-6}$.

3.2 Electromagnetic force

The force $\vec{F}_{QQ}$ represents Coulomb's law for the electromagnetic interaction between two electric charges. Electric charges have two varieties and thus three types of interactions: 1) repelling between positive electric charges $\vec{F}_{++}$, 2) repelling between negative electric charges $\vec{F}_{--}$, and 3) attracting between positive and negative electric charges $\vec{F}_{+-}$. Figure 2 of [1] shows the three types of Coulomb interactions between two electric charges.

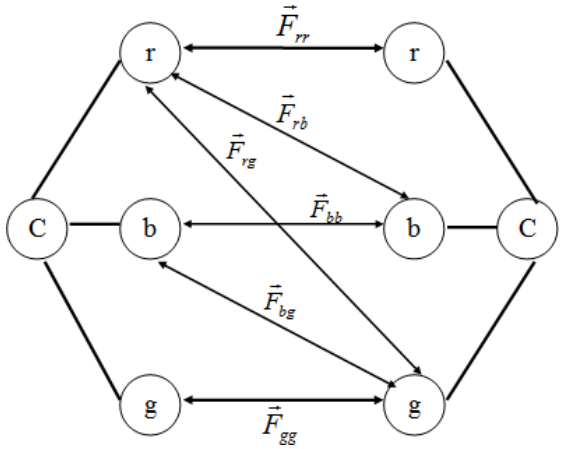

Fig. 2: Six types of strong interactions between color charges: red-red, green-green, blue-blue, red-green, red-blue, and green-blue interactions.

3.3 Strong force

The force $\vec{F}_{CC}$ is the strong interaction between color and color charges. Color charges have three varieties: red, blue, and green and thus six types of interactions: 1) the red-red interaction $\vec{F}_{rr}$, 2) the blue-blue interaction $\vec{F}_{bb}$, 3) the green-green interaction $\vec{F}_{gg}$, 4) the red-blue interaction $\vec{F}_{rb}$, 5) the red-green interaction $\vec{F}_{rg}$, and 6) the blue-green interaction $\vec{F}_{bg}$. Figure 2 shows these six types of color interactions.

Considering the strong interaction to be asymptotically free [19], we replace the color charge by

$$C \to r\,C\,; \qquad (18)$$

this assumption represents that the color charge becomes less colorful if it is closer to each other, i.e., asymptotically colorless. Then the strong interaction between color charges can be rewritten by

$$\vec{F}_{CC} = C_1 C_2\,\hat{\vec{r}}, \qquad (19)$$

which is independent of the radial distance and consistent with measurement.

The strong interaction is the only one that can change the color of quarks in a hadron. A typical strong interaction is proton-neutron scattering, $p + n \longrightarrow n + p$. This is an interaction between the color charge of one up quark in proton and the color charge of one down quark in neutron via exchanging a π^+ , $u + d \longrightarrow d + u$ (see Figure 2). In other words, during this proton-neutron scattering an up quark in the proton changes into a down quark by emitting a π^+, meanwhile a down quark in the neutron changes into an up quark by absorbing the π^+. Another typical strong interaction is delta decay, $\Delta^0 \longrightarrow p + \pi^-$. This is an interaction between the color

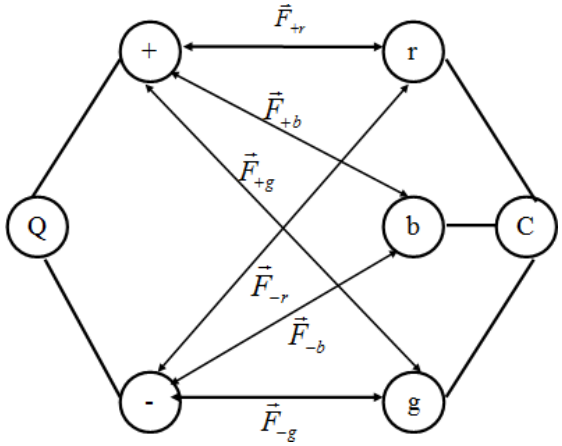

Fig. 3: Six types of weak interactions between electric and color charges: positive-red, positive-green, positive-blue, negative-red, negative-green, and negative-blue interactions.

charge of one down quark and the color charges of the other two quarks. In this interaction, a down quark emits a π^- and then becomes a up quark, $d \longrightarrow u + \pi^-$.

3.4 Weak force

The force $\vec{F}_{QC}$ is the weak interaction between electric and color charges. Considering electric charges with two varieties (positive and negative) and color charges with three varieties (red, blue, and green), we have also six types of weak interaction: 1) the positive-red interaction $\vec{F}_{+r}$, 2) the positive-blue interaction $\vec{F}_{+b}$, 3) the positive-green interaction $\vec{F}_{+g}$, 4) the negative-red interaction $\vec{F}_{-r}$, 5) the negative-blue interaction $\vec{F}_{-b}$, and 6) the negative-green interaction $\vec{F}_{-g}$. Figure 3 shows these six types of electric-color charge interactions.

Considering equation (18), we can represent the weak interaction by

$$\vec{F}_{QC} = \frac{QC}{r}\,\hat{\vec{r}}, \tag{20}$$

which is inversely proportional to the radial distance and consistent with measurement.

The weak interaction is the only one that can change the flavors of quarks in a hadron. A typical weak interaction is the neutron decay, $n \longrightarrow p + e^- + \bar{\nu}_e$. In this process, a down quark in the neutron changes into an up quark by emitting W^- boson, which lives about 10^{-26} seconds and then breaks into a high-energy electron and an electron antineutrino, i.e., $d \longrightarrow u + W^-$ and then $W^- \longrightarrow u + e^- + \bar{\nu}_e$. There are actually two interactions involved in this neutron decay. One is the interaction between electric and color charges inside the down quark, which is changed into an up quark by emitting a W^- boson. Another is the interaction inside W^-, which is broken into an electron and an electron antineutrino. Since W^- is composed of an up antiquark and a down quark ($\bar{u}d$), we suggest that the down quark changes into an up quark by emitting an electron and then the up antiquark and the up quark annihilate into an electron antineutrino. It should be noted that an upper antiquark and an up quark usually forms an η particle, which may live about a few tens of nanoseconds and decay into other particles such as photons and pions, which further decay to nuons and nuon neutrinos and antineutrinos. The formation of η and decay to photons and pions may explain the solar neutrino missing problem and neutrino oscillations, the detail of which leaves for a next study.

3.5 Imaginary force

The other terms with the imaginary number in Eq. (14) are imaginary forces between real and imaginary energies. These imaginary forces should play essential roles in combining or separating imaginary energies with or from real energies. The physics of imaginary forces needs further investigations.

4 Summary

As a summary, we have appropriately suggested mass, radiation, electric charge, and color charge as the four fundamental elements of nature. Mass and radiation are two types of real energy, while electric and color charges are considered as two forms of imaginary energy. we have described the nature as a system of complex energy and classically unified all the fundamental interactions of nature into a single interaction between complex energies. Through this classical unification theory, we provide a more general understanding of nature fundamental elements and interactions, especially the weak interaction as an interaction between electric and color charges without assuming a weak charge. The interaction between real energies is the gravitational force, which has three types: mass-mass, mass-radiation, and radiation-radiation interactions. Calculating the work done by the mass-radiation gravitation on a photon derives the Einsteinian gravitational redshift. Calculating the work done on a photon from an object by the radiation-radiation gravitation derives a radiation redshift, which is much smaller than the gravitational redshift. The interaction between imaginary energies is the electromagnetic (between electric charges), weak (between electric and color charges), and strong (between color charges) interactions. In addition, we have four imaginary forces between real and imaginary energies, which are mass-electric charge, radiation-electric charge, mass-color charge, and radiation-color charge interactions. Therefore, among the four fundamental elements, we have in total ten (six real and four imaginary) fundamental interactions. In addition, we introduce a three-dimensional energy space to describe all types of matter or particles including quarks and antiquarks.

Acknowledgement

This work was supported by the Title III program of Alabama A & M University, the NASA Alabama EPSCoR Seed grant (NNX07AL52A), and the National Natural Science Foundation of China (G40890161).

Submitted on January 21, 2010 / Accepted on January 25, 2010

References

1. Zhang T.X. Electric charge as a form of imaginary energy. *Progress in Phys.*, 2008, v.2, 79–83.
2. Newton I. Mathematical principles of nature philosophy. Book III 1687.
3. Hoskins L.M. Mass as quantity of matter. *Science*, 1915, v.42, 340–341.
4. Mach E. The science of mechanics. Reprinted by Open Court Pub. Co., 1960.
5. Einstein A. Ist die Trägheit eines Körpers von seinem Energieinhalt abhängig? *Ann. Phys.*, 1905, v.323, 639–641.
6. Einstein A. Über einen die Erzeugung und Verwandlung des Lichtes betreffenden heuristischen Gesichtspunkt. *Ann. Phys.*, 1905, v.322, 132–148.
7. Planck M. Ueber das Gesetz der Energieverteilung im Normalspectrum. *Ann. Phys.*, 1901, v.309, 553–563.
8. Coulomb C. Theoretical research and experimentation on torsion and the elasticity of metal wire. *Ann. Phys.*, 1802, v.11, 254–257.
9. Weinberg S. The first three minutes. Basic Books, New York, 1977.
10. Kaluza T. On the problem of unity in physics. *Sitz. Preuss. Aklad. Wiss. Berlin*, Berlin, 1921, 966–972.
11. Klein O. Quantum theory and five dimensional theory of relativity. *Z. Phys.*, 1926a, v.37, 895–906.
12. Klein O. The atomicity of electricity as a quantum theory law. *Nature*, 1926b, v.118, 516–520.
13. Zhang T.X. Electric redshift and quasars. *Astrophys. J. Letters*, 2006, v.636, 61–64.
14. Dirac P.A.M. The quantum theory of the electron. *Proc. R. Soc. London A*, 1928, v.117, 610–624.
15. Anderson C.D. The positive electron. *Phys. Rev.*, 1933, v.43, 491–498.
16. Zhang T.X. A new cosmological model: black hole universe. *Progress in Phys.*, 2009, v.3, 3–11.
17. Veltman M. Facts and mysteries in elementary particle physics. World Scientific Pub. Co. Pte. Ltd., 2003.
18. Finlay-Freundlich E. Red shift in the spectra of celestial bodies. *Phyl. Mag.*, 1954, v.45, 303–319.
19. Gross D.J. and Wilczek F. Asymptotically free gauge theories I. *Phys. Rev. D*, 1973, v.8, 3633–3652.

The Solar System According to General Relativity: The Sun's Space Breaking Meets the Asteroid Strip

Larissa Borissova

E-mail: borissova@ptep-online.com

This study deals with the exact solution of Einstein's field equations for a sphere of incompressible liquid without the additional limitation initially introduced in 1916 by Schwarzschild, by which the space-time metric must have no singularities. The obtained exact solution is then applied to the Universe, the Sun, and the planets, by the assumption that these objects can be approximated as spheres of incompressible liquid. It is shown that gravitational collapse of such a sphere is permitted for an object whose characteristics (mass, density, and size) are close to the Universe. Meanwhile, there is a spatial break associated with any of the mentioned stellar objects: the break is determined as the approaching to infinity of one of the spatial components of the metric tensor. In particular, the break of the Sun's space meets the Asteroid strip, while Jupiter's space break meets the Asteroid strip from the outer side. Also, the space breaks of Mercury, Venus, Earth, and Mars are located inside the Asteroid strip (inside the Sun's space break).

The main task of this paper is to study the possibilities of applying condensed matter models in astrophysics and cosmology. A cosmic object consisting of condensed matter has a constant volume and a constant density. A sphere of incompressible liquid, being in the weightless state (as any cosmic object), is a kind of condensed matter. Thus, assuming that a star is a sphere of incompressible liquid, we can study the gravitational field of the star inside and outside it.

The Sun orbiting the center of the Galaxy meets the weightless condition (see [1] for detail)

$$\frac{GM}{r} = \mathrm{v}^2,$$

where $G = 6.67{\times}10^{-8}$ cm^3/g$\times$sec^2 is the Newtonian gravitational constant, M is the mass of the Galaxy, r is the distance of the Sun from the center of the Galaxy, and v is the Sun's velocity in its orbit. The planets of the Solar System also satisfy the weightless condition. Assuming that the planets have a similar internal constitution as the Sun, we can consider these objects as spheres of incompressible liquid being in a weightless state.

I will consider the problems by means of the General Theory of Relativity. First, it is necessary to obtain the exact solution of the Einstein field equations for the space-time metric induced by the gravitational field of a sphere of incompressible liquid.

The regular field equations of Einstein, with the λ-field neglected, have the form

$$R_{\alpha\beta} - \frac{1}{2}\, g_{\alpha\beta} R = -\varkappa\, T_{\alpha\beta}\,, \qquad (1)$$

where $R_{\alpha\beta}$ is the Ricci tensor, R is the Riemann curvature scalar, $\varkappa = \frac{8\pi G}{c^2} = 18.6{\times}10^{-28}$ cm/g is the Einstein gravitational constant, $T_{\alpha\beta}$ is the energy-momentum tensor, and $\alpha, \beta = 0, 1, 2, 3$ are the space-time indices. The gravitational field of spherical island of substance should possess spherical symmetry. Thus, it is described by the metric of spherical kind

$$ds^2 = e^{\nu} c^2 dt^2 - e^{\lambda} dr^2 - r^2(d\theta^2 + \sin^2\theta\, d\varphi^2), \qquad (2)$$

where e^{ν} and e^{λ} are functions of r and t.

In the case under consideration the energy-momentum tensor is that of an ideal liquid (incompressible, with zero viscosity), by the condition that its density is constant, i.e. $\rho = \rho_0 = const$. As known, the energy-momentum tensor in this case is

$$T^{\alpha\beta} = \left(\rho_0 + \frac{p}{c^2}\right) b^{\alpha} b^{\beta} - \frac{p}{c^2}\, g^{\alpha\beta}, \qquad (3)$$

where p is the pressure of the liquid, while

$$b^{\alpha} = \frac{dx^{\alpha}}{ds}\,, \qquad b_{\alpha} b^{\alpha} = 1 \qquad (4)$$

is the four-dimensional velocity vector, which determines the reference frame of the given observer. Also, the energy-momentum tensor should satisfy the conservation law

$$\nabla_{\sigma} T^{\alpha\sigma} = 0\,, \qquad (5)$$

where ∇_{σ} is the four-dimensional symbol of covariant differentiation.

Formally, the problem we are considering is a generalization of the Schwarzschild solution produced for an analogous case (a sphere of incompressible liquid). Karl Schwarzschild [2] solved the Einstein field equations for this case, by the condition that the solution must be regular. He assumed that the components of the fundamental metric tensor $g_{\alpha\beta}$ must satisfy the signature conditions (the space-time metric must have no singularities). Thus, the Schwarzschild solution, according to his initial assumption, does not include space-time singularities.

This limitation of the space-time geometry, initially introduced in 1916 by Schwarzschild, will not be used by me in this study. Therefore, we will be able to study the singular properties of the space-time metric associated with a sphere of incompressible liquid. Then I will apply the obtained results to the cosmic objects such as the Sun and the planets.

The exact solution of the field equations (1) is obtained for the spherically symmetric metric (2) inside a sphere of incompressible liquid, which is described by the energy-momentum tensor (3). I consider here the reference frame which accompanies to the observer, consequently the components of his four-velocity vector are [3]

$$b^0 = \frac{1}{\sqrt{g_{00}}}\,, \quad b^i = 0\,, \quad i = 1,2,3, \tag{6}$$

while the physically observed components of the energy-momentum tensor $T_{\alpha\beta}$ has the form

$$\rho = \frac{T_{00}}{g_{00}} = \rho_0\,, \;\; J^i = \frac{c\,T^i_0}{\sqrt{g_{00}}} = 0\,, \;\; U^{ik} = c^2 T^{ik} = p h^{ik}, \tag{7}$$

where ρ is the density of the medium, J^i is the density of the momentum in the medium, U^{ik} is the stress-tensor, h^{ik} is the observable three-dimensional fundamental metric tensor [3].

Because we do not limit the solution by that the metric must be regular, the obtained metric has two singularities: 1) collapse by $g_{00} = 0$, and 2) break of the space by $g_{11} \to \infty$. It will be shown then that these singularities are irremovable, because the strong signature condition is also violated in both cases.

In order to obtain the exact internal solution of the Einstein field equations with respect to a given distribution of matter, it is necessary to solve two systems of equations: the Einstein field equations (1), and the equations of the conservation law (5).

After algebra we obtain the Einstein field equations in the spherically symmetric space (2) inside a sphere of incompressible liquid. The obtained equations, in component notation, are

$$e^{-\nu}\left(\ddot{\lambda} - \frac{\dot{\lambda}\dot{\nu}}{2} + \frac{\dot{\lambda}^2}{2}\right) - c^2 e^{-\lambda}\left[\nu'' - \frac{\lambda'\nu'}{2} + \frac{2\nu'}{r} + \frac{(\nu')^2}{2}\right] = \\ = -\varkappa\left(\rho_0 c^2 + 3p\right), \tag{8}$$

$$\frac{\dot{\lambda}}{r}\, e^{-\lambda - \frac{\nu}{2}} = \varkappa J^1 = 0\,, \tag{9}$$

$$e^{\lambda-\nu}\left(\ddot{\lambda} - \frac{\dot{\lambda}\dot{\nu}}{2} + \frac{\dot{\lambda}^2}{2}\right) - c^2\left[\nu'' - \frac{\lambda'\nu'}{2} + \frac{(\nu')^2}{2}\right] + \frac{2c^2\lambda'}{r} = \\ = \varkappa\left(\rho_0 c^2 - p\right) e^{\lambda}, \tag{10}$$

$$\frac{c^2\,(\lambda' - \nu')}{r}\, e^{-\lambda} + \frac{2c^2}{r^2}\left(1 - e^{-\lambda}\right) = \varkappa\left(\rho_0 c^2 - p\right). \tag{11}$$

The second equation manifests that $\dot{\lambda} = 0$ in this case. Hence, the space inside the sphere of incompressible liquid does not deform. Taking this circumstance into account, and also that the stationarity of λ, we reduce the field equations (8–11) to the final form

$$c^2 e^{-\lambda}\left[\nu'' - \frac{\lambda'\nu'}{2} + \frac{2\nu'}{r} + \frac{(\nu')^2}{2}\right] = \varkappa\left(\rho_0 c^2 + 3p\right) e^{\lambda}, \tag{12}$$

$$-c^2\left[\nu'' - \frac{\lambda'\nu'}{2} + \frac{(\nu')^2}{2}\right] + \frac{2c^2\lambda'}{r} = \varkappa\left(\rho_0 c^2 - p\right) e^{\lambda}, \tag{13}$$

$$\frac{c^2\,(\lambda' - \nu')}{r}\, e^{-\lambda} + \frac{2c^2}{r^2}\left(1 - e^{-\lambda}\right) = \varkappa\left(\rho_0 c^2 - p\right) e^{\lambda}. \tag{14}$$

To solve the equations (12–14), a formula for the pressure p is necessary. To find the formula, we now deal with the conservation equations (5). Because, as was found, $J^i = 0$ we obtain, this formula reduces to only a single nontrivial equation

$$p' e^{-\lambda} + \left(\rho_0 c^2 + p\right)\frac{\nu'}{2}\, e^{-\lambda} = 0\,, \tag{15}$$

where $p' = \frac{dp}{dr}$, $\nu' = \frac{d\nu}{dr}$, $e^{\lambda} \neq 0$. Dividing both parts of (15) by $e^{-\lambda}$, we arrive at

$$\frac{dp}{\rho_0 c^2 + p} = -\frac{d\nu}{2}\,, \tag{16}$$

which is a plain differential equation with separable variables. It can be easily integrated as

$$\rho_0 c^2 + p = B e^{-\frac{\nu}{2}}\,, \qquad B = const. \tag{17}$$

Thus we have to express the pressure p as the function of the variable ν,

$$p = B e^{-\frac{\nu}{2}} - \rho_0 c^2. \tag{18}$$

In look for an r-dependent function $p(r)$, we integrate the field equations (12–14), taking into account (18). We find finally expressions for e^{λ} and e^{ν}

$$g_{00} = e^{\nu} = \frac{1}{4}\left(3e^{\frac{\nu_a}{2}} - \sqrt{1 - \frac{\kappa\rho_0 r^2}{3}}\right)^2, \tag{19}$$

$$e^{\lambda} = -\,g_{11} = \frac{1}{1 - \frac{\kappa\rho_0 r^2}{3}}\,, \tag{20}$$

where $e^{\frac{\nu_a}{2}} = \sqrt{1 - \frac{2GM}{c^2 a}} = \sqrt{1 - \frac{r_g}{r}}$ is obtained from the boundary conditions, while r_g is the Hilbert radius.

Thus the space-time metric of the gravitational field inside a sphere of incompressible liquid is, since the formulae of ν and λ have already been obtained, as follows

$$ds^2 = \frac{1}{4}\left(3\,e^{\frac{\nu_a}{2}} - \sqrt{1 - \frac{\varkappa\rho_0 r^2}{3}}\right)^2 c^2 dt^2 - \\ - \frac{dr^2}{1 - \frac{\varkappa\rho_0 r^2}{3}} - r^2\left(d\theta^2 + \sin^2\theta\, d\varphi^2\right). \tag{21}$$

Taking into account that $M = \frac{4\pi a^3 \rho_0}{3}$ and $r_g = \frac{2GM}{c^2}$, we rewrite (21) in the form

$$ds^2 = \frac{1}{4}\left(3\sqrt{1-\frac{r_g}{a}} - \sqrt{1-\frac{r^2 r_g}{a^3}}\right)^2 c^2 dt^2 - \\ - \frac{dr^2}{1-\frac{r^2 r_g}{a^3}} - r^2\left(d\theta^2 + \sin^2\theta\, d\varphi^2\right). \quad (22)$$

It is therefore obvious that this "internal" metric completely coincides with the Schwarzschild metric in emptiness on the surface of the sphere of incompressible liquid ($r = a$). This study is a generalization of the originally Schwarzschild solution for such a sphere [2], and means that Schwarzschild's requirement to the metric to be free of singularities will not be used here. Naturally, the metric (22) allows singularities. This problem will be solved by analogy with the singular properties of the Schwarzschild solution in emptiness [4] (a mass-point's field), which already gave black holes.

Consider the collapse condition for the space-time metric of the gravitational field inside a sphere of incompressible liquid (21). The collapse condition $g_{00} = 0$ in this case is

$$3e^{\frac{\nu_a}{2}} = \sqrt{1-\frac{\varkappa\rho_0 r^2}{3}}\,, \quad (23)$$

or, in terms of the Hilbert radius, when the metric takes the form (22), the collapse condition is

$$3\sqrt{1-\frac{r_g}{a}} = \sqrt{1-\frac{r_g r^2}{a^3}}\,. \quad (24)$$

We obtain that the numerical value of the radial coordinate r_c, by which the sphere's surface meets the surface of collapse, is

$$r_c = a\sqrt{9-\frac{8a}{r_g}}\,. \quad (25)$$

Because we keep in mind really cosmic objects, the numerical value of r_c should be real. This requirement is obviously satisfied by

$$a < 1.125\, r_g\,. \quad (26)$$

If this condition holds not ($a \geqslant r_g$), the sphere, which is a spherical liquid body, has not the state of collapse. It is obvious that the condition $a = r_g$ satisfies to (26). It is obvious that r_c is imaginary for $r_g \ll a$, so collapse of such a sphere of incompressible liquid is impossible.

For example, consider the Universe as a sphere of incompressible liquid (the liquid model of the Universe). Assuming, according to the numerical value of the Hubble constant (17), that the Universe's radius is $a = 1.3{\times}10^{28}$ cm, we obtain the collapse condition, from (26),

$$r_g > 1.2{\times}10^{28}\ \text{cm}, \quad (27)$$

and immediately arrive at the following conclusion:

> The observable Universe as a whole, being represented in the framework of the liquid model, is completely located inside its gravitational radius. In other words, the observable Universe is a collapsar — a huge black hole.

In another representation, this result means that a sphere of incompressible liquid can be in the state of collapse only if its radius approaches the radius of the observable Universe.

Let's obtain the condition of spatial singularity — space breaking. As is seen, the metric (21) or its equivalent form (22) has space breaking if its radial coordinate r equals to

$$r_{br} = \sqrt{\frac{3}{\kappa\rho_0}} = a\sqrt{\frac{a}{r_g}}. \quad (28)$$

For example, considering the Sun as a sphere of incompressible liquid, whose density is $\rho_0 = 1.4$ g/cm^3, we obtain

$$r_{br} = 3.4{\times}10^{13}\ \text{cm}, \quad (29)$$

while the radius of the Sun is $a = 7{\times}10^{10}$ cm and its Hilert radius $r_g = 3{\times}10^5$ cm. Therefore, the surface of the Sun's space of breaking is located outside the surface of the Sun, far distant from it in the near cosmos.

Another example. Assume our Universe to be a sphere of incompressible liquid, whose density is $\rho_0 = 10^{-31}$ g/cm^3. The radius of its space breaking, according to (28), is

$$r_{br} = 1.3{\times}10^{29}\ \text{cm}. \quad (30)$$

Observational astronomy provides the following numerical value of the Hubble constant

$$H = \frac{c}{a} = (2.3 \pm 0.3){\times}10^{18}\ \text{sec}^{-1}, \quad (31)$$

where a is the observed radius of the Universe. It is easily obtain from here that

$$a = 1.3{\times}10^{28}\ \text{cm}. \quad (32)$$

This value is comparable with (30), so the Universe's radius may meet the surface of its space breaking by some conditions. We calculate the mass of the Universe by $M = \frac{4\pi a^3\rho_0}{3}$, where a is (32). We have $M = 5{\times}10^{54}$ g. Thus, for the liquid model of the Universe, we obtain $r_g = 7.4{\times}10^{26}$ cm: the Hilbert radius (the radius of the surface of gravitational collapse) is located inside the liquid spherical body of the Universe.

A few words more on the singularities of the liquid sphere's internal metric (21). In this case, the determinant of the fundamental metric tensor equals

$$g = -\frac{1}{4}\left(3e^{\frac{\nu_a}{2}} - \sqrt{1-\frac{\varkappa\rho_0 r^2}{3}}\right)^2 \frac{r^4\sin^2\theta}{\sqrt{1-\frac{\varkappa\rho_0 r^2}{3}}}\,, \quad (33)$$

so the strong signature condition $g < 0$ is always true for a sphere of incompressible liquid, except in two following

cases: 1) in the state of collapse ($g_{00} = 0$), 2) by the breaking of space ($g_{11} \to \infty$). These particular cases violate the weak signature conditions $g_{00} > 0$ and $g_{11} < 0$ correspondingly. If both weak signature conditions are violated, g has a singularity of the kind $\frac{0}{0}$. If collapse occurs in the absence of the space breaking, we have $g = 0$. If no collapse, while the space breaking is present, we have $g \to \infty$. In all the cases, the singularity is non-removable, because the strong singular condition $g < 0$ is violated.

So, as was shown above, a spherical object consisting of incompressible liquid can be in the state of gravitational collapse only if it is as large and massive as the Universe. Meanwhile, the space breaking realizes itself in the fields of all cosmic objects, which can be approximated by spheres of incompressible liquid. Besides, since $r_{br} \sim \frac{1}{\sqrt{\rho_0}}$, the r_{br} is then greater while smaller is the ρ_0. Assuming all these, we arrive at the following conclusion:

> A regular sphere of incompressible liquid, which can be observed in the cosmos or an Earth-bound laboratory, cannot collapse but has the space breaking — a singular surface, distantly located around the liquid sphere.

First, we are going to consider the Sun as a sphere of incompressible liquid. Schwarzschild [2] was the first person who considered the gravitational field of a sphere of incompressible liquid. He however limited this consideration by an additional condition that the space-time metric should not have singularities. In this study the metric (21) will be used. It allows singularities, in contrast to the limited case of Schwarzschild: 1) collapse of the space, and 2) the space breaking.

Calculating the radius of the space breaking by formula (28), where we substitute the Sun's density $\rho_0 = 1.41$ g/cm^3, we obtain

$$r_{br} = 3.4{\times}10^{13} \text{ cm} = 2.3 \text{ AU}, \qquad (34)$$

where 1 AU $= 1.49{\times}10^{13}$ cm (Astronomical Unit) is the average distance between the Sun and the Earth. So, we have obtained that the spherical surface of the Sun's space breaking is located inside the Asteroid strip, very close to the orbit of the maximal concentration of substance in it (as is known, the Asteroid strip is hold from 2.1 to 4.3 AU from the Sun). Thus we conclude that:

> The space of the Sun (its gravitational field), as that of a sphere of incompressible liquid, has a breaking. The space breaking is distantly located from the Sun's body, in the space of the Solar System, and meets the Asteroid strip near the maximal concentration of the asteroids.

In addition to it, we conclude:

> The Sun, approximated by a mass-point according to the Schwarzschild solution for a mass-point's field in emptiness, has a space breaking located inside the Sun's body. This space breaking coincides with the Schwarzschild sphere — the sphere of collapse.

What is the Schwarzschild sphere? It is an imaginary spherical surface of the Hilbert radius $r_g = \frac{2GM}{c^2}$, which is not a radius of a physical body in a general case (despite it can be such one in the case of a black hole — a physical body whose radius meets the Hilbert radius calculated for its mass). The numerical value of r_g is determined only by the mass of the body, and does not depend on its other properties. The physical meaning of the Hilbert radius in a general case is as follows: this is the boundary of the region in the gravitational field of a mass-point M, where real particles exist; particles in the boundary (the Hilbert radius) bear the singular properties. In the region wherein $r \leqslant r_g$, real particles cannot exist.

Let us turn back to the Sun approximated by a sphere of incompressible liquid. The space-time metric is (21) in this case. Substituting into (25) the Sun's mass $M = 2{\times}10^{33}$ g, radius $a = 7{\times}10^7$ cm, and the Hilbert radius $r_g = 3{\times}10^5$ cm calculated for its mass, we obtain that the numerical value of the radial coordinate r_c by which the Sun's surface meets the surface of collapse of its mass is imaginary. Thus, we arrive at the conclusion that a sphere of incompressible liquid, whose parameters are the same as those of the Sun, cannot collapse.

Thus, we conclude:

> A Schwarzschild sphere (collapsing space breaking) exists inside any physical body. The numerical value of its radius r_g is determined only by the body's mass M. We refer to the space-time inside the Schwarzschild sphere ($r < r_g$) as a "black hole". This space-time does not satisfy the singular conditions of the space-time where real observers exist. Schwarzschild sphere (internal black hole) is an internal characteristic of any gravitating body, independent on its internal constitution.

One can ask: then what does the Hilbert radius r_g mean for the Sun, in this context? Here is the answer: r_g is the photometric distance in the radial direction, separating the "external" region inhabited with real particles and the "internal" region under the radius wherein all particles bear imaginary masses. Particles which inhabit the boundary surface (its radius is r_g) bear singular physical properties. Note that no one real (external) observer can register events inside the singularity.

What is a sphere of incompressible liquid of the radius $r = r_c$? This is a "collapsar" — the object in the state of gravitational collapse. As it was shown above, not any sphere of incompressible liquid can be collapsar: the possibility of its collapse is determined by the relation between its radius a and its Hilbert radius r_g, according to formula (25). It was shown above that the Universe considered as a sphere of incompressible liquid is a collapsar.

Now we apply this research method to the planets of the Solar System. Thus, we approximate the planets by spheres

of incompressible liquid. The numerical values of r_c, calculated for the planets according to the same formula (25) as that for the liquid model of the Sun, are imaginary. Therefore, the planets being approximated by spheres of incompressible liquid cannot collapse as well as the Sun.

The Hilbert radius r_g calculated for the planets is much smaller than the sizes of their physical bodies, and is in the order of 1 cm. This means that, given any of the planets of the Solar System, the singulary surface separating our world and the imaginary mass particles world in its gravitational field draws the sphere of the radius about one centimetre around its centre of gravity.

The numerical values of the radius of the space breaking are calculated for each of the planets through the average density of substance inside the planet according to the formula (28).

The results of the summarizing and substraction associated with the planets lead to the next conclusions:

1. The spheres of the singularity breaking of the spaces of Mercury, Venus, and the Earth are completely located inside the sphere of the singularity breaking of the Sun's space;
2. The spheres of the singularity breaking of the internal spaces of all planets intersect among themselves, when being in the state of a "parade of planets";
3. The spheres of the singularity breaking of the Earth's space and Mars' space reach the Asteroid strip;
4. The sphere of the singularity breaking of Mars' space intersects with the Asteroid strip near the orbit of Phaeton (the hypothetical planet which was orbiting the Sun, according to the Titius–Bode law, at $r = 2.8$ AU, and whose distraction in the ancient time gave birth to the Asteroid strip).
5. Jupiter's singularity breaking surface intersects the Asteroid strip near Phaeton's orbit, $r = 2.8$ AU, and meets Saturn's singularity breaking from the outer side;
6. The singularity breaking surface of Saturn's space is located between those of Jupiter and Uranus;
7. The singularity breaking surface of Uranus's space is located between those of Saturn and Neptune;
8. The singularity breaking surface of Neptune's space meets, from the outer side, the lower boundary of the Kuiper belt (the strip of the aphelia of the Solar System's comets);
9. The singularity breaking surface of Pluto is completely located inside the lower strip of the Kuiper belt.

Just two small notes in addition to these. The intersections of the space breakings of the planets, discussed here, take place for only that case where the planets thenselves are in the state of a "parade of planets". However the conclusions concerning the location of the space breaking spheres, for instance — that the space breaking spheres of the internal planets are located inside the sphere of the Sun's space breaking, while the space breaking spheres of the external planets are located outside it, — are true for any position of the planets.

The fact that the space breaking of the Sun meets the Asteroid strip, near Phaeton's orbit, allows us to say: yes, the space breaking considered in this study has a really physical meaning. As probable the Sun's space breaking did not permit the Asteroids to be joined into a common physical body, Phaeton. Alternatively, if Phaeton was an already existing planet of the Solar System, the common action of the space breaking of the Sun and that of another massive cosmic body, appeared near the Solar System in the ancient ages (for example, another star passing near it), has led to the distraction of Phaeton's body.

Thus the internal constitution of the Solar System was formed by the structure of the Sun's space (space-time) filled with its gravitational field, and according to the laws of the General Theory of Relativity.

These and related results will be published in necessary detail later [5]*.

Submitted on October 31, 2009 / Accepted on January 27, 2010

References

1. Rabounski D. and Borissova L. Particles Here and Beyond the Mirror. Svenska fysikarkivet, Stockholm, 2008.
2. Schwarzschild K. Über das Gravitationsfeld einer Kugel aus incompressiebler Flüssigkeit nach der Einsteinschen Theorie. *Sitzungsberichte der Königlich Preussischen Akademie der Wissenschaften*, 1916, 424–435 (published in English as: Schwarzschild K. On the gravitational field of a sphere of incompressible liquid, according to Einstein's theory. *The Abraham Zelmanov Journal*, 2008, vol. 1, 20–32).
3. Zelmanov A. L. Chronometric invariants and accompanying frames of reference in the General Theory of Relativity. *Soviet Physics Doklady*, 1956, vol. 1, 227–230 (translated from *Doklady Academii Nauk USSR*, 1956, vol. 107, no. 6, 815–818).
4. Schwarzschild K. Über das Gravitationsfeld eines Massenpunktes nach der Einsteinschen Theorie. *Sitzungsberichte der Königlich Preussischen Akademie der Wissenschaften*, 1916, 196–435 (published in English as: Schwarzschild K. On the gravitational field of a point mass according to Einstein's theory. *The Abraham Zelmanov Journal*, 2008, vol. 1, 10–19).
5. Borissova L. The gravitational field of a condensed matter model of the Sun: the space breaking meets the Asteroid strip. Accepted to publication in *The Abraham Zelmanov Journal*, 2009, v.2, 224–260.

*The detailed presentation of the results [5] was already published at the moment when this short paper was accepted.

The Matter-Antimatter Concept Revisited

Patrick Marquet

Postal address: 7, rue du 11 nov, 94350 Villiers/Marne, Paris, France
Email: patrick.marquet6@wanadoo.fr

In this paper, we briefly review the theory elaborated by Louis de Broglie who showed that in some circumstances, a particle tunneling through a dispersive refracting material may reverse its velocity with respect to that of its associated wave (phase velocity): this is a consequence of Rayleigh's formula defining the group velocity. Within his "Double Solution Theory", de Broglie re-interprets Dirac's aether concept which was an early attempt to describe the matter-antimatter symmetry. In this new approach, de Broglie suggests that the (hidden) sub-quantum medium required by his theory be likened to the dispersive and refracting material with identical properties. A Riemannian generalization of this scheme restricted to a space-time section, and formulated within an holonomic frame is here considered. This procedure is shown to be founded and consistent if one refers to the extended formulation of General Relativity (EGR theory), wherein pre-exists a persistent field.

1 Introduction

The original wave function first predicted by Louis de Broglie [1] in his famous *Wave Mechanics Theory*, then was detected in 1927 by the American physicists Davisson and Germer in their famous experiment on electrons diffraction by a nickel crystal lattice.

In the late 1960's, Louis de Broglie improved on his first theory which he called *Double Solution Interpretation of Quantum Mechanics* [2, 3].

His successive papers actually described the massive particle as being much closely related to its physical wave and constantly in phase with it.

The theory which grants the wave function a true physical reality as it should be, necessarily requires the existence of an underlying medium that permanently exchanges energy and momentum with the guided particle [4].

The hypothesis of such a concealed "thermostat" was brought forward by D. Bohm and J. P. Vigier [5] who referred to it as the *sub-quantum medium*.

They introduced a hydrodynamical model in which the (real) wave amplitude is represented by a fluid endowed with some specific irregular fluctuations so that the quantum theory receives a causal interpretation.

Francis Fer [6] successfully extended the double solution theory by building a non-linear and covariant equation wherein the "fluid" is taken as a physical entity. In the recent paper [7], the author proposed to generalize this model to an extended formulation of General Relativity [8], which allows to provide a physical solution to the fluid random perturbation requirement.

Based on his late conceptions, Louis de Broglie then completed a subsequent theory [9] on the guided particle: under specific circumstances the particle tunneling through a dispersive refracting material is shown to reverse velocity with respect to the associated wave phase velocity.

As a further assumption, Louis de Broglie identified the dispersive refracting material with the hidden medium [10] considered above.

In this case, the theoretical results obtained are describing the behavior of a pair particle-antiparticle which is close to the Stuckelberg-Feynmann picture [11], in which antiparticles are viewed as particles with negative energy that move backward in time.

Within this interpretation, the sub-quantum medium as derived from de Broglie's theories, appears to provide a deeper understanding of Dirac's aether theory [12], once popular before.

In this paper, we try to generalize this new concept by identifying the hidden medium with the persistent energy-momentum field tensory inherent to the EGR theory.

Such a generalization is here only restricted to a Riemannian space-time section ($t = const$), where the integration is further performed over a spatial volume. By doing so, we are able to find back the essential formulas set forth by Louis de Broglie in the Special Relativity formulation.

We assumed here a limited extension without loss of generality: a fully generalized therory is desirable, as for example the attempt suggested by E. B. Gliner [13], who has defined a "μ-medium" entirely derived from General Relativity considerations.

2 Short overview of the Double Solution Theory within wave mechanics (Louis de Broglie)

2.1 The reasons for implementing the theory

As an essential contribution to quantum physics, Louis de Broglie's wave mechanics theory has successfully extended the wave-particle duality concepts to the whole physics.

Double solution theory which aimed at confirming the

true physical nature of the wave function is based on two striking observations: within the Special Theory of Relativity, the frequency ν_0 of a plane monochromatic wave is transformed as

$$\nu = \frac{\nu_0}{\sqrt{1-\beta^2}}\,,$$

whereas a clock's frequency ν_0 is transformed according to $\nu_c = \nu_0\sqrt{1-\beta^2}$ with the phase velocity

$$\tilde{\mathrm{v}} = \frac{c}{\beta} = \frac{c^2}{\mathrm{v}}\,.$$

The 4-vector defined by the gradient of the plane monochromatic wave is linked to the energy-momentum 4-vector of a particle by introducing Planck's constant h as

$$W = h\nu\,, \quad \lambda = \frac{h}{p}\,, \tag{1}$$

where p is the particle's momentum and λ is the wave length.

If the particle is considered as that containing a rest energy $M_0c^2 = h\nu_0$, it is likened to a small clock of frequency ν_0 so that when moving with velocity $\mathrm{v} = \beta c$, its frequency different from that of the wave is then

$$\nu = \nu_0\sqrt{1-\beta^2}\,.$$

In the spirit of the theory, the wave is a physical entity having a very small amplitude not arbitrarily normed and which is distinct from the ψ-wave reduced to a statistical quantity in the usual quantum mechanical formalism.

Let us call ϑ the physical wave which is connected to the ψ-wave by the relation $\psi = C\vartheta$, where C is a normalizing factor.

The ψ-wave has then nature of a subjective probability representation formulated by means of the objective ϑ-wave.

Therefore wave mechanics is complemented by the double solution theory, for ψ and ϑ are two solutions of the same equation.

If the complete solution of the equation representing the ϑ-wave (or, if preferred, the ψ-wave, since both waves are equivalent according to $\psi = C\vartheta$), is written as

$$\vartheta = a(x,y,z,t)\,\exp\left[\frac{i}{\hbar}\,\phi(x,y,z,t)\right], \quad \hbar = \frac{h}{2\pi}\,, \tag{2}$$

where a and ϕ are real functions, while the energy W and the momentum p of the particle localized at point (x,y,z), at time t are given by

$$W = \partial_t\phi\,, \qquad p = -\operatorname{grad}\phi\,, \tag{3}$$

which in the case of a plane monochromatic wave, where one has

$$\phi = h\left[\nu - \frac{(\alpha x+\beta y+\gamma z)}{\lambda}\right]$$

yields equation (1) for W and p.

2.2 The guidance formula and the quantum potential

Taking Schrodinger's equation for the scalar wave ϑ, and U being the external potential, we get

$$\partial_t\vartheta = \frac{\hbar}{2im}\,\Delta\vartheta + \frac{i}{\hbar}\,U\vartheta\,. \tag{4}$$

This complex equation implies that ϑ be represented by two real functions linked by these two real equations which leads to

$$\vartheta = a\,\exp\left(\frac{i\phi}{\hbar}\right), \tag{5}$$

where a the wave's amplitude, and ϕ its phase, both are real. Substituting this value into equation (4), it gives two important equations

$$\left.\begin{aligned} &\partial_t\phi - U - \frac{1}{2m}\,(\operatorname{grad}\phi)^2 = -\frac{\hbar^2}{2m}\,\frac{\Delta a}{a} \\ &\partial_t(a^2) - \frac{1}{m}\,\operatorname{div}(a^2\operatorname{grad}\phi) = 0 \end{aligned}\right\}. \tag{6}$$

If terms involving Planck 's constant $\hbar$ in equation (6) are neglected (which amounts to disregard quanta), and if we set $\phi = S$, this equation becomes

$$\partial_t S - U = \frac{1}{2m}\,(\operatorname{grad} S)^2\,.$$

As S is the Jacobi function, this equation is the Jacobi equation of Classical Mechanics.

Only the term containing $\hbar^2$ is responsible for the particle's motion being different from the classical motion.

The extra term in (6) can be interpreted as another potential Q distinct from the classical U potential

$$Q = -\frac{\hbar^2}{2m}\,\frac{\Delta a}{a}\,. \tag{7}$$

One has thus a variable proper mass

$$M_0 = m_0 + \frac{Q_0}{c^2}\,, \tag{8}$$

where, in the particle's rest frame, Q_0 is a positive or negative variation of this rest mass and it represents the "quantum potential" which causes the wave function 's amplitude to vary.

By analogy with the classical formula $\partial_t S = E$, and $p = -\operatorname{grad} S$, E and p being the classical energy and momentum, one may write

$$\partial_t\phi = E\,, \qquad -\operatorname{grad}\phi = p\,. \tag{9}$$

As in non-relativistic mechanics, where p is expressed as a function of velocity by the relation $p = m\mathrm{v}$, one eventually finds the following results

$$\mathrm{v} = \frac{p}{m} = -\frac{1}{m}\,\operatorname{grad}\phi\,, \tag{10}$$

which is the *guidance formula*.

It gives the particle' s velocity, at position (x, y, z) and time t as a function of the local phase variation at this point.

Inspection shows that relativistic dynamics applied to the variable proper mass M_0 eventually leads to the following result

$$W = \frac{M_0c^2}{\sqrt{1-\beta^2}} = M_0c^2\sqrt{1-\beta^2} + \frac{M_0\mathrm{v}^2}{\sqrt{1-\beta^2}} \qquad (11)$$

known as the Planck-Laue formula.

Here, the quantum force results from the variation of M_0c^2 as the particle moves.

2.3 Particles with internal vibration and the hidden thermodynamics

The idea of considering the particle as a small clock is of central importance here.

Let us look at the self energy M_0c^2 as the hidden heat content of a particle. One easily conceives that such a small clock has (in its proper system) an internal periodic energy of agitation which does not contribute to the whole momentum. This energy is similar to that of a heat containing body in the state of thermal equilibrium.

Let Q_0 be the heat content of the particle in its rest frame, and viewed in a frame where the body has a velocity βc, the contained heat will be

$$Q = Q_0\sqrt{1-\beta^2} = M_0c^2\sqrt{1-\beta^2} = h\nu_0\sqrt{1-\beta^2}\,. \qquad (12)$$

The particle thus appears as being at the same time a small clock of frequency

$$\nu = \nu_0\sqrt{1-\beta^2}$$

and a small reservoir of heat

$$Q = Q_0\sqrt{1-\beta^2}$$

moving with velocity βc. If ϕ is the wave phase $a\exp(\frac{i\phi}{\hbar})$, where a and ϕ are real, the guidance theory states that

$$\partial_t\phi = \frac{M_0c^2}{\sqrt{1-\beta^2}}\,, \quad -\operatorname{grad}\phi = \frac{M_0\mathrm{v}}{\sqrt{1-\beta^2}}\,. \qquad (13)$$

The Planck-Laue equation may be written

$$Q = M_0c^2\sqrt{1-\beta^2} = \frac{M_0c^2}{\sqrt{1-\beta^2}} - \mathrm{v}\,p\,. \qquad (14)$$

Combining (13) and (14) results in

$$M_0c^2\sqrt{1-\beta^2} = \partial_t\phi + \mathrm{v}\operatorname{grad}\phi = \frac{d\phi}{dt}\,.$$

Since the particle is regarded as a clock of proper frequency $M_0\frac{c^2}{h}$, the phase of its internal vibration expressed with $a_i\exp(\frac{i\phi_i}{\hbar})$ and a_i and ϕ_i real will be

$$\phi_i = h\nu_0\sqrt{1-\beta^2}\,t = M_0c^2\sqrt{1-\beta^2}\,t\,,$$

thus we obtain

$$d\,(\phi_i - \phi) = 0\,. \qquad (15)$$

This fundamental result agrees with the assumption according to which the particle as it moves in its wave, remains constantly in phase with it.

3 Propagation in a dispersive refracting material

3.1 Group velocity

The classical wave is written as

$$a\,\exp[2\pi i(\nu t - kr)]\,; \qquad (16)$$

it propagates along the direction given by the unit vector n.

We next introduce the phase velocity $\tilde{\mathrm{v}}$ of the wave, which determines the velocity between two "phases" of the wave.

Consider now the superposition of two stationary waves having each a very close frequency: along the x-axis, they have distinct energies

$$E_1 = A\sin 2\pi(\nu + d\nu)\left[t - \frac{x}{\mathrm{v} + d\mathrm{v}}\right],$$

$$E_2 = A\sin 2\pi(\nu - d\nu)\left[t - \frac{x}{\mathrm{v} - d\mathrm{v}}\right],$$

thus next we have

$$\frac{\nu + d\nu}{\mathrm{v} + d\mathrm{v}} = \frac{\nu}{\mathrm{v}} + d\left(\frac{\nu}{\mathrm{v}}\right), \quad \frac{(\nu - d\nu)}{\mathrm{v} - d\mathrm{v}} = \frac{\nu}{\mathrm{v}} - d\left(\frac{\nu}{\mathrm{v}}\right),$$

and by adding both waves

$$E = 2A\cos 2\pi d\nu\left[t - x\left(\frac{d}{d\nu}\right)\left(\frac{\nu}{\mathrm{v}}\right)\right]\sin 2\pi\nu\left(t - \frac{x}{\mathrm{v}}\right). \qquad (17)$$

The term

$$2A\cos 2\pi d\nu\left[t - x\left(\frac{d}{d\nu}\right)\left(\frac{\nu}{\mathrm{v}}\right)\right] \qquad (18)$$

may be regarded as the resulting amplitude that varies along with the so-called "group velocity" $[\mathrm{v}]_g$ and such that

$$\frac{1}{[\mathrm{v}]_g} = \left(\frac{d}{d\nu}\right)\left(\frac{\nu}{\mathrm{v}}\right). \qquad (19)$$

Recalling the relation between the wave length λ and the material refracting index n

$$\lambda = \frac{\tilde{\mathrm{v}}}{\nu} = \frac{\mathrm{v}_0}{\mathrm{n}\nu} \qquad (20)$$

where v_0 is the wave velocity in a given reference material (c in vacuum), we see that

$$\mathrm{n} = \frac{\mathrm{v}_0}{\tilde{\mathrm{v}}}\,, \quad \text{i.e. in vacuum } \mathrm{n} = \frac{c}{\tilde{\mathrm{v}}}\,. \qquad (21)$$

Now, we have the Rayleigh formulae

$$\frac{1}{[\mathrm{v}]_g} = \frac{d}{d\nu}\left(\frac{\nu}{\mathrm{v}}\right) = \frac{1}{\nu_0}\left(\frac{\partial}{\partial\nu}\right)\mathrm{n}\nu = \left(\frac{\partial}{\partial\nu}\right)\left(\frac{1}{\lambda}\right). \qquad (22)$$

It is then easy to show that $[v]_g$ coincides with the velocity v of the particle, which is also expressed in term of the wave energy W as

$$[\mathrm{v}]_g = \frac{\partial W}{\partial k}\,.$$

The velocity of the particle v may be directed either in the propagating orientation of the wave in which case

$$p = k = \left(\frac{h}{\lambda}\right) n\,,$$

or in the opposite direction $p = -k = -\left(\frac{h}{\lambda}\right) n$.

When the particle's velocity $\mathrm{v} > 0$, and $p = k$, we have the Hamiltonian form

$$\mathrm{v} = \frac{\partial W}{\partial p}\,.$$

3.2 Influence of the refracting material

Let us recall the relativistic form of the Doppler's formulae:

$$\nu_0 = \frac{\nu\left(1 - \frac{\mathrm{v}}{\tilde{\mathrm{v}}}\right)}{\sqrt{1-\beta^2}}\,, \tag{23}$$

where as usual ν_0 is the wave's frequency in the frame attached to the particle.

Considering the classical relation $W = h\nu$ connecting the particle energy and its wave frequency, and taking into account (23), we have

$$W = W_0\sqrt{1-\beta^2}\left(1 - \frac{\mathrm{v}}{\tilde{\mathrm{v}}}\right).$$

However, inspection shows that the usual formula

$$W = \frac{W_0}{\sqrt{1-\beta^2}}$$

holds only if

$$1 - \frac{\mathrm{v}}{\tilde{\mathrm{v}}} = 1 - \beta^2,$$

which implies

$$\tilde{\mathrm{v}} = c^2$$

and this latter relation is satisfied provided we set

$$W = \frac{M_0c^2}{\sqrt{1-\beta^2}}\,, \quad p = \frac{M_0\mathrm{v}}{\sqrt{1-\beta^2}}\,,$$

where M_0 is the particle's proper mass which includes an extra term δM_0 resulting from the quantum potential Q contribution.

When the particule whose internal frequency is $\nu_0 = \frac{M_0c^2}{h}$ has travelled a distance dn during dt, its internal phase ϕ_i has changed by

$$d\phi_i = M_0c^2\sqrt{1-\beta^2}\,dt = d\phi\,,$$

where n is the unit vector normal to the phase surface.

The identity of the corresponding wave phase variation

$$d\phi = \partial_t\phi\,dt + \partial_n\phi\,dn = (\partial_t\phi + \mathrm{v}\,\mathrm{grad}\,\phi)\,dt$$

is also expressed by

$$\partial_t\phi + \partial_n\phi\,d_t n = d_t\phi_i\,, \tag{24}$$

and it leads to

$$\frac{M_0c^2}{\sqrt{1-\beta^2}} - \frac{M_0\mathrm{v}^2}{\sqrt{1-\beta^2}} = M_0c^2\sqrt{1-\beta^2}\,.$$

The situation is different in a refracting material which is likened to a "potential" P acting on the particle so that we write

$$W = \frac{M_0c^2}{\sqrt{1-\beta^2}} + P\,, \tag{25}$$

$$p = \frac{M_0\mathrm{v}}{\sqrt{1-\beta^2}} = \mathrm{v}\,\frac{W-P}{c^2}\,. \tag{26}$$

Now taking into account equation (23), the equation (24) reads (re-instating $\hbar$)

$$\frac{1}{\hbar}\,d_t\phi_i = \nu_0\sqrt{1-\beta^2} = \nu\left(1 - \frac{\mathrm{v}}{\tilde{\mathrm{v}}}\right)$$

yielding

$$W - \mathrm{v}^2\,\frac{W-P}{c^2} = W\left(1 - \frac{\mathrm{v}}{\tilde{\mathrm{v}}}\right) \tag{27}$$

from which we infer the expression of the potential P

$$P = W\left(1 - \frac{c^2}{\tilde{\mathrm{v}}}\,\mathrm{v}\right) = h\nu\left(1 - \frac{c^2}{\tilde{\mathrm{v}}}\,\mathrm{v}\right) \tag{28}$$

and with the Rayleigh formulae (22)

$$P = W\left[1 - \mathrm{n}\,\frac{\partial(\mathrm{n}\nu)}{\partial\nu}\right] \tag{29}$$

(we assume $\mathrm{v}_0 = c$), for the phase ϕ of the wave along the x-axis we find $d\phi = Wdt - kdx$ with

$$k = \mathrm{v}\,\frac{W-P}{c^2} = \frac{h}{\lambda}\,. \tag{30}$$

The phase concordance $hd\phi_i = hd\phi$ readily implies

$$(W - k\mathrm{v})\,dt = \left(W - \mathrm{v}^2\,\frac{W-P}{c^2}\right)dt \tag{31}$$

and taking into account (28),

$$d\phi_i = \frac{W}{h}\left(1 - \frac{\mathrm{v}}{\tilde{\mathrm{v}}}\right)dt = 2\pi\mathrm{v}\left(1 - \frac{\mathrm{v}}{\tilde{\mathrm{v}}}\right)dt\,. \tag{32}$$

Now applying the Doppler formulae (23), and bearing in mind the transformation $dt_0 = dt\sqrt{1-\beta^2}$, we can write

$$d\phi = 2\pi\nu_0 dt_0 = 2\pi\nu\left(1 - \frac{\mathrm{v}}{\tilde{\mathrm{v}}}\right)dt\,. \tag{33}$$

One easily sees that the equivalence of (32) and (33) fully justifies the form of the "potential" P.

4 The particle-antiparticle state

4.1 Reduction of the EGR tensor to the Riemannian scheme

4.1.1 Massive tensor in the EGR formulation

Setting the 4-unit velocity $u^a = \frac{dx^a}{ds}$ which obeys here

$$g_{ab}\, u^a u^b = g^{ab} u_a u_b = 1\,.$$

Expressed in mixed indices, the usual Riemannian massive tensor is well known

$$(T_a^b)_{\text{Riem}} = \rho_0 c^2 u^b u_a\,, \tag{34}$$

where ρ_0 is the proper density of the mass.

In the EGR formulation, the massive tensor is given by

$$(T_a^b)_{\text{EGR}} = (\rho_0)_{\text{EGR}} c^2 (u^b)_{\text{EGR}} (u_a)_{\text{EGR}} + (T_a^b)_{\text{field}}\,. \tag{35}$$

The EGR world velocity is not explicitly written but it carries a small correction w.r.t. to the regular Riemannian velocity u^a.

The EGR density ρ_0 is also modified, as was shown in our paper [8] which explains the random perturbation of the fluid.

Let us now express $(T_a^b)_{\text{EGR}}$ in terms of the Riemannian representation

$$(T_a^b)_{\text{EGR}} = (T_a^b)^\star_{\text{Riem}}\,. \tag{36}$$

With respect to $(T_a^b)_{\text{Riem}}$, the tensor $(T_a^b)^\star_{\text{Riem}}$ is obviously only modified through the Riemannian proper density ρ we denote $\rho^\star$ since now.

Having said that, we come across a difficulty since the quantity $(T_a^b)_{\text{EGR}}$ is antisymmetric whereas $(T_a^b)^\star_{\text{Riem}}$ is symmetric.

In order to avoid this ambiguity, we restrict ourselves to a space-time section $x^4 = const$. In this case, we consider the tensor $(T_4^b)_{\text{EGR}}$ which we split up into

$$(T_4^\alpha)_{\text{EGR}} = (T_4^\alpha)^\star_{\text{Riem}}\,, \tag{37}$$

$$(T_4^4)_{\text{EGR}} = (T_4^4)^\star_{\text{Riem}}\,. \tag{38}$$

Inspection shows that each of the EGR tensors components when considered separately in (37) and (38) is now symmetric.

4.1.2 The modified proper mass

We write down the above components

$$(T_4^\alpha)^\star_{\text{Riem}} = \rho_0^\star c^2 u^\alpha u_4\,, \tag{39}$$

$$(T_4^4)^\star_{\text{Riem}} = \rho_0^\star c^2 u^4 u_4\,. \tag{40}$$

This amounts to state that the proper density ρ_0 is modified by absorbing the EGR free field component $(T_a^b)_{\text{field}}$ tensor.

By the modification, we do not necessarily mean an "increase", as will be seen in the next sections.

4.2 Refracting material

4.2.1 Energy-momentum tensor

We now consider a dispersive refracting material which is characterized by a given (variable) index denoted by n.

Unlike a propagation in vacuum, a particle progressing through this material will be subject to a specific "influence" which is acting upon the tensor $(T_4^b)^\star_{\text{Riem}}$. Thus, the energy-momentum tensor of the system will thus be chosen to be

$$(T_4^b)^\star_{\text{Riem}} = \rho_0^\star c^2 u^b u_4 - \delta_4^b b(\text{n})\,, \tag{41}$$

where $b(\text{n})$ is a scalar term representing the magnitude of the influence and which is depending on the refracting index n.

The tensor $\delta_4^b b(\text{n})$ is reminiscent of a "pressure term" which appears in the perfect fluid solution except that no equation of state exists.

Equation (41) yields

$$(T_4^\alpha)^\star_{\text{Riem}} = \rho_0^\star c^2 u^\alpha u_4\,, \tag{42}$$

$$(T_4^4)^\star_{\text{Riem}} = \rho_0^\star c^2 + b(\text{n})\,, \tag{43}$$

Applying the relation $u^\alpha c = \text{v}^\alpha u^4$, equation (42) becomes

$$(T_4^\alpha)^\star_{\text{Riem}} = \rho_0^\star c\, \text{v}^\alpha. \tag{44}$$

4.2.2 Integration over the hypersurface $x^4 = const$

Integration of (43) over the spatial volume V yields

$$(P^4)^\star_{\text{Riem}} = \frac{1}{c}\int \rho_0^\star c^2 \sqrt{-g}\, d\text{V} + \frac{1}{c}\int b(\text{n})\sqrt{-g}\, d\text{V}, \tag{45}$$

$$c\,(P^4)^\star_{\text{Riem}} = m_0^\star c^2 + B(\text{n})\,, \tag{46}$$

while integrating (44), we get a 3-momentum vector

$$(P^\alpha)^\star_{\text{Riem}} = \frac{1}{c}\int \rho_0^\star c\, \text{v}^\alpha \sqrt{-g}\, d\text{V}, \tag{47}$$

$$(P^\alpha)^\star_{\text{Riem}} = m_0^\star \text{v}^\alpha. \tag{48}$$

4.2.3 Matching the formulas of de Broglie

Let us multiply, respectively, (46) and (48) by u^4

$$u^4 c\,(P^4)^\star_{\text{Riem}} = u^4 m_0^\star c^2 + u^4 B(\text{n})\,; \tag{49}$$

if we set $P = u^4 B(\text{n})$, we retrieve de Broglie's first formula (25)

$$u^4 c\,(P^4)^\star_{\text{Riem}} = W = \frac{m_0^\star c^2}{\sqrt{1-\beta^2}} + P(\text{n}) \tag{50}$$

as well as the second formula (26)

$$u^4\,(P^\alpha)^\star_{\text{Riem}} = p = \frac{m_0^\star \text{v}^\alpha}{\sqrt{1-\beta^2}}\,. \tag{51}$$

5 A new aspect of the antiparticle concept

5.1 Proper mass

In §4.1.2 we have considered the modified proper density $\rho_0^\star$, resulted from the EGR persistent free field "absorbed" by the tensor in the Riemannian scheme.

Having established the required generalization, we now revert to the classical formulation as suggested by de Broglie.

The corresponding modified proper mass $m_0^\star$ should always be positive, therefore we are bound to set

$$p = k \ \text{ if } \ \mathrm{v} > 0\,, \qquad p = -k \ \text{ if } \ \mathrm{v} < 0\,. \tag{52}$$

With these, we infer

$$\frac{m_0^\star}{\sqrt{1-\beta^2}} = \pm\frac{W-P}{c^2} \tag{53}$$

that is

$$m_0^\star = \pm\,\frac{W}{\tilde{\mathrm{v}}\mathrm{v}}\sqrt{1-\beta^2}\,. \tag{54}$$

For propagation in vacuum we have $P = 0$, $\mathrm{v} = \mathrm{v}_0 = c^2/\tilde{\mathrm{v}}$, and $W = m_0c^2/\sqrt{1-\beta^2}$ which implies, a expected,

$$m_0^\star = m_0\,.$$

5.2 Antiparticles state

The early theory of antiparticles is due to P. A. M. Dirac after he derived his famous relativistic equation revealing the electron-positon symmetric state. In order to explain the production of a pair "electron-positon", Dirac postulated the presence of an underlying medium filled with electrons e bearing a negative energy $-m_0c^2$.

An external energy input $2m_0c^2$ would cause an negative energy electron to emerge from the medium as a positive energy one, thus become observable. The resulting "hole" would constitute, in this picture, an "observable" particle, positon, bearing a positive charge.

With Louis de Broglie, we follow this postulate: we consider that the hidden medium should also be filled with particles bearing a negative proper energy. Therefore the proper mass "modification" discussed above is expressed by

$$m_0^\star = -\,m_0 \tag{55}$$

and is true in the medium.

At this point, two fundamental situations are to be considered as follows:

a) The "normal" situation where $P = 0$, $m_0^\star$, and $\mathrm{v} = \mathrm{v}_0$;

b) The "singular" situation where $P = 2W$, in which case, according to (28) and (29), the following relations are obtained

$$\mathrm{n}\,\frac{\partial(\mathrm{n}\nu)}{\partial\nu} = -1.$$

Hence, in the "singular" situation b),

$$\frac{1}{[\mathrm{v}]_g} = \frac{\partial\left(\frac{1}{\lambda}\right)}{\partial\nu} = -\frac{\tilde{\mathrm{v}}}{c^2} = -\frac{1}{\mathrm{v}_0}\,,$$

from which is inferred

$$W = \frac{m_0^\star c^2}{\sqrt{1-\beta^2}} + P = -\frac{m_0^\star c^2}{\sqrt{1-\beta^2}}\,, \quad W = \frac{m_0^\star c^2}{\sqrt{1-\beta^2}}\,. \tag{56}$$

On the other hand

$$\left.\begin{aligned} k = \mathrm{v}_0\,\frac{(W-P)}{c^2} = \frac{m_0^\star \mathrm{v}_0}{\sqrt{1-\beta^2}}\,, \quad k = \frac{m_0\mathrm{v}_0}{\sqrt{1-\beta^2}} \\ p = -\,k = -\frac{m_0\mathrm{v}_0}{\sqrt{1-\beta^2}} \end{aligned}\right\}. \tag{57}$$

Within this interpretation, the *observed* antiparticle has an opposite charge, a positive rest mass m_0 and a reversed velocity v_0 with respect to the phase wave propagation.

The state of electron-positon requires negative energies *bounded* to the sub-quantum medium which can be now further explicited.

The external energy input $2m_0c^2$ causes a positive (observable) energy of the electron to emerge from the medium according to

$$-\,m_0c^2 + 2m_0c^2 = m_0c^2. \tag{58}$$

However, the charge conservation law requires the simultaneous emergence of an electron with positive rest energy m_0c^2 implying for the hidden medium to supply a *total* energy of $2m_0c^2$. In other words, we should have

$$Q = 2m_0c^2. \tag{59}$$

5.3 Introducing the quantum potential

Following the same pattern as above, the quantum potential Q is now assumed to act as a dispersive refracting material.

This means that $Q = P$ where the definition (8) holds now, for $m_0^\star$,

$$Q = M_0c^2 - m_0^\star c^2. \tag{60}$$

Since $m_0^\star c^2 = -\,m_0c^2$, we have with (59)

$$M_0 = m_0\,.$$

The energy and the momentum of the antiparticle are now given by

$$W = \frac{M_0c^2}{\sqrt{1-\beta^2}} = \frac{m_0c^2}{\sqrt{1-\beta^2}}\,, \tag{61}$$

$$p = \frac{M_0\mathrm{v}}{\sqrt{1-\beta^2}} = -\frac{m_0\mathrm{v}_0}{\sqrt{1-\beta^2}} = -\,k. \tag{62}$$

Clearly, the value obtained here for p characterizes a particle whose velocity direction v is opposite to that of the associated wave $-\,\mathrm{v}_0$.

This result perfectly matches the equation (57), which is physically satisfied.

6 Concluding remarks

According to the double solution theory, there exists a close relationship between the guidance formula, and the relativistic thermodynamics.

Following this argument, it is interesting to try to connect the entropy with the particle/antiparticle production process as it is derived above.

We first recall the classical action integral for the free particle :

$$\mathfrak{a} = \int L\,dt = -\int M_0c^2\sqrt{1-\beta^2}\,dt\,. \tag{63}$$

If we choose a period T_i of the particle's internal vibration (its proper mass is M_0) as the intergration interval, from (12) we have

$$\frac{1}{T_i} = \frac{m_0c^2}{h}\sqrt{1-\beta^2} \tag{64}$$

so that a "cyclic" action integral be defined as

$$\frac{\mathfrak{a}}{h} = -\int_0^{T_i} M_0c^2\sqrt{1-\beta^2}\,dt = -\frac{M_0c^2}{m_0c^2} \tag{65}$$

(T_i is assumed to be always short so that M_0 and $\beta^2 = \frac{v^2}{c^2}$ can be considered as constants over the integration interval).

Denoting the hidden thermostat's entropy by $\mathfrak{s}$, we set

$$\frac{\mathfrak{s}}{\Re} = \frac{\mathfrak{a}}{h}\,, \tag{66}$$

where $\Re$ is Boltzmann's constant.

Since

$$\delta Q_0 = \delta m_0c^2,$$

we obtain

$$\delta\mathfrak{s} = -\,\Re\,\frac{\delta Q_0}{m_0c^2}\,. \tag{67}$$

An entropy has thus been determined for the single particle surrounded by its guiding wave. According to Boltzmann's relation

$$\mathfrak{s} = \Re\ln\mathcal{P},$$

where $\mathcal{P} = \exp\left(\frac{\mathfrak{s}}{\Re}\right)$ is the probability characterizing the system.

In this view, the prevailing plane monochromatic wave representing the quantized (stable) stationary states corresponds to an entropy maxima, whereas the other states also exist but with a much reduced probability.

Now, we revert to the hidden sub-quantum medium which thus supplies the equivalent heat quantity

$$Q_0 = Q\,. \tag{68}$$

The definition (8) can be re-written as

$$Q_0 = M_0c^2 - m_0c^2. \tag{69}$$

Therefore, according to the formula (67), the medium is needed to supply an energy of $2m_0c^2$ that is characterized by an entropy decrease of $2\Re$.

Its probability being reduced, this explains why an antiparticle is *unstable*.

So, the thermodynamics approach, which could at first glance seem strange in quantum theory, eventually finds here a consistent ground. It is linked to "probability" situations which fit in the physical processes involving wave "packet" propagations within the guidance of the single particle.

We have tried here to provide a physical interpretation of the sub-quantum medium from which the particle-antiparticle symmetry originates within the double solution theory elaborated by Louis de Broglie. In the Riemannian approximation which we have presented above, the introduction of a term generalizing the quantum potential would appear as that having a somewhat degree of arbitrariness. However, if one refers to our extended general relativity theory (EGR theory), the introduction of this term is no longer arbitrary as it naturally arises from its main feature.

Submitted on January 22, 2010 / Accepted on January 29, 2010

References

1. De Broglie L. Eléments de la théorie des quantas et de mécanique ondulatoire. Gauthier-Villars, Paris, 1959.
2. De Broglie L. Une interprétation causale et non linéaire de la mécanique ondulatoire: la théorie de la double solution. Gauthier-Villars, Paris, 1960.
3. De Broglie L. La réinterprétation de la mécanique ondulatoire. Gauthier-Villars, Paris, 1971.
4. De Broglie L. Thermodynamique relativiste et mécanique ondulatoire. *Ann. Inst. Henri Poincaré*, 1968, v.IX, no.2, 89–108.
5. Bohm D. and Vigier J.P. Model of the causal interpretation of quantum theory in terms of a fluid with irregular fluctuations. *Physical Review*, 1954, v.96, no.1, 208–216.
6. Fer F. Construction d'une équation non linéaire en théorie de la double solution. *Séminaire Louis de Broglie*, Faculté des Sciences de Paris, 1955, exposé no.3.
7. Marquet P. The EGR theory: an extended formulation of General Relativity. *The Abraham Zelmanov Journal*, 2009, v.2, 148–170.
8. Marquet P. On the physical nature of the wave function: a new approach through the EGR theory. *The Abraham Zelmanov Journal*, 2009, 195–207.
9. De Broglie L. Etude du mouvement des particules dans un milieu réfringent. *Ann. Inst. Henri Poincaré*, 1973, v.XVIII, no.2, 89–98.
10. De Broglie L. La dynamique du guidage dans un mileu réfringent et dispersif et la théorie des antiparticules. *Le Journal de Physique*, 1967, tome 28, no.5–6, 481–486.
11. Greiner W. and Reinhardt J. Field quantization. Springer, Berlin, 1996, p.108–109.
12. Dirac P.A.M. Is there an aether? *Nature*, 1951, v.168, 906–907.
13. Gliner E.B. Algebraic properties of the energy-momentum tensor and vacuum like state of matter. *Soviet Physics JETP*, 1966, v.22, no.2, 378–383.

A Derivation of $\pi(n)$ Based on a Stability Analysis of the Riemann-Zeta Function

Michael Harney* and Ioannis Iraklis Haranas†

*841 North 700 West, Pleasant Crove, Utah, 84062, USA. E-mail: michael.harney@signaldisplay.com
†Department of Physics and Astronomy, York University, 314 A Pertie Science Building North York, Ontario, M3J-1P3, Canada. E-mail: ioannis@yorku.ca

The prime-number counting function $\pi(n)$, which is significant in the prime number theorem, is derived by analyzing the region of convergence of the real-part of the Riemann-Zeta function using the unilateral z-transform. In order to satisfy the stability criteria of the z-transform, it is found that the real part of the Riemann-Zeta function must converge to the prime-counting function.

1 Introduction

The Riemann-Zeta function, which is an infinite series in a complex variable s, has been shown to be useful in analyzing nuclear energy levels [1] and the filling of s_1-shell electrons in the periodic table [2]. The following analysis of the Riemann-Zeta function with a z-transform shows the stability zones and requirements for the real and complex variables.

2 Stability with the z-transform

The Riemann-Zeta function is defined as

$$\Gamma(s) = \sum_{n=1}^{\infty} n^{-s}. \tag{1}$$

We start by setting the following equality

$$\Gamma(s) = \sum_{n=1}^{\infty} n^{-s} = \sum_{n=1}^{\infty} e^{-as}. \tag{2}$$

Then by simplifying

$$n^{-s} = e^{-as} = e^{-a(r+j\omega)} \tag{3}$$

and taking natural logarithm of both sides we obtain

$$-s\ln(n) = -as. \tag{4}$$

We then find the constant a such that

$$a = \ln(n). \tag{5}$$

We then apply the unilateral z-transform on (1):

$$\Gamma(s) = \sum_{n=1}^{\infty} n^{-s} z^{-n} = \sum_{n=1}^{\infty} e^{-as} z^{-n} = \sum_{n=1}^{\infty} e^{-a(r+j\omega)} z^{-n}. \tag{6}$$

Substituting (5), the real part of (6) becomes:

$$\mathrm{Re}\,[\Gamma(s)] = \sum_{n=1}^{\infty} e^{-ar} z^{-n} = \sum_{n=1}^{\infty} e^{-r\ln(n)} z^{-n}. \tag{7}$$

In order to find the region of convergence (ROC) of (7), we have to factor (7) to the common exponent $-n$, which requires

$$r = n/\ln(n), \tag{8}$$

which is the same as saying that the real part of $\Gamma(s)$ must converge to the prime-number counting function $\pi(n)$. With (8) satisfied, (7) becomes

$$\mathrm{Re}\,[\Gamma(s)] = \sum_{n=1}^{\infty} (ez)^{-n}. \tag{9}$$

which has a region of convergence (ROC)

$$\mathrm{ROC} = \frac{1}{1 - \dfrac{1}{ez}}. \tag{10}$$

To be within the region of convergence, z must satisfy the following relation

$$|z| > e^{-1} \quad \text{or} \quad |z| > 0.368. \tag{11}$$

which, places z within the critical strip. It can also be shown that the imaginary part of (6)

$$\mathrm{Im}\,[\Gamma(s)] = \sum_{n=1}^{\infty} e^{-aj\omega} z^{-n} = \sum_{n=1}^{\infty} e^{-j\omega\ln(n)} z^{-n}. \tag{12}$$

converges based on the Fourier series of $\sum e^{-j\omega\ln(n)}$.

3 Conclusions

The prime number-counting function $\pi(n)$ has been derived from a stability analysis of the Riemann-Zeta function using the z-transform. It is found that the real part of the roots of the zeta function correspond to $\pi(n)$ under the conditions of stability dictated by the unit-circle of the z-transform. The distribution of prime numbers has been found to be useful in analyzing electron and nuclear energy levels.

Submitted on November 11, 2009 / Accepted on December 16, 2009

References

1. Dyson F. Statistical theory of the energy levels of complex systems. III. *Journal of Mathematical Physics*, 1962, v. 3, 166–175.
2. Harney M. The stability of electron orbital shells based on a model of the Riemann-Zeta function. *Progress in Physics*, 2008, v. 1, 1–5.

On the Significance of the Upcoming Large Hadron Collider Proton-Proton Cross Section Data

Eliahu Comay

Charactell Ltd., PO Box 39019, Tel-Aviv, 61390, Israel. E-mail: elicomay@post.tau.ac.il

The relevance of the Regular Charge-Monopole Theory to the proton structure is described. The discussion relies on classical electrodynamics and its associated quantum mechanics. Few experimental data are used as a clue to the specific structure of baryons. This basis provides an explanation for the shape of the graph of the pre-LHC proton-proton cross section data. These data also enable a description of the significance of the expected LHC cross section measurements which will be known soon. Problematic QCD issues are pointed out.

1 Introduction

Scattering experiments are used as a primary tool for investigating the structure of physical objects. These experiments can be divided into several classes, depending on the kind of colliding particles. The energy involved in scattering experiments has increased dramatically during the previous century since the celebrated Rutherford experiment was carried out (1909). Now, the meaningful value of scattering energy is the quantity measured in the rest frame of the projectile-target center of energy. Therefore, devices that use colliding beams enable measurements of very high energy processes. The new Large Hadron Collider (LHC) facility at CERN, which is designed to produce 14 TeV proton-proton (pp) collisions, will make a great leap forward.

This work examines the presently available pp elastic and total cross section data (denoted by ECS and TCS, respectively) and discusses the meaning of two possible alternatives for the LHC pp ECS values which will be known soon. The discussion relies on the Regular Charge-Monopole Theory (RCMT) [1,2] and its relevance to strong interactions [3,4].

Section 2 contains a continuation of the discussion presented in [4]. It explains the meaning of two possible LHC results of the pp ECS. Inherent QCD difficulties to provide an explanation for the data are discussed in section 3. The last section contains concluding remarks.

2 The proton-proton elastic cross section

The discussion carried out below is a continuation of [4]. Here it aims to examine possible LHC's ECS results and their implications for the proton structure. Thus, for the reader's convenience, the relevant points of [4] are presented briefly in the following lines.

RCMT is the theoretical basis of the discussion and strong interactions are regarded as interactions between magnetic monopoles which obey the laws derived from RCMT. Two important results of RCMT are described here:

1. Charges do not interact with bound fields of monopoles and monopoles do not interact with bound fields of charges. Charges interact with all fields of charges and with radiation fields emitted from monopoles. Analogously, monopoles interact with all fields of monopoles and with radiation fields emitted from charges.
2. The unit of the elementary magnetic charge g is a free parameter. However, hadronic data indicate that this unit is much larger than that of the electric charge: $g^2 \gg e^2 \simeq 1/137$. (Probably $g^2 \simeq 1$.)

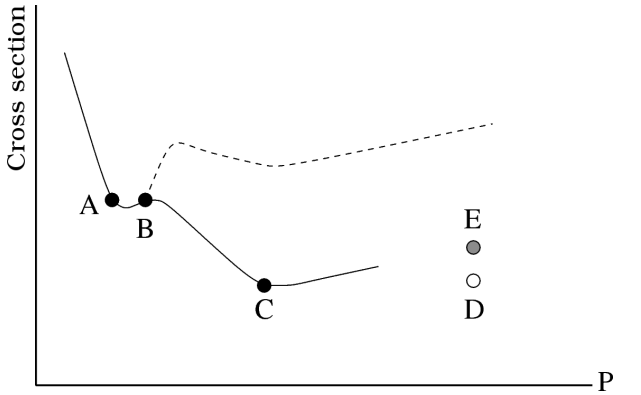

Fig. 1: A qualitative description of the pre-LHC proton-proton cross section versus the laboratory momentum P. Axes are drawn in a logarithmic scale. The solid line denotes elastic cross section and the broken line denotes total cross section. (The accurate figure can be found in [5]). Points A-E help the discussion (see text).

The application of RCMT to strong interactions regards quarks as spin-1/2 Dirac particles that carry a unit of magnetic monopole. A proton has three valence quarks *and* a core that carries three monopole units of the opposite sign. Thus, a proton is a magnetic monopole analogue of a nonionized atom. By virtue of the first RCMT result, one understands why electrons (namely, pure charges) do not participate in strong interactions whereas photons do that [6]. Referring to the pre-LHC data, it is shown in [4] that, beside the three valence quarks, a proton has a core that contains inner closed shells of quarks.

Applying the correspondence between a nonionized atom and a proton, one infers the validity of screening effects and of an analogue of the Franck-Hertz effect that takes place for the

proton's quarks. Thus, quarks of closed shells of the proton's core behave like inert objects for cases where the projectile's energy is smaller than the appropriate threshold.

The pre-LHC pp scattering data is depicted in Fig. 1. Let ep denote both electron-proton and positron-proton interaction. Comparing the ep scattering data with those of pp, one finds a dramatic difference between both the ECS and the TCS characteristics of these experiments. Thus, the deep inelastic and the Rosenbluth ep formulas respectively show that TCS *decreases* together with an increase of the collision energy and that at the high energy region, ECS decreases even faster and takes a negligible part of the entire TCS events (see [7], p. 266). The pp data of Fig. 1 show a completely different picture. Indeed, for high energy, both the TCS and the ECS pp graphs *go up* with collision energy and ECS takes about 15% of the total events.

The last property proves that a proton contains a quite solid component that can take the heavy blow of a high energy pp collision and leave each of the two colliding protons intact. Valence quarks certainly cannot do this, because in the case of a high energy ep scattering, an electron collides with a valence quark. Now, in this case, deep inelastic scattering dominates and elastic events are very rare. The fact that the quite solid component is undetected in an ep scattering experiment, proves that it is a spinless electrically neutral component. This outcome provides a very strong support for the RCMT interpretation of hadrons, where baryons have a core [3,4].

The foregoing points enable one to interprete the shape of the pp ECS graph of Fig. 1. Thus, for energies smaller than that of point A of the figure, the wave length is long and effects of large distance between the colliding protons dominate the process. Here the ordinary Coulomb potential, $1/r$, holds and the associated $1/p^2$ decrease of the graph is in accordance with the Rutherford and Mott formulas (see [7], p. 192)

$$\left(\frac{d\sigma}{d\Omega}\right)_{\text{Mott}} = \frac{\alpha^2 \cos^2\left(\frac{\theta}{2}\right)}{4p^2 \sin^4\left(\frac{\theta}{2}\right)\left[1 + \frac{2p}{M}\sin^2\left(\frac{\theta}{2}\right)\right]}\,. \qquad (1)$$

At the region of points A-B, the rapidly varying nuclear force makes the undulating shape of the graph. Results of screening effects of the valence quarks are seen for momentum values belonging to the region of points B-C. Indeed, a correspondence holds for electrons in an atom and quarks (that carry a monopole unit) in a proton. Hence, for a core-core interaction, the screening associated with the valence quarks weakens as the distance from the proton's center becomes smaller. It means that the strength of the core's monopole potential arises faster than the Coulomb $1/r$ formula. For this reason, the decreasing slope of the graph between points B-C is smaller than that which is seen on the left hand side of point A.

The ECS graph stops decreasing and begins to increase on the right hand side of point C. This change of the graph's slope indicates that for this energy a new effect shows up. Indeed, assume that the proton consists of just valence quarks and an elementary pointlike core which is charged with three monopole units of the opposite sign. Then, as the energy increases and the wave length decreases, the contribution of the inner proton region becomes more significant. Now, at inner regions, the valence quarks' screening effect fades away and the potential tends to the Coulomb formula $1/r$. Hence, in this case, the steepness of the decreasing graph between points B-C *should increase* near point C and tend to the Coulomb-like steepness of the graph on the left hand side of point A. The data negate this expectation. Thus, the increase of the graph on the right hand side of point C indicates the existence of inner closed shells of quarks at the proton. It is concluded that at these shells, a new screening effect becomes effective.

It is interesting to note that at the same momentum region also the TCS graph begins to increase and that on the right hand side of point C, the vertical distance between the two graphs is uniform. The logarithmic scale of the figure proves that, at this region, the ratio ECS to TCS practically does not change. The additional TCS events are related to an analogue of the Franck-Hertz effect. Here a quark of the closed shells is struck out of its shell. This effect corresponds to the ep deep inelastic process and it is likely to produce an inelastic event.

The main problem to be discussed here is *the specific structure of the proton's closed shells of quarks.* One may expect that the situation takes the simplest case and that the core's closed shells consist of just two u quarks and two d quarks that occupy an S shell. The other extreme is the case where the proton is analogous to a very heavy atom and the proton's core contains many closed shells of quarks. Thus, the energy of the higher group of the core's shells takes quite similar value and their radial wave functions partially overlap. (Below, finding the actual structure of the proton's core is called Problem *A*.) The presently known pp ECS data which is depicted in Fig. 1 is used for describing the relevance of the LHC future data to Problem *A*.

The rise of the pp ECS graph on the right hand side of point C is related to a screening effect of the proton's inner closed shells that takes a repulsive form. An additional contribution is the repulsive phenomenological force that stems from Pauli's exclusion principle which holds for quarks of the inner shells of the two colliding protons. Now, if the simplest case which is described above holds then, for higher energies, this effect should diminish and the graph is expected to stop rising and pass near the open circle of Fig. 1, which is marked by the letter D. On the other hand, if the proton's core contains several closed shells having a similar energy and a similar radial distribution, then before the screening contribution of the uppermost closed shell fades away another shell is expected to enter the dynamics. In this case, the graph is expected to continue rising up to the full LHC energy and pass near the gray circle of Fig. 1, which is marked by the letter E [8].

The foregoing discussion shows one example explaining how the LHC data will improve our understanding of the proton's structure.

3 Inherent QCD difficulties

Claims stating that QCD is unable to provide an explanation for the pp cross section data have been published in the last decade [9]. Few specific reasons justifying these claims are listed below. The examples rely on QCD's main property where baryons consist of three valence quarks, gluons and possible pairs of quark-antiquark:

- Deep inelastic ep scattering proves that for a very high energy, elastic events are very rare (see [7], p. 266). It means that an inelastic event is found for nearly every case where a quark is struck violently by an electron. On the other hand, Fig. 1 proves that for high energy, elastic pp events take about 15% of the total events. Therefore, one wonders what is the proton's component that takes the heavy blow of a high energy pp collision and is able to leave the two colliding protons intact? Moreover, why this component is not observed in the corresponding ep scattering?
- A QCD property called Asymptotic Freedom (see [10], p. 397) states that the interaction strength tends to zero at a very small vicinity of a QCD particle. Thus, at this region, a QCD interaction is certainly much weaker than the corresponding Coulomb-like interaction. Now, the general expression for the elastic scattering amplitude is (see [7], p. 186)

$$M_{if} = \int \psi_f^* V \psi_i \, d^3x \,, \qquad (2)$$

  where V represents the interaction. Evidently, for very high energy, the contribution of a very short distance between the colliding particles dominates the process. Therefore, if asymptotic freedom holds then the pp ECS line is expected to show a *steeper decrease* than that of the Coulomb interaction, which is seen on the left hand side of point A of Fig. 1. The data of Fig. 1 proves that for an energy which is greater than that of point C of Fig. 1, the pp ECS line *increases*. Hence, the data completely contradict this QCD property.
- A general argument. At point C of Fig. 1, the ECS graph changes its inclination. Here it stops decreasing and begins to increase. This effect proves that for this energy value, *something new shows up in the proton.* Now, QCD states that quarks and gluons are elementary particles that move quite freely inside the proton's volume. Therefore, one wonders how can QCD explain why a new effect shows up for this energy?

Each of these specific points illustrates the general statement of [9], concerning QCD's failure to describe the high energy pp cross section data.

4 Concluding remarks

The following lines describe the logical structure of this work and thereby help the reader to evaluate its significance.

A construction of a physical theory must assume the validity of some properties of the physical world. For example, one can hardly imagine how can a person construct the Minkowski space with *three* spatial dimensions, if he is not allowed to use experimental data. Referring to the validity of a physical theory, it is well known that unlike a mathematical theory which is evaluated just by pure logics, a physical theory must also be consistent with well established experimental data that belong to its domain of validity. The Occam's razor principle examines another aspect of a theory and prefers a theory that relies on a minimal number of assumptions. Thus, the Occam's razor can be regarded as a "soft" acceptability criterion for a theory.

Following these principles, the assumptions used for the construction of RCMT and of its application to strong interactions are described below. The first point has a theoretical character and the rest rely on experimental results that serve as a clue for understanding the specific structure of baryons:

- A classical regular charge-monopole theory is built on the basis of duality relations which hold between ordinary Maxwellian theory of charges together with their fields and a monopole system together with its associated fields [2]. (In [1], it is also required that the theory be derived from a regular Lagrangian density.) Like ordinary electrodynamics, this theory is derived from the variational principle where regular expressions are used. Therefore, the route to quantum mechanics is straightforward.
- In RCMT, the value of the elementary monopole unit g is a free parameter. Like the case of the electric charge, it is assumed that g is quantized. It is also assumed that its elementary value $g^2 \gg e^2 \simeq 1/137$. (Probably, $g^2 \simeq 1$.).
- It is assumed that strong interactions are interactions between monopoles. The following points describe the specific systems that carry monopoles.
- It is assumed that quarks are spin 1/2 Dirac particles that carry a unit of magnetic monopole. (As a matter of fact, it can be *proved* that an elementary massive quantum mechanical particle is a spin-1/2 Dirac particle [11].)
- It is assumed that baryons contain *three* valence quarks. It follows that baryons must have a core that carries three monopole units of the opposite sign.
- It is assumed that the baryonic core contains closed shells of quarks.

The discussion carried out in [4] and in section 2 of this work explains how RCMT can be used for providing a qualitative interpretation of the shape of the graph that describes

the elastic pp scattering data. In particular, an explanation is provided for the relation between the pre-LHC pp elastic cross section data and the existence of closed shells of quarks at the baryonic core. It is also explained how the upcoming LHC data will enrich our understanding of the structure of baryonic closed shells of quarks by providing information on whether there are just two active closed shells of u and d quarks or there are many shells having a quite similar energy value and radial distribution.

QCD's inherent difficulties to provide an explanation for the high energy pre-LHC pp scattering data are discussed in the third section. Screening effects of proton's quarks are used in the Regular Charge-monopole Theory's interpretation of the elastic cross section pp scattering. It is interesting to note that this kind of screening also provides an automatic explanation for the first EMC effect [12]. This effect compares the quarks' Fermi motion in deuteron and iron (as well as other heavy nuclei). The data show that the Fermi motion is smaller in hevier nuclei. This experimental data and the Heisenberg uncertainty relations prove that the quarks' self-volume increases in heavier nuclei. In spite of the quite long time elapsed, QCD supporters have not yet provided an adequate explanation for the first EMC effect [13].

Submitted on January 23, 2010 / Accepted on February 09, 2010

References

1. Comay E. Axiomatic deduction of equations of motion in Classical Electrodynamics. *Nuovo Cimento B*, 1984, v. 80, 159–168.
2. Comay E. Charges, monopoles and duality relations. *Nuovo Cimento B*, 1995, v. 110, 1347–1356.
3. Comay E. A regular theory of magnetic monopoles and its implications. In: *Has the Last Word Been Said on Classical Electrodynamics?* ed. A. Chubykalo, V. Onochin, A. Espinoza and R. Smirnov-Rueda. Rinton Press, Paramus, NJ, 2004.
4. Comay E. Remarks on the proton structure. *Apeiron*, 2009, v. 16, 1–21.
5. Amsler C. et al. (Particle Data Group) Review of particle properties. *Phys. Lett. B*, 2008, v. 667, 1–1340. (See p. 364).
6. Bauer T. H., Spital R. D., Yennie D. R. and Pipkin F. M. The hadronic properties of the photon in high-energy interactions. *Rev. Mod. Phys.*, 1978, v. 50, 261–436.
7. Perkins D. H. Introduction to high energy physics. Addison-Wesley, Menlo Park, CA, 1987.
8. This possibility has been overlooked in [4].
9. Arkhipov A. A. On global structure of hadronic total cross-sections. arXiv: hep-ph/9911533.
10. Frauenfelder H. and Henley E. M. Subatomic physics. Prentice Hall, Englewood Cliffs, 1991. (see pp. 296–304.)
11. Comay E. Physical consequences of mathematical principles. *Progress in Physics*, 2009, v. 4, 91–98.
12. Arrington J. et al. New measurements of the EMC effect in few-body nuclei. *J. Phys. Conference Series,* 2007, v. 69, 012024, 1–9.

The Intensity of the Light Diffraction by Supersonic Longitudinal Waves in Solid

Vahan Minasyan and Valentin Samoilov
Scientific Center of Applied Research, JINR, Dubna, 141980, Russia
E-mails: mvahan@scar.jinr.ru; scar@off-serv.jinr.ru

First, we predict existence of transverse electromagnetic field created by supersonic longitudinal waves in solid. This electromagnetic wave with frequency of ultrasonic field is moved by velocity of supersonic field toward of direction propagation of one. The average Poynting vector of superposition field is calculated by presence of the transverse electromagnetic and the optical fields which in turn provides appearance the diffraction of light.

1 Introduction

In 1921 Brillouin have predicted that supersonic wave in ideal liquid acts as diffraction gratings for optical light [1]. His result justify were confirmed by Debay and Sears [2]. Further, Schaefer and Bergmann had shown that supersonic waves in crystal leads to light diffraction [3]. The description of latter experiment is that the diffraction pattern is formed by passing a monochromatic light beam through solid perpendicular to direction of ultrasonic wave propagation. Furthermore, the out-coming light is directed on diffraction pattern. As results of these experiment, a diffraction maximums of light intensity represent as a sources of light with own intensities. Each intensity of light source depends on the amplitude of acoustical power because at certain value of power ultrasound wave there is vanishing of certain diffraction maxima. Other important result is that the intensity of the first positive diffraction maximum is not equal to the intensity of the first negative minimum, due to distortion of the waveform in crystals by the departures from Hooke's law as suggested [4]. For theoretical explanation of experimental results, connected with interaction ultrasonic and optical waves in isotropy homogenous medium, were used of so called the Raman-Nath theory [5] and theory of photo-elastic linear effect [6] which were based on a concept that acoustic wave generates a periodical distribution of refractive index in the coordinate-time space. For improving of the theory photo-elastic effect, the theories were proposed by Fues and Ludloff [7], Mueller [8] as well as Melngailis, Maradudin and Seeger [9]. In this letter, we predict existence of transverse electromagnetic radiation due to strains created by supersonic longitudinal waves in solid. The presence of this electromagnetic field together with optical one provides appearance of superposition wave which forms diffracted light with it's maxima.

2 Creation of an electromagnetic field

A model of solid is considered as lattice of ions and gas of free electrons. Each ion coupled with a point of lattice knot by spring, creating of ion dipole. The knots of lattice define a position equilibrium of each ion which is vibrated by own frequency Ω_0.

The electron with negative charge $-e$ and ion with positive charge e are linked by a spring which in turn defines the frequency ω_0 of electron oscillation in the electron-ion dipole. Obviously, such dipoles are discussed within elementary dispersion theory [10]. Hence, we suggest that property of springs of ion dipole and ion-electron one is the same.

Now we attempt to investigate an acoustic property of solid. By under action of longtidunal acoustic wave which is excited into solid, there is an appearance of vector displacement $\vec{u}$ of each ions.

Consider the propagation of an ultrasonic plane traveling wave in cubic crystal. Due to laws of elastic field for solid [11], the vector vector displacement $\vec{u}$ satisfies to condition which defines a longitudinal supersonic field

$$\operatorname{curl} \vec{u} = 0 \tag{1}$$

and is defined by wave-equation

$$\nabla^2 \vec{u} - \frac{1}{c_l^2} \frac{d^2 \vec{u}}{dt^2} = 0 , \tag{2}$$

where c_l is the velocity of a longitudinal ultrasonic wave which is determined by elastic coefficients.

The simple solution of (2) in respect to $\vec{u}$ has a following form

$$\vec{u} = \vec{u}_0 \vec{e}_x \sin(Kx + \Omega t) , \tag{3}$$

where u_0 is the amplitude of vector displacement; $\vec{e}_x$ is the unit vector determining the direction of axis OX in the coordinate system XYZ.

The appearance of the vector displacement for ions implies that each ion acquires the dipole moment $\vec{p} = e\vec{u}$ in of ion dipole. Consequently, we may argue that there is a presence of the electromagnetic field which may find by using of a moving equation for ion in the ion dipole

$$M \frac{d^2 \vec{u}}{dt^2} + q\vec{u} = e\vec{E}_l , \tag{4}$$

where $\vec{E}_l$ is the vector electric field which is induced by longitudinal ultrasonic wave; M is the mass of ion; the second term $q\vec{u}$ in left part represents as changing of quasi-elastic force which acts on ion in ion dipole, in this respect

$\Omega_0 = \sqrt{\frac{q}{M}} = \omega_0 \sqrt{\frac{m}{M}}$ which is the resonance frequency or own frequency of ion determined via a resonance frequency ω_0 of electron into electron-ion dipole [10].

Using of the operation *rot* of the both part of (4) together with (1), we obtain a condition for longitudinal electromagnetic wave

$$\operatorname{curl} \vec{E}_l = 0 \,. \tag{5}$$

Now, substituting solution $\vec{u}$ from (3) in (4), we find the vector longitudinal electric field of longitudinal electromagnetic wave

$$\vec{E}_l = E_{0,l}\, \vec{e}_x \sin(Kx + \Omega t) \,, \tag{6}$$

where

$$E_{0,l} = \frac{M(\Omega_0^2 - \Omega^2) u_0}{e} \tag{7}$$

is the amplitude of longitudinal electric field.

On other hand, the ion dipole acquires a polarizability α, which is determined by following form

$$\vec{p} = \alpha \vec{E}_l = \frac{M(\Omega_0^2 - \Omega^2)\, \alpha \vec{u}}{e} \,. \tag{8}$$

The latter is compared with $\vec{p} = e\vec{u}$, and then, we find a polarizability α for ion dipole as it was made in the case of electron-ion one presented in [10]

$$\alpha = \frac{e^2}{M(\Omega_0^2 - \Omega^2)} \,. \tag{9}$$

Thus, the dielectric respond ε of ion medium takes a following form

$$\varepsilon = 1 + 4\pi N_0 \alpha = 1 + \frac{4\pi N_0 e^2}{M(\Omega_0^2 - \Omega^2)} \,, \tag{10}$$

where N_0 is the concentration of ions.

The dielectric respond ε of acoustic medium likes to optical one, therefore,

$$\sqrt{\varepsilon} = \frac{c}{c_l} \,, \tag{11}$$

where c is the velocity of electromagnetic wave in vacuum.

We note herein that a longitudinal electric wave with frequency Ω is propagated by velocity c_l of ultrasonic wave in the direction OX. In the presented theory, the vector electric induction $\vec{D}_l$ is determined as

$$\vec{D}_l = 4\pi \vec{P}_l + \vec{E}_l \,, \tag{12}$$

and

$$\vec{D}_l = \varepsilon \vec{E}_l \,, \tag{13}$$

where $\vec{P}_l = N_0 \vec{p}$ is the total polarization created by ion dipoles in acoustic medium.

Furthermore, the Maxwell equations for electromagnetic field in acoustic medium with a magnetic penetration $\mu = 1$ take following form

$$\operatorname{curl} \vec{E} + \frac{1}{c} \frac{d\vec{H}}{dt} = 0 \,, \tag{14}$$

$$\operatorname{curl} \vec{H} - \frac{1}{c} \frac{d\vec{D}}{dt} = 0 \,, \tag{15}$$

$$\operatorname{div} \vec{H} = 0 \,, \tag{16}$$

$$\operatorname{div} \vec{D} = 0 \tag{17}$$

with

$$\vec{D} = \varepsilon \vec{E} \,, \tag{18}$$

where $\vec{E} = \vec{E}(\vec{r}, t)$ and $\vec{H} = \vec{H}(\vec{r}, t)$ is the vectors of local electric and magnetic fields in acoustic medium; $\vec{D} = \vec{D}(\vec{r}, t)$ is the local electric induction in the coordinate-time space; $\vec{r}$ is the coordinate; t is the current time in space-time coordinate system.

As we see in above, due to action of ultrasonic wave on the solid there is changed a polarization of ion dipole by creation electric field $\vec{E}_l$ and electric induction $\vec{D}_l$. Therefore, we search a solution of Maxwell equations by introducing the vector electric field by following form

$$\vec{E} = \vec{E}_t + \vec{E}_l - \operatorname{grad} \phi \tag{19}$$

and

$$\vec{H} = \operatorname{curl} \vec{A} \,, \tag{20}$$

where

$$\vec{E}_t = -\frac{d\vec{A}}{cdt} \,, \tag{21}$$

where ϕ and $\vec{A}$ are, respectively, the scalar and vector potential of electromagnetic wave.

As result, the solution of Maxwell equations leads to following expression

$$\operatorname{grad} \phi = \vec{E}_l \,. \tag{22}$$

In turn, using of (6) we find a scalar potential

$$\phi = \phi_0 \cos(Kx + \Omega t) \,, \tag{23}$$

where $\phi_0 = -\frac{E_{0,l}}{K}$.

As we see the gradient of scalar potential $\operatorname{grad} \phi$ of electromagnetic wave neutralizes the longitudinal electric field $\vec{E}_l$.

After simple calculation, we obtain a following equations for vector potential $\vec{A}$ of transverse electromagnetic field

$$\nabla^2 \vec{A} - \frac{\varepsilon}{c^2} \frac{d^2 \vec{A}}{dt^2} = 0 \tag{24}$$

with condition of plane transverse wave

$$\operatorname{div} \vec{A} = 0 \,. \tag{25}$$

The solution of (24) and (25) may present by plane transverse wave with frequency Ω which is moved by velocity c_l along of direction of unit vector $\vec{s}$

$$\vec{A} = \vec{A}_0 \sin(K\vec{s}\vec{r} + \Omega t) \tag{26}$$

and

$$\vec{A} \cdot \vec{s} = 0 \,, \tag{27}$$

where $K = \frac{\Omega\sqrt{\varepsilon}}{c}$ is the wave number of transverse electromagnetic wave; $\vec{s}$ is the unit vector in direction of wave normal; $\vec{A}_0$ is the vector amplitude of vector potential. In turn, the vector electric transverse wave $\vec{E}_t$ takes a following form

$$\vec{E}_t = \vec{E}_0 \cos(K\vec{s}\vec{r} + \Omega t)\,, \tag{28}$$

where the vector amplitude $\vec{E}_0$ of vector electric wave equals to

$$\vec{E}_0 = -\frac{\Omega\vec{A}_0}{c}\,.$$

Consequently, we found a transverse electromagnetic radiation which is induced by longitudinal ultrasonic wave. To find the vector amplitude $\vec{E}_0$, we using of the law conservation energy. In turn, the energy W_a of ultrasonic wave is transformed by energy W_t of transverse electromagnetic radiation, namely, there is a condition $W_a = W_t$ because there is absence the longitudinal electric field $\vec{E}_l$ which was neutralized by the gradient of scalar potential grad ϕ of electromagnetic wave as it was shown in above

$$W_a = \frac{M}{2}\left[\left(\frac{d\vec{u}}{dt}\right)^2 + \frac{1}{c_l^2}\left(\frac{d\vec{u}}{dx}\right)^2\right] = M\,\Omega^2 u_0^2 \cos^2(Kx + \Omega t)\,, \tag{29}$$

$$W_t = \frac{\varepsilon}{4\pi}\,E_0^2 \cos^2(K\vec{s}\vec{r} + \Omega t)\,. \tag{30}$$

At comparing of (29) and (30), we may argue that vector of wave normal $\vec{s}$ is directed along of axis OX or $\vec{s} = \vec{e}_x$, and then, we arrive to finally form of

$$\vec{E}_t = \vec{E}_0 \cos(Kx + \Omega t) \tag{31}$$

with condition

$$\frac{\varepsilon}{4\pi}\,E_0^2 = M\Omega^2 u_0^2\,. \tag{32}$$

Obviously, the law conservation energy plays an important role for determination of the transverse traveling plane wave.

3 Diffraction of light

First step, we consider an incident optical light into solid which is directed along of axis OZ in the coordinate space XYZ with electric vector $\vec{E}_e$

$$\vec{E}_e = \vec{E}_{0,e} \cos(kz + \omega t)\,, \tag{33}$$

where $k = \frac{\omega\sqrt{\varepsilon_0}}{c}$ is the wave number; ω is the frequency of light; ε_0 is the dielectric respond of optical medium created by electron dipoles [10]

$$\frac{\varepsilon_0 - 1}{\varepsilon_0 + 2} = \frac{4\pi N_0 e^2}{3m(\omega_0^2 - \omega^2)}\,, \tag{34}$$

where ω_0 is the own frequency of electron in electron-ion dipole; m is the mass of electron.

The interaction of ultrasonic waves with incident optical light in a crystal involves the relation between intensity of out coming light from solid and the strain created by ultrasonic wave.

Consequently, the superposition vector electric $\vec{E}_s$ field in acoustic-optical medium is determined by sum of vectors of electric transverse $\vec{E}_t$ and optical $\vec{E}_e$ waves

$$\vec{E}_s = \vec{E}_0 \cos(Kx + \Omega t) + \vec{E}_{0,e} \cos(kz + \omega t)\,. \tag{35}$$

The average Poynting vector of superposition field $\langle\vec{S}\rangle$ in acoustic-optical medium is expressed via the average Poynting vectors of $\langle\vec{S}_e\rangle$ and $\langle\vec{S}_t\rangle$ corresponding to the optical and the transverse electromagnetic waves

$$\langle\vec{S}\rangle = \frac{c}{\sqrt{\varepsilon_0}}\,w_e\vec{e}_z + \frac{c}{\sqrt{\varepsilon}}\,w_t\vec{e}_x\,, \tag{36}$$

where w_e and w_t are, respectively, the average density energies of the optical and the transverse electromagnetic waves

$$w_e = \frac{\varepsilon_0 E_{0,e}^2}{4\pi} \cdot \lim_{T\to\infty}\frac{1}{2T}\int_{-T}^{T}\cos^2(kz + \omega t)\,dt = \frac{\varepsilon_0 E_{0,e}^2}{8\pi} \tag{37}$$

and

$$w_t = \frac{\varepsilon E_0^2}{4\pi} \cdot \lim_{T\to\infty}\frac{1}{2T}\int_{-T}^{T}\cos^2(Kx + \Omega t)\,dt = \frac{M\Omega^2 u_0^2}{2} \tag{38}$$

by using of condition (32).

Thus, the average Poynting vector of superposition field $\langle\vec{S}\rangle$ is presented via intensities of the optical I_e and the transverse electromagnetic wave I_t

$$\langle\vec{S}\rangle = I_e\vec{e}_z + I_t\vec{e}_x\,, \tag{39}$$

where

$$I_e = \frac{E_{0,e}^2\, c\,\sqrt{\varepsilon_0}}{8\pi} \tag{40}$$

and

$$I_t = \frac{M\Omega^2 u_0^2 c_l}{2}\,. \tag{41}$$

This result shows that the intensity of transverse electromagnetic wave I_t represents as amplitude of acoustic field.

Obviously, we may rewrite down (39) by complex form within theory function of the complex variables

$$\langle\vec{S}\rangle = I_e + iI_t = \sqrt{I_e^2 + I_t^2}\,\exp(i\theta)\,, \tag{42}$$

where θ is the angle propagation of observation light in the coordinate system XYZ in regard to OZ

$$\theta = \operatorname{arcctg}\left(\frac{I_e}{I_t}\right), \tag{43}$$

which is chosen by the condition $0 \leqslant \operatorname{arcctg}\left(\frac{I_e}{I_t}\right) \leqslant \pi$.

Using of identity

$$\exp(iz\cos\psi) = \sum_{m=-\infty}^{m=\infty} J_m(z)\, i^m \exp(im\psi)\,, \qquad (44)$$

where $\psi = \arccos\theta$.

The average Poynting vector of superposition field $\langle\vec{S}\rangle$ is explicated on the spectrum of number m light sources with intensity I_m

$$\langle\vec{S}\rangle = \sum_{m=-\infty}^{m=\infty} I_m\,, \qquad (45)$$

where

$$I_m = \sqrt{I_t^2 + I_e^2}\, J_m\left(\operatorname{arcctg}\left(\frac{I_e}{I_t}\right)\right) i^m \exp(im\psi)\,, \qquad (46)$$

but $J_m(z)$ is the Bessel function of m order.

Thus, there is a diffraction of light by action of ultrasonic wave. In this respect, the central diffraction maximum point corresponds to $m = 0$ with intensity $I_{m=0}$

$$I_{m=0} = \sqrt{I_t^2 + I_e^2}\, J_0\left(\operatorname{arcctg}\left(\frac{I_e}{I_t}\right)\right). \qquad (47)$$

In the case, when $\operatorname{arcctg}\frac{I_e}{I_t} = 2.4$ (at $z = 2.4$, the Bessel function equals zero $J_0(z) = 0$, that implies $I_{m=0} = 0$. In this respect, there is observed a vanishing of central diffraction maximum at certainly value of amplitude I_t acoustic field.

The main result of above-mentioned experiment [4,9] is that the intensity of the first positive diffraction maximum $I_{m=1}$ is not equal to the intensity of the first negative minimum $I_{m=-1}$. Due to presented herein theory, the intensity of the first positive diffraction maximum is

$$I_{m=1} = i\sqrt{I_t^2 + I_e^2}\, J_1\left(\operatorname{arcctg}\left(\frac{I_e}{I_t}\right)\right)\exp(\psi)\,, \qquad (48)$$

but the intensity of the first negative diffraction maximum is

$$I_{m=-1} = -i\sqrt{I_t^2 + I_e^2}\, J_{-1}\left(\operatorname{arcctg}\left(\frac{I_e}{I_t}\right)\right)\exp(-\psi)\,. \qquad (49)$$

It is easy to show that $I_{m=1} \neq I_{m=-1}$. Indeed, at comparing $I_{m=1}$ and $I_{m=-1}$, we have

$$J_{-1} = -J_1$$

and

$$\exp(\psi) \neq \exp(-\psi)\,,$$

which is fulfilled always because the there is a condition for observation angle $\theta \neq \frac{\pi}{2}$. Consequently, we proved that evidence $I_{m=1} \neq I_{m=-1}$ confirms the experimental data.

Thus, as we have been seen the longitudinal ultrasonic wave induces the traveling transverse electromagnetic field which together with optical light provides an appearance diffraction of light.

Submitted on February 04, 2010 / Accepted on February 09, 2010

References

1. Brillouin L. *Ann. de Physique*, 1921, v. 17, 102.
2. Debay P. and Sears F.W. Scattering of light by supersonic waves. *Proc. Nat. Acad. Sci. Wash.*, 1932, v. 18, 409.
3. Schaefer C. and Bergmann L. *Naturuwiss*, 1935, v. 23, 799.
4. Seeger A. and Buck O. *Z. Natureforsch*, 1960, v. 15a, 1057.
5. Raman C.V., Nath N.S.N. *Proc. Indian. Acad. Sci.*, 1935, v. 2, 406.
6. Estermann R. and Wannier G. *Helv. Phys. Acta*, 1936, v. 9, 520; Pockels F. Lehrduch der Kristalloptic. Leipzig, 1906.
7. Fues E. and Ludloff H. *Sitzungsber. d. press. Akad. Math. phys. Kl.*, 1935, v. 14, 222.
8. Mueller M. *Physical Review*, 1937, v. 52, 223.
9. Melngailis J., Maradudin A.A., and Seeger A. *Physical Review*, 1963, v. 131, 1972.
10. Born M. and Wolf E. Principles of optics. Pergamon press, Oxford, 1964.
11. Landau L.D. and Lifshiz E.M. Theory of elasticity. (Course of Theoretical Physics, v. 11.) Moscow, 2003.

Oscillations of the Chromatic States and Accelerated Expansion of the Universe

Gunn Quznetsov

Chelyabinsk State University, Chelyabinsk, Ural, Russia
E-mail: gunn@mail.ru, quznets@yahoo.com

It is known (Quznetsov G. Higgsless Glashow's and quark-gluon theories and gravity without superstrings. *Progress in Physics*, 2009, v. 3, 32–40) that probabilities of point-like events are defined by some generalization of Dirac's equation. One part of such generalized equation corresponds to the Dirac's leptonic equation, and the other part corresponds to the Dirac's quark equation. The quark part of this equation is invariant under the oscillations of chromatic states. And it turns out that these oscillations bend space-time so that at large distances the space expands with acceleration according to Hubble's law.

1 Introduction

In 1998 observations of Type Ia supernovae suggested that the expansion of the universe is accelerating [1]. In the past few years, these observations have been corroborated by several independent sources [2]. This expansion is defined by the Hubble rule [3]

$$V(r) = Hr, \tag{1}$$

where $V(r)$ is the velocity of expansion on the distance r, H is the Hubble's constant ($H \approx 2.3{\times}10^{-18}c^{-1}$ [4]).

It is known that Dirac's equation contains four anticommutive complex 4×4 matrices. And this equation is not invariant under electroweak transformations. But it turns out that there is another such matrix anticommutive with all these four matrices. If additional mass term with this matrix will be added to Dirac's equation then the resulting equation shall be invariant under these transformations [5]. I call these five of anticommutive complex 4×4 matrices *Clifford pentade*. There exist only six Clifford pentads [7, 8]. I call one of them the light pentad, three — the chromatic pentads, and two — the gustatory pentads.

The light pentad contains three matrices corresponding to the coordinates of 3-dimensional space, and two matrices relevant to mass terms — one for the lepton and one for the neutrino of this lepton.

Each chromatic pentad also contains three matrices corresponding to three coordinates and two mass matrices — one for top quark and another — for bottom quark.

Each gustatory pentad contains one coordinate matrix and two pairs of mass matrices [9] — these pentads are not needed yet.

It is proven [6] that probabilities of pointlike events are defined by some generalization of Dirac's equation with additional gauge members. This generalization is the sum of products of the coordinate matrices of the light pentad and covariant derivatives of the corresponding coordinates plus product of all the eight mass matrices (two of light and six of chromatic) and the corresponding mass numbers.

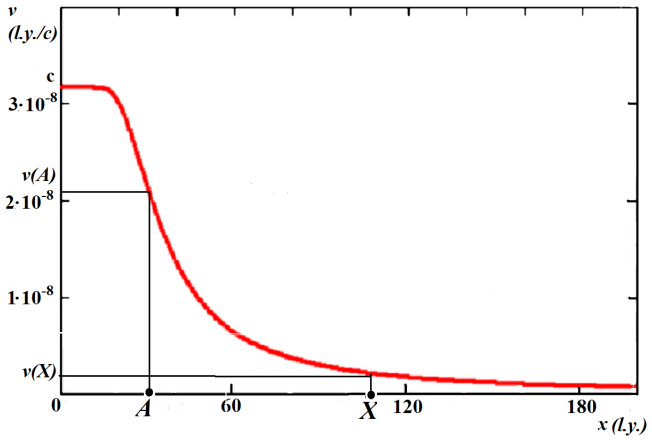

Fig. 1: Dependence of $v(t, x)$ from x [8].

If lepton's and neutrino's mass terms are equal to zero in this equation then we obtain the Dirac's equation with gauge members similar to eight gluon's fields [8]. And oscillations of chromatic states of this equation bend space-time.

2 Chromatic oscillations and the Hubble's law

Some oscillations of chromatic states bend space-time as follows [8]

$$\left.\begin{aligned} \frac{\partial t}{\partial t'} &= \cosh 2\sigma \\ \frac{\partial x}{\partial t'} &= \mathrm{c}\sinh 2\sigma \end{aligned}\right\}. \tag{2}$$

Hence, if v is the velocity of a coordinate system $\{t', x'\}$ in the coordinate system $\{t, x\}$ then

$$\sinh 2\sigma = \frac{\left(\frac{v}{\mathrm{c}}\right)}{\sqrt{1-\frac{v^2}{\mathrm{c}^2}}}, \qquad \cosh 2\sigma = \frac{1}{\sqrt{1-\frac{v^2}{\mathrm{c}^2}}}.$$

Therefore,

$$v = \mathrm{c}\tanh 2\sigma. \tag{3}$$

Let

$$2\sigma := \omega(x)\,\frac{t}{x}$$

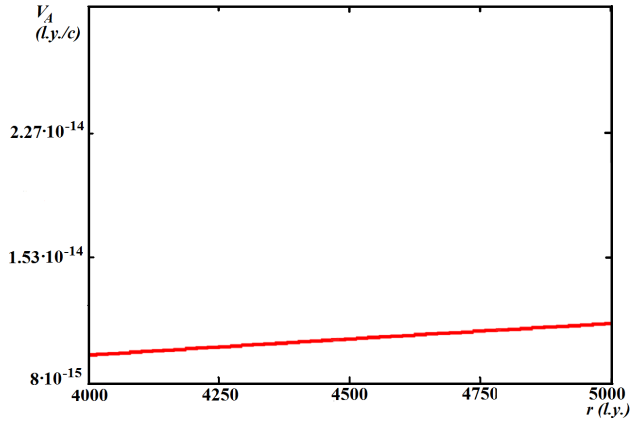

Fig. 2: Dependence of $V_A(r)$ on r with $x_A = 25 \times 10^3$ l.y.

with

$$\omega(x) = \frac{\lambda}{|x|},$$

where λ is a real constant with positive numerical value.

In that case

$$v(t, x) = \mathrm{c} \tanh\left(\frac{\lambda}{|x|}\frac{t}{x}\right). \tag{4}$$

Let a black hole be placed in a point O. Then a tremendous number of quarks oscillate in this point. These oscillations bend time-space and if t has some fixed volume, $x > 0$, and $\Lambda := \lambda t$ then

$$v(x) = \mathrm{c} \tanh\left(\frac{\Lambda}{x^2}\right). \tag{5}$$

A dependency of $v(x)$ (light years/c) from x (light years) with $\Lambda = 741.907$ is shown in Fig. 1.

Let a placed in a point A observer be stationary in the coordinate system $\{t, x\}$. Hence, in the coordinate system $\{t', x'\}$ this observer is flying to the left to the point O with velocity $-v(x_A)$. And point X is flying to the left to the point O with velocity $-v(x)$.

Consequently, the observer A sees that the point X flies away from him to the right with velocity

$$V_A(x) = \mathrm{c} \tanh\left(\frac{\Lambda}{x_A^2} - \frac{\Lambda}{x^2}\right) \tag{6}$$

in accordance with the relativistic rule of addition of velocities.

Let $r := x - x_A$ (i.e. r is distance from A to X), and

$$V_A(r) := \mathrm{c} \tanh\left(\frac{\Lambda}{x_A^2} - \frac{\Lambda}{(x_A + r)^2}\right). \tag{7}$$

In that case Fig. 2 demonstrates the dependence of $V_A(r)$ on r with $x_A = 25{\times}10^3$ l.y.

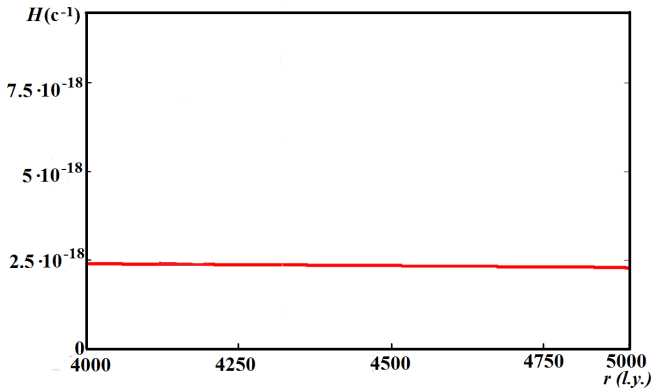

Fig. 3: Dependence of H on r.

Hence, X runs from A with almost constant acceleration

$$\frac{V_A(r)}{r} = H. \tag{8}$$

Fig. 3 demonstrates the dependence of H on r (the Hubble constant).

3 Conclusion

Therefore, the phenomenon of the accelerated expansion of Universe is explained by oscillations of chromatic states.

Submitted on February, 12, 2009 / Accepted on February 16, 2009

References

1. Riess A. et al. *Astronomical Journal*, 1998, v. 116, 1009–1038.
2. Spergel D.N., et al. *The Astrophysical Journal Supplement Series*, 2003, September, v. 148, 175–194; Chaboyer B. and Krauss L.M. *Astrophys. J. Lett.*, 2002, v. 567, L45; Astier P., et al. *Astronomy and Astrophysics*, 2006, v. 447, 31–48; Wood-Vasey W.M., et al. *The Astrophysical Journal*, 2007, v. 666, no. 2, 694–715.
3. Coles P., ed. Routledge critical dictionary of the new cosmology. Routledge, 2001, 202.
4. Chandra confirms the Hubble constant. Retrieved on 2007-03-07. http://www.universetoday.com/2006/08/08/chandra-confirms-the-hubble-constant/
5. Quznetsov G. Probabilistic treatment of gauge theories. In series: *Contemporary Fundamental Physics*, ed. V. Dvoeglazov, Nova Sci. Publ., NY, 2007, 95–131.
6. Quznetsov G. Higgsless Glashow's and quark-gluon theories and gravity without superstrings. *Progress in Physics*, 2009, v. 3, 32–40.
7. Madelung E. Die Mathematischen Hilfsmittel des Physikers. Springer Verlag, 1957, 29.
8. Quznetsov G. 4×1-marix functions and Dirac's equation. *Progress in Physics*, v. 2, 2009, 96–106.
9. Quznetsov G. Logical foundation of theoretical physics. Nova Sci. Publ., NY, 2006, 143–144.

LETTERS TO PROGRESS IN PHYSICS

LETTERS TO PROGRESS IN PHYSICS

Smarandache Spaces as a New Extension of the Basic Space-Time of General Relativity

Dmitri Rabounski

E-mail: rabounski@ptep-online.com

This short letter manifests how Smarandache geometries can be employed in order to extend the "classical" basis of the General Theory of Relativity (Riemannian geometry) through joining the properties of two or more (different) geometries in the same single space. Perspectives in this way seem much profitable: the basic space-time of General Relativity can be extended to not only metric geometries, but even to non-metric ones (where no distances can be measured), or to spaces of the mixed kind which possess the properties of both metric and non-metric spaces (the latter should be referred to as "semi-metric spaces"). If both metric and non-metric properties possessed at the same (at least one) point of a space, it is one of Smarandache geometries, and should be referred to as "Smarandache semi-metric space". Such spaces can be introduced according to the mathematical apparatus of physically observable quantities (chronometric invariants), if we consider a breaking of the observable space metric in the continuous background of the fundamental metric tensor.

When I was first acquainted with Smarandache geometries many years ago, I immediately started applying them, in order to extend the basic geometry of Einstein's General Theory of Relativity.

Naturally, once the General Theory of Relativity was established already in the 1910's, Albert Einstein stated that Riemannian geometry, as advised to him by Marcel Grossmann, was not the peak of excellence. The main advantage of Riemannian geometry was the invariance of the space metric and also the well-developed mathematical apparatus which allowed Einstein to calculate numerous specific effects, unknown or unexplained before (now, they are known as the effects of General Relativity). Thus, Einstein concluded, the basic spacetime of General Relativity would necessarily be extended in the future, when new experiments would overcome all the possibilities provided by the geometry of Riemannian spaces. Many theoretical physicists and mathematicians tried to extend the basic space-time of General Relativity during the last century, commencing in the 1910's. I do not survey all the results obtained by them (this would be impossible in so short a letter), but only note that they all tried to get another basic space, unnecessary Riemannian one, then see that effects manifest themselves in the new geometry. No one person (at least according to my information on this subject, perhaps incomplete) did consider the "mixed" geometries which could possess the properties of two or more (different in principle) geometries at the same point.

This is natural, because a theoretical physicist looks for a complete mathematical engine which could drive the applications to physical phenomena. What would have happened had there been no Bernhard Riemann, Erwin Christoffel, Tullio Levi-Civita, and the others; could Einstein have been enforced to develop Riemannian geometry in solitude from scratch? I think this would have been a "dead duck" after all. Einstein followed a very correct way when he took the well-approved mathematical apparatus of Riemannian geometry. Thus, a theoretical physicist needs a solid mathematical ground for further theoretical developments. This is why some people, when trying to extend the basis of General Relativity, merely took another space instead the four-dimensional pseudo-Riemannian space initially used by Einstein.

Another gate is open due to Smarandache geometries, which can be derived from any of the known geometries by the condition that one (or numerous, or even all) of its axioms is both true and violated in the space. This gives a possibility to create a sort of "mixed" geometries possessing the properties of two or more geometries in one. Concerning the extensions of General Relativity, this means that we can not refuse the four-dimensional pseudo-Riemannian space in place of another single geometry, but we may create a geometry which is common to the basic one, as well as one or numerous other geometries in addition to it. As a simplest example, we can create a space possessing the properties of both the curved Riemannian and the flat Euclidean geometries. So forth, we can create a space, every point of which possesses the common properties of Riemannian geometry and another geometry which is non-Riemannian.

Even more, we can extend the space geometry in such a way that the space will be particularly metric and particularly non-metric. In the future, I suggest we should refer to such spaces as semi-metric spaces. Not all semi-metric spaces manifest particular cases of Smarandache geometries. For example, a space wherein each pair of points is segregated from the others by a pierced point, i.e. distances can be determined only within diffeerential fragments of the space segregated by pierced points. This is undoubtely a semi-metric space, but is

not a kind of Smarandache geometries. Contrarily, a space wherein at least one pair of points possesses both metric and non-metric properties at the same time is definitely that of Smarandache geometries. In the future, I suggest, we should refer to such spaces as *Smarandache semi-metric spaces*, or *ssm-spaces* in short.

Despite the seeming impossibility of joining metric and non-metric properties in "one package", Smarandache semi-metric spaces can easily be introduced even by means of "classical" General Relativity. The following is just one example of how to do it. Regularly, theoretical physicists are aware of the cases where the signature conditions of the space are violated. They argue that, because the violations produce a breaking of the space, the cases have not a physical meaning in the real world and, hence, should not be considered. Thus, when considering a problem of General Relativity, most theoretical physicists artificially neglect, from consideration, those solutions leading to the violated signature conditions and, hence, to the breaking of the space. On the other hand, we could consider these problems by means of the mathematical apparatus of chronometric invariants, which are physically observable quantities in General Relativity. In this way, we have to consider the observable (chronometrically invariant) metric tensor on the background of the fundamental (general covariant) metric tensor of the space. The signature conditions of the metrics are determined by different physical requirements. So, in most cases, the violated signature conditions of the observable metric tensor, i.e. breaking of the observable space, can appear in the continuous background of the fundamental metric tensor (and vice versa). This is definitely a case of Smarandache geometries. If a distance (i.e. a metric, even if non-Riemannian) can be determined on the surface of the space breaking, this is a metric space of Smarandache geometry. I suggest we should refer to such spaces as *Smarandache metric spaces*. However, if the space breaking is incapable of determining a distance inside it, this is a Smarandache semi-metric space: the space possesses both metric and non-metric properties at all points of the surface of the space breaking.

A particular case of this tricky situation can be observed in Schwarzschild spaces. There are two kinds of these: a space filled with the spherically symmetric gravitational field produced by a mass-point (the center of gravity of a spherical solid body), and a space filled with the spherically symmetric gravitational field produced by a sphere of incompressible liquid. Both cases manifest the most apparent metrics in the Universe: obviously, almost all cosmic bodies can be approximated by either a sphere of solid or a sphere of liquid. Such a metric space has a breaking along the spherical surface of gravitational collapse, surrounding the center of the gravitating mass (a sphere of solid or liquid). This space breaking originates in the singularity of the fundamental metric tensor. In the case of regular cosmic bodies, the radius of the space breaking surface (known as the gravitational radius, it is determined by the body's mass) is many orders smaller than the radius of such a body itself: it is 3 km for the Sun, and only 0.9 cm for the Earth. Obviously, only an extremely dense cosmic body can completely be located under its gravitational radius, thus consisting a gravitational collapsar (black hole). Meanwhile, the space breaking at the gravitational radius really exists inside any continuous body, close to its center of gravity. Contrary, the space breaking due to the singularity of the observable metric tensor is far distant from the body; the sphere of the space breaking is huge, and is like a planetary orbit. Anyhow, in the subspace inside the Schwarzschild space breaking, distances can be determined between any two points (but they are not those of the Schwarzschild space distances). Thus, when considering a Schwarzschild space without any breaking, as most theoretical physicists do, it is merely a kind of the basic space-time of General Relativity. Contrarily, being a Schwarzschild space considered commonly with the space breaking in it, as a single space, it is a kind of Smarandache metric spaces — a *Schwarzschild-Smarandache metric space*, which generalizes the basic space-time of General Relativity. Moreover, one can consider such a space breaking that no distance (metric) can be determined inside it. In this case, the common space of the Schwarzschild metric and the non-metric space breaking in it is a kind of Smarandache semi-metric spaces — a *Schwarzschild-Smarandache semi-metric space*, and is an actual semi-metric extension of the basic space-time of General Relativity.

So, we see how Smarandache geometries (both metric and semi-metric ones) can be a very productive engine for further developments in the General Theory of Relativity. Because the Schwarzschild metrics lead to consideration of the state of gravitational collapse, we may suppose that not only regular gravitational collapsars can be considered (the surface of a regular black hole possesses metric properties), but even a much more exotic sort of collapsed objects — a collapsar whose surface cannot be presented with metric geometries. Because of the absence of metricity, the surface cannot be inhabited by particles (particles, a sort of discrete matter, imply the presence of coordinates). Only waves can exist there. These are standing waves: in the metric theory, time cannot be introduced on the surface of gravitational collapse due to the collapse condition $g_{00} = 0$; the non-metric case manifests the state of collapse by the asymptopic conditions from each side of the surface, while time is not determined in the non-metric region of collapse as well. In other words, the non-metric surface of such a collapsar is filled with a system of standing waves, i.e. holograms. Thus, we should refer to such objects — the collapsars of a Schwarzschild-Smarandache semi-metric space — as *holographic black holes*. All these are in the very course of the paradoxist mathematics, whose motto is "impossible is possible".

Submitted on February 12, 2010 / Accepted on February 18, 2010

The Journal on Advanced Studies in Theoretical and Experimental Physics, including Related Themes from Mathematics

PROGRESS IN PHYSICS

A quarterly issue scientific journal, registered with the Library of Congress (DC, USA). This journal is peer reviewed and included in the abstracting and indexing coverage of: Mathematical Reviews and MathSciNet (AMS, USA), DOAJ of Lund University (Sweden), Zentralblatt MATH (Germany), Scientific Commons of the University of St. Gallen (Switzerland), Open-J-Gate (India), Referativnyi Zhurnal VINITI (Russia), etc.

To order printed issues of this journal, contact the Editors. Electronic version of this journal can be downloaded free of charge:
http://www.ptep-online.com

Postal address

Department of Mathematics and Science,
University of New Mexico,
200 College Road,
Gallup, NM 87301, USA

ISSN: 1555-5534 (print)
ISSN: 1555-5615 (online)

Standard Address Number: 297-5092
Printed in the United States of America

JULY 2010 **VOLUME 3**

CONTENTS

Information for Authors and Subscribers

Progress in Physics has been created for publications on advanced studies in theoretical and experimental physics, including related themes from mathematics and astronomy. All submitted papers should be professional, in good English, containing a brief review of a problem and obtained results.

All submissions should be designed in LaTeX format using *Progress in Physics* template. This template can be downloaded from *Progress in Physics* home page http://www.ptep-online.com. Abstract and the necessary information about author(s) should be included into the papers. To submit a paper, mail the file(s) to the Editor-in-Chief.

All submitted papers should be as brief as possible. We accept brief papers, no larger than 8 typeset journal pages. Short articles are preferable. Large papers can be considered in exceptional cases to the section *Special Reports* intended for such publications in the journal. Letters related to the publications in the journal or to the events among the science community can be applied to the section *Letters to Progress in Physics*.

All that has been accepted for the online issue of *Progress in Physics* is printed in the paper version of the journal. To order printed issues, contact the Editors.

This journal is non-commercial, academic edition. It is printed from private donations. (Look for the current author fee in the online version of the journal.)

Calibration of Microwave Reference Blackbodies and Targets for Use in Satellite Observations: An Analysis of Errors in Theoretical Outlooks and Testing Procedures

Pierre-Marie Robitaille

Department of Radiology, The Ohio State University, 395 W. 12th Ave, Suite 302, Columbus, Ohio 43210, USA
E-mail: robitaille.1@osu.edu

Microwave reference blackbodies and targets play a key role in astrophysical and geophysical studies. The emissivity of these devices is usually inferred from return-loss experiments which may introduce at least 10 separate types of calibration errors. The origin of these inaccuracies depends on test conditions and on the nature of each target. The most overlooked errors are related to the geometry adapted in constructing reference loads and to the effects of conduction or convection. Target shape and design can create an imbalance in the probabilities of absorption and emission. This leads to loss of radiative equilibrium, despite the presence of a thermodynamic steady state. Heat losses or gains, through conduction and convection, compensate for this unexpected physical condition. The improper calibration of blackbodies and targets has implications, not only in global climate monitoring, but also relative to evaluating the microwave background.

1 Introduction

Blackbodies [1–4] can be difficult to construct and analyze. For example, by unknowingly pumping normal radiation [2, 3] into cavities using their detectors, scientists can easily make the interior of enclosures appear black [4]. They thereby create the illusion that all cavities emit normal radiation [1–3]. Relative to microwave reference targets, the situation is further complicated by the realization that these devices are pseudo-cavities and become subject to geometrical considerations. These problems are important as microwave targets are present on numerous satellites monitoring the microwave background [5–7] and global climate (e.g. [8]).

Calibration targets for microwave frequencies [9–15] are typically made from carbon or iron containing foams and epoxy resins, such as Eccosorb foams and Eccosorb CR-110 and 117 [Emerson and Cuming, Randolph, MA]. Recently, an aqueous blackbody has been proposed for calibration purposes [16]. Such a device takes advantage of the powerful microwave absorbance of water. As for Eccosorb surfaces used in the microwave [5,7], unlike graphite and carbon black paints in the infrared [3, 17–20], they manifest significantly increased absorbance as a function of thickness. Therefore, it is impossible to obtain a blackbody emission from a thin layer of Eccosorb, irrespective of claims to the contrary. For example, a 1 cm layer of Eccosorb CR-110 has an absorbance of only ~6 dB at 18 GHz [21]. Despite this reality, space restrictions aboard spacecraft often limit the volume available for satellite reference targets [7]. Further complicating the situation, these materials permit transmission at microwave frequencies and are not opaque. Consequently, the correct treatment of their properties involves the consideration of transmission. Unfortunately, since reference targets are often backed by highly reflective metal casings [10–15], it becomes easy to ignore the effects of transmission in the absorber. This can lead to a serious overestimation of calibrator emissions, as will be demonstrated.

2 The testing of reference targets

Almost without exception, the testing of microwave reference targets involves their placement within an anechoic chamber (e.g. [10–15]). Here, they are subjected to incident microwave radiation emitted from a test horn, typically driven at the frequency of interest by a network analyzer. This is achieved while making the assumption that the target, with its absorbing material and metal casing (e.g. [10–15]), can be treated as a single opaque unit. By measuring the return-loss produced in this configuration, the emissivity of the target can be inferred, but not without risk of error.

Return loss measurements are based on the validity of Stewart's formulation, which advances the equivalence of emission and absorption under conditions of thermal equilibrium [22, 23]. This statement is commonly viewed by the scientific community as Kirchhoff's law [1]. However, Kirchhoff's law differs from Stewart's formulation by advocating that all radiation within cavities must be black. Such a concept is demonstrably false [4, 17, 23]. As a result, the law of equivalence between emissivity and absorptivity, must be attributed uniquely to Stewart [22, 23].

The emissivity of a target is usually estimated through the relationship $\varepsilon_t = 1 - \sigma_{tn}$, where ε_t and σ_{tn} represent target emissivity and normal reflectivity, respectively (i.e. [10–15]. This treatment assumes that only normal reflection takes place and also constitutes an implicit formulation of Stewart's law [23]. Nonetheless, in this discussion, we will consider the

measurement of absorption, rather than emission, and write $\kappa_t = 1 - \sigma_{tn}$, where κ_t represents the absorptivity of the target. In the end, it is demonstrated that the measurement of absorptivity from return loss measurements in no way implies that the emissivity of the target has been properly evaluated.

2.1 Type-1, -2, -3 and -4 errors

The first error in the determination of emissivity using return loss measurements, involves leakage of incident radiation from the horn, directly into the anechoic chamber, without ever striking the target. This will be referred to as a Type-1 error (see Figure 1A) and symbolized as Γ_{bp}, as it depends on the beam pattern of the horn. Type-2 errors can occur when incident radiation is diffracted around the edges of the horn on transmission, as shown in Figure 1A. Type-2 errors will be symbolized as Γ_{dh} as they represent diffraction on the horn. These errors are also associated with the beam pattern. Since corrugated edging can be placed on a horn to minimize the effects of diffraction, it is treated as a separate error. Type-3 errors are similar in nature to Type-2 errors, but involve the diffraction of incoming radiation on the edges of the target, Γ_{dt}. This term also includes radiation which is scattered by the target. Finally, a Type-4 error results from the neglect of diffuse reflection off the target surface, σ_{td}.

Each of these error types result in radiation being lost to the walls of the anechoic chamber. Such radiation will not be available to the horn and will subsequently contribute to lowering the measured return radiation. In order to overcome this problem, it is important to numerically evaluate the beam pattern of the horn, thereby inferring the percentage of incident radiation that does, in fact, strike the target. It is also possible to place pick-up horns in the anechoic chamber and evaluate the beam patterns directly, in the absence of a target. Thus, whether through calculations or direct measurement, the magnitude of these errors can be understood and are usually properly addressed. Nonetheless, and for the sake of completeness, it is clear that the absorptivity of the target is actually given by:

$$\kappa_t = 1 - \sigma_{tn} - \sigma_{td} - \Gamma_{bp} - \Gamma_{dh} - \Gamma_{dt} \,. \qquad (1)$$

When viewing the target as a single unit, Type-1, -2, -3, and -4 errors can lead to the inaccurate assessment of target emissivity from return-loss experiments. Yet, it is the effect of using a transmissive absorber, in the presence of a metal casing or support, which can lead to the greatest errors in evaluating emissivity.

2.2 Type-5 and -6 errors

The emissivity of microwave targets is exclusively dominated by an absorbing material, like Eccosorb, which is also transmissive [9, 21]. Accordingly, it is unwise to treat these devices as single units. Instead, clearer insight into the problem can be gained if one views the target as made from its two components: the absorbent material and the perfectly reflective metallic backing. In this scenario, the absorbent material can be considered as possessing absorptivity, κ_a, and emissivity, ε_a, equal to one another ($\kappa_a = \varepsilon_a$), along with normal reflectivity, σ_{an}, diffuse reflectivity, σ_{ad}, and transmissivity, τ_a. The metallic casing, c, often constructed from aluminum, is viewed as having perfect reflectivity ($\sigma_c = 1$).

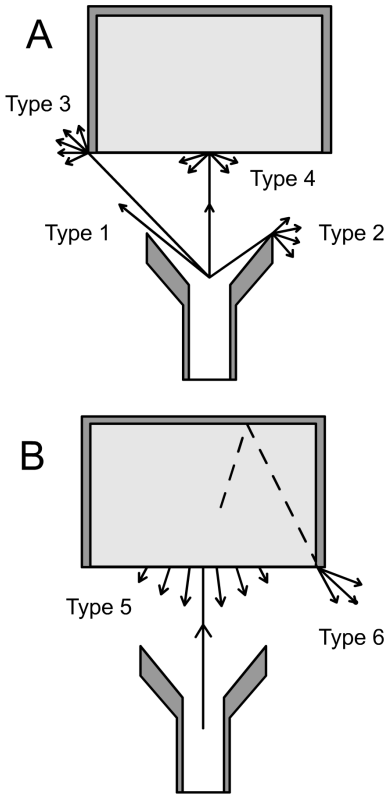

Fig. 1: Schematic representation of error types when assessing effective emissivity using return-loss measurements.

Under such conditions, the difficulties in ascertaining the emissivity of the target become evident, since for any non-opaque substance, $\varepsilon = 1 - \sigma - \tau$, rather than $\varepsilon = 1 - \sigma$. Because the absorber has transmittance, it can permit microwave energy to pass through its body and strike the metallic backing at virtually any angle. While an object transmits incident radiation, it is not required to preserve either phase or angle of incidence. As such, when the transmitted component strikes the casing, it can do so in a manner whereby the microwave energy, following reflection, re-enters the absorber only to be absorbed, transmitted towards the horn, scattered into space, or diffracted by the edge of the casing. This would lead to a good return-loss measurement on the network analyzer; but it would be improper to assume that $\varepsilon = 1 - \sigma$. Therefore, it becomes nearly impossible to measure emissivity, as will be demonstrated.

In reality, by treating the target as an opaque unit made up of two components (i.e. the absorber and the reflective

casing), it is apparent that its absortivity is now given by:

$$\kappa_t = 1 - \sigma_{an} - \sigma_{ad} - \Gamma_{bp} - \Gamma_{dh} - \Gamma_{dc} - \\ - \kappa_a \tau_a \sigma_c - \tau_a \tau_a \sigma_c - s_a \tau_a \sigma_c - d_a \tau_a \sigma_c \,, \quad (2)$$

where the normal and diffuse reflection of the absorber are now being considered (σ_{an} and σ_{ad}), along with the diffraction of incident radiation on the casing, Γ_{dc} (previously viewed as Γ_{dt}), and four new terms arise, whose coefficients sum to 1 (i.e. $\kappa_a + \tau_a + s_a + d_a = 1$). The seventh term, $\kappa_a \tau_a \sigma_c$, corresponds to that fraction of transmitted power which is reflected by the casing, σ_c, and absorbed, κ_a, upon reentry into the absorber. The eighth term, $\tau_a \tau_a \sigma_c$, represents that fraction of the transmitted power which is reflected by the casing and is subsequently re-transmitted, τ_a, towards the horn. The seventh term, like the eighth term, has been innocently considered when treating the target as an opaque unit in section 2.1. These terms introduce no errors in the return-loss measurement itself. For instance, it is evident that, with rearrangement, Eq. (2) becomes:

$$\kappa_{t_{\text{eff}}} = (\kappa_t + \kappa_a \tau_a \sigma_c) = 1 - (\sigma_{an} + \tau_a \tau_a \sigma_c) - \sigma_{ad} - \\ - \Gamma_{bp} - \Gamma_{dh} - \Gamma_{dc} - s_a \tau_a \sigma_c - d_a \tau_a \sigma_c \,. \quad (3)$$

In this expression, the seventh term in Eq. (2), $\kappa_a \tau_a \sigma_c$, is moved to the left as it makes a positive contribution to the effective absorptivity of the target, where on measurement, κ_t is indistinguishable from $\kappa_a \tau_a \sigma_c$. Unfortunately, we must now consider the effective absorptivity, $\kappa_{t_{\text{eff}}}$, from the target. In fact, the seventh term, $\kappa_a \tau_a \sigma_c$, brings such difficulty in the determination of emissivity that it will be considered below separately as a Type-7 problem. This occurs as the targets permit repeated cycles of absorption and reflection. The associated Type-7 errors experience geometric growth. It is also clear that, in Eq. (2), the eighth term, $\tau_a \tau_a \sigma_c$, can be paired with normal reflection, σ_{an}, the two being indistinguishable.

The ninth term in Eq. (2), $s_a \tau_a \sigma_c$, generates a Type-5 error as shown in Figure 1B. It accounts for that fraction of the transmitted power which is reflected by the casing, re-enters the absorber, and is then scattered, s_a, into the anechoic chamber. The term resembles a Type-4 error, σ_{td}, involving the effect of diffuse reflection when considering the entire target. However, it is not diffuse reflection, though indistinguishable from such a process. It is properly viewed, as a Type-5 error, as it involves scattering by the absorber following reflection on the casing.

Finally, the tenth term in Eq. (2), $d_a \tau_a \sigma_c$, introduces a Type-6 error. It corresponds to that fraction of the transmitted power which is reflected by the aluminum casing, re-enters the Eccosorb and is then diffracted, d_a, by the edge of the casing into the anechoic chamber (see Figure 1B). The tenth term involves diffraction on the casing from a direction opposite to the incident radiation. It resembles a Type-3 error, Γ_{dc} (previously referred to as Γ_{dt}), in being indistinguishable from it on measurement, but is distinct in its origin. It is really a "reverse diffraction" since it is produced from radiation which was previously reflected by the metallic casing. It will be properly viewed as a Type-6 error. The distinction is important because, while corrugations can be placed on horns to minimize diffractions on their edges during transmission, they are often not present on the metallic casings of their reference targets [7]. Hence, the diffraction produced as radiation exits the interior of the target is often ignored [7].

If we now represent the seventh through the tenth terms as $\Gamma_{\kappa\sigma}$, $\Gamma_{\tau\sigma}$, $\Gamma_{s\sigma}$, and $\Gamma_{d\sigma}$, Eq. (2) can be re-expressed, with pairing of indistinguishable terms, as follows:

$$\kappa_{t_{\text{eff}}} = (\kappa_t + \Gamma_{\kappa\sigma}) = 1 - (\sigma_{an} + \Gamma_{\tau\sigma}) - (\sigma_{ad} + \Gamma_{s\sigma}) - \\ - (\Gamma_{bp} + \Gamma_{dh}) - (\Gamma_{dc} + \Gamma_{d\sigma}) \,. \quad (4)$$

2.3 Type-7 errors

The most serious problem with microwave target return-loss measurements can be viewed as Type-7 errors which involve the geometry of the targets themselves. This problem exists in all determinations of emissivity from return-loss measurements in the presence of a metal casing. In reality, we are returning to the $\kappa_a \tau_a \sigma_c$, or $\Gamma_{\kappa\sigma}$ term. As previously mentioned, this term does not lead to an error in the return-loss measurement. But, it can cause an enormous error in the determination of emissivity from such measurements. This is a geometric effect, which is best understood by considering targets of varying geometry.

2.3.1 The Planck LFI

Consider, for instance, the target geometry for the ~4 K references on the Planck LFI [7]. These targets are box-like in appearance. They are composed of various layers of Eccosorb, including a small pyramid, enclosed on 5 sides by an aluminum casing (see Figures 8, 10 and 12 in [7]). Given incident radiation from the test horn and neglecting Type-1 through -4 errors, the layer of Eccosorb can initially absorb some of the microwave power. The radiation which is not absorbed is transmitted through the Eccosorb and strikes the aluminum casing. At this point, it ideally experiences normal reflection on the casing and travels back through the absorber. If this radiation is not absorbed following reentry, it travels into space. There, neglecting Type-5 and -6 errors, it can be detected by the horn and registered as return radiation. Note that, now, there are two chances for the incident microwave radiation to be absorbed: first on incidence and then following reflection on the metal casing (term $\kappa_a \tau_a \sigma_c$ above). The situation is not balanced on emission.

Relative to pure emission, the absorber is unable to provide the same performance. For instance, microwaves emitted from the upper surface of the absorber can travel uninterrupted towards the detector. Conversely, radiation emitted through the lower surface of the absorber immediately encounters reflection on striking the metal casing and then re-

enters the material of origin. Once in the absorber, the radiation which had been emitted from the lower surface has a chance of being absorbed before exiting towards the test horn. Furthermore, it is unlikely that the lower surface of such a test target can emit any photons towards the casing, since conduction is also taking place at the interface of the Eccosorb and the aluminum casing (see section 2.4). The effective emissivity, ε_{eff}, of the absorber is reduced by the presence of the metal casing, whereas the effective absorptivity, κ_{eff}, is being increased.

Speaking in quantum mechanical terms, the presence of the metal casing has created a condition where the probability of absorption is no longer equal to the probability of emission. Herein lays the major flaw associated with such approaches. Geometry has produced a condition where return-loss measurements can no longer properly evaluate the effective emissivity of the target. The effective absorbtivity has been enhanced by geometry and the effective emissivity reduced. This is a Type-7 error. Effective radiative equilibrium is being destroyed by geometry and $\varepsilon_{\text{eff}} \neq \kappa_{\text{eff}}$. This occurs precisely because the highly conductive metallic casing ensures that thermodynamic steady state remains. Conduction now compensates for the imbalance created in effective absorptivity and emissivity. In fact, conduction and convection can introduce Type-8 and 9 errors, respectively, as will be discussed in section 2.4.

2.3.2 Pyramidal targets

In order to emphasize the effect of geometry, consider a target where a metal casing is built, composed of a group of small pyramidal structures [10–12]. Such targets are important on geophysical satellites and in radiometry standards laboratories [8, 10–12]. In these targets, each pyramid is about 4 cm in height with a 1×1 cm base [10–12]. A large array of such pyramids, coated with a thin layer of absorber, will form the target. Often, the aluminum casing supports a thin layer of Eccosorb, as seen in the ARIS instrument [8] and other calibration sources [10–12]. In Figure 2A and B, a section of these calibrators is expanded, displaying only the valley created by two adjacent pyramids. Figure 2A treats the situation experienced in measuring absorption from such a target. Conversely, in Figure 2B, emission from a small surface element, at the bottom of the valley, is being considered. In order to simplify the presentation, only absorption and emission towards or away from a single element at the bottom of the valley is considered.

Thus, when radiation is incident on such a structure (see Figure 2A), it has an initial probability of being absorbed when it first enters the Eccosorb, P_1. If the radiation is not absorbed at this interface, it is transmitted to the metal casing where it is immediately reflected. At this point, the radiation re-enters the Eccosorb, where it still has another probability of being absorbed, P_2. Should the photons not be absorbed, the radiation travels to the adjacent pyramid. Here, once again, it has a probability of being absorbed, P_3. This scenario continues through many reflections and absorptions. As the photons travel towards the element at the bottom of the valley, a tremendous increase in the probability of being absorbed is generated. This effective absorptivity is made up of the sum of all individual absorption probabilities created from geometry in the presence of the casing. Because of repeated chances of absorption and reflection, the total probability for effective absorptivity, κ_{eff}, is tremendous as shown in Table 1. In fact, this represents geometric growth. For instance, if one permits a total of 8 interactions with the Eccosorp on the way to the small element (9 interactions in total), any photon will have nearly an 87% chance of being absorbed even if the emissivity of the Eccosorb layer (in isolation) was only 0.2. To make matters worse, if that same photon then tries to leave the valley, it must do so while dealing with the probabilities of absorption on exit. Other examples are provided in Table 1. Of course, the effective absorptivity of the target involves the sum of all probabilities for all photons and for all elements. The path through the Eccosorb layers will also be slightly different with each crossing. Nonetheless, it is easy to visualize why these geometric configurations give such outstanding results for effective absorptivity. This is true, even when extremely thin layers of absorber are placed on the surfaces of the metal casing.

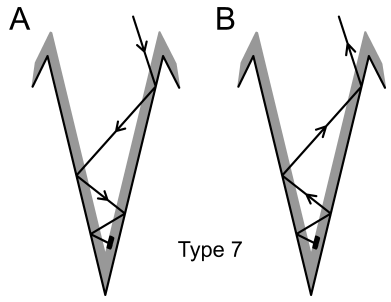

Fig. 2: Schematic representation of geometric, or Type-7 errors, in the assessment of effective emissivity. A) Path of a photon towards an absorptive element at the bottom of the valley. B) Path of a photon emitted by an element at the bottom of the valley. See Table 1 for the effect of geometries on effective emissivity of this element.

Unfortunately, while this situation is outstanding for absorption, it is suboptimal relative to emission. Consequently, a photon produced by a surface element at the bottom of the valley, which is not emitted directly in the direction of the horn, will be subject to repeated chances of being absorbed as it tries to make its way out of this microwave "death valley" (see Table 1). For instance, in considering the reverse path of Figure 2B, we can see that an element with an emissivity of 0.2, will be able to contribute an effective emissivity of only 0.034 after 8 interactions with the Eccosorb (4 changes in direction). Just 4 interactions would more than half the effective emissivity from this element. Once again, the effec-

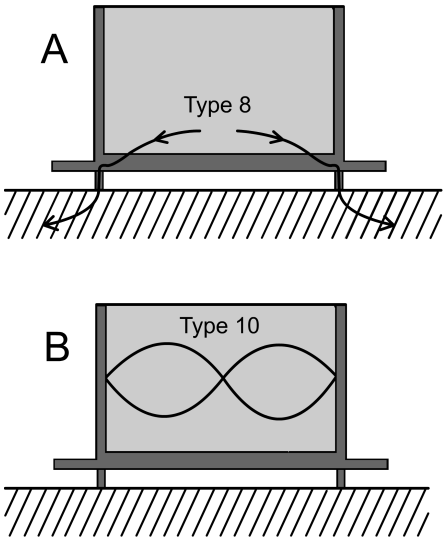

Fig. 3: Schematic representation of A) Type-8, or conductive, errors and B) Type-10, or standing wave errors. These errors can occur when assessing effective emissivity using return-loss measurements.

tive emissivity must include emission over all possible angles. Nonetheless, the situation is unfavorable, as geometry is hindering free emission from most elements.

Moreover, the situation is greatly accentuated if each element of the Eccosorb has a real emissivity of 0.7. In this case, after only 4 interactions with the Eccosorb (2 changes in direction), a photon leaving the bottom of the valley would contribute an effective emissivity of only 0.006. As such, superior absorptive characteristics of the surface absorber lead to inferior performance on effective emission. Furthermore, even a photon emitted near the tips of the pyramid has a chance of doing so in the direction of the valley, not the detector. Such a photon would have almost no chance of escaping the valley. This demonstrates the profoundness of Type-7 errors and the impact of geometry on calibration targets.

It is clear that the probability of absorption or the effective absorptivity, in this geometry, far surpasses the effective emissivity and all return-loss measurements involving such configurations improperly overestimate emission. In fact, rather than building a calibration target which ensures good emission, scientists unknowingly accomplished exactly the opposite. For instance, using infrared imaging, thermal variations in the targets are revealed, wherein the pyramidal tips display a reduced temperature (see Figure 5 in [10]). Such temperature distributions within calibration targets point to the presence of conductive and radiative imbalances which prove that the targets are not black (see section 2.4.1). Figure 5 in [10] constitutes a direct manifestation of Type-7 errors. Relative to emission, it would have been better to provide a very thick surface of Eccosorb. Unfortunately, return-loss measurement would indicate considerable diffuse reflection from such a surface. This had been circumvented by using valleys.

κ_{eff}	κ	N	ε_{eff}	ε	N
0.865	0.2	8	0.034	0.2	8
0.672	0.2	4	0.082	0.2	4
0.488	0.2	2	0.128	0.2	2
0.2	0.2	0	0.2	0.2	0
0.99	0.4	8	0.0067	0.4	8
0.922	0.4	4	0.0518	0.4	4
0.784	0.4	2	0.144	0.4	2
0.4	0.4	0	0.4	0.4	0
0.99998	0.7	8	0.00005	0.7	8
0.9975	0.7	4	0.00567	0.7	4
0.973	0.7	2	0.063	0.7	2
0.7	0.7	0	0.7	0.7	0

Table 1: Summary of calculated effective absorptivity and emissivity. In this table, κ_{eff} represents the effective absorptivity obtained after N interactions of an incoming photon with the absorber and 1 interaction with the element at the bottom of the valley (see Figure 2). It is assumed that Eccosorb is coating the 4×1×1 cm metallic pyramids [10–12]. The process involves geometric growth as given by $\kappa_{\text{eff}} = 1 - (1 - \kappa)^{N+1}$. Similarly, ε_{eff} represents the effective emissivity from a single element obtained after N interactions of an emitted photon with the Eccosorb. If the emitted photon travels directly to the detector, without further interactions with the Eccosorb, then $N = 0$. For effective emissivity, geometric decay is occurring corresponding to $\varepsilon_{\text{eff}} = \varepsilon - \varepsilon[1 - (1 - \kappa)^N]$. As a consequece of thermodynamic steady state, it is assumed that the ability of an individual element to absorb or emit radiation remains equal ($\kappa = \varepsilon$). The total effective emissivity of the target constitutes the summation of effective emissivities over all elements, e, and angles (θ and φ): $\varepsilon_{\text{eff}_T} = \Sigma\Sigma\Sigma\, \varepsilon_{\text{eff}}$.

2.4 Type-8, -9 errors

Type-8 and -9 errors can occur when heat flows out of the target through either conductive or convective paths, respectively. To ensure that radiative heat transfer dominates the equilibrium thermodynamics of the target, it is important to minimize all contacts.

A conductive path out of the reference target created with metallic fixtures can set up a Type-8 error as shown in Figure 3A. In this case, it is possible to produce an imbalance between thermal absorption and emission which immediately renders return-loss measurements invalid.

It is evident that a target bombarded with incident microwave radiation on absorption can dissipate such energy through conduction out of the target. It does not need to resort to emission. In this situation, the effective absorptivity of the target will not be equal to its effective emissivity ($\varepsilon_{\text{eff}} \neq \kappa_{\text{eff}}$), even though thermodynamic steady state is being maintained. This also explains why geometry can produce imbalances in effective emissivity and absorptivity while still maintaining a fixed target temperature.

In theory, a Type-9 error could also be produced, with the same consequences, if convective paths out of the target are

present. Such effects are unlikely to be significant in most scenarios as convective heat transfer is usually ineffective relative to conductive mechanisms.

Consequently, the presence of conduction and convection can introduce two new error terms, Γ_{cond} and Γ_{conv}, such that Eq. (4) now becomes:

$$\kappa_{t_{\text{eff}}} = (\kappa_t + \Gamma_{\kappa\sigma}) = 1 - (\sigma_{an} + \Gamma_{\tau\sigma}) - (\sigma_{ad} + \Gamma_{s\sigma}) - \\ - (\Gamma_{bp} + \Gamma_{dh}) - (\Gamma_{dc} + \Gamma_{d\sigma}) - \Gamma_{\text{cond}} - \Gamma_{\text{conv}} . \quad (5)$$

Conductive and convective errors in target calibration are often not properly addressed and the use of conduction to "cool the target" unwisely advocated [7]. Such approaches highlight elementary errors relative to the understanding of heat transfer. For instance, it is true that conductive paths can be used to heat a target to steady state with all heat being dissipated through radiation. In fact, this was the approach first used to make radiant cavities isothermal [24] in the days which led to Planck's formulation of the blackbody relationship [2, 3]. In this case, conductive paths bring heat into the device which is then forced to escape through radiation. It is quite another matter to permit conductive or convective paths to bring heat out of a target. In the former case, heat leaves the target exclusively through radiation. In the later, it can leave either through radiation or conduction. Accordingly, there is no reason to expect that brightness temperatures in the second setting will be correct.

2.4.1 Max Planck and heat radiation

Relative to this question, Max Planck insists that blackbodies be isolated from the surrounding system. He writes: "*A system of bodies of arbitrary nature, shape, and position which is at rest and is surrounded by a rigid cover impermeable to heat will, no matter what its initial state may be, pass in the course of time into a permanent state, in which the temperature of all bodies of the system is the same. This is the state of thermodynamic equilibrium, in which the entropy of the system has the maximum value compatible with the total energy of the system as fixed by the initial conditions. This state being reached, no further increase in entropy is possible*" [3]. In this treatment, Planck is really making a statement of Prévost's theory of exchanges [25, 26]. However, he is moving beyond Prévost, because he is considering the entropy of the radiation itself. For Planck, the normal spectrum is obtained when the entropy of radiation is maximized [3]. In any case, he continues: "*We shall begin with the simplest case, that of a single medium extending very far in all directions of space, and like all systems we shall here consider, being surrounded by a rigid cover impermeable to heat*" [3]. Finally, Planck makes the point relative to conduction: "*Now the condition of thermodynamic equilibrium requires that the temperature shall be everywhere the same and shall not vary with time. Therefore in any arbitrary time just as much radiant heat must be absorbed as is emitted in each volume-element of the medium. For the heat of the body depends only on the heat radiation, since on account of the uniformity of temperature, no conduction of heat takes place*" [3]. Remember, in this case, that Planck is dealing with a closed system. As such, once thermal equilibrium exists in such a system, there can be no net conduction.

Nonetheless, in open systems, an object can assume a fixed temperature, even if net conduction takes place. Such a situation can be devastating to the production of thermal photons as seen in section 2.4.2.

2.4.2 An example from the remote sensing of soil moisture

Soil moisture can be evaluated through emission profiles in the microwave region [27]. It is well known that the brightness temperature of soil drops dramatically with moisture content [27]. Given the presence of water, the soil can dissipate its heat through conduction, directly into the water, or through convection, as the liquid evaporates. In response, brightness temperatures drop [27]. When soil moisture is removed, brightness temperatures recover, for the simple reason that thermal emission now becomes the primary means of dissipating heat. Placing a body in direct contact with conductive or convective paths, allows heat to escape using non-radiative means, resulting in the lowering of brightness temperatures. In such a scenario, the brightness temperature recorded will be unrelated to the actual temperature of the object of interest. This is precisely what has been done in the case of the LFI reference targets on the Planck satellite [7,28].

2.5 Type-10 errors

In addition to all of the issues discussed so far, a Type-10 error can exist when standing waves are able to form inside the metal casing, enclosing the absorber (see Figure 3B). Thus, since the casing is made of metal, often possessing a backing along with small walls [7], it introduces the possibility of forming a pseudo-cavity in front of the horn wherein standing waves can build [4]. This leads to a Type-10 error. Such waves would trap energy into the target, making it unavailable to return-loss measurements. Nonetheless, absorption has not occurred. Standing waves simply confine the microwaves [4] and the return-loss measurements suggest an emissivity which is superior to that actually present.

As a result, a complete expression for the determination of absorptivity is as follows:

$$\kappa_{t_{\text{eff}}} = (\kappa_t + \Gamma_{\kappa\sigma}) = 1 - (\sigma_{an} + \Gamma_{\tau\sigma}) - (\sigma_{ad} + \Gamma_{s\sigma}) - \\ - (\Gamma_{bp} + \Gamma_{dh}) - (\Gamma_{dc} + \Gamma_{d\sigma}) - \Gamma_{\text{cond}} - \Gamma_{\text{conv}} - \Gamma_{sw} , \quad (6)$$

where Γ_{sw} accounts for the presence of standing waves. Once again, this term is important in addressing the reference targets on the Planck satellite [28].

3 Conclusions

Much can be gained by carefully considering all thermal components in a heat transfer problem. A complete analysis of error leads to the realization that progress must be made in the fabrication and testing of microwave reference loads and targets. At the same time, these considerations also impact the design of test facilities and anechoic chambers. Ideally, by lining room surfaces with temperature controlled metallic pyramids covered with Eccosorb, it should be possible to simultaneously create tremendous effective absorptivity by the walls and bring their effective emissivity down to very low levels. Such conditions would be ideal in many test scenarios involving anechoic chambers.

At the same time, the measurement of emissivity from microwave targets is a complex problem, wherein up to 10 or more, error types can be identified. Most of these errors are familiar to the geosciences and astrophysics communities. Some may have escaped analysis. Often though, calibration errors have been inappropriately dismissed as insignificant [7]. This is true for Type-10 errors, as the presence of standing waves in the metal casing is almost always ignored [7]. Nonetheless, a greater concern rests in the Type-7 errors which alter the effective radiative balance of the target due to geometrical arguments. Such errors can also be present in calibration blackbodies for use in the infrared [18, 19]. Targets are not enclosures [4] and are never blackbodies. Hence, they become subject to geometrical considerations. In addition, Type-8 errors can easily occur raising the possibility that conduction itself, by allowing heat to flow out of the target, is creating an imbalance between effective target emission and absorption. If heat can be funneled out of a target through conduction, its emissivity will fall. This can constitute an important limitation in building calibration targets.

As a result, though attempts have been made to quantify error sources in microwave calibration targets [13–15], it appears that many of the devices used as emissivity references on satellites and in the laboratory (e.g. [4–15] are inaccurate. They are simply unable to provide the emissivity believed to exist using return-loss measurements. This is a significant scientific oversight which affects the monitoring of global climate change (e.g. [8]) and the microwave background [5, 7]. Perhaps it is for this reason that geoscientists are now turning to Earth surfaces as potential calibration sources [29]. Nonetheless, this solution is not available to satellites such as Planck [7, 28] which must rely on their internal reference targets. The proper functioning of spacecraft internal reference targets can have the most profound consequences on scientific advancement, as will be discussed in the accompanying work [28].

Acknowledgements

The author would like to thank Luc and Christophe Robitaille for figure preparation and computer assistance, respectively.

Dedication

This work is dedicated to Barbara Anne Helgeson.

Submitted on February 15, 2010 / Accepted on February 19, 2010
Published online on February 22, 2010

References

1. Kirchhoff G. Über das Verhältnis zwischen dem Emissionsvermogen und dem Absorptionsvermögen der Körper für Wärme und Licht. *Poggendorfs Annalen der Physik und Chemie*, 1860, v. 109, 275–301 (English translation by F. Guthrie: Kirchhoff G. On the relation between the radiating and the absorbing powers of different bodies for light and heat. *Phil. Mag.*, 1860, ser. 4, v. 20, 1–21).
2. Planck M. Über das Gesetz der Energieverteilung im Normalspektrum. *Annalen der Physik*, 1901, v. 4, 553–563 (English translation by ter Haar D.: Planck M. On the theory of the energy distribution law in the normal spectrum. The old quantum theory. Pergamon Press, 1967, 82–90; also Planck's December 14, 1900 lecture "Zur Theorie des Gesetzes der Energieverteilung in Normalspectrum", which stems from this paper, can be found in either German, or English, in: Kangro H. Classic papers in physics: Planck's original papers in quantum physics. Taylor & Francis, London, 1972, 6–14 or 38–45).
3. Planck M. The theory of heat radiation. Philadelphia, PA., P. Blakiston's Son, 1914, 22–23.
4. Robitaille P.M. Kirchhoff's law of thermal emission: 150 Years. *Progr. Phys.*, 2009, v. 4, 3–13.
5. COBE website, http://lambda.gsfc.nasa.gov/product/cobe
6. Robitaille P.M. COBE: A radiological analysis. *Progr. Phys.*, 2009, v. 4, 17–42.
7. Valenziano L., Cuttaia F., De Rosa A., Terenzi L., Brighenti A., Cazzola G.P., Garbesi A., Mariotti S., Orsi G., Pagan L., Cavaliere F., Biggi M., Lapini R., Panagin E., Battaglia P., Butler R.C., Bersanelli M., D'Arcangelo O., Levin S., Mandolesi N., Mennella A., Morgante G., Morigi G., Sandri M., Simonetto A., Tomasi M., Villa F., Frailis M., Galeotta S., Gregorio A., Leonardi R., Lowe S.R., Maris M., Meinhold P., Mendes L., Stringhetti L., Zonca A. and Zacchei A. Planck-LFI: design and performance of the 4 Kelvin Reference Load Unit. *JINST*, 2009, v. 4, T12006.
8. Lambrigtsen B.H. Calibration of the AIRS microwave instruments. *IEEE Trans. Geosc. Rem. Sens.*, 2003, v. 41, 369–378.
9. Cox A.E. and Janezic M.D. Preliminary studies of electromagnetic properties of microwave absorbing materials used in calibration targets. *IGARSS*, 2006, 3467–3469.
10. Cox A.E., O'Connell J.J., and Rice J.P. Initial results from the infrared calibration and infrared imaging of a microwave calibration target. *IGARSS*, 2006, 3463–3465.
11. Randa J., Cox A.E, Francis M., Guerrieri J. and MacReynolds K. Standard radiometers and targets for microwave remote sensing. *IGARSS*, 2004, v. 1, 698.
12. Feng N. and Wei W. The optimization design for microwave wide band blackbody calibration targets. *International Conference on Microwave and Millimeter Wave Technology* (ICMMT), 2008, v. 4, 1695–1698.
13. Randa J., Walker D.K., Cox A.E., and Billinger R.L. Errors resulting from the reflectivity of calibration targets. *IEEE Trans. Geosc. Rem. Sens.*, 2005, v. 43, 50–58.
14. Li Z., Peng Y., Miao J., Wang Z. Evaluation of disturbance in the antenna calibration of the microwave radiometer. *International Conference on Microwave and Millimeter Wave Technology* (ICMMT), 2008, v. 4, 810–813.
15. Cheng C.Y., Li F., Yang Y.J. and Chen Y.M. Emissivity measurement study on wide aperture microwave radiometer. *International Conference on Microwave and Millimeter Wave Technology* (ICMMT), 2008, v. 4, 914–917.

16. Dietlein C., Popović Z., and Grossman E.N., Aqueous blackbody calibration source for millimeter-wave/terahertz metrology. *Appl. Opt.*, 2008, v. 47, 5604–5615.

17. Robitaille P.M. Blackbody radiation and the carbon particle. *Prog. Phys.*, 2008, v. 1, 36–55.

18. Fowler J.B. A third generation water bath based blackbody source. *J. Res. Nat. Inst. Stand. Technol.*, 1995, v. 100, 591–599.

19. Fowler J.B. An oil-bath-based 293 K to 473 K blackbody source. *J. Res. Natl. Inst. Stand. Technol.*, 1996, v. 101, 629–637.

20. Murphy A.V., Tsai B.K., Saunders R.D. Transfer calibration validation tests on a heat flux sensor in the 51 mm high temperature blackbody. *J. Res. Nat. Inst. Stand. Technol.*, 2001, v. 106, 823–831.

21. Emerson and Cuming Microwave Products. Technical Reference: ECCOSORB CR Two-Part Castable Load Absorber Series. http://www.eccosorb.com/file/958/cr.pdf

22. Stewart B. An account of some experiments on radiant heat, involving an extension of Prévost's theory of exchanges. *Trans. Royal Soc. Edinburgh*, 1858, v. 2(1), 1–20 (also found in Harper's Scientific Memoirs, edited by J. S. Ames: *The laws of radiation and absorption: memoirs of Prévost, Stewart, Kirchhoff, and Kirchhoff and Bunsen*, translated and edited by D. B. Brace, American Book Company, New York, 1901, 21–50).

23. Robitaille P.M. A critical analysis of universality and Kirchhoff's law: a return to Stewart's law of thermal emission. *Prog. in Phys.*, 2008, v. 3, 30–35; arXiv: 0805.1625.

24. Hoffmann D. On the experimental context of Planck's foundation of quantum theory. *Centaurus*, 2001, v. 43(3–4), 240–259.

25. Prévost P. Mémoire sur l'équilibre du feu. Journal de Physique, 1791, v. 38, 314–322 (translated in Harper's Scientific Memoirs (J. S. Ames, Ed.) — *The laws of radiation and absorption: memoirs of Prévost, Stewart, Kirchhoff, and Kirchhoff and Bunsen*, translated and edited by D. B. Brace, American Book Company, New York, 1901, 1–13).

26. Prévost P. Du calorique rayonnant. J. J. Paschoud, Geneva & Paris, 1809 (Sections are translated in Harper's Scientific Memoirs (J. S. Ames, Ed.) — *The laws of radiation and absorption: memoirs of Prévost, Stewart, Kirchhoff, and Kirchhoff and Bunsen*, translated and edited by D. B. Brace, American Book Company, New York, 1901, 15–20).

27. Ulaby F.T., Moore R.K., Fung A.K. Microwave remote sensing active and passive — Volume 2: Radar remote sensing and surface scattering and emission theory. London, Addison-Wesley Publishing Company, 1982, p.884–887.

28. Robitaille P.M. The Planck Satellite LFI and the microwave background: Importance of the 4 K references targets. *Prog. Phys.*, 2010, v. 2, 11–18.

29. Rüdiger C., Walker J.P., Allahmoradi M., Barrett D., Costelloe J., Gurney R., Hacker J., Kerr Y.H., Kim E., Le Marshall J., Lieff W., Marks A., Peisch S., Ryu D., and Ye N. Identification of spaceborne microwave radiometer calibration sites for satellite missions. *Proc. Intern. Congr. Modelling and Simulation* (MODSIM), Cairns, Australia, 2009, 3740–3746.

The Planck Satellite LFI and the Microwave Background: Importance of the 4 K Reference Targets

Pierre-Marie Robitaille

Department of Radiology, The Ohio State University, 395 W. 12th Ave, Suite 302, Columbus, Ohio 43210, USA
E-mail: robitaille.1@osu.edu

Armed with ∼4 K reference targets, the Planck satellite low frequency instrument (LFI) is intended to map the microwave anisotropies of the sky from the second Lagrange point, L2. Recently, the complete design and pre-flight testing of these ∼4 K targets has been published (Valenziano L. et al., JINST 4, 2009, T12006). The receiver chain of the LFI is based on a pseudo-correlation architecture. Consequently, the presence of a ∼3 K microwave background signal at L2 can be established, if the ∼4 K reference targets function as intended. Conversely, demonstration that the targets are unable to provide the desired emission implies that the ∼3 K signal cannot exist, at this location. Careful study reveals that only the second scenario can be valid. This analysis thereby provides firm evidence that the monopole of the microwave background, as initially detected by Penzias and Wilson, is being produced by the Earth itself.

1 Introduction

Over the years, I have expressed growing concern [1] about the origin of the microwave background [2]. My evaluation has focused on three fronts. First, I have highlighted that errors exist in the derivation of Kirchhoff's law of thermal emission (e.g. [3, 4] and references therein) which renders its use inappropriate in physics. The universality of blackbody radiation is invalid on both theoretical and experimental grounds [3, 4], making it impossible to assign an absolute temperature to the Penzias and Wilson [2] signal. At the same time, I have emphasized that the law of equivalence between emission and absorption, under conditions of thermal equilibrium, remains valid [4]. This is properly referred to as Stewart's law [5]. Second, I have questioned the assignment of the microwave background to the cosmos [6], invoking (see [1] and references therein), along with Borissova and Rabounski [7], that the Earth's oceans are responsible for this signal. It is the presence of the hydrogen bond within water which gives cause for reconsideration [8]. The emission of this bond has not yet been assigned for the Earth's spectrum, despite the reality that our planet is 70% water. Finally, I have outlined shortcomings in the measurements of the microwave background, especially relative to the COBE [9] and WMAP [10] satellites. Concern, relative to the results of these satellites, has also been voiced by a number of other groups [11–18]. Now, the Planck mission [19] is drawing the attention of the scientific community. But early reports [20] and system evaluations [21] should provoke uneasiness. This can only be appreciated when the function of the low frequency instrument (LFI) is understood [22–26]. It is through the analysis of the LFI's performance that the origin of the microwave background can be established [27].

On July 30, 2009 the ESA Planck team wrote: "*In the case of LFI, the results show even better than expected performances due to benign space environment and an improved tuning process*" [20]. On first consideration, it would seem that the monopole of the microwave background was present at L2, as expected by the astrophysics community. Unfortunately, upon careful review, this statement directly implies that the opposite situation has taken place. There can be no 3 K signal at this location. The arguments center on the functioning of the ∼4 K targets, whose full description only recently became available [21]. When the performance of these references is considered, in combination with the function of the pseudo-correlation receivers [22–26], solid evidence emerges that there can be no ∼3 K signal permeating space.

2 The performance of the Planck LFI

The proper characterization of the ∼4 K reference loads [21] and LFI [22–26] on the Planck satellite is critical to understanding whether the monopole of the 2.7 K microwave background is present at L2 [27]. This situation occurs, since the presence of a monopole cannot be ascertained with the high frequency instrument, HFI [28]. Relative to the HFI, the Planck team writes: "*Plank cannot measure accurately the monopole (uniform part of the emission) because many sources contribute (telescope, horns, filters,...)*" [29]. Thus, the HFI bolometers, though operating in absolute mode, can receive thermal photons from the spacecraft itself much of which is in a 50 K environment. As Planck's mirrors are exposed to 300 K at L2, photons of instrumental origin can enter the bolometers, making it difficult for the HFI to extract the ∼3 K background signal from instrumental foregrounds. It is anticipated that such effects are less important at the frequencies of the LFI. Consequently, it seems that only the LFI [22–26] can properly address the existence of a monopole at L2. The issue is critical since, in the absence of the monopole, any anisotropy measurements by this satellite would have little or no scientific value.

Expected performance of the PLANCK LFI receivers		
	Sky Temperature ~3 K	Sky Temperature ~0 K
Reference ~4 K	As expected	Poor
Reference ~0 K	Poor	Better than expected

Table 1: Summary of the scenarios which impact the expected performance of the pseudo-correlation receivers on the Planck satellite. Four possibilities exist depending on the actual brightness temperatures of the sky and the reference targets. It is assumed that the sky can be either at ~3 K (the Penzias and Wilson temperature [2]) or at ~0 K [1]. Similarly, the reference targets can be either operating as intended near 4 K [21], or are unable to generate a meaningful blackbody spectrum, ~0 K (as proposed herein).

As discussed in considerable detail [22–26], the low frequency instrument (LFI) functions as a pseudo-correlation receiver, wherein the sky signal is constantly being compared against a ~4 K reference signal. In this configuration, the receiver displays optimal performance only when the two input signals display approximately the same amplitude. Under these conditions, the input offsets are nearly identically zero, the knee frequency of the receiver is minimized and so is the $1/f$ noise [22–27]. The LFI team states, "*to minimize the 1/f noise of the radiometers, the reference blackbody temperature should be as close as possible to the sky temperatures (~3K)*" [21]. This represents an ideal situation, wherein the mechanical configurations of both receiver chains are identical. In practice, this cannot be achieved, as the reference horns are much smaller than the sky horns. Thus, a gain modulation factor is utilized to partially account for such effects [21–27]. In any case, the radiometric temperature difference between the signals captured by the sky and the reference horns constitutes a critical element in receiver performance. In order for the LFI to function properly, the sky signal must balance the reference signal.

There are four scenarios which need to be considered relative to the performance of the LFI receiver chains. These scenarios are summarized in Table 1 and are described as follows:

2.1 Sky at ~3 K, reference loads at ~4 K

The cosmology community is expecting a 2.7 K monopole signal at L2 [2]. In addition, some thermal photons might be expected from the galactic foreground and the spacecraft itself. As a result, the receiver would have optimal performance, if the sky signal was being compared with a reference signal at 2.7 K. However, the LFI group mentions that "*there is no convenient spacecraft source of 2.7 K with sufficient cooling power*" [21], and chose to passively cool the reference loads to ~4 K by mounting them on the 4 K thermal shield of the HFI. At first glance, this appears to be an elegant solution. But in actuality, as will be seen in section 3, this placement demonstrates suboptimal conditions relative to the principles of heat transfer. In any event, should the sky be at 2.7 K and the ~4 K load properly constructed, the receiver performance would be as expected from pre-flight modeling. Being approximately balanced, the sky and reference signals would generate a receiver performance matching the pre-flight technical specifications [22–26].

2.2 Sky at ~0 K, reference loads at ~4 K

Alternatively, if the monopole signal does not exist at L2 and *if the reference loads are truly acting as ~4 K blackbody sources*, a tremendous input offset would be generated in the receiver. The knee frequencies would rise, as would the $1/f$ noise. The result would be significant stripes in the maps generated by the satellite. These concerns were previously outlined in detail [27], *on the assumption that the ~4 K reference loads would be properly designed and able to provide the needed emission*.

2.3 Sky at ~3 K, reference loads acting as ~0 K sources

An interesting case can also manifest itself if the microwave sky is indeed at 2.7 K, but the reference loads, due to improper fabrication, do not produce an emission corresponding to a ~4 K blackbody source. In the extreme, the reference loads might be considered as producing no valuable emission signal. This would produce an emission from the loads indistinguishable from a ~0 K source, despite their ~4 K actual temperature. Under such a scenario, a tremendous imbalance would once again be produced in the receivers, the knee frequencies would rise, and $1/f$ noise would be manifested in the resultant maps.

2.4 Sky at ~0 K, reference loads acting as ~0 K sources

Finally, there is the possibility that the microwave sky is at ~0 K and that improperly manufactured reference loads produce a signal much inferior to the expected ~4 K source. Once again, in the extreme, the reference loads might be considered as producing no valuable emission signal, thereby behaving as ~0 K sources. Interestingly, in the case, the performance of the spacecraft would be better than expected. Only relatively small microwave emissions from the sky would be observed, and their lack of power would be complemented by the lack of power coming from the reference loads.

Of these four scenarios, only the first and last can be valid, given what we now know [20] about the performance of the LFI [22–26]. In fact, assuming that the ~4 K references were properly constructed, the performance of the LFI receivers,

by themselves, would prove that there is indeed a monopole signal at L2 [27]. Everything hinges on the quality of the ∼4 K reference blackbodies [21]. But given that "*even better than expected performances*" [20] were obtained, there is concern that the ∼4 K reference loads are not functioning as they should and that the last scenario (Sky at ∼0 K, reference loads ∼0 K) is the one which will prevail. Unfortunately, a detailed description of the ∼4 K loads was not available to the general public until December 29, 2009 [21]. The materials contained in this work provide enough information to resolve the question.

3 The ∼4 K Reference Loads on the PLANCK LFI

A schematic representation of a ∼4 K reference load system for the LFI is displayed in Figure 1. Each reference load system is comprised of a small horn, separated from a target by a 1.5 mm gap in order to preserve thermal isolation between the 20 K shield which houses the LFI and the ∼4 K shield housing the HFI [21]. The Planck team states: "*One of the main requirements of the 4KRL design was to minimize the heat load on the HFI to a value lower than 1 mW. Safety considerations (a thermal short between the two instruments will prevent the HFI to work) lead to mechanically decouple the loads, mounted on the HFI external shield, from the LFI radiometers, at 20 K*" [21]. They continue: "*This solution implies the presence of a gap in the radiometer reference arm, through which external spurious signals can leak in the radiometers*" [21]. They attempt to address this issue, by introducing grooves on the edge of the horn, in order to limit spillover. In addition, they state: "*Targets also need to be small and placed in the very near field of the reference horns to reduce the leak from the gap*" [21]. The LFI group notes that: "*the conceptual design is therefore based on small absorbing targets, mounted inside a metal enclosure ("case") to confine the radiation...*" [21].

The satellite team relays that: "*Each target is basically a rectangular Eccosorb™ CR block, shaped for optimal matching with the incoming field. The back part is made of highly absorbing CR117, while the front sector, made from CR 110, reduces the mismatch*" [21]. The absorbing material for each target is then enclosed on 5 sides, within an aluminum casing. These targets are mounted on the 4 K shield of the HFI using "*stainless steel (AISI304) thermal washers*" which are "*interposed between the loads and the interface points to the HFI*" [21]. The LFI group explains that: "*These are small cylinders (typically 5 mm long, 1 mm wall thickness) whose dimensions are optimized to dump temperature fluctuations in order to meet requirements*" [21]. Apparently, the ∼4 K reference loads are then attached directly through the washers onto the HFI 4 K shield with "*screws (mounted on the HFI)*" [21].

The designers opt to conduct heat out of the ∼4 K reference loads into the 4 K shield of the HFI in order to achieve a stable temperature. They enclose the Eccosorb material in an aluminum casing to help ensure that conductive paths are open which can suppress any thermal fluctuations within the loads. In so doing, they have introduced Type-8 errors into their system [30]. In fact, the LFI group, during the testing stage, observes that they must work to better suppress thermal fluctuations. Therefore, they attempt to increase thermal fluctuation damping. They write: "*the RF and thermal test results were used to further refine the design (i.e. thermal dumping was increased, mounting structure was slightly modified to facilitate integration)*" [21] and "*The optimization of the thermal washers allowed to increase the damping factor...*" [21]. Thus, they are trying to adopt a delicate balance between the necessity to cool the references on the 4 K shield and the need to efficiently address heat fluctuations: "*Cases, supported by an Al structure, are mounted on the HFI using Stainless Steel thermal decouplers (washers), which allows to carefully control the thermal behavior*" [21]. In reality, while the presence of the washers and their construction primarily impacts the time constants for damping heat fluctuations, they still provide a very efficient conductive heat path out of the targets. After all, the references remain cooled by conductive mechanisms which rely on thermal contact with the 4 K HFI shield. Herein is found the central design flaw of the Planck LFI.

3.1 Conductive paths and Type-8 errors

The Planck reference loads are cooled by conduction, not self-radiation. As a consequence, there is no reason to expect that the reference loads can output any photons at ∼4 K. Being cooled by conduction, the references do not need to invoke thermal radiation in achieving steady state. Indeed, the Planck team writes: "*Thermal interface is dominated by conduction through thermal washers*" [21]. They continue: "*Metal parts are assembled using Stainless Steel screws at high torque, to make thermal contact as close as possible to an ideal value*" [21]. Relative to thermal modeling they write: "*the 70 GHz loads are assumed to be perfect thermal conductors, due to their small thickness and mass*" [21]. Hence, the LFI group members, by introducing conduction directly into their loads, have rendered them ineffective as ∼4 K blackbody sources.

Certainly, in order for an object to act as a true blackbody, it must be devoid of all outgoing conductive paths of heat transfer. Reference targets must be spatially isolated from their surroundings, such that only radiation can dominate [30]. Yet, the ∼4 K targets on the Planck satellite are configured such that net conduction of heat out of the target is allowed to take place. The targets are mounted onto the 4 K shield of the HFI, and heat can flow continuously using conduction into that heat sink. Since the targets are continually exposed to a 20 K environment, their temperature is being ensured by conduction, not heat radiation. In this manner, thermodynamic steady state and a stable temperature is maintained, but through conduction, not heat radia-

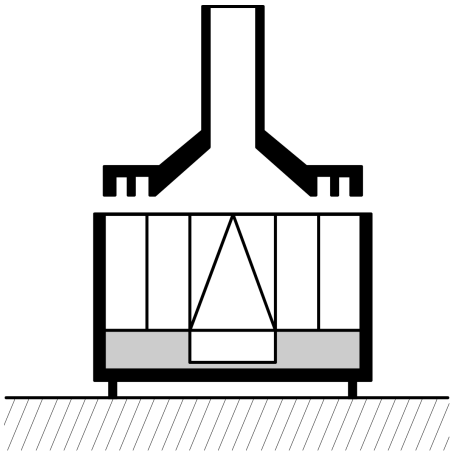

Fig. 1: Schematic representation of a Planck LFI reference load. Each load is comprised of a horn (upper section) and a target (middle section) separated by a 1.5 mm gap. The targets are constructed from molded Eccosorb (CR-110 or 117) absorber surrounded by an aluminum casing which acts to preserve thermodynamic steady state within each unit, using conduction. Heat is allowed to flow out of the target casing through a conductive path into the 4 K shield of the HFI (represented by the cross hatched area in the lower section). This path is provided by stainless steel cylindrical washers (see text and [21] for more detail). By providing a conductive path out of the target, the Planck LFI team has created a situation wherein a Type-8 error is introduced [30]. By itself, such a design ensures that these targets cannot operate as ∼4 K loads as intended (see text).

tion. The Planck LFI ∼4 K targets are directly linked, which good thermal contact, through stainless steel washers, onto a 4 K shield. Such a scenario will not only reduce the brightness temperature, relative to the real temperature, it is likely to completely inhibit the emission of photons [30]. In this respect, the presence of conductive paths in the Planck LFI ∼4 K targets provides a much worse scenario for achieving the expected brightness temperature, then when water permeates soil [30].

Rather than using conductive washers, stainless steel screws, and an aluminum casing, it would have been preferable to encase the Eccosorb in a strong insulator suspended in air with thin non-conducting support rods. Such a load could then be enclosed in a perfectly reflective shield at 4 K. It is only through this kind of geometry that a ∼4 K load can suitably act as a reference.

By itself, the Type-8 error indicates that no 3K signal exists at L2. The loads do not need to cool by radiation. Accordingly, they do not need to emit a single photon. They are unable to act as blackbodies in the intended capacity. Still, beyond the Type-8 error, there are sufficient concerns with the ∼4 K reference loads, that their lack of functionality can be established. In order to properly follow these issues, it is important to consider all of the potential errors related to measuring emissivity using return-loss methods on microwave targets [30].

3.2 Type-3, -4, -5, -6, and -7 errors

First, the ∼4 K reference loads are subject to a Type-3 error [30]. Radiation from the horn during testing can be diffracted on the edge of the target casing through the 1.5 mm thermal gap into the surroundings. This is because, unlike the horns, the casing contains no edge structure which can minimize diffraction. Secondly, the ∼4 K reference systems are subject to a Type-4 error, wherein incident radiation from the horn, experiences diffuse reflection on the surface of the Eccosorb, and is lost through the gap into space [30]. Similarly, Type-5 errors can occur. Incident radiation, in this case, enters the Eccosorb, is reflected on the casing, and then, after reentry into the absorber, becomes scattered into space through the gap. In the same way, a Type-6 error can occur [30]. That is, incident radiation which traverses the Eccosorb layer can be reflected by the casing, and on re-entry into the absorber, is diffracted upon striking the edge of the casing. Once more, such radiation could exit the system through the 1.5 mm thermal gap which separates the horn and the target (see Figure 1). In addition, Type-7 errors exist as previously discussed in detail [30]. These are errors which depend on the geometry of the target. They occur when a transmissive absorber is mounted on a reflective metallic casing and their characteristics have been addressed [30].

3.2.1 Planck test data, calculations, and Type-10 errors

There is also the possibility of a Type-10 error [30]. Namely, because the Planck team chose to use so little material in their casings, they have enclosed only weak absorbers. In so doing, they introduce the likelihood of generating standing waves within the casings during testing. This would represent a Type-10 error [30].

A careful study of Planck LFI return-loss traces provides strong evidence that such standing waves do exist. For instance, the Planck team presents Figure 26 [21], wherein the return-loss is measured. A single such tracing, obtained from a 30 GHz horn-target assembly, is extracted from this Figure to generate Figure 2 herein. Note that the network analyzer tracing has pronounced resonances extending as low as −50 dB at some frequencies. These resonances should not be present if the target is black [3]. In fact, the presence of such resonances, by itself, provides ample evidence that the 30 GHz targets are far from being black.

As a result, it is clear that the return-loss measurements published by the Planck team [21] far overstate the actual performance of the reference targets, if these values are directly utilized to calculate emissivity. In fact, this is evident by examining data provided by the Planck team. Consider, for instance, Figure 10 in [21] which is reproduced herein as Figure 3. This represents a computational analysis of field distributions that takes place both inside and around the targets, during testing with microwave radiation. It is evident, from this figure, that the targets are unable to localize microwave

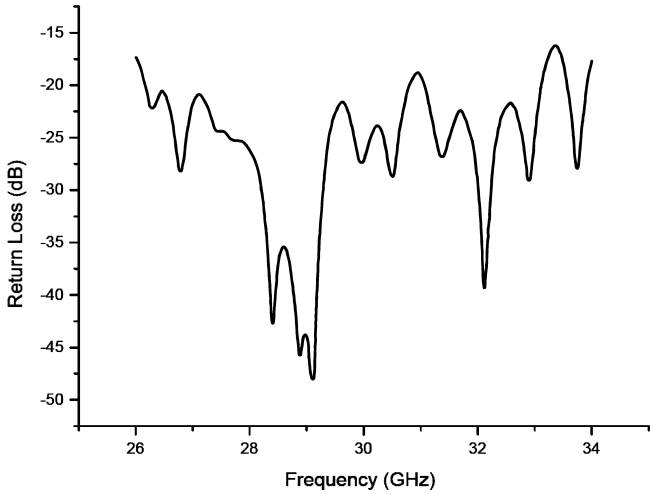

Fig. 2: Schematic representation of a network analyzer tracing for a 30 GHz reference target system, as provided by the Planck LFI team [21]. This particular tracing was extracted from Figure 26 in [21] in order to better visualize its features. Note the presence of significant resonances on this tracing, indicating the existence of standing waves within the horn-target system. It is well known, based on elementary considerations in electromagnetics [3], that cavities, waveguides, and enclosures, at microwave frequencies, can sustain standing waves in a manner depending on their size and geometry (see [3] and references therein). This problem is particularly important when the dimensions of the target approach the wavelengths of interest. In this case, 30 GHz corresponds to a wavelength of ∼1 cm in vacuum. The target casings are $3.3 \times 3.3 \times (\sim 2)$ cm (see Table 1 and Figure 12 in [21]). The presence of such resonances in the ∼4 K reference loads, demonstrates unambiguously that the targets are not black. In fact, the targets are still acting as resonant devices [3]. For a blackbody to exist, all such resonances must be suppressed (i.e. as ideally seen by a constant −50 dB tracing across the spectral range). In this case however, and when combined with the data in Figure 3, it appears that approximately −15 to −20 dB of return loss can be accounted for by leakage from the 1.5 mm gap. Then, between −20 to −25 dB of return loss can be attributed, at certain frequencies, to the existence of resonance features. Note that 29 GHz gives a wavelength of ∼1.03 cm in vacuum, and perhaps a little more in Eccosorb (see [30] and references therein). As such, the resonances at 28.5–29.2 GHz correspond almost exactly to 3 wavelengths in a square 3.3 cm enclosure. Reproduced from [21] with permission of the IOP and L.Valenziano on behalf of the authors and the Planck LFI consortium.

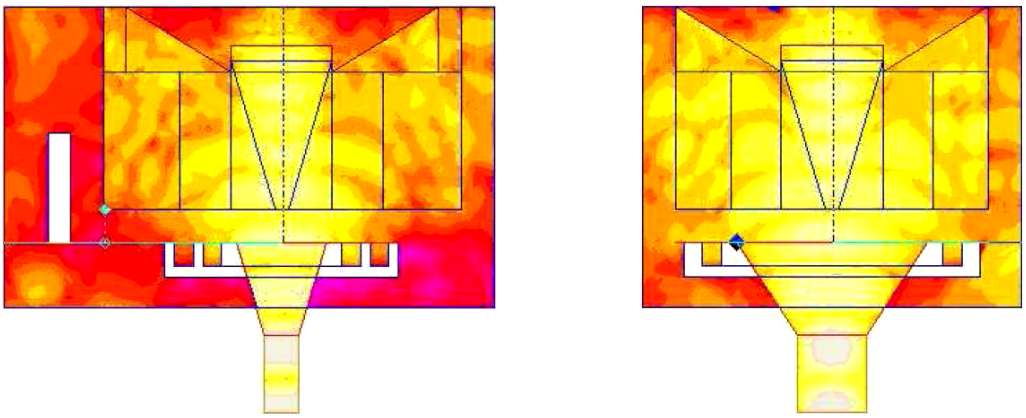

Fig. 3: Computational determination of the E-field distribution at 70 GHz for a horn-target assembly as reproduced from Figure 10 in [21]. White areas represent perfect conductors, whereas regions of increased brightness depict more intense fields [21]. The left panel corresponds to PHI = 90 while the right panel to PHI = 0. Further details are available in [21]. Note how the target is unable to localize microwave energy. Leakage of radiation beyond the 1.5 mm gap separating the horn and the target is evident, especially in the right panel. If leakage appears to be less intense in the left panel (examine the left edge of the casing), it is because the horn dimension in this cut is substantially smaller than the target. Nonetheless, some restriction of radiation is visible on the left edge of the casing in the left panel. This acts to confirm that none of the other edges are able to confine the radiation. Note also that the section of CR-117 absorber below the pyramid is actually acting to reflect rather than absorb the radiation. This is especially evident in the left panel (note red area beneath the central pyramid (see [21] for more detail). From these calculations, it is apparent that the Planck LFI targets at 70 GHz are not black, enabling dissipation of energy well beyond the horn-target assembly. Unfortunately, the Planck team does not display corresponding results at 30 and 44 GHz. Reproduced from [21] with permission of the IOP and L.Valenziano on behalf of the authors and the Planck LFI consortium.

energy within the casing. In fact, especially in the PHI = 0 cut (see Figure 3, right side), microwave power is flowing freely throughout the space in front and around the target. No localization of energy is evident. This provides solid evidence that the return-loss measurements far overstate the performance of these devices when attempting to evaluate emissivity.

4 Discussion

Consequently, the Planck LFI group has not properly measured the emission of their reference loads. "*Indeed, Valenziano et al. [21] do not even provide the estimated emissivity of their targets. By itself, this constitutes an implicit indication that these values cannot be properly determined, with such methods, as I previously stated*" [9].

Faced with Type-3, -4, -5, -6, -7 and -10 errors, the target is unable to absorb the microwave energy from the horn and the latter is able to leak out of the gap into the surrounding space. This occurs even though the horn has edge structure to prevent leakage into the gap as such a configuration neglects the chaotic propagation of microwave energy which can occur within the target. Nonetheless, the Planck team assumes that, in making their return-loss measurements, no leakage into the gap takes place, even though such phenomena is evident in their own calculations (see Figure 3). They further assume that their casing cannot support any standing waves (see Figure 2).

As such, relative to the Planck satellite LFI, the published return-loss values, do not properly represent the emissive power of their reference targets. The latter is much less than expected, both due to gap leaks, as mentioned above, and because return-loss methods overestimate the true emission in the presence of metal casings (Type-7 errors). The presence of the aluminum casings provides ample opportunities to set up standing waves in front of the horn (Type-10 errors). Such waves are present in the traces displayed by the Planck team (see Figure 2 herein and Figure 26 in [21]). This further illustrates that these reference blackbodies are not black. Ultimately, the most serious concern is the presence of a Type-8 error [30]. Conduction has been allowed as the key means of establishing thermodynamic steady state. Subsequently, it can be said that reference blackbodies do not even exist on the Planck satellite.

Given this information, the members of the scientific community, independent of the Planck team, can now either confirm or refute the existence of a monopole at L2. They may do so by concurring with this analysis and establishing the emissivity of the ∼4 K reference loads on the LFI. If the loads truly act as ∼4 K references, then the monopole signal must be present at L2. Conversely, as suggested by this work, if the ∼4 K references are unable to emit properly as ∼4 K blackbodies, then the excellent performance of the LFI implies that there is no monopole at L2 and that this signal does indeed arise from the Earth itself [1].

Unfortunately, it is rather difficult to establish the extent to which a reference target is black in the microwave. However, the following approaches might be considered. At the onset, the measurements must not occur inside an anechoic chamber. Such chambers suppress leaked signals and thereby overstate the emissivity of the target obtained with return-loss measurements. Therefore, such a setting should be avoided. Relative to a small target, like those on the Planck satellite [21], it might be possible to ascertain that they are very poor emitters in the following way. First, a duplicate horn must be placed inside a perfectly reflecting enclosure. The return-loss perfomance in such a case will be poor. This is because virtually all the energy emitted by the horn becomes trapped by the enclosure. This energy would then be able to return to the network analyzer, provided that it is not involved in the formation of standing waves either in the enclosure or within the horn [3].

Once this has been accomplished, the experiment must be repeated, but this time, the target must be placed in front of the horn with a 1.5 mm spacing, as noted by the Planck team. The entire assembly must be once again positioned inside a perfectly reflecting enclosure, wherein the horn and target geometry are preserved. A single drive mechanism must enter the enclosure. As for the target, two cases should be considered: one where a conductive path to the enclosure exists and one where it is suppressed. Once again, the network analyzer would be connected. But this time, any power incident on the target which is not absorbed will be reflected by the walls. Indeed, standing waves will be set up inside either the aluminum casing itself, or the enclosure [3], both of which are acting now as microwave cavities. These standing waves will create oscillations on the network analyzer tracing. By constructing a box whose dimensions can be gradually modified, it should be possible to alter the pattern of standing waves in the cavity. A target will be considered black only when all modifications of the enclosure dimensions, or that of the casings, can yield no changes on the return-loss signal proving that no standing waves exist. Ideally, in this case, the return-loss tracing will display a constant value across the spectral range with no trace of resonance. This can solely occur if all radiation, incident on the target, is absorbed. In this fashion, the blackness of a radiator can be established. Interestingly, this test, so critical to the proper scientific evaluation of the Planck mission, is readily accessible, and at low cost, by most of the electromagnetic laboratories of the world.

However, given our current knowledge of the LFI reference loads [21–27], it is already evident that the Planck targets within this test setting will display strong resonances. Indeed, from the analysis provided above, the references cannot be operating as blackbodies relative to the frequencies of interest. The Planck team has permitted conduction in their system. As a result, the reference targets are envisioned to have constant uniformity of temperature. In fact, this is assured by dumping heat through conduction into the 4 K shield

at all times during flight, in violation of Planck's requirement that conduction not transpire. Max Planck writes: "*For the heat of the body depends only on heat radiation, since, on account of the uniformity in temperature, no conduction of heat takes place*" [31]. To complicate matters, the Planck team ignores the reality that good conductors make poor emitters (see [3] and references therein). This fact has been known for more than 100 years. Yet, the LFI consortium unknowingly has created a situation where they believe that their reference loads can be treated as perfect conductors. They write that: "*the 70 GHz loads are assumed to be perfect thermal conductors, due to their small thickness and mass*" [21]. They have created these "perfect conductors" by enclosing a small amount of absorber within a metallic enclosure. This issue is discussed in greater detail in [30], but nonetheless, the design of the Planck LFI reference targets reflects a sidestep of elementary thermodynamic principles.

In closing, for nearly 50 years, the microwave signal first detected by Penzias and Wilson [2], has fascinated scientists. Yet, all too quickly, its cosmological nature was embraced [6]. In fact, the publication of the interpretation [6] preceded the discovery itself [2]. Now, with the aid of the Planck satellite, the electromagnetics laboratories of the world should be able to confirm or refute the existence of a ∼3 K cosmic signal. The key to this puzzle rests in the understanding of the LFI and reference targets [21–27]. Soon, scientists should reach the definitive answer. In the end, in this age of concern for the global climate, mankind cannot long afford to maintain that a signal of Earthly origin [1] is, in fact, cosmic [6]. Enough evidence is already beginning to build [1, 3, 4, 7–18] indicating that physics, astrophysics, and geophysics stand on the verge of a significant reformulation. In any event, the definitive proof that the monopole of microwave background belongs to the Earth has now been provided.

Acknowledgements

The author would like to thank Luc and Christophe Robitaille for figure preparation and computer assistance, respectively.

Dedication

This work is dedicated to Thomas Kerner Helgeson.

Submitted on February 15, 2010 / Accepted on February 19, 2010
Published online on February 22, 2010

References

1. Robitaille P.-M. A radically different point of view on the CMB. In: *Questions of Modern Cosmology — Galileo's Legacy*, ed. by M. D'Onofrio and C. Burigana, Springer, New York, N.Y., 2009.
2. Penzias A.A. and Wilson R.W. A measurement of excess antenna temperature at 4080 Mc/s. *Astrophys. J.*, 1965, v. 1, 419–421.
3. Robitaille P.M. Kirchhoff's law of thermal emission: 150 years. *Progr. Phys.*, 2009, v. 4, 3–13.
4. Robitaille P.M. A critical analysis of universality and Kirchhoff's law: a return to Stewart's law of thermal emission. *Prog. Phys.*, 2008, v. 3, 30–35; arXiv: 0805.1625.
5. Stewart B. An account of some experiments on radiant heat, involving an extension of Prévost's theory of exchanges. *Trans. Royal Soc. Edinburgh*, 1858, v. 22(1), 1–20 (also found in Harper's Scientific Memoirs, edited by J. S. Ames: *The laws of radiation and absorption: memoirs of Prévost, Stewart, Kirchhoff, and Kirchhoff and Bunsen*, translated and edited by D. B. Brace, American Book Company, New York, 1901, 21–50).
6. Dicke R.H., Peebles P.J.E., Roll P.G., and Wilkinson D.T. Cosmic black-body radiation. *Astrophys. J.*, 1965, v. 1, 414–419.
7. Borissova L. and Rabounski D. PLANCK, the satellite: a new experimental test of General Relativity. *Progr. Phys.*, 2008, v. 2, 3–14.
8. Robitaille P.M. Water, hydrogen bonding, and the microwave background. *Progr. Phys.*, 2009, v. 2, L5–L8.
9. Robitaille P.M. COBE: A radiological analysis. *Progr. Phys.*, 2009, v. 4, 17–42.
10. Robitaille P.M. WMAP: A radiological analysis. *Progr. Phys.*, 2007, v. 1, 3–18.
11. García-García A. Finite-size corrections to the blackbody radiation laws. *Phys. Rev. A*, 2008, v. 78(2), 023806.
12. Verschuur G.L. High Galactic latitude interstellar neutral hydrogen structure and associated (WMAP) high-frequency continuum emission. *Astrophys. J.*, 2009, v. 671, 447–457.
13. Cover K.S. Sky maps without anisotropies in the cosmic microwave background are a better fit to WMAP's uncalibrated time-ordered data than the official sky maps. *Europhys. Lett.*, 2009, v. 87, 69003.
14. Copi C.J., Huterer D., Schwarz D.J. and Starkman G.D. On the large-angle anomalies of the microwave sky. *Mon. Not. R. Astron. Soc.*, 2006, v. 367, 79–102.
15. Schwarz D.J., Starkman G.D., Huterer D. and Copi C.J. Is the low-ℓ microwave background cosmic? *Phys. Rev. Lett.*, 2004, v. 93, 221301.
16. Lieu R., Mittaz J.P.D. and Zhang S.N. The Sunyaev-Zel'dovich effect in a sample of 31 clusters: a comparison between the X-ray predicted and WMAP observed Cosmic Microwave Background temperature decrement. *Astrophys. J.*, 2006, v. 648, 176–199.
17. Jiang B.Z., Lieu R., Zhang S.N. and Wakker B. Significant foreground unrelated non-acoustic anisotropy on the 1 degree scale in Wilkinson Microwave Anisotropy Probe 5-year observations. *Astrophys. J.*, 2010, v. 708, 375–380.
18. Sawangwit U. and Shanks T. Beam profile sensitivity of the WMAP CMB power spectrum. 2009, arXiv:0912.0524.
19. Planck website: http://www.rssd.esa.int/index.php?project=Planck
20. http://twitter.com/Planck/status/2936389049
21. Valenziano L., Cuttaia F., De Rosa A., Terenzi L., Brighenti A., Cazzola G.P., Garbesi A., Mariotti S., Orsi G., Pagan L., Cavaliere F., Biggi M., Lapini R., Panagin E., Battaglia P., Butler R.C., Bersanelli M., D'Arcangelo O., Levin S., Mandolesi N., Mennella A., Morgante G., Morigi G., Sandri M., Simonetto A., Tomasi M., Villa F., Frailis M., Galeotta S., Gregorio A., Leonardi R., Lowe S.R., Maris M., Meinhold P., Mendes L., Stringhetti L., Zonca A. and Zacchei A. Planck-LFI: design and performance of the 4 Kelvin Reference Load Unit. *JINST*, 2009, v. 4, T12006.
22. Cuttaia F., A. Mennella A., Stringhetti L., Maris M., Terenzi L., Tomasi M., Villa F., Bersanelli M., Butler R.C., Cappellini B., Cuevas L.P., D'Arcangelo O., Davis R., Frailis M., Franceschet C., Franceschi E., Gregorio A., Hoyland R., Leonardi R., Lowe S., Mandolesi N., Meinhold P., Mendes L., Roddis N., Sandri M., Valenziano L., Wilkinson A., Zacchei A., Zonca A., Battaglia P., De Nardo S., Grassi S., Lapolla M., Leutenegger P., Miccolis M. and Silvestri R.. Planck-LFI radiometers tuning. *JINST*, 2009, v. 4, T12013.
23. Maino D., Burigana C., Maltoni M., Wandelt D.B., Gorski K.M., Malaspina M., Bersanelli M., Mandolesi N., Banday, A.J., and Hivon E. The Planck-LFI instrument: analysis of the $1/f$ noise and implications for the scanning strategy. *Astrophys. J. Suppl. Series*, 1999, v. 140, 383–391.

24. Sieffert M., Mennella A., Burigana C., Mandolesi N. Bersanelli M., Meinhold P., and Lubin P. $1/f$ noise and other systematic effects in the PLANCK-LFI radiometers. *Astron. Astrophys.*, 2002, v. 391, 1185–1197.

25. Bersanelli M., Aja B., Artal E., Balasini M., Baldan G., Battaglia P., Bernardino T., Bhandari P., Blackhurst E., Boschini L., Bowman R., Burigana C., Butler R.C., Cappellini B., Cavaliere F., Colombo F., Cuttaia F., Davis R., Dupac X., Edgeley J., D'Arcangelo O., De La Fuente L., De Rosa A., Ferrari F., Figini L., Fogliani S., Franceschet C., Franceschi E., Jukkala P., Gaier T., Galtress A., Garavaglia S., Guzzi P., Herreros J.M., Hoyland R., Huges N., Kettle D., Kilpelä V.H., Laaninen M., Lapolla P.M., Lawrence C.R., Lawson D., Leonardi F., Leutenegger P., Levin S., Lilje P.B., Lubin P.M., Maino D., Malaspina M., Mandolesi M., Mari G., Maris M., Martinez-Gonzalez E., Mediavilla A., Meinhold P., Mennella A., Miccolis M., Morgante G., NashA., Nesti R., Pagan L., Paine C., Pascual J.P., Pasian F., Pecora M., Pezzati S., Pospieszalski M., Platania P., Prina M., Rebolo R., Roddis N., Sabatini N., Sandri M., Salmon M.J., Seiffert M., Silvestri R., Simonetto A., Smoot G.F., Sozzi C., Stringhetti L., Terenzi L., Tomasi M., Tuovinen J., Valenziano L., Varis J., Villa F.,Wade L., Wilkinson A., Winder F., and Zacchei A. PLANCK-LFI: instrument design and ground calibration strategy. *Proc. Eur. Microwave Assoc.*, 2005, v. 1, 189–195.

26. Mennella A., Bersanelli M., Seiffert M., Kettle D., Roddis N., Wilkinson A., and Meinhold P. O set balancing in pseudocorrelation radiometers for CMB measurements. *Astro. Astrophys.*, 2003, v. 410, 1089–1100.

27. Robitaille P.M., On the Nature of the Microwave Background at the Lagrange 2 Point. Part I. *Progr. Phys.*, 2007, v. 4, 74-83.

28. Lamarre J.M., Puget J.L., Bouchet F., Ade P.A.R., Benoit A., Bernard J.P., Bock J., De Bernardis P., Charra J., Couchot F., Delabrouille J., Efstathiou G., Giard M., Guyot G., Lange A., Maffei B., Murphy A., Pajot F., Piat M., Ristorcelli I., Santos D., Sudiwala R., Sygnet J.F., Torre J.P., Yurchenko V., Yvon D., The Planck High Frequency Instrument, a third generation CMB experiment, and a full sky submillimeter survey. *New Astronomy Rev.*, 2003, v. 47, 1017–1024.

29. http://herschel.esac.esa.int/Hcal/documents/Lamarre.pdf (accessed January 24th, 2010).

30. Robitaille P.M. Calibration of microwave reference blackbodies and targets for use in satellite observations: An analysis of errors in theoretical outlooks and testing procedures. *Prog. Phys.*, 2010, v. 3, 3–10.

31. Planck M. The theory of heat radiation. Philadelphia, PA., P. Blakiston's Son, 1914, 23.

A Numerical Experiment with the Double Slit Geometry

Riadh H. Al Rabeh
Department of Mechanical Engineering, University of Basra, Iraq
Present address: Lydgate Close, Manningtree, Essex, UK
E-mail: alrabeh_rh@yahoo.com

Young's double slit experiment performed in 1801 was a milestone in the history of physics. The passing of light through two narrow slits creates interference patterns that sums up the diffraction patterns from each slit when separately uncovered. The experiment was later repeated by others using single photons, single electrons, atoms and even molecules producing similar effects. The present interpretation of the results is that photons and all other particles behave like waves and particles at the same time (the wave-particle duality principle). Further explanations were also given, including notions like particles can exist in more than one position at the same time and interfere with itself, and that the classical laws of physics are not applicable in an atomic scale. In this work we perform a numerical experiment in which a single charged particle is fired at a wall of (fixed) charged particles containing gaps to mimic slits, and collect the results over many events in time. Assuming only a classical inverse square relation to hold between the particles- including those of the wall, the results show clear diffraction and interference patterns indicating that the wave behaviour of the bullet particles arises simply from such interactions- hence providing a pure classical interpretation to the problem. That is; particles follow classical laws and produce waves only when interacting with each others. An analytical treatment of this subject is further required to remove the effects of a finite time step inherent in a numerical solution.

1 Introduction

The double slit experiment is considered an important milestone in the history of physics. It was first conducted by Thomas Young in 1801. In Young's experiment, light was made to pass through two narrow slits in an opaque barrier (wall) and collect on a photographic plate behind the barrier. The picture obtained with any one slit open, was that of diffraction in the form of one bright line in the middle of fading alternating dark and bright lines. When two slits are open, the picture changes into an interference pattern that can be explained by the addition of two diffraction patterns from the two slits separately. The double slit experiment was originally performed to settle the argument at the time of whether light- seen to travel along straight lines and reflect like being composed of particles (or corpuscles), and as suggested by Newton, or as waves like Huygens was advocating in his new theory for waves. The interference obtained were taken to favour the wave theory- since the effects of having particles should be producing only positive additions and no annihilation- as the slit experiment seemed to be suggesting [1].

As evidence from experiments in different fields and theoretical work started to accumulate in favour of the particle nature of light, there was a return to the slit experiment to be conducted this time using particles like electrons, neutrons, atoms and molecules [2, 3]. This is to establish if all particles do exhibit a wave-like behaviour as that of the photon particle. The results were again all positive prompting a new explanation to the results, namely that: particles have a dual particle-wave nature. Further tests were subsequently conducted using single photons, electrons and other particles fired one at a time. The interference pattern persisted in all these cases as well- prompting the conclusion that atomic scale particles do not obey the laws of classical mechanics [3–5]. In all these explanations however, the interaction between the barrier particles and those of the bullets are only taken to be of the go no-go relation with no regard to the possibility of some inverse square type forces being involved. Random scatter at the edges of the slits might have also been considered but thought not being capable of producing such consistent wave behaviour. The main thinking instead was concentrated on the interference pattern as being the result of an interaction between the bullet particles alone.

In this article we shall assume that the barrier particles do interact with the bullet particles through a simple inverse square relation. To do this we shoot a charged bullet particle at a wall composed of fixed and similarly or oppositely charged particles (with gaps to mimic the presence of slits). The path of the bullet particle is to be predicted by numerically integrating the equation of motion for a single path at a time and collect the paths over time. An interaction between the barrier particles and the bullet is a must of course, since otherwise there is no meaning to the word slit at all. The type of interaction however, is what is new in the present work. The results seem to show that an inverse square interaction is capable of producing the wave behaviour required to explain the results using pure classical laws and interpretations. A major drawback of the present numerical solution however, is that it is discrete and hence can be affected by the size of the time step. Further analytical treatment of the subject (in the

light of the present results) will be needed before a concrete conclusion can be made on this matter. Such work is not expected to contradict the vivid wave and interference patterns observed in the numerical results.

To be able to cover two slits and to produce different wave patterns, the axial velocity of the bullet was changed in a systemic manner in the experiment and the vertical (transverse) component of the bullet velocity was changed randomly by a very small amount around zero. This allows the accumulating beam to cover both slits over time.

2 Theory

For Coulomb forces, the expression for the acceleration is given by;

$$a = \frac{d^2r}{dt^2} = \frac{k}{r^2}\,, \tag{1}$$

where $a = a(t)$, $r = r(t)$ are the acceleration and separation distances between any isolated pair of particles as a function of time t, and k is the coupling constant (negative for attractive, and positive for repulsive forces) and in which the masses and charges of all particles are unity. The magnitude of k is dependent on the type of interaction. For example, in the case of a repulsive Coulomb forces $k = 1/4\pi\varepsilon_0$, where ε_0 is the permittivity of empty space. In the case the number of interacting particles is small; the Coulomb forces by far dominate other forces as assumed here. As the interacting masses are points, there is no need to consider angular velocity, spin, angular momentum or any form of moments of forces on the particle. For a group of interacting particles, the net acceleration of particle j is given by;

$$\mathbf{a}_j = \frac{d\mathbf{v}_j}{dt} = \sum_i \frac{k_{ij}\mathbf{r}_{ij}}{r_{ij}^3}\,;\;\; r_{ij} = |\mathbf{r}_{ij}|,\;\; i, j = 1, 2, \cdots N\,, \tag{2}$$

where $\mathbf{a}_j$ is the resultant acceleration, $\mathbf{v}$ is velocity, k_{ij} is the total coupling constant between particles i and j, and $\mathbf{r}_{ij} = \mathbf{r}_j - \mathbf{r}_i$ is the vector from i to j positions and N is the total number of particles. Equation (2) is a set of simultaneous ode's that must be integrated once in order to find $\mathbf{v}_j(t)$ and again to find the position $\mathbf{r}_j(t)$ giving;

$$\mathbf{r}_j = \mathbf{r}_{j0} + (dt)\mathbf{v}_{j0} + (dt)^2 \sum_i \frac{\mathbf{r}_j - \mathbf{r}_i}{|\mathbf{r}_j - \mathbf{r}_i|^3}\,;\;\; j = 1 : N;\;\; i \neq j. \tag{3}$$

If we know the initial position $\mathbf{r}_{j0}$, the initial velocity $\mathbf{v}_{j0}$, and the time step dt, we can find the new position of the bullet $\mathbf{r}_j$. This is to be repeated for different initial velocities and the resulting trajectories are collected over time and plotted. The values chosen for the various parameters do not necessarily correspond to particular physical values, but rather chosen to accentuate the resulting picture and make it clearer. The actual values used are given. A simple one step method is chosen for the integration as in equation (3) to avoid any erroneous contributions from any extra terms contained in a more refined integration procedure.

If we hope to produce results showing a wave behaviour using only inverse square relations, we should be able to show that this is possible in theory. In fact [6] states that the potential equation of motion becomes a spring like relation in the case of small displacements together with a large number of interacting particles. In the present case, we assume the wall particles are fixed in space, which is equivalent to a presence of a large number of particles in a small space making the group massive and well connected to resist the effects of the bullet particle approaching the barrier. We further confirm this in Fig. 1, where a spring type relation results from fixing two particles and allowing a third to experience a small displacement in the middle under an inverse square force. The algorithm needed to implement equation (3) is fairly straight forward as shown below;

```
Algorithm to compute the trajectory of a charged
particle fired at a wall containing slits and composed
of similarly (or oppositely) charged fixed particles.
Total number of particles nb=10 at position r(x,y),
velocity (vx,vy), acc.  (ax,ay)
and force (fx,fy)=acc.
For a fixed wall, x,y are calculated only
for the 1st particle.

ee=1e-100;X=[];Y=[];dt0=.01; v01=3.2; nb=12;
nbv=1:nb;x(nbv)=0;x=x';y=x;vx=x;
vy=x;kb(1:nb)=2e-3;kb(5:9)=0;
for ii=1:250;
y(1)=0; vy(1)=0.08*(rand-0.5); x(1)=-1;
vx(1)=v01;x(2:nb)=-0.25;
y(2:end)=0.002*((2:nb)-nb/2 -1);
for kk=1:100; for jj=1:nb; xj=x(jj); yj=y(jj);
vxj=vx(jj);vyj=vy(jj); xb=xj-x;yb=yj-y;
rb2=ee+xb.^ 2+yb.^ 2; rb=sqrt(rb2);
fb=kb'./rb2; fxb=fb.*xb./rb; fyb=fb.*yb./rb;
fx=sum(fxb);fy=sum(fyb);
ax=fx;ay=fy; dt=dt0;
if jj > 1;dt=0;end;
vxj=vxj+dt*ax; vyj=vyj+dt*ay; xj=xj+dt*vxj;
yj=yj+dt*vyj;x(jj)=xj; y(jj)=yj;
vx(jj)=vxj; vy(jj)=vyj;
end;
if abs(x(1)) > 1.5 | abs(y(1)) > 1;break;end;
X=[ X;x'];Y=[Y;y'];end;end;
figure(1);plot(X,Y);
```

The inner loop jj adds the forces over all the particles, then we advance in time in the kk loop to give one path (trajectory). The ii loop repeats this many times to arrive at the final picture. The rest of the algorithm is self explanatory.

3 Results

The values of the coupling constant k, (units m^3/s^2 as in (1)), the horizontal and vertical velocity components, the distances between slits and between the particles making the wall, the time step and other constants are clearly referenced in the al-

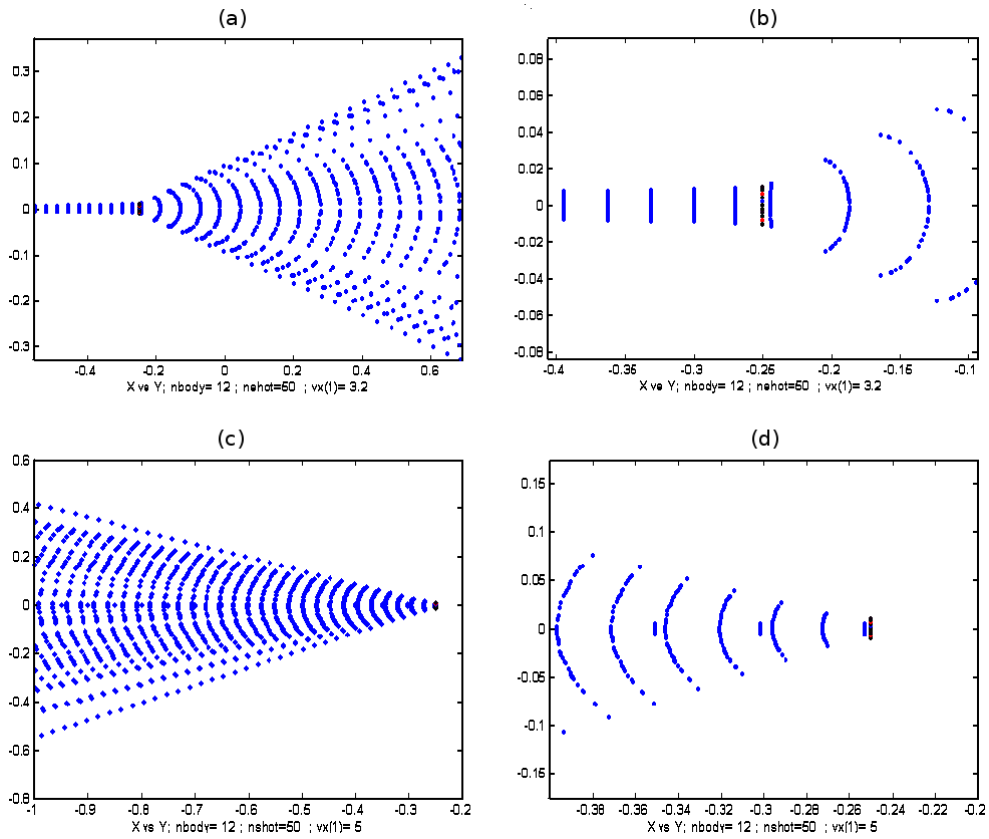

Fig. 2: Time collection of an electron fired (from left) against a fixed column barrier of loose electrons with a random small vel. component in the vertical direction. Total of 50 events are collected. Wave–front plane in (a), (b) changing to circular after the barrier. At another speed, the wave-front is completely reflected (b), (c) and also changed to circular.

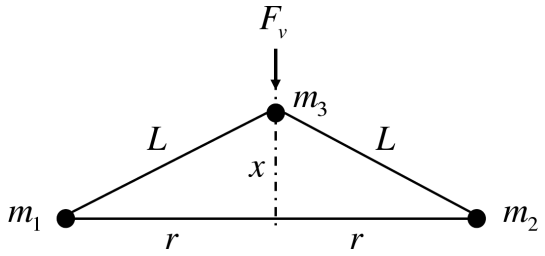

Fig. 1: A spring like force relation capable of producing a wave behavior can result from the interaction of particles under an inverse square relation. $F_{31} = F_{32} = k/r^2$; for small deflection x; $L = r$. $F_v = 2\frac{k}{r^2}\frac{x}{r} = 2\frac{k}{r^3}x = Kx$; k, r, K are constants. Therefore, force on m_3 is a spring type force.

gorithm given above. It is again stressed that the different constants are chosen so as to produce a clear picture rather than correspond to certain physical values. The main goal of this article is to show the wave phenomenon of diffraction and interference happening in a purely inverse square environment and with bullet particles that do not know of each other and hence never have a chance to interact as they exist in different times.

Fig. 2(a) shows a plot collecting 50 events and showing that what was originally a plane wave-front (elements of the front exist at different times) have been changed by the barrier to a circular wave-front as one would expect of a true wave. A magnified scale of the same is shown in the next figure. In Figs. 2(c),(d) the wave front is reflected completely as what could happen with real waves when the wavelength compared to the sparseness of the particle of the wall is of the correct order. In Fig. 3(a) few of the wall particles are assumed to be inert to mimic the presence of a slits. The result as expected is a superposition of two circular waves producing an interference pattern. It is seen that a single bullet collected over time is behaving like a true beam composed of many particles. The presence of the one barrier in all the shooting events is what unifies all the outputs and creates the observed effects.

4 Conclusions

The results shown indicate clearly that the passage of a bullet particle through a slit modifies its path and the wave-front composed of many particles, which need not exist at the same time, can change from plane to circular if the force between the barrier and the bullet particles is that of an inverse square type. In [6] and in Fig. 1 in this article, it is shown how a change from an inverse square to a spring relation can result

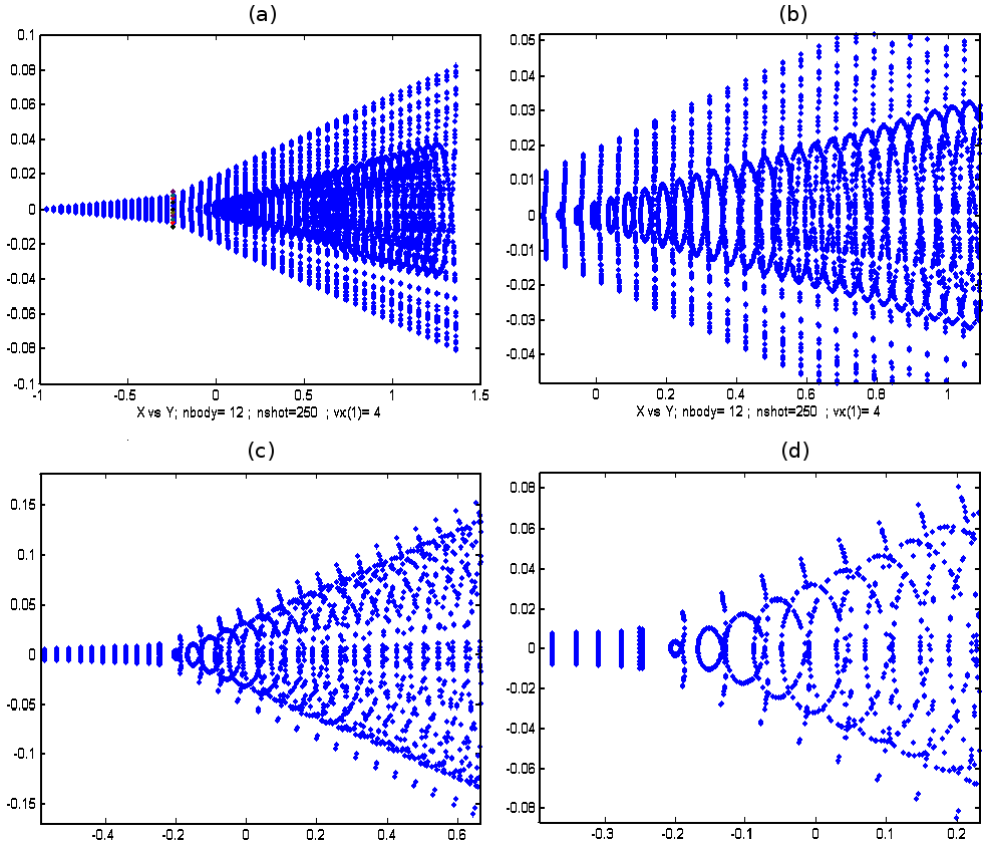

Fig. 3: Wall particles 5:9 (out of 11) are made neutral to mimic a slit. This causes two diffraction patterns interfering with each other. The last two (c), (d), are plotted using the algorithm given in this article with bullet horizontal speed $v_x = 3.2$.

in the case of large interacting particles as those of the barrier (and mimicked here by having fixed particles). This picture is equivalent to what happens in field theory in which a potential equation (resulting from inverse square relation) acquires wave solutions due to the presence of a boundary. This effect occurs in the case of waves in fluids and solids which are composed essentially of particles interacting under an inverse square environment.

The present results upholds the fact that particles behave like waves and particles, but differs in giving a more natural explanation that agrees with common logic and classical laws. It is difficult to believe at the end that classical laws that apply to planets composed of trillions of particles fail when considering few of them. The particle picture is simple to comprehend and can also afford to explain many of the relativistic and quantum findings in physics (see [7, 8] by this author for more on this).

For deeper understanding of the present results, it is useful to do a complementary theoretical analysis to overcome the finite time step effects inherent in any numerical solution. Further understanding of the problem may be achieved by using more elaborate particles where spin and moments are to be taken into consideration.

Submitted on February 09, 2010 / Accepted on February 16, 2010

References

1. Feynman, Richard P. The Feynman lectures on physics. *Addison-Wesley*, 1965, v. 3.
2. Jönsson C. Electron diffraction at multiple slits. *American Journal of Physics*, 1974, v. 4.
3. Nairz O., Arndt M., and Zeilinger A. Quantum interference experiments with large molecules. *American Journal of Physics*, 2003, v. 71.
4. Summhammer J., Rauch H., Tuppinger D. *Phys. Rev. A*, 1987, v. 36.
5. Greene B. The fabric of the cosmos: space, time, and the texture of reality. Vintage, 2000.
6. Landau L. D., Lifshitz E. M. Mechanics. Pergamon press, 1960.
7. Al Rabeh R. H. Primes, geometry and condensed matter. *Progress in Physics*, 2009, v. 3.
8. Al Rabeh R. H. New ideas for the extra dimensions and for deriving the basic laws of physics. *Progress in Physics*, 2010, v. 1.

Some Unsolved Problems, Questions, and Applications of the Brightsen Nucleon Cluster Model

Florentin Smarandache

Department of Mathematics, University of New Mexico, Gallup, NM 87301, USA. E-mail: smarand@unm.edu

Brightsen Model is opposite to the Standard Model, and it was build on John Weeler's Resonating Group Structure Model and on Linus Pauling's Close-Packed Spheron Model. Among Brightsen Model's predictions and applications we cite the fact that it derives the average number of prompt neutrons per fission event, it provides a theoretical way for understanding the low temperature / low energy reactions and for approaching the artificially induced fission, it predicts that forces within nucleon clusters are stronger than forces between such clusters within isotopes; it predicts the unmatter entities inside nuclei that result from stable and neutral union of matter and antimatter, and so on. But these predictions have to be tested in the future at the new CERN laboratory.

According to the Brightsen Nucleon Cluster Model [1] all nuclides of beta stable isotopes can be described by three fundamental nucleon clusters (NPN, PNP, NP), with halo clusters (NN, PP, NNN) now experimentally observed. The Brightsen model builds on the early cluster models of the Resonating Group Structure of John Wheeler [2] and the Linus Pauling Close-Packed Spheron Model [3], which predict mathematically that the wave function of a composite nucleus can be viewed quantum mechanically as a combination of partial wave functions that correspond to the multiple ways nucleons (protons, neutrons) can be distributed into close-packed clusters, thus rejecting the standard model Hartree-Fock formalism of average field interactions between independent nucleons in nuclear shells. Presented in this section are a number of unsolved problems, questions, and future experimental pathways based on the Brightsen Nucleon Cluster Model formalism–many additional applications can be gleamed from careful study of the literature cited in the references provided:

1. The Brightsen Model derives the average number of prompt neutrons per fission event for many radioactive isotopes of human importance (U-235, U-233, Pu-239, Pu-241) as well as emission of light charged particles, suggesting that all modes of fission derive from a four step process [4]. Further study of these claims are warranted given the importance of understanding the fission of radioactive isotopes for energy production.

2. The Brightsen Model provides a theoretical pathway for experimentalists to understand the numerous laboratory results of low temperature transformation/low energy reactions, such as the well studied ^{104}Pd (p, alpha) ^{101}Rh reaction [5]. Application of the Brightsen Model to low energy fusion reactions as a possible result of interactions between nucleon clusters is of fundamental importance to human energy demands.

3. The Brightsen Model predicts the existence of "unmatter entities" inside nuclei [6], which result from stable and neutral union of matter and antimatter nucleon clusters. As a result, the Brightsen Model predicts that antimatter has corresponding antigravity effects [7]. This prediction can be tested in the future at CERN beginning 2008 using antihydrogen. Once accurate measurements can be made of the gravitational acceleration of antihydrogen, and the results compared with matter hydrogen, if the two forms have opposite acceleration, then a major prediction of the Brightsen Model will be confirmed (e.g., that antimatter has both anti-gravity effect and anti-mass). If experimentally confirmed, then predictive equations will need to be developed using the Brightsen Model formalism of union of matter and antimatter clusters (e.g., the unsolved mathematical formation of unmatter entities inside nuclei). The importance of this aspect of the Brightsen Model links to the current problem in physics of the missing matter of the universe and possible unification of gravity at relativistic (macroscopic) and quantum (microscopic) states.

4. The Brightsen Model offers a theoretical approach for artificially induced fission of dangerous radioactive nuclei to produce relatively stable elements [5]. In theory, if externally produced electromagnetic radiation can be caused to resonate with the exact magnetic moment of a specific sub-nuclear nucleon cluster (e.g., NPN, PNP, NP nucleon clusters), than an individual nucleon cluster can in theory be excited to a energy such that it is expelled from the nucleus, resulting in transmutation of the parent isotope via fission and/or beta or alpha decay to less radioactive daughter structures. The applications of this process for nuclear energy production are clear and worthy of experimental test.

5. The Brightsen Model predicts that one sub-cluster isodyne [5] of the very stable Helium-4 isotope consists of two weakly stable deuteron [NP] clusters, each with their own distinct energy level, spin, magnetic moment, etc. Experimental tests are needed to confirm this fundamental model prediction. If confirmed, new physics mathematical description of shell structure of isotopes would follow.

6. The Brightsen Model predicts that forces "within" nucleon clusters (NPN,PNP,NP) are stronger that forces "between" such clusters within isotopes, a result of different combinations of the spin doublet and triplet clusters. It is predicted that research here would result in new measurable macroscopic properties of atomic nuclei including new fundamental force interactions.

7. The Brightsen Model predicts that the next "magic number" will be found at $N = 172$, $Z = 106$, $A = 278$ (Seaborgium-278). Experimental confirmation of this prediction would require a revised explanation of magic numbers in isotopes based on nucleon clusters as the fundamental building blocks of shell structure in atomic nuclei, as opposed to independent nucleons in an average field.

8. The Brightsen Model predicts that the large cross section of Boron-10 (as opposed to the small cross section of Boron-11) results from the presence of a stable and independent nucleon cluster structure [PNP], which coexists with two [NP] and one [NPN] clusters that maintain very small cross sections. Thus the vast majority of the cross section dynamics of Boron-10 is predicted by the Brightsen Model to derive from a strongly interacting [PNP] cluster. This four cluster formalism for Boron-10 (e.g., 1PNP, 2NP, 1NPN) also correctly derives the $I = 3$ spin experimentally observed.

Submitted on February 18, 2010 / Accepted on February 22, 2010

References

1. Brightsen R. A. Nucleon cluster structures in beta-stable nuclides. *Infinite Energy*, 1995, v. 1, no. 4, 55.
2. Wheeler J. A. On the mathematical description of light nuclei by the method of resonating group structure. *Physical Review*, 1937, v. 52, 1107.
3. Pauling L. The close-packed spheron theory and nuclear fission. *Science*, 1965, v. 150, no. 3694, 297.
4. Brightsen R. A. The nucleon cluster model and thermal neutron fission. *Infinite Energy*, 2000, v. 6, no. 31, 55.
5. Bass R. A. Experimental evidence favoring Brightsen's nucleon cluster model. *Infinite Energy*, 1996, v. 2, no. 11, 78.
6. Smarandache F., Rabounski D. Unmatter entities inside nuclei, predicted by the Brightsen nucleon cluster model. *Progress in Physics*, 2006, v. 1, 14.
7. Nelson W. D. New astronomical data finds support in the nucleon cluster model. *Journal of New Energy*, 1998. v. 3. no. 1, 1.

Cosmophysical Factors in the Fluctuation Amplitude Spectrum of Brownian Motion

Alexander V. Kaminsky* and Simon E. Shnoll†

*Elfi-tech Ltd., Rekhovot, Israel
†Department of Physics, Moscow State University, Moscow 119992, Russia
†Inst. of Theor. and Experim. Biophysics, Russian Acad. of Sci., Pushchino, Moscow Region, 142290, Russia
†Puschino State University, Prospect Nauki 3, Pushchino, Moscow Region, 142290, Russia
E-mail: shnoll@mail.ru

Phenomenon of the regular variability of the fine structure of the fluctuation in the amplitude distributions (shapes of related histograms) for the case of Brownian motion was investigated. We took an advantage of the dynamic light scattering method (DLS) to get a stochastically fluctuated signal determined by Brownian motion. Shape of the histograms is most likely to vary, synchronous, in two proximally located independent cells containing Brownian particles. The synchronism persists in the cells distant at 2 m from each other, and positioned meridionally. With a parallel-wise positioning of the cells, high probability of the synchronous variation in the shape of the histograms by local time has been observed. This result meets the previous conclusion about the dependency of histogram shapes ("fluctuation amplitudes" of the spectra of stochastic processes) upon rotation of the Earth.

1 Introduction

The works surveyed in [1–3] revealed a determinate variation in the spectra of the fluctuation amplitudes (these are the shapes of the related histograms in the characteristics of the various processes under measurement, ranging from the rates of chemical and biochemical reactions to the noises in gravity-gradient antennae and semiconductor circuits, and to radioactive decay). This paper represents data of a similar study of the process of Brownian motion.

2 Subject, materials, and methods

In 2006, we studied variations in the shapes of the histograms obtained from measurements of the fluctuations of the velocity of Brownian motion in an aqueous suspension of ZnO (average particle size: 5 μm). We obtained proofs of the synchronous variations in the histograms plotted according to the measurement data in independent "generators", placed on a lab bench.

In 2009, the same experiments were retried using 450-nm polystyrene microspheres (manufactured by Polysciences Inc.) with applying an improved measurement technique. The known method of dynamic light scattering (DLS) [4] was applied to measure the fluctuations of the velocity of Brownian motion. The method is based on the measurement of the fluctuations in coherent light scattering across an ensemble of the moving particles. In practice, a collimated laser beam was passed through a glass cell containing suspension of Brownian particles.

Electromagnetic waves, diffracted on the suspended particles, give a rise to a stochastically fluctuating intensity at the detector plane and corresponding photocurrent

$$i(t) \sim \langle E(t)\, E(t)\rangle.$$

Here, the angle parentheses denote the average of the rapid optical oscillations. A schematic diagram of the experimental installation is shown in Fig. 1.

We took an advantage of the "backscatter" geometry and a multiple scattering mode in our installation. Two identical optical cells (we refer to these as *Brownian signal generators*) were used. Each cell consisted of a 1-mm-spacing glass cell filled with a suspension, and an optoelectronic unit comprising a laser diode, a photodiode, and a preamplifier. Photo currents $i_1(t)$ and $i_2(t)$ of the detector were converted into voltage by trans-impedance amplifiers, whose conversion factor is $r = 10$ MOhm, then were saved on a PC hard disk following digitization in a 42 KHz 12-digit two-channel analog-to-digital converter. The detectors were differential pin photodiodes by Hamamatsu Co. Ltd. The lasers were single-mode VCSEL structures (wavelength: $\lambda = 850$ nm; emission bandwidth: ~100 MHz; radiant energy: 1 mW) manufactured by RayCan. Special steps were taken to exclude potential synchronous interference: the sensors were placed on a vibroisolated table; both lasers and the power supply circuits of the amplifiers were separated and duly filtered. A high-pass filter with cutoff frequency below 30 Hz was used in the amplification path to minimize vibration-related synchronous interference.

Fig. 2 shows a segment of photocurrent time series $i_1(t)$ in one of the Brownian generators. The signal's shape is typical of persistent signals.

The above autocorrelation function of the signal, for moderately large numerical values of τ, is described by an exponent $C(\tau) = \exp(-q^2 D\tau)$ with die-away time determined by the geometry of the scattering and diffusion coefficient $D = kT/3\pi\eta d$ (Stokes-Einstein formula), where k is Boltzmann's constant, T is temperature, η is viscosity, and d is the

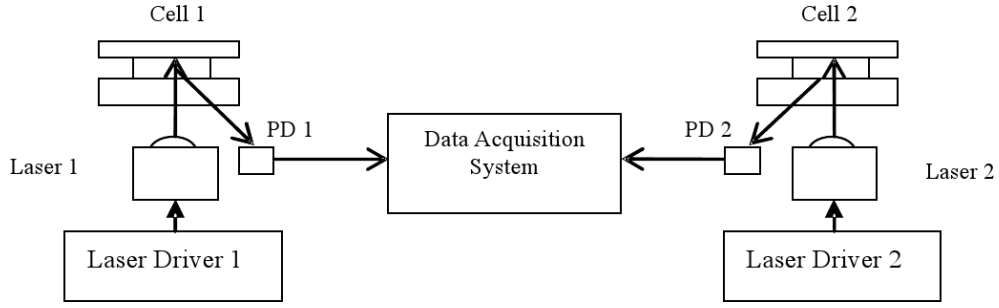

Fig. 1: A schematic diagram of the experimental installation.

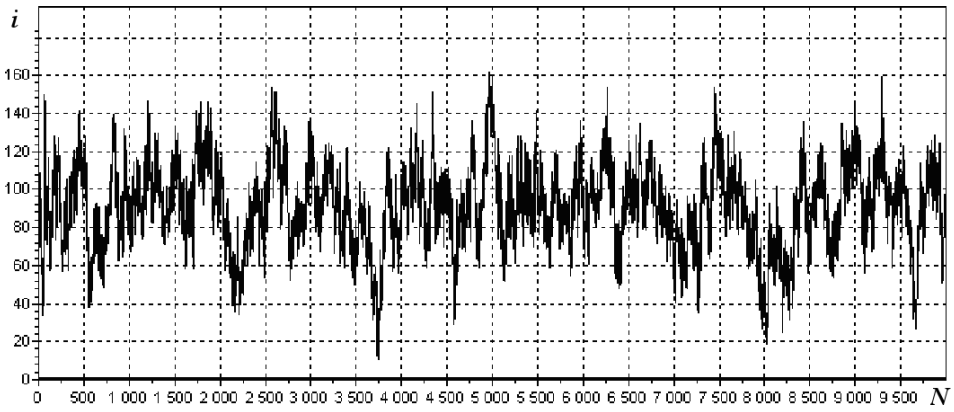

Fig. 2: A segment of time series: a result of DLS signal measurements taken from 1 "generator": 10,000 measurements of $1/8,000 = 1.2 \times 10^{-4}$ duration each.

particle's diameter. The numerical value of q determines the momentum transfer of a photon in scattering on the Brownian particles. The power spectrum is of Lorentzian-like shape is $S(\varpi) \sim \varpi_0/(\varpi_0^2 + \varpi^2)$, where $\varpi_0 = 1/T_0$ is the relaxation frequency. With $\varpi \gg \varpi_0$, the spectrum is approximated by a power-law dependence. Similarly, in the time-domain representation, the correlation function may be approximated by the power-law dependence in the area of $\tau \ll T_0$.

In our case, the DLS signal is described by a fractional Brownian motion model [5]. The signal is self-similar at the high-frequency range of >100 Hz, and an asymptotic behavior of the correlation function under $\tau' = q^2 D\tau \to 0$ is of the power-law nature: $C(\tau) = 1 - |\tau'|^\alpha$. Here α is a scaling parameter related to the fractal dimension $D = 2 - \frac{1}{2}\alpha$. At low frequencies we have $\tau \to \infty$ and $C(\tau) = |\tau'|^{-\beta}$, where β is the scaling parameter related to the Hurst coefficient: $\beta = 2 - 2H$.

The following characteristics of the time series were obtained for the DLS signal of the Brownian generators. They are: $\alpha \approx 0.7$, $D \approx 1.65$, $H = 0.82 \pm 0.1$.

Fig. 3a shows the autocorrelation function of a signal for one of the channels: $g_{11} = \langle i_1(t)\, i_1(t+\tau)\rangle$, while Fig. 3b shows the cross-correlation function between the channels: $g_{12} = \langle i_1(t)\, i_2(t+\tau)\rangle$.

As seen in 3b, there is no significant physical link between the channels. This might lead to a correlation moment different from 0. Insignificant near-zero-line fluctuations of the cross-correlation function g_{12} tend to 0 under bigger statistics figures.

3 Histogram plotting and shape examination

Amplitude distribution of the histograms were plotted using 30 or 60-measurement series segments. For better convenience of visual comparing, the said histograms were made smooth by the moving summation technique. All the procedures of histogram plotting, smoothing, and scaling were carried out using *Histogram Manager* software developed by Edwin Pozharsky (see [1] for detail).

We consider the histograms to be similar if visual similarity of their shapes can be attained by applying admissible expansion and mirror reflection operations. In other words, the "hystogram shape" can be articulated as an invariant of a subgroup of affine transformations in a plane involving operations of scaling, parallel translation, and X-axis reflection.

The histogram plotting and shape examination methods are given with requisite particularization used in the studies published in [1].

Fig. 4 shows a chunk of a computer archives: a sequence of the histograms based on the data obtained from the measurements produced in two independent Brownian generators. The histograms were plotted according to the data of

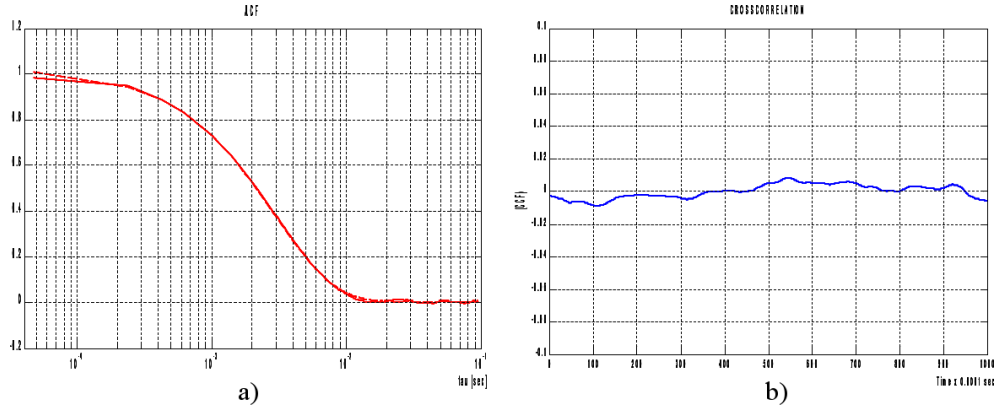

a) b)

Fig. 3: Autocorrelation (a) and cross-correlation (b) functions for the signals of two "Brownian generators" in our experiment.

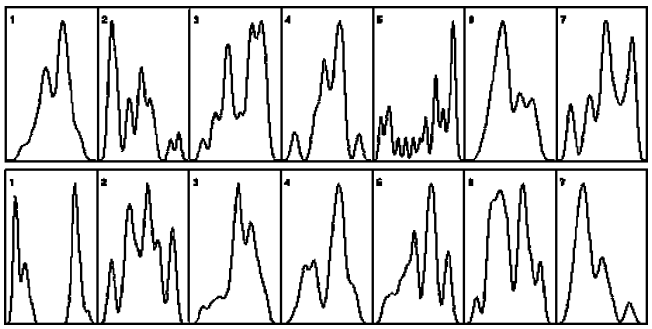

Fig. 4: A chunk of a computer archives: a sequence of the histograms based on the data obtained from the measurements produced in two independent Brownian generators. X-axis in each histogram represents values (in relative units) of the photocurrent in the mesurement of Brownian motion. Y-axis gives the number of similar pairs which correspond to the specific values of the photocurrent. The histograms are given after a 17-fold moving-summation smoothing.

30 measurements, and given a 17-fold smoothing. The upper and lower rows show No. 1 and No. 2 generator's histograms, correspondingly. Numbers of the sequential histograms are shown. The total of the sequential histograms amounted to several thousands.

4 Synchronous variation of the shape of the histograms in the measurements of Brownian motion on the independent "generators" in the same location

Fig. 5 shows a chunk of computer archives representing the pairs of *synchronous* histograms plotted on the basis of the data obtained by independent measurements in two installations found to be similar by experts. Numbers of the histograms in the time series are given. As seen in Fig. 5, the synchronous histograms turn out to be similar in shape.

In plotting a distribution of the number of similar pairs of the histograms, according to the values of the related separating intervals, a particularly large number of the similar pairs corresponds to some intervals. This is in exact a core evidence of a non-random nature of the similarity of the histograms in independent processes.

Nos. of synchronous histograms in two arrays	N_1 (array 1)	$P_1 = \frac{N_1}{720}$	N_2 (array 2)	$P_2 = \frac{N_2}{720}$
8	6	0.008	5	0.007
59	1	0.001	3	0.004
232	4	0.006	6	0.008
294	17	0.024	7	0.010
457	2	0.003	13	0.018
		3×10^{-12}		4×10^{-11}

Table 1: Occurrence frequency of the histograms of the shape under measurements produced in two independent Brownian generators during 24.09.2009 experiment (Fig. 8).

Fig. 6 shows a distribution of the number of similar pairs of the histograms plotted according to the data obtained by the measurements of Brownian motion in two independent generators.

As seen in Fig. 6, the number of the synchronous pairs is definitely above the "background". The height of the central log is equal to 89 pairs with 720 histograms in the rows, that is about 12% of the maximumally possible height. In the other intervals, the height of the logs is about 2.5% of the maximumally possible height. Making the use of majorizing estimation by $\sqrt{N}$ criterion is enough to evaluate the reliability of the inference on the synchronous variation of the histogram shape in independent Brownian generators. The figure shows that the central crest's height differs from the "background" by around 6 $\sqrt{N}$ which corresponds to a 10^{-11} probability for obtaining such a result at random.

It should be noted that according to Fig. 5 the histograms, forming the central log in Fig. 6 and evidencing the synchronous nature of the shape variation of the histograms in independent processes, do not have an apparent difference from the histograms that would correspond to other intervals. In other words, there is no definite shape specifically corresponding to the synchronous variation of the histogram shape.

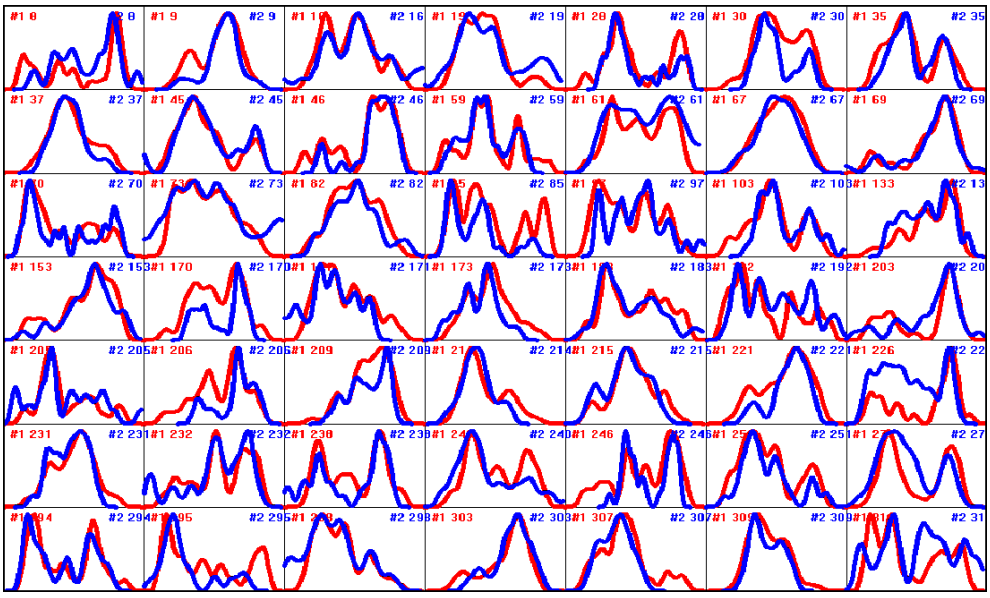

Fig. 5: A log piece: pairs of the histograms plotted on the basis of the data obtained by independent synchronous measurements in two independent Brownian generators found to be similar by an expert evaluation. Numbers of the histograms in the time series are given. Coordinate axes are the same as in Fig. 4.

However, a relatively small number of rare, "exotic" shapes can be found among the histograms that correspond to the central log. The pairs of such histograms can be used for an additional evaluation of the reliability of the core inferences.

At this point, we assume that realization of a complex-shaped histogram is per se an unlikely event to occur. A simultaneous occurrence of rare events in independent measurements is even a less probable event to happen. This evaluation has proven to be very strong. Illustration to this evaluation is given in Fig. 7 and Table 1. Fig. 7 shows 5 pairs of rare-shape histograms obtained synchronously during the 24.09.2009 experiment (there was 89 similar synchronous pairs, all-in-all). We can see, for example, that out of these 720 possible histograms, there was 6 No. 8 histograms in row 1 of the first array, and 5 ones in row 2, thus constituting 0.008 and 0.007 fractions out of the maximal values, respectively.

These fractions do come as an evaluation of the probability of a random occurrence of the given-shape histograms at this particular spot. The general probability of the uncertainty of the inference on a synchronous occurence of similarly-shaped histograms in two independent rows of measurement is equal to the product of these special-case probabilities. For example, given the 5 rare-shape histograms, this general probability constitutes $P_1 = 3{\times}10^{-12}$ for the first array, and $P_2 = 4{\times}10^{-11}$ for the second one, i.e., vanishing small values. It should be noted, however, that the number of the synchronous pairs of the rare-shape histograms is considerably large. Thus, the reliability of the inference on the synchronous occurrence of the similarly-shaped histograms in the independent Brownian generators is proven by these two types of evaluation.

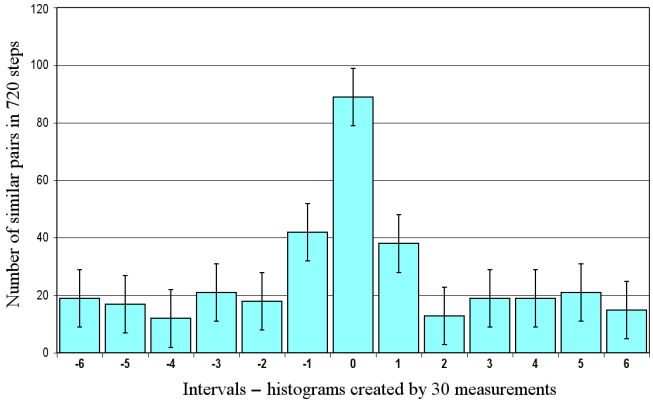

Fig. 6: Shapes of the histograms in the independent Brownian generators vary synchronously. Similar pairs of the histograms are distributed according to the values of the respective separating intervals of time. Date of the experiment: 24.09.2009. Each histogram is plotted according to the data of 30 measurements. X-axis shows values of the time intervals separating similar histograms. One interval is equal to 3.6×10^{-3} seconds.

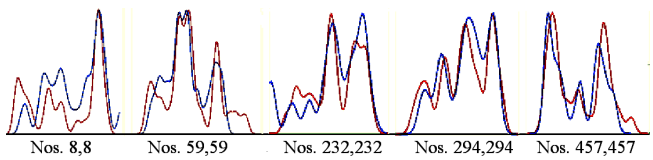

Fig. 7: Examples of the similarity in the rare-shape synchronous histograms according to the occurrence frequency shown in Table 1.

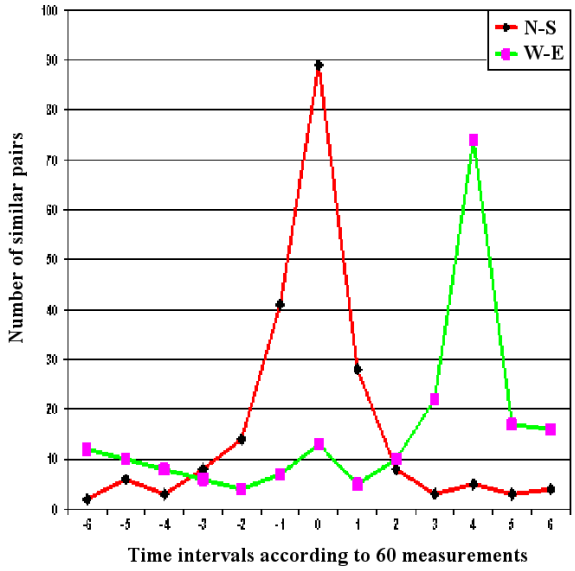

Fig. 8: Interval distribution of the number of similar pairs of the histograms plotted according to the results of 60 measurements produced in two independent Brownian generators which were distant at 200 cm from each other. A) Meridian (from North to South) positioning of the generators; B) Parallel-wise positioning of the generators. In the meridian positioning, the similar histograms occur in the two generators simultaneously. In the parallel-wise positioning, similar histograms of West generator occur 4 interval (11.6 msec) later than they do in the East one.

5 Synchronism in different locations

Similarity of the shape of the histograms obtained during independent measurements taken in *different locations at the same local time* comes as an evidence of the dependency of the histogram shape upon rotation of the Earth. Earlier we obtained this evidence by conducting experiments measuring radioactivity at an extremely near distance between the laboratories: at Pustchino (54°N, 37°E) and in Antarctic (Novolazarevskaya Station, 70°S, 11.5°E), so the distance is about 14,000 km. In the works [6–9], when measuring the noise in semiconductor circuits, a "local time effect" was obtained at a distance of about 1 meter. We carried out similar measurements using the "Brownian generators".

Figs. 8 and 9 show results of the experiments conducted at the town of Rekhovot, Israel (31.89°N, 34.80°E) on October 11, 2009. Two Brownian generators were distant as $\Delta L = 2$ meters from each other, and were first oriented by the Meridian, then by the Parallel. The signals were recorded for 4 minutes. Local time delay for the said latitude with the basic East-West orientation constitutes $\Delta T = \Delta L/V$ sec, where $V \approx 2\pi 6378000 \cos(31.89\pi/180)/86400$ m/sec is the speed of the present point of the Earth's surface bearing the above specified coordinates. With sampling frequency of 42 KHz, this delay value corresponds to 3.6 histograms plotted by 60 points, and to 7.1 histograms plotted by 30 points. As seen in the drawings below, the time intervals, where the maximal

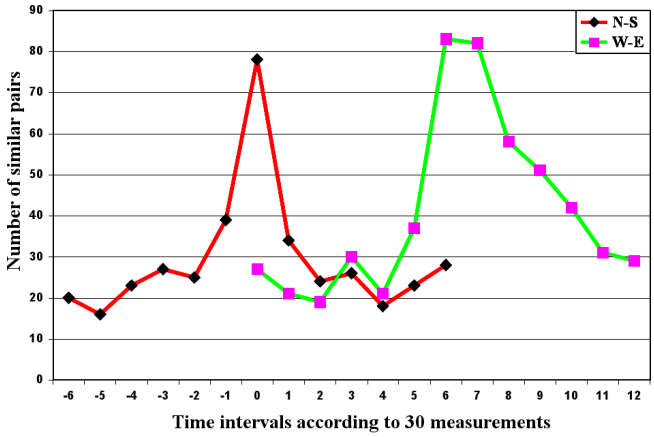

Fig. 9: Interval distribution of the number of similar pairs of the histograms plotted according to the results of 30 measurements produced in two independent Brownian generators at a distance of 200 cm from each other. The local-time synchronism has a more distinct manifestation under the 30-result plotting. In the meridian positioning of the independent generators, similar histograms occur simultaneously. In the parallel-wise positioning, similar histograms of West generator occur in West generator 7–8 intervals later than they do in the East one.

number of the similarly-shaped histograms is found, are close to the estimated values.

6 Discussion

Our study of Brownian motion by means of the dynamic light scattering method showed that the fine structure of the distribution of intensity fluctuations of the light, scattered by Brownian particles (shapes of the corresponding histograms) varies synchronously by local time. In other words, Brownian motion is specific for the same regularities as those found previously during examination of stochastic processes of a different nature, namely — those of chemical reactions, thermal fluctuation in resistors, radioactive decay etc. Thus, the similar regularities in the processes, where the energy changing range varies by many orders, show up the same space-time being the only thing in common. Proceeding from this fact, a conclusion was made according to which the observed regularities were explained by the space-time fluctuations determined by the motion of the Earth in a surrounding inhomogeneous gravitational field [1–3].

Acknowledgements

We are grateful to Prof. P. S. Lande for her valuable discussion and interpretation of the results. Our thanks also come to Head of the Chair of Biophysics of Department of Physics of the Moscow State University Prof. V. A. Tverdislov, and to the workers of the Laboratory of Physical Biochemistry of Institute of Theoretical and Experimental Biophysics of the Russian Academy of Science (Prof. D. P. Kharakoz) for their very valuable discussion. We are tremendously grateful to

Ms. Anna A. Andreyeva for her mission as the second independent expert who compared the histograms in this study.

Submitted on January 21, 2010 / Accepted on February 04, 2010

References

1. Shnoll S. E. Cosmic physical factors in random processes. Svenska fysikarkivet, Stockholm, 2009, 388 pages.
2. Shnoll S.E. and Rubinstein I.A. Regular changes in the fine structure of histograms revealed in the experiments with collimators which isolate beams of alpha-particles flying at certain directions. *Progress in Physics*, 2009, v. 2, 83–95.
3. Shnoll S.E. The "scattering of the results of measurements" of processes of diverse nature is determined by the Earth's motion in the inhomogeneous space-time continuum. The effect of "half-year palindromes". *Progress in Physics*, 2009, v. 1, 3–7.
4. Goldburg W. I. Dynamic light scattering. *Am. J. Phys.*, 1999, v. 67, no. 12.
5. Beran J. Statistics for long-memory processes. Chapman & Hall, New York, 1994.
6. Panchelyuga V.A., KolombetV.A., Pancheluga M.S., and Shnoll S.E. Local-time effect on small space-time scale. In: *Space-Time Structure*, collected papers, Tetru, Moscow, 2006, 344–350.
7. Panchelyuga, Kolombet V.A., Kaminsky A.V., Pancheluga M.S., and Shnoll S.E. Experimental investigation of the existence of a local-time effect on the laboratory scale and the heterogenety of space-time. *Progress in Physics*, 2007, v. 1, 64–69.
8. Kaminsky A.V., Shnoll S.E. The study of synchronous (by local time) changes of the statistical properties of thermal noise and alpha-activity fluctuations of a 239-Pu sample. arXiv: physics/0605056.
9. Panchelyuga V.A., Kolombet V.A., Kaminsky A.V., Pancheluga M.S., and Shnoll S.E. Local-time effect observed in noise processes. *Bull. of Kaluga University*, 2006, no. 2b, 3–8.

Strong Nuclear Gravitational Constant and the Origin of Nuclear Planck Scale

U. V. S. Seshavatharam* and S. Lakshminarayana†

*Spun QA Engineer, Lanco Industries Ltd, Srikalahasti, A.P, 517641, India. E-mail: seshavatharam.uvs@gmail.com

†Department of Nuclear Physics, Andhra University, Visakhapatnam, AP, 530003, India. E-mail: lnsrirama@yahoo.com

Whether it may be real or an equivalent, existence of strong nuclear gravitational constant G_S is assumed. Its value is obtained from Fermi's weak coupling constant as $G_S = 6.9427284\times10^{31}$ m^3/kg sec^2 and thus "nuclear planck scale" is defined. For strong interaction existence of a new integral charged "confined fermion" of mass 105.383 MeV is assumed. Strong coupling constant is the ratio of nuclear planck energy = 11.97 MeV and assumed 105.383 MeV. $\frac{1}{\alpha_s} = X_s$ is defined as the strong interaction mass generator. With 105.383 MeV fermion various nuclear unit radii are fitted. Fermi's weak coupling constant, strong interaction upper limit and Bohr radius are fitted at fundamental level. Considering Fermi's weak coupling constant and nuclear planck length a new number $X_e = 294.8183$ is defined for fitting the electron, muon and tau rest masses. Using X_s, X_e and α 105.32 = 0.769 MeV as the Coulombic energy constant = E_c, energy coefficients of the semi-empirical mass formula are estimated as $E_v = 16.32$ MeV, $E_s = 19.37$ MeV, $E_a = 23.86$ MeV and $E_p = 11.97$ MeV where Coulombic energy term contains $[Z]^2$. Starting from $Z = 2$ nuclear binding energy is fitted with two terms along with only one energy constant = 0.769 MeV. Finally nucleon mass and its excited levels are fitted.

1 Introduction

It can be supposed that elementary particles construction is much more fundamental than the black hole's construction. If one wishes to unify electroweak, strong and gravitational interactions it is a must to implement the classical gravitational constant G in the sub atomic physics. By any reason if one implements the planck scale in elementary particle physics and nuclear physics automatically G comes into subatomic physics. Then a large arbitrary number has to be considered as a proportionality constant. After that its physical significance has to be analyzed. Alternatively its equivalent "strong nuclear gravitational constant G_S can also be assumed. Some attempts have been done in physics history [1–5]. Whether it may be real or an equivalent if it is existing as a "single constant" its physical significance can be understood. "Nuclear size" can be fitted with "nuclear Schwarzschild radius". "Nucleus" can be considered as "strong nuclear black hole". This idea requires a basic nuclear fermion! Nuclear binding energy constants can be generated directly. Proton-neutron stability can be studied. Origin of "strong coupling constant" and "Fermi's weak coupling constant" can be understood. Charged lepton masses can be fitted. Authors feel that these applications can be considered favorable for the proposed assumptions and further analysis can be carried out positively for understanding and developing this proposed "nuclear planck scale"

2 Proposed assumptions

1. Strong nuclear gravitational constant can be given as $G_S = 6.94273\times10^{31}$ m^3/kg sec^2;
2. There exists a strongly interacting "confined" Fermionic mass unit $M_{Sf}c^2 = 105.383$ MeV. With this assumption in particle physics "super symmetry in strong and weak interactions" can be understood very easily [6];
3. Strong interaction mass generator $X_S = 8.8034856$ and Lepton mass generator $X_E = 294.8183$;
4. In the semi-empirical mass formula ratio of "Coulombic energy coefficient" and the proposed 105.383 MeV is equal to α. The Coulombic energy constant E_C = 0.769 MeV.

2.1 Planck scale Coulombic energy and the unified force

Let

$$M_Pc^2 = \text{planck energy} = \sqrt{\frac{\hbar c^5}{G}} = \sqrt{\hbar c\,\frac{c^4}{G}}\,. \qquad (1)$$

Multiplying this energy unit with $\sqrt{\alpha}$, we get

$$\sqrt{\alpha}M_Pc^2 = \sqrt{\frac{e^2}{4\pi\epsilon_0}\frac{c^4}{G}}\,, \qquad (2)$$

where $\sqrt{\alpha}M_Pc^2$ can be termed as "Coulombic energy", $\frac{c^4}{G}$ is having the dimensions of force and can be considered as the classical limit of any force. This classical force limit $\frac{c^4}{G}$ and the classical power limit $\frac{c^5}{G}$ plays a very vital role in black hole formation and planck scale generation [7]. These are two very important observations to be noted here: $\frac{c^5}{G}$ plays a very crucial role in "gravitational radiation"; using $\frac{c^4}{G}$ minimum distance r_{min} between any two charged particles is given as

$$\frac{e^2}{4\pi\epsilon_0 r_{min}^2} \leqslant \frac{c^4}{G}\,, \qquad (3)$$

$$r_{min} \geqslant \sqrt{\frac{e^2}{4\pi\epsilon_0}\frac{G}{c^4}}\,, \qquad (4)$$

planck mass can be generated if it is assumed that

$$\frac{GM_Pc^2}{r_{min}^2} \leqslant \frac{c^4}{G}\,, \tag{5}$$

$$2\pi r_{min} = \lambda_P = \text{planck wave length}, \tag{6}$$

where, M_P= planck mass and r_{min}= minimum distance between two planck particles. With these two conditions, planck mass can be obtained as

$$M_P = \text{planck mass} = \frac{h}{c\lambda_P} = \sqrt{\frac{\hbar c}{G}}\,. \tag{7}$$

Aim of equations (3, 4, 5, 6 and 7) is to show that there exists a fundamental force of the form $k\frac{c^4}{G} \cong 1.21027{\times}10^{44}$ Newton, where k is a proportionality ratio and is close to unity. This can be considered as the "unified force" of "true grand unification". In the foregoing sections authors show how it changes into the "strong nuclear force".

2.2 Strong nuclear gravitational constant G_S and strong nuclear force

Let the classical gravitational constant be represented by G_C and the assumed strong nuclear gravitational constant be represented by G_S. The most important definition is that

$$\frac{c^4}{G_S} = 116.3463 \text{ Newton} \tag{8}$$

can be called as the "nuclear strong force". This is the beginning of this "nuclear planck scale". Authors request the science community to analyze this equation positively. Magnitude of force of attraction or repulsion in between two nucleons when their distance of separation is close to 1.4 Fermi is

$$\frac{e^2}{4\pi\epsilon_0 R_0^2} \cong \frac{c^4}{G_S}\,, \tag{9}$$

$$R_0 \cong \sqrt{\frac{e^2}{4\pi\epsilon_0}\frac{G_S}{c^4}}\,. \tag{10}$$

If a nucleon of mass m_n revolves at a radius of R_0,

$$\text{potential energy} = E_P = -\frac{e^2}{4\pi\epsilon_0 R_0}\,, \tag{11}$$

$$\text{kinetic energy} = E_K = \frac{m_n v^2}{2} = \frac{e^2}{8\pi\epsilon_0 R_0}\,, \tag{12}$$

$$\text{total energy} = E_T = E_P + E_K = \frac{m_n v^2}{2} = -\frac{e^2}{8\pi\epsilon_0 R_0}\,. \tag{13}$$

We know that the characteristic size of nucleus is 1.3 to 1.4 Fermi. For $R_0 = 1.4$ Fermi total energy of revolving nucleon is close to the rest "energy of electron". This is still a mystery. Hence

$$\frac{e^2}{8\pi\epsilon_0 R_0} \cong \frac{1}{2}\sqrt{\frac{e^2}{4\pi\epsilon_0}\frac{c^4}{G_S}} \cong m_e c^2. \tag{14}$$

Here $m_e c^2$ is the rest energy of electron. Half the classical radius of electron can also be considered as the unit size of nucleus. If so with the assumed strong nuclear gravitational constant G_S it is noticed that

$$R_0 \cong \sqrt{\frac{e^2}{4\pi\epsilon_0}\frac{G_S}{c^4}} \cong \frac{e^2}{8\pi\epsilon_0 m_e c^2} \cong \frac{2G_S m_e}{c^2}\,. \tag{15}$$

This equation (15) clearly suggests that nucleus that we are observing or studying is not a simple object. It is a strange object and can be considered as an "electronic black hole" and works at strong nuclear gravitational constant G_S. Experimentally knowing the (exact) characteristic size of nucleus one can easily estimate the value of proposed G_S. Alternatively its value can be estimated form the famous Fermi weak coupling constant F_W. Considering "planck mass" and "electron mass" in view in a unified manner value of G_S can be obtained from the following 3 semi-empirical relations

$$F_W \cong \frac{1}{3}\left[\ln\left(\frac{\hbar c}{G_C m_e^2}\right)\right]^{-2}\left(\frac{e^2}{4\pi\epsilon_0}\right)^2\left(\frac{G_S}{c^4}\right). \tag{16}$$

This can be obtained from eq. (42, 31, 36, 43, 44 and 28)

$$G_S \cong 3\left[\ln\left(\frac{\hbar c}{G_C m_e^2}\right)\right]^2\left(\frac{4\pi\epsilon_0}{e^2}\right)^2 F_W c^4. \tag{17}$$

Its obtained value is $6.9427284{\times}10^{31}$ $\mathrm{m^3/kg\,sec^2}$. This value is considered in this paper

$$F_W \cong \frac{16\alpha^2}{27}\left(\frac{e^2}{4\pi\epsilon_0}\right)^2\left(\frac{G_S}{c^4}\right). \tag{18}$$

This can be obtained from eq. (42, 31, 36, 43, 44, and 10)

$$G_S \cong \left(\frac{27}{16\alpha^2}\right)\left(\frac{4\pi\epsilon_0}{e^2}\right)^2 F_W c^4. \tag{19}$$

Its obtained value is $6.9052{\times}10^{31}$ $\mathrm{m^3/kg\,sec^2}$. This method is independent of the classical gravitational constant G_C. Another interesting idea is

$$\frac{e^2}{4\pi\epsilon_0 G_S m_e^2} \cong 4, \tag{20}$$

$$G_S \cong \frac{1}{4}\left(\frac{e^2}{4\pi\epsilon_0 m_e^2}\right) \cong 6.9506{\times}10^{31}\ \mathrm{m^3/kg\,sec^2}. \tag{21}$$

Here m_e = rest mass of electron. If this is having any physical meaning without considering the classical gravitational constant G_C value of G_S can be calculated from electron mass directly. Not only that in quark physics in our paper [6] it is assumed that

$$\frac{\text{DCT geometric ratio}}{\text{USB geometric ratio}} \cong 4. \tag{22}$$

2.3 "Strong nuclear force" and "nuclear planck scale"

Similar to the planck scale in unified nuclear physics nuclear scale planck energy can be given as

$$M_n c^2 = \sqrt{\frac{\hbar c^5}{G_S}} = \sqrt{\hbar c \frac{c^4}{G_S}} \cong 11.9705568 \text{ MeV}. \quad (23)$$

These 4 energy coefficients of the semi-empirical mass formula lies in between 11.97 MeV and 2×11.97 = 23.94 MeV. Not only that using this expression in particle physics [6] it can be shown that strongly interacting particles follows energy levels as $[n(n+1)]^{\frac{1}{4}}$ and $\left[\frac{n(n+1)}{2}\right]^{\frac{1}{4}}$ where, n =1, 2, 3... We know that

$$\text{planck length} = \sqrt{\frac{\hbar G_C}{c^3}} = 1.616244\times10^{-35} \text{ meter}. \quad (24)$$

Nuclear planck length can be given as

$$L_n = \sqrt{\frac{\hbar G_S}{c^3}} = 1.664844\times10^{-14} \text{ meter}. \quad (25)$$

Nuclear scale Coulombic energy can be given as

$$M_e c^2 = \sqrt{\frac{e^2}{4\pi\epsilon_0}\frac{c^4}{G_S}} \cong 1.02258 \text{ MeV}. \quad (26)$$

These energy units directly can be implemented in nuclear physics for understanding nuclear structure. Nuclear planck energy $M_n c^2$ or nuclear planck length L_n plays an interesting role in understanding the origin of strong coupling constant [8] and energy coefficients of the semi-empirical mass formula. Lepton masses can also be fitted. It is also noticed that

$$M_{Sf} c^2 E_P^2 \cong \left(M_n c^2\right)^2 E_C. \quad (27)$$

where $M_{sf}c^2$ = proposed new strongly interacting 105.383 MeV, E_P = nucleon's potential energy close to 1.4 Fermi = 2×0.511 MeV, $M_n c^2$ = proposed nuclear scale planck energy = 11.97 MeV, E_C = assumed Coulombic energy coefficient of the semi-empirical mass formula $\alpha M_{Sf} c^2 = \alpha 105.383$ = 0.769 MeV.

3 New strongly interacting fermion (105.38 MeV) and Fermi's weak coupling constant (F_W)

It is assumed that 105.383 MeV is a strongly interacting particle. Authors request that this should not be confused with weakly interacting muon. This particle can be called as sion. Its charge is $\pm e$. Just like quarks it is a confined fermion. It plays a crucial part in understanding the nuclear size, nuclear binding energy, magnetic moments of nucleons and weak interaction. Along with the strong coupling constant it plays a heuristic role in understanding "super symmetry" in strong and weak interactions [6]. Considering "planck mass" and "electron mass" in a unified manner it is empirically defined as

$$\ln\left(\frac{M_P c^2}{m_e c^2}\right)^2 \sqrt{\frac{e^2}{4\pi\epsilon_0}\frac{c^4}{G_S}} \cong 105.3826 \text{ MeV}. \quad (28)$$

Here $M_P c^2$ = planck energy and $m_e c^2$ = rest energy of electron. Classical radius of $M_{Sf} c^2$ can be given as

$$\frac{e^2}{4\pi\epsilon_0 M_{Sf} c^2} = 1.3664\times10^{-17} \text{ meter}. \quad (29)$$

Compton length of $M_{Sf} c^2$ can be given as

$$\frac{\hbar}{M_{Sf} c} = 1.87245\times10^{-15} \text{ meter}. \quad (30)$$

This length can be considered as the strong interaction upper limit.

3.1 Various nuclear unit sizes and the mystery of 1.4 Fermi

Let

$$\frac{\hbar}{M_{Sf} c} = 1.87245\times10^{-15} \text{ meter} = a\,, \quad (31)$$

$$\frac{\hbar}{2M_{Sf} c} = 0.93624\times10^{-15} \text{ meter} = b\,. \quad (32)$$

Here a can be considered as the upper limit of strong interaction range and b can be considered as lower limit of strong interaction. Considering these two lengths as the semi-major axis and semi-minor axis of the nucleus it is noticed that

$$\text{arthematic mean of } (a,b) = \left[\frac{a+b}{2}\right] \cong 1.404 \text{ Fermi}, \quad (33)$$

$$\text{geometric mean of } (a,b) = \left[\sqrt{ab}\right] \cong 1.324 \text{ Fermi}, \quad (34)$$

$$\text{harmonic mean of } (a,b) = \left[\frac{2ab}{a+b}\right] \cong 1.248 \text{ Fermi}. \quad (35)$$

These sizes can be compared with the experimental values of various nuclear unit or characteristic sizes. From equation (33) it is noticed that arithmetic mean of semi-major and semi-minor axis of the assumed nuclear size = 1.404 Fermi. From this coincidence "existence of the strongly interacting 105.383 MeV" can be justified

$$R_0 \cong \frac{3}{4}\frac{\hbar}{M_{Sf} c} \cong 1.40436 \text{ Fermi}, \quad (36)$$

$$E_T = \frac{e^2}{8\pi\epsilon_0 R_0} \cong \frac{2}{3}\left(\alpha M_{Sf} c^2\right) \cong 0.512676 \text{ MeV}. \quad (37)$$

This idea suggests that a nucleon revolving at 1.404 Fermi having a total energy of 0.51267 MeV which is close to the electron rest energy 0.511 MeV. This small energy difference 0.51267−0.511= 0.00167 MeV may be related with origin of massive neutrino. It is assumed that

$$\alpha M_{Sf} c^2 = 0.769 \text{ MeV}, \quad (38)$$

$$\frac{E_T}{E_C} \cong \frac{0.511\ \text{MeV}}{0.769\ \text{MeV}} \cong 0.66445 \cong \frac{2}{3}. \tag{39}$$

Considering $E_T = m_e c^2$ and rearranging this equation we get

$$\frac{M_{Sf}c^2}{E_T} \cong \frac{M_{Sf}c^2}{m_e c^2} \cong \frac{3}{2\alpha}, \tag{40}$$

and from literature [9] it is noticed that

$$\frac{\text{muon mass}}{\text{electron mass}} \cong \left(\frac{3}{2\alpha} + 2\right). \tag{41}$$

Authors here suggest that in equation (41) it is not the muon mass but it is the strongly interacting proposed 105.383 MeV particle.

3.2 Fermi's weak coupling constant and estimation of 105.383 MeV

Empirically Fermi's weak coupling constant F_W [10] can be fitted as

$$F_W \cong \left(\frac{\alpha^2}{2}\right)\left(\frac{e^2}{8\pi\epsilon_0 R_0}\right)a^3. \tag{42}$$

Authors request the science community to consider this equation positively. It has interesting applications. Electron's "total energy" in hydrogen atom can be related with the strong interaction range! From equations (31 and 36)

$$F_W \cong \left(\frac{\alpha^3}{3}\right)\left(M_{Sf}c^2\right)a^3 \cong \frac{1}{3}\left(M_{Sf}c^2\right)\left(\frac{e^2}{4\pi\epsilon_0 M_{Sf}c^2}\right)^3. \tag{43}$$

Experimentally $F_W = 1.435841179{\times}10^{-62}$ J×meter^3

$$\therefore M_{Sf}c^2 \cong \left(\frac{e^2}{4\pi\epsilon_0}\right)\left(\frac{e^2}{12\pi\epsilon_0 F_W}\right)^{\frac{1}{2}} \cong 105.38\ \text{MeV}. \tag{44}$$

3.3 Strong interaction mass generator X_S

Based on nuclear planck scale it is assumed that strong interaction mass generator is

$$X_S \cong \frac{M_{Sf}c^2}{M_n c^2} \cong 8.803486 \cong \frac{L_n}{a}, \tag{45}$$

$$X_S \cong \sqrt{\frac{G_S M_{Sf}^2}{\hbar c}} \cong 8.803486, \tag{46}$$

$$\alpha_s(M_Z) \cong \sqrt{\frac{\hbar c}{G_S M_{Sf}^2}} \cong 0.11359. \tag{47}$$

It is noticed that $X_S = 8.803486 = \frac{1}{0.11359}$ seems to be the "inverse" of the strong coupling constant [8] $\alpha_s(M_Z) = 0.1186 \pm 0.0011\,(\text{exper}) \pm 0.0050\,(\text{theor})$. Considering the lower limits of this value we get $0.1186 - 0.0050\,(\text{theor}) = 0.1136$. We know the importance of the "strong coupling constant" in particle physics. If the proposed definition is found to be true and meaningful one has to accept the existence of proposed "nuclear planck scale". In the sense one must accept the existence of "strong nuclear gravitational constant G_S and existence of 105.383 MeV". This number X_S plays a very interesting role in correlating the energy coefficients of the semi-empirical mass formula and proton-neutron stability. This number plays a crucial role in understanding super symmetry in strong and weak interactions [8].

Based on X_S it is noticed that, $X_S M_{Sf}c^2 = 927.737$ MeV. This is roughly close to proton mass. $X_S M_{Sf}c^2 + M_n c^2 = 939.7$ MeV. This is close to the neutron mass = 939.57 MeV. Some how 105.383 MeV and X_S plays a vital role in "weighing" of the nucleon mass. See Section 5 for "nucleon mass fitting" and nucleon's basic excited levels.

3.4 Fermi's weak coupling constant and the Bohr radius

By any reason for the nucleus if

$$\frac{e^2}{8\pi\epsilon_0 R_0} \cong m_e c^2, \tag{48}$$

$$\frac{e^2}{4\pi\epsilon_0 R_0} \cong 2m_e c^2. \tag{49}$$

Equation(42) takes the following interesting form as

$$F_W \cong \left(\frac{\alpha^2}{2}\right)\left(\frac{e^2}{8\pi\epsilon_0 R_0}\right)a^3 \cong \left(\frac{\alpha^2}{2}\right)\left(m_e c^2\right)a^3. \tag{50}$$

At a glance equation (50) suggests that

$$\left(\frac{\alpha^2}{2}\right)\left(m_e c^2\right) \cong \frac{F_W}{a^3} \cong \left(\frac{\alpha^3}{3}\right)M_{Sf}c^2 \cong 13.65\ \text{eV}. \tag{51}$$

In this equation (51) "left hand side" is nothing but the "total energy of electron" in hydrogen atom. This is a very simple and strange relation! Based on the unification of strong and weak interactions "Bohr radius" of hydrogen atom can be given as

$$a_0 \cong \left(\frac{e^2}{8\pi\epsilon_0}\right)\left(\frac{a^3}{F_W}\right) \cong 5.27745{\times}10^{-11}\ \text{meter}. \tag{52}$$

This is matching with $a_0 = 5.29177{\times}10^{-11}$ meter. This idea suggests that existence of the proposed nuclear strong interaction upper limit a=1.8725 Fermi and strongly interacting $M_{Sf}c^2 = 105.383$ MeV seems to be true and can be considered for further analysis. Their direct existence strongly supports the hidden existence of the proposed strong nuclear gravitational constant G_S.

3.5 Lepton mass generator X_E and electron, muon and tau rest mass fitting

A new number (X_E) is empirically defined [1] as

$$X_E \cong \left[\frac{e^2}{8\pi\epsilon_0 R_0}\frac{L_n^3}{F_W}\right]^{\frac{1}{3}} \cong X_S\left[\frac{e^2}{8\pi\epsilon_0 R_0}\frac{a^3}{F_W}\right]^{\frac{1}{3}}. \tag{53}$$

n	Obtained lepton mass, MeV	Exp. lepton mass, MeV
0	0.5127	0.510998922
1	105.86	105.658369
2	1775.506	1776.9
3	42206.19	Not discovered

Table 1: Fitting of charged lepton rest masses.

Its obtained value is 294.8183. Here L_n = proposed nuclear planck length, a = strong interaction upper limit and F_W = Fermi's weak coupling constant.

This number can be called as "lepton mass generator". It has wide applications in nuclear and particle physics. It is noticed that $(\alpha X_E) = 2.1514$ plays a very interesting role in estimating the quark masses [6]. The weak coupling angle can be considered as $(\alpha X_E)^{-1} = \sin(\theta_W) = 0.4648$. It plays a crucial role in estimating the charged lepton rest masses. It plays a very interesting role in fitting energy coefficients of the semi-empirical mass formula. It can be used for fitting the nuclear size with "Compton wavelength of nucleon". It is noticed that ratio of "nuclear volume" and "A nucleons Compton volume" is X_E. It can be called as the nuclear "volume ratio" factor.

Till now no mechanism is established for the generation of the charged lepton rest masses [11]. Considering equation (39) an interesting empirical relation is given for fitting electron, muon and tau particle rest masses as

$$m_l c^2 \cong \frac{2}{3}\left[E_C^3 + \left(n^2 X_E\right)^n E_A^3\right]^{\frac{1}{3}}, \tag{54}$$

where E_C = Coulombic energy coefficient of the semi-empirical mass formula, E_A = asymmetry energy coefficient of the semi-empirical mass formula and X_E = proposed lepton mass generator = 294.8183 and $n = 0, 1, 2$.

If $E_C = 0.769$ MeV and $E_A = 23.86$ MeV obtained charged lepton masses are shown in the following Table 1. It is known that these two coefficients plays a vital role in nuclear stability. It is well known that in weak decay for getting stability neutron in an unstable nuclide emits electron. If our study is focused on why and how a charged lepton is coming out from the nucleus this idea can be adapted. For any model data fitting is the first successful step in its implementation in the actual field.

3.6 Role of X_E in estimating the nuclear size R_0

Compton wave length of nucleon is

$$\frac{\hbar}{m_n c} = 2.1016{\times}10^{-16} \text{ meter}, \tag{55}$$

where m_n is the average mass of nucleon = 938.92 MeV. It is noticed that

$$R_0 \cong (X_E)^{\frac{1}{3}} \frac{\hbar}{m_n c} = 1.399{\times}10^{-15} \text{ meter}. \tag{56}$$

This is very close to the estimated nuclear characteristic size. With reference to Rutherford's alpha scattering experiments size of a nucleus that contains A nucleons can be given as

$$R_A \cong (AX_E)^{\frac{1}{3}} \frac{\hbar}{m_n c}. \tag{57}$$

Hence ratio of "nuclear volume" and "A nucleons Compton volume" = X_E.

4 Relations between energy coefficients of the semi-empirical mass formula

We know that the best energy coefficients of the semi-empirical mass formula [12–14] are, Coulombic energy coefficient $E_C = 0.71$ MeV, volume energy coefficient $E_V = 15.78$ MeV, surface energy coefficient $E_S = 18.34$ MeV, asymmetry energy coefficient $E_A = 23.21$ MeV and pairing energy coefficient $E_{EO} = 12.0$ MeV. The 4 major energy coefficients of the semi-empirical mass formula lies in between 11.97 MeV and $2{\times}11.97 = 23.94$ MeV. Really this is a very interesting case. If one proceeds further for analyzing this strange observation possibly role of "strong coupling constant" or "strong interaction mass generator" can be understood in the "nuclear mass generation". Thus unification of "gravitation" with "nuclear physics" may be possible. Authors proposal may be given a chance. See the following Table 2. In this context it is assumed that

$$\frac{M_{Sf} c^2}{E_C} \cong \frac{1}{\alpha} \quad \text{and} \quad E_C \cong \alpha M_{Sf} c^2 = 0.769 \text{ MeV}. \tag{58}$$

From equations (23, 46, 53 and 58) empirically it is noticed that

$$E_V \cong M_n c^2 + \left(X_E^{\frac{1}{3}} - 1\right) E_C \cong 16.32 \text{ MeV}, \tag{59}$$

$$E_S \cong M_n c^2 + \left(X_E^{\frac{1}{3}} + \sqrt{X_S}\right) E_C \cong 19.37 \text{ MeV}, \tag{60}$$

$$E_A \cong M_n c^2 + \left(X_E^{\frac{1}{3}} + X_S\right) E_C \cong 23.86 \text{ MeV} \cong 2M_n c^2, \tag{61}$$

$$E_A - E_S \cong \left(X_S - \sqrt{X_S}\right) E_C, \tag{62}$$

$$E_{EO} \cong M_n c^2 \cong 11.97 \text{ MeV}. \tag{63}$$

It is also noticed that

$$X_E \cong \frac{E_S}{E_C} \sqrt{\frac{M_{Sf} c^2}{E_C}} \cong \frac{E_S}{E_C} \sqrt{\frac{1}{\alpha}}. \tag{64}$$

This is another interesting guess. This successfully implements the new number X_E. It is observed that proposed E_V-existing $E_V = 16.32{-}15.78 = 0.54$ MeV $\approx E_T = 0.511$ MeV. Proposed E_S — existing $E_S = 19.37 - 18.34 = 1.03$ MeV $\approx 2E_T = 2{\times}0.511$ MeV. Proposed E_A-existing $E_A = 23.86 - 23.21 = 0.65$ MeV $\approx E_T = 0.511$ MeV.

Please note that asymmetry energy coefficient is matching with twice of $M_n c^2 = 23.94$ MeV. This is very interesting. If proposed ideas has no significance here why and how it is happening like this? This data coincidence indicates that proposed scheme of energy coefficients can be applied in the

Z	A	Obtained Be, MeV	Be, MeV [13, 14]
8	16	121.6	118.13, 128.57
20	44	382.7	377.66, 382.78
28	62	543.7	538.85, 544.41
50	118	1003.4	1000.22, 1004.74
82	208	1620.6	1618.41, 1635.36
108	292	2089.6	2082.53, 2089.48

Table 2: Fitting of nuclear binding energy with proposed coefficients.

semi-empirical formula for understanding the significance of proposed 105.383 MeV and $X_S = 8.803486$ in the context of strong interaction. The semi-empirical mass formula is

$$Be = AE_V - A^{\frac{2}{3}}E_S - \frac{Z^2}{A^{\frac{1}{3}}}E_C - \frac{(A-2Z)^2}{A}E_A \pm \sqrt{\frac{1}{A}}E_{EO}. \quad (65)$$

Here $E_V = 16.32$ MeV, $E_S = 19.37$ MeV, $E_C = 0.769$ MeV, $E_A = 23.86$ MeV and $E_{EO} = 11.97$ MeV can be considered as the unified energy coefficients of the semi-empirical formula [13, 14] where Coulombic energy term contains $[Z]^2$.

If one wants to retain $[Z(Z-1)]$ energy coefficients can be fine tuned in the following way

$$E_{EO} \cong M_n c^2 \cong 11.97 \text{ MeV}, \quad (66)$$

$$E_A \cong 2M_n c^2 \cong 23.94 \text{ MeV}, \quad (67)$$

$$\frac{E_A}{E_V} \cong \sqrt{\alpha X_E} \text{ and } E_V \cong 16.322 \text{ MeV}, \quad (68)$$

$$E_V + E_S \cong E_A + E_{EO} \cong 3E_{EO}, \quad (69)$$

$$E_S \cong 3E_{EO} - E_V \cong 35.91 - 16.322 \cong 19.59 \text{ MeV}. \quad (70)$$

Alternatively

$$E_V \cong \left(\frac{3E_{EO}}{2}\right) - (\alpha X_E)E_C \cong 16.30 \text{ MeV}, \quad (71)$$

$$E_S \cong \left(\frac{3E_{EO}}{2}\right) + (\alpha X_E)E_C \cong 19.61 \text{ MeV}, \quad (72)$$

with $E_V = 16.30$ MeV, $E_S = 19.61$ MeV and with $E_V = 16.32$ MeV, $E_S = 19.59$ MeV,

- for $Z = 26$ and $A = 56$, $Be = 489.87$ MeV and 491.40 MeV,
- for $Z = 50$ and $A = 118$, $Be = 1002.88$ MeV and 1005.96 MeV,
- for $Z = 79$ and $A = 197$, $Be = 1547.96$ MeV and 1552.97 MeV,
- for $Z = 92$ and $A = 238$, $Be = 1794.87$ MeV and 1800.87 MeV.

Taking mean values of E_V and E_S, energy coefficients can be given as $E_V = 16.31$ MeV, $E_S = 19.60$ MeV, $E_C = 0.769$ MeV, $E_A = 23.94$ MeV and $E_{EO} = 11.97$ MeV.

4.1 Nuclear binding energy with two terms and one energy constant 0.769 MeV

An empirical method is proposed here for fitting the nuclear binding energy. This method contains two terms. For these two terms, Coulombic energy constant $E_C = 0.769$ MeV is applied. In this method the important point is at first for any Z its stable mass number A_S has to be estimated. Strong interaction mass generator X_S plays a crucial role in this method. For any Z error in binding energy is very small near the stable isotope A_S and increasing above and below A_S. Unifying 5 terms having 5 energy constants into two terms with one energy constant which are related with strong interaction mass generator is not a simple task. Authors proposal can be given a chance.

This method is applicable for light atoms also. For light atoms, when $A = 2Z$, obtained binding energy is very close to the actual value. For $Z = 2$ and $A = 4$ is 28.86 MeV, $Z = 4$, $A = 8$ is 59.57 MeV, $Z = 6$, $A = 12$ is 92.63 MeV $Z = 7$, $A = 14$ is 114.0 MeV, $Z = 8$ $A = 16$ is 127.14 MeV, $Z = 9$, $A = 19$ is 149.72 MeV and $Z = 10$, $A = 20$ is 155.06 MeV. For very light odd elements error is due to estimation of their stable mass numbers

$$T_1 = \left[(A+1)\left(1 + \frac{2Z}{A_S}\right)\right] \ln\left[(A+1)X_S\right] E_C. \quad (73)$$

Stable isotope of any Z can be estimated as

$$A_S \cong 2Z + \frac{Z^2}{S_f} \cong 2Z + \frac{Z^2}{155.72}. \quad (74)$$

Here S_f can be called as the nuclear stability factor. It can be given as

$$S_f \cong \frac{E_A}{E_C}\sqrt{\frac{E_S}{E_C}} \cong 155.72 \cong 2X_S^2 \cong 155.00. \quad (75)$$

After rounding off for even Z values, if obtained A_S is odd consider $A_S + 1$, for odd Z values if obtained A_S is even, consider $A_S - 1$. For very light odd elements this seems to be not fitting.

Term T_1 indicates the factors for increase in binding energy. Another observation is $[(A+1)X_S]$. This factor plays a key role in the saturation of the binding energy. It is observed that for any Z at its stable isotope A_S

$$T_1 \cong [A_S + 2Z + (1 \text{ or } 2)] \ln\left[(A_S + 1)X_S\right] E_C. \quad (76)$$

The basic question is that how to extrapolate from the stable isotope A_S of any Z to above and below its stable and unstable isotopes? Authors are working in this direction also

$$T_2 \cong \left[\frac{A^2 + \left(fZ^2\right)}{X_S^2}\right] E_C, \quad (77)$$

where

$$f \cong 1 + \frac{2Z}{A_S} \cong \text{ a factor} \leqslant 2. \quad (78)$$

Z	A_S	Obtained Be, MeV
2	4	28.9
8	16	127.1
20	44	368.4
26	56	481.6
44	100	856.2
68	166	1347.1
83	209	1623.5
92	238	1775.5

Table 3: Fitting of nuclear binding energy with two terms and one energy constant.

Term T_2 indicates the factors for decrease in binding energy. Both of these terms has to be analyzed at fundamental level. T_1 and T_2 indicates the importance of the number $X_S = 8.8034856$ in strong interaction mass generation

$$Be = T_1 - T_2. \tag{79}$$

Whether this is the total binding energy that includes shell effects or liquid drop energy has to be decided with observations and analysis. This method has to be analyzed and extended for isotopes above and below the stable mass number A_S of any Z value. With reference to A_S and by considering shell effects error in finding the first term can be eliminated. In the second term by selecting a suitable expression for f error can be minimized. The advantage of this method is that number of energy constants can be minimized. See the following Table 3.

5 Rest mass of nucleon

Let m_nc^2 = rest mass of nucleon. Semi-empirically it is observed that

$$m_nc^2 \cong \ln\left(M_nc^2\frac{8\pi\epsilon_0R_0}{e^2}\right)^2\sqrt{\frac{R_S}{a}}\,M_nc^2. \tag{80}$$

Here a is the Compton length of M_{Sf} and R_S is the black hole radius of M_{Sf} and is given by

$$R_S = \frac{2G_SM_{Sf}}{c^2} = 2.9023\times10^{-13}\text{ meter}, \tag{81}$$

$$m_nc^2 \cong \ln\left(\frac{8\pi\epsilon_0R_0M_nc^2}{e^2}\right)^2\sqrt{\frac{2G_SM_{Sf}^2}{\hbar c}}\,M_nc^2. \tag{82}$$

From equation (48)

$$m_nc^2 \cong \ln\left(\frac{M_nc^2}{m_ec^2}\right)^2\sqrt{\frac{2G_SM_{Sf}^2}{\hbar c}}\,M_nc^2. \tag{83}$$

5.1 Nucleon stability relation

If it is assumed that

$$A_S \cong 2Z + \frac{Z^2}{155.00} \cong 2Z + \frac{Z^2}{2X_S^2}, \tag{84}$$

significance of $2X_S^2$ can be given as

$$2X_S^2 \cong \frac{2G_SM_{Sf}^2}{\hbar c} \cong \frac{R_S}{a} \cong 155.00 \tag{85}$$

Hence

$$A_S \cong 2Z + \frac{Z^2}{S_f} \cong 2Z + \left(\frac{a}{R_S}\right)Z^2. \tag{86}$$

For example, if $Z = 47$, $A_S = 108.25$, $Z = 82$, $A_S = 207.38$ and $Z = 92$, $A_S = 238.6$. This clearly indicates the beautiful role of $2X_S^2$ in nuclear stability.

5.2 Excited levels of nucleon

From quantum mechanics quantized angular momentum is given by $\sqrt{n(n+1)}.\hbar$ where $n = 0, 1, 2\ldots$ Some how if $\hbar$ goes under a "square root" like the planck energy, $M_Pc^2 = \sqrt{\frac{\hbar c^5}{G_C}}$ as a ground state energy level in a heuristic way its massive excited levels are given by [6]

$$\left(M_Pc^2\right)_I = [n(n+1)]^{\frac{1}{4}}\sqrt{\frac{\hbar c^5}{G_C}}. \tag{87}$$

Here $n = 0, 1, 2, 3\ldots$ and $I = n(n+1)$. Keeping this idea in view it is assumed that "if m_0c^2 is the rest energy of a particle then its massive excited levels are given by

$$mc^2 = [n(n+1)]^{\frac{1}{4}}\,m_0c^2 \tag{88}$$

and each excited state can be seen as a new massive particle". The surprising observation is that in particle physics excited massive states are following two types of discrete levels. They are

$$[n(n+1)]^{\frac{1}{4}}\,m_0c^2 \text{ and } \left[\frac{n(n+1)}{2}\right]^{\frac{1}{4}}m_0c^2. \tag{89}$$

Presently understood "Regge trajectory" of some of the baryons and mesons are fitted in this way. These levels can be called as Fine rotational levels. If the proposed idea is correct nucleon must show excited levels as

$$\left(m_nc^2\right)_I = [I]^{\frac{1}{4}}\,939 \text{ and } \left(m_nc^2\right)_{\frac{I}{2}} = \left[\frac{I}{2}\right]^{\frac{1}{4}}939, \tag{90}$$

where $I = n(n+1)$ and n =1, 2, 3, ...

At $I = 2$, 1117 MeV, $\frac{I}{2} = 3$, 1236 MeV, at $I = \frac{I}{2} = 6$, 1470 MeV, at $\frac{I}{2} = 10$, 1670 MeV, $I = 12$, 1748 MeV levels are obtained. This is a great coincidence and is a true reflection of the correctness of the proposed assumptions. Hence the proposed ideas can be given a chance in "final grand unified physics".

Conclusions

Nucleus has strong nuclear gravitational mechanism. Some how electron plays a crucial role in its structural formation. Just like quark masses $M_{Sf}c^2$ can be considered as a strongly

interacting "confined" fermion. Whether G_S is really existing or an equivalent value it plays a heuristic role in understanding the experimental things and can be considered for further analysis. Based on the proposed data fitting results existence of the proposed strong interaction fermion $M_{Sf}c^2$ and the strong interaction mass generator $X_S = 8.8034856$ can be confirmed. 0.769 MeV can be considered as the unified Coulombic energy coefficient.

Two most important and interesting observations are as follows

$$\alpha X_E \cong \sqrt{\ln \sqrt{\frac{4\pi\epsilon_0 G_S M_{Sf}^2}{e^2}}} \cong 2.153. \qquad (91)$$

This expression clearly demonstrates the hidden existence of $M_{Sf}c^2$ and G_S in nuclear and particle physics. In our paper [6] it is assumed that there exists a strongly interacting fermion 11450 MeV which plays a crucial role in estimating quark-gluon masses. Empirically it is noticed that

$$(11450)^{\frac{14}{30}}\,(105.38)^{\frac{16}{30}} \cong 939.54 \text{ MeV}. \qquad (92)$$

This is very close to the neutron mass. Since both are integral charged particles and giving importance to the charged proton mass it can be written as

$$\left(\frac{11450}{105.38}\right)^{\frac{14}{30}}(105.38) \cong 939.54 \text{ MeV}, \qquad (93)$$

where

$$\left(\frac{11450}{105.38}\right)^{\frac{14}{30}} \cong 8.9157 \cong X_S\,. \qquad (94)$$

This number is very close to the proposed strong interaction mass generator X_S. It is noticed that $\frac{14}{30} \cong 0.4666$ and $\frac{16}{30} \cong 0.5333$. Comparing $\left(\frac{14}{30}\right)$ with $\left(\frac{1}{\alpha X_E}\right)$ one can see the significance of (αX_E) in deciding the mass of proton.

Even though this is an unconventional paper number of inputs are only two and they are assumed $M_{Sf}c^2$ and strong nuclear gravitational constant G_S. The main advantage of this paper is that there is no need to go beyond 4 dimensions. Authors humbly request the world science community to kindly look into these new and heuristic ideas for further analysis and development.

Acknowledgements

The first author is very much thankful to Prof. S. Lakshminarayana, Department of Nuclear Physics, Andhra University, Visakhapatnam, India, Dr. P. K. Panigrahi, PRL, India and Mr. N. Phani Raju, principal, SSN PG college, Ongole, AP, India for their kind, immense and precious encouragement and guidance at all times. The same author is very much thankful to Dr. Rukmini Mohanta, UoH, India and the organising committee for considering this for poster presentation in DAE-BRNS 2008 HEP Physics symposium, Banaras, India. Finally the first author is very much thankful to his loving brother B. Vamsi Krishna (Software professional) and boyhood friend T. Anand Kumar (software professional) for encouraging, providing technical and financial support.

Submitted on January 26, 2009 / Accepted on February 20, 2010

References

1. Stone R. A. Jr. Quark confinement and force unification. *Progress in Physics*, 2010, v. 2, 19–22.
2. Oldershaw R. L. Hadrons as Kerr-Newman black holes. arXiv: astro-ph/0701006.
3. Raut U. and Sinha K. P. Strong gravity and the Yukawa field. *International Journal of Theoretical Physics*, 1981, v 20, no. 1, 69–77.
4. Perng J. J. Strong gravitation and elementary particles. *Nuovo Cimento Lettere*, Serie 2, 1978, v. 23, 552–554.
5. Salam A. and Sivaram C. Strong gravity approach to QCD and confinement. *Mod. Phys. Lett. A*, 1993, v.8, no. 4, 321–326.
6. Seshavatharam U. V. S. and Lakshminarayana S. Super symmetry in strong and weak interactions. *IJMPE*, 2010, v. 19, no. 2, 263–280.
7. Seshavatharam U. V. S. Physics of rotating and expanding black hole universe. *Progress in Physics*, 2010, v. 2, 7–14.
8. Glasman C. Precision measurements of alphas at HERA. arXiv: hep-ex/0506035.
9. Nambu Y. *Prog. Theor. Phys.*, 1952, v. 7, 595.
10. Quigg C. The electroweak theory. arXiv: hep-ph/0204104.
11. Koschmieder E. L. The mass and spin of the mesons, baryons and leptons. arXiv: physics/0408070.
12. Roy Chowdhury P. et al. Modified Bethe-Weizsacker mass formula with isotonic shift and new driplines. arXiv: nucl-th/0405080.
13. Myers W. D. et al. Table of nuclear masses according to the 1994 Thomas-Fermi model. http://nsdssd.lbl.gov
14. Audi G. and Wapstra A. H. The 1995 update to the atomic mass evaluation. *Nuclear Physics A*, 1995, v. 595, no. 4, 409–480; arXiv: 0903.5141.

SPECIAL REPORT

Relativity in Combinatorial Gravitational Fields

Linfan Mao
Chinese Academy of Mathematics and System Science,
Beijing 100080, P. R. China
E-mail: maolinfan@163.com

A combinatorial spacetime $(\mathscr{C}_G|\bar{t})$ is a smoothly combinatorial manifold $\mathscr{C}$ underlying a graph G evolving on a time vector $\bar{t}$. As we known, Einstein's general relativity is suitable for use only in one spacetime. *What is its disguise in a combinatorial spacetime*? Applying combinatorial Riemannian geometry enables us to present a combinatorial spacetime model for the Universe and suggest a generalized Einstein gravitational equation in such model. For finding its solutions, a generalized relativity principle, called *projective principle* is proposed, i.e., *a physics law in a combinatorial spacetime is invariant under a projection on its a subspace* and then a spherically symmetric multi-solutions of generalized Einstein gravitational equations in vacuum or charged body are found. We also consider the geometrical structure in such solutions with physical formations, and conclude that an ultimate theory for the Universe maybe established if all such spacetimes in $\mathbf{R}^3$. Otherwise, our theory is only an approximate theory and endless forever.

1 Combinatorial spacetimes

The multi-laterality of our Universe implies the best spacetime model should be a combinatorial one. However, classical spacetimes are all in solitude. For example, the Newton spacetime $(\mathbf{R}^3|t)$ is a geometrical space $(x_1, x_2, x_3) \in \mathbf{R}^3$ with an absolute time $t \in \mathbf{R}^+$. With his deep insight in physical laws, Einstein was aware of that all reference frames were established by human beings, which made him realized that *a physics law is invariant in any reference frame*. Whence, the Einstein spacetime is $(\mathbf{R}^3|t) \cong \mathbf{R}^4$ with $t \in \mathbf{R}^+$, i.e., a warped spacetime generating gravitation. In this kind of spacetime, its line element is

$$ds^2 = \sum_{0\leqslant\mu,\nu\leqslant 3} g_{\mu\nu}(\overline{x})dx_\mu dx_\nu\,,$$

where $g_{\mu\nu}$, $0 \leqslant \mu, \nu \leqslant 3$ are Riemannian metrics with local flat, i.e., the Minkowskian spacetime

$$ds^2 = -c^2dt^2 + dx_1^2 + dx_2^2 + dx_3^2\,,$$

where c is the light speed. *Wether the spacetime of Universe is isolated*? In fact, there are no justifications for Newton's or Einstein's choice but only dependent on mankind's perception with the geometry of visible, i.e., the spherical geometry(see [1–4] for details).

Certainly, different standpoints had unilaterally brought about particular behaviors of the Universe such as those of electricity, magnetism, thermal, optics... in physics and their combinations, for example, the thermodynamics, electromagnetism, ..., etc. But the true colours of the Universe should be hybrid, not homogeneous or unilateral. They should be a union or a combination of all these features underlying a combinatorial structure. That is the origin of combinatorial spacetime established on smoothly combinatorial manifolds following ([5–9]), a particular case of Smarandache multi-space ([10–11]) underlying a connected graph.

Definition 1.1 *Let $n_i, 1 \leqslant i \leqslant m$ be positive integers. A combinatorial Euclidean space is a combinatorial system $\mathscr{C}_G$ of Euclidean spaces $\mathbf{R}^{n_1}$, $\mathbf{R}^{n_2}$, $\cdots$, $\mathbf{R}^{n_m}$ underlying a connected graph G defined by*

$$V(G) = \{\mathbf{R}^{n_1}, \mathbf{R}^{n_2}, \cdots, \mathbf{R}^{n_m}\}\,,$$

$$E(G) = \{\,(\mathbf{R}^{n_i}, \mathbf{R}^{n_j}) \mid \mathbf{R}^{n_i} \bigcap \mathbf{R}^{n_j} \neq \emptyset, 1 \leqslant i, j \leqslant m\}\,,$$

denoted by $\mathscr{E}_G(n_1, \cdots, n_m)$ and abbreviated to $\mathscr{E}_G(r)$ if $n_1 = \cdots = n_m = r$.

A *combinatorial fan-space* $\widetilde{\mathbf{R}}(n_1, \cdots, n_m)$ is a combinatorial Euclidean space $\mathscr{E}_{K_m}(n_1, \cdots, n_m)$ of $\mathbf{R}^{n_1}$, $\mathbf{R}^{n_2}$, $\cdots$, $\mathbf{R}^{n_m}$ such that for any integers i, j, $1 \leqslant i \neq j \leqslant m$, $\mathbf{R}^{n_i} \bigcap \mathbf{R}^{n_j} = \bigcap_{k=1}^{m} \mathbf{R}^{n_k}$, which is in fact a *p-brane* with $p = \dim \bigcap_{k=1}^{m} \mathbf{R}^{n_k}$ in *string theory* ([12]), seeing Fig. 1.1 for details.

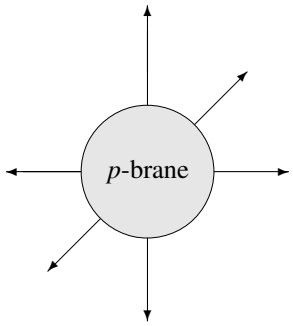

Fig. 1.1

For $\forall p \in \widetilde{\mathbf{R}}(n_1, \cdots, n_m)$ we can present it by an $m \times n_m$

coordinate matrix $[\overline{x}]$ following with $x_{il} = \dfrac{x_l}{m}$ for $1 \leqslant i \leqslant m, 1 \leqslant l \leqslant \widehat{m}$,

$$[\overline{x}] = \begin{bmatrix} x_{11} & \cdots & x_{1\widehat{m}} & \cdots & x_{1n_1} & \cdots & 0 \\ x_{21} & \cdots & x_{2\widehat{m}} & \cdots & x_{2n_2} & \cdots & 0 \\ \cdots & \cdots & \cdots & \cdots & \cdots & \cdots & \cdots \\ x_{m1} & \cdots & x_{m\widehat{m}} & \cdots & \cdots & \cdots & x_{mn_m} \end{bmatrix}.$$

A topological combinatorial manifold $\widetilde{M}$ is defined in the next.

Definition 1.2 *For a given integer sequence $0 < n_1 < n_2 < \cdots < n_m$, $m \geqslant 1$, a topological combinatorial manifold $\widetilde{M}$ is a Hausdorff space such that for any point $p \in \widetilde{M}$, there is a local chart (U_p, φ_p) of p, i.e., an open neighborhood U_p of p in $\widetilde{M}$ and a homeomorphism $\varphi_p : U_p \to \widetilde{\mathbf{R}}(n_1(p), \cdots, n_{s(p)}(p))$ with*

$$\{n_1(p), \cdots, n_{s(p)}(p)\} \subseteq \{n_1, \cdots, n_m\},$$
$$\bigcup_{p\in\widetilde{M}} \{n_1(p), \cdots, n_{s(p)}(p)\} = \{n_1, \cdots, n_m\},$$

denoted by $\widetilde{M}(n_1, n_2, \cdots, n_m)$ or $\widetilde{M}$ on the context and

$$\widetilde{\mathcal{A}} = \{(U_p, \varphi_p) | p \in \widetilde{M}(n_1, n_2, \cdots, n_m))\}$$

an atlas on $\widetilde{M}(n_1, n_2, \cdots, n_m)$.

A topological combinatorial manifold $\widetilde{M}$ is finite if it is just combined by finite manifolds without one manifold contained in the union of others.

For a finite combinatorial manifold $\widetilde{M}$ consisting of manifolds M_i, $1 \leqslant i \leqslant m$, we can construct a vertex-edge labeled graph $G^L[\widetilde{M}]$ defined by

$$V(G^L[\widetilde{M}]) = \{M_1, M_2, \cdots, M_m\},$$
$$E(G^L[\widetilde{M}) = \{ (M_i, M_j) \mid M_i \bigcap M_j \neq \emptyset, 1 \leqslant i, j \leqslant n\}$$

with a labeling mapping

$$\Theta : V(G^L[\widetilde{M}]) \bigcup E(G^L[\widetilde{M}]) \to \mathbf{Z}^+$$

determined by

$$\Theta(M_i) = \dim M_i, \quad \Theta(M_i, M_j) = \dim M_i \bigcap M_j$$

for integers $1 \leqslant i, j \leqslant m$, which is inherent structure of combinatorial manifolds. A differentiable combinatorial manifold is defined by endowing differential structure on a topological combinatorial manifold following.

Definition 1.3 *For a given integer sequence $1 \leqslant n_1 < n_2 < \cdots < n_m$, a combinatorial C^h-differential manifold $(\widetilde{M}(n_1, n_2 \cdots, n_m); \widetilde{\mathcal{A}})$ is a finite combinatorial manifold $\widetilde{M}(n_1, \cdots, n_m)$, $\widetilde{M}(n_1, \cdots, n_m) = \bigcup_{i\in I} U_i$, endowed with an atlas $\widetilde{\mathcal{A}} = \{(U_\alpha; \varphi_\alpha) | \alpha \in I\}$ on $\widetilde{M}(n_1, \cdots, n_m)$ for an integer $h, h \geqslant 1$ with conditions following hold.*

(1) *$\{U_\alpha; \alpha \in I\}$ is an open covering of $\widetilde{M}(n_1, n_2, \cdots, n_m)$.*

(2) *For $\forall \alpha, \beta \in I$, local charts $(U_\alpha; \varphi_\alpha)$ and $(U_\beta; \varphi_\beta)$ are equivalent, i.e., $U_\alpha \bigcap U_\beta = \emptyset$ or $U_\alpha \bigcap U_\beta \neq \emptyset$ but the overlap maps*

$$\varphi_\alpha\varphi_\beta^{-1} : \varphi_\beta(U_\alpha \bigcap U_\beta) \to \varphi_\beta(U_\beta),$$
$$\varphi_\beta\varphi_\alpha^{-1} : \varphi_\alpha(U_\alpha \bigcap U_\beta) \to \varphi_\alpha(U_\alpha)$$

both are C^h-mappings, such as those shown in Fig. 1.2 following.

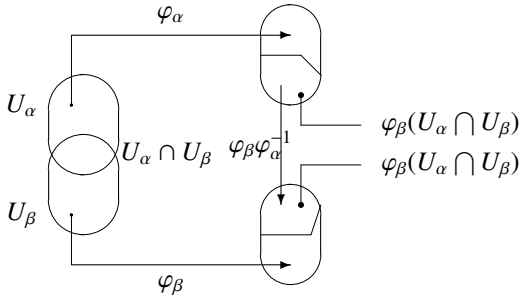

Fig. 1.2

(3) *$\widetilde{\mathcal{A}}$ is maximal, i.e., if $(U; \varphi)$ is a local chart of $\widetilde{M}(n_1, \cdots, n_m)$ equivalent with one of local charts in $\widetilde{\mathcal{A}}$, then $(U; \varphi) \in \widetilde{\mathcal{A}}$.*

A finite combinatorial manifold $\widetilde{M}(n_1, \cdots, n_m)$ is *smooth* if it is endowed with a C^∞-differential structure. Now we are in the place introducing combinatorial spacetime.

Definition 1.4 *A combinatorial spacetime $(\mathscr{C}_G|\bar{t})$ is a smooth combinatorial manifold $\mathscr{C}$ underlying a graph G evolving on a time vector $\bar{t}$, i.e., a geometrical space $\mathscr{C}$ with a time system $\bar{t}$ such that $(\overline{x}|\bar{t})$ is a particle's position at a time $\bar{t}$ for $\overline{x} \in \mathscr{C}$.*

The existence of combinatorial spacetime in the Universe is a wide-ranging, even if in the society science. By the explaining in the reference [13], there are four-level hierarchy of parallel universes analyzed by knowledge of mankind already known, such as those of *Hubble volumes, chaotic inflation, wavefunction* and *mathematical equations*, etc. Each level is allowed progressively greater diversity.

Question 1.5 *How to deal behaviors of these different combinatorial spacetimes definitely with mathematics, not only qualitatively?*

Recently, many researchers work for brane-world cosmology, particular for the case of dimensional $\leqslant 6$, such as those researches in references [14–18] and [3] etc. This brane-world model was also applied in [19] for explaining a black hole model for the Universe by combination. Notice

that the underlying combinatorial structure of brane-world cosmological model is essentially a tree for simplicity.

Now we have established a differential geometry on combinatorial manifolds in references [5–9], which provides us with a mathematical tool for determining the behavior of combinatorial spacetimes. The main purpose of this paper is to apply it to combinatorial gravitational fields combining with spacetime's characters, present a generalized relativity in combinatorial fields and use this principle to solve the gravitational field equations. We also discuss the consistency of this combinatorial model for the Universe with some observing data such as the cosmic microwave background (CMB) radiation by WMAP in 2003.

2 Curvature tensor on combinatorial manifolds

Applying combinatorial spacetimes to that of gravitational field needs us to introduce curvature tensor for measuring the warping of combinatorial manifolds. In this section, we explain conceptions with results appeared in references [5–8], which are applied in this paper.

First, the structure of tangent and cotangent spaces $T_p\widetilde{M}$, $T_p^*\widetilde{M}$ at any point $p \in \widetilde{M}$ in a smoothly combinatorial manifold $\widetilde{M}$ is similar to that of differentiable manifold. It has been shown in [5] that $\dim T_p\widetilde{M}(n_1, \cdots, n_m) = \widehat{s}(p) + \sum\limits_{i=1}^{s(p)} (n_i - \widehat{s}(p))$ and $\dim T_p^*\widetilde{M}(n_1, n_2, \cdots, n_m) = \widehat{s}(p) + \sum\limits_{i=1}^{s(p)} (n_i - \widehat{s}(p))$ with a basis

$$\left\{\frac{\partial}{\partial x^{i_0 j}}|_p | 1 \leqslant j \leqslant \widehat{s}(p)\right\} \bigcup \left(\bigcup_{i=1}^{s(p)} \left\{\frac{\partial}{\partial x^{ij}}|_p \mid \widehat{s}(p)+1 \leqslant j \leqslant n_i\right\}\right),$$

$$\{dx^{i_0 j}|_p | 1 \leqslant j \leqslant \widehat{s}(p)\} \bigcup \left(\bigcup_{i=1}^{s(p)} \{dx^{ij}|_p \mid \widehat{s}(p)+1 \leqslant j \leqslant n_i\}\right)$$

for any integer $i_0, 1 \leqslant i_0 \leqslant s(p)$, respectively. These mathematical structures enable us to construct tensors, connections on tensors and curvature tensors on smoothly combinatorial manifolds.

Definition 2.1 *Let $\widetilde{M}$ be a smoothly combinatorial manifold, $p \in \widetilde{M}$. A tensor of type (r, s) at the point p on $\widetilde{M}$ is an $(r+s)$-multilinear function τ,*

$$\tau : \underbrace{T_p^*\widetilde{M} \times \cdots \times T_p^*\widetilde{M}}_{r} \times \underbrace{T_p\widetilde{M} \times \cdots \times T_p\widetilde{M}}_{s} \to \mathbf{R}.$$

Let $\widetilde{M}(n_1, \cdots, n_m)$ be a smoothly combinatorial manifold. Denoted by $T_s^r(p, \widetilde{M})$ all tensors of type (r, s) at a point p of $\widetilde{M}(n_1, \cdots, n_m)$. Then for $\forall p \in \widetilde{M}(n_1, \cdots, n_m)$, we have known that

$$T_s^r(p, \widetilde{M}) = \underbrace{T_p\widetilde{M} \otimes \cdots \otimes T_p\widetilde{M}}_{r} \otimes \underbrace{T_p^*\widetilde{M} \otimes \cdots \otimes T_p^*\widetilde{M}}_{s},$$

where

$$T_p\widetilde{M} = T_p\widetilde{M}(n_1, \cdots, n_m),$$
$$T_p^*\widetilde{M} = T_p^*\widetilde{M}(n_1, \cdots, n_m),$$

particularly,

$$\dim T_s^r(p, \widetilde{M}) = \left(\widehat{s}(p) + \sum_{i=1}^{s(p)} (n_i - \widehat{s}(p))\right)^{r+s}$$

by argumentation in [5–7].

A connection on tensors of a smooth combinatorial manifold is defined by

Definition 2.2 *Let $\widetilde{M}$ be a smooth combinatorial manifold. A connection on tensors of $\widetilde{M}$ is a mapping $\widetilde{D} : \mathscr{X}(\widetilde{M}) \times T_s^r\widetilde{M} \to T_s^r\widetilde{M}$ with $\widetilde{D}_X\tau = \widetilde{D}(X, \tau)$ such that for $\forall X, Y \in \mathscr{X}\widetilde{M}$, $\tau, \pi \in T_s^r(\widetilde{M}), \lambda \in \mathbf{R}$ and $f \in C^\infty(\widetilde{M})$,*

(1) $\widetilde{D}_{X+fY}\tau = \widetilde{D}_X\tau + f\widetilde{D}_Y\tau$ and $\widetilde{D}_X(\tau + \lambda\pi) = \widetilde{D}_X\tau + \lambda\widetilde{D}_X\pi$;

(2) $\widetilde{D}_X(\tau \otimes \pi) = \widetilde{D}_X\tau \otimes \pi + \sigma \otimes \widetilde{D}_X\pi$;

(3) *for any contraction C on $T_s^r(\widetilde{M})$,*

$$\widetilde{D}_X(C(\tau)) = C(\widetilde{D}_X\tau).$$

For a smooth combinatorial manifold $\widetilde{M}$, we have shown in [5] that there always exists a connection $\widetilde{D}$ on $\widetilde{M}$ with coefficients $\Gamma^{\kappa\lambda}_{(\sigma\varsigma)(\mu\nu)}$ determined by

$$\widetilde{D}_{\frac{\partial}{\partial x^{\mu\nu}}} \frac{\partial}{\partial x^{\sigma\varsigma}} = \Gamma^{\kappa\lambda}_{(\sigma\varsigma)(\mu\nu)} \frac{\partial}{\partial x^{\sigma\varsigma}}.$$

A combinatorially connection space $(\widetilde{M}, \widetilde{D})$ is a smooth combinatorial manifold $\widetilde{M}$ with a connection $\widetilde{D}$.

Definition 2.3 *Let $\widetilde{M}$ be a smoothly combinatorial manifold and $g \in A^2(\widetilde{M}) = \bigcup\limits_{p \in \widetilde{M}} T_2^0(p, \widetilde{M})$. If g is symmetrical and positive, then $\widetilde{M}$ is called a combinatorially Riemannian manifold, denoted by $(\widetilde{M}, g)$. In this case, if there is also a connection $\widetilde{D}$ on $(\widetilde{M}, g)$ with equality following hold*

$$Z(g(X, Y)) = g(\widetilde{D}_Z, Y) + g(X, \widetilde{D}_Z Y),$$

then $\widetilde{M}$ is called a combinatorially Riemannian geometry, denoted by $(\widetilde{M}, g, \widetilde{D})$.

It has been proved in [5] and [7] that there exists a unique connection $\widetilde{D}$ on $(\widetilde{M}, g)$ such that $(\widetilde{M}, g, \widetilde{D})$ is a combinatorially Riemannian geometry.

Definition 2.4 *Let $(\widetilde{M}, \widetilde{D})$ be a combinatorially connection space. For $\forall X, Y \in \mathscr{X}(\widetilde{M})$, a combinatorially curvature operator $\widetilde{\mathcal{R}}(X, Y) : \mathscr{X}(\widetilde{M}) \to \mathscr{X}(\widetilde{M})$ is defined by*

$$\widetilde{\mathcal{R}}(X, Y)Z = \widetilde{D}_X\widetilde{D}_Y Z - \widetilde{D}_Y\widetilde{D}_X Z - \widetilde{D}_{[X,Y]}Z$$

for $\forall Z \in \mathscr{X}(\widetilde{M})$.

Definition 2.5 *Let $(\widetilde{M}, \widetilde{D})$ be a combinatorially connection space. For $\forall X, Y, Z \in \mathscr{X}(\widetilde{M})$, a linear multi-mapping $\widetilde{\mathcal{R}} : \mathscr{X}(\widetilde{M}) \times \mathscr{X}(\widetilde{M}) \times \mathscr{X}(\widetilde{M}) \to \mathscr{X}(\widetilde{M})$ determined by*

$$\widetilde{\mathcal{R}}(Z, X, Y) = \widetilde{\mathcal{R}}(X, Y)Z$$

is said a curvature tensor of type $(1, 3)$ *on* $(\widetilde{M}, \widetilde{D})$.

Calculation in [7] shows that for $\forall p \in \widetilde{M}$ with a local chart $(U_p; [\varphi_p])$,

$$\widetilde{\mathcal{R}} = \widetilde{\mathcal{R}}^{\eta\theta}_{(\sigma\varsigma)(\mu\nu)(\kappa\lambda)} dx^{\sigma\varsigma} \otimes \frac{\partial}{\partial x^{\eta\theta}} \otimes dx^{\mu\nu} \otimes dx^{\kappa\lambda}$$

with

$$\widetilde{\mathcal{R}}^{\eta\theta}_{(\sigma\varsigma)(\mu\nu)(\kappa\lambda)} = \left(\frac{\partial \Gamma^{\eta\theta}_{(\sigma\varsigma)(\kappa\lambda)}}{\partial x^{\mu\nu}} - \frac{\partial \Gamma^{\eta\theta}_{(\sigma\varsigma)(\mu\nu)}}{\partial x^{\kappa\lambda}} + \right.$$
$$\left. + \Gamma^{\vartheta\iota}_{(\sigma\varsigma)(\kappa\lambda)} \Gamma^{\eta\theta}_{(\vartheta\iota)(\mu\nu)} - \Gamma^{\vartheta\iota}_{(\sigma\varsigma)(\mu\nu)} \Gamma^{\eta\theta}_{(\vartheta\iota)(\kappa\lambda)} \right) \frac{\partial}{\partial x^{\vartheta\iota}} ,$$

where $\Gamma^{\sigma\varsigma}_{(\mu\nu)(\kappa\lambda)} \in C^\infty(U_p)$ is determined by

$$\widetilde{D}_{\frac{\partial}{\partial x^{\mu\nu}}} \frac{\partial}{\partial x^{\kappa\lambda}} = \Gamma^{\sigma\varsigma}_{(\kappa\lambda)(\mu\nu)} \frac{\partial}{\partial x^{\sigma\varsigma}} .$$

Particularly, if $(\widetilde{M}, g, \widetilde{D})$ is a combinatorially Riemannian geometry, we know the combinatorially Riemannian curvature tensor in the following.

Definition 2.6 *Let $(\widetilde{M}, g, \widetilde{D})$ be a combinatorially Riemannian manifold. A combinatorially Riemannian curvature tensor $\widetilde{R} : \mathscr{X}(\widetilde{M}) \times \mathscr{X}(\widetilde{M}) \times \mathscr{X}(\widetilde{M}) \times \mathscr{X}(\widetilde{M}) \to C^\infty(\widetilde{M})$ of type* $(0, 4)$ *is defined by*

$$\widetilde{R}(X, Y, Z, W) = g(\widetilde{R}(Z, W)X, Y)$$

for $\forall X, Y, Z, W \in \mathscr{X}(\widetilde{M})$.

Now let $(\widetilde{M}, g, \widetilde{D})$ be a combinatorially Riemannian manifold. For $\forall p \in \widetilde{M}$ with a local chart $(U_p; [\varphi_p])$, we have known that ([8])

$$\widetilde{R} = \widetilde{R}_{(\sigma\varsigma)(\eta\theta)(\mu\nu)(\kappa\lambda)} dx^{\sigma\varsigma} \otimes dx^{\eta\theta} \otimes dx^{\mu\nu} \otimes dx^{\kappa\lambda}$$

with

$$\widetilde{R}_{(\sigma\varsigma)(\eta\theta)(\mu\nu)(\kappa\lambda)} = \frac{1}{2} \left(\frac{\partial^2 g_{(\mu\nu)(\sigma\varsigma)}}{\partial x^{\kappa\lambda} \partial x^{\eta\theta}} + \frac{\partial^2 g_{(\kappa\lambda)(\eta\theta)}}{\partial x^{\mu\nu\nu} \partial x^{\sigma\varsigma}} - \right.$$
$$\left. - \frac{\partial^2 g_{(\mu\nu)(\eta\theta)}}{\partial x^{\kappa\lambda} \partial x^{\sigma\varsigma}} - \frac{\partial^2 g_{(\kappa\lambda)(\sigma\varsigma)}}{\partial x^{\mu\nu} \partial x^{\eta\theta}} \right) + \Gamma^{\vartheta\iota}_{(\mu\nu)(\sigma\varsigma)} \Gamma^{\xi o}_{(\kappa\lambda)(\eta\theta)} g_{(\xi o)(\vartheta\iota)} -$$
$$- \Gamma^{\xi o}_{(\mu\nu)(\eta\theta)} \Gamma_{(\kappa\lambda)(\sigma\varsigma)^{\vartheta\iota}} g_{(\xi o)(\vartheta\iota)} ,$$

where $g_{(\mu\nu)(\kappa\lambda)} = g\left(\frac{\partial}{\partial x^{\mu\nu}}, \frac{\partial}{\partial x^{\kappa\lambda}} \right)$.

Application of these mechanisms in Definitions 2.1–2.6 with results obtained in references [5–9], [20–23] enables us to find physical laws in combinatorial spacetimes by mathematical equations, and then find their multi-solutions in following sections.

3 Combinatorial gravitational fields

3.1 Gravitational equations

The essence in Einstein's notion on the gravitational field is known in two principles following.

Principle 3.1 *These gravitational forces and inertial forces acting on a particle in a gravitational field are equivalent and indistinguishable from each other.*

Principle 3.2 *An equation describing a law of physics should have the same form in all reference frame.*

By Principle 3.1, one can introduce inertial coordinate system in Einstein's spacetime which enables it flat locally, i.e., transfer these Riemannian metrics to Minkowskian ones and eliminate the gravitational forces locally. Principle 3.2 means that a physical equation should be a tensor equation. But *how about the combinatorial gravitational field*? We assume Principles 3.1 and 3.2 hold in this case, i.e., a physical law is characterized by a tensor equation. This assumption enables us to deduce the gravitational field equation following.

Let $\mathscr{L}_{G^L[\widetilde{M}]}$ be the Lagrange density of a combinatorial spacetime $(\mathscr{C}_G|\bar{t})$. Then we know equations of the combinatorial gravitational field $(\mathscr{C}_G|\bar{t})$ to be

$$\partial_\mu \frac{\partial \mathscr{L}_{G^L[\widetilde{M}]}}{\partial \partial_\mu \phi_{\widetilde{M}}} - \frac{\partial \mathscr{L}_{G^L[\widetilde{M}]}}{\partial \phi_{\widetilde{M}}} = 0 , \tag{3.1}$$

by the Euler-Lagrange equation, where $\phi_{\widetilde{M}}$ is the wave function of $(\mathscr{C}_G|\bar{t})$. Choose its Lagrange density $\mathscr{L}_{G^L[\widetilde{M}]}$ to be

$$\mathscr{L}_{G^L[\widetilde{M}]} = \widetilde{R} - 2\kappa \mathscr{L}_F ,$$

where $\kappa = -8\pi G$ and $\mathscr{L}_F$ the Lagrange density for all other fields with

$$\widetilde{R} = g^{(\mu\nu)(\kappa\lambda)} \widetilde{R}_{(\mu\nu)(\kappa\lambda)}, \quad \widetilde{R}_{(\mu\nu)(\kappa\lambda)} = \widetilde{R}^{\sigma\varsigma}_{(\mu\nu)(\sigma\varsigma)(\kappa\lambda)} .$$

Applying the Euler-Lagrange equation we get the equation of combinatorial gravitational field following

$$\widetilde{\mathcal{R}}_{(\mu\nu)(\kappa\lambda)} - \frac{1}{2} \widetilde{R}\, g_{(\mu\nu)(\kappa\lambda)} = \kappa \mathscr{E}_{(\mu\nu)(\kappa\lambda)} , \tag{3.2}$$

where $\mathscr{E}_{(\mu\nu)(\kappa\lambda)}$ is the energy-momentum tensor.

The situation for combinatorial gravitational field is a little different from classical field by its combinatorial character with that one can only determines unilateral or part behaviors of the field. We generalize the Einstein notion to combinatorial gravitational field by the following projective principle, which is coordinated with one's observation.

Principle 3.3 *A physics law in a combinatorial field is invariant under a projection on its a field.*

By Principles 3.1 and 3.2 with combinatorial differential geometry shown in Section 2, Principle 3.3 can be rephrased as follows.

Projective principle *Let $(\widetilde{M}, g, \widetilde{D})$ be a combinatorial Riemannian manifold and $\mathscr{F} \in T^r_s(\widetilde{M})$ with a local form*

$$\mathscr{F}^{(\kappa_1\lambda_1)\cdots(\kappa_r\lambda_r)}_{(\mu_1\nu_1)\cdots(\mu_s\nu_s)} e_{\kappa_1\lambda_1} \otimes \cdots \otimes e_{\kappa_r\lambda_r} \omega^{\mu_1\nu_1} \otimes \cdots \otimes \omega^{\mu_s\nu_s}$$

in $(U_p, [\varphi_p])$. If

$$\mathscr{F}^{(\kappa_1\lambda_1)\cdots(\kappa_r\lambda_r)}_{(\mu_1\nu_1)\cdots(\mu_s\nu_s)} = 0$$

for integers $1 \leqslant \mu_i \leqslant s(p), 1 \leqslant \nu_i \leqslant n_{\mu_i}$ with $1 \leqslant i \leqslant s$ and $1 \leqslant \kappa_j \leqslant s(p), 1 \leqslant \lambda_j \leqslant n_{\kappa_j}$ with $1 \leqslant j \leqslant r$, then for any integer $\mu, 1 \leqslant \mu \leqslant s(p)$, there must be

$$\mathscr{F}^{(\mu\lambda_1)\cdots(\mu\lambda_r)}_{(\mu\nu_1)\cdots(\mu\nu_s)} = 0$$

for integers ν_i, $1 \leqslant \nu_i \leqslant n_\mu$ with $1 \leqslant i \leqslant s$.

Certainly, we can only determine the behavior of space which we live. Then *what is about these other spaces in* $(\mathscr{C}_G|\bar{t})$? Applying the projective principle, we can simulate each of them by that of our living space. In other words, combining geometrical structures already known to a combinatorial one $(\mathscr{C}_G|\bar{t})$ and then find its solution for equation (3.2).

3.2 Combinatorial metric

Let $\widetilde{\mathcal{A}}$ be an atlas on $(\widetilde{M}, g, \widetilde{D})$. Choose a local chart $(U; \varpi)$ in $\widetilde{\mathcal{A}}$. By definition, if $\varphi_p : U_p \to \bigcup_{i=1}^{s(p)} B^{n_i(p)}$ and $\widehat{s}(p) = \dim(\bigcap_{i=1}^{s(p)} B^{n_i(p)})$, then $[\varphi_p]$ is an $s(p) \times n_{s(p)}$ matrix. A *combinatorial metric* is defined by

$$ds^2 = g_{(\mu\nu)(\kappa\lambda)} dx^{\mu\nu} dx^{\kappa\lambda}, \tag{3.3}$$

where $g_{(\mu\nu)(\kappa\lambda)}$ is the Riemannian metric in the combinatorially Riemannian manifold $(\widetilde{M}, g, \widetilde{D})$. Generally, we choose a orthogonal basis

$$\{\overline{e}_{11}, \cdots, \overline{e}_{1n_1}, \cdots, \overline{e}_{s(p)n_{s(p)}}\}$$

for $\varphi_p[U]$, $p \in \widetilde{M}(t)$, i.e., $\left\langle \overline{e}_{\mu\nu}, \overline{e}_{\kappa\lambda} \right\rangle = \delta^{(\kappa\lambda)}_{(\mu\nu)}$. Then the formula (3.3) turns to

$$\begin{aligned} ds^2 &= g_{(\mu\nu)(\mu\nu)}(dx^{\mu\nu})^2 \\ &= \sum_{\mu=1}^{s(p)} \sum_{\nu=1}^{\widehat{s}(p)} g_{(\mu\nu)(\mu\nu)} (dx^{\mu\nu})^2 + \\ &\quad + \sum_{\mu=1}^{s(p)} \sum_{\nu=1}^{\widehat{s}(p)+1} g_{(\mu\nu)(\mu\nu)} (dx^{\mu\nu})^2 \\ &= \frac{1}{s^2(p)} \sum_{\nu=1}^{\widehat{s}(p)} \left(\sum_{\mu=1}^{s(p)} g_{(\mu\nu)(\mu\nu)} \right) dx^\nu + \\ &\quad + \sum_{\mu=1}^{s(p)} \sum_{\nu=1}^{\widehat{s}(p)+1} g_{(\mu\nu)(\mu\nu)} (dx^{\mu\nu})^2 . \end{aligned}$$

We therefore find an important relation of combinatorial metric with that of its projections following.

Theorem 3.1 *Let ${}_\mu ds^2$ be the metric in a manifold $\phi_p^{-1}(B^{n_\mu(p)})$ for integers $1 \leqslant \mu \leqslant s(p)$. Then*

$$ds^2 = {}_1ds^2 + {}_2ds^2 + \cdots + {}_{s(p)}ds^2 .$$

Proof Applying the projective principle, we immediately know that

$${}_\mu ds^2 = ds^2|_{\phi_p^{-1}(B^{n_\mu(p)})}, \qquad 1 \leqslant \mu \leqslant s(p) .$$

Whence, we find that

$$\begin{aligned} ds^2 &= g_{(\mu\nu)(\mu\nu)} (dx^{\mu\nu})^2 \\ &= \sum_{\mu=1}^{s(p)} \sum_{\nu=1}^{n_i(p)} g_{(\mu\nu)(\mu\nu)} (dx^{\mu\nu})^2 \\ &= \sum_{\mu=1}^{s(p)} ds^2|_{\phi_p^{-1}(B^{n_\mu(p)})} = \sum_{\mu=1}^{s(p)} {}_\mu ds^2 . \end{aligned}$$

□

This relation enables us to find the line element of combinatorial gravitational field $(\mathscr{C}_G|\bar{t})$ by applying that of gravitational fields.

3.3 Combinatorial Schwarzschild metric

Let $(\mathscr{C}_G|\bar{t})$ be a gravitational field. We know its Schwarzschild metric, i.e., a spherically symmetric solution of Einstein's gravitational equations in vacuum is

$$\begin{aligned} ds^2 &= \left(1 - \frac{r_s}{r}\right) dt^2 - \frac{dr^2}{1 - \frac{r_s}{r}} - \\ &\quad - r^2 d\theta^2 - r^2 \sin^2\theta d\phi^2 , \end{aligned} \tag{3.4}$$

where $r_s = 2Gm/c^2$. Now we generalize it to combinatorial gravitational fields to find the solutions of equations

$$R_{(\mu\nu)(\sigma\tau)} - \frac{1}{2} g_{(\mu\nu)(\sigma\tau)} R = -8\pi G \mathscr{E}_{(\mu\nu)(\sigma\tau)}$$

in vacuum, i.e., $\mathscr{E}_{(\mu\nu)(\sigma\tau)} = 0$. Notice that the underlying graph of combinatorial field consisting of m gravitational fields is a complete graph K_m. For such a objective, we only consider the homogeneous combinatorial Euclidean spaces $\widetilde{M} = \bigcup_{i=1}^m \mathbf{R}^{n_i}$, i.e., for any point $p \in \widetilde{M}$,

$$[\varphi_p] = \begin{bmatrix} x^{11} & \cdots & x^{1n_1} & \cdots & 0 \\ x^{21} & \cdots & x^{2n_2} & \cdots & 0 \\ \cdots & \cdots & \cdots & \cdots & \cdots \\ x^{m1} & \cdots & \cdots & \cdots & x^{mn_m} \end{bmatrix}$$

with $\widehat{m} = \dim(\bigcap_{i=1}^m \mathbf{R}^{n_i})$ a constant for $\forall p \in \bigcap_{i=1}^m \mathbf{R}^{n_i}$ and $x^{il} = \frac{x^l}{m}$ for $1 \leqslant i \leqslant m, 1 \leq l \leqslant \widehat{m}$.

Let $(\mathscr{C}_G|\bar{t})$ be a combinatorial field of gravitational fields $M_1, \cdots, M_m$ with masses $m_1, \cdots, m_m$ respectively. For usually undergoing, we consider the case of $n_\mu = 4$ for $1 \leqslant \mu \leqslant m$ since line elements have been found concretely in classical gravitational field in these cases. Now establish m spherical coordinate subframe $(t_\mu; r_\mu, \theta_\mu, \phi_\mu)$ with its originality at the center of such a mass space. Then we have known its a spherically symmetric solution by (3.4) to be

$$\begin{aligned} ds_\mu^2 &= \left(1-\frac{r_{\mu s}}{r_\mu}\right)dt_\mu^2 - \left(1-\frac{r_{\mu s}}{r_\mu}\right)^{-1} dr_\mu^2 - \\ &\quad - r_\mu^2(d\theta_\mu^2 + \sin^2\theta_\mu d\phi_\mu^2) \end{aligned}$$

for $1 \leqslant \mu \leqslant m$ with $r_{\mu s} = 2Gm_\mu/c^2$. By Theorem 3.1, we know that

$$ds^2 = {}_1ds^2 + {}_2ds^2 + \cdots + {}_mds^2\,,$$

where ${}_\mu ds^2 = ds_\mu^2$ by the projective principle on combinatorial fields. Notice that $1 \leqslant \widehat{m} \leqslant 4$. We therefore get the geometrical of $(\mathscr{C}_G|\bar{t})$ dependent on $\widehat{m}$ following.

Case 1. *$\widehat{m} = 1$, i.e., $t_\mu = t$ for $1 \leqslant \mu \leqslant m$.*

In this case, the combinatorial metric ds is

$$\begin{aligned} ds^2 &= \sum_{\mu=1}^m \left(1-\frac{2Gm_\mu}{c^2 r_\mu}\right)dt^2 - \\ &\quad - \sum_{\mu=1}^m \left(1-\frac{2Gm_\mu}{c^2 r_\mu}\right)^{-1} dr_\mu^2 - \\ &\quad - \sum_{\mu=1}^m r_\mu^2\left(d\theta_\mu^2 + \sin^2\theta_\mu d\phi_\mu^2\right). \end{aligned}$$

Case 2. *$\widehat{m} = 2$, i.e., $t_\mu = t$ and $r_\mu = r$, or $t_\mu = t$ and $\theta_\mu = \theta$, or $t_\mu = t$ and $\phi_\mu = \phi$ for $1 \leqslant \mu \leqslant m$.*

We consider the following subcases.

Subcase 2.1. *$t_\mu = t$, $r_\mu = r$.*

In this subcase, the combinatorial metric is

$$\begin{aligned} ds^2 &= \sum_{\mu=1}^m \left(1-\frac{2Gm_\mu}{c^2 r}\right)dt^2 - \\ &\quad - \left(\sum_{\mu=1}^m \left(1-\frac{2Gm_\mu}{c^2 r}\right)^{-1}\right)dr^2 - \\ &\quad - \sum_{\mu=1}^m r^2\left(d\theta_\mu^2 + \sin^2\theta_\mu d\phi_\mu^2\right), \end{aligned}$$

which can only happens if these m fields are at a same point O in a space. Particularly, if $m_\mu = M$ for $1 \leqslant \mu \leqslant m$, the masses of $M_1, M_2, \cdots, M_m$ are the same, then $r_{\mu g} = 2GM$ is a constant, which enables us knowing that

$$\begin{aligned} ds^2 &= \left(1-\frac{2GM}{c^2 r}\right)mdt^2 - \\ &\quad - \left(1-\frac{2GM}{c^2 r}\right)^{-1} mdr^2 - \\ &\quad - \sum_{\mu=1}^m r^2\left(d\theta_\mu^2 + \sin^2\theta_\mu d\phi_\mu^2\right). \end{aligned}$$

Subcase 2.2. *$t_\mu = t$, $\theta_\mu = \theta$.*

In this subcase, the combinatorial metric is

$$\begin{aligned} ds^2 &= \sum_{\mu=1}^m \left(1-\frac{2Gm_\mu}{c^2 r_\mu}\right)dt^2 - \\ &\quad - \sum_{\mu=1}^m \left(1-\frac{2Gm_\mu}{c^2 r_\mu}\right)^{-1} dr_\mu^2 - \\ &\quad - \sum_{\mu=1}^m r_\mu^2\left(d\theta^2 + \sin^2\theta d\phi_\mu^2\right). \end{aligned}$$

Subcase 2.3. *$t_\mu = t$, $\phi_\mu = \phi$.*

In this subcase, the combinatorial metric is

$$\begin{aligned} ds^2 &= \sum_{\mu=1}^m \left(1-\frac{2Gm_\mu}{c^2 r_\mu}\right)dt^2 - \\ &\quad - \left(\sum_{\mu=1}^m \left(1-\frac{2Gm_\mu}{c^2 r_\mu}\right)^{-1}\right)dr_\mu^2 - \\ &\quad - \sum_{\mu=1}^m r_\mu^2\left(d\theta_\mu^2 + \sin^2\theta_\mu d\phi^2\right). \end{aligned}$$

Case 3. *$\widehat{m} = 3$, i.e., $t_\mu = t$, $r_\mu = r$ and $\theta_\mu = \theta$, or $t_\mu = t$, $r_\mu = r$ and $\phi_\mu = \phi$, or $t_\mu = t$, $\theta_\mu = \theta$ and $\phi_\mu = \phi$ for $1 \leqslant \mu \leqslant m$.*

We consider three subcases following.

Subcase 3.1. *$t_\mu = t$, $r_\mu = r$ and $\theta_\mu = \theta$.*

In this subcase, the combinatorial metric is

$$\begin{aligned} ds^2 &= \sum_{\mu=1}^m \left(1-\frac{2Gm_\mu}{c^2 r}\right)dt^2 - \\ &\quad - \sum_{\mu=1}^m \left(1-\frac{2Gm_\mu}{c^2 r}\right)^{-1} dr^2 - \\ &\quad - mr^2 d\theta^2 - r^2\sin^2\theta \sum_{\mu=1}^m d\phi_\mu^2\,. \end{aligned}$$

Subcase 3.2. *$t_\mu = t$, $r_\mu = r$ and $\phi_\mu = \phi$.*

In this subcase, the combinatorial metric is

$$\begin{aligned} ds^2 &= \sum_{\mu=1}^{m}\left(1-\frac{2Gm_\mu}{c^2r}\right)dt^2 - \\ &\quad -\sum_{\mu=1}^{m}\left(1-\frac{2Gm_\mu}{c^2r}\right)^{-1}dr^2 - \\ &\quad -r^2\sum_{\mu=1}^{m}\left(d\theta_\mu^2+\sin^2\theta_\mu d\phi^2\right). \end{aligned}$$

There subcases 3.1 and 3.2 can be only happen if the centers of these m fields are at a same point O in a space.

Subcase 3.3. *$t_\mu = t$, $\theta_\mu = \theta$ and $\phi_\mu = \phi$.*

In this subcase, the combinatorial metric is

$$\begin{aligned} ds^2 &= \sum_{\mu=1}^{m}\left(1-\frac{2Gm_\mu}{c^2r_\mu}\right)dt^2 - \\ &\quad -\sum_{\mu=1}^{m}\left(1-\frac{2Gm_\mu}{c^2r_\mu}\right)^{-1}dr_\mu^2 - \\ &\quad -\sum_{\mu=1}^{m}r_\mu\left(d\theta^2+\sin^2\theta d\phi^2\right). \end{aligned}$$

Case 4. *$\widehat{m} = 4$, i.e., $t_\mu = t$, $r_\mu = r$, $\theta_\mu = \theta$ and $\phi_\mu = \phi$ for $1 \leqslant \mu \leqslant m$.*

In this subcase, the combinatorial metric is

$$\begin{aligned} ds^2 &= \sum_{\mu=1}^{m}\left(1-\frac{2Gm_\mu}{c^2r}\right)dt^2 - \\ &\quad -\sum_{\mu=1}^{m}\left(1-\frac{2Gm_\mu}{c^2r}\right)^{-1}dr^2 - \\ &\quad -mr^2\left(d\theta^2+\sin^2\theta d\phi^2\right). \end{aligned}$$

Particularly, if $m_\mu = M$ for $1 \leqslant \mu \leqslant m$, we get that

$$\begin{aligned} ds^2 &= \left(1-\frac{2GM}{c^2r}\right)mdt^2 - \\ &\quad -\left(1-\frac{2GM}{c^2r}\right)^{-1}mdr^2 - \\ &\quad -mr^2\left(d\theta^2+\sin^2\theta d\phi^2\right). \end{aligned}$$

Define a coordinate transformation

$$(t, r, \theta, \phi) \to ({}_st,\ {}_sr,\ {}_s\theta,\ {}_s\phi) = (t\sqrt{m}, r\sqrt{m}, \theta, \phi).$$

Then the previous formula turns to

$$\begin{aligned} ds^2 &= \left(1-\frac{2GM}{c^2r}\right)d_st^2 - \frac{d_sr^2}{1-\frac{2GM}{c^2r}} - \\ &\quad -{}_sr^2\left(d_s\theta^2+\sin^2{}_s\theta d_s\phi^2\right) \end{aligned}$$

in this new coordinate system $({}_st,\ {}_sr,\ {}_s\theta,\ {}_s\phi)$, whose geometrical behavior likes that of the gravitational field.

3.4 Combinatorial Reissner-Nordström metric

The Schwarzschild metric is a spherically symmetric solution of the Einstein gravitational equations in conditions $\mathscr{E}_{(\mu\nu)(\sigma\tau)} = 0$. In some special cases, we can also find their solutions for the case $\mathscr{E}_{(\mu\nu)(\sigma\tau)} \neq 0$. The *Reissner-Nordström metric* is such a case with

$$\mathscr{E}_{(\mu\nu)(\sigma\tau)} = \frac{1}{4\pi}\left(\frac{1}{4}\,g_{\mu\nu}F_{\alpha\beta}F^{\alpha\beta} - F_{\mu\alpha}F^{\alpha}_{\nu}\right)$$

in the Maxwell field with total mass m and total charge e, where $F_{\alpha\beta}$ and $F^{\alpha\beta}$ are given in Subsection 7.3.4. Its metrics takes the following form:

$$g_{\mu\nu} = \begin{bmatrix} x_{11} & 0 & 0 & 0 \\ 0 & x_{22} & 0 & 0 \\ 0 & 0 & -r^2 & 0 \\ 0 & 0 & 0 & -r^2\sin^2\theta \end{bmatrix},$$

where $r_s = 2Gm/c^2$, $r_e^2 = 4G\pi e^2/c^4$, $x_{11} = 1 - \dfrac{r_s}{r} + \dfrac{r_e^2}{r^2}$ and $x_{22} = -\left(1 - \dfrac{r_s}{r} + \dfrac{r_e^2}{r^2}\right)^{-1}$. In this case, its line element ds is given by

$$\begin{aligned} ds^2 &= \left(1-\frac{r_s}{r}+\frac{r_e^2}{r^2}\right)dt^2 - \\ &\quad -\left(1-\frac{r_s}{r}+\frac{r_e^2}{r^2}\right)^{-1}dr^2 - \\ &\quad -r^2\left(d\theta^2+\sin^2\theta d\phi^2\right). \end{aligned} \tag{3.5}$$

Obviously, if $e = 0$, i.e., there are no charges in the gravitational field, then the equations (3.5) turns to that of the Schwarzschild metric (3.4).

Now let $(\mathscr{C}_G|\bar{t})$ be a combinatorial field of charged gravitational fields $M_1, M_2, \cdots, M_m$ with masses $m_1, m_2, \cdots, m_m$ and charges $e_1, e_2, \cdots, e_m$, respectively. Similar to the case of Schwarzschild metric, we consider the case of $n_\mu = 4$ for $1 \leqslant \mu \leqslant m$. We establish m spherical coordinate subframe $(t_\mu; r_\mu, \theta_\mu, \phi_\mu)$ with its originality at the center of such a mass space. Then we know its a spherically symmetric solution by (3.5) to be

$$\begin{aligned} ds_\mu^2 &= \left(1-\frac{r_{\mu s}}{r_\mu}+\frac{r_{\mu e}^2}{r_\mu^2}\right)dt_\mu^2 - \\ &\quad -\left(1-\frac{r_{\mu s}}{r_\mu}+\frac{r_{\mu e}^2}{r_\mu^2}\right)^{-1}dr_\mu^2 - \\ &\quad -r_\mu^2\left(d\theta_\mu^2+\sin^2\theta_\mu d\phi_\mu^2\right). \end{aligned}$$

Likewise the case of Schwarzschild metric, we consider combinatorial fields of charged gravitational fields dependent on the intersection dimension $\widehat{m}$ following.

Case 1. $\widehat{m} = 1$, *i.e.,* $t_\mu = t$ *for* $1 \leqslant \mu \leqslant m$.

In this case, by applying Theorem 3.1 we get the combinatorial metric

$$\begin{aligned} ds^2 &= \sum_{\mu=1}^{m}\left(1-\frac{r_{\mu s}}{r_\mu}+\frac{r_{\mu e}^2}{r_\mu^2}\right)dt^2- \\ &\quad -\sum_{\mu=1}^{m}\left(1-\frac{r_{\mu s}}{r_\mu}+\frac{r_{\mu e}^2}{r_\mu^2}\right)^{-1}dr_\mu^2- \\ &\quad -\sum_{\mu=1}^{m} r_\mu^2\left(d\theta_\mu^2+\sin^2\theta_\mu d\phi_\mu^2\right). \end{aligned}$$

Case 2. $\widehat{m} = 2$, *i.e.,* $t_\mu = t$ *and* $r_\mu = r$, *or* $t_\mu = t$ *and* $\theta_\mu = \theta$, *or* $t_\mu = t$ *and* $\phi_\mu = \phi$ *for* $1 \leqslant \mu \leqslant m$.

Consider the following three subcases.

Subcase 2.1. $t_\mu = t$, $r_\mu = r$.

In this subcase, the combinatorial metric is

$$\begin{aligned} ds^2 &= \sum_{\mu=1}^{m}\left(1-\frac{r_{\mu s}}{r}+\frac{r_{\mu e}^2}{r^2}\right)dt^2- \\ &\quad -\sum_{\mu=1}^{m}\left(1-\frac{r_{\mu s}}{r}+\frac{r_{\mu e}^2}{r^2}\right)^{-1}dr^2- \\ &\quad -\sum_{\mu=1}^{m} r^2\left(d\theta_\mu^2+\sin^2\theta_\mu d\phi_\mu^2\right), \end{aligned}$$

which can only happens if these m fields are at a same point O in a space. Particularly, if $m_\mu = M$ and $e_\mu = e$ for $1 \leqslant \mu \leqslant m$, we find that

$$\begin{aligned} ds^2 &= \left(1-\frac{2GM}{c^2 r}+\frac{4\pi G e^4}{c^4 r^2}\right)mdt^2- \\ &\quad -\frac{mdr^2}{1-\frac{2GM}{c^2 r}+\frac{4\pi G e^4}{c^4 r^2}}- \\ &\quad -\sum_{\mu=1}^{m} r^2\left(d\theta_\mu^2+\sin^2\theta_\mu d\phi_\mu^2\right). \end{aligned}$$

Subcase 2.2. $t_\mu = t$, $\theta_\mu = \theta$.

In this subcase, by applying Theorem 3.1 we know that the combinatorial metric is

$$\begin{aligned} ds^2 &= \sum_{\mu=1}^{m}\left(1-\frac{r_{\mu s}}{r_\mu}+\frac{r_{\mu e}^2}{r_\mu^2}\right)dt^2- \\ &\quad -\sum_{\mu=1}^{m}\left(1-\frac{r_{\mu s}}{r_\mu}+\frac{r_{\mu e}^2}{r_\mu^2}\right)^{-1}dr_\mu^2- \\ &\quad -\sum_{\mu=1}^{m} r_\mu^2\left(d\theta^2+\sin^2\theta d\phi_\mu^2\right). \end{aligned}$$

Subcase 2.3. $t_\mu = t$, $\phi_\mu = \phi$.

In this subcase, we know that the combinatorial metric is

$$\begin{aligned} ds^2 &= \sum_{\mu=1}^{m}\left(1-\frac{r_{\mu s}}{r_\mu}+\frac{r_{\mu e}^2}{r_\mu^2}\right)dt^2- \\ &\quad -\sum_{\mu=1}^{m}\left(1-\frac{r_{\mu s}}{r_\mu}+\frac{r_{\mu e}^2}{r_\mu^2}\right)^{-1}dr_\mu^2- \\ &\quad -\sum_{\mu=1}^{m} r_\mu^2\left(d\theta_\mu^2+\sin^2\theta_\mu d\phi^2\right). \end{aligned}$$

Case 3. $\widehat{m} = 3$, *i.e.,* $t_\mu = t$, $r_\mu = r$ *and* $\theta_\mu = \theta$, *or* $t_\mu = t$, $r_\mu = r$ *and* $\phi_\mu = \phi$, *or or* $t_\mu = t$, $\theta_\mu = \theta$ *and* $\phi_\mu = \phi$ *for* $1 \leqslant \mu \leqslant m$.

We consider three subcases following.

Subcase 3.1. $t_\mu = t$, $r_\mu = r$ *and* $\theta_\mu = \theta$.

In this subcase, by applying Theorem 3.1 we obtain that the combinatorial metric is

$$\begin{aligned} ds^2 &= \sum_{\mu=1}^{m}\left(1-\frac{r_{\mu s}}{r}+\frac{r_{\mu e}^2}{r^2}\right)dt^2- \\ &\quad -\sum_{\mu=1}^{m}\left(1-\frac{r_{\mu s}}{r}+\frac{r_{\mu e}^2}{r^2}\right)^{-1}dr^2- \\ &\quad -\sum_{\mu=1}^{m} r^2\left(d\theta^2+\sin^2\theta d\phi_\mu^2\right). \end{aligned}$$

Particularly, if $m_\mu = M$ and $e_\mu = e$ for $1 \leqslant \mu \leqslant m$, then we get that

$$\begin{aligned} ds^2 &= \left(1-\frac{2GM}{c^2 r}+\frac{4\pi G e^4}{c^4 r^2}\right)mdt^2- \\ &\quad -\frac{mdr^2}{1-\frac{2GM}{c^2 r}+\frac{4\pi G e^4}{c^4 r^2}}- \\ &\quad -\sum_{\mu=1}^{m} r^2\left(d\theta^2+\sin^2\theta d\phi_\mu^2\right). \end{aligned}$$

Subcase 3.2. $t_\mu = t$, $r_\mu = r$ *and* $\phi_\mu = \phi$.

In this subcase, the combinatorial metric is

$$\begin{aligned} ds^2 &= \sum_{\mu=1}^{m}\left(1-\frac{r_{\mu s}}{r}+\frac{r_{\mu e}^2}{r^2}\right)dt^2- \\ &\quad -\sum_{\mu=1}^{m}\left(1-\frac{r_{\mu s}}{r}+\frac{r_{\mu e}^2}{r^2}\right)^{-1}dr^2- \\ &\quad -\sum_{\mu=1}^{m} r^2\left(d\theta_\mu^2+\sin^2\theta_\mu d\phi^2\right). \end{aligned}$$

Particularly, if $m_\mu = M$ and $e_\mu = e$ for $1 \leqslant \mu \leqslant m$, then we get that

$$\begin{aligned} ds^2 &= \left(1 - \frac{2GM}{c^2 r} + \frac{4\pi G e^4}{c^4 r^2}\right) m dt^2 - \\ &- \frac{m dr^2}{1 - \frac{2GM}{c^2 r} + \frac{4\pi G e^4}{c^4 r^2}} - \\ &- \sum_{\mu=1}^{m} r^2 \left(d\theta_\mu^2 + \sin^2\theta_\mu d\phi^2\right). \end{aligned}$$

Subcase 3.3. *$t_\mu = t$, $\theta_\mu = \theta$ and $\phi_\mu = \phi$.*

In this subcase, the combinatorial metric is

$$\begin{aligned} ds^2 &= \sum_{\mu=1}^{m}\left(1 - \frac{r_{\mu s}}{r_\mu} + \frac{r_{\mu e}^2}{r_\mu^2}\right) dt^2 - \\ &- \sum_{\mu=1}^{m}\left(1 - \frac{r_{\mu s}}{r_\mu} + \frac{r_{\mu e}^2}{r_\mu^2}\right)^{-1} dr_\mu^2 - \\ &- \sum_{\mu=1}^{m} r_\mu^2 \left(d\theta^2 + \sin^2\theta d\phi^2\right). \end{aligned}$$

Case 4. *$\widehat{m} = 4$, i.e., $t_\mu = t, r_\mu = r, \theta_\mu = \theta$ and $\phi_\mu = \phi$ for $1 \leqslant \mu \leqslant m$.*

In this subcase, the combinatorial metric is

$$\begin{aligned} ds^2 &= \sum_{\mu=1}^{m}\left(1 - \frac{r_{\mu s}}{r} + \frac{r_{\mu e}^2}{r^2}\right) dt^2 - \\ &- \sum_{\mu=1}^{m}\left(1 - \frac{r_{\mu s}}{r} + \frac{r_{\mu e}^2}{r^2}\right)^{-1} dr^2 - \\ &- m r^2 \left(d\theta^2 + \sin^2\theta d\phi^2\right). \end{aligned}$$

Furthermore, if $m_\mu = M$ and $e_\mu = e$ for $1 \leqslant \mu \leqslant m$, we obtain that

$$\begin{aligned} ds^2 &= \left(1 - \frac{2GM}{c^2 r} + \frac{4\pi G e^4}{c^4 r^2}\right) m dt^2 - \\ &- \frac{m dr^2}{1 - \frac{2GM}{c^2 r} + \frac{4\pi G e^4}{c^4 r^2}} - \\ &- m r^2 \left(d\theta^2 + \sin^2\theta d\phi^2\right). \end{aligned}$$

Similarly, we define the coordinate transformation

$$(t, r, \theta, \phi) \to ({}_s t,\ {}_s r,\ {}_s\theta,\ {}_s\phi) = (t\sqrt{m}, r\sqrt{m}, \theta, \phi).$$

Then the previous formula turns to

$$\begin{aligned} ds^2 &= \left(1 - \frac{2GM}{c^2 r} + \frac{4\pi G e^4}{c^4 r^2}\right) d_s t^2 - \\ &- \frac{d_s r^2}{1 - \frac{2GM}{c^2 r} + \frac{4\pi G e^4}{c^4 r^2}} - \\ &- {}_s r^2 \left(d_s\theta^2 + \sin^2\ {}_s\theta d_s\phi^2\right) \end{aligned}$$

in this new coordinate system $({}_s t,\ {}_s r,\ {}_s\theta,\ {}_s\phi)$, whose geometrical behavior likes a charged gravitational field.

4 Multi-time system

A *multi-time system* is such a combinatorial field $(\mathscr{C}_G|\bar{t})$ consisting of fields $M_1, M_2, \cdots, M_m$ on reference frames

$$(t_1, r_1, \theta_1, \phi_1), \cdots, (t_m, r_m, \theta_m, \phi_m)$$

and there are always exist two integers $\kappa,\ \lambda,\ 1 \leqslant \kappa \neq \lambda \leqslant m$ such that $t_\kappa \neq t_\lambda$. Notice that these combinatorial fields discussed in Section 3 are all with $t_\mu = t$ for $1 \leqslant \mu \leqslant m$, i.e., we can establish a time variable t for all fields in this combinatorial field. But if we can not determine all the behavior of living things in the Universe implied in the *weak anthropic principle*, we can not find such a time variable t for all fields. If so, we need a multi-time system for describing the Universe.

Among these multi-time systems, an interesting case appears in $\widehat{m} = 3,\ r_\mu = r,\ \theta_\mu = \theta,\ \phi_\mu = \phi$, i.e., beings live in the same dimensional 3 space, but with different notions on the time. Applying Theorem 3.1, we discuss the Schwarzschild and Reissner-Nordström metrics following.

4.1 Schwarzschild multi-time system

In this case, the combinatorial metric is

$$\begin{aligned} ds^2 &= \sum_{\mu=1}^{m}\left(1 - \frac{2Gm_\mu}{c^2 r}\right) dt_\mu^2 - \\ &- \sum_{\mu=1}^{m}\left(1 - \frac{2Gm_\mu}{c^2 r}\right)^{-1} dr^2 - \\ &- m r^2 \left(d\theta^2 + \sin^2\theta d\phi^2\right). \end{aligned}$$

Applying the projective principle to this equation, we get metrics on gravitational fields $M_1, M_2, \cdots, M_m$ following:

$$\begin{aligned} ds_1^2 &= \left(1 - \frac{2Gm_1}{c^2 r}\right) dt_1^2 - \\ &- \left(1 - \frac{2Gm_1}{c^2 r}\right)^{-1} dr^2 - \\ &- r^2 \left(d\theta^2 + \sin^2\theta d\phi^2\right), \end{aligned}$$

$$\begin{aligned} ds_2^2 &= \left(1 - \frac{2Gm_2}{c^2 r}\right) dt_2^2 - \\ &- \left(1 - \frac{2Gm_2}{c^2 r}\right)^{-1} dr^2 - \\ &- r^2 \left(d\theta^2 + \sin^2\theta d\phi^2\right), \end{aligned}$$

$$\cdots\cdots\cdots\cdots\cdots\cdots,$$

$$\begin{aligned} ds_m^2 &= \left(1-\frac{2Gm_m}{c^2r}\right)dt_m^2 - \\ &-\left(1-\frac{2Gm_m}{c^2r}\right)^{-1}dr^2 - \\ &-r^2\left(d\theta^2+\sin^2\theta d\phi^2\right). \end{aligned}$$

Particularly, if $m_\mu = M$ for $1 \leqslant \mu \leqslant m$, we then get that

$$\begin{aligned} ds^2 &= \left(1-\frac{2GM}{c^2r}\right)\sum_{\mu=1}^{m} dt_\mu^2 - \\ &-\left(1-\frac{2GM}{c^2r}\right)^{-1} m dr^2 - \\ &- mr^2\left(d\theta^2+\sin^2\theta d\phi^2\right). \end{aligned}$$

Its projection on the gravitational field M_μ is

$$\begin{aligned} ds_\mu^2 &= \left(1-\frac{2GM}{c^2r}\right)dt_\mu^2 - \\ &-\left(1-\frac{2GM}{c^2r}\right)^{-1}dr^2 - \\ &- r^2\left(d\theta^2+\sin^2\theta d\phi^2\right), \end{aligned}$$

i.e., the Schwarzschild metric on M_μ, $1 \leqslant \mu \leqslant m$.

4.2 Reissner-Nordström multi-time system

In this case, the combinatorial metric is

$$\begin{aligned} ds^2 &= \sum_{\mu=1}^{m}\left(1-\frac{2Gm_\mu}{c^2r}+\frac{4\pi Ge_\mu^4}{c^4r^2}\right)dt_\mu^2 - \\ &- \sum_{\mu=1}^{m}\left(1-\frac{2Gm_\mu}{c^2r}+\frac{4\pi Ge_\mu^4}{c^4r^2}\right)^{-1}dr^2 - \\ &- mr^2\left(d\theta^2+\sin^2\theta d\phi^2\right). \end{aligned}$$

Similarly, by the projective principle we obtain the metrics on charged gravitational fields $M_1, M_2, \cdots, M_m$ following

$$\begin{aligned} ds_1^2 &= \left(1-\frac{2Gm_1}{c^2r}+\frac{4\pi Ge_1^4}{c^4r^2}\right)dt_1^2 - \\ &-\left(1-\frac{2Gm_1}{c^2r}+\frac{4\pi Ge_1^4}{c^4r^2}\right)^{-1}dr^2 - \\ &- r^2\left(d\theta^2+\sin^2\theta d\phi^2\right), \end{aligned}$$

$$\begin{aligned} ds_2^2 &= \left(1-\frac{2Gm_2}{c^2r}+\frac{4\pi Ge_2^4}{c^4r^2}\right)dt_2^2 - \\ &-\left(1-\frac{2Gm_2}{c^2r}+\frac{4\pi Ge_2^4}{c^4r^2}\right)^{-1}dr^2 - \\ &- r^2\left(d\theta^2+\sin^2\theta d\phi^2\right), \end{aligned}$$

$$\cdots\cdots\cdots\cdots\cdots\cdots\cdots,$$

$$\begin{aligned} ds_m^2 &= \left(1-\frac{2Gm_m}{c^2r}+\frac{4\pi Ge_m^4}{c^4r^2}\right)dt_m^2 - \\ &-\left(1-\frac{2Gm_m}{c^2r}+\frac{4\pi Ge_m^4}{c^4r^2}\right)^{-1}dr^2 - \\ &- r^2\left(d\theta^2+\sin^2\theta d\phi^2\right). \end{aligned}$$

Furthermore, if $m_\mu = M$ and $e_\mu = e$ for $1 \leqslant \mu \leqslant m$, we obtain that

$$\begin{aligned} ds^2 &= \left(1-\frac{2GM}{c^2r}+\frac{4\pi Ge^4}{c^4r^2}\right)\sum_{\mu=1}^{m} dt^2 - \\ &- \left(1-\frac{2GM}{c^2r}+\frac{4\pi Ge^4}{c^4r^2}\right)^{-1} m dr^2 - \\ &- mr^2\left(d\theta^2+\sin^2\theta d\phi^2\right). \end{aligned}$$

Its projection on the charged gravitational field M_μ is

$$\begin{aligned} ds_\mu^2 &= \left(1-\frac{2GM}{c^2r}+\frac{4\pi Ge^4}{c^4r^2}\right)dt_\mu^2 - \\ &-\left(1-\frac{2GM}{c^2r}+\frac{4\pi Ge^4}{c^4r^2}\right)^{-1}dr^2 - \\ &- r^2\left(d\theta^2+\sin^2\theta d\phi^2\right), \end{aligned}$$

i.e., the Reissner-Nordström metric on M_μ, $1 \leqslant \mu \leqslant m$.

As a by-product, these calculations and formulas mean that these beings with time notion different from that of human beings will recognize differently the structure of our universe if these beings are intellectual enough to do so.

5 Discussions

5.1 Geometrical structure

A simple calculation shows that the dimension of the combinatorial gravitational field $(\mathscr{C}|\bar{t})$ in Section 3 is

$$\dim(\mathscr{C}|\bar{t}) = 4m + (1-m)\widehat{m}. \tag{5.1}$$

For example, $\dim(\mathscr{C}|\bar{t}) = 7,\ 10,\ 13,\ 16$ if $\widehat{m} = 1$ and $6,\ 8,\ 10$ if $\widehat{m} = 1$ for $m = 2,\ 3,\ 4$. In this subsection, we analyze these geometrical structures with metrics appeared in Section 3.

As we have said in Section 1, the visible geometry is the spherical geometry of dimensional 3. That is why the sky looks like a spherical surface. In this geometry, we can only see the images of bodies with $\dim \geqslant 3$ on our spherical surface (see [1–2] and [4] in details). But the situation is a little difference from that of the transferring information, which is transferred in all possible routes. In other words, a geometry of dimensional $\geqslant 1$. Therefore, not all information transferring can be seen by our eyes. But some of them can be felt by

our six organs with the help of apparatus if needed. For example, the *magnetism* or *electromagnetism* can be only detected by apparatus. These notions enable us to explain the geometrical structures in combinatorial gravitational fields, for example, the Schwarzschild or Reissner-Nordström metrics.

Case 1. $\widehat{m} = 4$.

In this case, by the formula (5.1) we get $\dim(\mathscr{C}|\bar{t}) = 4$, i.e., all fields $M_1, M_2, \cdots, M_m$ are in $\mathbf{R}^4$, which is the most enjoyed case by human beings. We have gotten the Schwarzschild metric

$$\begin{aligned} ds^2 &= \sum_{\mu=1}^{m}\left(1-\frac{2Gm_\mu}{c^2r}\right)dt^2 - \\ &\quad -\sum_{\mu=1}^{m}\left(1-\frac{2Gm_\mu}{c^2r}\right)^{-1}dr^2 - \\ &\quad - mr^2(d\theta^2+\sin^2\theta d\phi^2) \end{aligned}$$

or the Reissner-Nordström metric

$$\begin{aligned} ds^2 &= \sum_{\mu=1}^{m}\left(1-\frac{r_{\mu s}}{r}+\frac{r_{\mu e}^2}{r^2}\right)dt^2 - \\ &\quad -\frac{dr^2}{\sum\limits_{\mu=1}^{m}\left(1-\frac{r_{\mu s}}{r}+\frac{r_{\mu e}^2}{r^2}\right)} - \\ &\quad - mr^2\left(d\theta^2+\sin^2\theta d\phi^2\right) \end{aligned}$$

for non-charged or charged combinatorial gravitational fields in vacuum in Sections 3. If it is so, the behavior of Universe can be realized finally by human beings. This also means that the discover of science will be ended, i.e., we can established the *Theory of Everything* finally for the Universe.

Case 2. $\widehat{m} \leqslant 3$.

If the Universe is so, then $\dim(\mathscr{C}|\bar{t}) \geqslant 5$. In this case, we know the combinatorial Schwarzschild metrics and combinatorial Reissner-Nordström metrics in Section 3, for example, if $t_\mu = t$, $r_\mu = r$ and $\phi_\mu = \phi$, the combinatorial Schwarzschild metric is

$$\begin{aligned} ds^2 &= \sum_{\mu=1}^{m}\left(1-\frac{r_{\mu s}}{r}\right)dt^2 - \sum_{\mu=1}^{m}\frac{dr^2}{\left(1-\frac{r_{\mu s}}{r}\right)} - \\ &\quad -\sum_{\mu=1}^{m} r^2\left(d\theta_\mu^2+\sin^2\theta_\mu d\phi^2\right) \end{aligned}$$

and the combinatorial Reissner-Nordström metric is

$$\begin{aligned} ds^2 &= \sum_{\mu=1}^{m}\left(1-\frac{r_{\mu s}}{r}+\frac{r_{\mu e}^2}{r^2}\right)dt^2 - \\ &\quad -\sum_{\mu=1}^{m}\frac{dr^2}{\left(1-\frac{r_{\mu s}}{r}+\frac{r_{\mu e}^2}{r^2}\right)} - \\ &\quad -\sum_{\mu=1}^{m} r^2\left(d\theta_\mu^2+\sin^2\theta_\mu d\phi^2\right). \end{aligned}$$

Particularly, if $m_\mu = M$ and $e_\mu = e$ for $1 \leqslant \mu \leqslant m$, then we get that

$$\begin{aligned} ds^2 &= \left(1-\frac{2GM}{c^2r}\right)mdt^2 - \frac{mdr^2}{\left(1-\frac{2GM}{c^2r}\right)} - \\ &\quad -\sum_{\mu=1}^{m} r^2\left(d\theta_\mu^2+\sin^2\theta_\mu d\phi^2\right) \end{aligned}$$

for combinatorial gravitational field and

$$\begin{aligned} ds^2 &= \left(1-\frac{2GM}{c^2r}+\frac{4\pi Ge^4}{c^4r^2}\right)mdt^2 - \\ &\quad -\frac{mdr^2}{\left(1-\frac{2GM}{c^2r}+\frac{4\pi Ge^4}{c^4r^2}\right)} - \\ &\quad -\sum_{\mu=1}^{m} r^2\left(d\theta_\mu^2+\sin^2\theta_\mu d\phi^2\right) \end{aligned}$$

for charged combinatorial gravitational field in vacuum. In this case, the observed interval in the field M_O where human beings live is

$$\begin{aligned} ds_O &= a(t,r,\theta,\phi)dt^2 - b(t,r,\theta,\phi)dr^2 - \\ &\quad - c(t,r,\theta,\phi)d\theta^2 - d(t,r,\theta,\phi)d\phi^2. \end{aligned}$$

How to we explain the differences $ds - ds_O$ in physics? Notice that we can only observe the line element ds_O, a projection of ds on M_O. Whence, all contributions in $ds - ds_O$ come from the spatial direction not observable by human beings. In this case, we are difficult to determine the exact behavior. Furthermore, if $\widehat{m} \leqslant 3$ holds, because there are infinite combinations $(\mathscr{C}_G|\bar{t})$ of existent fields underlying a connected graph G, we can not find an ultimate theory for the Universe, i.e., there are no a *Theory of Everything* for the Universe and the science established by ours is approximate, holds on conditions and the discover of science will be endless forever.

5.2 Physical formation

A generally accepted notion on the formation of Universe is the Big Bang theory ([24]), i.e., the origin of Universe is from an exploded at a singular point on its beginning. Notice that the geometry in the Big Bang theory is just a Euclidean $\mathbf{R}^3$ geometry, i.e., a visible geometry by human beings. Then *how is it came into being for a combinatorial spacetime*? *Weather it is contradicts to the experimental data*? We will explain these questions following.

Realization 5.1 *Any combinatorial spacetime was formed by $|G|$ times Big Bang in an early space.*

Certainly, if there is just one time Big Bang, then there exists one spacetime observed by us, not a multiple or combinatorial spacetime. But there are no arguments for this claim.

It is only an assumption on the origin of Universe. If it is not exploded in one time, but in $m \geqslant 2$ times in different spatial directions, *what will happens for the structure of spacetime*?

The process of Big Bang model can be applied for explaining the formation of combinatorial spacetimes. Assume the dimension of original space is bigger enough and there are m explosions for the origin of Universe. Then likewise the standard process of Big Bang, each time of Big Bang brought a spacetime. After the m Big Bangs, we finally get a multi-spacetime underlying a combinatorial structure, i.e., a combinatorial spacetime $(\mathscr{C}_G|\bar{t})$ with $|G| = m$, such as those shown in Fig. 5.1 for $G = C_4$ or K_3.

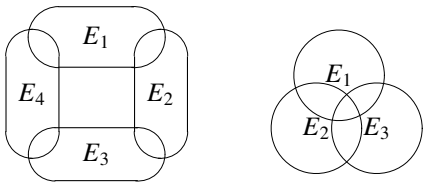

Fig. 5.1

where E_i denotes i^{th} time explosion for $1 \leq i \leqslant 4$. In the process of m Big Bangs, we do not assume that each explosion E_i, $1 \leqslant i \leqslant m$ was happened in a Euclidean space $\mathbf{R}^3$, but in $\mathbf{R}^n$ for $n \geqslant 3$. Whence, the intersection $E_i \cap E_j$ means the same spatial directions in explosions E_i and E_j for $1 \leqslant i, j \leqslant m$. Whence, information in E_i or E_j appeared along directions in $E_i \cap E_j$ will both be reflected in E_j or E_i. As we have said in Subsection 5.1, if $\dim E_i \cap E_j \leqslant 2$, then such information can not be seen by us but only can be detected by apparatus, such as those of the *magnetism* or *electromagnetism*.

Realization 5.2 *The spacetime lived by us is an intersection of other spacetimes.*

This fact is an immediately conclusion of Realization 5.1.

Realization 5.3 *Each experimental data on Universe obtained by human beings is synthesized, not be in one of its spacetimes.*

Today, we have known a few datum on the Universe by COBE or WMAP. In these data, the one well-known is the 2.7^oK cosmic microwave background radiation. Generally, this data is thought to be an evidence of Big Bang theory. If the Universe is a combinatorial one, *how to we explain it*? First, the 2.7^oK is not contributed by one Big Bang in $\mathbf{R}^3$, but by many times before 137 light years, i.e., it is a synthesized data. Second, the 2.7^oK is surveyed by WMAP, an explorer satellite in $\mathbf{R}^3$. By the projective principle in Section 3, it is only a projection of the cosmic microwave background radiation in the Universe on the space $\mathbf{R}^3$ lived by us. In fact, all datum on the Universe surveyed by human beings can be explained in such a way. So there are no contradiction between combinatorial model and datum on the Universe already known by us, but it reflects a combinatorial behavior of the Universe.

Submitted on February 22, 2010 / Accepted March 12, 2010

References

1. Belot G. Remarks on the geometry of visibles. *Philosophical Quarterly*, 2003, v. 53, 581–586.
2. Reid T. An inquiry into the human mind on the principles of common sense. In D. Brookes ed., Edinburgh University Press, 1997.
3. Shtanov Y.V. On brane-world cosmology. arXiv: hep-th/0005193.
4. Yaffe G. Reconsidering Reid's geometry of visibles. *Philosophical Quarterly*, 2002, v. 52, 602–620.
5. Mao L.F. Geometrical theory on combinatorial manifolds. *JP J. Geometry and Topology*, 2007, v. 7, no. 1, 65–114.
6. Mao L.F. An introduction to Smarandache multi-spaces and mathematical combinatorics. *Scientia Magna*, 2007, v. 3, no.1, 54–80.
7. Mao L.F. Curvature equations on combinatorial manifolds with applications to theoretical physics. *International J. Mathematical Combinatorics*, 2008, v. 1, 1–25.
8. Mao L.F. Combinatorially Riemannian submanifolds. *International J. Mathematical Combinatorics*, 2008, v. 2, 1–25.
9. Mao L.F. Combinatorial fields-an introduction. *International J. Mathematical Combinatorics*, 2009, v. 3, 1–22.
10. Rabounski D. Smarandache spaces as a new extension of the basic space-time of general relativity. *Progress in Physics*, 2010, v. 2, L1–L2.
11. Smarandache F. Mixed noneuclidean geometries. arXiv: math/0010119.
12. Moorw G.W. What is a brane? *Notices of the AMS*, 2005, v. 52, no. 2, 214–215.
13. Tegmark M. Parallel universes. In J. D. Barrow, P. C. W. Davies and C. L. Harper eds., *Science and Ultimate Reality: From Quantum to Cosmos*, Cambridge University Press, 2003.
14. Gunther U. and Zhuk A. Phenomenology of brane-world cosmological models. arXiv: gr-qc/0410130.
15. Ida D. Brane-world cosmology. arXiv: gr-qc/9912002.
16. Kanti P. Madden R. and Olive K.A. A 6-d brane world model. arXiv: hep-ph/0104177.
17. Papantonopoulos E. Braneworld cosmological models. arXiv: gr-qc/0410032.
18. Papantonopoulos E. Cosmology in six dimensions. arXiv: gr-qc/0601011.
19. Zhang T.X. A new cosmological model: black hole universe. *Progress in Physics*, 2009, v. 3, 3–11.
20. Mao L.F. Combinatorial geometry with applications to field theory. InfoQuest, USA, 2009.
21. Mao L.F. A combinatorial decomposition of Euclidean spaces $\mathbf{R}^n$ with contribution to visibility. To be submitted to publication.
22. Mao L.F. Lie multi-groups underlying graphs. To be submitted to publication.
23. Mao L.F. Constructing principal fiber bundles by voltage assignment. To be submitted to publication.
24. Peacock J.A. Cosmological physics. Cambridge University Press, 1999.

The "Proton Spin Crisis" — a Quantum Query

Johan Hansson

Department of Physics Luleå University of Technology, SE-97187 Luleå, Sweden. E-mail: c.johan.hansson@ltu.se

The "proton spin crisis" was introduced in the late 1980s, when the EMC-experiment revealed that little or nothing of a proton's spin seemed to be carried by its quarks. The main objective of this paper is to point out that it is wrong to assume that the proton spin, as measured by completely different experimental setups, should be the same in all circumstances, an assumption explicitly made in all present theoretical treatments of the "crisis". As spin is a genuine quantum property, without any objective existence outside its measuring apparatus context, proper account of quantum mechanical measurement theory must be taken.

The "proton spin crisis" [1] essentially refers to the experimental finding that very little of the spin of a proton seems to be carried by the quarks from which it is supposedly built. This was a very curious and unexpected experimental result of the European Muon Collaboration, EMC [2] (later consolidated by other experiments), as the whole idea of the original quark model of Gell-Mann [3] and Zweig [4] was to account for 100 percent of the hadronic spins, solely in terms of quarks. Although "improved" parton models can just about accomodate the experimental results, the purpose of this paper is to point out that the "proton spin crisis" may be due to a misinterpretation of the underlying, quantum mechanical theory. As spin is a fundamentally quantum mechanical entity, without any classical analog, special care must be taken to treat it in a correct quantum mechanical manner.

According to Niels Bohr, *the whole experimental setup* must be considered when we observe quantum mechanical systems. It means that a quantal object does not "really exist" independently of how it is observed. This notion was later quantified by Bell [5], and verified experimentally by Clauser and Freedman [6], Aspect, Dalibard and Roger [7] and others. These experimentally observed violations of Bell's theorem [5] are in accordance with quantum mechanics, but incompatible with a locally realistic world view, proving that quantum objects do not have objective properties unless and until they are actually measured*. The quantum states are not merely unknown, but completely undecided until measured. It is important to stress that *this is not merely a philosophical question, but an experimentally verified prediction based upon the very foundations of quantum theory itself*. To quote John Wheeler: "No elementary quantum phenomenon is a phenomenon until it is a registered (observed) phenomenon" [8]. Unless a specific observable is actually measured, it really does not exist. This means that we should not *a priori* assume that different ways of probing the system will give the same results, as the *system itself* will change when we change the method of observation.

*To be exact, also the possibility exists of non-local "hidden variable" theories, where objects *do* exist at all times. However, such theories manifestly break Lorentz-covariance.

To exemplify this for the spin of the proton, let us compare two different experimental setups designed to measure it:

i) The Stern-Gerlach (SG) experiment, which uses an inhomogeneous magnetic field to measure the proton spin state;

ii) Deep inelastic scattering (DIS), which uses an elementary probe (electron or neutrino) that inelastically scatters off the "proton" (actually elastically off partons).

We should at once recognize i) and ii) as different, or — in the words of Bohr — "complementary", physical setups. If one measures the first, the other cannot be measured simultaneously, and vice versa. DIS disintegrates the proton and produces "jets" of, often heavier, hadrons as the collision energy is much larger than the binding energy, so there is no proton left to measure. Also, the very fact that the hard reaction in DIS is describable in perturbation theory means that we are dealing with a different quantum mechanical object than an undisturbed proton.

In the case of using a SG apparatus to measure the spin, the proton is intact both before and after the measurement, potential scattering being by definition elastic. SG thus measures the total spin state of the proton, but does not resolve any partons. It therefore seems natural to identify the spin of an undisturbed proton with the result from a Stern-Gerlach type of experiment.

As we have seen, i) and ii) simply do not refer to the same physical system, but the "fundamental spin sum-rule", always assumed to hold in treatments of the spin crisis, explicitly equates the spin of the proton, i), with the sum-total of the measured partonic spins and orbital angular momenta, ii). Instead, it should generally read

$$\frac{\Sigma}{2} + L_q + L_G + \Delta G \neq \frac{1}{2}\,, \tag{1}$$

as the left hand side describes the measured spin of the partons, while the right hand side describes the spin of the proton. (Remember that the left and right hand sides correspond to different physical systems, as defined by the respective *complementary* experimental setups used to measure them.) The quantities above stand for: Σ = fraction of proton's spin

carried by the spin of quarks and anti-quarks, L_q = quark orbital angular momentum contribution, L_G = gluon orbital angular momentum contribution, ΔG = gluon spin contribution.

An additional complication is the following: While in quantum electrodynamics (QED) an atomic wave function can approximately be separated into independent parts due to the weak interaction, and the spins of the constituents (nuclei and electrons) can be measured separately as they can be studied in isolation*, in quantum chromodynamics (QCD) it fails as the interactions between fields in an undisturbed proton are much stronger than in the QED case, making even an approximate separation impossible. Still worse, in QCD at low momentum transfers†, like in an undisturbed proton, the particles "quarks" and "gluons" cannot even be defined [9] and thus do not "exist" within the proton, even when disregarding the quantum mechanical measurement process described above. The simple parton model (with or without orbital angular momenta) is simply not tenable in strong QCD.

However, even if we would assume, as is conventional, that ("clothed") partons within the proton *are* defined, the proton wave function, Ψ, could not be factorized into separate valence quark spin wave functions ($|\chi_1\rangle, |\chi_2\rangle, |\chi_3\rangle$) as this would not result in an eigenstate of the strongly spin-dependent Hamiltonian, entering the energy eigenvalue equation

$$H\psi_n = E_n\psi_n. \tag{2}$$

The proton wave function could as usual be written as a superposition of energy eigenstates

$$\Psi = \sum_n c_n\psi_n\,, \tag{3}$$

but

$$\Psi^{SG}(\mathbf{x}_1, \mathbf{x}_2, \mathbf{x}_3, s_1, s_2, s_3) \neq u(\mathbf{x}_1, \mathbf{x}_2, \mathbf{x}_3)\,|\chi_1\rangle|\chi_2\rangle|\chi_3\rangle, \tag{4}$$

where s_1, s_2, s_3 encodes the spin-dependence, and $u(\mathbf{x}_1, \mathbf{x}_2, \mathbf{x}_3)$ would be the space-part of a spin-independent system. In reality the quarks would always be correlated and the wave function could never be separated into product states, except as an approximation if the interaction would be sufficiently small, as in DIS

$$\Psi^{DIS}(\mathbf{x}_1, \mathbf{x}_2, \mathbf{x}_3, s_1, s_2, s_3) \simeq u(\mathbf{x}_1, \mathbf{x}_2, \mathbf{x}_3)\,|\chi_1\rangle|\chi_2\rangle|\chi_3\rangle. \tag{5}$$

Note that $\Psi^{SG} \neq \Psi^{DIS}$ as they describe *different* physical systems, defined by their different modes of observation. In SG there would be an intrinsic, unavoidable *interference effect* for the spin (much like in the famous double-slit experiment for position) which is lost when DIS experiments measure spin structure functions of the "proton". The DIS structure functions are proportional to cross sections, which by necessity are classical quantities incapable of encoding quantum interference. As each individual experimental data point is a classical (non-quantum) result, structure functions are by construction related to incoherent sums of individual probability distributions. Thus, even if we (wrongly) would assume the parton model to be applicable in both cases i) and ii), SG would result from adding spin *amplitudes* (taking full account of quantum interference terms), while DIS would result from adding spin *probabilities* (absolute squares of amplitudes). However, we emphasize again that in the case of SG the parton spins are not merely unknown, but actually *undefined*. An experiment like SG probes the spin state of the *proton*, while an experiment like DIS probes the spin state of the *partons* and the final (= observed) system is not a proton at all but "jets" of hadrons. These two experiments are disjoint, or complementary in the words of Bohr, and do *not* describe the same physical object.

In conclusion, we have explained why the "proton" tested by different experimental setups in general *cannot* be considered as the same physical object. Rather, the whole experimental situation must be taken into account, as quantum mechanical objects and observables do not have an objective existence unless measured. We should thus not enforce, by the "spin sum-rule", the same spin (1/2) for the "proton" when measured by DIS as when it is directly measured on the proton as a whole, *e.g.* by SG. The "proton" as measured by deep inelastic scattering is a *different* physical system than a (virtually) undisturbed proton. There is no reason why spin measurements on one should apply to the other. Especially, there is no need for parton spins, as measured by DIS, to add up to the polarized spin of an otherwise undisturbed proton, just like the EMC-experiment [2] and its successors show. On a more pessimistic note, DIS spin data can never directly unravel the spin of the proton because the two are mutually incompatible. At best, DIS can only serve as an indirect test of QCD by supplying asymptotic boundary conditions to be used in future non-perturbative QCD calculations of the proton spin. If the result of those calculations does not come out spin-1/2, QCD is not the correct theory of strong interactions.

Submitted on March 05, 2010 / Accepted on March 08, 2010

*Wigner's classification of particles according to their mass and spin is given by irreducible representations of the Poincaré group, *i.e.* noninteracting fields.

†More precisely, the elementary quanta of QCD are defined only as the momentum transfer goes to infinity.

References

1. Leader E., Anselmino M. *Z. Phys. C*, 1988, v. 41, 239.
2. Ashman J., *et al. Phys. Lett. B*, 1988, v. 206, 364; *Nucl. Phys. B*, 1989, v. 328, 1.
3. Gell-Mann M. *Phys. Lett.*, 1964, v. 8, 214.
4. Zweig G. *CERN reports*, TH-401, TH-412, 1964.
5. Bell J. S. *Physics*, 1964, v. 1, 195.
6. Freedman S. J., Clauser J. F. *Phys. Rev. Lett.*, 1972, v. 28, 938.
7. Aspect A., Dalibard J., Roger G. *Phys. Rev. Lett.*, 1982, v. 49, 91; 1804.
8. In preface to *The Quantum Theory of Measurement*, Eds. Wheeler J. A. and Zurek W. H., Princeton University Press, New Jersey, 1983.
9. Hansson J. *Can. J. Phys.*, 2002, v. 80, 1093.

Is the Field of Numbers a Real Physical Field? On the Frequent Distribution and Masses of the Elementary Particles

Anatoly V. Belyakov
E-mail: belyakov.lih@gmail.com

Frequent distributions of the databases of the numerical values obtained by resolving algorithms, which describe physical and other processes, give a possibility for bonding the probability of that results the algorithms get. In the frequent distribution of the *fractions* of integers (rational numbers), local maxima which meet the ratios of masses of the elementary particles have been found.

Consider a general case of an arbitrary function $F(x, y, z, \dots)$. Take under consideration a region of the values of this function, split into numerous intervals. Filling up the intervals by item-by-item examination of the possible numerical values of the parameters $x, y, z, \dots$, expressed with integers, will be non-uniform.

Any algorithm has its own individual *frequent distribution*. The distributions can be created* for any formula, which has two or more free parameters (the distributions of the parameters can sometimes have unexpected or complicate form, containing both minima and peaks of the probability).

Frequent distributions give a possibility for bonding the probability of the appearance of numerical values of a function in the region of its existence. This is because the number of the numerical values of the function, hitting into a respective interval, in by item-by-item examination of the possible numerical values of the function's arguments, is proportional to the probability of an average numerical value of the function in the interval. The frequent distributions manifest the reproductivity of numerical values of the function due to the possible variations of its arguments. A frequent distribution itself cannot provide exact numerical solutions. However, if the object or process under consideration is described by not a single function but a few ones, the frequent distributions of these functions can logically be summarized or multiplied in order to manifest, more clear, such regions wherein the probability is high to that in the rest regions. Form of the distribution depends on both the form of the function and the dependencies among the positive integers; in the distribution obtained as above, the properties of the integers become not limited by the plain function of their item-by-item examination, but are more complicate thus an *individualization* of the integers occurs.

Once sharp manifested maxima, attractors, or regions of zero probability appear, it is important to find what peculiarities the algorithm bears. This however can be done only through respective analysis of a large number of the calculation results. In early years, this problem was unable to be considered in serious: processing so large numerical databases, and enforced extracting the probability from chaos, require huge time of routine job; therefore this job became accessed only due to the computer techniques.

It should be noted that the discrete nature of experimental results was discovered in the background of normal distribution of their numerical values (fine structure of the histograms) in already many years ago, by experimental studies conducted, commencing in 1951, by Simon E. Shnoll and his experimental team (see his monograph [1] and bibliography therein). As a result, Shnoll suggested that form of the histograms is connected with the mathematical algorithms, which express the respective processes we measure.

Below are specific examples, which illustrate the connexion of the frequent distributions and the real physical processes and phenomena.

There is a very interesting property of the frequent distributions: several kinds of the distributions include the *ratios of masses of the elementary particles*. This property is attributed to the frequent distributions of the databases of numerical values of the functions, constructed on *fractions*. We found these are plain exponential functions $A^{x/y}$, where A is presented by special numbers $\pi = 3.1416\dots$, $e = 2.17183\dots$, and the reverse fine structure constant $\alpha = 137.036\dots$ In a few cases (hyperons), we mean A the relative mass of the proton $m_p/m_e = 1836$.

In order to be sure in it, we should do follows. Collect a database of numerical values of such a function in the framework of the complete item-by-item examination of its arguments x and y presented by integers, and in the scale which is enough large for covering the necessary scale of masses of the elementary particles (in the units of mass of the electron). Then we should distribute the numerical values along the axis of abscissas, covering numerous intervals by them. Once the distribution done, we will see that it has local maxima (peaks) in numerous locations of the scale, which meet the numerical values of masses of the elementary particles. Peaks of the distributions have a delta-like form.

Distributions of fractions along the numerical axis are self-similar. They reproduce themselves in the peaks of the first, the second and higher orders upto most small segments of the scale. It is possible to see that there is a fractal struc-

*There is a ready-to-use function "frequency" in MS Excel; another software can be applied as well.

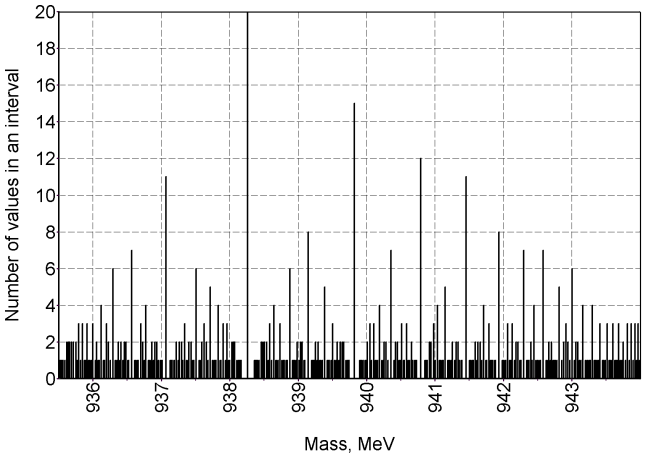

Fig. 1: Mass of the proton (938.27) in distribution 0.511 $\pi^{x/y}$.

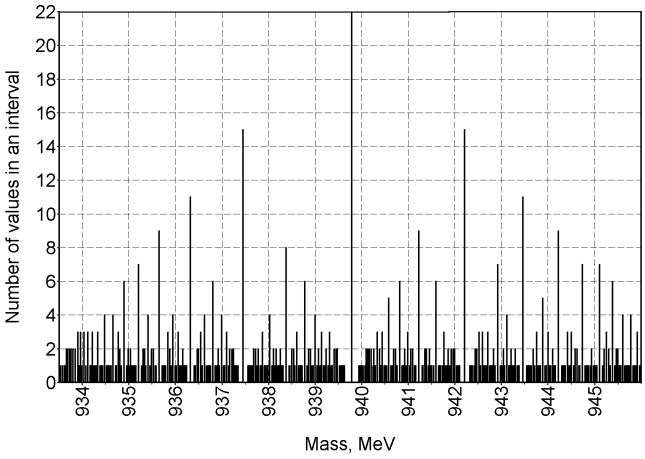

Fig. 2: Mass of the neutron (939.57) in distribution 0.511 $a^{x/y}$.

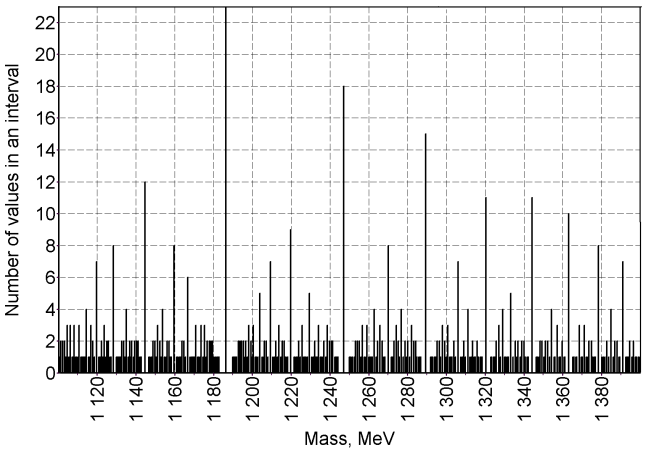

Fig. 3: Mass of the Σ^+ (1189) particle in distribution 0.511 $e^{x/y}$.

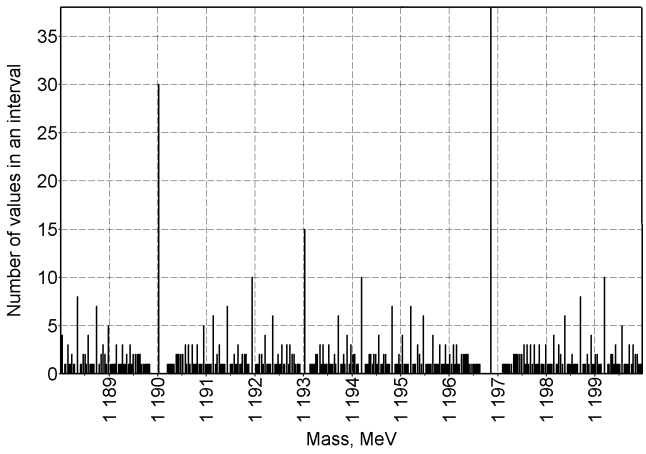

Fig. 4: Masses of the Σ^+ (1189.4), Σ^0 (1192.5), Σ^- (1197.3) particles in distribution 0.511 $a^{x/y}$.

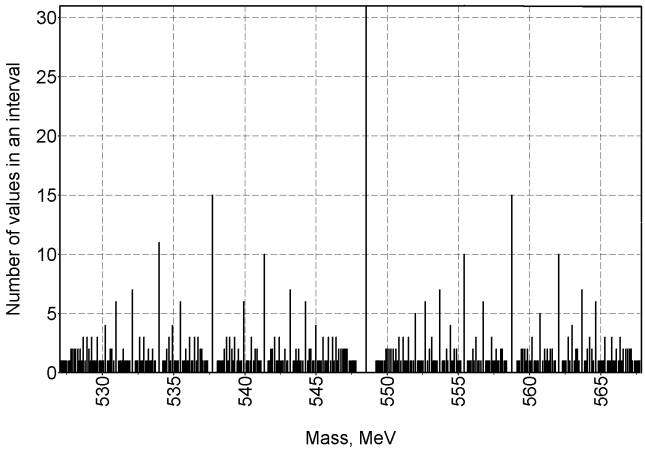

Fig. 5: Mass of the η (548.8) particle in 0.511 $(m_p/m_e)^{x/y}$ distribution.

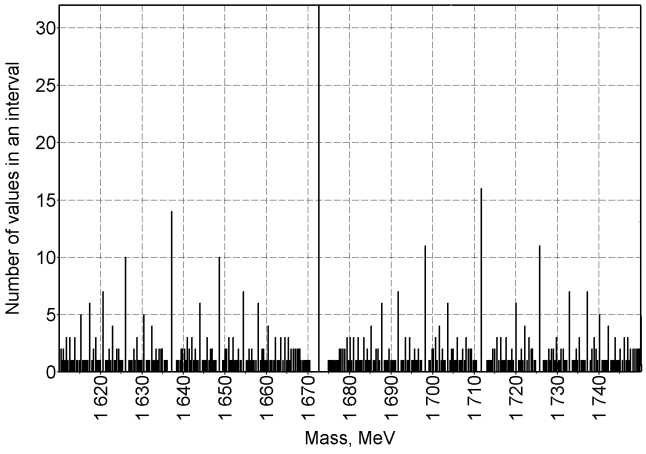

Fig. 6: Masses of the Ω^-, Σ_1 (1672, 1670) particles in distribution 0.511 $(m_p/m_e)^{x/y}$.

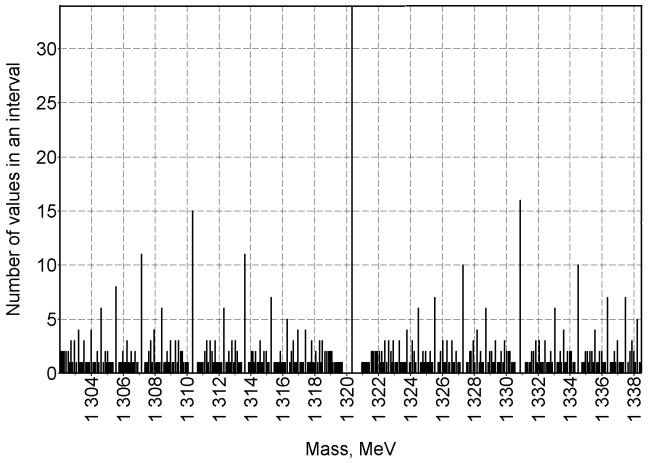

Fig. 7: Mass of the Ξ^-- (1321) particle in 0.511 $(m_p/m_e)^{x/y}$ distribution.

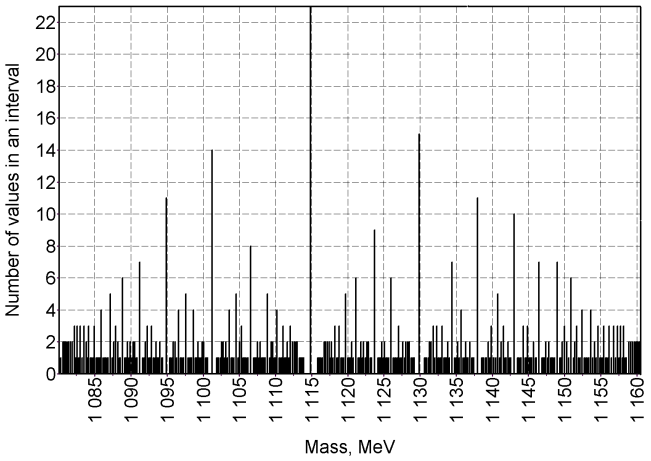

Fig. 8: Mass of the Λ (1115) particle in distribution 0.511 $a^{x/y}$.

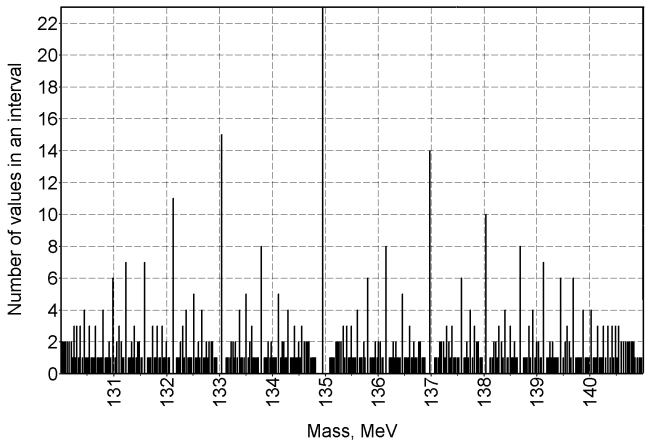

Fig. 9: Mass of the π^0 (134.9) particle in distribution 0.511 $a^{x/y}$.

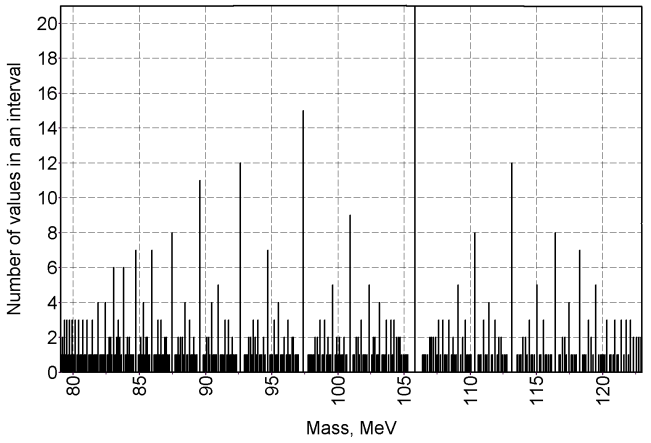

Fig. 10: Mass of the μ^- (105.7) particle in distribution 0.511 $e^{x/y}$.

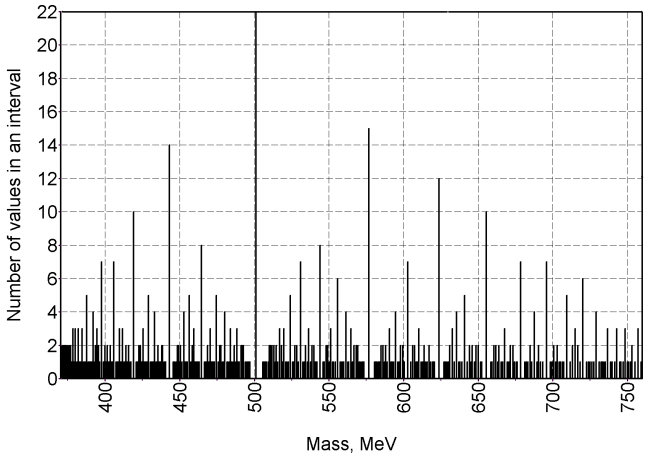

Fig. 11: Mass of the K^0 (498.7) particle in distribution 0.511 $a^{x/y}$.

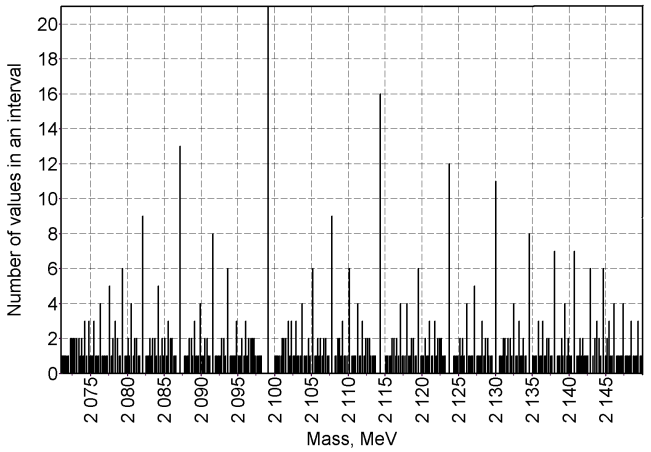

Fig. 12: Mass of the Λ_4 (2100) particle in 0.511 $(m_p/m_e)^{x/y}$ distribution.

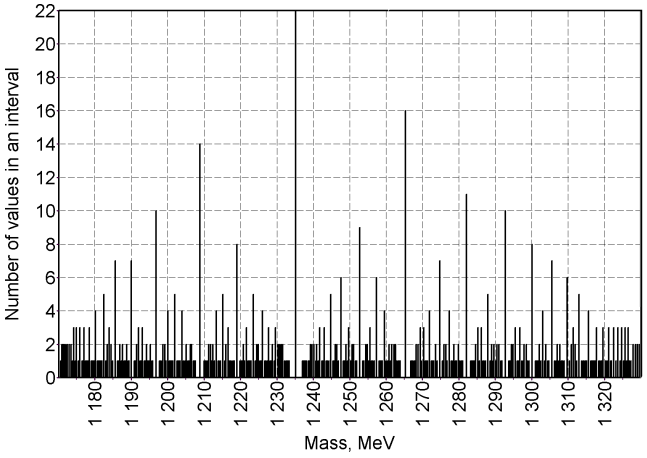

Fig. 13: Masses of the b_1^0, Δ_1 (1233, 1232) particles in distribution $0.511\,a^{x/y}$.

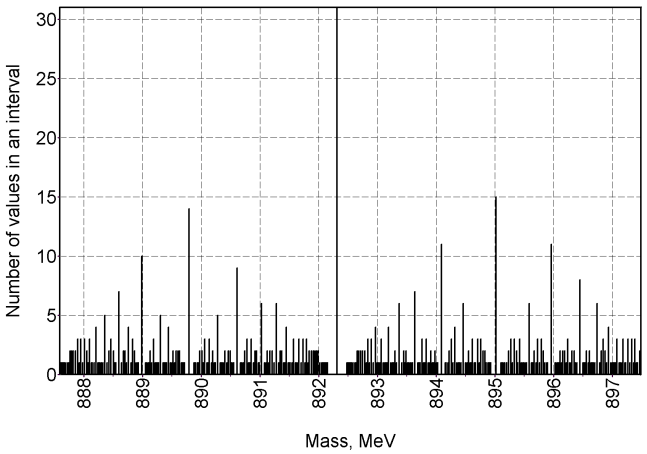

Fig. 14: Mass of the K^* (892.2) particle in distribution $0.511\,a^{x/y}$.

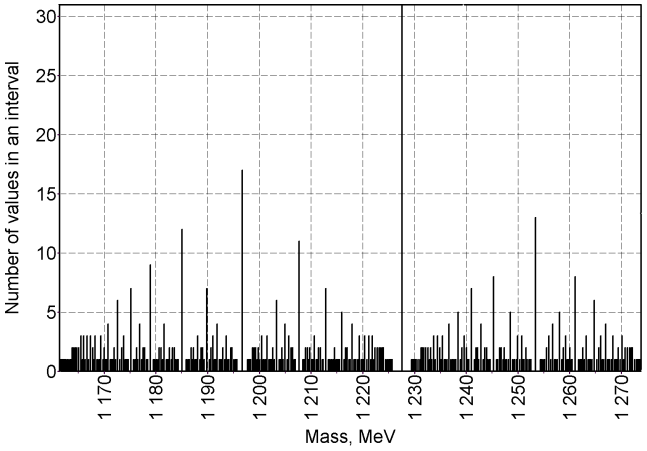

Fig. 15: Mass of the B (1230) particle in distribution $0.511\,\pi^{x/y}$.

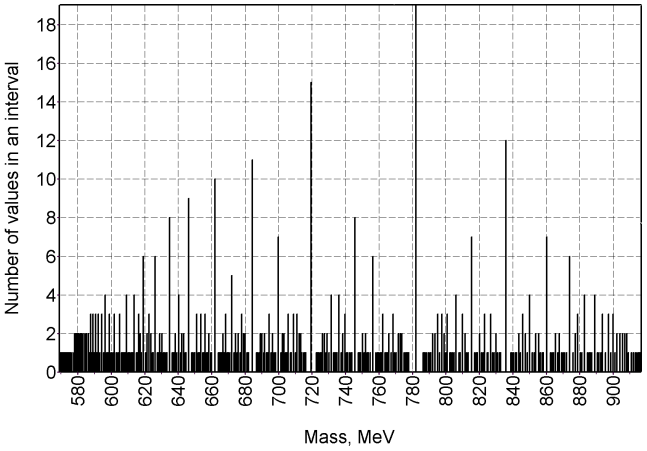

Fig. 16: Mass of the ω (782.7) particle in distribution $0.511\,e^{x/y}$.

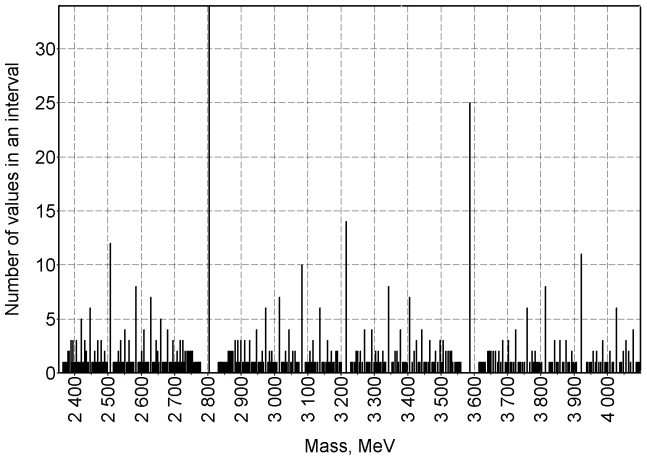

Fig. 17: Masses of the η_c (2820), χ (3556) particles in distribution $0.511\,a^{x/y}$.

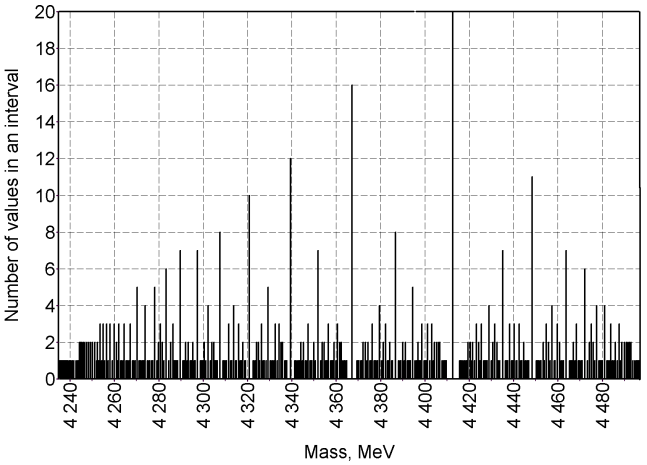

Fig. 18: Mass of the ψ''' (4414) particle in distribution $0.511\,a^{x/y}$.

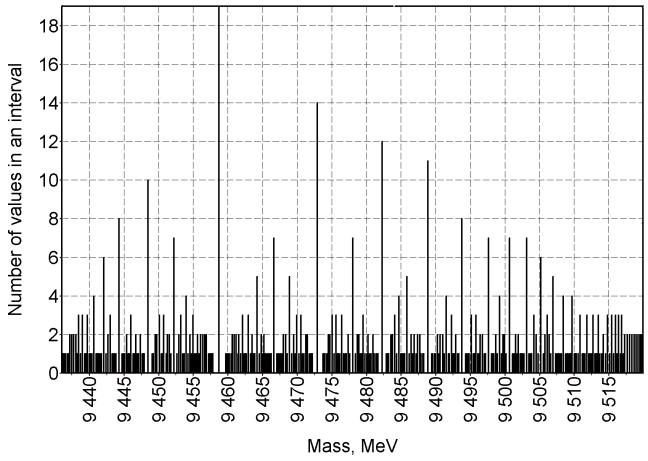

Fig. 19: Mass of the Y (9460) particle in distribution 0.511 $e^{x/y}$.

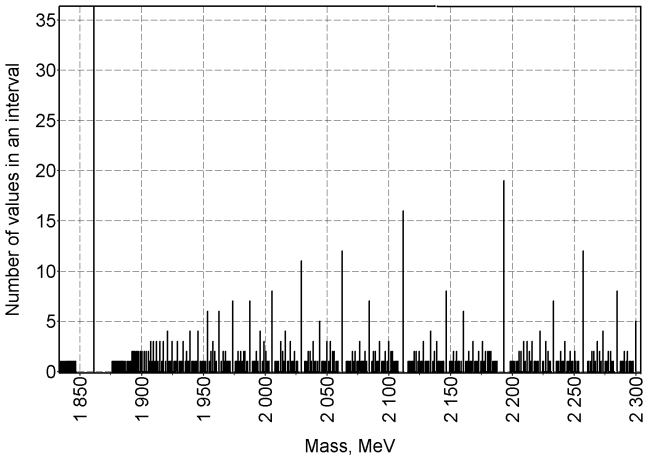

Fig. 20: Some main peaks correspond with masses of the D^0 (1863), D^{*0} (2006), Σ_3 (2030), N_4 (2190), Λ_c^+ (2260) particles in distribution 0.511 $a^{x/y}$.

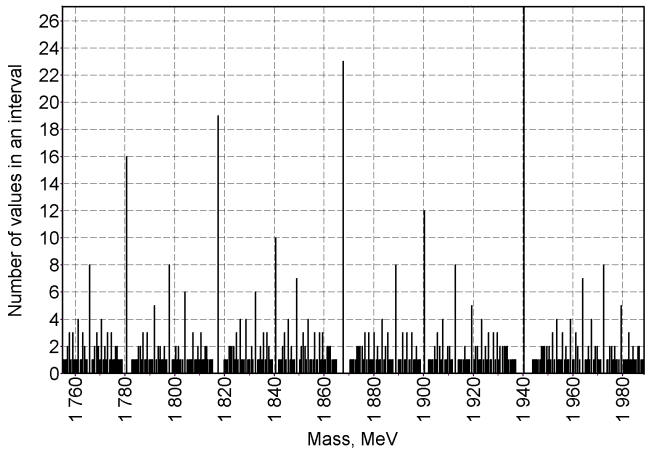

Fig. 21: Main peaks correspond with masses of the τ^- (1782), Λ_3, Ξ_1 (1820, 1820), D^+ (1868), S (1940) particles in distribution 0.511 $\pi^{x/y}$.

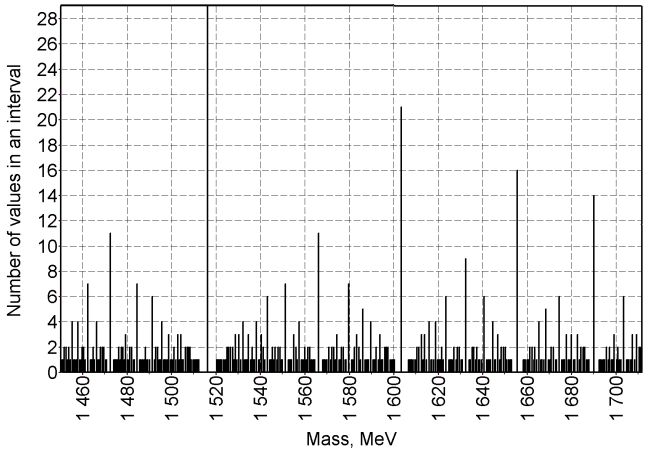

Fig. 22: Main peaks correspond with masses of the f′, Λ_2, N_2 (1516, 1518, 1520), ρ' (1600), Δ_2 (1650), N_3, g (1688, 1690) particles in distribution 0.511 $a^{x/y}$.

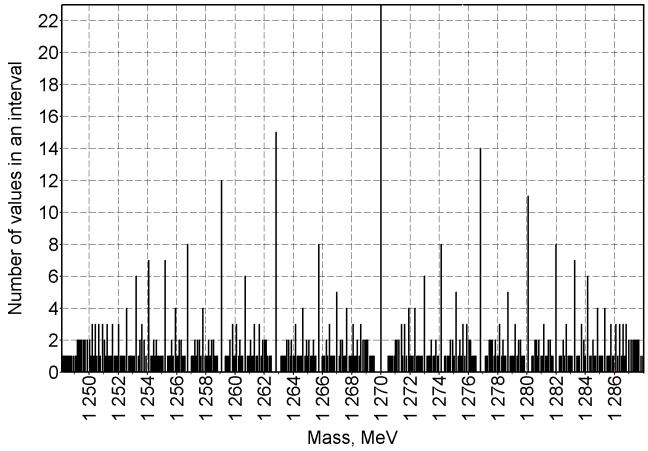

Fig. 23: Mass of the f (1270) particle in distribution 0.511 $e^{x/y}$.

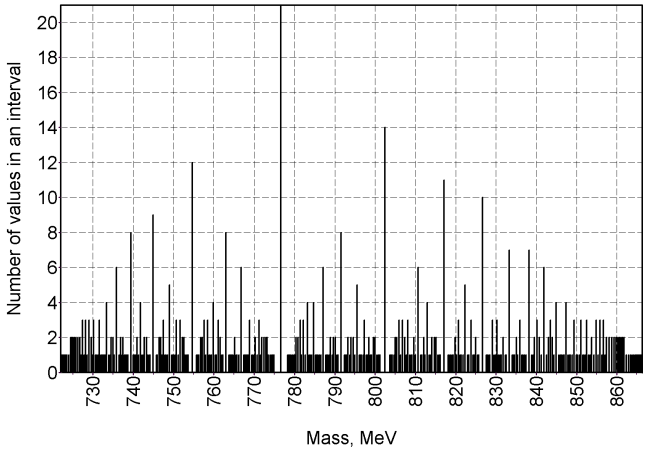

Fig. 24: Mass of the ρ (773) particle in distribution 0.511 $\pi^{x/y}$.

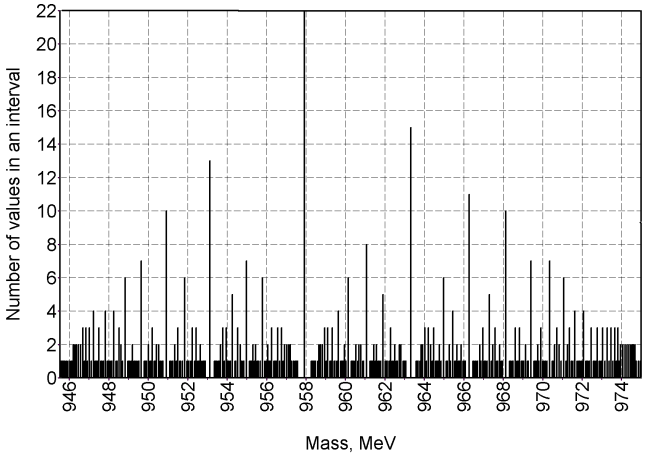

Fig. 25: Mass of the η' (958) particle in distribution 0.511 $\pi^{x/y}$.

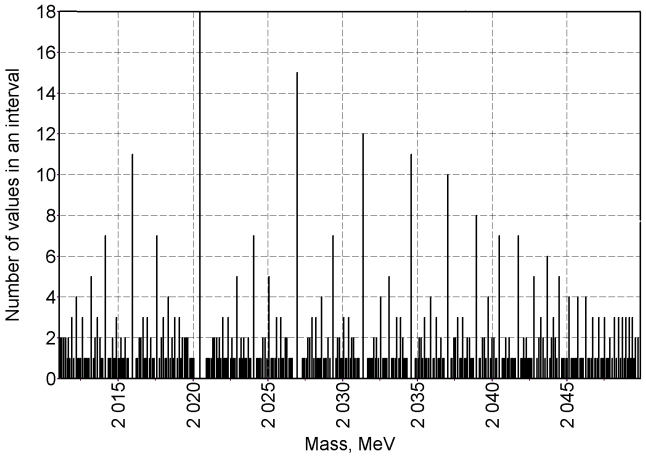

Fig. 26: Mass of the h (2020) particle in distribution 0.511 $\pi^{x/y}$.

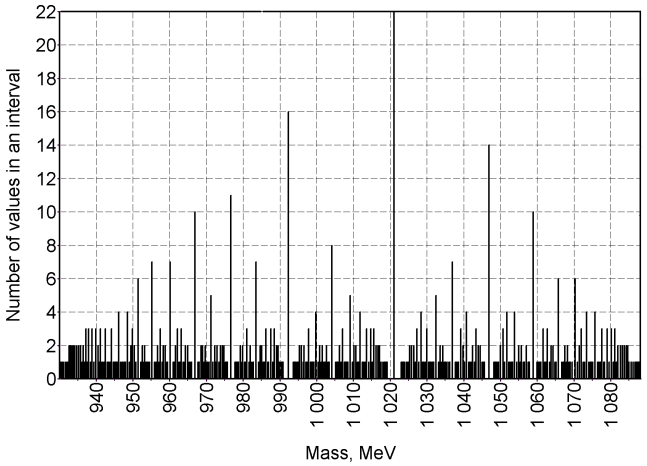

Fig. 27: Mass of the φ (1020) particle in distribution 0.511 $e^{x/y}$.

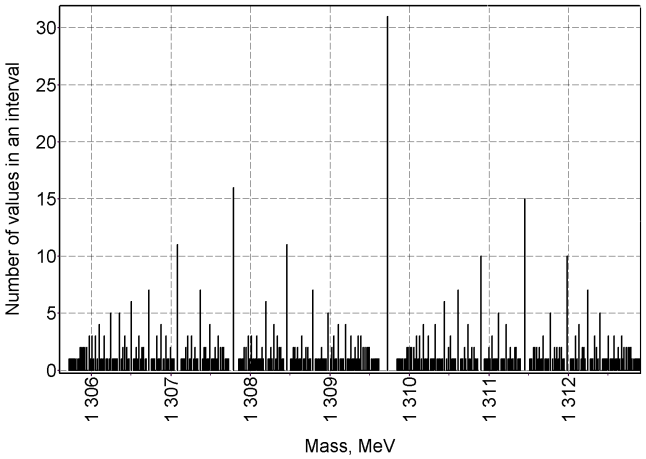

Fig. 28: Mass of the A (1310) particle in distribution 0.511 $a^{x/y}$.

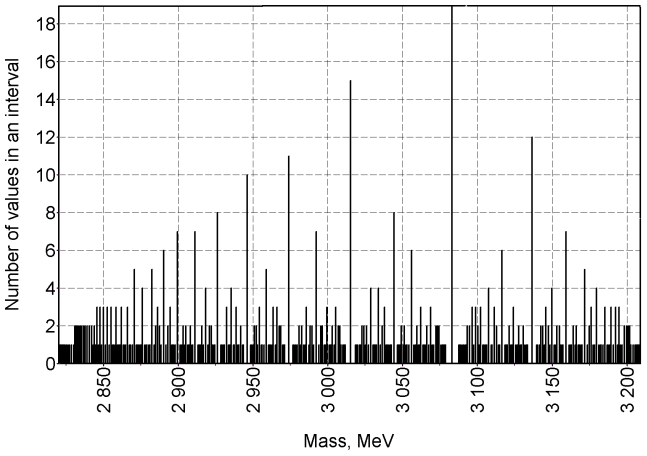

Fig. 29: Mass of the J/ψ (3096) particle in distribution 0.511 $a^{x/y}$.

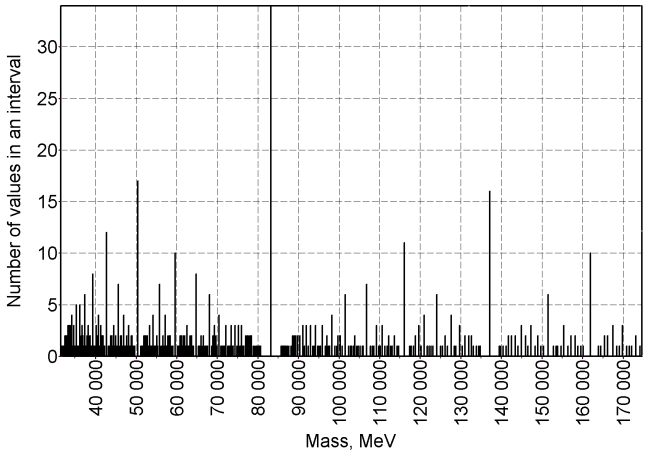

Fig. 30: Mass of the W (82000) particle in distribution 0.511 $e^{x/y}$.

ture of the distribution, when compressing the scale of the diagram by respective changing the variations by x and y (with the same number of the interval unchanged). Therefore, generally speaking, any arbitrary numerical value of the mass could meet, in the diagram, a peak of the first or higher orders. An objective criterion can be a relative error of the calculation, which is the ratio of the error of our calculation by the length of the respective local interval (or the distance between the peaks of the same order; the peak heights differ from each other as seen in Fig. 21 and Fig. 22). I checked about 50 numerical values of the masses; the relative error of the calculation was under a few percents only.

Figures 1–30 show specific examples of my calculations: these are frequent distributions, local maxima of which meet the relative masses of very different particles. The axis of abscissas is given in MeV. The histograms are created in the same way; they have 1000 numerical values distributed along 350 intervals.

It is probable, all the masses meet respective peaks in the distributions. This is not a result of my "passion" to numerology. This also does not mean that the masses of the particles are expressed just by the same functions. Meanwhile, these correspondences appear with so high precision and so often that they cannot be random, absolutely. On the other hand, the numerical values of some masses meet not the peaks, whose height is proportional to the number of the pairs x and y producing the same fraction, but empty spaces neighbouring the peaks (the spaces are presented by most rare appeared ratios of the prime numbers). As is obvious, the empty space neighbouring the peaks manifest minima of the relative density of rational numbers in their distribution along the numerical axis. Connexion of the spaces with the most stable states of oscillation processes was shown by Kyril I. Dombrowski [2, 3].

Is there a spectrum of masses of the elementary particles, if we mean it as the presence of the cross-dependency of the masses, and a possible algorithm of their calculation? I think that not. This is despite we can suppose that the numerical values of the masses constitute the "fine structure" of a distribution according to an unknown algorithm.

It is likely as the numerical values of the masses have a probabilistic origin, and are connected somehow with the properties of the prime numbers. It is probable, a rôle is played here by the fact that the prime number fractions or ratios are more fundamental quantities than the prime numbers themselves. This is because each single fraction of the infinite row is a result of ratios of infinite number of the pairs of arbitrary prime numbers.

At present time, many elementary particles were experimentally discovered. The particles have very different lifespans. This fact and also the shape of distributions constructed on fractions lead us to a conclusion that the first order masses "create" the second order masses, the second order masses "create" the third order masses, and so on to infinity. Such a process is specific to a continuous non-viscous medium, when perturbations appear in it. We cannot except that physical experiments can produce infinite variety of the elementary particles.

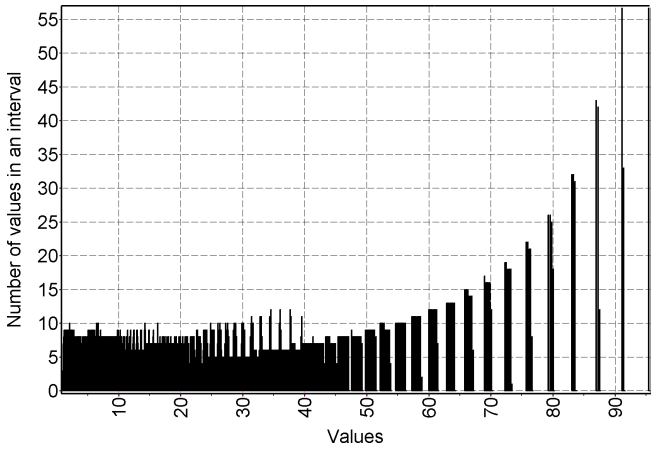

Fig. 31: Distribution on the function $100 \exp\left(-ax(b-y)^{0.5}\right)$, where $a = 0.00147$, $b = 1000$.

Another example is provided by frequent distribution of the exponent (Fig. 31)

$$100 \exp\left(-ax(b-y)^{0.5}\right),$$

modelling the well-known formula which expresses the transparency of the potential barrier of the tunnelling effect, where x and y are variables characterizing mass and energy of the particle. Shape of the distribution is very dependent on the numerical coefficients a and b. Moreover, several numerical values of the function are not realized at all. This form of histograms is specific to those functions, which do not contain ratios or fractions.

In this case, in item-by-item examination of the integers x and y along an abstract scale from 1 to 100, there is about 10,000 numerical values of the exponent. The axis of ordinates means the number of the coinciding numerical values of the function along the interval.

As we found, the distribution of the exponent has the most number of the intervals (nonzero numerical values of the ordinate, whose common number is as well dependent also on the given length of the unit interval) with several specific numerical values a and b. For instance, Fig. 31. With $b = 1000$ and $a = 0.00147$, difference between the neighboring intervals (i.e. the relative length of the interval) is 0.003 of the current numerical value f the function, while this is in the background of 1124 nonzero intervals (the graph has 10,000 intervals totally).

With these parameters, the term under the exponent approaches numerically to -1 independent from the "size" of the database. On the other hand, the *tunnelling effect* appears with the *same condition* in an analogous physical formula! I also attempted to employ frequent distributions in order to

explain the most brighty lines of the radiation spectra for different kinds of radiation [4].

Thus I suggest that, aside for the known physical fields, the field of the positive integers exists as a physical field of the Nature. Pattern of this field has concentrations (peaks) and rarefractions of integers, which determine special numbers such as e, π, and, probable, the fundamental physical constants (the fine structure constant, the gravitational constant, and the others). Physical phenomena process in the inhomogeneous background of this field; any function using the field of integers (database of integers) produces surfs of probability in it (a relative analogy). We should not except that the stable orbits of the cosmic bodies originate from the probabilistic frequent distributions in the gravitational field (the field of the gravitational potential) of the attracting masses they orbit.

It is obvious that the discrete distributions of experimental data, and also their connexion with the aforementioned frequent distributions, are true for the microscales in the first row. There in the microscales, physical quantities exist in the boundary of their decay, thus the possibility of this solution is due to the discrete origin of physical phenomena, which is manifested in the microscales very much. On the other hand, our conclusion are most probable true for a general case as well: non-prime numbers can be represented as the ratios of primes, so the aforementioned frequent distributions are still true for even smallest intervals.

Are we lawful to claim that the parameters of physical or other processes, which are described as above, have not only the quantitative expression but also the probabilistic expression as just said before?

Should we, within the given dependencies which describe some processes or phenomena, find out a possibility for the prediction of the regions of the most probable solutions as those most rational to the others, or for the prediction of those intervals of numerical values, where the considered phenomenon processes most intense (all these not only in the microscales)?

If so, we get a possibility for solving the reverse problems, which target re-construction of the probabilistic distribution of the primary experimental results on the basis of a respective algorithm. This is related first of all to those problems, which are based on the discrete data (primes). This is, for instance, industry or economics: the number of working sections, workgroups, units of equipment, produced units, the number of working personell, and so on.

If all that has been said above is true, and the results of solving similar algorithms (in the case where the algorithms are expressed by the functions whose arguments are more than two) can bear not only a numerical meaning but also a probabilistic meaning, this fact leads to important sequels. There are many problems where numerous parameters are unknown, or cannot be determined in exact. This is economics, game theory, military, meteorology, and many others. In such a case, given a respective algorithm, we could replace the unknown parameters in it with the numbers taken in the respective interval then create frequent distributions thus obtaining probabilistic solutions. Experimental tests are needed in this direction.

Finally, I would like to attract attention of physicists to this problem surveyed here. As is probable, this problem draws that dialectic boundary where chaos meets order, and chance meets regularity.

Submitted on February 14, 2010 / Accepted on February 18, 2010

References

1. Shnoll S. E. Cosmic physical factors in random processes. Svenska fysikarkivet, Stockholm, 2009, 388 pages.
2. Dombrowski K. I. *Bulletin of Soviet Atron. Geodesical Society*, 1956, no. 17(24), 46–50.
3. Dombrowski K. I. Rational numbers distribution and resonance. *Progress in Physics*, 2005, v. 1, 65–67.
4. Belyakov A. V. Geometrodynamics and elements of the matrix calculus of spectra. *Proceedings of Vladimir State Teacher University, the Scientific Didactic Journal*, 2002, no. 7, 29–37 (*in Russian*).

Fractal Scaling Models of Natural Oscillations in Chain Systems and the Mass Distribution of Particles

Hartmut Müller

Global Scaling Research Institute in memoriam Leonhard Euler, Munich, Germany. E-mail: info@globalscaling.de

The paper presents a fractal scaling model of a chain system of quantum harmonic oscillators, that reproduces some systematic features in the mass distribution of hadrons, leptons and gauge bosons.

1 Introduction

The origin of particle masses is one of the most important unsolved problems of modern physics. Also the discrete character of the distribution of particle masses is untreated. In this paper we won't discuss the current situation in the standard theory. Based on a fractal scaling model [1] of natural oscillations in chain systems of harmonic quantum oscillators we will analyze the distributions of particles in dependence on their masses to find out systematic features.

Fractal scaling models [2] of natural oscillations are not based on any statements about the nature of the link or interaction between the elements of the oscillating chain system. Therefore the model statements are quite generally, what opens a wide field of possible applications. Logarithmic scaling is a well known property of inclusive distributions in high energy particle reactions [3]. The quantity of secondary particles increases in dependence on the logarithm of the collision energy.

In the framework of the standard theory, the electron is stable because it's the least massive particle with non-zero electric charge. Its decay would violate charge conservation. The proton is stable, because it's the lightest baryon and the baryon number is conserved. Therefore the proton is the most important baryon, while the electron is the most important lepton and the proton-to-electron mass ratio can be understood as a fundamental physical constant. In the framework of the standard theory, the W- and Z-bosons are elementary particles that mediate the weak force. The rest masses of all theses particles are measured with high precision. The masses of other elementary or stable particles (quarks, neutrinos) are unknown.

In the framework of our model [1], particles are resonance states in chain systems of harmonic quantum oscillators and the masses of fundamental particles are connected by the scaling exponent $\frac{3}{2}$. For example, the proton-to-electron mass ratio is $7\frac{1}{2}$, but the W-boson-to-proton mass ratio is $4\frac{1}{2}$. This means, they are connected by the equation:

$$\ln\left(\frac{m_w}{m_p}\right) = \ln\left(\frac{m_p}{m_e}\right) - 3\,. \tag{1}$$

Therefore the W-boson-to-electron mass ratio corresponds to $4\frac{1}{2} + 7\frac{1}{2} = 12$:

$$\ln\left(\frac{m_w}{m_e}\right) = 12. \tag{2}$$

Already within the eighties the scaling exponent $\frac{3}{2}$ was found in the distribution of particle masses by Valery A. Kolombet [4]. In addition, we have shown [2] that the masses of the most massive celestial bodies in the Solar System are connected by the same scaling exponent $\frac{3}{2}$. The scaling exponent $\frac{3}{2}$ arises as consequence of natural oscillations in chain systems of similar harmonic oscillators [1]. If the natural frequency of one harmonic oscillator is known, one can calculate the complete fractal spectrum of natural frequencies of the chain system, in which spectral nodes arise on the distance of 1 and $\frac{1}{2}$ logarithmic units.

Near spectral nodes the spectral density reaches local maximum and natural frequencies are distributed maximum densely. The energy efficiency of natural oscillations is very high. Therefore one can expect that spectral nodes represent states of the oscillating chain system, which have the highest degree of effectiveness. For this reason we suspect, that stable particles correspond to main spectral nodes.

2 Methods

Based on the continued fraction method [5] we will search the natural frequencies of a chain system of many similar harmonic oscillators in this form:

$$f_{jk} = f_{00} \exp\left(S_{jk}\right). \tag{3}$$

f_{jk} is a set of natural frequencies of a chain system of similar harmonic oscillators, f_{00} is the natural oscillation frequency of one oscillator, S_{jk} is a set of finite continued fractions with integer elements:

$$S_{jk} = n_{j0} + \cfrac{1}{n_{j1} + \cfrac{1}{n_{j2} + \ddots + \cfrac{1}{n_{jk}}}} = [n_{j0}; n_{j1}, n_{j2}, \ldots, n_{jk}]\,, \tag{4}$$

where $n_{j0}, n_{j1}, n_{j2}, \ldots, n_{jk} \in Z$, $j = 0\,, \infty$. We investigate continued fractions (4) with a finite quantity of layers k, which generate discrete spectra, because in this case all S_{jk} represent rational numbers. Therefore the free links n_{j0} and the partial denominators $n_{j1}, n_{j2}, \ldots, n_{jk}$ can be interpreted as "quantum

Particle	Rest mass m, MeV/c^2 [6]	$\ln(m/m_{00})$	S	d
electron (m_{00})	0.510998910 ± 0.000000013	0	[0]	0.000
proton	938.27203 ± 0.00008	7.515	[7; 2]	0.015
neutron	939.565346 ± 0.000023	7.517	[7; 2]	0.017
W-boson	80398 ± 25	11,966	[12]	−0.034
Z-boson	91187.6 ± 2.1	12.092	[12]	0,092

Table 1: The rest masses of well measured stable and fundamental particles and the S-values (4) of the nearest main spectral nodes for the electron calibrated model spectrum. The deviation $d = (\ln(m/m_{00}) - S)$ is indicated.

numbers". The present paper follows the Terskich [5] definition of a chain system, where the interaction between the elements proceeds only in their movement direction. Model spectra (4) are not only logarithmic-invariant, but also fractal, because the discrete hyperbolic distribution of natural frequencies f_{jk} repeats itself on each spectral layer. The partial denominators run through positive and negative integer values. Ranges of relative low spectral density (spectral gaps) and ranges of relative high spectral density (spectral nodes) arise on each spectral layer. In addition to the first spectral layer, Fig. 1 shows the second spectral layer $k = 2$ with $|n_{j1}| = 2$ (logarithmic representation). Maximum spectral density areas (spectral nodes) arise automatically on the distance of integer and half logarithmic units.

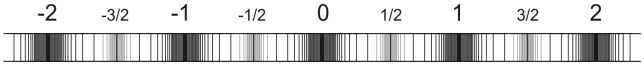

Fig. 1: The spectrum (4) on the first layer $k = 1$, for $|n_{j0}| = 0,\ 1\ 2, \ldots$ and $|n_{j1}| = 2,\ 3,\ 4, \ldots$ and, in addition, the second spectral layer $k = 2$, with $|n_{j1}| = 2$ and $|n_{j2}| = 2,\ 3,\ 4, \ldots$ (logarithmic representation).

Fractal scaling models of natural oscillations are not based on any statements about the nature of the link or interaction between the elements of the oscillating chain system. For this reason we assume that our model could be useful also for the analysis of natural oscillations in chain systems of harmonic quantum oscillators. We assume that in the case of natural oscillations the amplitudes are low, the oscillations are harmonic and the oscillation energy E depends only on the frequency (h is the Planck constant):

$$E = hf\,. \tag{5}$$

In the framework of our model (3) all particles are resonances, in which to the oscillation energy (5) corresponds the particle mass m:

$$m = f\frac{h}{c^2}\,. \tag{6}$$

In this connection the equation (6) means that quantum oscillations generate mass. Under consideration of (3) now we can create a fractal scaling model of the mass spectrum of model particles. This mass spectrum is described by the same continued fraction (4), for $m_{00} = f_{00}\frac{h}{c^2}$:

$$\ln\left(\frac{m_{jk}}{m_{00}}\right) = [n_{j0}; n_{j1}, n_{j2}, \ldots, n_{jk}]\,. \tag{7}$$

The frequency spectrum (4) and the mass spectrum (7) are isomorphic. The mass spectrum (7) is fractal and consequently it has a clear hierarchical structure, in which continued fractions (4) of the form $[n_{j0}]$ and $[n_{j0}; 2]$ define main spectral nodes, as Fig. 1 shows.

3 Results

In the present paper we will compare the scaling model mass spectrum (7) in the range of 100 KeV/c^2 to 100 GeV/c^2 with the mass distribution of well-known particles — hadrons, leptons and gauge bosons.

The model mass spectrum (7) is logarithmically symmetrical and the main spectral nodes arise on the distance of 1 and $\frac{1}{2}$ logarithmic units, as fig. 1 shows. The mass m_{00} in (7) corresponds to the main spectral node $S_{00} = [0]$, because $\ln(m_{00}/m_{00}) = 0$. Let's assume that m_{00} is the electron rest mass 0.510998910(13) MeV/c^2 [6]. In this case (7) describes the mass spectrum that corresponds to the natural frequency spectrum (4) of a chain system of vibrating electrons. Further stable or fundamental model particles correspond to further main spectral nodes of the form $[n_{j0}]$ and $[n_{j0}; 2]$. Actually, near the node [12] we find the W- and Z-bosons, but near the node [7; 2] the proton and neutron masses, as Table 1 shows.

Theoretically, a chain system of vibrating protons generates the same spectrum (7). Also in this case, stable or fundamental model particles correspond to main spectral nodes of the form $[n_{j0}]$ and $[n_{j0}; 2]$, but relative to the electron calibrated spectrum, they are moved by $-7\frac{1}{2}$ logarithmic units. Actually, if m_{00} is the proton rest mass 938.27203(8) MeV/c^2 [6], then the electron corresponds to the node $[-7; -2]$, but the W- and Z-bosons correspond to node [4; 2].

Consequently, the core claims of our model don't depend on the selection of the calibration mass m_{00}, if it is the rest mass of a fundamental resonance state that corresponds to a main spectral node. As mentioned already, this is why the model spectrum (7) is logarithmically symmetrical.

Because a chain system of any similar harmonic oscillators generates the spectrum (7), m_{00} can be much more smaller than the electron mass. Only one condition has to be fulfilled: m_{00} has to correspond to a main spectral node of the model spectrum (7). On this background all particles

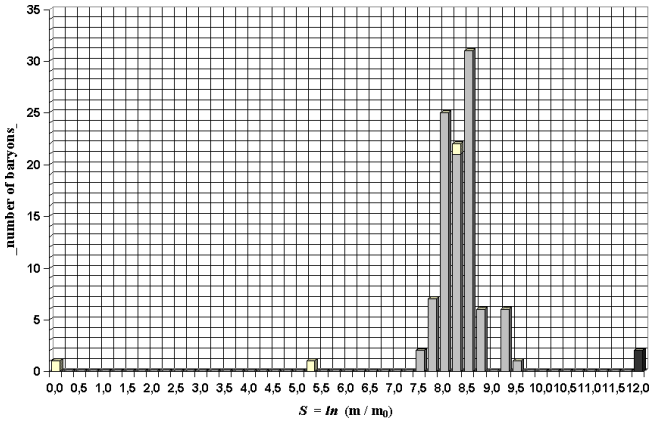

Fig. 2: This histogram was built based on Table 2 and shows the distribution of baryons (grey bars) and leptons (white bars) over $\frac{1}{4}$ logarithmic units wide S-intervals in the range of the electron mass ($S = 0$, white bar) to the W- and Z-bosons ($S = 12$, black bar).

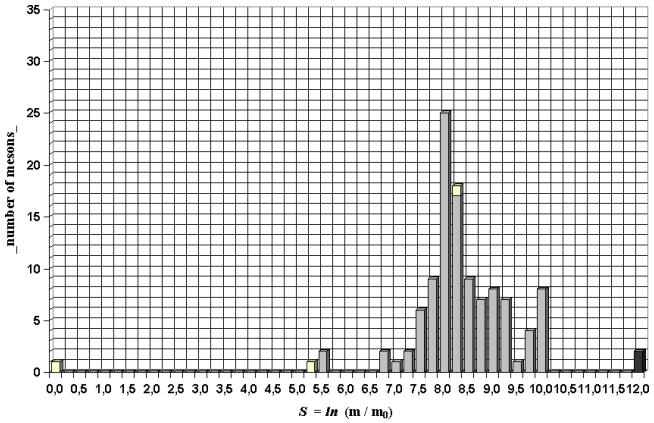

Fig. 3: This histogram was built based on Table 3 and shows the distribution of mesons (grey bars) and leptons (white bars) over $\frac{1}{4}$ logarithmic units wide S-intervals in the range of the electron mass ($S = 0$, white bar) to the W- and Z-bosons ($S = 12$, black bar).

can be interpreted as resonance states in a chain system of harmonic quantum oscillators, in which the rest mass of each single oscillator goes to zero. In the framework of our oscillation model this way can be understood the transition of massless to massive states.

In our model massive particles don't arise because of a symmetry violation. Massive particles arise as resonance states and their mass distribution is logarithmically symmetric.

Further we will investigate the distribution of hadrons (baryons and mesons) in dependence on their rest masses. For this we will split up the mass spectrum (7) into equal in size logarithmic intervals and build histograms. To separate clear the main spectral nodes $[n_{j0}]$ and $[n_{j0}; 2]$, we have to split up the spectrum (7) into S-intervals of $\frac{1}{4}$ logarithmic units.

Table 2 shows the measured masses of baryons, the calculated S-intervals of $\frac{1}{4}$ logarithmic units width and the corresponding calculated mass-intervals. Based on Table 2 a histogram was built (Fig. 2) that shows the distribution of baryons over the $\frac{1}{4}$ logarithmic S-intervals. Based on Table 3,

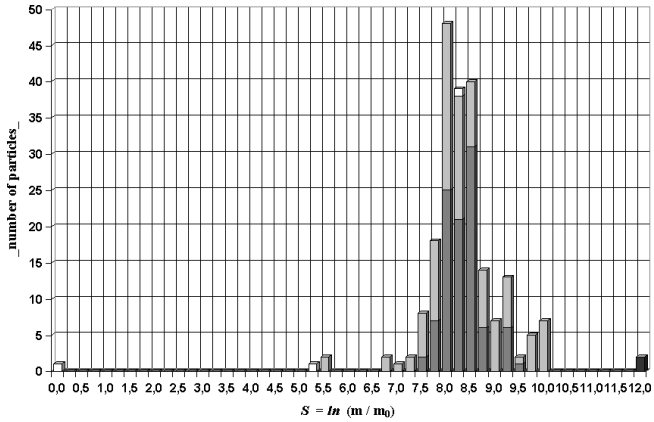

Fig. 4: This histogram was built based on tables 2, 3, 4, 5 and shows the distribution of baryons (dark grey bars), mesons (light grey bars) and leptons (white bars) over $\frac{1}{4}$ logarithmic units wide S-intervals in the range of the electron mass ($S = 0$, white bar) to the W- and Z-bosons ($S = 12$, black bar).

Figure 3 shows the distribution of mesons, but Figure 4 shows the distribution of baryons, mesons, leptons and gauge bosons over the $\frac{1}{4}$ logarithmic S-intervals in the range of 0 to 12 logarithmic units.

All known baryons are distributed over an interval of 2 logarithmic units, of $S = [7; 2]$ to $S = [9; 2]$, as Figure 2 shows. Maximum of baryons occupy the logarithmic center $S = [8; 2]$ of this interval. Figure 3 shows that maximum of mesons occupy the spectral node $S = [8]$ that split up the interval of $S = [0]$ to $S = [12]$ between the electron and the W- and Z-bosons proportionally of $\frac{2}{3}$.

The mass distribution of leptons isn't different of the baryon and meson mass distributions, but follows them, as Figure 4 shows. The mass of the most massive lepton (tauon) is near the maximum of the baryon and meson mass distributions, as Figures 2–4 show.

4 Resume

In the framework of the present model discrete scaling mass distributions arise as result of natural oscillations in chain systems of harmonic quantum oscillators. The observable mass distributions of baryons, mesons, leptons and gauge bosons are connected by the model scaling exponent $\frac{2}{3}$. In addition, with high precision, the masses of known fundamental and stable particles are connected by the model scaling exponent $\frac{3}{2}$. Presumably, the complete mass distribution of particles is logarithmically symmetric and, possibly, massive particles don't arise because of a symmetry violation, but as resonance states in chain systems of quantum oscillators.

Acknowledgements

The author is deeply grateful to S. E. Shnoll, V. A. Panchelyuga and V. A Kolombet for valuable discussions and support.

Submitted on March 13, 2010 / Accepted on March 22, 2010

References

1. Müller H. Fractal scaling models of natural oscillations in chain systems and the mass distribution of the celestial bodies in the Solar System. *Progress in Physics*, 2010.
2. Müller H. Fractal scaling models of resonant oscillations in chain systems of harmonic oscillators. *Progress in Physics*, 2009.
3. Feynman R. Very High-Energy Collisions of Hadrons. *Phys. Rev. Lett.*, 1969, v. 23, 1415.
4. Kolombet V. Macroscopic fluctuations, masses of particles and discrete space-time, *Biofizika*, 1992, v. 36, 492–499 (in Russian).
5. Terskich V. The continued fraction method. Leningrad, 1955 (in Russian).
6. Particle listings. Particle Data Group, www.pdg.lbl.gov

Table 2. The measured masses of baryons [6], the calculated *S*-intervals of $\frac{1}{4}$ logarithmic units width and the corresponding calculated mass-intervals.

baryons	measured mass MeV/c^2	mass interval MeV/c^2	*S*-interval	*S*
N-baryons, $S=0$, $I=1/2$				
proton	938.27203 ± 0.00008	815 – 1047	7.375 – 7.625	[7; 2]
neutron	939.565346 ± 0.000023	815 – 1047	7.375 – 7.625	[7; 2]
N(1440)	1420 – 1470	1344 – 1726	7.875 – 8.125	[8]
N(1520)	1515 – 1525	1344 – 1726	7.875 – 8.125	[8]
N(1650)	1645 – 1670	1344 – 1726	7.875 – 8.125	[8]
N(1675)	1670 – 1680	1344 – 1726	7.875 – 8.125	[8]
N(1680)	1680 – 1690	1344 – 1726	7.875 – 8.125	[8]
N(1710)	1680 – 1740	1344 – 1726	7.875 – 8.125	[8]
N(1720)	1700 – 1750	1344 – 1726	7.875 – 8.125	[8]
N(2190)	2100 – 2200	1726 – 2216	8.125 – 8.375	[8; 4]
N(2220)	2200 – 2300	2216 – 2846	8.375 – 8.625	[8; 2]
N(2250)	2200 – 2350	2216 – 2846	8.375 – 8.625	[8; 2]
N(2600)	2550 – 2750	2216 – 2846	8.375 – 8.625	[8; 2]
Δ-baryons, $S=0$, $I=1/2$				
Δ(1232)	1231 – 1233	1047 – 1344	7.625 – 7.875	[8; −4]
Δ(1600)	1550 – 1700	1344 – 1726	7.875 – 8.125	[8]
Δ(1620)	1600 – 1660	1344 – 1726	7.875 – 8.125	[8]
Δ(1700)	1670 – 1750	1344 – 1726	7.875 – 8.125	[8]
Δ(1905)	1865 – 1915	1726 – 2216	8.125 – 8.375	[8; 4]
Δ(1910)	1870 – 1920	1726 – 2216	8.125 – 8.375	[8; 4]
Δ(1920)	1900 – 1970	1726 – 2216	8.125 – 8.375	[8; 4]
Δ(1930)	1900 – 2020	1726 – 2216	8.125 – 8.375	[8; 4]
Δ(1950)	1915 – 1950	1726 – 2216	8.125 – 8.375	[8; 4]
Δ(2420)	2300 – 2500	2216 – 2846	8.375 – 8.625	[8; 2]
Λ-baryons, $S=-1$, $I=0$				
Λ	1115.683 ± 0.006	1047 – 1344	7.625 – 7.875	[8; −4]
Λ(1405)	1406 ± 4	1344 – 1726	7.875 – 8.125	[8]
Λ(1520)	1519.5 ± 1.0	1344 – 1726	7.875 – 8.125	[8]
Λ(1600)	1560 – 1700	1344 – 1726	7.875 – 8.125	[8]
Λ(1670)	1660 – 1680	1344 – 1726	7.875 – 8.125	[8]
Λ(1690)	1685 – 1695	1344 – 1726	7.875 – 8.125	[8]
Λ(1800)	1720 – 1850	1726 – 2216	8.125 – 8.375	[8; 4]
Λ(1810)	1750 – 1850	1726 – 2216	8.125 – 8.375	[8; 4]
Λ(1820)	1815 – 1825	1726 – 2216	8.125 – 8.375	[8; 4]
Λ(1830)	1810 – 1830	1726 – 2216	8.125 – 8.375	[8; 4]
Λ(1890)	1850 – 1910	1726 – 2216	8.125 – 8.375	[8; 4]
Λ(2100)	2090 – 2110	1726 – 2216	8.125 – 8.375	[8; 4]
Λ(2110)	2090 – 2140	1726 – 2216	8.125 – 8.375	[8; 4]
Λ(2350)	2340 – 2370	2216 – 2846	8.375 – 8.625	[8; 2]
Σ-baryons, $S=-1$, $I=1$				
Σ^+	1189.37 ± 0.07	1047 – 1344	7.625 – 7.875	[8; −4]
Σ^0	1192.642 ± 0.024	1047 – 1344	7.625 – 7.875	[8; −4]
Σ^-	1197.449 ± 0.030	1047 – 1344	7.625 – 7.875	[8; −4]
$\Sigma(1385)^+$	1382.8 ± 0.4	1344 – 1726	7.875 – 8.125	[8]
$\Sigma(1385)^0$	1383.7 ± 1.0	1344 – 1726	7.875 – 8.125	[8]
$\Sigma(1385)^-$	1387.2 ± 0.5	1344 – 1726	7.875 – 8.125	[8]
Σ(1660)	1630 – 1690	1344 – 1726	7.875 – 8.125	[8]
Σ(1670)	1665 – 1685	1344 – 1726	7.875 – 8.125	[8]
Σ(1750)	1730 – 1800	1726 – 2216	8.125 – 8.375	[8; 4]
Σ(1775)	1770 – 1780	1726 – 2216	8.125 – 8.375	[8; 4]
Σ(1915)	1900 – 1935	1726 – 2216	8.125 – 8.375	[8; 4]
Σ(1940)	1900 – 1950	1726 – 2216	8.125 – 8.375	[8; 4]
Σ(2030)	2025 – 2040	1726 – 2216	8.125 – 8.375	[8; 4]
Σ(2250)	2210 – 2280	2216 – 2846	8.375 – 8.625	[8; 2]
Ξ-baryons, $S=-2$, $I=1/2$				
Ξ^0	1314.86 ± 0.20	1047 – 1344	7.625 – 7.875	[8; −4]
Ξ^-	1321.71 ± 0.07	1047 – 1344	7.625 – 7.875	[8; −4]
$\Xi(1530)^0$	1531.80 ± 0.32	1344 – 1726	7.875 – 8.125	[8]
$\Xi(1530)^-$	1535.0 ± 0.6	1344 – 1726	7.875 – 8.125	[8]
Ξ(1690)	1690 ± 10	1344 – 1726	7.875 – 8.125	[8]
Ξ(1820)	1823 ± 5	1726 – 2216	8.125 – 8.375	[8; 4]
Ξ(1950)	1950 ± 15	1726 – 2216	8.125 – 8.375	[8; 4]
Ξ(2030)	2025 ± 5	1726 – 2216	8.125 – 8.375	[8; 4]

baryons	measured mass MeV/c^2	mass interval MeV/c^2	S-interval	S
Ω-baryons, $S=-3$, $I=0$				
Ω^-	1672.45 ± 0.29	1344 – 1726	7.875 – 8.125	[8]
$\Omega(2250)^-$	2252 ± 9	2216 – 2846	8.375 – 8.625	[8; 2]
charmed baryons, $C=+1$				
Λ_c^+	2286.46 ± 0.14	2216 – 2846	7.375 – 8.625	[8; 2]
$\Lambda_c(2595)^+$	2595.4 ± 0.6	2216 – 2846	7.375 – 8.625	[8; 2]
$\Lambda_c(2625)^+$	2628.1 ± 0.6	2216 – 2846	7.375 – 8.625	[8; 2]
$\Lambda_c(2880)^+$	2881.53 ± 0.35	2846 – 3654	8.625 – 8.875	[9; −4]
$\Lambda_c(2940)^+$	2939.3 ± 1.5	2846 – 3654	8.625 – 8.875	[9; −4]
$\Sigma_c(2455)^{++}$	2454.02 ± 0.18	2216 – 2846	8.375 – 8.625	[8; 2]
$\Sigma_c(2455)^+$	2452.9 ± 0.4	2216 – 2846	8.375 – 8.625	[8; 2]
$\Sigma_c(2455)^0$	2453.76 ± 0.18	2216 – 2846	8.375 – 8.625	[8; 2]
$\Sigma_c(2801)^{++}$	2801 ± 6	2216 – 2846	8.375 – 8.625	[8; 2]
$\Sigma_c(2800)^+$	2792 ± 14	2216 – 2846	8.375 – 8.625	[8; 2]
$\Sigma_c(2800)^0$	2802 ± 7	2216 – 2846	8.375 – 8.625	[8; 2]
Ξ_c^+	2467.8 ± 0.6	2216 – 2846	8.375 – 8.625	[8; 2]
Ξ_c^0	2470.88 ± 0.8	2216 – 2846	8.375 – 8.625	[8; 2]
$\Xi_c^{\prime+}$	2575.6 ± 3.1	2216 – 2846	8.375 – 8.625	[8; 2]
$\Xi_c^{\prime0}$	2577.9 ± 2.9	2216 – 2846	8.375 – 8.625	[8; 2]
$\Xi_c(2645)^+$	2645.9 ± 0.6	2216 – 2846	8.375 – 8.625	[8; 2]
$\Xi_c(2645)^0$	2645.9 ± 0.5	2216 – 2846	8.375 – 8.625	[8; 2]
$\Xi_c(2790)^+$	2789.1 ± 3.2	2216 – 2846	8.375 – 8.625	[8; 2]
$\Xi_c(2790)^0$	2791.8 ± 3.3	2216 – 2846	8.375 – 8.625	[8; 2]
$\Xi_c(2815)^+$	2816.6 ± 0.9	2216 – 2846	8.375 – 8.625	[8; 2]
$\Xi_c(2815)^0$	2819.6 ± 1.2	2216 – 2846	8.375 – 8.625	[8; 2]
$\Xi_c(2980)^+$	2971.4 ± 3.3	2846 – 3654	8.625 – 8.875	[9; −4]
$\Xi_c(2880)^0$	2968.0 ± 2.6	2846 – 3654	8.625 – 8.875	[9; −4]
$\Xi_c(3080)^+$	3077.0 ± 0.4	2846 – 3654	8.625 – 8.875	[9; −4]
$\Xi_c(3080)^0$	3079.9 ± 1.4	2846 – 3654	8.625 – 8.875	[9; −4]
Ω_c^0	2695.2 ± 1.7	2216 – 2846	8.375 – 8.625	[8; 2]
$\Omega_c(2770)^0$	2765.9 ± 2.0	2216 – 2846	8.375 – 8.625	[8; 2]
bottom baryons, $B=-1$				
Λ_b^0	5620.2 ± 1.6	4692 – 6025	9.125 – 9.375	[9; 4]
Σ_b^+	5807.8 ± 2.7	4692 – 6025	9.125 – 9.375	[9; 4]
Σ_b^-	5815.2 ± 2.0	4692 – 6025	9.125 – 9.375	[9; 4]
Σ_b^{*+}	5829.0 ± 3.4	4692 – 6025	9.125 – 9.375	[9; 4]
Σ_b^{*-}	5836.4 ± 2.8	4692 – 6025	9.125 – 9.375	[9; 4]
Ξ_b	5792.4 ± 3.0	4692 – 6025	9.125 – 9.375	[9; 4]
Σ_b^-	6165 ± 16	6025 – 7736	9.375 – 9.625	[9; 2]

Table 3. The measured masses of mesons [6], the calculated S-intervals of $\frac{1}{4}$ logarithmic units width and the corresponding calculated mass-intervals.

mesons	measured mass MeV/c^2	mass interval MeV/c^2	S-interval	S
light unflavored mesons $S=C=B=0$				
$\pi^\pm$	139.57018 ± 0.00035	110 – 142	5.375 – 5.625	[5; 2]
π^0	134.9766 ± 0.0006	110 – 142	5.375 – 5.625	[5; 2]
η	547.853 ± 0.024	495 – 635	6.875 – 7.125	[7]
$\rho(770)$	775.49 ± 0.34	635 – 815	7.125 – 7.375	[7; 4]
$\omega(782)$	782.65 ± 0.12	635 – 815	7.125 – 7.375	[7; 4]
$\rho'(958)$	957.78 ± 0.06	815 – 1047	7.375 – 7.626	[7; 2]
$f_0(980)$	980 ± 10	815 – 1047	7.375 – 7.626	[7; 2]
$a_0(980)$	980 ± 20	815 – 1047	7.375 – 7.626	[7; 2]
$\phi(1020)$	1019.455 ± 0.020	815 – 1047	7.375 – 7.626	[7; 2]
$a_0(980)$	980 ± 20	815 – 1047	7.375 – 7.626	[7; 2]
$\phi(1020)$	1019.455 ± 0.020	815 – 1047	7.375 – 7.626	[7; 2]
$h_1(1170)$	1170 ± 20	1047 – 1344	7.626 – 7.875	[8; −4]
$b_1(1235)$	1229.5 ± 3.2	1047 – 1344	7.626 – 7.875	[8; −4]
$a_1(1260)$	1230 ± 40	1047 – 1344	7.626 – 7.875	[8; −4]
$f_2(1270)$	1275.1 ± 1.2	1047 – 1344	7.626 – 7.875	[8; −4]
$f_1(1285)$	1281.8 ± 0.6	1047 – 1344	7.626 – 7.875	[8; −4]
$\eta(1295)$	1294 ± 4	1047 – 1344	7.626 – 7.875	[8; −4]
$h_1(1170)$	1170 ± 20	1047 – 1344	7.626 – 7.875	[8; −4]
$b_1(1235)$	1229.5 ± 3.2	1047 – 1344	7.626 – 7.875	[8; −4]
$a_1(1260)$	1230 ± 40	1047 – 1344	7.626 – 7.875	[8; −4]
$f_2(1270)$	1275.1 ± 1.2	1047 – 1344	7.626 – 7.875	[8; −4]
$f_1(1285)$	1281.8 ± 0.6	1047 – 1344	7.626 – 7.875	[8; −4]
$\eta(1295)$	1294 ± 4	1047 – 1344	7.626 – 7.875	[8; −4]
$\pi(1300)$	1300 ± 100	1047 – 1344	7.626 – 7.875	[8; −4]
$a_2(1320)$	1318.3 ± 0.6	1047 – 1344	7.626 – 7.875	[8; −4]
$f_0(1370)$	1200 – 1500	1344 – 1726	7.875 – 8.125	[8]
$\pi_1(1400)$	1351 ± 30	1344 – 1726	7.875 – 8.125	[8]
$\eta(1450)$	1409.8 ± 2.5	1344 – 1726	7.875 – 8.125	[8]
$f_1(1420)$	1426.4 ± 0.9	1344 – 1726	7.875 – 8.125	[8]
$\omega(1400)$	1400 – 1450	1344 – 1726	7.875 – 8.125	[8]
$a0(1450)$	1474 ± 19	1344 – 1726	7.875 – 8.125	[8]
$\rho(1450)$	1465 ± 25	1344 – 1726	7.875 – 8.125	[8]
$\eta(1475)$	1476 ± 4	1344 – 1726	7.875 – 8.125	[8]
$f_0(1500)$	1505 ± 6	1344 – 1726	7.875 – 8.125	[8]
$f_2(1525)$	1525 ± 5	1344 – 1726	7.875 – 8.125	[8]
$\pi_1(1600)$	1662 ± 15	1344 – 1726	7.875 – 8.125	[8]
$\eta_2(1645)$	1617 ± 5	1344 – 1726	7.875 – 8.125	[8]
$\omega(1650)$	1670 ± 30	1344 – 1726	7.875 – 8.125	[8]
$\omega_3(1670)$	1667 ± 4	1344 – 1726	7.875 – 8.125	[8]
$\pi_2(1670)$	1672.4 ± 3.2	1344 – 1726	7.875 – 8.125	[8]
$\phi(1680)$	1680 ± 20	1344 – 1726	7.875 – 8.125	[8]
$\rho_3(1690)$	1688.8 ± 2.1	1344 – 1726	7.875 – 8.125	[8]
$\rho(1700)$	1720 ± 20	1344 – 1726	7.875 – 8.125	[8]
$f_0(1710)$	1720 ± 6	1344 – 1726	7.875 – 8.125	[8]
$\pi(1800)$	1816 ± 14	1726 – 2216	8.125 – 8.375	[8; 4]
$\phi_3(1850)$	1854 ± 7	1726 – 2216	8.125 – 8.375	[8; 4]
$\pi_2(1880)$	1895 ± 16	1726 – 2216	8.125 – 8.375	[8; 4]
$f_2(1950)$	1944 ± 12	1726 – 2216	8.125 – 8.375	[8; 4]
$f_2(2100)$	2011 ± 80	1726 – 2216	8.125 – 8.375	[8; 4]
$a_4(2040)$	2001 ± 10	1726 – 2216	8.125 – 8.375	[8; 4]
$f_4(2050)$	2018 ± 11	1726 – 2216	8.125 – 8.375	[8; 4]
$f_2(2300)$	2297 ± 28	2216 – 2846	8.375 – 8.625	[8; 2]
$f_2(2340)$	2339 ± 60	2216 – 2846	8.375 – 8.625	[8; 2]
strange mesons $S=\pm 1 C=B=0$				
$K^\pm$	493.677 ± 0.016	385 – 495	6.625 – 6.875	[7; −4]
K^0	497.614 ± 0.024	385 – 495	6.625 – 6.875	[7; −4]
$K^*(892)^\pm$	891.66 ± 0.26	815 – 1047	7.375 – 7.625	[7; 2]
$K^*(892)^0$	896.00 ± 0.25	815 – 1047	7.375 – 7.625	[7; 2]
$K_1(1270)$	1272 ± 7	1047 – 1344	7.625 – 7.875	[8; −4]
$K_1(1400)$	1403 ± 7	1344 – 1726	7.875 – 8.125	[8]
$K^*(1410)$	1414 ± 15	1344 – 1726	7.875 – 8.125	[8]
$K_0^*(1430)$	1425 ± 50	1344 – 1726	7.875 – 8.125	[8]
$K_2^*(1430)^\pm$	1425.6 ± 1.5	1344 – 1726	7.875 – 8.125	[8]
$K_2^*(1430)^0$	1432.4 ± 1.3	1344 – 1726	7.875 – 8.125	[8]
$K^*(1680)$	1717 ± 27	1344 – 1726	7.875 – 8.125	[8]
$K_2(1770)^\pm$	1773 ± 8	1726 – 2216	8.125 – 8.375	[8; 4]
$K_3^*(1780)$	1776 ± 7	1726 – 2216	8.125 – 8.375	[8; 4]
$K_2(1820)$	1816 ± 13	1726 – 2216	8.125 – 8.375	[8; 4]
$K_4^*(2045)$	2045 ± 9	1726 – 2216	8.125 – 8.375	[8; 4]
charmed mesons $S=\pm 1$				
$D^\pm$	1869.62 ± 0.20	1726 – 2216	8.125 – 8.375	[8; 4]
D^0	1864.84 ± 0.17	1726 – 2216	8.125 – 8.375	[8; 4]
$D^*(2007)^0$	2006.97 ± 0.19	1726 – 2216	8.125 – 8.375	[8; 4]
$D^*(2010)^\pm$	2010.27 ± 0.17	1726 – 2216	8.125 – 8.375	[8; 4]
$D_1(2420)^0$	2423.3 ± 1.3	2216 – 2846	8.375 – 8.625	[8; 2]
$D_2^8(2460)^0$	2461.1 ± 1.6	2216 – 2846	8.375 – 8.625	[8; 2]
$D_2^8(2460)^\pm$	2460.1 ± 3.5	2216 – 2846	8.375 – 8.625	[8; 2]

mesons	measured mass MeV/c^2	mass interval MeV/c^2	S-interval	S
charmed, strange mesons $C = S = \pm 1$				
$D_S^{\pm}$	1968.49 ± 0.34	1726 – 2216	8.125 – 8.375	[8; 4]
$D_S^{*\pm}$	2112.3 ± 0.5	1726 – 2216	8.125 – 8.375	[8; 4]
$D_{S0}^{*}(2317)^{\pm}$	2317.8 ± 0.6	2216 – 2846	8.375 – 8.625	[8; 2]
$D_{S1}(2460)^{\pm}$	2459.6 ± 0.6	2216 – 2846	8.375 – 8.625	[8; 2]
$D_{S1}(2536)^{\pm}$	2535.35 ± 0.34	2216 – 2846	8.375 – 8.625	[8; 2]
$D_{S2}(2573)^{\pm}$	2572.6 ± 0.9	2216 – 2846	8.375 – 8.625	[8; 2]
bottom mesons $B = \pm 1$				
$B^{\pm}$	5279.17 ± 0.29	4692 – 6025	9.125 – 9.375	[9; 4]
B^0	5279.50 ± 0.3	4692 – 6025	9.125 – 9.375	[9; 4]
B^*	5325.1 ± 0.5	4692 – 6025	9.125 – 9.375	[9; 4]
$B_1(5721)^0$	5723.4 ± 2.0	4692 – 6025	9.125 – 9.375	[9; 4]
$B_2^*(5747)^0$	5743 ± 5	4692 – 6025	9.125 – 9.375	[9; 4]
bottom, strange mesons $B = \pm 1, S = \pm 1$				
B_S^0	5366.3 ± 0.6	4692 – 6025	9.125 – 9.375	[9; 4]
B_S^*	5415.4 ± 1.4	4692 – 6025	9.125 – 9.375	[9; 4]
bottom, charmed mesons $B = S = \pm 1$				
$B_c^{\pm}$	6277 ± 6	6025 – 7736	9.375 – 9.625	[9; 2]
cc-mesons $B = S = \pm 1$				
$\eta_c(1S)$	2980.5 ± 1.2	2846 – 3654	8.625 – 8.875	[9; −4]
$J/psi(1S)$	3096.916 ± 0.011	2846 – 3654	8.625 – 8.875	[9; −4]
$X_{c0}(1P)$	3414.75 ± 0.31	2846 – 3654	8.625 – 8.875	[9; −4]
$X_{c1}(1P)$	3510.66 ± 0.07	2846 – 3654	8.625 – 8.875	[9; −4]
$h_c(1P)$	3525.67 ± 0.32	2846 – 3654	8.625 – 8.875	[9; −4]
$X_{c2}(1P)$	3556.20 ± 0.09	2846 – 3654	8.625 – 8.875	[9; −4]
$\eta_c(2S)$	3637 ± 4	2846 – 3654	8.625 – 8.875	[9; −4]
$\psi(2S)$	3686.09 ± 0.04	3654 – 4692	8.875 – 9.125	[9]
$\psi(3770)$	3772.92 ± 0.35	3654 – 4692	8.875 – 9.125	[9]
$X(3872)$	3872.3 ± 0.8	3654 – 4692	8.875 – 9.125	[9]
$X(3945)$	3916 ± 6	3654 – 4692	8.875 – 9.125	[9]
$\psi(4400)$	4039 ± 1	3654 – 4692	8.875 – 9.125	[9]
$\psi(4160)$	4153 ± 3	3654 – 4692	8.875 – 9.125	[9]
$\psi(4260)$	4263 ± 9	3654 – 4692	8.875 – 9.125	[9]
$\psi(4415)$	4421 ± 4	3654 – 4692	8.875 – 9.125	[9]
bb-mesons				
$Y(1S)$	9460.30 ± 0.26	7736 – 9933	9.625 – 9.875	[10; −4]
$\chi_{b0}(1P)$	9859.44 ± 0.42	7736 – 9933	9.625 – 9.875	[10; −4]
$\chi_{b1}(1P)$	9892.78 ± 0.26	7736 – 9933	9.625 – 9.875	[10; −4]
$\chi_{b2}(1P)$	9912.21 ± 0.26	7736 – 9933	9.625 – 9.875	[10; −4]
$Y(2S)$	10023.26 ± 0.31	9933 – 12754	9.875 – 10.125	[10]
$\chi_{b0}(2P)$	10232.5 ± 0.4	9933 – 12754	9.875 – 10.125	[10]
$\chi_{b1}(2P)$	10255.46 ± 0.22	9933 – 12754	9.875 – 10.125	[10]
$\chi_{b2}(2P)$	10268.65 ± 0.22	9933 – 12754	9.875 – 10.125	[10]
$Y(3S)$	10355.2 ± 0.5	9933 – 12754	9.875 – 10.125	[10]
$Y(4S)$	10579.4 ± 1.2	9933 – 12754	9.875 – 10.125	[10]
$Y(10860)$	10865 ± 8	9933 – 12754	9.875 – 10.125	[10]
$Y(11020)$	11019 ± 8	9933 – 12754	9.875 – 10.125	[10]

Table 4. The measured masses of leptons [6], the calculated S-intervals of $\frac{1}{4}$ logarithmic units width and the corresponding calculated mass-intervals.

leptons	measured mass MeV/c^2	mass interval MeV/c^2	S-interval	S
electron	0.510998910 ± 0.000000013	0	0	[0]
μ	105.658367 ± 0.000004	86 – 110	5.125 – 5.375	[5; 4]
τ	1776.84 ± 0.17	1726 – 2216	8.125 – 8.375	[8; 4]

Table 5. The measured masses of gauge bosons [6], the calculated S-intervals of $\frac{1}{4}$ logarithmic units width and the corresponding calculated mass-intervals.

gauge bosons	measured mass MeV/c^2	mass interval MeV/c^2	S-interval	S
W	80398 ± 25	73395 – 94241	11.875 – 12.125	[12]
Z	91187, 6 ± 2.1	73395 – 94241	11.875 – 12.125	[12]

Schrödinger-Langevin Equation with PT-Symmetric Periodic Potential and its Application to Deuteron Cluster

Vic Christianto* and Florentin Smarandache†

*Present address: Institute of Gravitaion and Cosmology, PFUR, Moscow, 117198, Russia. E-mail: admin@sciprint.org
†Department of Mathematics, University of New Mexico, Gallup, NM 87301, USA. E-mail: smarand@unm.edu

In this article, we find out some analytical and numerical solutions to the problem of barrier tunneling for cluster deuterium, in particular using Langevin method to solve the time-independent Schrödinger equation.

1 Introduction

One of the most reported problem related to the CMNS (condensed matter nuclear science, or LENR), is the low probability of Coulomb barrier tunneling. It is supposed by standard physics that tunneling is only possible at high enough energy (by solving Gamow function).

However, a recent study by Takahashi (2008, 2009) and experiment by Arata etc. (2008) seem to suggest that it is not impossible to achieve a working experiment to create the CMNS process.

In accordance with Takahashi's EQPET/TSC model [1–3], the proposed study will find out some analytical and numerical solutions to the problem of barrier tunneling for cluster deuterium, in particular using Langevin method to solve the time-independent Schrödinger equation. It is hoped that the result can answer some of these mysteries.

One of the results of recent experiments is the lack of signature of D-D reaction as in standard fusion process; this is part of the reason to suggest that D-D fusion doesn't take place [1]. However, Takahashi suggests new possible reaction in the context of cluster deuterium, called 4D fusion [1–3], this mechanism seems to enable reaction at low temperature (CMNS). His result (2009) can be summarized as follows:

> "The ultimate condensation is possible only when the double Platonic symmetry of 4D/TSC is kept in its dynamic motion. The sufficient increase (super screening) of barrier factor is also only possible as far as the Platonic symmetric 4D/TSC system is kept. Therefore, there should be always 4 deuterons in barrier penetration and fusion process, so that 4d simultaneous fusion should take place predominantly. The portion of 2D (usual) fusion rate is considered to be negligible".

In this respect it can be noted that there are recent reports suggesting that hydrogen cluster can get reaction at very low temperature, forming the condition of superfluidity [4]. This seems to happen too in the context of Takahashi TSC condensate dynamics. Other study worth mentioning here is one that discussed molecular chessboard dynamics of deuterium [5].

The difference between this proposed study and recent work of Takahashi based on Langevin equation for cluster deuterium is that we focus on solution of Schrödinger-Langevin equation [6, 7] with PT-Symmetric periodic potential as we discussed in the preceding paper and its Gamow integral. The particular implications of this study to deuteron cluster will be discussed later.

Another differing part from the previous study is that in this study we will also seek clues on possibility to consider this low probability problem as an example of self-organized criticality phenomena. In other words, the time required before CMNS process can be observed is actually the time required to trigger the critical phenomena. To our present knowledge, this kind of approach has never been studied before, although self-organized criticality related to Schrödinger equation approximation to Burger's turbulence has been discussed in Boldyrev [8]. Nonetheless there is recent study suggesting link between diffusion process and the self-organized criticality phenomena.

The result of this study will be useful to better understanding of anomalous phenomena behind Condensed matter nuclear science.

2 Schrödinger-Langevin equation

The Langevin equation is considered as equivalent and therefore has often been used to solve the time-independent Schrödinger, in particular to study molecular dynamics.

Here we only cite the known Langevin equation [3, p. 29]

$$dX_t = p_t dt\,, \tag{1}$$

$$dp = -\partial_x \lambda_0(X_t)dt + Kp_t dt + dW_t\sqrt{2TK}\,. \tag{2}$$

Takahashi and Yabuuchi also used quite similar form of the stochastic non-linear Langevin equation [7] in order to study the dynamics of TSC condensate motion.

3 Schrödinger equation with PT-symmetric periodic potential

Consider a PT-Symmetric potential of the form [9, 10]

$$V = K_1 \sin(br)\,, \tag{3}$$

where

$$b = \frac{|m|}{\sqrt{-i-1}}\,. \tag{4}$$

Hence, the respective Schrödinger equation with this potential can be written as follows

$$\Psi''(r) = -k^2(r)\,\Psi(r)\,, \tag{5}$$

where

$$k(r) = \frac{2m}{\hbar^2}[E - V(r)] = \frac{2m}{\hbar^2}\left[E - k_1 \sin(br)\right]. \tag{6}$$

For the purpose of finding Gamow function, in area near x=a we can choose linear approximation for Coulomb potential, such that

$$V(x) - E = -\alpha(x - a)\,. \tag{7}$$

Substitution to Schrödinger equation yields

$$\Psi'' + \frac{2m\alpha}{\hbar^2}(x - a)\,\Psi = 0\,, \tag{8}$$

which can be solved by virtue of Airy function.

4 Gamow integral

In principle, the Gamow function can be derived as follows [11]

$$\frac{d^2y}{dx^2} + P(x)y = 0\,. \tag{9}$$

Separating the variables and integrating, yields

$$\int \frac{d^2y}{y} = \int -P(x)\,dx \tag{10}$$

or

$$y\,dy = \exp\left(-\int P(x)\,dx + C\right). \tag{11}$$

To find solution of Gamow function, therefore the integral below must be evaluated:

$$\gamma = \sqrt{\frac{2m}{\hbar^2}\left[V(x) - E\right]}\,. \tag{12}$$

For the purpose of analysis we use the same data from Takahashi's EQPET model [3,12], i.e. $b = 5.6$ fm, and $r_0 = 5$ fm. Here we assume that $E = V_b = 0.257$ MeV. Therefore the integral becomes

$$\Gamma = 0.218\,\sqrt{m}\int_{r_0}^{b}\sqrt{k_1 \sin(br) - 0.257}\,dr\,. \tag{13}$$

By setting boundary condition (either one or more of these conditions)

(a) at $r = 0$ then $V_0 = -V_b - 0.257$MeV;

(b) at $r = 5.6fm$ then $V_1 = k_1 \sin(br) - 0.257 = 0.257$MeV, therefore, one can find estimate of m;

(c) Using this procedure solution of the equation (11) can be found.

The interpretation of this Gamow function is the tunneling rate of the fusion reaction of cluster of deuterium (for the given data) corresponding to Takahashi data [12], with the difference that here we consider a PT-symmetric periodic potential.

The numerical study will be performed with standard package like Maxima etc. Some plausible implications in cosmology modeling should also be discussed in the future.

Submitted on January 20, 2010 / Accepted on March 04, 2010

References

1. Takahashi A. Basics of the deuteron-cluster dynamics by Langevin equation. In: *Low-Energy Nuclear Reactions and New Energy Technologies Sourcebook*, v. 2, 2010, Chapter 11, 193–217, (*ACS Symposium Series*, v. 1029).
2. Takahashi A. and Yabuuchi N. Study on 4D/TSC condensate motion using non-linear Langevin equation. In: *Low-Energy Nuclear Reactions Sourcebook*, 2008, Chapter 4, 57–83 (*ACS Symposium Series*, v. 998).
3. Takahashi A. Dynamic mechanism of TSC condensation motion. *Proc. Intern. Conf. of Condensed Matter Nuclear Science*, Washington DC, 2008.
4. Mezzacapo F. and Boninsegni M. Structure, superfluidity and quantum melting of hydrogen clusters. arXiv: cond-mat/0611775.
5. Calvert C.R., et al. Quantum chessboards in the deuterium molecular ion. arXiv: quantph/08062253.
6. Zsepessy A. Stochastic and deterministic molecular dynamics derived from the time independent Schrödinger equation. arXiv: cond-mat/0812.4338.
7. Rusov V.D. et al. Schrödinger-Chetaev equation. arXiv: 0810.2860.
8. Boldyrev S. arXiv: hep-th/9610080.
9. Christianto V. and Smarandache F. On PT-symmetric periodic potential, quark confinement, and other impossible pursuits. *Progress in Physics*, 2009, v. 1.
10. Christianto V. and Smarandache F. Numerical solution of biquaternion radical Klein-Gordon equation. *Progress in Physics*, 2008, v. 1; also in: Smarandache F. and Christianto V. (eds.) Hadron models and related new energy issues. InfoLearnQuest Publ., USA, 2008.
11. Coddington E. A. and Levinson N. Theory of ordinary differential equations. Mc Graw-Hill, New York, 1955.
12. Takahashi A. Summary of condensed matter nuclear reactions. *J. Cond. Matter Nuclear Science*, 2007, v. 1.

Smarandache's Cevian Triangle Theorem in The Einstein Relativistic Velocity Model of Hyperbolic Geometry

Cătălin Barbu

"Vasile Alecsandri" College — Bacău, str. Iosif Cocea, nr. 12, sc. A, apt. 13, Romania. E-mail: kafka_mate@yahoo.com

In this note, we present a proof of Smarandache's cevian triangle hyperbolic theorem in the Einstein relativistic velocity model of hyperbolic geometry.

1 Introduction

Hyperbolic geometry appeared in the first half of the 19^{th} century as an attempt to understand Euclid's axiomatic basis for geometry. It is also known as a type of non-Euclidean geometry, being in many respects similar to Euclidean geometry. Hyperbolic geometry includes such concepts as: distance, angle and both of them have many theorems in common.There are known many main models for hyperbolic geometry, such as: Poincaré disc model, Poincaré half-plane, Klein model, Einstein relativistic velocity model, etc. The hyperbolic geometry is a non-Euclidian geometry. Here, in this study, we present a proof of Smarandache's cevian triangle hyperbolic theorem in the Einstein relativistic velocity model of hyperbolic geometry. Smarandache's cevian triangle theorem states that if $A_1B_1C_1$ is the cevian triangle of point P with respect to the triangle ABC, then $\frac{PA}{PA_1}\cdot\frac{PB}{PB_1}\cdot\frac{PC}{PC_1}=\frac{AB\cdot BC\cdot CA}{A_1B\cdot B_1C\cdot C_1A}$ [1].

Let D denote the complex unit disc in complex z - plane, i.e.

$$D=\{z\in\mathbb{C}:|z|<1\}.$$

The most general Möbius transformation of D is

$$z\to e^{i\theta}\frac{z_0+z}{1+\overline{z}_0z}=e^{i\theta}(z_0\oplus z),$$

which induces the Möbius addition $\oplus$ in D, allowing the Möbius transformation of the disc to be viewed as a Möbius left gyrotranslation

$$z\to z_0\oplus z=\frac{z_0+z}{1+\overline{z}_0z}$$

followed by a rotation. Here $\theta\in\mathbb{R}$ is a real number, $z,z_0\in D$, and $\overline{z}_0$ is the complex conjugate of z_0. Let $Aut(D,\oplus)$ be the automorphism group of the grupoid $(D,\oplus)$. If we define

$$gyr:D\times D\to Aut(D,\oplus),\quad gyr[a,b]=\frac{a\oplus b}{b\oplus a}=\frac{1+a\overline{b}}{1+\overline{a}b},$$

then is true gyrocommutative law

$$a\oplus b=gyr[a,b](b\oplus a).$$

A gyrovector space $(G,\oplus,\otimes)$ is a gyrocommutative gyrogroup $(G,\oplus)$ that obeys the following axioms:

(1) $gyr[\mathbf{u},\mathbf{v}]\mathbf{a}\cdot gyr[\mathbf{u},\mathbf{v}]\mathbf{b}=\mathbf{a}\cdot\mathbf{b}$ for all points $\mathbf{a},\mathbf{b},\mathbf{u},\mathbf{v}\in G$;

(2) G admits a scalar multiplication, $\otimes$, possessing the following properties. For all real numbers $r,r_1,r_2\in\mathbb{R}$ and all points $\mathbf{a}\in G$:

G1 $1\otimes\mathbf{a}=\mathbf{a}$,

G2 $(r_1+r_2)\otimes\mathbf{a}=r_1\otimes\mathbf{a}\oplus r_2\otimes\mathbf{a}$,

G3 $(r_1r_2)\otimes\mathbf{a}=r_1\otimes(r_2\otimes\mathbf{a})$,

G4 $\frac{|r|\otimes\mathbf{a}}{\|r\otimes\mathbf{a}\|}=\frac{\mathbf{a}}{\|\mathbf{a}\|}$,

G5 $gyr[\mathbf{u},\mathbf{v}](r\otimes\mathbf{a})=r\otimes gyr[\mathbf{u},\mathbf{v}]\mathbf{a}$,

G6 $gyr[r_1\otimes\mathbf{v},r_1\otimes\mathbf{v}]=I$;

(3) Real vector space structure $(\|G\|,\oplus,\otimes)$ for the set $\|G\|$ of onedimensional "vectors"

$$\|G\|=\{\pm\|\mathbf{a}\|:\mathbf{a}\in G\}\subset\mathbb{R}$$

with vector addition $\oplus$ and scalar multiplication $\otimes$, such that for all $r\in\mathbb{R}$ and $\mathbf{a},\mathbf{b}\in G$:

G7 $\|r\otimes\mathbf{a}\|=|r|\otimes\|\mathbf{a}\|$,

G8 $\|\mathbf{a}\oplus\mathbf{b}\|\leqslant\|\mathbf{a}\|\oplus\|\mathbf{b}\|$.

Theorem 1 The Hyperbolic Theorem of Ceva in Einstein Gyrovector Space *Let* $\mathbf{a}_1,\mathbf{a}_2$, *and* $\mathbf{a}_3$ *be three non-gyrocollinear points in an Einstein gyrovector space* $(V_s,\oplus,\otimes)$. *Furthermore, let* $\mathbf{a}_{123}$ *be a point in their gyroplane, which is off the gyrolines* $\mathbf{a}_1\mathbf{a}_2,\mathbf{a}_2\mathbf{a}_3$, *and* $\mathbf{a}_3\mathbf{a}_1$. *If* $\mathbf{a}_1\mathbf{a}_{123}$ *meets* $\mathbf{a}_2\mathbf{a}_3$ *at* $\mathbf{a}_{23}$, *etc., then*

$$\frac{\gamma_{\ominus\mathbf{a}_1\oplus\mathbf{a}_{12}}\|\ominus\mathbf{a}_1\oplus\mathbf{a}_{12}\|}{\gamma_{\ominus\mathbf{a}_2\oplus\mathbf{a}_{12}}\|\ominus\mathbf{a}_2\oplus\mathbf{a}_{12}\|}\cdot\frac{\gamma_{\ominus\mathbf{a}_2\oplus\mathbf{a}_{23}}\|\ominus\mathbf{a}_2\oplus\mathbf{a}_{23}\|}{\gamma_{\ominus\mathbf{a}_3\oplus\mathbf{a}_{23}}\|\ominus\mathbf{a}_3\oplus\mathbf{a}_{23}\|}\times\\ \times\frac{\gamma_{\ominus\mathbf{a}_3\oplus\mathbf{a}_{13}}\|\ominus\mathbf{a}_3\oplus\mathbf{a}_{13}\|}{\gamma_{\ominus\mathbf{a}_1\oplus\mathbf{a}_{13}}\|\ominus\mathbf{a}_1\oplus\mathbf{a}_{13}\|}=1,$$

(here $\gamma_{\mathbf{v}}=\frac{1}{\sqrt{1-\frac{\|\mathbf{v}\|^2}{s^2}}}$ *is the gamma factor).* (See [2, pp. 461].)

Theorem 2 The Hyperbolic Theorem of Menelaus in Einstein Gyrovector Space *Let* $\mathbf{a}_1,\mathbf{a}_2$, *and* $\mathbf{a}_3$ *be three non-gyrocollinear points in an Einstein gyrovector space* $(V_s,\oplus,\otimes)$. *If a gyroline meets the sides of gyrotriangle* $\mathbf{a}_1\mathbf{a}_2\mathbf{a}_3$ *at points* $\mathbf{a}_{12},\mathbf{a}_{13},\mathbf{a}_{23}$, *then*

$$\frac{\gamma_{\ominus\mathbf{a}_1\oplus\mathbf{a}_{12}}\|\ominus\mathbf{a}_1\oplus\mathbf{a}_{12}\|}{\gamma_{\ominus\mathbf{a}_2\oplus\mathbf{a}_{12}}\|\ominus\mathbf{a}_2\oplus\mathbf{a}_{12}\|}\cdot\frac{\gamma_{\ominus\mathbf{a}_2\oplus\mathbf{a}_{23}}\|\ominus\mathbf{a}_2\oplus\mathbf{a}_{23}\|}{\gamma_{\ominus\mathbf{a}_3\oplus\mathbf{a}_{23}}\|\ominus\mathbf{a}_3\oplus\mathbf{a}_{23}\|}\times\\ \times\frac{\gamma_{\ominus\mathbf{a}_3\oplus\mathbf{a}_{13}}\|\ominus\mathbf{a}_3\oplus\mathbf{a}_{13}\|}{\gamma_{\ominus\mathbf{a}_1\oplus\mathbf{a}_{13}}\|\ominus\mathbf{a}_1\oplus\mathbf{a}_{13}\|}=1.$$

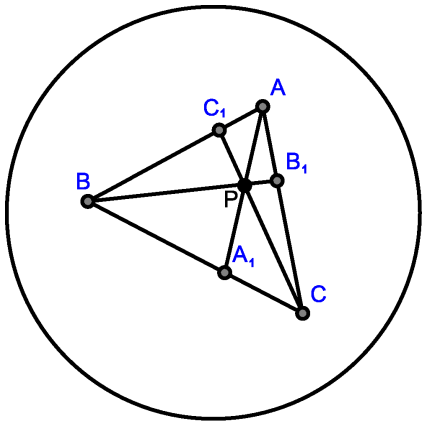

(See [2, pp. 463].) For further details we refer to A. Ungar's recent book [2].

2 Main result

In this section, we present a proof of Smarandache's cevian triangle hyperbolic theorem in the Einstein relativistic velocity model of hyperbolic geometry.

Theorem 3 *If $A_1B_1C_1$ is the cevian gyrotriangle of gyropoint P with respect to the gyrotriangle ABC, then*

$$\frac{\gamma_{|PA|}|PA|}{\gamma_{|PA_1|}|PA_1|}\cdot\frac{\gamma_{|PB|}|PB|}{\gamma_{|PB_1|}|PB_1|}\cdot\frac{\gamma_{|PC|}|PC|}{\gamma_{|PC_1|}|PC_1|}=\frac{\gamma_{|AB|}|AB|\cdot\gamma_{|BC|}|BC|\cdot\gamma_{|CA|}|CA|}{\gamma_{|AB_1|}|AB_1|\cdot\gamma_{|BC_1|}|BC_1|\cdot\gamma_{|CA_1|}|CA_1|}.$$

Proof *If we use a theorem 2 in the gyrotriangle ABC (see Figure), we have*

$$\gamma_{|AC_1|}|AC_1|\cdot\gamma_{|BA_1|}|BA_1|\cdot\gamma_{|CB_1|}|CB_1|=\gamma_{|AB_1|}|AB_1|\cdot\gamma_{|BC_1|}|BC_1|\cdot\gamma_{|CA_1|}|CA_1|. \quad (1)$$

If we use a theorem 1 in the gyrotriangle AA_1B, cut by the gyroline CC_1, we get

$$\gamma_{|AC_1|}|AC_1|\cdot\gamma_{|BC|}|BC|\cdot\gamma_{|A_1P|}|A_1P|=\gamma_{|AP|}|AP|\cdot\gamma_{|A_1C|}|A_1C|\cdot\gamma_{|BC_1|}|BC_1|. \quad (2)$$

If we use a theorem 1 in the gyrotriangle BB_1C, cut by the gyroline AA_1, we get

$$\gamma_{|BA_1|}|BA_1|\cdot\gamma_{|CA|}|CA|\cdot\gamma_{|B_1P|}|B_1P|=\gamma_{|BP|}|BP|\cdot\gamma_{|B_1A|}|B_1A|\cdot\gamma_{|CA_1|}|CA_1|. \quad (3)$$

If we use a theorem 1 in the gyrotriangle CC_1A, cut by the gyroline BB_1, we get

$$\gamma_{|CB_1|}|CB_1|\cdot\gamma_{|AB|}|AB|\cdot\gamma_{|C_1P|}|C_1P|=\gamma_{|CP|}|CP|\cdot\gamma_{|C_1B|}|C_1B|\cdot\gamma_{|AB_1|}|AB_1|. \quad (4)$$

We divide each relation (2), (3), and (4) by relation (1), and we obtain

$$\frac{\gamma_{|PA|}|PA|}{\gamma_{|PA_1|}|PA_1|}=\frac{\gamma_{|BC|}|BC|}{\gamma_{|BA_1|}|BA_1|}\cdot\frac{\gamma_{|B_1A|}|B_1A|}{\gamma_{|B_1C|}|B_1C|}, \quad (5)$$

$$\frac{\gamma_{|PB|}|PB|}{\gamma_{|PB_1|}|PB_1|}=\frac{\gamma_{|CA|}|CA|}{\gamma_{|CB_1|}|CB_1|}\cdot\frac{\gamma_{|C_1B|}|C_1B|}{\gamma_{|C_1A|}|C_1A|}, \quad (6)$$

$$\frac{\gamma_{|PC|}|PC|}{\gamma_{|PC_1|}|PC_1|}=\frac{\gamma_{|AB|}|AB|}{\gamma_{|AC_1|}|AC_1|}\cdot\frac{\gamma_{|A_1C|}|A_1C|}{\gamma_{|A_1B|}|A_1B|}. \quad (7)$$

Multiplying (5) by (6) and by (7), we have

$$\frac{\gamma_{|PA|}|PA|}{\gamma_{|PA_1|}|PA_1|}\cdot\frac{\gamma_{|PB|}|PB|}{\gamma_{|PB_1|}|PB_1|}\cdot\frac{\gamma_{|PC|}|PC|}{\gamma_{|PC_1|}|PC_1|}= \\ =\frac{\gamma_{|AB|}|AB|\cdot\gamma_{|BC|}|BC|\cdot\gamma_{|CA|}|CA|}{\gamma_{|A_1B|}|A_1B|\cdot\gamma_{|B_1C|}|B_1C|\cdot\gamma_{|C_1A|}|C_1A|}\cdot\frac{\gamma_{|B_1A|}|B_1A|\cdot\gamma_{|C_1B|}|C_1B|\cdot\gamma_{|A_1C|}|A_1C|}{\gamma_{|A_1B|}|A_1B|\cdot\gamma_{|B_1C|}|B_1C|\cdot\gamma_{|C_1A|}|C_1A|}. \quad (8)$$

From the relation (1) we have

$$\frac{\gamma_{|B_1A|}|B_1A|\cdot\gamma_{|C_1B|}|C_1B|\cdot\gamma_{|A_1C|}|A_1C|}{\gamma_{|A_1B|}|A_1B|\cdot\gamma_{|B_1C|}|B_1C|\cdot\gamma_{|C_1A|}|C_1A|}=1, \quad (9)$$

so

$$\frac{\gamma_{|PA|}|PA|}{\gamma_{|PA_1|}|PA_1|}\cdot\frac{\gamma_{|PB|}|PB|}{\gamma_{|PB_1|}|PB_1|}\cdot\frac{\gamma_{|PC|}|PC|}{\gamma_{|PC_1|}|PC_1|}=\frac{\gamma_{|AB|}|AB|\cdot\gamma_{|BC|}|BC|\cdot\gamma_{|CA|}|CA|}{\gamma_{|AB_1|}|AB_1|\cdot\gamma_{|BC_1|}|BC_1|\cdot\gamma_{|CA_1|}|CA_1|}.$$

Submitted on March 05, 2010 / Accepted on March 26, 2010

References

1. Smarandache F. Eight solved and eight open problems in elementary geometry. arXiv: 1003.2153.
2. Ungar A.A. Analytic hyperbolic geometry and Albert Einstein's Special Theory of Relativity. World Scientific Publishing Co., Hackensack (NJ), 2008.

The Journal on Advanced Studies in Theoretical and Experimental Physics, including Related Themes from Mathematics

PROGRESS IN PHYSICS

A quarterly issue scientific journal, registered with the Library of Congress (DC, USA). This journal is peer reviewed and included in the abstracting and indexing coverage of: Mathematical Reviews and MathSciNet (AMS, USA), DOAJ of Lund University (Sweden), Zentralblatt MATH (Germany), Scientific Commons of the University of St. Gallen (Switzerland), Open-J-Gate (India), Referativnyi Zhurnal VINITI (Russia), etc.

To order printed issues of this journal, contact the Editors. Electronic version of this journal can be downloaded free of charge:
http://www.ptep-online.com

This journal is powered by LaTeX

A variety of books can be downloaded free from the Digital Library of Science:
http://www.gallup.unm.edu/~smarandache

ISSN: 1555-5534 (print)
ISSN: 1555-5615 (online)

Standard Address Number: 297-5092
Printed in the United States of America

OCTOBER 2010 **VOLUME 4**

CONTENTS

Information for Authors and Subscribers

Progress in Physics has been created for publications on advanced studies in theoretical and experimental physics, including related themes from mathematics and astronomy. All submitted papers should be professional, in good English, containing a brief review of a problem and obtained results.

All submissions should be designed in LaTeX format using *Progress in Physics* template. This template can be downloaded from *Progress in Physics* home page http://www.ptep-online.com. Abstract and the necessary information about author(s) should be included into the papers. To submit a paper, mail the file(s) to the Editor-in-Chief.

All submitted papers should be as brief as possible. We accept brief papers, no larger than 8 typeset journal pages. Short articles are preferable. Large papers can be considered in exceptional cases to the section *Special Reports* intended for such publications in the journal. Letters related to the publications in the journal or to the events among the science community can be applied to the section *Letters to Progress in Physics*.

All that has been accepted for the online issue of *Progress in Physics* is printed in the paper version of the journal. To order printed issues, contact the Editors.

This journal is non-commercial, academic edition. It is printed from private donations. (Look for the current author fee in the online version of the journal.)

Formation of Singlet Fermion Pairs in the Dilute Gas of Boson-Fermion Mixture

Vahan Minasyan and Valentin Samoilov
Scientific Center of Applied Research, JINR, Dubna, 141980, Russia
E-mails: mvahan@scar.jinr.ru; scar@off-serv.jinr.ru

We argue the formation of a free neutron spinless pairs in a liquid helium -dilute neutron gas mixture. We show that the term, of the interaction between the excitations of the Bose gas and the density modes of the neutron, meditate an attractive interaction via the neutron modes, which in turn leads to a bound state on a spinless neutron pair. Due to presented theoretical approach, we prove that the electron pairs in superconductivity could be discovered by Frölich earlier then it was made by the Cooper.

1 Introduction

In 1938, the connection between the ideal Bose gas and superfluidity in helium was first made by London [1]. The ideal Bose gas undergoes a phase transition at sufficiently low temperatures to a condition in which the zero-momentum quantum state is occupied by a finite fraction of the atoms. This momentum-condensed phase was postulated by London to represent the superfluid component of liquid ^{4}He. With this hypothesis, the beginnings of a two- fluid hydrodynamic model of superfluids was developed by Landau [2] where he predicted the notation of a collective excitations so- called phonons and rotons.

The microscopic theory most widely- adopted was first described by Bogoliubov [3], who considered a model of a non-ideal Bose-gas at the absolute zero of temperature. In 1974, Bishop [4] examined the one-particle excitation spectrum at the condensation temperature T_c.

The dispersion curve of superfluid helium excitations has been measured accurately as a function of momentum [5]. At the lambda transition, these experiments show a sharp peak inelastic whose neutron scattering intensity is defined by the energy of the single particle excitations, and there is appearing a broad component in the inelastic neutron scattering intensity, at higher momenta. To explain the appearance of a broad component in the inelastic neutron scattering intensity, the authors of papers [6–7] proposed the presence of collective modes in superfluid liquid ^{4}He, represented a density excitations. Thus the collective modes are represent as density quasiparticles [8]. Such density excitations and density quasiparticles appear because of the remaining density operator term that describes atoms above the condensate, a term which was neglected by Bogoliubov [3].

Previously, the authors of ref [9] discovered that, at the lambda transition, there was scattering between atoms of the superfluid liquid helium, which is confirmed by the calculation of the dependence of the critical temperature on the interaction parameter, here the scattering length. On other hand, as we have noted, there are two types of excitation in superfluid helium at lambda transition point [5]. This means it is necessary to revise the conditions that determine the Bose-Einstein condensation in the superfluid liquid helium. Obviously, the peak inelastic neutron scattering intensity is connected with the registration of neutron modes in a neutron-spectrometer which, in turn, defines the nature of the excitations. So we may conclude that the registration of single neutron modes or neutron pair modes occurs at the lambda transition, from the neutron-spectrometer.

In this letter, we proposed new model for Bose-gas by extending the concept of a broken Bose-symmetry law for bosons in the condensate within applying the Penrose-Onsager definition of the Bose condensation [10]. After, we show that the interaction term between Boson modes and Fermion density modes is meditated by an effective attractive interaction between the Fermion modes, which in turn determines a bound state of singlet Fermion pair in a superfluid Bose liquid- Fermion gas mixture.

We investigate the problem of superconductivity presented by Frölich [11]. Hence, we also remark the theory of superconductivity, presented by Bardeen, Cooper and Schrieffer [12], and by Bogoliubov [13] (BCSB). They asserted that the Frölich effective attractive potential between electrons leads to shaping of two electrons with opposite spins around Fermi level into the Cooper pairs [14]. However, we demonstrate the term of the interaction between electrons and ions of lattice meditates the existence of the Frölich singlet electron pairs.

2 New model of a superfluid liquid helium

First, we present new model of a dilute Bose gas with strongly interactions between the atoms, to describe the superfluid liquid helium. This model considers a system of N identical interacting atoms via S-wave scattering. These atoms, as spinless Bose-particles, have a mass m and are confined to a box of volume V. The main part of the Hamiltonian of such system is expressed in the second quantization form as:

$$\hat{H}_a = \sum_{\vec{p}\neq 0} \frac{p^2}{2m} \hat{a}^+_{\vec{p}} \hat{a}_{\vec{p}} + \frac{1}{2V} \sum_{\vec{p}\neq 0} U_{\vec{p}} \hat{\varrho}_{\vec{p}} \hat{\varrho}^+_{\vec{p}} . \qquad (1)$$

Here $\hat{a}^+_{\vec{p}}$ and $\hat{a}_{\vec{p}}$ are, respectively, the "creation" and "annihilation" operators of a free atoms with momentum $\vec{p}$; $U_{\vec{p}}$ is the Fourier transform of a S-wave pseudopotential in the

momentum space:

$$U_{\vec{p}} = \frac{4\pi d\hbar^2}{m}\,, \tag{2}$$

where d is the scattering amplitude; and the Fourier component of the density operator presents as

$$\hat{\varrho}_{\vec{p}} = \sum_{\vec{p}_1} \hat{a}^+_{\vec{p}_1-\vec{p}}\,\hat{a}_{\vec{p}_1}\,. \tag{3}$$

According to the Bogoliubov theory [3], it is necessary to separate the atoms in the condensate from those atoms filling states above the condensate. In this respect, the operators $\hat{a}_0$ and $\hat{a}^+_0$ are replaced by c-numbers $\hat{a}_0 = \hat{a}^+_0 = \sqrt{N_0}$ within the approximation of the presence of a macroscopic number of condensate atoms $N_0 \gg 1$. This assumption leads to a broken Bose-symmetry law for atoms in the condensate state. To extend the concept of a broken Bose-symmetry law for bosons in the condensate, we apply the Penrose-Onsager definition of Bose condensation [10]:

$$\lim_{N_0,N\to\infty} \frac{N_0}{N} = const. \tag{4}$$

This reasoning is a very important factor in the microscopic investigation of the model non-ideal Bose gas because the presence of a macroscopic number of atoms in the condensate means new excitations in the model Bose-gas for superfluid liquid helium:

$$\frac{N_{\vec{p}\neq 0}}{N_0} = \alpha \ll 1\,,$$

where $N_{\vec{p}\neq 0}$ is the occupation number of atoms in the quantum levels above the condensate; α is the small number. Obviously, conservation of the total number of atoms suggests that the number of the Bose-condensed atoms N_0 essentially deviates from the total number N:

$$N_0 + \sum_{\vec{p}\neq 0} N_{\vec{p}\neq 0} = N\,,$$

which is satisfied for the present model. In this context,

$$\alpha = \frac{N - N_0}{N_0 \sum_{\vec{p}\neq 0} 1} \to 0\,,$$

where $\sum_{\vec{p}\neq 0} 1 \to \infty$.

For futher calculations, we replace the initial assumptions of our model by the approximation

$$\lim_{N_0\to\infty} \frac{N_{\vec{p}}}{N_0} \approx \delta_{\vec{p},0} \tag{5}$$

The next step is to find the property of operators $\frac{\hat{a}^+_{\vec{p}_1-\vec{p}}}{\sqrt{N_0}}$, $\frac{\hat{a}_{\vec{p}_1-\vec{p}}}{\sqrt{N_0}}$ by applying (5). Obviously,

$$\lim_{N_0\to\infty} \frac{\hat{a}^+_{\vec{p}_1-\vec{p}}}{\sqrt{N_0}} = \delta_{\vec{p}_1,\vec{p}} \tag{6}$$

and

$$\lim_{N_0\to\infty} \frac{\hat{a}_{\vec{p}_1-\vec{p}}}{\sqrt{N_0}} = \delta_{\vec{p}_1,\vec{p}}\,. \tag{7}$$

Excluding the term $\vec{p}_1 = 0$, the density operators of bosons $\hat{\varrho}_{\vec{p}}$ and $\hat{\varrho}^+_{\vec{p}}$ take the following forms:

$$\hat{\varrho}_{\vec{p}} = \sqrt{N_0}\,\left(\hat{a}^+_{-\vec{p}} + \sqrt{2}\,\hat{c}_{\vec{p}}\right) \tag{8}$$

and

$$\hat{\varrho}^+_{\vec{p}} = \sqrt{N_0}\,\left(\hat{a}_{-\vec{p}} + \sqrt{2}\,\hat{c}^+_{\vec{p}}\right) \tag{9}$$

where $\hat{c}_{\vec{p}}$ and $\hat{c}^+_{\vec{p}}$ are, respectively, the Bose-operators of density-quasiparticles presented in reference [8], which in turn are the Bose-operators of bosons used in expressions (6) and (7):

$$\hat{c}_{\vec{p}} = \frac{1}{\sqrt{2N_0}} \sum_{\vec{p}_1\neq 0} \hat{a}^+_{\vec{p}_1-\vec{p}}\,\hat{a}_{\vec{p}_1} = \frac{1}{\sqrt{2}} \sum_{\vec{p}_1\neq 0} \delta_{\vec{p}_1,\vec{p}}\,\hat{a}_{\vec{p}_1} = \frac{\hat{a}_{\vec{p}}}{\sqrt{2}} \tag{10}$$

and

$$\hat{c}^+_{\vec{p}} = \frac{1}{\sqrt{2N_0}} \sum_{\vec{p}_1\neq 0} \hat{a}^+_{\vec{p}_1}\,\hat{a}_{\vec{p}_1-\vec{p}} = \frac{1}{\sqrt{2}} \sum_{\vec{p}_1\neq 0} \delta_{\vec{p}_1,\vec{p}}\,\hat{a}^+_{\vec{p}_1} = \frac{\hat{a}^+_{\vec{p}}}{\sqrt{2}}\,. \tag{11}$$

Thus, we reach to the density operators of atoms $\hat{\varrho}_{\vec{p}}$ and $\hat{\varrho}^+_{\vec{p}}$, presented by Bogoliubov [3], at approximation $\frac{N_0}{N}$=$const$, which describes the gas of atoms ^{4}He with strongly interaction via S-wave scattering:

$$\hat{\varrho}_{\vec{p}} = \sqrt{N_0}\,\left(\hat{a}^+_{-\vec{p}} + \hat{a}_{\vec{p}}\right) \tag{12}$$

and

$$\hat{\varrho}^+_{\vec{p}} = \sqrt{N_0}\,\left(\hat{a}_{-\vec{p}} + \hat{a}^+_{\vec{p}}\right) \tag{13}$$

which shows that the density quasiparticles are absent.

The identical picture is observed in the case of the density excitations, as predicted by Glyde, Griffin and Stirling [5–7] proposing $\hat{\varrho}_{\vec{p}}$ in the following form:

$$\hat{\varrho}_{\vec{p}} = \sqrt{N_0}\,\left(\hat{a}^+_{-\vec{p}} + \hat{a}_{\vec{p}} + \tilde{\varrho}_{\vec{p}}\right) \tag{14}$$

where terms involving $\vec{p}_1 \neq 0$ and , $\vec{p}_1 \neq \vec{p}$ are written separately; and the operator $\tilde{\varrho}_{\vec{p}}$ describes the density-excitations:

$$\tilde{\varrho}_{\vec{p}} = \frac{1}{\sqrt{N_0}} \sum_{\vec{p}_1\neq 0,\vec{p}_1\neq\vec{p}} \hat{a}^+_{\vec{p}_1-\vec{p}}\,\hat{a}_{\vec{p}_1}\,. \tag{15}$$

After inserting (6) and (7) into (15), the term, representing the density-excitations vanishes because $\tilde{\varrho}_{\vec{p}} = 0$.

Consequently, the Hamiltonian of system, presented in (1) with also (12) and (13), represents an extension of the Bogoliubov Hamiltonian, with the approximation $\frac{N_0}{N} = const$, which in turn does not depend on the actual amplitude of interaction. In the case of strongly interacting atoms, the Hamiltonian takes the following form:

$$\hat{H}_a = \sum_{\vec{p}\neq 0} \left(\frac{p^2}{2m} + mv^2\right) \hat{a}^+_{\vec{p}}\,\hat{a}_{\vec{p}} + \frac{mv^2}{2} \sum_{\vec{p}\neq 0} \left(\hat{a}^+_{-\vec{p}}\,\hat{a}^+_{\vec{p}} + \hat{a}_{\vec{p}}\,\hat{a}_{-\vec{p}}\right), \tag{16}$$

where $v = \sqrt{\frac{U_{\vec{r}} N_0}{mV}} = \sqrt{\frac{4\pi d\hbar^2 N_0}{m^2 V}}$ is the velocity of sound in the Bose gas, and which depends on the density atoms in the condensate $\frac{N_0}{V}$.

For the evolution of the energy level, it is a necessary to diagonalize the Hamiltonian $\hat{H}_a$ which is accomplished by introduction of the Bose-operators $\hat{b}^+_{\vec{p}}$ and $\hat{b}_{\vec{p}}$ by using of the Bogoliubov linear transformation [3]:

$$\hat{a}_{\vec{p}} = \frac{\hat{b}_{\vec{p}} + L_{\vec{p}}\,\hat{b}^+_{-\vec{p}}}{\sqrt{1 - L^2_{\vec{p}}}}\,, \tag{17}$$

where $L_{\vec{p}}$ is the unknown real symmetrical function of a momentum $\vec{p}$.

Substitution of (17) into (16) leads to

$$\hat{H}_a = \sum_{\vec{p}} \varepsilon_{\vec{p}}\,\hat{b}^+_{\vec{p}}\,\hat{b}_{\vec{p}} \tag{18}$$

hence we infer that $\hat{b}^+_{\vec{p}}$ and $\hat{b}_{\vec{p}}$ are the "creation" and "annihilation" operators of a Bogoliubov quasiparticles with energy:

$$\varepsilon_{\vec{p}} = \left[\left(\frac{p^2}{2m}\right)^2 + p^2 v^2\right]^{1/2}. \tag{19}$$

In this context, the real symmetrical function $L_{\vec{p}}$ of a momentum $\vec{p}$ is found

$$L^2_{\vec{p}} = \frac{\frac{p^2}{2m} + mv^2 - \varepsilon_{\vec{p}}}{\frac{p^2}{2m} + mv^2 + \varepsilon_{\vec{p}}}\,. \tag{20}$$

As is well known, the strong interaction between the helium atoms is very important and reduces the condensate fraction to 10 percent or $\frac{N_0}{N} = 0.1$ [5], at absolute zero. However, as we suggest, our model of dilute Bose gas may be valuable in describing thermodynamic properties of superfluid liquid helium, because the S-wave scattering between two atoms, with coordinates $\vec{r}_1$ and $\vec{r}_2$ in coordinate space, is represented by the repulsive potential delta-function $U_{\vec{r}} = \frac{4\pi d\hbar^2 \delta_{\vec{r}}}{m}$ from $\vec{r} = \vec{r}_1 - \vec{r}_2$. The model presented works on the condensed fraction $\frac{N_0}{N} \ll 1$ and differs from the Bogoliubov model where $\frac{N_0}{N} \approx 1$.

3 Formation singlet spinless neutron pairs

We now attempt to describe the thermodynamic property of a helium liquid-neutron gas mixture. In this context, we consider a neutron gas as an ideal Fermi gas consisting of n free neutrons with mass m_n which interact with N interacting atoms of a superfluid liquid helium. The helium-neutron mixture is confined in a box of volume V. The Hamiltonian of a considering system $\hat{H}_{a,n}$ consists of the term of the Hamiltonian of Bogoliubov excitations $\hat{H}_a$ in (18) and the term of the Hamiltonian of an ideal Fermi neutron gas as well as the term of interaction between the density of the Bogoliubov excitations and the density of the neutron modes:

$$\begin{aligned}\hat{H}_{a,n} &= \textstyle\sum_{\vec{p},\sigma} \frac{p^2}{2m_n}\,\hat{a}^+_{\vec{p},\sigma}\,\hat{a}_{\vec{p},\sigma} + \\ &+ \sum_{\vec{p}} \varepsilon_{\vec{p}}\,\hat{b}^+_{\vec{p}}\,\hat{b}_{\vec{p}} + \frac{1}{2V}\sum_{\vec{p}\neq 0} U_0\,\hat{\varrho}_{\vec{p}}\,\hat{\varrho}_{-\vec{p},n}\,,\end{aligned} \tag{21}$$

where $\hat{a}^+_{\vec{p},\sigma}$ and $\hat{a}_{\vec{p},\sigma}$ are, respectively, the operators of creation and annihilation for free neutron with momentum $\vec{p}$, by the value of its spin z-component $\sigma = {}^+_- \frac{1}{2}$; U_0 is the Fourier transform of the repulsive interaction between the density of the Bogoliubov excitations and the density modes of the neutrons:

$$U_0 = \frac{4\pi d_0 \hbar^2}{\mu}\,, \tag{22}$$

where d_0 is the scattering amplitude between a helium atoms and neutrons; $\mu = \frac{m \cdot m_n}{m + m_n}$ is the relative mass.

Hence, we note that the Fermi operators $\hat{a}^+_{\vec{p},\sigma}$ and $\hat{a}_{\vec{p},\sigma}$ satisfy to the Fermi commutation relations $[\cdots]_+$ as:

$$\left[\hat{a}_{\vec{p},\sigma},\ \hat{a}^+_{\vec{p}',\sigma'}\right]_+ = \delta_{\vec{p},\vec{p}'}\ \delta_{\sigma,\sigma'}\,, \tag{23}$$

$$[\hat{a}_{\vec{p},\sigma}, \hat{a}_{\vec{p}',\sigma'}]_+ = 0\,, \tag{24}$$

$$[\hat{a}^+_{\vec{p},\sigma}, \hat{a}^+_{\vec{p}',\sigma'}]_+ = 0\,. \tag{25}$$

The density operator of neutrons with spin σ in momentum $\vec{p}$ is defined as

$$\hat{\varrho}_{\vec{p},n} = \sum_{\vec{p}_1,\sigma} \hat{a}^+_{\vec{p}_1-\vec{p},\sigma}\,\hat{a}_{\vec{p}_1,\sigma}\,, \tag{26}$$

where $\hat{\varrho}^+_{\vec{p},n} = \hat{\varrho}_{-\vec{p},n}$.

The operator of total number of neutrons is

$$\sum_{\vec{p},\sigma} \hat{a}^+_{\vec{p},\sigma}\,\hat{a}_{\vec{p},\sigma} = \hat{n}; \tag{27}$$

on other hand, the density operator, in the term of the Bogoliubov quasiparticles $\hat{\varrho}_{\vec{p}}$ included in (21), is expressed by following form, to application (17) into (12):

$$\hat{\varrho}_{\vec{p}} = \sqrt{N_0}\,\sqrt{\frac{1 + L_{\vec{p}}}{1 - L_{\vec{p}}}}\left(\hat{b}^+_{-\vec{p}} + \hat{b}_{\vec{p}}\right). \tag{28}$$

Hence, we note that the Bose- operator $\hat{b}_{\vec{p}}$ commutates with the Fermi operator $\hat{a}_{\vec{p},\sigma}$ because the Bogoliubov excitations and neutrons are an independent.

Now, inserting of a value of operator $\hat{\varrho}_{\vec{p}}$ from (28) into (21), which in turn leads to reducing the Hamiltonian of system $\hat{H}_{a,n}$:

$$\begin{aligned}\hat{H}_{a,n} &= \textstyle\sum_{\vec{p},\sigma} \frac{p^2}{2m_n}\,\hat{a}^+_{\vec{p},\sigma}\,\hat{a}_{\vec{p},\sigma} + \sum_{\vec{p}} \varepsilon_{\vec{p}}\,\hat{b}^+_{\vec{p}}\,\hat{b}_{\vec{p}} + \\ &+ \frac{U_0\sqrt{N_0}}{2V}\sum_{\vec{p}} \sqrt{\frac{1 + L_{\vec{p}}}{1 - L_{\vec{p}}}}\left(\hat{b}^+_{-\vec{p}} + \hat{b}_{\vec{p}}\right)\hat{\varrho}_{-\vec{p},n}\,.\end{aligned} \tag{29}$$

Hence, we note that the Hamiltonian of system $\hat{H}_{a,n}$ in (29) is a similar to the Hamiltonian of system an electron gas-phonon gas mixture which was proposed by Frölich at solving of the problem superconductivity (please, see the Equation (16) in Frölich, *Proc. Roy. Soc. A*, 1952, v.215, 291–291 in the reference [11]), contains a subtle error in the term of the interaction between the density of phonon modes and the density of electron modes which represents a third term in right side of Equation (16) in [11] because the later is described by two sums, one from which goes by the wave vector $\vec{w}$ but other sum goes by the wave vector $\vec{k}$. This fact contradicts to the definition of the density operator of the electron modes $\hat{\varrho}_{\vec{w}}$ (please, see the Equation (12) in [11]) which in turn already contains the sum by the wave vector $\vec{k}$, and therefore, it is not a necessary to take into account so-called twice summations from $\vec{k}$ and $\vec{w}$ for describing of the term of the interaction between the density of phonon modes and the density of electron modes Thus, in the case of the Frölich, the sum must be taken only by wave vector w, due to definition of the density operator of electron modes with the momentum of phonon $\vec{w}$.

To allocate anomalous term in the Hamiltonian of system $\hat{H}_{a,n}$, which denotes by third term in right side in (29), we apply the Frölich approach [11] which allows to do a canonical transformation for the operator $\hat{H}_{a,n}$ within introducing an operator $\tilde{H}$:

$$\tilde{H} = \exp\left(\hat{S}^{+}\right)\ \hat{H}_{a,n} \exp\left(\hat{S}\right), \tag{30}$$

which is decayed by following terms:

$$\begin{aligned} \tilde{H} &= \exp\left(\hat{S}^{+}\right)\ \hat{H}_{a,n} \exp\left(\hat{S}\right) = \\ &= \hat{H}_{a,n} - \left[\hat{S}, \hat{H}_{a,n}\right] + \frac{1}{2}\left[\hat{S}, \left[\hat{S}, \hat{H}_{a,n}\right]\right] - \cdots , \end{aligned} \tag{31}$$

where the operators represent as:

$$\hat{S}^{+} = \sum_{\vec{p}} \hat{Sp} \tag{32}$$

and

$$\hat{S} = \sum_{\vec{p}} \hat{Sp} \tag{33}$$

and satisfy to a condition $\hat{S}^{+} = -\hat{S}$.

In this respect, we assume that

$$\hat{Sp} = A_{\vec{p}}\left(\hat{\varrho}_{\vec{p},n}\hat{b}_{\vec{p}} - \hat{\varrho}^{+}_{\vec{p},n}\hat{b}^{+}_{\vec{p}}\right), \tag{34}$$

where $A_{\vec{p}}$ is the unknown real symmetrical function from a momentum $\vec{p}$. In this context, at application $\hat{Sp}$ from (34) to (33) with taking into account $\hat{\varrho}^{+}_{-\vec{p},n} = \hat{\varrho}_{\vec{p},n}$, then we obtain

$$\hat{S} = \sum_{\vec{p}} \hat{Sp} = \sum_{\vec{p}} A_{\vec{p}}\,\hat{\varrho}_{\vec{p},n}\left(\hat{b}_{=\vec{p}} - \hat{b}^{+}_{\vec{p}}\right). \tag{35}$$

In analogy manner, at $\hat{\varrho}^{+}_{-\vec{p},n} = \hat{\varrho}_{\vec{p},n}$, we have

$$\begin{aligned} \hat{S}^{+} &= \textstyle\sum_{\vec{p}} \hat{Sp} = \sum_{\vec{p}} A_{\vec{p}}\,\hat{\varrho}^{+}_{\vec{p},n}\left(\hat{b}^{+}_{\vec{p}} - \hat{b}_{-\vec{p}}\right) = \\ &= -\sum_{\vec{p}} A_{\vec{p}}\,\hat{\varrho}_{\vec{p},n}\left(\hat{b}_{-\vec{p}} - \hat{b}^{+}_{\vec{p}}\right). \end{aligned} \tag{36}$$

To find $A_{\vec{p}}$, we substitute (29), (35) and (36) into (31). Then,

$$\begin{aligned} \left[\hat{S}, \hat{H_{a,n}}\right] &= \tfrac{1}{V}\textstyle\sum_{\vec{p}} A_{\vec{p}}\, U_0 \sqrt{N_0}\sqrt{\frac{1+L_{\vec{p}}}{1-L_{\vec{p}}}}\,\hat{\varrho}_{\vec{p},n}\hat{\varrho}_{-\vec{p},n} + \\ &+ \sum_{\vec{p}} A_{\vec{p}}\,\varepsilon_{\vec{p}}\left(\hat{b}^{+}_{\vec{p}} + \hat{b}_{-\vec{p}}\right)\hat{\varrho}_{-\vec{p},n}, \end{aligned} \tag{37}$$

$$\frac{1}{2}\left[\hat{S}, \left[\hat{S}, \hat{H}_{a,n}\right]\right] = \sum_{\vec{p}} A^{2}_{\vec{p}}\,\varepsilon_{\vec{p}}\,\varrho_{\vec{p},n}\,\hat{\varrho}_{-\vec{p},n} \tag{38}$$

and $[\hat{S}, [\hat{S}, [\hat{S}, \hat{H}_{a,n}]]] = 0$ within application a Bose commutation relations as $[\varrho_{\vec{p}_1,n}, \hat{\varrho}_{\vec{p}_2,n}] = 0$ and $[\hat{a}^{+}_{\vec{p}_1,\sigma}\hat{a}_{\vec{p}_1,\sigma}, \hat{\varrho}_{\vec{p}_2,n}] = 0$.

Thus, the form of new operator $\tilde{H}$ in (31) takes a following form:

$$\begin{aligned} \tilde{H} &= \textstyle\sum_{\vec{p}} \varepsilon_{\vec{p}}\,\hat{b}^{+}_{\vec{p}}\,\hat{b}_{\vec{p}} + \sum_{\vec{p},\sigma} \frac{p^2}{2m_n}\,\hat{a}^{+}_{\vec{p},\sigma}\,\hat{a}_{\vec{p},\sigma} + \\ &+ \frac{1}{2V}\sum_{\vec{p}} U_0\sqrt{N_0}\sqrt{\frac{1+L_{\vec{p}}}{1-L_{\vec{p}}}}\left(\hat{b}^{+}_{-\vec{p}} + \hat{b}_{\vec{p}}\right)\hat{\varrho}_{-\vec{p},n} - \\ &- \sum_{\vec{p}} A_{\vec{p}}\,\varepsilon_{\vec{p}}\left(\hat{b}^{+}_{-\vec{p}} + \hat{b}_{\vec{p}}\right)\hat{\varrho}_{-\vec{p},n} + \sum_{\vec{p}} A^{2}_{\vec{p}}\,\varepsilon_{\vec{p}}\,\hat{\varrho}_{\vec{p},n}\,\hat{\varrho}_{-\vec{p},n} - \\ &- \frac{1}{V}\sum_{\vec{p}} A_{\vec{p}} U_0\sqrt{N_0}\sqrt{\frac{1+L_{\vec{p}}}{1-L_{\vec{p}}}}\,\hat{\varrho}_{\vec{p},n}\,\hat{\varrho}_{-\vec{p},n}\,. \end{aligned} \tag{39}$$

The transformation of the term of the interaction between the density of the Bogoliubov modes and the density neutron modes is made by removing of a second and fifth terms in right side of (39) which leads to obtaining of a quantity for $A_{\vec{p}}$:

$$A_{\vec{p}} = \frac{U_0\sqrt{N_0}}{2\varepsilon_{\vec{p}}V}\sqrt{\frac{1+L_{\vec{p}}}{1-L_{\vec{p}}}}\,. \tag{40}$$

In this respect, we reach to reducing of the new Hamiltonian of system (39):

$$\begin{aligned} \tilde{H} &= \textstyle\sum_{\vec{p}}\,\varepsilon_{\vec{p}}\,\hat{b}^{+}_{\vec{p}}\,\hat{b}_{\vec{p}} + \sum_{\vec{p},\sigma}\frac{p^2}{2m_n}\,\hat{a}^{+}_{\vec{p},\sigma}\hat{a}_{\vec{p},\sigma} - \\ &- \frac{1}{V}\sum_{\vec{p}} A_{\vec{p}} U_0\sqrt{N_0}\sqrt{\frac{1+L_{\vec{p}}}{1-L_{\vec{p}}}}\,\hat{\varrho}_{\vec{p},n}\,\hat{\varrho}_{-\vec{p},n} + \\ &+ \sum_{\vec{p}} A^{2}_{\vec{p}}\,\varepsilon_{\vec{p}}\,\hat{\varrho}_{\vec{p},n}\,\hat{\varrho}_{-\vec{p},n}\,. \end{aligned} \tag{41}$$

As result, the new form of Hamiltonian system takes a following form:

$$\tilde{H} = \sum_{\vec{p}}\varepsilon_{\vec{p}}\,\hat{b}^{+}_{\vec{p}}\,\hat{b}_{\vec{p}} + \hat{H}_n\,, \tag{42}$$

where $\hat{H}_n$ is the effective Hamiltonian of a neutron gas which contains an effective interaction between neutron modes:

$$\hat{H}_n = \sum_{\vec{p},\sigma} \frac{p^2}{2m_n} \hat{a}^+_{\vec{p},\sigma} \hat{a}_{\vec{p},\sigma} + \frac{1}{2V} \sum_{\vec{p}} V_{\vec{p}} \hat{\varrho}_{\vec{p},n} \hat{\varrho}_{-\vec{p},n} , \qquad (43)$$

where $V_{\vec{p}}$ is the effective potential of the interaction between neutron modes which takes a following form at substituting a value of $A_{\vec{p}}$ from (40) into (41):

$$\begin{aligned} V_{\vec{p}} &= -2A_{\vec{p}} U_0 \sqrt{N_0} \sqrt{\tfrac{1+L_{\vec{p}}}{1-L_{\vec{p}}}} + 2A^2_{\vec{p}} \varepsilon_{\vec{p}} V = \\ &= -\frac{U_0^2 N_0 \left(1 + L_{\vec{p}}\right)}{V\varepsilon_{\vec{p}} \left(1 - L_{\vec{p}}\right)} . \end{aligned} \qquad (44)$$

In this letter, we consider following cases:

1. At low momenta atoms of a helium $p \ll 2mv$, the Bogoliunov's quasiparticles in (19) represent as the phonons with energy $\varepsilon_{\vec{p}} \approx pv$ which in turn defines a value $L^2_{\vec{p}} \approx \frac{1-\frac{p}{mv}}{1+\frac{p}{mv}} \approx \left(1 - \frac{p}{mv}\right)^2$ in (20) or $L_{\vec{p}} \approx 1 - \frac{p}{mv}$. In this context, the effective potential between neutron modes takes a following form:

$$V_{\vec{p}} \approx -\frac{2mU_0^2 N_0}{Vp^2} = -\frac{4\pi\hbar^2 e_1^2}{p^2} . \qquad (45)$$

The value e_1 is the effective charge, at a small momenta of atoms:

$$e_1 = \frac{U_0}{\hbar} \sqrt{\frac{mN_0}{2V\pi}} .$$

2. At high momenta atoms of a helium $p \gg 2mv$, we obtain $\varepsilon_{\vec{p}} \approx \frac{p^2}{2m} + mv^2$ in (19) which in turn defines $L_{\vec{p}} \approx 0$ in (20). Then, the effective potential between neutron modes presents as:

$$V_{\vec{p}} \approx -\frac{mU_0^2 N_0}{Vp^2} = -\frac{4\pi\hbar^2 e_2^2}{p^2} , \qquad (46)$$

where e_2 is the effective charge, at high momenta of atoms:

$$e_2 = \frac{U_0}{2\hbar} \sqrt{\frac{mN_0}{V\pi}} .$$

Consequently, in both cases, the effective scattering between two neutrons is presented in the coordinate space by a following form:

$$V(\vec{r}) = \frac{1}{V} \sum_{\vec{p}} V_{\vec{p}} \, e^{i\frac{\vec{p}\vec{r}}{\hbar}} = -\frac{e_*^2}{r} , \qquad (47)$$

where $e_* = e_1$, at small momenta of atoms; and $e_* = e_2$, at high momenta.

The term of the interaction between two neutrons $V(\vec{r})$ in the coordinate space mediates the attractive Coulomb interaction between two charged particles with mass of neutron m_n, having the opposite effective charges e_* and $-e_*$, which together create a neutral system. Indeed, the effective Hamiltonian of a neutron gas in (43) is rewrite down in the space of coordinate by following form:

$$\hat{H}_n = \sum_{i=1}^{\frac{n}{2}} \hat{H}_i = -\frac{\hbar^2}{2m_n} \sum_{i=1}^{n} \Delta_i - \sum_{i<j} \frac{e_*^2}{\mid \vec{r}_i - \vec{r}_j \mid} , \qquad (48)$$

where $\hat{H}_i$ is the Hamiltonian of system consisting two neutron with opposite spin which have a coordinates $\vec{r}_i$ and $\vec{r}_j$:

$$\hat{H}_i = -\frac{\hbar^2}{2m_n} \Delta_i - \frac{\hbar^2}{2m_n} \Delta_j - \frac{e_*^2}{\mid \vec{r}_i - \vec{r}_j \mid} . \qquad (49)$$

The transformation of considering coordinate system to the relative coordinate $\vec{r} = \vec{r}_i - \vec{r}_j$ and the coordinate of center mass $\vec{R} = \frac{\vec{r}_i + \vec{r}_j}{2}$, we have

$$\hat{H}_i = -\frac{\hbar^2}{4m_n} \Delta_R - \frac{\hbar^2}{m_n} \Delta_r - \frac{e_*^2}{r} . \qquad (50)$$

In analogy of the problem Hydrogen atom, two neutrons with opposite spins is bound as a spinless neutron pair with binding energy:

$$E_n = -\frac{m_n e_*^4}{4\hbar^2 n^2} = -\frac{const}{n^2} \left(\frac{N_0}{V}\right)^2 , \qquad (51)$$

where n is the main quantum number which determines a bound state on a neutron pair, at $const > 0$.

Thus, a spinless neutron pair with mass $m_0 = 2m_n$ is created in a helium liquid-dilute neutron gas mixture.

4 Formation of the Frölich electron pairs in superconductivity

We now attempt to describe the thermodynamic property of the model a phonon-electron gas mixture confined in a box of volume V. In this context, we consider an electron gas consisting of n free electrons with mass m_e which interact with phonon modes of lattice by constancy interaction [11]. The Frölich Hamiltonian has a following form:

$$\hat{H} = \hat{H}_0 + \hat{H}_1 + \hat{H}_2 \qquad (52)$$

with

$$\hat{H}_0 = \sum_{\vec{k},\sigma} \varepsilon_{\vec{k}} \hat{d}^+_{\vec{k},\sigma} \hat{d}_{\vec{k},\sigma} , \qquad (53)$$

$$\hat{H}_1 = \sum_{\vec{w}} \hbar w s \, \hat{b}^+_{\vec{w}} \hat{b}_{\vec{w}} , \qquad (54)$$

$$\hat{H}_2 = i \sum_{\vec{w}} D_w \left(\hat{b}_{\vec{w}} \hat{\varrho}^+_{\vec{w}} - \hat{b}^+_{\vec{w}} \hat{\varrho}_{\vec{w}}\right), \qquad (55)$$

where $\hat{d}^+_{\vec{k},\sigma}$ and $\hat{d}_{\vec{k},\sigma}$ are, respectively, the Fermi operators of creation and annihilation for free electron with wave-vector

$\vec{k}$ and energy $\varepsilon_{\vec{k}} = \frac{\hbar^2 k^2}{2m_e}$, by the value of its spin z-component $\sigma = {}^{+}_{-}\frac{1}{2}$; s is the velocity of phonon; $\hat{b}^{+}_{\vec{w},\sigma}$ and $\hat{b}_{\vec{w},\sigma}$ are, respectively, the Bose operators of creation and annihilation for free phonon with wave-vector $\vec{w}$ and energy$\hbar ws$; D_w is the constant of the interaction between the density of the phonon excitations and the density modes of the electrons which equals to $D_w = \sqrt{\frac{\alpha\hbar ws}{V}}$ (where $\alpha = \frac{C^{"2}}{2Ms^2\frac{n}{V}}$ is the constant characterizing of the metal; $C^{"}$ is the constant of the interaction; M is the mass of ion); $\hat{\varrho}_{\vec{w}}$ is the density operator of the electron modes with wave vector $\vec{w}$ which is defined as:

$$\hat{\varrho}_{\vec{w}} = \sum_{\vec{k},\sigma} \hat{d}^{+}_{\vec{k}-\vec{w},\sigma}\hat{d}_{\vec{k},\sigma} \tag{56}$$

and

$$\hat{\varrho}^{+}_{\vec{w}} = \sum_{\vec{k},\sigma} \hat{d}^{+}_{\vec{k},\sigma}\hat{d}_{\vec{k}-\vec{w},\sigma}\,, \tag{57}$$

where $\hat{\varrho}^{+}_{\vec{w}} = \hat{\varrho}_{-\vec{w}}$.

Hence, we note that the Fermi operators $\hat{d}^{+}_{\vec{k},\sigma}$ and $\hat{d}_{\vec{k},\sigma}$ satisfy to the Fermi commutation relations $[\cdots]_+$ presented in above for neutrons (23–25).

Obviously, the Bose- operator $\hat{b}_{\vec{w}}$ commutates with the Fermi operator $\hat{d}_{\vec{k},\sigma}$ because phonon excitations and electron modes are an independent.

Now, we introduce new transformation of the Bose-operators of phonon modes $\hat{b}^{+}_{\vec{w}}$ and $\hat{b}_{\vec{w}}$ by the new Bose - operators of phonon excitations $\hat{c}^{+}_{\vec{w}}$ and $\hat{c}_{\vec{w}}$ which help us to remove an anomalous term:

$$\hat{b}_{\vec{w}} = -i\hat{c}_{\vec{w}} \tag{58}$$

and

$$\hat{b}^{+}_{\vec{w}} = i\hat{c}^{+}_{\vec{w}}\,. \tag{59}$$

Then, $\hat{H}_1$ in (56) and $\hat{H}_2$ in (57) take following forms:

$$\hat{H}_1 = \sum_{\vec{w}} \hbar ws\,\hat{c}^{+}_{\vec{w}}\hat{c}_{\vec{w}}\,, \tag{60}$$

$$\hat{H}_2 = \sum_{\vec{w}} D_w\left(\hat{c}_{\vec{w}}\,\hat{\varrho}^{+}_{\vec{w}} + \hat{c}^{+}_{\vec{w}}\,\hat{\varrho}_{\vec{w}}\right) = \sum_{\vec{w}} D_w\,\hat{\varrho}_{\vec{w}}\left(\hat{c}_{\vec{w}} + \hat{c}^{+}_{\vec{w}}\right). \tag{61}$$

To allocate anomalous term in the Hamiltonian of system $\hat{H}$ in (54), presented by the term in (63), we use of the canonical transformation for the operator $\hat{H}$ presented by formulae (30). Due to this approach, we obtain new form for operator Hamiltonian $\tilde{H}$:

$$\tilde{H} = \sum_{\vec{w}} \hbar ws\,\hat{b}^{+}_{\vec{w}}\,\hat{b}_{\vec{w}} + \hat{H}_e\,, \tag{62}$$

where

$$\hat{H}_e = \sum_{\vec{k},\sigma} \varepsilon_{\vec{k}}\,\hat{d}^{+}_{\vec{k},\sigma}\hat{d}_{\vec{k},\sigma} + \frac{1}{2V}\sum_{\vec{w}} V_{\vec{w}}\,\hat{\varrho}_{\vec{w}}\,\hat{\varrho}_{-\vec{w}}\,, \tag{63}$$

hence $V_{\vec{w}}$ is the effective potential of the interaction between electron modes, which at taking into account $D_w = \sqrt{\frac{\alpha\hbar ws}{V}}$, has the form:

$$V_{\vec{w}} = -\frac{2D_w^2 V}{\hbar ws} = -2\alpha\,. \tag{64}$$

Consequently, the effective scattering between two electrons in the coordinate space takes a following form:

$$V(\vec{r}) = \frac{1}{V}\sum_{\vec{w}} V_{\vec{w}}\,e^{i\vec{w}\vec{r}} = -2\alpha\delta(\vec{r}) \tag{65}$$

at using of $\frac{1}{V}\sum_{\vec{w}} e^{i\vec{w}\vec{r}} = \delta(\vec{r})$.

Using of the relative coordinate $\vec{r} = \vec{r}_i - \vec{r}_j$ and the coordinate of center mass $\vec{R} = \frac{\vec{r}_i+\vec{r}_j}{2}$, we reach to the Hamiltonian of system consisting two electron with opposite spins:

$$\hat{H}_i = -\frac{\hbar^2}{4m_e}\Delta_R - \frac{\hbar^2}{m_e}\Delta_r + V(\vec{r})\,. \tag{66}$$

To find the binding energy $E < 0$ of electron pair, we search the solution of the Schrödinger equation with introduction of wave function $\psi(\vec{r})$:

$$\hat{H}_i\,\psi_s(\vec{r}) = E\psi_s(\vec{r})\,.$$

In this respect, we have a following equation

$$-\frac{\hbar^2}{m_e}\Delta_r\psi_s(\vec{r}) + V(\vec{r})\,\psi_s(\vec{r}) = E\psi(\vec{r}) \tag{67}$$

which may determine the binding energy $E < 0$ of electron pair, if we claim that the condition $\frac{p_f d}{\hbar} \ll 1$ always is fulfilled. This reasoning implies that the effective scattering between two electrons is presented by the coordinate space:

$$V(\vec{r}) = \frac{1}{V}\sum_{\vec{w}} V_{\vec{w}}\,e^{i\vec{w}\vec{r}} = 4\pi\int_0^{w_f} V_{\vec{w}}\,w^2\,\frac{\sin(wr)}{wr}\,dw\,, \tag{68}$$

where we introduce a following approximation as $\frac{sin(wr)}{wr} \approx 1 - \frac{w^2r^2}{6}$ at conditions $w \le w_f$ and $w_f d \ll 1$ ($w_f = \left(\frac{3\pi^2 n}{V}\right)^{\frac{1}{3}}$ is the Fermi wave number). The later condition defines a state for distance r between two neighboring electrons which is a very small $r \ll \frac{1}{w_f} = \left(\frac{V}{3\pi^2 n}\right)^{\frac{1}{3}}$ where $\frac{4\pi w_f^3}{3} = \frac{n}{2V}$. Then,

$$V(\vec{r}) \approx -\frac{\alpha n}{V} + \alpha\left(\frac{n}{V}\right)^{\frac{5}{3}}\,r^2. \tag{69}$$

Thus, the effective interaction between electron modes $V(\vec{r}) = -2\alpha\delta(\vec{r})$, presented in (65) is replaced by a screening effective scattering presented by (69). This approximation means that there is an appearance of a screening character in the effective scattering because one depends on the density electron modes. Now, denoting $E = E_s$, and then, we arrive

to an important equation for finding a binding energy E_s of singlet electron pair:

$$\left[-\frac{\hbar^2}{m_e}\Delta_r - \frac{n\alpha}{V} + \alpha\left(\frac{n}{V}\right)^{\frac{5}{3}} r^2\right]\psi_s(r) = E_s\,\psi_s(r)\,, \qquad (70)$$

which we may rewrite down as:

$$\frac{d^2\psi_s(r)}{dr^2} + \left(\lambda - \theta^2 r^2\right)\psi_s(r) = 0\,, \qquad (71)$$

where we take $\theta = -\sqrt{\frac{m_e\alpha}{\hbar^2}\left(\frac{n}{V}\right)^{\frac{5}{3}}}$, and $\lambda = \frac{m_e E_s}{\hbar^2} - \frac{\alpha m_e n}{\hbar^2 V}$.

Now, introducing the wave function $\psi_s(r)$ via the Chebishev-Hermit function $H_s(it)$ from an imaginary number as argument it [15] (where i is the imaginary one; t is the real number; $s = 0; 1; 2; \ldots$), the equation (71) has a following solution:

$$\psi_s(\vec{r}) = e^{-\theta\cdot r^2} H_s\left(\sqrt{\theta}\, r\right),$$

where

$$H_s(it) = i^s e^{-t^2}\,\frac{d^s e^{t^2}}{dt^s}$$

at $\theta < 0$, where

$$\lambda = \theta\left(s + \frac{1}{2}\right).$$

Consequently, the quantity of the binding energy E_s of electron pair with mass $m_0 = 2m_e$ takes a following form:

$$E_s = -\sqrt{\frac{\alpha\hbar^2}{m_e}\left(\frac{n}{V}\right)^{\frac{5}{3}}}\left(s + \frac{1}{2}\right) + \frac{\alpha n}{V} < 0 \qquad (72)$$

at $s = 0; 1; 2; \ldots$.

The normal state of electron pair corresponds to quantity $s = 0$ which defines maximal binding energy of electron pair:

$$E_0 = -\sqrt{\frac{\alpha\hbar^2}{m_e}\left(\frac{n}{V}\right)^{\frac{5}{3}}} + \frac{\alpha n}{V} < 0\,. \qquad (73)$$

This fact implies that the formation of the superconducting phase in superconductor is appeared by condition for density of metal $\frac{n}{V}$:

$$\frac{n}{V} > \left(\frac{C^2 m_e}{2Ms^2\hbar^2}\right)^{\frac{3}{2}}.$$

At choosing $C \approx 10$ eV [11]; $M \approx 5{\times}10^{-26}$ kg; $s \approx 3{\times}10^3$ m, we may estimate density of electron $\frac{n}{V} > 10^{27}$ m^{-3} which may represent as superconductor.

Acknowledgements

We thank Professor Marshall Stoneham for help with the English.

Submitted on April 12, 2010 / Accepted on April 19, 2010

References

1. London F. *Nature*, 1938, v. 141, 643.
2. Landau L. *Journal of Physics (USSR)*, 1941, v. 5, 77.
3. Bogoliubov N.N. On the theory of superfludity. *Journal of Physics (USSR)*, 1947, v. 11, 23.
4. Bishop R.F. *J. Low Temp. Physics*, 1974, v. 15, 601.
5. Blagoveshchenskii N.N. et al. *Physical Review B*, 1994, v. 50, 16550.
6. Glyde H.R., Griffin A. *Physical Review Letters*, 1990, v. 65, 1454.
7. Stirling W.G.,Griffin A., Glyde H.R. *Physical Review B*, 1990, v. 41, 4224.
8. Minasyan V.N. et al. *Physical Review Letters*, 2003, v. 90, 235301.
9. Morawetz K. et al. *Physical Review B*, 2007, v. 76, 075116.
10. Penrose O., Onsager L. *Physical Review*, 1956, v. 104, 576.
11. Frölich H. *Proc. Roy. Soc.*, 1952, v. A215, 576.
12. Bardeen J., Cooper L.N., and Schrieffer J.R. *Physical Review*, 1957, v. 108, 1175.
13. Bogoliubov N.N. *Nuovo Cimento*, 1958, v. 7, 794.
14. Cooper L.N. *Physical Review*, 1956, v. 104, 1189.
15. Lavrentiev N.A. and Shabat B.V. Methods of the theory of a function of a complex variable. Nauka, Moscow, 1972.

Dispersion of Own Frequency of Ion-Dipole by Supersonic Transverse Wave in Solid

Vahan Minasyan and Valentin Samoilov
Scientific Center of Applied Research, JINR, Dubna, 141980, Russia
E-mails: mvahan@scar.jinr.ru; scar@off-serv.jinr.ru

First, we predict an existence of transverse electromagnetic field formed by supersonic transverse wave in solid. This electromagnetic wave acquires frequency and speed of sound, and it propagates along of direction propagation of supersonic wave. We also show that own frequency of ion-dipole depends on frequency of supersonic transverse wave.

1 Introduction

In our latest paper [1], we investigated the light diffraction by supersonic longitudinal waves in crystal. In this respect, we predicted an existence of transverse electromagnetic field created by supersonic longitudinal waves in solid. This electromagnetic wave with frequency of ultrasonic field is moved by speed of supersonic field toward to direction propagation of sound. There was shown that the average Poynting vector of superposition field involves the intensities of the transverse electromagnetic and the optical fields which form the intensity of light diffraction. We considered a model of solid as lattice of ions and gas of free electrons. Each ion of lattice coupled with a point of lattice knot by spring, creating of ion dipole. The knots of lattice define a position dynamical equilibrium of each ion which is vibrated by own frequency Ω_0. Hence, we may argue that the presented new model of solid leads to the same results which may obtain for solid by one dimensional model of single atomic crystal representing as model of continuum elastic medium which is described by chain of ions [2]. The vibration of ion occurs near position of equilibrium corresponding to minimum of potential energy (harmonic approximation of nearing neighbors).

Thus, the existence of transverse electromagnetic field is an important factor for correction so called the Raman-Nath theory [3] and the theory of photo-elastic linear effect [4] which were based on a concept that acoustic wave generates a periodical distribution of refractive index in the coordinate-time space.

In this letter, we attempt to investigate a property of solid by under action of supersonic transverse wave. In this context, we find dispersion law for own frequency of ion-dipole which depends on frequency of supersonic transverse wave.

2 Formation of transverse electromagnetic field

Let's consider the coupled ions with points of lattice knots. These ions are vibrated by own frequency Ω_0 into ion-dipoles. We note that ion-dipole is differ from electron-ion dipole which was discussed within elementary dispersion theory [5]. Hence, we assume that property of springs of ion dipole and ion-electron one are the same. This assumption allows us to obtain a connection between own frequencies of electron ω_0 and ion Ω_0 by condition $\Omega_0 = \sqrt{\frac{q}{M}} = \omega_0 \sqrt{\frac{m}{M}}$ where q is the rigidity of spring; m is the mass of electron.

By under action of transverse acoustic wave, there is an appearance of vector displacement $\vec{u}$ of each ions in solid.

Consider the propagation of an ultrasonic transverse plane traveling wave in cubic crystal. Due to laws of elastic field for solid [6], the vector displacement $\vec{u}$ satisfies to condition which defines property of transverse supersonic field

$$\operatorname{div} \vec{u} = 0 \tag{1}$$

and is defined by wave-equation

$$\nabla^2 \vec{u} - \frac{1}{c_t^2} \frac{d^2 \vec{u}}{dt^2} = 0 , \tag{2}$$

where c_t is the velocity of a transverse ultrasonic wave which is determined by elastic coefficients.

The simple solution of (2) in respect to $\vec{u}$ has a following form

$$\vec{u} = \vec{u}_0 \sin (Kx + \Omega t) , \tag{3}$$

where $\vec{u}_0$ is the amplitude of vector displacement; $K = \frac{\Omega \sqrt{\varepsilon}}{c}$ is the wave number of transverse electromagnetic wave.

Thus each ion acquires the dipole moment of ion $\vec{p} = -e\vec{u}$. Now, we may argue that there is a presence of transverse electromagnetic field with vector of electric field $\vec{E}$ due to displacement of ion:

$$M \frac{d^2 \vec{u}}{dt^2} + q\vec{u} = -e\vec{E} , \tag{4}$$

where $\vec{E}$ is the vector electric field which is induced by transverse ultrasonic wave; M is the mass of ion; the second term $q\vec{u}$ in left part represents as changing of quasi-elastic force which acts on ion.

Using of the operation div of the both part of (4) together with (1), we obtain a condition for Transverse electromagnetic wave

$$\operatorname{div} \vec{E} = 0 . \tag{5}$$

Now, substituting solution $\vec{u}$ from (3) in (4), we find the vector transverse electric wave

$$\vec{E} = \vec{E}_0 \sin (Kx + \Omega t) , \tag{6}$$

where

$$\vec{E}_0 = \frac{M\left(\Omega_0^2 - \Omega^2\right)\vec{u}_0}{e} \tag{7}$$

is the amplitude of transverse electric field which acts on ion into ion dipole.

The ion dipole acquires a polarizability α, which is determined via total dipole moment:

$$\vec{P} = N\alpha\vec{E}\,. \tag{8}$$

where N is the concentration of ion dipoles.

In the presented theory, the vector electric induction $\vec{D}$ is determined as

$$\vec{D} = 4\pi\vec{P} + \vec{E}\,, \tag{9}$$

and

$$\vec{D} = \varepsilon\vec{E}\,, \tag{10}$$

where $\vec{P}$=$N_0\vec{p}$ is the total polarization created by ion-dipoles.

It is easy to find the dielectric respond ε of acoustic medium which takes a following form

$$\varepsilon = 1 + 4\pi N\alpha = 1 + \frac{4\pi N e^2}{M\left(\Omega_0^2 - \Omega^2\right)}\,, \tag{11}$$

This formulae is also obtained by model of ions chain [2].

The dielectric respond ε of acoustic medium is similar to optical one, therefore,

$$\sqrt{\varepsilon} = \frac{c}{c_t}\,, \tag{12}$$

where c is the velocity of electromagnetic wave in vacuum.

Thus, we found that transverse electric wave with frequency Ω is propagated by velocity c_t of ultrasonic transverse wave in the direction OX.

Furthermore, we present the Maxwell equations for electromagnetic field in acoustic medium with a magnetic permittivity $\mu = 1$:

$$\operatorname{curl}\vec{E} + \frac{1}{c}\frac{d\vec{H}}{dt} = 0\,, \tag{13}$$

$$\operatorname{curl}\vec{H} - \frac{1}{c}\frac{d\vec{D}}{dt} = 0\,, \tag{14}$$

$$\operatorname{div}\vec{H} = 0\,, \tag{15}$$

$$\operatorname{div}\vec{D} = 0 \tag{16}$$

where $\vec{E} = \vec{E}(\vec{r}, t)$ and $\vec{H} = \vec{H}(\vec{r}, t)$ are the vectors of local electric and magnetic fields in acoustic medium; $\vec{D} = \vec{D}(\vec{r}, t)$ is the local electric induction in the coordinate-time space; $\vec{r}$ is the coordinate; t is the current time in space-time coordinate system.

We search a solution of Maxwell equations by introducing the vectors of magnetic and electric fields by following way

$$\vec{H} = \operatorname{curl}\vec{A}\,, \tag{17}$$

where

$$\vec{E} = -\frac{d\vec{A}}{cdt}\,, \tag{18}$$

where $\vec{A}$ is the vector potential of electromagnetic wave.

After simple calculation, we reach to following equation for vector potential $\vec{A}$ of transverse electromagnetic field

$$\nabla^2\vec{A} - \frac{\varepsilon}{c^2}\frac{d^2\vec{A}}{dt^2} = 0 \tag{19}$$

with condition of plane transverse wave

$$\operatorname{div}\vec{A} = 0\,. \tag{20}$$

The solution of (24) and (25) may present by plane transverse wave with frequency Ω which is moved by speed c_t along of direction of unit vector $\vec{s}$:

$$\vec{A} = \vec{A}_0\cos\left(Kx + \Omega t\right)\,, \tag{21}$$

and

$$\vec{A}\cdot\vec{s} = 0\,, \tag{22}$$

where $K = \frac{\Omega\sqrt{\varepsilon}}{c}$ is the wave number of transverse electromagnetic wave; $\vec{s}$ is the unit vector in direction of wave normal; $\vec{A}_0$ is the vector amplitude of vector potential. In turn, at comparting (23) and (6), we may argue that the vector of wave normal $\vec{s}$ is directed along of axis OX ($\vec{s} = \vec{e}_x$), because the vector electric transverse wave $\vec{E}$ takes a form presented in (6):

$$\vec{E} = \vec{E}_0\sin\left(Kx + \Omega t\right)\,, \tag{23}$$

where

$$\vec{E}_0 = \frac{\Omega\vec{A}_0}{c}\,.$$

To find a connection between vector amplitude of electric field $\vec{E}_0$ and vector amplitude of acoustic field $\vec{u}_0$, we use of the law conservation energy. The average density energy w_a of ultrasonic wave is transformed by one w_t of transverse electromagnetic radiation. In turn, there is a condition $w_a = w_t$ where Thus,

$$\begin{aligned} w_a &= MN\Omega^2u_0^2\lim_{T\to\infty}\tfrac{1}{2T}\int_{-T}^{T}\cos^2\left(Kx + \Omega t\right)dt = \\ &= \frac{MN\Omega^2u_0^2}{2}\,, \end{aligned} \tag{24}$$

In analogy manner,

$$w_t = \frac{\varepsilon}{4\pi}\,E_0^2\lim_{T\to\infty}\frac{1}{2T}\int_{-T}^{T}\sin^2\left(Kx + \Omega t\right)dt = \frac{\varepsilon}{8\pi}\,E_0^2\,. \tag{25}$$

Thus, at comparing (24) and (25), we arrive to an important expression which leads to foundation of dispersion law for own frequency of ion-dipole:

$$\frac{\varepsilon}{4\pi}\,E_0^2 = MN\Omega^2u_0^2\,, \tag{26}$$

where introducing meanings of $\vec{E}_0$ and ε from (7) and (11) into Eq.(26), we obtain a dispersion equation:

$$\left(\Omega_0^2 - \Omega^2\right)^2 + 2\Omega_p^2\left(\Omega_0^2 - \Omega^2\right) - \Omega_p^2\Omega^2 = 0\,, \qquad (27)$$

where $\Omega_p = \sqrt{\frac{4\pi N e^2}{M}} = \omega_p\sqrt{\frac{m}{M}}$ is the classic plasmon frequency of ion but ω_p is the plasmon frequency of electron. For solid $\omega_p \sim 10^{16}$ s^{-1}, therefore, at $\sqrt{\frac{m}{M}} \sim 10^{-2}$), it follows $\Omega_p \sim 10^{14}$ s^{-1}.

The solution of Eq.(27) in regard to own frequency of ion Ω_0 take following forms:

1. At $\Omega_0 \geqslant \Omega$

$$\Omega_0 = \sqrt{\Omega^2 - \Omega_p^2 + \sqrt{\Omega_p^4 + \Omega_p^2\Omega^2}}\,. \qquad (28)$$

2. At $\Omega_0 \leqslant \Omega$

$$\Omega_0 = \sqrt{\Omega^2 - \Omega_p^2 - \sqrt{\Omega_p^4 + \Omega_p^2\Omega^2}}\,. \qquad (29)$$

Now, consider following solutions of above presented equations:

1. At $\Omega \ll \Omega_p$, $\Omega_0 \geqslant \Omega$, we obtain $\Omega_0 \approx \sqrt{\frac{3}{2}}\Omega$ but at $\Omega_0 \leqslant \Omega$, it follows $\Omega_0 \approx \sqrt{\frac{1}{2}}\Omega$. This condition implies that we may consider model of solid as ideal gas of atoms at smaller Ω. 2. At $\Omega \gg \Omega_p$, $\Omega_0 \geqslant \Omega$ we obtain $\Omega_0 \approx \Omega + \frac{\Omega_p}{2}$ but at $\Omega_0 \leqslant \Omega$, it follows that $\Omega_0 \approx \Omega - \frac{\Omega_p}{2}$. 3. At $\Omega \approx \Omega_p$, $\Omega_0 \approx 2^{\frac{1}{4}}\Omega_p$.

In conclusion, we may note that the action of ultrasonic transverse wave in solid leads to new property as determination of own frequency of ion-dipole. This fact is useful because in the case of action of ultrasonic longitudinal wave in solid, the own frequency of ion-dipole can not be determined. However, knowledge of value of own frequency of ion-dipole allows us to calculate the intensity of sound by formulae (26) (at known meaning of intensity of transverse electromagnetic field excited by ultrasonic longitudinal wave in solid). In turn, it determines the resonance frequency ω_0 of optical light in solid because $\omega_0 = \Omega_0\sqrt{\frac{M}{m}}$ due to condition that the rigidity of spring is the same for ion-dipole and electron-ion dipole. Thus, the action of ultrasonic transverse wave on solid may change an optical property of solid.

Submitted on April 12, 2010 / Accepted on April 19, 2010

References

1. Minasyan V.N. and Samoilov V.N. The intensity of the light diffraction by supersonic longitudinal waves in solid. *Progress in Physics*, 2010, v. 2, 63.
2. Vonsovsky S.V. and Kasnelson M.N. Quantum physics of solid. Nauka, Moscow, 1983.
3. Raman C.V., Nath N.S.N. *Proc. Indian. Acad. Sci.*, 1935, v. 2, 406.
4. Estermann R. and Wannier G. *Helv. Phys. Acta*, 1936, v. 9, 520; Pockels F. Lehrduch der Kristalloptic. Leipzig, 1906.
5. Born M. and Wolf E. Principles of optics. Pergamon Press, Oxford, 1964.
6. Landau L.D. and Lifshiz E.M. Theory of elasticity. (Theoretical Physics, v. 11), Nauka, Moscow, 2003.

Predictions of High Energy Experimental Results

Eliahu Comay

Charactell Ltd., PO Box 39019, Tel-Aviv, 61390, Israel. E-mail: elicomay@post.tau.ac.il

Eight predictions of high energy experimental results are presented. The predictions contain the Σ^+ charge radius and results of two kinds of experiments using energetic pionic beams. In addition, predictions of the failure to find the following objects are presented: glueballs, pentaquarks, Strange Quark Matter, magnetic monopoles searched by their direct interaction with charges and the Higgs boson. The first seven predictions rely on the Regular Charge-Monopole Theory and the last one relies on mathematical inconsistencies of the Higgs Lagrangian density.

1 Introduction

A person who studies a well established physical theory becomes acquainted with its mathematical structure and with results of key experiments that are consistent with it. Here one generally does not pay much attention to the historical order of the development of theory and experiment. The situation is different in the case of a theory which has not yet passed the test of time. In the case of such a theory, one generally compares its conclusions with already known experimental results. However, in this situation, experiments that have not yet been performed play a specific role and one is generally inclined to be convinced of the theory's merits, if it predicts successfully experimental results that are obtained later.

This work describes eight predictions of high energy experimental results. All but one of the predictions rely on the Regular Charge-Monopole Theory (RCMT) [1, 2] and on its application to hadronic structure and processes [3]. From this point of view, the prediction of the failure to find a genuine Higgs boson makes an exception, because it relies on the inherently problematic structure of the Higgs Lagrangian density [4]. Some of the predictions refer to experiments that have not yet been carried out, whereas others refer to experiments that are performed for decades and failed to detect special objects. The second set contains the search for a monopole by means of its direct interaction with charge, glueballs, pentaquarks, nuggets of Strange Quark Matter (SQM) and the Higgs boson. In spite of a long list of experimental attempts that have ended in vain, searches for these objects still continue. The predictions made herein state that genuine particles of these kinds will not be found.

The second section presents a detailed phenomenological calculation that yields a prediction of the charge radius of the Σ^+ baryon. This outcome is higher than that of a QCD based prediction that has been published recently [5]. All other predictions are derived briefly or have already been published elsewhere. The third section contains a list of short descriptions of each of these predictions. Concluding remarks are included in the last section.

2 The Σ^+ charge radius

The prediction of the Σ^+ charge radius relies on phenomenological estimates of expectation value of spatial variables of baryonic quarks. Here the RCMT indicates a similarity between electrons in an atom and quarks in a baryons [3]. Appropriate phenomenological assumptions are explained and it is shown how their application yields the required prediction of the Σ^+ charge radius. The procedure used herein relies on the currently known data of the proton, the neutron and the Σ^- baryons [6]. The π and the k meson data are used as a justification for the calculations.

Particle	Mass (MeV)	$\langle \rho r^2 \rangle$	$\langle r \rangle$	Error
p	938.3	0.766	0.875	
n	939.6	−0.116		
Σ^-	1197.4	−0.61	0.78	0.15
π^+	139.6	0.452	0.672	
k^+	493.7	0.314	0.56	

Table 1: Known mean square charge radius ($\langle \rho r^2 \rangle$) and charge radius ($\langle r \rangle$) of hadrons.

Table 1 contains the presently known data of the mean square charge radius ($\langle \rho r^2 \rangle$) and of the corresponding charge radius of several hadrons, written in units of *fm*.

Remarks: *The experimental error refers to* $\langle \rho r^2 \rangle$. *Here the error of the* Σ^- *data is much larger than that of the other baryons. Therefore, only the* Σ^- *error is mentioned. The* π^- *and* k^- *are antiparticles of their respective positively charged counterparts and have the same spatial data.*

The three valence quarks of baryons make an important contribution to the quantities described in Table 1. Beside these quarks, it is well known that pairs of $\bar{q}q$ are found in baryons. The graphs of Fig. 1 describe the distribution of quarks and antiquarks in the proton. Two physically important properties of the proton (and of all other baryons) are inferred from the data of Fig. 1.

A. Antiquarks (namely, additional $\bar{q}q$ pairs) are explicitly seen in baryons and their probability is not negligible.

B. The x-width of antiquarks is much smaller than that of quarks. This property also proves that the Fermi motion of antiquarks is much smaller than that of quarks. Using the Heisenberg uncertainty principle, one finds that,

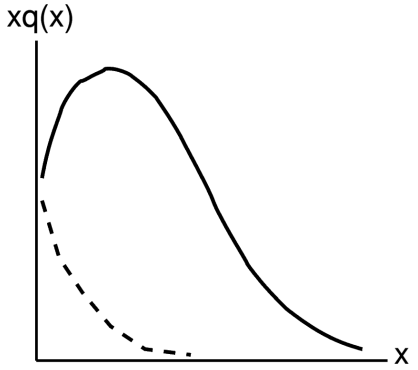

Fig. 1: The quantity $xq(x)$ is describes qualitatively as a function of x ($q(x)$ denotes quark/antiquark distribution, respectively). The solid line represents quarks and the broken line represents antiquarks. (The original accurate figure can be found on [7, see p. 281]).

> in a baryon, the volume of antiquarks is much larger than that of quarks.

These conclusions are called below Property A and Property B, respectively.

Property B is consistent with the RCMT hadronic model [3]. Indeed, in this model baryons have a core. The model assigns three positive monopole units to the baryonic core and one negative monopole unit to every quark. Now, by analogy with the electronic structure of atoms, one infers that, at the inner baryonic region, the potential of the baryonic core is not completely screened by quarks. For this reason, antiquarks, whose monopole unit has the same sign as that of the baryonic core, are pushed out to the baryonic external region and are enclosed inside a larger volume. (Property B is not discussed in QCD textbooks.)

An evaluation of experimental data of the proton indicates that the u, d quark flavors make the dominant contribution to the $\bar{q}q$ pairs and that, in the proton, the ratio between the probability of these kinds of quarks is [8]

$$\frac{\langle \bar{d} \rangle}{\langle \bar{u} \rangle} \simeq 3/2. \tag{1}$$

This ratio is used later in this work. Obviously, isospin symmetry shows that this ratio is reversed for the neutron. The excess of the additional $\bar{d}d$ quark pairs in the proton is consistent with the Pauli exclusion principle, which RCMT ascribes to the spin-1/2 quarks. Indeed, a proton contains uud valence quarks. Hence, it is energetically easier to add a $\bar{d}d$ pair than a $\bar{u}u$ pair.

The following assumption relies on Property A of Fig. 1.

I. It is assumed that, on the average, a baryon contains one additional $\bar{q}q$ pair. Thus, in the discussion carried out below, baryons contain four quarks and one antiquark. In particular, a proton contains an additional 0.6 $\bar{d}d$ fraction of a pair and 0.4 $\bar{u}u$ fraction of a pair. Isospin symmetry indicates that for a neutron, the corresponding quantities are reversed.

The calculation of the baryonic *charge radius* is not very sensitive to the accuracy of Assumption I. Indeed, each member of a $\bar{q}q$ has an opposite electric charge and their contributions partially cancel each other. Moreover, the ud quarks carry charge of opposite sign. This property further reduces the effect of the additional pairs. The discussion of the neutron data, which is carried out later, illustrates these issues.

The baryonic mean square charge radius is obtained below as a sum of the contribution of the baryon's individual quarks. Thus, the following notation is used for a quark q and a baryon b

$$R^2(q_i, b) \equiv \int r^2 \psi_i^\dagger \psi_i \, d^3x, \tag{2}$$

where $\psi_i^\dagger \psi_i$ represents the single particle density of a q_i quark. (Below, ψ is not used explicitly, and the value of $R^2(q, b)$ is derived phenomenologically from the data of Table 1.) Thus, $R^2(u, p)$ denotes the value of (2) for one of the proton's u quarks. Analogous expressions are used for other quark flavors and for other baryons. It follows that the contribution of each quark to the baryonic *mean square charge radius* is obtained as a product $QR^2(q, b)$, where Q denotes the charge of the respective quark. Relying on isospin symmetry, one defines Assumption II:

$$R^2(u, p) = R^2(d, p) = R^2(u, n) = R^2(d, n) \equiv R^2, \tag{3}$$

where the last symbol is used for simplifying the notation.

As explained above, both the data depicted in Fig. 1 and the RCMT model of hadrons [3], indicate that the volume of baryonic antiquarks is larger than that of the corresponding quarks (herein called Property B). Therefore, by analogy of (3), the following definition is used for the proton/neutron antiquarks

$$R^2(\bar{u}, p) = R^2(\bar{d}, p) = R^2(\bar{u}, n) = R^2(\bar{d}, n) = \lambda R^2, \tag{4}$$

where $\lambda > 1$ is a numerical parameter.

The foregoing arguments and the data of Table 1 enable one to equate the experimental value of the proton's mean square charge radius with the quantities defined above

$$0.766 = 2\,\frac{2}{3}R^2 - \frac{1}{3}R^2 - 0.4\,(\lambda - 1)\,\frac{2}{3}R^2 + 0.6\,(\lambda - 1)\,\frac{1}{3}R^2 =$$
$$= R^2 - 0.2\,(\lambda - 1)\,\frac{1}{3}R^2. \tag{5}$$

The terms on the right hand side of the first line of (5) are defined as follows. The first term represents the contribution of the two uu valence quarks; the second term is for the single d quark; the third term is for the $\bar{u}u$ pair; the last term is for the $\bar{d}d$ pair.

An analogous treatment is applied to the neutron and the result is

$$-0.116 = \frac{2}{3}R^2 - 2\,\frac{1}{3}R^2 - 0.6\,(\lambda - 1)\,\frac{2}{3}R^2 + 0.4\,(\lambda - 1)\,\frac{1}{3}R^2 =$$
$$= -0.8\,(\lambda - 1)\,\frac{1}{3}R^2. \tag{6}$$

Here one sees once again the merits of the RCMT model of hadrons [3]. Thus, the fact that the proton's antiquarks volume is larger than that of its quarks means that $\lambda > 1$, as seen in (4). Obviously, the final result of (6) proves that this relation is mandatory for explaining the *sign* of the experimental value of the neutron's mean square charge radius. It is also evident that the contribution of the quark-antiquark pair to R^2 is small.

The neutron relation (6) enables the removal of the λ parameter from (5). Thus, one finds that

$$R^2 = 0.766 + 0.116/4 = 0.795. \tag{7}$$

This value of R^2 will be used in the derivation of the prediction for the charge radius of the Σ^+ baryon.

Let us turn to the Σ^- baryon whose valence quarks are dds. The u, d quarks of the previous discussion are regarded as particles having (practically) the same mass and a different electric charge. This is the underlying basis of isospin symmetry. It is also agreed that the s quark is heavier. Indeed, the following data support this statement. Thus, the experimental mass difference (in MeV) of the k, π mesons is [6]

$$M(k^+) - M(\pi^+) = 493.7 - 139.6 = 354.1 \tag{8}$$

and the difference between the isospin average of the $\Sigma^{\pm}$ and the nucleons is

$$\frac{1}{2}\left(M(\Sigma^+) + M(\Sigma^-) - M(p) - M(n)\right) = \\ = \frac{1}{2}(1197.4 + 1189.4 - 938.3 - 939.6) = 254.5. \tag{9}$$

In each of the previous relations, the mass difference between two hadrons, where an s quark replaces a u (or d) quark is positive. This outcome indicates that the s quark is indeed heavier than the u quark.

The RCMT model of baryons and mesons [3] is analogous to the atomic structure of electrons and to the positronium, respectively. The results of (8) and (9) show that replacing a u (or d) quark by an s quark in a nucleon yields more binding energy than doing it in a pion. This outcome is consistent with the RCMT model. Indeed, in a meson, an s quark is attracted just by the field of one antiquark that carries *one* monopole unit. On the other hand, in a nucleon, the s quark is attracted by the baryonic core that carries *three* monopole units. Like in the atomic case, the field of the core is not completely screened by the other quarks. (A QCD explanation of this phenomenon is certainly less obvious.)

Let us turn to the problem of the s quark single particle radial distribution. Thus, if a u (or d) quark is replaced by the heavier s quark, then the s quark mean radius will be smaller than that of the u quark. This conclusion is supported both by the mass dependence of the radial function of a Dirac solution of the Hydrogen atom (see [9, see p. 55] and by a comparison of the experimental k and π radii of Table 1. For this reason, it is defined here that

$$R^2(s, \Sigma^-) = \eta R^2, \tag{10}$$

where $0 < \eta < 1$ is a yet undefined parameter.

By analogy with the case of atomic electrons, one should expect that the negative monopole of the s quark, which is closer to the core, partially *screens* the potential of the positive monopole at the baryonic core. Therefore, one may expect a somewhat larger size for the d quarks of the Σ^- baryon

$$R^2(d, \Sigma^-) = \xi R^2, \tag{11}$$

where $\xi > 1$ is another undefined parameter.

Like the neutron, whose valence quarks are udd, the Σ^- valence quarks dds contains a pair of d quarks. Hence, it is assumed here that the contribution of a quark-antiquark pair to the Σ^- mean square charge radius is the same as that of the neutron (6). (As shown above, the contribution of this effect is relatively small, and the final result is not sensitive to a small change of this quantity.) Taking the experimental value of the Σ^- from Table 1, one uses (6), (7), (10), and (11) and writes the following relation for the two undetermined parameters ξ, η

$$-0.61 \pm \delta = -2\,\frac{1}{3}\,0.795\,\xi - \frac{1}{3}\,0.795\,\eta - 0.116, \tag{12}$$

where δ is related to the error assigned to the measurement of the mean square charge radius of the Σ^- baryon (see Table 1).

Taking into account the constraint on ξ, η, one finds that relation (12) does not hold for $\delta = 0$. Table 2 describes some pairs of values of the parameters ξ, η and their relation to δ. It is shown below how each pair of the ξ, η parameters of Table 2 yields a prediction of the Σ^+ mean square charge radius.

The Σ^+ baryon contains the uus valence quarks and it is the isospin counterpart of the Σ^- baryon. Hence, the spatial properties of its u quarks are the same as those of the d quarks of the Σ^- baryon. Also the s quark of these baryons is assumed to have the same spatial properties. The small effect of the quark-antiquark pairs is equated to that of the proton, because both have a pair of uu valence quarks. Thus, the phenomenological formula for the mean square charge radius of the Σ^+ baryon is

$$R^2(\Sigma^+) = 2\,\frac{2}{3}\,0.795\,\xi - \frac{1}{3}\,0.795\,\eta - 0.029, \tag{13}$$

where $R^2(b)$ denotes the mean square charge radius of the baryon b. Substituting the values of each pair of the parameters ξ, η into (13), one obtains a predictions for $R^2(\Sigma^+)$. It is clear from the details of the discussion presented above that a prediction of $R^2(\Sigma^+)$ must carry the estimated experimental error of the mean square charge radius of the Σ^- baryon *and*

δ	ξ	η
−15	1.0	0.43
−15	1.05	0.33
−15	1.1	0.23
−10	1.12	0.0
−5	1.03	0.0

Table 2: Several values of ξ and η of (12).

the uncertainties of the assumptions used herein. Thus, the final prediction is given (in fm^2):

$$0.85 \leqslant R^2(\Sigma^+) \leqslant 1.17. \quad (14)$$

The prediction for the charge radius (in fm) is

$$0.91 \leqslant R(\Sigma^+) \leqslant 1.12. \quad (15)$$

The range of these predictions is higher than that of a QCD dependent prediction which has been published recently [5].

3 The other seven high energy predictions

This section presents seven predictions of high energy experimental results.

- High Energy pion beams exist. Thus, in principle, the experiment described here can be performed in the near future. The RCMT basis for a prediction of the elastic $\pi - \pi$ cross section is explained. Unlike protons (see [10] and references therein), pions are characterized by a pair of quark-antiquark and *they do not have inner quark shells*. Moreover, in a deep inelastic $e - p$ experiment, the electron collides with one quark at a time. This property should also hold for the quark-quark interaction in a $\pi-\pi$ collision. Therefore, relying on RCMT, where quarks carry one monopole unit, the $\pi - \pi$ elastic cross section is analogous to the elastic cross section of colliding charges. It is well known that this cross section decreases with the increase of the collision energy (see chapter 6 of [7]).

  Prediction: Unlike the proton case, where the elastic cross section increases for collision energy which is greater than that of point C of Fig. 2, a decrease of the elastic cross section is predicted for a $\pi - \pi$ scattering. Hence, its graph will not increase for energies which are not too close to a resonance. In particular, no similar effect like the rise of the $p - p$ cross section on the right hand side of point C will be found in a $\pi - \pi$ collision. By the same token, for a very high energy $\pi - \pi$ scattering, the ratio of the elastic cross section to the total cross section will be much smaller then that of the $p - p$ cross section of Fig. 2, which is about 1/6.

- The problem of the portion of the pion's momentum carried by quarks. The deep inelastic $e - p$ scattering data are used for calculating the relative portion of the proton's momentum carried by quarks, as seen in a frame where the proton's momentum is very very large. It turns out that for a proton, the overall quarks' portion is about one half of the total momentum. The RCMT proves that baryons have a core and that this is the reason for the effect. Mesons are characterized as a bound $\bar{q}q$ pair and they *do not have a core*. This is the basis for the following prediction:

  Unlike the proton case, it is predicted that an analogous experiment of deep inelastic $e - \pi$ scattering will prove that in this case the pion's quarks carry all (or nearly all) the pion's momentum.

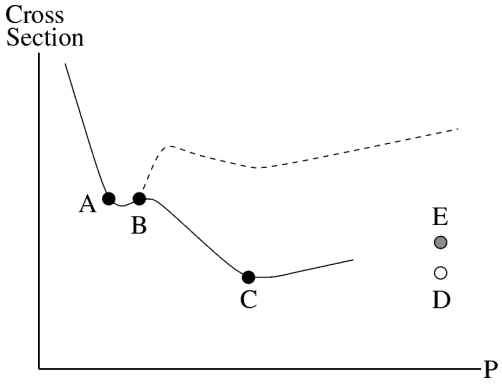

Fig. 2: A qualitative description of the pre-LHC proton-proton cross section versus the laboratory momentum P. Axes are drawn in a logarithmic scale. The solid line denotes the elastic cross section and the broken line denotes the total cross section. (The accurate figure can be found in [6].)

- Several decades ago, claims concerning the existence of glueballs have been published by QCD supporters (see [11], p. 100). RCMT describes the strong interactions as interactions between monopoles that satisfy the RCMT equations of motion. Here, no gluon exist. A fortiori, a genuine glueball does not exist. On April 14, 2010, Wikipedia says that glueballs "have (as of 2009) so far not been observed and identified with certainty."

- Several decades ago, claims concerning the existence of pentaquarks have been published by QCD supporters [12, 13]. Pentaquarks are supposed to be strongly bound states of a baryon and a meson. RCMT clearly contradicts the existence of these kinds of objects. Indeed, like nucleons, all hadrons are neutral with respect to monopoles. Hence, like the nuclear force, a hadron-hadron interaction has residual features. In a deuteron the proton-neutron binding energy is about 2.2 MeV. Let us compare this value to what is expected for a baryon-meson binding energy. For each flavor, the lightest meson, which is the best candidate for assembling a pentaquark, is a spin-0 particle, which resembles a noble gas. Hence, the binding energy of a nucleon with this kind of meson should be even smaller

than the 2.2 MeV binding energy of the deuteron. For this reason, strongly bound pentaquarks should not exist. Experimental results are consistent with this theoretical conclusion [14].

- Several decades ago, claims concerning the existence of SQM have been published by QCD supporters [15]. RCMT clearly contradicts the existence of this kind of matter. Indeed, an SQM is a nugget of Λ baryons. Now the mass of a Λ baryon is greater than the nucleon mass by more than 170 MeV. On the other hand, the Λ binding energy in an SQM should be similar to the nucleon binding energy in a nucleus, which is about 8 MeV per nucleon. This very large difference between energy values proves that the SQM is unstable and will disintegrate like a free Λ. Experimental results are consistent with this theoretical conclusion [16].
- RCMT proves that there is no *direct* charge-monopole interaction. Radiation fields (namely, real photons) interact with charges *and* with monopoles. As of today, experimental attempts to detect monopoles rely on a direct interaction of the monopole fields with charges of the measuring device. As stated above, such an interaction does not exist. Hence, no genuine monopole will be detected. This prediction has been made about 25 years ago [17]. In spite of a very long search, all attempts to detect monopoles have ended in vain [6, see p. 1209]. Monopole search continues [18].
- A genuine Higgs boson will not be found. For a theoretical discussion, see the first four sections of [4]. This conclusion relies on inherent inconsistencies of the Higgs Lagrangian density.

4 Concluding remarks

A physical theory is tested by its consistency with experimental results that belong to the theory's domain of validity. A second kind of test is the demand that the examined theory has a solid mathematical structure. However, one does not really think that a theory having an erroneous mathematical structure can fit all experimental data. Therefore, one may argue that a test of the theory's mathematical structure plays an auxiliary role. On the other hand, an analysis of the mathematical structure can provide convincing arguments for disqualifying incorrect theories. The present work concentrates on the examination of the fit of high energy theories to the data.

In undertaking this task, one realizes that the historical order of formulating the theory's predictions and carrying out the required experiments bears no fundamental meaning. Thus, at this point, one may state that making a prediction that is later found to be successful is *at least* as good as deriving a theoretical result that fits a known measurement. This is certainly an incomplete description of the problem. Indeed, many predictions depend on numerical value of adjustable parameters that yield the required quantity. Therefore, in the case of a theory that is not fully established, a successful prediction that is *later* confirmed by measurement provides a significantly better support for it. This aspect is one of the motivations for writing the present work which contains eight different predictions. Let us wait and see what will come out of the experimental work.

Submitted on April 19, 2010 / Accepted on April 23, 2010

References

1. Comay E. Axiomatic deduction of equations of motion in Classical Electrodynamics. *Nuovo Cimento B*, 1984, v. 80, 159–168.
2. Comay E. Charges, Monopoles and duality relations. *Nuovo Cimento B*, 1995, v. 110, 1347–1356.
3. Comay E. A regular theory of magnetic monopoles and its implications. In: *Has the Last Word Been Said on Classical Electrodynamics?* Editors: Chubykalo A., Onoochin V., Espinoza A.R. and Smirnov-Rueda R. Rinton Press, Paramus (NJ), 2004.
4. Comay E. Physical consequences of mathematical principles. *Prog. in Phys.*, 2009, v. 4, 91–98.
5. Wang P., Leinweber D. B., Thomas A. W. and Young R. D. Chiral extrapolation of octet-baryon charge radii. *Phys. Rev. D*, 2009, v. 79, 094001-1–094001-12.
6. Amsler C. et al. Review of particle physics. *Phys. Lett. B*, 2008, v. 667, 1–1340.
7. Perkins D. H. Introduction to high energy physics. Addison-Wesley, Menlo Park (CA), 1987.
8. Alberg M. Parton distributions in hadrons. *Prog. Part. Nucl. Phys.*, 2008, v. 61, 140–146.
9. Bjorken J. D. and Drell S. D. Relativistic quantum mechanics. McGraw-Hill, New York, 1964.
10. Comay E. On the significance of the upcoming large hadron collider proton-proton cross section data. *Prog. in Phys.*, 2010 v. 2, 56–59.
11. Frauenfelder H. and Henley E. M. Subatomic physics. Prentice Hall, Englewood Cliffs, 1991.
12. Gignoux C., Silvestre-Brac B. and Richard J.M. Possibility of stable multiquark baryons. *Phys. Lett.*, 1987, v. 193, 323–326.
13. Lipkin H.J. New possibilities for exotic hadrons — anticharmed strange baryons. *Phys. Lett.*, 1987, v. 195, 484–488.
14. Whole C.G. (in the 2009 report of PDG). See: http://pdg.lbl.gov/2009/reviews/rpp2009-rev-pentaquarks.pdf
15. Witten E. Cosmic separation of phases. *Phys. Rev. D*, 1984, v. 30, 272–285.
16. Han K. et al. Search for stable strange quark matter in Lunar soil. *Phys. Rev. Lett.*, 2009, v.103, 092302-1–092302-4.
17. Comay E. Will magnetic monopoles be detected in our instruments? *Lett. Nuovo Cimento*, 1985, v. 43, 150–152.
18. A monopole search is planned to be carried out at the LHC. See: http://cdsweb.cern.ch/record/1243082

Neutrosophic Diagram and Classes of Neutrosophic Paradoxes or to the Outer-Limits of Science

Florentin Smarandache

Department of Mathematics, University of New Mexico, Gallup, NM 87301, USA. E-mail: smarand@unm.edu

These paradoxes are called "neutrosophic" since they are based on indeterminacy (or neutrality, i.e. neither true nor false), which is the third component in neutrosophic logic. We generalize the Venn diagram to a Neutrosophic Diagram, which deals with vague, inexact, ambiguous, illdefined ideas, statements, notions, entities with unclear borders. We define the neutrosophic truth table and introduce two neutrosophic operators (neuterization and antonymization operators) give many classes of neutrosophic paradoxes.

1 Introduction to the neutrosophics

Let <*A*> be an idea, or proposition, statement, attribute, theory, event, concept, entity, and <*non A*> what is not <*A*>.

Let <*anti A*> be the opposite of <*A*>. We have introduced a new notation [1998], <*neut A*>, which is neither <*A*> nor <*anti A*> but in between. <*neut A*> is related with <*A*> and <*anti A*>.

Let's see an example for vague (not exact) concepts: if <*A*> is *"tall"* (an attribute), then <*anti A*> is *"short"*, and <*neut A*> is *"medium"*, while <*non A*> is *"not tall"* (which can be *"medium or short"*). Similarly for other <*A*>, <*neut A*>, <*anti A*> such as: <*good*>, <*so so*>, <*bad*>, or <*perfect*>, <*average*>, <*imperfect*>, or <*high*>, <*medium*>, <*small*>, or respectively <*possible*>, <*sometimes possible and other times impossible*>, <*impossible*>, etc.

Now, let's take an exact concept / statement: if <*A*> is the statement "1 + 1 = 2 *in base* 10" , then <*anti A*> is "1 + 1 ≠ 2 *in base* 10", while <*neut A*> is undefined (doesn't exist) since it is not possible to have a statement in between "1 + 1 = 2 *in base* 10" and "1 + 1 ≠ 2 *in base* 10" because in base 10 we have 1+1 is either equal to 2 or 1+1 is different from 2. <*non A*> coincides with <*anti A*> in this case, <*non A*> is "1 + 1 ≠ 2 *in base* 10".

Neutrosophy is a theory the author developed since 1995 as a generalization of dialectics. This theory considers every notion or idea <*A*> together with its opposite or negation <*anti A*>, and the spectrum of "neutralities" in between them and related to them, noted by <*neut A*>.

The Neutrosophy is a new branch of philosophy which studies the origin, nature, and scope of neutralities, as well as their interactions with different ideational spectra.

Its Fundamental Thesis:
Any idea <*A*> is *T*% true, *I*% indeterminate (i.e. neither true nor false, but neutral, unknown), and *F*% false.

Its Fundamental Theory:
Every idea <*A*> tends to be neutralized, diminished, balanced by <*non A*> ideas (not only by <*anti A*> as Hegel asserted) — as a state of equilibrium.

In between <*A*> and <*anti A*> there may be a continuous spectrum of particular <*neut A*> ideas, which can balance <*A*> and <*anti A*>.

To neuter an idea one must discover all its three sides: of sense (truth), of nonsense (falsity), and of undecidability (indeterminacy) — then reverse/combine them. Afterwards, the idea will be classified as neutrality.

There exists a *Principle of Attraction* not only between the opposites <*A*> and <*anti A*> (as in dialectics), but also between them and their neutralities <*neut A*> related to them, since <*neut A*> contributes to the *Completeness of Knowledge*.

Hence, neutrosophy is based not only on analysis of oppositional propositions as dialectic does, but on analysis of these contradictions together with the neutralities related to them.

Neutrosophy was extended to Neutrosophic Logic, Neutrosophic Set, Neutrosophic Probability and Neutrosophic Statistics, which are used in technical applications.

In the *Neutrosophic Logic* (which is a generalization of fuzzy logic, especially of intuitionistic fuzzy logic) every logical variable x is described by an ordered triple $x = (T, I, F)$, where T is the degree of truth, F is the degree of falsehood, and I the degree of indeterminacy (or neutrality, i.e. neither true nor false, but vague, unknown, imprecise), with T, I, F standard or non-standard subsets of the non-standard unit interval $]^{-}0, 1^{+}[$. In addition, these values may vary over time, space, hidden parameters, etc.

Neutrosophic Probability (as a generalization of the classical probability and imprecise probability) studies the chance that a particular event <*A*> will occur, where that chance is represented by three coordinates (variables): *T*% chance the event will occur, *I*% indeterminate (unknown) chance, and *F*% chance the event will not occur.

Neutrosophic Statistics is the analysis of neutrosophic probabilistic events.

Neutrosophic Set (as a generalization of the fuzzy set, and especially of intuitionistic fuzzy set) is a set such that an element belongs to the set with a neutrosophic probability,

i.e. T degree of appurtenance (membership) to the set, I degree of indeterminacy (unknown if it is appurtenance or non-appurtenance to the set), and F degree of non-appurtenance (non-membership) to the set.

There exist, for each particular idea: PRO parameters, CONTRA parameters, and NEUTER parameters which influence the above values.

Indeterminacy results from any hazard which may occur, from unknown parameters, or from new arising conditions. This resulted from practice.

2 Applications of neutrosophics

Neutrosophic logic/set/probability/statistics are useful in artificial intelligence, neural networks, evolutionary programming, neutrosophic dynamic systems, and quantum mechanics.

3 Examples of neutrosophy used in Arabic philosophy (F. Smarandache and S. Osman)

- While Avicenna promotes the idea that the world is contingent if it is necessitated by its causes, Averroes rejects it, and both of them are right from their point of view.

  Hence <*A*> and <*anti A*> have common parts.
- Islamic dialectical theology (*kalam*) promoting creationism was connected by Avicenna in an extraordinary way with the opposite Aristotelian-Neoplatonic tradition.

  Actually a lot of work by Avicenna falls into the frame of neutrosophy.
- Averroes's religious judges (*qadis*) can be connected with atheists' believes.
- al-Farabi's metaphysics and general theory of emanation vs. al-Ghazali's Sufi writings and mystical treatises [we may think about a coherence of al-Ghazali's "Incoherence of the Incoherence" book].
- al-Kindi's combination of Koranic doctrines with Greek philosophy.
- Islamic Neoplatonism + Western Neoplatonism.
- Ibn−Khaldun's statements in his theory on the cyclic sequence of civilizations, says that:

  Luxury leads to the raising of civilization (because the people seek for comforts of life) but also Luxury leads to the decay of civilization (because its correlation with the corruption of ethics).
- On the other hand, there's the method of absent−by−present syllogism in jurisprudence, in which we find the same principles and laws of neutrosophy.
- In fact, we can also function a lot of Arabic aphorisms, maxims, Koranic miracles (Ayat Al- Qur'an) and Sunna of the prophet, to support the theory of neutrosophy.

Take the colloquial proverb that "The continuance of state is impossible" too, or "Everything, if it's increased over its extreme, it will turn over to its opposite"!

4 The Venn diagram

In a Venn diagram we have with respect to a universal set U the following:

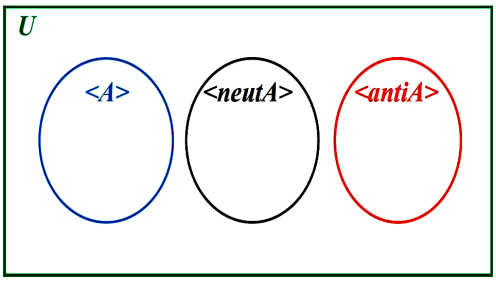

Fig. 1: Venn diagram

Therefore, there are no common parts amongst <*A*>, <*neut A*>, and <*anti A*>, and all three of them are (completely) contained by the universal set U. Also, all borders of these sets <*A*>, <*neut A*>, <*anti A*>, and U are clear, exact. All these four sets are well−defined.

While <*neut A*> means neutralities related to <*A*> and <*anti A*>, what is outside of <*A*> U <*neut A*> U <*anti A*> but inside of U are other neutralities, not related to <*A*> or to <*anti A*>.

Given <*A*>, there are two types of neutralities: those related to <*A*> (and implicitly related to <*anti A*>), and those not related to <*A*> (and implicitly not related to <*anti A*>)

5 The neutrosophic diagram, as extension of the Venn diagram

Yet, for ambiguous, vague, not-well-known (or even unknown) imprecise ideas / notions / statements / entities with unclear frontiers amongst them the below relationships may occur because between an approximate idea noted by <*A*> and its opposite <*anti A*> and their neutralities <*neut A*> there are not clear delimitations, not clear borders to distinguish amongst what is <*A*> and what is not <*A*>. There are buffer zones in between <*A*> and <*anti A*> and <*neut A*>, and an element x from a buffer zone between <*A*> and <*anti A*> may or may not belong to both <*A*> and <*anti A*> simultaneously. And similarly for an element y in a buffer zone between <*A*> and <*neut A*>, or an element z in the buffer zone between <*neut A*> and <*anti A*>. We may have a buffer zone where the confusion of appurtenance to <*A*>, or to <*neut A*>, or to <*anti A*> is so high, that we can consider that an element w belongs to all of them simultaneously (or to none of them simultaneously).

We say that all four sets <*A*>, <*neut A*>, <*anti A*>, and the neutrosophic universal set U are illdefined, inexact, unknown (especially if we deal with predictions; for example

if <*A*> is a statement with some degree of chance of occurring, with another degree of change of not occurring, plus an unknown part). In the general case, none of the sets <*A*>, <*neut A*>, <*anti A*>, <*non A*> are completely included in *U*, and neither *U* is completely known; for example, if *U* is the neutrosophic universal set of some specific given events, what about an unexpected event that might belong to *U*? That's why an approximate *U* (with vague borders) leaves room for expecting the unexpected.

The *Neutrosophic Diagram* in the general case is the following (Fig. 2): the borders of <*A*>, <*anti A*>, and <*neut A*> are dotted since they are unclear.

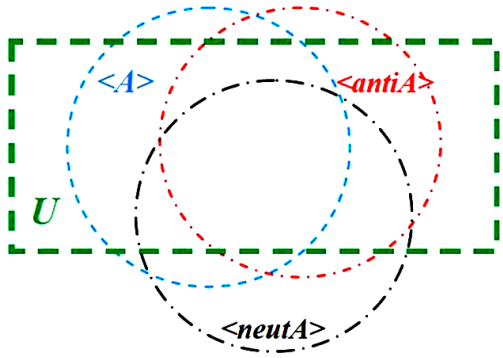

Fig. 2: Neutrosophic Diagram

Similarly, the border of the neutrosophic universal set *U* is dotted, meaning also unclear, so *U* may not completely contain <*A*>, nor <*neut A*> or <*anti A*>, but *U* "approximately" contains each of them. Therefore, there are elements in <*A*> that may not belong to *U*, and the same thing for <*neut A*> and <*anti A*>. Or elements, in the most ambiguous case, there may be elements in <*A*> and in <*neut A*> and in <*anti A*> which are not contained in the universal set *U*.

Even the neutrosophic universal set is ambiguous, vague, and with unclear borders.

Of course, the intersections amongst <*A*>, <*neut A*>, <*anti A*>, and *U* may be smaller or bigger or even empty depending on each particular case.

See below an example of a particular neutrosophic diagram (Fig. 3), when some intersections are contained by the neutrosophic universal set:

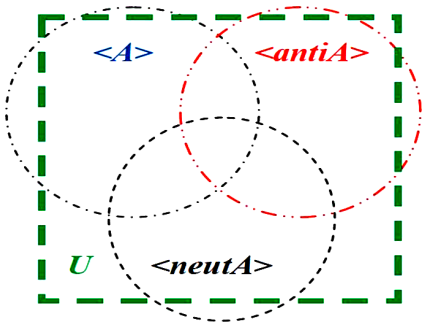

Fig. 3: Example of a particular neutrosophic diagram

A neutrosophic diagram is different from a Venn diagram since the borders in a neutrosophic diagram are vague. When all borders are exact and all intersections among <*A*>, <*neut A*>, and <*anti A*> are empty, and all <*A*>, <*neut A*>, and <*anti A*> are included in the neutrosophic universal set *U*, then the neutrosophic diagram becomes a Venn diagram.

The neutrosophic diagram, which complies with the neutrosophic logic and neutrosophic set, is an extension of the Venn diagram.

6 Classes of neutrosophic paradoxes

The below classes of neutrosophic paradoxes are not simply word puzzles. They may look absurd or unreal from the classical logic and classical set theory perspective. If <*A*> is a precise / exact idea, with well-defined borders that delimit it from others, then of course the below relationships do not occur.

But let <*A*> be a vague, imprecise, ambiguous, not-well-known, not-clear-boundary entity, <*non A*> means what is not <*A*>, and <*anti A*> means the opposite of <*A*>. <*neut A*> means the neutralities related to <*A*> and <*anti A*>, neutralities which are in between them.

When <*A*>, <*neut A*>,<*anti A*>,<*non A*>, *U* are uncertain, imprecise, they may be selfcontradictory. Also, there are cases when the distinction between a set and its elements is not clear.

Although these neutrosophic paradoxes are based on "pathological sets" (those whose properties are considered atypically counterintuitive), they are not referring to the theory of Meinongian objects (*Gegenstandstheorie*) such as round squares, unicorns, etc. Neutrosophic paradoxes are not reported to objects, but to vague, imprecise, unclear ideas or predictions or approximate notions or attributes from our everyday life.

7 Neutrosophic operators

Let's introduce for the first time two new Neutrosophic Operators:

1. An operator that "neuterizes" an idea. To **neuterize** [*neuter+ize*, transitive verb; from the Latin word *neuter* = neutral, in neither side], $\mathfrak{n}(.)$, means to map an entity to its neutral part. [We use the Segoe Print for "*n*(.)".]
   "To neuterize" is different from "to neutralize" [from the French word *neutraliser*] which means to declare a territory neutral in war, or to make ineffective an enemy, or to destroy an enemy.
   $\boldsymbol{n}$(<*A*>) = <*neut A*>. By definition $\mathfrak{n}$(<*neut A*>) = <*neut A*>.
   For example, if <*A*> is "tall", then $\boldsymbol{n}(tall) = medium$, also $\boldsymbol{n}(short) = medium$, $\boldsymbol{n}(medium) = medium$.
   But if <*A*> is "1 + 1 = 2 *in base* 10" then $\mathfrak{n}$(<1 + 1 = 2 *in base* 10>) is undefined (does not exist), and similarly $\mathfrak{n}$(<1 + 1 ≠ 2 *in base* 10>) is undefined.

2. And an operator that "antonymizes" an idea. **To antonymize** [*antonym+ize*, transitive verb; from the Greek work *antōnymia* = instead of, opposite], $\mathfrak{a}(.)$, means to map an entity to its opposite. [We use the Segoe Print for $\mathfrak{a}(.)$] $\mathfrak{a}(<A>) = <anti\ A>$.

   For example, if $<A>$ is "*tall*", then $\mathfrak{a}(tall) = short$, also $\mathfrak{a}(short) = tall$, and $\mathfrak{a}(medium) = tall\ or\ short$.

   But if $<A>$ is "$1 + 1 = 2\ in\ base\ 10$" then $\mathfrak{a}(<1 + 1 = 2\ in\ base\ 10>) = <1+1 \neq 2\ in\ base\ 10>$ and reciprocally $\mathfrak{a}(<1 + 1 \neq 2\ in\ base\ 10>) = <1 + 1 = 2\ in\ base\ 10>$.

The classical operator for *negation / complement* in logics respectively in set theory, "*to negate*" ($\neg$), which is equivalent in neutrosophy with the operator " *to nonize*" (i.e. to *non+ize*) or *nonization* (i.e. *non+ization*), means to map an idea to its neutral or to its opposite (a union of the previous two neutrosophic operators: *neuterization and antonymization*):
$\neg<A> = <non\ A> = <neut\ A> \cup <anti\ A> = \mathfrak{n}(<A>) \cup \mathfrak{a}(<A>)$.

Neutrosophic Paradoxes result from the following *neutrosophic logic / set connectives* following all apparently impossibilities or semi-impossibilities of neutrosophically connecting $<A>$, $<anti\ A>$, $<neut\ A>$, $<non\ A>$, and the neutrosophic universal set U.

8 Neutrosophic truth tables

For $<A>$ = "*tall*":

$<A>$	$\mathfrak{a}(<A>)$	$\mathfrak{n}(<A>)$	$\neg<A>$
tall	short	medium	short or medium
medium	short or tall	medium	short or tall
short	tall	medium	tall or medium

To remark that $\boldsymbol{n}(<medium>) \triangleq medium$. If $<A> = tall$, then $<neut\ A> = medium$, and $<neut(neut\ A)> = <neut\ A>$, or $\boldsymbol{n}(<\boldsymbol{n}(<A>)>) = n(<A>)$.

For $<A>$ = "$1 + 1 = 2\ in\ base\ 10$" we have $<anti\ A> = <non\ A>$ = "$1 + 1 \neq 2\ in\ base\ 10$", while $<neut\ A>$ is undefined (N/A) — whence the neutrosophic truth table becomes:

$<A>$	$\boldsymbol{a}(<A>)$	$\boldsymbol{n}(<A>)$	$\neg<A>$
True	False	N/A	False
False	True	N/A	True

In the case when a statement is given by its neutrosophic logic components $<A> = (T, I, F)$, i.e. $<A>$ is $T\%$ true, $I\%$ indeterminate, and $F\%$ false, then the neutrosophic truth table depends on the defined neutrosophic operators for each application.

9 Neutrosophic operators and classes of neutrosophic paradoxes

a) **Complement/Negation**
$\neg<A> \neq <non\ A>$ and reciprocally $\neg<non\ A> \neq <A>$.
$\neg(\neg<A>) \neq <A>$
$\neg(\neg<anti\ A>) \neq <anti\ A>$
$\neg(\neg<non\ A>) \neq <non\ A>$
$\neg(\neg<neut\ A>) \neq <neut\ A>$
$\neg(\neg U) \neq U$, where $U$is the neutrosophic universal set. $\neg(\neg<\varnothing>) \neq <\varnothing>$, where $<\varnothing>$ is the neutrosophic empty set.

b) **Neuterization**
$\boldsymbol{n}(<A>) \neq <neut\ A>$
$\boldsymbol{n}(<anti\ A>) \neq <neut\ A>$
$\boldsymbol{n}(<non\ A>) \neq <neut\ A>$
$\boldsymbol{n}(\boldsymbol{n}(<A>)) \neq <A>$

c) **Antonymization**
$\boldsymbol{a}(<A>) \neq <anti\ A>$
$\boldsymbol{a}(<anti\ A>) \neq <A>$
$\boldsymbol{a}(<non\ A>) \neq <A>$
$\boldsymbol{a}(\boldsymbol{a}(<A>)) \neq <A>$

d) **Intersection/Conjunction**
$<A> \cap <non\ A> \neq \varnothing$ (neutrosophic empty set) [symbolically $(\exists x)(x \in A \wedge x \in \neg A)$],
or even more $<A> \cap <anti\ A> \neq \varnothing$ [symbolically $(\exists x)(x \in A \wedge x \in \boldsymbol{a}(A))$],
similarly $<A> \cap <neut\ A> \neq \varnothing$ and $<anti\ A> \cap <neut\ A> \neq \varnothing$,
up to $<A> \cap <neut\ A> \cap <anti\ A> \neq \varnothing$.
The symbolic notations will be in a similar way.
This is *Neutrosophic Transdisciplinarity*, which means to find common features to uncommon entities.
For examples:
There are things which are good and bad in the same time.
There are things which are good and bad and medium in the same time (because from one point of view they may be god, from other point of view they may be bad, and from a third point of view they may be medium).

e) **Union / Weak Disjunction**
$<A> \cup <neut\ A> \cup <anti\ A> \neq U$.
$<anti\ A> \cup <neut\ A> \neq <non\ A>$.
Etc.

f) **Inclusion/Conditional**
$<A> \subset <anti\ A>$
$(\forall x)(x \in A \rightarrow x \in \boldsymbol{a}(A))$
All is $<anti\ A>$, the $<A>$ too.
All *good* things are also *bad*.
All is *imperfect*, the *perfect* too.

$<anti\ A> \subset <A>$
$(\forall x)(x \in \boldsymbol{a}(A) \rightarrow x \in A)$
All is $<A>$, the $<anti\ A>$ too.
All *bad* things have something *good* in them [this is rather a fuzzy paradox].
All is *perfect* things are *imperfect* in some degree.

$<non\ A> \subset <A>$
$(\forall x)(x \in \neg A \rightarrow x \in A)$
All is $<A>$, the $<non\ A>$ too.
All *bad* things have something *good* and something *medium* in them [this is a neutrosophic paradox, since it is based on good, bad, and medium].
All is *perfect* things have some *imperfectness* and *mediocrity* in them at some degree.
$<A> \subset <neut\ A>$
$(\forall x)(x \in A \rightarrow x \in \boldsymbol{n}(A))$
All is $<neutA>$, the $<A>$ too.

$<non\ A> \subset <neutA>$ [partial neutrosophic paradox of inclusion]
$(\forall x)(x \in \neg A \rightarrow x \in \boldsymbol{n}(A))$
All is $<neutA>$, the $<non\ A>$ too.
$<non\ A> \subset <antiA>$ [partial neutrosophic paradox of inclusion]
$(\forall x)(x \in \neg A \rightarrow x \in \boldsymbol{a}(A))$
All is $<antiA>$, the $<non\ A>$ too.
$<antiA> \subset <neut\ A>$
$(\forall \mathtt{x})(\mathtt{x} \in \boldsymbol{a}(A) \rightarrow \mathtt{x} \in \boldsymbol{n}(\mathtt{A}))$
All is $<neut\ A>$, the $<anti\ A>$ too.
$<A> \cup <anti\ A> \subset <neut\ A>$
$(\forall \mathtt{x})((x \in \mathtt{A} \vee \mathtt{x} \in \boldsymbol{a}(\mathtt{A})) \rightarrow \mathtt{x} \in \boldsymbol{n}(\mathtt{A}))$
All is $<neutA>$, the $<A>$ and $<antiA>$ too.

Paradoxes of some Neutrosophic Arguments
$<A> \Rightarrow <B>$
$<B> \Rightarrow <anti\ A>$
$\therefore <A> \Rightarrow <anti\ A>$
Example: too much work produces sickness; sickness produces less work (absences from work, low efficiency); therefore, too much work implies less work (this is a *Law of Self-Equilibrium*).
$<A> \Rightarrow <B>$
$<B> \Rightarrow <non\ A>$
$\therefore <A> \Rightarrow <non\ A>$

$<A> \Rightarrow <B>$
$<B> \Rightarrow <neut\ A>$
$\therefore <A> \Rightarrow <neut\ A>$

g) **Equality/Biconditional**
Unequal Equalities
$<A> \neq <A>$
which symbolically becomes $(\exists x)(x \in \neg A \leftrightarrow x \notin \neg A)$ or even stronger inequality $(\forall x)(x \in \neg A \leftrightarrow x \notin \neg A)$.
Nothing is $<A>$, nor even $<A>$.
$<anti\ A> \neq <anti\ A>$
which symbolically becomes $(\exists x)(x \in A \leftrightarrow x \notin A)$ or even stronger inequality $(\forall x)(x \in A \leftrightarrow x \notin A)$.

$<neut\ A> \neq <neut\ A>$
which symbolically becomes $(\exists x)(x \in \upsilon A \leftrightarrow x \notin \upsilon A)$ or even stronger inequality $(\forall x)(x \in \upsilon A \leftrightarrow x \notin \upsilon A)$.

$<non\ A> \neq <non\ A>$
which symbolically becomes $(\exists x)(x \in \neg A \leftrightarrow x \notin \neg A)$ or even stronger inequality $(\forall x)(x \in \neg A \leftrightarrow x \notin \neg A)$.

Equal Inequalities
$<A> = <anti\ A>$
$(\forall x)(x \in A \leftrightarrow x \in \boldsymbol{a}(A))$
All is $<A>$, the $<anti\ A>$ too; and reciprocally, all is $<anti\ A>$, the $<A>$ too. Or, both combined implications give: All is $<A>$ is equivalent to all is $<anti\ A>$.

And so on:
$<A> = <neut\ A>$
$<anti\ A> = <neut\ A>$
$<non\ A> = <A>$

Dilations and Absorptions
$<anti\ A> = <non\ A>$,
which means that $<anti\ A>$ is dilated to its neutrosophic superset $<non\ A>$, or $<non\ A>$ is absorbed to its neutrosophic subset $<anti\ A>$.
Similarly for:
$<neut\ A> = <non\ A>$
$<A> = U$
$<neut\ A> = U$
$<anti\ A> = U$
$<non\ A> = U$

h) Combinations of the previous single neutrosophic operator equalities and/or inequalities, resulting in more neutrosophic operators involved in the same expression.
For examples:
$<neut\ A> \cap (<A> \cup <anti\ A>) \neq \varnothing$ [two neutrosophic operators].
$<A> \cup <anti\ A> \neq \neg <neut\ A>$ and reciprocally $\neg(<A> \cup <anti\ A>) \neq <neut\ A>$.
$<A> \cup <neut\ A> \neq \neg <anti\ A>$ and reciprocally.
$\neg(<A> \cup <neut\ A> \cup <anti\ A>) \neq \varnothing$ and reciprocally.
Etc.

i) We can also take into consideration other logical connectors, such as strong disjunction (we previously used the *weak disjunction*), *Shaffer's connector, Peirce's connector*, and extend them to the neutrosophic form.

j) We may substitute $<A>$ by some entities, attributes, statements, ideas and get nice neutrosophic paradoxes, but not all substitutions will work properly.

10 Some particular paradoxes

Quantum Semi-Paradox
Let's go back to 1931 Schrödinger's paper. Saul Youssef writes (flipping a *quantum coin*) in arXiv.org at quant-ph/9509004:

> "The situation before the observation could be described by the distribution (1/2,1/2) and after observing heads our description would be adjusted to (1,0). The problem is, what would you say to a student who then asks: "Yes, but what causes (1/2,1/2) to evolve into (1,0)? How does it happen?"

It is interesting. Actually we can say the same for any probability different from 1: If at the beginning, the probability of a quantum event, P(*quantum event*) = p, with $0<p<1$, and if later the event occurs, we get to P(*quantum event*) = 1; but if the event does not occur, then we get P(*quantum event*) = 0, so still a kind of contradiction.

Torture's paradox

An innocent person P, who is tortured, would say to the torturer T whatever the torturer wants to hear, even if P doesn't know anything.

So, T would receive incorrect information that will work against him/her. Thus, the torture returns against the torturer.

Paradoxist psychological behavior

Instead of being afraid of something, say <*A*>, try to be afraid of its opposite <*anti A*>, and thus− because of your fear − you'll end up with the <*anti*<*anti A*>>, which is <*A*>.

Paradoxically, *negative publicity* attracts better than positive one (enemies of those who do negative publicity against you will sympathize with you and become your friends).

Paradoxistically [word coming etymologically from *paradoxism, paradoxist*], to be in opposition is more poetical and interesting than being opportunistic.

At a sportive, literary, or scientific competition, or in a war, to be on the side of the weaker is more challenging but on the edge of chaos and, as in Complex Adoptive System, more potential to higher creation.

Law of Self-Equilibrium

(Already cited above at the Neutrosophic Inclusion/Conditional Paradoxes) <*A*> → <*B*> and <*B*> → <*anti A*>, therefore <*A*> → <*anti A*> !

Example: too much work produces sickness; sickness produces less work (absences from work, low efficiency); therefore, too much work implies less work.

Submitted on April 25, 2010 / Accepted on April 30, 2010

References

1. Weisstein E.W. Smarandache paradox. *CRC Concise Enciclopedia of Mathematics*, CRC Press, Boca Raton, FL, 1998, 1661.
2. Begay A. The Smarandache Semantic Paradox. *Humanistic Mathematics Network Journal*, Harvey Mudd College, Claremont (CA), 1998, no. 17, 48.
3. Greenstein C.H. Dictionary of logical terms and symbols. Van Nostrand Reinhold Co., 1978.
4. Devaraj Ramasamy. Florentin Smarandache set up the paradoxist literary movement. In *Parnassus of World Poets 1994*, Madras, India, September 1994.
5. Dale J. Logic: the semantics of existence and nonexistence. Berlin, de Gruyter, 1996.
6. Le C.T. The Smarandache class of paradoxes. *Bulletin of the Transylvania University of Brasov*, New Series, Series B, 1994, v.1(36), 7–8.
7. Le C.T. The Smarandache class of paradoxes. *Bulletin of Pure and Applied Sciences E*, 1995, v.14(2), 109–110.
8. Le C.T. The most paradoxist mathematician of the world: Florentin Smarandache. *Bulletin of Pure and Applied Sciences E*, 1996, v.15(1), 81–100.
9. Le C.T. The Smarandache class of paradoxes. *Journal of Indian Academy of Mathematics*, 1996, v.18, no.1, 53–55.
10. Le C.T. The Smarandache class of paradoxes (mathematical poem). In: Bunner H.C. An anthology in memoriam. Bristol Banner Books, Bristol (IN), 1996, 94.
11. Le C.T. Clasa de paradoxuri Smarandache. *Tempus*, 1994, anul III, no.2(5), 4.
12. Mitroiescu I. The Smarandache class of paradoxes applied in computer sciences. *Abstracts of Papers Presented to the American Mathematical Society*, 1995, v.16, no.3, issue 101, 651.
13. Mitroiescu I. The Smarandache class of paradoxes. *The Mathematical Gazette*, 1995, v.79, no.484, 125.
14. Popescu M. A model of the Smarandache paradoxist geometry. *Abstracts of Papers Presented to the American Mathematical Society*, 1996, v.17, no.1, issue 103, 265.
15. Smarandache F. Neutrosophy. Neutrosophic probability, set, and logic. American Research Press, Rehoboth (NM), 1998; Republished in 2000, 2003, 2005 as Smarandache F. A unifying field in logics: neutrosophic logic. Neutrosophy, neutrosophic set, neutrosophic probability and statistics. American Research Press, Rehoboth (NM).
16. Smarandache F. Mixed non-Euclidean geometries. Arhivele Statului, Filiala Vâlcea, Rm. Vâlcea, 1969.
17. Smarandache F., Osman S. Neutrosophy in Arabic philosophy. Renaissance High Press (Ann Arbor), 2007.
18. Smarandache F. Mathematical fancies and paradoxes. *The Eugene Strens Memorial on Intuitive and Recreational Mathematics and its History*, University of Calgary, Alberta, Canada, 27 July — 2 August, 1986.
19. Tilton H.B. Smarandache's paradoxes. *Math Power*, Tucson (AZ), 1996, v.2, no.9, 1–2.

Five Paradoxes and a General Question on Time Traveling

Florentin Smarandache

Department of Mathematics, University of New Mexico, Gallup, NM 87301, USA. E-mail: smarand@unm.edu

These are five paradoxes on time traveling, which come from Neutrosophy and Neutrosophic Logics applied to the theory of relativity.

1 Traveling to the past

Joe40, who is 40 years old, travels 10 years back to the past when he was 30 years old. He meets himself when he was 30 years old, let's call this Joe30.

Joe40 kills Joe30.

If so, we mean if Joe died at age 30 (because Joe30 was killed), how could he live up to age 40?

2 Traveling to the future

Joe30, who is 30 years old, travels 10 years in the future and meats himself when he will be 40 years old, let's call him Joe40.

Joe40 kills Joe30.

At what age did Joe die, at 30 or 40?

If Joe30 died, then Joe40 would not exist.

3 Traveling pregnant woman

a) A 3-month pregnant woman, Jane3, travels 6 months to the future where she gives birth to a child Johnny3.
b) Then she returns with the child back, and after 1 month she travels 5 months to the future exactly at the same time as before.

Then how is it possible to have at exactly the same time two different situations: first only the pregnant woman, and second the pregnant woman and her child?

4 Traveling in the past before birth

Joe30, who is 30 years old, travels 40 years in the past, therefore 10 years before he was born.

How is it possible for him to be in the time when he did not exist?

5 Traveling in the future after death

Joe30, who is 30 years old, travels 40 years in the future, 10 years after his death. He has died when he was 60 years old, as Joe60.

How is it possible for him to be in the time when he did not exist any longer?

6 A general question about time traveling

When traveling say 50 years in the past [let's say from year 2010 to year 1960] or 50 years in the future [respectively from year 2010 to year 2060], how long does the traveling itself last?

If it's an instantaneous traveling in the past, is the time traveler jumping from year 2010 directly to year 1960, or is he continuously passing through all years in between 2010 and 1960? Similar question for traveling in the future.

If the traveling lasts longer say, a few units (seconds, minutes, etc.) of time, where will be the traveler at the second unit or third unit of time? I mean, suppose it takes 5 seconds to travel from year 2010 back to year 1960; then in the 1st second is he in year 2000, in the 2nd second in year 1990, in the 3rd second in year 1980, in the 4st second in year 1970, and in the 5st second in year 1960? So, his speed is 10 years per second?

Similar question for traveling in the future.

Submitted on April 25, 2010 / Accepted on April 30, 2010

References

1. Weisstein E.W. Smarandache paradox. *CRC Concise Enciclopedia of Mathematics*, CRC Press, Boca Raton, FL, 1998, 1661.
2. Smarandache F. Neutrosophy. Neutrosophic probability, set, and logic. American Research Press, Rehoboth (NM), 1998; Republished in 2000, 2003, 2005 as Smarandache F. A unifying field in logics: neutrosophic logic. Neutrosophy, neutrosophic set, neutrosophic probability and statistics. American Research Press, Rehoboth (NM).
3. Smarandache F. Mixed non-Euclidean geometries. Arhivele Statului, Filiala Vâlcea, Rm. Vâlcea, 1969.
4. Smarandache F. Mathematical fancies and paradoxes. *The Eugene Strens Memorial on Intuitive and Recreational Mathematics and its History*, University of Calgary, Alberta, Canada, 27 July — 2 August, 1986.

Do the Uncertainty Relations Really have Crucial Significances for Physics?

Spiridon Dumitru

Department of Physics (retired), Transilvania University, B-dul Eroilor 29, 500036 Braşov, Romania
E-mail: s.dumitru42@yahoo.com

It is proved the falsity of idea that the Uncertainty Relations (UR) have crucial significances for physics. Additionally one argues for the necesity of an UR-disconnected quantum philosophy.

1 Introduction

The Uncertainty Relations (UR) enjoy a considerable popularity, due in a large measure to the so called Conventional (Copenhagen) Interpretation of UR (CIUR). The mentioned popularity is frequently associated with the idea (which persist so far) that UR have crucial significances for physics (for a list of relevant references see [1–3]). The itemization of the alluded idea can be done through the following more known Assertions (***A***):

• $\boldsymbol{A}_1$: In an experimental reading the UR are crucial symbols for measurement characteristics regarding Quantum Mechanics (QM) in contrast with non-quantum Classical Physics (CP). The pointed characteristics view two aspects: (i) the so called "observer effect" (i.e. the perturbative influence of "observation"/measuring devices on the investigated system), and (ii) the measurement errors (uncertainties). Both of the alluded aspects are presumed to be absolutely notable and unavoidable in QM contexts respectively entirely negligible and avoidable in CP situations. ■

• $\boldsymbol{A}_2$: From a theoretical viewpoint UR are essential distinction elements between the theoretical frameworks of QM and CP. This in sense of the supposition that mathematically UR appear only in QM pictures and have not analogues in the CP representations. ■

• $\boldsymbol{A}_3$: In both experimental and theoretical acceptions the UR are in an indissoluble connection with the description of uncertainties (errors) specific for Quantum Measurements (QMS). ■

• $\boldsymbol{A}_4$: As an esential piece of UR, the Planck's constant $\hbar$, is appreciated to be exclusively a symbol of quanticity (i.e. a signature of QM comparatively with CP), without any kind of analogue in CP. ■

• $\boldsymbol{A}_5$: UR entail [4] the existence of some "impossibility" (or "limitative") principles in foundational physics. ■

• $\boldsymbol{A}_6$: UR are regarded [5] as expression of *"the most important principle of the twentieth century physics"*. ■

To a certain extent the verity of the idea itemized by assertions $\boldsymbol{A}_1 - \boldsymbol{A}_6$ depends on the entire truth of CIUR. That is why in the next section we present briefly the CIUR untruths which trouble the mentioned verity. Subsequently, in Section 3, we point out a lot of Observations (***O***) which invalidate completely and irrefutably the items $\boldsymbol{A}_1 - \boldsymbol{A}_6$. The respective invalidation suggests a substitution of UR-subordinate quantum philosophy with an UR-disconnected conception. Such a suggestion is consolidated by some additional Comments (***C***) given in Section 4. So, in Section 5, we can conclude our considerations with: (i) a definitely negative answer to the inquired idea, respecively (ii) a pleading for a new quantum philosophy. Such conclusions argue for the Dirac's intuitional guess about the non-survival of UR in the physics of future.

2 Shortly on the CIUR untruths

In its essence the CIUR doctrine was established and disseminated by the founders and subsequent partisans of Copenhagen School in QM. The story started from the wish to give out an unique and generic interpretation for the thought-experimental (*te*) formula

$$\Delta_{te}A \cdot \Delta_{te}B \geqslant \hbar \tag{1}$$

(A and B being conjugated observables) respectively for the QM theoretical formula

$$\Delta_{\psi}A \cdot \Delta_{\psi}B \geqslant \frac{1}{2}\left|\left\langle\left[\hat{A},\hat{B}\right]\right\rangle_{\psi}\right| \tag{2}$$

(where the notations are the usual ones from usual QM — see also [3]). Both the above two kind of formulas are known as UR.

The alluded doctrine remains a widely adopted conception which, in various manners, dominates to this day the questions regarding the foundation and interpretation of QM. However, as a rule, a minute survey of the truths-versus-untruths regarding its substance was (and still is) underestimated in the main stream of publications (see the literature mentioned in [1, 2]). This in spite of the early known opinions like [6]: *"the idea that there are defects in the foundations of orthodox quantum theory is unquestionable present in the conscience of many physicists"*.

A survey of the mentioned kind was approached by us in the report [3] as well as in its precursor papers [7–15] and preprints [16]. Our approaches, summarized in [3], disclose the fact that each of all basic elements (presumptions) of CIUR are troubled by a number of insurmountable shortcomings (unthruths). For that reason we believe that CIUR must be wholly abandoned as a wrong construction which, in its substance, has no noticeable value for physics. The disclosures from [3] were carried out by an entire class of well

argued remarks ($\boldsymbol{R}$). From the mentioned class we compile here only the following ones:

• $\boldsymbol{R}_a$: Formula (1) is mere provisional fiction without any durable physical significance. This because it has only a transitory/temporary character, founded on old resolution criteria from optics (introduced by Abe and Rayleigh). But the respective criteria were surpassed by the so called super-resolution techniques worked out in modern experimental physics.
Then, instead of CIUR formula (1), it is possible to imagine some "improved relations" (founded on some super-resolution thought-experiments) able to invalidate in its very essence the respective formula. ■

• $\boldsymbol{R}_b$: From a theoretical perspective the formula (2) is only a minor and deficient piece, resulting from the genuine Cauchy-Schwarz relation

$$\Delta_\psi A \cdot \Delta_\psi B \geqslant \left|\left(\delta_\psi \hat{A}\,\psi, \delta_\psi \hat{B}\,\psi\right)\right| \tag{3}$$

written in terms of usual QM notations (see [3]).
As regards their physical significance the formulas (2) and (3) are nothing but simple (second order) fluctuations relations from the same family with the similar ones [3, 7–9, 12, 15] from the statistical CP. ■

• $\boldsymbol{R}_c$: In a true approach the formulas (1) and (2) as well as their "improvised adjustments" have no connection with the description of QMS. ■

• $\boldsymbol{R}_d$: The Planck's constant $\hbar$ besides its well-known quanticity significance is endowed also [3, 12] with the quality of generic indicator for quantum randomness (stochasticity) — i.e. for the random characteristics of QM observables. Through such a quality $\hbar$ has [3, 12] an authentic analogue in statistical CP. The respective analogue is the Boltzmann's constant k_B which is an authentic generic indicator for thermal randomness. Note that, physically, the randomness of an observable is manifested through its fluctuations [3, 7–9, 12, 15]. ■

• $\boldsymbol{R}_e$: The formula (2) is not applicable for the pair of (conjugated) observables $t - E$ (time-energy). In other words [3] a particularization of (2) in the form

$$\Delta_\psi t \cdot \Delta_\psi E \geqslant \frac{\hbar}{2} \tag{4}$$

gives in fact a wrong relation. This because in usual QM the time t is a deterministic variable but not a random one. Consequently for any QM situation one finds the expressions $\Delta_\psi t \equiv 0$ respectively $\Delta_\psi E = a\ finite\ quantity$.
Note that in a correct mathematical-theoretical approach for the $t-E$ case it is valid only the Cauchy Schwarz formula (3), which degenerate into trivial relation $0 = 0$. ■

Starting from the above remarks $\boldsymbol{R}_a$–$\boldsymbol{R}_e$ in the next section we add an entire group of Observations ($\boldsymbol{O}$) able to give a just estimation of correctness regarding the assertions $\boldsymbol{A}_1 - \boldsymbol{A}_6$.

3 The falsity of assertions $\boldsymbol{A}_1 - \boldsymbol{A}_6$

The above announced estimation can be obtained only if the mentioned remarks are supplemented with some other notable elements. By such a supplementation one obtains a panoramic view which can be reported through the whole group of the following Observations ($\boldsymbol{O}$) :

• $\boldsymbol{O}_1$: The remark $\boldsymbol{R}_a$, noted in previous section, shows irrefutably the falsity of the assertion $\boldsymbol{A}_1$. The same falsity is argued by the fact that the referred "observer effect" and corresponding measuring uncertainties can be noticeable not only in QMS but also in some CP measurements (e.g. [17] in electronics or in thermodynamics) ■

• $\boldsymbol{O}_2$: On the other hand the remark $\boldsymbol{R}_b$ points out the evident untruth of the assertion $\boldsymbol{A}_2$. ■

• $\boldsymbol{O}_3$: Furthermore the triplet of remarks $\boldsymbol{R}_a - \boldsymbol{R}_c$ infringes the essence of the assertion $\boldsymbol{A}_3$. ■

• $\boldsymbol{O}_4$: The exclusiveness feature of Planck's constant $\hbar$, asserted by $\boldsymbol{A}_4$, is evidently contradicted by the remark $\boldsymbol{R}_d$. ■

• $\boldsymbol{O}_5$: Assertion $\boldsymbol{A}_5$ was reinforced and disseminated recently [4] thrugh the topic:

> *"What role do 'impossibility' principles or other limits (e.g., sub-lightspeed signaling,* ***Heisenberg uncertainty****, cosmic censorship, the second law of thermodynamics, the holographic principle,* ***computational limits****, etc.) play in foundational physics and cosmology?"*.

Affiliated oneself with the quoted topic the assertion $\boldsymbol{A}_5$ implies two readings: (i) one which hints at Measuring Limits (ML), respectively (ii) another associated with the so called "Computational Limits" (CL). ■

• $\boldsymbol{O}_6$: In the reading connected with ML the assertion $\boldsymbol{A}_5$ presumes that the QMS accuracies can not surpass "Heisenberg uncertainties" (1) and (2). Such a presumption is perpetuated until these days through sentences like: *"The uncertainty principle of quantum mechanics places a fundamental limitation on what we can know"* [18].
Now is easy to see that the above noted remarks $\boldsymbol{R}_a$ and $\boldsymbol{R}_c$ reveal beyond doubt the weakness of such a presumption. Of course that, as a rule, for various branches of physics (even of CP nature such are [17] those from electronics or thermodynamics), the existence of some specific ML is a reality. The respective existence is subordinate to certain genuine elements such are the accuracy of experimental devices and the competence of the theoretical approaches. But note that as it results from the alluded remarks the formulas (1) and (2) have nothing to do with the evaluation or description of the ML (non-performances or uncertainties) regarding QMS. ■

• $\boldsymbol{O}_7$: The reading which associate the UR with CL sems to refer mainly to the Bremermann's limit (i.e. to the maximum computational speed of a self-contained system in the universe) [19, 20]. But it is easy to see from [19, 20] that the aludded association is builded in fact on the wrong relations (1) and (4) written for the observables pair $t - E$. Conse-

quently such an association has not any real value for appreciation of UR significance as CL. Add here the remark that, nevertheless, the search [20] for finding the ultimate physical limits of computations remains a subject worthy to be investigated. This because, certainly, that what is ultimately permissible in practical computational progresses depends on what are the ultimate possibilities of real physical artifacts (experiences). However, from our viewpoint, appraisals of the alluded possibilities do not require any appeal to the relations (1, 2, 4). ■

• $\boldsymbol{O}_8$: For a true judgment regarding the validity of assertion $\boldsymbol{A}_6$ can be taken into account the following aspects:

(i) In its essence $\boldsymbol{A}_6$ prove oneself to be nothing but an unjustifiable distortion of the real truths. Such a proof results directly from the above remarks $\boldsymbol{R}_a - \boldsymbol{R}_c$. According to the alluded remarks in reality the UR (1) and (2) are mere provisional fictions respectively minor (and restricted) QM relations. So it results that, in the main, UR are insignificant things comparatively with the true important principles of the 20th century physics (such are the ones regarding *Noether's theorem*, *mass-energy equivalence*, *partricle-wave duality* or *nuclear fission*).

(ii) It is wrongly to promote the assertion $\boldsymbol{A}_6$ based on the existent publishing situation where, in the mainstream of QM text-books, the UR (1) and/or (2) are amalgamated with the basic quantum concepts. The wrongness is revealed by the fact that the alluded situation was created through an unjustified perpetuance of the writing style done by the CIUR partisans.

(iii) The assertion $\boldsymbol{A}_6$ must be not confused with the history confirmed remark [21] : *UR "are probably the most controverted formulae in the whole of the theoretical physics"*. With more justice the respective remark has to be regarded as accentuating the weakness of concerned assertion.

Together the three above noted aspects give enough reasons for an incontestable incrimination of the assertion under dicussion. ■

The here detailed observations $\boldsymbol{O}_1 - \boldsymbol{O}_8$ assure sufficient solid arguments in order to prove the indubitable incorrectness for each of the assertions $\boldsymbol{A}_1 - \boldsymbol{A}_6$ and, consequently, the falsity of the idea that UR really have crucial significances for physics. But the alluded proof conflicts with the UR-subordinate quantum philosophy in which the interpretational questions of QM and debates about QMS description are indissolubly associated with the formulas (1) and/or (2). The true (and deep) nature of the respective conflict suggests directly the necesity of improvements by substituting the alluded philosophy with another UR-disconnected conception.

Of course that the before-mentioned substitution necessitates further well argued reconsiderations, able to gain the support of mainstream scientific communities and publications. Note that, in one way or other, elements of the UR-subordinate philosophy are present in almost all current QM interpretations [22]. We think that among the possible multitude of elements belonging to the alluded reconsiderations can be included the additional group of comments from the next section.

4 Some additional comments

The Comments ($\boldsymbol{C}$) from the foregoing announced group, able to suggest also improvements in quantum philosophy, are the following ones:

• $\boldsymbol{C}_1$: Firstly we note that the substance of above presented remarks $\boldsymbol{R}_a - \boldsymbol{R}_b$ respectively observations $\boldsymbol{O}_1 - \boldsymbol{O}_3$ can be fortified by means of the following three our views:

(i) In its bare and lucrative framework, the usual QM offers solely theoretical models for own characteristics of the investigated systems (microparticles of atomic size).

(ii) In the alluded framework QM has no connection with a natural depiction of QMS.

(iii) The description of QMS is an autonomous subject, investigable in addition to the bare theoretical structure of usual QM.

We think that, to a certain extent, our above views find some support in the Bell's remark [23]: *"the word (**measurement**) has had such a damaging efect on the discussions that ... it should be banned altogether in quantum mechanics"*. (It happened that, in a letter [24], J.S.Bell comunicated us early the essence of the alluded remark together with a short his personal agreement with our incipient opinions about UR and QMS). ■

• $\boldsymbol{C}_2$: In its substance the view (i) from $\boldsymbol{C}_1$ regards the bare QM as being nothing but an abstract (mathematical) modeling of the properties specific to the atomic-size sytems (microparticles). For a given system the main elements of the alluded modeling are the wave functions ψ_α, respectively the quantum operators $\hat{A}_j$. On the one hand ψ_α describes the probabilistic situation of the system in α state. Mathematically ψ_α is nothing but the solution of the corresponding Schrodinger equation. On the other hand each of the operators $\hat{A}_j$ ($j = 1, 2, \ldots, n$) is a generalised radom variable associated to a specific observable A_j (e.g. coordinate, momentum, angular momentum or energy) of the system. Then in a probabilistic sense the global characterization of the observables A_j is given by the expected parameters:
(i) the mean values $\left\langle A_j \right\rangle_\psi = \left(\psi, \hat{A}_j \psi\right)$ wherre $\psi \equiv \psi_\alpha$ while (f, g) denotes the scalar product of functions f and g,
(ii) the $(r + s)$-order correlations

$$\mathrm{K}_\psi(i, j; r, s) = \left(\left(\delta_\psi \hat{A}_i\right)^r \psi, \left(\delta_\psi \hat{A}_j\right)^s \psi\right),$$

with $\delta_\psi \hat{A}_j = \hat{A}_j - \left\langle A_j \right\rangle_\psi$ and $r + s \geqslant 2$.
So the definitions of parameters $\langle A_a \rangle_\psi$ and $\mathrm{K}_\psi(i, j; r, s)$ appeal to the usual notations from QM texts (see [3, 25, 26]). ■

• $\boldsymbol{C}_3$: The before mentioned QM entities are completely similar with the known things from statistical CP (such are the phenomenological theory of fluctuations [27, 28] respectively the classical statistical mechanics [29, 30]). So the wave functions ψ_α correspond to the probability distributions w_α while the operators $\hat{A}_j$ are alike the macroscopic random observables $\mathbb{A}_j$. Moreover the QM probabilistc expected parameters $\langle A_a \rangle_\psi$ and $\mathrm{K}_\psi(i, j; r, s)$ are entirely analogous with the mean values respectively the second and higher order fluctuations correlations regarding the macroscopic observables $\mathbb{A}_j$ [3, 7–10, 12, 15, 27–31] ■

• $\boldsymbol{C}_4$: It is interesting to complete the above comment with the following annotations. Undoubtedly that, mathematically, the QM observables have innate characteristics of random variables. But similar characteristics one finds also in the case of statistical CP observables. Then it is surprisingly that the two kinds of random observables (from QM and CP) in their connection with the problem of measurements are approached differently by the same authors [25, 29] or teams [26, 30]. Namely the alluded problem is totally neglected in the case of CP observables [29, 30], respectively it is regarded as a capital question for QM observables [25, 26]. Note that the mentioned differentiation is not justified [25, 26, 29, 30] by any physical argument. We think that, as regard the description of their measurements, the two kinds of random observables must be approached in similar manners.
In the context of above annotations it is interesting to mention the following very recent statement [32]: *"To our best current knowledge the measurement process in quantum mechanics is non-deterministic"*. The inner nature of the mentioned statement strengthens our appreciation [3] that a measurement of a (random) quantum observable must be understood not as a single trial (which give a unique value) but as a statistical sampling (which yields a spectrum of values). Certainly that in such an understanding the concept of "wave function collapse" [33] becomes an obsolete thing. ■

• $\boldsymbol{C}_5$: A credible tentative in approaching similarly the description of measurements regarding random observables from both QM and CP was promoted by us in [3, 34]. Our approach was done according the views (ii) and (iii) noted in the above comment $\boldsymbol{C}_1$. Mainly the respective approach aims to obtain a well argued (and consequently credible) description of QMS. So, in papers [3, 34], a QMS was depicted as a distortion of the information about the measured system. For a given system the respective distortion is described (modeled) as a process which change linearly the probability density and current (given in terms of wave function) but preserve the mathematical expressions of QM operators regarded as generalised random variables. Note that an analogous description of measurements concerning the random observables from CP was done by us formerly in [35]. ■

• $\boldsymbol{C}_6$: Other open question of quantum philosophy regards the deterministic subjacency of QM randomness. The question, of great interest [36], aims to clarify if the respective randomness has an irreducible nature or otherwise it derives from the existence of some subjacent hidden variables of deterministic essence. Then it appears as a notable aspect the fact that, in so reputable report [36] about the alluded question, the possible involvement of UR (1) and/or (2) is completely omited. Such a remarkable omission show clearly that the UR (1) and/or (2) do not present any interest for one of the most thought-provoking subject regarding quantum philosophy. ■

• $\boldsymbol{C}_7$: Here is the place to refer comparatively to the deterministic subjacency regarding CP kind of randomness. The respective kind is associated (both theoretically and experimentally) with a class of subjacent deterministic variables, specific to the molecular and atomic motions [27–30]. The important feature of the alluded CP subjacency is the fact that it does not annul at all the corresponding randomness. Namely the respective deterministic subjacency do not revoke at all the random entities such are the probability distributions w_α and macroscopic observables $\mathbb{A}_j$, mentioned above in $\boldsymbol{C}_3$. The respective entities keep the essence of the CP randomness revealed physically through the corresponding global fluctuations of macroscopic observables.
We think that the noted classical feature must be taken as a reference element in managing the discussions regarding the deterministic subjacency of QM (i.e. the question of hidden variables — versus — QM randomness) and, generally speaking, the renovation of quantum philosophy. More exactly it is of direct interest to see if the existence of hidden variables removes or keeps the QM randomness incorporated within the wave functions ψ_α and operators $\hat{A}_j$. We dare to believe that the alluded QM randomness will persist, even if the existence of some subjacent hidden variables would be evidenced (first of all experimentally). ■

• $\boldsymbol{C}_8$: Now some other words about the question of "impossibility" principles in foundational physics, discussed above in observations $\boldsymbol{O}_5 - \boldsymbol{O}_7$. The respective principles were mentioned in connection with questions like: ' What is Ultimately Possible in Physics?' (see [4]). To a deeper analysis the alluded connection calls attention to 'the frontier of knowledge'. In scrutinizing the respective frontier it was acknowledged recently [32] that: *"Despite long efforts, no* ***progress*** *has been made...* for *... the understanding of quantum mechanics, in particular its measurement process and interpretation"*. What is most important in our opinion is the fact that, in reality, for the sought ***"progress"*** the UR (1) and (2) are of no interest or utility. ■

By ending this section it is easy to see that the here added comments $\boldsymbol{C}_1 - \boldsymbol{C}_8$ give supports to the before suggested proposal for a UR-disconnected quantum philosophy.

5 Conclusions

A survey, in Section 3, of the observations $\boldsymbol{O}_1 - \boldsymbol{O}_8$ discloses that ***in fact the UR (1) and (2) have not any crucial significance for physics***. Additionally, in Section 4, an examination of the comments $\boldsymbol{C}_1 - \boldsymbol{C}_8$ provides supporting elements for a UR-disconnected quantum philosophy.

So we give forth a class of solid arguments which come to advocate and consolidate the Dirac's intuitional guess [37] that: ***"uncertainty relations in their present form will not survive in the physics of future"***.

Submitted on May 04, 2010 / Accepted on May 05, 2010

References

1. Auletta G. Foundations and interpretation of Quantum Mechanics. World Scientific, Singapore, 2000.
2. Cabello A. Bibliographic guide to the foundations of quantum mechanics and quantum information. arXiv: quant-ph/0012089.
3. Dumitru S. Reconsideration of the Uncertainty Relations and Quantum Measurements. *Progress in Physics*, v.2, 2008, 50–68.
4. The pretext of A_5 is comprised in a topic circulated through the web page of "*FQXi 2009 Essay Contest: What's Ultimately Possible in Physics? (Introduction)*", promoted by Foundational Questions Institute (FQXi). The respective page was disponible during the Spring 2009 but is now closed However the home one of FQXi is: http://www.fqxi.org/community. But note that the before mentioned topic is entirely quoted by us above in observation O_5 from Section 3.
5. Martens H. Uncertainty Principle, *Ph.D. Thesis*. Tehnical University, Eidhoven, 1991.
6. Piron C. What is wrong in Orthodox Quantum Theory. *Lect. Notes. Phys.*, Springer, v.153, 1982, 179–182.
7. Dumitru S. Fluctuations and Thermodynamic Inequalities. *Physica Scripta*, v.10, 1974, 101–103.
8. Dumitru S. Uncertainty relations or correlation relations? *Epistemological Letters*, Issue 15, 1977, 1–78.
9. Dumitru S. Fluctuations but not uncertainities deconspiration of some confusions. In: *Recent Advances in Statistical Physics*, ed. by B. Datta and M. Dutta, World Scientific, Singapore, 1987, 122–151.
10. Dumitru S. $L_z - \varphi$ uncertainty relation versus torsion pendulum example and the failure of a vision. *Revue Roumaine de Physique*, v.33, 1988, 11–45.
11. Dumitru S. Compatibility versus commutativity — the intriguing Ccse of angular momentum-azimuthal angle. In: *Symmetries and Algebraic Structures in Physics — Proceedings of the XVIII International Colloquium on Group Theoretical Methods in Physics*, Moscow, 4–9 June, 1990, ed.by V.V.Dodonov and V.I.Manko, Nova Science Publishers, Commack, N.Y., 1991, 243–246.
12. Dumitru S. The Planck and Boltzmann constants as similar generic indicators of stochasticity: some conceptual implications of quantum-nonquantum analogies. *Physics Essays*, v.6, 1993, 5–20.
13. Dumitru S., Verriest E.I. Behaviour patterns of observables in quantum-classical limit. *Int. J. Theor. Physics*, v.34, 1995, 1785–1790.
14. Dumitru S. A possible general approach regarding the conformability of angular observables with the mathematical rules of Quantum Mechanics. *Progress in Physics* v.1, 2008, 25–30.
15. Dumitru S., Boer A. Fluctuations in the presence of fields — phenomenological Gaussian approximation and a class of thermodynamic inequalities. *Phys. Rev. E*, v.64, 2001, 021108.
16. Dumitru S. The preprints deposited in E-Print Libraries at: (i) the Cornell University arXiv and CERN Library (CDS CERN).
17. *Wikipedia*, Observer effect (physics), http://en.wikipedia.org/wiki/Observer_effect_(physics); Dated: May 04, 2010.
18. Gleiser M. Unification and the limits of knowledge. Preprint of Foundational Questions Institute, http://www.fqxi.org/community/essay/winners/2009.1#Gleiser
19. Bremermann H.J. Optimization through evolution and recombination. In: *Self-Organizing systems*, ed. M.C. Yovitts et al., Spartan Books, Washington, DC, 1962, 93–106.
20. Lloyd S. Ultimate physical limits to computation. *Nature*, v.406, 2000, 1047–1054.
21. Bunge M. Interpretation of Heisenberg's Inequalities. In: *Denken und Umdenken (zu Werk und Werkung von Werner Heisenberg)*, ed. by H. Pfepfer, Piper R., Munchen, 1977.
22. Ismael J. Quantum Mechanics. In: *The Stanford Encyclopedia of Philosophy*, Edward N. Zalta (ed.), Winter 2009 Edition.
23. Bell J.S. Against "measurement". *Physics World*, v.3, 1990, 33–40. Reprinted also in some books containing J.S.Bell's writings.
24. A letter to the present author from J.S.Bell, dated 1985, Jan 29: arXiv: quant-ph/0004013.
25. Schwabl F. Quantum Mecanics. 2nd rev. ed., Springer, Berlin, 1995.
26. Cohen-Tannoudji C., Diu B., Laloe F. Quantum Mechanics, vol. I, II. J. Wiley, 1977.
27. Munster A. Statistical thermodynamics, vol. I. Springer, Berlin, 1969.
28. Landau L., Lifchitz E. Physique statistique. Mir, Moscou, 1984.
29. Schwabl F. Statistical mechanics. Springer, Berlin, 2002.
30. Diu B., Guthmann C., Lederer D., Roulet B. Elements de physique statistique. Herman, Paris, 1989.
31. Boer A., Dumitru S. Higher order correlations in the presence of fields. *Phys. Rev. E*, v.66, 2002, 046116.
32. Hossenfelder S. At the frontier of knowledge. arXiv: physics.pop-ph/1001.3538.
33. Ghirardi G. Collapse theories. In: *The Stanford Encyclopedia of Philosophy*, Edward N. Zalta (ed.), Fall 2008 Edition.
34. Dumitru S., Boer A. On the measurements regarding random observables. *Rom. Journ. Phys.*, v.53, 2008, 1111–1116.
35. Dumitru S. Phenomenological theory of recorded fluctuations. *Phys. Lett. A*, v.48, 1974, 109-110.
36. Genovese M. Research on Hidden Variable Theories: a review of recent progresses. *Phys. Rep.*, v.413, 2005, 319–396; arXiv: quant-ph/0701071.
37. Dirac P.A.M. The evolution of physicist's picture of nature. *Scientific American*, v.208, May 1963, 45–53.

Lunar Laser Ranging Test of the Invariance of c: a Correction

Ulrich E. Bruchholz

Wurzen, Germany. E-mail: Ulrich.Bruchholz@t-online.de; http://www.bruchholz-acoustics.de

In the APOLLO test, a speed of light was found, which seemingly supports a Galileian addition theorem of velocities [1]. However, the reported difference of 200 ± 10 m/s is based on a simple error. The correct evaluation of this test leads to the known value of c within the given precision. This correction does not mean an impossibility of detecting spatial anisotropies or gravitational waves.

The Apache Point Lunar Laser-ranging Operation (APOLLO) provides a possibility of directly testing the invariance of light speed [1, 2]. Gezari [1] reported a difference of 200 ± 10 m/s to the known value ($c = 299,792,458$ m/s according to [1]), which is in accordance with the speed of the observatory on the earth to the retro-reflector on the moon. That would support rather a Galileian addition theorem of velocities than the local invariance of light speed. Let us follow up the path of light, Figure 1.

The way from the Apache Point Observatory (APO) to the retro-reflector and back to APO assumed by Gezari (see also Figure 2 in [1]) is $D_{LB} + D_{BR}$ (dotted lines). Gezari [1] wrote:

> Note that the Earth and Moon are moving together as a binary system at ∼30 km/s in that frame, as the Earth orbits the Sun, and relative to each other at much smaller speeds of order ∼10 m/s due to the eccentricity of the lunar orbit.

This "much smaller speed" may be the vertical speed of the moon relative to the earth. However, the moon moves irregularly in the used frame. This motion is not straight-line, that means, there is no relativity of motion between earth and moon. Therefore, we have to consider the horizontal speed (speed of revolution) of $v_{hor} \approx 1$ km/s. In the test constellation, the moon covers smaller distances parallel to the earth than the earth itself, Figure 1. It is false to set a unitary velocity of the "binary system" of ∼ 30 km/s. If we define a "binary system" with power (what is an unfortunate step), this unitary velocity becomes here smaller.

Therefore, the path of light from APO to retro-reflector is shorter than assumed by Gezari. It is now D'_{LB} (full line), because the earth takes another position in the chosen frame at launch, see Figure 1. — The elapsed time $t_{LB} + t_{BR}$ was measured correctly but the calculation of the light speed gave a false (greater) value. As well, the way back via D_{BR} does not differ from that reported by Gezari. With it, the difference of the path of light is (Figure 1)

$$D_{LB} - D'_{LB} \approx \Delta l \cos\theta \tag{1}$$

with

$$\Delta l = v_{hor}\, t_{LB}\, \sin\theta\,, \tag{2}$$

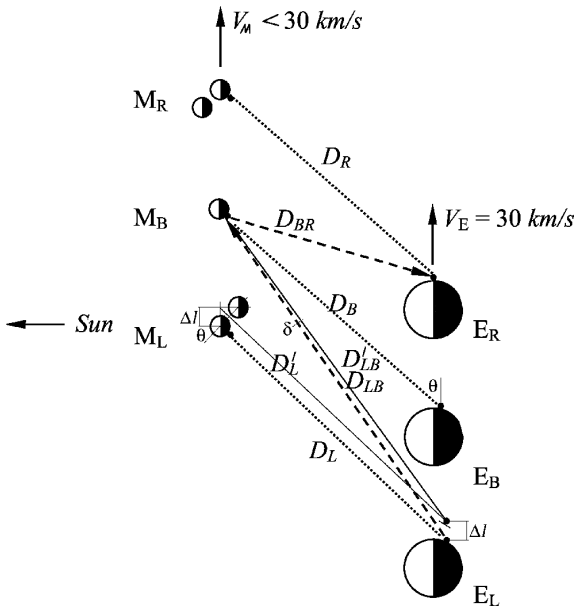

Fig. 1: Corrected path of light.

i.e.

$$D_{LB} - D'_{LB} \approx \frac{1}{2}\, v_{hor}\, t_{LB}\, \sin 2\theta\,, \tag{3}$$

with the numerical values

$$D_{LB} - D'_{LB} < \frac{1}{2}\ \text{km/s} \times 1.3\ \text{s} \approx 650\ \text{m}\,. \tag{4}$$

This difference becomes maximal with $\theta = 45°$.

The reported value of the light speed c has to be corrected for a difference (with the ratio of path difference to whole path)

$$\Delta c < \frac{300000\ \text{km/s} \times 650\ \text{m}}{780000\ \text{km}} \approx 250\ \text{m/s}\,. \tag{5}$$

We get the reported difference of 200 m/s for $\theta = 27°$ and for $\theta = 63°$. That means a coincidence within a tolerance of ±20%. — Thus, we have to take this result as negative regarding a verification of a violation of *local* invariance of c.

This from now on negative result does *not* rule out the possible existence of spatial anisotropies, as dependences of stochastic processes on direction [3] or measurements with

gas interferometers [2] demonstrate. The observed effects like anisotropic light speed in gas could be based on anisotropic material properties, which come from anisotropic metrics. The reason is explained in [4]:

The universal (according to author's opinion) field equations as quoted in [4, 5] (Eq. (1),(2),(3) in [5]) involve 10 independent equations for 14 components of metrics and electromagnetic vector potential. If one considers only gravitation, that become 6 independent equations for 10 components of metrics. This means, four components of metrics are ambiguous *in first order*. Since our existence is time-like, these ambiguous components are space-like. For example in central-symmetric and time-independent solutions, vertical metric (first order) results according to

$$\gamma_{(vert)} = +\frac{\kappa\, m}{4\pi\, r}\,, \tag{6}$$

which comes from Eq. (35) in [4], during horizontal metrics can have any value, i.e. Eq. (35) in [4] is correct only for $\gamma_{(vert)}$. On the earth is $\gamma_{(vert)} \approx 1.5{\times}10^{-9}$, but $\gamma_{(hor)}$ could be just zero. — An upgrade APOLLO equipment could be suited for direct detection of such differences in metrics, if exist.

Submitted on March 01, 2010 / Accepted on May 14, 2010

References

1. Gezari D.Y. Lunar laser ranging test of the invariance of c. arXiv: 0912.3934
2. Cahill R.T. Lunar laser-ranging detection of light-speed anisotropy and gravitational waves. *Progress in Physics*, 2010, v. 2, 31–35.
3. Shnoll S.E., Rubinstein I.A., Vedenkin N.N. "The arrow of time" in the experiments in which alpha-activity was measured using collimators directed at East and West. *Progress in Physics*, 2010, v. 1, 26–29.
4. Bruchholz U.E. Key notes on a geometric theory of fields. *Progress in Physics*, 2009, v. 2, 107–113.
5. Bruchholz U.E. Geometry of space-time. *Progress in Physics*, 2009, v. 4, 65-66.

Demonstrating Gravitational Repulsion

Pieter Cornelius Wagener

Department of Physics, Nelson Mandela Metropolitan University, Port Elizabeth, South Africa
E-mail: Pieter.Wagener@nmmu.ac.za

In previous papers we showed that a classical model of gravitation explains present gravitational phenomena. This paper deals with gravitational repulsion and it shows how it manifests in black holes and particle pair production. We also suggest a laboratory experiment to demonstrate gravitational repulsion.

1 Introduction

In previous papers [1–5] we showed that a Lagrangian

$$L = -m_0(c^2 + v^2)\exp R/r, \tag{1}$$

where

m_0 = *gravitational rest mass* of a test body moving at velocity $\mathbf{v}$ in the vicinity of a massive, central body of mass M,
γ = $1/\sqrt{1 - v^2/c^2}$,
R = $2GM/c^2$ is the Schwarzschild radius of the central body.

gives rise to the following conservation equations:

$$E = mc^2 e^{R/r} = \text{total energy} = \text{constant}, \tag{2}$$
$$\mathbf{L} = e^{R/r}\mathbf{M}, \tag{3}$$
$$L = \text{magnitude of } \mathbf{L} = \text{constant}, \tag{4}$$
$$L_z = M_z e^{R/r} = e^{R/r} m_0 r^2 \sin^2\theta\dot{\phi}, \tag{5}$$
$$= z \text{ component of } \mathbf{L} = \text{constant},$$

where

$$m = m_0/\gamma^2, \tag{6}$$

is a *variable gravitational mass* and

$$\mathbf{M} = (\mathbf{r} \times m_0\mathbf{v}), \tag{7}$$

is the total angular momentum of the test body. Eqs. (3) and (4) are amendments to the equations in the previous articles.

The above equations give rise to equations of motion that satisfy all tests for present gravitational phenomena.

2 Gravitational repulsion

Eq. (2) shows that gravitational repulsion occurs between bodies when their masses m are increased by converting radiation energy into mass. This conversion occurs according to the photoelectric effect,

$$h\nu \to mc^2. \tag{8}$$

This is the reverse of what occurs during nuclear fission.

In a previous paper [4, §3] we proposed that this accounts for the start of the Big Bang as well as the accelerating expansion of the universe. We now consider other effects.

2.1 Black holes

With black holes the reverse of repulsion occurs. According to (2) and (6) matter is converted into radiation energy ($v \to c$) as $r \to 0$. Conversely, as radiation is converted into mass, matter should be expelled from a black hole. This phenomenon has been observed [6].

In this regard our model of a black hole differs from that of general relativity (GR) in that our model does not approach a mathematical singularity as $r \to 0$, whereas GR does approach one as $r \to R$.

2.2 Pair production

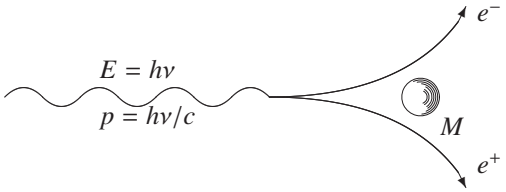

Fig. 1: A high-energy gamma ray passing near matter can create an electron-positron pair.

In pair production a gamma ray converts into a positron and an electron, with both particles moving away from one another. Pair production only occurs in the presence of a heavy mass. The explanation for the required presence of the mass is generally given in texts as:

> The process as we have assumed it to occur is impossible. This is because energy and momentum cannot simultaneously be conserved in free space in this process. ...
>
> However, if the high-energy gamma ray passes near a very heavy particle, then the heavy particle can soak up all the momentum without carrying away a significant amount of energy [7, §5.6].

We aver that the explanation is contrived. The last sentence is too inexact for a rigorous mathematical formulation. Although we do not submit a formulation at this stage, we suggest that repulsion occurs between the particles and the heavy mass.

2.3 Laboratory demonstration

It should be possible to demonstrate gravitational repulsion in a laboratory. A suggestion on how to do this is provided by Jennison and Drinkwater [8]. Their experiment was not designed to demonstrate gravitational repulsion, but to demonstrate how the properties of mass, or inertia, are simulated by phase-locked standing waves in a microwave transmitter/receiver system mounted on a frictionless air track. It should be possible to modify their experiment to show that gravitational repulsion would occur if the frequencies of the standing waves were increased. As a prototype we propose a modification of their experimental setup as depicted in Fig. 2. Two microwave transmitters/receivers lock a standing wave of frequency ν near a large mass M. Increasing the frequency of the standing wave should push it away from M.

From (2) and (8) an increase of $\Delta\nu$ will cause a separation of the microwave system from M equal to

$$\Delta r = A/(B - \ln h\Delta\nu), \tag{9}$$

where A, B are constants.

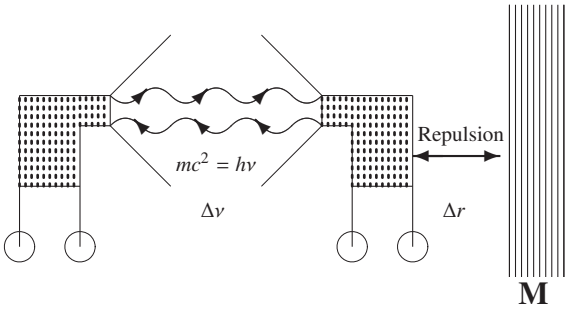

Fig. 2: Repulsion of a trapped wave. Repulsion $\Delta r = A/(B - \ln \Delta mc^2)$ where A, B = constant and $\Delta m = h\Delta\nu/c^2$.

The repulsive effect can also be measured by a sensitive gravimeter placed between M and the standing wave system.

Setting up the above experiment could be cumbersome on a macro scale. The author is investigating demonstrating the repulsive effect at nano scales.

3 Conclusion

The success of the proposed theory to explain present gravitational phenomena supports the above proposal to demonstrate gravitational repulsion.

Submitted on April 28, 2010 / Accepted on May 17, 2010

References

1. Wagener P.C. A classical model of gravitation. *Progress in Physics*, v.3, 2008, 21–23.
2. Wagener P.C. A unified theory of interaction: gravitation and electrodynamics. *Progress in Physics*, v.4, 2008, 3–9.
3. Wagener P.C. A unified theory of interaction: gravitation, electrodynamics and the strong force. *Progress in Physics*, v.1, 2009, 33–35.
4. Wagener P.C. Experimental verification of a classical model of gravitation. *Progress in Physics*, v.3, 2009, 24–26.
5. Wagener P.C. From inspired guess to physical theory: finding a theory of gravitation. *Progress in Physics*, v.1, 2010, 11–14.
6. Elbaz D., Jahnke K., Pantin E., Le Borgne D. and Letawe G. Quasar induced galaxy formation: a new paradigm? *Astronomy & Astrophysics*, v.507, 2009, 1359–1374.
7. Ashby N. and Miller S.C. Principles of Modern Physics. Holden-Day, 1970.
8. Jennison R.C. and Drinkwater A.J. An approach to the understanding of inertia from the physics of the experimental method. *J. Phys. A. Math. Gen.*, v.10, 1977, 167–179.

The Relativity Principle: Space and Time and the Planck Vacuum

William C. Daywitt

National Institute for Standards and Technology (retired), Boulder, Colorado, USA.
E-mail: wcdaywitt@earthlink.net

This short paper examines the Relativity Principle in light of the emerging Planck Vacuum (PV) theory and shows that Special and General Relativity are based physically on the Relativity Principle and the dynamics of the PV.

The idea that absolute motion through space is undetectable has been around for a long time, spanning the work of Galileo and Newton, and the Special and General theories of Relativity [1]. The Relativity Principle asserts that the cosmos is so constituted that it is impossible to detect absolute motion by any type of experiment whatsoever, or in more modern terms, that the equations of physics must be fundamentally covariant [2]. It is important to note, however, that this principle *does not* imply that a fundamental reference frame does not exist. In fact, the following discussion indicates that there may be a hierarchy of reference frames that are hidden from our view.

The PV theory views the cosmos as consisting of an omnipresent, negative-energy, degenerate collection of Planck particles known as the PV; *and* free space which is the void of classical physics [3]. Uniformly spread throughout this free space is the quantum vacuum [4] which consists of an omnipresent field of virtual photons and massive virtual particles whose source is the PV [5]. The free-space vacuum state is not empty, but as Davies puts it, "[this living vacuum] holds the key to a full understanding of the forces of nature" [6, p.104]. How the PV and free space manage to coexist is not known, but the equations of modern physics strongly suggest that some type of active vacuum state does indeed exist, when Newton's gravitational constant, Planck's constant, and the fine structure constant are replaced by their more fundamental counterparts

$$G = \frac{e_*^2}{m_*^2} \qquad \hbar = \frac{e_*^2}{c} \qquad \alpha = \frac{e^2}{e_*^2} \tag{1}$$

in those equations. The universality of this suggestion can be seen by combining the relationships in (1) to yield the string of equalities

$$m_*^2 G = c\hbar = \frac{e^2}{\alpha} \tag{2}$$

where e_* and m_* are the charge and mass of the Planck particles making up the PV. These equations imply that gravitational physics ($m_*^2 G$), quantum physics ($c\hbar$), and electromagnetics (e^2/α) belong to a *single physics*, and their arrangement in the string suggests the central position occupied by the quantum theory in uniting mass and charge. The latter suggestion is realized in the equality between the two particle forces that perturb the PV

$$\frac{mc^2}{r} = \frac{e_*^2}{r^2} \qquad \text{at } r = r_c \tag{3}$$

leading to the particle's Compton radius $r_c\,(= e_*^2/mc^2)$ [3], where mc^2/r and e_*^2/r^2 are the curvature force (a gravitational force) and the polarization force (an electrical force) the particle exerts on the PV. That mc^2/r is a gravitational type of force can be seen from Newton's expression for the gravitational force between two masses m and M separated by a distance r

$$\frac{mMG}{r^2} = \frac{(mc^2/r)(Mc^2/r)}{(m_*c^2/r_*)} \tag{4}$$

where $c^4/G = m_*c^2/r_*$ is used to remove G from the left side of the equation. The ratios mc^2/r and Mc^2/r are the curvature forces the masses m and M exert on the PV, while $m_*c^2/r_* = e_*^2/r_*^2$ is the maximum force sustainable by the PV. One of the e_*s in the product e_*^2 comes from the charge on the free particle and the other represents the charge on the individual Planck particles within the PV.

The reaction of the PV to the uniform motion of a free charge is such that an iterative process taking place between 'the magnetic and Faraday fields produced by the PV' and the charge results in the well known relativistic electric and magnetic fields commonly ascribed to the charge as a single entity [3, Sec. 4]. Since these magnetic and Faraday fields emerge from the PV, it is reasonable to suggest that the Maxwell equations themselves must owe their existence to a perturbed PV. If it is then assumed that the tensor forms of the Maxwell equations are *the* covariant equations for electromagnetics, the corresponding coordinate transformation that leaves these equations covariant is the coordinate transformation that satisfies the Relativity Principle. This will be the Lorentz transformation assuming the result is unique. With this transformation in hand, the constancy of the speed of light can be deduced and the Michelson-Morley experiments [7] satisfied. From that point on relativistic kinematics can be derived in the usual way [2, p.9]. Special Relativity is now based on (1) relativity and (2) the dynamics of the PV state, rather than the standard postulates including (1) relativity and (2) the constancy of the speed of light. In this PV formulation of Special Relativity the constancy of the speed of light is a *derived* result, not a postulate.

The presence of the PV in the kinematic picture causes a mix-up in the classical position and time coordinates (r, t), resulting in the differential interval

$$ds^2 = c^2dt^2 - dr^2 \tag{5}$$

between the two events in spacetime at (r, t) and $(r+dr, t+dt)$. However, with the PV in the picture: the mixing of space and time is no longer the mystery that it is in the pre-PV formalism where the equations in (1) are unknown; and (r, t) is still just the bookkeeping entry it is in pre-relativistic physics.

The mixing of coordinates and time in Special Relativity is necessarily carried over into the equations of General Relativity to insure covariance of those equations. But now the effects of a mass perturbing the PV show up in the equations. For a point mass the force perturbation is mc^2/r and the resulting differential-interval equation is the Schwarzschild line element [8]

$$ds^2 = (1 - 2n_r)\, c^2dt^2 - \frac{dr^2}{(1 - 2n_r)} \tag{6}$$

where

$$n_r \equiv \frac{mc^2/r}{m_*c^2/r_*} \tag{7}$$

is the relative curvature force the mass m exerts on the PV. If there were no perturbing mass ($m = 0$), the line element would reduce to that of the Special Relativity result in (5) as it should.

Expressing the Einstein field equation in the following way [9]

$$G_{\mu\nu} = \frac{8\pi G}{c^4}\, T_{\mu\nu} \qquad \rightarrow \qquad \frac{G_{\mu\nu}/6}{1/r_*^2} = \frac{T_{\mu\nu}}{\rho_*} \tag{8}$$

shows that it, and those equations like (6) that follow from it, owe their existence to the PV as implied by the presence of the Planck-particle Compton radius r_* $(= e_*^2/m_*c^2)$ and the energy density

$$\rho_* = \frac{m_*c^2}{4\pi r_*^3/3} = \frac{e_*^2/r_*}{4\pi r_*^3/3} \tag{9}$$

in the final equation of (8). The ratio $1/r_*^2$ in (8) is the Gaussian curvature of a spherical volume of the PV equal to $4\pi r_*^3/3$.

Although it is accepted knowledge that absolute motion through free space is undetectable, such motion is clearly suggested by the equations of modern physics as seen above. The assumed existence of the PV implies that extra-free-space (XFS) reference frames must exist, at least those reference frames that describe the dynamics taking place within the PV for example. From this point it is easy to speculate that some XFS frames might be associated with levels of reality more fundamental than both the free-space and the PV frames. Thus the picture emerges of a cosmos possibly occupied by successive sets of XFS reference frames, in addition to the free-space frames in which we live, that belong to deeper levels of reality yet to be discovered.

The coexistence of the free-space and PV reference frames on top of each other is easily seen in equation (4), where the Newtonian force on the LHS belongs to the free-space frame and the three PV-curvature forces on the RHS to the PV reference frame. The reference frame for both sides of equations (5) through (9) is the PV reference frame. The presence of the PV frame in the equations indicates that, although it may be impossible to detect an absolute frame experimentally, there is abundant evidence that at least XFS reference frames do exist.

Finally, it is worth noting that there may exist only one reference frame (the absolute frame) in which there are successively more complicated states of existence figuratively "piled on top of each other like the skins of an onion" with the free-space state at the top of the pile.

Submitted on May 11, 2010 / Accepted on May 17, 2010

References

1. Møller C. The Theory of Relativity. Oxford Clarendon Press, First Addition, NY, Toronto, London, . . . , 1952–1962.
2. Leighton R.B. Principles of modern physics. McGraw-Hill Book Co., NY, Toronto, London, 1959.
3. Daywitt W.C. The Planck vacuum. *Progress in Physics*, v. 1, 2009, 20.
4. Milonni P.W. The quantum vacuum — an introduction to Quantum Electrodynamics. Academic Press, New York, 1994.
5. Daywitt W.C. The source of the quantum vacuum. *Progress in Physics*, v. 1, 2009, 27.
6. Davies P. Superforce — the search for a Grand Unified Theory of Nature. Simon and Schuster, New York, 1984.
7. Michelson A.A., Morley E.W. Relative motion of earth and luminiferous ether. *Silliman J.*, v. 34, 1887, 333, 427.
8. Daywitt W.C. The Planck vacuum and the Schwarzschild metrics. *Progress in Physics*, v. 3, 2009, 30.
9. Daywitt W.C. Limits to the validity of the Einstein field equations and General Relativity from the viewpoint of the negative-energy Planck vacuum state. *Progress in Physics*, v. 3, 2009, 27.

Finding the Fine Structure of the Solutions of Complicate Logical Probabilistic Problems by the Frequent Distributions

Anatoly V. Belyakov
E-mail: belyakov.lih@gmail.com

The Author suggests that frequent distributions can be applied to the modelling the influences of stochastically perturbing factors onto physical processes and situations, in order to look for most probable numerical values of the parameters of the complicate systems. In this deal, very visual spectra of the particularly undetermined complex problems have been obtained. These spectra allows to predict the probabilistic behaviour of the system.

Normal distribution, also known as the Gauss distribution, is a distribution of the probabilities ruling physical quantities and any other parameters in general, if the parameters are affected by a large number of purely stochastic processes. The normal distribution plays a highly important rôle in many fields of knowledge and activity of the Mankind. This is because of all distributions, which may be met in the Nature, the most frequent is the normal distribution. In particular, the normal distribution sets up the law of the Brownian motion — the fluctuations of Brownian particles being affected by the probabilistically perturbing factors such as the heat motion of molecules. In these fluctuations, the consecutive changes of the particles' location are independent from the last events in them, and their any current location can be assumed to be the initially start-point.

As an example of another sort, a simplest situation of the theory of games can be provided. In this example, an initially rate S_0 increases proportionally to the progression coefficient q_1 with a probability of p_1, or decreases proportionally the progression coefficient q_2 with a probability of p_2. As is obvious, the pair of these numerical values are connected to each other here: these are the current and past values connected as $S_{i+1} = S_i\, q_i$.

However in the core of this problem, the examples are a manifestation of the same situation, because S_0 can be meant as any parameter under consideration in a process being affected by perturbing factors.

It is clear that, having duration of the process unbounded, the numerical value of the parameter S_0 will vary near an average value, then filling, step-by-step, the arc of the normal distribution.

The current value S_i should return back to this average value each time after a number of the steps passed in the ways of different lengthes under stochastic alternating q_1 and q_2. Therefore, concerning the parameters of the perturbing effects in the perturbation series, the set of the current numerical values of the parameters is different in the cases of both sequent and parallel observations. Thus, it seems that there should not be "spectra" or "non-uniformities" in the Gauss arc. On the other hand, the Gauss distribution is a particular case of more complicate distributions, where the smooth form of the Gauss distribution is only an idealisation of those. Because some numerical values can meet each other in the series of the observations, the frequent distribution* of the *sum of all numerical values registered in many series* manifests the preferred numerical values of S_i thus producing by this its own specific spectrum.

Note that the discrete nature of normal distributions was experimentally discovered in different physical processes in already the 1950's by S. E. Shnoll [1].

Figures 1–3 show examples of the frequent spectra which came from the normal distributions being affected by two, three, and four perturbing factors (the progression coefficients q_i). The ordinate axis shows the number of coincident numerical values. The axis of abscissas shows the current values of S_i in doles of the initially value. These numerical values were given, for more simple and convenient comparing the histograms, in the same interval of abscissas from 0.0001 to 10000, while the initially parameters were assumed to be such that the axis of the distribution crosses the initially sum S_0. The diagrams were obtained by summing 500 series of 500 steps in each (so the common number of the values is $500 \times 500 = 250000$). The relative length of the current interval q was assumed 10^{-6} of the current value S_i. The algorithmic language C++ was used in the calculation.

This is a fragment of a computer program

```
for ( int t = 1; t < 500; t ++ )   {
double  Si = 1;
for ( int u = 1; u < 500; u ++ )   {

if ( a >=  b && a >= c ) {qi = q1 ; goto nn ; }
if ( b >=  a && b >= c ) {qi = q2 ; goto nn ; }
if ( c >=  a && c >= b ) {qi = q3 ; goto nn ; }
nn:    Si = Si*qi ;
if ( Si < 10000 && Si > 0.0001 )
i++ ,  m[ i ] = Si ;               }
                                   }
```

*Frequent distributions provide a possibility for bonding the probability of the appearance of numerical values of a function in the area where it exists. That is, the frequent distributions show the reproducibility of numerical values of the function due to allowed varying its arguments. There is a ready-to-use function "frequency" in MS Excel; any other software can be applied as well.

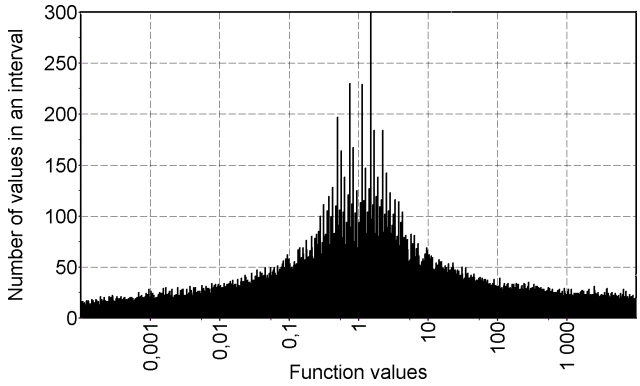

Fig. 1: Frequent distribution obtained with $q_1 = 1.5$, $q_2 = 0.5$, $p_1 = 0.555$, $p_2 = 0.444$; number of steps in the series is 500, number of the series is 500; number of the numerical values in the scale 190,000 (of those, nonzero intervals are 8,000).

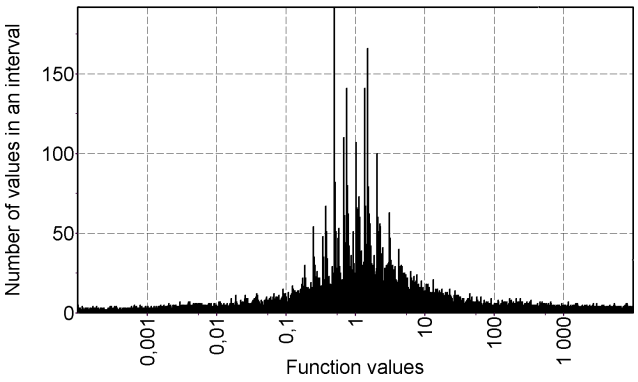

Fig. 2: Frequent distribution obtained with $q_1 = 1.5$, $q_2 = 0.5$, $q_3 = 1.37$, $p_1 = 0.333$, $p_2 = 0.333$, $p_3 = 0.333$; number of the steps in the series is 500, number of the series is 500; number of the numerical values in the scale is 180,000 (of those, nonzero intervals are 62,000).

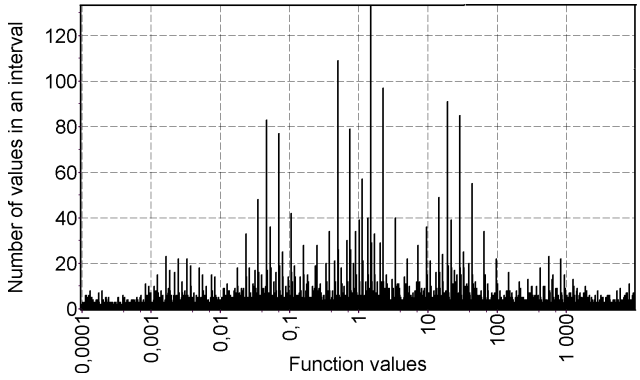

Fig. 3: Frequent distribution obtained with $q_1 = 1.5$, $q_2 = 0.5$, $q_3 = 19.3$, $q_4 = 0.047$, $p_1 = 0.294$, $p_2 = 0.235$, $p_3 = 0.235$, $p_4 = 0.235$; number of the steps in the series is 500, number of the series is 500; number of the numerical values in the scale is 67,000 (of those, nonzero intervals are 28,000).

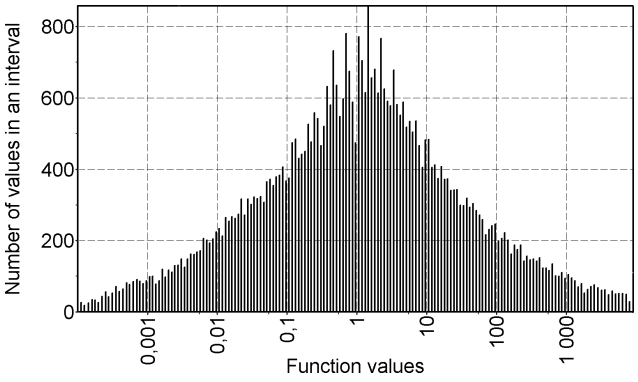

Fig. 4: Frequent distribution obtained with $g = 0.1$ from the current numerical value S_i; here $q_1 = 1.5$, $q_2 = 0.5$, $p_1 = 0.555$, $p_2 = 0.444$; number of the steps in the series is 100, number of the series is 500; number of the numerical values in the scale is 48,000 (of those, nonzero intervals are 173).

modelling the change of the parameter S_i and the set of a massive data of S_i, in look for the frequent distributions obtained due to three perturbing factors q_1, q_2, q_3. Here a, b, c are prime numbers which stochastically change (the computer program contains a function which generates random numbers), in each single cycle of the observation, along the intervals whose length is proportional to their probabilities p_1, p_2, p_3.

The graphs manifest that fact that, in the common background of the numerical values of the current parameters, there is only minor number of those whose probability exceeds the average value in many times. Besides that, the exceeding numerical values depend on the numerical values of the progression coefficients, but are independent from the length of the series (the number of the steps). Increasing the number of the perturbing factors does not make the non-uniform distribution more smooth, as it should be expected. Contrary, the non-uniformity of the distribution increases: in this process the allowed current values S_i occupy more square of the graph, while their number in the given section of the axis x decreases. Therefore a small probability of that the current values S_i will valuable shift from their average positions appear due to the appearance of the long chains of the co-multipliers which have the progression coefficients larger (or lesser) than unit. If the progression coefficients differ valuable from each other, the histogram manifest distributions of high orders (see Figure 3).

Consider an ultimate case where all perturbing factors, i.e. the progression coefficients q_i, differ from each other by the numerical values, and there is not their coinciding numerical values in the series. This situation can easy be modelled, if setting up in the computer program that the progression coefficients have a connexion with the counters of the cycles t and u, or that they are varied by any other method. In this case, in a limit, the amplitude of the numerical values in the histogram will never exceed unit, nowhere, while the *frequent non-uniformity* will still remain in the distribution. Therefore, even if extending the length of the unit interval, the same dis-

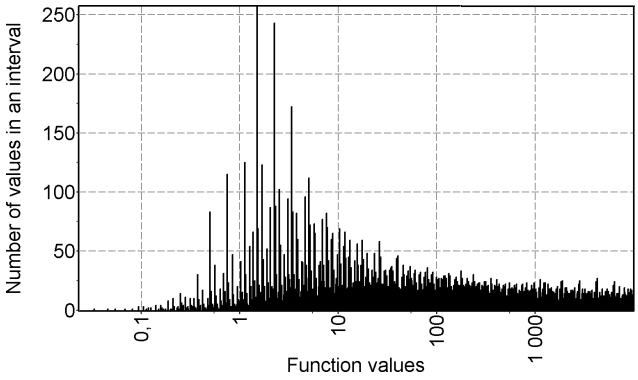

Fig. 5: Non-symmetric frequent distribution obtained according to the data of Fig. 2; number of the numerical values in the scale is 22,000 (of those, nonzero intervals are 2,400).

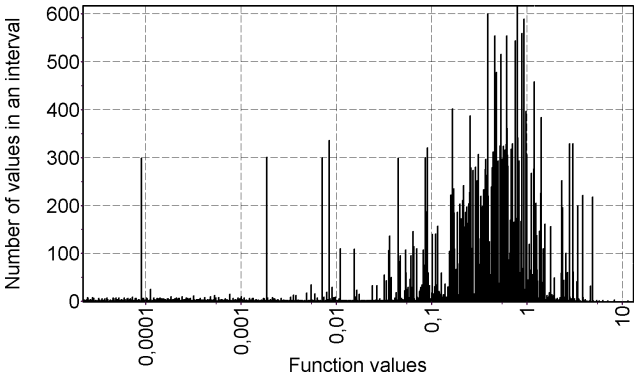

Fig. 6: Frequent distribution of the solutions of the quadratic equation $x^2 - 2Bx + C = 0$ with $q_1 = 1.33$, $q_2 = 0.71$, $q_3 = 1.33$, $q_4 = 0.71$; here $p_1 = p_2 = p_3 = p_4 = 0.25$; number of the steps in the series is 300, number of the series is 300; number of nonzero intervals is 16,000. All geometric coefficients of the progression are independent from each other.

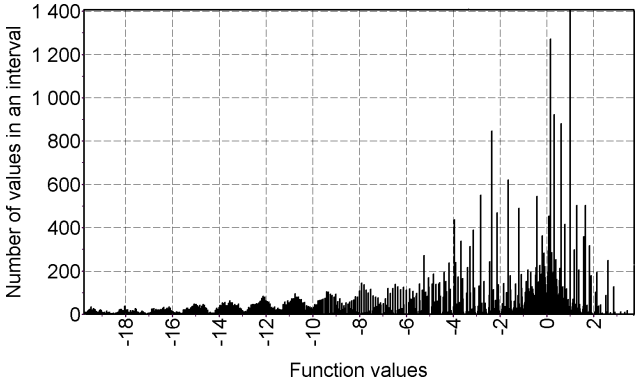

Fig. 7: Frequent distribution of the solutions of the quadratic equation $x2 - 2Bx + C = 0$ with $q_1 = 0.71$, $q_2 = -0.71$, $q_3 = 0.71$, $q_4 = -0.71$; here $p_1 = p_2 = p_3 = p_4 = 0.25$; number of the steps in the series is 250, number of the series is 250, number of nonzero intervals is 1,800. All arithmetic coefficients of the progression are independent from each other.

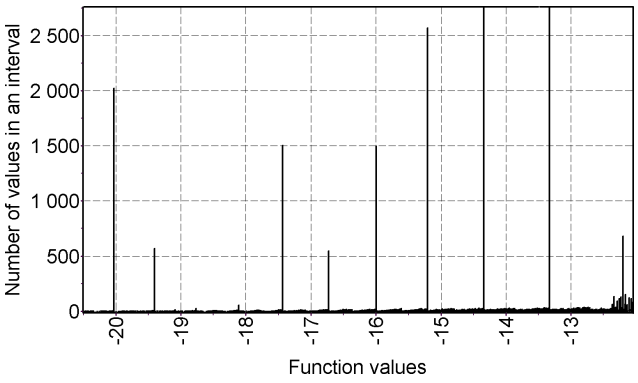

Fig. 8: Frequent distribution of the solutions of the quadratic equation $x2 - 2Bx + C = 0$ with $q_1 = 0.127$, $q_2 = 1.13$; $p_1 = 0.465$, $p_2 = 0.535$; number of the steps in the series is 500, number of the series is 10,000; number of the numerical values in the scale is 27,000, number of nonzero intervals is 1,350. All arithmetic coefficients of the progression are dependent on each other.

tribution takes the amplitudal discrete shape again. Finally, under truncating the number of the intervals (this, generally speaking, means analysis of the given process with a lower precision), the graph takes a shape of almost the smooth normal distribution (see Figure 4).

It is possible to suppose that the discreteness of normal distributions (and, as is obvious, any other distributions as well) is their core property originated from that the rational numbers are distributed with different density along the axis of numbers [2, 3].

Shapes of the histograms depend on specific parameters; they may be very spectacular. So, in the bit of the computer program that was given above, each perturbing factor realizes itself independent from the others. If however, for instance in the first condition, one replaces the logical "and" with the logical "or", the distribution changes its shape very much (see Figure 5).

So forth, Figures 6–9 show illustrative examples of the versions of the frequent distributions of one of the solutions of a quadratic equation $x^2 - 2Bx + C = 0$, where we see iterrationally correcting two parameters B and C whose initially numerical values are units.

In the example shown in Figure 6, the progression coefficients are geometric, and are independent from each other. The parameter B is under a correction by the coefficients q_1 and q_2, while the parameter C is under a symmetrical correction by the coefficients q_3 and q_4. Specific to the graph is that, somewhere left from the main distribution, in the background of many dense numerical values whose probabilities are very small, a small number of the numerical values having a very high probability appear (they experience a shift to the side of small numerical values of the function).

In the other examples shown in Figures 7 and 8, the progression coefficients are arithmetic. In the distribution shown

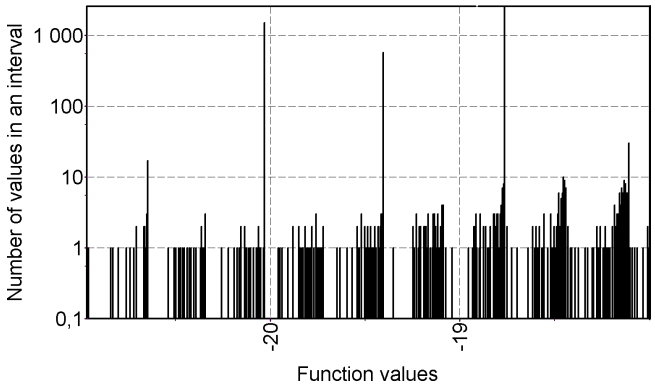

Fig. 9: A fragment of the frequent distrinution according to the data of Fig. 8; number of the numerical values in the scale is 5,300 (of those, nonzero intervals are 220).

in Figure 7, four progression coefficients are present; they are symmetric. The histogram is built by a set of the Gauss arcs of the first, second, and higher orders which fill the side of negative numerical values. The distance between the arcs, and their shape depend on the numerical value of the progression coefficients. In Figure 8, we give a part of the quadratic function distribution in the region of negative numerical values of its solutions taken under two coefficients q_1 and q_2, where the parameters B and C are additionally connected to each other, and their correction is produced commonly for them. The respective bit of the algorithm has the form:

```
for ( int t = 1; t < 10000; t ++ )      {
double  B  =  C = 1;
for ( int u = 1; u < 500; u ++ )        {

if ( a >=  b )   B = B + q1 , C = C - sqrt(q2) ;
if ( b >=  a )   C = C + q2 , B = B -  q1 ;
if ( B*B - C > 0 )
Si =  B - sqrt ( B*B - C ) ;
i++ ,  m[ i ] = Si ;                    }
                                        }
```

Here, as well as in the example shown in Figure 7 (but with more obvious visibility), that fact is manifested that the overwhelming number of the numerical values, i.e. the probable solutions of the function obtained under the variation of the parameters B and C, have an infinitesimally small probability in the scale, while the probability of the solutions is concentrated in a very small number of the solutions where it thus is very high. In the fragment of the histogram taken in a semi-logarithmic scale (Figure 9), is is clearly seen that the peaks of the maxima "grow up" from the frequent concentrations of the numerical values of the functions in the axis x. Should this mean that, in the case of similar distributions of a macroscopic system having an arbitrary number of solutions (degrees of freedom), the macroscopic system under a specific set of the parameters acting in it can be in selected special discrete (quantum) states, i.e. the system can have discrete solutions?

It is absolutely obvious that, first, such maximally probable solutions are mostly interested in processes and phenomena we study. Finding these solutions by some other methods that the method given above would be very complicate. Of course, in formulating algorithms for similar problems (obtaining the massive of the required values and their distribution by the algorithm) it is expedient to introduce reasonable limitations on the intervals of the parameters, their relations, etc., in order to excluse some extra calculations non-useful in the problems.

The simple examples we considered here show that the logical mathematical models similar to those we considered can contain actually unbounded number (with a limit provided by the computer techniques only) of both stochastic influences (the parameters q_i) and the conditions of their appearance (the logical and other relations between the coefficients q_i and also the parameters of the system). In the same way, very complicate complex influences of very different stochastic factors affecting any processes we study (not only physical processes) can be modelled if their formalization is possible. Moreover, it is probably we can set up the probabilistic system or process to be into a small number of stable states, which are necessary to our needs in the problem, by respective choice of the parameters affecting it.

Concerning the Brownian motion as a particular case of normal distributions, it can be also analysed if we know the spectrum of the factors perturbing it (the dole of each factor in their common sum, and the goal of each factor into the commonly perturbing influence). Concentration of the Brownian molecules and their momentum can be such factors in the problem.

Generalizing all that has been presented in this paper, I would like to say that frequent distributions provide a possibility for bonding the reaction of different parameters of a complicate system being affected by stochastic factors of the surrounding world, and also finding most probable states of the system thus predicting its behaviour. Having any problem, both those of physics, industry, economics, game, and others where numerous parameters are unknown, non-sufficiently determined, or are affected by stochastic changes, the method that presented in the paper leads to a spectrum of the most probable solutions of the problem.

Submitted on April 24, 2010 / Accepted on May 17, 2010

References

1. Shnoll S. E. Cosmic physical factors in random processes. Svenska fysikarkivet, Stockholm, 2009, 388 pages.
2. Dombrowski K. I. *Bulletin of Soviet Atron. Geodesical Society*, 1956, no. 17(24), 46–50.
3. Dombrowski K. I. Rational numbers distribution and resonance. *Progress in Physics*, 2005, v.1, 65–67.

On the Necessity of Using Element No.155 in the Chemical Physical Calculations: Again on the Upper Limit in the Periodic Table of Elements

Albert Khazan
E-mail: albkhazan@gmail.com

It is shown how the properties of different elements of the Periodic System of Elements can be obtained using the properties of the theoretically predicted heaviest element No.155 (it draws the upper principal limit of the Table, behind which stable elements cannot exist). It is suggested how the properties of element No.155 can be used in the synthesis of superheavy elements. An analysis of nuclear reactions is also produced on the same basis.

1 Introduction

At the present time, we know about 20 lists of chemical elements (representing their most important properties such as atomic mass and radius, density, temperatures of melting and boiling, energy of ionization, etc.), which were suggested by their authors as periodic tables of the elements. These data were however obtained for, mainly, stable isotopes and numerous other radioactive isotopes that makes further interpolation of these properties onto superheavy elements quite complicate.

This is most important for planning further experiments whose task is synthesis new superheavy elements which approach to the recently predicted heaviest element No.155, whose atomic mass is 411.66 (the upper limit of elements in Mendeleev's Table of Elements behind which stable elements cannot exist). Thus, using the parameters of element 155 in the analysis of other elements, we will see in this paper how the properties of the elements behave with increasing their number in the Table.

2 Some peculiarities of the dependency between atomic mass of the elements and their numbers in the Table of Elements

Consider the dependency between atomic mass of the elements and their number in the Table of Elements. This dependency is well known in science and industry and is presented as numerous lists and tables. As is seen in Fig. 1, this dependency is well described by the exponential equation of the line of the trend. However, if we take more attention to this figure, we find numerous areas which destroy the common picture. Approximately smooth line continues from the origin of coordinates to almost the end of Period 6 (No.83, 208.98, Bismuth). This is the last stable isotope, after whom all elements of the Table have an artificial (radioactive) origin, except of Thorium (No.90, 232.038), Protactinium (No.91, 231.036) and Uranium (No.92, 238.029). This is their order in the family of actinides. Period of half-decay of these natural elements consists many thousand years. It is easy to find in the figure that valuable deviations from the line of the trend are present in the region from Bismuth to element 104, then to element 119 where the deviations from the line of the trend are high (especially — in the region of the already synthesized superheavy elements 104–118).

This is seen more obvious in Fig. 2, where the absolute deviations of the atomic masses are presented. These are deviations between the data of the Table of elements and the result obtained after the equation

$$y = 1.6143\, x^{1.0981}, \qquad R^2 = 0.9969, \tag{1}$$

where y is the atomic mass, while x is the number in the Table of Elements.

It should be noted that mass number is an integer equal to the common number of nucleons in the nucleus. Mass number of an isotope is equal to the numerical value of its mass, measured in atomic mass units (a.m.u.) and approximated to a near integer. A difference between the mass numbers of different isotopes of the same element is due to the different number of neutrons in their nuclei.

It is seen in the figure that this difference does not exceed 4 a.m.u. in the first five periods and in lanthanides. This tendency still remain upto Bismuth after whom the deviations of actinides experience a positive shift: this means that the numerical values of the atomic masses presented in the Periodic Table are overstated for the region.

Then, after actinides, a region of the atomic masses of the elements of Period 7 (elements 104–118) is located. These elements were obtained as a result of nuclear reactions. As is seen, all deviations in this region are negative: this can mean a large deficiency of the numerical values of the atomic masses obtained in the nuclear synthesis producing these elements, incorrect calculations, or a lack of neutrons in the nuclei. All these in common resulted large deviations of the atomic masses upto 10–12 a.m.u.

Look at Fig. 1 and Fig. 2 again. Section of the line of the trend in the interval No.119–155 is manifested in Fig. 1 as a very straight line without any deviation, while the same section in Fig. 2 manifests deviations from 0.63 to 1.28. Once we get a ratio of the difference between the table and calculated numerical values of the atomic masses to the respective a.m.u., we obtain Fig. 3 which shows the respective de-

viations in percents. As is seen in the figure, most valuable deviations are located in the left side (upto the first 20 numbers). This is because the respective elements of the Table of Elements bear small atomic masses under high difference of a.m.u., i.e. the larger numerator results the larger ratio. It is necessary to note that the results presented in this figure are within 3–5%. Most lower results are located in the scale from element 104 to element 118: according to our calculation, the deviations are only 0.2–0.3% there.

In order to exclude any influence of our calculations onto the creation of the line of the trend, we study the dependency "atomic mass — number in the Table" in the scale from element 1 to element 118 according to the equation

$$y = 1.6153\, x^{1.0979}, \qquad R^2 = 0.9966. \tag{2}$$

As a result we obtain that the general shape of the deviations and their numerical values are actually the same as the results obtained due to equation (1). So forth, the next particular equations were taken under analysis:

$$\text{elements 1–54:} \quad y = 1.6255\, x^{1.0948}, \quad R^2 = 0.9922, \tag{3}$$

$$\text{elements 55–118:} \quad y = 1.8793\, x^{1.0643}, \quad R^2 = 0.9954, \tag{4}$$

$$\text{elements 119–155:} \quad y = 1.5962\, x^{1.1009}, \quad R^2 = 1.0\,. \tag{5}$$

These sections gave no any substantial change to the previous: the ultimate high difference of the deviations taken in 3 points of 120 was 0.7% for element 111, 0.95% for element 118, and 1.5% for element 57.

3 Why one third of the elements of the Table of Elements is taken into square brackets?

94 chemical elements of 118 already known elements are natural substances (contents of several of them consists, however, of only traces). Rest 24 superheavy elements were obtained artificially as a result of nuclear reactions. Atomic mass of an element in Table of Elements is presented by the average atomic mass of all stable isotopes of the element with taking their content in the lithosphere. This average mass is presented in each cell of the Table, and is used in calculations.

If an elements has not stable isotopes, it is taken into square brackets that means the atomic mass of most long living isotope or the specific isotope contents. There are 35 such elements. Of those 35, elements from 93 to 118 are actinides and artificially synthesized superheavy elements. Hence, one third of 118 elements (known in science at the present time) bears undetermined atomic masses.

Fig. 4 shows common number of isotopes of all elements of the Table of Elements. Location of all elements can be described by the equation of parabola with a high coefficient of real approximation. As is seen, the descending branch of the parabola manifest that fact that the heavier element in the Table (the larger is its number) the lesser number of its isotopes. This tendency lads to decreasing the number of isotopes upto 1 at element 118.

4 Synthesis of superheavy elements and the upper limit of the Periodic Table

Because number of the isotopes reduces to 1 in the end of Period 7, the possibility of Period 8 and Period 9 (each consisting of 50 elements) in the Table of Elements suggested earlier by Seaborg and Goldanskii [1, 2] seems non-real. At the same time, Seaborg suggested a possibility of the synthesis of a "magic nucleus" consisting of 114 protons and 184 neutrons: according to his suggestion, this nucleus should be the centre of a large "island of stability" in the sea of spontaneous decay. Goldanskii told that the "isthmus of stability" may be a region where isotopes of the elements bearing nuclear charges 114, 126, and even 164 may be located. Flerov [3], when analysed studies on the synthesis of superheavy elements, claimed that the elements should give us a possibility for answering the question: are the elements bearing nuclear charges 100–110 located at the real end of the Table of Elements, or more heavy nuclei exist in the Nature? There are many studies of the conditions of nuclear reactions. For instance, in already 1966, Strutinski [4] theoretically predicted a valuable increase of stability of nuclei near the "magic numbers" $Z = 114$ and $N = 184$. His calculation was based on the shell model of nucleus (this model won Nobel Prize in physics in 1963 [5, 6, 7]).

In 1973, Oganesyan in Dubna (Russia) and a group of German scientists in Darmstadt (Germany) first used cold synthesis, where the "magic nuclei" were used as both a target and bombing particles [8]. In 1973, Oganesyan claimed that elements with atomic numbers 160 and, maybe, 170, are hypothetically possible. However only two years later, he claimed that the properties of an element with number 400 and bearing 900 neutrons in its nucleus were theoretically discussed [9].

In addition to the indeterminacy of atomic masses in the synthesis of superheavy elements, Oganesyan also told, in his papers, that we do not know limits in the Table of Elements behind whom superheavy elements cannot exist. According to his own words, "the question about limits of the existence of the elements should be addressed to nuclear physics" [10]. A few years later, in 2005, Oganesyan claimed "this question is still open: where is the limit of chemical elements?" [11]. In 2006, in his interview to *Moscow News*, he set up the questions again: "is a limit there?" and "how many elements can exist?". So forth, he tells in the interview: "We use modelling instead a theory. Each models approaches this system in a form of those known to us in analogy to the macroscopic world. However we still do not understand what is nuclear substance. Thus the question asked about a limit of the Periodic System is still open for discussion" [12].

In January 20–21, 2009, in Dubna, the international symposium celebrating the 175th birthday of Dmitri Mendeleev set up the question about limits of the Table of Elements, and the complete number of elements in it again. Some-

one suggested even a possibility of the synthesis of elements with numbers 150–200 [13]. However a few weeks later, in February 09, at a press-conference in Moscow, the participants claimed that "at present the scientists discuss a theoretical possibility of extending Mendeleev's Periodic Table upto **150 elements**" [14].

In April 07, 2010, the world press claimed about the end of an experiment in which element 117 was synthesized (this experiment continued from July 27, 2009, until February 28, 2010). During these seven months, the experimentalists registered six cases where nuclei of the new element were born. This experiment was also based on the supposition that there is an "island of stability" near an element bearing parameters $Z = 114$ and $N = 184$. Lifespan of this island should be a few million years. However this target was not reached in the experiment. The research group of experimentalists in Dubna prepares next experiments which target synthesis of element 119 and element 120 [15].

In this connexion it is interesting those words said by Sigurd Hofman (the GSI Helmholtz Centre for Heavy Ion Research, Darmstadt), where he claimed about filling the Table of Elements upto its end in the close time. According to his opinion, atomic nuclei heavier than No.126 cannot exist, because they should have not the shell effect [16].

5 Discussion of the results

1. The considered dependency of atomic masses of the elements on their numbers in the Table of Elements cannot answer the question "where is the upper limit of the Table".

Despite the coefficient of the line of the trend is very close to unit, it is easy to see that there are large deviations of the data, especially starting from the numbers of actinides and then so forth. Because all actinides bear similar chemical properties, selecting a segregate element in this group is quite complicate task. Besides, the possibility of different isotopic content in samples of the elements leads to a large deviation of the calculated atomic masses from the atomic masses given by the Table of Elements. This is related to one third part of all elements of the Table.

2. Next elements to actinides, i.e. a group of elements 104–118, were synthesized as a result of nuclear reactions, in a very small portions (only segregate atoms were produced). The way how the elements were produced makes a problem in the identification of them, and the large deviations of the data of the Table of Elements from the line of the trend. Hence, atomic masses attributed to these numbers in the Table of Elements, are determined very approximate. The line of the trend, which includes element 155, gives a possibility to exclude the deviations of the atomic masses.

3. Section 4 gave a survey of opinions on the structure of the Table of Elements, its limits, superheavy elements (their synthesis and the products of the synthesis), the search for an "island of stability", and the technical troubles with the nuclear reactions.

Many questions could be removed from discussion, if my recommendations suggested in [17], where I suggested the last (heaviest) element of the Table of Elements as a reference point in the nuclear reactions, would be taken into account. This survey manifests that the quantum mechanical approach does not answer the most important question: **where is the limit of the Periodic Table of Elements?** Only our theory gives a clear answer to this question, commencing in the **pioneering paper of 2005**, where the **hyperbolic law** — a new fundamental law discovered in the Table of Elements — was first claimed. This theory was never set up under a substantially criticism.

It should be noted that the word "discovery" is regularly used in the press when telling on the synthesis of a new element. This is incorrect in the core, because "discovery" should mean finding new dependencies, phenomena, or properties, while the synthesis of a new element is something like an invention in the field of industry, where new materials are under development.

4. Taking all that has been said above, I suggest to IUPAC that they should produce a legal decision about the use of element 155, bearing atomic mass 411.66, as a reference point in the synthesis of new superheavy elements, and as an instrument correcting their atomic masses determined according to the Table of Elements.

My theory I used in the calculations differs, in principle, from the calculations produced by the quantum mechanical methods, which were regularly used for calculations of the stability of elements. The theory was already approved with the element Rhodium that verified all theoretical conclusions produced in the framework of the theory with high precision to within thousandth doles of percent. Therefore there is no a reason for omiting the theory from scientific consideration.

6 Conclusions

Having all that has been said above as a base, I suggest an open discussion of the study **Upper Limit in Mendeleev's Periodic Table — Element No.155** at scientific forums with participation of the following scientific organizations:

— International Union of Pure and Applied Chemistry (IUPAC);

— International Council for Science (ICSU);

— American Physical Society (APS).

This step should allow to give a correct identification to the chemical elements and substances, and also to plan new reactions of nuclear reactions with a well predicted result. In this deal, financial spends on the experimental research in nuclear reactions could be substantially truncated, because the result would be well predicted by the theory. The experimental studies of nuclear reactions could be continued as a verification of the theory, and aiming the increase of the experimental techniques. Thus, according to the last data of the

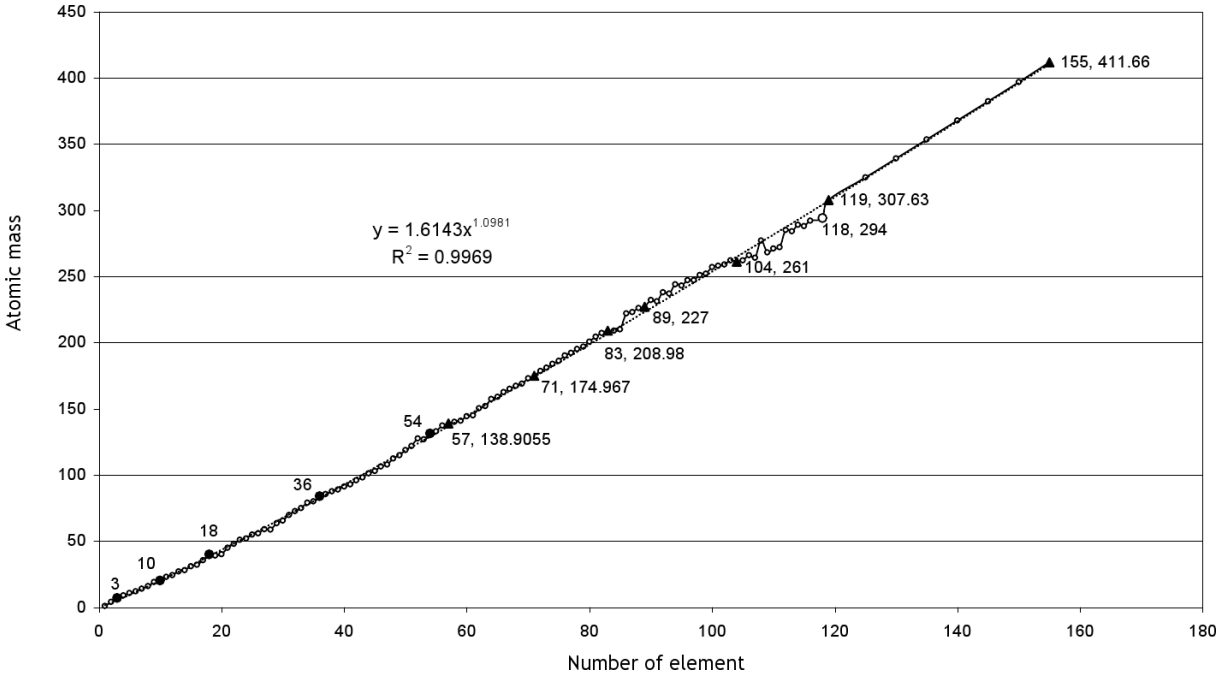

Fig. 1: Dependency between the atomic mass of the elements and their number in the Table of Elements (including element 155).

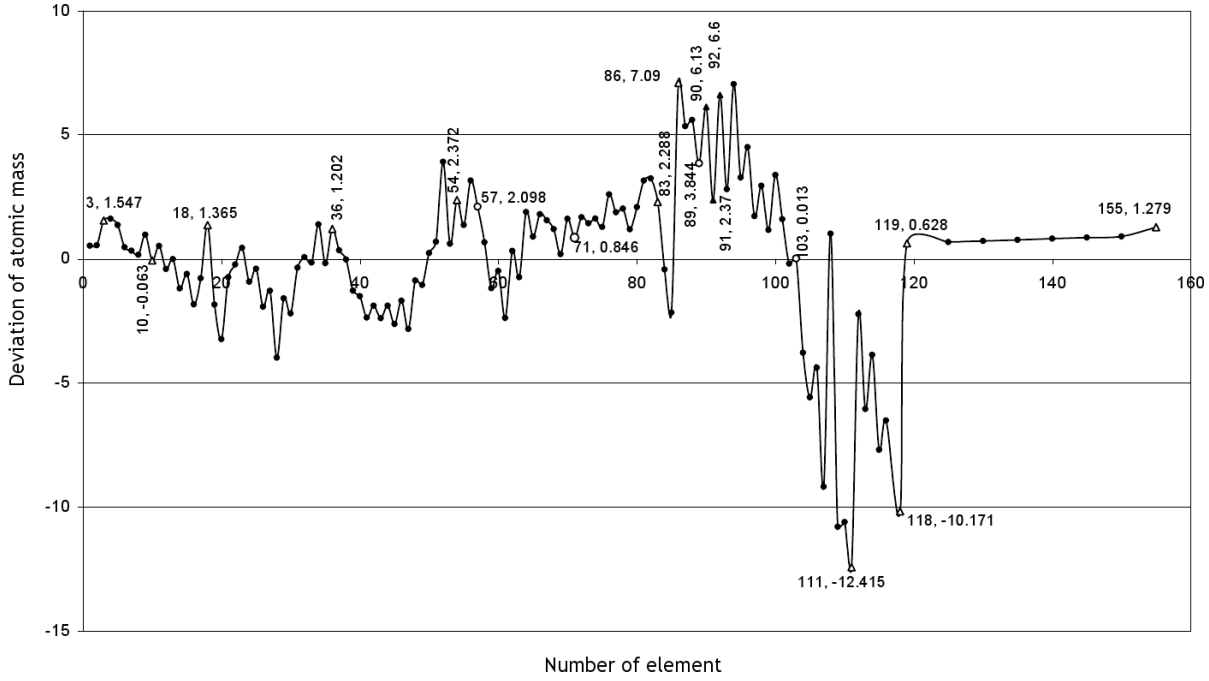

Fig. 2: Absolute deviations of atomic masses of the elements from the line of the trend (including element 155).

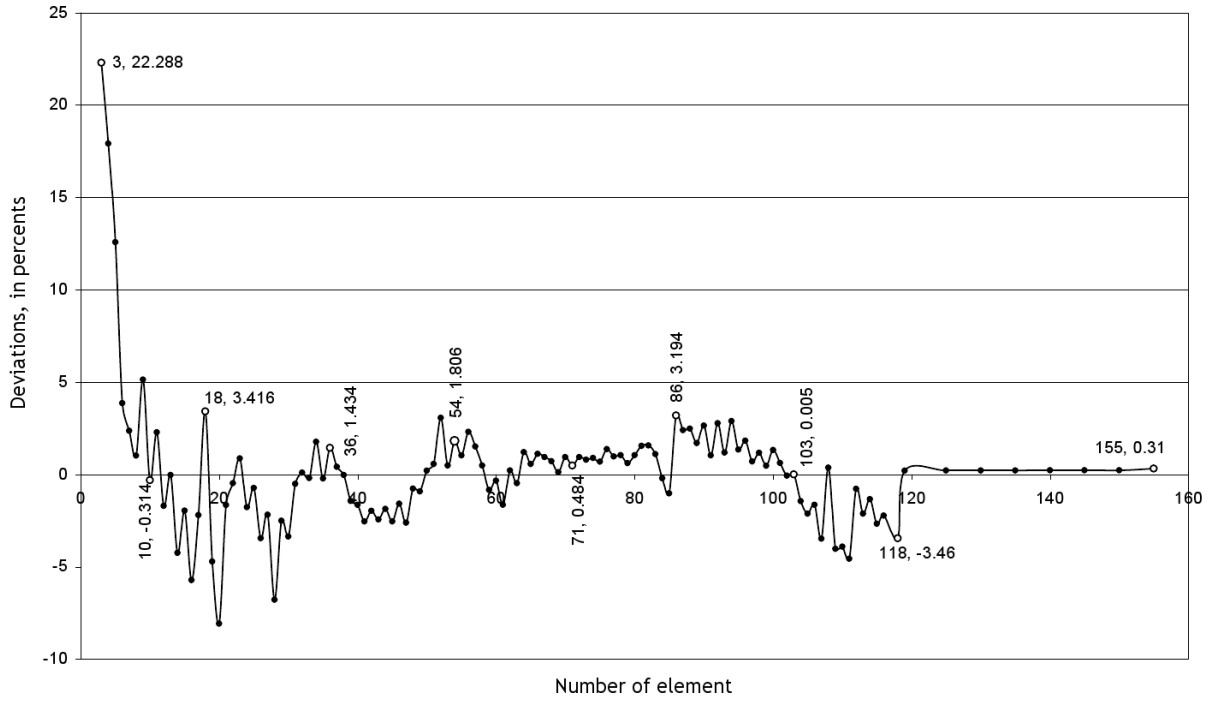

Fig. 3: Relative deviation of the atomic masses from the line of the trend, in percents.

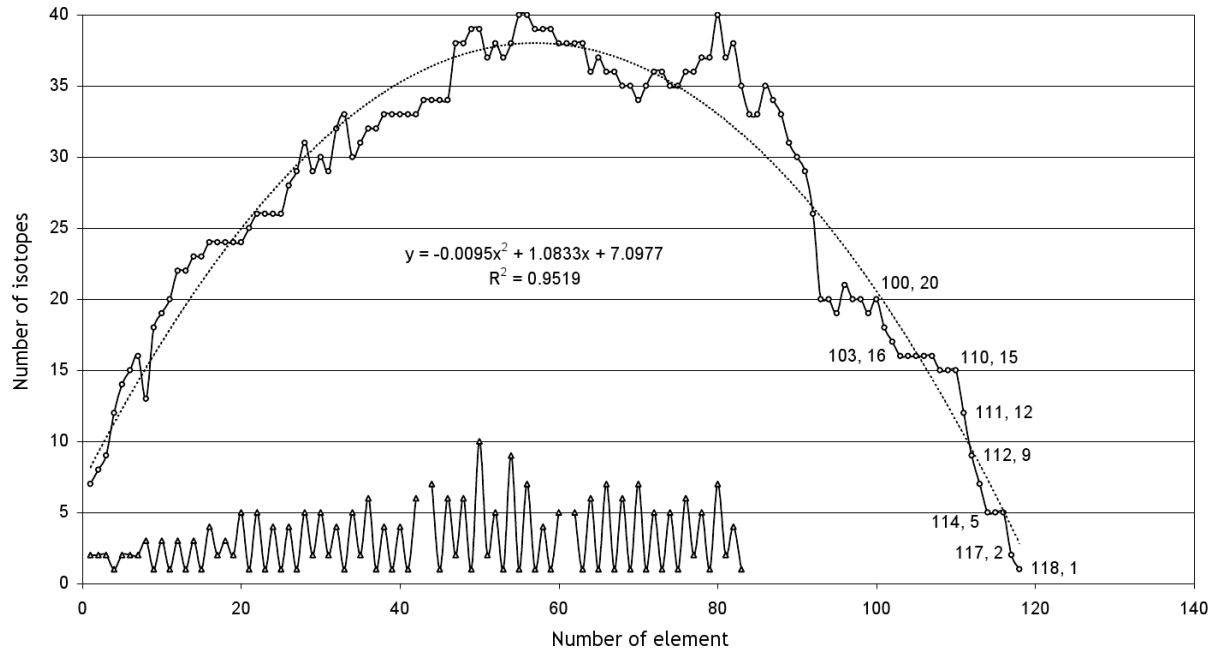

Fig. 4: Dependency between the number of the isotopes (3180) and the number of element in the Table of Elements. Location of the stable isotopes (256) is also shown. The data of Brookhaven National Laboratory, National Nuclear Data Center.

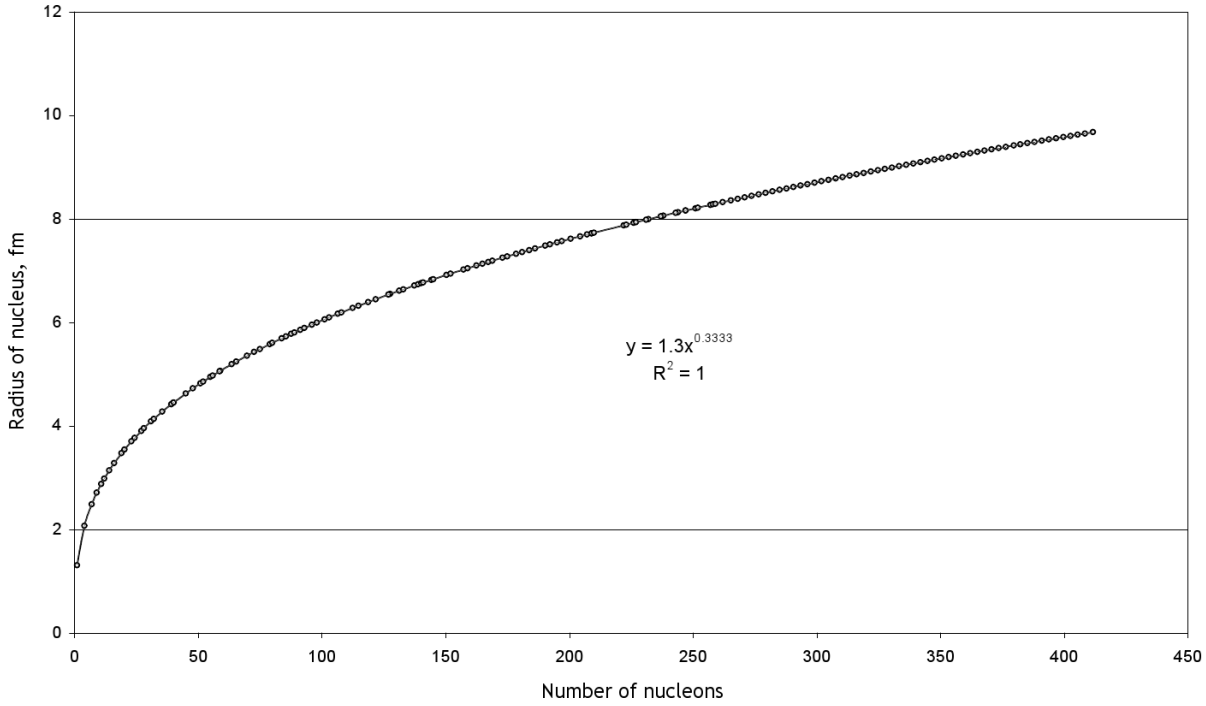

Fig. 5: Empirical dependency between the radius of the nuceus (fm) and the number of the nucleons.

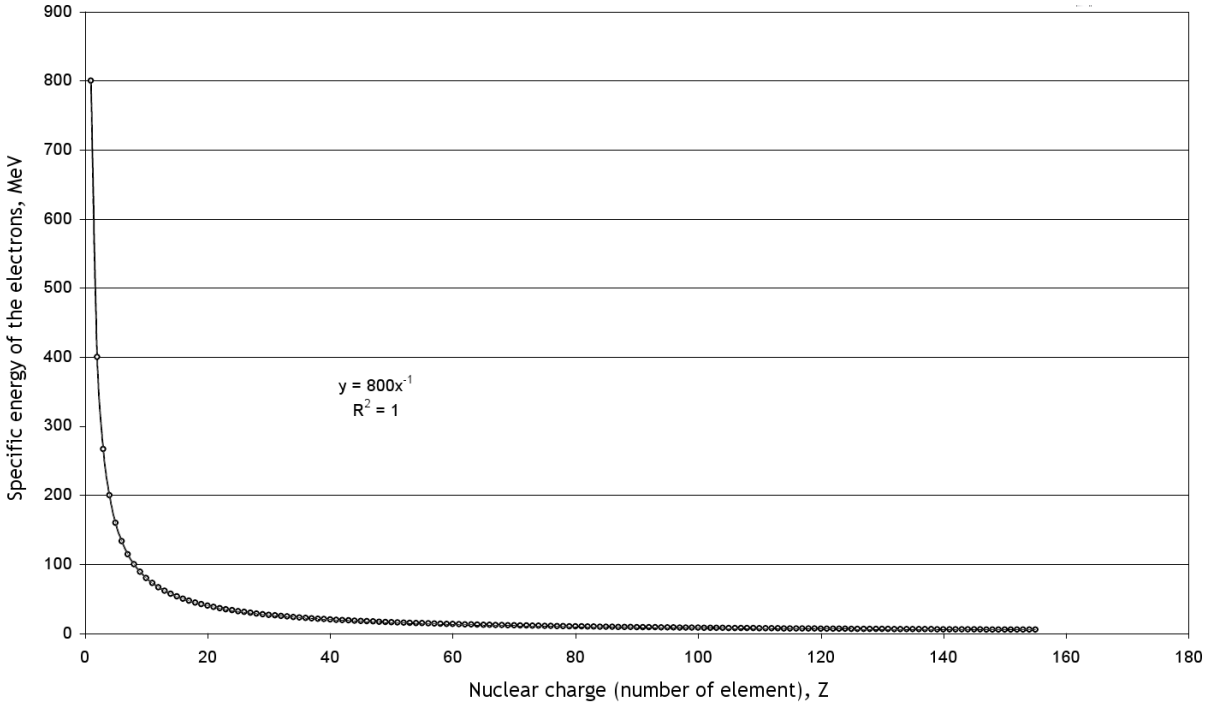

Fig. 6: Dependency beween the critical energy of the electrons and the nuclear charge, according to formula $T = 800/Z$.

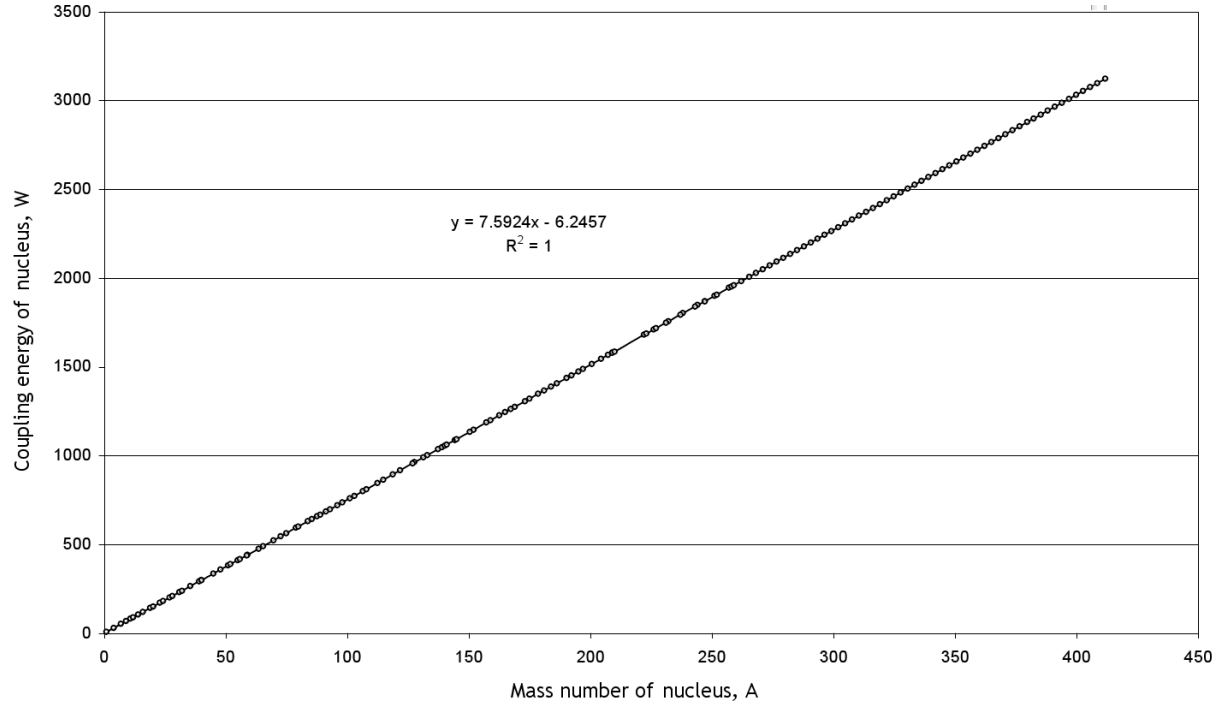

Fig. 7: Dependency between the coupling energy of the nuclei and the mass number (number of nucleons).

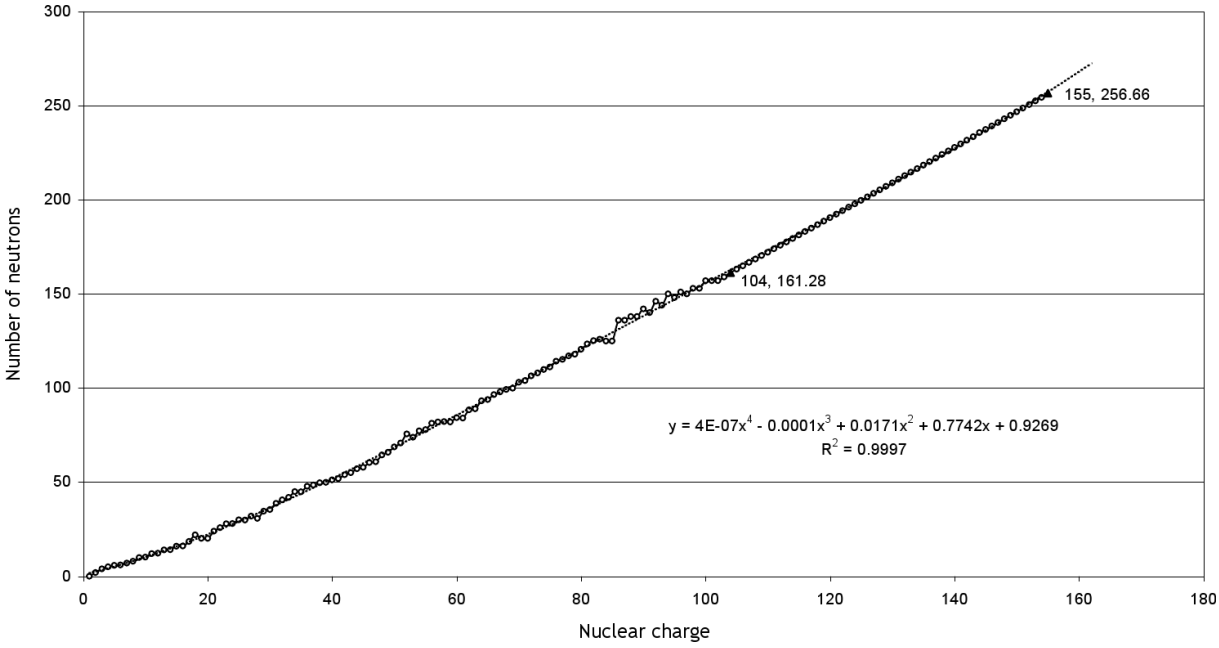

Fig. 8: Dependency between the number of neutrons and the number of protons in the atomic mass, for all elements of the Table of Elements. Our calculation data are given beginning from element 104.

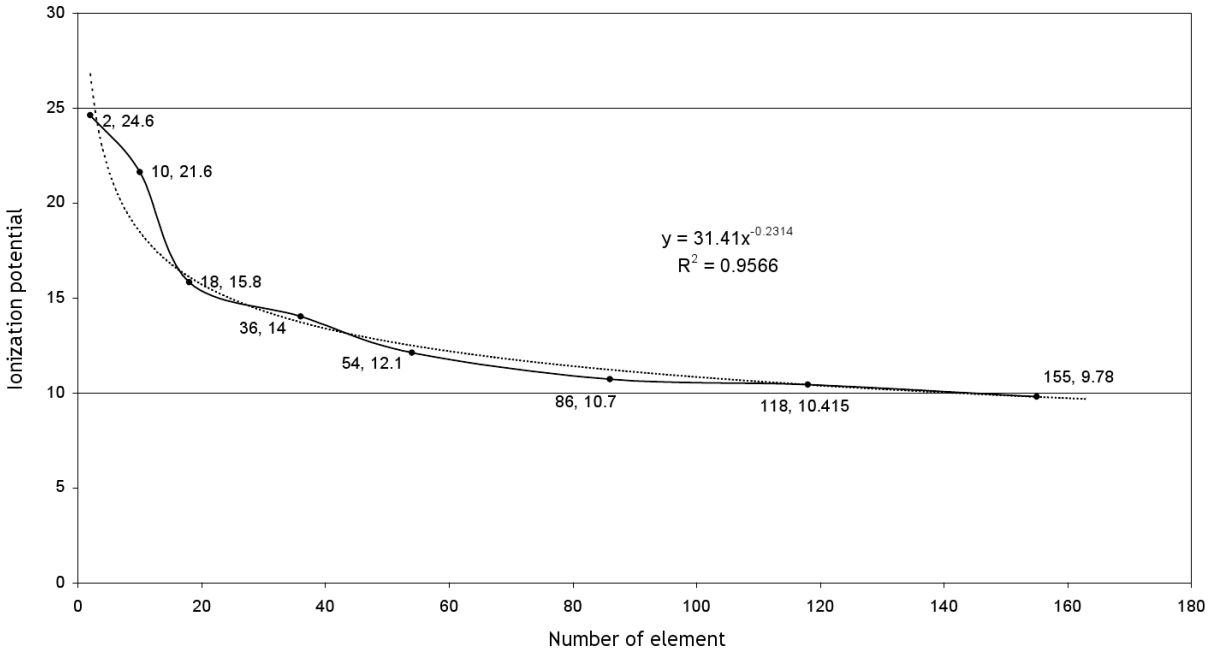

Fig. 9: Dependency between the ionization potential and the number of the elements (nuclear charge), for the neutral atoms of the elements ending the periods of the Table of Elements (including calculated element 118 and element 155).

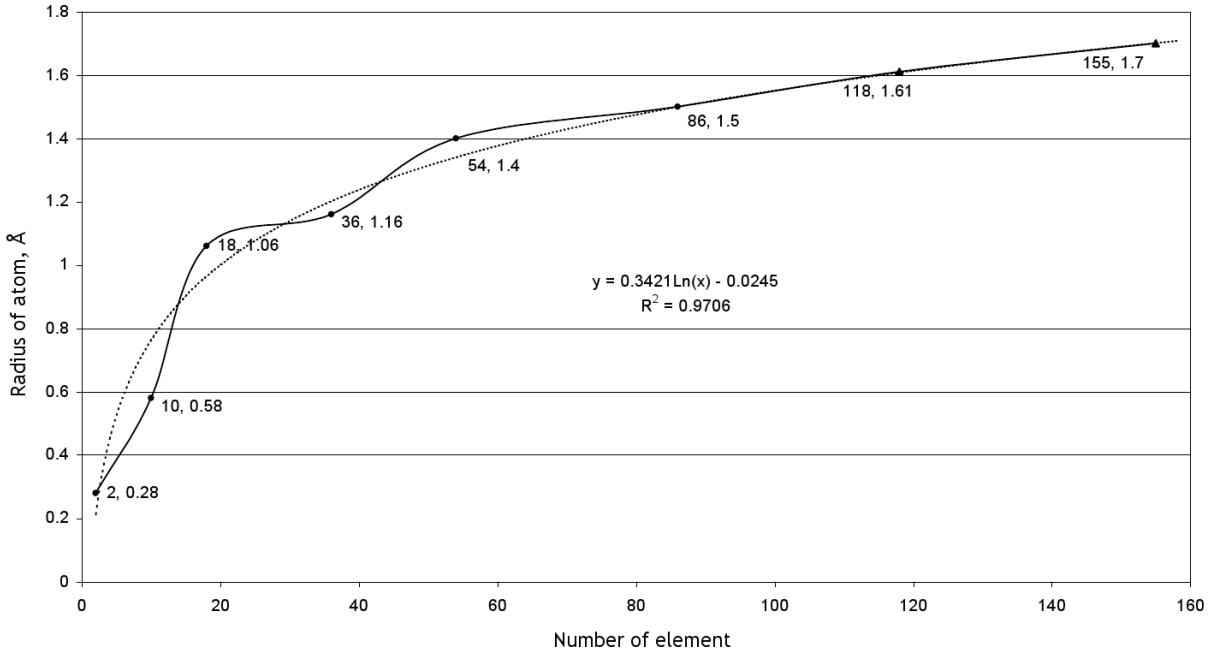

Fig. 10: Dependency between the atomic radius and the number of the elements in all periods of the Table of Elements, including the calculated elements No.188 in Period 7 and No.155 in Period 8.

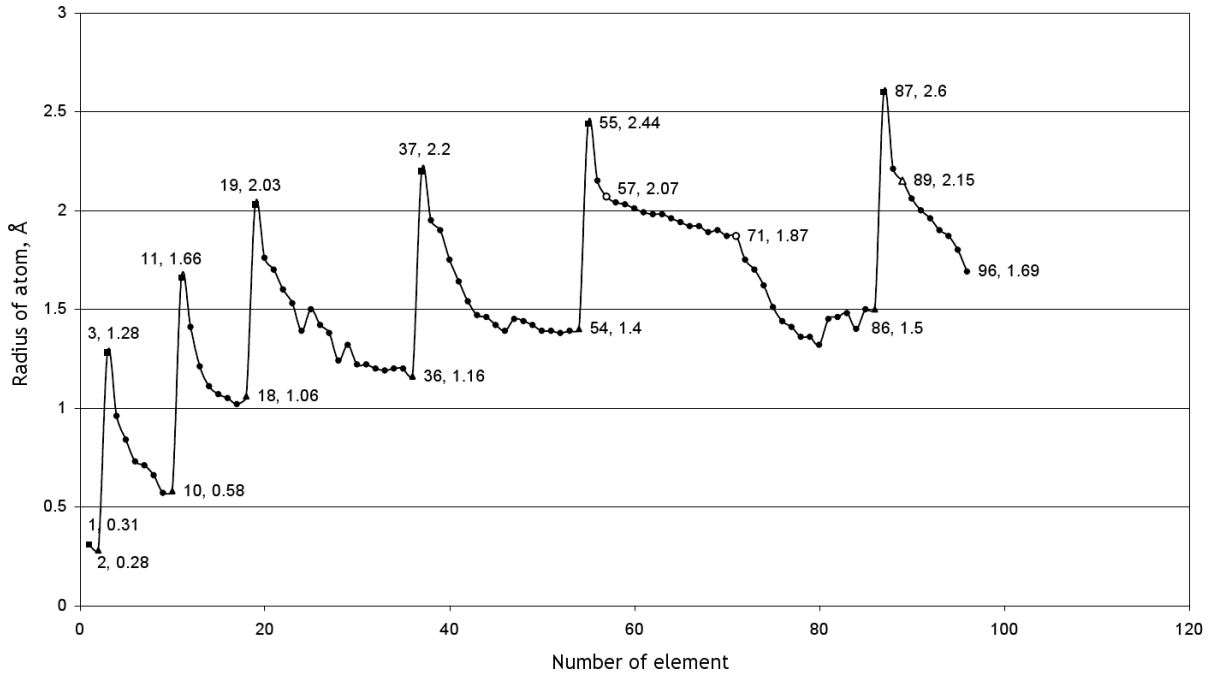

Fig. 11: Change of the numerical value of the atomic radius in each period with increasing number in the Table of Elements.

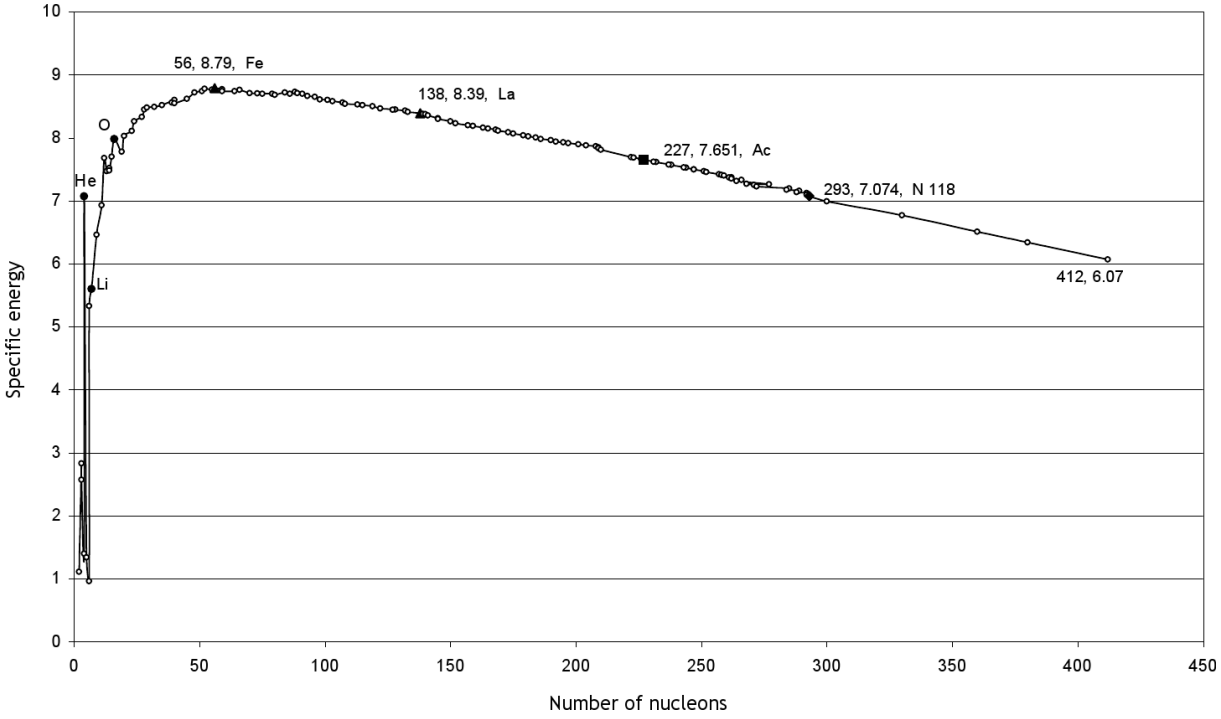

Fig. 12: Dependency between the specific energy of ther coupling in an atomic nuclei and the number of the nucleons in it.

List of Chemical Elements (on April 08, 2010), Ununseptium (No.117) bears atomic mass [295], while atomic mass of Ununoctium (No.118) is [294]. According to the calculation, produced in the framework of my theory, these quantities should be 301.95 and 304.79 respectively.

As was shown the theoretical studies according to the theory, and its comparing to the experimental data, the element bearing number 155 and atomic mass 411.66 a.m.u. answers all conditions necessary for including it into the Periodic Table of Elements.

Appendix I

As was already noted above, we took much attention to the dependency between atomic mass of the elements and their number in the Table of Elements. It was shown that the line of the trend continued upto No.155 provides obtaining very correct results. In verification of this fact, additional dependencies concerning the last element No.155 were studied [18].

Fig. 5 shows an empirical dependency between the radius of a nucleus and the number of nucleons in it (mass number). This graph manifests that this dependency is true upto element 155: the arc has the same shape without deviation along all its length.

Fig. 6 shows an arc, which manifests critical energies of the electrons for all elements of the Table of Elements, including No.155. A critical is that energy with whom energy loss for ionization and radiation become equal to each other. Formula for the critical energy is $T_{\text{crit}} = 800/Z$, where Z is the charge the nucleus (in units of the charge of the electron). As is seen from the graph, this formula is applicable to all elements of the Table of Elements.

Fig. 7 gives calculations of the coupling energy in nuclei. This graph shows that minimally energy required for destruction of the nucleus into its nucleons. It is seen, from the graph, that this dependency is strictly straight along all Table of Elements, including element 155.

Dependency between the number of the neutrons and the charge of the nucleus is shown in Fig. 8. As is seen, equation of the line of the trend describes, with a high level of probability ($R^2 = 0.9997$), the polynomial of the fourth order presented in the graph. This equation covers a large region along the axis x, from element 1 upto element 155 including. This dependency was also calculated, in order to compare it with the previous result, for a truncated region of the protons from element 1 upto element 104:

$$Y = 4E - 0.7x^4 + 2E - 0.5x^3 + 0.007x^2 + \\ + 1.0014x - 0.2176, \quad (6)$$

where $R^2 = 0.999$.

As is seen, certainty the level of the approximation differs only in 0.0007 from the previous. This manifests that fact that this dependency is as well true for the elements heavier than No.104, including element 155.

Appendix II

At the present time there are many versions of the periodic tables of elements, where each cell contains a property of a respective element (such as atomic radius, volume, density, first ionization potential, etc.). This information can also be obtained from the regular lists of the properties of chemical elements. This information has, however, a substantially lack: most data end in the beginning or the middle of Period 7.

Here we target continuing the list of numerous properties of the elements upto element 155, and also the compatibility of the properties with the reference data.

Fig. 9 shows a dependency between the ionization potential of the neutral atoms of the elements and the change of their nuclei. Each point corresponds to the last element of the period, from Period 1 to Period 6. The end of Period 7 and that of Period 8 were calculated according to the equation of the trend. As is seen, the points corresponding element 118 and element 155 are completely correlated with the initially data.

An important characteristic of atomic nucleus is the numerical value of its radius (see Fig. 10). This graph was created on the basis of the reference data known at the present time. This dependency between the atomic radius and the number of the last element in the period was created for all periods of the Table of Elements where it was possible. Coordinates of the points for Period 7 and Period 8 were calculated according to the equation of the line of the trend. As is easy to see, even the point of Period 6 meets the calculated data in complete.

Fig. 11 shows how the atomic radii change from period to period and inside each period of the Table of Elements (i.e. in the columns of the Table from up to down, and along the horizontal line). The upper maxima represent the beginning of the periods, while the lower points represent their ends. It should be noted that in lanthanides, which are No.57–No.71, a linear dependency between the radius and the number is observed. Further study of the correlation shows that there is a change of the linearity upto No.80 (Mercury). Another very interesting detail is that fact that, in the transfer from the alkaline to the alkaline earth elements, a valuable lowering the numerical values of the radii (for 0.3Å on the average) is observed in the periods.

In the calculations of nuclear reactions, the information about the stability of the nuclei as the systems consisting of protons and neutrons has a valuable maning. The forces joining the partcles altogether are known as nuclear forces; they exceed the forces of electrostatic and gravitational interactions in many orders.

The "resistance" of a nucleus can be bond by their coupling energy which shows the energy required for destroying the nucleus into its consisting nucleons (their number in the nucleus is equal to the mass number A expressed in atomic units of mass, a.m.u.). It is known that the sum of the masses

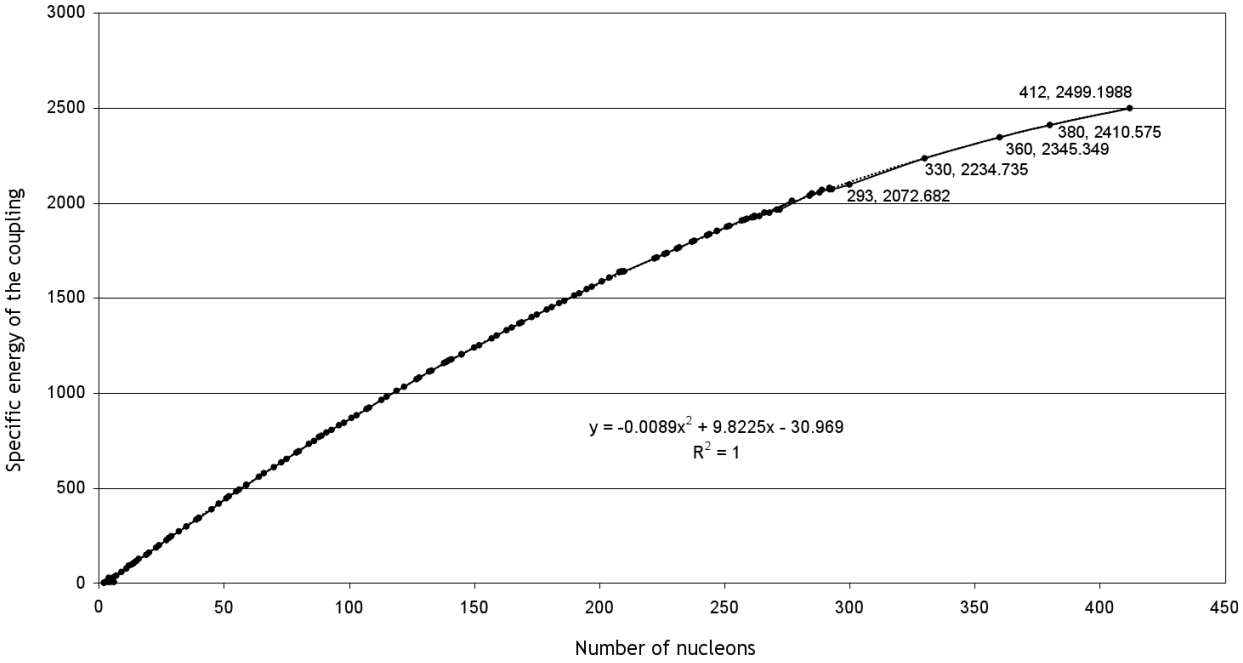

Fig. 13: Dependency between the specific energy of ther coupling in an atomic nuclei and the number of the nucleons in it.

of the free nucleons is already larger than the mass of the nucleus they consist. The difference of the masses is known as the mass defect, according to which Einstein's formula $E = \Delta mc^2$ gives a possibility for calculating the coupling energy of the nucleus, thus the specific energy in it per one nucleon.

Fig. 12 shows an arc, created according to the table data, which manifests the dependency between the specific energy of the coupling in a nucleus and the number of nucleons in it [19]. The left side of the graph shows several isotopes of Hydrogen and the nucleus of several light elements, which bear close numerical values of the specific energy of the coupling and, thus, a large deviation of the data. The arc become more smooth with increasing the number of the nucleons. The maximum is reached in a region of $A = 50$–60, then the falls slow down. The main advantage of this graph is that we produced the calculation beyond element 118 (at which the table data ended): we showed that the results of our calculation *completely meet* the table data known from the reference literature. Decreasing the specific energy of the coupling in the region of heavy nuclei is explained by increasing the number of protons that leads to increasing the Coulomb forces thus the need of additional neutrons apprears.

This is well manifested in Fig. 13. The arc described by the quadratic three-term equation has the numerical value of real approximation $R^2 = 1$. In the region of the nuclei consisting about 120 nucleons, this dependency is actually linear. Then this dependency transforms into an arc of a very large curvature radius. Data bofore the point of the nuclear charge 118 (203, 2072.582) were taken from the previous Fig. 12, then the calculation was produced on the basis of the coordinaters of the suggested last element No.155. As is seen, the arc approaches the horizontal location, where the number of nucleons in a nucleus is not affected by its coupling energy. Accordimng to our calculation, this happens in a region of the coordinates (530, 2670) — (550, 2673) — (600, 2659). This is the ultimate high energy of the coupling of nuclei. If a nucleus has a higher coupling energy, is becomes instable: even a small external influence is needed in order to destry it.

Therefore, Oganesyan's claim that the theoretical physicists discuss the properties of an element with number 400 and bearing 900 neutrons in its nucleus [9] has not any ground or reason.

Submitted on May 01, 2010 / Accepted on May 21, 2010

References

1. Seaborg G.T. and Bloom J.L. The synthetic elements, *Scientific American*, 1969, v.220, no.4, 56.
2. Goldanskii V.I. About connections nuclear and chemical physics. *Progress in Physical Sciences*, 1976, v.118, issue 2.
3. Flerov G.N., Druin Z.A., and Pleve A.A. Stability of heavy nucleus and borders of Periodic System of elements. *Uspekhi Fizicheskikh Nauk*, 1970, v.100, no.11, 45–92.
4. Penionzhkevich Yu.E. Physics of exotics of nucleus. *Soros' Educational Journal*, 1995, 1.
5. Goeppert-Mayer M. Nuclear shell structure. In: *Modern Physics for the Engineer*, McGraw Hill, 1961, 40.
6. Goeppert-Mayer M., Jensen J.H.D. Elementary theory of nuclear of shell. Foreign Literature, Moscow, 1958.
7. Eisenbood L. and Wigner E.P. Structure of the nucleus. Foreign Literature, Moscow, 1959.

8. Oganesyan Yu. New area of the nucleus stability. *Herald of Russian Academy of Sci.*, 2001, v.71, no.7, 590–599.
9. Oganesyan Yu. Superheavy race. Flerov Laboratory, JINR, Dubna, Russia, Atomium 1 [5], 2003. http://flerovlab.jinr.ru/linkc/flerov/atomium/atomium_ogan.html
10. Scientific medium. *Literaturnaya Gazeta*, May 8–14, 2002, no.18–19 (5877), *in Russian*.
11. Oganesyan Yu. Islands of the stability. *Scientific American Russian Edition*, 2005, no.3.
12. Oganesyan Yu. We revive elements of the timeless of the creation of the world. *Moscow News*, December 15, 2006.
13. Mendeleev's year began in Dubna. Weekly of the United Institute of the Nucleus Research (UINR), February 06, 2009, no.5 (3944) *in Russian*; http://wwwinfo.jinr.ru/j̃inrmag/win/2009/5/me5.htm
14. The scientists try to extend Mendeleev's Table upto 150 elements. *Izvestiya*, February 09, 2009 *in Russian*; http://www.izvestia.ru/news/20/news197601/index.html
15. Prehistory of the synthesis of the 117th of the element. *Nezavisimaya Gazeta*, April 14, 2010 *in Russian*; http://www.ng.ru/science/2010-04-14/15_117th.html
16. *RIA News*, Science and Technologies, August 03, 2009 *in Russian*; http://rian.ru/science/20090803/179595691.html
17. Khazan A. Upper limit of the Periodic Table and synthesis of superheavy elements. *Progress in Physics*, 2007, v.2, 104–109.
18. Ishanov B.S., Kebin E.I. Nuclear physics on-line. Physics of nuclei and particles. XX century. Moscow, Moscow University Press, 2000.
19. Audi G., Wapstra A.H., and Thibault C. The AME2003 anomic mass evaluation (II). Tables, graphs, and references. *Nuclear Physics A*, 2003, v.729, 337–676.

An Experimental Proposal for Demonstration of Macroscopic Quantum Effects

Raymond Jensen

Department of Mathematics and Informatics, Trine University, Angola, Indiana, USA. E-mail: rjensen@allmail.net

An experiment is proposed, whose purpose is to determine whether quantum indeterminism can be observed on a truly macroscopic scale. The experiment involves using a double-slit plate or interferometer and a macroscopic mechanical switch. The objective is to determine whether or not the switch can take on an indeterminate state.

1 Introduction

Since the founding of quantum theory in the last century, there has been the question of what limit, if any, there is to the quantum effects which may be observed, in terms of size or number of particles of a system under observation. By *quantum effects*, it is meant in particular, phenomena such as entanglement or indeterminism. The most famous gedankenexperiment in quantum theory, *Schrödingers cat*, concerns this *macroscopic* question. This *cat paradox* argument was used by Schrödinger to ridicule the Copenhagen interpretation of quantum theory. [1]. Another well-known paradox was that of Einstein, Podolsky and Rosen [2] commonly referred to as the *EPR paradox*. This gedankenexperiment was also an attempt to discredit the Copenhagen interpretation, but for a different reason than that of the cat paradox.

Regrettably, there are few known experiments that demonstrate whither the macroscopic question, unlike with the EPR paradox. A recent experiment [3] has shown that quantum effects *i.e.* entanglement, can occur between systems of $O(10^{12})$ particles. Although these results are encouraging, such a system can hardly be termed macroscopic in spite of the title of the article in which it appears. Here, we consider a *macroscopic* system to be one clearly visible to the naked eye and in the solid state, such as Schrödingers cat. Another experiment, of Schmidt [4], seems to demonstrate that bits on a computer disk, even printouts of ones and zeros concealed in an envelope, take on indeterminate states. However, the desire remains for further proof of macroscopic quantum effects, in particular, absent of paranormal phenomena and resulting complications [5]. Perhaps the reason that evidence of macroscopic quantum effects is so few and far between is because macroscopic analogs to experiments such as the double-slit experiment are difficult to design. One cannot simply shoot cats through a double slit and expect to see an interference pattern!

Instead of shooting Schrödingers cat through the double slit, suppose the cat is kept in its box, but a large double slit plate is also placed inside the box. Things are arranged so that the cat in the alive state obstructs one slit, and the cat in the dead state obstructs the other. All in the box is concealed from the observer and also, many cats would need to be used. See Figure 1. Now the question arises: will an interference pattern be observed on the screen if individual photons are transmitted through the double slit and box, one by one? If interference is observed, would this indicate that the cats were in an alive-dead state? The answer is in the affirmative; for if the cats were each definitely either alive or dead when the photons passed through, then no interference pattern should be observed.

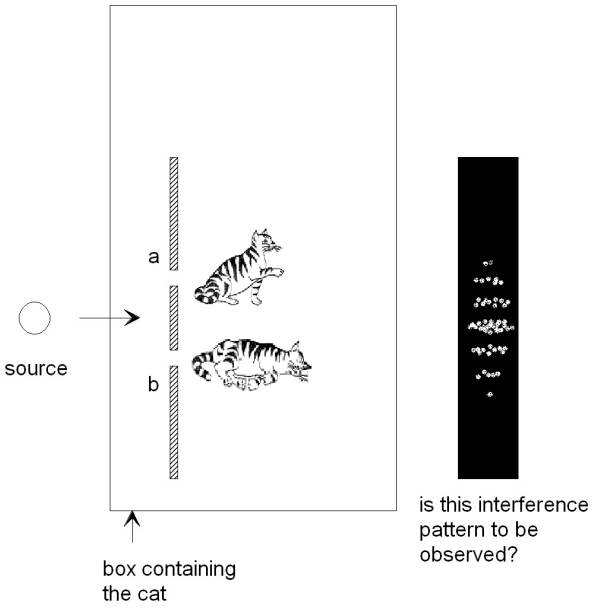

Fig. 1: An experiment with Schrödingers cat and a double slit. The experiment is designed so that if the cat is in the alive state, it obstructs slit **a** and if the cat is in the dead state it obstructs slit **b**. Many cats are needed for the experiment. If the cats remain unobserved and individual photons are transmitted through the double-slit and box, the question is: would an interference pattern be observed on the screen, and further, does this signify that the cats were in a superposition of alive and dead states?

In the next section, a more realizable (and cat-friendly) experimental set-up than the previous is proposed. This experiment will aid in answering the question of macroscopic indeterminism, as the accompanying calculations show. Although the set-up is quite simple by todays standards, it is not the intention of the author, a theorist, to carry out the experiment. Rather, it is hoped that an experimentalist is willing to carry out the necessary work.

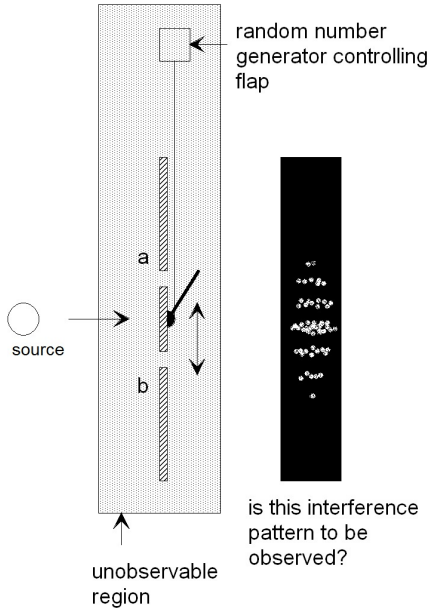

Fig. 2: The apparatus in Figure 1 is now modified so that a flap takes the place of Schrödingers cat. The flap position is controlled by an indeterministic random number generator, in order to put the flap in an indeterminate state with regard to which slit it covers. If measures are taken to destroy information about the flaps position before the photons reach the screen, the individual photons passing through the double slit apparatus should build up an interference pattern on the screen.

2 Double-slit experiment

Consider a set-up with a double slit, as in Figure 2. The difference between this set-up and the previous is that a flap takes the place of the cat. The flap covers either one slit or the other, and alternates between the two positions, controlled by a random-number generator.

The random number generator, flap and double-slit are concealed from the observer. The random number generator should be of the indeterministic type such as the one developed by Stipčević and Rogina [6]. The purpose of this is to put the flap into an indeterminate state. The set-up in Figure 2 is similar to one proposed by Mandel [7] which was carried out by Sillitto and Wykes [8]. However in that experiment, photons were *not* transmitted individually. So it is likely that the experiment was *not* free of photon-photon interference, whereas in the experiment under consideration here, such interference must be eliminated. Also, it is unclear if the electro-optic shutter used in that experiment could be said to be in an indeterminate state or to even be a mechanical macroscopic object.

Assuming that the flap in Figure 2 can be put into an indeterminate state, the flap can be represented by the equation

$$|\psi\rangle = \frac{1}{\sqrt{2}}\Big(|\mathbf{a}_f\rangle + |\mathbf{b}_f\rangle\Big), \qquad (1)$$

where $|\mathbf{a}_f\rangle$, $|\mathbf{b}_f\rangle$ are the basis states representing the flap f covering slits **a** and **b**, respectively. Now if a single photon p passes through the double-slit, say it passes through slit **b**, then the flap must be covering slit **a**, and *vice versa*. Thus, each photon passing through the double-slit is entangled together with the flap, and the flap-photon entangled state is:

$$|\psi\rangle = \frac{1}{\sqrt{2}}\Big(|\mathbf{a}_f\rangle|\mathbf{b}_p\rangle + |\mathbf{b}_f\rangle|\mathbf{a}_p\rangle\Big), \qquad (2)$$

where $|\mathbf{a}_p\rangle$, $|\mathbf{b}_p\rangle$ are the basis states for photon p. Equation (2) indicates that each photon passing through the double-slit takes on an indeterminate state with regards to which slit it passes through. Individual photons in the state (2) will build up an interference pattern if certain precautions are taken. Rather than using equation (2) to calculate the pattern which results from the set-up in Figure 2, we look at a variation of this experiment, for which it is easier to calculate interference. The apparatus is shown in Figure 3, in the next section.

3 Mach-Zehnder interferometer experiment

The set-up in Figure 3 essentially involves the same experiment as that shown in Figure 2, except that the isolated photons traverse a Mach-Zehnder interferometer (MZ) instead of a double-slit, and a moveable mirror (rm) replaces the flap. The rotation of the mirror rm switches the photon trajectory between two possible paths through MZ. The two different configurations are shown in the figure, top and bottom. Similar to the previous experiment, rm is to be put into an indeterminate state by controlling it with an indeterministic random number generator concealed from the observer (not shown in figure), and isolated photons can only be allowed to enter MZ through a gate. Further, position information of rm must be destroyed before each time a photon reaches the detectors. After such precautions are taken, the photons should each take an indeterminate path through MZ. Interference patterns of photon counts *vs.* relative length or phase between paths, the same observed by Aspect, Grangier and Roger [9] will then be seen. We next calculate these interference patterns.

Suppose first, rm is in the down position (upper diagram in Figure 3). This causes the photon to take the lower (–) path through MZ. Conversely, if the mirror is in the up position (lower diagram in Figure 3), the photon will take the upper (+) path through MZ. If rm can be prepared in an indeterminate state between up and down positions, then what results is the following entangled state between photon and mirror [*cf.* equation (2)]:

$$|\psi\rangle = \frac{1}{\sqrt{2}}\left(|\text{rm up}\rangle|+\rangle + |\text{rm down}\rangle|-\rangle\right), \qquad (3)$$

where $|\text{rm up}\rangle$, $|\text{rm down}\rangle$ are the two possible basis states for the moveable mirror rm and $|+\rangle$, $|-\rangle$ are the resultant basis states of the photon traversing MZ.

Let ϕ be the phase shift between arms of MZ, due to the presence of a phase shifter, or to a variation in the arms relative lengths. Using the rotation transformation equations

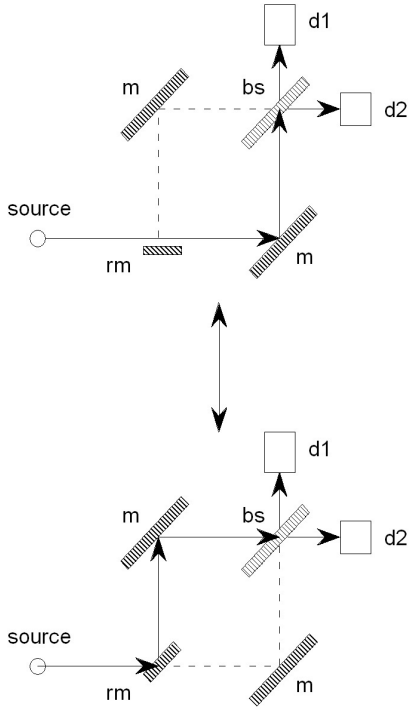

Fig. 3: A Mach-Zehnder (MZ) interferometer instead of the double slit of Figure 2. The moveable mirror rm acts as the former flap. The devices labeled m are fixed mirrors, bs, a beam splitter and d1, d2 are detectors. When rm is in the horizontal (down) position as at top, the photon takes the lower (–) path of mz (solid line with arrows). When rm is in the 45-degree position (up) as at bottom, then the photon takes the upper (+) path. If rm can take on an indeterminate state between these two configurations, then the photon paths will also be indeterminate, and thus interference patterns will result in d1 and d2, as variations of photon counts *vs.* relative length or phase ϕ between the two paths.

$|+\rangle = \sin\phi|\mathrm{d1}\rangle + \cos\phi|\mathrm{d2}\rangle$, $|-\rangle = \cos\phi|\mathrm{d1}\rangle - \sin\phi|\mathrm{d2}\rangle$ to put state (3) into the basis $|\mathrm{d1}\rangle$, $|\mathrm{d2}\rangle$ of the detectors, we obtain:

$$|\psi\rangle = \frac{1}{\sqrt{2}}\left(\sin\phi|\mathrm{rm\ up}\rangle|\mathrm{d1}\rangle + \cos\phi|\mathrm{rm\ up}\rangle|\mathrm{d2}\rangle + \right. \\ \left. + \cos\phi|\mathrm{rm\ down}\rangle|\mathrm{d1}\rangle - \sin\phi|\mathrm{rm\ down}\rangle|\mathrm{d2}\rangle\right). \quad (4)$$

If rm is successfully put into an indeterminate state, then the detector probabilities will be, using equation (4):

$$p\,(\mathrm{d1}) = |<\mathrm{rm\ up}, \mathrm{d1}|\psi\rangle + <\mathrm{rm\ down}, \mathrm{d1}|\psi\rangle|^2 = \\ = \frac{1}{2}\,(1+\sin 2\phi) \quad (5)$$

and

$$p(\mathrm{d2}) = \frac{1}{2}\,(1-\sin 2\phi)\,. \quad (6)$$

That is, interference fringes will be observed as oppositely-modulated signal intensity ($\propto$ probability) as a function of relative phase ϕ. These interference patterns; *i.e.* the interference patterns predicted by equations (5) and (6) are the same observed by Aspect and co-workers [9] using a similar set-up.

On the other hand, if rm remains in a *determinate* state, then *no* interference fringes will be observed; *i.e.* the signal intensity *vs.* phase-shift ϕ will be flat:

$$p\,(\mathrm{d1}) = |<\mathrm{rm\ up}, \mathrm{d1}|\psi\rangle|^2 + |<\mathrm{rm\ down}, \mathrm{d1}|\psi\rangle|^2 = \frac{1}{2} \quad (7)$$

and

$$p\,(\mathrm{d2}) = \frac{1}{2}\,. \quad (8)$$

Thus we have that: *the interference patterns* (5), (6) *result if and only if rm is in an indeterminate state. Presence of the interference patterns* (5), (6) *is therefore proof of macroscopic indeterminism, since the moveable mirror rm is a macroscopic object.*

It is emphasized again that it is important for the experimenter to take care that any information about the position of moveable mirror rm during the experiment is destroyed. This means that the random number generator should reset rm after each time an individual photon exits MZ, prior to the photon reaching detectors d1 or d2; otherwise in principle at least, the experimenter could discover which path the photon passed through, by uncovering rm. In that case, *no* interference [*i.e.* equations (7) and (8)] will be observed. Additional time to allow resetting rm can be obtained by placing d1 and d2 at some distance beyond the half-silvered mirror bs.

The experimental set-up of Figure 3 is similar to one proposed by Žukowski *et al.* [10], except that they propose to use a pair of electro-optical switches (one for each arm of MZ), instead of a moveable mirror before the arms. This is because the object of their proposal is to demonstrate whether or not the individual photons traverse MZ using both paths when the photon wave packet is cut in two using the switches as it passes though MZ. Their aim is to determine which of several interpretations of quantum theory is correct [11]. The purpose of that experiment is *not* to determine if the electro-optical switches take on an indeterminate state, even if again, such switches could be called mechanical and macroscopic.

4 Conclusion

An experiment involving individual photons passing through a double-slit plate or Mach-Zehnder interferometer apparatus has been proposed. Rather than keep both paths in the plate or apparatus open at all times however, one path or the other is kept closed by a macroscopic mechanical switch, controlled by an indeterministic device. The purpose of this is to determine whether the macroscopic switch can take on an indeterminate state: such indeterminism is detectible, dependent on whether an interference pattern results.

Acknowledgements

Thanks to C. Dumitrescu, who alerted the author to the third reference.

Submitted on June 21, 2010 / Accepted on June 25, 2010

References

1. Trimmer J. The present situation in Quantum Mechanics: a translation of Schrödingers Cat Paradox paper. *Proc. Am. Phil. Soc.*, 1980, v. 124, 323–338.
2. Einstein A., Podolsky B., Rosen N. Can quantum-mechanical description of physical reality be considered complete? *Phys. Rev.*, 1935, v. 47, 777–780.
3. Julsgaard B., Kozhekin A., Polzik E. Experimental long-lived entanglement of two macroscopic objects. *Nature*, 2001, v. 413, 400–403.
4. Schmidt H. Observation of a psychokinetic effect under highly controlled conditions. *J. Parapsychol.*, 1993, v. 57, 351–372.
5. Stapp H. Theoretical model of a purported empirical violation of the predictions of quantum theory. *Phys. Rev. A*, 1994, v. 50, 18–22.
6. Stipčević M., Rogina M. Quantum random number generator based on photonic emission in semiconductors. *Rev. Sci. Instr.*, 2007, v. 78, 45104.
7. Mandel L. On the possibility of observing interference effects with light beams divided by a shutter. *J. Opt. Soc. Am.*, 1959, v. 49, 931–932.
8. Sillitto R., Wykes C. An interference experiment with light beams modulated in anti-phase by an electro-optic shutter. *Phys. Lett. A*, 1972, v. 39, 333–334.
9. Grangier P., Roger G., Aspect A. Experimental evidence for a photon anticirrelation effect on a beam splitter: a new light on single-photon interferences. *Europhysics Lett.*, 1986, v. 1 (4), 173–179.
10. Žukowski M., Posiewnik A., Pykacz J. Interference in the double-slit experiment with only one slit open at a time. *Phys. Lett. A*, 1989, v. 135 (8,9), 411–416.
11. Posiewnik A., Pykacz J. Double-slit experiment, Copenhagen, neo-Copenhagen and stochastic interpretation of Quantum Mechanics. *Phys. Lett. A*, 1988, v. 128 (1,2), 5–8.

Gravitational Spectral Shift Exterior to the Sun, Earth and the Other Oblate Spheroidal Planets

Chifu Ebenezer Ndikilar*, Adam Usman†, and Osita C. Meludu†

*Department of Physics, Gombe State University, P.M.B 127, Gombe, Nigeria
†Department of Physics, Federal University of Technology, Yola, Adamawa State, Nigeria
E-mails: ebenechifu@yahoo.com; aausman@yahoo.co.uk; ocmeludu@yahoo.co.uk

Here, we use our new metric tensor exterior to homogeneous oblate spheroidal mass distributions to study gravitational spectral shift of light in the vicinity of the Sun, Earth and other oblate spheroidal planets. It turns out most profoundly that, this experimentally verified phenomenon holds good in the gravitational field exterior to an oblate spheroid using our approach. In approximate gravitational fields, our obtained theoretical value for the Pound-Rebka experiment on gravitational spectra shift along the equator of the Earth (2.578×10^{-15}) agrees satisfactorily with the experimental value of 2.45×10^{-15}. We also predict theoretical values for the Pound-Rebka experiment on the surface (along the equator) of the Sun and other oblate spheroidal planets.

1 Introduction

According to the General Theory of Gravitation, the rate of a clock is slowed down when it is in the vicinity of a large gravitating mass. Since the characteristic frequencies of atomic transitions are, in effect, clocks, one has the result that the frequency of such a transition occurring, say, on the surface of the Sun, should be lowered by comparison with a similar transition observed in a terrestrial laboratory. This manifests itself as a gravitational red shift in the wavelengths of spectral lines [1]. It has been experimentally and astrophysically observed that there is an increase in the frequency of light (photon) when the source or emitter is further away from the body than the receiver. The frequency of light will increase (shifting visible light towards the blue end of the spectrum) as it moves to lower gravitational potentials (into a gravity well). Also, there is a reduction in the frequency of light when the source or emitter is nearer the body than the receiver. The frequency of light will decrease (shifting visible light towards the red end of the spectrum) as it moves into higher gravitational potentials (out of a gravity well). This was experimentally confirmed in the laboratory by the Pound-Rebka experiment in 1959 (they used the Mossbauer effect to measure the change in frequency in gamma rays as they travelled from the ground to the top of Jefferson Labs at Havard University) [2]. This gravitational phenomenon was later confirmed by astronomical observations [3]. In this article, we verify the validity of our metric tensor exterior to a massive homogeneous oblate spheroid by studying gravitational spectral shift in the vicinity of the Sun, Earth and other oblate spheroidal planets. Basically, we assume that these gravitational sources are time independent and homogeneous distributions of mass within spheroids, characterized by at most two typical integrals of geodesic motion, namely, energy and angular momentum. From an astrophysical point of view, such an assumption, although not necessary, could, however, prove useful, because it is equivalent to the assumption that the gravitational source is changing slowly in time so that partial time derivatives are negligible compared to the spatial ones. We stress that the mass source considered is not the most arbitrary one from a theoretical point of view, but on the other hand, many astrophysically interesting systems are usually assumed to be time independent (or static from another point of view) and axially symmetric continuous sources.

2 Covariant metric tensor exterior to a massive homogeneous oblate spheroid

The covariant metric tensor in the gravitational field of a homogeneous oblate spheroid in oblate spheroidal coordinates (η, ξ, ϕ) has been obtained [4, 5] as;

$$g_{00} = \left(1 + \frac{2}{c^2} f(\eta,\xi)\right), \tag{2.1}$$

$$g_{11} = -\frac{a^2}{1+\xi^2-\eta^2}\left[\eta^2\left(1+\frac{2}{c^2} f(\eta,\xi)\right)^{-1} + \frac{\xi^2(1+\xi^2)}{(1-\eta^2)}\right], \tag{2.2}$$

$$g_{12} \equiv g_{21} = -\frac{a^2\eta\xi}{1+\xi^2-\eta^2}\left[1-\left(1+\frac{2}{c^2} f(\eta,\xi)\right)^{-1}\right], \tag{2.3}$$

$$g_{22} = -\frac{a^2}{1+\xi^2-\eta^2}\left[\xi^2\left(1+\frac{2}{c^2} f(\eta,\xi)\right)^{-1} + \frac{\eta^2(1-\eta^2)}{(1+\xi^2)}\right], \tag{2.4}$$

$$g_{33} = -a^2(1+\xi^2)(1-\eta^2), \tag{2.5}$$

$f(\eta,\xi)$ is an arbitrary function determined by the mass or pressure distribution and hence possesses all the symmetries of the latter, a priori. Let us now recall that for any gravitational field [4–7]

$$g_{00} \cong 1 + \frac{2}{c^2}\Phi \tag{2.6}$$

where Φ is Newton's gravitational scalar potential for the field under consideration. Thus we can then deduce that the unknown function in our field equation can be given approximately as

$$f(\eta,\xi) \cong \Phi(\eta,\xi)\ , \tag{2.7}$$

where $\Phi(\eta,\xi)$ is Newton's gravitational scalar potential exterior to a homogeneous oblate spheroidal mass. It has been shown that [8];

$$\Phi(\eta,\xi) = B_0 Q_0(-i\xi) P_0(\eta) + B_2 Q_2(-i\xi) P_2(\eta)\ , \tag{2.8}$$

where Q_0 and Q_2 are the Legendre functions linearly independent to the Legendre polynomials P_0 and P_2 respectively; B_0 and B_2 are constants given by

$$B_0 = \frac{4\pi G\rho_0 a^2\xi_0}{3\Delta_1}$$

and

$$B_2 = \frac{4\pi G\rho_0 a^2\xi_0}{9\Delta_2}\left[\frac{d}{d\xi}P_2(-i\xi)\right]_{\xi=\xi_0},$$

where Δ_1 and Δ_2 are defined as

$$\Delta_1 = \left[\frac{d}{d\xi}Q_0(-i\xi)\right]_{\xi=\xi_0}$$

and

$$\Delta_2 = Q_0\left[\frac{d}{d\xi}P_2(-i\xi)\right]_{\xi=\xi_0} - P_2(-i\xi)\left[\frac{d}{d\xi}Q_2(-i\xi)\right]_{\xi=\xi_0},$$

G is the universal gravitational constant, ρ_0 is the uniform density of the oblate spheroid and a is a constant parameter.

In a recent article [9], we obtained a satisfactory approximate expression for equation (2.8) as;

$$\Phi(\eta,\xi) \approx \frac{B_0}{3\xi^3}\left(1+3\xi^2\right)i - \frac{B_2}{30\xi^3}\left(7+15\xi^2\right)\left(3\eta^2-1\right)i \tag{2.9}$$

with

$$\Phi(\eta,\xi) \approx \frac{B_0}{3\xi^3}\left(1+3\xi^2\right)i + \frac{B_2}{30\xi^3}\left(7+15\xi^2\right)i$$

and

$$\Phi(\eta,\xi) \approx \frac{B_0}{3\xi^3}\left(1+3\xi^2\right)i - \frac{B_2}{15\xi^3}\left(7+15\xi^2\right)i$$

as the respective approximate expressions for the gravitational scalar potential along the equator and pole exterior to homogeneous oblate spheroidal bodies. These equations were used to compute approximate values for the gravitational scalar potential exterior to the Sun, Earth and other oblate spheroidal planets [9].

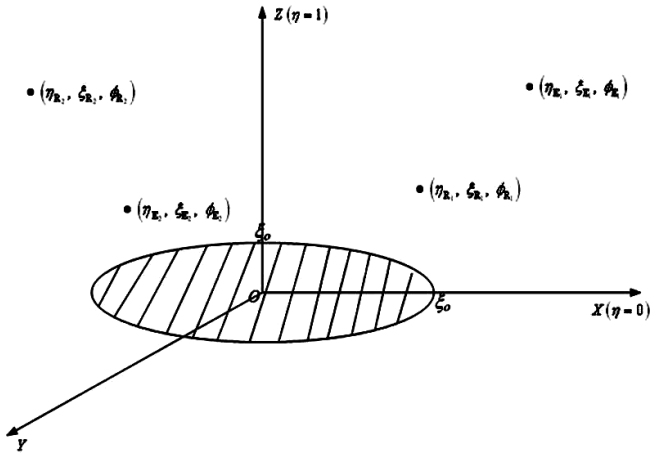

Fig. 1: Emission and reception space points of light (photon).

3 Gravitational spectral shift exterior to oblate spheroidal distributions of mass

Here, we consider a beam of light moving from a source or emitter at a fixed point in the gravitational field of the oblate spheroidal body to an observer or receiver at a fixed point in the same gravitational field. Einstein's equation of motion for a photon is used to derive an expression for the shift in frequency of a photon moving in the gravitational field of an oblate spheroidal mass.

Now, consider a beam of light moving from a source or emitter (E) at a fixed point in the gravitational field of an oblate spheroidal body to an observer or receiver (R) at a fixed point in the field as shown in Fig. 1.

Let the space time coordinates of the emitter and receiver be $(t_E,\ \eta_E,\ \xi_E, \phi_E)$ and $(t_R,\ \eta_R,\ \xi_R, \phi_R)$ respectively. It is well known that light moves along a null geodesic given by

$$d\tau = 0\,. \tag{3.1}$$

Thus, the world line element for a photon (light) takes the form

$$c^2 g_{00}\,dt^2 = g_{11}\,d\eta^2 + 2g_{12}\,d\eta\,d\xi + g_{22}\,d\xi^2 + g_{33}\,d\phi^2. \tag{3.2}$$

Substituting the covariant metric tensor for this gravitational field in equation (3.2) gives

$$\begin{aligned} c^2\left(1+\frac{2}{c^2}f(\eta,\xi)\right)dt^2 &= -\frac{a^2}{1+\xi^2-\eta^2}\times \\ &\times\left[\eta^2\left(1+\frac{2}{c^2}f(\eta,\xi)\right)^{-1} + \frac{\xi^2\left(1+\xi^2\right)}{\left(1-\eta^2\right)}\right]d\eta^2 - \\ &- \frac{2a^2\eta\xi}{1+\xi^2-\eta^2}\left[1-\left(1+\frac{2}{c^2}f(\eta,\xi)\right)^{-1}\right]d\eta\,d\xi - \\ &- \frac{a^2}{1+\xi^2-\eta^2}\left[\xi^2\left(1+\frac{2}{c^2}f(\eta,\xi)\right)^{-1} + \frac{\eta^2\left(1-\eta^2\right)}{\left(1+\xi^2\right)}\right]d\xi^2 - \\ &- a^2\left(1+\xi^2\right)\left(1-\eta^2\right)d\phi^2. \end{aligned} \tag{3.3}$$

Now, let u be a suitable parameter that can be used to study the motion of a photon in this gravitational field. Then equation (3.3) can be written as

$$c^2\left(1+\frac{2}{c^2}f(\eta,\xi)\right)\left(\frac{dt}{du}\right)^2 = -\frac{a^2}{1+\xi^2-\eta^2}\times$$
$$\times\left[\eta^2\left(1+\frac{2}{c^2}f(\eta,\xi)\right)^{-1}+\frac{\xi^2\left(1+\xi^2\right)}{(1-\eta^2)}\right]d\eta^2 -$$
$$-\frac{2a^2\eta\xi}{1+\xi^2-\eta^2}\left[1-\left(1+\frac{2}{c^2}f(\eta,\xi)\right)^{-1}\right]\left(\frac{d\eta}{du}\frac{d\xi}{du}\right) -$$
$$-\frac{a^2}{1+\xi^2-\eta^2}\left[\xi^2\left(1+\frac{2}{c^2}f(\eta,\xi)\right)^{-1}+\frac{\eta^2\left(1-\eta^2\right)}{(1+\xi^2)}\right]\times$$
$$\times\left(\frac{d\xi}{du}\right)^2 - a^2\left(1+\xi^2\right)\left(1-\eta^2\right)\left(\frac{d\phi}{du}\right)^2. \quad (3.4)$$

Equation (3.4) can be equally written as

$$\frac{dt}{du} = \frac{1}{c}\left(1+\frac{2}{c^2}f(\eta,\xi)\right)^{-\frac{1}{2}}ds, \quad (3.5)$$

where ds is defined as

$$ds^2 = -\frac{a^2}{1+\xi^2-\eta^2}\times$$
$$\times\left[\eta^2\left(1+\frac{2}{c^2}f(\eta,\xi)\right)^{-1}+\frac{\xi^2\left(1+\xi^2\right)}{(1-\eta^2)}\right]d\eta^2 -$$
$$-\frac{2a^2\eta\xi}{1+\xi^2-\eta^2}\left[1-\left(1+\frac{2}{c^2}f(\eta,\xi)\right)^{-1}\right]\left(\frac{d\eta}{du}\frac{d\xi}{du}\right) -$$
$$-\frac{a^2}{1+\xi^2-\eta^2}\left[\xi^2\left(1+\frac{2}{c^2}f(\eta,\xi)\right)^{-1}+\frac{\eta^2\left(1-\eta^2\right)}{(1+\xi^2)}\right]\times$$
$$\times\left(\frac{d\xi}{du}\right)^2 - a^2\left(1+\xi^2\right)\left(1-\eta^2\right)\left(\frac{d\phi}{du}\right)^2. \quad (3.6)$$

Integrating equation (3.5) for a signal of light moving from emitter E to receiver R gives

$$t_R - t_E = \frac{1}{c}\int_{u_E}^{u_R}\left[\left(1+\frac{2}{c^2}f(\eta,\xi)\right)^{-\frac{1}{2}}ds\right]du. \quad (3.7)$$

The time interval between emission and reception of all light signals is well known to be the same for all light signals in relativistic mechanics (constancy of the speed of light) and thus the integral on the right hand side is the same for all light signals. Consider two light signals designated 1 and 2 then

$$t_R^1 - t_E^1 = t_R^2 - t_E^2 \quad (3.8)$$

or

$$t_R^2 - t_R^1 = t_E^2 - t_E^1. \quad (3.9)$$

Thus,

$$\Delta t_R = \Delta t_E. \quad (3.10)$$

Hence, coordinate time difference of two signals at the point of emission equals that at the point of reception. From our expression for gravitational time dilation in this gravitational field [10], we can write

$$\Delta\tau_R = \left(1+\frac{2}{c^2}f_R(\eta,\xi)\right)^{\frac{1}{2}}\Delta t_R. \quad (3.11)$$

Equations (3.9), (3.10) and (3.11) can be combined to give

$$\frac{\Delta\tau_R}{\Delta\tau_E} = \left(\frac{1+\frac{2}{c^2}f_R(\eta,\xi)}{1+\frac{2}{c^2}f_E(\eta,\xi)}\right)^{\frac{1}{2}}. \quad (3.12)$$

Now, consider the emission of a peak or crest of light wave as one event. Let n be the number of peaks emitted in a proper time interval $\Delta\tau_E$, then, by definition, the frequency of the light relative to the emitter, ν_E, is given as

$$\nu_E = \frac{n}{\Delta\tau_E}. \quad (3.13)$$

Similarly, since the number of cycles is invariant, the frequency of light relative to the receiver, ν_R, is given as

$$\nu_R = \frac{n}{\Delta\tau_R}. \quad (3.14)$$

Consequently,

$$\frac{\nu_R}{\nu_E} = \frac{\Delta\tau_E}{\Delta\tau_R} = \left(1+\frac{2}{c^2}f_E(\eta,\xi)\right)^{\frac{1}{2}}\left(1+\frac{2}{c^2}f_R(\eta,\xi)\right)^{-\frac{1}{2}} \quad (3.15)$$

or

$$\frac{\nu_R}{\nu_E} \approx \left(1+\frac{2}{c^2}f_E(\eta,\xi)\right)\left(1-\frac{2}{c^2}f_R(\eta,\xi)\right) \quad (3.16)$$

or

$$\frac{\nu_R}{\nu_E} - 1 \approx \frac{1}{c^2}\left[f_E(\eta,\xi) - f_R(\eta,\xi)\right] \quad (3.17)$$

to the order of c^{-2}. Alternatively, equation (3.17) can be written as

$$z \equiv \frac{\Delta\nu}{\nu_E} \equiv \frac{\nu_R-\nu_E}{\nu_E} \approx \frac{1}{c^2}\left[f_E(\eta,\xi) - f_R(\eta,\xi)\right]. \quad (3.18)$$

It follows from equation (3.18) that if the source is nearer the body than the receiver then $f_E(\eta,\xi) < f_R(\eta,\xi)$ and hence $\Delta\nu < 0$. This indicates that there is a reduction in the frequency of light when the source or emitter is nearer the body than the receiver. The light is said to have undergone a red shift (that is the light moves toward red in the visible spectrum). Otherwise (source further away from body than receiver), the light undergoes a blue shift. Now, consider a signal of light emitted and received along the equator of the homogeneous oblate spheroidal Earth (approximate gravitational field where $f(\eta,\xi) \approx \Phi(\eta,\xi)$. The ratio of the shift

Emi Pt	Recep pt	$z\,(\times 10^{-10})$	Type of shift
ξ_0	ξ_0	0	none
$2\xi_0$	ξ_0	3.454804	blue
$3\xi_0$	ξ_0	4.603165	blue
$4\xi_0$	ξ_0	5.176987	blue
$5\xi_0$	ξ_0	5.521197	blue
$6\xi_0$	ξ_0	5.750643	blue
$7\xi_0$	ξ_0	5.914522	blue
$8\xi_0$	ξ_0	6.037426	blue
$9\xi_0$	ξ_0	6.133016	blue
$10\xi_0$	ξ_0	6.209486	blue

Fig. 2: Ratio of the shift in frequency of light to the frequency of the emitted light at points along equator and received on the surface of the Earth on the equator.

Emi Pt	Recep pt	$z\,(\times 10^{-10})$	Type of shift
ξ_0	ξ_0	0	none
ξ_0	$2\xi_0$	−3.454804	red
ξ_0	$3\xi_0$	−4.603165	red
ξ_0	$4\xi_0$	−5.176987	red
ξ_0	$5\xi_0$	−5.521197	red
ξ_0	$6\xi_0$	−5.750643	red
ξ_0	$7\xi_0$	−5.914522	red
ξ_0	$8\xi_0$	−6.037426	red
ξ_0	$9\xi_0$	−6.133016	red
ξ_0	$10\xi_0$	−6.209486	red

Fig. 3: Ratio of the shift in frequency of light to the frequency of the emitted light at points along equator and received on the surface of the Earth on the equator.

Body	Radial dist. (km)	ξ at pt	Φ_E ($\mathrm{N\,m\,kg^{-1}}$)	Φ_R ($\mathrm{N\,m\,kg^{-1}}$)	Predicted shift
Sun	700,022.5	241.527	-1.9375791×10^{11}	-1.9373218×10^{11}	-2.85889×10^{-21}
Earth	6,378.023	12.010	-6.2079113×10^{7}	-6.2078881×10^{7}	-2.57800×10^{-15}
Mars	3,418.5	9.231	-1.2401149×10^{7}	-1.2317966×10^{7}	-9.24256×10^{-20}
Jupiter	71,512.5	2.641	-1.4968068×10^{9}	-1.4958977×10^{9}	-1.010111×10^{-20}
Saturn	60,292.5	1.971	-4.8486581×10^{8}	-4.8484869×10^{8}	-1.902222×10^{-21}
Uranus	25,582.5	3.994	-2.1563913×10^{8}	-2.1522082×10^{8}	-4.647889×10^{-20}
Neptune	24,782.5	4.304	-2.5243240×10^{8}	-2.5196722×10^{8}	-5.168667×10^{-20}

Fig. 4: Predicted Pound-Rebka shift in frequency along the equator for the Sun, Earth and the other oblate spheroidal planets.

in frequency to the frequency of the emitted light at various points along the equator and received on the equator at the surface of the homogeneous oblate spheroidal Earth can be computed using equation (3.18). This yields Table 1. Also, the ratio of the shift in frequency of light to the frequency of the emitted light on the equator at the surface and received at various points along the equator of the homogeneous oblate spheroidal Earth can be computed. This gives Table 2.

Tables 1, thus confirms our assertion above that there is an increase in the frequency of light when the source or emitter is further away from the body than the receiver. The frequency of light will increase (shifting visible light toward the blue end of the spectrum) as it moves to lower gravitational potentials (into a gravity well). Table 2, also confirms our assertion above that there is a reduction in the frequency of light when the source or emitter is nearer the body than the receiver. The frequency of light will decrease (shifting visible light toward the red end of the spectrum) as it moves to higher gravitational potentials (out of a gravity well). Also, notice that the shift in both cases increases with increase in the distance of separation between the emitter and receiver. The value of the shift is equal in magnitude at the same separation distances for both cases depicted in Tables 1 and 2.

Now, suppose the Pound-Rebka experiment is performed at the surface of the Sun, Earth and other oblate spheroidal planets on the equator. Then, since the gamma ray frequency shift was observed at a height of 22.5m above the surface, we model our theoretical computation and calculate the theoretical value for this shift. This computation yields Table 3.

With these predictions, experimental astrophysicists and astronomers can now attempt carrying out similar experiments on these bodies. Although, the prospects of carrying out such experiments on the surface of some of the planets and Sun are less likely (due to temperatures on their surfaces and other factors); theoretical studies of this type helps us to understand the behavior of photons as they leave or approach these astrophysical bodies. This will thus aid in the development of future instruments that can be used to study these heavenly bodies.

4 Conclusion

The practicability of the findings in this work is an encouraging factor. More so, that in this age of computational precision, the applications of these results is another factor.

Submitted on June 01, 2010 / Accepted on June 05, 2010

References

1. Matolcsi T. and Matolcsi M. GPS revisited: the relation of proper time and coordinate time. arXiv: math-ph/0611086.
2. Pound R.V. and Rebka G.A. Jr. Gravitational red shift in nuclear resonance. *Physical Review Letters*, 1959, v. 3(9), 439–441.
3. Ohanian H.C. and Remo R. Gravitation and space-time. W.W. Norton and Company, 1994.

4. Howusu S.X.K. The 210 astrophysical solutions plus 210 cosmological solutions of Einstein's gravitational field equations. Natural Philosophy Society, Jos, 2007, 47–79.
5. Chifu E.N., Usman A. and Meludu O.C. Orbits in homogeneous oblate spheroidal gravitational space-time. *Progress in Physics*, 2009, v.3, 49–53.
6. Chifu E.N. and Howusu S.X.K. Gravitational radiation and propagation field equation exterior to astrophysically real or hypothetical time varying distributions of mass within regions of spherical geometry. *Physics Essays*, 2009, v.22(1), 73–77.
7. Chifu E.N. and Howusu S.X.K. Solution of Einstein's geometrical field equations exterior to astrophysically real or hypothetical time varying distributions of mass within regions of spherical geometry. *Progress in Physics*, 2009, v.3, 45–48.
8. Howusu S.X.K. Gravitational fields of spheroidal bodies-extension of gravitational fields of spherical bodies. *Galilean Electrodynamics*, 2005, v.16(5), 98–100.
9. Chifu E.N., Usman A., and Meludu O.C. Gravitational scalar potential values exterior to the Sun and planets. *Pacific Journal of Science and Technology*, 2009, v.10(1), 663–673.
10. Chifu E.N., Usman A., and Meludu O.C. Gravitational time dilation and length contraction in fields exterior to static oblate spheroidal mass distributions. *Journal of the Nigerian Association of Mathematical Physics*, 2009, v.15, 247–252.

Microwave Spectroscopy of Carbon Nanotube Field Effect Transistor

Aziz N. Mina*, Attia A. Awadalla*, Adel H. Phillips†, and Riham R. Ahmed*

*Faculty of Science, Beni-Suef University, Beni-Suef, Egypt. E-mail: attiamd2005@yahoo.com
†Faculty of Engineering, Ain-Shams University, Cairo, Egypt. E-mail: adel_phillips@yahoo.com

The quantum transport property of a carbon nanotube field effect transistor (CNTFET) is investigated under the effect of microwave radiation and magnetic field. The photon-assisted tunneling probability is deduced by solving Dirac equation. Then the current is deduced according to Landauer-Buttiker formula. Oscillatory behavior of the current is observed which is due to the Coulomb blockade oscillations. It was found, also, that the peak heights of the dependence of the current on the parameters under study are strongly affected by the interplay between the tunneled electrons and the photon energy. This interplay affects on the sidebands resonance. The results obtained in the present paper are found to be in concordant with those in the literature, which confirms the correctness of the proposed model. This study is valuable for nanotechnology applications, e.g., photo-detector devices and solid state quantum computing systems and quantum information processes.

5 Introduction

Carbon Nanotubes (CNTs) have been discovered by Sumio Iijim of the NEC Tsukuba Laboratory in HRTEM study of carbon filaments [1]. Carbon-based materials, clusters and molecules are unique in many ways [2]. One distinction related to the many possible configurations of the electronic states of carbon atom, which is known as the hybridization of atomic orbital. Electrical conductivity of carbon nanotube depending on their chiral vector carbon nanotube with a small diameter is metallic or semiconducting [2,3]. The differences in conducting properties are caused by the molecular structure that results in a difference band structure and thus a different band gap. The quantum electronic transport properties of carbon nanotubes have received much attention in recent years [4,5]. This is due to the very nice features of the band structure of these quasi-one dimensional quantum systems. The quantum mechanical behavior of the electronic transport in carbon nanotubes has been experimentally and theoretically investigated by many authors [6,7]. According to these investigations, the authors showed that carbon nanotube sandwiched between two contacts behaves as coherent quantum device. A microwave field with frequency, ω, can induce additional tunneling process when electrons exchange energy by absorbing or emitting photons of energy, $\hbar\omega$. This kind of tunneling is known as the photon-assisted tunneling [8]. The aim of the present paper is to investigate the quantum transport characteristics of a CNTFET under the microwave irradiation and the effect magnetic field.

6 CNTFET

A carbon nanotube field effect transistor (CNTFET) is modeled as: two metal contacts are deposited on the carbon nanotube quantum dot to serve as source and drain electrodes. The conducting substance is the gate electrode in this three-terminal device. Another metallic gate is used to govern the electrostatics and the switching of the carbon nanotube channel. The substrates at the nanotube quantum dot /metal contacts are controlled by the back gate. The tunneling through such device is induced by an external microwave field of different frequencies of the form $V = V_{ac}\cos(\omega t)$ where V_{ac} is the amplitude of the field and ω is its angular frequency, that is the photon-assisted tunneling process is achieved. One of the measurable quantities of the transport characteristic is the current which may be expressed in terms of the tunneling probability by the following Landauer-Buttiker formula [9]:

$$I=\left(\frac{4e}{h}\right)\int\left[f_{FD(s)}(E)-f_{FD(d)}(E-eV_{sd})\right]\Gamma_n(E)dE \qquad (1)$$

where $\Gamma(E)$ is the photon-assisted tunneling probability, $f_{FD(s/d)}$ are the Fermi-Dirac distribution function corresponding to the source (s) and drain (d) electrodes, while e and h are electronic charge and Planck's constant respectively. The tunneling probability $\Gamma_n(E)$ might be calculated by solving the following Dirac equation [7]

$$\left[i\upsilon_{F\hbar}\begin{pmatrix}0 & \partial_x-\partial_y\\ \partial_x-\partial_y & 0\end{pmatrix}-eV_{sd}+\right. \qquad (2)$$
$$\left.+(e\hbar B)(2m)^{-1}+eV_B+eV_{sd}\cos(\omega t)\right]\psi_{\frac{e}{\hbar}}=i\hbar\frac{\partial\psi_{\frac{e}{\hbar}}}{\partial E}$$

where υ_F is the Fermi velocity corresponding to Fermi-energy E_F, V_g is the gate voltage, V_{sd} is source-drain voltage, B is the applied magnetic field, m^* is the effective mass of the charge carrier, $\hbar$ is the reduced Planck ı́s constant, ω is the frequency of the applied microwave field with amplitude V_{ac} and V_b is the barrier height. The index e/h refers to electron like (with the energy > 0 with respect to the Dirac point) and hole-like (with energy < 0 with respect to the Dirac point) solutions to the eigenvalue differential equation (2).

The solution of equation (2) is given by [7]:

$$\Psi^{(ac)}_{+,n}(x,t) = \sum J_n\left(\frac{eV_{ac}}{\hbar\omega}\right)\Psi^{ac}_{0,e/h}(x,t)\, e^{(-in\omega t)} \tag{3}$$

where

$$\Psi^{(in)}_{0,e/h}(x,t) = \Psi^{(ac)}_{0,e/h}(x)\, e^{\mp iEt/h}. \tag{4}$$

Accordingly equation (2) will take the following form.

$$\left[i\nu_{F\hbar}\begin{pmatrix} 0 & \partial_x-\partial_y \\ \partial_x-\partial_y & 0 \end{pmatrix}-\varepsilon\right]\Psi^{ac}_{0.e/h} = \pm E\Psi_{0.e/h} \tag{5}$$

where the letter ε denotes the following

$$\varepsilon = E_F + eV_g + eV_{sd} + \left(\frac{e\hbar B}{2m^*}\right) + V_b + eV_{ac}\cos\omega t\,. \tag{6}$$

In Eq. (3), J_n is the n^{th} order Bessel function. Since in ballistic transport from one region of quantum dot to another one, charge carriers with a fixed energy (which can be either positive or negative with respect to the Dirac point) are transmitted and their energy is conserved. The desired state represents a superposition of positive and negative solution to the eigenvalue problem Eq. (5). The solution must be generated by the presence of the different side-bands, n, which come with phase factors $\exp(-in\omega t)$ that shift the center energy of the transmitted electrons by integer multiples of $\hbar\omega$ [8]. The complete solution of Eq. (5) is given by [7]:

(i) The incoming eigenfunction

$$\Psi^{(ac)}_{icome}(x,t) = \sum_{n=-\infty}^{\infty} J_n\left(\frac{eV_{ac}}{\hbar\omega}\right)\times \\ \times\Psi^{ac}_{0,+}\exp\left(i\left(\varepsilon + E + n\hbar\omega\right)t/h\right) \tag{7}$$

(ii) The reflected eigenfunction

$$\Psi^{\alpha}_{r}(x,t) = \sum_{n=-\infty}^{\infty} R_n(E)\, J_n\left(\frac{eV_{ac}}{\hbar\omega}\right)\times \\ \times\Psi^{ac}_{0,-}\exp\left(i\left(\varepsilon + E + n\hbar\omega\right)t/h\right) \tag{8}$$

where $R_n(E)$ is the energy-dependent reflection coefficient.

(iii) The transmitted eigenfunction

$$\Psi^{ac}_{tr}(x,t) = \sum_{n=-\infty}^{\infty} \Gamma_n(E)\, J_n\left(\frac{eV_{ac}}{\hbar\omega}\right)\times \\ \times\Psi^{in}_{+,n}\exp\left(i\left(\varepsilon + E + n\hbar\omega\right)t/h\right) \tag{9}$$

where $\Psi^{(ac)}_{0,+}, \Psi^{(ac)}_{0,-}$ are respectively given by

$$\Psi^{(ac)}_{0,+} = \frac{e^{iq_n y + ik_n x}}{\sqrt{\cos\alpha_{ac}}}\begin{pmatrix} \exp\left(-\frac{\alpha_{ac}}{2}\right) \\ -\exp\left(\frac{\alpha_{ac}}{2}\right) \end{pmatrix} \tag{10}$$

and

$$\Psi^{(ac)}_{0,-} = \frac{e^{iq_n y - ik_n x}}{\sqrt{\cos\alpha_{ac}}}\begin{pmatrix} \exp\left(\frac{\alpha_{ac}}{2}\right) \\ -\exp\left(-\frac{\alpha_{ac}}{2}\right) \end{pmatrix} \tag{11}$$

$\Psi^{(in)}_{+,n}$ in Eq. (9) is expressed as

$$\Psi^{(in)}_{+,n} = \frac{e^{iq,y-ik,x}}{\sqrt{\cos\alpha_{in,n}}}\begin{pmatrix} \exp\left(-\frac{\alpha_{in,n}}{2}\right) \\ \exp\left(\frac{\alpha_{in,n}}{2}\right) \end{pmatrix}. \tag{12}$$

In equations (10, 11, 12), the symbols α_{ac}, $\alpha_{in,n}$ are

$$\alpha_{ac} = \sin^{-1}\left(\frac{\hbar\nu q_n}{\varepsilon}\right) \tag{13}$$

and

$$\alpha_{in,n} = \sin^{-1}\left(\frac{\hbar\nu q_n}{\varepsilon + n\hbar\omega}\right) \tag{14}$$

where

$$q_n = \frac{n\pi}{W} \quad (n = 1, 2, 3, \ldots) \tag{15}$$

where W is the dimension of the nanotube quantum dot. The parameter k_n in Eqs. (10, 11, 12) is given by

$$k_n^2 = \left[\frac{V_b + eV_g + eV_{sd} + \frac{\hbar eB}{m^*}}{\hbar\omega}\right]^2 - q_n^2. \tag{16}$$

In order to get an explicit expression for the tunneling probability $\Gamma_n(E + n\hbar\omega)$ this can be achieved by applying the matching condition for the spatial eigenfunctions at the boundaries $x = 0$ and $x = L$. So, the tunneling probability $\Gamma_n(E+n\hbar\omega)$ will take the following form after some algebraic procedures, as

$$\Gamma_n(E + n\hbar\omega) = \\ = \left|\frac{k_n}{k_n\cos(k_nL) + i\left(\frac{eV_g + eV_{sd} + (\hbar eB/2m^*)}{\hbar\omega}\right)\sin(k_nL)}\right|^2. \tag{17}$$

The complete expression for the tunneling probability with the influence of the microwave field is given by [8]:

$$\Gamma_{withphoton}(E) = \sum J_n^2\left(\frac{eV_{ac}}{\hbar\omega}\right)\times \\ \times f_{FD}\left(E - \frac{C_g}{C}eV_g - n\hbar\omega - eV_{cd}\right)\Gamma(E - n\hbar\omega) \tag{18}$$

where C_g is the quantum capacitance of the nanotube quantum dot and C is the coupling capacitance between the nanotube quantum dot and the leads.

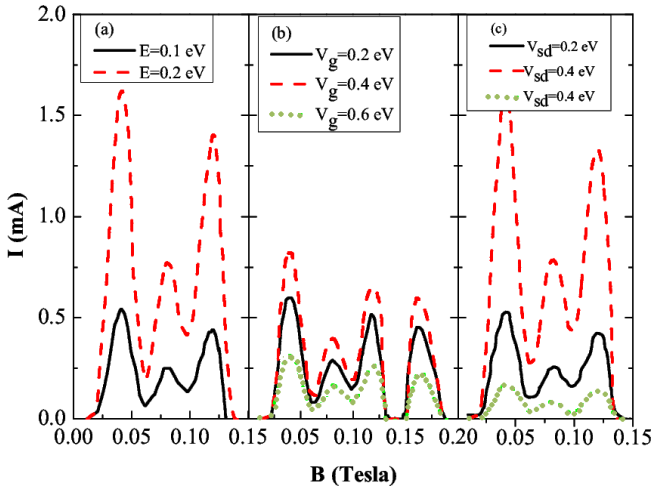

Fig. 1: The current as a function of the applied magnetic field (a) photon energy (b) gate voltage in energy units(c) source drain voltage in energy units.

7 Results and Discussions

Numerical calculations were performed according to the following:

(i) The electron transport through the present investigated device is treated as a stochastic process, so that the tunneled electron energy has been taken as a random number relative to the Fermi-energy of the carbon nanotube. The calculations had been conducted previously by the authors [9, 11].

(ii) The value of the quantum capacitance, C_g, is 0.25 nF.

(iii) The coupling capacitance between carbon nanotube quantum dot and the leads is calculated in the Coulomb blockade regime and in the charging energy of the quantum dot [9, 11]. Its value is found to be approximately equals $\sim$ 0.4 nF. The value of the Fermi energy, E_F is calculated using the values of the Fermi velocity, ν_F, and it was found to be approximately equals $\sim$ 0.125 eV. This value of the Fermi energy, E_F, was found to be consisted with those found in the literature [12, 13]. The effective mass of the charge carrier was taken as 0.054 m_e [12, 13].

The variation of the current, I, with the applied magnetic field, B, at difference values of the photon energy, E, gate voltage, V_g, and different values of the bias voltage, V_{sd}, is shown in Figs. (1a,b,c). It is known that the influence of an external magnetic field, B, will lead to a change in the energy level separation between the ground state and the first excited state [14] in the carbon nanotube quantum dot. We notice that the current dependence on the magnetic field oscillates with a periodicity of approximately equals $\sim$ 0.037 T. This value corresponds roughly to the addition of an extra flux quantum to the quantum dot. These results have been observed by the authors [12, 15]. The peak heights are different due the interplay between the tunneled electrons and the applied photons of the microwave field and also this flux quantum will affect on the photon–assisted tunneling rates between electronic states of the carbon nanotube quantum dot. The results obtained in the present paper are, in general, found to be in concordant with those in the literature [12–20].

8 Conclusion

We conclude from the present analysis of the proposed ccc theoretically and numerically that the present device could be used as photo-detector device for very wide range of frequencies. Some authors suggested that such mesoscopic device, i.e. cccc could be used for a solid state quantum computing system. Recently the investigation of the authors [20] shows that such carbon nanotubes (CNT's) could find applications in microwave communications and imaging systems.

Submitted on June 27, 2010 / Accepted on July 10, 2010

References

1. Iijma S. *Nature*, v.354, 1991, 56.
2. Harris F. Carbon nanotubes and related structures. Cambridge University Press, 1999.
3. Dresselhaus M. S. Dresselhaus G.,Eklund P. C., Science of fullerenes and carbon nanotubes. Academic Press, NY, 1996.
4. Javey A. and Keng Jing. Carbon nanotube electronics. Springer Science + Business Media LLC, 2009.
5. Dai Liming. Carbon nanotechnology Recent developments in chemistry, Physics, Materials Science and Device Applications. Elsevier, Amsterdam, 2006.
6. Saito R., Fujita M., Dresselhaus G., and Dresselhaus M. S. *Appl. Phys. Lett.*, v.60, 1992, 2204.
7. Tworzydlo J., Trauzett B, Titov M., Rycerz A., and Beenakker C. W. J. *Phys. Rev.Lett.*, v.96, 2006, 246802.
8. Platero G. and Aguado R. *Physics Reports*, v.395, 2004, 1.
9. Atallah A. S., Phillips A. H., Amin A. F. Semary M. A., *Nano 2006*, v.1, no. 3, 2006, 259 .
10. Phillips A. H., Mina A. N., Sobhy M. S., and Fouad E. A. *J. of Computational and theoretical nanoscience*, v.4 (1), 2007, 174 .
11. Phillips A. H., Aly N. A. I., Kirah K., El-Sayes H. E. *Chinese Physics Letters*, v.25, no. 1, 2008, 250.
12. Anantram M. P., Leonard F. *Rep. Prog. Phys.*, v.69, 2006, 507.
13. Durkop T., Getty S. A., Cobas E., Fuhrer M. S. *Nano Lett.*, v.4, 2004, 35.
14. Oosterkamp T. H., Kouwenhoven L. P., Koolen A. E. A., van der Vaart N. C. and Harmans C. J. P. M. *Semicond. Sci. Technol.*, v.11, 1996, 1512.
15. Meyer C., Elzerman J. M., and Kouwenhoven L. P. *Nano Lett.*, v.7, no. 2, 2007, 295.
16. Orellana P. A., Pacheco M. *Phys. Rev.*, v.B75, 2007, 115427.
17. Kim J., Hye–Miso, Kim Nam, Kim Ju–Ji, and Kicheon Kang. *Phys. Rev.*, v.B70, 2004, 153402.
18. Zhao Li–Na and Zhao Hong–Kang. *Phys. Lett.*, v.A325, 2004, 156.
19. Pan Hui, Li Tsung–Han, and Ya Dapeng. *Physica B*, v.369, 2005, 33.
20. Lin Y. M., Dimitrakpoulos C., Jenkins K. A., Farmer D. B., Chiu H. Y., Grill A., Avouris Ph. *Science, 2010*, v.327, no. 5966, 2010, 662.

On the Geometry of the Periodic Table of Elements

Albert Khazan
E-mail: albkhazan@gmail.com

The presented analytical research manifests a geometrical connexion existing among the elements of the Periodic Table of Elements, in addition to the known physical chemical connexion.

Despite the spectacular versions of the periodic tables of elements were suggested by the scientists, no one person did not state the following problem: how the elements are geometrically connected among each other in the groups and periods? As is known, the element are located in the cells, which are joined into 18 groups along the vertical axis in the Table of Elements, and into 7 periods (I suggested recently that 8 periods, see [1] and references therein) along the horizontal axis. Number of the elements rises from left to right in the periods, and from up to down in the groups. The periods begin with the elements of Group 1, and end with the elements of Group 18. Each column determines the main physical chemical properties of the elements, which change both from up to down and from left to right. For example, the elements of Group 1 are alkaline metals (the very active chemical elements), while Group 18 consists of inert gases which manifest a very low chemical activity under the regular physical conditions. In the end of the 20th century, IUPAC suggested a long period form of the Table of Elements, where Period 1 consists of 2 elements, Periods 2 and 3 consist of 8 elements in each, Periods 4 and 5 consist of 18 elements in each, while Periods 6 and 7 consist of 32 elements in each. Finally, Period 8 consisting of 37 elements was suggested on the basis of my theoretical studies [1].

This short study targets a search for the geometrical connexion among the elements of the Periodic Table.

Figure 1 in Page 65 shows that the elements of Group 18 are concentrated along the upper broken line, which is split into three straight lines joining three elements (four elements in the end) in each. The numbers indicate the periods and elements. Period 8, containing element No.155, is also shown here. Each straight section of these can easily be described by a straight line equation.

The lower broken line presents Group 1 (as seen according to the numbers of the elements). The space between the upper and lower straight lines is filled with the straight line of Group 13. It consists of Periods 2–4, 4–6, and 6–8 (Period 1 was omitted from the graph for simplicity). Besides, the points 6,67; 6,81; and 7, 99 which are related to actinides and lanthanides are shown inside the boundaries. Hence, we can suppose that the plane bounded by the lines of Group 1 and Group 18, and also by the points 8,155 and 8,119 on right and the points 1,2; 1,1 on left (and 2,3 of course) contains all known and unknown elements of the Periodic Table. Thus, this figure obtained as a result of the purely geometrical constructions, allows us to make the following conclusions:

- The Periodic Table should necessary contain Period 8, which begins with No.119 and ends by No.155;
- No elements can exists outside this figure;
- A strong geometrical connexion exists among the groups and periods.

Thus, this short study hints at a geometrical connection among the elements of the Table of Elements, which exists in addition to the known physical chemical properties of the elements. Note that the geometrical connexion manifests itself per se in the study, without any additional suggestions or constructions. Therefore, this does not change the form of the Periodic Table of Elements, which remains the same.

Submitted on June 29, 2010 / Accepted on July 12, 2010

References

1. Khazan A. Upper limit in Mendeleev's Periodic Table — Element No.155. 2nd expanded edition, Svenska fysikarkivet, Stockholm, 2010.

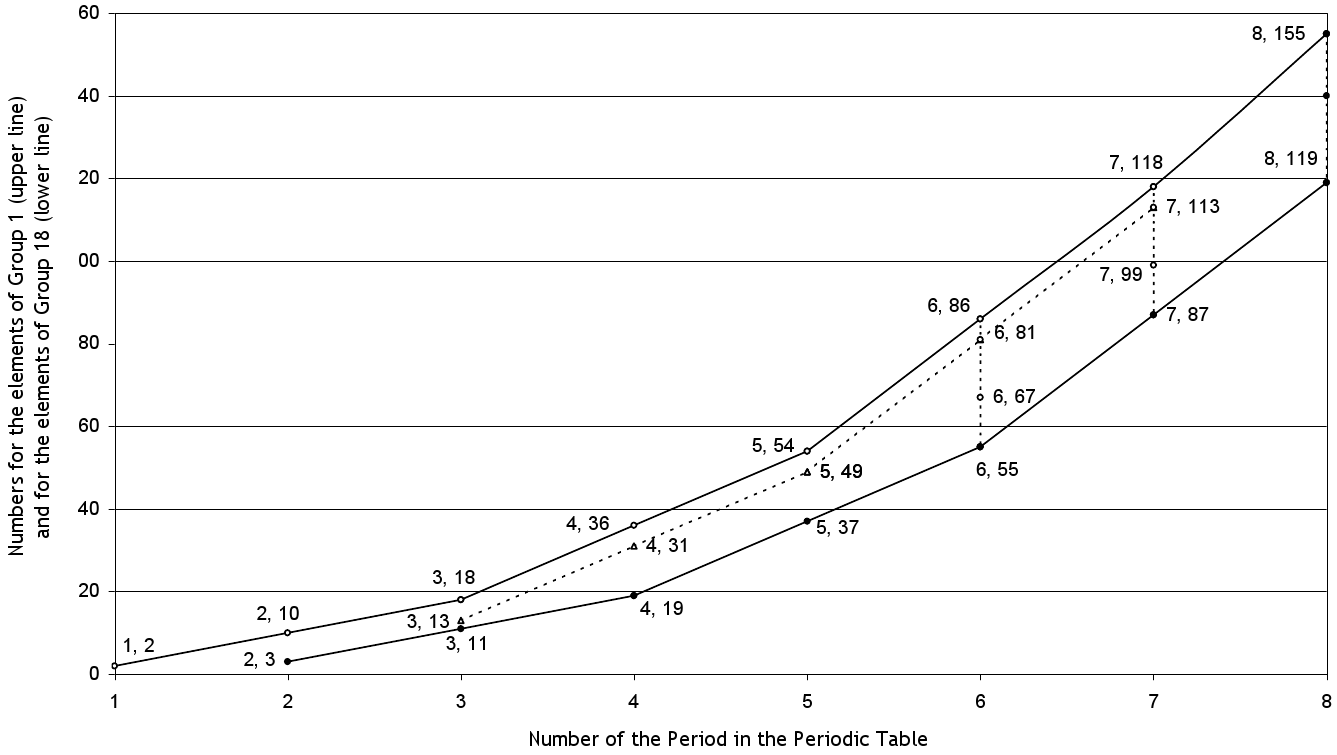

Fig. 1: Locations of the elements opening the Periods (the lower line) and those closing the Periods (the upper line).

On the Source of the Systematic Errors in the Quatum Mechanical Calculation of the Superheavy Elements

Albert Khazan
E-mail: albkhazan@gmail.com

It is shown that only the hyperbolic law of the Periodic Table of Elements allows the exact calculation for the atomic masses. The reference data of Periods 8 and 9 manifest a systematic error in the computer software applied to such a calculation (this systematic error increases with the number of the elements in the Table).

Most scientists who worked on the problems of the Periodic Table of Elements (G. T. Seaborg, J. T. Bloom, V. I. Goldanskii, F. W. Giacobbe, M. R. Kibler, J. A. Rihani et al.) attempted to construct new models of the Table with the use of quantum mechanical calculations. In this process, they used a complicate mathematical apparatus of Quantum Mechanics, and introduced additional conditions such as the periods, the number of the elements, and so on. In other word, they first set up a problem of introducing Periods 8 and 9 into the Table of Elements (50 elements in each), and predict the respective interior of the cells of the Table and the interior of the atoms. Only then, on the basis of the above data, they calculate the atomic mass and the number of the neutrons. However the main task — obtaining the exact numerical values of the atomic mass, corresponding to the numbers of the elements higher than period 8 — remains unsolved.

The core of my method for the calculation is the law of hyperbolas discovered in the Periodic Table [1]. Using the law, we first calculated the atomic mass of the upper (heaviest) element allowed in the Periodic Table (411.663243), then its number (155) was also calculated. According to the study [1], this element should be located in Group 1 of Period 8. The main parameters of the chemical elements were obtained in our study proceeding from the known data about the elements, not from the suggestions and the use of the laws specific to the microscale.

Figure 1 in Page 67 shows two dependencies. The first is based on the IUPAC 2007 data for elements 80–118 (line 1). The second continues upto element 224 (line 2). As is seen, there is a large deviation of the data in the section of the numbers 104–118. This is obviously due to the artificial synthesis of the elements, where the products o the nuclear reactions were not measured with necessary precision. Line 2 is strictly straight in all its length except those braking sections where it is shifted up along the ordinate axis. Is is easy to see that at the end of line 1, in the numbers 116–118, the atomic mass experiences a shift for 17 units. These shifts increase their value with the number of the elements: the next shift rises the line up for 20 units, and the last shift — for 25 units. In order to find the numerical values of the shifts more precisely, Figure 2 was created (see Page 67): this is the same broken line (the initially data) compared to itself being averaged by the equation of the line of trend (whose data were compared to the initial data). Hence, the difference between these lines should give the truly deviation of the numerical values f the atomic masses between the FLW Inc. data and our data (our data deviate from the equation of the line of trend for nothing but only one hundredth of 1 atomic mass unit). Figure 3 in Page 68 shows a shift of the atomic mass just element 104, before Period 8: in element 118 the atomic mass is shifted for 11 units; in Period 9 the shift exceeds 15 units, and then it increases upto 21 units. The respective data for Period 8 are shown in Figure 4.

These data lead to only a single conclusion. Any software application, which targets the quantum mechanical calculation for the atomic mass of the elements, and is constructed according to the suggested law specific to the microscale, not the known data about the chemical elements, will make errors in the calculation. The theory [1] referred herein manifested its correctness in many publications, and met no one negative review.

Submitted on July 06, 2010 / Accepted on July 12, 2010

References

1. Khazan A. Upper limit in Mendeleev's Periodic Table — Element No.155. 2nd expanded edition, Svenska fysikarkivet, Stockholm, 2010.

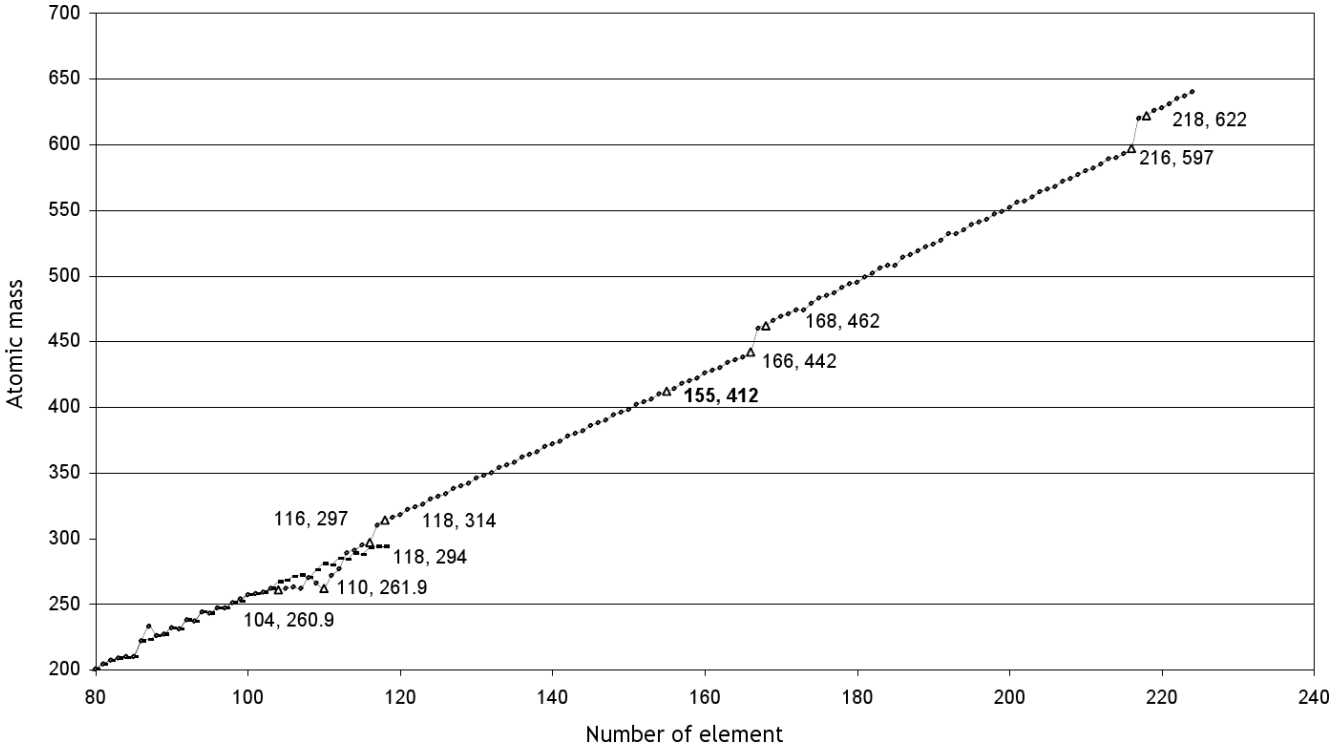

Fig. 1: Dependency between the atomic mass of the elements and their number in the Table of Elements. The IUPAC data and the FLW Inc. data begin from number 80, for more visibility of the dependency.

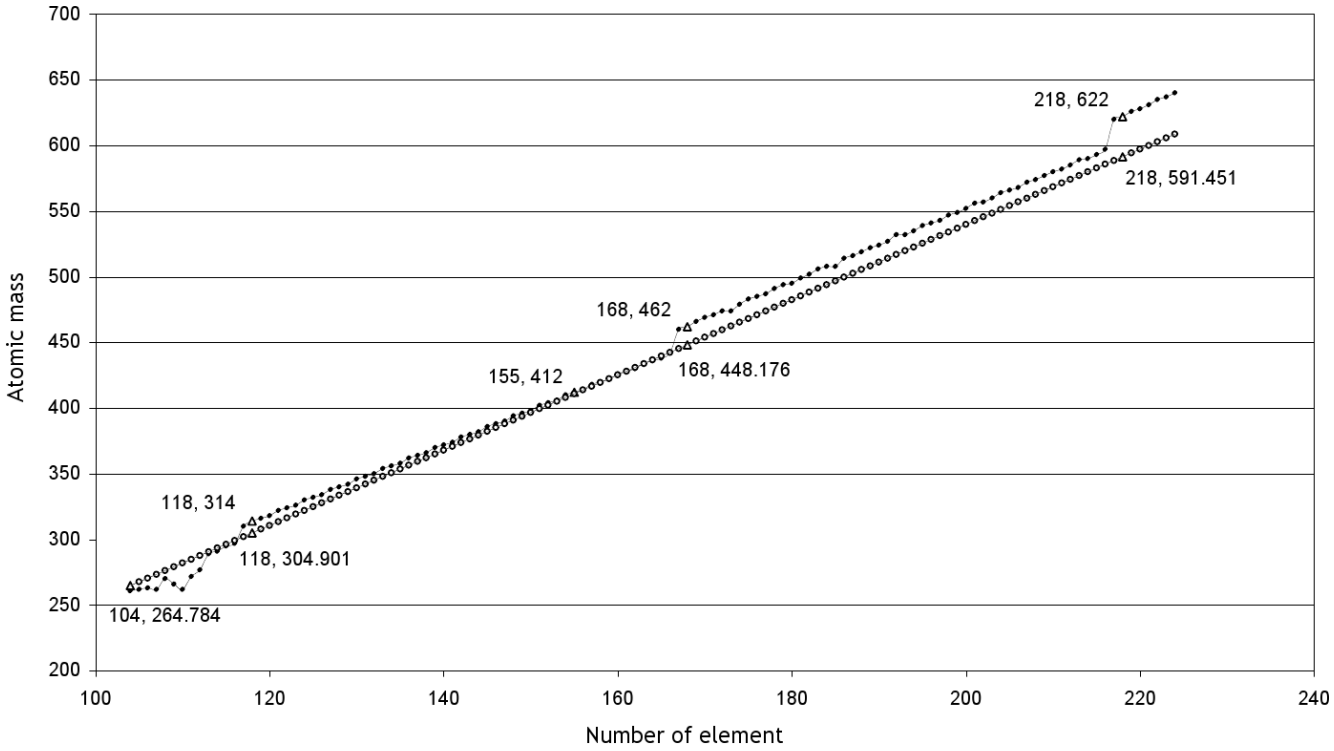

Fig. 2: Dependency between the atomic mass of the elements and their number in the Table of Elements. Black dots are the FLW Inc. data. Small circles — the averaged results according to the FLW Inc. data.

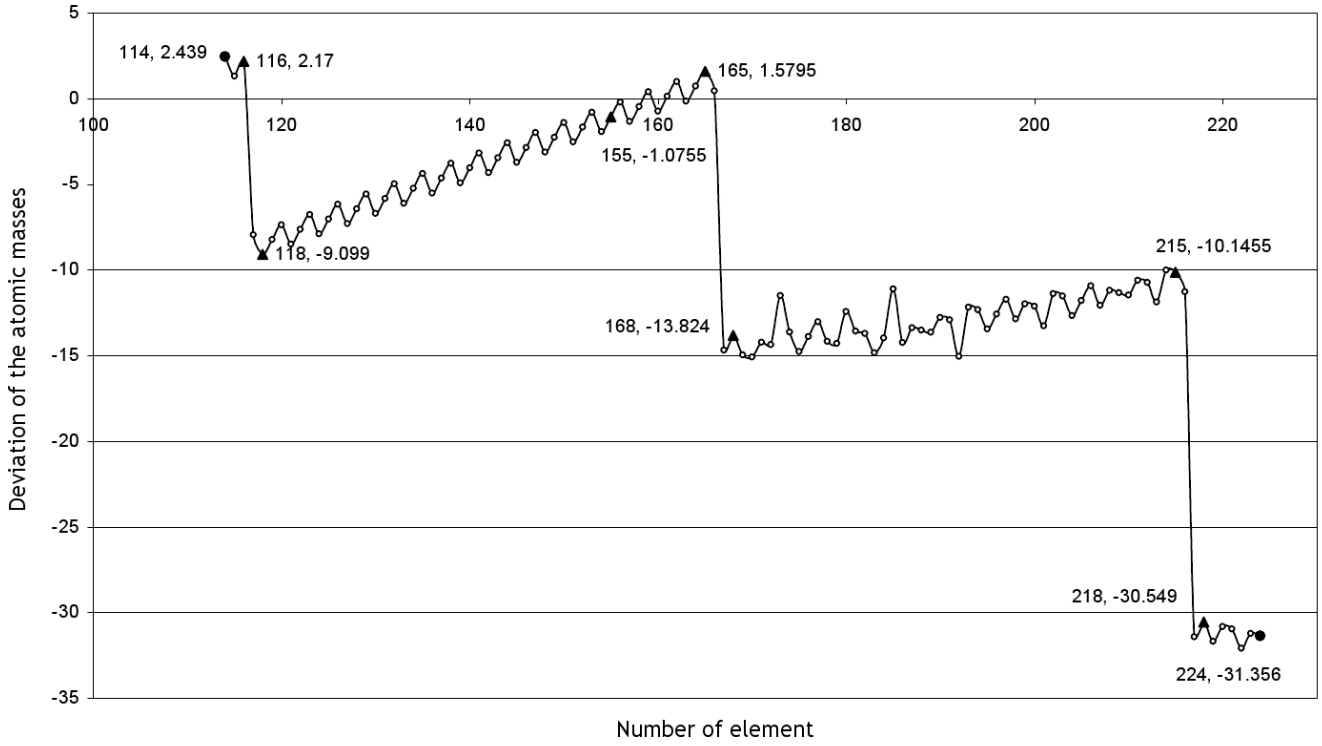

Fig. 3: Dependency between the atomic mass, calculated according to our theory and the FLW Inc. data, and their number in the Table of Elements.

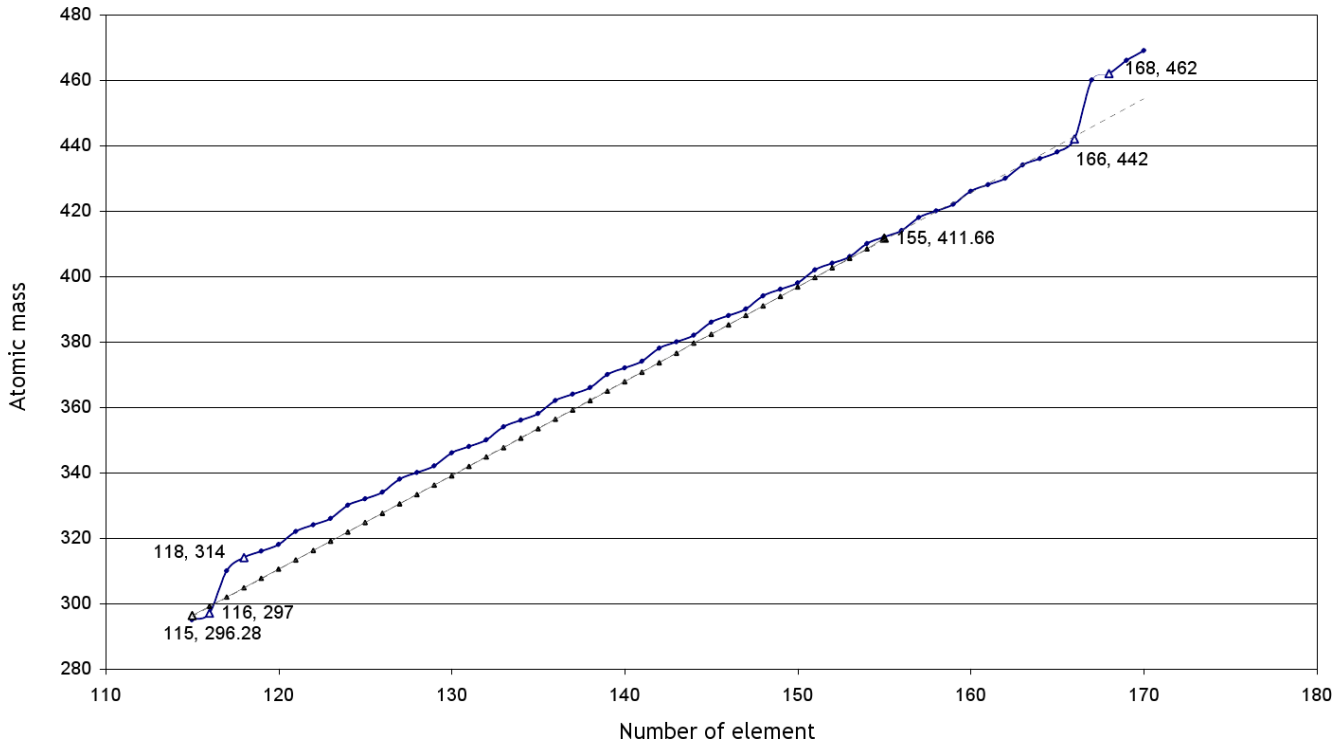

Fig. 4: Dependency between the atomic mass of the elements and their number in the Table of Elements, shown for Period 8. Black dots are the FLW Inc. data. Small triangles — the data according to our calculations.

The Dirac Electron in the Planck Vacuum Theory

William C. Daywitt

National Institute for Standards and Technology (retired), Boulder, Colorado, USA.
E-mail: wcdaywitt@earthlink.net

The nature of the Dirac electron (a massive point charge) and its negative-energy solutions are examined heuristically from the point of view of the Planck vacuum (PV) theory [1,2]. At the end of the paper the concept of the vacuum state as previously viewed by the PV theory is expanded to include the massive-particle quantum vacuum [3,4].

1 The Dirac equation

When a free, massless, bare charge travels in a straight line at a uniform velocity v, its bare Coulomb field e_*/r^2 perturbs (polarizes) the PV. If there were no PV, the bare field would propagate as a frozen pattern with the same velocity. However, the PV responds to the perturbation by producing magnetic and Faraday fields [1,5] that interact with the bare charge in a iterative fashion that leads to the well-known relativistic electric and magnetic fields [6] that are ascribed to the charge as a single entity. The corresponding force perturbing the PV is e_*^2/r^2, where one of the charges e_* in the product e_*^2 belongs to the free charge and the other to the individual Planck particles making up the degenerate negative-energy PV. By contrast, the force between two free elementary charges observed in the laboratory is $e^2/r^2\,(=\alpha e_*^2/r^2)$, where e is the observed electronic charge and α is the fine structure constant.

In the Dirac electron, where the bare charge has a mass m, the response of the PV to the electron's uniform motion is much more complicated as now the massive charge perturbs the PV with *two* forces, the polarization force e_*^2/r^2 and the attractive curvature force mc^2/r [1]. The radius at which the magnitudes of these two forces are equal

$$\frac{mc^2}{r} = \frac{e_*^2}{r^2} \qquad \text{at } r = r_c \tag{1}$$

is the electron's Compton radius $r_c\,(= e_*^2/mc^2)$. The string of Compton relations [4]

$$r_c\, mc^2 = r_*\, m_*\, c^2 = e_*^2 = c\hbar \tag{2}$$

tie the electron $(r_c mc^2)$ to the Planck particles $(r_* m_* c^2)$ within the PV, where r_* and m_* are the Compton radius and mass of those particles. The charges in the product e_*^2 of (2) are assumed to be massless point charges.

The Dirac equation for the electron is [3,7]

$$\left(c\,\widehat{\alpha}\,\widehat{p} + \beta mc^2\right)\psi = E\psi\,, \tag{3}$$

where the momentum operator and energy are given by

$$\widehat{p} = \hbar\,\nabla/i \qquad \text{and} \qquad E = \pm(m^2c^4 + c^2p^2)^{1/2} \tag{4}$$

and where $\widehat{\alpha}$ and β are defined in the references. The relativistic momentum is $p\,(= mv/\sqrt{1 - v^2/c^2})$.

As expressed in (3), the physics of the Dirac equation is difficult to understand. Using (2) to replace $\hbar$ in the momentum operator and inserting the result into (3), reduces (3) to

$$\left(\widehat{\alpha}\,\frac{e_*^2\nabla}{imc^2} + \beta\right)\psi = \frac{E}{mc^2}\,\psi\,, \tag{5}$$

where the charge product e_*^2 suggests the connection in (2) between the free electron and the PV. It is significant that neither the fine structure constant nor the observed electronic charge appear in the Dirac equation, for it further suggests that the bare charge of the electron interacts *directly* with the bare charges on the individual Planck particles within the PV, without the fine-structure-constant screening that leads to the Coulomb force e^2/r^2 in the first paragraph. Equation (5) leads immediately to the equation

$$\left(\widehat{\alpha}\,\frac{r_c\nabla}{i} + \beta\right)\psi = \frac{E}{mc^2}\,\psi \tag{6}$$

with its Del operator

$$r_c\,\nabla = \sum_{n=1}^{3} \widehat{x}_n\,\frac{\partial}{\partial x_n/r_c} \tag{7}$$

being scaled to the electron's Compton radius.

Through (2), (5), and (6), then, the connection of the Dirac equation to the PV is self evident — the Dirac equation represents the response of the PV to the two perturbations from the uniformly propagating electron. As an extension of this thinking, the quantum-field and Feynman-propagator formalisms of quantum electrodynamics are also associated with the PV response.

2 The Klein paradox

The "hole" theory of Dirac [7] that leads to the Dirac vacuum will be presented here along with the Klein paradox as the two are intimately related. Consider an electrostatic potential of the form

$$e\phi = \begin{cases} 0 & \text{for } z < 0 \ \text{(Region I)} \\ V_0 & \text{for } z > 0 \ \text{(Region II)} \end{cases} \tag{8}$$

acting on the negative-energy vacuum state (corresponding to the negative E in (4)) with a free electron from $z < 0$ being

scattered off the potential step at $z = 0$, beyond which $V_0 > E + mc^2 > 2mc^2$. This scattering problem leads to the Klein paradox that is reviewed below.

The scattering problem is readily solved [8, pp.127–131]. For the free electron in Region I, $E^2 = m^2c^4 + c^2p^2$; and for Region II, $(E - V_0)^2 = m^2c^4 + (cp')^2$, where E is the total electron energy in Region I, and p and p' are the z-directed electron momenta in Regions I and II respectively.

The Dirac equation (with motion in the z-direction) for $z < 0$ is

$$\left(c\,\alpha_z\,\widehat{p_z} + \beta mc^2\right)\psi = E\psi \tag{9}$$

and for $z > 0$ is

$$\left(c\,\alpha_z\,\widehat{p_z} + \beta mc^2\right)\psi = (E - V_0)\psi\,. \tag{10}$$

The resulting incident and reflected electron wavefunctions are

$$\psi_{\mathrm{I}} = A \begin{pmatrix} 1 \\ 0 \\ \frac{cp}{E+mc^2} \\ 0 \end{pmatrix} e^{ipz/\hbar} \tag{11}$$

and

$$\psi_{\mathrm{R}} = B \begin{pmatrix} 1 \\ 0 \\ \frac{-cp}{E+mc^2} \\ 0 \end{pmatrix} e^{-ipz/\hbar} \tag{12}$$

respectively, where $cp = \sqrt{E^2 - m^2c^4}$. The transmitted wave turns out to be

$$\psi_{\mathrm{T}} = D \begin{pmatrix} 1 \\ 0 \\ \frac{cp'}{V_0-E-mc^2} \\ 0 \end{pmatrix} e^{ip'z/\hbar}\,, \tag{13}$$

where $cp' = \sqrt{(V_0 - E)^2 - m^2c^4}$. It should be noted that the imaginary exponent in (13) represents a propagating wave which results from $V_0 > E + mc^2$; in particular, the particle motion in Region II is not damped as expected classically and quantum-mechanically when $V_0 < E + mc^2$.

The constants A, B, and D are determined from the continuity condition

$$\psi_{\mathrm{I}} + \psi_{\mathrm{R}} = \psi_{\mathrm{T}} \tag{14}$$

at $z = 0$ and lead to the parameter

$$\Gamma \equiv \left(\frac{V_0 - E + mc^2}{V_0 - E - mc^2}\,\frac{E + mc^2}{E - mc^2}\right)^{1/2} > 1\,. \tag{15}$$

The particle currents are calculated from the expectation values of

$$j_z(x) = c\,\psi^{\dagger}(x)\,\alpha_z\psi(x) \tag{16}$$

and yield j_I, j_R, and j_T for the incident, reflected, and transmitted currents respectively. The resulting normalized reflection and transmission currents become

$$\frac{j_R}{j_I} = -\left(\frac{1+\Gamma}{1-\Gamma}\right)^2\,, \tag{17}$$

$$\frac{j_T}{j_I} = -\frac{4\Gamma}{(1-\Gamma)^2}\,. \tag{18}$$

Since Γ is positive, (17) gives

$$\left|\frac{j_R}{j_I}\right| - 1 > 0 \tag{19}$$

for the excess reflected current; i.e., the reflected current is *greater* than the incident current! This seemingly irrational result is known as the Klein paradox.

The most natural and Occam's-razor-consistent conclusion to be drawn from (19), however, is that the excess electron (or electrons) in the reflected current is (are) coming from the right ($z > 0$) of the step at $z = 0$ and proceeding in the negative z direction away from the step. Furthermore, the minus sign on the normalized transmission current in (18) implies that no electrons are entering Region II — the total electron current (reflected plus "transmitted") travels in the negative z direction away from the step. Then, given the experimental fact of electron-positron pair creation, it is reasonable to conclude that the incident free electron creates such pairs when it "collides" with the stressed portion of the vacuum ($z > 0$), the positrons (Dirac "holes") proceeding to the right *into the vacuum* after the collision [8, fig. 5.6]. That is, positrons (like neutrinos [9]) travel within the vacuum, not free space!

The evidence of the created positrons is felt in free space as the positron fields, analogous to the zero-point fields whose source is the zero-point agitation of the Planck particles within the PV. The curving of the positrons in a laboratory magnetic field is due to that field permeating the PV and acting on the "holes" within. (In the PV-theory view of things, the free electron is not seen as propagating *within* the vacuum state — only the electron force-fields (e_*^2/r^2 and mc^2/r) permeate that vacuum; consequently, the electron is not colliding with the negative-energy Planck particles making up the vacuum.)

3 Summary and comments

The total r-directed perturbing force the electron exerts on the PV is

$$F_e = \frac{e_*^2}{r^2} - \frac{mc^2}{r} = \frac{e_*^2}{r^2}\left(1 - \frac{r}{r_c}\right), \tag{20}$$

where the force vanishes at the electron's Compton radius r_c. For $r > r_c$ the force compresses the vacuum and for $r < r_c$ the vacuum is forced to expand. Ignoring the second term in (20) for convenience and concentrating on the region $r < r_c$, the lessons from the preceding section can be applied to the internal electron dynamics.

Recalling that the bare charge of the free electron interacts directly with the individual Planck particles in the PV, the electron-Planck-particle potential (e_*^2/r) in the inequality $e_*^2/r > E + mc^2$ leads to

$$r < \frac{e_*^2}{E + mc^2} = \frac{r_c}{1 + E/mc^2} < \frac{r_c}{2}\,, \tag{21}$$

where the positive and negative energy levels in (4) now *overlap*, and where any small perturbation to the PV can result in an electron-positron pair being created (the electron traveling in free space and the positron in the PV). The smaller the radius r, the more sensitive the PV is to such disruption.

The electron mass results from the massless bare charge being driven by ultra-high-frequency photons of the zero-point electromagnetic vacuum [4, 10]; so the bear charge of the electron exhibits a small random motion about its center-of-motion. The resulting massive-charge collisions with the sensitized PV produce a cloud of electron-positron pairs around that charge. The massive free charge then exhibits an exchange type of scattering [3, p.323] with some of the electrons in the pairs, increasing the free electron's apparent size in the process.

In the current PV theory it is assumed that the total quantum vacuum, which consists of the electromagnetic vacuum and the massive-particle vacuum [3, 4], exists in free space as virtual particles. However, the simple picture presented in the previous paragraphs and in Section 2 concerning pair creation modifies that view significantly. It is the massive-particle quantum vacuum that overlaps the positive energy levels of the free-space electron in the previous discussion. Thus, as the appearance of this latter vacuum in free space requires a sufficiently stressed vacuum state (in the above region $r < r_c/2$ e.g.), it is more reasonable to assume that the massive-particle component of the quantum vacuum does not exist in free space except under stressful conditions.

Consequently, it seems reasonable to conclude that the PV is a composite state patterned, perhaps, after the hierarchy of Compton relations

$$r_e m_e c^2 = r_p m_p c^2 = \cdots = r_* m_* c^2 = e_*^2 , \qquad (22)$$

where the products $r_e m_e$, $r_p m_p$, and $r_* m_*$ refer to the electron, proton, and Planck particle respectively. The dots between the proton and Planck-particle products represent any number of heaver intermediate-particle states. The components of this expanded vacuum state correspond to the sub-vacua associated with these particles; e.g., the electron-positron Dirac vacuum ($r_e m_e c^2$) in the electron case. If these assumptions are correct, then the negative-energy states in (4) no longer end in a negative-energy infinity — as the energy decreases it passes through the succession of sub-vacuum states, finally ending its increasingly negative-energy descent at the Planck-particle stage $r_* m_* c^2$. In summary, the PV model now includes the massive-particle quantum vacuum which corresponds to the collection of sub-vacuum states in (22).

Submitted on July 13, 2010 /Accepted on July 16, 2010

References

1. Daywitt W.C. The Planck vacuum, *Progress in Physics*, v. 1, 20, 2009.
2. Daywitt W.C. A paradigm shift from quantum fields to the Planck vacuum. To be published in *Galilean Electrodynamics*. See also http://www.planckvacuum.com
3. Milonni P.W. The quantum vacuum — an introduction to Quantum Electrodynamics. Academic Press, New York, 1994.
4. Daywitt W.C. The source of the quantum vacuum. *Progress in Physics*, 2009, v. 1, 27.
5. Pemper R.R. A classical foundation for electrodynamics. Master Dissertation, U. of Texas, El Paso, 1977. Barnes T.G. Physics of the future — a classical unification of physics. Institute for Creation Research, California, 1983, 81.
6. Jackson J.D. Classical Electrodynamics. John Wiley & Sons, 1st ed., 2nd printing, NY, 1962.
7. Dirac P.A.M. A theory of electrons and protons. *Proc. Roy. Soc. Lond. A*, 1930, v.126, 360.
8. Gingrich D.M. Practical Quantum Electrodynamics. CRC, The Taylor & Francis Group, Boca Raton, London, New York, 2006.
9. Daywitt W.C. The neutrino: evidence of a negative-energy vacuum state. *Progress in Physics*, 2009, v. 2, 3.
10. Puthoff H.E. Gravity as a zero-point-fluctuation force. *Phys. Rev. A*, 1989, v. 39, no. 5, 2333–2342.

IN MEMORIAM OF NIKIAS STAVROULAKIS

On the Field of a Spherical Charged Pulsating Distribution of Matter

Nikias Stavroulakis*

In the theory of the gravitational field generated by an isotropic spherical mass, the spheres centered at the origin of $\mathbb{R}^3$ are non-Euclidean objects, so that each of them possesses a curvature radius distinct from its Euclidean radius. The classical theory suppresses this distinction and consequently leads to inadmissible errors. Specifically, it leads to the false idea that the field of a pulsating source is static. In a number of our previous publications (see references), we have exposed the inevitable role that the curvature radius plays and demonstrated that the field generated by a pulsating not charged spherical course is dynamical. In the present paper we prove that the curvature radius plays also the main role in the description of the gravitational field generated by a charged pulsating source.

1 Introduction

The manifold underlying the field generated by an isolated spherical distribution of matter is the space $\mathbb{R}\times\mathbb{R}^3$, considered with the product topology of four real lines. In fact, the distribution of matter is assumed to be located in a system represented topologically by the space $\mathbb{R}^3$ and moreover to every point of $\mathbb{R}^3$ there corresponds the real line described by the time coordinate t (or rather ct). In the general case, the investigation of the gravitational field by means of the Einstein equations is tied up with great mathematical difficulty. In order to simplify the problem, we confine ourselves to the case when the spherical distribution of matter is isotropic. The term "*isotropic*" refers classically to the action of the rotation group SO(3) on $\mathbb{R}^3$ and the corresponding invariance of a class of metrics on $\mathbb{R}^3$. But in our case we have to deal with a *space-time* metric on $\mathbb{R}\times\mathbb{R}^3$, so that its invariance must be conceived with respect to another group defined by means of SO(3) and acting on $\mathbb{R}\times\mathbb{R}^3$. This necessity leads to the introduction of the group SΘ(4), which consist of the matrices

$$\begin{pmatrix} 1 & 0_H \\ 0_V & A \end{pmatrix}$$

with $0_H = (0,0,0)$, $0_V = \begin{pmatrix} 0 \\ 0 \\ 0 \end{pmatrix}$ and $A \in \mathrm{SO}(3)$. It is also convenient to introduce the larger group $\Theta(4)$ consisting of the matrices of the same form for which $A \in \mathrm{O}(3)$.

From the general theory [10] of the SΘ(4)-invariant and $\Theta(4)$-invariant tensor fields on $\mathbb{R}\times\mathbb{R}^3$, we deduce the explicit form of an SΘ(4)-invariant space-time metric to be

$$ds^2 = [f(t,\|x\|)\,dt + f_1(t,\|x\|)\,(xdx)]^2 - l_1^2(t,\|x\|)dx^2 -$$

$$-\frac{l^2(t,\|x\|) - l_1^2(t,\|x\|)}{\|x\|^2}\,(xdx)^2$$

and the condition $l(t,0) = l_1(t,0)$ is satisfied, which is also $\Theta(4)$-invariant. The functions that appear in it, result from the functions of two variables

$$f(t,u)\,,\quad f_1(t,u)\,,\quad l(t,u)\,,\quad l_1(t,u)\,,$$

assumed to be C^∞ on $\mathbb{R}\times[0,+\infty[$, if we replace u by the norm

$$\|x\| = \sqrt{x_1^2 + x_2^2 + x_3^2}.$$

However, since the norm $\|x\|$ is not differentiable at the origin of $\mathbb{R}^3$, the functions

$$f(t,\|x\|)\,,\quad f_1(t,\|x\|)\,,\quad l(t,\|x\|)\,,\quad l_1(t,\|x\|)$$

are not either. So, without appropriate conditions on these functions in a neighborhood of the origin, the curvature tensor and hence the gravitational field, will present a singularity at the origin of $\mathbb{R}^3$, which would not have any physical meaning. In order to avoid the singularity, our functions must be **smooth functions of the norm** in the sense of the following definition:

*Professor Dr. Nikias Stavroulakis, born on the island of Crete on October 6, 1921, passed away in Athens, Greece, on December 20, 2009. A handwritten manuscript of this paper was found on his desk by his daughter Eleni, who gave it to Dr. Ioannis M. Roussos, Professor of Mathematics at Hamline University, Saint Paul, Minnesota, compatriot scientific collaborator and closed friend of her father, to fill in some gaps, rectify some imperfections existing in the manuscript and submit it for publication to *Progress in Physics*. At this point Dr. I. M. Roussos wishes to express that he considers it a great honor to himself the fact that his name will remain connected with this great and original scientist. This is a continuation of the 5 most recent research papers that have appeared in this journal since 2006, but as we shall see at the end of this paper, very unfortunately Professor Stavroulakis has left it unfinished. Some of the claimed final conclusions are still pending. We believe that an expert on this subject matter and familiar with the extensive work of Professor Stavroulakis, on the basis of the material provided here and in some of his previous papers, will be able to establish these claims easily. No matter what, these 6 papers make up his swan-song on his pioneering research on gravitation and relativity.

Definition 1. Let $\phi(t,u)$ be a function C^∞ on $\mathbb{R}\times[0,\infty[$. (This implies that the function $\phi(t,\|x\|)$ is C^∞ with respect to the coordinates $t,\ x_1,\ x_2,\ x_3$ on $\mathbb{R}\times\Big[\mathbb{R}^3\times\Big(\mathbb{R}^3-\{(0,\,0,\,0)\}\Big)\Big]$.) Then the function $\phi(t,u)$ will be called **smooth function of the norm**, if every derivative

$$\frac{\partial^{p_0+p_1+p_2+p_3}\,\phi\,(t,\|x\|)}{\partial t^{p_0}\partial x_1^{p_1}\partial x_2^{p_2}\partial x_3^{p_3}}$$

at the point $(t,\ x)\in\mathbb{R}^3\times\Big(\mathbb{R}^3-\{(0,\,0,\,0)\}\Big)$ tends to a definite value, as $(x_1,\ x_2,\ x_3)\to(0,\,0,\,0)$.

The following Theorem characterizes the smooth functions of the norm:

Theorem 1. Let $\phi(t,u)$ be a C^∞ function on $\mathbb{R}\times[0,\infty[$. Then $\phi\,(t,\|x\|)$ is a smooth function of the norm if and only if the right derivatives of odd order

$$\frac{\partial^{2s+1}\phi\,(t,u)}{\partial u^{2s+1}}\bigg|_{u=0}$$

vanish for every value of t.

We will not need this theorem in the sequel, because we confine ourselves to the gravitational field outside the spherical source, so that we have to do exclusively with functions whose restrictions to a compact neighborhood of the origin of $\mathbb{R}^3$ are not taken into account.

This is why we also introduce two important functions on account of their geometrical and physical significance. Namely:

$$h\,(t,\|x\|)=\|x\|\ f_1\,(t,\|x\|)$$

and

$$g\,(t,\|x\|)=\|x\|\ l_1\,(t,\|x\|)\ ,$$

although, considered globally on $\mathbb{R}\times\mathbb{R}^3$, they are not smooth functions of the norm. Then if we set $\|x\|=\rho$, we can conveniently rewrite the space-time metric in the form

$$ds^2=\left[fdt+\frac{h}{\rho}(xdx)\right]^2-\left(\frac{g}{\rho}\right)^2dx^2-\frac{1}{\rho^2}\left[l^2-\left(\frac{g}{\rho}\right)^2\right](xdx)^2 \quad (1)$$

under the condition $|h|\leqslant l$, as explained in [4]. We recall, [2], that with this metric, the field generated by a spherical charged, pulsating in general, distribution of matter, is determined by the system of equations

$$Q_{00}+\frac{v^2}{g^4}f^2=0\,, \quad (2)$$

$$Q_{01}+\frac{v^2}{g^4}\frac{fh}{\rho}=0\,, \quad (3)$$

$$Q_{11}+\frac{v^2}{g^2\rho^2}=0\,, \quad (4)$$

$$Q_{11}+\rho^2Q_{22}+\frac{v^2}{g^4}(-l^2+h^2)=0\,, \quad (5)$$

where $v^2=\frac{k}{c^4}\,\varepsilon^2$, ε being the charge of the source.

Regarding the function $Q_{00}\,,\ Q_{01}\,,\ Q_{11}\,,\ Q_{22}\,$, they occur in the definition of the Ricci tensor $R_{\alpha\beta}$ related to (1) and are given by:

$$R_{00}=Q_{00}\,,\quad R_{0i}=R_{i0}=Q_{01}x_i\,,$$
$$R_{ii}=Q_{11}+Q_{22}x_i^2\,,\quad R_{ij}=Q_{22}x_ix_j\,,$$

where $i,\ j=1,2,3$ and $i\neq j$.

This been said, before dealing with the solutions of the equations of gravitation, we have to clarify the questions related to the boundary conditions at finite distance.

Let S_m be the sphere be the sphere bounding the matter. S_m is an isotropic non-Euclidean sphere, characterized therefore by its radius and its curvature-radius, which, in the present situation, are both time dependent. Let us denote them by $\sigma(t)$ and $\zeta(t)$ respectively. Since the internal field extends to the external one through the sphere S_m, the non-stationary (dynamical) states outside the pulsating source are brought about by the radial deformations of S_m, which are defined by the motions induced by the functions $\sigma(t)$ and $\zeta(t)$. Consequently these functions are to be identified with the boundary conditions at finite distance.

How is the time occurring in the functions $\sigma(t)$ and $\zeta(t)$ defined? Since the sphere S_m is observed in a system of reference defined topologically by the space $\mathbb{R}^3$, the time t must be conceived in the same system. But the latter is not known *metrically* in advance (i.e., before solving the equations of gravitation) and moreover it is time dependent. Consequently the classical method of special relativity is not applicable to the present situation. It follows that the first principles related to the notion of time must be introduced axiomatically in accordance to the very definition of SΘ(4)-invariant metric. Their physical justification will be sought a-posteriori on the basis of results provided by the theory itself.

This been said, the introduction of the functions $\sigma(t)$ and $\zeta(t)$ is implicitly related to another significant notion, namely the notion of synchronization in S_m. If S_1 denotes the unit sphere

$$S_1=\{\ \alpha\in\mathbb{R}^3\quad|\quad\|\alpha\|=1\}\,,$$

the equation of S_m *at each distance* t is written as

$$x=\alpha\sigma(t)\,.$$

So the assignment of the value t at every point of S_m defines both the radius $\sigma(t)$ and the "*simultaneous events*"

$$\{\,[t,\ \alpha\sigma(t)]\quad|\quad\alpha\in S_1\,\}\,.$$

What do we mean exactly by saying that two events A and B in S_m are simultaneous? The identity of values of time at A and B does not imply by itself that we have to do with simultaneous events. The simultaneity is ascertained by the fact that the value of time in question corresponds to a definite

position of the advancing spherical gravitational disturbance which is propagated radially and isotropically according to the very definition of the SΘ(4)-invariant metric.

If $\sigma'(t) = \zeta'(t) = 0$ on a compact interval of time $[t_1, t_2]$, no propagation of gravitational disturbances takes place in the external space during $[t_1, t_2]$ (at least there is no diffusion of disturbances), so that the gravitational radiation outside the matter depends on the derivatives $\sigma'(t)$ and $\zeta'(t)$. It follows that we may identify the pair $[\sigma'(t)\,,\,\zeta'(t)]$ with the gravitational disturbance emitted radially from the totality of the points of S_m at the instant t. We assume that this gravitational disturbance is propagated as a spherical wave and reaches the totality of any of the spheres

$$S_\rho = \{\, x \in \mathbb{R}^3 \quad | \quad \|x\| = \rho > \sigma(t) \,\}$$

outside the matter, in consideration, at another instant.

2 Propagation function and canonical metric

A detailed study of the propagation process appears in the paper [2]. It is shown that the propagation of gravitation from a spherical pulsating source is governed by a function $\pi(t,\rho)$, termed **propagation function**, such that

$$\frac{\partial\pi(t,\rho)}{\partial t} > 0\,, \quad \frac{\partial\pi(t,\rho)}{\partial\rho} \leqslant 0\,, \quad \rho \geqslant \sigma(t)\,, \quad \pi[t,\sigma(t)] = t\,.$$

If the gravitational disturbance reaches the sphere

$$S_\rho = \{\, x \in \mathbb{R}^3 \quad | \quad \|x\| = \rho > \sigma(t) \,\}$$

at the instant t, then

$$\tau = \pi(t,\rho)$$

is the instant of its radial emission from the totality of the sphere S_m.

Among the infinity of possible choices for $\pi(t,\rho)$, we distinguish principally the one obtained in the limit case where $h = l$. Then $\pi(t,\rho)$ reduces to the time coordinate, denoted by τ, in the sphere that bounds the matter and the space-time metric takes the so-called **canonical form**

$$ds^2 = \left[f(t,\rho)d\tau + l(\tau,\rho)\frac{(xdx)}{\rho}\right]^2 - \tag{6}$$
$$-\left[\left[\frac{g(\tau,\rho)}{\rho}\right]^2 dx^2 + \left[l^2(\tau,\rho) - \left[\frac{g(\tau,\rho)}{\rho}\right]^2\right]\frac{(xdx)^2}{\rho^2}\right].$$

Any other Θ(4)-invariant metric is derived from (6) if we replace τ by a conveniently chosen propagation function $\pi(t,\rho)$. It follows that the general form of a Θ(4)-invariant metric outside the matter can be written as follows:

$$ds^2 = \left[f\,[\pi(t,\rho),\rho]\,\frac{\partial\pi(t,\rho)}{\partial t}\,dt + \right.$$
$$+\left.\left(f\,[\pi(t,\rho),\rho]\,\frac{\partial\pi(t,\rho)}{\partial t} + l\,[\pi(t,\rho),\rho]\right)\frac{(xdx)}{\rho}\right]^2 - \tag{7}$$
$$-\left[\left(\frac{g[\pi(t,\rho),\rho]}{\rho}\right)^2 dx^2 + \right.$$
$$+\left.\left(l^2[\pi(t,\rho),\rho] - \left(\frac{g[\pi(t,\rho),\rho]}{\rho}\right)^2\right)\frac{(xdx)^2}{\rho^2}\right].$$

We do not need to deal with the equations of gravitation related to (7). Their solution follows from that of the equations of gravitation related to (6), if we replace in it τ by the general propagation function $\pi(t,\rho)$. Each permissible propagation function is connected with a certain conception of time, so that, the infinity of possible propagation functions introduces an infinity of definitions of time with respect to (7). So, the notion of time involved in (7) is not quite clear.

Our study of the gravitational field must begin necessarily with the canonical form (6). Although the conception of time related to (6) is unusual, it is easily definable and understandable. The time in the bounding the matter sphere S_m as well as in any other sphere S_ρ outside the matter is considered as a time synchronization according to what has been said previously. But of course this synchronization cannot be extended radially. Regarding the time along the rays, it is defined by the radial motion of photons. The motion of a photon emitted radially at the instant τ_0 from the sphere S_m will be defined by the equation $\tau = \tau_0$. If we label this photon with indication τ_0, then as it travels to infinity, it assigns the value of time τ_0 to every point of the corresponding ray. **The identity values of τ along this ray does not mean "synchronous events"**. This conception of time differs radically from the one encountered in special relativity.

3 The equations related to (2.1)

Since $h = l$ the equations (2), (3), (4) and (5) are greatly simplified to:

$$Q_{00} + \frac{v^2}{g^4}f^2 = 0\,, \tag{8}$$

$$\rho\,Q_{01} + \frac{v^2}{g^4}fl = 0\,, \tag{9}$$

$$\rho^2 Q_{11} + \frac{v^2}{g^2} = 0\,, \tag{10}$$

$$Q_{11} + \rho^2 Q_{22} = 0\,. \tag{11}$$

Regarding the functions Q_{00}, Q_{01}, Q_{11} and Q_{22}, they are

already known, [3], to be:

$$Q_{00} = \frac{1}{l}\frac{\partial^2 f}{\partial\tau\partial\rho} - \frac{f}{l^2}\frac{\partial^2 f}{\partial\rho^2} + \frac{f}{l^2}\frac{\partial^2 l}{\partial\tau\partial\rho} + \frac{2}{g}\frac{\partial^2 g}{\partial\tau^2} -$$
$$- \frac{f}{l^3}\frac{\partial l}{\partial\tau}\frac{\partial l}{\partial\rho} + \frac{f}{l^3}\frac{\partial f}{\partial\rho}\frac{\partial l}{\partial\rho} + \frac{2f}{l^2 g}\frac{\partial l}{\partial\tau}\frac{\partial g}{\partial\rho} - \frac{2f}{l^2 g}\frac{\partial f}{\partial\rho}\frac{\partial g}{\partial\rho} - \quad (12)$$
$$- \frac{2}{fg}\frac{\partial f}{\partial\tau}\frac{\partial g}{\partial\tau} - \frac{2}{lg}\frac{\partial l}{\partial\tau}\frac{\partial g}{\partial\tau} + \frac{2}{lg}\frac{\partial f}{\partial\rho}\frac{\partial g}{\partial\tau} - \frac{1}{fl}\frac{\partial f}{\partial\tau}\frac{\partial f}{\partial\rho},$$

$$\rho Q_{01} = \frac{\partial}{\partial\tau}\left[\frac{1}{fl}\frac{\partial(fl)}{\partial\rho}\right] - \frac{\partial}{\partial\rho}\left(\frac{1}{l}\frac{\partial f}{\partial\rho}\right) + \frac{2}{g}\frac{\partial^2 g}{\partial\tau\partial\rho} - \frac{2}{lg}\frac{\partial f}{\partial\rho}\frac{\partial g}{\partial\rho}, \quad (13)$$

$$\rho^2 Q_{11} = -1 - \frac{2g}{fl}\frac{\partial^2 g}{\partial\tau\partial\rho} + \frac{g}{l^2}\frac{\partial^2 g}{\partial\rho^2} - \frac{2}{fl}\frac{\partial g}{\partial\tau}\frac{\partial g}{\partial\rho} -$$
$$- \frac{g}{l^3}\frac{\partial l}{\partial\rho}\frac{\partial g}{\partial\rho} + \frac{1}{l^2}\left(\frac{\partial g}{\partial\rho}\right)^2 + \frac{g}{fl^2}\frac{\partial f}{\partial\rho}\frac{\partial g}{\partial\rho}, \quad (14)$$

$$Q_{11} + \rho^2 Q_{22} = \frac{2}{g}\left[\frac{\partial^2 g}{\partial\rho^2} - \frac{\partial g}{\partial\rho}\frac{1}{fl}\frac{\partial(fl)}{\partial\rho}\right]. \quad (15)$$

From (8) and (9) we deduce the equation

$$lQ_{00} - f\rho\, Q_{01} = 0, \quad (16)$$

which is easier to deal with than (8) on account of the identity

$$lQ_{00} - f\rho\, Q_{01} = \frac{2l}{g}\frac{\partial^2 g}{\partial\tau^2} + \frac{2f}{lg}\frac{\partial l}{\partial\tau}\frac{\partial g}{\partial\rho} - \frac{2l}{fg}\frac{\partial f}{\partial\tau}\frac{\partial g}{\partial\tau} - \quad (17)$$
$$- \frac{2}{g}\frac{\partial l}{\partial\tau}\frac{\partial g}{\partial\tau} + \frac{2}{g}\frac{\partial f}{\partial\rho}\frac{\partial g}{\partial\tau} - \frac{2f}{g}\frac{\partial^2 g}{\partial\tau\partial\rho}$$

which follows from (12) and (13).

On account of (15), the equation (11) gives

$$\frac{\partial}{\partial\rho}\left(\frac{1}{fl}\frac{\partial g}{\partial\rho}\right) = 0$$

whence

$$\frac{1}{fl}\frac{\partial g}{\partial\rho} = \beta = \text{function of } \tau$$

and, more explicitly,

$$\frac{\partial g(\tau,\rho)}{\partial\rho} = \beta(\tau)\, f(\tau,\rho)\, l(\tau,\rho).$$

We contend that the function $\beta(\tau)$ cannot vanish. In fact, if $\beta(\tau_0) = 0$ for some value τ_0 of τ, then

$$\frac{\partial g(\tau_0,\rho)}{\partial\rho} = 0$$

from which it follows that

$$g(\tau_0,\rho) = \text{constant}.$$

This condition is un-physical: Since a photon traveling radially to infinity, assigns the values of time τ_0 to every point of a ray, this condition implies that the curvature radius $g(\tau_0,\rho)$ is constant outside the matter at the instant τ_0. Consequently $\beta(\tau) \neq 0$, so that

$$\text{either} \quad \beta(\tau) > 0 \quad \text{or} \quad \beta(\tau) < 0 \quad \text{for every value of} \quad \tau.$$

But, since $f(\tau,\rho) > 0$ and $l(\tau,\rho) > 0$, the condition $\beta(\tau) < 0$ implies

$$\frac{\partial g(\tau,\rho)}{\partial\rho} < 0$$

and so the curvature radius $g(\tau,\rho)$ is a strictly decreasing function of ρ. **This last conclusion is also un-physical**.

Consequently $\beta(\tau) > 0$ for every τ, so that we can define the positive function

$$\alpha = \alpha(\tau) = \frac{1}{\beta(\tau)}$$

and write

$$fl = \alpha\frac{\partial g}{\partial\rho}$$

and so

$$f = \frac{\alpha}{l}\frac{\partial g}{\partial\rho}. \quad (18)$$

Consequently

$$\frac{\partial f}{\partial\rho} = -\frac{\alpha}{l^2}\frac{\partial l}{\partial\rho}\frac{\partial g}{\partial\rho} + \frac{\alpha}{l}\frac{\partial^2 g}{\partial\rho^2} \quad (19)$$

and inserting this expression into (14) we obtain

$$\rho^2 Q_{11} = -1 - \frac{2g}{\alpha\frac{\partial g}{\partial\rho}}\frac{\partial^2 g}{\partial\tau\partial\rho} + \frac{2g}{l^2}\frac{\partial^2 g}{\partial\rho^2} -$$
$$- \frac{2}{\alpha}\frac{\partial g}{\partial\tau} - \frac{2g}{l^3}\frac{\partial l}{\partial\rho}\frac{\partial g}{\partial\rho} + \frac{1}{l^2}\left(\frac{\partial g}{\partial\rho}\right)^2.$$

On account of (10), we can deduce that

$$0 = \left(\rho^2 Q_{11} + \frac{v^2}{g^2}\right)\frac{\partial g}{\partial\rho} =$$
$$= -\frac{\partial g}{\partial\rho} - \frac{2g}{\alpha}\frac{\partial g^2}{\partial\tau\partial\rho} + \frac{2g}{l^2}\frac{\partial^2 g}{\partial\rho^2}\frac{\partial g}{\partial\rho} - \frac{2}{\alpha}\frac{\partial g}{\partial\tau}\frac{\partial g}{\partial\rho} -$$
$$- \frac{2g}{l^3}\frac{\partial l}{\partial\rho}\left(\frac{\partial g}{\partial\rho}\right)^2 + \frac{1}{l^2}\left(\frac{\partial g}{\partial\rho}\right)^3 + \frac{v^2}{g^2}\frac{\partial g}{\partial\rho} =$$
$$= \frac{\partial}{\partial\rho}\left[-g - \frac{2g}{\alpha}\frac{\partial g}{\partial\tau} + \frac{g}{l^2}\left(\frac{\partial g}{\partial\rho}\right)^2 - \frac{v^2}{g}\right],$$

whence

$$-g-\frac{2g}{\alpha}\frac{\partial g}{\partial\tau}+\frac{g}{l^2}\left(\frac{\partial g}{\partial\rho}\right)^2-\frac{v^2}{g}=-2\mu=\text{function of }\tau$$

and so

$$\frac{\partial g}{\partial\tau}=\frac{\alpha}{2}\left[-1+\frac{2\mu}{g}-\frac{v^2}{g^2}+\frac{1}{l^2}\left(\frac{\partial g}{\partial\rho}\right)^2\right]. \tag{20}$$

To continue our discussion we need the following derivatives obtained by direct computation:

$$\frac{\partial^2 g}{\partial\tau\partial\rho}=\alpha\left[-\frac{\mu}{g^2}\frac{\partial g}{\partial\rho}+\frac{v^2}{g^3}\frac{\partial g}{\partial\rho}-\frac{1}{l^3}\frac{\partial l}{\partial\rho}\left(\frac{\partial g}{\partial\rho}\right)^2+\frac{1}{l^2}\frac{\partial g}{\partial\rho}\frac{\partial^2 g}{\partial\rho^2}\right], \tag{21}$$

$$\begin{aligned}\frac{\partial^3 g}{\partial\tau\partial\rho^2}=&\alpha\left[\frac{2\mu}{g^3}\left(\frac{\partial g}{\partial\rho}\right)^2-\frac{\mu}{g^2}\frac{\partial^2 g}{\partial\rho^2}-\frac{3v^2}{g^4}\left(\frac{\partial g}{\partial\rho}\right)^2+\frac{v^2}{g^3}\frac{\partial^2 g}{\partial\rho^2}+\right.\\&+\frac{3}{l^4}\left(\frac{\partial l}{\partial\rho}\right)^2\left(\frac{\partial g}{\partial\rho}\right)^2-\frac{1}{l^3}\frac{\partial^2 l}{\partial\rho^2}\left(\frac{\partial g}{\partial\rho}\right)^2-\frac{4}{l^3}\frac{\partial l}{\partial\rho}\frac{\partial l}{\partial\rho}\frac{\partial^2 g}{\partial\rho^2}+\\&\left.+\frac{1}{l^2}\left(\frac{\partial^2 g}{\partial\rho^2}\right)^2+\frac{1}{l^2}\frac{\partial g}{\partial\rho}\frac{\partial^3 g}{\partial\rho^3}\right].\end{aligned} \tag{22}$$

Consider now the equation (9). Since

$$\frac{\partial}{\partial\tau}\left[\frac{1}{fl}\frac{\partial(fl)}{\partial\rho}\right]=\frac{\partial}{\partial\tau}\left(\frac{\frac{\partial^2 g}{\partial\rho^2}}{\frac{\partial g}{\partial\rho}}\right)=\frac{\frac{\partial g}{\partial\rho}\frac{\partial^3 g}{\partial\tau\partial\rho^2}-\frac{\partial^2 g}{\partial\rho^2}\frac{\partial^2 g}{\partial\tau\partial\rho}}{\left(\frac{\partial g}{\partial\rho}\right)^2}$$

by taking into account (21) and (22), we find after some computations

$$\begin{aligned}\frac{\partial}{\partial\tau}\left[\frac{1}{fl}\frac{\partial(fl)}{\partial\rho}\right]=&\alpha\left[\frac{2\mu}{g^3}\frac{\partial g}{\partial\rho}-\frac{3v^2}{g^4}\frac{\partial g}{\partial\rho}+\frac{3}{l^4}\left(\frac{\partial l}{\partial\rho}\right)^2\frac{\partial g}{\partial\rho}-\right.\\&\left.-\frac{3}{l^3}\frac{\partial l}{\partial\rho}\frac{\partial^2 g}{\partial\rho^2}-\frac{1}{l^3}\frac{\partial^2 l}{\partial\rho^2}\frac{\partial g}{\partial\rho}+\frac{1}{l^2}\frac{\partial g^3}{\partial\rho^3}\right].\end{aligned}$$

On the other hand (19) leads to the relation

$$\frac{\partial}{\partial\rho}\left[\frac{1}{l}\frac{\partial f}{\partial\rho}\right]=\alpha\left[\frac{3}{l^4}\left(\frac{\partial l}{\partial\rho}\right)^2\frac{\partial g}{\partial\rho}-\frac{1}{l^3}\frac{\partial^2 l}{\partial\rho^2}\frac{\partial g}{\partial\rho}-\frac{3}{l^3}\frac{\partial l}{\partial\rho}\frac{\partial^2 g}{\partial\rho^2}+\frac{1}{l^2}\frac{\partial^3 g}{\partial\rho^3}\right].$$

Moreover by (21)

$$\frac{2}{g}\frac{\partial^2 g}{\partial\tau\partial\rho}=\alpha\left[-\frac{2\mu}{g^3}\frac{\partial g}{\partial\rho}+\frac{2v^2}{g^4}\frac{\partial g}{\partial\rho}-\frac{2}{l^3 g}\frac{\partial l}{\partial\rho}\left(\frac{\partial g}{\partial\rho}\right)^2+\frac{2}{l^2 g}\frac{\partial g}{\partial\rho}\frac{\partial^2 g}{\partial\rho^2}\right]$$

and

$$\frac{2}{lg}\frac{\partial f}{\partial\rho}\frac{\partial g}{\partial\rho}=\alpha\left[-\frac{2}{l^3 g}\frac{\partial l}{\partial\rho}\left(\frac{\partial g}{\partial\rho}\right)^2+\frac{2}{l^2 g}\frac{\partial g}{\partial\rho}\frac{\partial^2 g}{\partial\rho^2}\right].$$

Inserting these expressions into (13) we find, after cancelations,

$$\rho Q_{01}=-\alpha\frac{v^2}{g^4}\frac{\partial g}{\partial\rho}$$

so that

$$\rho\,Q_{01}+\frac{v^2}{g^4}fl=-\alpha\frac{v^2}{g^4}\frac{\partial g}{\partial\rho}+\frac{v^2}{g^4}\alpha\frac{\partial g}{\partial\rho}=0\,.$$

Consequently the equation (9) is verified.

It remains to examine the equation (16), which amounts to transform the expression (17). In principle, we need the derivatives

$$\frac{\partial^2 g}{\partial\tau^2}\quad\text{and}\quad\frac{\partial f}{\partial\tau}$$

expressed by means of l and g.

First we consider the expression of $\frac{\partial^2 g}{\partial\tau^2}$ resulting from the derivative of (20) with respect to τ and then replace in it the $\frac{\partial g}{\partial\tau}$ and $\frac{\partial^2 g}{\partial\tau\partial\rho}$, given by their expressions (20) and (21). We get:

$$\begin{aligned}2\frac{\partial^2 g}{\partial\tau^2}=&\frac{d\alpha}{d\tau}\left[-1+\frac{2\mu}{g}-\frac{v^2}{g^2}+\frac{1}{l^2}\left(\frac{\partial g}{\partial\rho}\right)^2\right]+\\&+\alpha\left[-\frac{2}{l^3}\frac{\partial l}{\partial\tau}\left(\frac{\partial g}{\partial\rho}\right)^2+\frac{2}{g}\frac{d\mu}{d\tau}\right]+\\&+\alpha^2\left[\frac{\mu}{g^2}-\frac{2\mu^2}{g^3}+\frac{3\mu v^2}{g^4}-\frac{3\mu}{l^2 g^2}\left(\frac{\partial g}{\partial\rho}\right)^2-\frac{v^2}{g^3}-\frac{v^4}{g^5}+\right.\\&\left.+\frac{3v^2}{l^2 g^3}\left(\frac{\partial g}{\partial\rho}\right)^2-\frac{2}{l^5}\left(\frac{\partial g}{\partial\rho}\right)^3\frac{\partial l}{\partial\rho}+\frac{2}{l^4}\left(\frac{\partial g}{\partial\rho}\right)^2\frac{\partial^2 g}{\partial\rho^2}\right].\end{aligned}$$

On the other hand taking the derivative of

$$f=\frac{\alpha}{l}\frac{\partial g}{\partial\rho}$$

with respect to τ and then, in the resulting expression, replace the expression of $\frac{\partial^2 g}{\partial\tau\partial\rho}$ given by equation (21) , we obtain

$$\begin{aligned}\frac{\partial f}{\partial\tau}=&\frac{d\alpha}{d\tau}\frac{1}{l}\frac{\partial g}{\partial\rho}-\frac{\alpha}{l^2}\frac{\partial l}{\partial\tau}\frac{\partial g}{\partial\rho}+\\&+\frac{\alpha^2}{l}\left[-\frac{\mu}{g^2}\frac{\partial g}{\partial\rho}+\frac{v^2}{g^3}\frac{\partial g}{\partial\rho}-\frac{1}{l^3}\frac{\partial l}{\partial\rho}\left(\frac{\partial g}{\partial\rho}\right)^2+\frac{1}{l^2}\frac{\partial g}{\partial\rho}\frac{\partial^2 g}{\partial\rho^2}\right].\end{aligned}$$

So, we have already obtained f, $\frac{\partial f}{\partial\tau}$, $\frac{\partial f}{\partial\rho}$, $\frac{\partial^2 g}{\partial\tau\partial\rho}$, $\frac{\partial^2 g}{\partial\tau^2}$, by means of l and g. Inserting them into (21), we get after some computations and several cancelations the relation

$$lQ_{00}-f\rho Q_{01}=\frac{2\alpha l}{g^2}\frac{d\mu}{d\tau}\,,$$

so that the equation (16) is written as

$$\frac{2\alpha l}{g^2}\frac{d\mu}{d\tau}=0$$

which implies

$$\frac{d\mu}{d\tau}=0$$

and so μ is a constant.

Later on we will prove that this constant is identified with the mass that produces the gravitational field. . . *

Submitted on July 12, 2010 / Accepted on July 14, 2010

References

1. Stavroulakis, N. On the stationary charged spherical source. *Progress in Physics*, 2009, v.2, 66–71.
2. Stavroulakis, N. Gravitation and electricity. *Progress in Physics*, 2008, v.2, 91–96.
3. Stavroulakis, N. On the gravitational field of a pulsating source. *Progress in Physics*, 2007, v.4, 3–8.
4. Stavroulakis, N. On the propagation of gravitation from a pulsating source. *Progress in Physics*, 2007, v.2, 75–82.
5. Stavroulakis, N. Non-Euclidean geometry and gravitation. *Progress in Physics*, 2006, v.2, 68–75.
6. Stavroulakis, N. On a paper by J. Smoller and B. Temple. *Annales de la Fondation Louis de Broglie*, 2002, v.27, no.3, 511–521.
7. Stavroulakis, N. Matière cache et relatitité générale. *Annales de la Fondation Louis de Broglie*, 2001, v.26, no. spécial, 411–427.
8. Stavroulakis, N. Vérité scientifique et trous noirs (quatrième partie). Determination de métriques $\Theta(4)$-invariantes. *Annales de la Fondation Louis de Broglie*, 2001, v.26, no.4, 743–764.
9. Stavroulakis, N. Vérité scientifique et trous noirs (troisième partie). Équations de gravitation relatives à une métrique $\Theta(4)$-invariante. *Annales de la Fondation Louis de Broglie*, 2001, v.26, no.4, 605–631.
10. Stavroulakis, N. Vérité scientifique et trous noirs (deuxmième partie). Symétries relatives au groupe des rotations. *Annales de la Fondation Louis de Broglie*, 2000, v.25, no.2, 223–266.
11. Stavroulakis, N. Vérité scientifique et trous noirs (premième partie). Les abus du formalisme. *Annales de la Fondation Louis de Broglie*, 1999, v.24, no.1, 67–109.
12. Stavroulakis, N. On the principles of general relativity and the $S\Theta(4)$-invariant metrics. *Proceedings of the 3rd Panhellenic Congress of Geometry*, Athens, Greece, 1997, 169–182.
13. Stavroulakis, N. Sur la function de propagation des ébranlements gravitationnels. *Annales de la Fondation Louis de Broglie*, 1995, v.20, no.1, 1–31.

*At this point, Professor Dr Nikias Stavroulakis laid the pen down for good, before writing the proofs of this latter important assertion and some of the claims found in the abstract and thus completing this very interesting work. — I. M. Roussos.

Spin-Dependent Transport through Aharonov-Casher Ring Irradiated by an Electromagnetic Field

Walid A. Zein*, Nabil A. Ibrahim†, and Adel H. Phillips*

*Faculty of Engineering, Ain-Shams University, Cairo, Egypt
†Higher Technological Institute, Ramadan Tenth City, Egypt
E-mail: adel_phillips@yahoo.com

The spin dependent conductance of mesoscopic device is investigated under the effect of infrared and ultraviolet radiation and magnetic field. This device is modeled as Aharonov-Casher semiconducting ring and a quantum dot is embedded in one arm of the ring. An expression for the conductance is deduced. The results show oscillatory behavior of the conductance. These oscillations might be due to Coulomb blockade effect and the interplay of Rashba spin orbit coupling strength with the induced photons of the electromagnetic field. The present device could find applications in quantum information processing (qubit).

1 Introduction

Advances in nanotechnology opened the way for the synthesis of artificial nanostructures with sizes smaller than the phase coherence length of the carriers [1]. The electronic properties of these systems are dominated by quantum effects and interferences [2]. One of the goals of semiconductor spintronics [3,4] is to realize quantum information processing based on electron spin. In the last decades, much attention is attracted by many scientists to study the spin-dependent transport in diverse mesoscopic systems, e.g., junctions with ferromagnetic layers, magnetic semiconductors, and low-dimensional semiconducting nanostructures [5, 6]. Coherent oscillations of spin state driven by a microwave field have been studied extensively [7–11].

Many authors investigated the spin transport through quantum rings [12–18]. These rings are fabricated out of two dimensional electron gas formed between heterojunction of III–V and II–VI semiconductors. Spin-orbit interaction (SOI) is crucial in these materials. The purpose of the present paper is to investigate the quantum spin transport in ring made of semiconductor heterostructure under the effect of infrared and ultraviolet radiations.

2 Theoretical treatment

In order to study the quantum spin characteristics of a mesoscopic device under the effect of both infrared (IR) and ultraviolet (UV) radiation, we propose the following model:

A semiconductor quantum dot is embedded in one arm of the Aharonov-Casher ring with radius comparable with the Fermi-wavelength of semiconductor heterostructure. This ring is connected to two conducting leads. The form of the confining potential is modulated by an external gate electrode allowing for direct control of the electron spin-orbit interaction. By introducing an external magnetic field, we also calculate the combined Aharonov-Casher, and Aharonov-Bohm conductance modulations. The conductance G for the present investigated device will be calculated using Landauer formula [17–19] as:

$$G = \frac{2e^2}{h} \sin\phi \sum_{\mu=1,2} dE \left(-\frac{\partial j_{FD}}{\partial E} \right) \left| \Gamma_{\mu,with\ photon}(E) \right|^2 , \quad (1)$$

where f_{FD} is the Fermi-Dirac distribution function, e is the electron charge, h is Planck's constant, ϕ is the electron phase difference propagating through the upper and lower arms of the ring, and $\left|\Gamma_{\mu,with\ photon}(E)\right|^2$ is the tunneling probability induced by the external photons.

Now, we can find an expression for the tunneling probability $\left|\Gamma_{\mu,with\ photon}(E)\right|^2$ by solving the following Schrodinger equation and finding the eigenfunctions for this system as follows:

$$\left(\frac{P^2}{2m^*} + V_d + eV_g + E_F + eV_{ac}\cos(\omega t) + \right.$$
$$\left. + \frac{\hbar eB}{2m^*} + \widehat{H}_{Soc} + eV_{Sd} \right) \psi = E\psi , \quad (2)$$

where V_d is the barrier height, V_g is the gate voltage, m^* is the effective mass of electrons, E_F is the Fermi-energy, B is the applied magnetic field, and V_{ac} is the amplitude of the applied infrared, and ultraviolet electromagnetic field with frequency ω. In (2) $\widehat{H}_{Soc}$ is the Hamiltonian due to the spin-orbit coupling which is expressed as:

$$\widehat{H}_{Soc} = \frac{\hbar^2}{2m^*a^2} \left(-i\frac{\partial}{\partial\phi} - \frac{\Phi_{AB}}{2\pi} - \frac{\omega_{Soc} m^* a^2}{\hbar}\, \sigma_r \right), \quad (3)$$

where $\omega_{Soc} = \alpha/(\hbar a)$ and it is called the frequency associated with the spin-orbit coupling,α is the strength of the spin-orbit coupling, a is the radius of the Aharonov-Casher ring, and σ_r is the radial part of the Pauli matrices which expressed in the components of Pauli matrices σ_x, σ_y as:

$$\begin{aligned} \sigma_r &= \sigma_x \cos\phi + \sigma_y \sin\phi, \\ \sigma_\phi &= \sigma_y \cos\phi - \sigma_x \sin\phi . \end{aligned} \quad (4)$$

Due to the application of magnetic field B, normal to the plane of the device, the Aharonov-Bohm phase will be picked up by an electron which encircling the following magnetic flux Φ_{AB}, see Eq. (3), as:

$$\Phi_{AB} = \frac{\pi e B a^2}{\hbar} . \tag{5}$$

Now, the solution of Eq. (2) will consist of four eigenfunctions [17, 18, 20], where $\psi_L(x)$ is the eigenfunction for transmission through the left lead, $\psi_R(x)$ for the right lead, $\psi_{up}(\theta)$ for the upper arm of the ring, and $\psi_{low}(\theta)$ for the lower arm of the ring. Their expressions are:

$$\psi_L(x,t) = \sum_{\sigma} \sum_{n=-\infty}^{\infty} J_n\left(\frac{eV_{ac}}{\hbar\omega}\right)\left[Ae^{ikx} + Be^{-ikx}\right]\chi^{\sigma}(\pi)\, e^{-in\omega t}, \tag{6}$$

$\chi \in [-\infty, 0]$

$$\psi_R(x,t) = \sum_{\sigma} \sum_{n=-\infty}^{\infty} J_n\left(\frac{eV_{ac}}{\hbar\omega}\right)\left[Ce^{ik'x} + De^{-ik'x}\right]\chi^{\sigma}(0)\, e^{-in\omega t}, \tag{7}$$

$\chi \in [0, \infty]$,

$$\psi_{up}(\theta,t) = \sum_{\sigma,\mu} \sum_{n=-\infty}^{\infty} J_n\left(\frac{eV_{ac}}{\hbar\omega}\right) F_{\mu} e^{in'^{\sigma}_{\mu}\phi} e^{-in\omega t}\chi^{\sigma}(\phi), \tag{8}$$

$\phi \in [0, \pi]$,

$$\psi_{low}(\theta,t) = \sum_{\sigma,\mu} \sum_{n=-\infty}^{\infty} J_n\left(\frac{eV_{ac}}{\hbar\omega}\right) G_{\mu} e^{in^{\sigma}_{\mu}\phi} e^{-in\omega t}\chi^{\sigma}(\phi), \tag{9}$$

$\phi \in [\pi, 2\pi]$

were $J_n(eV_{ac}/(\hbar\omega))$, Eqs. (6–9), is the n^{th} order Bessel function. The solutions, Eqs. (6–9), must be generated by the presence of the different side-bands n, which come with phase factor $\exp(-in\omega t)$. The parameter $\chi^{\sigma}(\phi)$ is expressed as:

$$\chi^1_n(\phi) = \begin{pmatrix} \cos(\theta/2) \\ e^{i\phi}\sin(\theta/2) \end{pmatrix} \tag{10}$$

and

$$\chi^2_n(\phi) = \begin{pmatrix} \sin(\theta/2) \\ -e^{i\phi}\cos(\theta/2) \end{pmatrix} \tag{11}$$

where the angle θ [17, 18, 21] is given by

$$\theta = 2\tan^{-1}\left(\frac{\Omega - \sqrt{\Omega^2 + \omega^2_{Soc}}}{\omega_{Soc}}\right) \tag{12}$$

in which Ω is given by

$$\Omega = \frac{\hbar}{2m^* a^2}. \tag{13}$$

Also, the parameters n'^{σ}_{μ} and n^{σ}_{μ} expressed respectively as:

$$n'^{\sigma}_{\mu} = \mu k' a - \phi + \frac{\Phi_{AB}}{2\pi} + \frac{\Phi^{\sigma}_{AC}}{2\pi} , \tag{14}$$

$$n^{\sigma}_{\mu} = \mu k a - \phi + \frac{\Phi_{AB}}{2\pi} + \frac{\Phi^{\mu}_{AC}}{2\pi} , \tag{15}$$

in which $\mu = \pm 1$ corresponding to the spin-up, and spin-down of the transmitted phase, expressed as [17, 18, 20]:

$$\Phi^{\mu}_{AC} = \pi\left[1 + \frac{(-1)^{\mu}\left(\omega^2_{Soc} + \Omega^2\right)^{1/2}}{\Omega}\right] . \tag{16}$$

The wave numbers k' and k are given respectively by

$$k' = \sqrt{\frac{2m^*(E + n\hbar\omega)}{\hbar^2}} , \tag{17}$$

and

$$k = \sqrt{\frac{2m^*}{\hbar^2}\left(V_d + eV_g + \frac{N^2e^2}{2C} + E_F + n\hbar\omega - E\right)}, \tag{18}$$

where V_d is the barrier height, V_g is the gate voltage, N is the number of electrons entering the quantum dot, C is the total capacitance of the quantum dot, e is the electron charge, E_F is the Fermi energy, m^* is the effective mass of electrons with energy E, and $\hbar\omega$ is the photon energy of both infrared and ultraviolet electromagnetic field.

Now, the tunneling probability $\left|\Gamma_{\mu,with\ photon}(E)\right|^2$ could be obtained by applying the Griffith boundary condition [15, 17, 18, 20, 21] to Eqs. (6–9). The Griffith boundary condition states that the eigenfunctions, Eqs. (6–9), are continuous and their current density is conserved at each intersection. Accordingly therefore, the expression for the tunneling probability is given by:

$$\left|\Gamma_{\mu\ with\ photons}(E)\right|^2 = \tag{19}$$

$$= \sum_n J^2_n \left[\frac{8i\cos\left(\frac{\Phi_{AB}+\Phi^{\mu}_{AC}}{2}\right)\sin(\pi k a)}{4\cos(2\pi k' a) + 4\cos\left(\Phi_{AB} + \Phi^{\mu}_{AC}\right) + 4\sin(2\pi k' a)}\right]^2 .$$

Now, substituting $\left|\Gamma_{\mu\ with\ photons}(E)\right|^2$, into Eq. (1), we get a full expression for the conductance G, which will be solved numerically as will be seen in the next section.

3 Result and discussion

Numerical calculations are performed for the conductance G as function of the gate voltage V_g, magnetic field B, and function of ω_{Soc} frequency due to spin-orbit coupling at specific values of photon energies, e.g., energies of infrared and ultraviolet radiations. The values of the following parameters

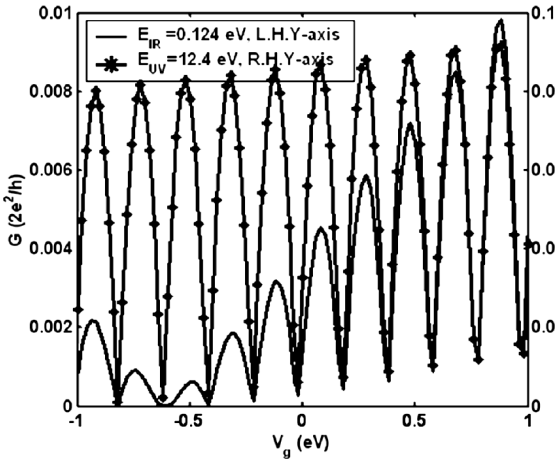

Fig. 1: The variation of the conductance G with the gate voltage V_g at different photon energy E_{IR} and E_{UV}.

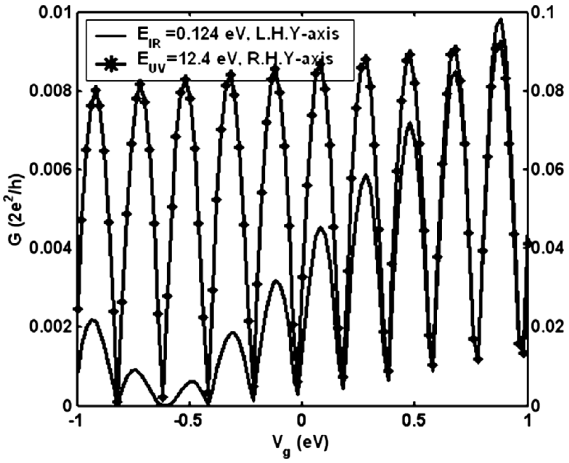

Fig. 3: The variation of the conductance G with the frequency ω_{Soc} at different photon energy E_{IR} and E_{UV}.

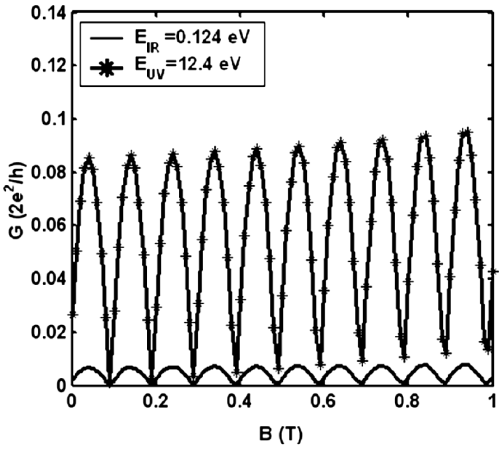

Fig. 2: The variation of the conductance G with the magnetic field B at different photon energy E_{IR} and E_{UV}.

have been found previous by the authors [22–24]. The values of $C \sim 10^{-16}$ F and $V_d \sim 0.47$ eV. The value of the number of electrons entering the quantum dot was varied as random number.

We use the semiconductor heterostructures as In Ga As/ In Al As. The main features of our obtained results are:

1. Fig. (1), shows the dependence of the conductance G, on the gate voltage V_g, at both photon energy of infrared (IR), and ultraviolet (UV) radiations. Oscillatory behavior is shown. For the case of infrared radiation, the peak height strongly increases as gate voltage increases from –0.5 to 1. But for the case ultraviolet, this increase in peak height is so small.
2. Fig. (2), shows the dependence of the conductance G, on the applied magnetic field B, at both the photon energies considered (IR and UV). A periodic oscillation is shown for the two cases, the periodicity equals the quantum flux h/e.
3. The dependence of the conductance G, on the frequency associated with the spin-orbit coupling, ω_{Soc}. at different values of the investigated applied photon energies is shown in Fig. 3.

The obtained results might be explained as follows: The oscillatory behavior of the conductance is due to spin-sensitive quantum interference effects caused by the difference in the Aharonov-Casher phase accumulated by the opposite spin states. The Aharonov-Casher phase arises from the propagation of the electron in the spin-orbit coupling. The quantum interference effect appears due to photon spin-up, and spin-down subbands coupling. Our results are found concordant with these in the literature [15, 16, 25].

4 Conclusion

The Aharonov-Casher, and Aharonov-Bohm effects are studied, taking into consideration the influence of both infrared (IR), and ultraviolet (UV) electromagnetic field. This could be realized by proposing a semiconducting quantum dot embedded in one arm of semiconducting ring. Spin filtering, and spin pumping due to the effect of photons are studied by deducing the spin transport conductance. The present results are valuable for the application in the field of quantum information processing (qubit) quantum bit read out, and writing.

Submitted on August 08, 2010 / Accepted on August 12, 2010

References

1. Heinzel T. Mesoscopic electronics in solid state nanostructures. Wiley-VCH Verlag Weinheim, 2003.
2. Mitin V.V., Sementsov D.I., and Vagidov N.Z. Quantum Mechanics for nanostructures. Cambridge University Press, Cambridge, 2010.
3. Awschalom D.D., Loss D., and Samart N., editors. Semiconductor spintronics and quantum computation. Spinger, New York, 2000.
4. Sahoo S., Kantos T., et al. *Nature Physics*, v.1, 2005, 99.
5. Zutic I., Fabian J., and Das Sarma S. *Rev. Mod. Phys.*, v.76, 2004, 323.

6. Parkin S.S.P. Applications of magnetic nanostructures. Taylor and Francis, NY, 2002.
7. Rashba E.J. and Efros A.L. *Phys. Rev. Lett.*, v.91, 2003, 126405.
8. Cheng J.L., Wu M.W. *Appl. Phys. Lett.*, v.86, 2005, 032107.
9. Jiang J.H., Weng M.Q., and Wu M.W. *J. Appl. Phys.*, v.100, 2006, 063709.
10. Tokura Y., van der Wiel W.G., Obata T., and Tarucha S, *Phys. Rev. Lett.*, v.96, 2006, 047202.
11. Duckheim M., and Loss D. *Nature Physics*, v.2, 2006, 195.
12. Meijer F.E., Morpurgo A.F., and Klapwijk T.M. *Phys. Rev. B*, v.66, 2002, 033107.
13. Frustaglia D. and Richter K. *Phys. Rev. B*, v.69, 2004, 235310.
14. Nitta J., Meijer F.E., and Takayanagi H. *Appl. Phys. Lett.*, v.75, 1999, 695.
15. Molnar B., Peeters F.M., and Vasilopoulos P. *Phys. Rev. B*, v.69, 2004, 155335.
16. Kovalev A.A., Borunda M.F., Jungwirth T., Molenkamp L.W., and Sinov J. *Phys. Rev. B*, v.76, 2007, 125307.
17. Zein W.A., Phillips A.H., and Omar O.A. *Progress in Physics*, v.4, 2007, 18.
18. Zein W. A., Phillips A.H. and Omar O.A. *NANO*, v.2, no.6, 2007, 389.
19. Datta S. Electronic transport in mesoscopic systems. Cambridge University Press, Cambridge, 1997.
20. Hentschel M., Schomerus H., Frustaglia D., and Richter K. *Phys. Rev. B*, v.69, 2004, 155326.
21. Goiffith S. *Trans. Faraday Soc.*, v.49, 1953, 345.
22. Phillips A.H., Mina A.N., Sobhy M.S., and Fouad E.A. *J. Computational and Theoretical Nanoscience*, v.4, 2007, 174.
23. Aly A.H., Hong J., and Phillips A.H. *International J. of Modern Phys. B*, v.20, no.16, 2006, 2305.
24. Aly A.H., and Phillips A.H. *Phys. Stat. Sol. B*, v.232, no.2, 2002, 283.
25. Moskalenko A.S., Matos-Abiague A., and Berakdar J. *Europhys. Lett.*, v.78, 2007, 57001.

Fractal Structure of Nature's Preferred Masses: Application of the Model of Oscillations in a Chain System

Andreas Ries and Marcus Vinicius Lia Fook

Universidade Federal de Campina Grande, Unidade Acadêmica de Engenharia de Materiais, Rua Aprígio Veloso 882, 58429-140 Campina Grande — PB, Brazil
E-mail: andreasries@yahoo.com, marcusvinicius@dema.ufcg.edu.br

A numerical analysis of elementary particle masses on the logarithmic number line revealed systematic mass gaps of $2e$, e, $\frac{e}{2}$, $\frac{e}{4}$, $\frac{e}{8}$ and $\frac{e}{16}$. Also in abundance data of the chemical elements, a repeated abundance gap of $\frac{e}{2}$ could be detected. This lead us to modify a fractal scaling model originally published by Müller in this journal, interpreting elementary particles as proton resonances. We express a set of 78 accurately determined particle masses on the logarithmic scale in a continued fraction form where all numerators are Euler's number.

1 Introduction

Recently in three papers of this journal, Müller [1–3] has proposed a chain of similar harmonic oscillators as a new model to describe the fractal properties of nature. For a specific process or data set, this model treats observables such as energies, frequencies, lengths and masses as resonance oscillation modes and aims at predicting naturally preferred values for these parameters. The starting point of the model is the fact that hydrogen is the most abundant element in the universe and therefore the dominant oscillation state. Consequently, Müller calculates the spectrum of eigenfrequencies of a chain system of many proton harmonic oscillators according to a continued fraction equation [2]

$$f = f_p \exp S \,, \tag{1}$$

where f is any natural oscillation frequency of the chain system, f_p the oscillation frequency of one proton and S the continued fraction corresponding to f. S was suggested to be in the canonical form with all partial numerators equal 1 and the partial denominators are positive or negative integer values

$$S = n_0 + \cfrac{1}{n_1 + \cfrac{1}{n_2 + \cfrac{1}{n_3 + \ldots}}} \,. \tag{2}$$

Particularly interesting properties arise when the nominator equals 2 and all denominators are divisible by 3. Such fractions divide the logarithmic scale in allowed values and empty gaps, i.e. ranges of numbers which cannot be expressed with this type of continued fractions. He showed that these continuous fractions generate a self-similar and discrete spectrum of eigenvalues [1], that is also logarithmically invariant. Maximum spectral density areas arise when the free link n_0 and the partial denominators n_i are divisible by 3.

This model was applied to the mass distribution of celestial bodies in our solar system [2] as well as to the mass distribution of elementary particles such as baryons, mesons, leptons and gauge bosons [3]. The masses were found to be located at or close to spectral nodes and definitively not random.

In this article we investigated the properties of masses in the micro-cosmos on the logarithmic scale by a graphical analysis with particular interest in detection of periodic trends. We analyzed abundance data of the chemical elements, atomic masses and the masses of elementary particles. Then we applied a slightly modified version of Müller's fractal model and demonstrate that there is a hidden structure in the masses of elementary particles.

2 Data sources and computational details

Solar system abundance data of chemical elements (with uncertainties of around 10%) were taken from reference [4]. High accuracy nuclide masses are given in an evaluation by Audi [5]. Relative isotope abundances for a selected chemical element can be found in the CRC Handbook of Chemistry and Physics [6]. Accurate masses of elementary particles are given in Müller's article [3] and were used for the calculation of continued fractions. In order to avoid machine based rounding errors, numerical values of continued fractions were always calculated using the the Lenz algorithm as indicated in reference [7].

3 Results

Figure 1 shows the relative abundance of the chemical elements in a less usual form. In textbooks or articles these data are normally presented as $log_{10}(abundance)$ versus atomic number on a linear scale. Here we adopted Müller's formalism and present the abundance data as a function of the natural logarithm of the atomic masses (here mean values from a periodic table were used) which were previously divided by the lowest atomic weight available (hydrogen). As can be seen, there is a general trend of decreasing abundance with increasing atomic mass, but the plot has a few remarkable extremities.

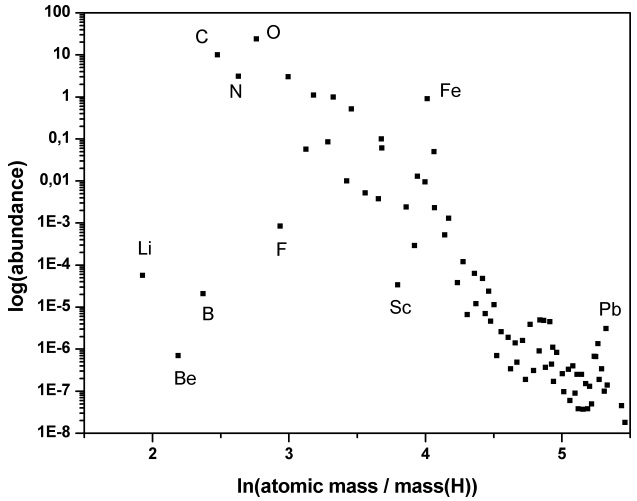

Fig. 1: Solar system abundance data of the chemical elements on a logarithmic scale. H and He omitted for clarity.

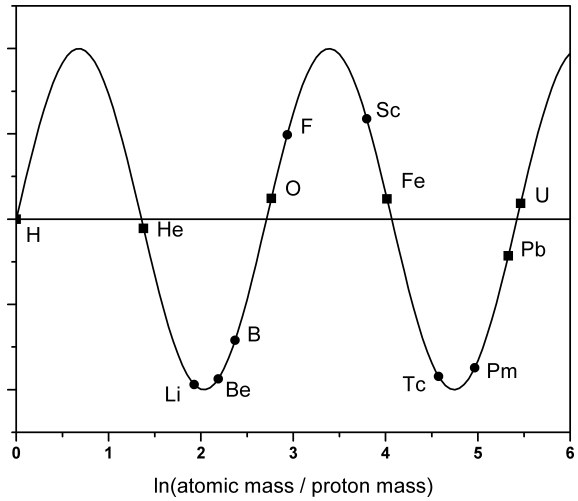

Fig. 2: Abundance maxima and minima of chemical elements on the logarithmic number line.

Nuclide	$\ln \frac{m(nuclide)}{m(\mathrm{H})}$	multiples of $\frac{e}{2}$
$^{1}_{1}$H	0.0	$0.0 \times \frac{e}{2}$
$^{4}_{2}$He	1.379	$1.015 \times \frac{e}{2}$
$^{16}_{8}$O	2.764	$2.034 \times \frac{e}{2}$
$^{56}_{26}$Fe	4.016	$2.955 \times \frac{e}{2}$
$^{208}_{82}$Pb	5.330	$3.921 \times \frac{e}{2}$

Table 1: $\ln \frac{m(nuclide)}{m(\mathrm{H})}$ of element abundance maxima expressed in multiples of $\frac{e}{2}$.

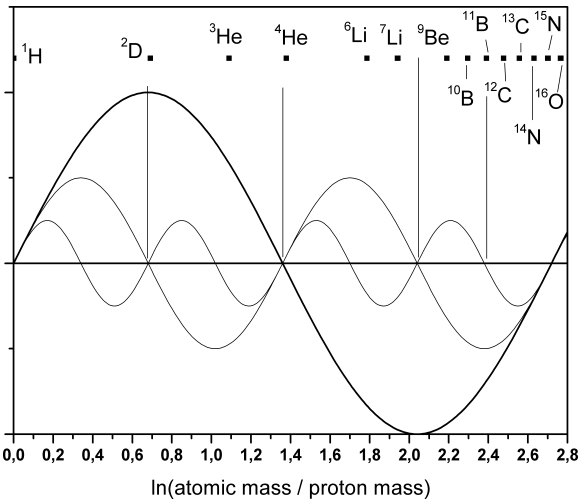

Fig. 3: Stable isotopes on the logarithmic scale in the range 0 to e.

Elements marking very clear maxima or minima are labeled with symbols. The most relevant maxima in graph are elements O, Fe and Pb. Of course, H and He, the most abundant elements in the universe (not shown in Fig. 1) must also be interpreted as maxima in the figure. From Figure 2 it becomes directly clear that these abundance maxima occur in almost equal distances on the logarithmic number line. The simple calculation $\ln \frac{m(^4_2\mathrm{He})}{m(^1_1\mathrm{H})} - \ln \frac{m(^1_1\mathrm{H})}{m(^1_1\mathrm{H})} = 1.37$ reveals that these distance seems to be $\frac{e}{2}$, where e is Euler's number. When drawing a sine function with period e, $f(x) = \sin(\frac{2\pi x}{e})$ on the logarithmic number line, the abundance maxima are closely located to the zeros of this function.

Table 1 summarizes the numerical deviations from multiples of $\frac{e}{2}$. The calculations were performed for the naturally most abundant isotope of the considered element.

Figure 2 has some analogy to Kundt's famous experiment with standing sound waves in a tube. It seems as a standing wave on the logarithmic number line supporting an accumulation of naturally preferred mass particles in the nodes, which are multiples of $\frac{e}{2}$. On the other hand these preferred masses are not exactly located in the notes, more evidently the less abundant chemical elements (Li, Be, B, F) are more distant from the bulges than H, He, O, Fe and U from the nodes. Pm and Tc are even completely absent in the abundance data due to their radioactivity.

Within the first period of the sine function in Fig. 2, very few stable isotopes are found. So it is possible to analyze the location of their isotope masses in relation to nodes of the previously constructed sine function including higher harmonics. Figure 3 displays the logarithmic axis from zero to e with a sine function of period e and two corresponding (2nd and 4th) higher harmonics defined through repeated frequency doubling. The location ($= \ln \frac{m_{nuclide}}{m_{proton}}$) of all existing stable isotopes in that range is indicated. From this, similar wave stabilizations regarding these light isotopes can be obtained:

1. Deuterium is a stable, but hardly abundant hydrogen isotope. It seems to be stabilized by the second harmonics with period $\frac{e}{2}$ due to location in the node (tritium does not fit in a node of this wave). Possibly hy-

drogen isotopes are principally governed by the basic wave with period e and the influence of higher harmonics is greatly reduced, which explains the low abundance.

2. Why is the isotope ^{4}He (99.999%) much more abundant than ^{3}He (0.0001%)? Assuming that He is principally governed as H by the wave with period e, the isotope ^{4}He is closer to the node than ^{3}He. In this case the higher stability of ^{4}He can also explained with the magic numbers for both, protons and neutrons.
3. Lithium is composed of 92.5% ^{7}Li and 7.5% ^{6}Li. The isotope ^{7}Li is more abundant and clearly closer to a node of the second harmonic (it has also a little higher bonding energy per nucleon than ^{6}Li).
4. The isotope ^{11}B is exactly located in the node of the third harmonic with period $\frac{e}{4}$. It is much more abundant (80.1%) than ^{10}B (19.9%).
5. The isotope ^{12}C is closer to the node of the fourth harmonics than ^{13}C. This is in agreement with the abundances of 98.0% for ^{12}C and 1.1% for ^{13}C.
6. Nitrogen is composed of 99.63% ^{14}N and 0.36% ^{15}N. The isotope ^{15}N is almost in the node of the basic wave and all higher harmonics. Here the model fails to predict the correct abundance order, but the isotope ^{15}N has the higher stability, which can be readily confirmed by the magic number of 8 neutrons in this nuclide. For a certain reason, the nuclide stability does not go along with the corresponding abundance. For an explanation of this fact must be considered that elements heavier than He cannot be built up in our sun or similar present-day (second generation) stars [8]. This is due to the fact that for all nuclei lighter than carbon, a nuclear reaction with a proton leads to the emission of an alpha particle disintegrating the original nucleus. So the heavier elements in stars must already have existed prior to the second generation star formation. Bethe [8] investigated possible nuclear reactions of both nitrogen isotopes and found that ^{15}N can give a $p-\alpha$ reaction

$$^{15}\mathrm{N} + {}^{1}\mathrm{H} \rightarrow {}^{4}\mathrm{He} + {}^{12}\mathrm{C}$$

while ^{14}N can only capture a proton

$$^{14}\mathrm{N} + {}^{1}\mathrm{H} \rightarrow {}^{15}\mathrm{O} + \gamma.$$

According to Bethe, such a $p-\alpha$ reaction is always more probable than a radiative capture. So we theorize that without existence of the above mentioned nuclear reaction, the abundance data would show an excess of ^{15}N.

A nuclear reaction also explains why lead is the element with the highest deviation from such a node (Fig. 2). We believe that Pb does actually not present its true abundance value as existed through stellar element formation, its abundance is increased since it is the end product of the 3 most important decay chains (thorium series, uranium series, actinium series). There are no stable isotopes between Pb and ^{238}U, which has a long half-life. The element uranium lies much more close to a node than Pb, and also because of its long half-life, we believe that this nuclide could be a former abundance maximum.

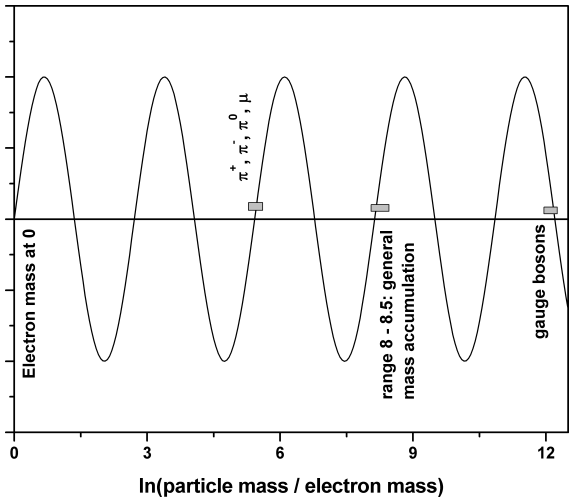

Fig. 4: Accumulation of particle masses on the logarithmic scale.

In order to find similar regularities for elementary particles we selected according to some physics textbooks a set of commonly discussed particles. Their importance was mainly justified by the relatively long lifetimes ($> 10^{-19}$ s). We believe that nature's preferred masses are the more stable particles and particularly for these masses some regularities could be expected. Table 2 presents the considered set of particles, their rest masses and positions on the logarithmic scale. It was found that the particles produce an interesting set of mass distances on the logarithmic number line: $2e$, e, $\frac{e}{2}$, $\frac{e}{4}$, $\frac{e}{8}$ and $\frac{e}{16}$. These mass gaps are listed in Table 3. There is, however, no standing wave analogy on the logarithmic scale that can be applied to all particles, consequently here, another model must be applied, which lead us to modify Müller's continued fraction term in an empirical way. However, the standing wave analogy is not completely absent. Müller [3] has shown that the majority of baryon and meson masses is in the range of 1300–8600 MeV/c^2. When scaling according to $\ln \frac{m_{particle}}{m_{electron}}$, this range translates to 8–8.5 on the logarithmic scale and it becomes clear that this range and as well as the masses of the electron, muon, pion and gauge bosons are in proximity of the zeros of the above considered sine function (see Figure 4).

Considering the framework of Müller's fractal scaling model, we interpret these numerical regularities as follows: Masses in nature are in relation to proton resonance states. Nature can realize various masses, only when they are close to proton resonance states, they are preferred masses. For stable particles such as nuclides, the term "preferred mass" translates to more abundance. For unstable particles, "preferred mass" translates to more realization probability. Un-

Particle	Rest mass m [MeV/c^2]	$\ln \frac{m(particle)}{m(proton)}$
Leptons:		
Electron	0.511	−7.515
μ	105.658	−2.183
τ	1776.84	0.638
Mesons:		
$\pi^{\pm}$	139.57	−1.905
π^0	134.9766	−1.939
$K^{\pm}$	493.677	−0.642
K^0_S, K^0_L	497.614	−0.634
η	547.853	−0.538
$\rho^{\pm}$	770	−0.198
ρ^0	775.5	−0.191
ω	782.6	−0.181
η^0	957.8	0.021
$K^{*\pm}$	891.7	−0.051
K^{*0}	896.0	−0.046
ϕ	1019.5	0.083
$D^{\pm}, D^0$	1869.6	0.689
$D^{\pm}_s$	1968.5	0.741
J/Ψ	3096.9	1.194
$B^{\pm}, B^0$	5279.2	1.727
Y	9460.3	2.311
Baryons:		
p	938.272	0
n	939.56	0.001
Λ^0	1115.6	0.173
Σ^+	1189.4	0.237
Σ^0	1192.5	0.240
Σ^-	1197.3	0.244
$\Delta^{\pm}, \Delta^{++}, \Delta^0$	1232	0.272
Ξ^0	1314.9	0.337
Ξ^-	1321.3	0.342
Ω	1672	0.578
Λ^+_C	2281	0.888
Λ^0_b	5624	1.791
Ξ_b	5774	1.817
Ξ^{-*}, Ξ^{0*}	15300	2.792

Table 2: Selected particles with rest masses and values on the logarithmic number line.

Particle mass step	Rest mass difference on logarithmic scale	Numerical result
Mass gap 2*e* (= 5.436):		
Electron → μ	$\lvert -7.515 - -2.183\rvert$	5.332
Mass gap *e* (= 2.718):		
$p \to \Xi^{-*}, \Xi^{0*}$	$\lvert 0 - 2.792\rvert$	2.792
Mass gap $\frac{e}{2}$ (= 1.359):		
$\pi^0 \to K^{\pm}$	$\lvert -1.939 - -0.642\rvert$	1.297
$\Xi^0 \to B^{\pm}, B^0$	$\lvert 0.337 - 1.727\rvert$	1.390
$\Lambda^+_C \to Y$	$\lvert 0.888 - 2.311\rvert$	1.423
Mass gap $\frac{e}{4}$ (= 0.68):		
$K^0_S, K^0_L \to p$	$\lvert -0.634 - 0\rvert$	0.634
$\Lambda^0 \to \Lambda^+_C$	$\lvert 0.173 - 0.888\rvert$	0.715
$p \to D^{\pm}, D^0$	$\lvert 0 - 0.689\rvert$	0.689
$p \to D^{\pm}_s$	$\lvert 0 - 0.741\rvert$	0.741
$p \to \tau$	$\lvert 0 - 0.638\rvert$	0.638
Mass gap $\frac{e}{8}$ (= 0.34):		
$\eta \to \rho^{\pm}$	$\lvert -0.538 - -0.198\rvert$	0.340
$p \to \Xi^0$	$\lvert 0 - 0.337\rvert$	0.337
$p \to \Xi^-$	$\lvert 0 - 0.342\rvert$	0.342
$\eta \to \rho^0$	$\lvert -0.538 - -0.191\rvert$	0.347
$\eta \to \rho^{\pm}$	$\lvert -0.538 - -0.198\rvert$	0.340
$\Sigma^+ \to \Omega$	$\lvert 0.237 - 0.578\rvert$	0.341
$\Sigma^0 \to \Omega$	$\lvert 0.240 - 0.578\rvert$	0.338
$\Sigma^- \to \Omega$	$\lvert 0.244 - 0.578\rvert$	0.334
$\Lambda^+_C \to J/\Psi$	$\lvert 0.888 - 1.194\rvert$	0.306
$\Omega \to \Lambda^+_C$	$\lvert 0.578 - 0.888\rvert$	0.310
Mass gap $\frac{e}{16}$ (= 0.17):		
$\omega \to p$	$\lvert -0.181 - 0\rvert$	0.181
$\rho^{\pm} \to p$	$\lvert -0.198 - 0\rvert$	0.198
$\rho^0 \to p$	$\lvert -0.191 - 0\rvert$	0.191
$p \to \Lambda^0$	$\lvert 0 - 0.173\rvert$	0.173
$\Lambda^0 \to \Xi^0$	$\lvert 0.173 - 0.337\rvert$	0.164
$\Lambda^0 \to \Xi^-$	$\lvert 0.173 - 0.342\rvert$	0.169
$\Omega \to D^{\pm}_s$	$\lvert 0.578 - 0.741\rvert$	0.163
$D^{\pm}_s \to \Lambda^+_C$	$\lvert 0.741 - 0.888\rvert$	0.147
$D^{\pm}, D^0 \to \Lambda^+_C$	$\lvert 0.689 - 0.888\rvert$	0.199

Table 3: Mass gaps between elementary particles on the logarithmic scale.

Particle	Particle mass with standard deviation. Continued fraction representation
N-baryons (S=0, I=1/2):	
p	938.27203 ±0.00008 [0; 0]
n	939.565346 ±0.000023 [0; 0 | 1973]
Λ-baryons (S=−1, I=0):	
Λ	1115.683 ±0.006 [0; 0 | 15, $e+1$, 15, −6]
$\Lambda(1520)$	1519.5 ±1.0 [0; 0 | 6, −9, $e+1$, $-e-1$, ***]
Σ-baryons (S=−1, I=1):	
Σ^+	1189.37 ±0.07 [0; 0 | 12, −6, $e+1$, $-e-1$, 6]
Σ^0	1192.642 ±0.024 [0; 0 | 12, $-e-1$, −9, $e+1$, $-e-1$, ***]
Σ^-	1197.449 ±0.03 [0; 0 | 12, $-e-1$, 6, $-e-1$, $e+1$, $-e-1$]
$\Sigma(1385)^+$	1382.8 ±0.4 [0; 0 | 6, $e+1$, $-e-1$, ***]
$\Sigma(1385)^0$	1383.7 ±1.0 [0; 0 | 6, $e+1$, $-e-1$, $e+1$, $-e-1$]
$\Sigma(1385)^-$	1387.2 ±0.5 [0; 0 | 6, $e+1$, $-e-1$, $e+1$, $e+1$]
Ξ-baryons (S=−2, I=1/2):	
Ξ^0	1314.86 ±0.2 [0; 0 | 9, $-e-1$, $e+1$, −6]
Ξ^-	1321.71 ±0.07 [0; 0 | 9, $-e-1$, $e+1$, ***]
$\Xi(1530)^0$	1531.8 ±0.32 [0; 0 | 6, −6]
$\Xi(1530)^-$	1535.0 ±0.6 [0; 0 | 6, −6, 9]
Ω-baryons (S=−3, I=0):	
Ω^-	1672.45 ±0.29 [0; 0 | $e+1$, $e+1$, $-e-1$, $e+1$, $-e-1$, $-e-1$] [1.5; 0 | $-e-1$, $e+1$, −15, 6]
charmed baryons (C = +1):	
Λ_C^+	2286.46 ±0.14 [1.5; 0 | $-e-1$, $-e-1$, 45, −15]
$\Lambda_C(2595)^+$	2595.4 ±0.6 [1.5; 0 | −6, 6, $e+1$, $-e-1$, ***]
$\Lambda_C(2625)^+$	2628.1 ±0.6 [1.5; 0 | −6, 12, 6]
$\Lambda_C(2880)^+$	2881.53 ±0.35 [1.5; 0 | −6, $-e-1$, $e+1$, ***]

Table 4: Continued fraction representation of particle masses according to equation (4).

Particle	Particle mass with standard deviation. Continued fraction representation
charmed baryons (C = +1):	
$\Sigma_C(2455)^{++}$	2454.02 ±0.18 [1.5; 0 | −6, $e+1$, $-e-1$, $e+1$, $e+1$, $-e-1$, $e+1$]
$\Sigma_C(2455)^+$	2452.9 ±0.4 [1.5; 0 | −6, $e+1$, $-e-1$, $e+1$, $e+1$]
$\Sigma_C(2455)^0$	2453.76 ±0.18 [1.5; 0 | −6, $e+1$, $-e-1$, $e+1$, $e+1$, $-e-1$]
Ξ_c^+	2467.8 ±0.6 [0; 0 | $e+1$, $-e-1$, $e+1$, 60] [1.5; 0 | −6, $e+1$, $-e-1$, −15]
Ξ_c^0	2470.88 ±0.8 [0; 0 | $e+1$, $-e-1$, $e+1$, −162] [1.5; 0 | −6, $e+1$, $-e-1$, −6]
$\Xi_c(2645)^+$	2645.9 ±0.6 [1.5; 0 | −6, 21, −6]
$\Xi_c(2645)^0$	2645.9 ±0.5 [1.5; 0 | −6, 21, −6]
$\Xi_c(2815)^+$	2816.6 ±0.9 [1.5; 0 | −6, $-e-1$, 12]
$\Xi_c(3080)^+$	3077.0 ±0.4 [1.5; 0 | −9, 9, 18]
light unflavored mesons (S = C = B = 0):	
$\pi^\pm$	139.57018 ±0.00035 [1.5; −3 | −6, $-e-1$, 18, $-e-1$, $e+1$, $-e-1$, $e+1$]
π^0	134.9766 ±0.0006 [1.5; −3 | −6, −15, $e+1$, $-e-1$, −33]
η	547.853 ±0.024 [0; 0 | −6, $e+1$, $-e-1$, 6, $-e-1$, 12] [1.5; −3 | $e+1$, $-e-1$, $e+1$, 9, $-e-1$, $-e-1$]
$\rho(770)$	775.49 ±0.34 [0; 0 | −15, $-e-1$]
$\omega(782)$	782.65 ±0.12 [0; 0 | −15]
$\rho'(958)$	957.78 ±0.06 [0; 0 | 132]
$\phi(1020)$	1019.455 ±0.02 [0; 0 | 33, −12, $e+1$]
$f_1(1285)$	1281.8 ±0.6 [0; 0 | 9, −9, −6]
$a_2(1320)$	1318.3 ±0.6 [0; 0 | 9, $-e-1$, $e+1$, $-e-1$, $e+1$, $-e-1$]
$f_1(1420)$	1426.4 ±0.9 [0; 0 | 6, 6, −6]
strange mesons (S =±1, C = B = 0):	
$K^\pm$	493.667 ±0.016 [0; 0 | $-e-1$, −6, $e+1$, 39]
K^0	497.614 ±0.024 [1.5; −3 | $e+1$, $-e-1$, $-e-1$, $e+1$, $-e-1$]

Particle	Particle mass with standard deviation. Continued fraction representation
strange mesons (S =±1, C = B = 0):	
$K^*(892)^{\pm}$	891.66 ±0.26 [0; 0 | −54, e+1]
$K^*(892)^0$	896.00 ±0.25 [0; 0 | −60, e+1]
charmed mesons (S =±1):	
$D^{\pm}$	1869.62 ±0.2 [0; 0 | e+1, 12, 24]
D^0	1864.84 ±0.17 [0; 0 | e+1, 12, −e−1, −e−1]
$D^*(2007)^0$	2006.97 ±0.19 [0; 0 | e+1, −18, −e−1, e+1, −e−1] [1.5; 0 | −e−1, 63]
$D^*(2010)^{\pm}$	2010.27 ±0.17 [0; 0 | e+1, −18, −216] [1.5; 0 | −e−1, 78]
charmed, strange mesons (C = S =±1):	
$D_s^{\pm}$	1968.49 ±0.34 [0; 0 | e+1, −54]
$D_s^{*\pm}$	2112.3 ±0.5 [1.5; 0 | −e−1, −12, 15]
$D_{S0}^*(2317)^{\pm}$	2317.8 ±0.6 [0; 0 | e+1, −e−1, −27] [1.5; 0 | −e−1, −e−1, 6, −e−1, −e−1]
$D_{S1}(2460)^{\pm}$	2459.6 ±0.6 [0; 0 | e+1, −e−1, e+1, 12] [1.5; 0 | −6, e+1, −e−1, 9]
$D_{S1}(2536)^{\pm}$	2535.35 ±0.34 [0; 0 | e+1, −e−1, e+1, −e−1, e+1, e+1] [1.5; 0 | −6, e+1, e+1, e+1]
$D_{S2}(2573)^{\pm}$	2572.6 ±0.9 [1.5; 0 | −6, 6, −15]
bottom mesons (B =±1):	
$B^{\pm}$	5279.17 ±0.29 [1.5; 0 | 12, −54]
B^0	5279.5 ±0.3 [1.5; 0 | 12, −51]
B^*	5325.1 ±0.5 [1.5; 0 | 12, −6, 6]
bottom, strange mesons (S = B =±1):	
B_S^0	5366.3 ±0.6 [1.5; 0 | 12, −e−1, 6, −e−1]
cc-mesons (S = B =±1):	
$J/\Psi(1S)$	3096.916 ±0.011 [1.5; 0 | −9, 24]
$X_{c0}(1P)$	3414.75 ±0.31 [1.5; 0 | 12, −e−1, e+1, ***]
$X_{c1}(1P)$	3510.66 ±0.07 [1.5; 0 | −15, −45]
$h_c(1P)$	3525.67 ±0.32 [1.5; 0 | −15, −6, −6]

Particle	Particle mass with standard deviation. Continued fraction representation
cc-mesons (S = B =±1):	
$X_{c2}(1P)$	3556.20 ±0.09 [1.5; 0 | −15, −e−1, e+1, ***]
$\Psi(2S)$	3686.09 ±0.04 [1.5; 0 | −21, 9, −e−1, e+1, ***]
$\Psi(3770)$	3772.92 ±0.35 [1.5; 0 | −24, −e−1, e+1, ***]
$X(3872)$	3872.3 ±0.8 [1.5; 0 | −33]
$Y(1S)$	9460.3 ±0.26 [0; 3 | −e−1, −12, −87]
$X_{b0}(1P)$	9859.44 ±0.42 [0; 3 | −e−1, −6, 9, −15] [1.5; 0 | e+1, −6, e+1, −6, e+1, −e−1]
$X_{b1}(1P)$	9892.78 ±0.26 [1.5; 0 | e+1, −6, e+1, −e−1, e+1, −9]
$X_{b2}(1P)$	9912.21 ±0.26 [0; 3 | −e−1, −6, e+1, 15, −e−1]
$Y(2S)$	10023.76 ±0.31 [0; 3 | −e−1, −e−1, −e−1, −e−1] [1.5; 0 | e+1, −e−1, −e−1, e+1, 12, −e−1]
$X_{b0}(2P)$	10232.5 ±0.4 [0; 3 | −e−1, −e−1, 327] [1.5; 0 | e+1, −e−1, −6, −e−1, e+1, −e−1]
$X_{b1}(2P)$	10255.46 ±0.22 [0; 3 | −e−1, −e−1, 30, 6]
$X_{b2}(2P)$	10268.65 ±0.22 [0; 3 | −e−1, −e−1, 21, −e−1] [1.5; 0 | e+1, −e−1, −9, 6, 6]
$Y(3S)$	10355.2 ±0.5 [0; 3 | −e−1, −e−1, 6, e+1, 6] [1.5; 0 | e+1, −e−1, −18, 9]
leptons:	
Electron	0.510998910 ±0.000000013 [1.5; −9 | −177]
μ	105.658367 ±0.000004 [0; −3 | e+1, −6, −e−1, e+1, ***]
τ	1776.84 ±0.17 [0; 0 | e+1, 6, −e−1, e+1, −e−1, −e−1]
gauge bosons:	
W	80398 ±25 [1.5; 3 | −54, −e−1, e+1]
Z	91187.6 ±2.1 [1.5; 3 | 36, −6, e+1]

fortunately, these simple graphs do not provide information to distinguish between stable and unstable particles. The repeatedly occurring mass gaps from $2e$ to $\frac{e}{16}$ strongly support the idea that masses in the micro-cosmos are not random and have a self-similar, fractal structure. However, we emphasize that this fractal behavior is only a statistical influence with low priority, since we know for instance that nature realizes with the chemical elements easily the whole logarithmic mass range from 0 to $2e$ without significant mass gaps. Also it should be noted that the logarithmic mass differences in Table 3 are always approximately multiples of the fractions of e. This means the fractal property provides only a signature of regularities, becoming visible only on the logarithmic number line.

Due to the fact that frequently mass distances occur which are close, but not exactly a fraction of e, we decided to modify Müller's continued fractions (given in equation(2)). Specifically we abandon the canonical form and change all partial numerators to Euler's number. Furthermore we follow results published by Müller in one of his patents [9] and introduce a phase shift p in equation (2). According to [9] the phase shift can only have the values 0 or ± 1.5. So we write

$$\ln \frac{particle\ mass}{proton\ mass} = p + S\ , \tag{3}$$

where S is the continued fraction

$$S = n_0 + \cfrac{e}{n_1 + \cfrac{e}{n_2 + \cfrac{e}{n_3 + \dots}}}\ . \tag{4}$$

We abbreviate $p + S$ as $[p; n_0 \mid n_1, n_2, n_3, \dots]$. Provided that our initial assumption is correct, and the particles are resonance states, their masses should be located in the maximum spectral density areas. Consequently we must require that the free link n_0 and the partial denominators n_i are integers divisible by 3. For convergence reason, we have to include $|e + 1|$ as allowed partial denominator. This means the free link n_0 is allowed to be $0, \pm 3, \pm 6, \pm 9 \dots$ and all partial denominators n_i can take the values $e + 1, -e - 1, \pm 6, \pm 9, \pm 12 \dots$ In order to test the model very critically for a more extended set of particles we followed Müller's article [3] and selected all elementary particles which have their masses determined with a standard deviation $\leqslant 1$ MeV/c^2 and included additionally the gauge bosons due to their special importance (78 particles altogether). For the calculation of the continued fractions we assumed first that the mass values were without any measurement error. This means, equation (3) does not hold and one ideally obtains a continued fraction with an infinite number of partial denominators. For practical reasons we determined only 18 partial denominators. Next we calculated repeatedly the particle mass from the continued fraction, every time considering one more partial denominator. As soon as the calculated mass value (on the linear scale) was in the interval "*mass* $\pm$ *standard deviation*", we stopped considering further denominators and gave the resulting fraction in Table 4. In special cases, where the particle mass is much more accurately determined than the proton mass (e.g. electron) the standard deviation was set to that of the proton.

It was found that the great majority of the particle masses could be expressed by a continued fraction, which means that they are localized in nodes or sub-nodes. Only 10 particles were found to be localized in a gap. In such a case the continued fraction turns into an alternating sequence of $-e-1$ and $e+1$ without any further significant approximation to the mass value. In Table 4, this sequence was then abbreviated by three stars. It should be noted that the particle mass calculated from such a fraction is still close to the experimental value, but has a difference from the experimental value higher than the standard deviation. For around 50% of the particles, it was required to set the phase shift to 1.5 in order to get the masses located in a node or sub-node. For 14 particles, their masses can even be located in sub-nodes for both phase shifts (0 and 1.5). If so, both continued fractions were indicated in Table 4. As can be seen, the continued fractions have seldom more than 5 partial denominators, they can be even shortened abandoning the standard deviation requirement and accepting a small percentage error on the logarithmic scale as it was done in Müller's article [2].

There are, however some general questions open. It is clear that the continued fraction analysis provides a new system to put the particles in groups regarding the length of the fraction (fractal layers), the phase shift, value of the free link and the value of the numerator. Which of these parameters have physical meaning and which ones are just mathematics?

Especially regarding the physical significance of the nominator, more research must be done. We believe that is not coincidence that most of the masses become localized in nodes or sub-nodes when calculating the fractal spectrum with nominator e, similar calculations have shown that the numerators 2 or the golden ratio do not work in this manner. This however, was here found empirically, to the best of our knowledge there is no way to calculate directly which nominator reproduces best the fractal distribution. It must still be done by trial and error combined with intuition. Anyway, we suggest to abandon the canonical form of the continued fractions whenever possible, since with numerator 1, actually some physical information of the fractal distribution is lost. It is known that continued fractions with arbitrary numerator $\neq 1$ can be transformed into fractions with numerator equal to 1, via Euler equivalent transformation.

From the presented numerical results, some ideas can be derived:

1. The three most stable here considered particles are the electron, proton and neutron with half-life of around 11 minutes. Their continued fraction representations are quite short, consisting only of the free link and one

partial denominator. Possibly short continued fractions indicate stability. Furthermore the very high values of the first partial denominators n_1 indicate two facts: a proximity to the node n_0 and an irrelevance of any further partial denominator which can change the value of the fraction only insignificantly. This means a high value of n_1 might also be considered as a criterion for stability.

2. According to reference [1], in a node, there is a change from spectral compression to spectral decompression, which means that with a certain probability a change in process trend can be observed. This statement is in agreement with the continued fraction representations of the electron and the neutron. The electron [1.5; −9 | −177] lies with a negative first partial denominator closely before the principal node [1.5; −9], whereas the neutron [0; 0 | 1973] is positioned right after the principal node [0; 0] due to its positive denominator. This means the electron in the compression range is stable whereas the neutron is in a decompression range and already exhibits decay property.

4 Resume

Numerical investigation of particle masses revealed that 87% of the considered elementary particles can be interpreted as proton resonance states. We cannot expect that all particle masses are only governed by proton resonance properties, other natural laws apply as well. The here presented mathematical model can be modified in various ways and future research should concentrate on identifying fractal properties in other data sets such as half-lifes of radioactive nuclides or mass defects, utilizing either our or similarly modified continued fractions. Only when multiple fractal data sets are known, the possible numerical values of the numerator or the phase shift can be adequately interpreted and maybe attributed to a physical property.

Acknowledgements

The authors greatly acknowledge the financial support from the Brazilian governmental funding agencies FAPESQ and CNPq.

Submitted on July 21, 2010 / Accepted on August 11, 2010

References

1. Müller H. Fractal scaling Models of resonant oscillations in chain systems of harmonic oscillators. *Progress in Physics*, 2009, v. 2, 72–76.
2. Müller H. Fractal scaling models of natural oscillations in chain systems and the mass distribution of the celestial bodies in the solar system. *Progress in Physics*, 2010, v. 1, 62–66.
3. Müller H. Fractal scaling models of natural oscillations in chain systems and the mass distribution of particles. *Progress in Physics*, 2010, v. 3, 61–66.
4. Anders E., Grevesse N. Abundances of the elements — meteoritic and solar. *Geochimica et Cosmochimica Acta*, 1989, v. 53, 197–214.
5. Audi G., Wapstra A. H., Thibault C. The AME2003 atomic mass evaluation (II). Tables, graphs and references. *Nuclear Physics A*, 2003, v. 729, 337–676.
6. Lide D. R. (Editor) CRC Handbook of Chemistry and Physics. CRC Press, Boca Raton, 2005.
7. Press W. H., Teukolsky S. A., Vetterling W. T., Flannery B. P. Numerical recipes in C. Cambridge University Press, Cambridge, 1992.
8. Bethe H. A. Energy production in stars. *Physical Review*, 1939, v. 55, 434–456.
9. Otte R., Müller H. German patent No. DE102004003753A1, date: 11.08.2005.

Charge of the Electron, and the Constants of Radiation According to J. A. Wheeler's Geometrodynamic Model

Anatoly V. Belyakov
E-mail: belyakov.lih@gmail.com

This study suggests a mechanical interpretation of Wheller's model of the charge. According to the suggested interpretation, the oppositely charged particles are connected through the vortical lines of the current thus create a close contour "input-output" whose parameters determine the properties of the charge and spin. Depending on the energetic state of the system, the contour can be structurized into the units of the second and thirs order (photons). It is found that, in the framework of this interpretation, the charge is equivalent to the momentum. The numerical value of the unit charge has also been calculated proceeding from this basis. A system of the relations, connecting the charge to the constants of radiation (the Boltzmann, Wien, and Stefan-Boltzmann constants, and the fine structure constant) has been obtained: this give a possibility for calculating all these constants through the unit charge.

William Thomson (Baron Kelvin), the prominent physicist of the 19th century, said: "we can mean a phenomenon to be clearly understood only if a mechanical model of it has been constructed". It would be fine if the famous phrase would be actual in the nowadays as well. This however meets some difficulties, in particular — in the case of the electron, despite its spin has the dimension of mechanical angular momentum, and the charge is not (at least) a special "entity" or "electric substance".

In order to explain the properties of the electric charge, John A. Wheeler suggested his own concept of geometrodynamics. According to the concept, the charged microparticles are special points in the three-dimensional spatial surface of our world, connected to each other through "wormholes" — vortical tubes analogous to the lines of current working according to the "input-output" ("source-drain") principle, but in an additional dimension of space.

Is the fourth dimension still necessary in this case?

Suppose that the world, being an entity in the limits of the three-dimensional continuum, is a really *surface* which is *topologically non-unitary coherent* and *fractalized* upto the parameters of the micro-world bearing a fraction dimension of the numerical value upto three. In this case, it is easy to see that the Wheeler vortical tube is located "under the surface" of our world, thus is "invisible" to us, the fragments of the fractalized surface.

Meanwhile numerous specific properties of the microworld do not manifest themselves into it, or are manifested being *distorted*, as if they were projected into our world from an "additional" dimension. In particular, this should be true in the charge and spin of the electron, which can be considered according to the mechanistic scheme as the respective momentum of the vortical tube and the angular momentum with respect to its longitudinal axis. So forth we will consider, for brevity, the close contour crossing the surface X of the our world in the points, say, p^+ and e^-. In the framework of this scheme, a free charged particle is presented as a section of the open contour, or as a single-pole curl directed along the "additional" direction; the electron can be presented as an object activating the motion of the medium (electric current).

Let S be the sinus of an angle determining the projection of the momentum onto the surface X, and also the projection of the circulation velocity v (this is also, in the same time, the velocity of the rotation around the longitudinal axis of the contour) onto the chosen direction, say the axis $p^+ - e^-$. In this case, S^i characterizes the ratio of the projection of the velocity to the velocity itself ($i = 1, 2, 3$ depending on the orientation of the velocity vector).

Let, according to our initially suggestion, the charge be equivalent to the momentum, thus be Coulomb = kg×m/sec. Replace the elementary charge with the ultimate momentum of the electron, $m_e c$, in the formulae of Coulomb and Ampere. With taking this into account, in order to arrive at the numerical coincidence with the electric and magnetic forces (determined by the classical formulae), it is sufficient to introduce new formulae for the electric and magnetic contants, ε_0 and μ_0, as follows

$$\varepsilon_0 = \frac{m_e}{r_e} = 3.233{\times}10^{-16}\ \left[\mathrm{kg/m}\right], \tag{1}$$

$$\mu_0 = \frac{1}{c^2\,\varepsilon_0} = 0.0344\ \left[\mathrm{N}^{-1}\right], \tag{2}$$

where m_e is the mass of the electron, while c is the velocity of light. The quantity r_e means the classical radius of the electron, which is, in SI units,

$$r_e = \frac{10^{-7}\,e_0^2}{m_e}, \tag{3}$$

where e_0 is the charge of the electron.

Thus, these constants get a clear physical meaning now. They characterize the vortical tube, because ε_0 has a dimen-

sion of its density per meter, while μ_0 is the quantity reciprocal to the centrifugal force which appears when the element of the vortical tube, whose mass is m_e, rotates with the radius r_e with the linear velocity c.

The contour's length can vary, depending on the energetic state of the system. Assume that its increase, according to the well-known analogy to hydrodynamics, results the decrease of the tube's radius upto an arbitrary numerical value r, and also the creation of the secondary and tertiary spiral structures, which fill the toroidal volume (the section of the torus is the same as the classical radius of the electron r_e).

Thus, the charge of a particle can be characterized by the projection of the longitudinal component of the momentum Mv onto the surface X, where the mass of the vortical tube (contour) is proportional to the tube's length, and is

$$M = \varepsilon_0 R = \varepsilon n^2 R_b \,, \tag{4}$$

where n is the leading quantum number, $R_b = \alpha^2 r_e$ is the Bohr 1st radius, while α is the reciprocal fine structure constant which is 137.036 (it will be shown below that α is also determined according to the suggested model).

Among the possible contours characterized by different masses and velocities, there is such a contour in which the energy of the unit charge (electron) reaches the maximal numerical value. We take into account that a potential, in the framework of the mechanistic "coulombless" system, corresponds to a velocity. Thus, in the case of this contour, we can write down

$$e\,v = m_e c^2 = E_{max} \,, \tag{5}$$

where e is the common charge, which is identical to the momentum (in contrast to its projection, the observed charge e_0). In this contour, we determine the standard unit of the potential (velocity) as follows

$$\mathrm{v} = \frac{m_e v^2}{e} = 1 \ \text{[m/sec]} \,. \tag{6}$$

Thus we obtain, from (5) and (6),

$$v = c_p^{2/3}\,\mathrm{v} \,, \tag{7}$$

where the dimensionless velocity of light $c_p = \frac{c}{\mathrm{v}}$ has been introduced, and also

$$e = M v = m_e c_p^{2/3} c_p^{2/3}\,\mathrm{v} \,. \tag{8}$$

In other word, we see that the mass M of the contour is the same as $m_e c_p^{2/3} = 4.48{\times}10^5\, m_e$ that is close to the *summary mass of the bosons* W^+, W^-, Z^0.

We will refer to the contour as the *standard contour*. In it, the maximal energy of the "point-like" electron, $m_e c^2$, is the same as that of the current tube, $M v^2$. The numerical values of the charge and spin remain unchanged for any contour, and have a common component — the contour's momentum Mv. It should be noted that, despite the dimension of electric charge corresponds to the dimension of momentum, it is not common to both entities, thus cannot be divided by the dimensions of mass and velocity.

The projection of the momentum, which is the *observed charge*, is

$$e_0 = m_e c_p^{4/3} S^i \mathrm{v} \,, \tag{9}$$

where, as is obvious, $i = 1$, while the complete momentum of the vortical tube (the Planck constant h) reduced to the radius of the electron can be determined as the vector recovered, on the basis of the projection, in the general way where $i = 3$. Thus

$$\frac{h}{r_e} = 2\pi\alpha\, m_e c = \frac{e_0}{S^3} \,. \tag{10}$$

Taking e_0 from (9), we obtain, through (10),

$$S = \frac{c_p^{1/6}}{\sqrt{2\pi\alpha}} = 0.881, \tag{11}$$

thus the *projective angle* is 61.82°, while the obtained numerical value of the observed charge $e_0 = 1.61{\times}10^{-19}$ kg/m×sec differs from the exact value (standard numerical value obtained in the experiments) for doles of the percent.

The charge of the "point-like" electron in the region X, we will denote as e_x, is substituted into the formulae of Coulomb and Ampere: under ε_0 and μ_0 assumed in the model, it consist a very small part of e_0, which is

$$e_x = m_e c = \frac{e_0}{c_p^{1/3} S} = \frac{e_0}{590} \,. \tag{12}$$

The *main standard quantum number* can be expressed through the mass M of the contour and its density per one meter (the electric constant ε_0)

$$n_s = \sqrt{\frac{m_e c_p^{2/3}}{\varepsilon_0 R_b}} = \frac{c_p^{1/3}}{\alpha} = 4.884; \tag{13}$$

the contour's size is $R_s = n_s^2 R_b = 1.26{\times}10^{-9}$ m.

The *number of the ordered structural units* z of the contour (we will refer to them as *photons*, for brevity) is determined, for an arbitrary quantum number, by the ratio between the full length of the contour and the length of the wave λ

$$z = \frac{n^2 R_b \left(\frac{r_e}{r}\right)}{\lambda} \,, \tag{14}$$

where

$$\lambda = \frac{W}{R_\infty} \,, \tag{15}$$

Rydberg's constant is expressed as

$$R_\infty = \frac{1}{4\pi\alpha^3 r_e} \,, \tag{16}$$

while Balmer's formula is

$$W = \frac{m^2 n^2}{m^2 - n^2}\,, \tag{17}$$

where $n, m = 1, 2, \ldots$ Here the ratio of the radii $\frac{r_e}{r}$ takes into account the increase of the length of the "stretched" contour in the case where the spiral structures of the second and third orders are created. Because $\varepsilon_0 = const$ and $\mu_0 = const$, in the case of arbitrary r and v the formulae (1) and (2) lead to

$$\frac{r_e}{r} = \left(\frac{c}{v}\right)^2. \tag{18}$$

We obtain the *velocity v* and *radius r of the vortical tube of the contour*, in the general case, from the condition of constancy of the momentum which is true for any contour having an arbitrary quantum number n. We obtain

$$M v = m_e c_p^{4/3} \mathrm{v} = n^2 R_b \varepsilon_0 v\,, \tag{19}$$

wherefrom, substituting the extended formulae of R_b and ε_0, and taking (18) into account, we obtain

$$v = \frac{c_p^{1/3} c}{(\alpha n)^2}\,, \tag{20}$$

$$r = \frac{c_p^{2/3} r_e}{(\alpha n)^4}\,. \tag{21}$$

As a result, with (15) and (16) taken into account, and having the velocity v replaced with its projection $v S^i$, we obtain the number of the photons in the arbitrary contour

$$z = \frac{n^6 \alpha^3}{4\pi W c_p^{2/3} S^{2i}}\,. \tag{22}$$

In particular, consider the standard contour (denote it by the index s). In the unitary transfer in it from n_s to $n_s + 1$, we obtain: $W_s = 76.7$, $\lambda_s = 7.0{\times}10^{-6}$ m, $v_s = 4.48{\times}10^5$ m/sec, $r_s = 6.3{\times}10^{-21}$ m, while the number of the photos z_s being calculated under $i = 2$ is close to $\alpha = 137$.

Thus, given a "standard" photon, the following relation

$$\frac{R_s}{r_e} = \frac{r_e}{r_s} = c_p^{2/3} = 448000 \tag{23}$$

is reproduced (that is specific to an atom).

The *Boltzmann, Wien, and Stefan-Boltzmann constants*, k, b, and σ, can be determined connecting the energy of the section of the contour in the region X taken per one photon, E_z, i.e. the energy of the structural unit, with the energy of the heat motion E_t (the average energy of the radiating oscillator) in the case of a specific particular conditions.

We express E_z and E_t as follows

$$E_z = \frac{e_x v S}{z}\,, \tag{24}$$

$$E_t = k\,T\,. \tag{25}$$

The numerical value of E_z decreases with the increase of the quantum number so that, with a numerical value of n, it becomes equal E_t taken with the wavelength λ of the photon emitted by a black body whose temperature is that of the scale unit

$$E_z = E_t \quad \text{under} \quad T = 1^\circ\ [\mathrm{K}]\,. \tag{26}$$

With decreasing n, the numerical value of E_z increases faster than E_t. Assume that, with taking (23) into account, the following ratio

$$(E_z)_s = z E_t \quad \text{under} \quad T = T_s \tag{27}$$

is true for the standard contour.

Using (12), (20), and (22), we modify (24) then re-write (26) and (27) for n and n_s assuming that the most large contour has been contracted into a tertiary structure

$$\frac{A W}{n^8} = k\,T\,, \qquad i = 3, \quad T = 1^\circ\ [\mathrm{K}]\,, \tag{28}$$

$$\frac{A_s W_s}{n_s^8} = k\,T_s\,z\,, \qquad i = 2. \tag{29}$$

where $A = 4\pi S^{2i} n_s^5 e_0 \mathrm{v}$. Taking into account that $\frac{A}{A_s} = S^2$ and also

$$1^\circ\ [\mathrm{K}] = \frac{b R_\infty}{W}\,, \tag{30}$$

$$T_s = \frac{b R_\infty}{W_s} \tag{31}$$

where Wien's constant is

$$b = T\lambda\,, \tag{32}$$

we obtain, from the common solution of (28) and (29),

$$\frac{n^4}{W} = \frac{S\,z^{1/2} n_s^4}{W_s}\,. \tag{33}$$

Assume $z = z_s = 137$. Taking (17) into account, we calculate, for the transfer from n to $n+1$: $n = 39.7$, $W = 32470$, $\lambda = 0.0030$ m, *Wien's constant* $b = 0.0030$ m×K. From (28), we obtain *Boltzmann's constant* $k = 1.38{\times}10^{-23}$ J/K. According (22), we obtain the *number of the photons* of the contour: $z = 117840$ under $i = 3$.

The number of the photons z of the given contour is very close to the numerical value of $2\pi\alpha^2$. This result does not follow from the initially assumptions, thus is absolutely independent. So, the presence of the secondary and tertiary structures has been confirmed. That is, there are three specific contours: the contour of the 1st order (the Bohr 1st radius, $n = 1$; the contour of the 2nd order (the standard contour, $n = 4.884$, containing α structural units, the photons); and the contour of the 3rd order ($n \approx 40$, containing $2\pi\alpha^2$ photons).

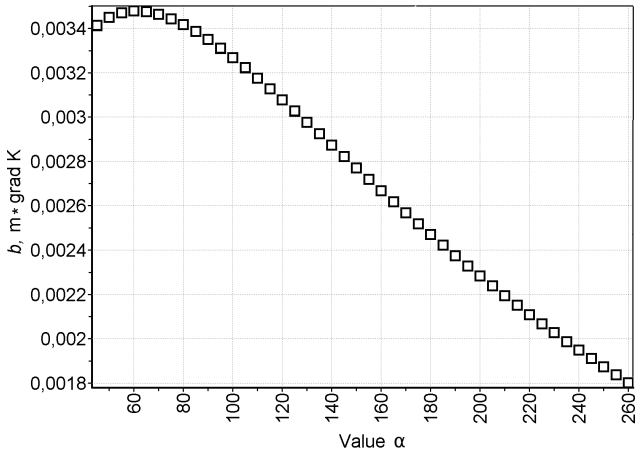

Fig. 1: Dependency of Wien's constant b on the reciprocal value of the fine structure constant α.

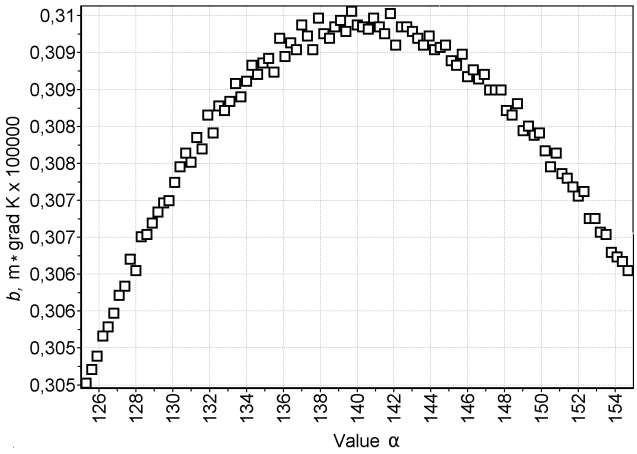

Fig. 2: Results of the numerical differentiation of the function $b(\alpha)$ in the region of the second singular point (inflection of the $b(\alpha)$ arc). The ordinate axis means the speed of the change of the parameter b.

Boltzmann's constant can be expressed also through the parameters of the standard contour

$$k = \frac{n_s e_0 \mathrm{v}}{\alpha T_s} = 1.38{\times}10^{-23} \text{ [J/K]} , \qquad (34)$$

where $T_s = \frac{b}{\lambda_s} = 414.7^\circ$ K.

Formula (34) can be transformed so that

$$\frac{kT}{n_s} = m_e \left(c_p^{2/3} \mathrm{v}\right)^2 \frac{S}{\alpha} , \qquad (35)$$

i.e. *given the standard contour, the energy of the radiating oscillator per the contour's quantum number is equal to the energy of the internal rotation of the "point-like" electron taken per the number of the structural units of the contour.*

It is interesting to compare the Planck entropy of the photon, S_h, to the entropy of the part of the contour related to the single photon, S_z, within the region X. The Planck entropy remains constant

$$S_h = \frac{E_h}{T} = \frac{hc}{\lambda T} = \frac{hc}{b} = 6.855{\times}10^{-23} \text{ [J/K]} , \qquad (36)$$

while S_z decreases rapidly with the increase of the leading quantum number

$$S_z = \frac{E_z}{T} = \frac{AW}{n^8 T} = \frac{AW^2}{n^8 b R_\infty} . \qquad (37)$$

Equalizing S_h to S_z, and expanding the formulae for h, R_∞, and A for the case of the ionization of the atom (that means the transfer from n to $m \to \infty$ under $W \to \infty$), we obtain, under $i = 1 \ldots 3$,

$$n_\infty = \sqrt[4]{8\pi n_s^3 S^{2i+1}} = 6.7 \ldots 5.9 . \qquad (38)$$

Because the common direction of the physical processes to the increase of entropy, thermodynamics prefers, with $n > 6.7$, that the structural units of the contour exist separately from each other, i.e. are the photons. It is probably, this result verifies the identity of the contour's structural units to the photons, and also manifests one of the causes of that the stable atoms have no more electronic shells than 6 or 7.

The *Stefan-Boltzmann constant* can be expressed as the projection of the unit energy of the heat motion per one photon and the unit square of the standard contour, i.e. as $k\Delta T S/(\alpha n_s^4 R_b^2)$, where $\Delta T = 1^\circ$K, and reduced to the unit of time and the unit of temperature (in the respective exponent). As a result, we obtain $\sigma = 5.56{\times}10^{-8}$ [W/m^{2}K^4].

The obtained formulae (34), (35), and (39) are actually definitions. They completely confirm the existence of the special standard contour.

Despite the fine structure constant was used in the calculation (the constant itself is meant to be derived from e_0 and h), the calculation was processed in independent way. Besides, assuming that α and all other quantities dependent on it (r_e, S, e_0, n_s, z, k, b) are variables, we can determine the numerical value of α according to the location of the second singular point (inflection of the $b(\alpha)$ arc in Fig. 1), where the change of b is proportional to the quantum number. Numerical differentiation, Fig. 2, manifest the numerical value of α within the boundaries 137–140 and, hence, it manifests the numerical values of all other parameters (for instance, k and z in Fig. 3 and Fig. 4 respectively). That is, finally, in order to calculate all the parameters we only need: the *mass of the electron*, the *velocity of light*, the *units of velocity and temperature*, and the *assumption that E_z is proportional to E_t in the standard contour*.

It is interesting that more precise numerical value of α arrives under the condition that m and n approach to infinity in the function $b(\alpha)$ and Balmer's formula (17). Thus Balmer's formula becomes $W = \frac{n^3}{2}$ under infinite large distance between the charges, that meets the determination of the textbook nu-

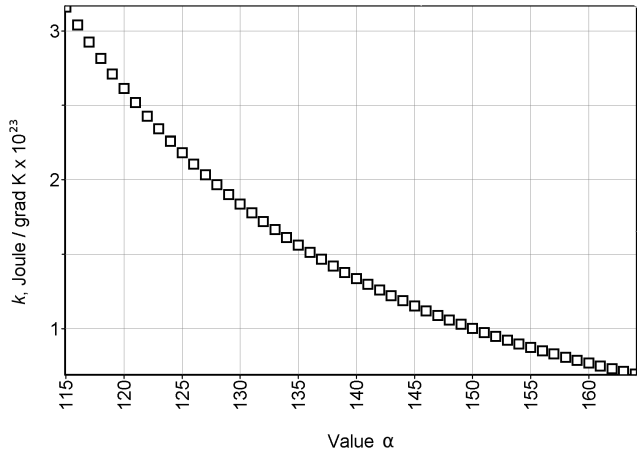

Fig. 3: Dependency of Boltzmann's constant k on the reciprocal value of the fine structure constant α.

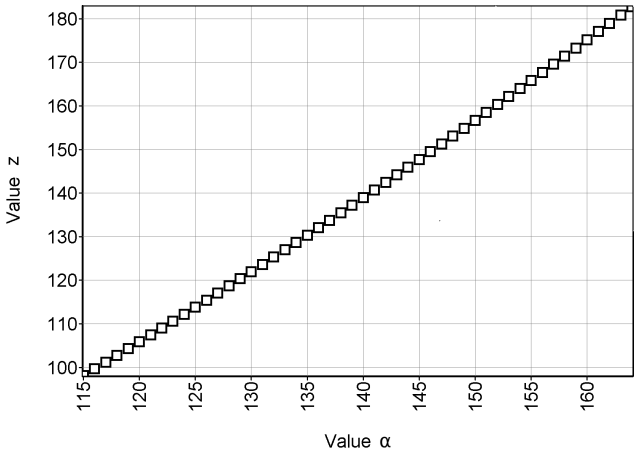

Fig. 4: Dependency of the number of the photons z of the standard contour on the reciprocal value of the fine structure constant α.

merical value of α. In the same time, we can obtain the exact numerical value of the charge from formula (1), by substituting α determined from the function $b(\alpha)$, Fig. 2.

Note that the validity of the suggested model is confirmed by that significant fact that the quantity kT, which is the unit of the work done by the structural unit of an ideal gas (this quantity is also interpreted, in the theory of heat radiation, as the energy of an elementary oscillator), is connected here with the charge of the electron. A connexion between Planck's constant and the quantity kT was found, as is known, in already a century ago by Max Planck, through the formula of the blackbody radiation. This formula is proportional to

$$\frac{1}{\lambda}\,\frac{1}{\lambda}\,\frac{1}{\lambda\,(e^{C/\lambda}-1)}\,,$$

where C is a constant. Taking all that has been obtained in our study, we understand follows. The first term here manifests the decrease of the intensity of the radiation with the increase of the wavelength of the photon. The second term manifests the decrease of the number of the photons per the unit of the full length of the contour. The third term manifests the change of the length of the contour itself, which reaches a contant with the increase of λ thus the Planck formula transforms into the Rayleigh-Jeans formula. With small numerical values of λ, the contour compresses upto the size of the photon. This gives an explanation to the decrease of the radiation power on high frequencies.

In the end, it should be noted that the properties of the charge are, of course, not limited by Wheeler's model in its mechanistic interpretation suggested here. Meanwhile, the unexpected relation between the charge of the electron and the molecular kinetic properties of the atoms and molecules manifests additional connexions between the elementary particles and macro-particles, thus this fact needs to be more studied in the future.

Submitted on July 24, 2010 / Accepted on August 17, 2010

LETTERS TO PROGRESS IN PHYSICS

Scientific Community of Valentin N. Samoilov

(On the Occasion of His 65th Birthday Anniversary)

Dmitri Rabounski
E-mail: rabounski@ptep-online.com

In this letter we celebrate the 65th birthday anniversary of Prof. Valentin N. Samoilov, a man of the Soviet scientific ancestry in the nuclear and space research, who is a pupil and follower of the famous Soviet engineer Sergey P. Korolev and the prominent Soviet nuclear physicist Michael G. Mescheryakov.

Prof. Valentin N. Samoilov. The back wall of his cabinet is curtained with photo portrait of Michael G. Mescheryakov.

On behalf of the Editorial Board of *Progress in Physics*, in April 25, 2010, I am pleased to celebrate the 65th birthday anniversary of Professor Valentin Nikolaevich Samoilov, ScD, Director of Scientific Centre of Applied Research, Joint Institute for Nuclear Research (JINR), Dubna, Russia. His more than 45 years of the successful work on science rose from that fact that he started his scientific activity being of a pupil of two famous persons of the Soviet scientific ancestry: Sergey P. Korolev, the engineer and rocket designer who headed the pioneering cosmic flights in the USSR, and Prof. Michail G. Mescheryakov, the nuclear physicist an close co-labour of Igor V. Kurchatov in the construction and launch of the first cyclotronic accelerator of particles in Leningrad, 1938–1940. According to the testament of his teachers, Prof. Samolilov spends his life in scentific research. He is still full of energy and creative scentific ideas until the present day.

In the row of Prof. Samoilov's scientific achievements, which are many, I would like to emphasize four fundamental discoveries in physics of solids and particles he did in common with Dr. Vahan N. Minasyan (reportas about these were published recently in *Progress in Physics* [4–7]). In these papers, they presented a new and very original approach to investigation of the excitation processes of electromagnetic surface shape resonances in lamellar metallic gratings by light, from the visible to near-infrared scale, based on the surface plasmon–polaritons, where they first argued that the smooth metal-air interface should be regarded as a distinct dielectric medium, the skin of the metal. They predicted the existence of light quasi-particles bearing spin equal to 1, and a finite effective mass $m = 2.5{\times}10^{-5}\, m_e$ (where m_e is the mass of the electron); these light quasi-particles should excite two type surface polaritons in the nanoholes in metal films. They also found, theoretically, that a transverse electromagnetic field should exist being formed by supersonic longitudinal and transverse waves in solids which acquire the frequency and the speed of sound. According to their theory, the transverse electromagnetic field should propagate along the direction the forming supersonic wave travels. In this context, another very interesting result obained in the paper [6] should also be noted: there they first proved that the property of the lambda-point of superliquid helium is determined by registering the single neutron modes or neutron pair modes in the neutron-spectrometer.

In addition to his scientific research, Prof. Valentin N. Samoilov is known as a successful organizer of science, and also as a designer of the space flight complexes and their segregate components. He was granted by the honorary title Merit Creator of Cosmical Techniques (2006) and by the international order Tsciolkovski Star (2002). He also was conferred with the order Beneficence, Honor and Glory (2006), Tsiolkovski Medal (2004), and Korolev Medal (2005). Due to his activity in astro-biology research, in 2005 he was elected to the International Academy of Information, Communica-

tion, Control, in Engineering, Nature, and Society (Pasadena, California, USA). Aside for these, during the last 15 years Prof. Samoilov governs numerous common scientific projects on the nuclear safety between JINR and DOE, which include close communications with the US National Laboratories such as BNL, SNL and PNNL. Also, during the last 20 years he governs communications between JINR and European Scientific Nuclear Research Centre in Geneva (CERN), in the framework of the scientific projects LHC, CMS, ATLAS, COMPASS, and CLIC. By governing of him, a joint scientific community is working amongst JINR, Institute of Particle and Nuclear Studies, and High Energy Accelerator Research Organization (Japan). Due to his international activity, connecting research scientists throughout the world, Prof. Samoilov was conferred with Order of People Friendship which was decorated upon him in 2006 by Vladimir V. Putin, President of Russia.

Prof. Valentin N. Samoilov authored two scientific monographs, *Technology Modeling of the Complicated Processes* [1] and *Theoretical Informational Analysis of the Complicated Systems* [2], and co-authored seven other scientific books. During his long term and successful scientific carrier, he also authored about 300 scientific publications, 20 registered inventions certified by patents, and 30 software application [3]. For several of these achievements, he was confered wth A. S. Popov Silver Medal (2006).

The decades of distinguished leadership and mutual cooperation in the field of nuclear material protection control and accountability between Russia and the USA are greatly recognized as his contribution to the global security. In the present time, Prof. Valentin N. Samoilov is still engaged for the nuclear and cosmic safety as an experienced veteran of the atomic industry.

I would like to wish Prof. Samoilov for long life and success in the future.

Submitted on April 29, 2010 / Accepted on April 30, 2010

References

1. Samoilov V.N. Technology modeling of the complicated processes. *Joint Institute for Nuclear Research*, Dubna, Russia, 2000.
2. Samoilov V.N. Theoretical informational analysis of the complicated systems. *Joint Institute for Nuclear Research*, 2000, Dubna, Russia.
3. Interacademic Information Bulletin, Saint Petersburg, *International Academia*, 2006, v. 22 anniversary, 316–325.
4. Minasyan V.N. and Samoilov V.N. Two type surface polaritons excited into nanoholes in metal films. *Progress in Physics*, 2010, v. 2, 3.
5. Minasyan V.N. and Samoilov V.N. The intensity of the light diffraction by supersonic longitudinal waves in solid. *Progress in Physics*, 2010, v. 2, 63.
6. Minasyan V.N. and Samoilov V.N. Formation of singlet fermion pairs in the dilute gas of boson-fermion mixture. *Progress in Physics*, 2010, v. 4, 3.
7. Minasyan V.N. and Samoilov V.N. Dispersion of own frequency of ion-dipole by supersonic transverse wave in solid. *Progress in Physics*, 2010, v. 4, 10.

LETTERS TO PROGRESS IN PHYSICS

Nikias Stavroulakis (1921–2009). In Memoriam

Ioannis M. Roussos

Dept. of Mathematics, Hamline University, 1536 Hewitt Avenue, Saint Paul, Minnesota 55104-1284, USA
E-mail: iroussos@gw.hamline.edu

This paper was written by Dr. Ioannis M. Roussos, Professor of Mathematics, Hamline University at Saint Paul, Minnesota, in honor and memoriam of the late Dr. Nikias Stavroulakis, Professor of Mathematical Physics. The included information is particularly based on the publications of the late professor, and was particularly collected through the various types of communication (personal visits with lengthy and extensive discussions, professional meetings, letters, telephone-calls, words of relatives and friends, etc.) Dr. Roussos had with and about him in the last 14 years. Dr. Roussos first met Dr. Stavroulakis in the 3rd Panhellenic Congress of Geometry, University of Athens, Greece, May 1996, and they became friends ever since.

Prof. Nikias Stavroulakis, Limoges, France, 1980.

Nikias Stavroulakis was born at the village Thronos Rethymnes of the Island of Crete, Greece, on October 2, 1921. In 1938 he finished high school (Lyceum) and then entered the National Technical University (E. M. Polytechnion), Athens, Greece, where he studied Civil Engineering.

Although World War II interrupted the smooth course of his studies, destroyed his country, and he escaped execution by the Nazis on account of their defeat and hasty retreat for a time-span of just a few days, he managed to continue his studies after the war was over, in 1945. He graduated from the National Technical University (E. M. Polytechnion), Athens, Greece, in 1947.

During the years 1949–1963 he worked as a civil engineer in Greece. His work, as civil engineer, was done under extremely trying and bad conditions, civil war, imprisonment, great difficulties and political turmoil, struggle and pressure.

The year 1963, he was released from a Greek prison in which he was kept because of ideological believes and political reasons, and went to Paris, France, to pursue graduate studies in mathematics. He eventually received Doctorat d'Etat from Faculté des Sciences of Paris in 1969. His advisor was the famous professor Charles Ehresmann. His dissertation was entitled *Substructure of Differentiable Manifolds and Riemannian Spaces with Singularities*.

Then, he was immediately hired as a professor of mathematics by the University of Limoges, France, from which he retired the year 1990. On his retirement he returned to Athens, Greece, where he mainly stayed and continued his research until the end of his life.

He is the author of numerous papers related to the subjects of: Geometry, algebraic topology, differential geometry, optimization problems, mathematical physics and general relativity. His scientific work and contributions were recognized internationally from the beginning.

Although he had retired for several years, he continued his scientific and mathematical research up to the end of his life in December 2009 at the ages of 88. His main purpose was to restore the theory of gravitational field by pointing out the misunderstandings and correcting the mathematical errors committed by relativists since the inception of general relativity and thus rejecting them right from the beginning of his carrier.

Unfortunately he died on the 20th of December 2009, due a chronic aneurism in the abdominal area. At that time he was working on several papers, but his untimely death left them unfinished. As he had told me, among other things, he was planning to write a few things about the use of the polar coordinates beyond those he had already exposed in his already published papers, write some expository papers and above all to finish especially the important paper *On the Filed of a Spherical Charged Pulsating Distribution of Matter*, which will appear (as he left it unfinished), as his sixth publication in the journal *Progress in Physics*. He will be greatly missed from his friends and scientific collaborators.

Nikias Stavroulakis at the age of 4 years, outside his house at the village Thronos, Crete, Greece, 1925.

Nikias Stavroulakis (center, 6th from the left in the middle row), with his classmates and teachers of the last grade of Lyceum of Rethymno, Crete, Greece, 1938.

Nikias Stavroulakis and Salomi in their wedding, Athens, Greece, 1958.

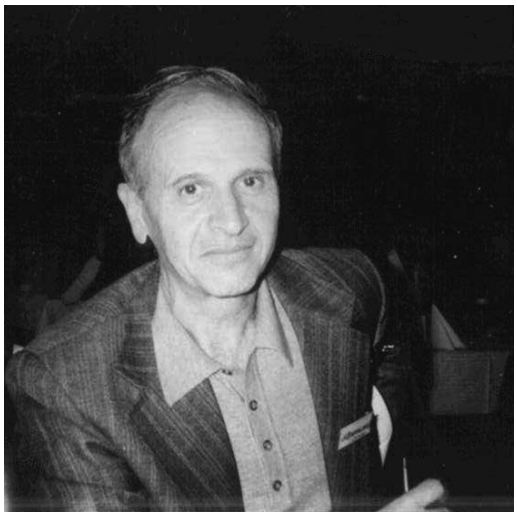

Prof. Nikias Stavroulakis on the 10th International Conference on General Relativity and Gravitation in Padova, Italy, July 4–9, 1983.

He was married to Salomi, who died four years earlier, with whom he had a daughter, Eleni.

Besides being a great, well published, voluminous and original scientist, Nikias Stavroulakis was always the polite man of principle and humility; seeking the truth and never being afraid to say "*we do not know yet*", when something was unknown, elusive or simply surmised.

Dr. Nikias Stavroulakis was Professor at Université de Limoges, Département de Mathématique, France, and Member of Faculté des Sciences de Limoges, U. E. R. des Sciences de Limoges and then Emeritus during his time of research in relativity and gravitation. He made an extensive and advanced contribution in:

1) the Birkhoff theorem in General Relativity;
2) the indiscriminate use of the polar coordinates, before knowing what the manifold in which we work is;
3) the static and dynamical field of a pulsating spherical mass;
4) the theory of black holes and the Big Bang theory.

Nikias Stavroulakis' publications on mathematical physics and General Relativity

1. A statical smooth extension of Schwarzschild's metric. *Lettere al Nuono Cimento*, 1974, v. 11, no. 8, 427–430.
2. Paramètres cachés dans les potentials des champs statiques. *Annales de la Fondation Louis de Broglie*, 1981, v. 6, no. 4, 287–327.
3. Mathématiques et trous noirs. *Gazette des mathematiciens*, Juillet 1986, no. 31, 119–132.
4. Solitons et propagation d'actions suivat la relativité générale. (Premième partie). *Annales de la Fondation Louis de Broglie*, 1987, v. 12, no. 4, 443–473.
5. Solitons et propagation d' actions suivat la relativité générale. (Deuxième partie). *Annales de la Fondation Louis de Broglie*, 1988, v. 13, no. 1, 7–42.
6. Sur quelques points de la theorie gravitationnelle d'Einstein. *Tiré à part de Sinsularité*, Lyon, France, Aout–Septembre 1991, v. 2, no. 7, 4–20.
7. Particules et particules test en relativité générale. *Annales de la Fondation Louis de Broglie*, 1991, v. 16, no. 2, 129–175.
8. Sur la function de propagation des ébranlements gravitationnels. *Annales de la Fondation Louis de Broglie*, 1995, v. 20, no. 1, 1–31.
9. On the principles of general relativity and the SΘ(4)-invariant metrics. *Proceedings of the 3rd Panhellenic Congress of Geometry*, Athens, Greece, 1997, 169–182.
10. Vérité scientifique et trous noirs (première partie). Les abus du formalisme. *Annales de la Fondation Louis de Broglie*, 1999, v. 24, no. 1, 67–109.
11. Vérité scientifique et trous noirs (deuxmième partie). Symétries relatives au groupe des rotations. *Annales de la Fondation Louis de Broglie*, 2000, v. 25, no. 2, 223–266.
12. Vérité scientifique et trous noirs (troisième partie). Équations de gravitation relatives à une métrique Θ(4)-invariante. *Annales de la Fondation Louis de Broglie*, 2001, v. 26, no. 4, 605–631.
13. Vérité scientifique et trous noirs (quatrième partie). Determination de métriques Θ(4)-invariantes. *Annales de la Fondation Louis de Broglie*, 2001, v. 26, no. 4, 743–764.
14. Matière cachée et relatitité générale. *Annales de la Fondation Louis de Broglie*, 2001, v. 26, no. spécial, 411–427.
15. On a paper by J. Smoller and B. Temple. *Annales de la Fondation Louis de Broglie*, 2002, v. 27, no. 3, 511–521.
16. Non-Euclidean geometry and gravitation. *Progress in Physics*, 2006, v. 2, 68–75.
17. On the propagation of gravitation from a pulsating source. *Progress in Physics*, 2007, v. 2, 75–82.
18. On the gravitational field of a pulsating source. *Progress in Physics*, 2007, v. 4, 3–8.
19. Gravitation and electricity. *Progress in Physics*, 2008, v. 2, 91–96.
20. On the stationary charged spherical source. *Progress in Physics*, 2009, v. 2, 66–71.
21. General Relativity and black holes. *The Hellenic Mathematical Review*, January–June 2009, no. 71, 43–83 (*in Greek*).
22. On the field of a spherical charged pulsating distribution of matter. *Progress in Physics*, 2010, v. 4, 72–77.

Submitted on July 20, 2010 / Accepted on August 22, 2010

Progress in Physics **is an American scientific journal on advanced studies in physics, registered with the Library of Congress (DC, USA): ISSN 1555-5534 (print version) and ISSN 1555-5615 (online version). The journal is peer reviewed and listed in the abstracting and indexing coverage of: Mathematical Reviews of the AMS (USA), DOAJ of Lund University (Sweden), Zentralblatt MATH (Germany), Scientific Commons of the University of St. Gallen (Switzerland), Open-J-Gate (India), Referential Journal of VINITI (Russia), etc.** ***Progress in Physics*** **is an open-access journal published and distributed in accordance with the Budapest Open Initiative: this means that the electronic copies of both full-size version of the journal and the individual papers published therein will always be acessed for reading, download, and copying for any user free of charge. The journal is issued quarterly (four volumes per year).**

Electronic version of this journal:
http://www.ptep-online.com

Postal address: Department of Mathematics and Science, University of New Mexico, 200 College Road, Gallup, NM 87301, USA

Printed in the United States of America

ISSN 1555-5534

9 771555 553907 >